


Alternative Plan for
Tahoe Valley South
Subbasin (6-005.01)
First Five-Year Update

Rybarski, S., M. Hausner and I. Bergsohn
4/22/2022
Volume I - Report

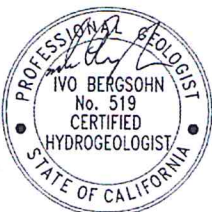

Respectfully Submitted,

Susan Rybarski Digitally signed by Susan Rybarski
Date: 2022.04.27 07:23:20 -07'00'

Susan Rybarski, Research Scientist
Desert Research Institute



Mark Hausner, PhD., Associate Research Professor
Desert Research Institute



Ivo Bergsohn, PG, HG, Hydrogeologist
South Tahoe Public Utility District

EXECUTIVE SUMMARY

The historic passage of the Sustainable Groundwater Management Act (SGMA) in 2014 set forth a statewide framework to help protect groundwater resources over the long-term. A core underpinning of SGMA is the concept of local control. SGMA requires local agencies to form a groundwater sustainability agency (GSA) for each high and medium priority basin. Each GSA then develops and implements a groundwater sustainability plan (GSP) or an alternative (Alternative) to avoid undesirable results and mitigate overdraft within 20 years.

The Tahoe Valley South Subbasin of the Tahoe Valley Groundwater Basin (TVS Subbasin) is classified by the California Department of Water Resources (DWR) as a medium priority basin. Because the TVS Subbasin is not critically overdrafted, the South Tahoe Public Utility District (District) elected to submit its 2014 Groundwater Management Plan (2014 GWMP) and additional plans reports, and other documents, referred to as Alternative Materials, as an Alternative to a GSP to DWR by January 1, 2017. DWR determined that the 2014 GWMP submitted by the District satisfied the objectives of SGMA pursuant to Water Code Section 10733.6 and approved it as the Alternative Plan for the TVS Subbasin. The following document is the first five-year update of this Alternative Plan and is referenced herein as the Alternative Plan.

SECTION ES-1: INTRODUCTION

Shortly after SGMA was enacted, the District and EDWA became GSAs within the TVS Subbasin. The agencies cooperate to ensure the entire TVS Subbasin is sustainably managed, with the District taking the primary management responsibility and the lead role in developing a plan compliant with SGMA.

Prior to SGMA's enactment, the District managed the TVS Subbasin under the 2014 GWMP. The District and EDWA continued to manage groundwater under the Alternative Plan since its submission to DWR in December 2016. This document is the first five-year update of the Alternative Plan and will be submitted to DWR for periodic review of the Alternative Plan.

Since it was submitted, the District and EDWA have continued to manage groundwater successfully within the TVS Subbasin. Major accomplishments included broadening the scope of basin monitoring; developing complex hydrologic models to calculate water budgets, evaluate future conditions, identify recharge areas, consider groundwater-surface water interactions, and evaluate remedial alternatives for the management of contaminated groundwater found within the TVS Subbasin. Investigations were performed to define the extent of groundwater contamination and assess the suitability of renewing the use of an impaired groundwater source for contaminant plume control and removal. Other investigations were used to inform possible management actions to address Basin Management Objectives (BMOs). Public outreach involving private well owner surveys were also performed to foster communications between private well owners and the District, inform private well owners about the District's role and responsibilities as a GSA and inform the District on the use of individual water system wells and the concerns of individual water system well owners. Under the Alternative Plan, the District

also satisfied all new annual reporting requirements under SGMA and continued to satisfy its monitoring entity requirements under the California State Groundwater Elevation Monitoring (CASGEM).

In addition to the groundwater management projects and activities conducted under the 2014 GWMP and Alternative Materials, the District undertook additional studies building on previous modeling analysis to address Recommended Actions identified in the DWR Statement of Findings, including but not limited to development of projected water budgets over the 50-year planning and implementation horizon, incorporating climate change effects, reconciling future water demand projections between the District's Urban Water Management Plan (UWMP) and the Alternative Plan; estimating quantity and timing of depletions of surface water; and development of sustainable management criteria to demonstrate sustainability within the TVS Subbasin.

The District will continue to update the Alternative Plan every five years as required by Water Code section 10733.6(c).

SECTION ES-2: TAHOE VALLEY SOUTH SUBBASIN

The TVS Subbasin (6-005.01) is the largest of three subbasins within the Tahoe Valley Groundwater Basin (6-005). The TVS Subbasin does not share a boundary with any other basin or subbasin identified in California's Groundwater (Bulletin 118).

TVS Subbasin Delineation

The TVS Subbasin is a triangular area bordering the southern shoreline of Lake Tahoe, underlying the City of South Lake Tahoe. The TVS Subbasin is bounded by the Sierra Nevada, the Carson Range, and Lake Tahoe.

Climate

Precipitation is greater in the Lake Tahoe Basin than in the Central Valley, California to the west or the Carson Valley, Nevada to the east. Storms in November through May account for over eighty-five (85) percent of precipitation within the Lake Tahoe Basin. On average, 334,000 acre-feet per year (AFY) of precipitation falls within the TVS Subbasin and its surrounding watersheds.

Climate change is expected to alter timing of snowmelt and streamflow, shifting peak snowpack runoff by approximately six (6) weeks and peak groundwater recharge by approximately four (4) weeks. Although changes in quantities of precipitation are highly uncertain, models agree precipitation is more likely to come as rain as opposed to snow.

Soils

The TVS Subbasin consists of three soil types at the order level: Alfisols are found under forest canopies, entisols associated with mountainous terrain, and inceptisols are located along riparian corridors of Trout Creek and the Upper Truckee River.

Geology

The regional geology is generally mountains composed of granitic rocks and valleys filled with basin-fill sedimentary deposits. The basin-fill deposits are primary sources of groundwater within the TVS Subbasin. Lake Tahoe rests within a fault-bounded structural basin, or graben, bordered by the Sierra Nevada and the Carson Range. Periods of glaciation created most of the canyons around Lake Tahoe and deposited large quantities of sediment, more than 1,000 feet thick in some places.

Within the TVS Subbasin, the geology consists of glacial, fluvial, and lacustrine basin fill deposits overlying the bedrock units. At least three areas of thick sediment (600-1,000 feet thick) occur within the TVS Subbasin: (1) underlying the City of South Lake Tahoe between Tahoe Keys development and Bijou Creek; (2) near the shore of Lake Tahoe, north of Fallen Leaf Lake, underlying the present drainages of Baldwin and Taylor Creeks; and (3) underlying the Meyers area south of Twin Peaks. These locations are also associated with the highest groundwater production. Glacial deposits formed coarse-grained glacial till composed of variable mixtures of silt and sand with cobble to boulder size material, as glaciers advanced north toward Lake Tahoe through the Upper Truckee River Valley. Glacial outwash of layered silt, sand and gravels were deposited from meltwaters as glaciers receded. Where glacial streams deposited sediment directly into Lake Tahoe, broad deltas were formed. Fine-grained lake deposits of silt and clay were deposited during high stands in lake level and are interlayered with coarse grained glacial and fluvial deposits. Alluvium are floodplain deposits composed of stratified silt and sand and channel deposits of stratified sand and gravel with locally interbedded lacustrine deposits.

Description of Basin Aquifers

Most wells drilled within the TVS Subbasins penetrate basin-fill deposits consisting of unconsolidated glacial, lake and stream sediments reaching thicknesses of 1,000 feet and varying in permeability. The basin-fill deposits include at least twenty-six (26) water bearing zones (WBZs) informally recognized within the TVS Subbasin. Relatively high permeability glacial outwash and delta deposits form the most productive WBZs within the basin-fill aquifer.

For ease of description, the TVS Subbasin is subdivided into six geographic subareas: Christmas Valley (CV), Meyers (M), Angora (A), South Lake Tahoe (SLT), Tahoe Keys (TK) and Bijou (B). WBZs recognized in the basin-fill are identified by the geographic subarea in which they are found and the stratigraphic order in which they occur from deep to shallow depth (1 = lowermost zone; 5 =-uppermost zone).

Surface Water Features

The Tahoe Regional Planning Agency recognizes eleven (11) priority watersheds within the TVS Subbasin and surrounding watersheds covering an area of 99,900 acres. Of these portions of seven watersheds lie within the TVS Subbasin. These watersheds all flow into Lake Tahoe. Average annual runoff from these watersheds to Lake Tahoe is estimated at about 124,000 AFY.

Lake Tahoe is the principal hydrologic feature, covering approximately 192 square miles. The Lake Tahoe Dam controls the surface elevation of Lake Tahoe, which has ranged from 6,220 to 6,229 feet over the last few decades. Numerous other lakes and tributary streams also occur within the TVS Subbasin.

Groundwater Dependent Ecosystems (GDEs) primarily occur within Stream Environment Zones (SEZs) which are areas that owe its biological and physical characteristics to the presence of surface or groundwater, generally along riparian corridors. GDEs within the TVS Subbasin are not only affected by groundwater management practices, but also climate change, land use changes, and other disturbances. There are one-hundred thirty (130) GDEs within the Lake Tahoe Basin of which forty-seven (47) occur within the TVS Subbasin.

An interagency Environmental Improvement Program (EIP) was developed in 1996 to improve watersheds and water quality, forest health, transportation, and sustainable recreation. Numerous projects have been achieved under this effort including stormwater management and erosion control, installation of wetland treatment systems, stream restoration, preservation of open space and retrofitting of properties with erosion control technology to enhance water quality. Within the TVS Subbasin, EIP projects are generally related to the Watersheds and Water Quality Focus area, implemented through the Stormwater Management, Watershed Restoration or Aquatic Invasive Species EIP Programs. Current projects include aquatic weed control, regional stormwater monitoring, and expansion of the Osgood stormwater retention basin.

ES-3: ALTERNATIVE PLAN AREA

Population and Economy

Most of the population within the greater South Lake Tahoe area lives within the residential areas of the City of South Lake Tahoe (CSLT) and the adjoining unincorporated communities of El Dorado County (County). The 50-year population growth rate for the County (0.37%) is used to project future groundwater extractions in water budgets calculated for the TVS Subbasin.

The economy of South Lake Tahoe is largely dependent on tourism. As a destination resort, South Lake Tahoe experiences large fluctuations in population and commensurate fluctuations in water demands.

Land Use

Tahoe Regional Planning Agency (TRPA) developed a depiction of approved land uses for the Lake Tahoe Basin. Land use within the TVS Subbasin is 52.8 percent residential, 22.5 percent conservation, 12.5 percent recreation, 9.4 percent mixed-use, 2.7 percent tourist, and 0.1 percent backcountry. Land use surrounding the TVS Subbasin is mostly undeveloped and are designated as Backcountry, Conservation, Wilderness or Mixed-Use. There are no agricultural or industrial land use types.

Groundwater Uses and Users

Drinking water is the primary use of groundwater within the TVS Subbasin. Users of groundwater in the TVS Subbasin include public water systems, domestic well owners, environmental users, the US Forest Service, and disadvantaged communities.

Large community water systems within the TVS Subbasin include the District, Tahoe Keys Water Company (TKWC), Lukins Brothers Water Company (LBWC) and Lakeside Park Association (LPA). The District, TKWC and LBWC are 100% reliant on groundwater sources. The primary source for LPA is surface water which is supplemented with groundwater. Together these community water systems are believed to account for more than ninety percent (90%) of the groundwater extracted from the TVS Subbasin on an annual basis. Further information about these water systems is provided in Sections 3.3.2. Table ES-1 shows the Safe Drinking Water Information System connection and population information for these four water systems.

Table ES-1. Water systems information for the four largest community water systems within the TVS Subbasin (Safe Drinking Water Information System S, downloaded October 12, 2021).

Water System	Water System No.	Primary Source	Population Served	Service Connections
South Tahoe PUD-Main (District)	0910002	Groundwater	33,124 – Residents 88,000 - Tourist	14,235
Tahoe Keys Water Company (TKWC)	0910015	Groundwater	1,420 - Residents	1,566
Lukins Brothers Water Company (LBWC)	0910007	Groundwater	3,200- Residents	982
Lakeside Park Association (LPA)	0910019	Surface Water	1,000 - Residents	139

Individual water systems within the TVS Subbasin include small community water systems, non-community water systems, state small water systems and domestic well owners. Current records indicate there are fifty-eight (58) individual water system wells regulated by the County within the TVS Subbasin. Further information about these water systems is provided in Sections 3.3.3 and 3.3.4.

In most of the TVS Subbasin, water well densities are less than 10 wells per square mile, but in some areas can exceed 50 wells per square mile. Areas of heightened well density include the northeastern portion and southern tip of the TVS Subbasin (Figure 3-9).

Demand Projection

Demand is artificially capped within the Lake Tahoe Basin and the State Water Resources Control Board policy allocates a maximum of 12,493 AFY for use within the greater South Lake Tahoe area. This volume is greater than the total projected water demand at total build-out estimated for the TVS Subbasin (10,808 AFY) and the total pumpage in the 50-year water budget (11,800 AFY) projected using the current County 50-year population growth rate.

Wastewater Management

Under the Porter-Cologne Water Quality Control Act, all sewage from within Lake Tahoe Basin must be collected, treated, and exported outside of the Lake Tahoe Basin. The District’s Wastewater Treatment Plant has a maximum treatment capacity of 7.7 million gallons per day (MGD). The District presently treats approximately 4 MGD in the winter and 5 MGD in the summer.

ES-4: LOCAL GOVERNMENT AGENCIES AND GROUNDWATER-RELATED PROGRAMS

History of Collaboration and Collaboration Opportunities

The Alternative Plan is developed within the context of existing, long-term coordination and collaboration among agencies regulating land use, groundwater quality, and hazardous materials management. Long-established relationships enhance implementation of the Alternative Plan.

Section 4.1 identifies potential opportunities for additional and continued collaboration in areas of groundwater protection, land use planning, and groundwater quality and management.

Groundwater Regulatory Authorities

Table ES-2 summarizes the agencies with jurisdiction and regulatory oversight related to groundwater quality, hazardous materials management, and land use management within the TVS Subbasin.

Table ES-2. List of Groundwater Related Governmental Agencies in the South Lake Tahoe Area.

Agency	Geographic Jurisdiction	Surface Water Quality	Ground Water Quality	Drinking Water	Land Use	Hazardous Materials
US EPA	Nationwide and some programs in California (CA)	Clean Water Act (CWA)	Underground Injection Control (UIC)	Safe Drinking Water Act (SDWA)	--	TSCA, CERCLA
Federal Water Master	CA and Nevada (NV)			Truckee River Operating		

Agency	Geographic Jurisdiction	Surface Water Quality	Ground Water Quality	Drinking Water	Land Use	Hazardous Materials
	within the Truckee River Basin, including Lake Tahoe Basin			Agreement (TROA)		
Tahoe Regional Planning Agency (TRPA)	CA and NV within the Lake Tahoe Basin	Lake Tahoe Water Quality Management Plan under Section 208 of CWA and TRPA Regional Plan		--	TRPA Regional Plan and associated Storm water BMP Handbook	
State Water Resources Control Board (SWRCB)	CA Statewide	With RWQCBs regulates discharges to surface water and groundwater statewide under CWA ¹ and Porter Cologne Water Quality Control Act (WQCA)		DDW ² - SDWA for large water systems	--	Brownfields and Land Disposal Program
Lahontan Regional Water Quality Control Board (LRWQCB)	Lahontan Region including CA portion of Lake Tahoe Basin	Basin Plan ³ /TM DL and Lake Tahoe Municipal Storm water Permit	Basin Plan, Underground Storage Tank (UST), Site cleanup Program,	--	--	
County Environmental Health Department	County portion of Lake Tahoe Basin	--	Water Well Program	SDWA for small water systems Water Well Program	County General Plan outside of City limits	CUPA, Hazardous waste/material generator permits
City of South Lake Tahoe (CSLT)	Within City Limits	Complies with Lake Tahoe Municipal Storm water Permit	--	--	City General Plan	--
US Forest Service – LTBMU	National Forest Lands in CA and NV within the Lake Tahoe Basin	Land and Resource Management Plan	Proposed Groundwater Directive FSM 2560	--	Land and Resource Management Plan	--
El Dorado Water Agency (EDWA) GSA	Portion of the TVS Subbasin outside the District's boundaries		El Dorado County Water Agency Act Water Resources Development and Management Plan	El Dorado County Water Agency Act Water Resources Development and Management Plan		
South Tahoe Public Utility District GSA	Portion of the TVS Subbasin inside the District's boundaries		Wat. Code §§ 10723 and 10753(a) Alternative	Wat. Code §§ 10723 and 10753(a) Alternative	Wat. Code §§ 10723 and 10753(a) Alternative	

Agency	Geographic Jurisdiction	Surface Water Quality	Ground Water Quality	Drinking Water	Land Use	Hazardous Materials
			Plan for TVS Subbasin	Plan for TVS Subbasin	Plan for TVS Subbasin	

- Notes:
- (1) SWRCB/RWQCB has primacy to implement much of CWA regulatory activity
- (2) SWRCB –Division of Drinking Water (DDW, formerly CDPH), El Dorado County is a Local Primacy Agency under contract to DDW for regulating small public water systems.
- (3) Basin Plan implements, for the Lahontan Region, state and federal laws including CWA, Porter Cologne WQCA, SDWA, and other hazardous material laws by setting water quality standards

Regulatory Programs and Policies

The UWMP generally guides actions of water management agencies and helps identify water supply issues. Consistent with DWR’s Recommended Actions, the District reconciled demand projections between the Alternative Plan and the UWMP and incorporated into the projected water budgets.

There is a rich and complex history of managing land use to protect Lake Tahoe water quality. Water clarity of the lake is the primary target of water quality regulation, as Lake Tahoe has impaired status under Water Code section 303(d). The Lahontan Regional Water Quality Control Board and Tahoe Regional Planning Agency are primarily responsible for regulating and managing the clarity of Lake Tahoe, cooperating with their Nevada counterparts.

The interagency Environmental Improvement Program has facilitated improvement of watersheds and water quality, forest health, transportation, and sustainable recreation since 1996. Review of the EIP project list by watershed shows a total of one hundred eighty-two (182) EIP projects within portions of the seven priority watersheds situated within the TVS Subbasin. Most of these projects are located within the Trout Creek and Upper Truckee River Watersheds.

The Tahoe-Sierra Integrated Regional Water Management (IRWM) Plan defines a vision for the management of water resources within the region and highlights important actions to accomplish the vision through 2035.

Analysis of Limits Imposed by Existing Water Resources Monitoring and Management Programs

The Truckee River Operating Agreement limits water use within the Lake Tahoe Basin and allocates that water between California and Nevada. The total annual allocation for the Lake Tahoe basin is 23,000 AFY and is an upper limit for total annual production from the California portion of the Lake Tahoe Basin. Estimated future water demands are projected to total slightly more than half of total annual allocation for the Lake Tahoe Basin.

Because the Porter Cologne Water Quality Act prohibits reuse of recycled water within the Lake Tahoe Basin, recycled water projects are not appropriate within the TVS Subbasin.

The District adopted a policy in 1999 prohibiting the supply of drinking water containing detectible levels of MtBE to its customers. Detectible levels for MtBE are significantly lower than state standards (maximum contaminant load [MCL] and secondary maximum contaminant level [SMCL]).

ES-5: STATE OF THE GROUNDWATER BASIN

Background

Management actions in the Alternative Plan are largely informed using an updated South Tahoe Groundwater Model. The model was updated and calibrated to match historical (WY 1985-2019) conditions. Following calibration, the updated model was run into the future to simulate expected groundwater conditions. Future groundwater conditions are largely dependent on future climate conditions. Both precipitation and temperature strongly affect recharge and evapotranspiration – two primary components of the total groundwater budget. Because of uncertainty associated with climate projections, multiple future scenarios were assessed to ensure that simulations would cover any anticipated condition. Future conditions and the impacts of climate change on the TVS Subbasin are discussed in detail in Section 5.7.

Groundwater Conditions

Groundwater level data is measured semi-annually by the District in forty-seven (47) wells located throughout the TVS Subbasin. The District well network includes thirty-two (30) observation wells and fifteen (15) community water system wells. Only the observation wells are used in the CASGEM program. Groundwater levels within the WBZs occurring in the Tahoe Keys, Bijou, South Tahoe, Angora, Meyers, and Christmas Valley subareas are generally stable or do not exhibit long-term downward trends. However, short periods of decline are present in the WBZs found in the Bijou and South Lake Tahoe subareas. Artesian flows within the Angora subarea peaked in 2011 and are now declining.

The general groundwater level pattern in the TVS Subbasin is high levels along basin margins where the majority of recharge enters the system from higher elevations. The highest groundwater levels occur in the Christmas Valley subarea, which is also the topographically highest portion of the TVS Subbasin floor. Groundwater flows from the Christmas Valley subarea northward where it converges with groundwater flowing southeast from the Angora subarea. Ultimately, groundwater discharges into local tributaries or to Lake Tahoe as underflow. Hydraulic conductivity values range from 0.5 to 210 feet per day with a median of 27 feet per day and a geometric mean of 20 feet per day.

Approximately 1,800,000 AF of groundwater storage is available, as calculated by the groundwater model for the TVS Subbasin from the water table to the bedrock contact.

Groundwater-Surface Water Interactions

Groundwater discharges to stream channels along the Upper Truckee River and Trout Creek, provide a substantial portion of total stream flow during late summer and fall. Groundwater pumping has the potential to reduce base flow to streams and impact GDEs. South

of the Lake Tahoe Airport, groundwater pumping has the potential to reduce base flow to streams. North of the Lake Tahoe Airport, capture of surface waters is from Lake Tahoe.

Groundwater Budget

Most recharge within the TVS Subbasin occurs in the mountains of the Sierra Nevada and Carson range. Groundwater in the TVS Subbasin is largely dependent on precipitation in high elevations. Average annual recharge over the last decade (2010 – 2019) is 48,300 AFY and the average over 1983– 2019 is 41,600 AFY.

Groundwater withdrawals averaged 7,660 AFY and 7,150 AFY over the periods 1983– 2019 and 2010–2019, respectively. Water use, including groundwater extraction, within the Lake Tahoe Basin is limited by the terms of the California-Nevada Interstate Compact Concerning Water of Lake Tahoe, Truckee River, Carson River, and Walker River Basins (Compact) approved in 1971. The Compact allots 23,000 AFY for the California side of the Lake Tahoe Basin. California SWRCB policy recommends 12,493 AFY of the California allocation for use in the South Lake Tahoe area, and 9,528 AFY for the District.

Over the historical period (1983-2019), total baseflow to streams in the model domain averaged approximately 30,100 AFY, with 12,700 AFY occurring within the TVS Subbasin. Over the last decade (2010-2019), average annual baseflow within the subbasin remained stable at 12,700 AFY. Over the historical period (1983-2019), annual net groundwater discharge from the subbasin to Lake Tahoe was 3,300 AFY. Over the last decade (2010-2019), average outflow reduced to 3,000 AFY.

Annual change in groundwater storage for the subbasin varies from -7,400 AFY (meaning water levels are falling) to 12,100 AFY (meaning groundwater levels are rising). On average, groundwater storage changes are near zero (-200 AFY), meaning groundwater storage changes tend to even out over periods of higher and lower recharge. Over the last decade (2010-2019), groundwater in storage has increased an average of 1,700 AFY.

Sustainable Yield

Under SGMA sustainable yield is explicitly defined as “the maximum quantity of water calculated over a base period that is representative of long-term conditions in the basin and including any temporary surplus, that can be withdrawn annually from a groundwater supply without causing an undesirable result.” The sustainable yield must be, at a minimum, less than or equal to the amount of groundwater recharge. Groundwater recharge in the TVS Subbasin is from areal recharge and recharge from the surrounding mountain block, averaging about 21,500 AFY over the historical period (1983 – 2019).

Although the exact amount of baseflow required to avoid an undesirable result is not known, a minimum ‘safe’ baseflow was estimated at 8,300 AFY for the TVS Subbasin based on climate modeling results. Average recharge less this estimated minimum ‘safe’ baseflow gives a sustainable yield of 13,200 AFY. Projected 50-year flow budget terms suggest that average recharge to the TVS Subbasin may vary, depending on climate scenario, from 20,600 AFY

(baseline) to 14,400 AFY (Q2 hot and dry). Comparison of historical and projected water demands to historical and projected average recharge estimates derived from model flow budgets, indicate that total groundwater pumpage in the TVS Subbasin has and will likely continue to operate within its sustainable yield under the baseline scenario, but recharge may not be adequate to sustain both projected groundwater pumpage and minimum “safe” baseflow under the Q2 hot and dry scenario.

Assessment of Potential Overdraft Issues

Overdraft can cause groundwater levels to decline, reduced baseflow in interconnected surface waters, reduced availability to support groundwater dependent ecosystems, and land subsidence. The potential impacts to wells and interconnected surface waters due to pumping alone are negligible. The potential effects only become significant where the rate of extraction leading to an overdraft condition occurs in conjunction with sustained reduction in groundwater recharge. The potential for land subsidence in the TVS Subbasin under current groundwater conditions is negligible because the fine-grained lacustrine deposits are relatively thin and discontinuous, and historical groundwater levels have been stable.

Potential Climate Change Impacts

Climate change in the TVS Subbasin will disrupt processes that have historically been assumed to be stable or at equilibrium. Climate changes will likely lead to a higher rain-snow line, decreased snowpack, increased wildfires, and increased evapotranspiration within the TVS Subbasin. These disruptions are described in the statewide and regional reports produced by the California Fourth Climate Change Assessments, and guidance for preventing, quantifying, and assessing vulnerability is provided in California’s Climate Action Plans.

Climate data for the plan area is available from a variety of sources that are listed in Table ES-3.

Table ES-3: Basin Monitoring Plan Data Sources

Organization	Contact	Data
District	Ivo Bergsohn 1275 Meadow Crest Drive South Lake Tahoe, CA 530-544-6474	Groundwater levels Groundwater quality Pumping volumes
Lukins Brothers Water Company	Jennifer Lukins 2013 West Way South Lake Tahoe, CA 530-541-2606	Pumping volumes Groundwater levels

Organization	Contact	Data
Tahoe Keys Water Company	Jennifer Lukins (Interim) 356 Ala Wai Blvd. South Lake Tahoe, CA 530-542-6451	Pumping volumes Groundwater levels
Lakeside Mutual Water Company	Nakia Foskett 4077 Pine Avenue South Lake Tahoe, CA 530-542-2314	Pumping volumes Groundwater levels
USGS	National Water Information System http://waterdata.usgs.gov/nwis/	Groundwater levels Surface water flow and quality
DWR	Groundwater Information Center http://water.ca.gov/groundwater/ Water Data Library http://www.water.ca.gov/waterdatalibrary/index.cfm CASGEM http://www.water.ca.gov/groundwater/casgem/	Groundwater and climate data
SWRCB	GeoTracker http://geotracker.waterboards.ca.gov Groundwater Ambient Monitoring & Assessment Program (GAMA) http://geotracker.waterboards.ca.gov/gama/	Groundwater levels Groundwater quality Pumping data
TRCD	Regional Storm Water Monitoring Program http://tahoercd.org/tahoe-stormwater-monitoring/	Storm water quality
Desert Research Institute	Tahoe Climate Information Management System http://www.tahoeclim.dri.edu/ California Data Exchange Center http://www.wrcc.dri.edu/summary/Climsmcca.html Western Regional Climate Center http://www.wrcc.dri.edu/summary/Climsmcca.html	Climate data
NOAA	National Climate Data Center Global Historical Climate Network http://www.ncdc.noaa.gov/oa/climate/ghcn-daily/	Climate data
USDA	Natural Resources Conservation Service http://www.wcc.nrcs.usda.gov/ SNOTEL http://www.wcc.nrcs.usda.gov/snow/	Total Precipitation

Precipitation is the primary component of the climate data that is regularly used in the TVS Subbasin to describe water year type (see Section 2.2.2) and calculate groundwater recharge (Section 5.4.1). Total precipitation measured at National Resources Conservation Service snow telemetry station 508: Hagan's Meadow, CA is used as a reference station for the plan area, as this station was found to have the best correlation with simulated groundwater recharge for the South Tahoe Groundwater Model domain (Carroll et al., 2016).

ES-6: GROUNDWATER QUALITY

Section 6 of this Alternative Plan provides an overview of current groundwater quality and groundwater quality issues recognized within the TVS Subbasin based on available water quality records collected over the past ten years (2011–2020). Limitations of the water quality data used to describe groundwater quality are discussed in Section 6.1.2.

Groundwater Quality

Groundwater in the TVS Subbasin is generally of excellent chemical quality, suitable for the designated beneficial uses of municipal and industrial water use and for any other uses to which it might be put. Dissolution of minerals in the basin-fill deposits cause natural accumulation of salts. Groundwater collected from private wells (16 in total) classified by water type show calcium-bicarbonate (Ca-HCO₃) is the predominant water type, followed by sodium bicarbonate (Na-HCO₃) and calcium-chloride (Ca-Cl).

Inorganic constituents listed in drinking water standards generally include various metals, halogens, and cyanide. Of these constituents, aluminum and arsenic are the only constituents found at concentrations exceeding a primary MCL. Iron and manganese are the only constituents found at concentrations exceeding secondary MCLs (SMCLs).

Radioactive constituents are present in groundwater within the TVS Subbasin. Radiological substances include radium isotopes (Ra-226 and Ra-228), total soluble uranium, gross alpha activity and radon. Incidences of radiological substances exceeding the gross alpha MCL of 15 pCi/L and total uranium MCL of 20 pCi/L have been found in water supply wells within the TVS Subbasin

Man-made contaminants which occur most frequently in the TVS Subbasin include petroleum hydrocarbon and chlorinated hydrocarbon compounds. Petroleum hydrocarbon compounds are from spills and releases associated with the operation of gasoline storage and fueling facilities. Contaminants of concern from these releases include benzene, toluene, ethylbenzene, and total xylenes (BTEX) and the gasoline additives used as fuel oxygenates and octane enhancers including Methyl tert- Butyl Ether (MtBE), Tert-Butyl Alcohol (TBA), Tertiary-Amyl Methyl Ether (TAME), and ethanol. Chlorinated hydrocarbon compounds are most often industrial agents used for degreasing metals, cleaning electronic parts, and dry-cleaning fabrics. They are also contained in many household products such as oil-based paints, drain cleaners, spot removers, engine degreasers and paint removers. Contaminants of concern from these releases include Tetrachloroethylene (PCE); Trichloroethylene (TCE); 1,2-Dichloroethane (1,2-DCA); 1,2 Dichloroethylene (1,2-DCE); Vinyl Chloride (VC); and 1,4-Dichlorobenzene (1,4-DCB).

Groundwater Quality Issues

Groundwater quality issues in the TVS Subbasin include (1) migration of contaminated groundwater; (2) emerging contaminants; and (3) potential groundwater contamination via stormwater infiltration.

The Alternative Plan (Section 6.3.1) discusses three examples of contaminant plume migration: the south “Y” regional contamination, a private residence site in the Bijou subarea, and the Meyers Landfill site. Section 6.3.1.4 discusses the potential impacts of pumping on the south “Y” plume migration. Models under three targeted pumping scenarios showed reductions in maximum concentrations at downgradient wells and a faster basin-wide reduction in PCE.

Emerging contaminants include Radon 222 and PFAS substances. Because the United States Environmental Protection Agency has not yet set a final MCL for Radon 222, the impact to drinking water supply wells in the TVS Subbasin is unclear. In May 2021, PFAS compounds were detected in monitoring wells for the first time in the TVS Subbasin.

Stormwater is treated primarily with infiltration through detention basins. The greatest risk of stormwater infiltration is to the shallow groundwater zones beneath infiltration basins, not deeper groundwater supplies.

Groundwater Vulnerability Assessment

Where pollutants are present at the land surface or within the pore spaces of the vadose zone, groundwater recharge can introduce contaminants to the groundwater system. The highest densities of possible contaminating activity (PCA) sites are located along Highways 50 and 89, especially within the Bijou, South Lake Tahoe, and Meyers subareas (Figure 6-16). Well source areas overlap these sites within the South Lake Tahoe subarea. A large proportion of small water system and domestic wells across the Bijou and South Lake Tahoe subareas are within areas of relatively high PCA site densities.

ES-7: STAKEHOLDER INVOLVEMENT

The Alternative Plan was developed within the context of an existing, on-going coordination and collaboration on water issues in the TVS Subbasin.

Stakeholder Advisory Group

Since adoption of the existing GWMP, the District has continually engaged stakeholders through a Stakeholder Advisory Group (SAG). The current SAG is composed of the original SAG formed in 2014 supplemented with new members as representatives of general interest categories change. General interest categories are used to capture a broad spectrum of community, business, and agency interests to provide meaningful input during the development and implementation of the Alternative Plan. The current SAG has a roster of fourteen members representing Agency, Real Property Owner, Water Purveyor and Non-Business Community Rate Payer interest categories. Workshops were held in 2019, 2020 and 2021 to present information to the SAG as the first five-year update of the Alternative Plan was being developed.

Groundwater Management Collaboration

The SAG identified three primary collaboration goals for groundwater protection: (1) integrate groundwater protection inspection protocol of the several agencies already conducting site inspections; (2) create a private well owner education and cooperation campaign; and (3) maintain an inventory of infiltration basins and dry wells, inform spill responders of these locations, and communicate spill events to water purveyors. SGMA provides further opportunity for collaboration among water management agencies and land use planning agencies. The SAG continues to be an important vehicle to share information for water management. The SAG has achieved several accomplishments involving enhanced data collection and use, improved hydrologic modeling, and improved relationships with the public.

Future/Ongoing Stakeholder Involvement Opportunities

Future SAG topics include emerging contaminants, specifically PFAS, illicit discharges to stormwater infiltration systems, drought, inorganic contaminants, and climate change, among others.

Public Participation in the Five-Year Update of the Alternative Plan

The District and EDWA began procedural, technical, and public outreach activities for the first five-year update of the Alternative Plan starting in 2020. The members of the SAG representing the public have contributed to the development of the Alternative Plan. A list of the public notices, communications and public meetings conducted for the Alternative Plan is provided below.

ITEM	DATE (S)
Public Hearing to receive public comment to adopt Resolution No. 3140-20 to draft an update to the 2014 Groundwater Management Plan	5/21/2020
Notice of Intent to Draft an Updated Groundwater Management Plan	6/25/2020
2020 Stakeholder Advisory Group Workshop 1	7/29/2020
District Regular Board Meeting Staff Report – Stakeholder Advisory Group Update	8/6/2020
2020 Stakeholder Advisory Group Workshop 2	12/17/2020
District Regular Board Meeting Staff Report – Alternative Plan Update	12/17/2020
Public Notice of Opportunities to Participate in the Development of the five-year update to the Alternative Plan	1/7/2021
2021 Stakeholder Advisory Group Workshop 1	3/25/2021

ITEM	DATE (S)
District Regular Board Meeting Staff Report – Alternative Plan Update	4/1/2021
2021 Stakeholder Advisory Group Workshop 2	6/30/2021
District Regular Board Meeting Staff Report – Alternative Plan Update	7/1/2021
90-Day Notice to Cities and Counties (WCS 10728.4)	10/1/2021
District Regular Board Meeting Staff Report – Alternative Plan Update	11/4/2021
Draft Alternative Plan to SAG	12/17/2021
2022 SAG Workshop 1 – Alternative Plan Review	1/12/2022
District Regular Board Meeting Staff Report – Alternative Plan Update	2/3/2022
Draft Alternative Plan – SAG Comment Period	12/17/2021 - 1/17/2022
Post Public Draft Alternative Plan Notice of Availability (30-Day Comment Period)	1/31/2022
Notice of Availability Draft Alternative Plan to Cities and Counties	2/9/2022
Public Draft Alternative Plan 30-Day Comment Period	2/9/2022 - 3/11/2022
EDWA Board Presentation: Alternative Plan Update	3/9/2022
EDWA Public Hearing: Consider to Adopt the first five-year update of the Alternative Plan	4/13/2022
STPUD Public Hearing: Consider to Adopt the first five-year update of the Alternative Plan	4/21/2022

Table ES-4. Public notices and opportunities for participation during development of the first five-year update of the Alternative Plan.

Under SGMA, GSAs are required to engage the public during the development of a GSP (Wat. Code § 354.10). As part of its public outreach the District developed an engagement chart organized by stakeholders groups and communication methods to be employed for each group

(Table 7-5), updated lists of possible stakeholders within each group, and development of various communication tools including: participation notice, stakeholder survey, media release, on-line web postings and a power point presentation targeted to the general public explaining the Alternative Plan, the update process and opportunities for engagement in this process.

The stakeholders list has 286 entries and was developed in accordance with DWR guidance (DWR, 2018). The participation notice was developed to satisfy SGMA public notification and participation requirements (Wat. Code §10727.8). The stakeholder survey was developed for the Alternative Plan using the Stakeholder Survey Template available from the DWR engagement tools. The participation notice was posted on the District and EDWA web sites and mailed along with the stakeholder survey to Group A and Group B stakeholders. Only the participation notice was emailed to all possible stakeholders with email contact information. The District power point presentation was posted on the Groundwater Management Plan web page of the District's website. Copies of the outreach materials developed for the Alternative Plan are provided in Appendix D.

ES-8: CHARACTERIZATION OF UNDESIRABLE RESULTS

Section 8 of the Alternative Plan outlines the sustainable management criteria developed for the TVS Subbasin. Through this analysis, each undesirable result is described and a sustainability indicator and a minimum threshold that would trigger an undesirable result are defined within a framework of BMOs. Comparison of current groundwater conditions to minimum thresholds demonstrates that the sustainability goal for the TVS Subbasin is currently being met.

BMO #1: Maintain a Sustainable Long-Term Groundwater Supply

Undesirable results related to the long-term groundwater supply occur when regional water levels decline such that water demands cannot be met, or when water level declines result in substantial land subsidence. Quantitative thresholds are developed in Section 8.1 to avoid both results. Thresholds are based on upper elevations of screened intervals in public supply wells and expected drawdowns at these wells while pumping. Resultant freeboard calculations provide a threshold water level decline that would render each well inactive, thus reducing the accessible supply of groundwater. There is currently a sufficient supply of groundwater adequate to meet the drinking water needs of beneficial users in the TVS Subbasin.

Estimated drawdowns that would result in substantial land subsidence were defined using Terzaghi's Law. For subsidence to occur, drawdowns must far exceed thresholds based on screened intervals in most cases.

BMO #2: Maintain and Protect Groundwater Quality

Undesirable results related to degraded water quality occur when water at public supply wells exceeds the MCL for a given contaminant, reducing the ability to produce groundwater of sufficient quality and quantity such that demands cannot be met. Quantitative thresholds are developed in Section 8.2 to avoid this result. There is currently a sufficient supply of high-

quality water adequate to meet the drinking water needs of beneficial users of groundwater in the TVS Subbasin. Seawater intrusion is not an undesirable result posed within the TVS Subbasin.

BMO #5: Assess the Interaction of Water Supply Activities on Environmental Conditions

Undesirable results stemming from interconnectedness of surface and groundwater takes one of two forms: a depletion in surface flow in a stream or a negative impact to a groundwater dependent ecosystem (GDE). Quantitative thresholds are developed in Section 8.3 to avoid both results. Based on guidance from California Department of Fish and Wildlife (DFW), seasonally varying minimum in-stream flows are established for the Upper Truckee River and Trout Creek. These flows follow DFW recommendations based on the flows needed for successfully spawning and rearing of the salmonids that occur in those streams.

GDEs occur where the plant community can directly access groundwater as a source of water. GDEs are generally characterized by riparian vegetation and shallow groundwater, as the depth of the water table determines whether plants can directly utilize groundwater. Therefore, thresholds for the conservation of GDEs center on water level observations and detecting and mitigating any declines in the shallow water table in or around the identified GDEs. There is little or no long-term data on GDEs in the TVS subbasin, and the lack of data for this threshold poses a challenge in monitoring these thresholds.

To support monitoring and potential mitigation of undesirable results, a provisional management area is delineated based on groundwater capture. The provisional management area, which is defined based on the potential to affect interconnected surface waters, will be evaluated over the next five years to determine its utility in monitoring and mitigating undesirable impacts to streamflow and GDEs.

ES-9: GROUNDWATER MONITORING

Section 9 of this Alternative Plan presents a description of the monitoring network and the data used to regularly assess groundwater conditions in the TVS Subbasin.

Groundwater Monitoring

The District has long monitored groundwater conditions within the TVS Subbasin. The District collected spot readings of static and pumping water levels prior to 2001. Since 2001, the District has collected groundwater level data in the fall and spring of each year from each well in a monitoring network within the District's service area, consisting of thirty-two (32) observation wells and fifteen (15) community water supply wells (Figure 9-1).

In 2010, the District volunteered to be a monitoring entity within the California Statewide Groundwater Elevation Monitoring Program (CASGEM). Since 2011, the District has monitored and reported static groundwater elevation data collected from observation wells within the monitoring network semi-annually to DWR. Since adoption of the 2014 GWMP, the District has used groundwater level data collected from the monitoring network to prepare annual reports assessing groundwater conditions and has submitted these reports to DWR, in satisfaction of GSA reporting requirements (Wat. Code § 10728) (Annual Reports).

As part of the Basin Monitoring Plan, the District will reach out to other water purveyors and other governmental agencies about sharing data within the TVS Subbasin. The District will work with other agencies to identify data that will help support the Basin Monitoring Program for all stakeholders.

Identification and Description of Data Gaps

The monitoring network successfully monitors all sustainability indicators except degraded groundwater quality and depletion of interconnected surface water. The District addressed the groundwater quality data gaps by collecting samples of groundwater from fifteen (15) active production wells on at least an annual basis (from June to August) and submitting those samples for analysis of the full suite of Title 22 analyses. The District plans to collaborate with the SAG to identify further groundwater quality data regularly collected within the TVS Subbasin that may be used to supplement available state groundwater quality data sets. The District manages the depletion of interconnected surface water data gaps by leveraging surface water monitoring efforts by USGS on the Upper Truckee River and Trout Creek. The District also plans to monitor GDEs annually using selected monitoring wells near delineated GDEs.

ES-10: IMPLEMENTATION PLAN

The District has long managed groundwater in the TVS Subbasin. Section 10 analyzes and proposes implementation actions building on prior and ongoing management efforts.

This section provides a schedule (Appendix M) to assist with the implementation of the Alternative Plan organized by BMO and actions tied to sustainable management criteria developed for the TVS Subbasin. Specific areas of focus include groundwater contamination, the effect of groundwater pumping on GDEs, and engaging private well owners. The goal of implementation is to maintain a sustainable source of drinking water for all beneficial users and uses of groundwater within the TVS Subbasin.

Over the past five years the cost of implementation for the Alternative Plan averaged about \$415,000 per annum. A general description of funding options for future implementation of the Alternative Plan are discussed in Section 10.2

The District has fulfilled its annual reporting obligations and will continue to do so. This five-year assessment and update of the Alternative Plan meets SGMA requirements and will continue to be reviewed at least every five years.

**GROUNDWATER SUSTAINABILITY AGENCY
INFORMATION**

Mailing Address:

South Tahoe Public Utility District
1275 Meadow Crest Drive
South Lake Tahoe, CA
96150-7401

El Dorado Water Agency
4330 Golden Center Drive
Placerville, CA
95667 - 6232

Plan Manager:

Ivo Bergsohn, PG, HG
Hydrogeologist
South Tahoe Public Utility District
1275 Meadow Crest Drive
South Lake Tahoe, CA 96150
(530) 543-6204
ibergsohn@stpud.us

Volume I - Report

SECTION 1: INTRODUCTION	1
1.1 Background.....	3
1.1.1 Plan Authorization and Legal Authority.....	3
1.1.2 TVS Subbasin GSA Formation.....	5
1.1.3 Plan Manager and Contact Information.....	6
1.2 Development and Adoption Process.....	7
1.2.1 2014 GWMP.....	7
1.2.2 Alternative Plan and DWR Approval.....	9
1.3 Recommended Actions Identified by DWR.....	10
1.4 Alternative Plan Changes.....	11
SECTION 2: TAHOE VALLEY SOUTH SUBBASIN.....	17
2.1 Delineation.....	17
2.1.1 Basin Boundaries.....	17
2.1.2 Geographic Sub-Areas.....	19
2.1.3 Provisional Management Area.....	20
2.2 Climate.....	20
2.2.1 Climatology.....	20
2.2.2 Water Year Classification.....	22
2.2.3 Climate Change.....	22
2.3 Soils.....	25
2.4 Geology.....	26
2.5 TVS Subbasin Aquifer.....	30
2.6 Surface Water Features.....	32
2.6.1 Watersheds.....	32
2.6.2 Lakes.....	36
2.6.3 Groundwater Dependent Ecosystems (GDEs).....	37
SECTION 3: ALTERNATIVE PLAN AREA.....	41
3.1 Population and Economy.....	41
3.2 Land Use.....	42
3.2.1 Land Use Designations.....	44
3.3 Groundwater Uses and Users.....	45
3.3.1 Groundwater Uses.....	45
3.3.2 Community Water Systems.....	46
3.3.3 Individual Water Systems.....	53
3.3.4 Well Owners Survey Results.....	56
3.3.5 Groundwater Pumpage/Well Densities.....	63
3.4 Demand Projections.....	67
3.5 Wastewater Management.....	68
SECTION 4: LOCAL GOVERNMENTAL AGENCIES AND GROUNDWATER-RELATED PROGRAMS.....	69
4.1 History of Collaboration and Collaboration Opportunities.....	69
4.1.1 Potential Collaboration on Groundwater Protection.....	69

4.1.2	Potential Collaboration on Land Use Planning.....	70
4.1.3	Potential Collaboration on Groundwater Quality Monitoring and Management .	71
4.2	Overlying Jurisdictions	72
4.3	Regulatory Agencies.....	72
4.3.1	Groundwater Sustainability Agencies.....	73
4.3.2	State Water Resources Control Board and Lahontan Regional Water Quality Control Board.....	74
4.3.3	El Dorado County	76
4.3.4	El Dorado Water Agency.....	77
4.3.5	South Tahoe Public Utility District.....	79
4.3.6	Tahoe Regional Planning Agency (TRPA).....	80
4.3.7	City of South Lake Tahoe	82
4.3.8	United States Forest Service	83
4.3.9	TROA: Office of the Federal Watermaster.....	84
4.3.10	Tahoe Resource Conservation District	84
4.4	Regulatory Programs and Policies.....	85
4.4.1	Urban Water Management Plan.....	85
4.4.2	Lake Tahoe TMDL	86
4.4.3	Stormwater Management and Monitoring.....	86
4.4.4	Environmental Improvement Program – Stream and Wetland Restoration	87
4.4.5	Integrated Regional Water Management Planning.....	89
4.5	Analysis of Limits Imposed by Existing Water Resources Monitoring and Management Programs	89
SECTION 5: STATE OF THE GROUNDWATER BASIN.....		92
5.1	Background.....	92
5.1.1	South Tahoe Groundwater Model.....	92
5.1.2	Identification of Data Gaps/Uncertainty.....	94
5.2	Groundwater Conditions.....	95
5.2.1	Groundwater Level History	95
5.2.2	Groundwater Flow Directions.....	103
5.2.3	Hydraulic Parameters.....	109
5.2.4	Groundwater-Storage.....	112
5.3	Groundwater-Surface Water Interactions	112
5.4	Groundwater Budget.....	113
5.4.1	Recharge	113
5.4.2	Groundwater Withdrawals.....	117
5.4.3	Discharges to Streams and Lakes	118
5.4.4	Increases from Streams and Lakes.....	118
5.4.5	Changes in Groundwater Storage	120
5.4.6	Historical Groundwater Budgets.....	124
5.4.7	Current Groundwater Budget.....	126
5.4.8	Projected Water Budget	127
5.5	Sustainable Yield	131
5.6	Assessment of Potential Overdraft Issues.....	132
5.6.1	Assessment of Potential Overdraft.....	132
5.6.2	Assessment of Land Subsidence.....	140

5.7	Potential Climate Change Impacts	140
5.7.1	CCCA4 Sierra Nevada Region	141
5.7.2	Climate Action Plans	141
SECTION 6: GROUNDWATER QUALITY		143
6.1	Background	143
6.1.1	Overview and Data Sources	143
6.1.2	Identification of Data Gaps/Uncertainty	144
6.2	Groundwater Quality	144
6.2.1	General Water Quality	145
6.2.2	Inorganic Constituents	148
6.2.3	Radioactive Constituents	153
6.2.4	Regulated Chemicals	156
6.3	Groundwater Quality Issues	166
6.3.1	Migration of Contaminated Groundwater	166
6.3.2	Emerging Contaminants	175
6.3.3	Stormwater Infiltration	179
6.4	Groundwater Vulnerability Assessment	184
6.4.1	Importance of Protecting Groundwater Quality	184
6.4.2	Groundwater Recharge Areas	184
6.4.3	Delineation of Well Source Area Zones	186
6.4.4	Possible Contaminating Activity (PCA) Sites	187
6.4.5	Groundwater Vulnerability Map	188
SECTION 7: STAKEHOLDER INVOLVEMENT		193
7.1	Stakeholder Advisory Group	193
7.1.1	SAG Workshops	194
7.2	Groundwater Management Collaboration	196
7.2.1	Protect Groundwater	196
7.2.2	Coordination with Land Use Planning Agencies	198
7.2.3	Sharing Data and Information	198
7.2.4	SAG Accomplishments	199
7.3	Future/Ongoing Stakeholder Involvement Opportunities	200
7.3.1	Future SAG Topics	200
7.4	Public Participation in the Five-Year Update of the Alternative Plan	201
7.4.1	Public Notice and Comment	202
7.4.2	Public Outreach and Engagement	203
SECTION 8: CHARACTERIZATION OF UNDESIRABLE RESULTS		207
8.1	BMO #1: Maintain a Sustainable Long-Term Groundwater Supply	210
8.1.1	Chronic Lowering of Groundwater Levels	210
8.1.2	Reduction of Groundwater Storage	218
8.1.3	Land Subsidence	220
8.2	BMO #2: Maintain and Protect Groundwater Quality	222
8.2.1	Seawater Intrusion	222
8.2.2	Water Quality	222

8.3	BMO #5: Assess the Interaction of Water Supply Activities on Environmental Conditions	226
8.3.1	Interconnected Surface Waters	227
8.3.2	Groundwater Dependent Ecosystems	233
SECTION 9: GROUNDWATER MONITORING		238
9.1	Groundwater Monitoring	238
9.1.1	Monitoring Network	240
9.1.2	Monitoring Protocols	243
9.2	Identification and Description of Data Gaps	249
9.2.1	Monitoring for Degraded Water Quality	249
9.2.2	Monitoring for Depletions of Interconnected Surface Water	249
SECTION 10: IMPLEMENTATION PLAN		252
10.1	Projects and Management Actions.....	252
10.1.1	Circumstances for Implementation.....	252
10.1.2	Approval of Implementation Actions	252
10.1.3	Expected Benefits	253
10.2	Funding Alternative Plan Implementation.....	253
10.2.1	Budget and Funding for Past Groundwater Projects.....	253
10.2.2	Projected Budget and Future Funding Opportunities	255
10.3	Reporting.....	257
10.3.1	Annual Report.....	257
10.3.2	5-Year Assessment and Resubmittal	257

ABBREVIATIONS

1,2-DCA	1,2-Dichloroethane
1,2-DCE	1,2 Dichloroethylene
AF	Acre-feet
AFY	Acre-feet per year
AMSL	Above Mean Sea Level
Annual Report	Report assessing groundwater conditions submitted annually to DWR, in satisfaction of GSA reporting requirements (Wat. Code § 10728; 23 Cal. Code Regs., § 356.2)
Basin Plan	The Water Quality Control Plan for the Lahontan Region
BGS	Below Groundwater Surface
BMOs	Basin management objectives specified in the 2014 Groundwater Management Plan prepared and adopted by the South Tahoe Public Utility District in 2014
BMPs	Best Management Practices
BTEX	Benzene, toluene, ethylbenzene, and total xylenes
CASGEM	California State Groundwater Elevation Monitoring Program
CFR	Calculated Fixed Radius
CFS	Cubic Feet Per Second
CFD	Cubic Feet per Day
County	El Dorado County
CSLT	City of South Lake Tahoe
CUPA	Certified Unified Program Agency
CWA	Clean Water Act
CWS	Community Water System
DAC	Disadvantaged Community
DDW	State Water Resources Control Board Division of Drinking Water

DEM	Digital Elevation Model
DFA	State Water Resources Control Board Division of Financial Assistance
DFW	California Department of Fish and Wildlife
District	South Tahoe Public Utility District
DOF	California Department of Finance
DRI	Desert Research Institute
DSWAP	Drinking Source Water Assessment and Protection
DWR	California Department of Water Resources
EDCEMD	El Dorado County Environmental Management Department
EDWA	El Dorado County Water Agency
EIP	Environmental Improvement Program.
EPA	United States Environmental Protection Agency
FS	South Y Feasibility Study
FT/D	Feet per day
GAC	Granular Activated Carbon
GAMA	Groundwater Ambient Monitoring and Assessment
GCM	Global Climate Model
GDEs	Groundwater Dependent Ecosystems
GPM	Gallons per Minute
GSA	Groundwater Sustainability Agency
GSFLOW	Groundwater and Surface Water Flow Model
GSFRM	GSFLOW Regional Model
GSP	Groundwater Sustainability Plan
GWMP	Groundwater Management Plan
IRWM	Tahoe-Sierra Integrated Regional Water Management

ISW	Interconnected Surface Water
LBWC	Lukins Brothers Water Company
LCT	Lahontan cutthroat trout
LMP	USFS LTBMU Land Management Plan
LPA	Lakeside Park Association (aka Lakeside Mutual Water Company)
LRWQCB	Lahontan Regional Water Quality Control Board
LTBMU	US Forest Service, Lake Tahoe Basin Management Unit
LTCP	Low-Threat UST Case Closure Policy
LULC	Land Use Land Cover
MBR	Mountain Block Recharge
MCLs	Maximum Contaminant Levels
MDD	Maximum Daily Demand
MG/L	Milligrams per Liter
MGD	Million gallons per day
MODFLOW	Modular Groundwater Flow Model
MODFLOW-NWT	Modular Groundwater Flow Model – Newton Solver
MOU	The Second Amended and Restated Memorandum of Understanding between the South Tahoe Public Utility District and the El Dorado County Water Agency
MtBE	Methyl tert-Butyl Ether
MT3DMS	Modular three-dimensional transport model
NPDES	National Pollutant Discharge Elimination System
PAH	Polycyclic aromatic hydrocarbons
PCA	Possible Contaminating Activity
PCE	Tetrachloroethylene
pCi/L	Picocuries per Liter

PDI	South Y Predesign Investigation
PFAS	Per- and polyfluoroalkyl substances
PFOA	Perfluorooctanoic acid
PFOS	Perfluorooctane sulfonic acid
PHG	Public Health Goal
PPT	Parts per trillion
PWOS	Private Well Owner Survey
RWQCB	Regional Water Quality Control Board
SAG	Stakeholders Advisory Group
SDWA	Safe Drinking Water Act, 42 U.S.C. §300f et seq. (1974)
SEZ	Stream Environment Zone
SGMA	Sustainable Groundwater Management Act
SMCLs	Secondary Maximum Contaminant Levels
SNOTEL	National Resources Conservation Service snow telemetry station
South Y	Area south of the junction of State Route 89 and US Highway 50
STGM	South Tahoe Groundwater Model
SWRCB	California State Water Resources Control Board
TCE:	Trichloroethylene
TKWC	Tahoe Keys Water Company
TMDL	Total Maximum Daily Load
TRCD	Tahoe Resource Conservation District
TROA	Truckee River Operating Agreement
TRPA	Tahoe Regional Planning Agency
Tucker Basin	Tucker Avenue Stormwater Detention Basin

TVS Subbasin	Tahoe Valley South Subbasin of the Tahoe Valley Groundwater Basin, Subbasin No. 6-005.01
UG/L	Micrograms per Liter, equivalent to parts per billion
USFS	United States Forest Services
USGS	U.S. Geological Survey
UST	Underground Storage Tank
UWMP	South Tahoe Public Utility District 2020 Urban Water Management Plan
VC	Vinyl Chloride
WBZs	Water-bearing zones
WRDMP	Water Resources Development and Management Plan
WWTP	Districts Wastewater Treatment Plant
WY	Water Year

TABLES

- 1-1 Summary of Recommended Actions identified during DWR assessment of the 2014 GWMP and Alternative Materials submitted to DWR in 2016 (DWR, 2019).
- 1-2 Major plan components presented in the 2014 GWMP and Alternative Materials and the first five-year update of the Alternative Plan.
- 2-1 Estimates of average annual runoff for eleven South Lake Tahoe watersheds either directly overlying or neighboring the TVS Subbasin.
- 3-1 P-1 projected long-term population growth rates for El Dorado County, California (DOF, 2020d).
- 3-2 Land use types and areas within the South Lake Tahoe area.
- 3-3 2020 water uses by sector for the District water system, in acre feet (AF). The total volume accounts for about 97 percent of the Districts total water accounts which were metered in 2020. Losses were estimated using the difference between District groundwater production and consumption from the meter data.
- 3-4 Water systems information for the four largest community water systems within the TVS Subbasin (Safe Drinking Water Information System, downloaded October 12, 2021).
- 3-5 Well and source capacity information for District wells.
- 3-6 Number and type of properties with individual water system wells within the District's service area as of February 2020.
- 3-7 Assigned well usage values based on survey responses for active wells.
- 3-8 Total water production requirements estimated from future water demand analysis for the District's service area (adapted from Kennedy Jenks, 2020).
- 4-1. List of Groundwater Related Governmental Agencies in the South Lake Tahoe Area.
- 4-2 EIP projects by watershed in the South Lake Tahoe Area, as of January 31, 2022 (<https://www.laketahoeinfo.org/Watershed/Index>).
- 5-1 Pre-development flow budget, segregated into components for the TVS Subbasin (Zone 10) and the surrounding mountain block (Zone 1).
- 5-2 Average flow budget terms for the historical period WY 1983 to WY 2019, segregated into components for the TVS Subbasin (Zone 10) and the surrounding mountain block (Zone 1).

- 5-3 Average flow budget terms for the period WY 2010 WY 2019, segregated into components for the TVS Subbasin (Zone 10) and the surrounding mountain block (Zone 1).
- 5-4 Areal recharge rates and lake stages used in future predictive climate scenarios. Recharge rates listed are for the model domain.
- 5-5 Projected flow budget terms from the Baseline climate scenario for WY 2070, segregated into components for the TVS Subbasin (Zone 10) and the Mountain Block (Zone 1).
- 5-6 Projected flow budget terms from the Q2 (hot and dry) climate scenario for WY 2070, segregated into components for the TVS Subbasin (Zone 10) and the Mountain Block (Zone 1).
- 6-1 Types and numbers of water quality records used for describing groundwater quality in the TVS Subbasin.
- 6-2. General water quality for water supply and environmental wells within the TVS Subbasin (6-005.01) sampled over the past ten years (2011–2020).
- 6-3. Inorganic water quality for water supply and environmental wells within the TVS Subbasin (6-005.01) sampled over the past ten years (2011 – 2020).
- 6-4 Radionuclide water quality in water supply wells within the TVS Subbasin (6-005.01) sampled over the past ten years (2011–2020).
- 6-5 Chemical water quality in water supply and environmental wells within the TVS Subbasin (6-005.01) sampled over the past ten years (2011–2020).
- 6-6 Clean-up sites with water quality records of petroleum hydrocarbon contaminants detected in groundwater within the TVS Subbasin over the past ten years (2011–2020).
- 6-7 Clean-up sites with water quality records of chlorinated hydrocarbon contaminants detected in groundwater within the TVS Subbasin over the past ten years (2011 – 2020).
- 6-8 Pumping rates used for four pumping scenarios.
- 6-9 Number of years after 2018 each well drops below 4 UG/L for all pumping scenarios. N.E. = Never Exceeds 4 UG/L.
- 6-10 Groundwater discharge limits per Chapter 60.1.3.B, TRPA Code of Ordinances.
- 6-11 Numbers and types of PCA sites located within source protection zones delineated within the TVS Subbasin.
- 7-1 Current members of the Stakeholder Advisory Group (SAG) for the Alternative Plan.
- 7-2 SAG workshops convened since adoption of the 2014 GWMP through June 2021.

- 7-3 Major groundwater management activities completed since 2015.
- 7-4 Potential topics for future discussion with the SAG.
- 7-5 Alternative Plan stakeholder engagement chart.
- 7-6 Public notices and opportunities for participation during development of the first five-year update of the Alternative Plan.
- 8-1 Assessment of undesirable results for the TVS Subbasin (6-005.01)
- 8-2 Source capacity for active wells in the District, TKWC, and LBWC.
- 8-3 Maximum day demands (MDD) calculated for community water systems operating within the TVS Subbasin (WY 2011 – WY 2020) and minimum threshold value for lowering groundwater levels based on water demands. The minimum threshold for lowering groundwater levels is the total MDD, in MGD, for community water systems reliant on groundwater operating within the TVS Subbasin.
- 8-4 Minimum water level targets for active production wells within the TVS Subbasin. Red line indicates drawdown required to reach a condition where the MDD could not be met.
- 8-5 Water levels targets for land subsidence and chronic lowering of water levels.
- 8-6 Threshold discharges and current (WY 2011 – WY 2020) 10-year average flows in cfs for each season and gage.
- 9-1 Screen intervals for selected monitoring wells presented in the Annual Reports for the TVS Subbasin. Hydrographs for these wells showing groundwater level trends within each subarea are presented in Section 5.2 and included in Appendix L.
- 9-2 Classification system for water year type based on observed accumulated precipitation at Hagan’s Meadows, CA, SNOTEL 508. Upper bound of z-statistic and ranges in precipitation (inches) (Adapted from Carroll *et al.*, 2016b)
- 10-1 Funding sources and amounts used to support groundwater management through December 2020.

FIGURES

- 1-1 Lake Tahoe area regional map and groundwater subbasin designations.
- 1-2 Jurisdictional and TVS Subbasin boundaries within the TVS Subbasin.
- 2-1 Tahoe Valley South Subbasin (6-005.01). The Nevada portion of this subbasin is not considered within the scope of this Alternative Plan.
- 2-2 Geographic subarea designations and provisional management area proposed in the Alternative Plan.
- 2-3 Average annual precipitation (in) isohyets and location of climate stations within the analysis area. Annual precipitation data (1981-2010) derived from PRISM Climate Group, Oregon State University, <http://prism.oregonstate.edu>, Copyright © 2016.
- 2-4 Annual water year precipitation measured at Hagan’s Meadow SNOTEL Station 508.
- 2-5 Time series of simulated yearly average hydrologic variables for Incline Creek, Third Creek, and Galena Creek watersheds from Huntington and Niswonger (2012). Simulated hydrologic variables for different GCMs (colored lines) and for greenhouse gas emission scenarios A2.
- 2-6 Soil types at the order level within the TVS Subbasin (NRCS, 2021).
- 2-7 Hydrogeologic map of the South Lake Tahoe area derived from USGS Scientific Investigations Map 3063 (Plume et al., 2009). Mapped faults are from the Geologic Map of the Lake Tahoe Basin (CGS CD 2008-01) (Saucedo et al, 2008). Lines of section shown are for subsurface cross-sections included in Appendix F.
- 2-8 Geologic cross section D’ – D’’/F’ trending south to north across the north half of the TVS Subbasin (from Kennedy Jenks, 2014).
- 2-9 Geologic cross section I’ – E’/I’ trending west to east near the north margin of the TVS Subbasin (from Kennedy Jenks, 2014).
- 2-10 Conceptual hydrogeologic section trending east -west near the north margin of the TVS Subbasin.
- 2-11 Watersheds, lakes, streams, and USGS gaging stations within the South Lake Tahoe area.

- 2-12 Relationship between watershed area and average annual runoff for Edgewood Creek, Trout Creek, and the Upper Truckee River watersheds.
- 2-13 Hydrograph showing historic elevations for Lake Tahoe measured at the Tahoe City, CA gage (USGS 10337000).
- 2-14 Stream Environment Zones as mapped by the Tahoe Regional Planning Agency using land capability. Mapping is for general use only, requiring verification at the individual parcel scale.
- 3-1 TRPA land use types recognized within the TVS Subbasin.
- 3-2 Groundwater production trends for community water system wells in the TVS Subbasin since WY 2005, in AFY.
- 3-3 Water system services areas and annual groundwater pumpage from the four largest community well water systems for WY 2020, in AF.
- 3-4 Parcels with County Well Permits issued for new construction or deepening in the TVS Subbasin.
- 3-5 Small water system wells regulated by El Dorado County within the TVS Subbasin.
- 3-6 Domestic wells in-use based on private well owner survey responses collected in 2017 and 2020.
- 3-7 Confirmed private well locations situated within Disadvantaged Community census blocks within the City of South Lake Tahoe.
- 3-8 Pumpage from active wells based on the combined results of the survey of private well owners.
- 3-9 Water well density per square mile in the TVS Subbasin, including community water supply wells, small water system wells, and private wells (*de minimus* extractors).
- 5-1 Selected monitoring well locations and geographic sub-area designations.
- 5-2 Groundwater hydrograph for the Valhalla Well (6,257 feet AMSL) within the Tahoe Keys sub-area. Also shown is the water level (stage) of Lake Tahoe measured at USGS 10337000.
- 5-3 Groundwater hydrograph for the Blackrock #1 (6,241 feet AMSL) and Glenwood #3 (6,260 feet AMSL) wells within the Bijou sub-area.
- 5-4 Groundwater hydrograph for the Paloma (6,267 feet AMSL); Sunset (6,249 feet AMSL) and CL-1 (6,279 feet AMSL) wells in the South Lake Tahoe sub-area.

- 5-5 Groundwater hydrograph for the Mountain View (6,313 feet AMSL) well (artesian flowing well) in the Angora sub-area.
- 5-6 Groundwater hydrograph for the Bakersfield (6,311 feet AMSL); Elks Club #1 (6,283 feet AMSL) and Washoan (6,308 feet AMSL) wells in the Meyers sub-area.
- 5-7 Groundwater hydrograph for the Henderson Well (6,366 feet AMSL) within the Christmas Valley sub-area.
- 5-8 Shallow aquifer (upper 300 ft) water levels and flow directions (based on steady-state MODFLOW model). Contour interval is 10 ft.
- 5-9 Shallow aquifer (upper 300 ft) water levels as measured in October 2019 and May 2020. Contour interval is 10 ft.
- 5-10 Location of wells used to calculate vertical hydraulic head gradients.
- 5-11 Groundwater hydrograph for the USGS TCF nested well (6,296 feet AMSL) within the South Lake Tahoe sub-area. Total well depths for the observation wells completed within the common borehole are as indicated.
- 5-12 Groundwater hydrograph for the Clement Well cluster (6,279 feet AMSL) within the South Lake Tahoe sub-area. Total well depths for the observation wells comprising the well cluster are as indicated.
- 5-13 Hydraulic conductivity (FT/D) within the TVS Subbasin.
- 5-14 Hydraulic conductivity field (FT/D) used in the uppermost layer of the groundwater flow model.
- 5-15 Groundwater recharge rates for 2010 as simulated with the GSFLOW model.
- 5-16 Hagan's Meadow annual precipitation versus groundwater recharge within the hydrologic analysis area. Also shown is a non-linear regression.
- 5-17 Groundwater recharge to the TVS Subbasin from water year 1983–2019, including mountain block recharge and direct areal recharge, compared to water year type.
- 5-18 Annual pumpage in AFY from community water system and individual water system wells within the TVS Subbasin used in the MODFLOW model.
- 5-19 Simulated baseflow to streams within the TVS Subbasin for 1983-2019, not including the surrounding watershed.
- 5-20 Simulated net groundwater flow from the TVS Subbasin to Lake Tahoe for 1983-2019.
- 5-21 Simulated change in storage for the TVS Subbasin (Zone 10) for 1983-2019, not including the surrounding watershed.

- 5-22 Annual groundwater production from public water supply wells and modeled annual and cumulative change in groundwater storage, in AFY, for the TVS Subbasin (WY 2005 through WY 2020). Water year type using the classification developed for the TVS Subbasin (Section 9.1.2.1 is indicated on the vertical axis along the right-side of the graph. Positive changes in groundwater storage indicate periods of rising groundwater level.
- 5-23 Hagan's Meadow precipitation versus groundwater storage change through WY 2015.
- 5-24 Summary of historical inflows and outflows (not including changes in storage) for WY 1983 to WY 2019, and the annual change in storage for the TVS Subbasin.
- 5-25 Cumulative change in storage within the TVS Subbasin for all climate scenarios, WY 2020 – WY 2070.
- 5-26 Baseflow to streams within the TVS Subbasin for all climate scenarios, WY 2020 – WY 2070.
- 5-27 Discharge to Lake Tahoe from the TVS Subbasin for all climate scenarios, WY 2020 – WY 2070. Negative flow rates indicate lake water flowing into the TVS Subbasin.
- 5-28 Simulated drawdown from WY 2019 to WY 2070 for the baseline climate model.
- 5-29 Simulated drawdown from WY 2019 to WY 2070 for the Q2 (hot and dry) climate model.
- 5-30 Simulated depth to water and locations of individual water system wells for WY 2070 for the baseline climate model.
- 5-31 Simulated depth to water and locations of individual water system wells for WY 2070 for the Q2 (hot and dry) climate model.
- 5-32 Locations and magnitudes of baseflow depletion due to pumping in the baseline climate model in cubic feet per day (CFD).
- 5-33 Locations and magnitudes of baseflow depletion due to pumping and climate change in the Q2 (hot and dry) climate model in cubic feet per day (CFD).
- 6-1 Major ion compositions for groundwater samples collected from private wells during the Phase II survey of private well owners.
- 6-2 Incidences of inorganic chemical constituents above MCLs detected in water samples collected from water supply wells within the TVS Subbasin (Data Source: GAMA Groundwater Information System, June 2021).
- 6-3 Incidences of radionuclide constituents above MCLs detected in water samples collected from water supply wells within the TVS Subbasin (Data Source: GAMA Groundwater Information System, June 2021).

- 6-4 Incidences of regulated chemical constituents above MCLs detected in water samples collected from water supply wells within the TVS Subbasin (Data Source: GAMA Groundwater Information System, June 2021).
- 6-5 Incidences of petroleum hydrocarbon constituents above MCLs detected in water samples collected from environmental wells within the TVS Subbasin (Data Source: GAMA Groundwater Information System, June 2021).
- 6-6 Incidences of chlorinated hydrocarbon constituents above MCLs detected in water samples collected from environmental wells within the TVS Subbasin (Data Source: GAMA Groundwater Information System, June 2021).
- 6-7 Location of the South Y plume within the South Lake Tahoe subarea, as defined by PCE in groundwater detected above 5 micrograms per liter (UG/L), provisional data provided by LRWQCB.
- 6-8 Breakthrough curves at TKWC 1 for four pumping scenarios.
- 6-9 Breakthrough curves at TKWC 2 for four pumping scenarios.
- 6-10 Breakthrough curves at TKWC 3 for four pumping scenarios.
- 6-11 Breakthrough curves at LBWC 1 for four pumping scenarios.
- 6-12 Breakthrough curves at LBWC 5 for four pumping scenarios.
- 6-13 Incidences of Radon 222 in water samples collected from water supply wells within the TVS Subbasin (Data Source: GAMA Groundwater Information System, June 2021).
- 6-14 Locations of CSLT stormwater detention basins and dry wells in the TVS Subbasin.
- 6-15 Mean annual recharge rates over the TVS Subbasin extracted from the GSFRM.
- 6-16 Source area zones delineated using the modified CFR method and possible contaminating activity sites identified within the TVS Subbasin.
- 8-1 Beneficial users of groundwater within the TVS Basin (6-5.01) as a percent of the total groundwater production produced during WY 2020. Number of wells for each user is also shown.
- 8-2 Source capacity trends for community water system wells in the TVS Subbasin and the minimum threshold (in MGD) for degraded water quality.
- 8-3 Average daily flows, WY 1991 – WY 2020 at each USGS stream gage along with the DFW-recommended daily threshold values. The indicated interannual variability (the shaded gray area) represents ± 1 standard deviation from the mean flow.

- 8-4 Based on baseline simulations, the GDEs (as mapped by TRPA) indicated here are vulnerable to exceeding the threshold value in the timeframe indicated by their color. Mapping is for general use only, requiring verification at the individual parcel scale.
- 9-1 Locations of wells used in the TVS Subbasin monitoring network, USGS stream gage stations and NRCS snow telemetry stations.
- 9-2 Elevation ranges of the perforated intervals for all wells included in the monitoring network for the TVS Subbasin.
- 9-3 Hagans Meadow, CA SNOTEL 508 annual precipitation versus modeled groundwater recharge within the South Lake Tahoe area (G. Pohl et al., 2016).
- 9-4 Hand readings collected during the May groundwater elevation monitoring event for WY2015 through WY 2020 compared to the record of hand readings for the same wells collected during WY 2001 through WY 2010 base period for groundwater elevations.
- 9-5 Model simulated groundwater elevations (upper 300 ft), representing seasonal low (October 2019) and seasonal high (May 2020) groundwater conditions. Contour interval is 10 ft.
- 10-1 Expended costs for groundwater management in the TVS Subbasin through December 2020.

Volume II
APPENDICES

- A. Authorizing Resolutions
 - A01 – STPUD Notice of Intent to Serve as Groundwater Sustainability Agency (August 12, 2015) with STPUD Resolution No. 2986-15
 - A02 – STPUD Resolution No. 3055-17 of Withdraw as Groundwater Sustainability Agency (May 4, 2017)
 - A03 – EDWA Resolution No. WA-11-2017 to Serve as Groundwater Sustainability Agency (June 14, 2017)
 - A04 – STPUD_EDCWA Second Amended MOU (June 4, 2020)
 - A05 – DWR Notification- Resolution of Intent to Draft GMP (Jun 25, 2020)
 - A06 – EDWA Resolution No. WA-6-2020 Intent to Draft an Updated Groundwater Management Plan Pursuant to Groundwater Management Act (July 8, 2020)
 - A07 – SGMA 90 Day NOI to Adopt TVS Subbasin Alternative (October 1, 2021)
 - A08 – EDCWA Resolution WA -07-2022 to Adopt Alternative Plan (April 13, 2022)
 - A09 – STPUD Resolution No. 3215-22 to Adopt Alternative Plan (April 21, 2022)

- B. District Organization Chart
 - B01 – STPUD Org Chart – Official with Names (January 24, 2022)

- C. Alternative Plan Functional Equivalency Analysis
 - C01 – STPUD GSP Alternative Checklist (23156562.11) (April 8, 2022)

- D. Public Outreach and Engagement Materials
 - D01 – Tahoe Daily Tribune Affidavit of Publication (May 2020)
 - D02 – Tahoe Daily Tribune Affidavit of Publication (June 2020)
 - D03 – STPUD Notice to Participate in the Five-Year Update to the 2014 GMP_final_2021.01.07
 - D04 – 2014 GMP Update Presentation _2020.11.23
 - D05 – TVS Alternative Stakeholder Engagement Chart
 - D06 – TVS Stakeholder Survey
 - D07 – TVS Alternative Stakeholders List (March 2021)
 - D08 – SGMA 90-Day NOI to Adopt TVS Subbasin Alternative (October 1, 2021)
 - D09 – Notice of Availability Draft Alternative Plan (January 31, 2022)
 - D10 – Notice of Availability Draft Alternative Plan to Cities and Counties (February 9, 2022)
 - D11 – Proof of Publication Mountain Democrat NOA (February 2022)
 - D12 – Tahoe Daily Tribune Affidavit NOA (February 2022)
 - D13 – Notice of Public Hearings to Adopt the first five-year update of the Alternative Plan (March 17, 2022)
 - D14 – Proof of Publication Mountain Democrat Notice of Public Hearings (March 23, March 30, 2022)
 - D15 – Tahoe Daily Tribune Affidavit Notice of Public Hearings (April 8, April 15, 2022)

- E. Groundwater Management Ordinances
 - E01 – Ordinance No. 558-14 (December 4, 2014)
 - E02 – Ordinance No. 580-22 (April 21, 2022)
- F. Subsurface Sections
 - F01 – Regional Subsurface Cross-Sections (Sept. 2006)
- G. Assessment of Groundwater Dependent Ecosystems
 - G01 – Assessment of Groundwater Dependent Ecosystems within the Tahoe Valley South Subbasin (Hausner and Rybarski, 2022)
- H. Survey of Private Well Owners
 - H01 – Laketahoenews.net (August 2017)
 - H02 – Groundwater Well Survey Nes Release (Jun 2020)
 - H03 – WOS Questions
 - H04 – Analyze- Well Owner Survey Combined (2/24/2021)
- I. South Tahoe Groundwater Model
 - I01– South Tahoe Groundwater Model Update (Rybarski and Hausner, 2022)
- J. TVS Subbasin Water Budget Tables
 - J01 – TVS Subbasin (Zone 10) Flow Budget Tables (01/25/2022)
- K. Groundwater Elevation Monitoring Plan
 - K01-Groundwater Elevation Monitoring Plan -Tahoe Valley South (Basin No. 6-5.01).
Version 1.0 (December 2011)
- L. TVS Subbasin Hydrographs (WY 2000 – WY 2020)
 - L01 – GW Level Hydrographs thru Nov 2020
- M. 2021 Implementation Plan
 - M01 – Implementation Plan 11 x 17 Table (04/08/2022)
 - M02 – Component Requirements 5year Plan Assessment (12/16/2021)
- N. Summary of Comments and Responses
 - N01 – Draft Alternative Plan (12172021) – SAG Comment Log and Responses
(2022.02.07)
 - N02a – TVS Subbasin draft Alternative Plan Response to SSLP Comments_04.01.2022
 - N02a – 102100101L017 _SSLP Comments (03/11/2022)

SECTION 1: INTRODUCTION

The State of California enacted the Sustainable Groundwater Management Act (SGMA), effective January 1, 2015, as the first legislation in the state's history to mandate comprehensive sustainable groundwater resources management. SGMA requires local agencies to develop Groundwater Sustainability Plans (GSPs) outlining the basin's strategies for obtaining sustainability. SGMA permits a Groundwater Management Plan (GWMP) developed under AB 3030 to serve as an Alternative to a GSP. While SGMA will revolutionize groundwater management in California, the South Tahoe Public Utility District (District) has been managing the Tahoe Valley South Subbasin (6-005.01) (TVS Subbasin) of the Tahoe Valley Groundwater Basin (No.6-005) (TV Groundwater Basin) (Figure 1-1) long before SGMA was passed into law.

The TVS Subbasin has been managed under a GWMP prepared in accordance with AB 3030, also known as the Groundwater Management Act (Wat. Code Section 10750 *et. seq.*), since 2000. The GWMP adopted in 2000 was updated in 2014 (2014 GWMP). In late 2016, pursuant to Water Code section 10733, the District timely submitted to the California Department of Water Resources (DWR) two potential Alternatives to a GSP to meet the TVS Subbasin's new obligations under SGMA: (1) its 2014 GWMP and additional plans, reports and other documents related to the 2014 GWMP (Alternative Materials); and (2) an Analysis of Basin Conditions.¹ On July 17, 2019, DWR determined that the 2014 GWMP and Alternative Materials satisfied the objectives of the SGMA and approved the 2014 GWMP and Alternative Materials as the Alternative Plan. During DWR's evaluation and assessment of the 2014 GWMP eight recommended actions (Recommended Actions) were identified for inclusion of the first five-year update of the Alternative Plan to facilitate DWR's ongoing evaluation of the Alternative Plan and whether implementation of the Alternative Plan is achieving the sustainability goal, and recommendations for improvements to the Alternative Plan. The first five-year update of the Alternative Plan is to be resubmitted to DWR by January 1, 2022, for periodic review and every five-years thereafter. The following Alternative Plan for the TVS Subbasin has been prepared to satisfy this requirement.

The Alternative Plan is a product of both the groundwater management actions implemented by the District and El Dorado County Water Agency (EDWA) since adoption of the 2014 GWMP, as well as the on-going collaboration with local stakeholders to manage groundwater in a sustainable manner for all users and beneficial uses of groundwater within the TVS Subbasin. The Alternative Plan provides new information and data, describes proposed implementation actions, and evaluates progress towards meeting the sustainability goals for the TVS Subbasin.

This document is the first required five-year update to the approved Alternative Plan.

¹ As noted in correspondence transmitting both of its GSP Alternatives to DWR, the District requested DWR to first review its 2014 GWMP and Alternative Materials and to only review the analysis of basin conditions if it were to find that the 2014 GWMP and Alternative Materials were not functionally equivalent to a GSP.

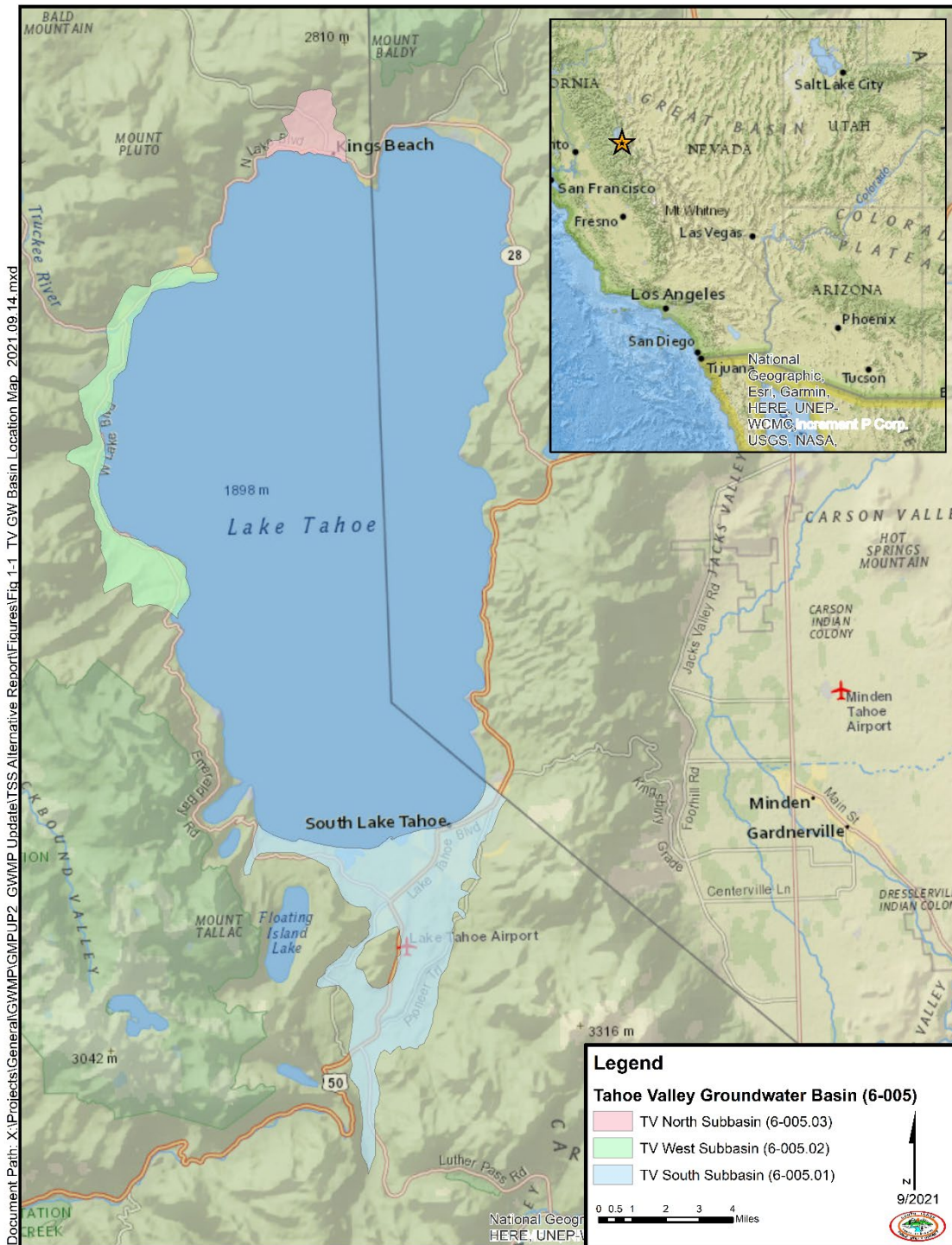


Figure 1-1. Lake Tahoe area regional map and groundwater subbasin designations.

The following section describes the submission and approval process of the Alternative Plan, presents the findings from the DWR assessment of the Alternative Plan (DWR, 2019), and

outlines the subsequent legal and administrative requirements completed for the first five-year update of the Alternative Plan. Basin Management Objectives (BMOs) of the 2014 GWMP serve as the foundation for the Alternative Plan.

1.1 **Background**

SGMA required basins that DWR designated to be medium- or high-priority to create Groundwater Sustainability Agencies (GSAs) to develop plans for sustainably managing groundwater (i.e., Groundwater Sustainability Plans GSPs)). In 2015, DWR used the 2014 Basin Prioritization completed under the California State Groundwater Elevation Monitoring (CASGEM) Program as the initial SGMA basin prioritization. Under the 2014 Basin Prioritization the TVS Subbasin was ranked medium priority based on population density, total number of public supply wells, total number of wells, groundwater reliance and documented impacts of groundwater contamination. In 2018, DWR used the same process to reprioritize groundwater basins for the 2018 SGMA Basin Prioritization as was used for the 2014 CASGEM Basin Prioritization and the TVS Subbasin was again ranked medium priority (DWR, 2020). As described above, local agencies had the ability to comply with SGMA requirements using an existing groundwater management plan developed and implemented by groundwater management agencies.

1.1.1 **Plan Authorization and Legal Authority**

This Alternative Plan covers the entirety of the TVS Subbasin, as defined in Bulletin 118.² The TVS Subbasin lies entirely within El Dorado County (County) and largely within the jurisdiction of the District (Figure 1-2). While the entire TVS Subbasin is within the County, only that portion of the TVS Subbasin outside the District’s jurisdiction is within the jurisdiction of EDWA for the Alternative Plan. Both the District and EDWA are local agencies within the meaning of Water Code section 10721(n) and are thus eligible to be a GSA for the TVS Subbasin. Both agencies are GSAs pursuant to California Water Code Section 10723 and are authorized groundwater management agencies within the meaning of California Water Code Section 10753(a). Additionally, the Public Utility District Act authorizes the District to manage local groundwater resources, including developing, adopting, and implementing a groundwater management plan (*see* Pub. Util. Code. §§ 15501–18055). A copy of the District’s authorizing legislation is provided in Appendix A. Similarly, EDWA has the power to “do any and every lawful act necessary in order that sufficient water may be available for any present or future beneficial use or uses of the lands or inhabitants within the agency.” (Cal. Wat. Code § 96-11; *see* Cal. Wat. Code § 96-1 *et seq.*) A copy of EDWA’s authorizing legislation is also provided in Appendix A.

The District is primarily responsible for Alternative Plan development and implementation through the MOU (see below for discussion) with EDWA. With the District assuming primary responsibility for managing the quantity and quality of the groundwater resources within the TVS Subbasin pursuant to the Alternative Plan, the District has the authority

² A portion of the physical subbasin extends into the State of Nevada and is therefore beyond the scope of SGMA and the Alternative Plan.

to adopt rules, regulations, and procedures to implement and enforce the Alternative Plan pursuant to California Water Code section 10750 *et seq.* and SGMA.

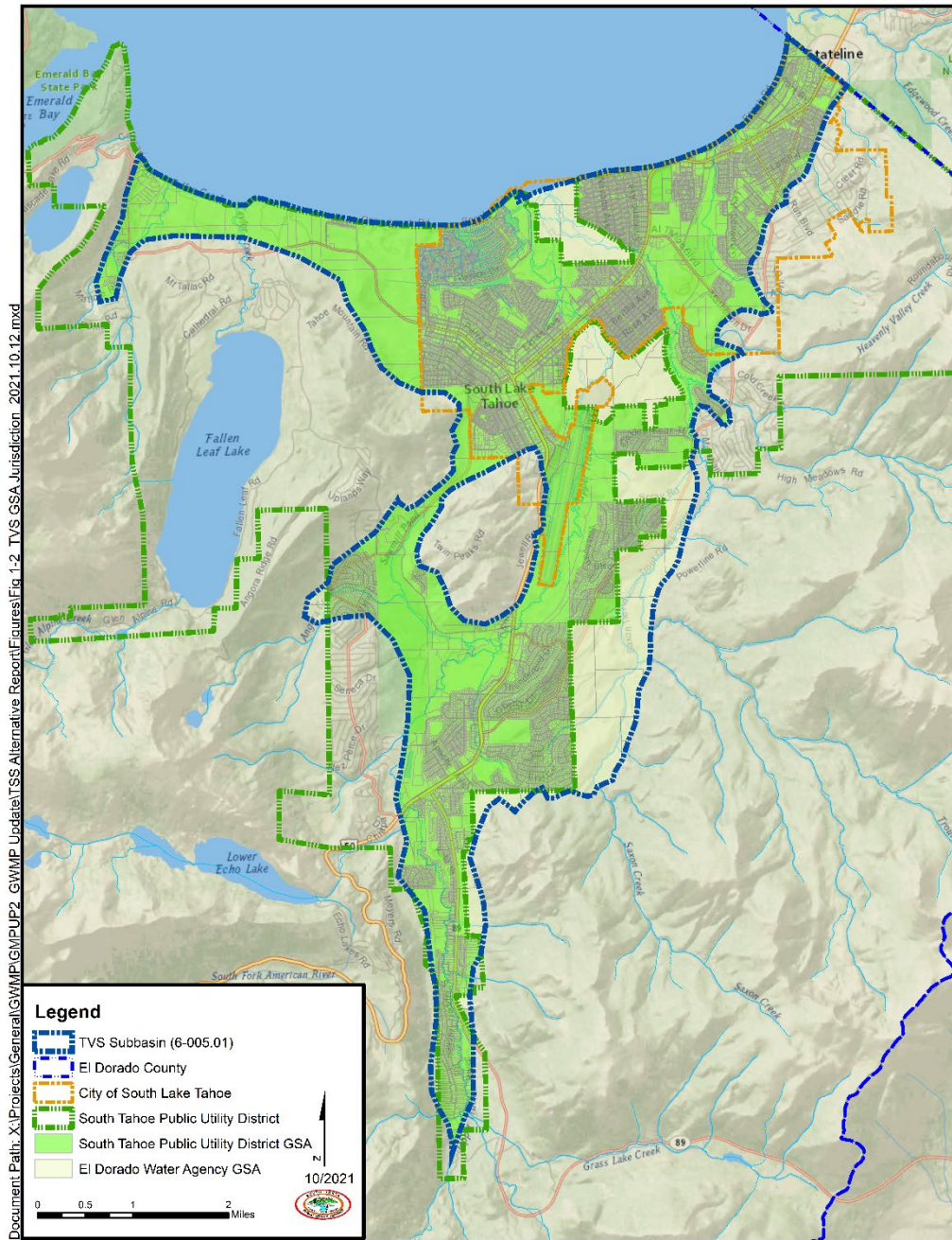


Figure 1-2. Jurisdictional and TVS Subbasin boundaries within the TVS Subbasin.

This Alternative Plan is a regional effort facilitated by the District and EDWA. In developing this Alternative Plan, the District has collaborated with other South Lake Tahoe area water purveyors, including Lukins Brothers Water Company (LBWC) and Tahoe Keys Water

Company (TKWC), along with other governmental agencies and authorities, including the City of South Lake Tahoe (CSLT), County Environmental Management Department (EDCEMD), the Tahoe Regional Planning Agency (TRPA) and the Lahontan Regional Water Quality Control Board (LRWQCB). This collaboration has been undertaken to better achieve comprehensive groundwater management, minimize duplication of effort, and apply consistent standards to the extent reasonably possible.

1.1.2 **TVS Subbasin GSA Formation**

As described in further detail below, the District has been recognized by DWR as the exclusive GSA for the portion of the Subbasin within its jurisdictional boundaries. EDWA has been recognized by DWR as the exclusive GSA for the remaining portion of the TVS Subbasin. EDWA and the District cooperate through a Second Amended and Restated Memorandum of Understanding (MOU) to sustainably manage groundwater resources and implement SGMA consistently throughout the entire TVS Subbasin.

1.1.2.1 **South Tahoe Public Utility District GSA**

During the summer of 2016, the District and EDWA began discussing options to form a GSA in the portion of the TVS Subbasin outside of the District's jurisdiction. Concurrent with this decision, EDWA and the District entered into a memorandum of understanding setting forth EDWA's and the District's agreement to cooperatively manage and coordinate implementation and enforcement of SGMA in this portion of the Basin. Under this memorandum of understanding, the District and EDWA agreed that the District should become the exclusive GSA for the entire TVS Subbasin. As a result, the District submitted GSA formation notices to DWR for both the portion of the TVS Subbasin within its jurisdictional boundaries as well as the area that extends into the County's jurisdiction. The District was recognized as the exclusive GSA for both areas on November 17, 2015, and December 28, 2016, respectively. The District's Notice of Intent (NOI) to form a GSA is provided in Appendix A1.³

Due to concerns raised by the State Water Resources Control Board (SWRCB) about a GSA exercising regulatory authority outside of its jurisdictional boundary, the District notified DWR that it would be rescinding its GSA formation notice for the portion of the TVS Subbasin outside of its jurisdiction (see Appendix A2) and that EDWA had agreed to become the GSA for this portion of the TVS Subbasin.⁴

1.1.2.2 **El Dorado Water Agency (EDWA) GSA**

In response to the above concerns, on June 14, 2017, EDWA held a public hearing and elected to become the GSA for the portion of the TVS Subbasin outside of the District's jurisdictional boundaries. On June 15, 2017, EDWA was recognized by DWR as the GSA for the

³ Appendix A2 includes the District's Notice of Intent to Withdraw as GSA for the portion of the TVS Subbasin outside the District's jurisdiction.

⁴ The withdrawal notice had no effect on formation or recognition of the District as the exclusive GSA for the portion of the TVS Subbasin within its jurisdictional boundaries.

portion of the TVS Subbasin outside of the District’s jurisdiction. EDWA’s Notice of Intent (NOI) to form a GSA is provided in Appendix A3.

1.1.2.3 **Second Amended and Restated MOU**

Concurrent with EDWA’s GSA formation notice for the portion of the TVS Subbasin outside of the District’s jurisdiction, the District and EDWA entered an amended and restated memorandum of understanding to work collaboratively as separate GSAs to sustainably manage groundwater resources and implement SGMA throughout the entire TVS Subbasin. With the execution of the amended and restated memorandum of understanding on June 14, 2017, the TVS Subbasin was in full compliance with SGMA’s GSA formation requirements.

On July 17, 2019, DWR determined that the 2014 GWMP and the Alternative Materials satisfied the objectives of SGMA and accepted the 2014 GWMP and Alternative Materials as an approved Alternative for the TVS Subbasin. In its approval, DWR also included a set of eight Recommended Actions recommending the District and EDWA to provide additional information in the first five-year update (discussed in Section 1.3). The District and EDWA subsequently amended the memorandum of understanding a second time (MOU) to acknowledge DWR’s approval of the Alternative Plan and formalize the District’s and EDWA’s agreement to continue to manage groundwater resources cooperatively and sustainably within the TVS Subbasin and to jointly implement the Alternative Plan in accordance with SGMA (District, 2020a). A copy of the MOU is included in Appendix A4.

1.1.3 **Plan Manager and Contact Information**

The District is the lead GSA for the Alternative Plan. The name and mailing address of the District is presented in the Groundwater Sustainability Information provided following the Executive Summary. Organization and management structure is shown using the District Organization Chart (with names) provided in Appendix B. Mr. Ivo Bergsohn, PG, HG serves as the Plan Manger for implementation of the TVS Subbasin Alternative Plan. Management and implementation authority, however, resides with various members of District staff including Julie Ryan, PE, Engineering Department Manager. Staff reports back to John Thiel, PE, General Manager, and the District’s Board of Directors for final authorization.

As noted above Ivo Bergsohn has been designated as the Plan Manager for implementation of the TVS Subbasin Alternative Plan. The following contact information is available on the District’s website:

Ivo Bergsohn, P.G., HG. Hydrogeologist
South Tahoe Public Utility District
1275 Meadow Crest Drive,
South Lake Tahoe, CA 96150
(530) 543-6204
ibergsohn@stpud.us

1.2

Development and Adoption Process

The 2014 GWMP is foundational to both the Alternative Plan and the first five-year update to the Alternative Plan. The following section describes the submittal and approval processes for the Alternative Plan, outlines the contents of the Alternative Plan and the accomplishments under the plan, and describes updates incorporated into the first five-year update to the Alternative Plan.

1.2.1

2014 GWMP

The 2014 GWMP was prepared in accordance with Assembly Bill 3030 (AB 3030) pursuant to California Water Code Section 10750 *et seq.* The 2014 GWMP was adopted by the District and an accompanying Groundwater Ordinance was added as Division 7 to the District's Administrative Code on December 4, 2014.

The 2014 GWMP centered around eight BMOs. BMOs are flexible guidelines for the management of groundwater resources that describe specific actions to be taken by the District to meet locally developed objectives at the basin or sub-area scale. Under the 2014 GWMP, eight BMOs were defined for groundwater management of the TVS Subbasin.

- BMO #1 – Maintain a sustainable long-term groundwater supply.
- BMO #2 – Maintain and protect groundwater quality.
- BMO #3 – Strengthen collaborative relationships with local water purveyors, governmental agencies, businesses, private property owners and the public.
- BMO #4 – Integrate groundwater quality protection into local land use planning activities.
- BMO #5 – Assess the interaction of water supply activities with environmental conditions.
- BMO #6 – Convene an ongoing Stakeholder's Advisory Group (SAG) as a forum for future groundwater issues.
- BMO #7 – Conduct technical studies to assess future groundwater needs and issues.
- BMO #8 - Identify and obtain funding for groundwater projects.

Using this framework, the District successfully managed groundwater within the TVS Subbasin. Major accomplishments include: (1) broadening the scope of basin monitoring to include precipitation, groundwater pumpage, recharge and storage, and (2) developing complex hydrologic models to calculate water budgets, evaluate future conditions, identify recharge areas, consider groundwater-surface water interactions, and evaluate remedial alternatives for the management of contaminated groundwater within the TVS Subbasin. Investigations were also

performed to define the extent of groundwater contamination and assess the suitability of renewing the use of an impaired groundwater source for contaminant plume control and removal.

Newly developed hydrologic models were used to address the following management actions:

- Providing water balance estimates (BMO #7, Action 3);
- Conducting a regional groundwater vulnerability assessment (BMO #4, Action 2);
- Identifying recharge areas;
- Identifying amounts and capture zones for public supply wells;
- Assessing the effects of groundwater pumping on habitats in lakes, streams, and wetlands (BMO #5, Action 1);
- Determining stream depletion rates; and
- Creating capture maps to show surface water withdrawals.

The District developed six climate scenarios using global climate models (GCMs) to assess potential effects of climate change pursuant to BMO #5, Action 3. The District also developed a historically based drought model to assess the impact of a changing climate on the groundwater conditions in the TVS Subbasin. In alignment with BMO #7, Action 4, the District expanded its monitoring well network to evaluate recharge areas and other key areas. The District also identified two areas in need of additional monitoring. (DRI, 2018).

Public outreach involving private well owner surveys were also performed to foster communications between private well owners and the District, inform private well owners about the District's role and responsibilities as a GSA and inform the District on the use of private water system wells and the concerns of private well owners. The District also satisfied all of the new annual reporting requirements under SGMA and continued to satisfy its monitoring entity requirements under the California State Groundwater Elevation Monitoring (CASGEM).

Following adoption of the 2014 GWMP, the District undertook various studies and reports, as well as completed Annual Reports as part of implementation of the 2014 GWMP. These additional plans, reports and other documents were submitted to DWR as Alternative Materials. DWR determined these Alternative Materials, outlined in bullet points below, sufficiently related to the 2014 GWMP to warrant consideration as part of the Alternative Plan (DWR, 2019).

- Bergsohn, I. (Mar. 11, 2016). South Tahoe Public Utility District: Tahoe Valley South Basin (6-5.01) Annual Report – 2015 Water Year. (2015 Water Year Report). The 2015 Water Year Report was prepared by the District to track progress on the implementation of the Groundwater Management Plan through an assessment of the groundwater supplies and conditions, review of monitoring data, and progress reporting on implementation of BMOs.

- Carrol, R. W.H., Pohll, G., & Rajagopal, S. (Feb. 25, 2016). Desert Research Institute: South Lake Tahoe Groundwater Model. (DRI Phase 1 Memo). The DRI Phase 1 Memo was prepared at the request of the District to develop a numerical groundwater model to calculate a water budget for the water years 1983 to 2014 for the Tahoe South Subbasin. Refinement of a groundwater model is included in the implementation plan for the Groundwater Management Plan and addresses one of the District’s BMOs.
- Carrol, R. W.H., Pohll, G., & Rajagopal, S. (Aug. 26, 2016). Desert Research Institute: South Lake Tahoe Groundwater Model Update. (DRI Phase 2 Memo). The DRI Phase 2 Memo was prepared at the request of the District to extend the numerical groundwater model through water year 2015 for the TVS Subbasin.
- J. Crowley Group, ECORP Consulting, Inc. (Jun. 2016), South Tahoe Public Utility District: 2015 Urban Water Management Plan. (UWMP). The UWMP was prepared at the request of the District and is used by the District in the Groundwater Management Plan for future water demand projections for the TVS Subbasin.

1.2.2 **Alternative Plan and DWR Approval**

Under SGMA, local agencies are authorized to submit an Alternative, in lieu of a GSP, for review by DWR. SGMA identifies the following three Alternatives to a GSP: (1) a GWMP developed pursuant to Part 2.75 of Division 6 of the Water Code (Section 10750 *et seq.*), (2) management pursuant to an adjudication action, or (3) an analysis of basin conditions (Wat. Code § 10733.6(b).)

To be eligible to submit any of the above Alternatives, the local agency must be able to demonstrate that (1) the Alternative applies to the entire basin, and (2) the basin is compliant with section 10733.6 of the Water Code. (23 Cal. Code Regs., § 358.2(a).) Additionally, the local agency must demonstrate that its Alternative is “functionally equivalent to the elements of a [GSP] required by Articles 5 and 7... [and is] sufficient to demonstrate the ability of the [Alternative] to achieve the objectives of [SGMA].” (23 Cal. Code Regs., § 358.2(d).)

On December 28, 2016, the District concurrently submitted (1) its 2014 GWMP and Alternative Materials to DWR as an existing plan Alternative pursuant to Water Code section 10733.6(b)(1) and (2) an analysis of basin conditions pursuant to Water Code section 10733.6(b)(2) to DWR for evaluation and assessment.⁵

On July 17, 2019, DWR determined that the 2014 GWMP and Alternative Materials satisfied SGMA’s requirements for an existing plan Alternative and approved it as an Alternative Plan for the TVS Subbasin in compliance with Water Code section 10733.6(b). (DWR, 2019a.) In its approval of the Alternative Plan, DWR issued a set of Recommended Actions to be

⁵ As part of its submittals, the District indicated its preference to DWR that the review be sequenced in such a manner that its 2014 GWMP and Alternative Materials be reviewed first and should DWR agree that the 2014 GWMP and Alternative Materials are functionally equivalent to a GSP, review of the analysis of basin conditions would not be necessary.

addressed in the first five-year update of the Alternative Plan. These Recommended Actions are summarized below in Section 1.3.

Similarly, this first five-year update to the Alternative Plan will be resubmitted to DWR for evaluation upon its completion pursuant to the requirement that the GSA resubmit its Alternative Plan for periodic review at least every five years after initial submission (January 1, 2022) and every five-years thereafter (Cal. Water Code § 10733.8.). The Alternative Plan Functional Equivalency Matrix in Appendix C demonstrates the Alternative Plan’s compliance with SGMA as a “functional equivalent” of a GSP.⁶

1.3 Recommended Actions Identified by DWR

During evaluation and assessment of the 2014 GWMP and Alternative Materials, DWR identified eight Recommended Actions to facilitate further development of the Alternative Plan and its implementation in a Statement of Findings. The Recommended Actions involve information needed to facilitate DWRs ongoing evaluation of the Alternative Plan and whether implementation of the Alternative Plan is achieving the sustainability goal, and recommendations for improvement to the Alternative Plan (DWR, 2019). Table 1-1 provides a summary of these Recommended Actions and the sections where they are implemented in this first five-year update to the Alternative Plan.

Table 1-1. Summary of Recommended Actions identified during DWR assessment of the 2014 GWMP and Alternative Materials submitted to DWR in 2016 (DWR, 2019).

Recommended Action	Description	Section(s)
1	Provide water budget information in Tabular Form for historical, current, and projected water budgets.	Sections 5.4.6; 5.4.7; and 5.4.8. Appendix J
2	Provide a projected water budget over the 50-year planning and implementation horizon, incorporating climate change effects.	Section 5.4.8 Appendix J
3	Reconcile the different future water demand projections between the Groundwater Management Plan (GWMP) and Urban Water Management Plan (UWMP) and incorporate the reconciliation in the projected water budget.	Section 4.4.1

⁶ The District has included in the Alternative Plan Functional Equivalency Matrix both original GSP submission requirements and five-year update requirements. This first five-year update to the Alternative Plan involved broad revisions to overlay SGMA on top of the existing BMOs. This comprehensive update necessitated a restating of the Alternative Plan rather than a narrow evaluation of new information, monitoring data from the previous five years, etc.

Recommended Action	Description	Section(s)
4	To understand change in groundwater storage for the TVS Subbasin, the water budget calculated by the South Tahoe Groundwater Model should be calculated within the TVS Subbasin boundary rather than the surrounding watershed area inclusive of the TVS Subbasin.	Section 5.2.4
5	Provide additional explanation in the first five-year update for how pumping may impact plume migration or cause degraded water quality.	Section 6.3.1
6	Provide estimates of the quantity and timing of depletions of interconnected surface water; define what would cause depletions to become significant and unreasonable.	Sections 5.3 and 8.3
7	Define quantitative criteria for groundwater levels, storage and depletion of interconnected surface water that can be used to objectively determine compliance of the Plan with the objectives of SGMA on an on-going basis.	Sections 8.1.1, 8.1.2 and 8.3.
8	Provide a description of how the data gaps identified will be addressed; specifically, the projects identified in Appendix M for BMO 5 - dependent upon District funding.	Section 5.1.1, 5.3, 5.4, 5.7, 7.2.4, and 8.3

The District undertook studies building on previous modeling and analyses to address the Recommended Actions identified in the DWR Statement of Findings. The District also developed projected water budgets over the 50-year planning and implementation horizon, incorporating climate change effects and reconciling future water demand projections with the District’s Urban Water Management Plan (UWMP). Additionally, the District estimated quantity and timing of depletions of interconnected surface water. Finally, the District developed sustainable management criteria to demonstrate sustainability within the TVS Subbasin.

1.4 Alternative Plan Changes

As the first five-year update of the Alternative Plan proceeded, numerous changes were made to the 2014 GWMP and Alternative Materials approved by DWR in 2019. These changes involved incorporating new information developed since adoption of the 2014 GWMP and Alternative Materials in 2014, incorporating new data developed during periodic review of groundwater conditions within the TVS Subbasin and incorporating findings from new hydrologic analyses completed to satisfy the Recommended Actions identified by DWR (Section 1.3).

Table 1-2 lists the major plan components (in terms of major headings and subheadings) presented in the 2014 GWMP and Alternative Materials alongside the major plan components contained in this first five-year update of the Alternative Plan. The most significant changes to the Alternative Plan components between these two documents occur in Section 8 of this Alternative Plan. In the 2014 GWMP and Alternative Materials, Section 8 provides a description of basin management objectives, strategies, and actions for qualitative management of groundwater resources within the TVS Subbasin. Under this first five-year update of the Alternative Plan, Section 8 has been updated using a characterization of undesirable results with quantitative sustainable management criteria consistent with SGMA and developed for the TVS Subbasin within the framework of BMOs. The sustainable management criteria presented in the Alternative Plan are quantitative metrics used to demonstrate the current status towards attainment of the sustainability goal for the TVS Subbasin under SGMA.

Other important changes in plan components from the 2014 GWMP and Alternative Materials to this first five-year update of the Alternative Plan, include the following.

- Section 1: Information has been updated and reorganized into Sections 1.1 Background, and Section 1.2 Development and Adoption Process. New Sections 1.3 Recommended Actions Identified by DWR and 1.4 Alternative Plan Changes have been added; Plan requirements and organization are presented below in Table 1-2.
- Section 2: A new Section 2.3 Soils and 2.5 Description of Basin Aquifers has been added. Surface Features and ecological resources are discussed under Section 2.6 Surface Water Features. All subsections have been updated.
- Section 3: Information has been updated and reorganized into new Sections 3.1 Population and Economy; and Section 3.2 Land Use. Water purveyors are discussed under new Section 3.3 Groundwater Uses and Users. A new Section 3.4 Demand Projections has been added.
- Section 4: Information has been updated and reorganized into new Section 4.2 Overlying Jurisdictions, Section 4.3 Regulatory Agencies, Section 4.4 Regulatory Programs and Policies, and Section 4.5 Analysis of Limits Imposed by Existing Water Resource Monitoring and Management Programs.
- Section 5: A new Section 5.5 Sustainable Yield has been added. All subsections have been updated.
- Section 6: Groundwater Contamination and Stormwater Infiltration Potential are discussed under new Section 6.3 Groundwater Quality Issues. All subsections have been updated.
- Section 7: Convene an Ongoing SAG has been updated and discussed under new Section 7.3 Future/Ongoing Stakeholder Involvement Opportunities.

- Section 8: Information has been updated and reorganized into new Sections 8.1 Maintain a Sustainable Long-Term Groundwater Supply; 8.2 Maintain and Protect Groundwater Quality; and 8.3 Assess the Interaction of Water Supply Activities with Environmental Conditions.
- Section 9: Information has been updated and reorganized into Sections 9.1 Groundwater Monitoring and Section 9.2. Identification and Description of Data Gaps.
- Section 10: Information has been updated and reorganized into Sections 10.1 Projects, Section 10.2. Funding the Alternative Plan and 10.3 Reporting.

Table 1-2. Major plan components presented in the 2014 GWMP and Alternative Materials and the first five-year update of the Alternative Plan.

2014 GWMP and Alternative Materials Tahoe Valley South Basin (6-5.01) 2014 Groundwater Management Plan (KJC, 2014)	First Five-Year Update of the Alternative Plan Alternative Plan for Tahoe South Subbasin (6-005.01) First Five Year Update (This Document)
Executive Summary Stakeholder Involvement State of the Groundwater Basin Basin Management Objectives Monitoring and Reporting	Executive Summary ES-1 Introduction ES-2 Groundwater Basin ES-3 Groundwater management Area ES-4 Overview of Local Government Agencies ES-5 State of the Groundwater Basin ES-6 Groundwater Quality ES-7 Stakeholder Involvement ES-8 Characterization of undesirable Results ES-9 Groundwater Monitoring ES-10 Implementation Plan
1. Introduction	1. Introduction
1.1 Introduction 1.2 Plan Authorization 1.3 Background 1.4 Updated Goals and Objectives 1.5 Plan Requirements & Organization 1.6 Plan Preparation & Adoption Process	1.1. Background 1.2. Development and Adoption Process 1.3. Recommended Actions identified by DWR 1.4. Alternative Plan Changes
2. Groundwater Basin	2. Tahoe Valley South Subbasin
2.1. TVS Basin Delineation 2.2. Geology 2.3. Climate 2.4. Surface Features 2.5. Ecological Resources	2.1 Delineation
3. Groundwater Management Area	3. Alternative Plan Area
3.1 GWMP Area 3.2 Water Purveyors 3.3 Wastewater Management	3.1 Population and Economy 3.2 Land Use 3.3 Groundwater Uses and Users 3.4 Demand Projections 3.5 Wastewater Management
4. Overview of Local Governmental Agencies	4. Local Government Agencies and Groundwater-Related Programs
4.1 History of Collaboration 4.2 Groundwater Regulatory Authorities 4.3 Land Use Planning Agencies and Programs 4.4 Oversight of Drinking Water Supply and Wells 4.5 Lake Tahoe Water Quality Management and TMDL	4.1 History of Collaboration and Collaboration Opportunities 4.2 Overlying Jurisdictions 4.3 Regulatory Agencies 4.4 Regulatory Programs and Policies

<p>2014 GWMP and Alternative Materials Tahoe Valley South Basin (6-5.01) 2014 Groundwater Management Plan (KJC, 2014)</p>	<p>First Five-Year Update of the Alternative Plan Alternative Plan for Tahoe South Subbasin (6-005.01) First Five Year Update (This Document)</p>
<p>4.6 Integrated Regional Water Management Planning</p>	<p>4.5 Analysis of Limits Imposed by Existing Water Resources Monitoring and Management Programs</p>
<p>5. State of the Groundwater Basin</p>	<p>5. State of the Groundwater Basin</p>
<p>5.1 Description of the Aquifers 5.2 Groundwater Conditions 5.3 Groundwater – Surface Water Interactions 5.4 Preliminary Groundwater Budget 5.5 Assessment of Potential Overdraft Issues 5.6 Potential Climate Change Impacts</p>	<p>5.1 Background 5.2 Groundwater Conditions 5.3 Groundwater-Surface Water Interactions 5.4 Groundwater Budget 5.5 Sustainable Yield 5.6 Assessment of Potential Overdraft Issues 5.7 Potential Climate Change Impacts</p>
<p>6. Groundwater Quality</p>	<p>6. Groundwater Quality</p>
<p>6.1 Background 6.2 General Groundwater Quality 6.3 Groundwater Contamination 6.4 GWMP Aquifer Vulnerability Assessment 6.5 Stormwater Infiltration and Potential for Groundwater Contaminations</p>	<p>6.1 Background 6.2 Groundwater Quality 6.3 Groundwater Quality Issues 6.4 Groundwater Vulnerability Assessment</p>
<p>7. Stakeholder Involvement</p>	<p>7. Stakeholder Involvement</p>
<p>7.1 Stakeholders Advisory Group 7.2 Groundwater Management Collaboration Opportunities 7.3 Convene an Ongoing SAG</p>	<p>7.1 Stakeholder Advisory Group 7.2 Groundwater Management Collaboration 7.3 Future/Ongoing Stakeholder Involvement Opportunities 7.4 Public Participation in the Five-Year Update of the Alternative Plan</p>
<p>8. Basin Management Objectives, Strategies and Actions</p>	<p>8. Characterization of Undesirable Results</p>
<p>8.1 BMO #1 - Maintain a Sustainable Long-Term Groundwater Supply 8.2 BMO #2 -Maintain and Protect Groundwater Quality 8.3 BMO #3- Integrate Groundwater Protection into Local Land Use Planning Activities 8.4 BMO#4 - Integrate Groundwater Protection into Local Land Use Planning Activities 8.5 BMO#5 - Assess the Interaction of Water Supply Activities with Environmental Conditions 8.6 BMO#6 - Convene an Ongoing Stakeholders Advisory Group 8.7 BMO#7 - Conduct Technical Studies to Assess Future Groundwater Needs and Issues</p>	<p>8.1 BMO #1: Maintain a Sustainable Long-Term Groundwater Supply 8.2 BMO #2: Maintain and Protect Groundwater Quality 8.3 BMO#5: Assess the Interaction of Water Supply Activities with Environmental Conditions</p>

2014 GWMP and Alternative Materials Tahoe Valley South Basin (6-5.01) 2014 Groundwater Management Plan (KJC, 2014)	First Five-Year Update of the Alternative Plan Alternative Plan for Tahoe South Subbasin (6- 005.01) First Five Year Update (This Document)
8.8 BMO#8 - Conduct Technical Studies to Assess Future Groundwater Needs and Issues	
9. Basin Monitoring Program	9. Groundwater Monitoring
9.1 Groundwater Management Monitoring 9.2 Additional Groundwater Quality Monitoring 9.3 Compilation of Data from Other Sources	9.1 Groundwater Monitoring 9.2 Identification and Description of Data Gaps
10. Implementation Plan	10. Implementation Plan
10.1 Approach for Implementation 10.2 Annual Report 10.3 Compliance with SGMA	10.1 Projects and Management Actions 10.2 Funding Alternative Plan Implementation 10.3 Reporting
References	References
Appendices	Appendices
A. GWMP Preparation and Adoption Resolutions B. Additional Information Regarding Water Quality and Land Use Planning Agencies C. Draft Hydrogeological Cross Sections for the Tahoe Valley South Basin D. Tahoe Valley South Basin Groundwater Monitoring Plan and Protocols E. Stakeholder Advisory Group Meeting Documentation F. Preliminary Groundwater-Related Agency Programs Table G. STPUD Groundwater Ordinance No. 558-14	A. Authorizing Resolutions B. District Organization Chart C. Alternative Plan Functional Equivalency Analysis D. Public Outreach and Engagement Materials E. Groundwater Management Ordinances F. Subsurface Sections G. Assessment of Groundwater Dependent Ecosystems H. Surveys of Private Well Owners I. South Tahoe Groundwater Model J. TVS Subbasin Water Budget Tables K. Groundwater Level Elevation Monitoring Plan L. TVS Subbasin Hydrographs (WY 2000 – WY 2020) M. 2021 Implementation Plan N. Summary of Comments and Responses

SECTION 2: TAHOE VALLEY SOUTH SUBBASIN

The Tahoe Valley South Subbasin (6-005.01) is part of the larger Tahoe Valley Groundwater Basin (6-005), which is located within the Lake Tahoe Hydrologic Basin and incorporates the sediment-filled basins bordering Lake Tahoe. The Tahoe Valley Groundwater Basin is subdivided into three subbasins: Tahoe North (6-005.03), Tahoe West (6-005.02), and Tahoe South (6-005.01) (Figure 1-1). Of these three subbasins, the Tahoe Valley South Subbasin (TVS Subbasin) is the largest and most productive. This subbasin is about 150 miles east of the San Francisco Bay Area and about 90 miles east of Sacramento.

2.1 Delineation

The TVS Subbasin underlies an area of approximately 23 square miles in El Dorado County, California (Figure 2-1). Elevations range from 6,223 feet at lake level rising to above 6,500 feet to the south along the mountain front (DWR, 2003). Portions of seven Priority Watersheds defined by the Tahoe Regional Planning Agency (TRPA) overlie the TVS Subbasin, the largest of which include the Upper Truckee River watershed. The Upper Truckee River flows north across the entire length of the basin and drains into Lake Tahoe through the Upper Truckee Marsh. The Upper Truckee River is joined by Grass Lake and Big Meadow Creeks along the southern extent of its course, Angora Creek centrally, and Trout Creek near to Lake Tahoe.

2.1.1 Basin Boundaries

The TVS Subbasin is a roughly triangular area that is bounded on the southwest by the Sierra Nevada, on the southeast by the Carson Range, and on the north by the southern shore of Lake Tahoe. The TVS Subbasin generally conforms to the valleys of the Upper Truckee River and Trout Creek. The TVS Subbasin does not share a boundary with any other basin or subbasin identified in California's Groundwater (Bulletin 118). The City of South Lake Tahoe overlies the northern portion of the TVS Subbasin. The southern boundary extends about 3 miles south of the town of Meyers. The northeast boundary of the TVS Subbasin is defined by the California-Nevada state line; however, a small portion of the physical groundwater basin extends beyond the state line into Nevada as shown on Figure 2-1. The Nevada portion of this subbasin is not considered within the scope of the Alternative Plan.

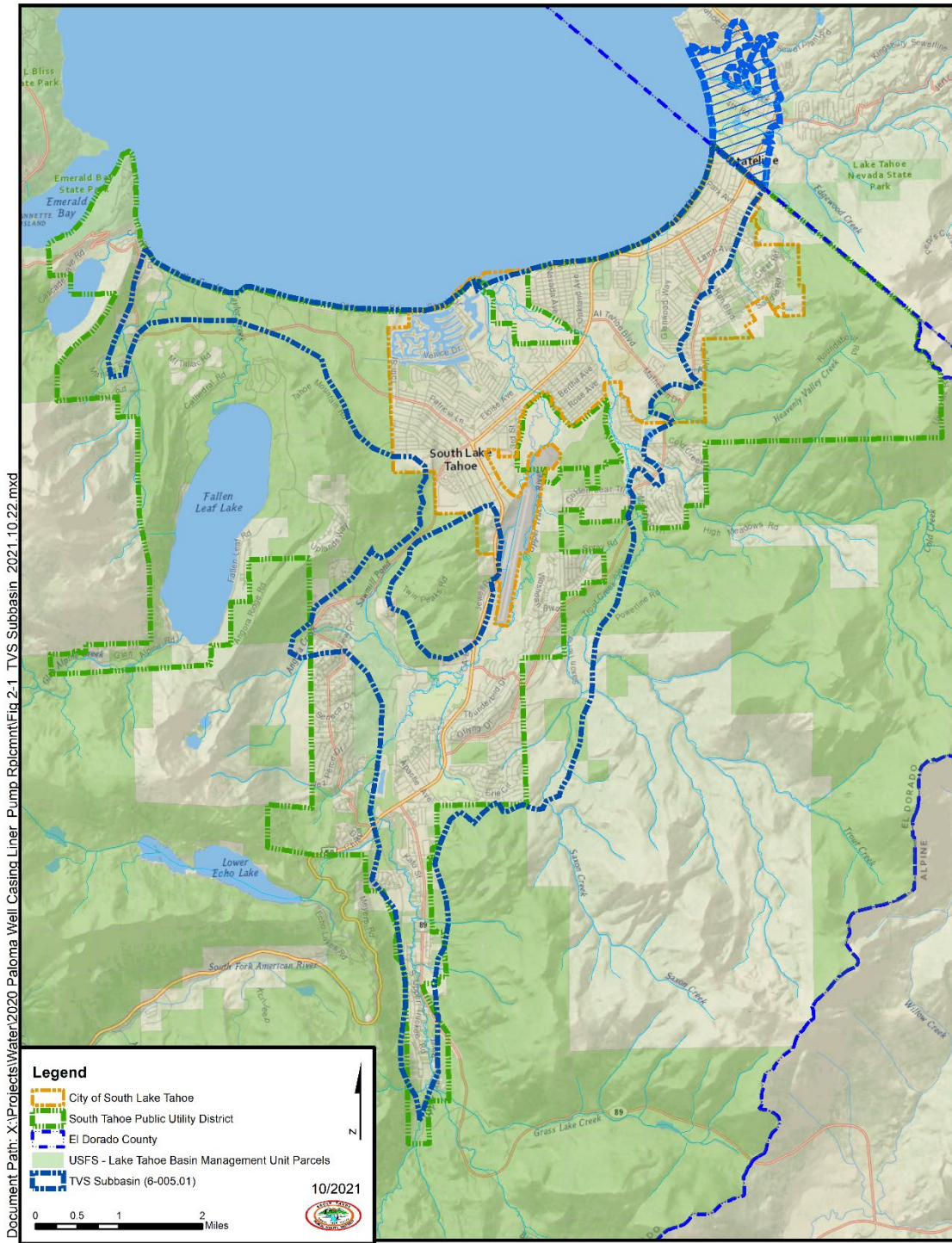


Figure 2-1. Tahoe Valley South Subbasin (6-005.01). The Nevada portion of this subbasin is not considered within the scope of this Alternative Plan.

2.1.2

Geographic Sub-Areas

For ease of description, the TVS Subbasin is subdivided into geographically based subareas: Christmas Valley, Meyers, Angora, South Lake Tahoe, Tahoe Keys and Bijou. The locations of these subareas are shown in Figure 2-2. These subareas are also used to name water-bearing zones recognized within the basin fill aquifer (Section 2.5).

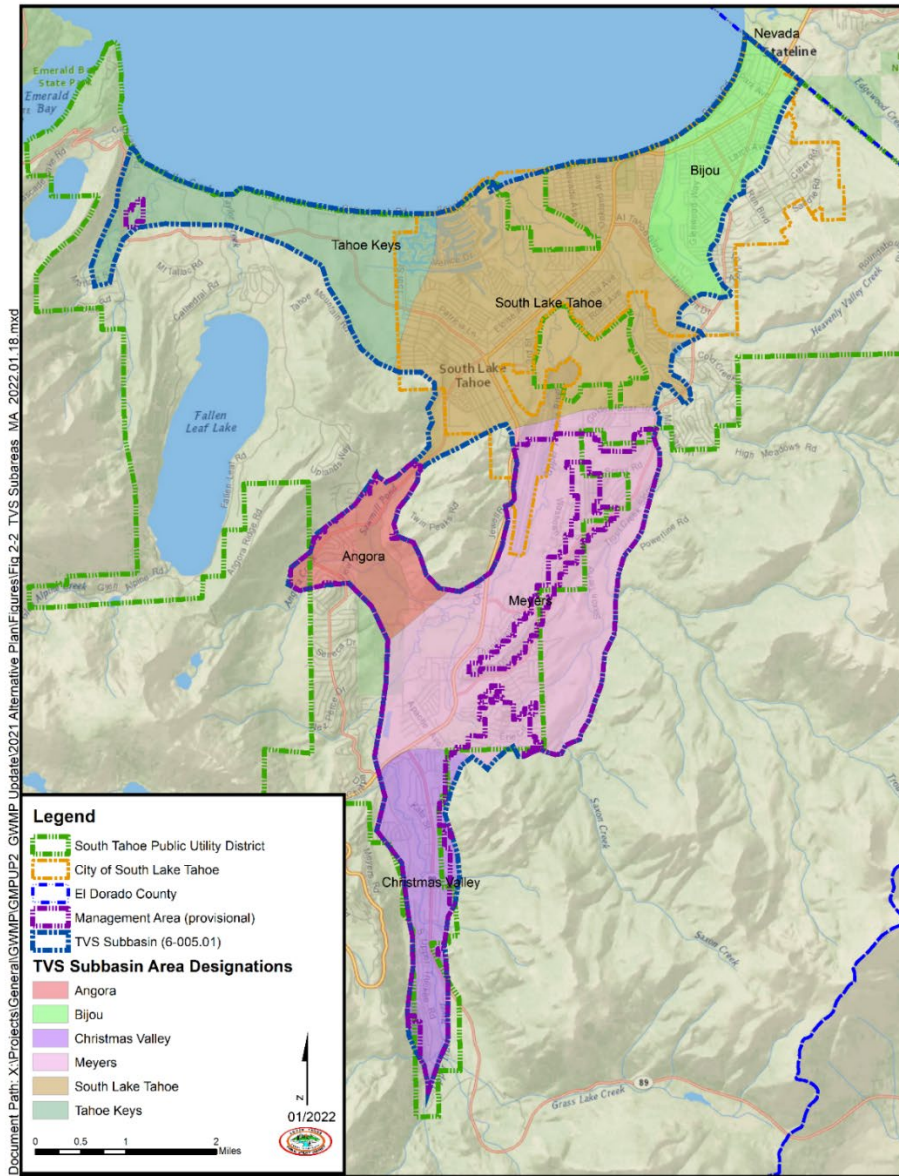


Figure 2-2. Geographic subarea designations and provisional management area proposed in the Alternative Plan.

2.1.3 **Provisional Management Area**

Under SGMA, a GSA may designate management areas within a basin for which the GSP or an Alternative identifies different minimum thresholds, measurable objectives, monitoring, or projects and management actions based on differences in water use sector, water source type, geology, aquifer characteristics, or other factors. (23 Cal. Code Regs., § 351(r).) The District has provisionally identified a potential management area generally located south of the Lake Tahoe Airport. The provisional management area is shown in Figure 2-2 and discussed in detail in Section 8.3.

2.2 **Climate**

Climate is the general prevailing weather conditions in an area over an extended period. The following section describes the climatology of the TVS Subbasin. Predicted impacts from climate change throughout the Sierra Nevada Region are discussed at the end of this section.

2.2.1 **Climatology**

In general, precipitation falls as weather systems transport moisture east from the Pacific Ocean (Crippen and Pavelka, 1970; Thodal, 1997). The Sierra Nevada forces these masses upward. As a result, precipitation is higher in the Lake Tahoe Basin than it is either in the Central Valley to the west, which lies at a low elevation, or the Carson City area to the east, which is in the rain shadow of the Sierra Nevada.

Due to the rain shadow effect, precipitation is generally greater in the western portion of the Lake Tahoe Basin as compared to the eastern portion (Figure 2-3). Frontal systems typically come from the west from November through May and account for over 85 percent of precipitation in the Lake Tahoe Basin. In some years, summertime monsoon storms from the Great Basin bring intense rainfall, especially to high elevations, primarily affecting areas to the northeast of South Lake Tahoe. Mean annual precipitation ranges from a low of 20 inches near Lake Tahoe to a high of 40 inches in the southwest. In the higher elevations annual precipitation can exceed 75 inches along the western flank near Echo Summit, 55 inches in the south, and only 35 inches along the eastern flank near Heavenly Valley Ski Resort. On average, 334,000 acre-feet per year (AFY) of precipitation falls within the hydrologic area being analyzed in this Alternative Plan.

Most annual precipitation is in the form of snow. In the Sierra Nevada, snow falls in great quantities from late November to early April. Winter snowpack in the mountains can exceed 20 feet. Figure 2-3 shows the locations of the National Resources Conservation Service (NRCS) snow telemetry stations (SNOTEL) in South Lake Tahoe. The Echo Peak station measures almost twice as much precipitation as the other three stations (Fallen Leaf, Heavenly Valley, and Hagan's Meadow) that are located at lower elevations or to the east.

The South Lake Tahoe area experiences considerable variability in annual precipitation as shown in Figure 2-4. Over the period from 1979 to 2020, annual precipitation ranged from just under 15 inches (1987) to over 67 inches (2017) at the Hagan's Meadow SNOTEL station. Although precipitation rates in the region are highly variable, the annual average precipitation

(33.8 inches) over the last ten years (2011 – 2020) is similar to the longer-term average (31.5 inches) over the period of 1979 through 2020. However, this comparison of averages is skewed by the two highest annual precipitation years in WY 2011 and WY 2017. Over the past ten years, the region has also experienced a Statewide Drought Emergency (2012–2016) and below average precipitation during the WY 2018 and WY 2020.

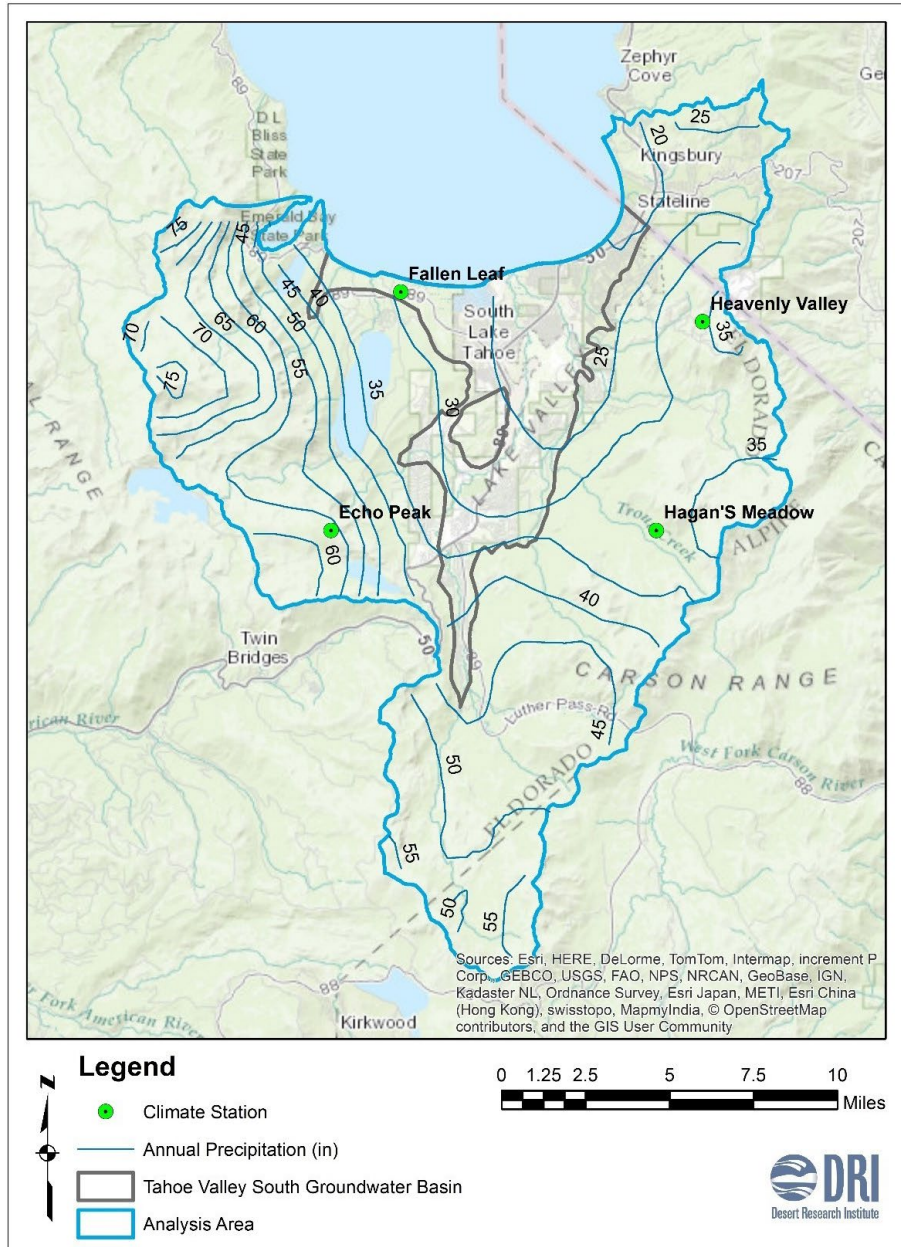


Figure 2-3. Average annual precipitation (in) isohyets and location of climate stations within the analysis area. Annual precipitation data (1981-2010) derived from PRISM Climate Group, Oregon State University, <http://prism.oregonstate.edu>, Copyright © 2016.

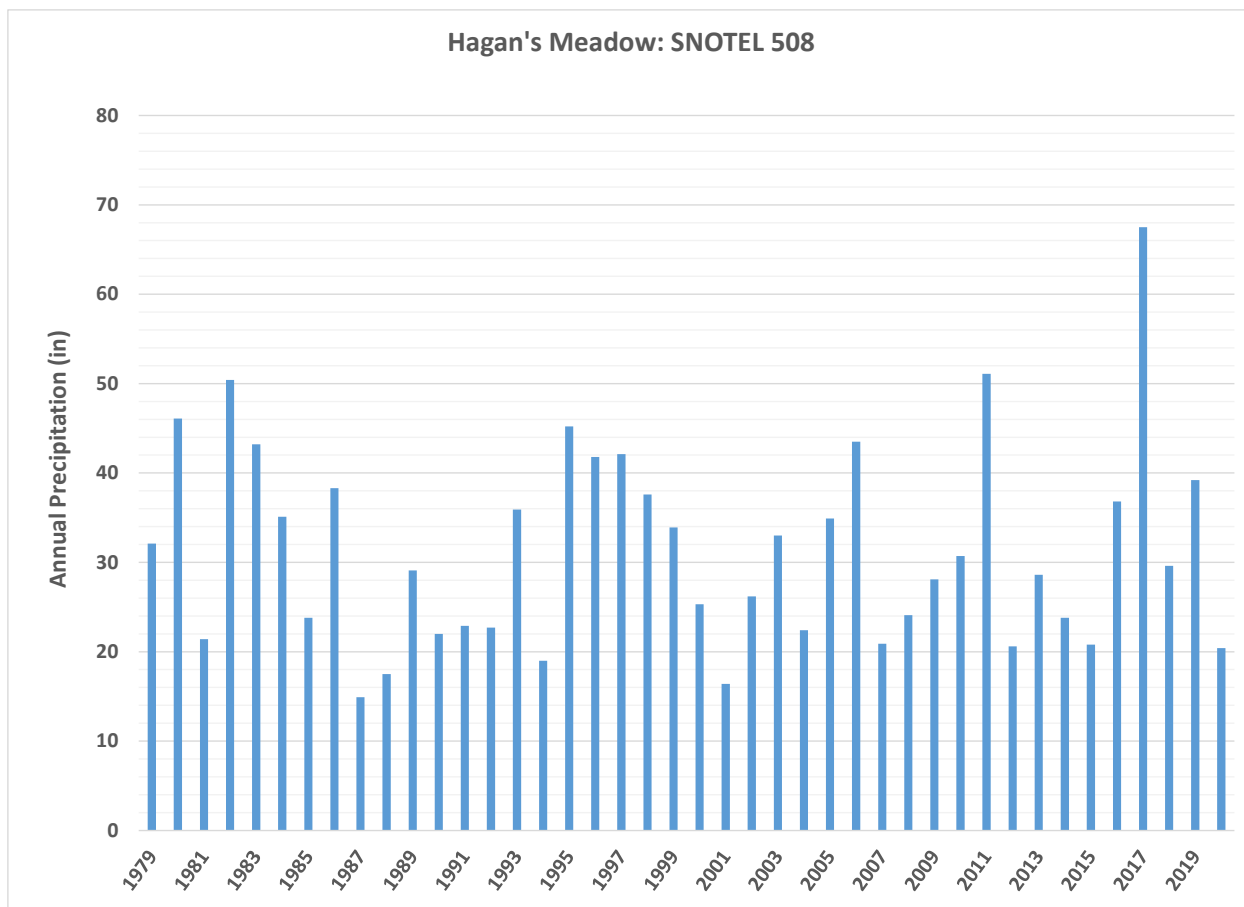


Figure 2-4. Annual water year precipitation measured at Hagan's Meadow SNOTEL Station 508.

2.2.2 Water Year Classification

Water year classification refers to the categories used to assess the amount of annual precipitation in a basin. DWR generally assigns water year type based on river flow indices or precipitation amounts. For example, in the Sacramento Valley, the SWRCB developed five categories based on runoff forecasts and previous water year's index: (1) wet, (2) above normal, (3) below normal, (4) dry, and (5) critical (SWRCB, 1978). A description of the water year classification developed for the TVS Subbasin is presented in Section 9.1.2.1.

2.2.3 Climate Change

Recent findings show significant shifts in the timing of snowmelt and observed streamflow in several watersheds in the Sierra Nevada (Coats, 2010), and vulnerability of groundwater to changing climate in the region (Singleton and Moran, 2010). A hydrologic modeling study was conducted in a nearby Lake Tahoe watershed (Incline Creek, Third Creek, and Galena Creek) to gain insight into mechanisms behind these potential changes (Huntington and Niswonger, 2012). An integrated surface and groundwater model was used to simulate climate impacts on surface water/groundwater interactions using projections of temperature and precipitation from 2010 to 2100. The model also evaluates the interplay between snowmelt

timing and streamflow, groundwater recharge, storage, groundwater discharge, and evapotranspiration.

Global Climate Models (GCMs) consistently indicate that increased carbon dioxide concentrations will lead to temperature increases within the study area of 2°C (3.6°F) – 4°C (7.2°F) from 2010 to 2100 relative to the base period of 1950 through 2010 (Christensen et al., 2007). The temperature increases predicted by any individual model are highly dependent on the carbon dioxide emission scenario used to drive the model, which relies on global assumptions of population growth and future reliance on fossil fuels.

The climate models do not agree on expected changes in precipitation. For one of the most aggressive greenhouse gas emissions scenarios (scenario A2: 4°C or 7.2°F increase in temperature by 2100), four GCMs predict a steady decrease in annual precipitation, while the other two predict a steady increase in precipitation. Predicted declines for four of the models are approximately 10 percent by 2100. The Geophysical Fluid Dynamics Laboratory (GFDL) Climate Model Version 2.1 model predicts the largest declines in precipitation on the order of 20 percent by the end of this century. Because of the large uncertainty in precipitation predictions, impacts to total groundwater recharge are difficult to predict.

Though changes in precipitation magnitude are highly uncertain, all models agree that the snowpack will decline significantly in the future due to precipitation falling mostly as rain instead of snow (Huntington and Niswonger, 2012). This result is seen clearly in Figure 2-5 which shows the predicted changes in various hydrologic variables for the emissions scenario A2. According to this scenario, the snow-water content, which is a measure of the amount of water contained within the snowpack, decreases by a factor of five between 2010 and 2100. Additionally, increasing temperatures will result in significant timing shifts of hydrologic response. In particular, the snowpack will begin to melt earlier and earlier, which will cause peak runoff to occur about six weeks earlier in 2100 than it did in 2010. The earlier runoff cascades through the hydrologic system and impacts the timing of all other important hydrologic processes, including groundwater recharge, which is expected to peak about one month earlier in 2100 as compared to 2010.

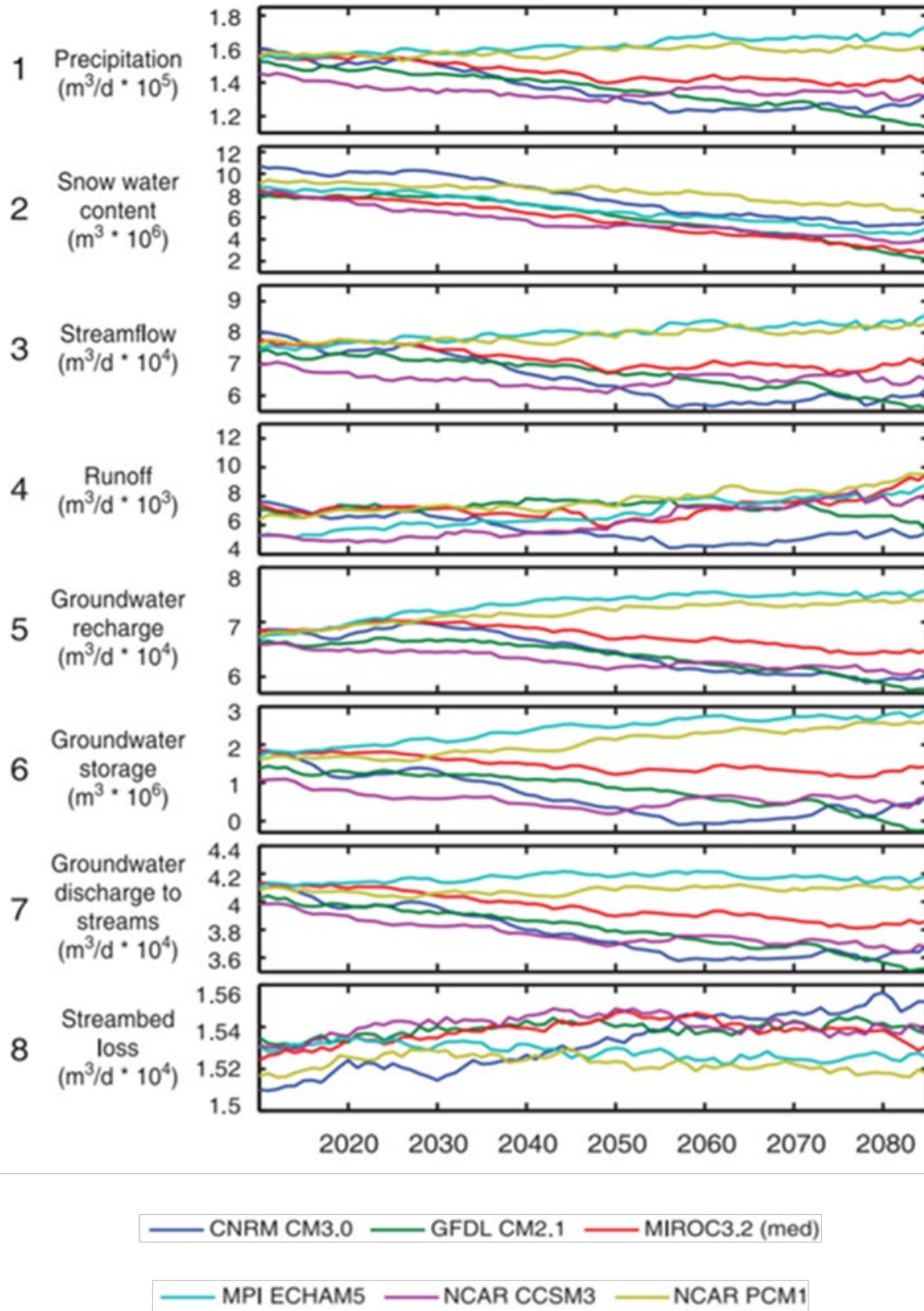


Figure 2-5. Time series of simulated yearly average hydrologic variables for Incline Creek, Third Creek, and Galena Creek watersheds from Huntington and Niswonger (2012). Simulated hydrologic variables for different GCMs (colored lines) and for greenhouse gas emission scenarios A2.

2.3

Soils

The TVS Subbasin consists of three soil types at the order level: alfisols, entisols, and inceptisols (NRCS, 2012). The spatial distribution of soil types is shown in Figure 2-6. Alfisols develop from weathering processes that leach clay minerals out of the surface layer and into the subsoil. These soil types tend to form under forest canopies and provide relatively high fertility to vegetation. Entisols are weakly-developed soils that are unaltered from their parent material. Inceptisols are better developed than entisols, but their lack of accumulated clays allows them to drain more freely than entisols. These soil types are found along riparian corridors of Trout Creek and the Upper Truckee River.

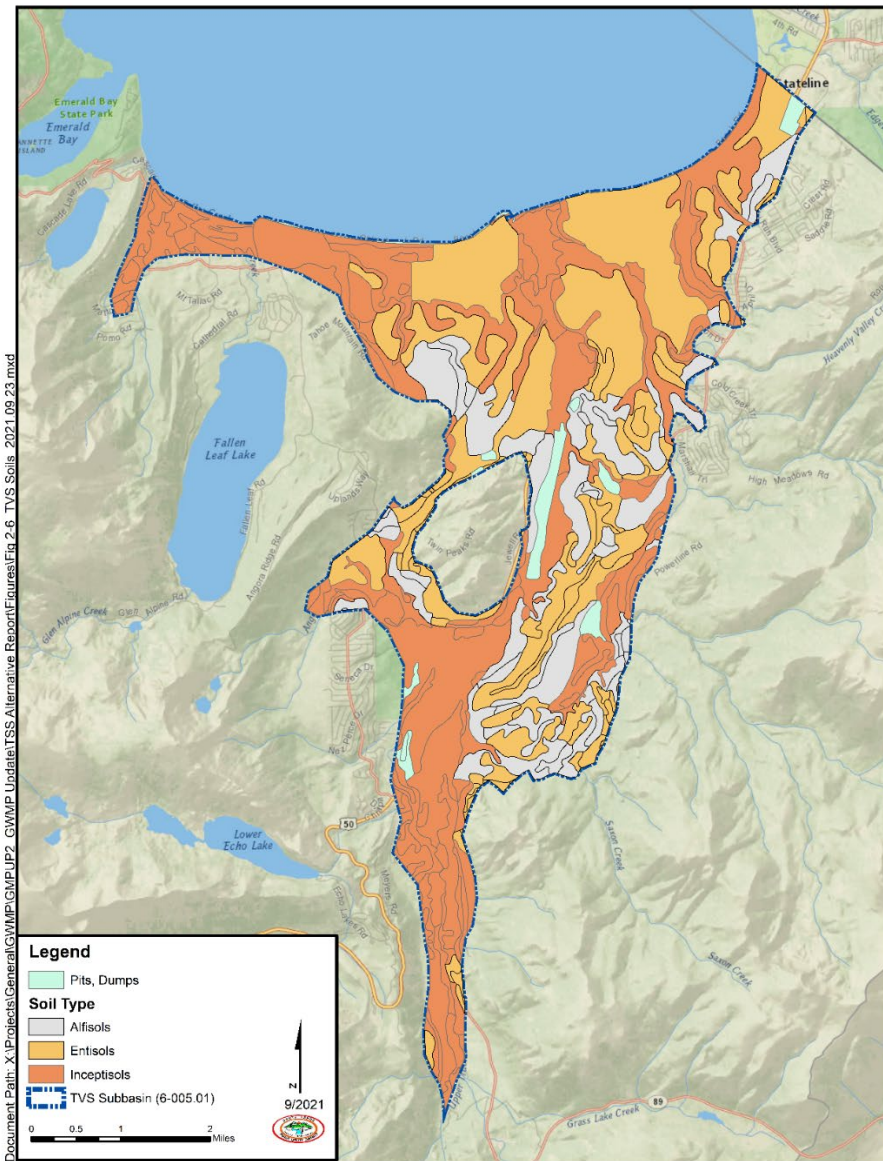


Figure 2-6. Soil types at the order level within the TVS Subbasin (NRCS, 2021).

The regional geology for the Lake Tahoe Basin can be generalized as surrounding mountains composed mainly of intrusive granitic rocks and metamorphic rocks; and valleys with basin-fill composed of glacial and alluvial deposits. The basin-fill deposits have been reworked by glacial activity, alluvial and fluvial processes, and by Lake Tahoe in response to fluctuations in lake levels. Figure 2-7 shows the distribution of these deposits in the southern Lake Tahoe area (Plume et al, 2009).

Lake Tahoe rests within a fault-bounded structural basin, or graben, bordered on the west by the Sierra Nevada and on the east by the Carson Range. The Tahoe graben formed about two to three million years ago, leading to the large elevation difference between the Lake and the surrounding mountains (U.S. Army Corps of Engineers, 2003). The Tahoe-Sierra Frontal Fault Zone defines the west side of the Tahoe graben and is described as a quaternary east-dipping normal fault, with east-side-down displacements (USGS, 2006). This western bounding fault zone is reflected as a northwest-southeast lineament along the mountain front of the Crystal Range from Emerald Bay toward Meyers, California (Figure 2-7). There are limited groundwater level and aquifer test data in the higher elevations where this fault is mapped so its effect on groundwater flow is not fully known. The East Tahoe Fault is inferred to form the eastern side of the Tahoe graben and is poorly characterized as a Quaternary west- or east-dipping normal fault (USGS, 2006). The bounding fault strikes north-south along the mountain front of the Carson Range, from Stateline toward Meyers. The Tahoe Valley Fault Zone is a poorly characterized Quaternary fault that strikes southwest-northeast in the TVS Subbasin (USGS, 2006). There is limited evidence that this feature acts as a barrier to groundwater flow.

Glaciation greatly modified the landscape in the Lake Tahoe Basin. At least four (4) periods of major glaciation and one minor glacial advance took place during the Pleistocene Epoch (about 2 million to about 10,000 years). Large valley glaciers formed in most of the canyons around the lake, except along the eastern shore where glaciation was limited to the northern sides of the highest peaks (Burnett, 1971). One major result of the glaciations was the deposition of large quantities of sediment in the form of till and outwash deposits, as well as discharge of considerable quantities of finer sediment into the lake. The deposits in Lake Tahoe and adjoining valleys can be greater than 1,000 feet thick in places (Hyne et al., 1972). Much of the glacially derived sediment is from decomposed granite that had been scoured away and reworked from the granitic slopes of the western and southern mountains.

The current outlet from Lake Tahoe, and the present-day Truckee River system, was formed between 10,000 - 75,000 years ago. Earlier, the elevation of the outlet was affected by the formation of ice dams. As a result of the formation of an ice dam at the natural outlet, the lake level during these events is believed to have risen to as high as 6,800 feet (Birkeland, 1962). The ice dam is believed to have been breached several times, resulting in periodic, catastrophic flooding down the valley and periodic lowering of the lake level. During the interglacial periods, the lake level would have been similar to today's level. Lava flows at the outlet of Lake Tahoe provide a minimum threshold for lake elevation at about 6,220 feet.

Within the TVS Subbasin, the geology consists of glacial till, outwash and alluvial deposits overlying the bedrock units (Figure 2-7). Basin-fill deposits range in thickness from less

than 100 feet along the basin margins to over 1,000 feet thick in the deeper portions of the TVS Subbasin. Gravity survey and well drilling information suggests that at least three areas of thick sediments occur within the TVS Subbasin. The largest of these underlies CSLT between the Tahoe Keys development and Bijou Creek. A second is located near the south shore of Lake Tahoe, north of Fallen Leaf Lake, underlying the present drainages of Baldwin and Taylor Creeks. A third underlies the Meyers area south of Twin Peaks. The areas where the basin-fill deposits are on the order of 600 feet to 1,000 feet thick generally correlate with the areas of the highest groundwater production.

Glacial deposits were formed as valley glaciers advanced north toward Lake Tahoe through the Upper Truckee River Valley during at least four episodes of glaciation during the Quaternary. As these glaciers advanced, they formed ground, lateral, and terminal moraines composed of glacial till. Glacial till in the TVS Subbasin consists of variable mixtures of silt and sand with cobble to boulders deposits. The glacial till is mounded to form moraines composed of poorly sorted and massive deposits consisting of variable mixtures of silt and sand with gravel to boulder size material. The Angora Ridge, located along the western side of the TVS Subbasin near the Angora subarea, is one of the most prominent glacial landforms within the TVS Subbasin.

Glacial outwash was formed as glaciers receded and meltwaters flowed downstream north toward Lake Tahoe. Meltwaters dropped their sediment loads along stream channels and in broad coalescing flood fans forming outwash plains. The channel and fan deposits are composed of layered beds of well sorted gravel, sand, and silt size material. Where glacial streams deposited sediment directly into Lake Tahoe, broad deltas were formed of interbedded sand with silt and clay. These delta sequences grade laterally with:

- lakeshore deposits consisting of moderately well sorted sand and gravel deposits with relatively high permeability.
- inter-fan and marsh deposits consisting of fine-grained sand, silt, and clay; and
- lake deposits, consisting of silt and clay.

Alluvium are primarily floodplain deposits composed of stratified silt and sand, and channel deposits consisting of stratified sand and gravel with locally interbedded lacustrine deposits composed of bedded silt and clay (Harrill, 1977). The alluvium consists mostly of decomposed granite from surrounding hillslopes and reworked glacial deposits and ranges from 10 – 20 feet thick near the basin margin and more than 500 feet thick near the south shore of Lake Tahoe.

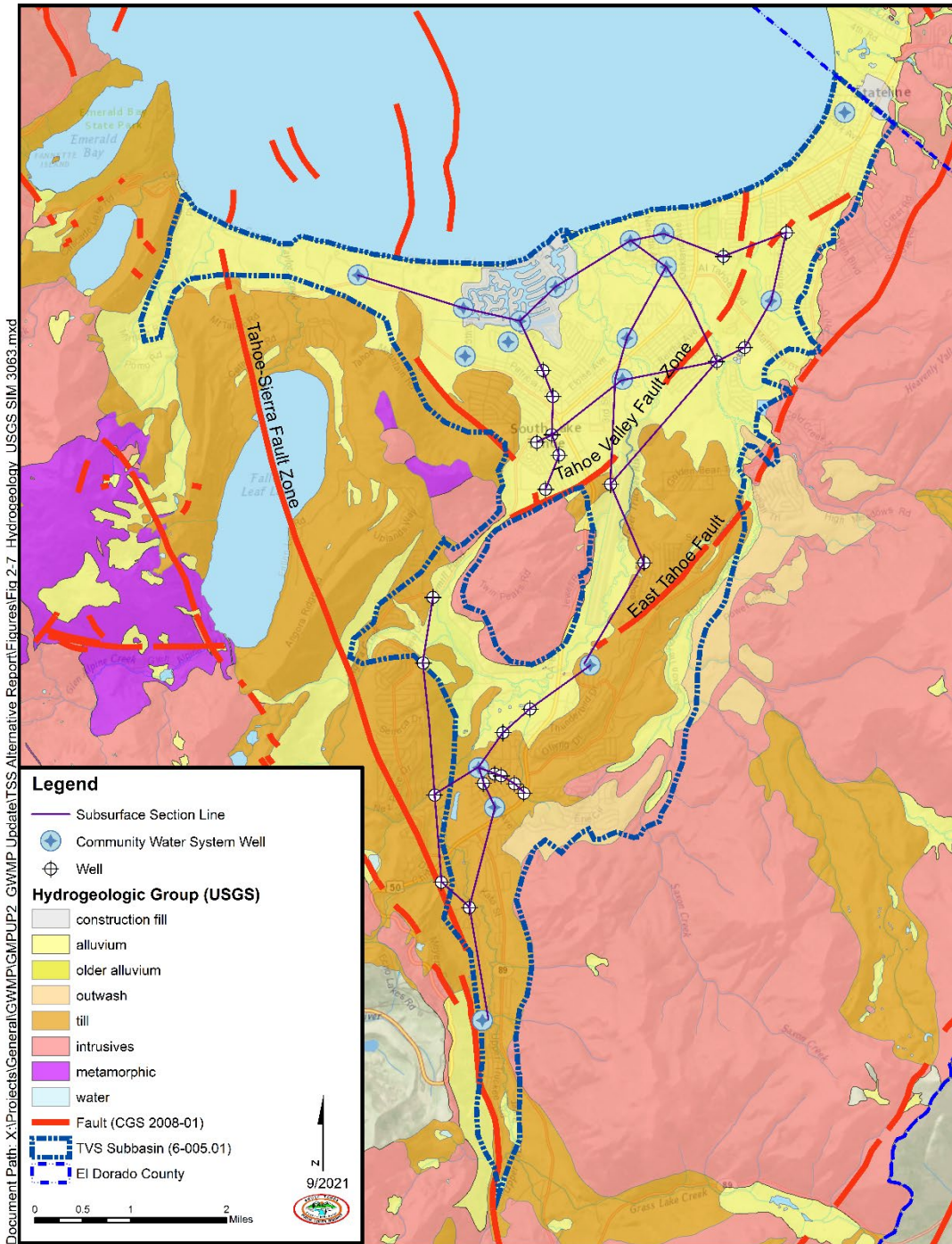


Figure 2-7. Hydrogeologic map of the South Lake Tahoe area derived from USGS Scientific Investigations Map 3063 (Plume et al., 2009). Mapped faults are from the Geologic Map of the Lake Tahoe Basin (CGS CD 2008-01) (Saucedo et al, 2008). Lines of section shown are for subsurface cross-sections included in Appendix F.

Two representative cross sections (Figure 2-8 and Figure 2-9) depict the interlayered character of the basin-fill within the TVS Subbasin. In general, the basin-fill is composed of coarse-grained glacial outwash, fluvial, and deltaic deposits, and fine-grained lacustrine sediment. Figure 2-8 shows a north-south cross section extending north of Meyers across the area of thick basin fill to the south shore of Lake Tahoe. Figure 2-9 shows an east-west cross section along the south shore of Lake Tahoe from near Camp Richardson on the west (Valhalla Well) to near Bijou Creek on the east (Bijou School Well).

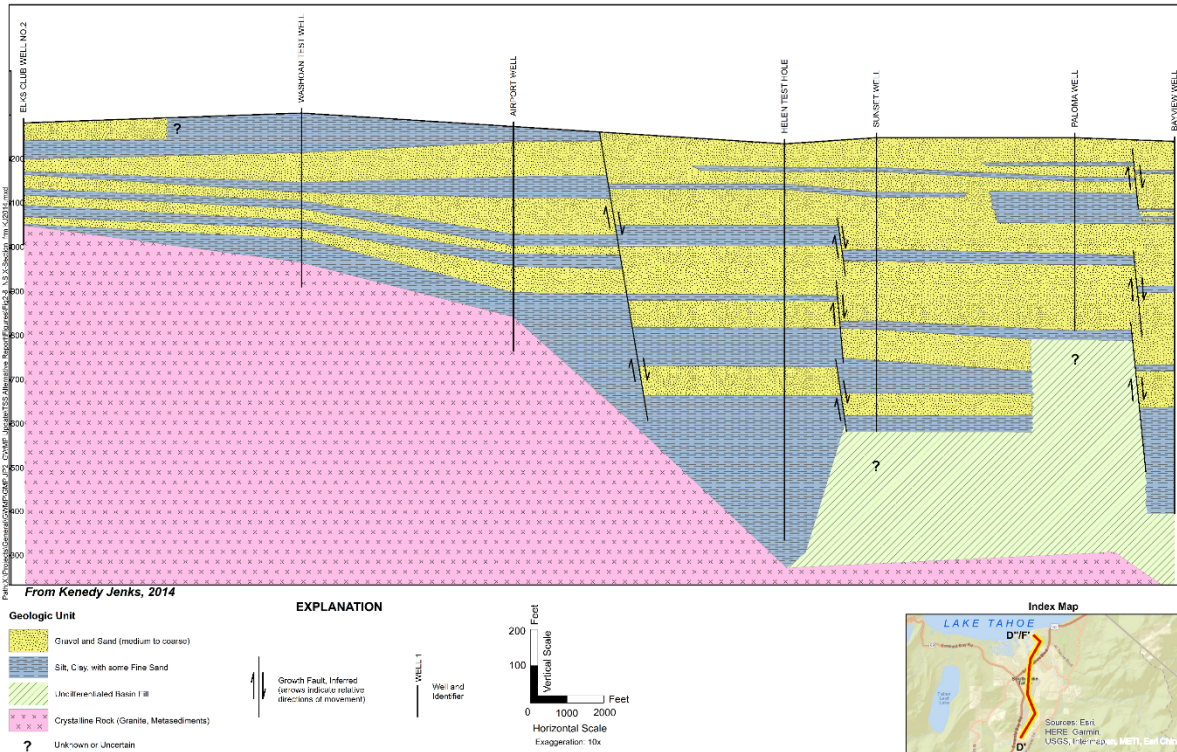


Figure 2-8. Geologic cross section D' – D''/F' trending south to north across the north half of the TVS Subbasin (from Kennedy Jenks, 2014).

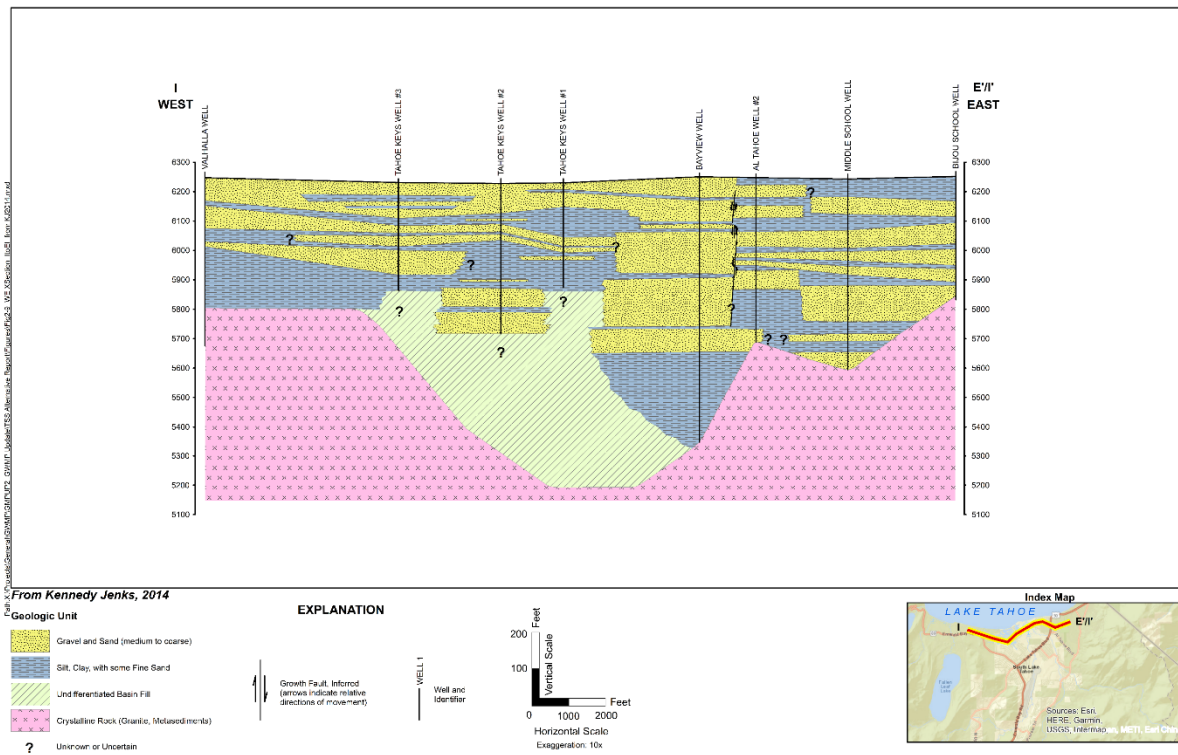


Figure 2-9. Geologic cross section I' – E'/I' trending west to east near the north margin of the TVS Subbasin (from Kennedy Jenks, 2014).

2.5 TVS Subbasin Aquifer

Most water wells drilled in the TVS Subbasin are completed in basin-fill deposits that generally consist of unconsolidated glacial, lake and stream sediments. These sedimentary deposits fill the lower reaches of the canyons that drain toward Lake Tahoe and underlie the relatively flat lying valley floors. These deposits can be over 1,000 feet thick in the deeper portions of the basin, but thin toward the basin margins where they are underlain by shallow bedrock.

Permeability of these sediments differs considerably, both spatially within each unit and between the different units. In general, glacial outwash and fluvial deposits are highly permeable, while glacial moraine and lacustrine deposits tend to have moderate and low permeability, respectively (Thodal, 1997; Fogg et al., 2007). Fogg et al. (2007) used lithologic and geophysical logs to construct a series of 10 regional cross-sections through the TVS Subbasin (Appendix F). They identified at least 26 water-bearing zones within the basin-fill aquifer using the logs and interpreted correlations to divide the basin-fill into multiple layers, representing regionally correlated units of high and low permeability. Units of relatively high permeability typically correspond to coarse-grained glacial outwash, fluvial and deltaic deposits forming the basin-fill aquifer. The laterally continuous fine-grained lacustrine (lakebed) deposits form local confining layers or aquitards that affect groundwater flow between these higher permeability deposits.

During 2019 and 2020, lithologic interpretation of shallow and deep boring logs collected during high density drilling of the basin-fill in the South Lake Tahoe subarea indicate that the lateral continuity of interlayered confining layers may be more limited than depicted in Figure 2-9(AECOM, 2021). As the lateral extent of confining layers are reduced the potential for vertical movement of groundwater within the basin-fill increases. This also increases the susceptibility of deeper water-bearing zones to contamination.

The relatively high permeability glacial outwash and delta deposits form excellent groundwater aquifers. The most transmissive of these aquifers has been found in the South Lake Tahoe subarea, primarily beneath the present-day Truckee Marsh. Both the inter-fan, marsh and lake deposits are fine-grained and have relatively low permeability. These fine-grained deposits form at least four locally extensive aquitards that separate the TVS Subbasin into at least five distinct water-bearing zones (WBZs). Where the sediment types are layered, the basin-fill aquifer can be characterized as different WBZs. Where the fine-grained confining layers are more discontinuous, the WBZs act as leaky or semi-confined aquifers. The shallowest intervals occur in the upper 200 feet. These WBZs are unconfined to semi-confined depending on the continuity and relative permeability of the overlying fine-grained layers. These shallow WBZs interact most with surface waters.

Figure 2-10 shows a conceptual hydrogeological cross section across the northern portion of the TVS Subbasin to illustrate these WBZs. Up to five of these zones have been identified as being practical for groundwater management (Bergsohn, 2011). The different WBZ designations are informal and are based on geographic subarea in which they are found and the stratigraphic order in which they occur from deep to shallow depth (1 = lowermost zone; 5 = uppermost zone). WBZs in the Christmas Valley subarea are designated CVZ1 through CVZ5. WBZs in the Meyers subarea are designated MZ1 through MZ5. WBZs in the Angora subarea are designated AZ1 and AZ2. WBZs in the South Lake Tahoe are designated SLTZ1 through SLTZ5. WBZs in the Tahoe Keys subarea are designated TKZ1 through TKZ5. WBZs in the Bijou subarea are designated BZ1 through BZ5.

The deepest zone (WBZ1) occurs in the deepest portions of the basin, generally at depths below 600 feet, and may act as a confined aquifer and may locally show artesian conditions. The middle two zones (WBZ2 and WBZ3) represent the interval at depths between 200 to 600 feet and the shallowest two zones (WBZ4 and WBZ5) represent depths up to 200 feet.

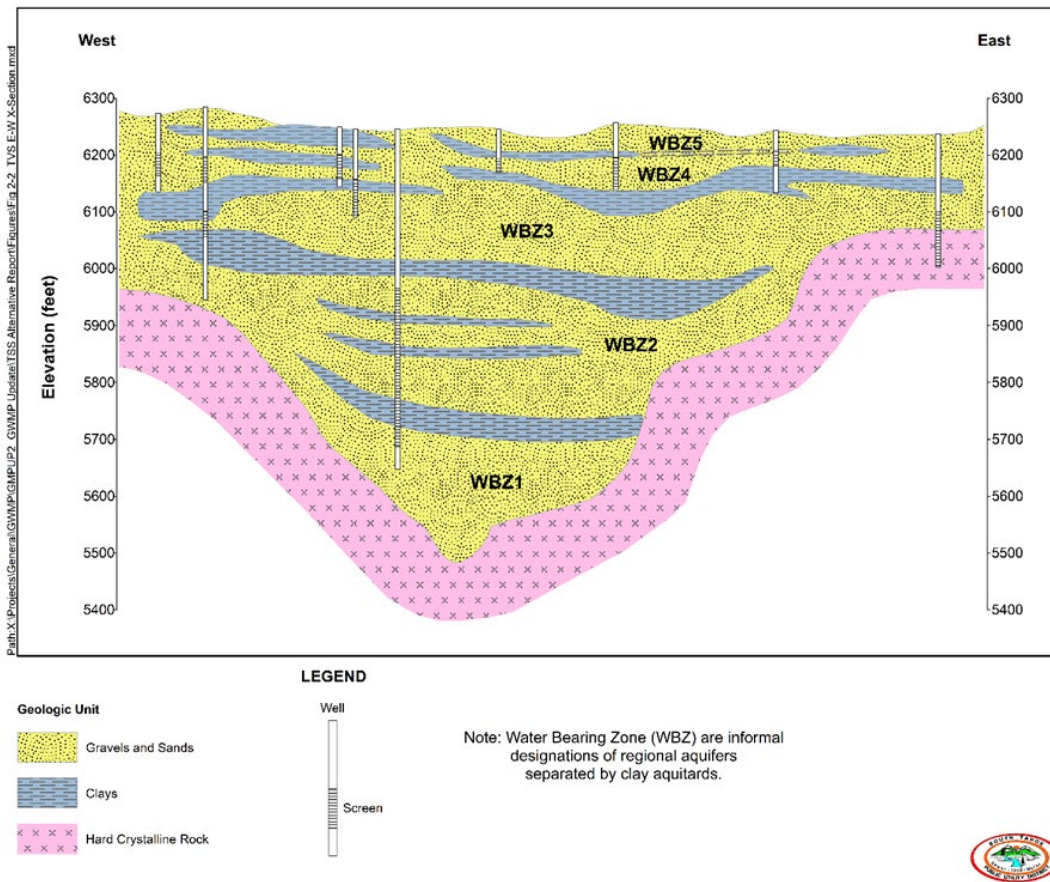


Figure 2-10. Conceptual hydrogeologic section trending east -west near the north margin of the TVS Subbasin.

2.6 Surface Water Features

Surface water features within the South Lake Tahoe area include 11 watersheds that feed streams and numerous lakes. Alongside many of these surface features are delineated stream environment zones (SEZs), defined as areas “that owe their biological and physical characteristics to the presence of surface or ground water.” The SEZs delineated by the TRPA comprise not only streams, but also meadows, marshes, wetlands, and other riparian habitats. These established SEZs are used as a proxy for Groundwater Dependent Ecosystems (GDE) (Section 2.6.3).

2.6.1 Watersheds

TRPA has defined 11 priority watersheds within the South Lake Tahoe area; of these portions of seven watersheds fall within the TVS Subbasin (Figure 2-11). These include Tallac Creek, Taylor Creek, Camp Richardson, Upper Truckee River, Trout Creek, Bijou Creek, and Bijou Park Watershed. The total watershed area for the South Lake Tahoe area is 99,900 acres, all of which flow into Lake Tahoe. The area for the TVS Subbasin is 14,800 acres.

There are seven USGS stream gages within the southern Lake Tahoe area (Figure 2-11). For the Taylor Creek Watershed, the Taylor Creek gage (10336626) is located at the outlet of Fallen Leaf Lake and has daily discharge data available from 1968 – 1992. In the Upper Truckee River Watershed there are two gages. One gage is located at Highway 50 above Meyers, California (103366092) with a period of record from 1990 – present, and another downstream in CSLT (10336610) with data from 1971 – present. In the Trout Creek Watershed there are three (3) gages. The upstream gage is at U.S. Forest Service Road 12N01 (10336770) with data from 1990 – 2011. Downstream there is a gage at Pioneer Trail (10336775) with data from 1997 – 2003 and again from 2007 – 2014. Further downstream the third gage is located near Tahoe Valley (10336780) with discharge data from 1960 – present. On the Nevada side of the analysis area, a gage exists on Edgewood Creek at Stateline, Nevada (10336760) with data from 1992 – 2012.

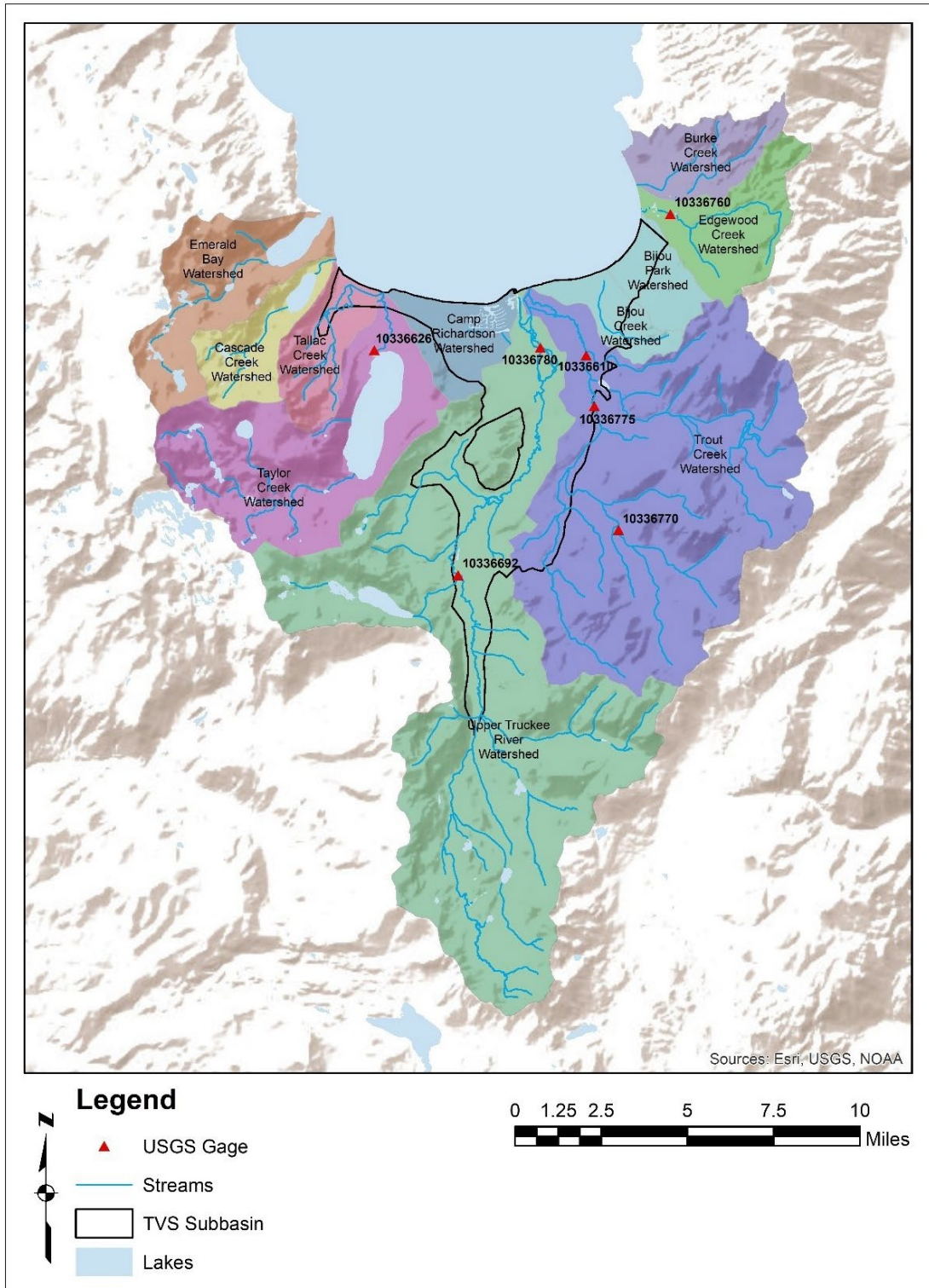


Figure 2-11. Watersheds, lakes, streams, and USGS gaging stations within the South Lake Tahoe area.

Discharge data from the downstream gages at Edgewood Creek (10336760), Trout Creek (10336780) and the Upper Truckee River (10336610) were used to develop a regression between watershed area and average annual runoff (Figure 2-12). The regression equation was used to estimate average annual runoff for the eight remaining watersheds in the southern Lake Tahoe area (Table 2-1.). Total average annual runoff from the South Lake Tahoe watersheds to Lake Tahoe is estimated to be 124,000 AFY.

Table 2-1. Estimates of average annual runoff for eleven South Lake Tahoe watersheds either directly overlying or neighboring the TVS Subbasin.

Watershed	Area (acres)	Runoff (af)	Method
Burke Creek	3,179	2,936	Regression
Edgewood Creek	4,275	3,243	Measurements (2007-2012)
Emerald Bay	5,639	3,755	Regression
Bijou Park	1,974	2,603	Regression
Cascade Creek	3,019	2,889	Regression
Tallac Creek	2,932	2,864	Regression
Bijou Creek	1,807	2,560	Regression
Camp Richardson	2,651	2,785	Regression
Taylor Creek	11,787	6,943	Regression
Trout Creek	26,428	25,361	Measurements (1960-2016)
Upper Truckee	36,216	68,400	Measurements (2007-2016)
Total:	99,907	124,339	

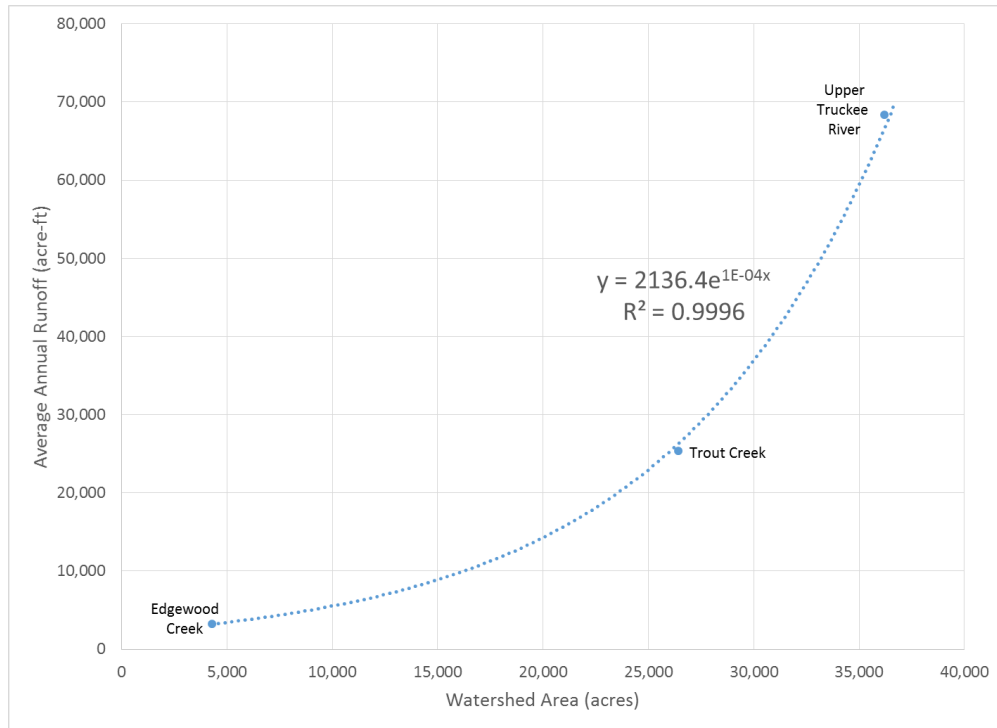


Figure 2-12. Relationship between watershed area and average annual runoff for Edgewood Creek, Trout Creek, and the Upper Truckee River watersheds.

2.6.2 Lakes

Lake Tahoe is the principal hydrologic feature covering approximately 192 square miles in total area within the Lake Tahoe Hydrologic Basin. In addition to Lake Tahoe, there are numerous other lakes and tributary streams in the South Lake Tahoe area (Figure 2-11). Some of the larger lakes in the area include Emerald Bay, which is part of Lake Tahoe, Cascade Lake, Fallen Leaf Lake, and Echo Lake.

Over the last few decades, the water surface elevation of Lake Tahoe ranged from 6,220 to 6,229 feet above mean sea level (AMSL), and is controlled by the Lake Tahoe Dam, which regulates discharge into the Truckee River near Tahoe City. The natural sill (i.e., rim) of the basin is at 6,223 feet AMSL and once lake level drops below this elevation water is unable to be released to the Truckee River. Figure 2-13 provides a hydrograph for Lake Tahoe from 1968 to 2020. During this period, the Lake elevation has fallen below the natural rim nine times in response to drought periods.

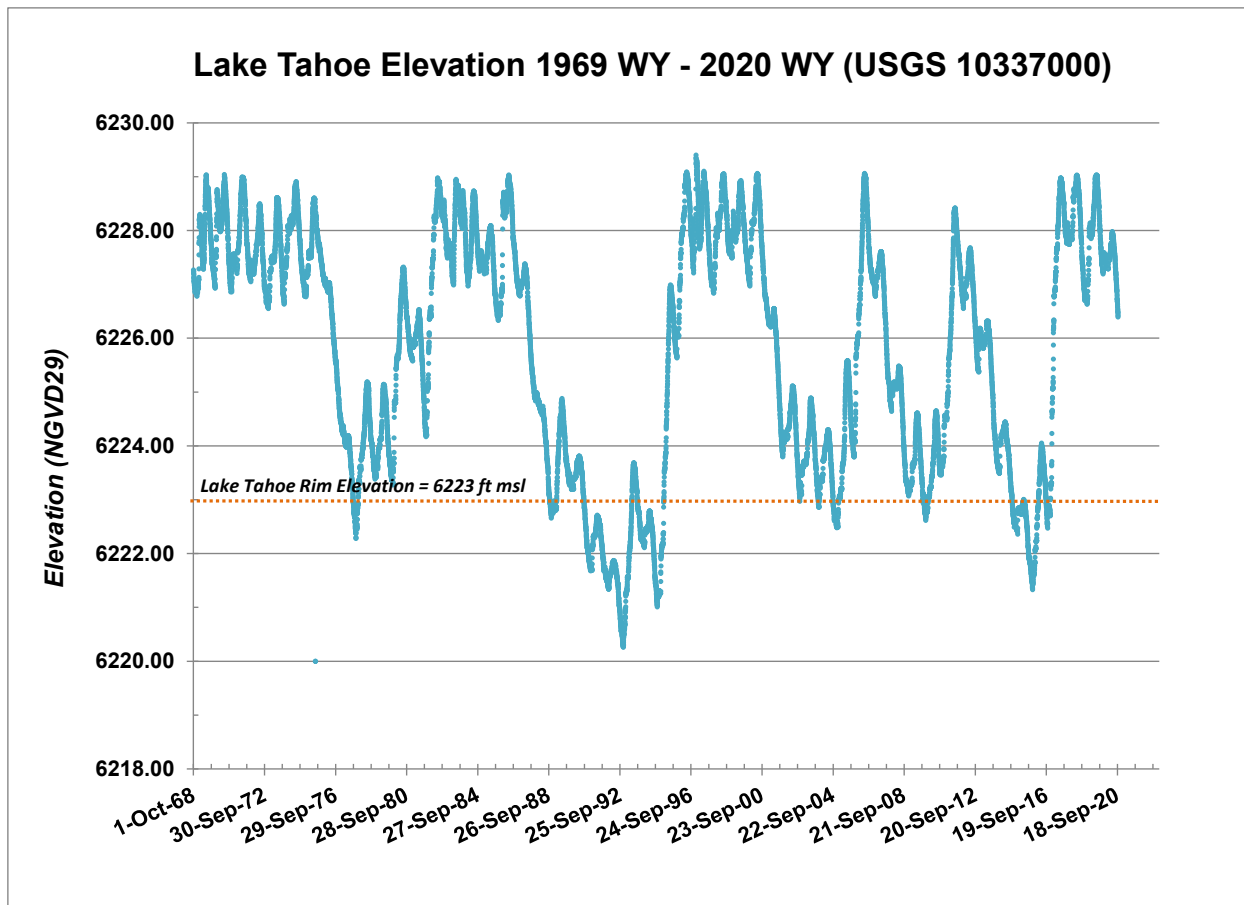


Figure 2-13. Hydrograph showing historic elevations for Lake Tahoe measured at the Tahoe City, CA gage (USGS 10337000).

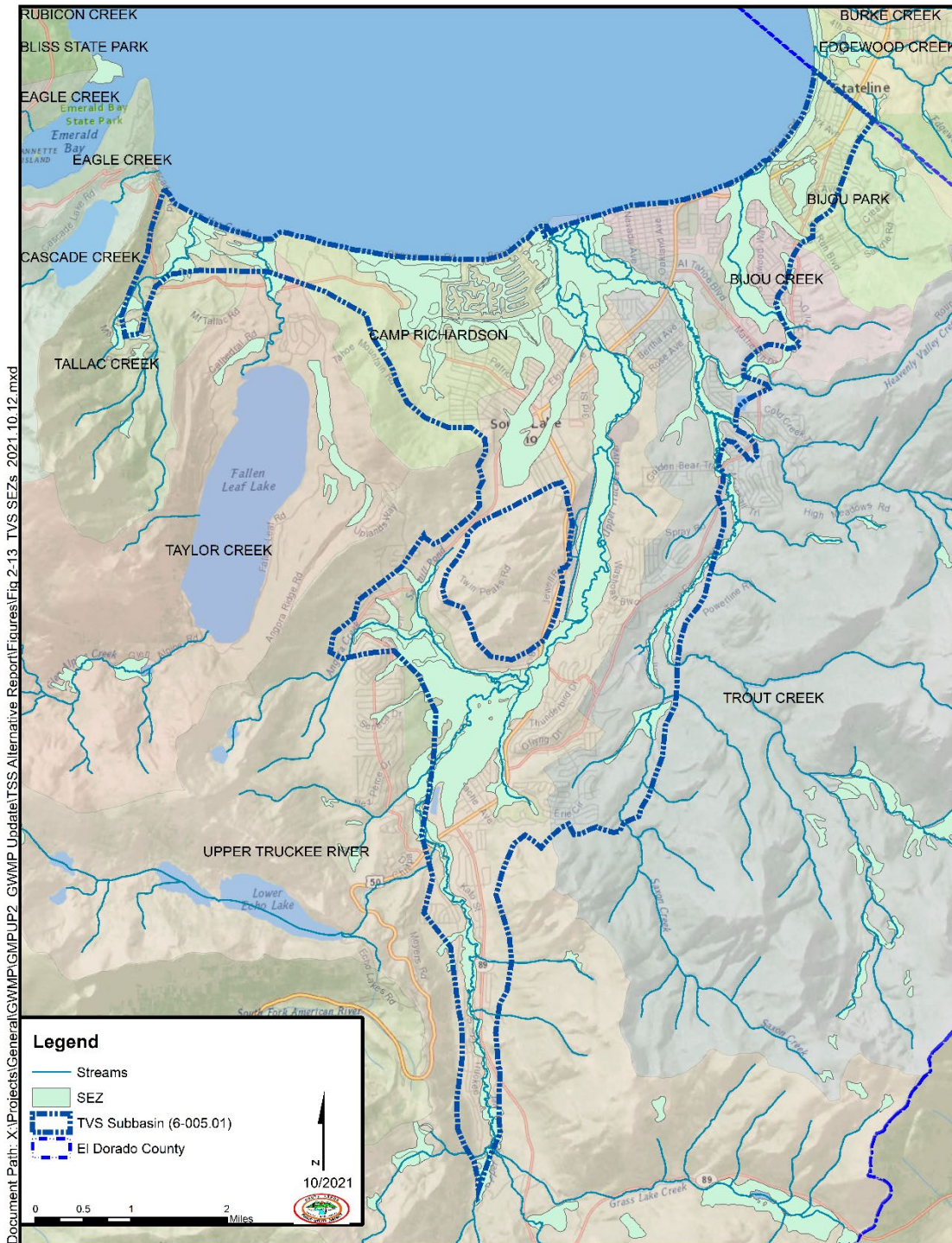
2.6.3 Groundwater Dependent Ecosystems (GDEs)

Groundwater dependent ecosystems (GDEs) are ecological communities or species that depend on groundwater emerging from aquifers or on groundwater occurring near the ground surface (23 Cal. Code Regs., § 351 (m)). GSAs are responsible for identifying GDEs within a groundwater basin. As stream environment zones (SEZs) and GDEs are both dependent on the presence of groundwater there is substantial overlap in the spatial distributions of SEZs as mapped by the TRPA and of GDEs as delineated by The Nature Conservancy in the TVS Subbasin. Because SEZ is an established term, commonly used in land planning and environmental resource management across regulatory and environmental agencies working within the TVS Subbasin, SEZ is used as a proxy for describing the spatial distribution of GDEs in the Alternative Plan.

Surface water features help to filter water and provide critical habit. The most important of these features are recognized by the TRPA as SEZs. SEZs are defined in the TRPA Code of Ordinances as an area that owes its biological and physical characteristics to the presence of surface or groundwater. This term was developed by TRPA to denote perennial, intermittent and ephemeral streams, and drainages, as well as marshes and meadows. SEZs generally possess the

characteristics of riparian or hydric (wet site) vegetation, alluvial, hydric soils, and/or the presence of surface water or near-surface groundwater at least part of the year. As shown on Figure 2-14, the SEZs in the TVS Subbasin generally occur along riparian corridors. The SEZs help protect water quality because as the surface water flows slow in these areas, natural processes of infiltration, nutrient uptake, denitrification, and sediment capture help to reduce sediment and nutrients in the surface water.

As mapped by TRPA, 130 SEZs (Figure 2-14) fall completely or partially within the South Lake Tahoe area, and 52 wholly or partially within the TVS Subbasin. Any use of the terms “groundwater dependent ecosystem” or “GDE” in the Alternative Plan will be in reference to these mapped SEZs, unless otherwise stated.



Document Path: X:\Projects\General\GWMP\GMP\UP2_GWMP_Update\TSS\Alternative_Report\Figures\Fig 2-13_TVSEZs_2021_10_12.mxd

Figure 2-14. Stream Environment Zones as mapped by the Tahoe Regional Planning Agency using land capability. Mapping is for general use only, requiring verification at the individual parcel scale.

GDEs provide numerous ecosystem services, ranging from recreation and flood mitigation to biodiversity and carbon sequestration, and provide habitat for a wide range of species, including protected species. Within the TVS Subbasin, these ecosystems primarily occur as riparian areas or meadows alongside stream channels or lakes. Lahontan cutthroat trout, federally listed as a threatened species, occur in the streams within the basin, and the adjacent riparian ecosystems support populations of endangered Sierra Nevada yellow-legged frogs. GDEs are also home to species protected by the state of California, including bald eagles, great gray owls, and Sierra Nevada red fox (Rohde et al. 2019).

Like other salmonids, Lahontan cutthroat trout are sensitive to water temperature – they begin to exhibit acute stress at temperatures greater than 72 °F (22 °C) (Rohde et al. 2019). Similarly, Sierra Nevada yellow-legged frog populations require surface water features that do not freeze during the winter (Rohde et al. 2019). Both warm summer temperatures and freezing winter temperatures can be mitigated by baseflow to streams and meadows. Groundwater impacts that may affect the Lahontan cutthroat trout and Sierra Nevada yellow-legged frog populations are addressed in the thresholds for interconnected surface water. Bald eagles and great gray owls nest and feed in and around GDEs, and the Sierra Nevada red fox depends on GDEs for both its habitat and its forage range (Rohde et al. 2019). The conservation of these ecosystems also supports the conservation and recovery of these protected species.

The GDEs within the TVS Subbasin are affected not only by groundwater management practices, but also by climate change, land use changes (i.e., nearby development) and disturbances such as floods and fires. The status of these systems is monitored by TRPA using a range of metrics that include both physical (e.g., headcuts, incision, gullies) and biological (e.g., vegetation vigor, conifer encroachment, biotic integrity) indicators (TRPA 2020). To avoid duplicating those monitoring efforts, this plan focuses on the groundwater levels and connections to surface waters as indicators of GDE impacts. Appendix G details an assessment of the historical status of GDEs within the TVS Subbasin, as well as projections of future conditions. Over the past 30 years, groundwater levels in the 130 GDEs within the model domain have fluctuated with changes in precipitation but have generally not exhibited statistically significant trends over time. When statistically significant trends have been observed, those trends have been towards higher groundwater levels.

SECTION 3: ALTERNATIVE PLAN AREA

The following section describes the factors affecting use of the TVS Subbasin, including information regarding population, land use, groundwater uses and users and drinking water demand projections.

3.1 Population and Economy

Most of the population within the greater South Lake Tahoe area lives within the residential areas of CSLT and the adjoining unincorporated communities of the County. Because of land use and development restrictions, projected population growth in the greater South Lake Tahoe area is low, generally less than one percent.

The California Department of Finance (DOF) is designated as the official source of demographic data for state planning and budgeting. Demographic data from the Demographic Research Unit of the California Department of Finance were reviewed for current and future population growth estimates for the County and the CSLT (DOF, 2020 a; 2020b; 2020c and 2020d). These data were reviewed prior to the 2020 Census.

Population for the CSLT through 2019 is estimated at approximately 22,800. Since 2000, population in the CSLT has decreased at a rate of approximately 0.18% annually. County population projections (2010–2060) estimate the 2020 County population at approximately 193,000. Table 3-1 shows the annual growth rates for the County over the current 50-year forecast period (2010–2060). The County 50-year population growth rate (0.37%) is used to project future groundwater extractions within the TVS Subbasin for the projected water budgets presented in Section 5.4.8 of this report.

Table 3-1. P-1 projected long-term population growth rates for El Dorado County, California (DOF, 2020d).

PERIOD	ANNUAL GROWTH RATE
Population Growth (2010–2020)	0.66%
Population Growth (2020–2030)	0.75%
Population Growth (2030–2040)	0.27%
Population Growth (2040–2050)	-0.10%
Population Growth (2050–2060)	0.17%
Population Growth (2010–2030)	0.73%
Population Growth (2010–2040)	0.59%
Population Growth (2040–2060)	0.04%
Population Growth (2010–2060)	0.37%

The economy of South Lake Tahoe is largely dependent upon tourism. As a destination resort, the South Lake Tahoe area experiences large fluctuations in population on a regular basis. Because of this, water purveyors experience fluctuations in the water demand corresponding to

the summer tourist season and must meet maximum water demands on long weekends and holidays.

3.2 **Land Use**

TRPA developed a generalized depiction of the approved land uses for the Lake Tahoe Basin (TRPA, 2012). TRPA land-use types recognized within the TVS Subbasin are shown in Figure 3-1. Land use is primarily designated as Residential (7,823 acres or 52.8 percent); Recreation (1,855 acres or 12.5 percent); Mixed-Use (1,390 acres or 9.4 percent) or Tourist (396 acres or 2.7 percent); with the remaining 3,349 acres designated as either Conservation (3,330 acres or 22.5 percent) or Backcountry (19 acres or 0.1 percent). Land use within the surrounding watersheds neighboring the TVS Subbasin are designated as either Backcountry (33,287 acres); Conservation (30,359 acres); Wilderness (15,586 acres); or Mixed –Use (5,832 acres). Agricultural or industrial land use types do not occur within the TVS Subbasin or surrounding watershed areas. Areas (in acres) for each land use type is presented in Table 3-2.

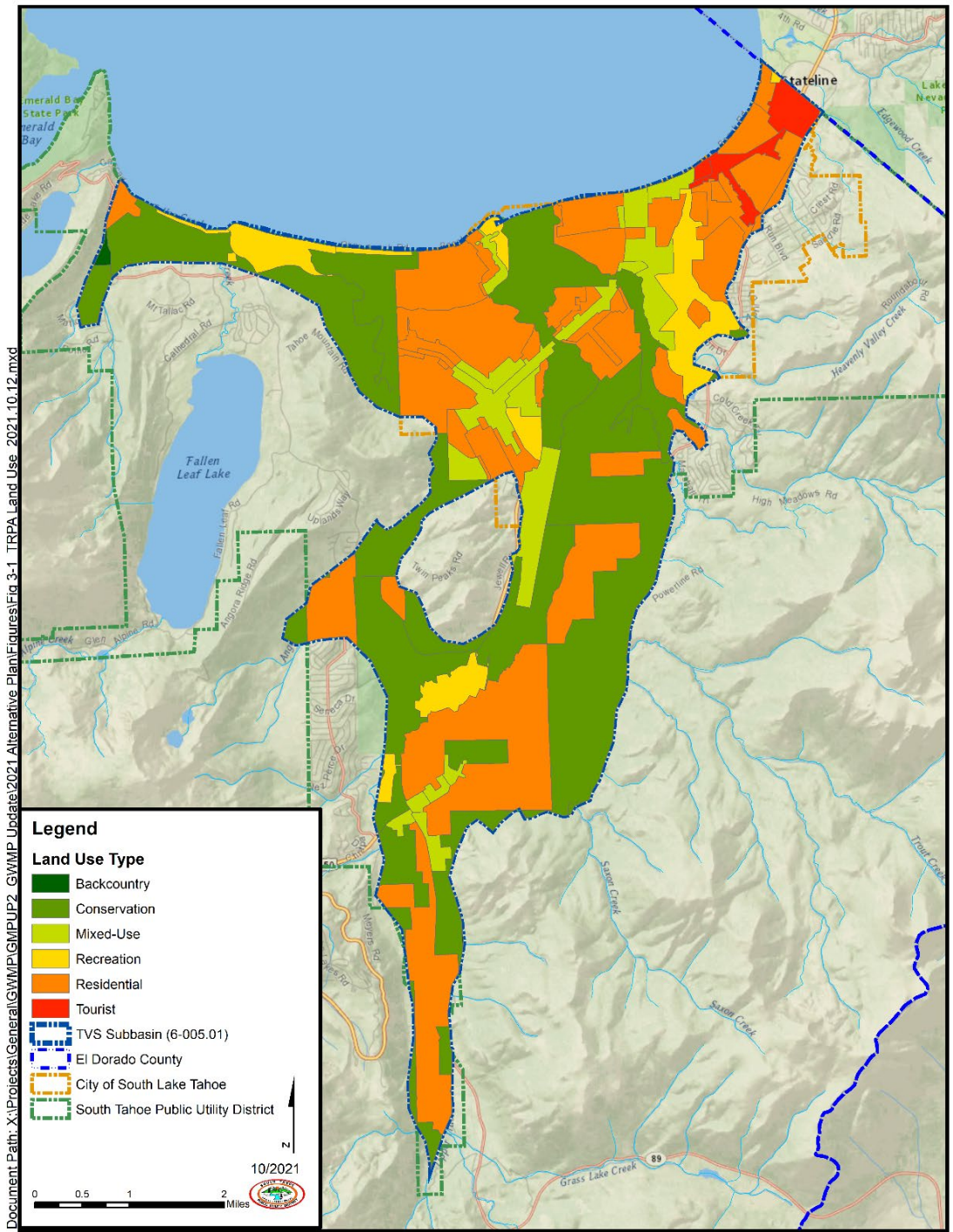


Figure 3-1. TRPA land use types recognized within the TVS Subbasin.

Table 3-2. Land use types and areas within the South Lake Tahoe area.

TVS SUBBASIN	
TYPE	Area (acres)
Backcountry	19
Conservation	3,330
Mixed-Use	1,390
Recreation	1,855
Residential	7,823
Tourist	396
TOTAL	14,814
SURROUNDING WATERSHEDS	
TYPE	Area (acres)
Backcountry	33,287
Conservation	30,359
Wilderness	15,586
Mixed-Use	5,832
TOTAL	85,064
TVS SUBBASIN + WATERSHEDS	99,878

3.2.1 Land Use Designations

Land use designations are defined by TRPA in the 2012 Regional Plan for Lake Tahoe (TRPA, 2012). Wilderness Areas are designated and defined by the U.S. Congress as part of the National Wilderness Preservation System. These lands offer outstanding opportunities for solitude and primitive, unconfined recreation experiences. They also contain ecological, geological, and other features of scientific, educational, scenic, and historic value. Backcountry Areas are designated and defined by the U.S. Forest Service as part of their Resource Management Plans. These lands are roadless areas where natural ecological processes are primarily free from human influences. Conservation Areas are non-urban areas with value as primitive or natural areas, with strong environmental limitations on use, and with a potential for dispersed recreation or low intensity resource management. Recreation Areas are non-urban areas with good potential for developed outdoor recreation, park use, or concentrated recreation. Resort Recreation Areas are the specific Edgewood and Heavenly parcels. Residential Areas are urban areas having potential to provide housing for the residents of the region. In addition, the purpose of the residential classification is to identify density patterns related to both the physical and manmade characteristics of the land and to allow accessory and non-residential uses that complement the residential neighborhood. Mixed-Use Areas are urban areas that have been designated to provide a mix of commercial, public services, light industrial, office, and residential uses or have the potential to provide future commercial, public service, light industrial, office, and residential uses. Tourist Areas are urban areas that have the potential to provide intensive tourist accommodations and services or intensive recreation.

3.3 Groundwater Uses and Users

Drinking water is the primary use of groundwater within the TVS Subbasin. Users of groundwater in the TVS Subbasin include public water systems, individual well owners, environmental users, the US Forest Service, and disadvantaged communities. Collaboration with these interest groups is discussed in Section 7.

Community water systems within the TVS Subbasin include the District, TKWC, LBWC and LPA. The District, TKWC and LBWC are 100 percent reliant on groundwater sources. The primary source for LPA is surface water which is supplemented with groundwater. Together these community water systems are believed to account for more than 90 percent of the groundwater annually extracted from the TVS Subbasin. Further information about these water systems is provided in Section 3.3.2. Individual water systems within the TVS Subbasin include small community and non-community water systems, state small water systems and domestic wells.

3.3.1 Groundwater Uses

The primary use of groundwater in the TVS Subbasin is as drinking water for residential and commercial water uses. Water use information provided in this section is from the District’s customer service database. The District produces most of the drinking water used within the TVS Subbasin (see Figure 3-2). Although information from the District’s customer service database does not capture all water use in the TVS Subbasin, it is believed to be adequate to show the general pattern of water use within the TVS Subbasin.

Table 3-3 shows water uses by sector from metered data for the District’s water system during the 2020 calendar year. The District is in the process of installing meters on all connections and is planned to be fully metered before the end of this year (2022). The 2020 data captures about 97 percent of the total number of water accounts in the District’s water system. The majority of the District’s customers are residential. The District’s commercial category includes office and retail, resorts including hotels, restaurants, and snowmaking and government customers. The “Other” category consists of water transfers through the District’s intertie to the LBWC water system under its Mutual Aid and Assistance Agreement. “Losses” are the non-revenue water system losses calculated from the difference between total groundwater production from District wells and consumption from the District meter data.

Table 3-3. 2020 water uses by sector for the District water system, in acre feet (AF). The total volume accounts for about 97 percent of the Districts total water accounts which were metered in 2020. Losses were estimated using the difference between District groundwater production and consumption from the meter data.

Use Type	Additional Description	Level of Treatment When Delivered	Volume, AF
Single Family	RES	Drinking Water	3,258.7
Multi-Family	MFR	Drinking Water	739.38
Commercial	COM +MHT+ GOV	Drinking Water	703.00

Use Type	Additional Description	Level of Treatment When Delivered	Volume, AF
Other	Mutual Aid Transfers	Drinking Water	0.10
Losses	Non-Revenue Water	Drinking Water	1,076.8
TOTAL			5,778

3.3.2 Community Water Systems

Community water systems (CWS) in the TVS Subbasin include both public utility water purveyors and community water purveyors that are not public utilities. CWSs that are public utility water purveyors are regulated water systems with more than 250 connections. CWSs that are community water purveyors that are not public utilities supply water to the same population of at least 25 people year-round at their primary residences or at least 15 residences that are primary residences (for example, municipalities, mobile home parks, and sub-divisions).

Groundwater production from the four largest CWSs is estimated to account for more than 90 percent of the groundwater extracted from the TVS Subbasin. Table 3-4 shows the connection and population information for these four water systems.

Table 3-4. Water systems information for the four largest community water systems within the TVS Subbasin (Safe Drinking Water Information System, downloaded October 12, 2021).

Water System	Water System No.	Primary Source	Population Served	Service Connections
South Tahoe PUD-Main (District)	0910002	Groundwater	33,124 – Residents 88,000 – Tourists	14,235
Tahoe Keys Water Company (TKWC)	0910015	Groundwater	1,420 – Residents	1,566
Lukins Brothers Water Company (LBWC)	0910007	Groundwater	3,200- Residents	982
Lakeside Park Association (LPA)	0910019	Surface Water	1,554 – Residents	139

Groundwater extractions from the District, TKWC, LBWC and LPA wells are metered using propeller or turbine type flowmeters with a register for total flow and a flow rate indicator.

Totalizer readings are recorded daily by the District and monthly by TKWC, LBWC and LPA. Accuracy of measurement for these flow meters is typically within two percent.

Groundwater production trends for the District, TKWC, LBWC and LPA water systems are shown below in Figure 3-2. Since WY 2005, groundwater pumpage by these water systems has ranged from a low of approximately 6,306 AF during WY 2015 to a high of approximately 9,652 AF during WY 2007. Since 2005, total annual groundwater pumpage by these water systems averaged 7,631 AFY. During WY 2020, total groundwater production (6,791 AF) was about 10 percent below average.

Service areas for the District, TKWC, LBWC and LPA water systems as well as the locations of active wells and their annual pumpage for WY 2020 are shown on Figure 3-3. Slightly more than 70 percent of the total groundwater pumpage for WY 2020 was extracted from the South Lake Tahoe sub-area.

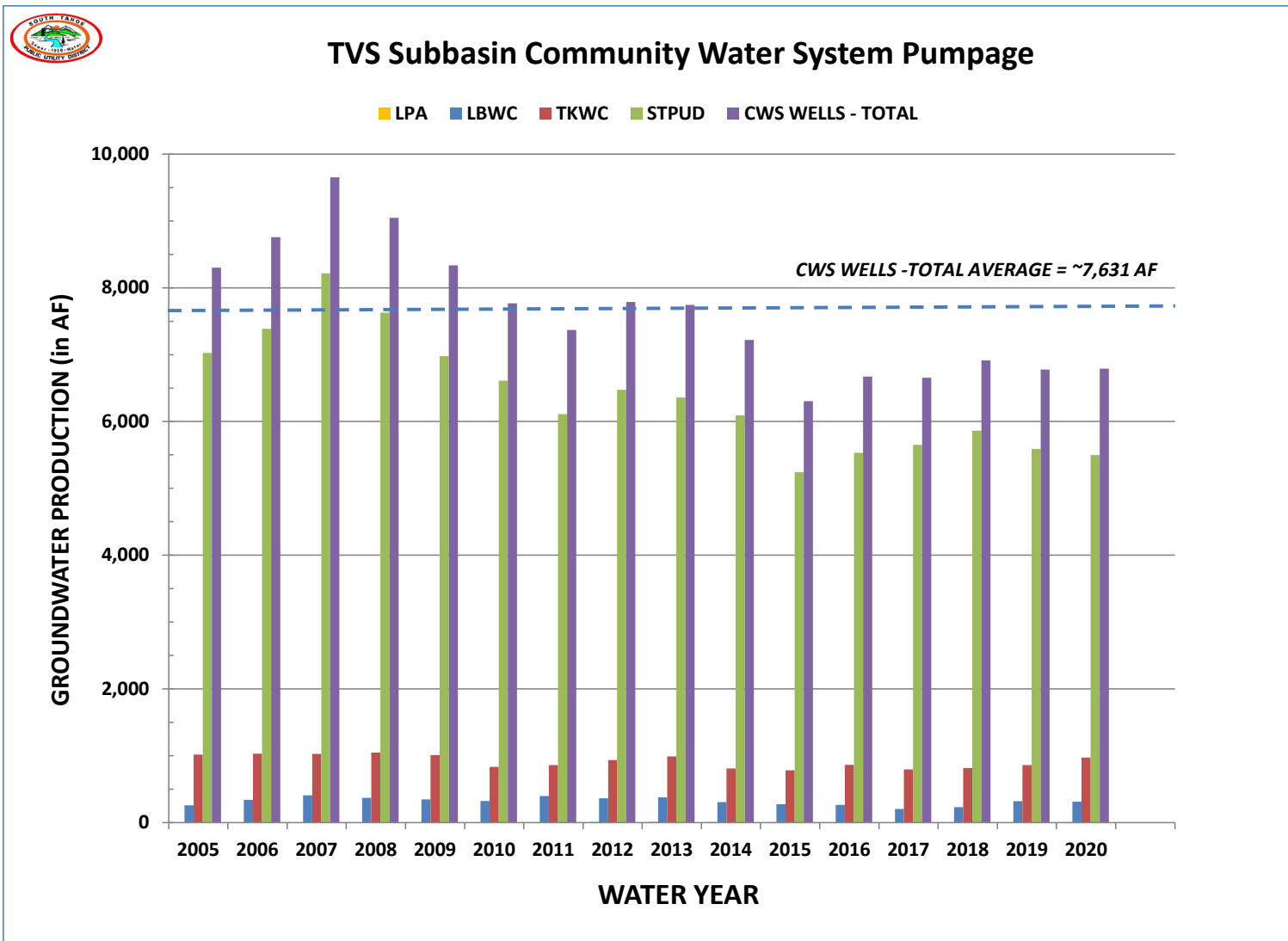


Figure 3-2. Groundwater production trends for community water system wells in the TVS Subbasin since WY 2005, in AFY.

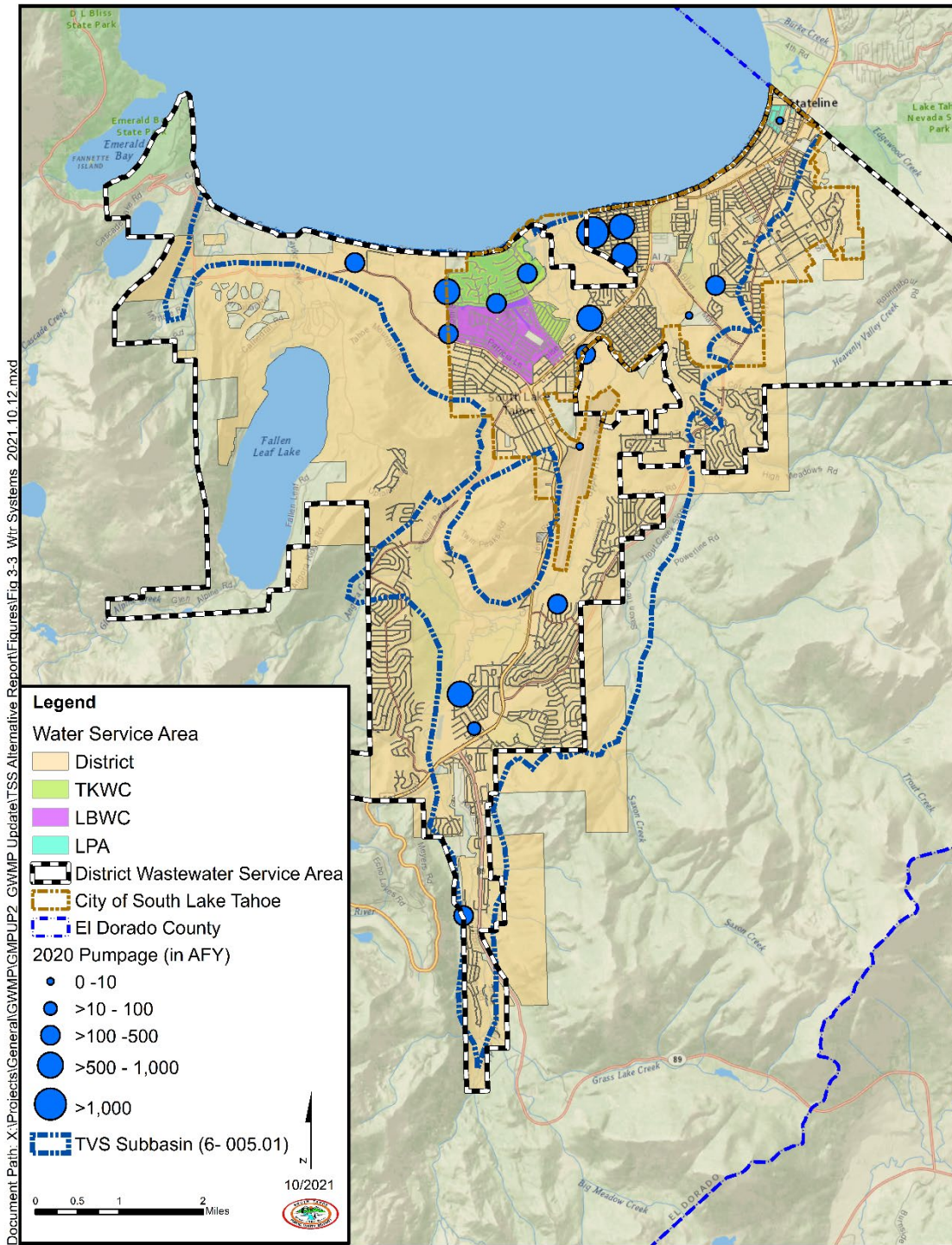


Figure 3-3. Water system services areas and annual groundwater pumpage from the four largest community well water systems for WY 2020, in AF.

3.3.2.1 South Tahoe Public Utility District

The District was established in 1950 and is the only public utility district water purveyor within the TVS Subbasin. The service area is largely residential with a relatively small number of connections to commercial businesses. The District generally controls groundwater pumping by changing water storage reservoir levels in response to water system demands within the pressure zone served by the reservoir within which it is located. The booster stations and pressure reducing valves are used to distribute water between pressure zones.

The District owns, operates, and maintains a medium size water system consisting of 14,235 service connections that include businesses, single-family, and multi-family dwellings within a 20,480-acre service area. The District’s service area covers the majority of the TVS Subbasin extending from the California-Nevada state line on the east to Emerald Bay on the west, and from Christmas Valley on the south, to the south shore of Lake Tahoe to the north. Drinking water for the District water system is currently provided by 11 active groundwater wells and three stand-by wells. Operation of stand-by sources is limited for short-term emergencies of five consecutive days or fewer and for fewer than a total of fifteen calendar days a year (H&S Code §64414(c)). Table 3-5 provides well and current source capacity information for the District’s active and stand-by wells.

Table 3-5. Well and source capacity information for District wells.

Well	Well Year	Well Depth	Well Status	Source Capacity	
				GPM	AFY
Al Tahoe Well #2	1978	400	Active	2,500	4,033
Arrowhead Well #3	1998	290	Active	775	1,250
Bakersfield Well	1994	253	Active	1,450	2,339
Bayview Well	2004	550	Active	3,600	5,807
Elks Club Well #2	2003	228	Active	300	484
Glenwood Well #5	2002	230	Active	1,037	1,673
Helen Avenue Well #2	1966	150	Active	242	390
Paloma Well	1994	418	Active	1,825	2,944
South Upper Truckee Well #3	2004	320	Active	850	1,371
Sunset Well	1990	440	Active	600	968
Valhalla Well	1999	190	Active	600	968

Well	Well Year	Well Depth	Well Status	Source Capacity	
				GPM	AFY
Airport Well	1978	380	Stand-By	500	807
Blackrock Well #2	1959	240	Stand-By	90	145
College Well	1981	365	Stand-By	1,100	1,774

District water production information (2005–2020) shows groundwater pumpage ranging from 5,241 to 8,216 AFY, with an annual average of approximately 6,391 AFY. Groundwater production from the District wells is believed to account for about 81 to 85 percent of the total annual volume of groundwater extracted by CWS wells within the TVS Subbasin.

3.3.2.2 Tahoe Keys Water Company

The TKWC is a community water purveyor that is a mutual water company owned and operated by Tahoe Keys Property Owners Association. The Tahoe Keys Property Owners Association was organized as a mutual-benefit nonprofit corporation 501(c)(4) in November 1963 to provide for management, maintenance and architectural control of the individual units and the common area property within the Tahoe Keys. The primary function and responsibility of the TKWC is to operate and maintain all wells, pipe delivery systems and monitoring equipment to consistently provide safe drinking water throughout the Tahoe Keys development.

TKWC operates and maintains a small water system consisting of 1,566 service connections that includes 1,532 residential customers and 34 commercial customers northwest of the CSLT. The residential customers are Tahoe Keys owners and renters, consisting of approximately 1,194 single family homes and 335 townhouses. The commercial customers include the Tahoe Keys Marina and Tahoe Keys Office Center.

Drinking water for the TKWC water system is provided by three groundwater sources: TKWC01, TKWC02, and TKWC03. TKWC01 casing depth is at 318 feet and can produce 1,000 gallons per minute (GPM). This well acts as the primary well and is equipped with a back-up generator in case of a power outage. TKWC02 casing depth is at 501 feet and can produce 1,800 GPM. Since 2012, this well has been equipped with a Granular Activated Carbon (GAC) system for the removal of tetrachloroethylene (PCE) from groundwater. Operation of the treatment system limits current water production from this well to 550 GPM. TKWC03 casing depth is at 320 feet and can produce 1,750 GPM. Historically, TKWC has operated TKWC 01 as a lead well with TKWC03 operated as a lag well. TKWC02 is operated during the summer months to meet peak water demands.

Water production information provided by TKWC (2005–2020) shows groundwater pumpage ranging from 782 to 1,047 AFY, with an average production of about 916 AFY. Groundwater production from the TKWC wells is believed to account for about 10 to 14 percent of the total annual volume of groundwater extracted by CWS wells within the TVS Subbasin.

In 2020, elevated levels of naturally occurring uranium above MCLs were detected in raw water samples collected from TKWC02 and TKWC03. Arsenic below MCLs was detected in all three TKWC wells. TKWC is in the process of developing both near-term interim and emergency plans for provision of drinking water to meet its immediate summer water demands; and long-term facility plans to prevent PCE, uranium and arsenic from entering its water distribution system. Current interim plans are relying on strict landscape irrigation restrictions and emergency water purchase(s) from neighboring District and LBWC water systems.

3.3.2.3 **Lukins Brothers Water Company**

Established in 1942, LBWC is an investor-owned public utility regulated by the California Public Utility Commission. The LBWC owns, operates, and maintains a small water system consisting of 982 service connections that include businesses, single-family and multi-family dwellings within a 320-acre service area in the northwest portion of the CSLT. Historically, drinking water for the LBWC water system has been provided by three groundwater sources: LBWC01, LBWC02 and LBWC05. Of these sources, only LBWC01 is active. LBWC01 casing depth is at 182 feet and can produce 700 GPM. This well is equipped with a back-up generator in case of a power outage. LBWC03 and LBWC04 were destroyed in 1989 and 2020, due impairment by PCE contamination.

In 2014, PCE contamination impaired LBWC02 and LBWC05 (both wells share the same well site). In 2020, LBWC02 was properly destroyed and a groundwater treatment facility consisting of a two 8,800-gallon GAC treatment vessels were installed to remove PCE from groundwater pumped by LBWC05. A 98,000-gallon storage tank, a 250-kW emergency power generator, and four booster pumps (2 x 15 Hp; 2 x 30 Hp) were also installed to provide storage and redundancy for the LBWC water system. The GAC treatment system is designed to remove PCE to non-detect levels at a design flow rate of up to 700 GPM at PCE concentrations up to 300 parts per billion. With SWRCB Division of Drinking Water (DDW) approval, and start-up testing of the groundwater treatment system completed, LBWC05 went back on-line in July 2021. LBWC05 is operated as a lead well with LBWC01 operated as a lag well. LBWC05 casing depth is at 255 feet and can produce 620 GPM.

Water production information provided by LBWC (2005–2020) shows groundwater pumpage ranging from 206 to 408 AFY, with an average production of about 319 AFY. Groundwater production from the LBWC wells is believed to account for about three to five percent of the total annual volume of groundwater extracted by CWS wells within the TVS Subbasin.

3.3.2.4 **Lakeside Park Association**

Established in 1909, LPA was the first subdivision on the south shore of Lake Tahoe. The Lakeside Park Mutual Water Company was first started in 1938 to serve the LPA service area. The Lakeside Park Mutual Water Company is a community water purveyor which is not a public utility, serving 139 largely non-residential connections in a roughly 70-acre area in the northeast corner of the CSLT, north of Highway 50, adjacent to the state line. The system's original source came from a spring that was developed in 1908. Water storage capacity was provided by four

7,000-gallon redwood tanks located near the spring, and water flowed downstream to the LPA service area.

As the LPA service area developed, two groundwater wells were constructed as the primary source of drinking water and the spring was maintained as a backup supply. In the 1960s, LPA obtained water rights to Lake Tahoe. An intake line was constructed, and surface water became the primary source of water for the LPA service area. By the 1980s the first two wells were abandoned, and a third well (LPA03) was constructed with a casing depth of 339 feet and a production capacity of about 250 GPM. This well is currently used to supplement surface water use and typically accounts for less than two percent of the system's total water production. Water production information provided by LPA (2010–2020) shows groundwater pumpage ranging from 0.5 to 15 AFY, with an average production of about 7 AFY. Groundwater production from this well is believed to account for less than 1 percent of the total annual volume of groundwater extracted by CWS wells within the TVS Subbasin.

3.3.3 Individual Water Systems

Individual water systems consist of community water systems with less than 250 connections, non-community water systems, state small water systems regulated by El Dorado County, and domestic wells. Non-community water systems are composed of transient and non-transient water systems. Transient non-community water systems provide water to 25 or more people for at least 60 days per year, but not to the same people and not on a regular basis (for example, gas stations, campgrounds). Non-transient non-community water systems regularly supply water to at least 25 of the same people at least six months per year, but not year-round (for example, schools, factories, office buildings, and hospitals which have their own water systems). State small water systems consist of water systems for the provision of piped water to the public for human consumption that serves at least five, but not more than 14, service connections and does not regularly serve drinking water to more than an average of 25 individuals daily for more than 60 days out of the year. Domestic wells supply water to an individual residence. Some individual residences are supplied by springs and along the south shore of Lake Tahoe some residences are supplied by freshwater intakes to Lake Tahoe. However, most private residences are supplied by a domestic well.

As indicated in Section 4.3.3, the County Environmental Management Division, Environmental Health Department (County Environmental Health Department) is responsible for implementing the County Water Well Program. Information gathered from completed Well Permit applications has been mapped by the County Surveyors office to show the spatial distribution of wells within the County (last updated in 2018). Review of these data indicate that from 1990 through 2018, forty-six permits for new well construction; and five permits for well deepening were issued for properties within the TVS Subbasin. Another nine well permit applications were issued for new well construction on parcels neighboring the TVS Subbasin. Figure 3-4 shows the distribution of these well locations inferred from County well permit applications.

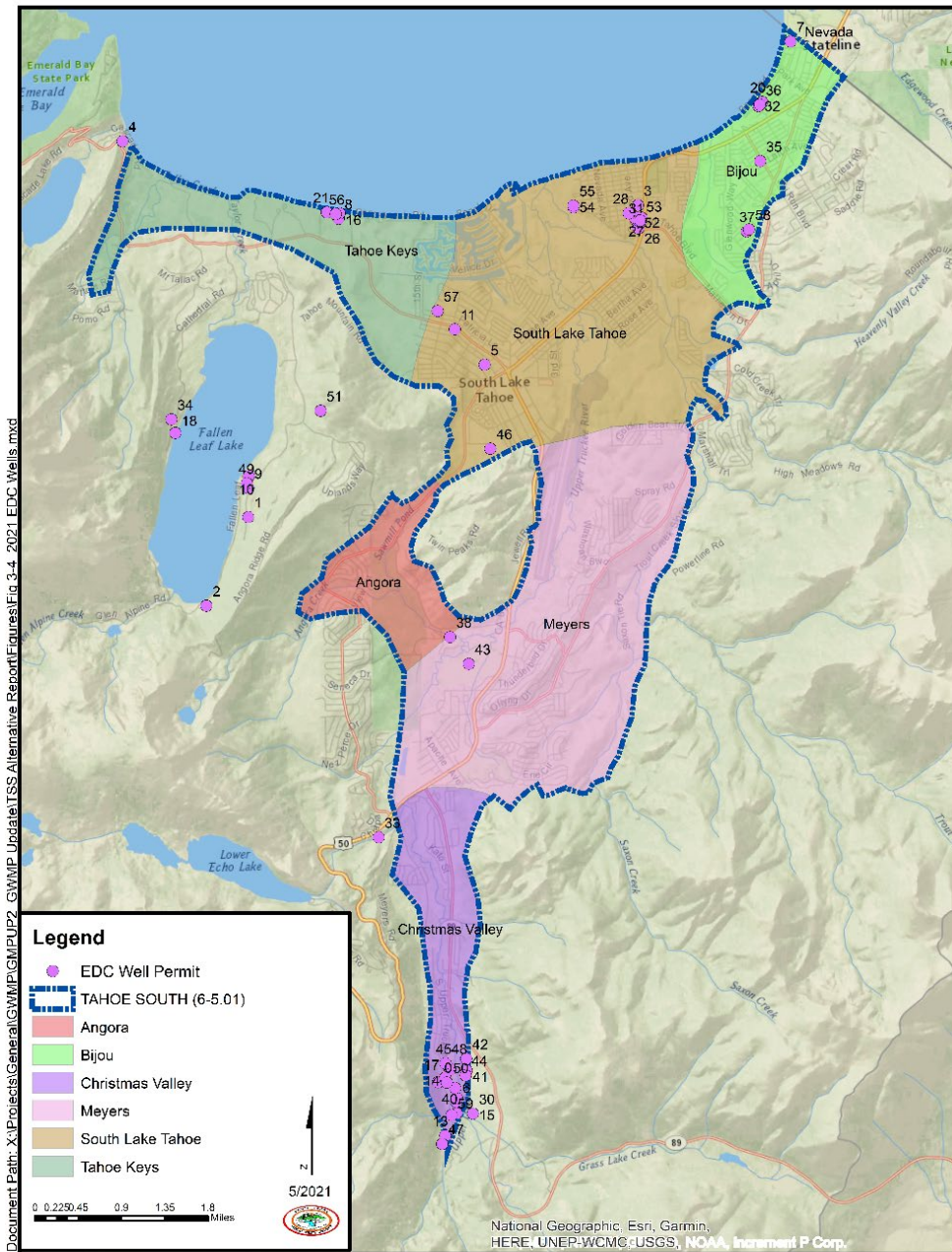


Figure 3-4. Parcels with County Well Permits issued for new construction or deepening in the TVS Subbasin.

As indicated in Section 4.3.3, the County Environmental Health Department is also responsible for implementing the County Small Water System Program. Lists of small water systems in the South Lake Tahoe area regulated under this program were obtained from the South Lake Tahoe office of the El Dorado County Environmental Management Department (EDCEMD). Most of the small water systems on the list are reliant on groundwater sources. Review of the County small water systems list indicates that there are 58 private wells regulated

by the County within the TVS Subbasin. These include 38 non-community water systems; 14 state small water systems; 3 community water systems; and 3 non-transient non-community water systems. Figure 3-5 shows the spatial distribution of the County-regulated small water system wells within and neighboring the TVS Subbasin.

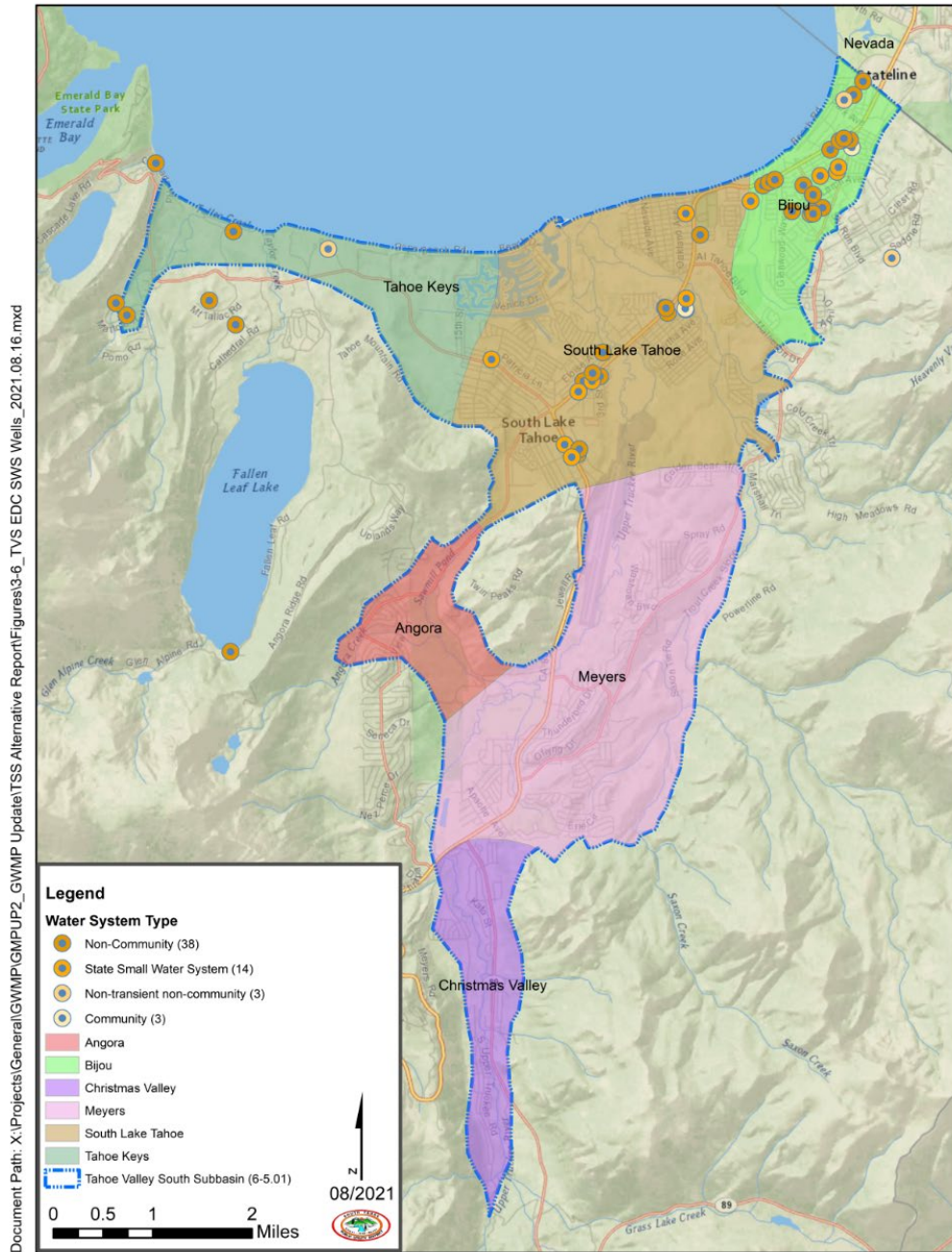


Figure 3-5. Small water system wells regulated by El Dorado County within the TVS Subbasin.

3.3.3.1 Domestic Water Systems

Domestic wells usually supply water to an individual residence. The occurrence of high-quality water at shallow depth led to the early use of domestic wells throughout the TVS Subbasin. Use of domestic wells are known prior to 1908 serving individual residential and commercial units (Brown and Caldwell, 1961). The South Lake Tahoe area was strongly affected by the growth of automobile transportation in the 1920s and 1930s. Many of the domestic wells within the TVS Subbasin are in older neighborhoods clustered along the U.S. Highway 50 corridor, California’s first state highway, established in 1896. In 1924, Tahoe Meadows was founded as the first private summer resort community on the south shore of Lake Tahoe. Most of the cabins within Tahoe Meadows were built from 1925 to 1941 (NPS, 1990). Potable water for many of these cabins is provided by domestic wells.

Through the District’s customer service database, the District can recognize parcels with individual water system wells within its service area as parcels which have sewer connections but no water connection to the District’s water system. From this list the District can identify whether the parcel is supplied by a well and the property type (based on Class Code). Using this method, the District has identified 390 parcels within its service area supplied by an individual water system well, spring, or freshwater intake. Table 3-6 shows a breakdown of these wells based on Class Code. Based on property type, as many as 310 domestic wells are within the District’s service area.

Table 3-6. Number and type of properties with individual water system wells within the District’s service area as of February 2020.

Class Code	Number of Parcels with a Well
Single-Family Dwelling (SFD)	310
Multi-Family Dwelling (MFD)	35
Motel/Hotel (MHT)	16
Commercial (COMM)	15
Government (GOV)	14
TOTAL	390

3.3.4 Well Owners Survey Results

As part of its outreach efforts, the District conducted a survey of individual water system well owners and users of wells not connected to community water systems within the TVS Subbasin. The purposes of this well survey were to: (1) inform well owners of groundwater management planning and implementation efforts; (2) encourage participation of individual well owners in the SAG; and (3) confirm the inferred location and use of individual water system wells.

The initial phase of the well survey (PWOS-I) spanned a two-month period from August 2017 through October 2017. Planning for the survey involved the development of the survey questionnaire, survey team recruitment, preparation of outreach materials and compilation of available well owner lists from the District and SAG members, including the County and the United States Forest Service –Lake Tahoe Basin Management Unit (USFS LTBMU). The District inferred there to be 578 domestic and 56 small community water system wells located on parcels within or surrounding the TVS Subbasin.

The well survey was advertised using local media, public service announcements, direct mail notification letters, door hangers and the District’s website. Participation in the well survey was made available through a URL for direct access to the survey online, through paper copy on request from the District, and through direct door-to-door survey performed by a dedicated three-member survey team. The well survey was successful in collecting information from a total of 370 respondents. Of these respondents, 247 confirmed the presence of a well on their parcels, 77 indicated that there was no well on their parcels, and 2 were uncertain if a well was located on their parcels. Figure 3-6 shows the locations of the confirmed domestic locations from the well survey.

During WY 2018, a final report documenting the well survey was completed (Allegro Communications, 2018) and made available to the public through the District’s website (<http://stpud.us/news/groundwater-management-process/>).

Major findings from the TVS Groundwater Basin Survey of Well Owners report include:

- Private well geographic distribution reflects travel and settlement patterns of the one-hundred-year period prior to the District’s formation, from 1845 to 1950.
- Most respondents to the well survey were property owners (72%). Most of these properties were used as “secondary” residences.
- Most respondents (61%) indicated that the well on their property is currently in use. Most of this use is either daily or more than 90 days out of the year.
- Private well owners overwhelmingly “like” perceived “purity” of well water. “Taste, color and odor” of well water are perceived favorably. Well owners enjoy features of private well water such as “cold temperature”, “low cost”, “quality”, and “absence of chlorine”. They highly value well water while the system consistently delivers high quality water.
- Well owners indicating concern about well systems mention “pumps”, “wellhead connections”, “water production”, and “system maintenance.

Recommendations developed based on the information gathered during this survey include:

1. Create capacity within the groundwater community to make technical support available to private well owners.

2. Complete the assessment of the status of private wells.
3. Assess risk to groundwater resources from private wells.
4. Cultivate capacity to create and maintain collaborative ties in the groundwater community.
5. Communicate with private well owners.
6. Collaborate with national and state programs that support source water protection.
7. Share survey findings with Lake Tahoe Basin partner agencies.

During WY 2019, the District started planning a second phase of surveys to contact private well owners missed in 2017. The Phase II survey (PWOS-II) was conducted in 2020 to reach the nearly 300 private well owners that were not contacted during PWOS-I in 2017. PWOS-II began at the end of June 2020 with a direct mailer to property owners believed to have private wells on their property. Because of the COVID-19 Public Health Emergency, PWOS-II was dependent on direct mail with follow-up telephone calls and emails encouraging property owners to complete the well survey questionnaire. In appreciation for responding to the PWOS-II, the District offered:

- Guidance on maintaining private wells through the County Water Well Program website.
- Visual well checks to help property owners identify and prevent contamination from entering their well head.
- General water quality testing to check well water quality.

A copy of the survey questionnaire along with the combined results from PWOS-I(PWOS-II provided in Appendix H.

The survey questionnaire was the primary tool for gathering information from private well owners during PWOS-I and PWOS-II. The questionnaire was arranged around several topics: (1) property ownership and usage; (2) well location and usage; (3) well water quality; (4) well system condition; and (5) interest in receiving additional information concerning water wells and/or local groundwater management. A combined total of 509 responses were received during PWOS-I (375 responses) and PWOS-II (134 responses). Review of the combined responses show that many respondents (401 out of 507) were either the owner or manager of the property, owned the property since at least 1998 (183 out of 364), and used the property as a second home (192 out of 390). Another 107 out of 390 respondents indicated business as the primary use of the property (includes rental properties, apartments, hotels/motels, mobile home parks and restaurants).

Most respondents (335 of 503) indicated that a well was located on their property, 118 respondents indicated no knowledge of a well, and 50 respondents did not know. Of the respondents with a well on their property, 286 respondents confirmed that the well was actively

used: nearly every day (190); more than 90 days out of the year (58); infrequently (30); or rarely (5). Three respondents answered that their well was not used at all. Of respondents indicating a well was located on the property, the majority (244 out of 283) indicated that the well was the primary source of water; the other (39) respondents indicated that the well was used solely for irrigation.

In terms of well water quality, most respondents liked the aesthetic qualities (taste, color, and odor) and purity of their water. Most respondents (43 out of 85) identified contaminants as a well water concern. In terms of water well systems, pump failure was the most common concern (50 out of 103), followed by declining water production (15 out of 103), declining water quality (15 out of 103), and well in disrepair or lacking tight seal (12 out of 103).

Overall, the top three groundwater supply concerns identified during the survey were: groundwater contamination (183 out of 408), declining groundwater levels (97 out of 408), and population growth; future water demands (93 out of 408). A significant number of respondents (140 out of 408) did not believe there were any concerns related to groundwater.

In terms of interest in receiving additional information, most respondents appear content with their current level of information. Most respondents were not interested in receiving information about County guidelines and requirements for well abandonments, connection to a public water system, or receiving District emails about local groundwater management activities in the TVS Subbasin.

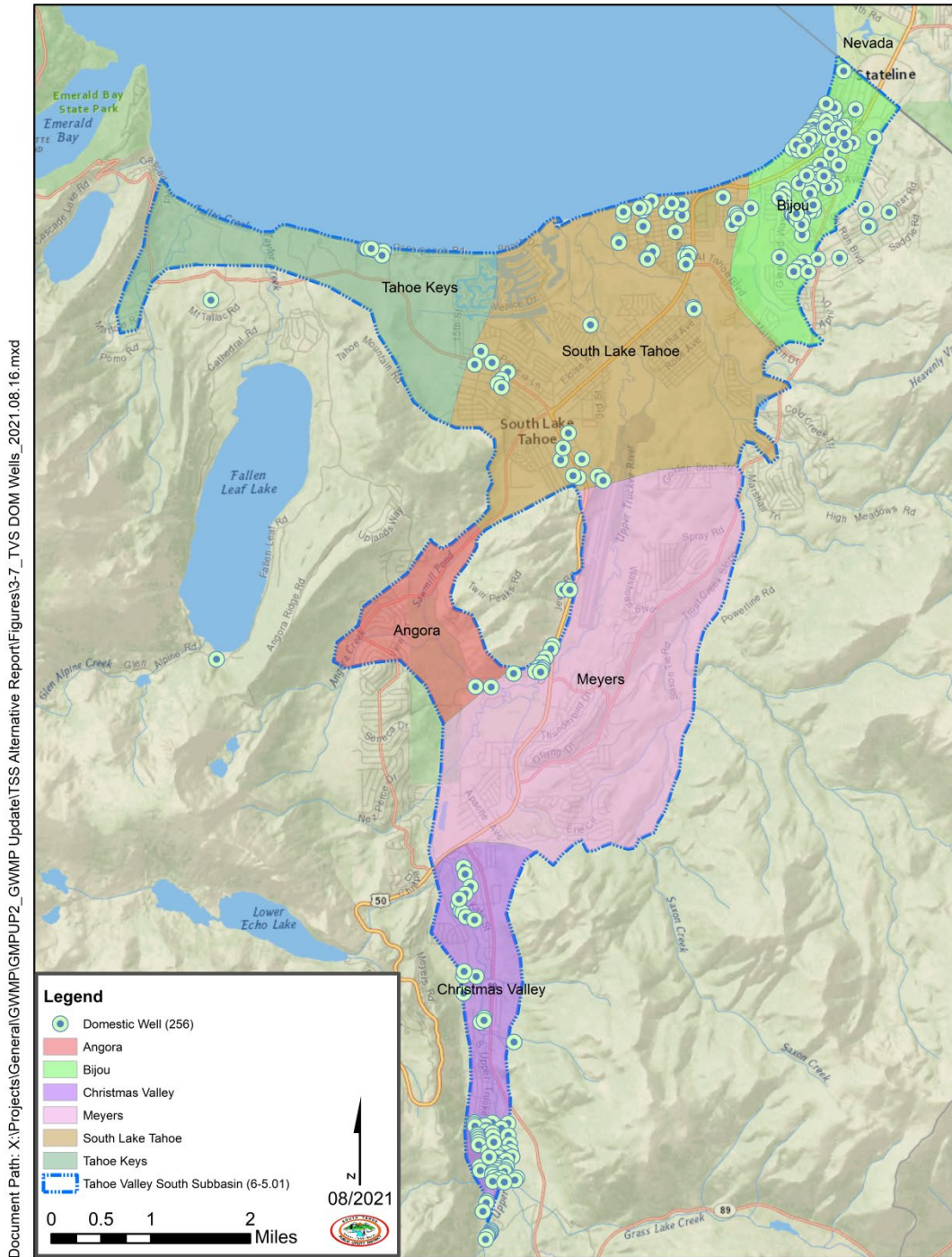


Figure 3-6. Domestic wells in-use based on private well owner survey responses collected in 2017 and 2020.

Spatial analysis of the well owner's survey data shows that most respondents with private wells on their property are located within Disadvantaged Community (DAC) Census Block Groups (Figure 3-7). Census blocks are the smallest geographic area for which the Bureau of the Census collects and tabulates decennial census data. A census block group is a cluster of census blocks having the same first digit of their four-digit identifying numbers within a census tract. Block groups generally contain between 600 and 3,000 people, with an optimum size of 1,500 people. DAC Block Groups depict data from the US Census ACS 2010–2014 showing census block groups identified as disadvantaged communities (less than 80% of the State's median household income) or severely disadvantaged communities (less than 60% of the State's median household income). Results of the analysis indicates that more than one-third of the total number of survey respondents are private well owners located with DAC Census Block Groups, accounting for nearly two-thirds of all respondents with an active well on their property. Relative to the 2016 California median household income (\$ 67,739), most survey respondents own or operate wells located within severely disadvantaged DAC Block Groups. The high level of engagement in the well survey suggests that this group has a significant level of interest in groundwater-related issues. The District recognizes well owners within DAC Block Groups as a significant stakeholder group within the TVS Subbasin.

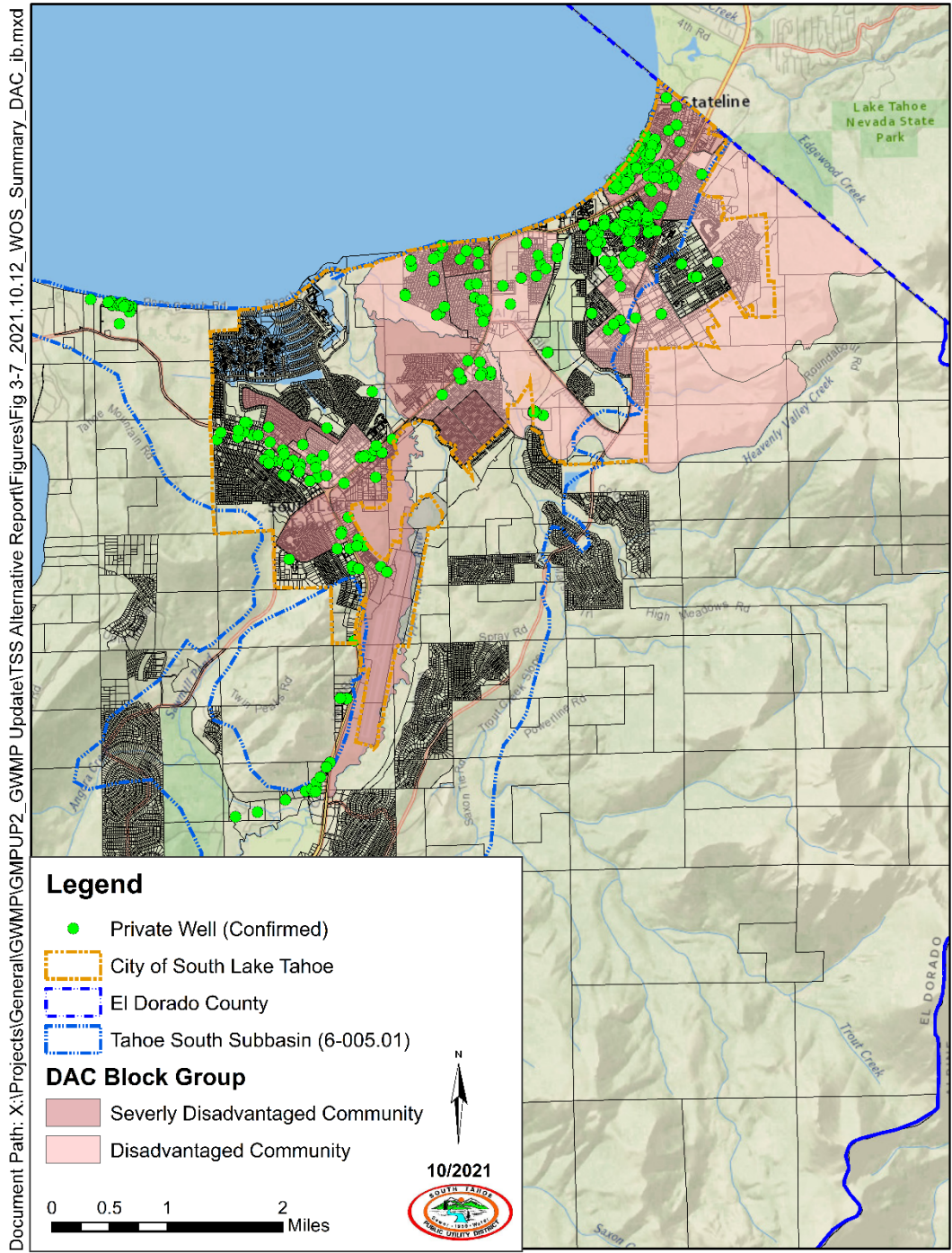


Figure 3-7. Confirmed private well locations situated within Disadvantaged Community census blocks within the City of South Lake Tahoe.

3.3.5 Groundwater Pumpage/Well Densities

Using the combined survey responses and available water use constants for private wells within the TVS Subbasin, estimates were developed for the total pumpage from active private wells captured in the surveys. Based on the survey responses, the following well usages, in days, were assigned for the active wells (Table 3-7).

Table 3-7. Assigned well usage values based on survey responses for active wells.

Survey Response	Annual Well Usage (in days)
Nearly Every Day	365
More than 90 days	180
Infrequently (15 < x < 90 days)	60
Rarely (< 15 days)	10
Not at all	0

The Truckee River Operating Agreement (TROA) is an interstate water agreement for the operation of the existing lakes and reservoirs in the Truckee River system from Lake Tahoe downstream to the river’s terminus at Pyramid Lake (see Section 4.3.9). Under TROA, annual diversions of water within the Truckee River Basin are calculated on an annual basis. For the Lake Tahoe Basin, the unmeasured water used for residential purposes (i.e., domestic wells) is presumed at 0.40 AFY per residential unit (TROA, Section 6.D.3). Under SGMA a “de minimis extractor” is a person who extracts, for domestic purposes, two acre-feet or less per year (SGMA § 10721(e)). For purposes of this water use analysis, both the TROA water and SGMA water use rates were applied to bracket the estimated range of possible water use represented by the domestic wells.

As indicated in Table 3-6, many of the domestic wells captured in the survey are situated on properties with multi-family residential, motel/hotel, or commercial uses. For multi-family dwellings, water usage was estimated using annual water use rates, estimated annual well usage and number of connections at the facility (from County small water system records). For motel/hotel properties, water use was estimated based on the number of rooms; an occupancy rate of 50 percent (conservative estimate based on Lake Tahoe Visitors Authority Transient Occupant Tax Reports for CSLT); and a water usage rate of 101 gallons per room per day for motels with less than 75 rooms (Murray, 2015). For commercial properties, water usage was estimated using annual water use rates, estimated annual well usage, a conservative occupancy rate of 50 percent (assuming business hours at 12 hours per day, 6 days per week, for 52 weeks per year).

Figure 3-8 shows the inferred spatial distribution of well pumpage from active wells identified during the private well owners’ surveys. The combined results included responses

from a total of 290 private well owners; of these 254 were for domestic wells; 28 were for non-community water system wells and 8 were for state small water system wells. Using the presumed TROA water usage rate for domestic wells, the total pumpage from the active private wells is estimated at about 126 AFY. Adjusting the well data for discrepancies between well owner responses and existing County well records for wells in the South Y area increased the total pumpage for private wells by 3.32 AF to about 129 AFY. If the SGMA water usage rate for domestic wells is used, the total pumpage from the active private wells is estimated at about 542 AFY.

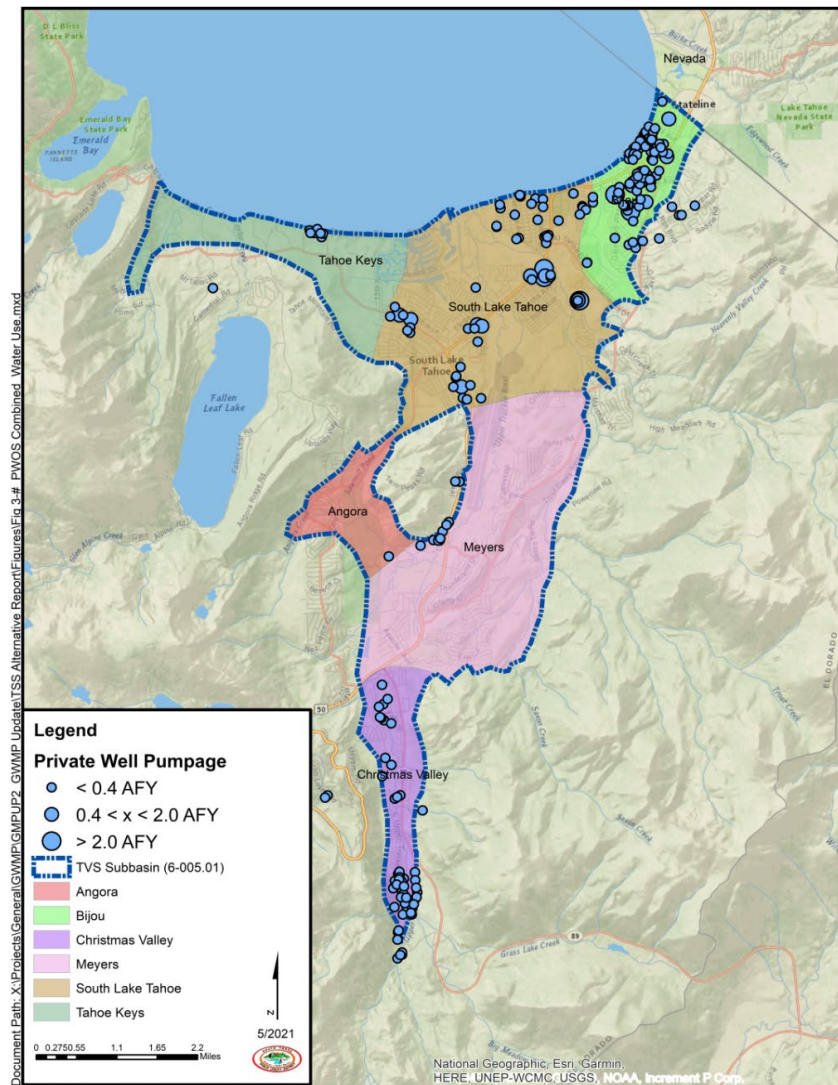


Figure 3-8. Pumpage from active wells based on the combined results of the survey of private well owners.

Using the survey results, the District generated a density map to show the active wells within the TVS Subbasin (Figure 3-9). As the well owners survey could not verify the locations

of all active wells within the TVS Subbasin, estimated well densities are regarded as minimum values and may be greater than indicated.

The well density map includes the CWS wells for the District, TKWC, LBWC, and LPA. In most of the TVS Subbasin, well densities are less than 10 wells per square mile. The areas of highest well densities include the northeast portion of the TVS Subbasin in the Bijou and South Lake Tahoe subareas with densities exceeding 50 wells per square mile near the Nevada border. Another high-density (11 to greater than 50 wells per square mile) area is located at the southern tip of the Christmas Valley subarea along Grass Lakes Road. Lower, but significant well densities (11 to 50 wells per square mile) are also found along CA-89 south of the Y and continuing along CA-89 north of the Y to the northwest, in the South Lake Tahoe and Tahoe Keys subareas.

Groundwater extractions at private wells within the TVS Subbasin are subject to some uncertainty in terms of rates and precise well locations. Pumpage estimates stated previously range from 142 AFY based on expected use, to 542 AFY based on maximum allowable use for domestic wells. These rates are small relative to the estimated sustainable yield for the TVS Subbasin of 13,200 AFY (Section 5.5), approximately 1.1 to 4.1%, respectively. Given the methods used, the true rate is likely much closer to 142 AFY than to 542 AFY. Error in these estimates can therefore be expected to be small and unlikely to have a significant effect on planning and water budget projections. Likewise, although the precise locations of all private wells may not be known, the general locations are known to the parcel level, and the well density analysis can be considered reasonable accurate.

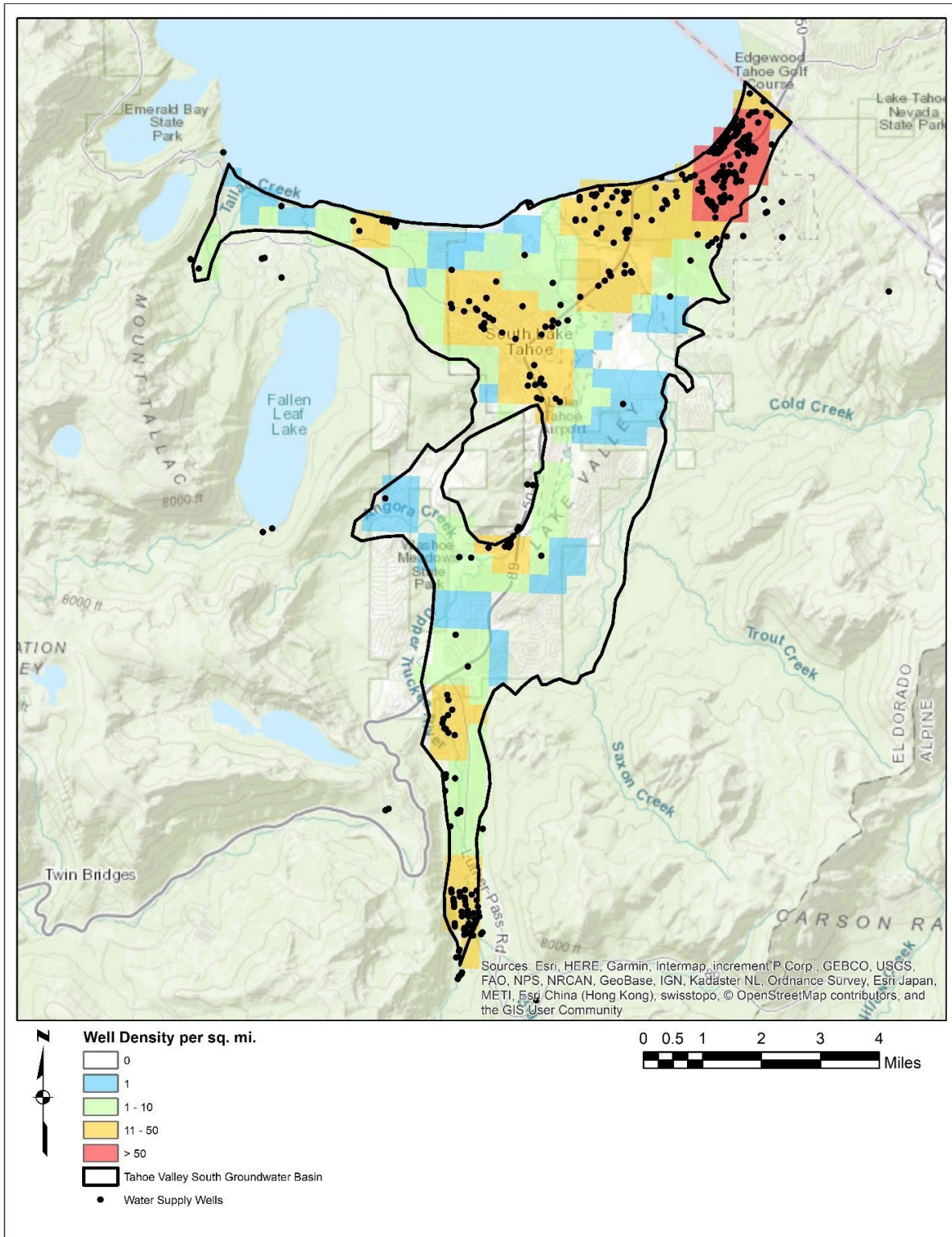


Figure 3-9. Water well density per square mile in the TVS Subbasin, including community water supply wells, small water system wells, and private wells (*de minimus* extractors).

3.4

Demand Projections

In January 2020, the District submitted a water demand analysis to the SWRCB-Division of Water Rights in support of its water rights application (A023393). The water demand analysis was prepared in collaboration with the North Tahoe and Tahoe City public utility districts to determine potential annual water production needs using a joint methodology for each respective agencies service area (Cotulla et al, 2021). The water demand analysis used water agency metered water demand and water production data, County parcel and ownership information, and TRPA land use information to determine the future water demand at total build-out for each service area. The water demand analysis completed for the District’s service area presented estimates of the total annual water production requirements for each of the four largest CWSs and other individual water users within the TVS Subbasin. Table 3-8 shows the estimated future water demands resulting from this analysis (Kennedy Jenks, 2020).

Table 3-8. Total water production requirements estimated from future water demand analysis for the District’s service area (adapted from Kennedy Jenks, 2020).

Water System	Baseline Water Production Requirement – Current (AFY)	Baseline Water Production Requirement – Future (AFY)	Total Water Production Requirement – Future (AFY)
South Tahoe Public Utility District	7,385	1,025	8,410
Tahoe Keys Water Company	1,018	28	1,046
Lukins Brothers Water Company	319	34	353
Lakeside Park Association	237	62	299
Other individual Water Users	676	24	700
<i>Estimated Totals</i>	<i>9,635</i>	<i>1,173</i>	<i>10,808</i>

Demand is artificially capped by the California-Nevada Interstate Compact Concerning Water of Lake Tahoe, Truckee River, Carson River, and Walker River Basins (Compact) approved in 1971, which allocates a total annual surface water and groundwater diversion of 23,000 AFY within the California side of the Lake Tahoe Basin. In 1972, the SWRCB adopted a Policy for the Administration of Water Rights in the Lake Tahoe Basin establishing that all surface water and groundwater diversions shall not exceed the allocations defined in the Compact. In 1979, the SWRCB issued a report on water rights and water use in the Lake Tahoe Hydrologic Basin. In this report SWRCB presented recommendation for the administration of water rights including an annual allocation of 12,100 AF for the South Lake Tahoe area referred to as South Tahoe Zone C (SWCB, 1979). In 1984 the SWRCB prepared a Draft Report titled, Policy for Water Allocation in the Lake Tahoe Basin (SWRCB Policy). This policy was termed

Draft since both the States of California and Nevada were using the Compact for water allocations within the Lake Tahoe Basin (Baer, 1994; Kennedy/Jenks, 2007). The Compact allocated a maximum of 23,000 AF for use on the California side of the Lake Tahoe Hydrologic Basin, however the SWRCB Policy recommended that the allocation be split between public (State and Federal) and private lands. Of the 23,000 AF allocated for the California side of the Lake Tahoe Hydrologic Basin, 12,100 AFY is recommended for use in the South Lake Tahoe area which is greater than the projected water demand at full build-out. Further information related to water right allocations is presented in Section 4.3.9 of this document.

3.5 **Wastewater Management**

Under the Porter-Cologne Water Quality Control Act all sewerage from within the Lake Tahoe Basin must be collected, treated, and exported outside of the Lake Tahoe Basin. The District is the largest wastewater utility provider for the greater South Lake Tahoe area. This regulation restricts the potential to reuse recycled wastewater to mitigate reductions of stored groundwater should that become necessary.

The District's sewer collection system services an area of approximately 42 square miles and includes the CSLT, USFS LTBMU-managed lands west of the CSLT, and unincorporated area of the County, south of the CSLT (Figure 3-3). The collection system includes 41 pumping station facilities, approximately 314 miles of gravity sewers that range in size from 4 inches to 24 inches in diameter, and approximately 22 miles of force mains that range in size from 2.5 inches to 18 inches in diameter. All sewage from the collection system is conveyed to the District's Wastewater Treatment Plant (WWTP) in South Lake Tahoe. The collected wastewater is treated to a secondary treatment standard and then disinfected with chlorine prior to being pumped out of the Lake Tahoe Basin to Alpine County for irrigation use. The WWTP has a treatment capacity of 7.7 million gallons per day (MGD) for dry-weather (sanitary) wastewater flows. It currently receives and treats approximately 4 MGD during the winter and about 5 MGD during the summer. The WWTP is also equipped to handle wet-weather flows more than 18 MGD that occur during storm events because of inflow and infiltration to the collection system. The export system originates at the WWTP and consists of about 27-miles of dedicated force and gravity pipelines that conveys the disinfected secondary-23 treated wastewater to neighboring Alpine County, where it is temporally stored in a recycled water reservoir before distribution for irrigation reuse.

The total number of connections in the District's sewer collection system is estimated at about 22,130 sewer connections. Of these, at least 18,277 are active, used by sewer customers. The remaining 3,855 sewer connections are inactive. Many of the District's sewer connections are over 40 years old. Less than 10 percent of these connections are less than 10 years old. While a lateral can last 50 to 100 years, its life expectancy is determined by its material, original installation, root intrusion or external pressure, soil stability and chemical makeup, high water tables, corrosion (sometimes from the hydrogen sulfide gas present in the sewer system), and forces leading to structural failure (CSLT, 2014). Because of the potential for leaks, sewer lines are considered a potential source of contamination. The Drinking Source Water Assessment and Protection (DSWAP) Program (CDPH, 2000) also identifies wastewater treatment facilities and conveyance as a potentially contaminating activity (Section 6.4). The District follows the

California State Water Well standards (DWR 1981, 1991) that includes mandatory setbacks of 50 feet from any sewer line.

SECTION 4: LOCAL GOVERNMENTAL AGENCIES AND GROUNDWATER-RELATED PROGRAMS

A key goal of the Alternative Plan is to further expand collaboration with local land use and regulatory agencies for groundwater management and water quality protection in the TVS Subbasin. The following section outlines the existing regulatory agencies and authorities to provide the context in which increased support for sustainable groundwater management can be built.

Groundwater is directly regulated by the GSAs pursuant to SGMA; however, many other agencies play a role in managing the TVS Subbasin by regulating groundwater and surface water, land use, drinking water supply, wells, and stormwater. Coordination of implementation of programs and policies of these agencies has enabled the TVS Subbasin to operate within its sustainable yield and address shared groundwater quality and quantity concerns.

4.1 History of Collaboration and Collaboration Opportunities

This Alternative Plan is updated within the context of an existing, on-going coordination and collaboration with water issues in the South Lake Tahoe area. Many long-established relationships already exist that form the foundation of coordination and collaboration which has expanded to include consideration of groundwater management issues with an emphasis on water quality. A key objective of this Alternative Plan is to continue to build off these existing relationships to further enhance groundwater management and continue to conform with the sustainability goal for the TVS Subbasin. Section 7.2 more fully describes opportunities for collaboration with environmental and land use planning agencies and private well owners.

4.1.1 Potential Collaboration on Groundwater Protection

All water purveyors in the TVS Subbasin have a vested interest in preserving groundwater quality in the TVS Subbasin. The key objectives for the water purveyors are the following:

- Protecting existing water supply infrastructure from groundwater contamination to avoid loss of production capacity and incurring costs of replacing impacted infrastructure;
- Maintaining the water quality of the available groundwater supply in the TVS Subbasin for providing drinking water to the community;
- Preserving potential future production well sites from being impacted by groundwater contamination;
- Sharing information from condition assessments at individual water system wells;
- Promoting best practices for well-head maintenance; and

- Increasing informal communications across agencies.

Historical issues have demonstrated the vulnerability of the aquifer in TVS Subbasin. Relict contamination from historic releases of PCE have impaired drinking water wells within the TVS Subbasin which is believed to be derived from the past use of this solvent at former commercial facilities dating back to the mid 1970's (LRWQCB, 2017). In the 1990s and early 2000s, releases of fuel hydrocarbons and Methyl tert-Butyl Ether (MtBE) from leaking underground tanks at gasoline stations resulted in several of the District's groundwater supply wells having to be taken offline when contamination levels exceeded drinking water standards. Contamination from the past use of both chemicals within the TVS Subbasin has resulted in a loss of the beneficial use of portions of the aquifer and caused water purveyors to incur additional costs for added treatment to remove these contaminants or the replacement of impacted wells.

The LRWQCB and County are the primary agencies for regulating groundwater in the TVS Subbasin and overseeing groundwater remediation. An objective of this Alternative Plan is for the District, EDWA, and water purveyors to continue to work with LRWQCB and the County to better achieve these objectives.

There are several areas for increased collaboration between the LRWQCB, County, District, and other water purveyors to ensure information about identification, site investigations, remediation, site inspections and case closures at groundwater cleanup sites is communicated to the potentially affected water purveyors, and that issues and concerns of the water purveyors is communicated to LRWQCB and County staff. It is anticipated that additional protocols will need to be established to identify who should be contacted in such an event.

4.1.2 **Potential Collaboration on Land Use Planning**

Several agencies have jurisdiction and programs for land use and resource management responsibilities. State law requires that every county and municipality adopt a long-term General Plan that includes seven required elements. Water-related issues are generally addressed directly in the Conservation element. Currently in California, general planning by counties and municipalities, and groundwater and urban water management planning by large water suppliers are the primary means of collaboration between water management and land use planning entities. The following provides a summary of the land use planning agencies for the South Lake Tahoe area.

Land use decisions can have significant effects on groundwater resources, yet coordinated and collaborative land use and groundwater management planning is uncommon. However, the Lake Tahoe region has a rich and complex history of managing land use to protect Lake Tahoe water quality. While source water protection has been an integrated theme in multi-decade, bi-state negotiations, it has received minor attention relative to groundwater quality subjects. There is opportunity to increase understanding of source water issues and to raise the profile of the subject in this region where water quality is the focus of much attention.

Coordination with TRPA on the update of the Regional Plan can better address the needs and issues of water purveyors for groundwater management and protection in the TVS Subbasin. There are other administrative activities that can also be done. For example, the District will provide TRPA with a recharge area map (Figure 6-15) and an updated map of water supply source area protection zones (Figure 6-16) that can be incorporated into the current TRPA planning, permitting and inspection process. Copies of these maps will be provided to the TRPA, County, CSLT, and LRWQCB following final adoption of this Alternative Plan. The USFS is another key agency active in the TVS Subbasin with land use planning and water resources protection. Addition of the USFS to the SAG has provided mutual benefits in the areas of data and information sharing and may provide further benefits in managing groundwater contaminants detected at the Meyers Landfill Site (Section 6.3.1.3).

4.1.3 **Potential Collaboration on Groundwater Quality Monitoring and Management**

All water purveyors have a shared interest in maintaining groundwater quality for all beneficial uses and users of groundwater within the TVS Subbasin. Since adoption of the 2014 GWMP the District has convened an on-going SAG consisting of local members representing collaborating business or government agencies with a demonstrated commitment to protecting groundwater resources. The SAG has met regularly to discuss pertinent groundwater concerns affecting local groundwater resources. Opportunities for increased collaboration regarding groundwater quality monitoring and management include.

- Developing and maintaining a comprehensive water quality database for the TVS Subbasin;
- Sharing of water quality data collected from existing water resource monitoring programs that could supplement the Basin Monitoring Program;
- Considering approaches to monitoring groundwater quality improvements as a metric for evaluating the efficacy of EIP projects;
- Using water quality parameters for evaluation of surface water quality data with groundwater quality data collected from water supply and environmental wells;
- Using existing environmental wells for possible long-term groundwater elevation and potential water quality monitoring in the Basin Monitoring Program;
- Considering use of the South Tahoe Groundwater Model as a foundation for contaminant fate and transport models developed within the TVS Subbasin; and
- Improving processes for notification of unauthorized releases and progress of groundwater clean-up from contamination assessment through corrective action and closure.

4.2

Overlying Jurisdictions

The TVS Subbasin underlies several different jurisdictions as shown on Figure 2-1. These include the CSLT, portions of unincorporated El Dorado County and federal lands managed by the U.S. Forest Service-Lake Tahoe Basin Management Unit (USFS LTBMU). The Nevada portion of the physical basin underlies a portion of the Cities of Stateline, Kingsbury, and Zephyr Cove-Round Hill Village. The Nevada jurisdictions are not included in this Alternative Plan.

4.3

Regulatory Agencies

The following section provides a summary of agencies involved in groundwater protection in the TVS Subbasin. These agencies include agencies directly involved in surface and groundwater regulation as well as those with land use authority impacting use of groundwater and sustainability of the TVS Subbasin.

Table 4-1 provides a summary of the many different agencies with jurisdictions and regulatory oversight related to groundwater quality, hazardous materials management, and land use management in the TVS Subbasin. The following discussion provides a summary of the roles and responsibilities for the various agencies that are relevant for managing and protecting groundwater in the TVS Subbasin.

Table 4-1. List of Groundwater Related Governmental Agencies in the South Lake Tahoe Area.

Agency	Geographic Jurisdiction	Surface Water Quality	Ground Water Quality	Drinking Water	Land Use	Hazardous Materials
US EPA	Nationwide and some programs in California (CA)	Clean Water Act (CWA)	Underground Injection Control (UIC)	Safe Drinking Water Act (SDWA)	--	TSCA, CERCLA
Federal Water Master	CA and Nevada (NV) within the Truckee River Basin, including Lake Tahoe Basin	--	--	Truckee River Operating Agreement (TROA)	--	--
Tahoe Regional Planning Agency (TRPA)	CA and NV within the Lake Tahoe Basin	Lake Tahoe Water Quality Management Plan under Section 208 of CWA and TRPA Regional Plan		--	TRPA Regional Plan and associated Storm water BMP Handbook	
State Water Resources Control Board (SWRCB)	CA Statewide	With RWQCBs regulates discharges to surface water and groundwater statewide under CWA ¹ and Porter Cologne Water Quality Control Act (WQCA). Waste Discharges that can be exempted from California Code of Regulation Requirements (CCRs) are regulated by		DDW ² - SDWA for large water systems	--	Brownfields and Land Disposal Program

Agency	Geographic Jurisdiction	Surface Water Quality	Ground Water Quality	Drinking Water	Land Use	Hazardous Materials
		the Waste Discharge Requirements (WDRs) Program.				
Lahontan Regional Water Quality Control Board (LRWQCB)	Lahontan Region including CA portion of Lake Tahoe Basin	Basin Plan ³ /TM DL and Lake Tahoe Municipal Storm water Permit	Basin Plan, Underground Storage Tank (UST), Site cleanup Program,	--	--	
County Environmental Health Department	County portion of Lake Tahoe Basin	--	Water Well Program	SDWA for small water systems Water Well Program	County General Plan outside of City limits	CUPA, Hazardous waste/material generator permits
City of South Lake Tahoe (CSLT)	Within City Limits	Complies with Lake Tahoe Municipal Storm water Permit	--	--	City General Plan	--
US Forest Service – LTBMU	National Forest Lands in CA and NV within the Lake Tahoe Basin	Land and Resource Management Plan	Proposed Groundwater Directive FSM 2560	--	Land and Resource Management Plan	--
EI Dorado County Water Agency	Portion of the TVS Subbasin outside the District's boundaries	--	EI Dorado County Water Agency Act Water Resources Development and Management Plan	EI Dorado County Water Agency Act Water Resources Development and Management Plan	--	--
South Tahoe Public Utility District	Portion of the TVS Subbasin inside the District's boundaries	--	Water Code §§ 10723 and 10753(a) Alternative Plan for TVS Subbasin	Water Code §§ 10723 and 10753(a) Alternative Plan for TVS Subbasin	Water Code §§ 10723 and 10753(a) Alternative Plan for TVS Subbasin	--

Notes:

- (1) SWRCB/RWQCB has primacy to implement much of CWA regulatory activity
- (2) SWRCB –Division of Drinking Water (DDW, formerly CDPH), the County is a Local Primacy Agency under contract to DDW for regulating small public water systems.
- (3) Basin Plan implements, for the Lahontan Region, state and federal laws including CWA, Porter Cologne WQCA, SDWA, and other hazardous material laws by setting water quality standards

4.3.1 Groundwater Sustainability Agencies

SGMA created a new structure for managing California’s groundwater resources at the local level. SGMA required GSAs to form in the State’s high- and medium-priority basins and subbasins by June 30, 2017. (Wat. Code § 10724(b)(2).) Local agencies are expected to

collaborate and coordinate GSA formation on a basin-wide scale to sustainably manage groundwater at a local level. A GSA may be formed by a single local agency or a combination of local agencies by using a joint powers agreement, a memorandum of agreement, or other legal agreement. (Wat. Code § 10723.6)

After formation, GSAs are tasked with development and implementation of GSPs or Alternatives to sustainably manage local groundwater resources and avoid six undesirable results. (Wat. Code § 10727.2; *see* 10721(u), (v), (x).) The planning deadline for an existing GWMP to be submitted as a GSP Alternative was January 1, 2017. (Wat. Code § 10733.6(c).)

The TVS Subbasin lies entirely within the County, and largely within the jurisdiction of the District. As discussed in Section 1.1.2, the District is the exclusive GSA within its jurisdiction but cooperates with EDWA to implement the Alternative Plan outside of the District's Jurisdiction (Section 1.1.2.3). The development and approval processes for this first five-year update of the Alternative Plan is described in Section 7.4 of this document.

4.3.2 **State Water Resources Control Board and Lahontan Regional Water Quality Control Board**

The primary responsibility for the protection of groundwater quality in California rests with the SWRCB and nine Regional Water Quality Control Boards. The SWRCB sets statewide policy for the implementation of federal and state laws and regulations. The Regional Water Quality Control Boards adopt and implement Water Quality Control Plans which recognize regional differences in natural water quality, actual and potential beneficial uses, and water quality problems associated with human activities. Chapter 5 of the Water Quality Control Plan for the Lahontan Region (Basin Plan), entitled "Water Quality Standards and Control Measures for the Lake Tahoe Basin", (CRWQCB, 1995) is the primary regional water quality planning document in the California portion of Lake Tahoe and is also the basis for regulation by the LRWQCB.

Chapter 5 of the Basin Plan establishes beneficial uses and water quality objectives of both surface water bodies and groundwater basins. It also outlines implementation programs such as control and enforcement action and describes current monitoring activities. Programs used to implement Basin Plan objectives include waste discharge prohibitions; spills, leaks, investigations, and cleanups; storm water, erosion, and sedimentation control measures; wastewater treatment, disposal, and reclamation measures; oversight of land disposal of solid and liquid waste; groundwater protection and management; Total Maximum Daily Loads (TMDLs); and other measures related to specific resource uses and development activities.

As described in the Basin Plan, the beneficial uses of groundwater in the TVS Subbasin are designated as municipal, industrial, and agricultural. Ground waters designated as municipal shall not contain concentrations of chemical constituents more than the MCL or SMCL based upon drinking water standards specified in Title 22 of the California Code of Regulations.

The enforcement of groundwater cleanup is primarily conducted through two LRWQCB programs in the TVS Subbasin, the Underground Storage Tank (UST) Program and the Site Cleanup Program (SCP). The UST Program addresses the potential for, and cleanup of,

groundwater contamination from leaking tanks (primarily at gasoline stations). The Low-Threat UST Case Closure Policy (LTCP) allows contamination to remain in place at time of closure of petroleum UST sites if LTCP criteria are met or is otherwise appropriate for closure based on a site-specific analysis.

The UST Program includes the following four program elements:

- Leak Prevention - The Leak Prevention Program element includes requirements for tank installation, construction, testing, leak detection, spill containment, and overflow protection (SWRCB responsibility; also see County responsibility under Certified Unified Program Agency (CUPA) in Section 4.3.3).
- Cleanup - Cleanup of leaking tanks often involves a soil and groundwater investigation and remediation, under the direction of a regulatory agency (Joint LRWQCB/County responsibility).
- Enforcement - The SWRCB UST Enforcement Unit aids local agencies enforcing UST requirements.
- Tank Tester Licensing - Tank integrity testing is required by law, must meet the requirements of the State Water Resources Control Board, and must be conducted by State-licensed tank testers (SWRCB responsibility).

Special programs also reside within the SWRCB's UST Cleanup Fund for a variety of situations involving underground storage tanks. These include the Comingled Plume Account; Emergency, Abandoned, and Recalcitrant Account; Removing, Replacing, or Upgrading USTs; and the Orphan Site Cleanup Fund.

The SCP regulates and oversees the investigation and cleanup of "non-federally owned" sites where recent or historical unauthorized releases of pollutants to the environment have occurred. The types of pollutants are varied and include solvents, pesticides, heavy metals, fuel constituents, etc. The LRWQCB oversees the investigation and remediation of pollution to ensure the dischargers cleanup and abate the effects of discharges to promote attainment of either background water quality, or the best water quality which is reasonable if background levels of water quality cannot be restored. Important SWRCB and LRWQCB policies used to protect groundwater resources include:

- SWRCB Resolution No. 68-16: Statement with Respect to Maintaining High Quality Water.
- SWRCB Resolution No. 92-49: Policies and Procedures for Investigation and Cleanup and Abatement of Discharges under Water Code Section 13304.
- SWRCB Resolution No. 2012-0016: Low Threat UST Case Closure Policy, adopted in November 2012.

The SWRCB Division of Drinking Water (DDW) classifies water systems based on the number of connections and whether the users are full time residents or short-term users. The Drinking Water Program is responsible for enforcing the federal and state Safe Drinking Water Acts. The main responsibilities are to: (1) issue permits to drinking water systems, (2) inspect water systems, (3) monitor drinking water quality, (4) set and enforce drinking water standards and requirements, and (5) award infrastructure loans and grants.

DDW Field Operation Branches are responsible for the enforcement of the federal and California Safe Drinking Water Acts and the regulatory oversight of public water supply systems. Water purveyors are required to submit regular water quality analysis data to DDW as part of the Consumer Confidence Reporting Requirements.

4.3.3 **El Dorado County**

The land area within the TVS Subbasin that is located outside of the City of South Lake Tahoe is located within the County. As a result, land use regulation outside of the City of South Lake Tahoe is shared by the County and TRPA. The County's General Plan regarding land area in the South Lake Tahoe area emphasizes coordination with TRPA and other state and federal agencies with land use jurisdiction in the TV Basin (Policies 2.10.1.1 through 5, Measure LU-O). The County's General Plan also requires buffers to be established around future water supplies (Policy 2.2.5.14).

The County Environmental Management Department (EDCEMD) is organized into five department units. The Environmental Health Department is responsible for regulating domestic wells and small water systems within the TVS Subbasin.

The Water Well Program is conducted to protect the health, safety, and general welfare of the people of the County by ensuring that the groundwater will not be impacted. Since 1990, this program has required permits for the construction, destruction, deepening, and repair of a water well. Well drillers are required to follow the California Water Well Standards (i.e., Bulletin 74-81 and supplements). EDCEMD staff reviews permit applications submitted by Licensed Well Drillers for setback and development issues and conducts inspections, as needed, on specific parcels prior to permit approval, during the placement of the annular seal, and at any other time deemed necessary. Well completion reports are required to be submitted within 60 days of well completion and are reviewed prior to issuing the final of the well permit.

The Small Water System Program permits, inspects, and monitors small public water systems. A small water system is a system for the provision of piped water to the public for human consumption that serves at least five, but not more than fourteen, service connections and does not regularly serve drinking water to more than an average of 25 individuals daily for more than 60 days of the year (CA Health and Safety Code §116275(n)). The County is the Local Primacy Agency, under contract with the DDW, to perform the program requirements that are specified in State and Federal Regulations. The purpose of the program is to ensure that small water systems deliver safe, adequate, and dependable potable water. Environmental Health reviews new applications and changes of ownership to verify that the system will be able to meet technical, managerial, and financial capabilities.

The County Hazardous Materials Department is responsible for implementing the hazardous materials and household hazardous waste programs to ensure that hazardous materials and hazardous waste are properly managed. EDCEMD, Hazardous Waste Division is also typically the lead agency for responding to hazardous waste issues. The objective of the Hazardous Materials Program is to protect human health and the environment by ensuring that hazardous materials and hazardous waste are properly managed. The Hazardous Materials Department meets this objective through permit and inspection processes, as well as public education programs.

The Hazardous Materials Program is approved by California Environmental Protection Agency as the CUPA for the County. The Unified Program is intended to provide relief to businesses complying with the overlapping and sometimes conflicting requirements of formerly independently managed programs. The CUPA Program includes the following:

- California Accidental Release Prevention Program
- UST Program
- Above ground Petroleum Storage Act Requirements for Spill Prevention, Control and Countermeasure Plans
- Hazardous Waste Generator and Onsite Hazardous Waste Treatment Programs, which has five tiers of permitting, including submittal of Hazardous Materials Business Plan, consisting of Hazardous Materials Release Response Plans and Hazardous Waste Contingency Plan and associated inspections.
- California Uniform Fire Code: Hazardous Material Management Plans and Hazardous Material Inventory Statements
- The County Hazardous Materials Emergency Response Program works in close cooperation with law enforcement, fire and allied health agency officers and staff. Special attention is given to the hazardous materials used and transported frequently in the county by local businesses.

4.3.4 **El Dorado Water Agency**

The Eldorado Water Agency (EDWA) was established in 1959 under the El Dorado County Water Agency Act to ensure that the County has adequate water supplies now and in the future. To meet its directive, EDWA is authorized to

- Be a political and corporate body
- Exercise authorized power and legal actions necessary for providing sufficient water for any present or future beneficial use, or for uses of the environment or inhabitants within EDWA

- Construct, operate, and maintain works to develop hydroelectric energy as a means of assisting in financing the construction, operation, and maintenance of its projects for the control, conservation, diversion, and transmission of water and to enter into contracts for the sale of such energy. Such energy may be marketed only at wholesale rates to any public agency or private entity engaged in the sale or use of electric energy, or to the federal or state government.
- Control the flood and stormwaters of EDWA and the flood and stormwaters of streams that have their sources outside of EDWA, which streams, and floodwaters flow into the agency, and to conserve such waters for beneficial and useful purposes
- Store, conserve, reclaim, appropriate, and import water; and prevent interference of water sources and prevent contamination/pollution
- Conduct water resources investigations and studies
- Sell, lease, or transfer water within/outside the County
- Cooperate with other federal, state, and local agencies to carry out EDWA's powers (<https://www.edwateragency.org/about-water-agency>).

In 2019, EDWA completed its Water Resources Development and Management Plan (WRDMP). The WRDMP provides a foundation to identify resource management strategies to counter the threats to the County, including droughts, wildfires, deteriorated headwaters, limited groundwater resources, and fragmented water management. The WRDMP identified seven water resource management challenges (C) along with eleven resource management strategies (RMS) grouped into five water agency implementation programs to address these challenges (EDWA, 2019).

Long-term water supply demand imbalance (C1), vulnerability during drought (C2) and limited groundwater resources (C6) are water-resource related challenges addressed under WRDMP Section 4.3 RMS3- Implement Sustainable Groundwater Management. Under RMS 3, two actions are identified in collaboration with the District (as Principal Implementing Agencies): RMS 3a. Implement sustainable groundwater management consistent with SGMA for major groundwater basins; and RMS 3b. Engage in the development of statewide sustainable groundwater management policies, regulations, and legislation related to the preservation of El Dorado County interests. Under these actions, EDWA serves in a facilitating role coordinating the development and implementation of this draft Alternative Plan and coordinating consistent messages and engagement approach with the District and other groundwater users in the County. EDWA also plays a supporting role in communications, information sharing and advocacy efforts (EDWA, 2019).

Long-term water supply demand imbalance (C1), vulnerability during drought (C2), water quality impacts due to stormwater runoff (C5), limited groundwater resources (C6) and vulnerability to flooding (C7) are addressed under WRDMP Section 4.10 RMS10- Prevent Contamination of Surface Water and Groundwater Resources. Under RMS 10, District

collaboration opportunities include: RMS 10b Implement Sewage System Management Plans in coordination with system owners including emergency response protocols and vulnerability assessment; and RMS 10e Conduct public outreach and education activities to encourage prevention of water supply contamination. Under RMS 10b EDWA serves in a facilitating role to coordinate with the County and water purveyors to identify vulnerable sewage lines with high risk of contaminating surface water or groundwater resources and in a supporting role in terms of communications, information sharing and advocacy efforts. Under RMS 10e, EDWA serves in supporting role in terms of communications, information sharing and advocacy efforts (EDWA, 2019).

To advance RMS and actions presented in Section 4.0 of the WRDMP, EDWA created five implementation programs including Governance and Partnership, Water Security, Watershed Management, Assistance and Innovation, and Communication and Advocacy. The Governance and Partnership Program focuses on how EDWA will function throughout implementation of the WRDMP in creating benefits for the entire County. The Water Security Program is focused ongoing water supply and demand gap analysis, water supply development, drought protection and response, developing stormwater as a resource, flood management, and water quality. The Watershed Management Program focuses on areas of headwater management, water quality management for rural and agricultural communities, and habitat and other ecosystem function enhancement. The Assistance and Innovation Program's purpose is to encourage the development and use of innovative ideas in water planning and management, as well as provide technical and educational assistance to other entities involved in RMS and action development and implementation. The Communication and Advocacy Program focuses on public information, countywide communications, and federal and state advocacy related to water resource issues and management (EDWA, 2019).

4.3.5 South Tahoe Public Utility District

In 1999, the District adopted a policy to not supply drinking water containing detectable concentrations of Methyl tert-butyl ether (MtBE) to its customers (STPUD, 2004). MtBE has a primary and secondary MCL of 13 and 5 micrograms per liter (UG/L), respectively. The District's MtBE policy is a self-imposed policy applicable only to the District and is not related to a state regulatory drinking water standard. This policy requires that any District well producing groundwater at a level of 0.5 UG/L of MtBE be placed on increased observation and testing to determine if the initial measurement is an anomaly. If the concentration of MtBE in the well continues to increase or average greater than 0.5 UG/L the District's Board determines appropriate management actions. These actions have included suspending production from the public water supply wells or adding wellhead treatment to remove MtBE below detectable levels. Because of the implementation of the District's MtBE policy, areas of degraded groundwater quality at levels below MCLs, have affected groundwater supplies in the TVS Subbasin.

In December 2000, the District enacted Ordinance No. 477-00 adding Division 7 to the Administrative Code. The ordinance was developed for the purposes of regulating, managing, conserving, and protecting local groundwater resources. A primary focus of Ordinance No. 477-00 was to establish a Basin Monitoring Program to provide a means for the early detection and immediate response to the release of petroleum products into groundwater, and

development of management plans to prevent or minimize the impact of contamination from possible contaminating activities.

Ordinance No. 477-00 was updated concurrently with the development of the 2014 GWMP. The updated ordinance (Ordinance No. 558-14) provided the District with an additional enforcement mechanism to protect the District’s beneficial use of the aquifer and the water supply infrastructure. The District, however, must first look to the regulatory authority of LRWQCB and County CUPA before exercising its own enforcement powers under the ordinance. SGMA provides separate powers to the District as a GSA. Another key modification reduced the prescriptive monitoring requirements included in the original ordinance.

On April 21, 2022, the District adopted Ordinance No. 580-22, which removed the Groundwater Management Ordinance from the District’s Administrative Code. The District’s Administrative Code includes topics relating to the District’s provision of services to customers. Groundwater and supply management are beyond the scope of direct services to customers, though they are connected. Moreover, SGMA grants GSAs authority to manage groundwater, making the Groundwater Management Ordinance redundant with the Alternative Plan. Although the Alternative Plan is not codified in the District’s Administrative Code, the Alternative Plan will continue to guide the District’s efforts to manage groundwater within the TVS Subbasin. Copies of the most recent Groundwater Management Ordinance No. 558-14 and Ordinance No. 580-22, removing the ordinance from the District’s Administrative Code, are included in Appendix E.

4.3.6 **Tahoe Regional Planning Agency (TRPA)**

All land surrounding Lake Tahoe, including the City of South Lake Tahoe, the County and the District’s service area, falls under the jurisdiction of the TRPA as defined in the Tahoe Regional Planning Compact (Compact) created in 1969. The Compact requires that all local jurisdiction planning be consistent with a series of environmental thresholds. Under the Compact, environmental thresholds are environmental standards necessary to maintain significant scenic, recreational, educational, scientific, or natural values of the region or to maintain public health and safety within the region, including but not limited to standards for air quality, water quality, soil conservation, vegetation preservation, and noise. The 2012 Regional Plan defines thresholds as “environmental standards for the region” which “indirectly define the capacity of the region to accommodate additional development” (TRPA, 2012). TRPA was granted the authority to adopt and implement environmental threshold carrying capacities for the entire Lake Tahoe Basin through the development and enforcement of a regional plan and ordinances. It is generally acknowledged that the TRPA Environmental Thresholds effectively provide a growth control mechanism for Lake Tahoe area.

Within the Lake Tahoe Basin, local land use planning has considered regional water issues for decades under the jurisdiction of the TRPA. The basic framework for review and approval of activities in the Lake Tahoe area is established by the following TRPA documents:

- The Tahoe Regional Planning Agency Bi-State Compact
- The Lake Tahoe Water Quality Management Plan (208 Plan),

- The TRPA Regional Plan Goals and Policies which includes
 - Environmental threshold carrying capacities for nine resource areas, including water quality
 - Best Management Practices (BMP) Handbook for storm water infiltration and hazardous material management
 - Environmental Improvement Plan (EIP)
 - Other regional-scale plans and reference documents
 - Plans for specific geographic areas within the region
 - TRPA Code of Ordinances
 - TRPA programs
 - TRPA Rules of Procedure and
 - Other administrative manuals.

The 208 Plan was updated by the TRPA in 2012, mandated by the CWA, and describes the framework for water quality management in the entire Lake Tahoe Basin, the desired water quality outcomes, and the methods to achieve those outcomes. The 208 Plan incorporates, by reference, many documents by local, state, and federal agencies including the TRPA Regional Plan and Regional Plan Environmental Impact Statement, LRWQCB Basin Plan, USFS LTBMU Land and Resource Management Plan, and General Plans for the CSLT and the County.

The 208 Plan includes regulatory protections and restoration of SEZs that provide significant filtering of nutrients and sediment. The BMP Handbook of the Regional Plan describes methods to help developed properties to function more like natural, undisturbed forest and meadowland. By implementing BMPs, property owners can help slow the loss of lake clarity. Owners of developed properties must ensure BMPs remain functional and effective to retain their BMP Certificate and comply with the TRPA Code of Ordinances. If BMPs are not functioning effectively due to property owner's failure to inspect, maintain, and monitor them, a BMP Certificate may be revoked by TRPA.

The Tahoe Regional Plan describes the needs and goals and of the Lake Tahoe Region provides statements of policy to guide decision making as it affects the Region's resources and remaining capacities. Chapter 2 Land Use Element presents land use goals and policies to ensure the desired equilibrium between the natural and manmade environments and attain and maintain the environmental thresholds within a specific time schedule. Environmental thresholds define the capacity of the natural environment and set specific environmental performance standards related to land use. However, environmental thresholds do not define the maximum buildout, densities, permitted uses, or other land use criteria for the manmade environment, which are provided in the Regional Plan. Land use goals that may affect water demands include Goal LU-2 which direct the amount and location of new land uses in conformance with the environmental

threshold carrying capacities and the other goals of the Tahoe Regional Planning agency bi-state compact. Under this goal Policy LU-2.1 development is limited using an allocation of development rights for residential, tourist accommodation, commercial, recreation, public service, and resource management categories (TRPA, 2012). Under Policy LU-2.9, development is further restricted by limiting allowable impervious land coverage associated with new development. Policy LU-2.10 caps allowed land coverage for all new projects based on land capability. All of these policies limit growth in the TVS Subbasin and are in alignment with the water demand projections presented in Section 3.4 and the projected water budgets presented in Section 5.4.8 of this Alternative Plan.

4.3.7 **City of South Lake Tahoe**

Land use regulation within the CSLT is shared by the City and TRPA. The CSLT General Plan (adopted 2011) contains many mutually adopted policies. In addition to coordination with TRPA, coordination with the District and other water providers is highlighted in the CSLT General Plan (Goal PQP-2 and Policies PQP-2.2, 2.5, and 2.7). Other CSLT land use policies in the CSLT General Plan related to protection of water quality include protection of the groundwater basin from overdraft and contamination (Policy PQP-2.9), protection of Lake Tahoe and other surface water streams from storm water pollution through storm water management (Goals PQP-4 and NCR-2, and Policies PQP-4.1 through 4.3, NCR2.1 through 2.5, NCR-2.13 and NCR-2.14), considerations of snow removal practices (Policy PQP-11.8), and protection and restoration of SEZs and floodplains (Goal HS-4, Policies HS-4.1, 4.2, and 4.4, NCR-2.9 and NCR-2.12). The CSLT is also a co-permittee to the Municipal NPDES Permit to reduce pollutants in storm water.

Incorporated in 1965, the CSLT is the most populous city in the Lake Tahoe Basin and the second most populous city in the County. The city extends about 5 miles west-southwest along U.S. Highway 50, also known as Lake Tahoe Boulevard. The east end of the city extends to the California-Nevada state line. The western end of the city is mainly residential, and clusters around "the Y", the Y-shaped intersection of U.S. Highway 50 and California State Route 89. The city extends about 3 miles north - south along State Route 89 from about 1 mile south of the south shore of Lake Tahoe to immediately south of the Lake Tahoe Airport. As a popular tourist destination and resort community, the economy of CSLT is largely dependent upon tourism and accompanying service industries, which fluctuates seasonally. Water service to the CSLT is provided by the District, TKWC, LBWC, and LPA.

The CSLT is organized around two primary functions: government and city services. City services include Development Services and Public Works. Development services include the Planning Division which is responsible for current and long-range planning activities which implement the CSLT General Plan. Current planning activities include reviewing and permitting development activities to ensure new development and redevelopment projects are consistent with the CSLT General Plan, Plan Area Statements, and Title 6, Development Services, of the South Lake Tahoe City Code. Public works include the Engineering Division which is responsible for safeguarding life, health, property, and public welfare through review, design, bid and construction of public improvement projects constructed on City property and within the City's right-of-way. The Engineering Division includes the City's Stormwater Management Program which works to control and reduce the discharge of fine sediment, nutrients, and other

pollutants from private lands and City streets and facilities into streams and beaches along the Lake Tahoe shoreline. The Stormwater Management Program is regulated under City Code Chapter 7.15, referred to as the City's Stormwater Ordinance. The City Manager is responsible for administration, implementation, and enforcement of the Stormwater Ordinance.

4.3.8 **United States Forest Service**

The portions of national forest lands that overlie the TVS Subbasin are managed by the U.S. Forest Service, Lake Tahoe Basin Management Unit (USFS LTBMU). Most of the managed lands of the USFS LTBMU are located outside of the TVS Subbasin, but USFS LTBMU jurisdiction includes large areas around the Camp Richardson/Fallen Leaf Lake area within the northwest portion of the TVS Subbasin and along the basin margins on the eastern side of the TVS Subbasin (Figure 2-1). As the USFS LTBMU, TRPA, and LRWQCB share the same planning area, these agencies cooperate with each other.

In 2016, the USFS LTBMU established the Land Management Plan (LMP) to create planning consistency within the portions of the National Forests that lie within the Lake Tahoe Basin. The management goal of the Basin Plan is to restore or maintain the health of the land, to promote a sustainable flow of uses, benefits, products, services, and visitor opportunities. The LMP has identified several desired conditions related to watershed resilience, stream channel geomorphic processes, and physical and chemical attributes of SEZs, as well as surface and ground water levels, groundwater recharge and discharge, and attenuation of peak flows. Among the relevant goals of the LMP are to preserve clarity in Lake Tahoe by maintaining or improving water quality, soil function, riparian areas, stream process to reduce erosion, and sustained aquatic habitats including for Lahontan cutthroat trout.

Any individual or entity other than the USFS must have a special use authorization to develop water wells or construct water pipelines on USFS lands. The Technical Guide to Managing Ground Water Resources (USFS, 2007) provides guidance for the authorization of water wells or injection wells and water pipelines. A permitting process for wells and pipelines is discretionary; a permit may be denied if the analysis indicates an adverse impact to the forest natural resources. The applicants must evaluate other reasonable alternatives before the USFS authorizes new or increased groundwater pumping on National Forest lands.

The USFS has an established Groundwater Management Program to maintain and enhance groundwater fed streams, springs, wells, and wetlands, which support healthy watersheds and communities. USFS works in partnership with local communities, states, and others to preserve these resources. FSM 2880 Geologic Resources, Hazards, and Services provides guidance on Forest management activities including developing geologic resources and groundwater dependent ecosystem within the floodplains and wetlands, identifying recharge areas and geologic and geomorphic factors influencing watershed function, and monitoring the cumulative effect of management activities on groundwater resources (USFS, 2008). The Technical Guide to Managing Ground Water Resources (USFS, 2007) also provides guidance on the National Forest groundwater policy in Land Management Planning, water development, water quality, groundwater dependent ecosystems, inventory and monitoring, data management, and partnership with other local, state, and federal agencies and tribes.

Within the TVS Subbasin, groundwater management at USFS LTBMU generally involves gathering information on water rights and water uses to populate the USFS Water Rights & Use Geospatial Database, assessing impacts to surface water resources from groundwater use, identifying and assessing of GDEs; determining water needs for watershed health and ecosystem sustainability, identifying surface water source and protection zones; and investigating groundwater contamination from the Meyers Landfill. The USFS LTBMU assesses potential impacts from groundwater pumping to surface water resources within one mile of the forest service boundary. When considering permits for new wells on USFS lands, USFS LTBMU requires applicants to consider alternative supply sources outside USFS boundaries. Other groundwater concerns involve development along stream courses, the impact of shallow wells (<50 feet depth) on surface waters and transferring riparian rights to groundwater.

4.3.9 **TROA: Office of the Federal Watermaster**

The interstate waters of the Lake Tahoe and Truckee River Basins have been the subject of dispute, controversy, and litigation for well over a century. These conflicts have been resolved through federal legislation, the 1990 Truckee-Carson-Pyramid Lake Water Rights Settlement Act (Settlement Act) (Pub. Law 101-618), and a negotiated agreement known as the Truckee River Operating Agreement (TROA). The Federal Water Master has primary responsibility for operating the Truckee River reservoir system and is responsible for the administration of TROA.

The Settlement Act provides for the permanent allocation of water between the States of California and Nevada in the Lake Tahoe, Truckee River, and Carson River Basins. For the Lake Tahoe Basin, the Settlement Act provides that the total gross diversions for use within the basin in the State of California, from all natural sources, including groundwater, and under all water rights shall not exceed 23,000 AFY. Of this amount, the SWRCB recommended allocation of 12,100 AF of water rights for South Tahoe Zone C (SWRCB, 1979). With the implementation of TROA on December 1, 2015, the interstate allocations under the Settlement Act for the Lake Tahoe, Truckee River, and Carson River Basins took effect. The SWRCB administers water rights actions in California assuring that surface water use is consistent with the Settlement Act and TROA.

The District filed for rights to divert surface water from Lake Tahoe under TROA for a total of 12,100 AFY. In January 2020, the District submitted a water demand analysis to the SWRCB Division of Water Rights in support of its water rights application (see Section 3.4). Estimated total annual water production requirements from this analysis for each of the four largest community water systems and other individual water users within the TVS Subbasin is 10,808 AFY (Table 3-8). The District's permit application for surface water rights is under review by the SWRCB and are therefore not currently regarded as a supply source in this Alternative Plan.

4.3.10 **Tahoe Resource Conservation District**

In 1974, the Tahoe Resource Conservation District (Tahoe RCD) was established under Division 9 of the California Public Resources Code and is a non-regulatory, grant-funded, local agency that works in the Lake Tahoe Basin. Current programs at Tahoe RCD focus on

stormwater management, aquatic invasive species control and prevention, land management, forestry, and conservation landscaping initiatives.

Tahoe RCD manages the Regional Stormwater Monitoring Program (RSWMP) and maintains a current network of 12 stormwater monitoring sites and 6 weather stations distributed around the perimeter of Lake Tahoe. Collected water quality samples are analyzed for fine sediment particles (FSP), Total Nitrogen (TN) and total phosphorus (TP). Automated samplers are used to collect stormwater quality samples and monitor continuous flow and selected weather data (precipitation, temperature). The collected data are analyzed for status (precipitation amounts, runoff volumes, and pollutant loads for a given water year) and trends to compare year-to-year changes in annual volumes and pollutant loads. Currently, Tahoe RCD dataset includes 6–7 water years of stormwater monitoring data. Data is reported annually to LRWQCB and Nevada Division of Environmental Protection.

4.4 **Regulatory Programs and Policies**

The following section describes a selection of programs and policies involved in groundwater protection in the TVS Subbasin. These programs and policies involve regulating surface and groundwater as well as land use impacting use of groundwater and sustainability of the TVS Subbasin.

4.4.1 **Urban Water Management Plan**

The Urban Water Management Act (Act) became part of the California Water Code with the passage of Assembly Bill 797 during the 1983–1984 regular session of the California Legislature. The California Water Code requires every urban water supplier providing water for municipal purposes either directly or indirectly to more than 3,000 customers or supplying more than 3,000 acre-feet of water annually to adopt and submit an UWMP every five years to DWR. The specific planning requirements are detailed in California Water Code Division 6, Part 2.6 Urban Water Management Planning. Subsequent legislation has been passed that updates and provides for additional requirements for UWMPs and water management. Senate Bill (SB) X7-7 Water Conservation calls for the state to achieve a 20 percent reduction in urban per capita water use by December 31, 2020, a requirement known as 20x2020. These mandates are incorporated into the 2015 UWMP requirements. In summary, the UWMP must include the baseline demand analysis, water use target analysis use for 2015 and 2020, and present a compliance plan to achieve the target demand reductions in the UWMP.

Recommended Action 3 suggested that the different future water demand projections between the 2014 GWMP and Alternative Materials and the District's 2015 UWMP be reconciled (DWR, 2019). DWR also recommended that the reconciled water demand projections be incorporated into the projected water budgets used in each document.

To satisfy Recommended Action 3, both this first five-year update of the Alternative Plan and the District's 2020 UWMP use the same County 50-year population growth rate (0.37%) as a basis for projecting future water demands (see Section 3.1). In addition, projected total supplies and supply/shortfall estimates provided in the 2020 UWMP are calculated using the same minimum threshold for groundwater storage (-32,050 AF) as presented in Section 8.1.2. The

storage threshold represents the total amount of groundwater available for groundwater extraction within the TVS Subbasin, without any undesirable results. As differences in Alternative Plan and UWMP reporting requirements (water year versus calendar year) and the periods used for projecting total water use (50-year versus 20-year) exist, projected future water demands presented in the 2020 UWMP differ from the projected water demands presented in this document.

4.4.2 **Lake Tahoe TMDL**

A large portion of water quality regulation in the Lake Tahoe Region is targeted at improving the clarity of Lake Tahoe which has impaired status under Water Code Section 303(d). LRWQCB leads Lake Tahoe TMDL implementation efforts by coordinating local government storm water treatment and erosion control projects, facilitating stream channel restoration work, and overseeing forest management practices. The LRWQCB is working closely with the TRPA to implement its Regional Plan and associated Environmental Improvement Program. In partnership with the Nevada Division of Environmental Protection (NDEP), the LRWQCB has developed a detailed TMDL accounting, tracking, and reporting program that provides for regular TMDL progress assessment and adaptive management. This information is provided through the Lake Clarity Tracker which is the central hub for information related to the Lake Tahoe TMDL Program (<https://clarity.laketahoeinfo.org/>).

The Basin Plan (LRWQCB, 1995) and TRPA Code of Ordinances (TRPA, 1987) provide several water quality standards and control measures to protect the beneficial uses of surface and groundwater. Previously, LRWQCB set maximum concentration limits for runoff discharged to infiltration systems. Amendments to the Basin Plan, including Basin Plan Section 5.6, describe the differing storm water treatment requirements for municipal and public roadways and new development, redevelopment, and existing development projects.

Other efforts to reduce potential contamination sources for Lake Tahoe clarity in many cases also reduce potential sources for groundwater contamination as well. For example, wastewater, which constitutes the largest potential source of nutrients, has been treated and exported out of the Lake Tahoe watershed since the 1960s. There are, however, other potential man-made chemical contaminants from uncontrolled releases from storage that are important to manage to preserve groundwater quality. Further integration of groundwater into the existing programs to protect surface waters can provide improved groundwater protection in the TVS Subbasin.

4.4.3 **Stormwater Management and Monitoring**

The LRWQCB has the obligation to implement and enforce the Lake Tahoe TMDL through NPDES storm water discharge permits issued to California governmental entities (CSLT, the County, and the California Department of Transportation). Efforts to improve lake clarity have included implementation of nonpoint source pollution BMPs for storm water management focused on reducing potential contamination sources.

Storm water management includes on-site infiltration. Infiltration to groundwater can be beneficial by providing additional recharge but may also provide a conduit for contaminants to

reach groundwater. The benefit from storm water management BMPs is to limit pollutants to storm water as well as to groundwater through source control, inspections, and other measures.

Both the LRWQCB and TRPA include vertical separation requirements for constructing infiltration basins to protect groundwater beneficial uses. The Basin Plan requires five feet of separation between the highest anticipated groundwater level and the bottom of an infiltration system. The TRPA recommends 12 inches between the bottom of dry wells and seasonal high groundwater. This requirement is set given the potentially higher risk of groundwater contamination in areas with high groundwater underlying infiltration basins.

The LRWQCB adopted the revised storm water municipal NPDES Permit (Board Order No. R6T-2010-1010) (Municipal Permit) for co-permittees that include the County and the CSLT. The Municipal Permit, which is consistent with the TRPA Regional Plan, includes particle number and mass-based load reduction requirements in accordance with the Lake Tahoe TMDL Implementation Schedule. The Municipal Permit required the submittal of a Storm Water Management Plan which describes a clear process to expand existing storm water related activities into a program that incorporates a minimum of twelve components.

Storm water for the California Department of Transportation (Caltrans) is regulated under statewide storm water permit Order No. 2012-0011-DWQ issued by the SWRCB. Caltrans is responsible for reducing sediments and nutrients by managing erosion and storm water runoff along US 50 and SR 89 under the TMDL. Caltrans has several erosion/sediment control projects underway to meet the TMDL as well as ongoing operations and maintenance work including street sweeping and abrasive management.

Storm water monitoring to evaluate the effectiveness of sediment and load reduction is conducted regionally in both California and Nevada by the Tahoe RCD (Section 4.3.10). The Tahoe RCD Regional Stormwater Monitoring Program represents eight agencies to fulfill NPDES permit requirements.

The Underground Injection Control regulations under the US EPA address the subsurface disposal of fluids through drains, pipes, and other constructed conveyances that are intended to permanently infiltrate water below ground surface. Drywells, unlined sumps, seepage pits, and infiltration galleries are some of the terms used to describe the subcategory of injection wells known as shallow Class V injection for non-hazardous fluids. EPA acknowledges that storm water wells can be a community asset or liability (USEPA, 2002).

4.4.4 **Environmental Improvement Program – Stream and Wetland Restoration**

In 1996, in advance of the 1997 Lake Tahoe Summit,⁷ an interagency Environmental Improvement Program (EIP) was initiated to improve watersheds and water quality, forest health, transportation, and sustainable recreation. As part of the effort, numerous projects have been completed, including stormwater management and erosion control, installation of wetland

⁷ The Lake Tahoe Summit is a bi-state summit bringing together elected officials, policy makers, federal agencies, the private sector, and local community leaders from California and Nevada to collaboratively address environmental problems facing the Lake Tahoe Basin.

treatments systems, stream restoration, preservation of open space, and retrofitting of properties with erosion control Best Management Practices (BMPs) to enhance watersheds and water quality.

TRPA is responsible for the development and administration of the EIP. Under TRPA Code of Ordinances, Chapter 15: Environmental Improvement Program, the EIP is defined as a process for identifying and implementing threshold improvements. Tools used in the process include the TRPA Code of Ordinances, capital improvement planning, programs, studies, a monitoring and tracking system, and a finance plan. The capital improvement component of the EIP identifies physical project needs related to adopted thresholds. Other needs are identified as continuing programs that typically require resources beyond a physical improvement project or require a long period of time to implement. Other needs also include studies to improve knowledge regarding threshold attainment.

The Lake Tahoe EIP Project Tracker provides public access to data showing the locations and status of EIP Projects in the Lake Tahoe Hydrologic Basin since 2007 (<https://eip.laketahoeinfo.org/>). These projects have been implemented through several lead implementer agencies including CSLT, El Dorado County, CTC, USFS LTBMU and others.

EIP Projects are assigned to a focus area, program, and action priority. While some projects have multiple benefits and thus could fit under various action priorities, for reporting purposes TRPA assigns each project to one action priority. Within the TVS Subbasin, EIP projects are predominantly assigned to the watersheds and water quality focus area and are implemented through the following EIP programs: stormwater management, watershed restoration, or aquatic invasive species. Review of the EIP project list by watershed shows a total of one hundred eighty-two (182) EIP projects within the seven priority watersheds situated within the South Lake Tahoe area. Most of these projects are located within the Trout Creek and Upper Truckee River Watersheds (Table 4-2). For detailed descriptions of these projects the reader is referred to EIP Project Tracker.

The Upper Truckee River is the largest watershed overlying the TVS Subbasin (Figure 2-11). River and floodplain restoration strategies have involved several techniques, but most aim to restore natural hydrologic processes and improve water quality by increasing floodplain connectivity, especially in meadows. This has been accomplished through channel reconstruction, placement of in-channel structures and biotechnical bank treatments and raising channel bed elevation and/or construction of new channels with lower bank heights, decreased overall channel capacity, and increased roughness to increase overbank flows.

Table 4-2. EIP projects by watershed in the South Lake Tahoe Area, as of January 31, 2022 (<https://www.laketahoeinfo.org/Watershed/Index>).

WATERSHED	NUMBER OF PROJECTS
Bijou Creek	15
Bijou Park	21

Camp Richardson	17
Tallac Creek	6
Taylor Creek	11
Trout Creek	29
Upper Truckee River	83
TOTAL	182

4.4.5 **Integrated Regional Water Management Planning**

Another activity with potential relevance to the Alternative Plan is the Tahoe-Sierra Integrated Regional Water Management (IRWM) Plan which defines a vision for the management of water resources in the IRWM Region. The IRWM Region is an area that extends from the Carson River watershed to the south to the Truckee River watershed to the north including the Lake Tahoe Basin. The IRWM Plan highlights important actions needed to accomplish a broad vision through the year 2035 planning horizon and is a planning tool that provides a framework to address the major water-related challenges facing the IRWM Region.

The updated IRWM Plan was completed in summer 2014 and was developed through the time and contributions of more than 30 water supply, wastewater treatment, land use management, public interest, and ecosystem-focused organizations with interests in the water resources of the IRWM Region.

The IRWM Plan process provides another venue for collaboration with other local water districts, land use planning and regulatory agencies in the area, and provides an opportunity developing and funding projects to support groundwater management.

4.5 **Analysis of Limits Imposed by Existing Water Resources Monitoring and Management Programs**

The TVS Subbasin is situated within the Lake Tahoe Basin Hydrologic Region. Water within the Lake Tahoe Basin is shared between California and Nevada. The TROA implements a federal settlement agreement that provides for allocation of the interstate waters of the Lake Tahoe and Truckee River Basins between California and Nevada (Section 4.3.9). Under TROA, California’s total annual allocation from surface and groundwater sources within the Lake Tahoe Basin is 23,000 AFY (DWR, 2019). As the TVS Subbasin is situated within the Lake Tahoe Basin, the total annual allocation of 23,000 AFY for the California portion of the Lake Tahoe Basin provides an upper limit on the total annual amount of groundwater that can be pumped from the TVS Subbasin.

In 2020, the District submitted a water demand analysis to DWR in support of its pending water rights applications estimating an estimated total annual water production requirement

10,808 AFY for all users of groundwater for drinking water purposes in the TVS Subbasin (Kennedy Jenks, 2020).

The future annual water demand requirements for the TKWC, LBWC and LPA water systems from the water demand analysis (Kennedy Jenks, 2020) were considered as future maximums in the projected pumping rates used in the 50-year water budgets developed for the TVS Subbasin. Applying the 50-year projected growth rate for the County, the projected pumping rate for the District increased above the estimated future maximum from the water demand analysis (8,410 AFY) to 10,128 AFY. The sum of the 50-year projected annual pumping rates used in the 50-year water budgets total 11,709 AFY which is slightly more than 50% of the total annual allocation for the California portion of the Lake Tahoe Basin.

As indicated in Section 3.5, over the past twenty years (2000–2020) the District has exported on average about 5,425 AFY of treated recycled water from the TVS Subbasin to Alpine County for agricultural reuse. Export of this recycled water is equal to more than half of the water pumped from within the TVS Subbasin on an annual basis. Because the Porter Cologne Water Quality Act restricts the reuse of recycled water in the Lake Tahoe Basin, groundwater replenishment projects utilizing recycled water are not possible within the TVS Subbasin.

The primary responsibility for the protection of groundwater quality in the TVS Subbasin is the LRWQCB (Section 4.3.2). LRWQCB implements water quality standards consistent with the beneficial uses of groundwater as described in the Basin Plan. Under the Basin Plan, groundwaters designated as municipal shall not contain concentrations of chemical constituents exceeding the MCL or SMCL based upon drinking water standards specified in the Title 22 of the California Code of Regulations. Under the Antidegradation Policy, continued maintenance of existing high-quality waters is required whenever the existing quality of water is better than the quality of water established in the Basin Plan. Drinking water standards, however, often serve as objectives for groundwater clean-up sites within the TVS Subbasin.

In response to groundwater quality concerns related to MtBE groundwater contamination and water quality impairments of its drinking water wells, the District's Board of Directors adopted a policy in 1999 prohibiting the supply of drinking water containing detectable levels of MtBE to its customers (Section 4.3.5). Detectable levels for MtBE are more than an order of magnitude lower than MCL and SMCL concentrations for this contaminant. The MtBE Policy was subsequently reviewed and readopted by the District Board of Directors in 2003 and 2012. Under this policy, wells with detectable levels of MtBE undergo increased observation and testing. If MtBE detections are confirmed, the District removes the impacted well from service using all reasonably available alternatives rather than continuing use of that well as a groundwater source (District, 2003).

Relict MtBE groundwater contamination is still detected in shallow environmental wells within the TVS Subbasin (Table 6-5). There are also clean-up sites which LRWQCB has closed with levels of MtBE groundwater contamination above MCLs (Table 6-6), highlighting differences between clean-up standards employed by the LRWQCB and the limits imposed by the Districts MtBE Policy on the use of impaired drinking water wells within the TVS Subbasin.

There are no other water resource monitoring or management programs that would limit the setting of measurable objectives to define quantifiable goals or minimum thresholds to define undesirable results for the TVS Subbasin.

SECTION 5: STATE OF THE GROUNDWATER BASIN

This section describes the recent data used to assess current conditions of the TVS Subbasin and the historical and baseline conditions of groundwater in the TVS Subbasin.

5.1 Background

The Alternative Plan is largely based on the South Tahoe Groundwater Model constructed and calibrated to match historical (WY 1985 – WY 2019) conditions. Following calibration, the model was run into the future to simulate projected groundwater conditions. Projected groundwater conditions are largely dependent on future climate conditions. Both precipitation and temperature strongly affect recharge and evapotranspiration – two primary components of the groundwater budget. Because of uncertainty associated with climate projections, multiple future scenarios were assessed to ensure that simulations would cover a range of potential conditions. Future conditions and the impacts of climate change on the TVS Subbasin are discussed in detail in Section 5.7.

5.1.1 **South Tahoe Groundwater Model**

The South Tahoe Groundwater Model (STGM) was originally developed by the Desert Research Institute (DRI) (Carroll, et al., 2016a; Carroll, et al., 2016b; Pohll, et al., 2018) to address BMOs identified in the 2014 GWMP and Alternative Materials. For use in this first five-year update of the Alternative Plan, it has been updated to include more recent years (WY 1983 - WY 2019) of the historical record and to extend predictive modeling scenarios further into the future (WY 2020 – WY 2099). The model is used to quantify the TVS Subbasin conditions and is based on the U.S. Geological Survey (USGS) Newton-Rhapson formulation for MODFLOW-2005, referred to as MODFLOW-NWT (Niswonger et al., 2011) software. MODFLOW-NWT relies on an unstructured, asymmetric matrix solver to calculate groundwater head. MODFLOW-NWT is specifically designed to work with the Upstream Weighting Package to solve complex, unconfined groundwater flow simulations to maintain numerical stability during the wetting and drying of model cells.

The model grid is oriented north-south and contains 342 rows and 251 columns. Horizontal cell size is 100 meters (328 feet) and is based on the need to capture steep topography, narrow canyons, and potentially steep hydrologic gradients. The model is subdivided into four subsurface layers to maintain reasonable computation time. Layers are determined based on production well screen intervals. Land surface elevations are based on 30-meter (98 feet) Digital Elevation Model (DEM) aggregated to a 100-meter (328 feet) spatial resolution. Layer thicknesses are 40 meters (131 feet) for layer one and layer two, and 100 meters (328 feet) for layer three. Layer four bottom elevation is set to a constant 1,600 meters (5,248 feet) to produce variable thickness ranging from approximately 114 meters (274 feet) along the northern boundary with Lake Tahoe to 1,300 meters (4,264 feet) at watershed divides.

The model grid (i.e., model domain) covers an area of 99,907 acres commensurate with the South Lake Tahoe area (Figure 2-11). For ease of reporting the model domain is differentiated into two spatial zones (Zone 1 and Zone 10). Zone 1, referred to as the Mountain Block, covers an area of 85,093 acres encompassing the surrounding watersheds outside the TVS

Subbasin within the South Lake Tahoe area (Section 2.6.1). Zone 10 covers an area of 14,814 acres encompassing the TVS Subbasin as delineated by DWR within the South Lake Tahoe area. Organization of the model domain into spatial zones allows for comparison and reporting of discrete water budgets (including changes of groundwater in storage) for the model domain (Zone 1 + Zone 10), the Mountain Block (Zone 1) and the TVS Subbasin (Zone 10). Reporting of water budgets specifically for the TVS Subbasin rather than the surrounding watershed area inclusive of the TVS Subbasin was a Recommended Action identified by DWR for this first five-year update of the Alternative Plan (see Section 1.3).

The STGM simulates three (3) distinct time periods. The first period (pre-1983) represents steady-state conditions prior to any significant groundwater production in the basin. Hydraulic conductivity was calibrated using the steady-state model configuration. A transient historic model simulates the second period (1983–2019) to calculate changes in groundwater levels and flux due to variations in climate and groundwater extractions. For the the third period (2020–2099), a series of predictive models simulate 2020 to 2099 to test the effects of a variety of potential future climate conditions and the potential for increased future groundwater extractions due to an increasing population.

A second model was developed to simulate surface and subsurface hydrologic processes for the entire Lake Tahoe Basin and was used to calculate rates of groundwater recharge for input into the Modular Groundwater Flow Model (MODFLOW). This model was developed by the DRI as part of a U.S. Department of Interior study looking at the historical and future water supply in the Truckee River Basin. The DRI model uses the numeric code Groundwater and Surface Water Flow (GSFLOW) (Markstrom et al., 2008), which combines the USGS Precipitation-Runoff Modeling System (PRMS) (Leavesley et al., 2005) with the MODFLOW (Harbaugh 2005; Niswonger et al., 2011). GSFLOW estimates energy and water budget partitioning to account for flow within and between the plant canopy and soil zone, streams, and the groundwater. GSFLOW is also used to understand effects of climate change on the hydrology of mountain catchments to Lake Tahoe. This model is generally referred to as the GSFLOW Regional Model (GSFRM).

For calculations of recharge, the GSFRM is parameterized from the National Elevation Dataset, State Soil Geographic soils database, and USGS land use land cover (LULC) dataset. The depth of the root or soil zone is determined by the LULC for each 300-meter grid. Five categories of LULC are used in each 300-meter grid-cell based on dominant vegetation category: bare soils, grasses, shrubs, trees, or water. The GSFRM simulates transient conditions from 1980 to 2015. A two-year warm-up period is used to remove the influence of initial conditions. Daily weather data from four Snow Telemetry sites (Echo Peak, Fallen Leaf Lake, Hagans Meadow and Heavenly Valley) are used to drive the model in the region of the TVS Subbasin. While stations give point climate, Parameter-elevation Regressions on Independent Slopes Model (PRISM Climate Group, 2016) data are used to distribute precipitation spatially over the entire basin. The four climate stations within the basin capture the gradient in precipitation from the west to the east side of the basin. This gradient is especially visible in wet and dry years, when the east side receives far less precipitation compared to the west side in dry years. A series of predictive models, each simulating a 33-year period, was also developed to generate spatial and temporal recharge rates and distributions assuming potential future climate conditions including increasing temperatures and both increasing and decreasing precipitation rates.

The GSFRM was not updated alongside the STGM. Instead, a regression developed by Carroll, et al., (2016) was used to estimate recharge rates and distributions through the year 2019. Similarly, mean recharge rates and distributions from the 33-year GSFRM climate scenarios were used to estimate predictive recharge rates for the TVS Subbasin groundwater predictive models for 2020 to 2099. The methods used to extend these simulations, along with other modifications made to improve the model as tool for assessing groundwater conditions in the TVS Subbasin, are provided in more detail in a Technical Memo (Rybarski and Hausner, 2021) provided in Appendix I of this document.

5.1.2 Identification of Data Gaps/Uncertainty

The primary data gaps revolve around projections of future climate change. Climate change scenarios in this effort are based on a suite of ten Global Climate Models (GCMs) identified by the California DWR Climate Change Technical Advisory Group as representative of future conditions in the Sierra Nevada (DWR 2015). Temperature increases across all these GCMs. Although the magnitude and rate of the projected temperature increase varies from model to model, the trend is consistent. Projected precipitation, however, is not consistent across those models, and even the direction of change (i.e., increasing or decreasing over time) varies from GCM to GCM. The uncertainty attached to precipitation requires a wide range of modeled scenarios to bracket potential climate effects, greatly complicating the planning process.

Groundwater modeling indicates that climate affects simulated groundwater levels as much as or more than simulated pumping does. In the north part of the TVS Subbasin, simulated groundwater heads match the stage of Lake Tahoe (incorporated into the model as a specified head boundary condition based on the climate scenario). In the higher elevation south part of the TVS Subbasin, groundwater heads are determined by the recharge, which is again prescribed in the model based on the climate scenario. These phenomena underscore the need for better constrained climate projections.

Since the inception of the previous model, a new suite of simulations has been released as part of the World Climate Research Program's Coupled Model Intercomparison Project (Eyring et al. 2018). These updated models may be able to better constrain the uncertainty surrounding future climate conditions in the Tahoe Basin – especially precipitation. Because the STGM relies on an existing model of the entire Tahoe Basin to provide boundary conditions under future climate scenarios, improved climate scenarios would require a revised Tahoe Basin model. This larger model is written in GSFLOW, a USGS product that integrates surface and subsurface processes. Such a model is needed to realistically simulate the effects of climate on groundwater recharge. As more certain climate projections become available, a revised GSFLOW model of the entire Lake Tahoe Hydrologic Basin will be needed to reassess recharge under the more constrained climate scenarios.

An additional source of uncertainty that should be addressed in future updates of the Alternative Plan centers on water quality. There is known PCE contamination stemming from former commercial sites at the South Y that has affected several production wells within the South Lake Tahoe subarea of the TVS Subbasin. Potential source areas for this contamination are presently being investigated by the LRWQCB (Section 6.3.1.1). Recent information indicates the presence of Per- and Polyfluoroalkyl Substances (PFAS) in groundwater within the TVS

Subbasin (Section 6.3.2.2). Other emerging contaminants such as microplastics have also been found in both the snowpack (Davidson et al. 2019) and surface waters (Collins et al. 2019) in the Tahoe Basin, and it is not clear whether these contaminants may be present in groundwater. Additionally, there are natural contaminants (arsenic, iron, manganese, and uranium) in the local groundwater that threaten the viability of several production wells within the TVS Subbasin (Section 6.2). Continuing to rely on groundwater for potable use likely requires consideration of new information on the occurrence of each of these substances in future updates of the Alternative Plan.

Recent fires in the Lake Tahoe basin (Gondola (2002), Angora (2007) and Caldor (2021) Fires) raise concerns about the effects of fire on groundwater recharge. After burning, soils often become hydrophobic for time, meaning that the soil repels water. This hydrophobicity leads to increased runoff and erosion, and a concurrent reduction in infiltration and groundwater recharge. Reported magnitudes and durations of decreased infiltration are highly variable (Robichaud 2000), with reported infiltration reductions ranging from 10% to 85% (Burch et al. 1989; Martin and Moody 2001) and effects lasting from months to years after burning (Huffman et al 2001). The length and severity of the annual fire season is projected to increase significantly over the 21st century (Flannigan et al 2012). In addition to infiltration reductions, wildfires have been reported to significantly increase concentrations of polycyclic aromatic hydrocarbons (PAHs) – carcinogenic organic contaminants produced during combustion – in shallow groundwater following wildfire (Mansilha et al 2014). The effects that recent and future wildfires may have on groundwater quantity and quality within the basin is largely unknown.

Groundwater simulations indicate that some groundwater dependent ecosystems in the northern part of the basin may be affected by pumping over the next ten years. Additional analysis is needed to better understand the spatial extent of interaction between groundwater pumping and these GDEs, and to formulate a management plan, as needed, to mitigate potential impacts.

5.2 **Groundwater Conditions**

The following section presents a description of current and historical groundwater conditions based on groundwater level data collected through the District’s groundwater monitoring program (Section 9). Groundwater flow information (Section 5.2.2) and water budget values (Section 5.4) were derived from complex hydrologic analysis conducted using the STGM (Section 5.1.1). Hydraulic parameters presented in this section were derived from aquifer tests performed on District wells which were also used during preparation of the STGM. All data provided in this section include data from January 1, 2015, to current conditions based on the best available data. Groundwater quality within the TVS Subbasin is discussed in Section 6.

5.2.1 **Groundwater Level History**

Groundwater level data is measured semi-annually by the District in 47 wells that are located in the TVS Subbasin (Section 9.1.2.2). The District well network includes 32 observation wells and 15 community water system wells. Most of the community water system wells are active and are used for public drinking water supply

Locations of selected wells for which hydrographs are provided are shown in Figure 5-1. As described in Section 2.5, WBZs are informal designations using geographically based subarea designations (Christmas Valley (CVZ), Meyers (MZ), Angora (AZ), South Lake Tahoe (SLTZ), Tahoe Keys (TKZ) and Bijou (BZ)).

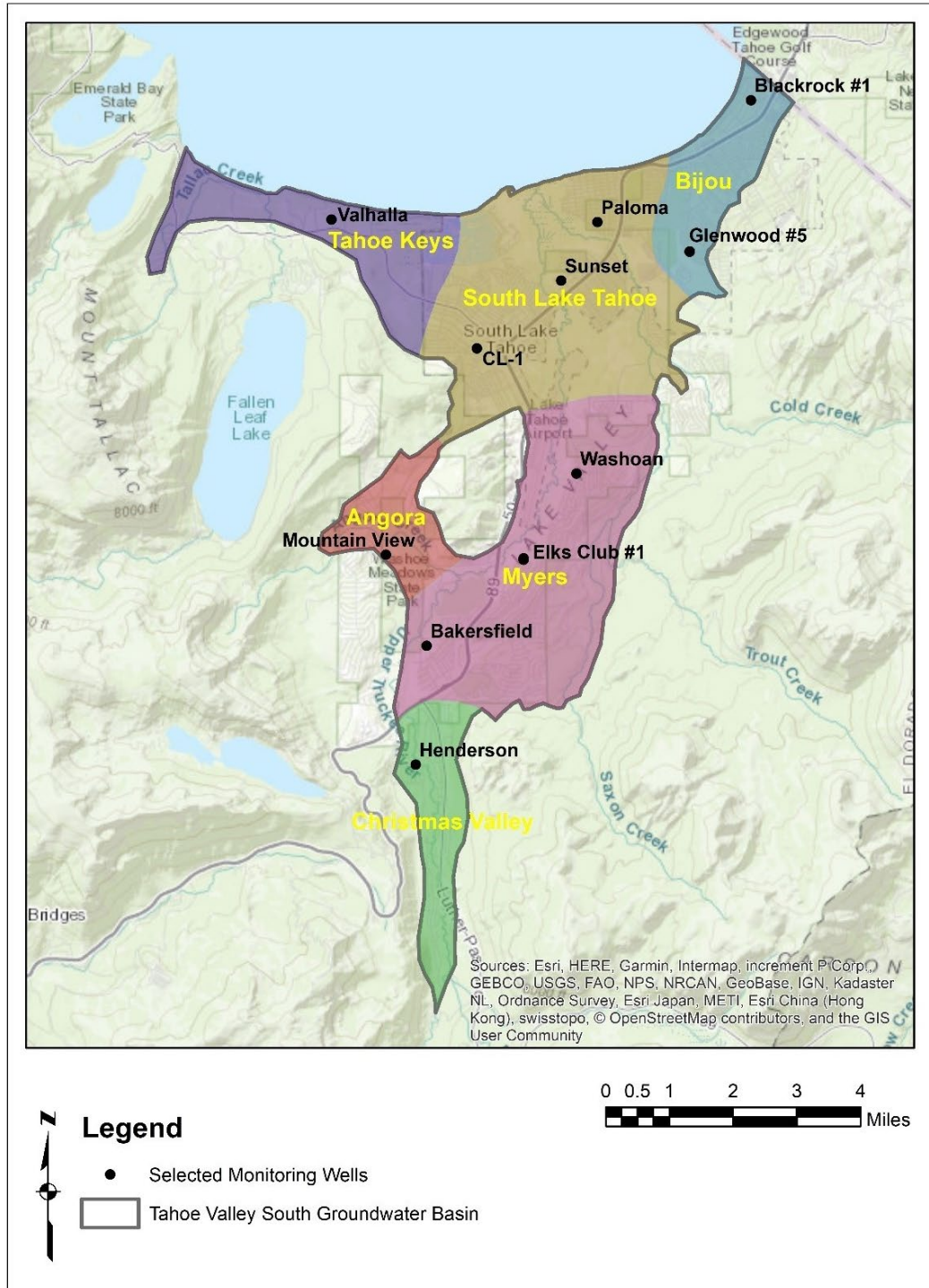


Figure 5-1. Selected monitoring well locations and geographic sub-area designations.

The District collects semi-annual measurements timed to coincide with seasonal low (November) and high (May) groundwater elevations and continuous readings daily from selected wells using dedicated water-level monitoring equipment. Figure 5-2 to Figure 5-7 present hydrographs for wells within each of the six subareas for the period 2000 to 2020 based on semi-annual hand readings. These semi-annual readings are collected over a two-day period to coordinate with water operations and allow production wells to be turned off for a minimum 12-hour recovery period prior to measurement. The descriptions below provide a brief interpretation of the water-level changes.

The District has one well in its basin monitoring network situated within the Tahoe Keys subarea. The Valhalla Well is an active water supply well-constructed to a depth of 190 feet below groundwater surface (BGS) and produces water from TKZ4. Static water levels from this well are typically collected following a minimum 12-hour recovery time, except for the May 2007 reading, which shows a pumping water level (6,161.81 feet AMSL) recorded at a well pumping rate of 700 GPM. With this pumping water level reading removed, groundwater elevations typically range from 6,210 to 6,235 feet AMSL (Figure 5-2), though groundwater elevations increased substantially during the very wet water year in 2017. This well is located 1,600 feet from Lake Tahoe but does not show a significant correlation with the Lake Tahoe stage (Figure 5-2). This is consistent with the slow recovery behavior of this well following pumping. The static water levels collected from this well indicate that water levels in this area are stable.

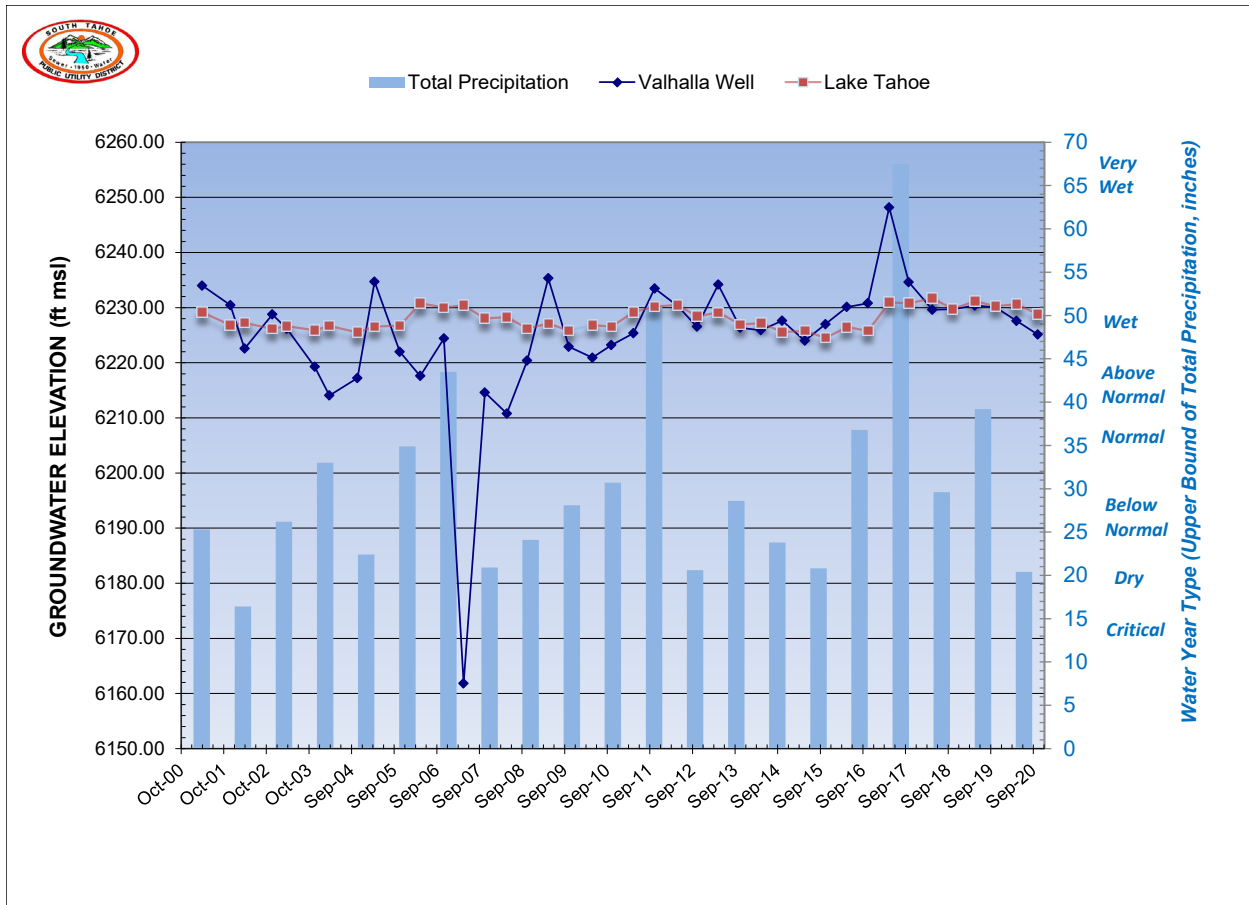


Figure 5-2. Groundwater hydrograph for the Valhalla Well (6,257 feet AMSL) within the Tahoe Keys sub-area. Also shown is the water level (stage) of Lake Tahoe measured at USGS 10337000.

Two types of groundwater level behavior are found in the Bijou subarea. The Blackrock Well #1 is a single observation well (converted from an inactive water supply well) constructed to a depth of 180 feet BGS and is screened through BZ4. Static water levels in this well are stable, typically rising slightly above ground surface elevation (6,240 feet AMSL) as shown in Figure 5-3). The Glenwood Well #3 is a single observation well (converted from an inactive water supply well) constructed to a depth of 192 feet BGS and is also screened through BZ4. This well is situated within 50 feet of the Glenwood Well #5, an active water supply well producing water from BZ3 and BZ4. The District uses the Glenwood Well #3 to monitor groundwater levels near the pumping well. In 2007, the District restricted pumping from the Glenwood Well #5 from late May through November in order to sustain production from BZ3 and BZ4. The water level response in the Glenwood Well #3 shows that this change in operation has been successful in allowing groundwater levels to recover to sustainable levels. Neither of the wells in the Bijou subarea responds to Lake Tahoe water levels. Regardless, these wells do not exhibit a long-term downward trend.

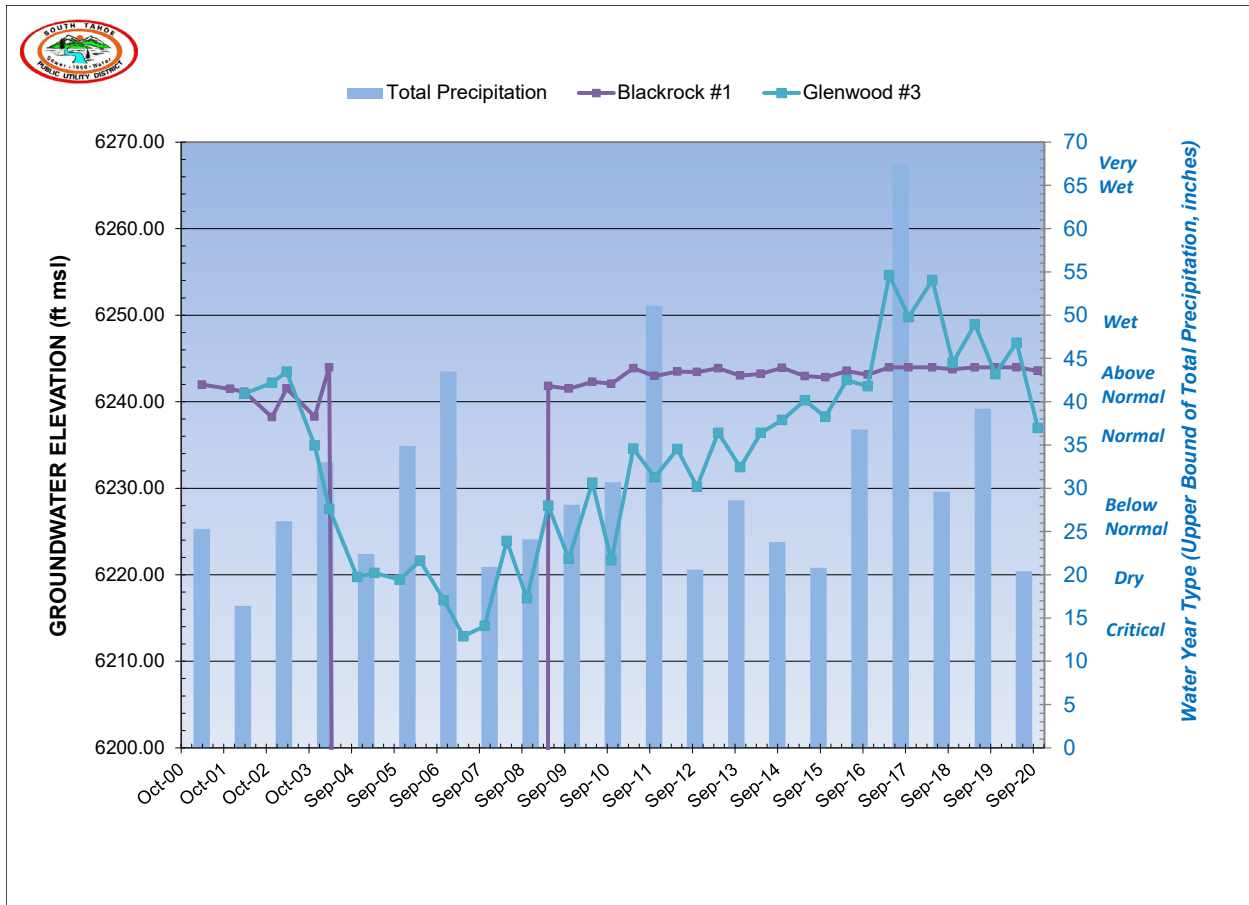


Figure 5-3. Groundwater hydrograph for the Blackrock #1 (6,241 feet AMSL) and Glenwood #3 (6,260 feet AMSL) wells within the Bijou sub-area.

All three monitoring wells within the South Tahoe subarea exhibit relatively stable water levels (Figure 5-4). The CL-1 Well is a single observation well constructed to a depth of 115 feet BGS and is screened through SLTZ5. This well was constructed to monitor water levels in the neighboring Clement Well (offline since 1999). Water levels in the CL-1 Well generally range in elevation from 6,242 to 6,250 feet AMSL in response to seasonal changes in groundwater levels with no long-term trend. The Sunset Well is an active water supply well constructed to a depth of 440 feet BGS and produces water from SLTZ2 and SLTZ3. Static water levels from this well are typically collected following a minimum 12-hour recovery time. Water levels in the Sunset Well generally range in elevation from 6,219 to 6,234 feet AMSL in strong correlation with pumping rates (not shown in Figure 5-4). The Paloma Well is an active water supply well constructed to a depth of 418 feet BGS and produces water from SLTZ2 and SLTZ3. Likewise, the Paloma Well has water levels varying from 6,216 to 6,226 feet AMSL in concert with pumping rates. None of the wells exhibit a long-term downward trend.

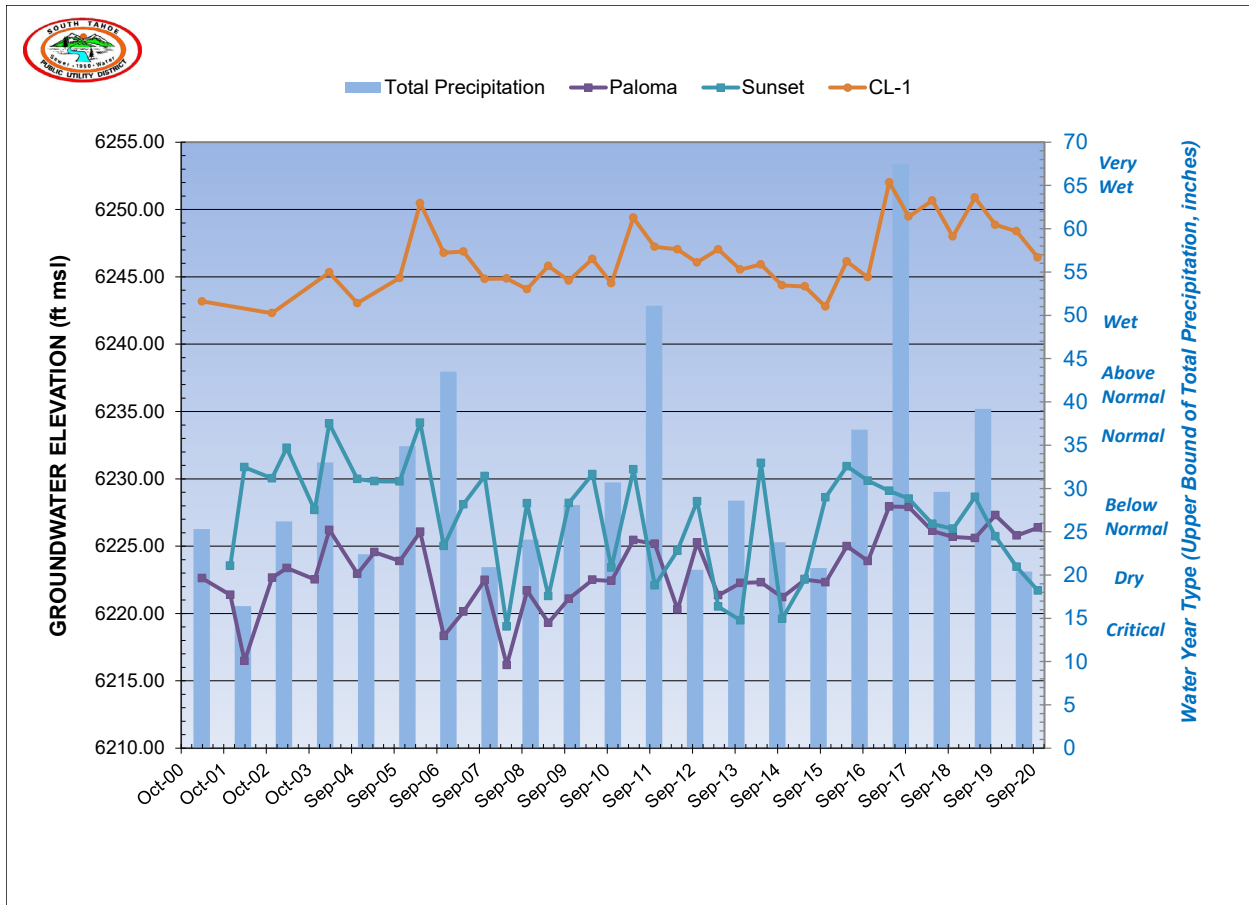


Figure 5-4. Groundwater hydrograph for the Paloma (6,267 feet AMSL); Sunset (6,249 feet AMSL) and CL-1 (6,279 feet AMSL) wells in the South Lake Tahoe sub-area.

The Mountain View Well within the Angora subarea is a single observation well (converted from an inactive artesian water supply well) constructed to a depth of 250 feet BGS and is screened through AZ1 and AZ2. Static water levels in this well are stable, typically rising slightly above ground surface elevation (6,313 feet AMSL) and flowing through an artesian overflow pipe to an adjoining meadow (Figure 5-5). In 2011, the Mountain View Well was removed from service and is now used as an observation well. Manual discharge measurements indicate that artesian flow measured from the overflow pipe peaked in November 2011 at about 43 gallons per minute (GPM) and has steadily declined to less than 10 GPM. Decline in artesian flow from this well is believed to be related to the accumulation of fill inhibiting groundwater flow through the perforated interval near the bottom of this well.

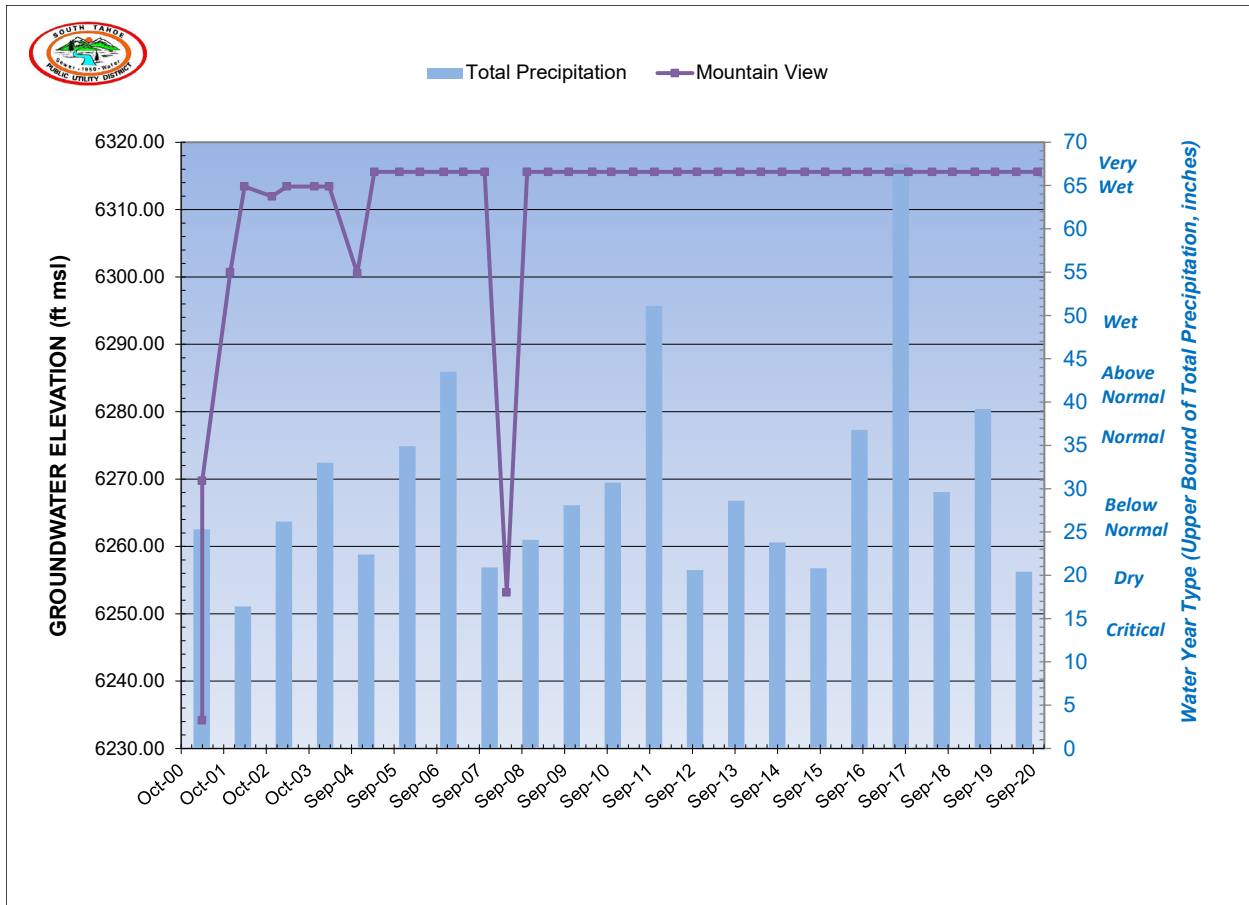


Figure 5-5. Groundwater hydrograph for the Mountain View (6,313 feet AMSL) well (artesian flowing well) in the Angora sub-area.

Groundwater levels within the Meyers subarea are generally stable with short periods of declining water levels due to increased pumping rates (Figure 5-6). The Bakersfield Well is an active water supply well constructed to a depth of 330 feet BGS and produces water from MZ3 and MZ4. Static water levels from this well are typically collected following a minimum 12-hour recovery time except for the May 2008 reading which is a pumping water level (6,239 feet AMSL) recorded at a well pumping rate of 1,500 GPM. With this pumping water level reading removed, groundwater elevations typically range between 6,278 to 6,289 feet AMSL. The Washoan Well is a single observation well constructed to a depth of 275 feet BGS and is screened through SLTZ1, SLTZ2, SLTZ3 and SLTZ4. Groundwater levels in this well are influenced by pumping of the Airport Well, which is evident in the initial static readings collected in 2001. The November 2015 water-level measurement is believed to be an errant reading. With these anomalous readings removed groundwater elevations typically range between 6,266 to 6,273 feet AMSL. The Elks Club Well #1 is a single observation well (converted from an inactive water supply well) constructed to a depth of 168 feet BGS and is screened through MZ4. This well is situated within 100 feet of the Elks Club Well # 2, an active water supply well producing water from MZ3 and MZ4. The District uses the Elks Club Well #1 to monitor groundwater levels near the pumping well (Elks Club Well #2). The Elks Club Well #2 replaced the Elks Club Well #1 as a production well in 2004. Using static water level readings

collected after 2004, groundwater levels range from 6,265 to 6,275 feet AMSL (average of 6,271 feet AMSL). None of these wells exhibit a long-term downward trend.

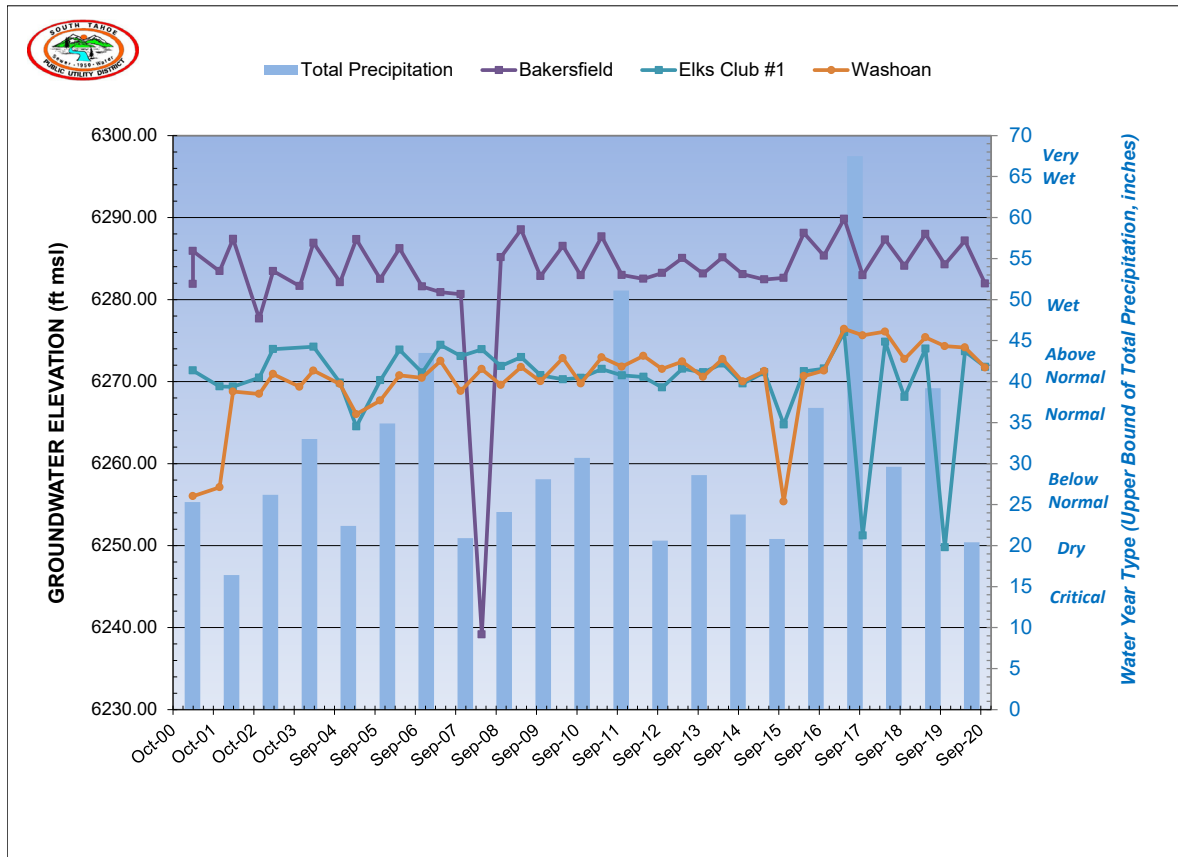


Figure 5-6. Groundwater hydrograph for the Bakersfield (6,311 feet AMSL); Elks Club #1 (6,283 feet AMSL) and Washoan (6,308 feet AMSL) wells in the Meyers sub-area.

The Henderson Well within the Christmas Valley subarea is a single observation well, constructed to a depth of 210 feet BGS. The Henderson Well is screened across CVZ3 and CVZ4, which are also used for water production at the South Upper Truckee Well #3. Water levels in the Henderson Well generally range in elevation from 6,242 to 6,252 feet AMSL with peaks in the spring when pumping is at a minimum and troughs in the fall following the peak summer pumping season (Figure 5-7). No long-term downward trend in water levels was observed in WBZs within this subarea.

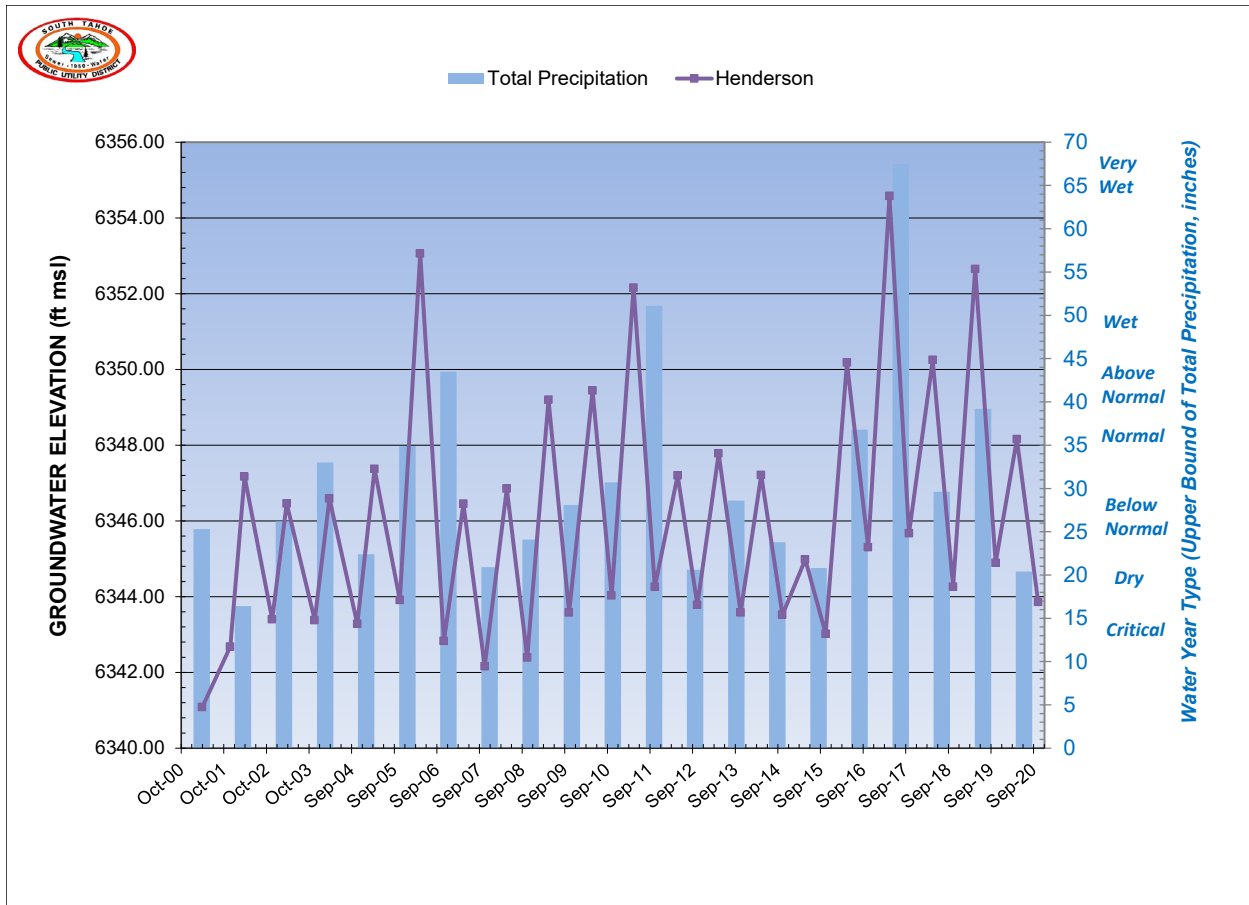


Figure 5-7. Groundwater hydrograph for the Henderson Well (6,366 feet AMSL) within the Christmas Valley sub-area.

5.2.2 Groundwater Flow Directions

Groundwater levels are shown in Figure 5-8 representing steady-state conditions (pre-1983) in the shallow aquifer (upper 300 feet) – as simulated from the STGM . Figure 5-8 also shows the general direction of groundwater flow. Groundwater generally flows from high to low groundwater elevations. The relative rate of groundwater flow is proportional to the hydraulic gradient and the hydraulic conductivity. The general groundwater level pattern observed in the TVS Subbasin is for higher groundwater levels to occur along the basin margins where a majority of recharge enters the groundwater system from higher elevations. Highest groundwater levels occur in the Christmas Valley subarea which also forms the topographically highest portion of the TVS Subbasin valley floor. From Christmas Valley, groundwater flows northward. Water from the Angora subarea flows southeast converging with flow from Christmas Valley and flow originating in the Carson Range to the east where groundwater flows around the lower permeable intrusive rocks forming the Twin Peaks to the north along the Upper Truckee River riparian corridor (Figure 2-7). Ultimately groundwater discharges in local tributaries or to Lake Tahoe as underflow.

Groundwater elevation contour maps for October 2019 and May 2020 are presented in Figure 5-9) and represent low and high groundwater level conditions, respectively. The typical

pattern is for the highest groundwater conditions to occur in the spring following the spring snowmelt and runoff. The lowest groundwater conditions typically occur in the late summer and early fall due to low recharge following the relatively dry summer months and increased groundwater pumping to meet seasonal demand.

Groundwater levels were contoured based on groundwater level measurements for all monitoring wells located in the TVS Subbasin. As indicated in Figure 2-10 the basin-fill deposits include a multitude of WBZs with inter-layered clay horizons of variable lateral extents. To make maximum use of the available data, all wells are contoured together regardless of the WBZ where they are located. This is appropriate to illustrate the general pattern of groundwater flow in the TVS Subbasin.

Comparison of contours from the two measurement periods shows that the generalized pattern of groundwater flow remained similar in October 2019 and May 2020. This is consistent with the hydrograph data that shows the typical variation in groundwater levels is on the order of a few feet. In most of the TVS Subbasin, the October 2019 water level contours progress southward, indicating a general lowering of water levels following the summer peak pumping months.

Vertical gradients were calculated for nested wells and clustered wells located throughout the TVS Subbasin (Figure 5-10). The clustered piezometers SW-1, IW-1, and DW-1 are ideal for calculating vertical gradients as these are located approximately 50 feet from each other with average screen depths of 25, 130, and 240 feet BGS, respectively. Hydraulic heads measured in May 2020 were 6,324.40, 6,314.28, and 6,296.87 feet AMSL, for SW-1, IW-1, and DW-1, respectively. These data were used to calculate downward vertical gradients of 0.096 and 0.158 ft/ft for the upper (SW-1 to IW-1) and lower (IW-1 to DW-1) sections, respectively.

Neighboring wells with shallow and deep screen intervals were used to calculate a vertical gradient in the northernmost part of the TVS Subbasin. The Sunset Well (average screen depth is 353 feet) is located approximately 2,200 feet west of the Chris Well (average screen depth is 121 feet), which is not ideal, but a general estimate of the vertical gradient can be made. In May 2020 the hydraulic head was measured at 6,223.46 and 6,228.32 feet AMSL for Sunset and Chris Wells, respectively. These data were used to calculate a downward vertical gradient of 0.02 ft/ft.

The USGS TCF Well is a nested well consisting of five observation wells completed in a single borehole that monitors groundwater levels at varying depths near Trout Creek in the South Lake Tahoe subarea (Figure 5-10). Each of the WBZs monitored by this nested well are confined or semi-confined by the intervening clay and peat layers. Comparing the vertical difference in groundwater levels (see Figure 5-11) indicates upward flow from BZ1 and BZ3 toward BZ4 and downward vertical flow from BZ5 toward BZ4. The complex vertical flow directions observed in the nested well may result from the lowered potentiometric head in BZ4 induced by pumping of the Glenwood Well #5.

CL-1 and CL-3 are observation wells which were constructed as a well cluster at the Clement Well site. Both CL-1 and CL-3 monitor groundwater levels from the uppermost WBZ (TKZ5). Comparison of the vertical difference in groundwater levels (see Figure 5-12) shows

higher groundwater levels in the shallow well indicating that vertical flow is directed downward through TKZ5 in this Groundwater Zone. Downward directed vertical flow through a WBZ is often a characteristic of recharge areas and is consistent with the spatial distribution of groundwater recharge depicted in Figure 5-15.

These vertical gradients are consistent with the conceptual model of the TVS Subbasin in which recharge is generally occurring in the higher elevations, then flowing laterally and then moving up from depth to ultimately discharge in Lake Tahoe. Pumping effects may locally influence vertical hydraulic gradients between water-bearing zones.

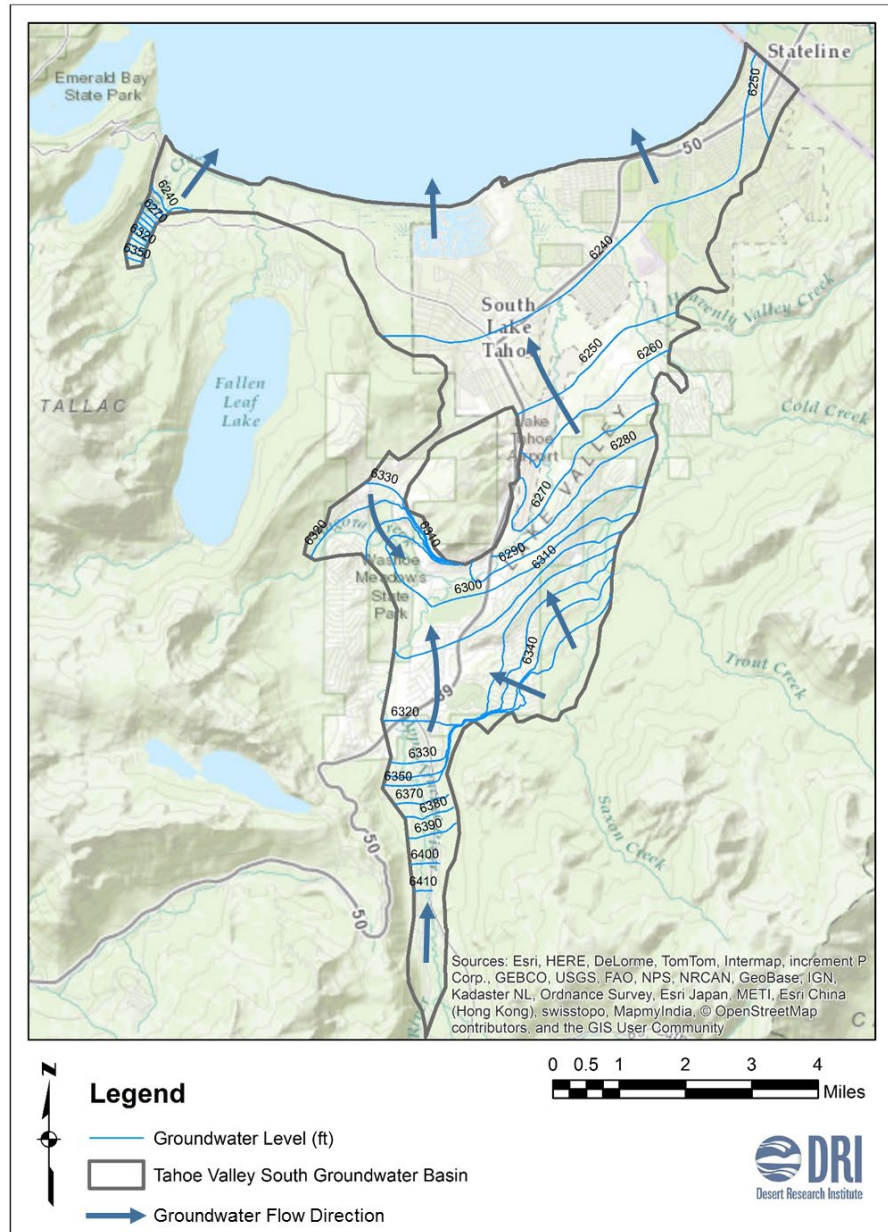


Figure 5-8. Shallow aquifer (upper 300 ft) water levels and flow directions (based on steady-state MODFLOW model). Contour interval is 10 ft.

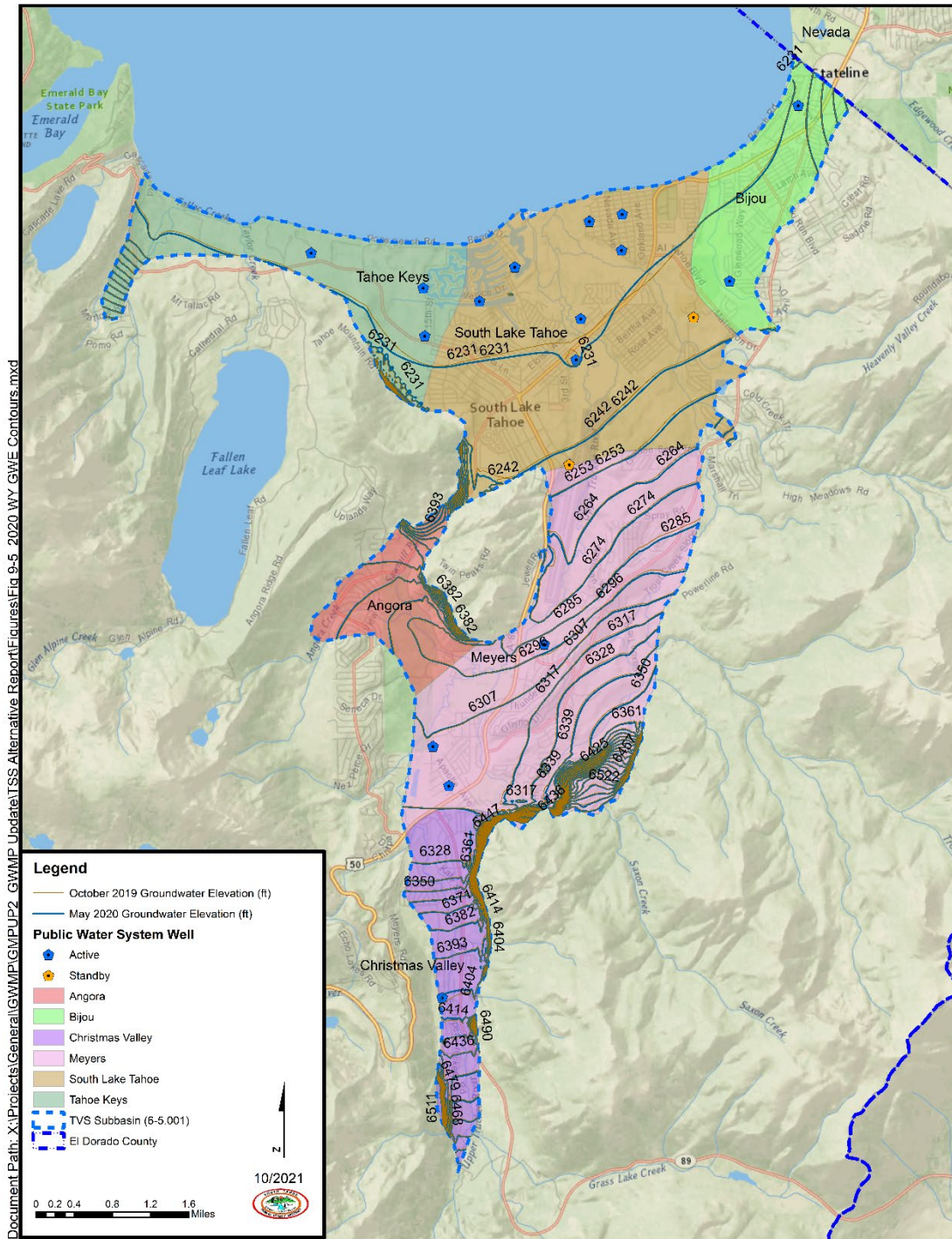


Figure 5-9. Shallow aquifer (upper 300 ft) water levels as measured in October 2019 and May 2020. Contour interval is 10 ft.

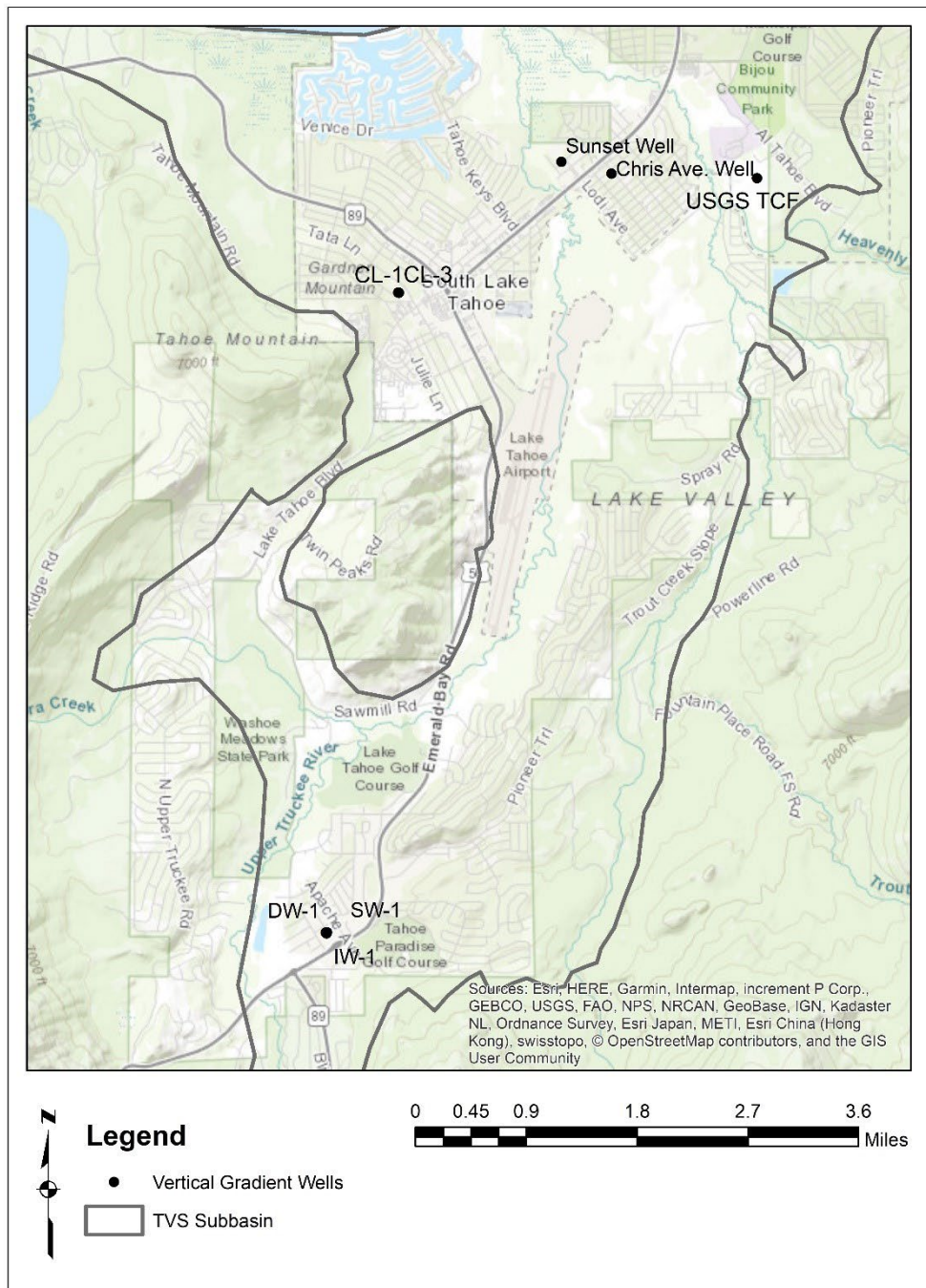


Figure 5-10. Location of wells used to calculate vertical hydraulic head gradients.

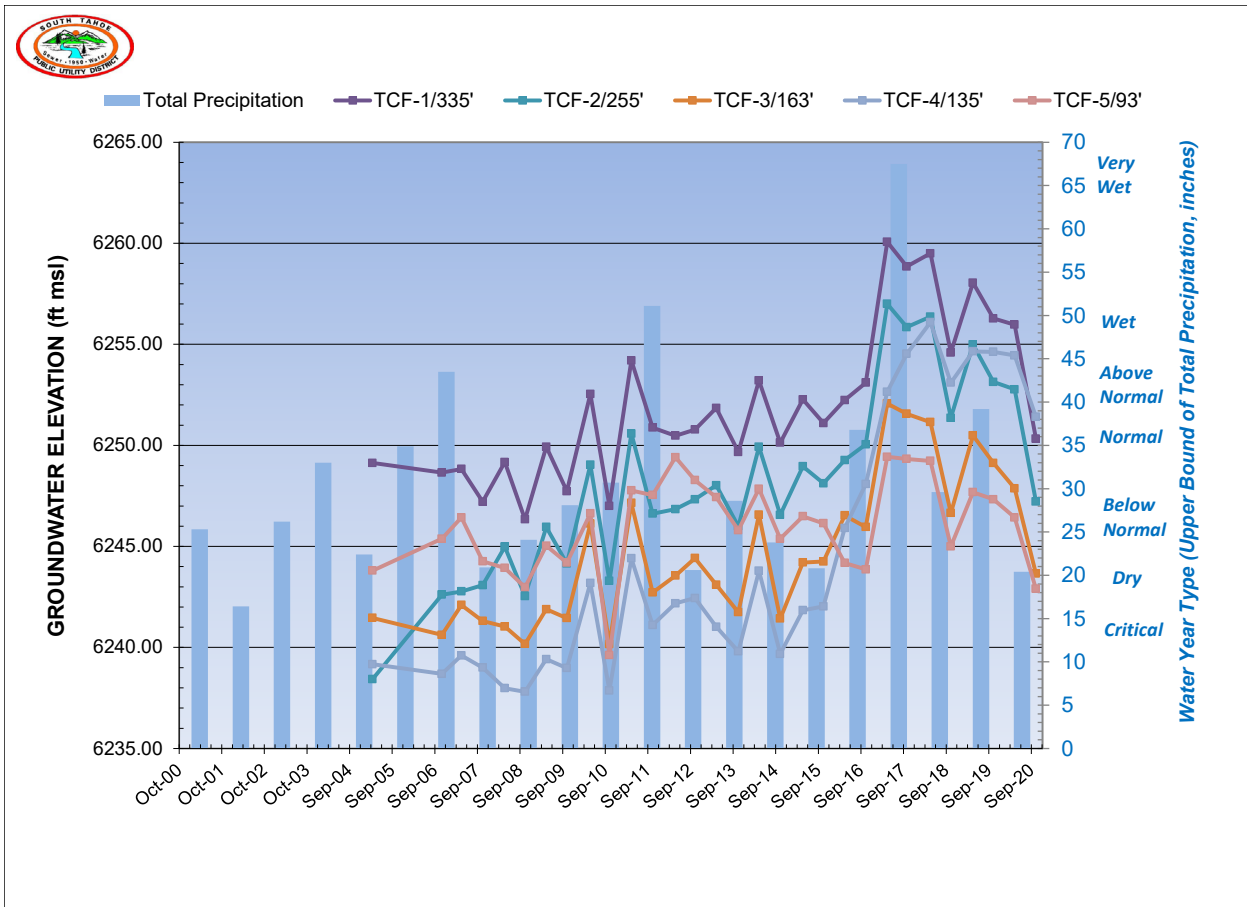


Figure 5-11. Groundwater hydrograph for the USGS TCF nested well (6,296 feet AMSL) within the South Lake Tahoe sub-area. Total well depths for the observation wells completed within the common borehole are as indicated.

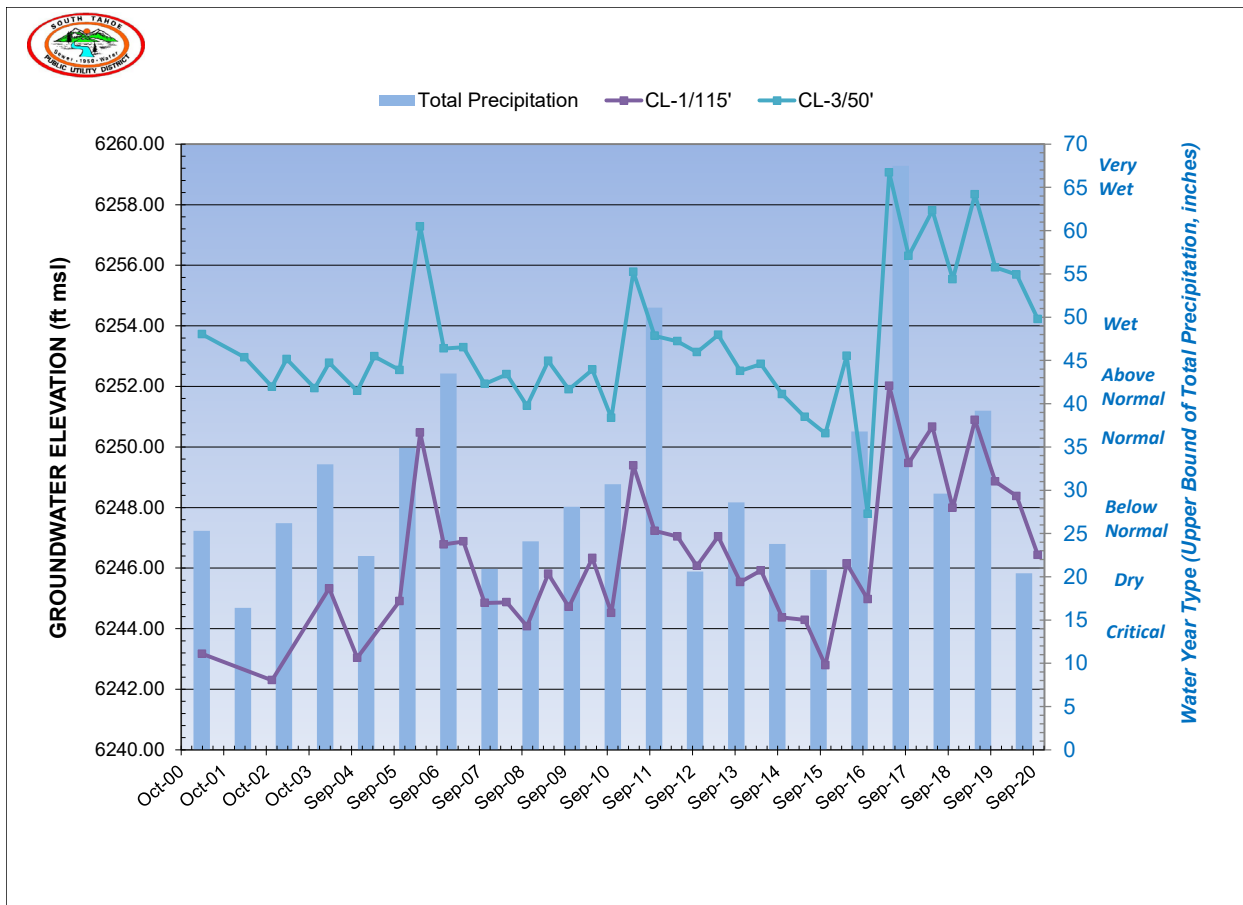


Figure 5-12. Groundwater hydrograph for the Clement Well cluster (6,279 feet AMSL) within the South Lake Tahoe sub-area. Total well depths for the observation wells comprising the well cluster are as indicated.

5.2.3 Hydraulic Parameters

Aquifer tests were conducted at numerous wells providing estimates of hydraulic conductivity throughout the TVS Subbasin. Hydraulic conductivity is a measure of an aquifer's capacity to transmit water. A map of hydraulic conductivity values is shown in Figure 5-13.

The aquifer materials in the TVS Subbasin are very permeable. The hydraulic conductivity values range from 0.5 to 210 feet per day (FT/D) with a median of 27 FT/D and geometric mean of 20 FT/D. Aquifers with hydraulic conductivities greater than 1 FT/D are considered productive for groundwater extraction purposes.

The measured hydraulic conductivities were used to aid the groundwater model calibration process using the Pilot Point Methodology (Doherty, 2008). The hydraulic conductivity remains fixed at measured locations and an automated calibration procedure was used to adjust hydraulic conductivity values at unmeasured locations. Bedrock hydraulic conductivity values were assumed to be homogeneous. The resulting hydraulic conductivity field is shown in Figure 5-14. Highest permeability values are associated with the basin-fill deposits in the valley and along the riparian corridors. Bedrock hydraulic conductivity is 0.26 FT/D in the uppermost layer and decreases to 5.6×10^{-3} FT/D in deeper layers. Highest hydraulic

conductivity values are located south of Twin Peaks near the Bakersfield and Arrowhead Wells in a region dominated by glacial deposits.

Storage parameters were determined through calibration of the transient groundwater flow model. A specific yield of 0.1 for bedrock and 0.3 for alluvium was used while specific storage was 3.0×10^{-7} for all geologic units to achieve an agreement between simulated and measured water levels. Note that the average of storage coefficients derived from aquifer tests is 0.078, which is likely a measure of both confined and unconfined conditions.

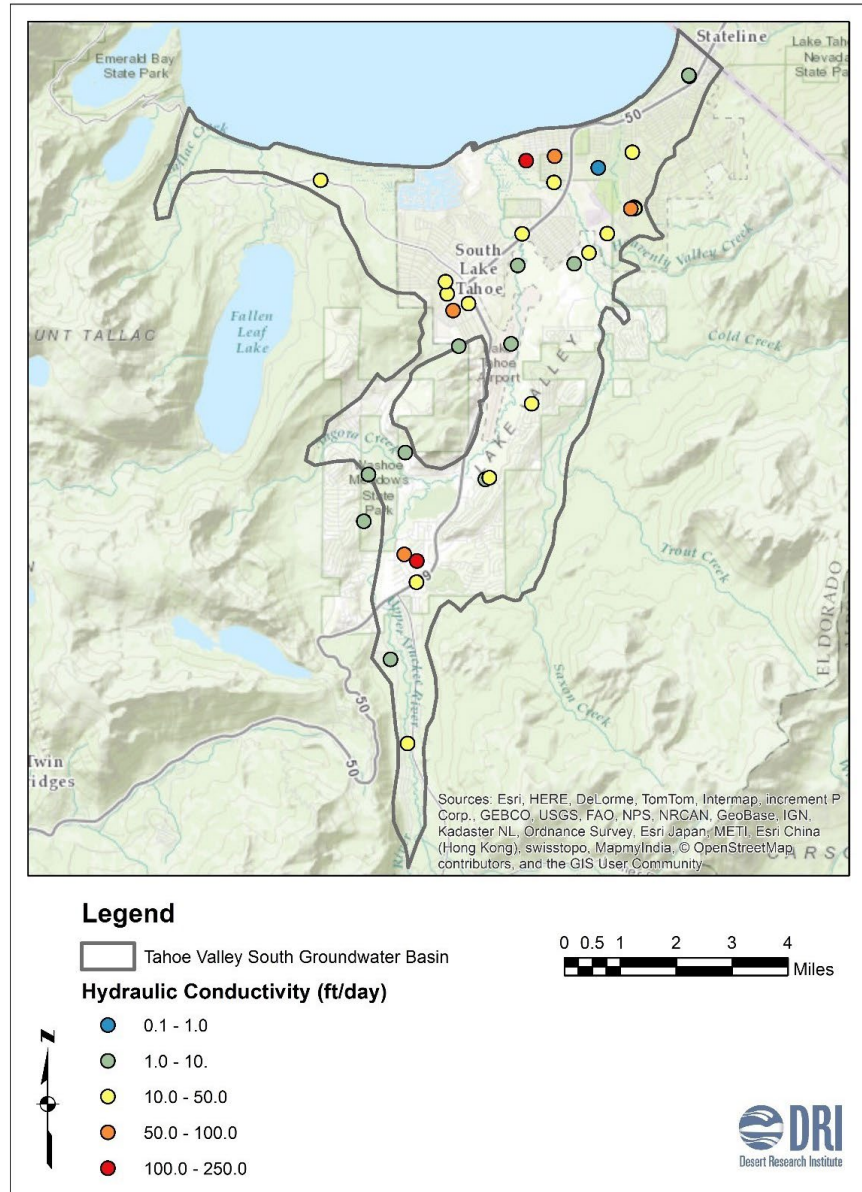


Figure 5-13. Hydraulic conductivity (FT/D) within the TVS Subbasin.

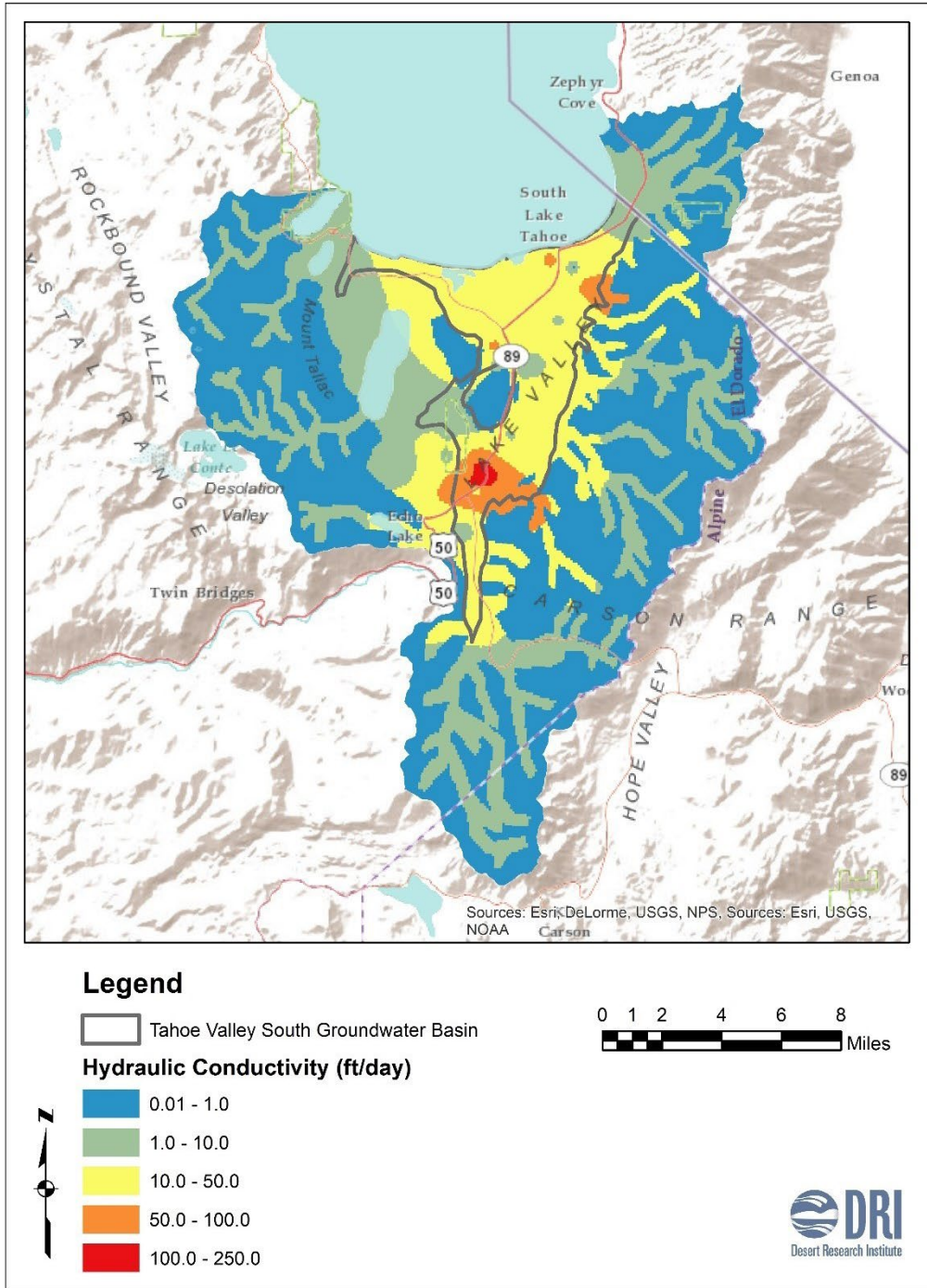


Figure 5-14. Hydraulic conductivity field (FT/D) used in the uppermost layer of the groundwater flow model.

5.2.4 **Groundwater-Storage**

A storage calculation was performed using the STGM but limited to the TVS Subbasin (Zone 10) and basin-fill sediments all the way to the bedrock contact. This calculation yielded total storage of 1,800,000 AF. Additional calculations were performed to include all simulated grid cells within the STGM model domain, including the Mountain Block (Zone 1) surrounding the TVS Subbasin and all cells representing bedrock (Zone 1 + Zone 10). These calculations yielded total storage values of 23,900,000 AF and 2,800,000 AF, respectively. For the purposes of this report, the 1,800,000 AF of groundwater storage derived from groundwater that is limited to the TVS Subbasin (Zone 10), from the water table to the bedrock contact, is used for analysis of groundwater storage.

The value of total groundwater storage (1,800,000 AF) used for this analysis is derived from the STGM from the water table to the bedrock contact. Storage calculations were done using a Python script which reads simulated groundwater levels at every cell within the TVS Subbasin. For each cell, the code calculates storage by multiplying the difference in water table elevation and the cell bottom by the specific yield (0.3) and the cell's surface area (~2.5 acres). In other words, it multiplies the saturated volume of the cell by the specific yield. The storage for any cells below that cell was calculated in the same way, using the total volume of each cell as the saturated volume. Storage for all cells in a column was then summed, and the storage values for all columns were converted to a georeferenced raster image and clipped to the shape of the basin sediments. The raster cell values within this clipped shape were then summed to reach the final storage value.

5.3 **Groundwater-Surface Water Interactions**

Groundwater-surface water interactions occur when the water table intersects with surface water features such as streams or lakes. These interactions comprise the movement of water between surface features and the underlying aquifer. The direction of flow depends on the head in the aquifer and the stage of the surface water feature: when the surface stage is greater than the groundwater head water flows from the surface feature to the aquifer, when the groundwater head is greater than the surface stage water flows from the aquifer to the surface feature. Flows between groundwater and surface waters exhibit a seasonal cycle and interannual variability.

Within the TVS Subbasin, groundwater discharges to the stream channels along much of the Upper Truckee River and Trout Creek. These groundwater discharges (i.e., base flow) provide a component of the total streamflow that accounts for a substantial proportion of total stream flow during the late summer and fall when runoff from the surrounding mountains has diminished. During the winter and spring, seasonal storm or melt waters provide the majority of total stream flows. The proportion of the total flow attributed to base flow is relatively low.

Groundwater pumping has the potential of reducing base flow to streams, which could affect GDEs and the aquatic and biologic resources dependent on the ecosystem services provided by these habitats. The potential impact of groundwater withdrawals on surface water systems depends on a multitude of variables including, but not limited to: the aquifer properties of the groundwater system; the arrangement of aquitards and confining layers between the water-

bearing zone(s) and the surface water system; the distribution and construction of neighboring drinking water production wells; and the timing and magnitude of groundwater withdrawals from those wells.

Surface water features and GDEs in the basin are described in Section 2.6 of this plan. The interactions between these features and the groundwater are briefly discussed below and are addressed in detail along with the sustainable management criteria presented in Section 8.3.

5.4 **Groundwater Budget**

This section addresses DWR Recommended Actions RA-1 and RA-2 (presented in Section 1.3), which recommend that water budget information be presented in tabular form (Sections 5.4.6, 5.4.7, and 5.4.8; and Appendix J), and that projected water budgets incorporate climate change over the planning and implementation horizon of 50 years (Section 5.4.8). These results also incorporate Recommended Action RA-4, which recommends that changes in storage be calculated within the TVS Subbasin boundary, rather than incorporating the surrounding watershed. A groundwater budget analysis balances sources of recharge and discharge for a given hydrologic basin and may be described with varying levels of detail for each component of flow. Within this report, historic, current, and projected water budgets are described for the TVS Subbasin based on simulation results from the STGM and in terms of the flow budget components simulated in that model. Simulated sources of groundwater include areal recharge, mountain-block recharge (MBR) and inflows from Lake Tahoe. Inflows to groundwater due to losses from streams are incorporated in the areal recharge term based on GSFLOW modeling results. Simulated groundwater sinks include baseflow to streams, outflows to Lake Tahoe, and groundwater pumping. Groundwater storage may act as either a source or a sink within the model, depending on initial conditions and stresses applied for each stress period. Each of these sources and sinks are described in more detail in the following sections.

5.4.1 **Recharge**

Recharge was extracted from the GSFRM and applied to the STGM model domain. Recharge is defined as the model computed excess water leaving the unsaturated root or soil zone and entering the saturated zone after accounting for abstractions of interception, sublimation, surface runoff and evapotranspiration. GSFLOW simulated recharge for the TVS hydrologic basin varies from year to year based on annual cycles of precipitation. The spatial distribution of groundwater recharge for WY 2010, which represents average precipitation conditions, is shown in Figure 5-15. Most of the recharge occurs in the mountains of the Sierra Nevada and Carson Range. Annual recharge ranges from 9 inches in the valley to upwards of 34 inches in the higher elevations. This result is consistent with observations of stable isotope levels in stream baseflow and of groundwater from numerous shallow and deep-screened wells which indicate that a significant fraction of groundwater present within the TVS Subbasin is sourced from precipitation in high elevation areas that recharges at the mountain front and/or in the mountain block as MBR (Fogg, et al., 2007). MBR is the subsurface inflow of groundwater to lowland basin-fill aquifers from adjacent mountains (Markovich et al., 2019). In the STGM, MBR is calculated in the groundwater budget as the difference between the areal recharge within the Mountain Block adjoining the TVS Subbasin and the sum of the base flow to streams, net discharge to Lake Tahoe, and net change in storage within the mountain block area. Fallen Leaf

and Cascade Lakes are simulated as lakes and therefore receive constant recharge of approximately 30 inches per year.

Groundwater recharge is largely dependent on annual precipitation, and it is important to understand how recharge changes over time. A regression equation was developed between annual precipitation at Hagan's Meadows climate station to groundwater recharge (Figure 5-16) with a coefficient of determination (R^2) of 0.92. The coefficient of determination describes how much of the variability in one variable can be predicted based on the value of another variable. In this case, more than 92% of the year-to-year variability in groundwater recharge (as derived from the groundwater flow model) can be predicted based on the observed precipitation at Hagan's Meadow. The Hagan's Meadow climate station resulted in the best correlation between precipitation at one station versus groundwater recharge.

Groundwater recharge to the TVS Subbasin (Zone 10) from WY 1983 to WY 2019 is shown in Figure 5-17 as the sum of areal recharge over the TVS Subbasin and MBR. Average annual recharge over the last decade (2010–2019) is 22,400 AFY and the average over the entire simulation period (1983–2019) is 21,400 AFY. MBR is typically 5% to 50% of the total recharge to basin-fill aquifers (Markovich et al, 2019). Groundwater budgets computed by the STGM show MBR annually accounts for about 75% of the total recharge to the TVS Subbasin.

The ratio of recharge computed by the GSFLOW model to annual precipitation, which is termed as "recharge efficiency," can be used to describe the fraction (or percentage) of precipitation that is converted to recharge. Mean estimated precipitation by GSFLOW for the model domain is approximately 344,000 AFY over the hydrologic analysis area. Computed recharge efficiency for the TVS Subbasin varies annually but on average (1983–2015) is approximately 11 percent. The fraction of precipitation that becomes recharge is consistent with other studies in the Sierra Nevada region (Flint and Flint, 2007).

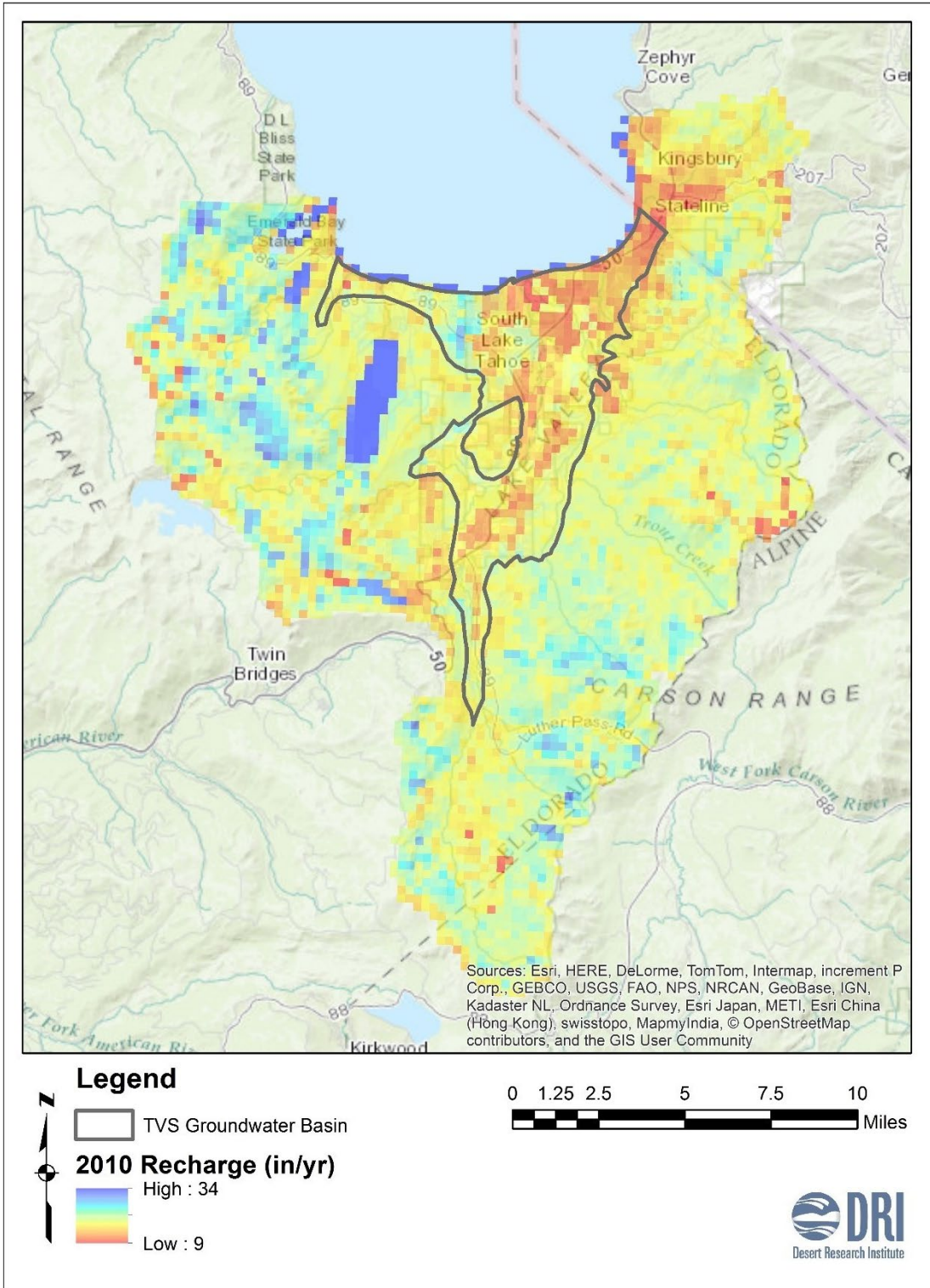


Figure 5-15. Groundwater recharge rates for 2010 as simulated with the GSFLOW model.

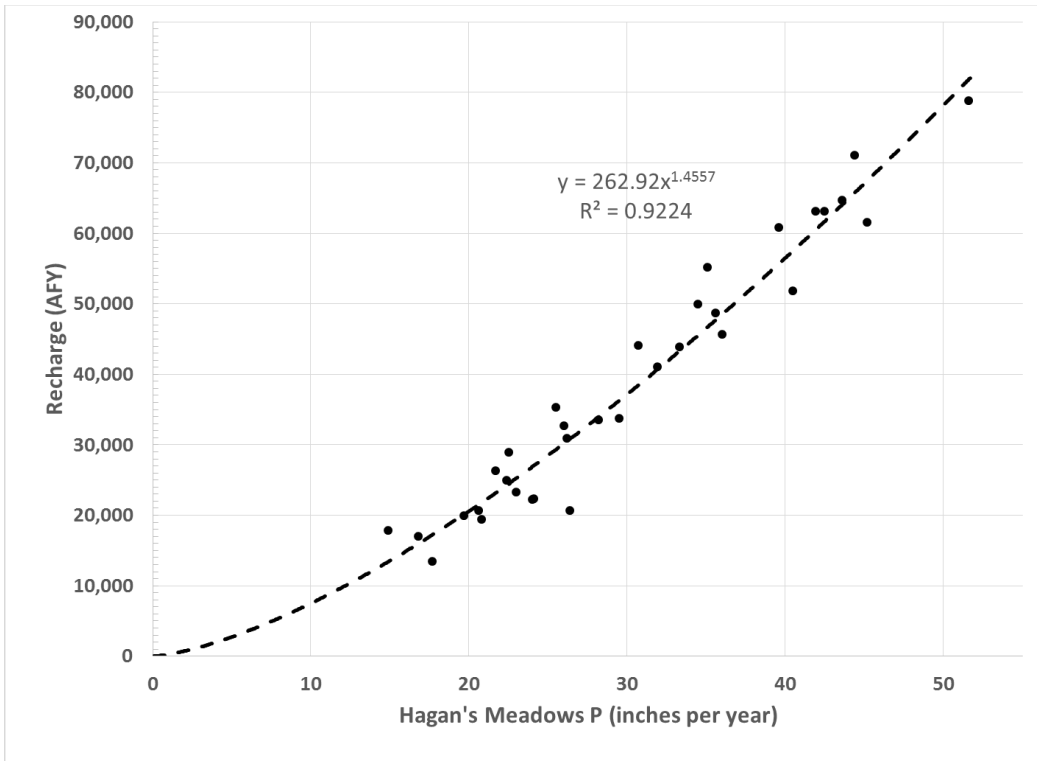


Figure 5-16. Hagan’s Meadow annual precipitation versus groundwater recharge within the hydrologic analysis area. Also shown is a non-linear regression.

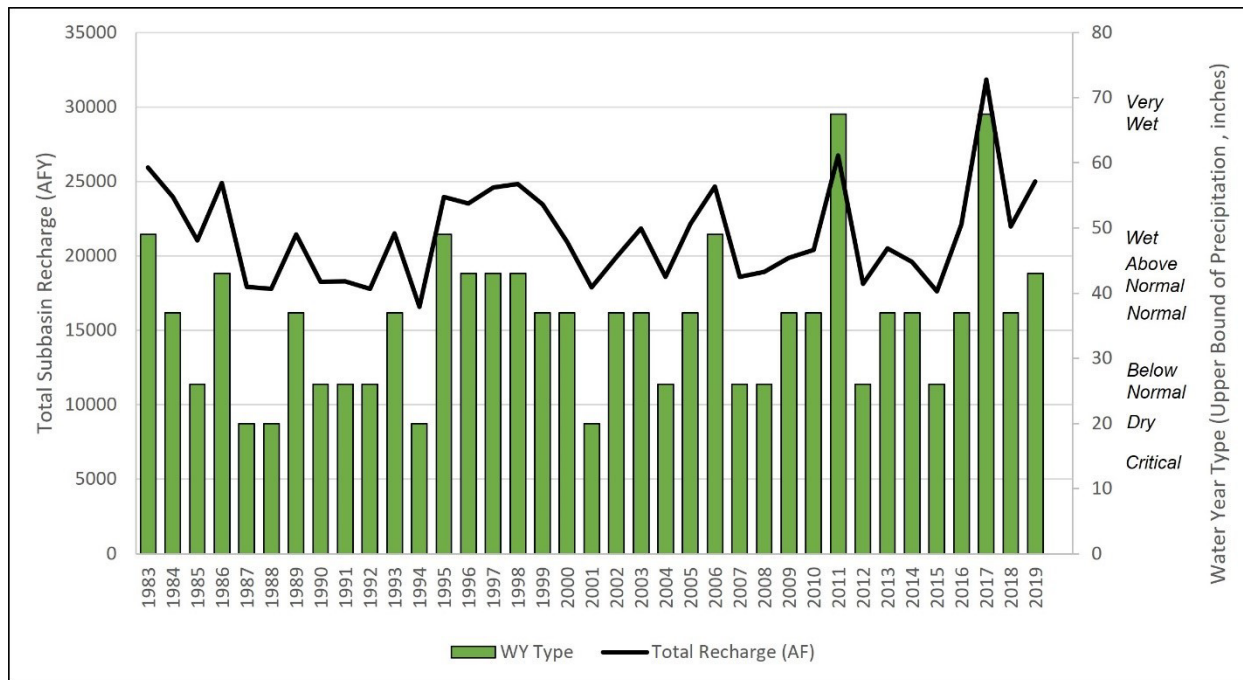


Figure 5-17. Groundwater recharge to the TVS Subbasin from water year 1983–2019, including mountain block recharge and direct areal recharge, compared to water year type.

5.4.2 Groundwater Withdrawals

Groundwater is the primary source of drinking water accounting for more than 95 percent of the potable water used within the TVS Subbasin. Surface water as a drinking water source is relatively minor and is provided through a surface water intake to Lake Tahoe by LPA (Section 3.3.2.4). Groundwater withdrawals from community and individual water systems are discussed in detail in Section 3.3. Groundwater production from the largest community water supply wells typically account for more than 95% of the total groundwater extracted on an annual basis from the TVS Subbasin. The remaining 5% is extracted from individual water system wells (Section 3.3.5).

Figure 5-18 shows the historical water use from the four largest water purveyors and estimated pumpage at all individual water system wells used in the historical MODFLOW model. Groundwater withdrawals averaged 7,660 AFY and 7,150 AFY over the periods 1983–2019 and 2010–2019, respectively. Note that total demand has decreased from 9,790 AFY in 2007 to 6,830 AFY in 2019.

For all climate scenarios, total pumpage at community water system wells was increased at an annual rate of 0.37%, using the 50-year population growth rate for the County (see Section 3.1). This population growth was expressed in the projected water budgets using initial total pumpage rates for each water provider from WY 2007, as this was the year with the greatest pumping volume in historical record and allowed for the most conservative estimate of future pumpage. LBWC, TKWC, and LPA all service smaller, discrete service areas with limited potential for growth, and pumpage from these systems was limited to a maximum rate, determined by a recent water demand projections (see Section 3.4). After these water systems reached their maximum pumping rate, excess pumpage that would otherwise have been assigned to them according to the 0.37% rate increase was instead added to pumpage at District wells. Total pumpage for each water system was distributed among that provider's wells according to the WY 2019 distribution and was temporally distributed according to historical seasonal pumping rates. Individual water system wells simulated in the historical model were assumed to continue pumping at the same rates and locations for the duration of the climate scenario models.

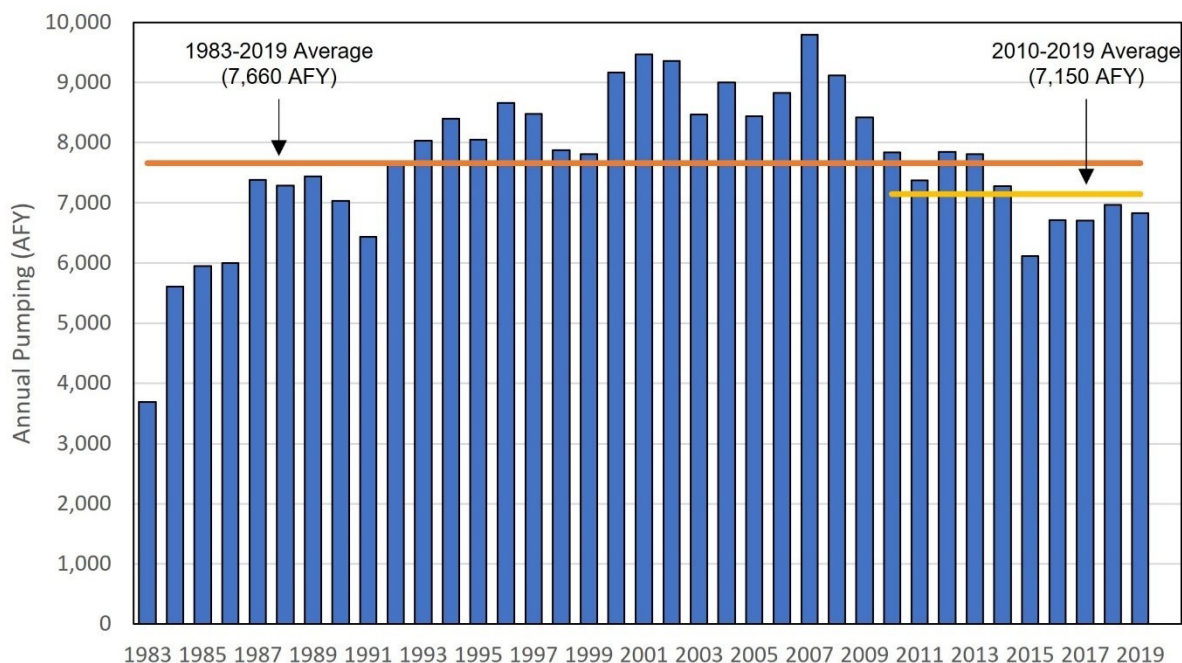


Figure 5-18. Annual pumpage in AFY from community water system and individual water system wells within the TVS Subbasin used in the MODFLOW model.

5.4.3 Discharges to Streams and Lakes

Groundwater discharges to streams and lakes are simulated using the MODFLOW stream package. During pre-1983 (steady state) period, total baseflow to streams in the model domain was approximately 34,400 AFY: 18,400 AFY in the Mountain Block and 16,000 AFY in the TVS Subbasin (Table 5-1). Annual net groundwater discharge to Lake Tahoe during this time was estimated at 7,900 AFY. Over the historical period (1983–2019), total baseflow to streams averaged approximately 30,100 AFY in the model domain: 17,300 AFY in the Mountain Block and 12,700 AFY in the TVS Subbasin (Table 5-2). Over the last decade (2010–2019), total baseflow to streams averaged 30,300 AFY in the model domain: 17,600 AFY in the Mountain Block and 12,700 AFY in the TVS Subbasin (Table 5-3). Simulated baseflow rates within the subbasin for 1983–2019 are shown in Figure 5-19. Over the historical period (1983–2019), annual net groundwater discharge from the model domain to Lake Tahoe was 5,600 AFY, of which 2,300 AFY was from the Mountain Block and 3,300 AFY was from the TVS Subbasin. Over the last decade (2010–2019), average outflow from the TVS Subbasin to Lake Tahoe reduced to 3,200 AFY. Net groundwater outflow from the TVS Subbasin to Lake Tahoe for 1983–2019 is shown in Figure 5-20.

5.4.4 Increases from Streams and Lakes

Flows from surface waters (i.e., streams and lakes) to groundwater are included in the STGM as areal recharge. Historical groundwater recharge is prescribed based on a linear regression between precipitation at Hagan’s Meadow and total recharge (Pohll et al. 2016). Groundwater recharge is prescribed for each climate scenario based on the GSFRM (see

Section 5.1.1). Total annual recharge to the groundwater basin is distributed spatially and temporally based on the output of that model and includes recharge from surface water features in contact with the water table. MODFLOW simulations show that inflows from Lake Tahoe occur in response to pumping, particularly in the summer months, but over the historical period 1983–2019 model results showed an annual net outflow for all but three years (1995, 1996, and 2006). During each of these years Lake Tahoe Elevations (stage) were at high levels (see Figure 2-13).

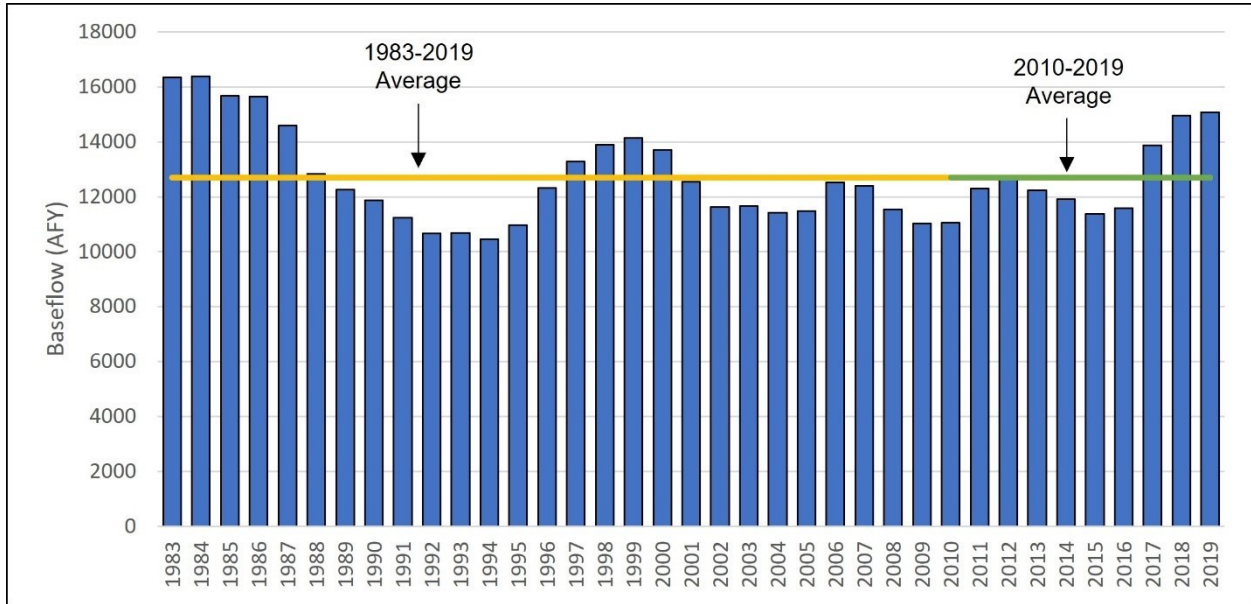


Figure 5-19. Simulated baseflow to streams within the TVS Subbasin for 1983-2019, not including the surrounding watershed.

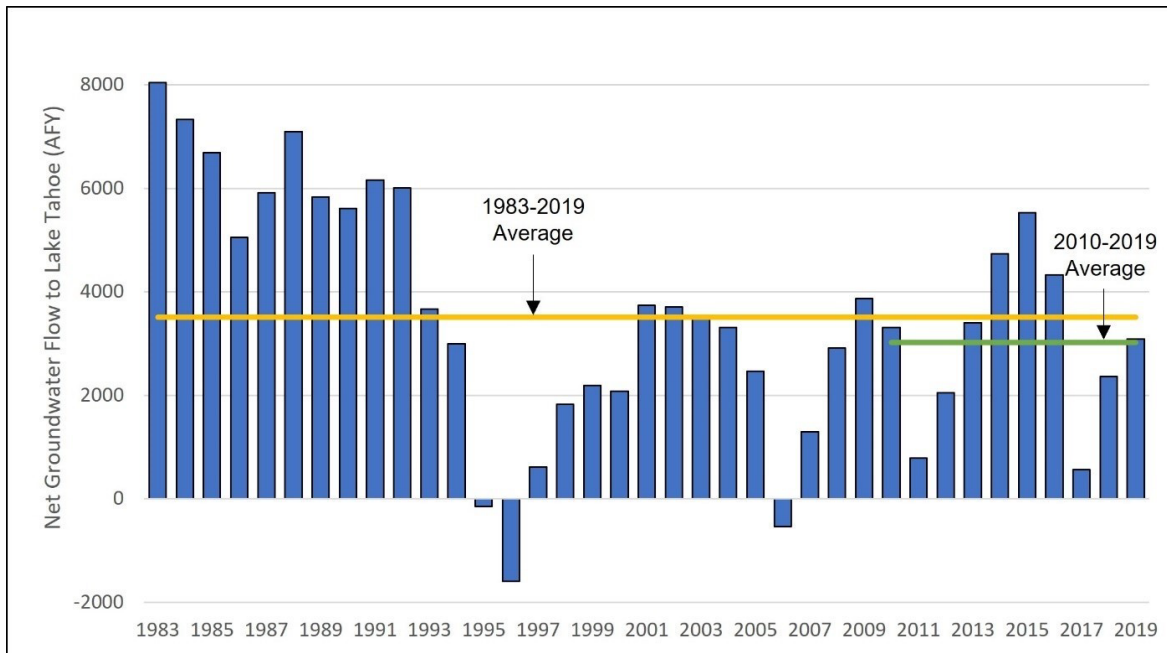


Figure 5-20. Simulated net groundwater flow from the TVS Subbasin to Lake Tahoe for 1983-2019.

5.4.5 Changes in Groundwater Storage

The STGM was used to calculate annual changes in groundwater storage for WY 1983 – WY 2019 (Figure 5-21) for the TVS Subbasin (Zone 10). Annual change in groundwater storage magnitudes vary from -7,400 AFY (meaning water levels are falling) to 12,100 AFY (meaning groundwater levels are rising). On average, groundwater storage changes are near zero (-200 AFY), meaning groundwater storage changes tend to even out over periods of higher and lower recharge. Over the last decade (2010–2019), storage has increased an average of 1,700 AFY.

Changes in groundwater storage are generally associated with variations in climate and/or pumping. Given that groundwater recharge is more than pumping, changes in groundwater storage are largely dependent on annual precipitation. Cumulative changes in storage for the TVS Subbasin relative to WY 2005 are presented alongside groundwater production and water year type (precipitation rate) in Figure 5-22. As of WY 2020, the cumulative change in storage for the TVS Subbasin relative to WY 2005 was approximately +5,300 AF.

A regression equation was developed between annual precipitation at Hagan’s Meadow climate station and changes in groundwater storage as calculated by STGM (Figure 5-23). Hagan’s Meadow climate station was chosen because it resulted in the best correlation between a single station’s annual precipitation and changes in groundwater storage. Note that this regression relates precipitation to changes in groundwater storage for the model domain which includes both the TVS Subbasin (Zone 10) and the Mountain Block (Zone 1), while storage change presented in Figure 5-21 and Figure 5-22 is for the TVS Subbasin only. The zero point occurs at approximately 31 inches of annual precipitation at Hagan’s Meadow, which is slightly less than the 30-year (1991–2020) mean annual precipitation of 31.9 inches. The zero point

represents the point at which groundwater storage does not change. Precipitation more than 31 inches causes groundwater storage to increase (positive storage change) and vice versa.

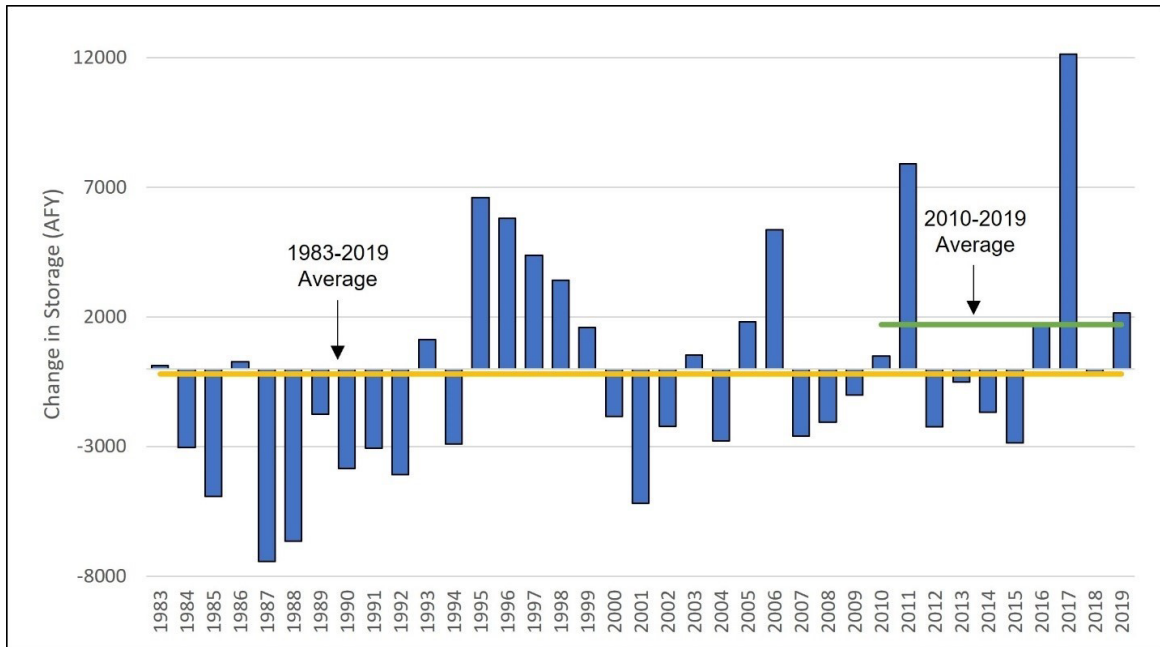


Figure 5-21. Simulated change in storage for the TVS Subbasin (Zone 10) for 1983-2019, not including the surrounding watershed.

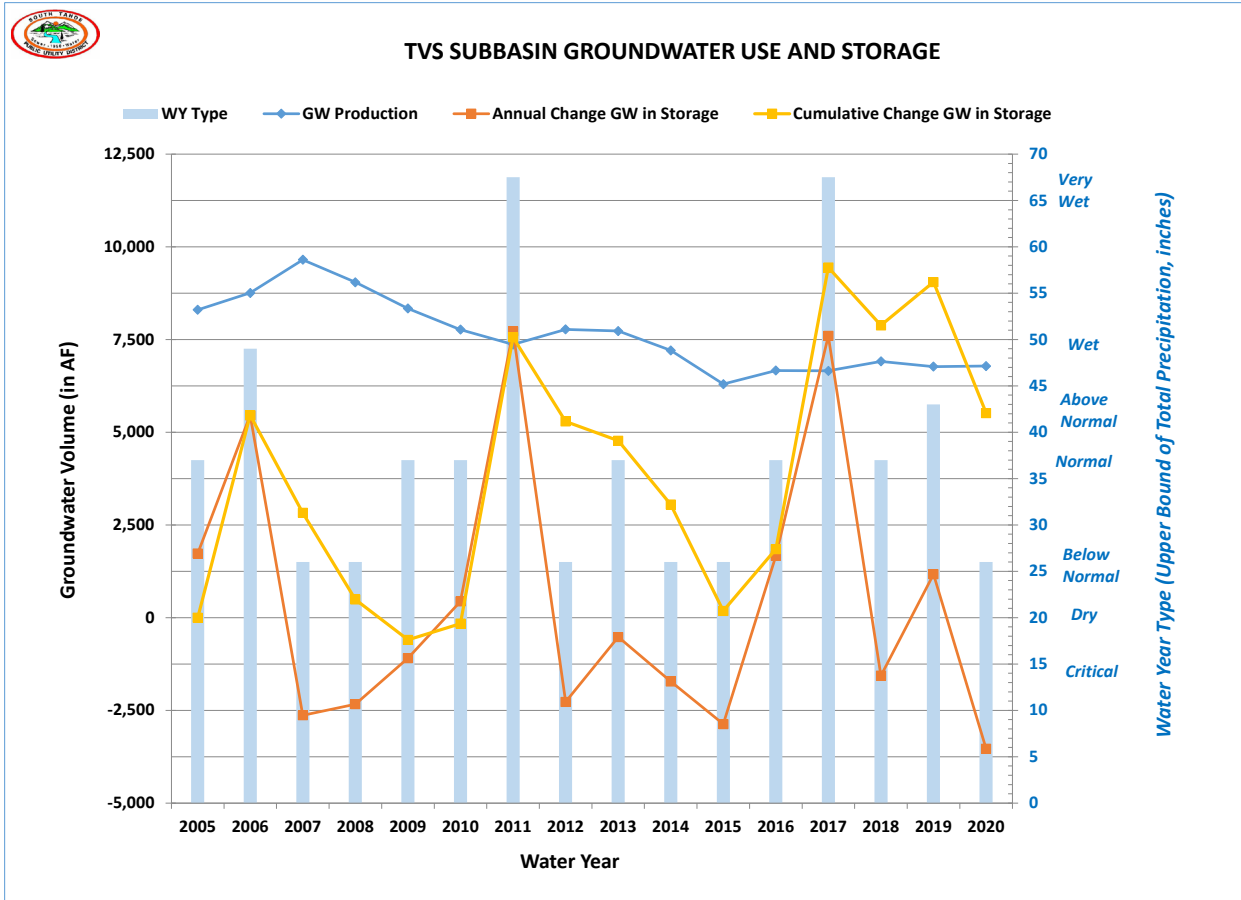


Figure 5-22. Annual groundwater production from public water supply wells and modeled annual and cumulative change in groundwater storage, in AFY, for the TVS Subbasin (WY 2005 through WY 2020). Water year type using the classification developed for the TVS Subbasin (Section 9.1.2.1) is indicated on the vertical axis along the right-side of the graph. Positive changes in groundwater storage indicate periods of rising groundwater level.

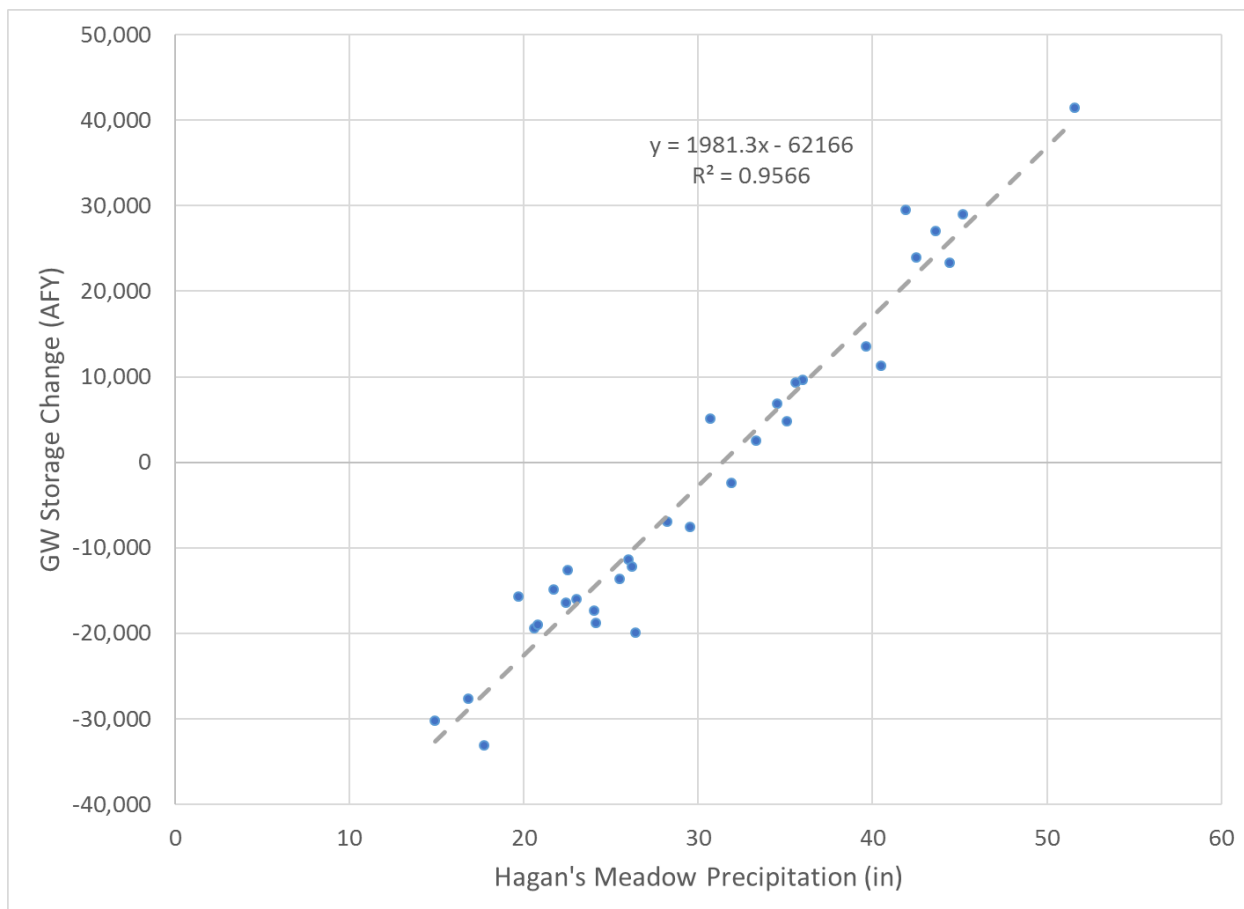


Figure 5-23. Hagan’s Meadow precipitation versus groundwater storage change through WY 2015.

5.4.6 Historical Groundwater Budgets

Prior to 1983, average groundwater recharge was likely similar to current conditions and has been estimated at approximately 42,300 AFY based on the average annual recharge estimate from the GSFRM for WY 1983 to WY 2011 (Carroll et al, 2016a). While groundwater pumping occurred prior to 1983, rates were not well recorded and were likely less than half of current averages. This summary can therefore be considered a good approximation of pre-development conditions for the basin. Under these conditions, most groundwater discharged either as baseflow to streams (34,400 AFY) or to Lake Tahoe (7,900 AFY).

These numbers represent the condition for the entire model domain; however, a more representative picture of available groundwater may be found by separating flow budget terms spatially for the TVS Subbasin (Zone 10) and the Mountain Block (Zone 1). Accordingly, the groundwater budget for each of these spatial zones for the period prior to WY 1983 is summarized in Table 5-1. The budget for the TVS Subbasin includes two recharge terms – one representing areal recharge occurring directly over the TVS Subbasin, and one representing recharge originating from the Mountain Block. This recharge term is calculated as areal recharge occurring over the mountain block, minus baseflow and discharge to Lake Tahoe that occur

within the mountain block. Recharge and discharge rates for the two spatial zones are discretized from the steady-state groundwater model (Carroll et al, 2016a; Carroll et al, 2016b). This analysis shows that under average pre-development conditions, the annual flow of groundwater into the TVS Subbasin was approximately 21,700 AFY.

Table 5-1. Pre-development flow budget, segregated into components for the TVS Subbasin (Zone 10) and the surrounding mountain block (Zone 1).

Item	Units	Mountain Block (Zone 1)	TVS Subbasin (Zone 10)	Model Domain (Zone 1 + Zone 10)
Area	AC	85,093	14,814	99,907
INFLOWS				
Areal Recharge	AFY	36,900	5,400	42,300
Recharge from Zone 1 to Zone 10 ¹	AFY	0	16,300	N/A
Inflow Total	AFY	36,900	21,700	42,300
OUTFLOWS				
Recharge from Zone 1 to Zone 10 ¹	AFY	16,300	0	N/A
Baseflow to Streams	AFY	18,400	16,000	34,400
Discharge to Lake Tahoe	AFY	2,200	5,700	7,900
Outflow Total	AFY	36,900	21,700	42,300

Note: All values are rounded to the nearest 100 AFY.

¹Recharge from Zone 1 to Zone 10 is an internal flux within the model domain rather than a simulated inflow or outflow, and is not summed within the model domain flow budget.

As groundwater pumping increased through the 1980s, baseflow to streams and discharge to Lake Tahoe decreased. Average flow budget results from the STGM are presented in Table 5-2 for the historical period (WY 1983 to WY 2019). These results are representative of the TVS subbasin and include a term for groundwater flow entering the subbasin from the Mountain Block, as defined above. A summary plot showing annual inflows and outflows, and the annual change in storage for WY 1883 to WY 2019 is presented in Figure 5-24. Annual flow budget results for the historical period WY 1983 to WY 2019 are presented in tabular form in Appendix J1.

Table 5-2. Average flow budget terms for the historical period WY 1983 to WY 2019, segregated into components for the TVS Subbasin (Zone 10) and the surrounding mountain block (Zone 1).

Item	Units	Mountain Block (Zone 1)	TVS Subbasin (Zone 10)	Model Domain (Zone 1 + Zone 10)
Area	AC	85,093	14,814	99,907
INFLOWS				
Areal Recharge	AFY	36,300	5,300	41,600
Recharge from Zone 1 to Zone 10 ¹	AFY	0	16,200	N/A

Item	Units	Mountain Block (Zone 1)	TVS Subbasin (Zone 10)	Model Domain (Zone 1 + Zone 10)
Area	AC	85,093	14,814	99,907
Lake Tahoe	AFY	100	2,000	2,200
Storage	AFY	7,300	2,700	10,000
Inflow Total	AFY	43,700	26,200	53,700
OUTFLOWS				
Recharge from Zone 1 to Zone 10 ¹	AFY	16,200	0	N/A
Pumping	AFY	0	7,700	7,700
Baseflow to Streams	AFY	17,300	12,700	30,100
Lake Tahoe	AFY	2,300	3,300	5,600
Storage	AFY	7,900	2,500	10,400
Outflow Total	AFY	43,700	26,200	53,700

Note: All values are rounded to the nearest 100 AFY.

¹Recharge from Zone 1 to Zone 10 is an internal flux within the model domain rather than a simulated inflow or outflow and is not summed within the model domain flow budget.

5.4.7 Current Groundwater Budget

Over the last decade (2010–2019), total baseflow rates for the model domain averaged 30,300 AFY, or 12,700 AFY within the TVS Subbasin. Over the same time period, total net outflow to Lake Tahoe averaged 3,100 AFY and 900 AFY solely within the TVS Subbasin. While the historical period WY 1983 to WY 2019 showed a slight average decline in subbasin storage of approximately 200 AFY, storage increased by an average of approximately 1,700 AFY between WY 2010 and WY 2019. A summary of average flow budget results for WY 2010 to WY 2019 is shown in Table 5-3.

Table 5-3. Average flow budget terms for the period WY 2010 WY 2019, segregated into components for the TVS Subbasin (Zone 10) and the surrounding mountain block (Zone 1).

Item	Units	Mountain Block (Zone 1)	TVS Subbasin (Zone 10)	Model Domain (Zone 1 + Zone 10)
Area	AC	85,093	14,814	99,907
INFLOWS				
Areal Recharge	AFY	42,100	6,300	48,400
Recharge from Zone 1 to Zone 10 ¹	AFY	0	16,100	N/A
Lake Tahoe	AFY	100	2,300	2,400
Storage	AFY	5,800	1,700	7,500
Inflow Total	AFY	48,000	26,400	58,300
OUTFLOWS				
Recharge from Zone 1 to Zone 10 ¹	AFY	16,100	0	N/A
Pumping	AFY	0	7,100	7,100
Baseflow to Streams	AFY	17,600	12,700	30,300

Item	Units	Mountain Block (Zone 1)	TVS Subbasin (Zone 10)	Model Domain (Zone 1 + Zone 10)
Lake Tahoe	AFY	2,300	3,200	5,500
Storage	AFY	12,000	3,400	15,400
Outflow Total	AFY	48,000	26,400	58,300

Note: All values are rounded to the nearest 100 AFY.

¹Recharge from Zone 1 to Zone 10 is an internal flux within the model domain rather than a simulated inflow or outflow, and is not summed within the model domain flow budget.

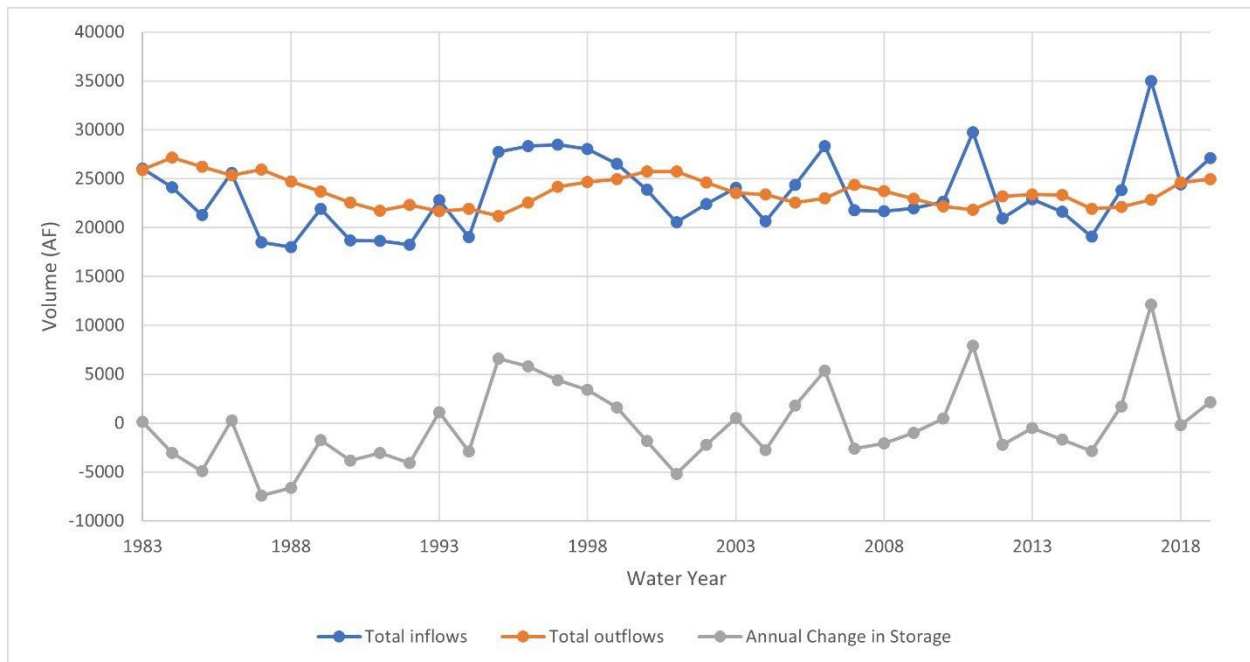


Figure 5-24. Summary of historical inflows and outflows (not including changes in storage) for WY 1983 to WY 2019, and the annual change in storage for the TVS Subbasin.

5.4.8 Projected Water Budget

Water budget projections depend greatly on expected groundwater withdrawals and on the effects of climate change. Six models were developed to simulate the potential impact of climate change and estimated future pumping rates for WY 2020 to WY 2070, based on a recommended subset of World Climate Research Program’s Coupled Model Intercomparison Project GCMs for 2075 to 2099 (DWR 2018). As there is some disagreement among climate models, these scenarios test the effect of warming temperatures and varying quantities of precipitation, both more and less than the historical average. For comparison, a future baseline model was also developed to include estimated future pumping rates, but with no simulated climate change effects. Because predicted climate change effects are based on the 2075–2099 period, the simulated climate scenarios represent a worst case scenario, such that the changes in temperature and precipitation occur immediately beginning in WY 2020, rather than the more

gradual change that would be expected to occur in reality. The climate scenarios tested, along with the corresponding changes in recharge and lake stage, are listed in Table 5-4. The methodology used to simulate recharge rates and lake stages for each of these climate scenarios is described in more detail in Appendix I.

Projected flow budget results for WY 2070 from the baseline and Q2 (hot and dry) climate scenarios are presented in Table 5-5 and Table 5-6, respectively. For the sake of brevity, flow budget results from the remaining climate scenarios are not presented in tabular form, but selected flow budget components are plotted for comparison. Cumulative change in storage within the TVS subbasin for all climate scenarios is shown in Figure 5-25. Though not depicted here, it is interesting to note that the cumulative change in storage for the entire model domain for scenario Q3 (hot and wet) is positive over the simulated period, while it can be seen to be negative for the TVS Subbasin alone in Figure 5-25. Baseflow to streams within the TVS Subbasin for all climate scenarios is shown in Figure 5-26 and shows an increase in baseflow for ‘wet’ scenarios (Q3 and Q4) relative to baseline, and a decrease in baseflow for the warmer and drier scenarios.

Discharge to Lake Tahoe originating from within the TVS Subbasin for all climate scenarios is shown in Figure 5-27. Warmer and drier scenarios show an interesting result of a sudden increase in outflow to Lake Tahoe at the beginning of the simulated period, followed by a decline in outflow, eventually reaching a negative outflow rate (i.e., inflow from the lake to the basin). This pattern is a result of the simulated changes to the lake stage corresponding to the various climate scenarios. As the stage of the lake declines during dry periods, the gradient between groundwater levels in the basin and the lake steepens, and outflow increases. When the simulated lake stage reaches a new equilibrium level for each climate scenario, the gradient re-equilibrates to the boundary condition and outflow to the lake begins to decline.

Table 5-4. Areal recharge rates and lake stages used in future predictive climate scenarios. Recharge rates listed are for the model domain.

Scenario	Recharge (AFA)	Lake Stage (ft)
Baseline	38,790	6,228.20
Q1 (warm/dry)	29,206	6,218.20
Q2 (hot/dry)	26,026	6,214.90
Q3 (hot/wet)	48,254	6,232.00
Q4 (warm/wet)	52,303	6,232.00
Q5 (warm)	36,564	6,225.90

Table 5-5. Projected flow budget terms from the Baseline climate scenario for WY 2070, segregated into components for the TVS Subbasin (Zone 10) and the Mountain Block (Zone 1).

Item	Units	Mountain Block (Zone 1)	TVS Subbasin (Zone 10)	Model Domain (Zone 1 + Zone 10)
Area	AC	85,093	14,814	99,907
INFLOWS				
Areal Recharge	AFY	33,900	4,900	38,800

Item	Units	Mountain Block (Zone 1)	TVS Subbasin (Zone 10)	Model Domain (Zone 1 + Zone 10)
Recharge from Zone 1 to Zone 10 ¹	AFY	0	15,600	N/A
Lake Tahoe	AFY	0	4,700	4,700
Storage	AFY	14,000	3,300	17,300
Inflow Total	AFY	47,900	28,500	60,800
OUTFLOWS				
Recharge from Zone 1 to Zone 10 ¹	AFY	15,600	0	N/A
Pumping	AFY	0	11,800	11,800
Baseflow to Streams	AFY	16,300	11,200	27,500
Lake Tahoe	AFY	2,200	2,300	4,500
Storage	AFY	13,800	3,200	17,000
Outflow Total	AFY	47,900	28,500	60,800

Note: All values are rounded to the nearest 100 AFY.

¹Recharge from Zone 1 to Zone 10 is an internal flux within the model domain rather than a simulated inflow or outflow, and is not summed within the model domain flow budget.

Table 5-6. Projected flow budget terms from the Q2 (hot and dry) climate scenario for WY 2070, segregated into components for the TVS Subbasin (Zone 10) and the Mountain Block (Zone 1).

Item	Units	Mountain Block (Zone 1)	TVS Subbasin (Zone 10)	Model Domain (Zone 1 + Zone 10)
Area	AC	85,093	14,814	99,907
INFLOWS				
Areal Recharge	AFY	23,400	2,600	26,000
Recharge from Zone 1 to Zone 10 ¹	AFY	0	11,800	N/A
Lake Tahoe	AFY	0	5,000	5,000
Storage	AFY	11,200	2,900	14,100
Inflow Total	AFY	34,600	22,300	45,100
OUTFLOWS				
Recharge from Zone 1 to Zone 10 ¹	AFY	11,800	0	N/A
Pumping	AFY	0	11,800	11,800
Baseflow to Streams	AFY	10,700	6,000	16,700
Lake Tahoe	AFY	1,800	1,700	3,500
Storage	AFY	10,300	2,800	13,100
Outflow Total	AFY	34,600	22,300	45,100

Note: All values are rounded to the nearest 100 AFY.

¹Recharge from Zone 1 to Zone 10 is an internal flux within the model domain rather than a simulated inflow or outflow, and is not summed within the model domain flow budget.

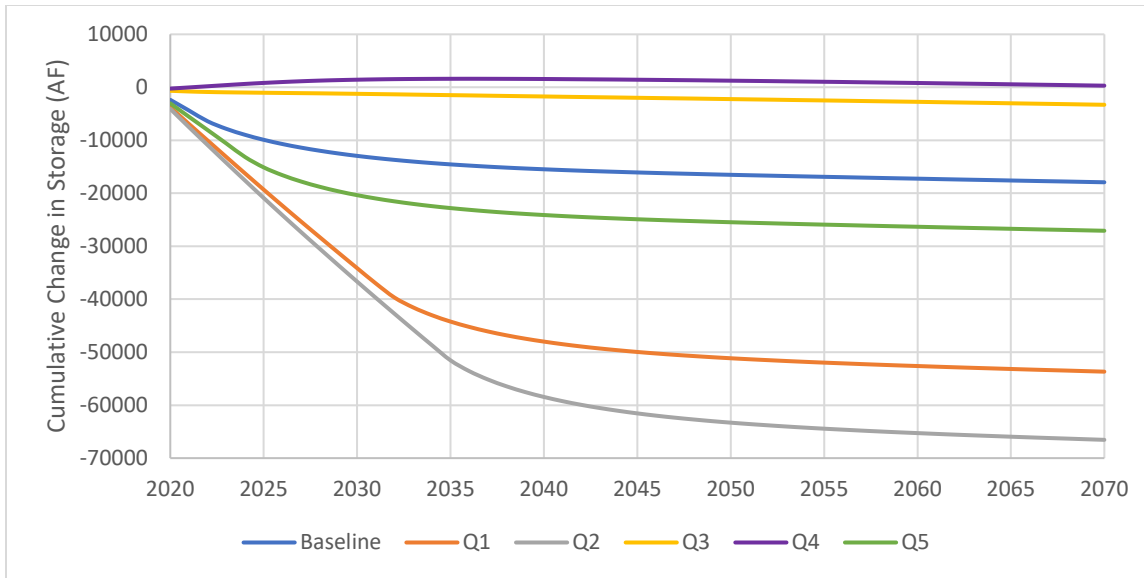


Figure 5-25. Cumulative change in storage within the TVS Subbasin for all climate scenarios, WY 2020 – WY 2070.

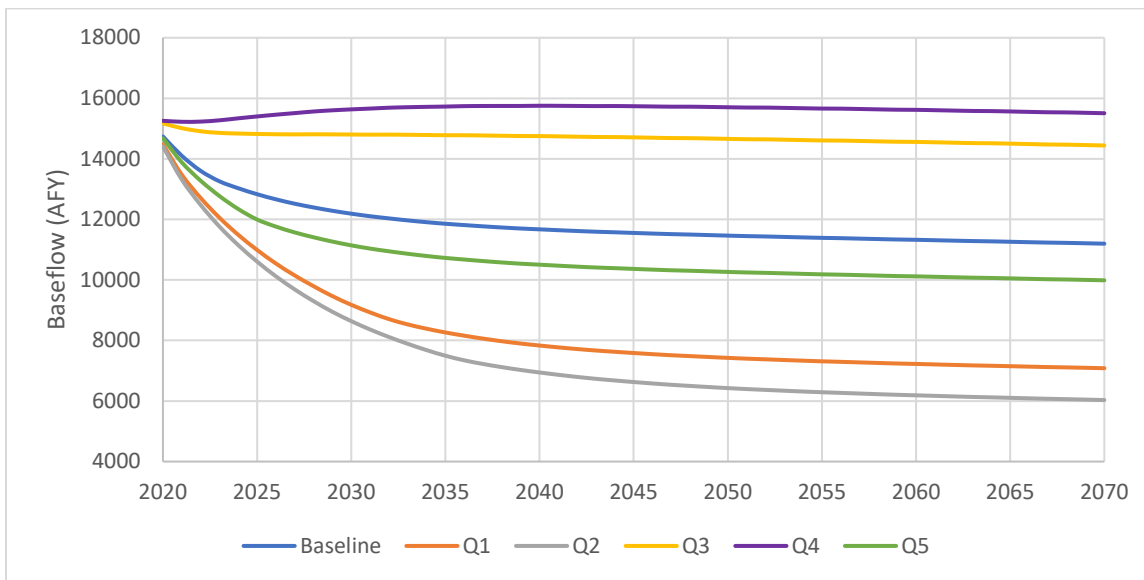


Figure 5-26. Baseflow to streams within the TVS Subbasin for all climate scenarios, WY 2020 – WY 2070.

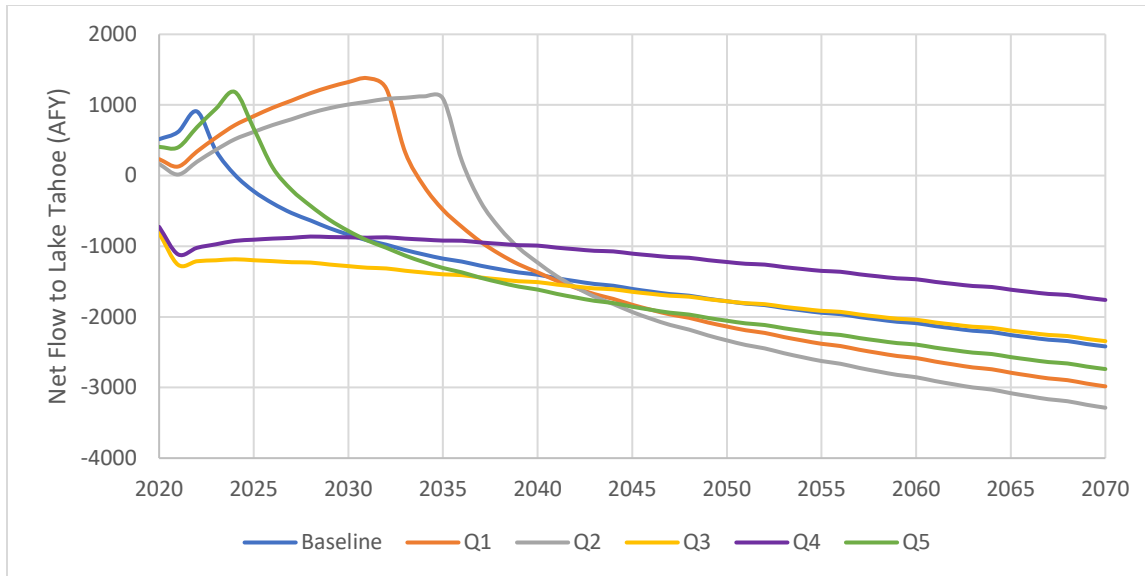


Figure 5-27. Discharge to Lake Tahoe from the TVS Subbasin for all climate scenarios, WY 2020 – WY 2070. Negative flow rates indicate lake water flowing into the TVS Subbasin.

5.5 Sustainable Yield

Under SGMA, sustainable yield is explicitly defined as “the maximum quantity of water calculated over a base period that is representative of long-term conditions in the basin and including any temporary surplus, that can be withdrawn annually from a groundwater supply without causing an undesirable result.” The sustainable yield must be, at a minimum, less than or equal to the amount of groundwater recharge. As noted above, groundwater recharge varies in response to annual precipitation, but on average (1983–2019) groundwater recharge for the model domain is 41,600 AFY, or 21,500 AFY for the TVS Subbasin, including both areal recharge and MBR (Table 5-2). When estimating sustainable yield, it is also important to consider that some amount of recharge must remain unwithdrawn to support GDEs in the form of baseflow to streams.

While the exact amount of baseflow to streams required to avoid an undesirable result is not known, minimum historical observed flow rates can be used as a reasonable estimate for the purpose of deriving a sustainable yield. Because gages are not maintained along all streams within the TVS Subbasin and the surrounding mountain block, simulated baseflow rates were used to define this value. A steady-state version of the STGM was developed representing recharge and lake stage conditions used in the transient Q2 (hot and dry) climate scenario but was run with no simulated pumping. The resultant baseflow to streams at each of the gages exceeds the historical minimum at that gage by at least 10 percent. Total simulated baseflow to streams over the model domain, including un-gaged streams, was 18,600 AFY: 10,300 AFY within the Mountain Block and 8,300 AFY within the TVS Subbasin. Average recharge less this estimated minimum ‘safe’ baseflow generates a sustainable yield of 20,190 AFY for the model domain: 6,990 AFY for the Mountain Block and 13,200 AFY for the TVS Subbasin. The sustainable yield estimate for the TVS Subbasin (13,200 AFY) is more than the allocations for the South Lake Tahoe area (12,100 AFY) defined in the Compact (Section 4.3.9). It is also more than the groundwater withdrawals which have been declining from a maximum of 9,800 AFY in

2007 to 6,800 AFY in 2019. The sustainable yield estimate is also more than the projected water demand of 11,800 AFY in 2070 using the 50-year population growth rates for the County (Table 5-5 and Table 5-6). Comparison of groundwater withdrawals to sustainable yield demonstrates that pumpage within the TVS Subbasin is currently within the sustainable yield and is projected to remain within the sustainable yield over the next 50-years.

5.6 Assessment of Potential Overdraft Issues

Overdraft occurs when groundwater extractions exceed the sustainable yield of an aquifer. As discussed in Section 5.5, projected groundwater extractions (11,800 AFY) are within the sustainable yield (13,200 AFY) for the TVS Subbasin. However, since the sustainable yield value is based on an average recharge rate, it is possible that an overdraft condition may still occur during years with reduced recharge, such as during a sustained drought or in response to a more permanent reduction in recharge rates because of climate change. Potential overdraft issues may include reduction of groundwater levels below the tops of well screens, reductions of groundwater in storage, reduction of baseflow to streams available to support GDEs and land subsidence. Characterization of undesirable results from chronic lowering of groundwater levels is considered in Section 8.1 and characterization of undesirable results relating to interconnected surface waters and GDEs is considered in Section 8.3.

5.6.1 Assessment of Potential Overdraft

The STGM was used to assess potential overdraft issues within the TVS Subbasin through WY 2070. The simulated change in groundwater levels between WY 2019 and WY 2070 are shown for the baseline (average current climate conditions) and the Q2 (hot and dry climate scenario) climate models in Figure 5-28 and Figure 5-29, respectively. The baseline results show an average drawdown within the TVS Subbasin of 4.3 feet over the simulated period, representative of the potential drawdown resulting from the conservative estimates of future pumping used in these models. The Q2 model results show an average drawdown within the TVS Subbasin of 15.4 feet over the simulated period. The additional drawdown shown in this model represents the contribution from a worst-case future climate change scenario. The average drawdown at community water system wells is 5.6 feet and 18.1 feet for the baseline and Q2 models, respectively.

As individual water system wells are typically much shallower than community water system wells, they are at greater risk of deleterious effects resulting from declining groundwater levels. The locations of active individual water system wells throughout the TVS Subbasin were derived from the Phase I and Phase II private well owner surveys described in Section 3.3.4. While the exact depths of these wells are not known for each location, they are assumed to have a minimum depth of 50 feet. In order to assess the number of individual water system wells that may be at risk from potential overdraft, the locations of all known active individual water system wells are compared to basin areas with simulated depth to water greater than 50 feet for WY 2070 for the baseline and Q2 models in Figure 5-30 and Figure 5-31, respectively. Simulated water levels for WY 2019 indicate 34 individual water system wells located in areas with depths to water greater than 50 feet. The baseline model WY 2070 indicates 38 individual water system wells located in these areas, an increase of 4 wells from present, while the Q2 model WY 2070 indicates 73 individual water system wells located in these areas, an increase of 39 wells.

Baseline and Q2 model results were also used to assess the potential effect of drawdown on baseflow to streams in interconnected surface waters. Baseflow depletion maps for WY 2070 for the baseline and Q2 models are presented in Figure 5-32 and Figure 5-33, respectively. These maps represent the difference in baseflow between a baseline model with no pumping, and baseline and Q2 models including pumping. Thus, the baseline depletion map represents depletions in baseflow to streams due to pumping only, while the Q2 depletion map represents the depletions in baseflow to streams due to both pumping and climate change. The locations of baseflow depletions are nearly identical between the two maps, with the Q2 map showing a slightly larger area affected by depletions, but the magnitude of these depletions is much greater for the Q2 model. Baseflow depletions for WY 2070 total 3,220 AF for the baseline model and 13,990 AF for the Q2 model, relative to a total simulated baseflow of 30,720 AF for the baseline model with no pumping.

These results indicate the potential impacts on wells and interconnected surface waters due to pumpage alone are negligible. At current rates of groundwater recharge, the potential effects of overdraft are not significant. If climate change results in a sustained reduction in groundwater recharge, overdraft may become a significant concern.

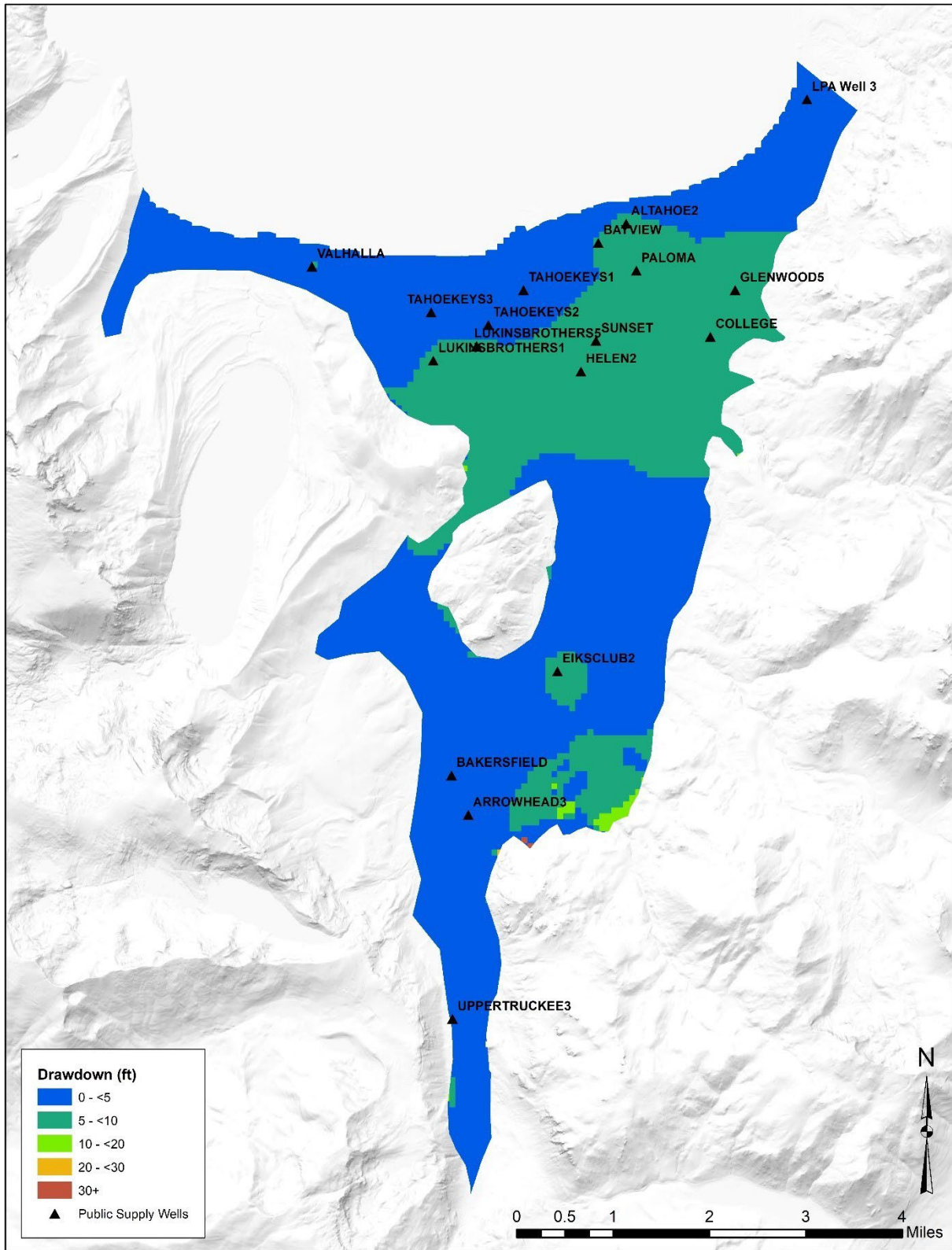


Figure 5-28. Simulated drawdown from WY 2019 to WY 2070 for the baseline climate model.

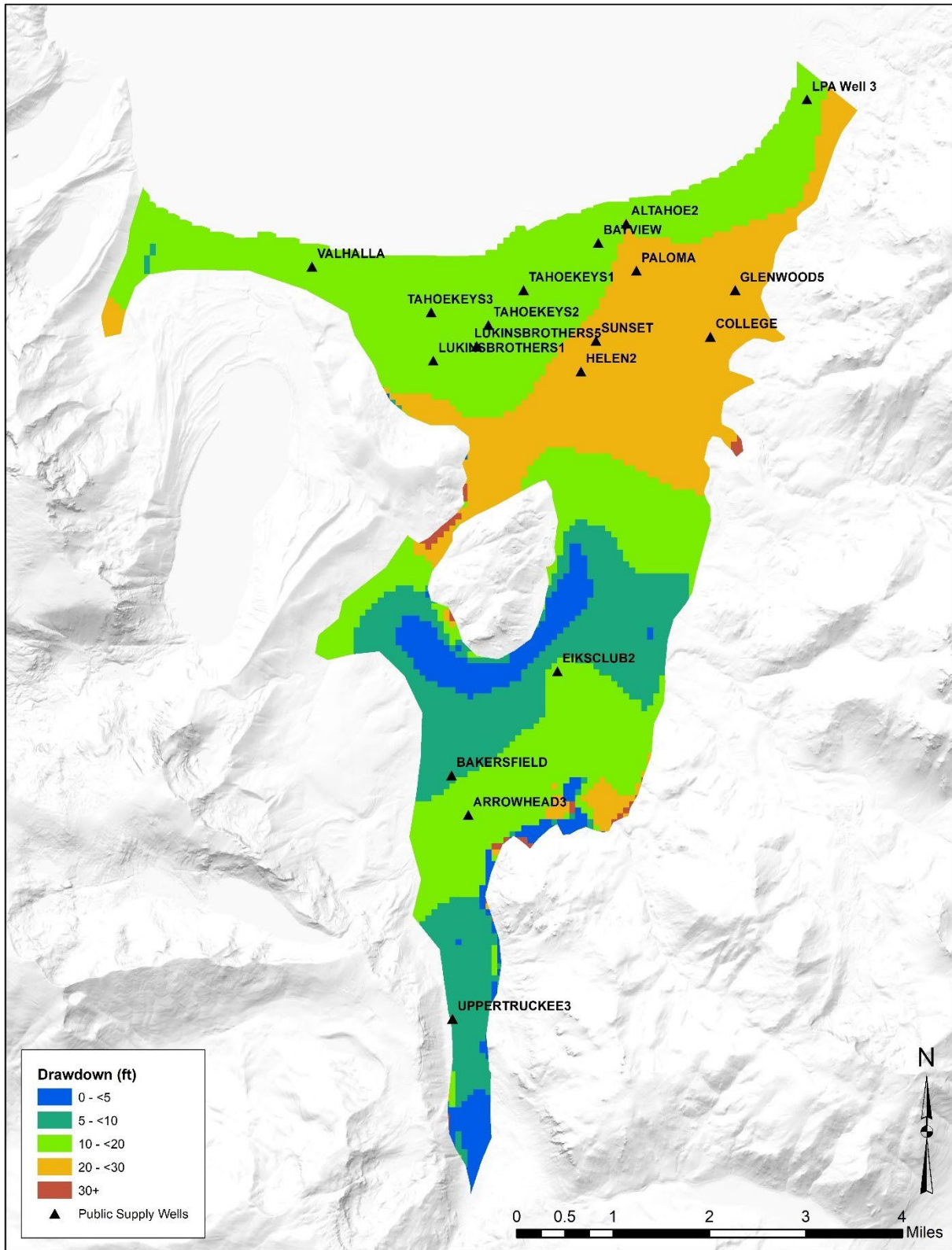


Figure 5-29. Simulated drawdown from WY 2019 to WY 2070 for the Q2 (hot and dry) climate model.

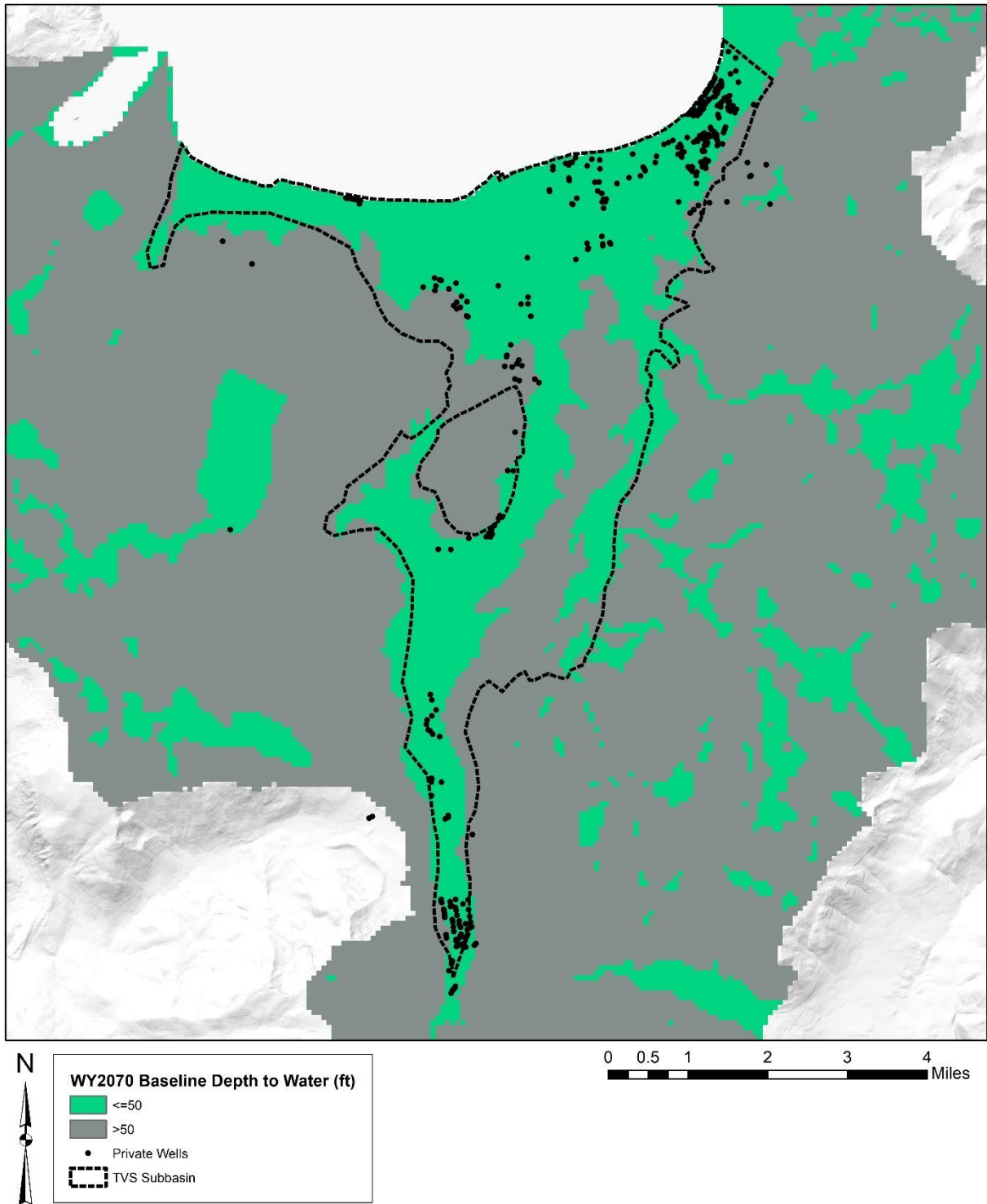


Figure 5-30. Simulated depth to water and locations of individual water system wells for WY 2070 for the baseline climate model.

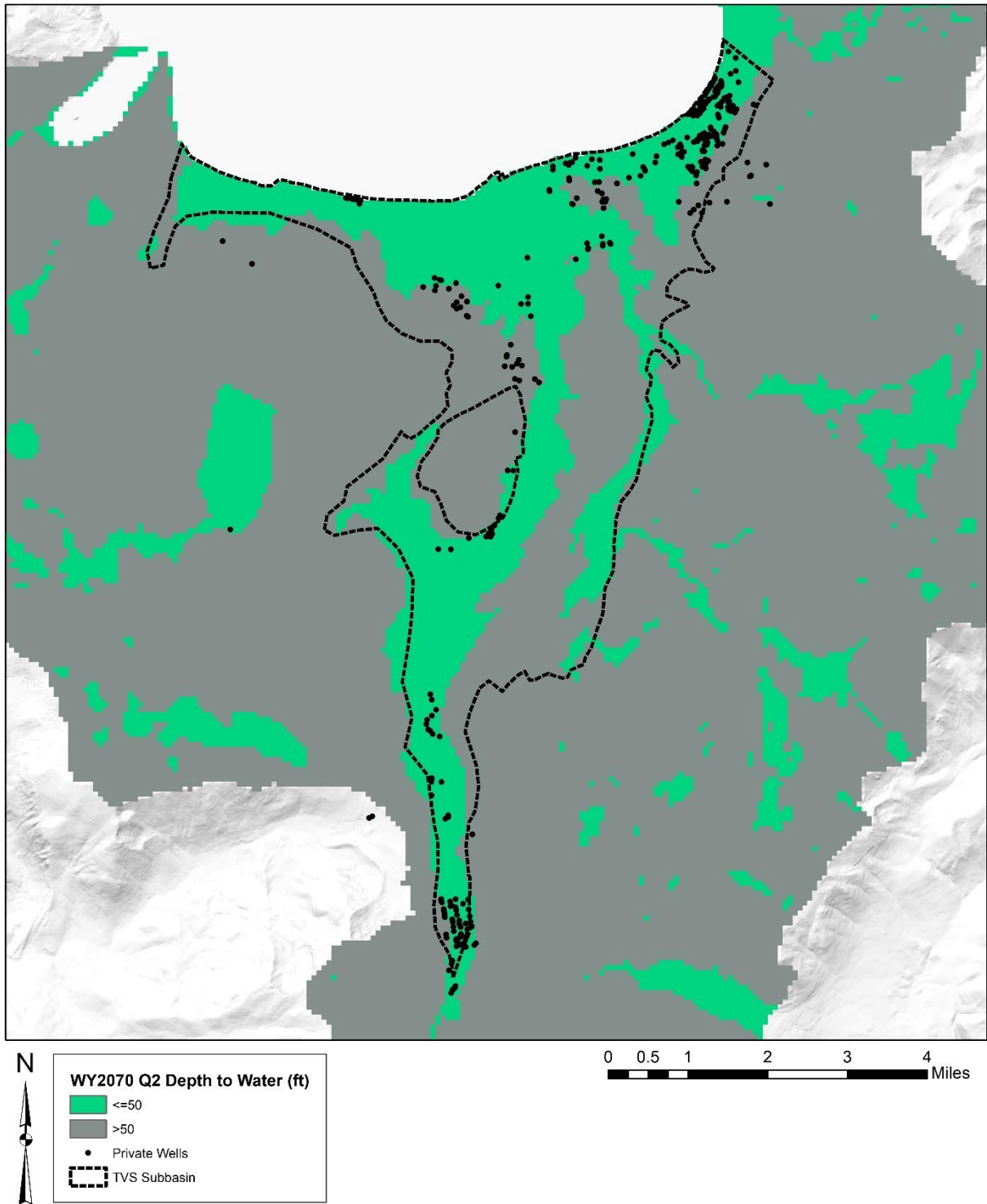


Figure 5-31. Simulated depth to water and locations of individual water system wells for WY 2070 for the Q2 (hot and dry) climate model.

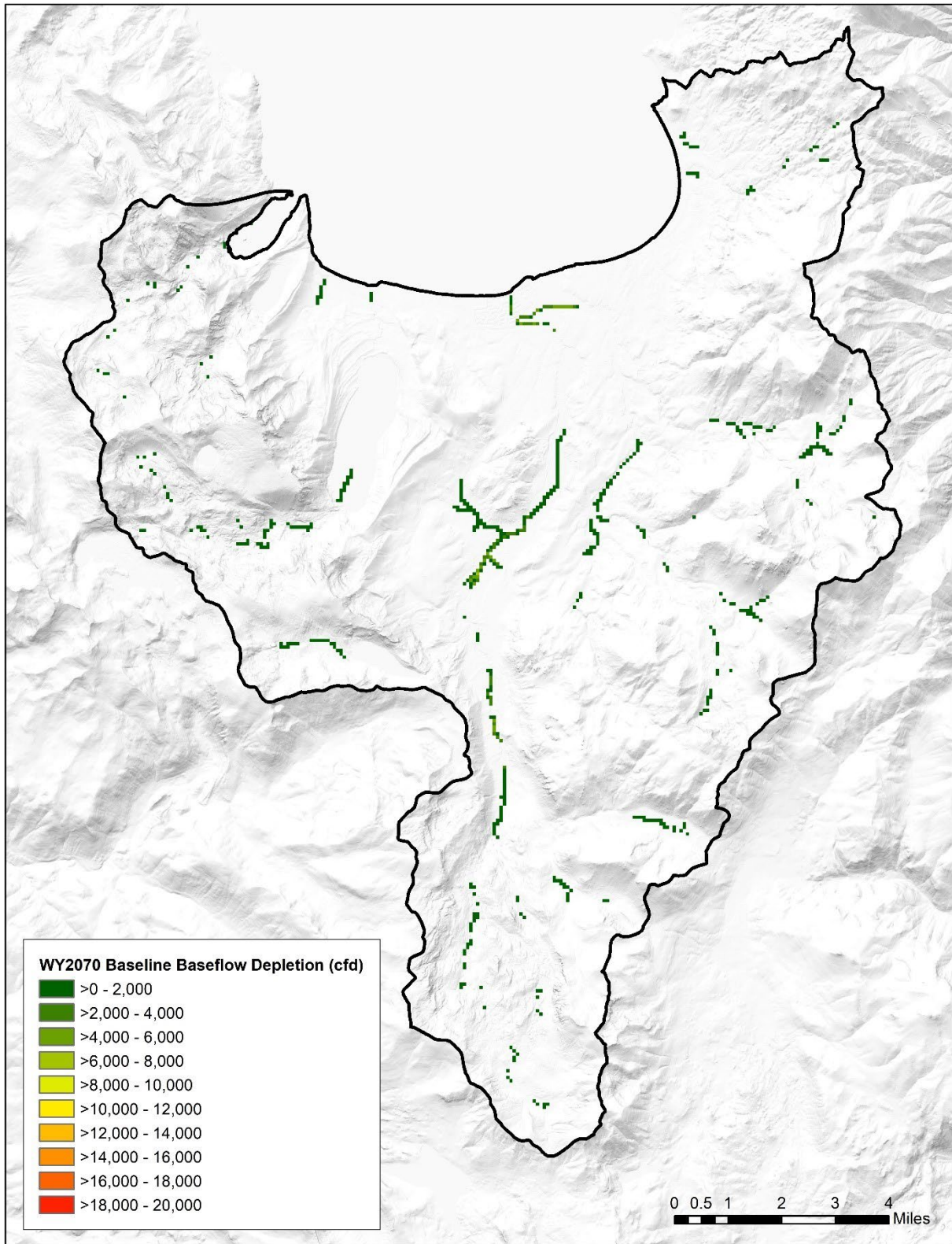


Figure 5-32. Locations and magnitudes of baseflow depletion due to pumping in the baseline climate model in cubic feet per day (CFD).

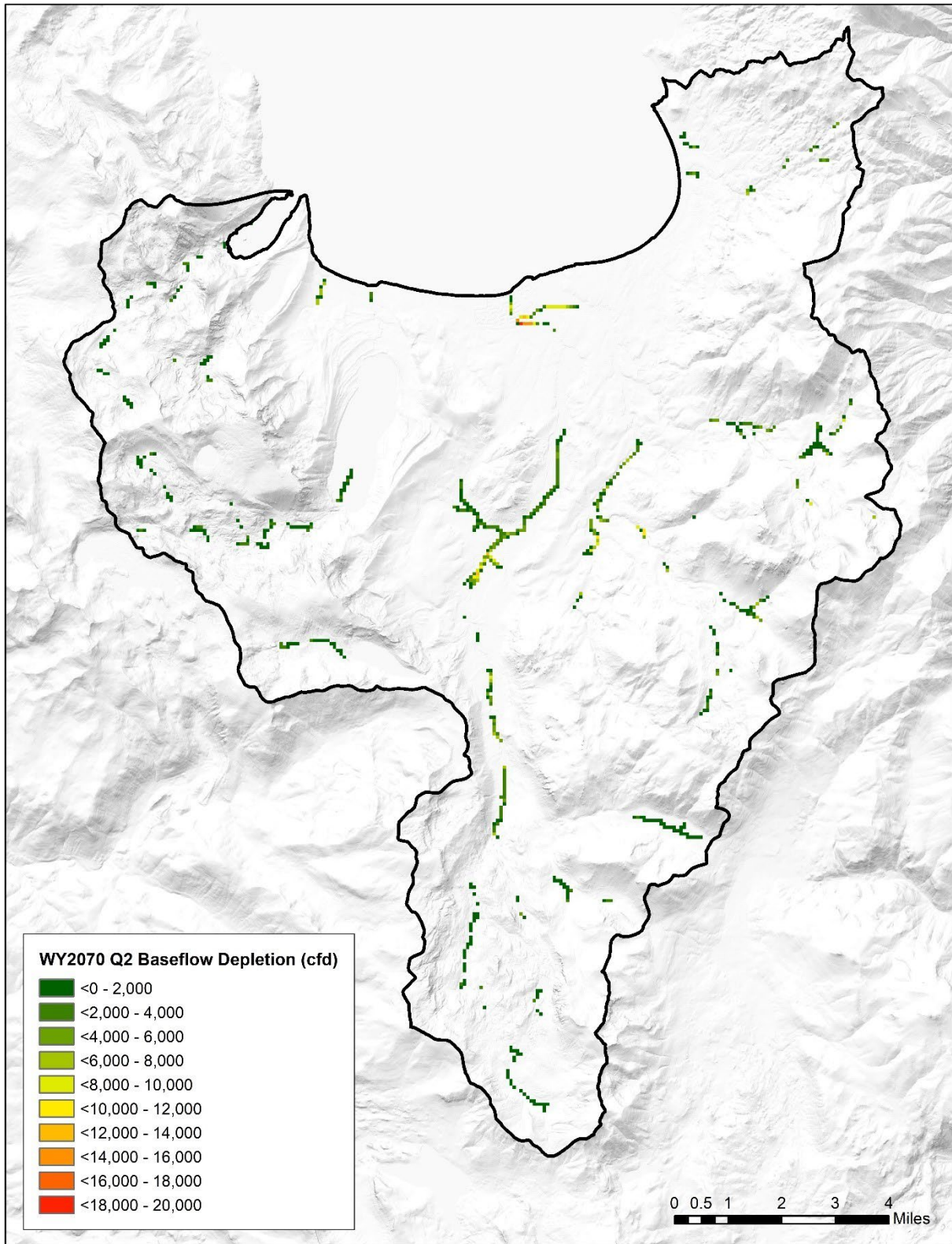


Figure 5-33. Locations and magnitudes of baseflow depletion due to pumping and climate change in the Q2 (hot and dry) climate model in cubic feet per day (CFD).

The TVS Subbasin consists mostly of coarse-grained glacial and alluvial/fluvial deposits and lesser fine-grained interbedded lacustrine layers (see Section 2.4). The coarse-grained deposits consist of variable mixtures of stratified and massive sand to boulders, which have sedimentologic characteristics that are less susceptible to compaction during deep declines in groundwater levels than the fine-grained lacustrine deposits composed of bedded silt and clay. The potential for land subsidence in the TVS Subbasin under current groundwater conditions is negligible because the fine-grained lacustrine deposits are relatively thin and discontinuous, and historical groundwater levels in the basin have been stable (e.g., Ireland et al., 1984).

Land subsidence can be induced by deep declines in groundwater levels that allow for compaction, particularly of fine-grained layers. This compaction occurs as pumping of groundwater reduces the fluid pressure in pore spaces between grains, which would otherwise oppose the normal stress caused by the weight of overlying sediments. The stress borne by a porous medium can be expressed by Terzaghi's Law, such that

$$\sigma = \sigma' + p \quad (1)$$

where σ is the vertical normal stress, σ' is the effective stress, or 'grain-to-grain' stress, and p is the fluid pressure. Thus, with an unchanging vertical normal stress, a reduction in fluid pressure necessitates an increase in the effective stress, which can induce a shifting or elastic compression of grains to reduce porosity (i.e., compaction). The degree of compaction resulting from a given increase in effective stress—caused by an equivalent decrease in pore fluid pressure—is a function of the compressibility (α) of the aquifer rock or sediment, such that

$$-(dz) = \alpha z (d\sigma') = -\alpha \rho_w g dh \quad (2)$$

where z is the saturated thickness, dz is the change in thickness (i.e., the compaction), $d\sigma'$ is the change in effective stress, and $\rho_w g dh$ is the drop in hydrostatic pressure due to a decrease in head (dh).

The compressibility of a dense, sandy gravel representative of the coarse glacial deposits making up much of the basin fill in the TVS Subbasin is 4×10^{-7} ft²/lb (Domenico and Mifflin, 1965). Deeper wells (e.g. Sunset Well) access approximately 400 feet of saturated thickness. To generate land subsidence of one foot in these sediments, a sustained head drop of 100 feet would be required. This exceeds the maximum simulated drawdown within the subbasin for WY 2070 for both the baseline and Q2 models. Characterization of undesirable results with respect to land subsidence are presented in Section 8.1.3.

Climate change in the Sierra Nevada Region will disrupt a wide range of processes that have historically been assumed to be stable or at equilibrium. Within this region, temperatures are generally warming while changes in overall precipitation remain uncertain. Anticipated climate changes will likely lead to a higher rain-snow line, decreased snowpack, reduced soil moisture, increased wildfires, and increased evapotranspiration within the Lake Tahoe Hydrologic Basin. These disruptions are described in the statewide and regional reports produced

by the California Fourth Climate Change Assessment, and guidance for preventing, quantifying, and assessing vulnerability to these impacts is provided in California’s Climate Action Plans.

5.7.1 **CCCA4 Sierra Nevada Region**

The California Climate Change Assessment projects 6 °F to 9 °F of warming in the Sierra Nevada region by the end of the century and highlights the uncertainty in future precipitation (Dettinger et al. 2018). Despite this uncertainty (projections of changes to precipitation range between ±10%–15% of historical averages), snowpack is expected to decline due to warming, and spring runoff will therefore occur earlier in the year. Shifts from snow to rain are likely to lead increases in spring and winter discharges with concurrent reductions in late season base flows, as well as reduced soil and vegetation moisture. These changes are already occurring and will continue even in the absence of development-induced stresses. Along with the long-term trend of temperatures, both temperatures and precipitation are expected to become increasingly variable. Prolonged drought conditions could lead to increased groundwater pumping to meet increased water demands.

The adaptation framework presented by the California Climate Change Assessment recognizes that not all changes can be countered with management actions. Adaptation will take one of four forms: resistance (trying to ward off climate change impacts), resilience (increasing the capacity of systems to absorb and recover from climate changes), orderly response (assisting transitions to avoid the least desirable outcomes), and realignment (facilitating major transitions to the most desirable new condition). These different strategies guide the mitigation efforts described in this Alternative Plan, in which the adaptations are primarily based around resistance and resilience.

Resistant strategies are used when the combination of climate change and groundwater management threatens the viability of existing infrastructure. For example, the thresholds presented in Section 8.1 for reductions in groundwater levels are based on the need to maintain sufficient freeboard above the top of screen for existing production wells. If this threshold is approached, the timing and location of groundwater withdrawals can be adjusted to minimize the risk of dropping groundwater levels too far. Environmental changes that may be caused or exacerbated by groundwater pumping (depletions in surface water, for example) can be addressed with resilience-based strategies, allowing some declines but managing withdrawals to ensure that environmental discharge does not fall too low to irrevocably damage the community.

5.7.2 **Climate Action Plans**

The California DWR’s Climate Action Plan (CAP) offers guidance on mitigating the effects of climate change on a variety of processes. The plan is divided into three phases: Greenhouse Gas Emissions Reduction Plan (Phase 1; DWR 2020), Climate Change Analysis (Phase 2; DWR 2018), and Climate Change Vulnerability Assessment (Phase 3; Selmon et al. 2019). The Phase 1 plan is incorporated into other management activities within the TVS Subbasin. While the formulation of climate scenarios for this planning effort followed previous DWR guidance (DWR 2018), future updates to this Alternative should follow the SGMA-specific guidance presented in the Phase 2 Climate Action Plan.

The Climate Change Vulnerability Assessment (Selmon et al. 2019) examines the effects of climate change on DWR assets. Mechanisms considered include, among others, long-term persistent hydrologic changes and habitat and ecosystems services degradation. Diminished snowpack and warmer temperatures will change the timing of spring runoff peaks and drive increased demand for both agricultural and municipal water. The DWR Phase 3 assessment focuses largely on the risks to the ability of the State Water Project to deliver agricultural flows, but the increased demand for water and changes in runoff timing are relevant to this Alternative Plan as well. Projected increases in water demand and changes to recharge induced by shifts in runoff timing are incorporated in the STGM that informs this Alternative Plan, as described in Section 5.4.8.

Climate change has already affected Sierra Nevada ecosystems, and these effects will continue (PRBO Conservation Science 2011). The distributions of plant and animal communities are shifting in response to climate changes, even in the absence of other anthropogenic disturbances (Selmon et al. 2019). When anthropogenic stressors are present, they are exacerbated by climate change (Selmon et al. 2019). Whereas the DWR Vulnerability Assessment considers these impacts qualitatively (Selmon et al. 2019), Section 8.3 of this Alternative Plan includes quantitative metrics to protect both terrestrial and aquatic communities that rely, in whole or in part, on the connections between groundwater and surface water.

SECTION 6: GROUNDWATER QUALITY

The following section provides an overview of current groundwater quality and groundwater quality issues recognized within the TVS Subbasin using available water quality records collected over the past ten years (2011–2020). Limitations of the water quality data used to describe groundwater quality are discussed in Section 6.1.2.

6.1 Background

The Safe Drinking Water Act (SDWA) defines a contaminant as any physical, chemical, biological, or radiological substance or matter present in any media at concentrations that may pose a threat to human health or the environment. Pursuant to the SDWA, EPA adopts and enforces standards for the amount of a contaminant that is allowed in public water systems. Maximum Contaminant Levels (MCLs) are enforceable standards established to protect the public against consumption of drinking water contaminants that present a risk to human health. MCLs are established for inorganic chemicals, organic chemicals, disinfection by-products and radioactivity. The EPA has also established National Secondary Drinking Water Regulations that set non-mandatory water quality standards. These secondary MCLs (SMCLs) are not enforceable but are established only as guidelines to assist public water systems in managing their drinking water for aesthetic considerations, such as taste, color, and odor. These contaminants are not considered to present a risk to human health at the SMCL. MCLs and SMCLs also serve as water quality objectives for groundwater designated for municipal and domestic supply under the Basin Plan (see Section 4.3.2).

6.1.1 Overview and Data Sources

The following analysis uses water quality data collected over the past 10 years (2011–2020) to describe current groundwater quality conditions within the TVS Subbasin. These data consist of water quality records downloaded on June 2, 2021, from the State Water Board Groundwater Ambient Monitoring and Assessment (GAMA) Groundwater Information System – which includes records from the Department of Health Services and USGS datasets for water supply wells – and records from the GAMA-Electronic Deliverable Format dataset for environmental monitoring wells (environmental wells).

Environmental wells typically sample groundwater quality from the uppermost water-bearing zones, while the water supply wells typically sample groundwater quality in the deeper water-bearing zones used for drinking water production. Chemical data for the water supply wells was supplemented with general and inorganic water quality data collected during private well water quality testing conducted during the Phase II survey (Section 3.3.4). Chemical data for the environmental wells was supplemented with chemical data available from site investigation reports through SWRCB-GeoTracker for the Meyers Landfill (SL0601724846) and Private Residence (SL0601714201) sites. For a detailed description of historical groundwater conditions, the reader is referred to Section 6.0 of the 2014 Groundwater Management Plan (Kennedy-Jenks, 2014).

6.1.2

Identification of Data Gaps/Uncertainty

Even though the total number of water quality records used for describing water quality in the TVS Subbasin is substantial (16,669 records), the data is inherently predisposed by the well type, sampling frequency and types of water quality constituents analyzed. For instance, in terms of the total number of records, there are about five times more water quality records available for water supply wells than environmental monitoring wells (Table 6-1). Within each well type, there is further bias in the types of wells from which water quality records are generated. For the drinking water supply wells, water quality records are predominantly from active wells within community water systems. There are a very limited number of water quality records from non-community and private wells. For the environmental monitoring wells, water quality records are from underground storage tank cleanup and cleanup program sites regulated by the LRWQCB including open site assessment, remediation, or verification monitoring sites; and case closed sites completed within the past ten years. These biases lead to substantially greater description of water quality within portions of TVS Subbasin areas where groundwater is actively used for drinking water and/or monitored as part of recent and/or active regulated groundwater investigation and remediation sites.

Table 6-1. Types and numbers of water quality records used for describing groundwater quality in the TVS Subbasin.

Water Quality Type	Drinking Water Supply Wells	Environmental Monitoring Wells
General	1,476	13
Inorganic	2,441	99
Chemical	9,425	2,581
Radionuclide	634	-
Total Number of Records	13,976	2,693

There are other biases, in terms of the types of water quality constituents analyzed. For example, PAHs have shown up in aquifers as byproducts of combustion during wildfires (see Section 5.1.2). PAHs are made whenever substances are burned and found in hundreds of chemicals that occur naturally in fossil fuels and are formed as by-products from their combustion. Only two of the most common PAHs (benzo (a) pyrene and naphthalene) are in the GAMA dataset. Search of the GAMA dataset for these compounds show that benzo (a) pyrene and naphthalene were not detected in groundwater samples collected from water supply wells in the TVS Subbasin. Naphthalene has been detected in groundwater samples collected from environmental wells at the Meyers Landfill site (Section 6.3.1.3).

6.2

Groundwater Quality

The following section describes groundwater quality in terms of general, inorganic, chemical and radionuclide constituents regulated by the SWRCB Division of Drinking Water and groundwater contaminants regulated by LRWQCB through underground storage tank and Site Cleanup Programs.

6.2.1 General Water Quality

Groundwater in the TVS Subbasin is generally of excellent chemical quality, suitable for the designated beneficial uses of municipal and industrial water use and for any other uses to which it might be put. Natural sources of salts are from the dissolution of minerals in the basin-fill deposits. Anthropogenic sources are from disposal of wastewater and infiltration of water containing fertilizers or other sources of salts, nitrates, or phosphates. All sewage from within the Lake Tahoe Basin must be collected, treated, and exported outside of the Lake Tahoe Basin. Spills and releases from the District's sewer collection system have the potential to contaminant surface water and groundwater quality. The District regularly performs inspections and maintenance on its sewer collection and recycled water export systems in order to prevent sewerage spills and releases.

A summary of the nutrient and general water quality data for water supply and environmental wells is provided in Table 6-2.

6.2.1.1 Water Supply Wells

Groundwater from water supply wells is relatively low in total dissolved solids with typical values on the order of 100 milligrams per liter (MG/L). Average values for chloride and sulfate are very low at about 10.4 MG/L and 3.3 MG/L, respectively. Maximum nutrient concentrations for Nitrate (NO₃ as N) and Nitrite (NO₂ as N) are also low at 1.36 MG/L and 0.07 mg/L, respectively, well within MCLs for these constituents.

A limited number of groundwater samples collected from private wells (16 in total) were further evaluated and plotted on a Piper trilinear diagram (Table 6-1) to show major ion compositions and water types occurring within the TVS Subbasin. From this evaluation, calcium-bicarbonate (Ca-HCO₃) is the predominant water type, followed by sodium bicarbonate (Na-HCO₃) and calcium-chloride (Ca-Cl). Two groundwater samples, one collected near the south shore of Lake Tahoe within the Bijou sub-area (Sample Id AG74113) and the other collected in the Christmas Valley sub-area (Sample Id AG73885) were classified as sodium-chloride (Na-Cl) water types.

Table 6-2. General water quality for water supply and environmental wells within the TVS Subbasin (6-005.01) sampled over the past ten years (2011–2020).

Constituent	MCL	Units	WATER SUPPLY WELLS					ENVIRONMENTAL WELLS				
			Wells Sampled	Average Conc.	Min. Conc.	Max. Conc.	Wells >MCL	Wells Sampled	Average Conc.	Min. Conc.	Max. Conc.	Wells >MCL
Constituents with Primary MCLs								Constituents with Primary MCLs				
Nitrate (NO ₃ as N) + Nitrate (NO ₂ as N)	45	mg/L	21	0.30	<0.02	1.36	0	0	-	-	-	-
Nitrite (NO ₂ as N)	1	mg/L	87	0.01	<0.01	0.07	0	0	-	-	-	-
Constituents with Secondary MCLs								Constituents with Secondary MCLs				
Chloride	250	mg/L	49	10.4	<0.5	66.7	0	0	-	-	-	-
Specific Conductance	900	μS/cm	36	188	60	528	0	0	-	-	-	-
Sulfate	250	mg/L	48	3.3	<0.5	28.8	0	4	11.87	1.9	32.4	0
Total Dissolved Solids	500	mg/L	50	133	37	308	0	0	-	-	-	-

Note: Bold is for constituents with concentrations above the MCL.

Source: GAMA Groundwater Information System Database for period from 2010 to 2020 for water supply wells and environmental wells within the TVS Subbasin (Downloaded June 2, 2021).

Piper Diagram - PWOS II

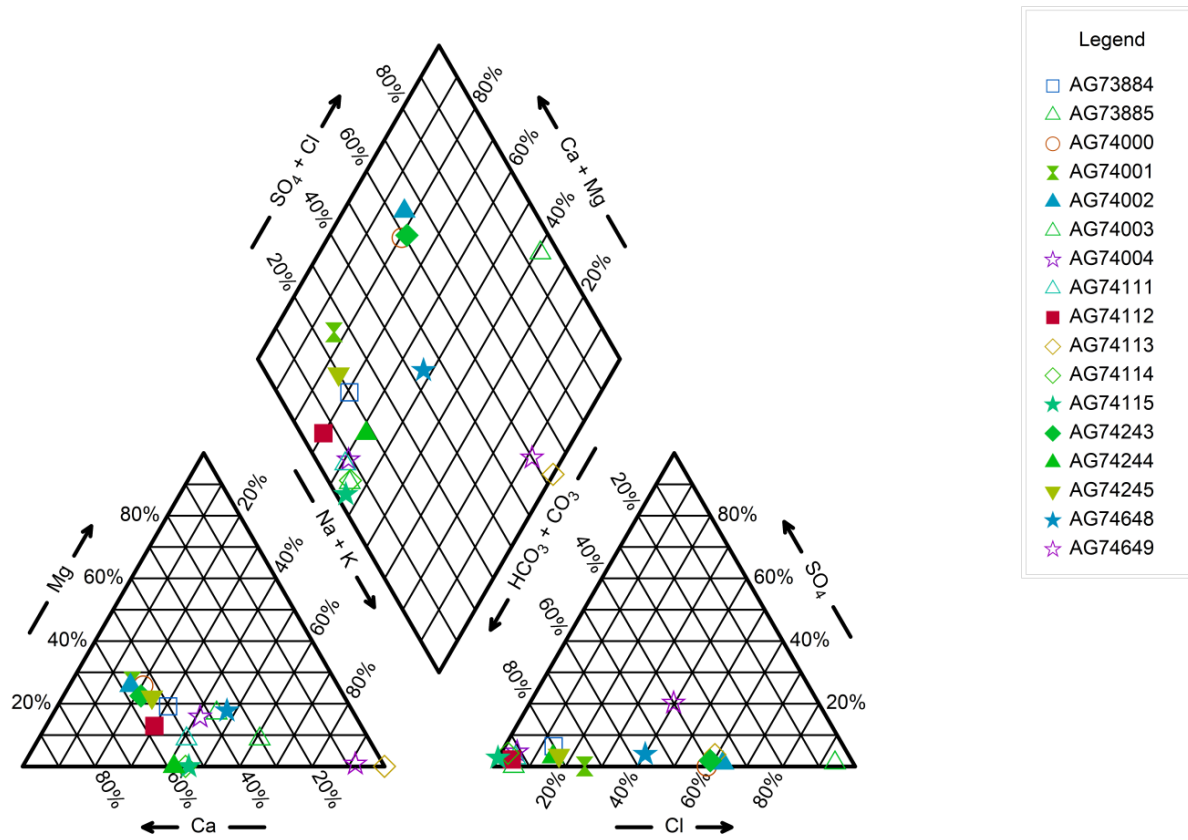


Figure 6-1. Major ion compositions for groundwater samples collected from private wells during the Phase II survey of private well owners.

6.2.1.2 Environmental Wells

General groundwater quality data for environmental wells is very limited to Sulfate values for groundwater samples collected from four monitoring wells from a single site (TO6017001). Sulfate in these monitoring wells average (11.8 MG/L) with a maximum concentration of 32.4 MG/L.

6.2.2 Inorganic Constituents

Inorganic constituents listed in drinking water standards generally include various metals, halogens and cyanide. Of these constituents, arsenic and chromium are the only constituents found at concentrations exceeding the primary MCL. Iron and manganese are the only constituents found at concentrations exceeding SMCLs.

6.2.2.1 Water Supply Wells

Table 6-3 presents a summary of the inorganic constituents detected in water samples collected from the water supply wells in the TVS Subbasin over the past 10 years. Of the wells sampled during this period, one well had a single instance of aluminum above the primary MCL of 1 milligram per liter (MG/L); and five wells had one or more instances of arsenic above the primary MCL of 10 micrograms per liter (UG/L). A total of eight wells had one or more instances of iron above the SMCL (300 UG/L) and three wells had one or more instances of manganese above the SMCL (50 UG/L). A map showing locations of incidences of inorganic chemical constituents above MCLs is shown in Figure 6-2

Based on the incidences of arsenic in the water supply wells and the WBZs from which these wells produce, arsenic above MCLs is found in relatively deep confined WBZs found in the Meyers (MZ3, MZ4), Angora (AZ1, AZ2), South Lake Tahoe (SLTZ1, SLTZ2, SLTZ3), and Tahoe Keys (TKZ2, TKZ3) subareas. Iron above MCLs is found in relatively shallow semi-confined and confined WBZs in the Bijou (BZ4, BZ5), South Lake Tahoe (SLTZ4, SLTZ5), and Christmas Valley (CV4) subareas, and in relatively deep confined water-bearing zones in the Meyers (MZ3, MZ4) and Angora (AZ1, AZ2) subareas. Manganese above MCLs is found in relatively shallow unconfined and semi-confined water-bearing zones in the Tahoe Keys (TKZ5) and Meyers (MZ5) subareas; and in relatively shallow semi-confined and confined WBZs in the Bijou (BZ4, BZ5) subarea.

The sources of the arsenic, iron and manganese are believed to be naturally occurring derived from the weathering of exposed bedrock within and surrounding the groundwater basin and/or the dissolution of arsenic and/or iron- and manganese-bearing materials within the basin-fill deposits. Iron in standby and offline wells may sometimes also be caused by biofilms or corrosion of metal casings within the well.

6.2.2.2 Environmental Wells

Although the number of environmental wells sampled for inorganic constituents is very limited, there was only one incidence of an inorganic constituent (Thallium at 10 UG/L) detected above an MCL (Thallium at 2 UG/L). However, the sampling result is suspect as the result is

below the reporting limit for the analysis. A summary of inorganic water quality sample results is presented in Table 6-3.

Table 6-3. Inorganic water quality for water supply and environmental wells within the TVS Subbasin (6-005.01) sampled over the past ten years (2011–2020).

Constituent	MCL	Units	WATER SUPPLY WELLS					ENVIRONMENTAL WELLS				
			Wells Sampled	Avg Conc.	Min. Conc.	Max. Conc.	Wells >MCL	Wells Sampled	Avg Conc.	Min. Conc.	Max. Conc.	Wells >MCL
Constituents with Primary MCLs								Constituents with Primary MCLs				
Aluminum	1	mg/L	35	0.05	ND	1.2	1	0	-	-	-	-
Antimony	0.006	mg/L	32	ND	ND	ND	0	7	ND	ND	ND	0
Arsenic	0.01	mg/L	56	0.006	<0.001	0.014	5	7	ND	ND	ND	0
Barium	1	mg/L	36	0.006	ND	0.05	0	7	0.14	0.06	0.5	0
Beryllium	0.004	mg/L	35	0.000001	ND	0.00001	0	7	ND	ND	ND	0
Cadmium	0.005	mg/L	35	0.00002	ND	0.0001	0	7	ND	ND	ND	0
Chromium	0.05	mg/L	36	0.0005	ND	0.001	0	7	0.003	0.001	0.005	0
Cyanide	0.15	mg/L	26	0.0006	ND	0.005	0	0	-	-	-	-
Fluoride	2	mg/L	34	0.12	ND	0.613	0	0	-	-	-	-
Hexavalent chromium	0.01	mg/L	23	0.001	0.001	0.001	0	7	0.003	0.003	0.003	0
Mercury	0.002	mg/L	29	ND	ND	ND	0	7	ND	ND	ND	0
Nickel	0.1	mg/L	35	ND	ND	ND	0	7	0.004	0.004	0.004	0
Perchlorate	0.006	mg/L	32	ND	ND	ND	0	0	-	-	-	-

Constituent	MCL	Units	WATER SUPPLY WELLS					ENVIRONMENTAL WELLS				
			Wells Sampled	Avg Conc.	Min. Conc.	Max. Conc.	Wells >MCL	Wells Sampled	Avg Conc.	Min. Conc.	Max. Conc.	Wells >MCL
Selenium	0.05	mg/L	35	0.00002	ND	0.0001	0	7	ND	ND	ND	0
Thallium	0.002	mg/L	31	ND	ND	ND	0	7	0.01	0.01	0.01	1
Constituents with Secondary MCLs							Constituents with Secondary MCLs					
Copper	1	mg/L	33	0.013	ND	0.16	0	7	0.005	0.003	0.011	0
Iron	0.3	mg/L	49	0.553	<0.003	6.7	8	0	-	-	-	-
Manganese	0.05	mg/L	49	0.020	<0.001	0.144	3	0	-	-	-	-
Silver	0.1	mg/L	32	0.000001	ND	0.00001	0	7	0.001	0.001	0.001	0
Zinc	5	mg/L	32	0.013	ND	0.10	0	7	0.03	0.01	0.06	0

Note: Bold is for constituents with concentration above the MCL

Source: GAMA Groundwater Information System Database for period from 2010 to 2020 for water supply wells and environmental wells within the TVS Subbasin (Downloaded June 2, 2021).

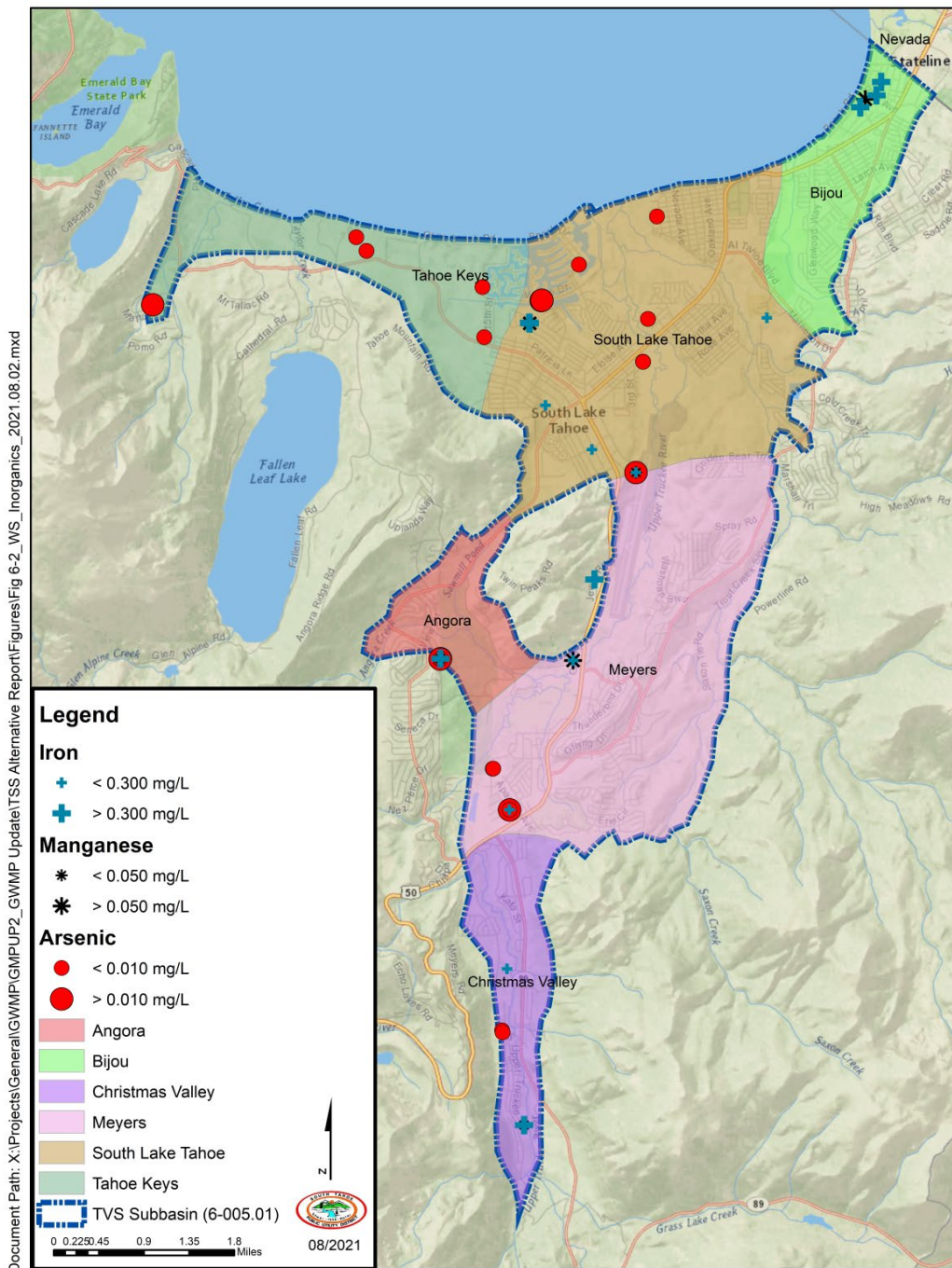


Figure 6-2. Incidences of inorganic chemical constituents above MCLs detected in water samples collected from water supply wells within the TVS Subbasin (Data Source: GAMA Groundwater Information System, June 2021).

6.2.3 **Radioactive Constituents**

Radioactive constituents are present in groundwater within the TVS Subbasin. Radiological substances include radium isotopes (Ra-226 and Ra-228), total soluble uranium, gross alpha activity and radon. Incidences of radiological substances exceeding the gross alpha MCL of 15 pCi/L and total uranium MCL of 20 pCi/L have been found in water supply wells within the TVS Subbasin (Figure 6-3).

6.2.3.1 **Water Supply Wells**

Table 6-4 presents a summary of the radioactive constituents detected in water samples collected from the water supply wells in the TVS Subbasin over the past 10 years. Of the wells sampled during this period, twelve wells had gross alpha activity above the MCL, and three wells had total uranium above the MCL.

Based on the incidences of radioactive constituents in the water supply wells and the water-bearing zones from which these wells produce, gross alphas activity above MCLs is found in relatively deep confined WBZs in the Meyers (MZ3), South Lake Tahoe (SLTZ1, SLTZ2, SLTZ3), and Tahoe Keys (TKZ2, TKZ3) subareas, and in confined WBZs in the Bijou (BZ4) and Christmas Valley (CVZ1) subareas. Incidences of uranium activity above MCLs is found in relatively deep confined water-bearing zones in the Bijou (BZ3) and Tahoe Keys (TKZ2, TKZ4) subareas (Figure 6-3). The source of the radioactivity is the naturally occurring radioactive isotopes found in granite and sediments derived from granite deposited in the basin-fill.

Radon 222 (Radon) is a radioactive gas formed by decay of small amounts of uranium and thorium naturally present in rock and soil and is found in groundwater throughout the TVS Subbasin. Investigation by the California Geological Survey shows that high radon potential is associated with granitic rock (certain granodiorite units), and lake terrace, glacial till and glacial outwash deposits. Moderate radon potential is associated with glacial till, outwash, and lake terrace deposits derived from the granodiorite (Churchill, 2009). Radon gas derived from these materials can move into the groundwater system. Currently, there are no Federal or State drinking water standards for radon (see Section 6.3.2.1).

6.2.3.2 **Environmental Wells**

Water quality records for radioactive constituents were not found for the environmental wells.

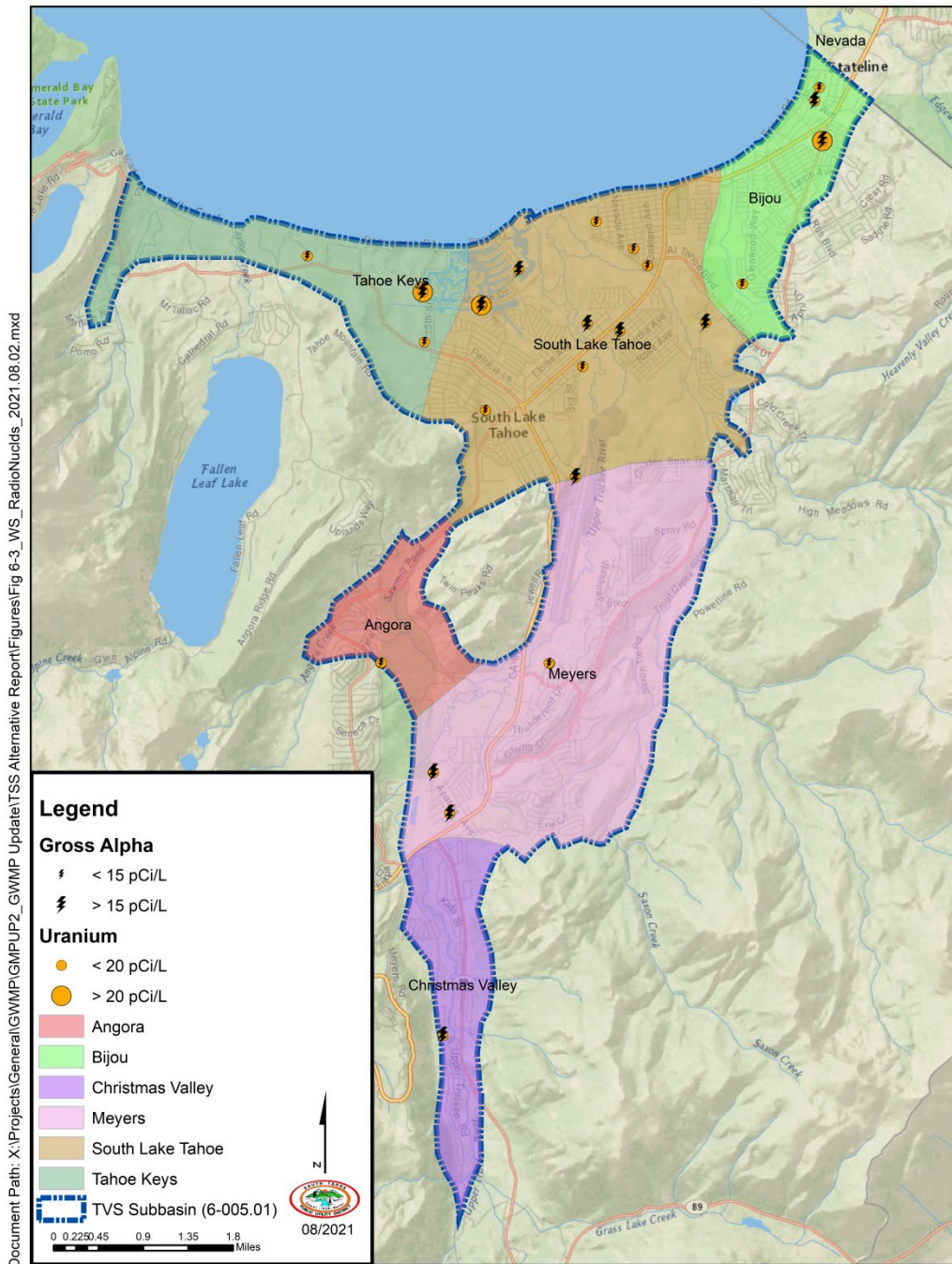


Figure 6-3. Incidences of radionuclide constituents above MCLs detected in water samples collected from water supply wells within the TVS Subbasin (Data Source: GAMA Groundwater Information System, June 2021).

Table 6-4. Radionuclide water quality in water supply wells within the TVS Subbasin (6-005.01) sampled over the past ten years (2011–2020).

Constituent	MCL	Units	WATER SUPPLY WELLS					ENVIRONMENTAL WELLS				
			Wells Sampled	Avg Conc.	Min. Conc.	Max. Conc.	Wells >MCL	Wells Sampled	Avg Conc.	Min. Conc.	Max. Conc.	Wells >MCL
Constituents with Primary MCLs								Constituents with Primary MCLs				
Radium-226	5	pCi/L	23	0.66	<1	3.99	0	-	-	-	-	
Radium-228	(combined Ra-226,228)	pCi/L	23	1.12	<1	3.97	0	-	-	-	-	
Gross Alpha particle activity	15	pCi/L	26	11.16	<3	29.7	11	0	-	-	-	
Radon 222	n/a	pCi/L	17	694	<100	6,700	n/a	0	-	-	-	
Uranium	20	pCi/L	24	7.4	<1	43	3	0	-	-	-	

Note: Bold is for constituents with concentrations above the MCL.

Source: GAMA Groundwater Information System Database for period from 2010 to 2020 for water supply wells and environmental wells within the TVS Subbasin (Downloaded June 2, 2021).

6.2.4 Regulated Chemicals

Man-made contaminants which occur most frequently in the TVS Subbasin include petroleum hydrocarbon and chlorinated hydrocarbon compounds. Petroleum hydrocarbon compounds are from spills and releases associated with the operation of gasoline storage and fueling facilities. Contaminants of concern from these releases often include the most soluble fraction of the gasoline released, including benzene, toluene, ethylbenzene and total xylenes (BTEX) and the gasoline additives used as fuel oxygenates and octane enhancers including MtBE, Tert-Butyl Alcohol (TBA), Tertiary-Amyl Methyl Ether (TAME), and ethanol. Chlorinated hydrocarbon compounds are most often used as industrial agents used for degreasing metals, cleaning electronic parts and dry-cleaning fabrics. They are also contained in many household products such as oil-based paints, drain cleaners, spot removers, engine degreasers and paint removers. Contaminants of concern from these releases often include Tetrachloroethylene (PCE); Trichloroethylene (TCE); 1,2-Dichloroethane (1,2-DCA); 1,2 Dichloroethylene (1,2-DCE); Vinyl Chloride (VC); and 1,4-Dichlorobenzene (1,4-DCB).

6.2.4.1 Water Supply Wells

Table 6-5 presents a summary of the regulated chemicals detected in water samples collected from water supply wells in the TVS Subbasin over the past 10 years. Of the wells sampled during this period, one well in the South Lake Tahoe subarea had one or more instances of 1,2-DCA above the MCL (0.5 UG/L); and five wells in the South Lake Tahoe and Bijou subareas had one or more instances of PCE above the MCL (5.0 UG/L).

Incidences of the regulated chemicals within the water supply wells are shown in Figure 6-4. Based on the incidences of regulated chemicals and the water-bearing zones from which these wells produce, chlorinated hydrocarbons above MCLs are inferred to be found in relatively shallow unconfined or semi-confined water-bearing zones near the south shore of Lake Tahoe in the Bijou (BZ5) subarea and in the Tahoe Keys (TKZ4) subarea. The source of these contaminants in the Bijou subarea is believed to be from the operation of former dry-cleaning facilities. The source of these contaminants in the South Lake Tahoe subarea is under investigation by the LRWQCB (see Section 6.3.1.1).

Table 6-5. Chemical water quality in water supply and environmental wells within the TVS Subbasin (6-005.01) sampled over the past ten years (2011–2020).

Constituent	WATER SUPPLY WELLS							ENVIRONMENTAL WELLS				
	MCL	Units	Wells Sampled	Avg Conc.	Min. Conc.	Max. Conc.	Wells >MCL	Wells Sampled	Avg Conc.	Min. Conc.	Max. Conc.	Wells >MCL
Constituents with Primary MCLs							Constituents with Primary MCLs					
Benzene	0.001	mg/L	36	ND	ND	0.0005	0	261	0.168	< 0.0005	23	46
Carbon Tetrachloride	0.0005	mg/L	36	ND	ND	ND	0	119	ND	ND	ND	0
1,2-Dichlorobenzene	0.6	mg/L	34	ND	ND	ND	0	119	ND	ND	ND	0
1,4-Dichlorobenzene (1,4 DCB)	0.005	mg/L	34	ND	ND	ND	0	119	ND	ND	0.0002	0
1,1-Dichloroethane	0.005	mg/L	36	ND	ND	ND	0	119	0.0004	0.0005	0.002	0
1,2-Dichloroethane (1,2-DCA)	0.0005	mg/L	36	0.0002	ND	0.0007	1	119	0.003	<0.0005	0.087	1
1,1-Dichloroethylene	0.006	mg/L	36	ND	ND	ND	0	119	0.003	0.0001	0.038	1
cis-1,2-Dichloroethylene (1,2-DCE)	0.006	mg/L	33	0.0002	ND	0.001	0	127	0.004	<0.0005	0.053	9
trans-1,2-Dichloroethylene	0.01	mg/L	36	ND	ND	ND	0	127	0.0002	<0.0005	0.003	0
Dichloromethane	0.005	mg/L	37	ND	ND	ND	0	11	ND	ND	ND	0

Constituent	MCL	Units	WATER SUPPLY WELLS					ENVIRONMENTAL WELLS				
			Wells Sampled	Avg Conc.	Min. Conc.	Max. Conc.	Wells >MCL	Wells Sampled	Avg Conc.	Min. Conc.	Max. Conc.	Wells >MCL
1,2-Dichloropropane	0.005	mg/L	36	ND	ND	0.00002	0	119	0.0002	<0.0005	0.002	0
1,3-Dichloropropene	0.0005	mg/L	34	ND	ND	ND	0	18	ND	ND	ND	0
Ethylbenzene	0.3	mg/L	36	ND	ND	ND	0	271	0.182	<0.0005	17	5
Methyl tert-butyl ether (MTBE)	0.013	mg/L	36	0.0003	ND	0.001	0	271	0.130	<0.0005	8.7	22
Chlorobenzene	0.07	mg/L	36	ND	ND	ND	0	1	0.049	0.049	0.049	0
Styrene	0.1	mg/L	36	ND	ND	ND	0	2	0.091	0.003	0.18	1
1,1,2,2-Tetrachloroethane	0.001	mg/L	36	ND	ND	ND	0	119	ND	ND	ND	0
Tetrachloroethylene (PCE)	0.005	mg/L	34	0.011	ND	0.046	5	120	0.051	<0.0005	1.58	80
Toluene	0.15	mg/L	37	0.000003	ND	0.00004	0	271	0.098	0.0001	10.0	9
1,2,4-Trichlorobenzene	0.005	mg/L	36	ND	ND	ND	0	109	ND	ND	ND	0
1,1,1-Trichloroethane	0.2	mg/L	36	ND	ND	ND	0	119	0.0001	<0.0005	0.002	0
1,1,2-Trichloroethane	0.005	mg/L	36	ND	ND	ND	0	119	ND	ND	ND	0
Trichloroethylene (TCE)	0.005	mg/L	34	0.0002	ND	0.001	0	127	0.005	<0.0005	0.13	14
Trichlorofluoromethane	0.15	mg/L	33	0.00003	0.00003	0.00003	0	119	ND	ND	ND	0

Constituent	MCL	Units	WATER SUPPLY WELLS					ENVIRONMENTAL WELLS				
			Wells Sampled	Avg Conc.	Min. Conc.	Max. Conc.	Wells >MCL	Wells Sampled	Avg Conc.	Min. Conc.	Max. Conc.	Wells >MCL
Vinyl Chloride (VC)	0.0005	mg/L	36	ND	ND	ND	0	127	0.018	<0.0005	0.053	12
Xylenes	1.75	mg/L	34	ND	ND	ND	0	122	0.221	<0.0005	2.4	3

Note: Bold is for constituents with concentrations above the MCL.

Source: GAMA Groundwater Information System Database for period from 2010 to 2020 for water supply wells and environmental wells within the TVS Subbasin (Downloaded June 2, 2021).

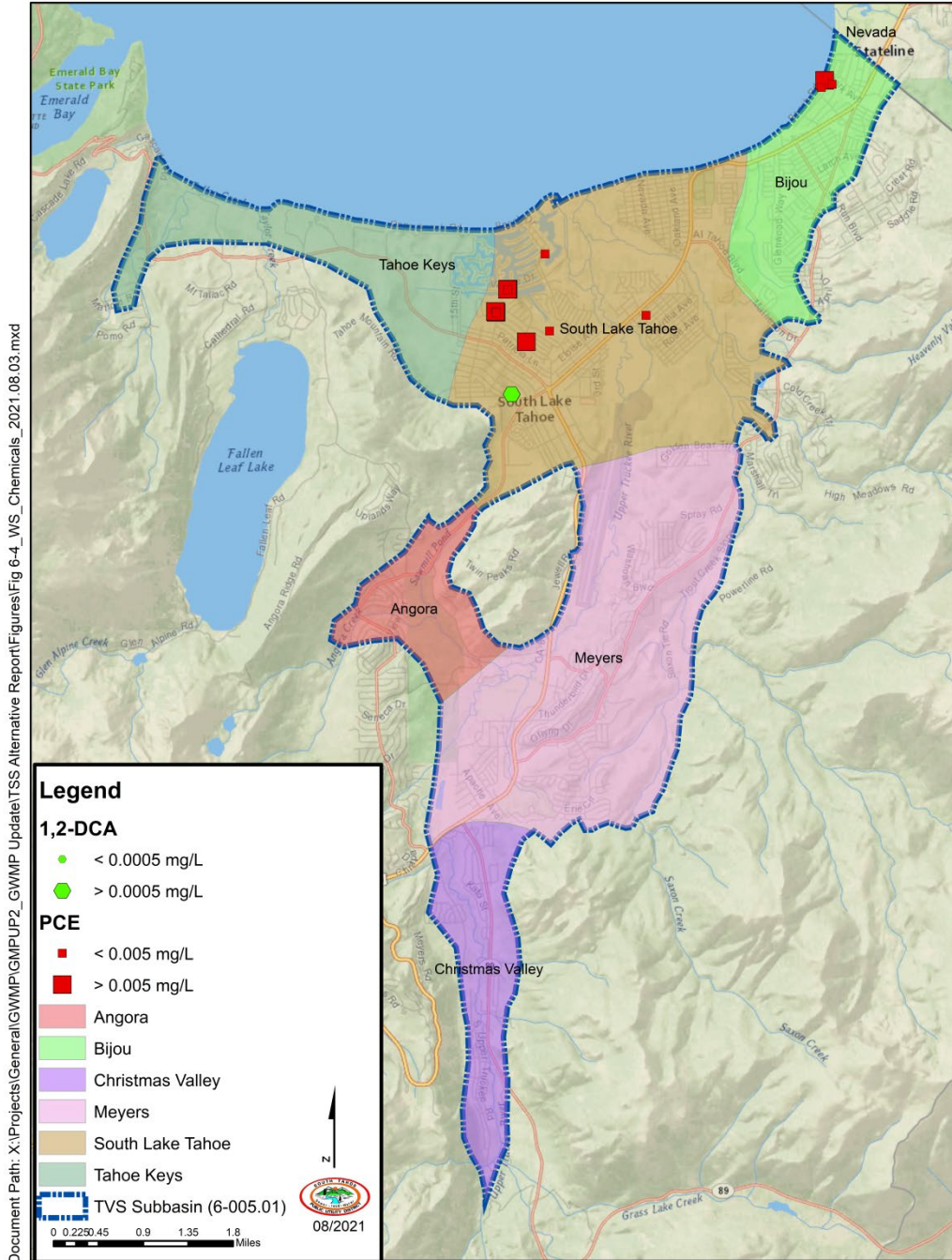


Figure 6-4. Incidences of regulated chemical constituents above MCLs detected in water samples collected from water supply wells within the TVS Subbasin (Data Source: GAMA Groundwater Information System, June 2021).

6.2.4.2 Environmental Wells

Table 6-5 presents a summary of the regulated chemicals detected in water samples collected from environmental wells in the TVS Subbasin over the past 10 years. In terms of petroleum hydrocarbon contaminants sampled during this period: 22 monitoring wells had one or more instances of MtBE above the MCL (13 UG/L); 46 monitoring wells had one or more instances of Benzene above the MCL (1 UG/L); 9 monitoring wells had one or more instances of toluene above the MCL (150 UG/L); and 5 monitoring wells had one or more instances of ethylbenzene above the MCL (300 UG/L). In terms of chlorinated hydrocarbon contaminants sampled during this period, 80 monitoring wells had one or more instances of PCE above the MCL (5.0 UG/L), 14 monitoring wells had one or more instances of TCE above the MCL (5.0 UG/L), 9 monitoring wells had one or more instances of 1,2-DCE above the MCL (6.0 UG/L), and 12 monitoring wells had one or more instances of Vinyl Chloride (VC) above the MCL (0.5 UG/L).

Incidences of petroleum hydrocarbon contaminants detected in groundwater samples collected from environmental monitoring wells are presented in Figure 6-5 and are associated with the clean-up sites in the Bijou, South Lake Tahoe and Meyers subareas presented in Table 6-6.

Table 6-6 shows the types and levels of petroleum hydrocarbon constituents with respect to MCLs detected in cleanup site environmental monitoring wells and the status of each clean-up site. For open sites, the groundwater quality with respect to MCLs is generally current through 2019 or 2020. For the closed sites, the groundwater quality with respect to MCLs is for the last groundwater monitoring event completed prior to case closure, except for the Meyers Landfill site, where groundwater monitoring continued into 2017, following case closure in 2012. Review of No Further Action Required Summaries for clean-up sites with levels of petroleum hydrocarbon constituents above MCLs indicate that these sites were recommended for closure based on site land use, the levels of petroleum contamination remaining in the vadose zone, the contaminant type(s), and lateral and vertical extent of the groundwater contamination. The distance to nearby groundwater and surface water receptors and the methods, duration and quantities of soil and groundwater contamination removed from the site consistent with LTCP criteria are also considered (Section 4.3.2).

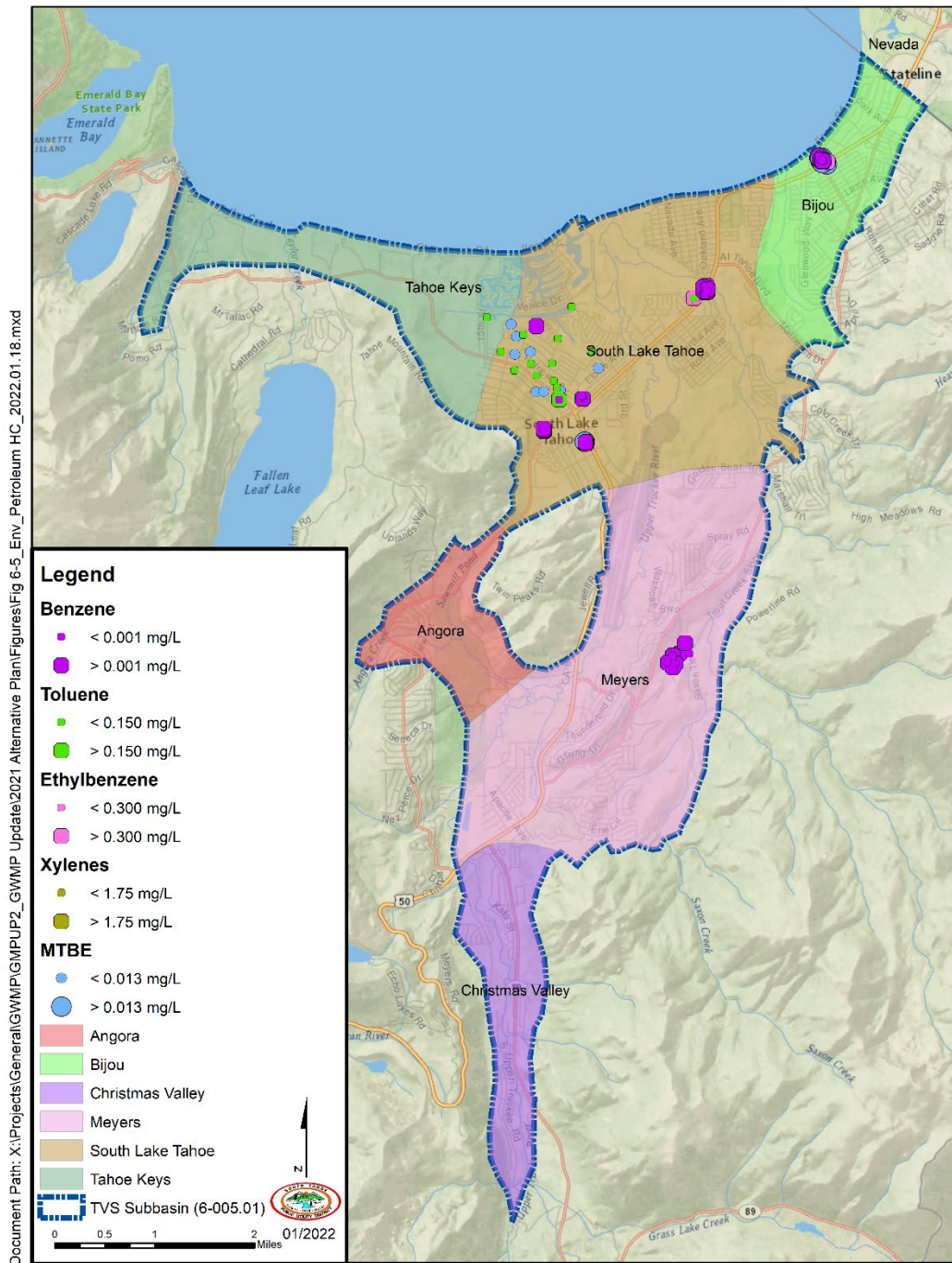


Figure 6-5. Incidences of petroleum hydrocarbon constituents above MCLs detected in water samples collected from environmental wells within the TVS Subbasin (Data Source: GAMA Groundwater Information System, June 2021).

Table 6-6. Clean-up sites with water quality records of petroleum hydrocarbon contaminants detected in groundwater within the TVS Subbasin over the past ten years (2011–2020).

Subarea	SWRCB Site Name	Site Number	Benzene	Toluene	Ethylbenzene	Xylenes	MtBE	Site Status
Bijou	Al's Ski Run Chevron (Former)	T0601700100	<MCL	<MCL	<MCL	<MCL	>MCL	Open
Bijou	Jet-Thru Gas and Car Wash	T0601700108	<MCL	<MCL	>MCL	<MCL	>MCL	Closed (2/27/2013)
South Lake Tahoe	Terrible Herbst Gas Station	T0601700090	>MCL	>MCL	>MCL	>MCL	<MCL	Closed (1/24/2019)
South Lake Tahoe	Berry Hinckley Bulk Fuel Plant	SL0601781518	>MCL	<MCL	<MCL	<MCL		Closed (1/21/2015)
South Lake Tahoe	Cardinale Way/Jim Bagan Toyota	T10000012529	>MCL	>MCL	>MCL	>MCL		Open
South Lake Tahoe	Former USA Gas #7	T0601700091	>MCL	>MCL	<MCL	<MCL	>MCL	Closed (2/24/2015)
South Lake Tahoe	South Y Regional Contamination	T10000007984	>MCL	>MCL	<MCL	<MCL	<MCL	Open
Meyers	Meyers Landfill	SL0601724846	>MCL	<MCL	<MCL	<MCL	<MCL	Open – Closed/with Monitoring (5/23/2012)

Incidences of chlorinated hydrocarbon contaminants detected in groundwater samples collected from environmental monitoring wells are presented in Figure 6-6 and are associated with the clean-up sites in the South Lake Tahoe and Meyers subareas presented in Table 6-7.

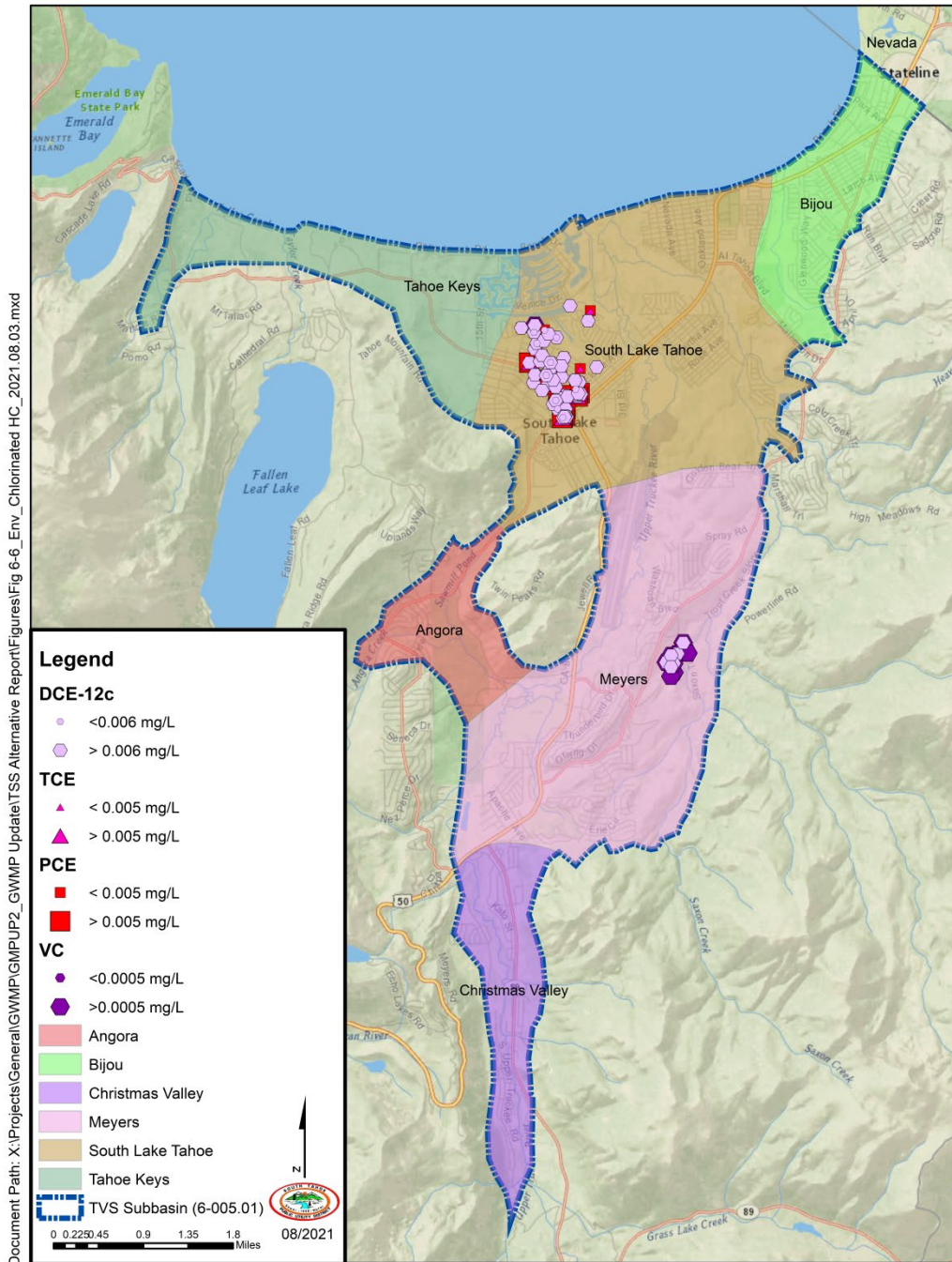


Figure 6-6. Incidences of chlorinated hydrocarbon constituents above MCLs detected in water samples collected from environmental wells within the TVS Subbasin (Data Source: GAMA Groundwater Information System, June 2021).

Table 6-7. Clean-up sites with water quality records of chlorinated hydrocarbon contaminants detected in groundwater within the TVS Subbasin over the past ten years (2011 – 2020).

Subarea	SWRCB Site Name	Site Number	DCE-12c	TCE	PCE	VCs	Site Status
South Lake Tahoe	Lake Tahoe Laundry Works	SL0601754315	>MCL	>MCL	>MCL	>MCL	Open
South Lake Tahoe	South Y Regional Contamination	T10000007984	>MCL	>MCL	>MCL	<MCL	Open
Meyers	Meyers Landfill	SL0601724846	>MCL	<MCL	<MCL	>MCL	Open – Closed/with Monitoring (5/23/2012)

Table 6-7 shows the types and levels of chlorinated hydrocarbon constituents with respect to MCLs detected in cleanup site environmental monitoring wells and the status for each clean-up site. For the Lake Tahoe Laundry Works site (SL0601754315), the groundwater quality with respect to MCLs is generally through 2020. The South Y Regional Contamination site (T10000007984) provides groundwater quality data collected during a regional plume characterization conducted by the LRWQCB. The regional plume investigation involved the drilling and groundwater sampling of 79 borings to determine the lateral and vertical extent of groundwater contamination recognized in the South Lake Tahoe subarea. Water quality records for these grab samples represent one-time events collected during 2019 and 2020. The Meyers Landfill site (SL0601724846) includes groundwater monitoring data collected through 2017.

6.3 **Groundwater Quality Issues**

The TVS Subbasin faces three primary groundwater quality challenges: (1) migration of contaminated groundwater; (2) emerging contaminants, specifically PFAS substances; and (3) potential groundwater contamination via stormwater infiltration.

6.3.1 **Migration of Contaminated Groundwater**

The following section presents three examples of contaminant plumes identified within the TVS Subbasin. The first two of these examples have impaired water quality in community water system and/or individual water system wells. Additional explanation on how groundwater pumping may impact plume migration to address Recommended Action RA-5 is presented at the end in Section 6.3.1.4.

6.3.1.1 **South “Y” Regional Contamination**

The South Y Regional Contamination site (T10000007984) is in the South Lake Tahoe subarea neighboring the intersection of US Route 50 and California State Highway 89, in the CSLT (locally referred to as the “Y”). This is an open Cleanup Program Site including the South Y PCE site (SL0601794942) which was an open Cleanup Program Site starting in October 1989 and which was closed in February 2015.

In 2016, the District, in partnership with LBWC and TKWC, undertook renewed investigations to describe the extent of PCE contamination and identify remedial measures that may be used to remove this contamination from groundwater to protect existing groundwater sources used for drinking water supply, consistent with BMO #2. This included completion of an engineering assessment of an inactive water supply well (LBWC #4) for use as a potential extraction well (GEI, 2016a); compilation of historical data to show the spatial and temporal distribution of PCE contamination in the South Y area (GEI, 2016b); and initial development of a modular three-dimensional transport model (MT3DMS) that could be used to evaluate various remedial alternatives designed to mitigate contamination from the South Y plume.

During 2017, the District, LBWC, and TKWC completed water quality monitoring to better understand the current extent of PCE contamination in community water system wells. The District also completed the preliminary MT3DMS model (South Y PCE Model) and initiated negotiations with the DFA to conduct a Feasibility Study under a Proposition 1 Groundwater Planning Grant, addressing this groundwater contaminant problem.

In May 2017, the LRWQCB issued a Clean Up and Abatement Order (CAO No. R6T-2017-0022) requiring remediation and additional investigation of PCE groundwater contamination resulting from historic PCE release from the former Lake Tahoe Laundry Works site (SL0601754315) (LRWQCB, 2017). During WY 2018, consultants for the working parties (Seven Springs Limited Partnership and Fox Capital Management Corporation), prepared work plans, planning reports and conducted initial contaminant investigations required in the Clean Up and Abatement Order. A full list of documents describing the regulatory activities performed at this site can be found online through the SWRCB GeoTracker website. (https://geotracker.waterboards.ca.gov/profile_report.asp?global_id=SL0601754315).

During 2018, the District entered into an agreement with DFA to complete a Feasibility Study of Remedial Alternatives to Mitigate Tetrachloroethylene Contamination (Agreement D1712508). Agreement D1712508 required the District to perform numerous activities including but not limited to: conducting a groundwater investigation near the inferred center of the plume (referred to as the pre-design investigation); completing a Baseline Human Health Risk Assessment; conducting groundwater modeling for the purposes of evaluating potential implementation projects that will prevent or clean-up groundwater contamination; completing a feasibility study to develop interim remedial alternatives that prevent or clean contamination of groundwater that serves or has served as a source of drinking water; develop an Interim Remedial Action Plan that will lead to the implementation of the preferred remedial action alternative; complete environmental analysis checklists and identify mitigation measures required for implementation of the preferred alternative; and perform public outreach to inform the public concerning the progress of these activities.

The pre-design investigation was conducted in the mid-section of the South Y plume and was completed during the summer of 2018. Activities completed for this investigation involved the drilling and logging of a borehole to a total depth of 150 feet, the drilling and construction of two test wells, aquifer and soil and groundwater testing, and collection of groundwater elevation readings. The data collection was used to characterize the vertical extent of PCE contamination in groundwater and inform the development of design strategies for hydraulic control and/or removal of PCE contamination from groundwater. The District also updated its Well Owners Survey for the South Y Area. The update was performed to gather information on private wells situated within or neighboring the South Y plume to identify potential wells that may serve as vertical conduits for contaminant migration and identify property owners with active wells that may be impacted by PCE groundwater contamination. Information from the pre-design investigation was used to inform the preliminary engineering design of extraction wells for the removal of PCE from groundwater. The South Y PCE Model was updated using 2018 water quality data; and management scenarios were developed for modeling and engineering evaluation.

Following performance of the PDI, KJC conducted a screening level Human Health Risk Assessment addressing risks associated with PCE impacted groundwater at CWS wells in the South Y area. The Human Health Risk Assessment was completed and submitted to the DFA in January 2019.

Groundwater modeling for the Feasibility Study resumed in 2018. During 2018, the South Y PCE Model was updated through 2018 and used to evaluate management scenarios developed for the Feasibility Study. Modeling evaluation used best- and worst-case conditions to forecast the effectiveness of management scenarios to prevent or clean-up groundwater contamination over the next twenty years, through 2038. Scenarios evaluated using the South Y PCE Model included: (1) no action; (2) use of new extraction wells to clean-up the PCE plume; (3) use of new CWS wells to prevent groundwater contamination and provide replacement water supply; and (4) use of existing CWS wells to clean-up the South Y plume.

During WY 2019, the District continued on-going activities to complete the Feasibility Study. Initial management scenarios were refined to interim remedial alternatives to manage on-going contamination from the PCE Plume. Six interim remedial alternatives were developed and

initially screened for effectiveness using the South Y Fate and Transport Model. The alternatives were also reviewed and screened for implementability using input from the water purveyors. Based on this screening three interim remedial alternatives were selected for detailed analysis, including 20-year project life cost analysis, to select a preferred remedy. Technical reports presenting information from the pre-design investigation; Baseline Human Health Risk Assessment; and South Y Fate and Transport Modeling were completed and are posted on the District's website (<https://stpud.us>). The Feasibility Study Report and accompanying Interim Remedial Action Plan were completed and posted on the District's website in May 2020.

In March 2019, the LRWQCB was awarded a \$4.6 million grant under the Site Cleanup Subaccount Program to investigate the South Y plume (Figure 6-7). The South Y plume is believed to have resulted from spills and releases associated with the use of commercial grade dry cleaning solvents in the South Y area during the 1970's. During 2019, the LRWQCB undertook a regional plume characterization that involved the drilling and sampling of 64 borings to determine the lateral and vertical extent of PCE contamination, identify contaminant pathways, and show the current distribution of PCE in groundwater using detailed graphics. During 2020, the LRWQCB continued regional plume characterization activities that involved the drilling and sampling of an additional 15 borings (79 borings total during 2019 and 2020). In June 2020, impaired public water supply well, LBWC #4 (situated within the PCE plume) was identified as a vertical conduit and was properly destroyed using Site Cleanup Subaccount Program grant funding. Future activities planned under this program include the installation of sentry wells up-gradient of threatened community water supply wells near the north end of the plume, soil-gas sampling to evaluate vapor-intrusion pathways at the south end of the plume and sampling of individual water system wells located within the plume.

Review of preliminary data collected during the regional plume characterization shows that the South Y plume extends more than 7,200 feet north from the South Y towards the south shore of Lake Tahoe. Within this plume, PCE concentrations above the MCL (5 UG/L) were detected in groundwater samples collected from subsurface depths to 185 feet below ground surface. PCE concentrations in groundwater samples collected from within the plume ranged from below the detection limit of 0.5 UG/L to greater than 500 UG/L. The isoconcentration map of PCE within the South Y plume show a broad area of PCE groundwater contamination greater than 50 UG/L extending from the south end of the plume (near inferred source areas) to the north end of the South Y plume (near the leading edge of the plume front).

Further investigations are being planned by the LRWQCB as part of the Regional Contamination Investigation to identify potential source areas for this plume. Information from these future source area investigations may help to provide detail about the composition of the South Y plume and its evolution from singular or multiple releases from singular or multiple sites. Regulatory activities and environmental data for the South Y Regional Contamination investigation (T10000007984) are available online through the SWRCB GeoTracker website (https://geotracker.waterboards.ca.gov/profile_report.asp?global_id=T10000007984).

The South Y plume has impaired three CWS wells (LBWC #2, LBWC #5 and TKWC #2) with a combined source capacity of 3.25 MGD. Potential impairment of TKWC #1 would further reduce the total production capacity of area drinking water sources by an additional 1.44 MGD. Two other CWS wells (LBWC #1 and TKWC #3) west of the South Y plume are

presently non-detect (LBWC #1) or below MCLs (TKWC #3) for PCE. However, the recent impairment of TKWC #2 and TKWC #3 by natural contaminants (uranium and arsenic) has further reduced source capacity for the TKWC water system to below its water system maximum day demand (2.383 MGD). TKWC is currently working on long-term facilities plan to address this apparent deficit of available water supply for its water system. In 2021, LBWC completed construction of a wellhead treatment system for the removal of PCE from groundwater at the LBWC #5 well site. DDW granted LBWC permission to place this facility in operation in advance of issuance of the final operating permit on July 2, 2021. In 2021, TKWC constructed an inter-tie connection with the LBWC water system for the emergency provision of drinking water to the TKWC water distribution system.

The District has mutual aid and assistance agreements for the emergency provision of drinking water using inter-tie connections from its water distribution system to both the LBWC and TKWC water systems. During WY 2020, the District provided 32,000 gallons of drinking water to LBWC through its inter-tie connection, which is less than 1% of LBWC's total water production for WY 2020. The District is also working with TKWC to confirm the volume of flow that the District's water system can currently supply to TKWC.

A file review of District and County records indicated that as many as 24 private wells and 14 small community water system wells may be located within or near the South Y plume (KJ, 2019). Most of these wells are relatively shallow, constructed to total depths of less than 100 feet and are believed to be susceptible to water quality impairment from this plume.

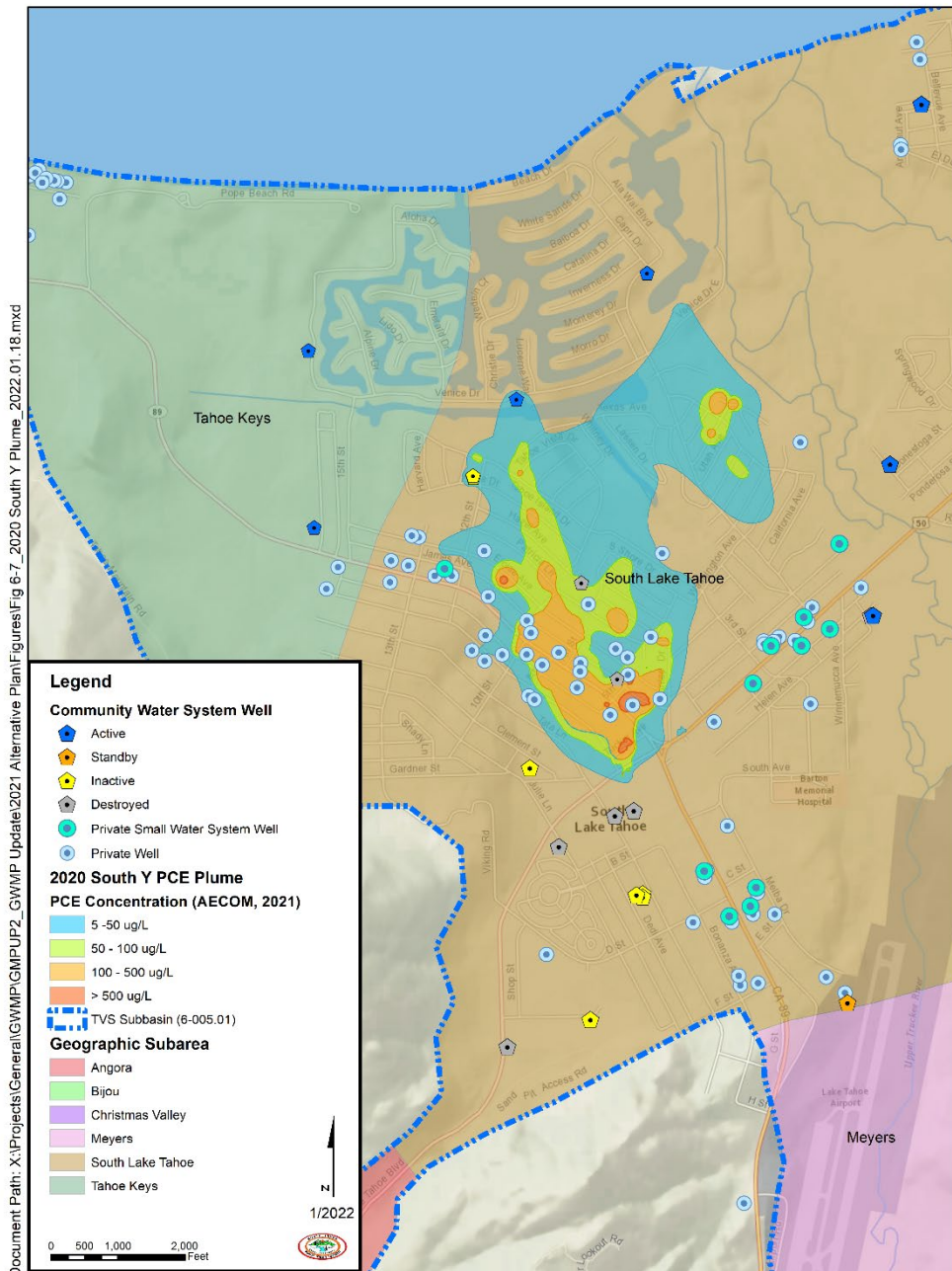


Figure 6-7. Location of the South Y plume within the South Lake Tahoe subarea, as defined by PCE in groundwater detected above 5 micrograms per liter (UG/L), provisional data provided by LRWQCB.

6.3.1.2 Private Residence Site

The Private Residence site (SL0601714201) is in the Bijou subarea and includes the private water supply wells that have been impacted by PCE and MtBE within the Tahoe Meadows subdivision. This site is currently in the verification monitoring stage. Current data suggest that the lateral extent of PCE and MtBE contamination is generally delineated, while the vertical extent of delineation is incomplete. The source(s) of MtBE and PCE contamination has not been identified (Fugro, 2014). In June 2016, LRWQCB sampled select domestic wells for the Private Residence site. PCE was detected above MCLs in one well and below MCLs in four other private wells. In June 2018, LRWQCB conducted another round of groundwater sampling on selected private wells. PCE was detected in one private well above MCLs and three other private wells below MCLs (LRWQCB, 2018).

6.3.1.3 Meyers Landfill Site

The Meyers Landfill site (SL601724846; T10000000216) is in the Meyers Subarea between Pioneer Trail and Saxon Creek. The nearest active drinking water well neighboring the Meyers Landfill is the Elks Club Well #2 located about 4,150 feet west of the Meyers Landfill. The nearest surface water feature is Saxon Creek, which is a main tributary to Trout Creek, flowing along the east margin of the Meyers Landfill site.

The Meyers Landfill was operated by private parties from 1946 to 1955 and the County from approximately 1955 to 1971 under USFS Special Use Permits. Water leaching through the landfill has impacted groundwater beneath the site, resulting in a plume of contaminated groundwater extending approximately 2,000 feet in a north-northeast direction, down-gradient of the site. The contaminants of concern include both petroleum and chlorinated hydrocarbons, including VC, BTEX and naphthalene. VC has also been detected in surface water samples collected from Saxon Creek, down gradient of the former landfill (Weston, 2012). Contamination at the site is being remediated using an impermeable cover to prevent surface water from percolating through the landfill waste. Groundwater monitoring is being performed to evaluate the effects of the cover on groundwater flow and water quality underlying the site (USFS, 2013).

In 2018, an updated groundwater characterization report was issued documenting methods and results of investigation activities at the Meyers Landfill from 2011 through 2017 (Weston, 2018). Major findings from the groundwater characterization report indicate that perched water is flowing toward the waste mass across sections of a new French drain installed to capture upgradient groundwater and divert it away from the waste mass. The VC plume in the upper groundwater zone extends at least 1,500 feet north-northeast of the north extent of the final cover over the Meyers Landfill and crosses Saxon Creek; the VC plume in the middle groundwater zone extends 1,700 feet north of the north extent of the final cover over the Meyers Landfill toward Hepka Drive. In 2019, a work plan for Remedial Investigation/Feasibility Study of groundwater at Meyers Landfill was completed. The objective of the Remedial Investigation/Feasibility Study is to delineate the nature and extent of groundwater contamination, identify whether the multilayered impermeable cap installed at OU-1 (i.e., the landfill waste mass) is affecting groundwater, and to develop and evaluate remedial alternatives for the contaminated groundwater (ERRG, 2019).

Potential Impacts of Groundwater Pumping on Plume Migration

The South Y PCE Model is a groundwater flow and transport model of the South Y PCE site developed for the purpose of assessing the flow path and time scale of PCE plume migration given current and expected pumping conditions in the TVS Subbasin, and to test the effects of several potential remediation plans (Rybarski et al, 2019a; Rybarski et al, 2019b). The model domain was derived as an inset within the original STGM (Carroll et al., 2016). A section of the original model grid covering the area of PCE plume and extending northward to Lake Tahoe was extracted, and the grid was refined in the existing plume and along the expected plume migration path, from a grid cell size of 100 meters in the original model to a refined size of 10 meters in the plume. To recreate the calibrated head field from the original model and simulate lateral flow from cells not represented in the new model domain, a constant head boundary was applied to the landward boundaries of the new model grid, with heads taken from the original model framework. Hydraulic conductivity, specific yield, and specific storage fields were also taken directly from the original model framework.

Transport simulations were run using MT3DMS, a modular three-dimensional transport model for the simulation of advection, dispersion, and chemical reactions of dissolved constituents in groundwater systems (Zheng and Wang, 1999). While the original transient model simulated WY 1983 to WY 2015, the updated South Tahoe flow and transport model was extended into the past and the future to simulate WY 1971 to WY 2068, to capture the genesis of the PCE plume as well to predict future plume migration pathways (2019a). Transport parameters including dispersivity, sorption, and biogenic degradation rates were calibrated within reasonable ranges given known and estimated aquifer parameters, organic carbon fraction, and levels of dissolved oxygen, to closely match observed trends in PCE concentrations over time.

Several management alternatives were simulated to assess the effects of various pumping regimes at LBWC and TKWC wells on plume migration. These include:

- 1) Base Treatment – this alternative acts as a baseline against which to compare other remedial action alternatives, maintaining current (WY 2018) lead/lag/lag-lag operations status for TKWC and LBWC wells. Produced water from both LBWC #5 and TKWC #2 is treated via a granular activated carbon (GAC) system. Simulation is run 50 years into the future (WY 2068) (Rybarski et al, 2019a).
- 2) Targeted Pumping – this alternative uses LBWC #5 and TKWC #2 as the lead wells for LBWC and TKWC, respectively, as these wells are positioned near the current simulated heart of the plume. Increased pumping at these wells is intended to remove mass from the system as well as limit potential plume migration towards TKWC #1, TKWC #3, and LBWC #1. Produced water from both LBWC #5 and TKWC #2 is treated via a GAC system. Simulation is run 50 years into the future (WY 2068) (Rybarski et al, 2019a).
- 3) Targeted Pumping, Option 1 – this alternative serves to identify the benefit of using LBWC #5 as the lead well for hydraulic control and PCE mass removal, as this well is positioned near the simulated center of mass of the plume. Increased pumping at this well is intended to remove mass from the system as well as limit potential plume migration towards TKWC #1, TKWC #3, and LBWC #1. Produced water from both LBWC #5 is

treated via a GAC system. Simulation is run 50 years into the future (WY 2068) (Rybarski et al, 2019b).

- 4) Targeted Pumping, Option 2 – this alternative serves to identify the benefit of adding a new extraction well at 843 Hazel Drive (LBWC #4 site) for plume control and PCE mass removal. Aside from the addition of this extraction well, all other pumping rates are identical to Option 1. Simulation is run 50 years into the future (WY 2068) (Rybarski et al, 2019b).

Pumping rates used for each of the four alternatives are listed in Table 6-8.

Table 6-8. Pumping rates used for four pumping scenarios.

Description	Pumping Rates (m ³ /d)										
	LBWC 1	LBWC 5	TKWC 1	TKWC 2	TKWC 3	Sunset	Paloma	Helen 2	Bayview	Al Tahoe 2	EW-1
Base Treatment	872.2	199.7	532.5	1,219.5	1,317.0	1,735.8	195.7	713.2	8,997.5	1,462.2	0
Targeted Pumping	199.7	872.2	532.5	1,317.0	1,219.5	1,735.8	195.7	713.2	8,997.5	1,462.2	0
Targeted Pumping, Option 1	199.7	872.2	532.5	1,219.5	1,317.0	1,735.8	195.7	713.2	8,997.5	1,462.2	0
Targeted Pumping, Option 2	199.7	872.2	532.5	1,219.5	1,317.0	1,735.8	195.7	713.2	8,997.5	1,462.2	872.2

Note: 1 cubic meter per day (m³/d) is equal to 0.1835 gallons per minute (gpm).

In general, relative to the Base Treatment scenario, the three targeted pumping scenarios showed a reduction in maximum concentrations at downgradient wells, and a more rapid return to PCE concentrations below 4 UG/L basin wide. Overall differences in the shape and migration pathway of the plume were relatively small between scenarios. No simulations resulted in concentrations at District wells meeting or exceeding 4 UG/L. Concentrations at TKWC #3 and LBWC #1, currently unaffected by the plume, also remained well below 4 UG/L for all scenarios. Comparisons of breakthrough curves for all scenarios for each of the TKWC and LBWC wells are shown in Figure 6-8 through Figure 6-12, and Table 6-9 shows the number of simulation years after WY 2018 required for the concentration at each well to drop below 4 UG/L.

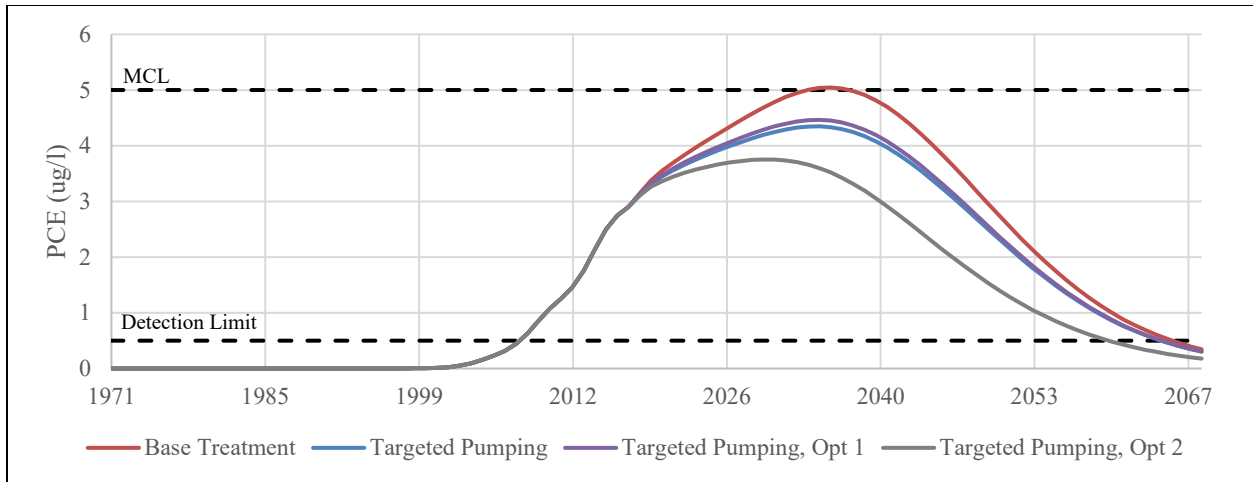


Figure 6-8. Breakthrough curves at TKWC 1 for four pumping scenarios.

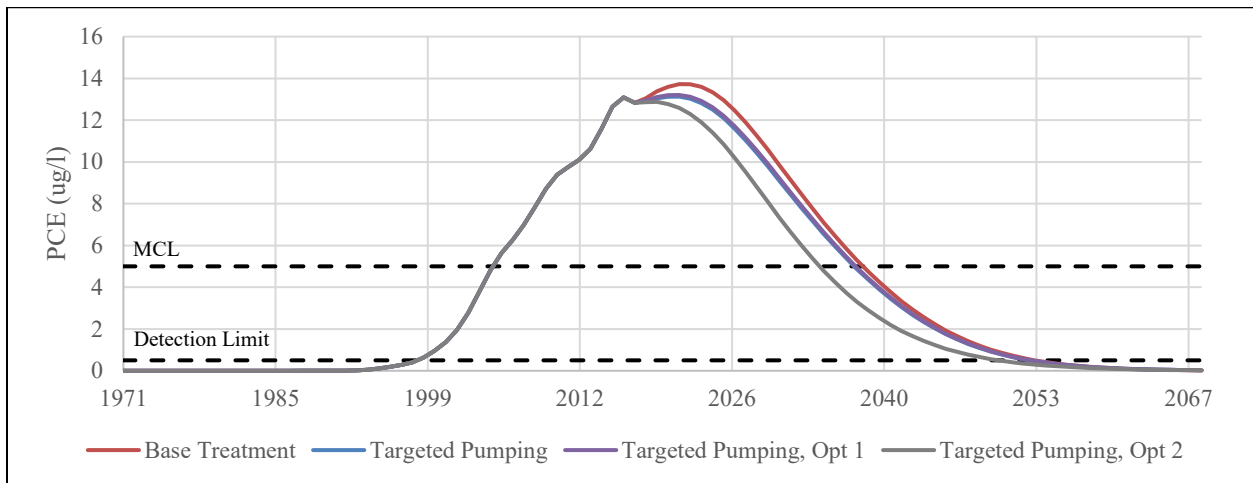


Figure 6-9. Breakthrough curves at TKWC 2 for four pumping scenarios.

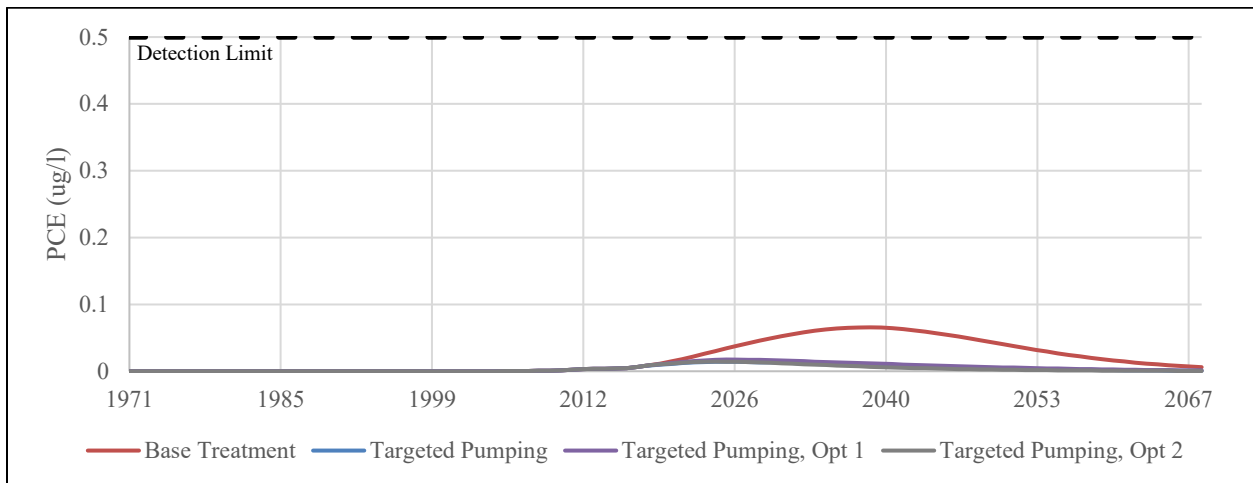


Figure 6-10. Breakthrough curves at TKWC 3 for four pumping scenarios.

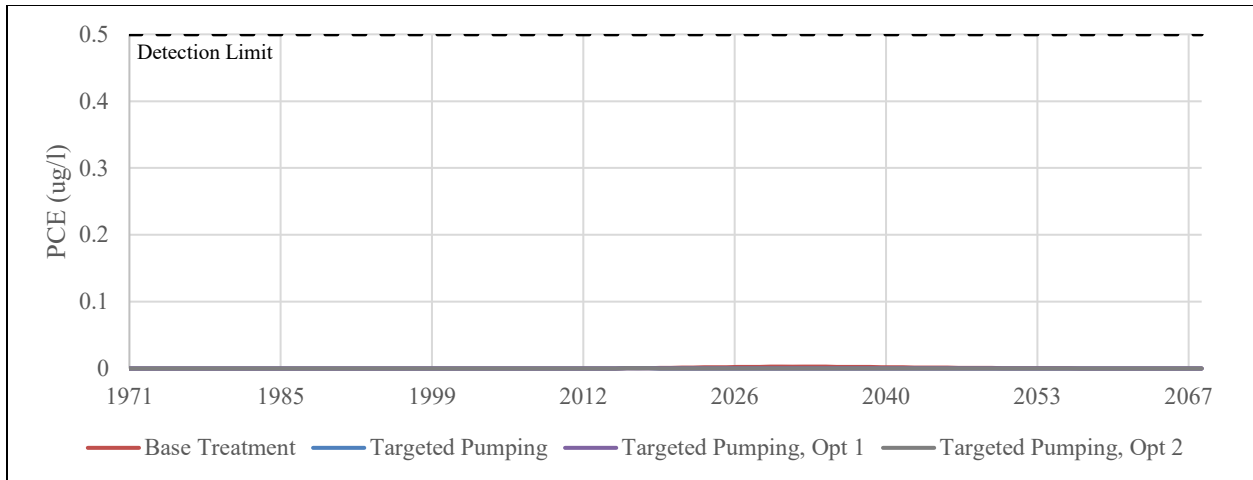


Figure 6-11. Breakthrough curves at LBWC 1 for four pumping scenarios.

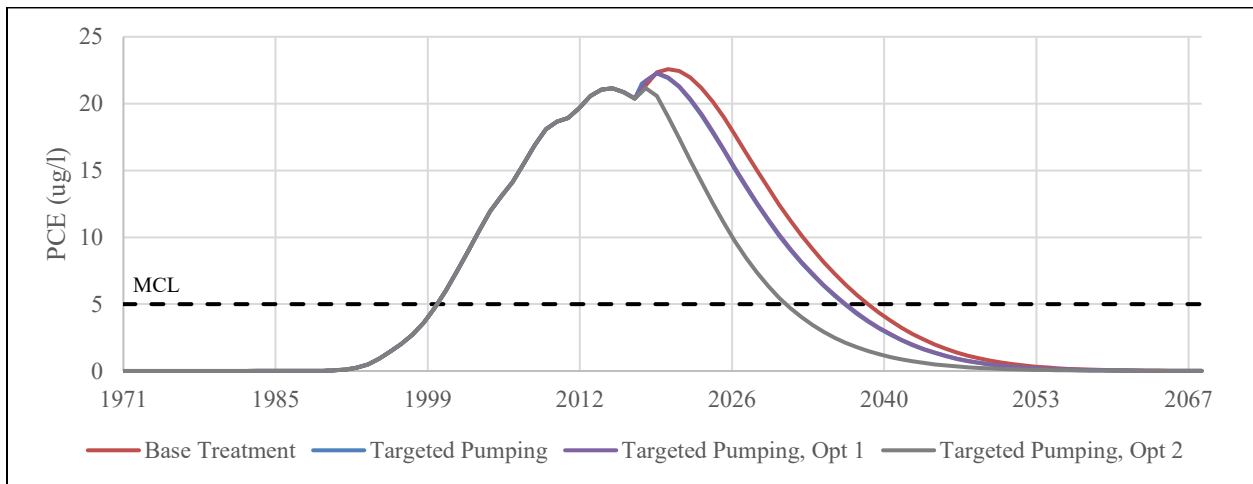


Figure 6-12. Breakthrough curves at LBWC 5 for four pumping scenarios.

Table 6-9. Number of years after 2018 each well drops below 4 UG/L for all pumping scenarios. N.E. = Never Exceeds 4 UG/L.

Description	Years after 2018 (PCE < 4 UG/L)				
	LBWC 1	LBWC 5	TKWC 1	TKWC 2	TKWC 3
Base Treatment	N.E.	22	27	22	N.E.
Targeted Pumping	N.E.	20	22	21	N.E.
Targeted Pumping, Option 1	N.E.	20	23	21	N.E.
Targeted Pumping, Option 2	N.E.	15	N.E.	18	N.E.

6.3.2 Emerging Contaminants

Emerging contaminants, as used in this Section, are contaminants that are known or may occur in groundwater used for drinking water within the TVS Subbasin and are not currently subject to federal or state drinking water regulation. These contaminants include Radon 222 (Radon) and per- and polyfluoroalkyl substances (PFAS).

6.3.2.1 **Radon 222**

On November 2, 1999, the EPA proposed the Radon in Drinking Water Rule in the Federal Register (64 Fed. Reg. 59246 (Nov. 2, 1999)). The proposed rule was designed to promote a multimedia approach to reduce radon risks in indoor air and in drinking water. The rule proposed an MCL of 300 picocuries per liter (pCi/L) and an Alternative MCL of 4000 pCi/L. The applicable drinking water standard would depend on whether the State or community water system develops a multimedia mitigation program to address radon entering indoor air from soil under homes and buildings.

In 2003, Congress directed EPA to (1) report on the pending radon in drinking water regulations; (2) to consult with the State drinking water, air, and radiation programs; and (3) evaluate options to implement a single drinking water standard for radon. State air and radiation representatives supported a single MCL for drinking water ranging from 4,000 to 40,000 pCi/L. State program representatives also expressed concern that a standard for radon in drinking water would mislead the public about the risks of radon in drinking water relative to the greater public health risk of radon in indoor air (EPA, 2012).

Table 6-4 shows levels of Radon 222 in water samples collected from drinking water wells averaged 694 pCi/L with maximum concentrations to 6,700 pCi/L. Figure 6-13 shows the incidences of radon in in water supply wells compared to the proposed MCL (300 pCi/L) and proposed alternative MCL (4,000 pCi/L). Inspection of Figure 6-13 shows that every water supply well sampled within the TVS Subbasin had incidences of radon above the proposed MCL, and only two wells (Airport Well and Blackrock Well No. 2) had incidences of radon above the proposed alternative MCL. Adoption of the proposed MCL would have a severe impact on groundwater production in the TVS Subbasin, while adoption of the proposed alternative MCL would have a minor impact.

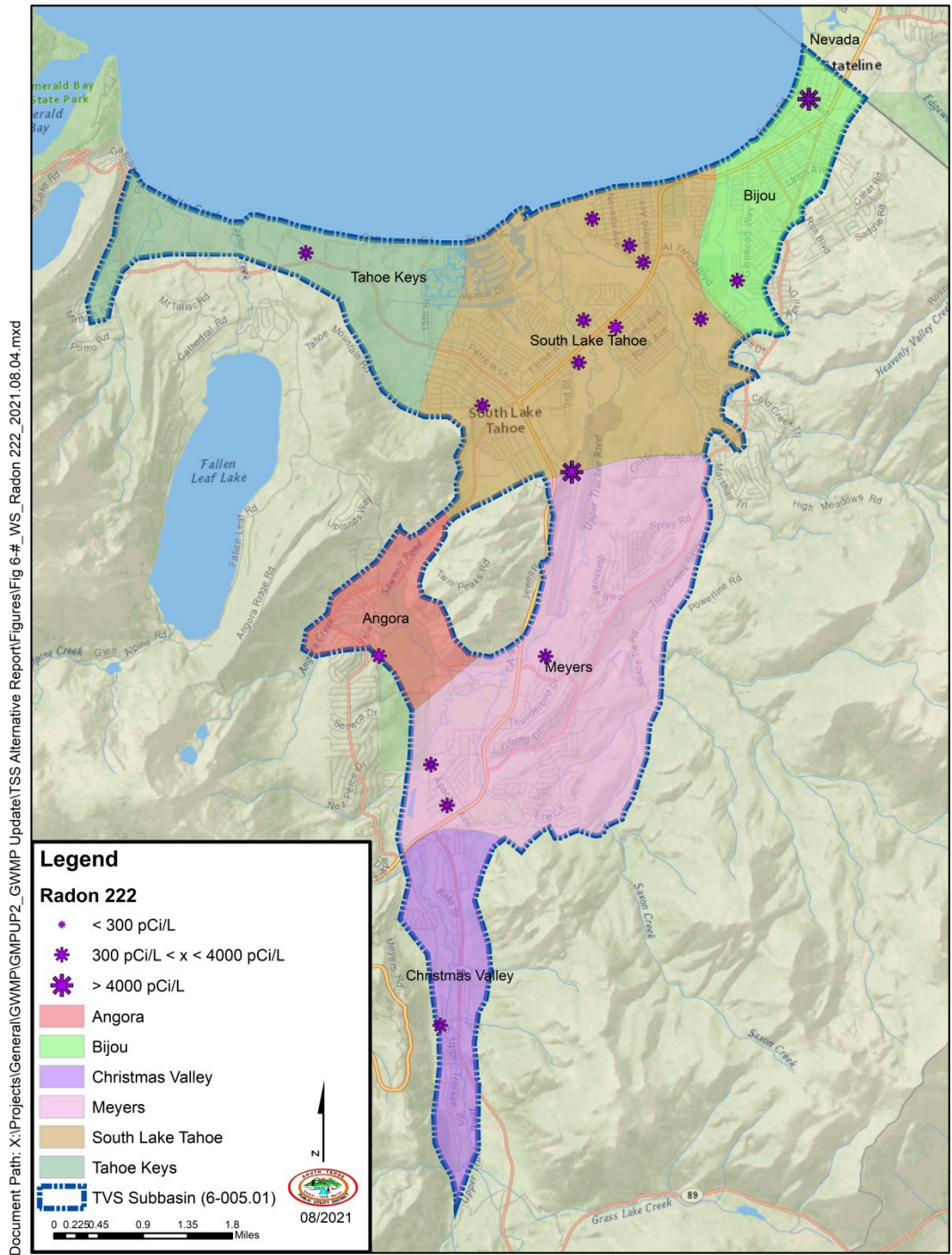


Figure 6-13. Incidences of Radon 222 in water samples collected from water supply wells within the TVS Subbasin (Data Source: GAMA Groundwater Information System, June 2021).

6.3.2.2 Per- and Polyfluoroalkyl Substances (PFAS)

PFAS are a group of nearly 5,000 manmade chemicals that are resistant to degradation in the environment and when degradation occurs, it often results in the formation of other PFAS compounds.

PFAS are found in many products such as dental floss, non-stick cookware, food packaging materials, non-stick products (e.g., Teflon™), waterproof and water repellent textiles, water repellent furniture, carpet, polishes, waxes, paints, cleaning products, medical garments, and fire-fighting foams (aqueous film-forming foams; AFFF). PFAS are used in the aerospace, automotive, chemical, electronics, metal coatings and plating, and textiles industries due to their friction-reducing characteristics. PFAS have the potential to enter the waste stream from many different sources. Potential sources of PFAS include airports and aviation facilities, military bases and training centers, petroleum refineries and terminals, and petrochemical production facilities. Non-industrial PFAS sources include waste disposal facilities, wastewater treatment plant operations, and biosolids application to land. Currently, the key chemicals of concern are Perfluorooctanoic acid (PFOA) and Perfluorooctane sulfonic acid (PFOS).

In 2012, “Revisions to the Unregulated Contaminant Monitoring Rule (UCMR 3) for Public Water Systems” was published in the Federal Register (77 Fed. Reg. 26072 (May 2, 2012)). UCMR 3 requires public water systems to conduct sampling and analyses for Assessment Monitoring (List 1), Screening Survey (List 2) and Pre-Screen Testing (List 3) contaminants. The Assessment Monitoring (List 1) includes six perfluorinated compounds; PFOA, PFOS, perfluorobutanesulfonic acid (PFBS), perfluorohexanesulfonic acid (PFHxS), perfluoroheptanoic acid (PFHpA), and perfluorononanoic acid (PFNA). Public Water Systems subject to Assessment Monitoring were required to test for these contaminants within a 12-month period during 2013–2015. To satisfy UCMR 3 Assessment Monitoring requirements, the District collected treated (i.e., chlorinated) water samples from each of its active and stand-by wells in August 2014 and February 2015. Two rounds of samples were collected from District wells to capture any potential seasonal variations in contaminant concentrations. All samples were analyzed for the full list of perfluorinated compounds (EPA Method 537). Perfluorinated compounds were not detected in any of the UCMR 3 Assessment Monitoring samples collected from District wells.

Data on PFAS detections from more than 600 water system sites in California have been reported to the SWRCB since August 2019 and continue to be collected on a quarterly basis and are available from the SWRCB PFAS website (<https://www.waterboards.ca.gov/pfas/>). As of August 2021, there was no data for these chemicals in this database for any well types situated within the TVS Subbasin.

In March 2021 the EPA proposed the fifth Unregulated Contaminant Monitoring Rule (UCMR 5). The proposed contaminant list in the draft UCMR 5 includes another twenty-nine (29) PFAS compounds which were not sampled under UCMR 3. Under UCMR 5, public water systems shall be required to collect samples between 2023 and 2025. EPA anticipates that the UCMR final rule to be published in December 2021 (EPA, 2020b). On December 27, 2021, EPA posted its final rule for the UCMR 5 and noted that it will become effective on January 26, 2022 (Federal Register / Vol. 86, No. 245, 12/27/2021).

In May 2021, USFS LTBMU informed the District it detected PFAS compounds in several groundwater monitoring wells located at the Meyers Landfill site (SL0601724846). These are believed to be the first incidences of PFAS compounds detected in groundwater within the TVS Subbasin. Laboratory results provided by the USFS LTBMU (Golder, 2021) show that levels of PFOA and PFOS in several monitoring wells were above DDW response level of 10 parts per trillion (PPT) for PFOA and 40 PPT for PFOS. Response levels are levels of detected contaminants that if exceeded require a community water system or a non-transient non-community public water system to:

- Report that detection in the water system’s annual consumer confidence report; and
- Take a water source where detected levels exceed the response level out of use or provide public notification (as specified in Health and Safety §116378) within 30 days of the confirmed detection.

In July 2021, the Office of Environmental Health Hazard Assessment of the California Environmental Protection Agency announced the release of a draft document for public review describing proposed Public Health Goals (PHGs) for PFOA and PFOS in drinking water. A PHG is the level of a drinking water contaminant at which adverse health effects are not expected to occur from a lifetime of exposure. The Office of Environmental Health Hazard Assessment is proposing a PHG of 0.007 PPT for PFOA based on kidney cancer in humans; and a PHG of 1.0 PPT for PFOS based on liver and pancreatic tumors in laboratory animals (SWRCB, 2021).

In July 2021, the House passed– the PFAS Action Act of 2021 (HR 2467), directing EPA to establish Federal MCLs for PFAS not later than two years after the date of enactment of the Act.

6.3.3 Stormwater Infiltration

Storm water infiltration through detention basins is one of the primary treatment processes utilized in the Lake Tahoe Basin to reduce storm water pollutant loads from urban runoff to Lake Tahoe. To prevent groundwater contamination, discharge limits are used to prevent pollutants in surface runoff from exceeding prescribed levels for dissolved inorganic nitrogen, dissolved phosphorus, dissolved iron, grease and oil and suspended sediment (TRPA Code of Ordinances Chapter 60.1.3-Water Quality Control). Table 6-10 lists the regulated constituents and concentration limits for discharges to groundwater from these systems. The following discussion summarizes some recent work illustrating the potential for contaminants to reach groundwater via stormwater.

Table 6-10. Groundwater discharge limits per Chapter 60.1.3.B, TRPA Code of Ordinances.

Constituent	Units	Maximum Concentration
Total Nitrogen as N	mg/L	5
Total Phosphate as P	mg/L	1

Constituent	Units	Maximum Concentration
Total Iron	mg/L	4
Turbidity	Jackson Turbidity Unit (JTU)	200
Oil and Grease	mg/L	40

Figure 6-14 shows the locations of 63 stormwater detention basins and 114 dry wells used to infiltrate stormwater from the CSLT stormwater collection system. Review of this figure shows that the majority of active CWS wells in the South Lake Tahoe and Bijou subareas lie near dry wells and detention basins used to discharge storm water to groundwater in the TVS Subbasin.

6.3.3.1 2nd Nature Inc. Studies

In 2006 and 2011 two detailed studies were conducted by 2nd Nature Inc. to evaluate the potential risk of several constituents related to storm water pollutants (hydrocarbon, oil and grease, turbidity, iron, nitrogen, phosphorous) to shallow groundwater resources because of urban storm water infiltration.

The main objective of the 2006 study was to identify whether the hydrocarbon contamination poses a threat to shallow groundwater quality due to infiltration of storm water. The 2006 study focused on stormwater infiltration through two dry detention basins (Eloise Basin and Industrial Basin) within the urban limits of the CSLT and included both storm water sampling and groundwater monitoring over two water years (WY 2004 and WY 2005). Shallow groundwater was monitored from 12 monitoring wells, installed to evaluate whether the local water table showed a hydrologic response to infiltration from the detention basin. Data showed urban storm water entering the detention basins consistently contained heavy petroleum hydrocarbons, with less frequent detections of oil and grease. The levels of TPH-diesel detected in the surface water samples exceeded the LRWQCB numerical groundwater quality objectives for petroleum hydrocarbons. Low level detections of VOCs (primarily toluene and xylenes) were observed in approximately 20% of the storm water samples collected. Other key petroleum constituents, including benzene, ethylbenzene, and oxygenates (MtBE, TBA, etc.) were not detected in any of the surface water samples collected. None of the monitoring wells installed for this project contained detectable levels of hydrocarbons, VOCs or oxygenates following the analysis of over 70 shallow groundwater samples collected in locations potentially impacted by detention basin infiltration. The lack of hydrocarbons and VOC detections in all groundwater samples indicates that gasoline surface spills are rapidly depleted in light-end petroleum hydrocarbons before they are entrained in storm water flows and that the soil horizon beneath the detention basins provides adequate treatment to reduce low level concentrations of heavy hydrocarbons, toluene, and xylene compounds that were detected in the infiltrating urban runoff.

The 2011 study further evaluated the vulnerability of groundwater aquifers in South Lake Tahoe from infiltrating urban storm water with a focus on several other constituents related to storm water pollutants (oil and grease, turbidity, iron, nitrogen, phosphorous). The study also

reported findings from other storm water infiltration studies from the scientific literature. According to the study findings, most of these chemicals are trapped within the upper portions of the soil column where infiltration occurs and extensive migration of pollutants in the subsurface is unlikely. Existing data indicates that constituents such as oil and grease, total iron, total nitrogen, and turbidity are unlikely to degrade groundwater quality because of storm water infiltration.

Among the chemicals evaluated, nitrate is considered a moderate risk, given its highly mobile state in the subsurface. Studies of infiltration basins indicated that the storm water infiltration discharge standard of 5 mg/L of total nitrogen was commonly exceeded in urban catchments containing a high proportion of impervious surfaces or recreational land uses. In addition, storm water infiltration studies identified relatively higher average nitrate concentrations measured in shallow monitoring wells located downgradient of infiltration basins relative to nitrate concentrations measured in shallow monitoring wells located upgradient. The mobility of nitrate in groundwater may warrant future monitoring to protect the beneficial uses of domestic and municipal water supply wells.

According to the study, the greatest potential risk resulting from storm water infiltration is to the shallow groundwater zones underneath infiltration basins, rather than deep groundwater used for water supply. Other studies of urban storm water infiltration suggest that the shallow groundwater (at a depth of about 3 feet below the water table) consisted almost entirely of storm water and storm water did not penetrate to depths greater than 9.9 feet below the water table. Among several results provided by this study, it is recommended for management purposes that infiltration practices should minimize the contact between inflow storm water and organic sediments retained in infiltration basins.

6.3.3.2 South Y Feasibility Study

In 2019, significant levels of PCE contamination (>500 UG/L) were detected in groundwater samples collected neighboring the Tucker Avenue Stormwater Detention Basin (Tucker Basin). Stormwater infiltrated through this basin is believed to be leaching PCE contamination from soils underlying the Tucker Basin, contributing to the regional PCE groundwater contamination (T10000007984). The CSLT storm drain system is believed to have been in place when the former Lake Tahoe Laundry Works site, (SL0601754315) was operating between 1972 and 1979. Spills from this site are believed to have flowed into the CSLT storm drain system contaminating the soils underlying the present-day Tucker Basin (Weiss, 2019).

In 2021, LRWQCB issued a Notice of Violation (NOV) to responsible parties of the Former Big O Tire Store (SL0601729739), requiring the submittal of a work plan including but not limited to determining if contamination originating from this site occurred along preferential pathways, including the CSLT storm drain system. Further investigations for this site have yet to be performed.

6.3.3.3 PFAS in Stormwater

PFAS substances have been detected in stormwater where PFAS-impacted media are exposed to rainwater. In 2020, EPA published a memorandum with interim requirements to

address point source discharges of PFAS substances in stormwater and wastewater discharges (EPA, 2020a). Major sources of PFAS in the environment include primary manufacturing facilities that produce PFAS and secondary manufacturing facilities that use PFAS to produce goods, such as use as surface coatings applied to textile and leather products, and paper products; corrosion prevention in metal plating; and as coatings and insulation in wire manufacturing (ITRC, 2020). PFAS substances have also been detected in stormwater associated with residential and commercial land uses. Literature review of studies focused on the occurrences of PFAS in stormwater show PFOS concentrations on the order of 15.5 PPT and PFOA concentrations on the order of 19.1 PPT in stormwater runoff from Residential land uses; and PFOS concentrations on the order of 42.5 PPT and PFOA concentrations on the order of 30.6 PPT in stormwater runoff from mixed Residential/Commercial land use areas (Geosyntec, 2020). Occurrences of PFAS in stormwater runoff have caused renewed concern about the infiltration of stormwater as a pathway for PFAS contamination of groundwater.

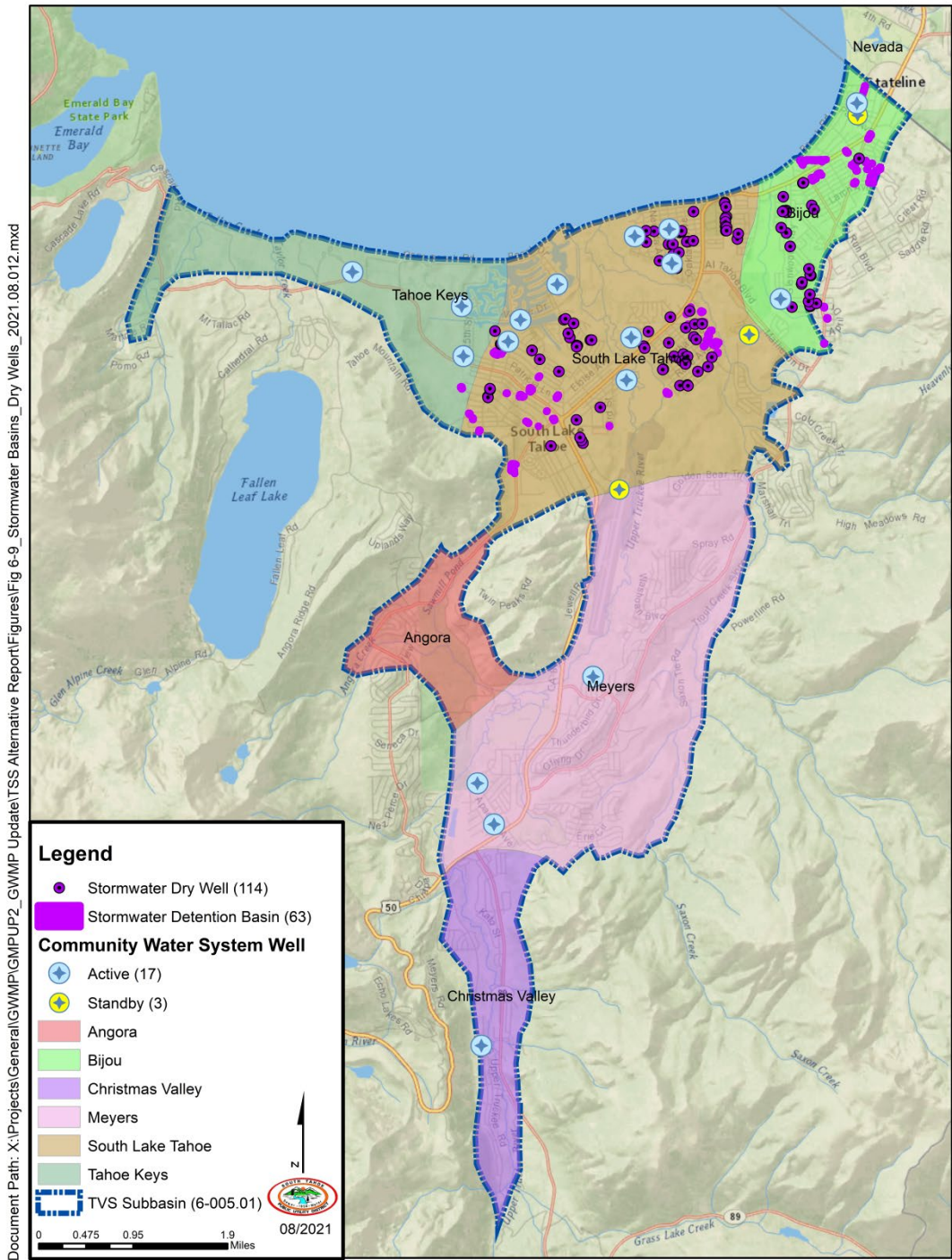


Figure 6-14. Locations of CSLT stormwater detention basins and dry wells in the TVS Subbasin.

6.4

Groundwater Vulnerability Assessment

The following section provides an overview of groundwater sensitivity to contamination in terms of groundwater recharge areas, and the susceptibility of groundwater sources to contamination using groundwater source area delineation and potential contamination activity site mapping. Locations of small water system and domestic wells are included on the vulnerability map to also consider the potential susceptibility of these wells to potential sources of contamination recognized within the TVS Subbasin.

6.4.1

Importance of Protecting Groundwater Quality

Maintaining high groundwater quality not only involves protection of drinking water wells themselves, but also extends to protection of all water-bearing zones used for water supply. Groundwater contamination resulting from leaks or spills has impaired groundwater wells in the TVS Subbasin (see Section 6.2.4 and 6.3.1.1). If the groundwater quality in a portion of the TVS Subbasin is not usable for water supply due to a contamination problem, it effectively reduces the total water supply, as wells cannot be placed in that area, and concentrating wells in non-impacted areas may lead to well interference effects that may have to be addressed.

6.4.2

Groundwater Recharge Areas

In areas where pollutants are present at the land surface or within the pore spaces of the vadose zone, groundwater recharge can serve as a pathway to introduce these contaminants into the groundwater system. While the majority of groundwater recharge flowing into the TVS Subbasin originates within the surrounding mountain block, groundwater recharge is believed to occur at some rate over the entirety of the subbasin area. Mean annual recharge rates extracted from the GSFRM over the TVS Subbasin are presented in Figure 6-15. Recharge rates range from 0.4 to 12.4 inches per year. Where streamflow is present, recharge rates tend to be low as most stream sections are gaining and are therefore less likely to act as contaminant pathways to the underlying aquifer. Recharge rates are notably higher along the western side of Trout Creek and in the South Y area. Most public water supply wells are in areas receiving 2 to 6 inches per year, though Arrowhead 3 and Tahoe Keys 3 are in somewhat more vulnerable areas expected to receive 6 to 8 inches year.

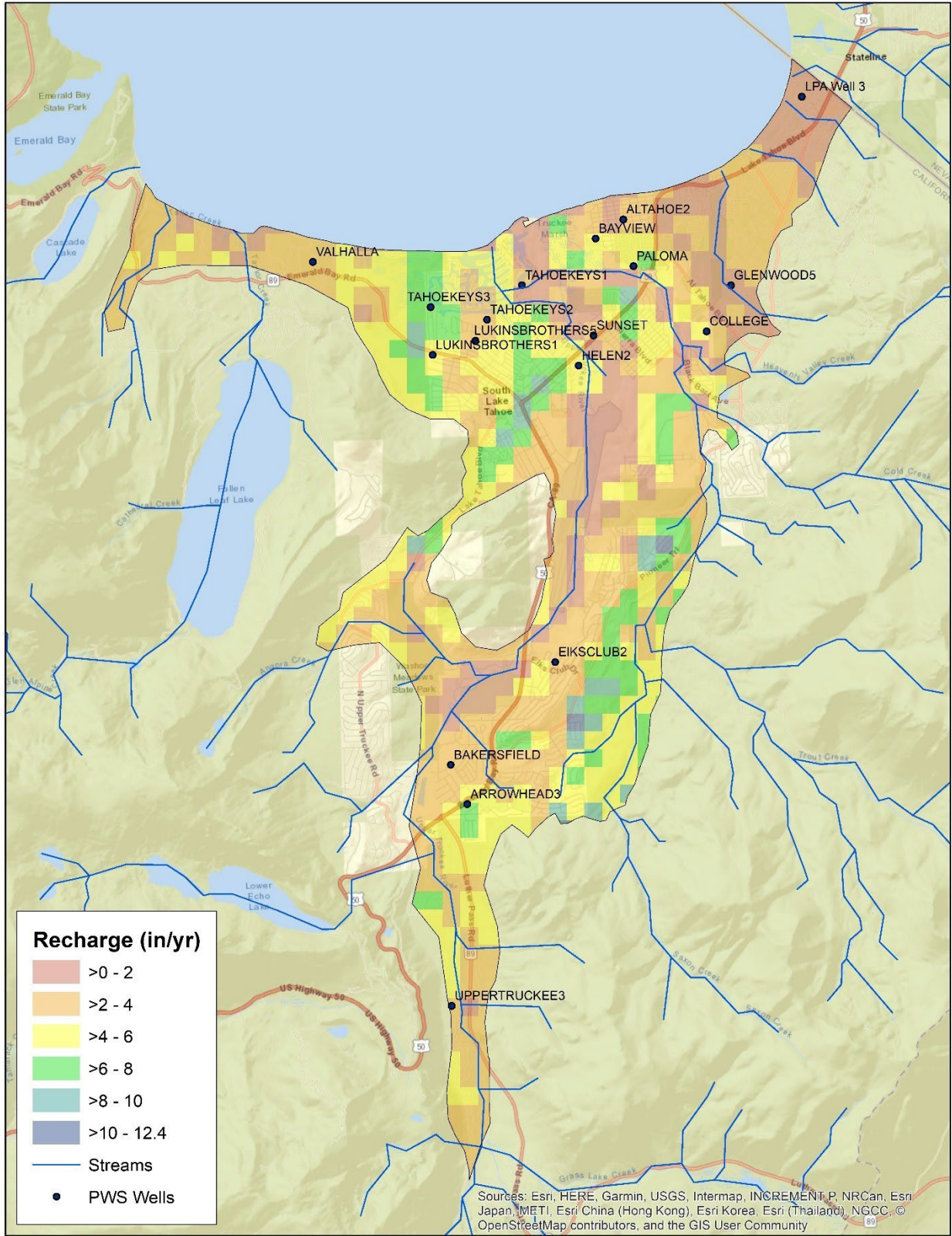


Figure 6-15. Mean annual recharge rates over the TVS Subbasin extracted from the GSFRM.

Delineation of Well Source Area Zones

The source area for a groundwater well represents the recharge area with permeable alluvial materials directly overlying an unconfined or semi-confined aquifer, where there is direct percolation of water into the unconfined or semi-confined aquifer. Recharge areas, which may be natural or artificial, are land areas that contribute water to an aquifer. Recharge occurs naturally from lakes, wetlands, direct precipitation, stream inflow, and subsurface inflow from upgradient sources of groundwater.

The delineation of source area zones was performed using the modified Calculated Fixed Radius (CFR) method (DDWEM-CDHS, 1999). Source area protection zones are concentric circles that represent the areas of groundwater that may be drawn to the well during two, five and ten years of pumping. The size of each protection zone is determined by the pumping rate of the well, the effective porosity of the formation that the well is completed in, the interval of pumping (two, five and ten years), and the screened interval of the well.

In the modified CFR method, source area protection zones are shifted in the upgradient direction to better represent the resulting geometry from the intersection of the capture zone of the well and the slope of the hydraulic gradient. The upgradient extent of the zone is determined as one and one-half times the calculated radius). The down-gradient extent of the zone is one-half the calculated radius. Three source area zones are defined. These zones are:

- Zone A : Microbial/Direct Chemical Contamination Zone. Protects the drinking water supply from viral, microbial and direct chemical contamination and is defined by the surface area overlying the portion of the aquifer that contributes water to the well within a two-year time-of-travel.
- Zone B5 : Chemical Contamination Zone. Prevents chemical contamination of the water supply, and protects drinking water sources for the long term, encompassing the area in between the two- and five-year time-of-travel. This zone provides for more response time for chemical spills.
- Zone B10 : Chemical Contamination Zone. Prevents chemical contamination of the water supply, and protects drinking water sources for the long term, encompassing the area in between the five- and ten-year time-of-travel. This zone allows for some attenuation or remediation of contaminant sites, or if necessary, time to develop alternate sources of water supply.

Source area zones for CWS wells in the TVS Subbasin were calculated using the modified CFR method and the average pumpage rate for each well over the preceding 10-year period (WY 2011–WY 2020). The California Drinking Water Source Assessment and Protection (DWSAP) Program requires a minimum radius for each protection zone: 600 feet for Zone A; 1,000 feet for Zone B5; and 1,500 feet for Zone B10. If the calculated radii of the protection zones are less than the DWSAP minimums, the minimum values are used instead. Source area zones are cropped at the basin margins. Figure 6-16 shows the modified CFR source area zones for these wells. Figure 6-16 also includes locations of small water system (Section 3.3.3) and domestic wells (Section 3.3.3.1). As pumpage data for these wells was not found, source area

zones for these wells were not calculated. However, these wells were plotted to consider the proximity of these wells to possible contaminating activity sites (see below Section 6.4.4).

6.4.4 Possible Contaminating Activity (PCA) Sites

Under the DWSAP Program, a Possible Contaminating Activity (PCA) is defined as human activities that are actual or potential origins of contamination for a drinking water source. PCAs include sources of both microbiological and chemical contaminants that could have adverse effects upon human health. PCAs are potential origins of contamination in drinking water source areas and protection zones. To develop an inventory of PCA sites in the TVS Subbasin, information was obtained from the following data management systems.

- GeoTracker: SWRCB' data management system for sites that impact, or have the potential to impact, water quality in California, with an emphasis on groundwater.
- CERS: California Environmental Protection Agency data management system for Unified Program information including, but not limited to, facility data regarding hazardous material regulatory activities (such as, hazardous materials business plans, site maps, and chemical inventories), underground and aboveground storage tanks, hazardous waste generation, inspection, compliance, and enforcement actions.

GeoTracker sites are environmental regulatory compliance sites that are under investigation or in remediation for contamination of soil and groundwater. Each site is designated as "open" or "closed". The open sites are categorized based on the status of site investigation or remediation activities as follows: site assessment, interim remedial action, remediation, or verification monitoring. Closed sites include any site with a status that suggests contaminated groundwater is no longer migrating offsite (e.g., case closed, no further action). A general summary of these data includes the following groupings:

- Moderate Threat – includes closed sites that affect groundwater not used for drinking water supply or involve soil contamination only.
- High Threat – includes closed sites that affect groundwater used for drinking water supplies, or open sites that affect groundwater not used for drinking water supply or involve soil contamination only.
- Very High Threat – includes open sites that affect groundwater used for drinking water supplies.

In addition to these data sources, listings of businesses regulated by the EDCEMD and business license information from the CSLT were reviewed to identify businesses activities involving PCAs. Business activity PCAs are assigned threat ranks by correlating with rankings used for the DWSAP program guidelines (DDWEM-CDHS, 1999). A general summary of these data includes the following groupings:

- Low Threat – includes parks, playgrounds, and schools.

- Moderately Low Threat – includes churches, schools with industrial arts facilities, general manufacturing, commercial and service industries which would not use chemicals.
- Moderate Threat – includes general manufacturing, commercial and service industries which generally use few chemicals, public areas and office buildings, hospitals, hotels, golf courses.
- Moderately High Threat – includes general manufacturing, commercial and service industries which generally use chemicals, non-retail fuel dispensers.
- High Threat – includes businesses with past histories of contamination including dry cleaners, airports, gasoline stations, automotive repair, chemical manufacturers, machine shops, pest control, and chemical manufacturers.
- Very High Threat – includes businesses with past histories of contamination that handle large volumes of hazardous materials including chemical and waste handling facilities, and bulk fuel storage facilities.

6.4.5 **Groundwater Vulnerability Map**

Information from the source area zone delineation and inventory of PCA sites is presented on Figure 6-16. The number and types of PCAs found within each source water protection zone are summarized below in Table 6-11. Highest densities of PCA sites are located along Highways 50 and 89 especially within the Bijou, South Lake Tahoe, and Meyers subareas. The well source areas within the South Lake Tahoe subarea overlap many of these PCA clusters, especially for the high-volume wells in the northern portion of the Subbasin indicated by the largest source area zones. Figure 6-16 also such a large proportion of small water system and domestic wells across the Bijou and South Lake Tahoe subareas are located within areas with relatively high PCA site densities.

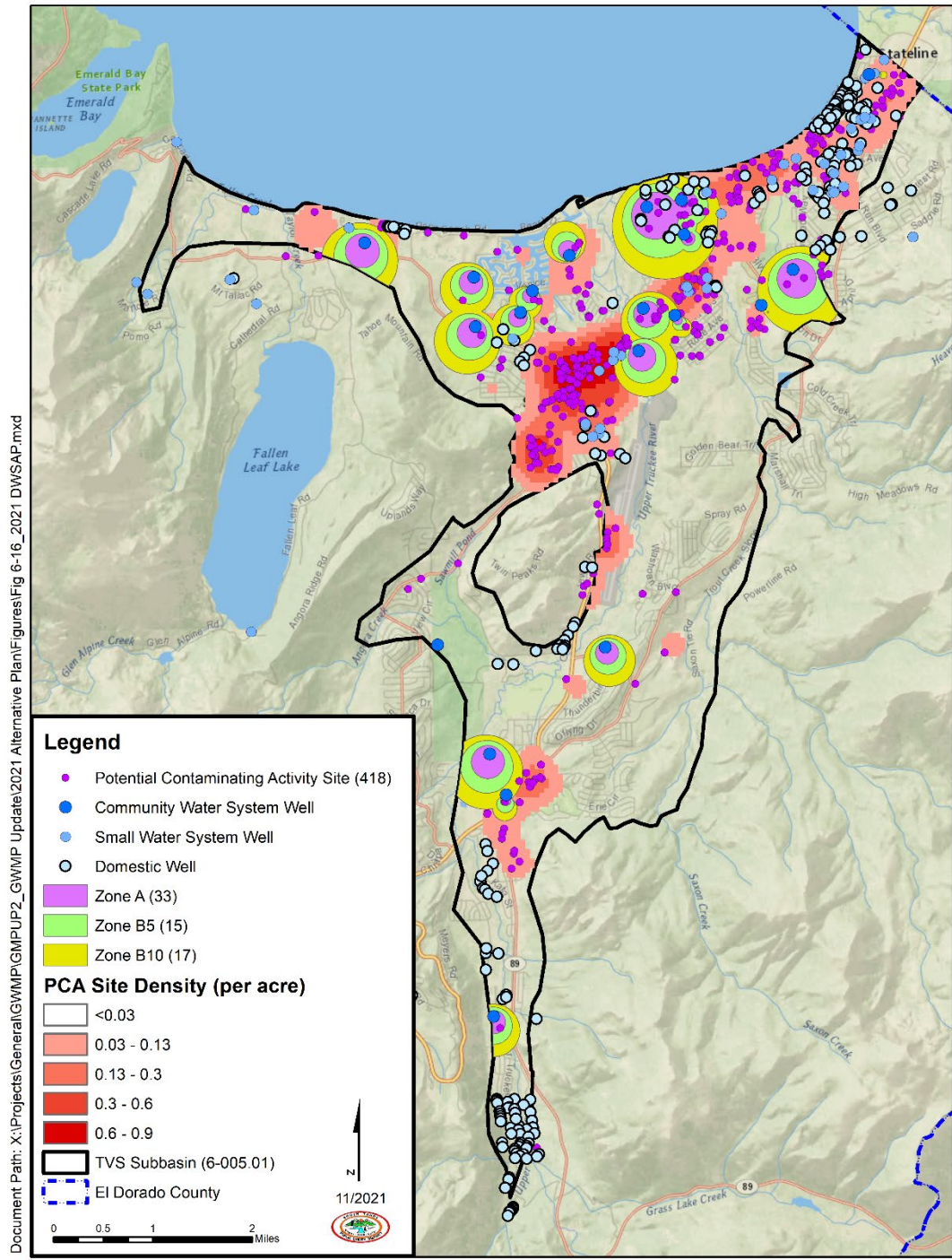


Figure 6-16. Source area zones delineated using the modified CFR method and possible contaminating activity sites identified within the TVS Subbasin.

Table 6-11. Numbers and types of PCA sites located within source protection zones delineated within the TVS Subbasin.

Number of Sites (Count)	Type(s)	Possible Contaminating Activity Sites
		Possible Contaminants (DDWEM-CDHS, 1999)
Zone A		
1	Apartments and condominiums	Swimming pool maintenance chemicals; pesticides for lawn and garden maintenance and cockroach, termite, ant, rodent, and other pest control wastes from on- site sewage treatment plants; household hazardous wastes.
1	Cellular Site	Diesel fuel (Diesel generator back-up); sulfuric acid (Battery back-up)
1	Clean-Up Program Site - Open	Diesel fuel; gasoline; kerosene
3	Clean-Up Program Site - Closed	Diesel fuel; gasoline; kerosene
2	Gas Stations/sumps	Soaps; detergents, waxes; miscellaneous chemicals, hydrocarbons
19	Injection Wells/ Dry Wells/ Sumps	Stormwater runoff; spilled liquids; used oils; antifreeze; gasoline; solvents; other petroleum products; pesticides; and a wide variety of other substances
1	Motor Pools	Automotive wastes: solvents; waste oils; hydrocarbons from storage tanks
3	Sewer Pump Station	Sewage, treatment chemicals
1	Utility Stations/ Maintenance Areas	PCBs from transformers and capacitors; oils; solvents; sludges; acid solution; metal plating solutions (chromium, nickel, cadmium); herbicides from utility rights-of-way
1	Wells	Storm water runoff; solvents; nitrates; septic tanks
Zone B5		

Possible Contaminating Activity Sites		
Number of Sites (Count)	Type(s)	Possible Contaminants (DDWEM-CDHS, 1999)
2	Boat Services/repair/refinishing	Diesel fuels; oil; septage from boat waste disposal area; wood preservative and treatment chemicals; paints; waxes; varnishes; automotive wastes
1	Body Shops/repair shops	Waste oils; solvents; acids; paints; automotive wastes; miscellaneous cutting oils
2	Clean-Up Program Site - Closed	Diesel fuel; gasoline; kerosene
1	Gas Stations/sumps	Soaps; detergents, waxes; miscellaneous chemicals, hydrocarbons
10	Injection Wells/ Dry Wells/ Sumps	Stormwater runoff; spilled liquids; used oils; antifreeze; gasoline; solvents; other petroleum products; pesticides; and a wide variety of other substances
1	Sewer Pump Station	Sewage, treatment chemicals
Zone B10		
1	Body Shops/repair shops	Waste oils; solvents; acids; paints; automotive wastes; miscellaneous cutting oils
1	Cellular Site	Diesel fuel (Diesel generator back-up); sulfuric acid (Battery back-up)
6	Clean-Up Program Site - Closed	Diesel fuel; gasoline; kerosene
2	Dry Cleaners	Solvents (perchloroethylene, petroleum solvents, Freon); spotting chemicals (trichloroethane, methylchloroform, ammonia, peroxides, hydrochloric acid, rust removers, amyl acetate)
1	Fire Station	General building wastes; hydrocarbons from test burn areas

Possible Contaminating Activity Sites		
Number of Sites (Count)	Type(s)	Possible Contaminants (DDWEM-CDHS, 1999)
1	Hardware/lumber/parts stores	Hazardous chemical products in inventories; heating oil and forklift fuel from storage tanks; wood-staining and treating products such as creosote; paints; thinners; lacquers; varnishes
3	Injection Wells/ Dry Wells/ Sumps	Stormwater runoff; spilled liquids; used oils; antifreeze; gasoline; solvents; other petroleum products; pesticides; and a wide variety of other substances

SECTION 7: STAKEHOLDER INVOLVEMENT

Public education, public participation, and community relations are integral elements to groundwater management in the TVS Subbasin. As such, the District is committed to involving the public and the commercial and industrial communities in the development and implementation of this Alternative Plan. Since adoption of the 2014 GWMP, the District has continually engaged stakeholders. The following section presents a brief description of the Stakeholders Advisory Group (SAG) formed for implementation of the 2014 GWMP and development of this first five-year update of the Alternative Plan, groundwater management activities conducted in collaboration with the SAG, the public adoption process of the first five-year update of the Alternative Plan, and opportunities for on-going and future stakeholder involvement.

7.1 Stakeholder Advisory Group

Within the South Lake Tahoe area, there is existing, on-going coordination and collaboration regarding water issues in the TVS Subbasin. A key objective of this Alternative Plan is to continue to build off existing relationships to further enhance groundwater management and protection.

Since adoption of the 2014 GWMP, the District has convened an ongoing SAG, which was supplemented with new members as representatives of the general interest categories changed. Participants on the SAG represent the interest categories called out in Section 7.4 of the District’s 2000 Groundwater Management Plan, Ordinance No. 477-00 (District, 2000). The interest categories are used to capture a broad spectrum of community, business, and agency interests to provide meaningful input in the development and implementation of the Alternative Plan. The District invites new or replacement members to join the SAG through an application process as circumstances change within the TVS Subbasin. Vacancies for the Business Rate Payer and Service Station Operator interest categories are currently open.

The current SAG has a roster of fourteen members (Table 7-1). District staff participating as SAG members includes the General Manager and District Hydrogeologist. The District Hydrogeologist serves as the Plan Manager and is the technical lead for the Alternative Plan and liaison to the SAG. The Plan Manager is also responsible for organizing and facilitating SAG workshops.

Table 7-1. Current members of the Stakeholder Advisory Group (SAG) for the Alternative Plan.

Interest Category	Name	Affiliation	Position
Agency	Brian Grey	Lahontan Regional Water Quality Control Board	Engineering Geologist
Agency	Ken Payne, PE	El Dorado County Water Agency	General Manager
Agency	Robert Lauritzen, PG	El Dorado County EMD	Geologist

Interest Category	Name	Affiliation	Position
Agency	Jason Burke	City of South Lake Tahoe	Storm Water Program Coordinator
Agency	Jacob Stock	Tahoe Regional Planning Agency	Senior Long-Range Planner
Agency	Nicole Bringolf	UDSA Forest Service LTBMU	Hydrologist
Real Property Owner	Scott Carroll	California Tahoe Conservancy	Associate Environmental Planner
Service Station Operator	Open		
Water Purveyor	Nakia Foskett	Lakeside Mutual Water Company	Water System Manager
Water Purveyor	Jennifer Lukins	Lukins Brothers Water Company	Vice President
Water Purveyor	Daniel Larson	Tahoe Keys Water Company	Water System Manager
Business Community Rate Payer	Open		
Non-Business Community Rate Payer	Harold Singer	Resident	Retired
Other	Andrea Buxton	Tahoe Resource Conservation District	Stormwater Program Manager
District	John Thiel, PE	South Tahoe Public Utility District	General Manager
District	Ivo Bergsohn, PG, HG	South Tahoe Public Utility District	Hydrogeologist/Plan Manager

7.1.1 SAG Workshops

The SAG meets on a semi-annual basis and may meet more frequently, as decided by a majority of members. These meetings are organized as workshops, providing a forum in which to discuss current groundwater issues and groundwater management activities associated with implementation of the Alternative Plan. Since 2015, the District has hosted 14 SAG Workshops discussing a variety of topics pertinent to groundwater management with the TVS Subbasin (Table 7-2). Notices of these workshops along with workshop agendas are emailed to interested parties approximately one week prior to the scheduled meeting date. During the COVID-19 Public Health Emergency, these workshops have been convened as virtual meetings since July

2020. Meeting notes and presentations discussed at each workshop are posted for public access following the workshop on the District’s Groundwater Management Plan web page:
<https://stpud.us/news/groundwater-management-plan/>

Table 7-2. SAG workshops convened since adoption of the 2014 GWMP through June 2021.

SAG WORKSHOP	DATE	TOPICS
2015 SAG Workshop 1	4/22/2015	<ul style="list-style-type: none"> • South Y PCE Site • TVS Subbasin Drinking Source Water Assessment and Protection (DSWAP) Improvements • SGMA - GSA Formation • 2015 Annual Report - Planning
2015 SAG Workshop 2	12/16/2015	<ul style="list-style-type: none"> • 2015 Annual Report - Planning • South Y Area PCE Contamination Update • SGMA – Update • TVS Subbasin Hydrologic Modeling Tools • 2015 TVS Subbasin Groundwater Levels
2016 SAG Workshop 1	5/27/2016	<ul style="list-style-type: none"> • 2016 GW Management Activities • South Y Extraction Well Study • Proposition 1 Groundwater Cleanup Program Funding • TRPA Regulations – Relevant Ordinances
2016 SAG Workshop 2	10/25/2016	<ul style="list-style-type: none"> • 2016 GW Management Activities • 2016 DSWAP Mapping Update • Tahoe Keys Property Owners Association South Y PCE Investigation • TVS Subbasin GW Modeling Evaluation Update
2017 SAG Workshop 1	4/26/2017	<ul style="list-style-type: none"> • Groundwater Dependent Ecosystems (GDE’s) • SGMA – GWMP Alternatives • South Y Activity - Updates • South Y Remedial Alternatives FS • 2017 Private Well Owner Survey • GSA Formation Coordination Agreement
2017 SAG Workshop 2	12/15/2017	<ul style="list-style-type: none"> • South Y Remedial Alternatives FS • South Y Activity - Updates • 2017 Private Well Owner Survey • USFS LTBMU Groundwater Resources Management • GWMP Activity Updates
2018 SAG Workshop 1	10/09/2018	<ul style="list-style-type: none"> • South Y Activity - Updates • SGMA – GWMP Alternatives • 2018 Draft SGMA Basin Prioritization
2018 SAG Workshop 2	12/21/2018	<ul style="list-style-type: none"> • South Y Activity - Updates • 2017 Survey of Well Owners Report • 2018 Closing Items
2019 SAG Workshop 1	7/23/2019	<ul style="list-style-type: none"> • South Y Activity - Updates • TVS Subbasin Stormwater Management

SAG WORKSHOP	DATE	TOPICS
		<ul style="list-style-type: none"> • 2019 Groundwater Management Activities
2019 SAG Workshop 2	11/22/2019	<ul style="list-style-type: none"> • Groundwater Management Plan – 5- Year Update • 2019 TVS Subbasin GW Conditions
2020 SAG Workshop 1	7/29/2020	<ul style="list-style-type: none"> • Private Well Owner Survey – Phase II • LRWQCB Regional Plume Characterization • DRI Model Evaluation – 50 Year Water Budget • Update to 2014 GWMP
2020 SAG Workshop 2	12/17/2020	<ul style="list-style-type: none"> • South Y PCE Contamination - Update • TVS Subbasin Alternative
2021 SAG Workshop 1	3/25/2021	<ul style="list-style-type: none"> • TVS Subbasin Alternative – Progress Update • Phase II Survey of Private Well Owners • Site Cleanup Subaccount Program Regional Plume Investigation • TVS Subbasin 50 Year Water Budget Projections
2021 SAG Workshop 2	6/30/2021	<ul style="list-style-type: none"> • TVS Subbasin Alternative – Sustainable Management Criteria • TVS Subbasin Alternative – Interconnected Surface Waters • TVS Subbasin Alternative – Implementation Plan (Section 10)

7.2 Groundwater Management Collaboration

The Alternative Plan is updated within the context of existing, on-going coordination and collaboration in groundwater issues within the TVS Subbasin. As noted in Section 4.1.2 of this Alternative Plan, water quality improvement programs, with a focus on Lake Tahoe clarity, and groundwater management issues have required the coordination and collaboration of many of the organizations and agencies within the Lake Tahoe Basin. The following section presents several examples showing how groundwater management through implementation of the Alternative Plan has benefited through collaboration and engagement with the SAG.

7.2.1 Protect Groundwater

The overall goals for groundwater protection discussed by the SAG during development of the Alternative included:

- Integrate groundwater protection into existing site inspection protocol of the several agencies already conducting site inspections;
- Create a private well owner education and cooperation campaign; and
- Maintain an inventory of infiltration basins and dry wells, inform spill responders of these locations, and communicate spill events to water purveyors.

Acting on the results of the private well owners' survey (see Section 3.3.4), the District has offered: guidance on well maintenance, site visits for basic assessment of wellhead conditions, and accredited laboratory testing of well water quality to improve private well owners' understanding on the importance of well maintenance on protecting groundwater quality. The District has also used these efforts to build relationships and establish communication with private well owners, promote guidance on well maintenance available through the County Water Well Program, and encourage engagement in groundwater management through participation on the SAG.

The District invited storm water program managers from SAG member agencies to describe their respective stormwater management programs and consider the connection(s) between storm water management and groundwater protection. During 2019 (2019 SAG Workshop 1), storm water managers proposed that parcels with known incidences of shallow soil contamination be mapped to prevent unintended infiltration of residual soil contamination to groundwater. Renewed public outreach and education was also proposed as the best approach to protecting groundwater quality by preventing illicit discharges to stormwater infiltration facilities. The locations of PCA sites (including sites that impact or have the potential to impact groundwater quality) and CSLT stormwater infiltration facilities are included on the updated 2021 DSWAP map (Figure 6-16) presented in Section 6.4.5 of this Alternative Plan. Locations of storm water infiltration facilities should be shared with spill responders to help prevent spills from entering these facilities. Spills entering storm water infiltration facilities should be reported to the LRWQCB and EDCEMD to investigate the extent of potential contamination within the receiving infiltration facility and to the water purveyors as a potential source of groundwater contamination within the TVS Subbasin.

Groundwater quality in the TVS Subbasin is typically of excellent quality, however, there is a legacy of groundwater contamination from regulated chemicals (see Section 6.2.4). Under the short-term implementation plan for BMO #2 (Maintain and Protect Groundwater Quality), the SAG supported renewed investigation and clean-up of relict groundwater contamination with special emphasis on PCE contaminant plume(s) in the South "Y" Area (Kennedy Jenks, 2014). A summary of the activities involved with this work is presented in Section 6.3.1.1. Given the need for interagency coordination and the importance of changes being considered by SAG water purveyors, SAG water purveyors participated as partners on the Technical Advisory Committee (TAC) organized for the South Y Feasibility Study.

7.2.1.1 **Site Inspections**

Findings of the well owners' surveys confirm that more than 340 private wells are currently active within the TVS Subbasin (Section 3.3.4). Private wells do not require operating permits or reporting; therefore, information on operational status is very limited along with the overall condition of the wellhead. TRPA Best Management Practice (BMP) Parcel permit applications, County well permit applications and County Small Water System Program inspections could be used to collect operational status information and build on the private well use and wellhead conditions data collected during the well owner's surveys. Building the private well inventory for domestic wells could be added to the County Water Well Program for continued use in the Alternative Plan.

7.2.2

Coordination with Land Use Planning Agencies

SGMA requires close coordination and consultation between water supply or management agencies and land use planning agencies to ensure that proper water supply and management planning occurs to accommodate projects that will result in increased demands on water supplies or impact water resource management. (Gov. Code § 65352.5(a).) Existing law requires a city or county upon adoption of its General Plan to use as a source document any Urban Water Management Plan (UWMP) submitted by an urban water supplier. (Gov. Code § 65352.5(c).) When a city or county adopts or substantially amends a general plan, GSAs or an entity that submits an Alternative must provide the planning agency a current version of the Groundwater Sustainability Plan or Alternative (Gov. Code § 65352.5(d)(1)), and, if needed, a report on the anticipated effect of proposed action to adopt or substantially amend a general plan on implementation of a GSP (Gov. Code § 65352.5(d)(3)).

Local land use planning agencies within the TVS Subbasin are described in Sections 4.3.3 (El Dorado County) 4.3.6 (TRPA); 4.3.7 (CSLT); and 4.3.8 (USFS) of this Alternative Plan. Agency members from El Dorado County, the TRPA, CSLT and USFS are represented on the SAG (Table 7-1) and have been regularly updated throughout the development of this Alternative Plan. In 2021, local land use planning agencies were formally contacted and provided copies of a participation notice and stakeholder survey by direct mailer and follow-up email as described in Section 7.4.1 of this Alternative Plan.

A key element of the Alternative includes an ongoing program of monitoring groundwater conditions. As part of this effort, the District regularly updates and maintains a groundwater vulnerability map. In 2017, the scope of the District's groundwater vulnerability map was expanded to include groundwater source information provided by SAG water purveyors and new PCA site information provided by SAG agencies. The 2017 vulnerability map was presented in WY 2017 Annual Report (District, 2018) and was shared with all SAG members for their use. This map was again updated in 2021 as part of this update to the Alternative Plan (see Section 6.4.5).

7.2.3

Sharing Data and Information

A key part of groundwater management is collecting data to monitor groundwater conditions. Multiple governmental agencies and water purveyors collect groundwater-related data in the TVS Subbasin. The SAG has been an important vehicle for the sharing of well location, construction, groundwater pumpage, and water quality information used in hydrologic models developed to calculate annual water budgets and assess groundwater conditions reported to DWR in Water Year Annual Reports.

The District's surveys of private well owners (Section 3.3.4) were the principal tool used by the District to receive input from more than 500 private well owners and users. Responses from surveys were used to identify individual private well owners to improve interested parties' lists; and better understand private well owners' groundwater use, private well system conditions and water quality concerns. The surveys were also used to inform private well owners on the importance of private well maintenance to protect groundwater quality.

7.2.4

SAG Accomplishments

Since adoption of the 2014 GWMP, the District, in collaboration with EDWA and the SAG, has achieved a substantial list of accomplishments to support the sustainable management of groundwater resources within the TVS Subbasin (Table 7-3). Several accomplishments involve enhanced data collection and use with applications ranging from basic monitoring of groundwater use, levels, and supply to development of complex hydrologic models. Advanced hydrologic models increased accuracy and reliability of model outputs – including calculation of annual water budgets, identification of recharge areas, effects of groundwater pumping on interconnected surface waters, impacts of climate change, and migration of PCE-contaminated groundwater.

Regular SAG meetings and SAG-recommended public outreach have helped build relationships, facilitated information sharing among interested parties, and increased awareness of sustainable groundwater management among private well owners.

Lastly, the District has continued to satisfy SGMA requirements by (1) acting as a GSA for TVS Subbasin; (2) cooperating with EDWA via the MOU to manage groundwater resources across the full extent of the TVS Subbasin; (3) submitting semi-annual reports of groundwater elevation data to DWR as a monitoring entity pursuant to CASGEM; and (4) submitting annual reports to DWR under SGMA (23 Cal. Code Regs., § 356.2) (Annual Reports).

Table 7-3. Major groundwater management activities completed since 2015.

CATEGORY	ACCOMPLISHMENT
Basin Monitoring	<ul style="list-style-type: none"> • Groundwater Monitoring– precipitation, elevations, groundwater pumpage, recharge, storage
Hydrologic Modeling	<ul style="list-style-type: none"> • Phase I Hydrologic Models– Water balance, future conditions • Phase II Hydrologic Models – Recharge areas, capture zones, baseflow depletion analysis and capture maps, climate change impacts, monitoring network evaluation • Updated Phase I Groundwater Model • South Y Fate & Transport Model
Investigations	<ul style="list-style-type: none"> • Analysis of Basin Conditions • South Y Extraction Well Suitability Investigation • Basin Management Objectives Analysis • Survey of Private Well Owners • South Y Feasibility Study – Baseline Health Risk Assessment, Pre-Design Investigation, Feasibility Study, Interim Remedial Action Plan
Public Outreach	<ul style="list-style-type: none"> • SAG Workshops • South Y Feasibility Study Workshops • PWOS I – Groundwater Well Survey • PWOS II – Groundwater Well Survey • Groundwater Web Page • Public Meeting Updates and Annual Reports
Reporting	<ul style="list-style-type: none"> • GSA Formation

CATEGORY	ACCOMPLISHMENT
	<ul style="list-style-type: none"> • MOU • CASGEM Reporting • SGMA Annual Reporting • TVS Subbasin Alternative Plan

7.3 Future/Ongoing Stakeholder Involvement Opportunities

The current SAG was convened to provide input during implementation of the 2014 GWMP and development of this first five-year update of the Alternative Plan. A new SAG may be formed following formal adoption of the first five-year update of this Alternative Plan. The District plans to conduct any new SAG in a similar manner as the current SAG: meet on a regular, ongoing basis to discuss and propose actions for sustainable groundwater management. Procedures for running the SAG will be reviewed and modified as needed to fulfill its purpose(s).

7.3.1 Future SAG Topics

The purpose of the SAG is to provide a forum to facilitate the discussion of groundwater related issues and sharing of information between water purveyors, land use planning agencies, regulatory agencies, businesses, and the public. Table 7-2 lists the numerous topics considered by the SAG since 2014. In the future, the SAG will be called upon to provide input on Recommended Actions for periodic review and assessment of this Alternative Plan and updates to the Implementation Plan (Section 10). The SAG will consider any modifications to sustainable management criteria, measurable objectives and minimum thresholds used to prevent the occurrence of undesirable results within the TVS Subbasin. Table 7-4 provides an initial list of future topics for potential discussion with the SAG.

Table 7-4. Potential topics for future discussion with the SAG.

TOPIC	DESCRIPTION
Emerging Contaminants– PFAS	<ul style="list-style-type: none"> • Occurrence <ul style="list-style-type: none"> • Meyers Landfill • WWTP Sampling (SWRCB Order WQ 2020-0015-DWQ) • Storm Water
Illicit Discharges to Storm Water Infiltration Systems	<ul style="list-style-type: none"> • Stormwater quality affecting groundwater • Public Outreach and Education • Basins and Dry Wells
Drought	<ul style="list-style-type: none"> • Water Supply and Demand Assessments • Coordinating Water Conservation Measures
Private Wells	<ul style="list-style-type: none"> • Dry Well Monitoring • Corrosivity in groundwater • Destruction of abandoned wells

TOPIC	DESCRIPTION
	<ul style="list-style-type: none"> Public Outreach and Education
Inorganic Contaminants	<ul style="list-style-type: none"> Radionuclide impacts on drinking water supply
Basin Monitoring Network	<ul style="list-style-type: none"> Opportunities for expanding basin monitoring network using existing wells
Integrated Regional Water Management (IRWM)	<ul style="list-style-type: none"> Opportunities for collaboration with the IRWM Region
Groundwater Dependent Ecosystems (GDEs)	<ul style="list-style-type: none"> Quantifying water use
Environmental Improvement Projects (EIP)	<ul style="list-style-type: none"> Benefits to groundwater replenishment
Climate Change	<ul style="list-style-type: none"> Lake Tahoe Basin agency efforts to assess climate change impacts on water resources. Operational Supply and Reliability <ul style="list-style-type: none"> Regional Power Outages (RPOs)/Wildfire Events
Funding for Groundwater Remediation	<ul style="list-style-type: none"> GSA role in pursuing funding opportunities and responsibilities

7.4 **Public Participation in the Five-Year Update of the Alternative Plan**

During WY 2020, the District and EDWA started the procedural, technical and public outreach activities needed for the first five-year update of the Alternative Plan⁸. In April 2020, the District and DRI met with DWR staff via conference call to discuss and consider approaches to address DWR’s Recommended Actions. In May 2020, the District adopted Resolution 3140-20 establishing its intent to update the Alternative Plan. In June 2020, the District submitted a Notice of Intent to DWR informing DWR of its intent to draft the first five-year update of the Alternative Plan (STPUD, 2020) (Appendix A05). In June 2020, the District and EDWA worked to develop the second amended and restated MOU between the District and EDWA to continue to coordinate and cooperate in the implementation of the SGMA within their respective jurisdictions of the TVS Subbasin. In July 2020, EDWA adopted its own Resolution WA-6-2020 establishing its intent to draft an updated Alternative Plan for implementation within the portion of the TVS Subbasin lying within the County and outside the District’s service area boundary.

The SAG and members of the SAG representing the public also contributed to development of the five-year update to the Alternative Plan, including advising the District regarding Plan content, offering information and insight of regional groundwater issues, and reviewing the Alternative Plan.

⁸ In addition to the public engagement outlined in this section, the District also held multiple public meetings during adoption of the 2014 GWMP and submission of the 2014 GWMP and Alternative Materials to DWR as a GSP Alternative in December 2016.

7.4.1 **Public Notice and Comment**

On October 1, 2021, the District and EDWA jointly issued 90-day notice of a hearing to adopt the five-year update to the Alternative Plan to CSLT and the County. On February 9, 2022, a follow-up letter was sent to CSLT and the County notifying these agencies of the availability of the draft of the first five-year update of the Alternative Plan for public comment.

On December 17, 2021, the District released a draft version of this five-year update to the Alternative Plan to the SAG for review and comment. The District received comments from the SAG and made responsive changes. A summary of comments and responses are included as Appendix N. On January 31, 2022, the District posted a notice of availability announcing a draft of the first five year of the Alternative Plan for public comment. The notice of availability was published in the Mountain Democrat and in the Tahoe Daily Tribune on February 4th and February 11th, 2022. The public comment period began February 9, 2022, and extended until March 11, 2022. A summary of comments and responses from the public comment period are also included in Appendix N.

On March 17, 2022, the District and EDWA jointly issued notice of the public hearings on April 13, 2022, and April 21, 2022, at which EDWA and the District, respectively, considered adoption of the first five-year update of the Alternative Plan. The notice of public hearings was published in the Mountain Democrat on March 23rd and March 30th, 2022; and was published in the Tahoe Daily Tribune on April 8th and April 15th, 2022. District staff advised the District's Board of Directors of the pending hearing date at the District Board's February 3, 2022, meeting and advised the EDWA's Board of Directors of the pending hearing date at the EDWA Board's March 9, 2022, meeting.

7.4.1.1 **Public Meeting**

The District Board of Directors held a public hearing on April 21, 2022 to solicit comments to the first five-year update of the Alternative Plan to consider adoption of the first five-year update of the Alternative Plan, enactment of Resolution No. 3215-22. The public was given an opportunity to ask questions and provide comment at the hearing. If the parties could not attend the public hearing, they could express their questions, interests, and concerns in writing to the District as explained in the public notice. The Notice of Availability and proof of publication for this notice are included in Appendix D. Following the public hearing, the first five-year update of the Alternative Plan was adopted by the District Board of Directors by passing Resolution No. 3215-22. A copy of this Resolution is provided in Appendix A. There were no public comments received during the public hearing.

At the Board's April 21, 2022 meeting, the District adopted Ordinance No. 580-22, removing the Groundwater Management Ordinance from the District's Administrative Code to allow this five-year update to the Alternative Plan to govern groundwater management in the TVS Subbasin. A copy of Ordinance No. 580-22 is included in Appendix E.

EDWA's Board of Directors held a public hearing on April 13, 2022 to solicit comments to the first five-year update of the Alternative Plan to consider adoption of the first five-year update of the Alternative Plan and adoption of Resolution No. WA-07-2022. The public was

given an opportunity to ask questions and provide comment at the hearing. If the parties could not attend the public hearing, they could express their questions, interests, and concerns in writing to EDWA as explained in the public notice. The Notice of Availability and proof of publication for this notice are included in Appendix D. Following the public hearing the first five-year update of the Alternative Plan was adopted by EDWA Board of Directors by passing Resolution No. WA-07-2022. A copy of this Resolution is provided in Appendix A. There were no public comments received during the public hearing.

7.4.2 Public Outreach and Engagement

Under SGMA, GSAs are required to engage the public during the development of a GSP or Alternative (Wat. Code § 354.10). As part of its public outreach the District developed a stakeholder engagement chart organized by stakeholders’ groups and communication methods to be employed for each group, updated lists of possible stakeholders within each group, and development of various communication tools. Communication tools developed include: participation notice, stakeholder survey, media release, on-line web postings, and a power point presentation targeted to the general public explaining the 2014 GWMP, the update process, and opportunities for engagement in this process. The stakeholders list has 286 entries and was developed in accordance with DWR guidance (DWR, 2018). Stakeholder Group A consists of regulatory bodies whose participation is specifically required by SGMA. Group B comprises other beneficial users of groundwater with the TVS Subbasin, and Group C includes civic groups, regulatory agencies and resource managers in the region that do not operate within the TVS Subbasin, and other interested parties. Stakeholders in Groups B and C were invited to participate in this process by the District. The participation notice was developed to satisfy SGMA public notification and participation requirements (Wat. Code § 10727.8). The stakeholder survey was developed for the Alternative Plan using the Stakeholder Survey Template available from the DWR engagement tools. The participation notice was posted on the District and EDWA web sites and mailed along with the stakeholder survey to Group A and Group B stakeholders. Only the Participation Notice was emailed to all possible stakeholders with email contact information. The District’s 2014 Groundwater Management Plan Update Presentation (District, 2020b) was posted on the Groundwater Management Plan web page of the District’s website. Copies of the outreach materials developed for the TVS Subbasin Alternative are provided in Appendix D.

Table 7-5. Alternative Plan stakeholder engagement chart.

Group	STAKEHOLDERS	METHOD(S)	Participation Notice	Stakeholder Survey
A	1) Legislative Bodies (§10727.8) <ul style="list-style-type: none"> a. County - Board of Supervisors b. CSLT – City Council 2) GW Elevation Monitoring and Reporting Entities (§10927) <ul style="list-style-type: none"> a. Federal Water Master 3) Local Land Use Planning Agencies <ul style="list-style-type: none"> a. TRPA 	1) Direct Mailer 2) Follow-Up Email 3) Interested Parties List 4) District Web Page	X X X	X X

Group	STAKEHOLDERS	METHOD(S)	Participation Notice	Stakeholder Survey
	<ul style="list-style-type: none"> b. County Planning c. CSLT Planning d. US Forest Service e. California State Parks 			
B	<ul style="list-style-type: none"> 1) Groundwater Users <ul style="list-style-type: none"> a. Domestic Well Owners b. Water Systems <ul style="list-style-type: none"> i. Community Water Systems (CWS) ii. Non-Transient Non-Community; iii. Transient Non-Community iv. State Small Water Systems 2) Environmental Users of Groundwater <ul style="list-style-type: none"> a. California Tahoe Conservancy 3) Surface Water Users <ul style="list-style-type: none"> a. Lakeside Park Association b. Tahoe Water Suppliers Association 	<ul style="list-style-type: none"> 1) Direct Mailer 2) Interested Parties List 3) District Web Page 	<ul style="list-style-type: none"> X X 	X
C	<ul style="list-style-type: none"> 1) Economic Development <ul style="list-style-type: none"> a. Tahoe Chambers of Commerce b. South Tahoe Chamber of Commerce 2) Environmental and Ecosystems <ul style="list-style-type: none"> a. State Agencies b. County Environmental Management District c. Environmental Groups 3) Federal and State Lands <ul style="list-style-type: none"> a. Federal Agency b. State Agency 4) General Public <ul style="list-style-type: none"> a. Community Leader 5) Human Right To Water <ul style="list-style-type: none"> a. See SSWS 6) Integrated Water Management <ul style="list-style-type: none"> a. Regional Water Management 7) Tribes <ul style="list-style-type: none"> a. Washoe Tribe 	<ul style="list-style-type: none"> 1) Interested Parties list 2) District Web Page 	X	

A complete list of the public notices, communications and public meetings conducted for the Alternative Plan is provided below.

Table 7-6. Public notices and opportunities for participation during development of the first five-year update of the Alternative Plan.

ITEM	DATE (S)
Public Hearing to receive public comment to adopt Resolution No. 3140-20 to draft an update to the 2014 Groundwater Management Plan	5/21/2020
Notice of Intent to Draft an Updated Groundwater Management Plan	6/25/2020
2020 Stakeholder Advisory Group Workshop 1	7/29/2020
District Regular Board Meeting Staff Report – Stakeholder Advisory Group Update	8/6/2020
2020 Stakeholder Advisory Group Workshop 2	12/17/2020
District Regular Board Meeting Staff Report – Alternative Plan Update	12/17/2020
Public Notice of Opportunities to Participate in the Development of the five-year update to the Alternative Plan	1/7/2021
2021 Stakeholder Advisory Group Workshop 1	3/25/2021
District Regular Board Meeting Staff Report – Alternative Plan Update	4/1/2021
2021 Stakeholder Advisory Group Workshop 2	6/30/2021
District Regular Board Meeting Staff Report – Alternative Plan Update	7/1/2021
90-Day Notice to Cities and Counties (WCS 10728.4)	10/1/2021
District Regular Board Meeting Staff Report – Alternative Plan Update	11/4/2021
Draft Alternative Plan to SAG	12/17/2021
2022 SAG Workshop 1 – Alternative Plan Review	1/12/2022

ITEM	DATE (S)
District Regular Board Meeting Staff Report – Alternative Plan Update	2/3/2022
Draft Alternative Plan – SAG Comment Period	12/17/2021 - 1/17/2022
Post Public Draft Alternative Plan Notice of Availability (30-Day Comment Period)	1/31/2022
Notice of Availability Draft Alternative Plan to Cities and Counties	2/9/2022
Public Draft Alternative Plan 30-Day Comment Period	2/9/2022 - 3/11/2022
EDWA Board Presentation: Alternative Plan Update	3/9/2022
EDWA Public Hearing: Consider to Adopt the first five-year update of the Alternative Plan	4/13/2022
STPUD Public Hearing: Consider to Adopt the first five-year update of the Alternative Plan	4/21/2022

SECTION 8: CHARACTERIZATION OF UNDESIRABLE RESULTS

Undesirable results occur when one or more significant and unreasonable effects are caused by groundwater conditions occurring throughout the basin: chronic lowering of groundwater levels, reduction of groundwater storage, seawater intrusion, degraded water quality, land subsidence, or depletion of interconnected surface water. To address and avoid any of these groundwater conditions, the District has defined sustainability goals, selected sustainability indicators, and developed minimum thresholds.

A sustainability goal is a goal that culminates in the absence of undesirable results within 20 years of GSP implementation. Minimum thresholds are defined as numeric values that, if exceeded, may cause an undesirable result. Two groundwater conditions—seawater intrusion and land subsidence related to groundwater extraction—were found not to be present and not likely to occur in the TVS Subbasin. Pursuant to section 354.28 of the GSP Regulations (23 Cal. Code Regs. § 354.28), a minimum threshold for sea water intrusion has not been developed. Even though not found within the TVS Subbasin, a sustainability indicator and minimum threshold has been developed for land subsidence out of an abundance of caution.

Characterization of undesirable results for the TVS Subbasin is considered within the framework of BMOs in the following sections. A table summarizing the current assessment of undesirable results for the TVS Subbasin is provided below in Table 8-1. Review of Table 8-1 shows that the quantitative criteria used as sustainability indicators do not exceed their corresponding minimum thresholds for each undesirable result assessed for the TVS Subbasin.

Table 8-1. Assessment of undesirable results for the TVS Subbasin (6-005.01)

SUSTAINABILITY INDICATOR			MINIMUM THRESHOLD (MT)		STATUS
Indicator (Wat. Code § 10721(x))	Description	Current Value	Description	Value	
Chronic lowering of groundwater levels (Section 8.1.11)	Total source capacity of CWS wells with pumping water levels above the top of well screen.	25.20 MGD	110% of the preceding ten-year average maximum day demand.	14.17 MGD	Not Exceeded
Reduction of Groundwater in Storage (Section 8.1.2)	Cumulative change in groundwater storage for the TVS Subbasin relative to WY 2005 levels	+5,300 AF	The cumulative change in groundwater storage corresponding to the groundwater level that would not allow total source capacity to be met	-32,050 AF	Not Exceeded
Seawater Intrusion (Section 8.2.1)	As the TVS Subbasin is in the Lake Tahoe Hydrologic Basin, outside the influence of seawater, a sustainability indicator for seawater intrusion does not exist.	Not Applicable	As a sustainability indicator for seawater intrusion does not exist, a minimum threshold for this indicator was not developed.	Not Applicable	Not Applicable
Degraded Water Quality (Section 8.2.2)	Total source capacity of CWS wells meeting federal and state drinking water standards.	25.20 MGD	110% of the preceding ten-year average maximum day demand.	14.17 MGD	Not Exceeded
Land Subsidence (Section 8.1.3)	Maximum negative change in groundwater level at any groundwater elevation monitoring well within the TVS Subbasin compared to May 2015 levels.	-0.85 ft	The sustained decline of groundwater level at any groundwater elevation monitoring well.	-100 ft	Not Exceeded

SUSTAINABILITY INDICATOR			MINIMUM THRESHOLD (MT)		STATUS
Indicator (Wat. Code § 10721(x))	Description	Current Value	Description	Value	
Interconnected Surface Waters (Section 8.3.1)	Current 10-year average stream discharge recorded at USGS Gage 103366092; 10336610 and 10336780 for Oct – Mar (winter)/ Apr – July (peak)/ and July – Sept (late season) flows.	USGS 103366092: 42.8/194.4/17.6 cfs; USGS 10336610: 61.3/226.8/19.3 cfs; USGS 10336780: 23.0/77.2/24.9 cfs;	10-year average (or 30-year median) stream discharge at selected USGS Gage Stations for each specified period.	USGS 103366092: 30/80/10 cfs; USGS 10336610: 40/240/10 cfs; USGS 10336780: 15/30/15 cfs;	Not Exceeded
Groundwater dependent ecosystems (GDEs) (Section 8.3.2)	Trends in water level in shallow aquifers underlying or adjacent to identified GDEs	[in progress] Existing monitoring wells to be identified and/or new monitoring wells to be installed No negative trend in modeled water level underlying any identified GDEs	No statistically significant ($p < 0.05$) negative trends using Mann-Kendall trend analysis over the last ten years	Kendall's tau less than zero and $p < 0.05$	Under Review

8.1 **BMO #1: Maintain a Sustainable Long-Term Groundwater Supply**

The purpose of BMO #1 is to implement measures to manage the groundwater levels for long-term sustainability and reliability of the water supply for all users within the TVS Subbasin. The measurable goal for tracking groundwater levels is to sustain groundwater levels within the range of historical data. If long-term groundwater levels show a consistent declining trend that falls below the historical range indicating a potential overdraft condition, then an assessment of the cause for the decline would be conducted. If excessive groundwater pumping is found to be the cause, then steps would need to be taken to either redistribute the pumping to other portions of the TVS Subbasin or reduce pumping at the implicated well(s). No action would be required if the condition described above is not observed.

8.1.1 **Chronic Lowering of Groundwater Levels**

- Sustainability Goal: To maintain a sustainable supply of groundwater by keeping groundwater water levels a safe distance above well screens.
- Undesirable Result: Regional water level declines such that water demands cannot be met.
- Sustainability Indicator: The total source capacity of community water supply wells
- Minimum Threshold: Having water levels above the screen intake at enough water supply wells such that the total source capacity meets or exceeds the Maximum Daily Demand (MDD).

8.1.1.1 **Sustainability Goal**

The first groundwater condition is the prevention of chronic lowering of groundwater levels in the TVS Subbasin. The goal is to implement measures to manage the groundwater levels for long-term sustainability and reliability of the water supply for all users within the TVS Subbasin. If long-term groundwater levels show a consistent declining trend that falls below the historical range, indicating a potential overdraft condition, then water supply wells are likely to fail and the needs of the beneficial users in the TVS Subbasin cannot be met.

The sustainability goal is to maintain a sustainable supply of groundwater by keeping groundwater water levels a safe distance above well screens.

8.1.1.2 **Undesirable Result – Chronic Lowering of Groundwater Levels**

The high reliance on groundwater necessitates active wells have sufficient source capacity to meet water demands within the TVS Subbasin. To remain active, groundwater levels must be sustained adequately above the pump intake and the top of the uppermost screen interval of water supply wells to reduce the risk of corrosion and pump cavitation as entrainment of air in the pumped water would lead to a loss of production.

8.1.1.3 **Sustainability Indicator**

Because of the high reliance on groundwater to meet the drinking water needs of the beneficial users in the TVS Subbasin and the need to have water levels above screen intakes to prevent corrosion and pump cavitation, the total source capacity of community water supply wells is selected as the indicator of chronic lowering of groundwater levels in the TVS Subbasin.

The sustainability indicator is determined by the source capacity of the active water supply wells operated by the District, TKWC and LBWC water systems. Source capacity values for current community water system wells operating in the TVS Subbasin are provided in Table 8-2.

Reasons for selection of this indicator for chronic lowering of groundwater levels are as follows:

1. The data required for this indicator are readily available from each of the community water systems.
2. The source capacities of the community water system wells are sensitive to nearby groundwater levels that threaten the beneficial users of groundwater within the basin. As such, it is believed to be representative of groundwater levels conditions within the TVS Subbasin.
3. The source capacities of community water system wells are significantly changed by adjacent groundwater levels and the subsequent actions needed to address this undesirable result. The rate of these changes can be quantified, and improvements can be detected over relatively short periods (less than five years).
4. The source capacities of the community water system wells are independent from the sustainable yield of the TVS Subbasin but are dependent on changes in groundwater storage. However, the level of dependence on these other indicators is not critical and does not diminish its utility as an independent indicator of groundwater levels.
5. Trends in source capacities of community water system wells can inform policy decisions in evaluating the impacts of lowering groundwater levels. It can also be used as a performance measure to evaluate the effectiveness of management decisions to mitigate lowering groundwater levels effecting beneficial users within the TVS Subbasin.

Table 8-2. Source capacity for active wells in the District, TKWC, and LBWC.

Well I.D.	WATER SYSTEM	SOURCE CAPACITY		STATUS
		(gpm)	(MGD)	
Al Tahoe Well #2	STPUD	2500	3.6000	Active
Bakersfield Well	STPUD	1450	2.0880	Active
Bayview Well	STPUD	3600	5.1840	Active
Elks Club Well #2	STPUD	300	0.4320	Active
Glenwood Well #5	STPUD	1037	1.4933	Active
Helen Ave. Well #2	STPUD	242	0.3485	Active
Paloma Well	STPUD	1825	2.6280	Active
Sunset Well	STPUD	600	0.8640	Active
SUT No. 3	STPUD	850	1.2240	Active - Treated
Valhalla Well	STPUD	600	0.8640	Active
Arrowhead Well #3	STPUD	775	1.1160	Active - Treated
STPUD SUB-TOTAL		13,779	19.8418	
TKWC No. 1	TKWC	1000	1.440	Active
TKWC No. 2	TKWC	400	0.576	Active-Treated (LP GAC; IX (Temporary))
TKWC No. 3	TKWC	800	1.152	Active-Treated (IX (Temporary))
TKWC SUB-TOTAL		2,200	3.168	
LBWC No. 1	LBWC	900	1.296	Active
LBWC No. 5	LBWC	620	0.8928	Active-Treated (LP GAC)
LBWC SUB-TOTAL		1,520	2.1888	
COMMUNITY WATER SYSTEMS TOTAL		17,499	25.1986	

8.1.1.4 **Minimum Threshold**

The minimum threshold is having water levels above the screen intake at enough water supply wells such that the total source capacity meets or exceeds the maximum daily demand (MDD). This threshold will be evaluated by monitoring static water levels in all active water supply wells semi-annually to ensure that levels are above the target levels in enough wells to meet the total MDD for the TVS Subbasin.

There is no indication that groundwater levels are on a long-term downward trend in the TVS Subbasin and therefore should not fall to a level that threatens the ability of groundwater sources (community water system wells) to meet water system demands. Demand requirements for community water systems are calculated in accordance with methods described under Section 64554 of the California Waterworks Standards (Chapter 16, Title 22, Cal. Code Regs.). Under these standards, community water system's water sources shall have the capacity to meet the system's MDD calculated using the water system's daily, monthly, or annual water use data, as available. These standards also include a water system's requirements for peak hourly demands, however peak hourly demand requirements are directed toward the adequacy of the water system's distribution system to provide sufficient flows. Therefore, only the MDD calculated for the community water systems reliant on groundwater are used to establish a minimum threshold for chronic lowering of water levels in the TVS Subbasin.

The data required for calculating the minimum threshold is the monthly water production data for the active wells in the District, TKWC and LBWC water systems. The LPA is primarily reliant on surface water to meet its water system demands. LPA has one active well (LPA Well #3). This well is used as a back-up source to augment or help temporarily replace surface water supplies. As the LPA is generally regarded as a surface water system and LPA Well # 3 is rarely used, production from the LPA Well #3 is not included in the minimum threshold calculations.

The MDD for the District, TKWC and LBWC are calculated using the month with the highest water usage (maximum month) for each water system over the preceding 10-years (WY 2011 – WY 2020). The maximum month is divided by the number of days within that month to derive an average daily usage for the maximum month. This value is then multiplied by a peaking factor which is the quotient of the average daily use for the maximum month and the average daily use for that year. For the minimum threshold calculation, peaking factors for each water system were derived for each year and then averaged over the 10-year period. Average peaking factors over the 10-year period for the District, TKWC and LBWC water systems were 1.68, 2.28 and 1.86, respectively.

As indicated in Figure 8-1, about 93 percent of the total water demand is satisfied by the community water system wells operated by the District, TKWC and LBWC water systems. To account for the beneficial users of groundwater not connected to these water systems, a 10 percent safety factor is added to the MDD derived for these water systems to determine the minimum threshold for the TVS Subbasin. Results of these calculations show that the current minimum threshold is a total source capacity of 14.166 MGD (Table 8-3).

Reasons for selection of this minimum threshold are as follows:

1. The data required for this minimum threshold is readily available from each of the community water systems.
2. The minimum threshold is calculated in a manner that is consistent with California Waterworks Standards and is representative of the volume of water needed to satisfy the water demands of the beneficial users of groundwater within the TVS Subbasin.
3. The minimum threshold is based on direct water use data which is sensitive to changes in population and water use in the TVS Subbasin. Therefore, it can be easily adjusted to reflect current beneficial user needs.
4. The volumes used for the sustainability indicator and accompanying minimum threshold are the same for ease of comparison.
5. The MDD is completely independent of the source capacity.
6. Groundwater levels do not fall in direct response to drought periods with the only exception being wells that are located a short distance from Lake Tahoe. Therefore, the minimum threshold defined above should be relatively insensitive to water year type.
7. The minimum threshold defined for groundwater levels would also be a useful indicator for groundwater storage, and to a lesser extent interconnected surface water. For example, if the minimum threshold for groundwater levels was violated this would also indicate that groundwater storage is declining at perhaps unsafe levels. If water level declines were such that the MDD could not be met, this would likely indicate increased loss from or reduced groundwater flow to surface water bodies but only for streams that are located near active production wells.

Minimum water level targets for individual wells are based on the depth to the top of screen plus an additional amount to account for drawdown while pumping at source capacity. Table 8-5 shows the calculations used to derive the target water levels for the sixteen major CWS wells used in the TVS Subbasin. It is assumed that water levels must remain above the top of the screen to ensure proper well-functioning. Depth to water is provided as the average water depth measured over the past ten water years (WY 2011 – WY 2020). Depth to water was not available during this period for four wells so they were estimated based on nearby wells because the semi-annual water level measurements represent static water levels (i.e., pumps are not running for 12 hours or more prior to taking the measurement). Specific capacity values represent either direct measurements at source capacity or calculations based on transmissivity estimates and source capacity rates (Cooper and Jacob, 1946). Transmissivity values were estimated using nearby wells for six of the production wells. The minimum water level target (Table 8-5) is calculated as the difference between depth from the top of screen and the additional drawdown expected at source capacity pumping rates.

The minimum threshold is defined as having enough wells meeting the water level target such that the MDD can be met for the entire TVS Subbasin. Currently the source capacity is 25.199 MGD and the MDD is 14.166 MGD, including a 10 percent safety factor, for a surplus of

11.032 MGD. Water levels would have to fall below the target level in enough wells for the source capacity to fall below the MDD.

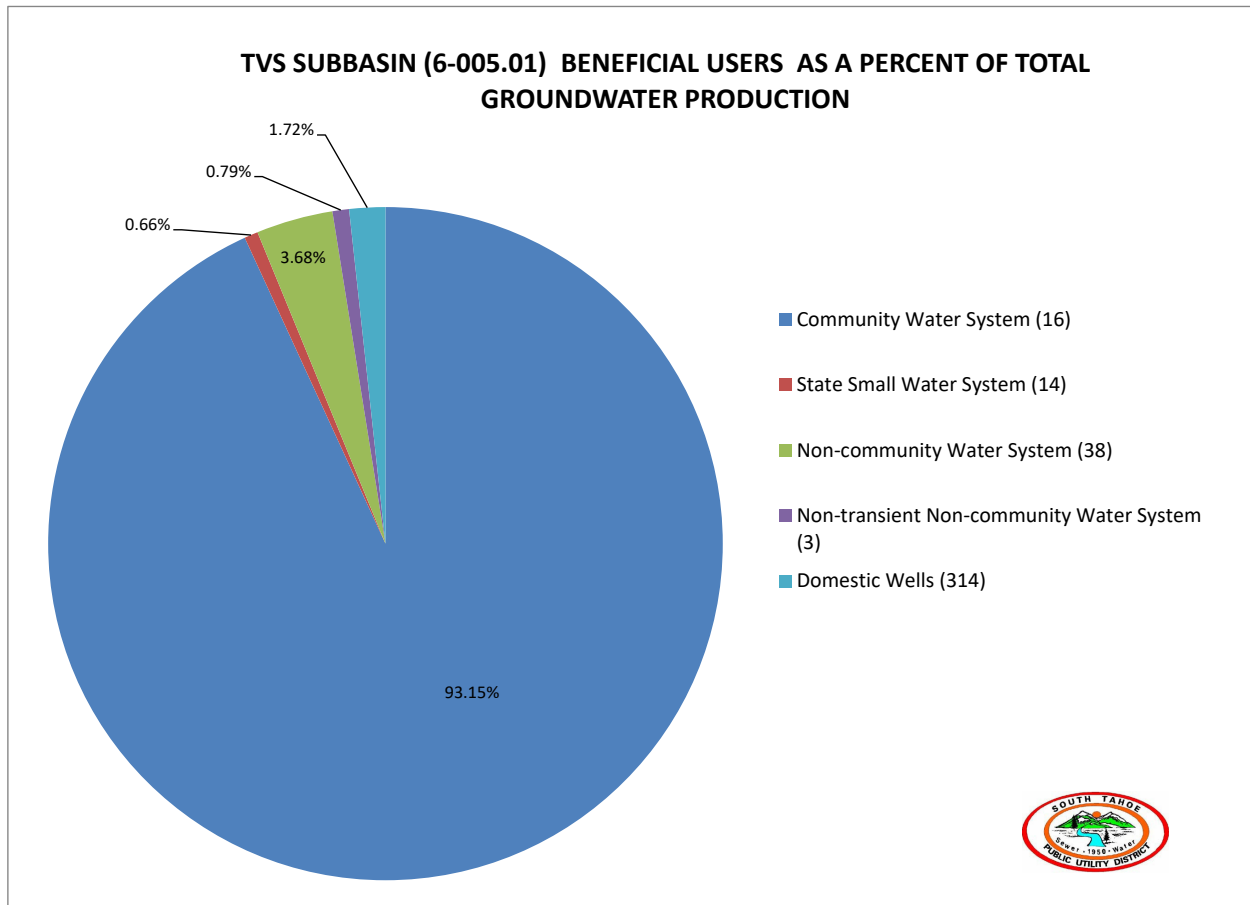


Figure 8-1. Beneficial users of groundwater within the TVS Basin (6-5.01) as a percent of the total groundwater production produced during WY 2020. Number of wells for each user is also shown.

Table 8-3. Maximum day demands (MDD) calculated for community water systems operating within the TVS Subbasin (WY 2011 – WY 2020) and minimum threshold value for lowering groundwater levels based on water demands. The minimum threshold for lowering groundwater levels is the total MDD, in MGD, for community water systems reliant on groundwater operating within the TVS Subbasin.

Community Water System	Ca Water System No.	Active Wells	Connections ₁	Population Served _{1,4}	Source Capacity (MGD) ₂	Maximum Day Demand (MGD) ₃	Surplus (+) Deficit (-) (MGD) ₄
South Tahoe Public Utility District	910002	11	14,235	33,124	19.8418	9.862	9.9798
Tahoe Keys Water Company	910015	3	1,566	1,420	3.168	2.383	0.785
Lukins Brother Water Company	910007	2	982	3,200	2.189	0.634	1.555
TVS SUBBASIN (6-5.001) TOTALS		16		37,744	25.199	12.879	12.320
Minimum Threshold (110% of MDD)						14.166	11.032

NOTES

- 1) Source: SWRCB Drinking Water Branch Drinking Water Watch (<https://sdwis.waterboards.ca.gov/PDWW/>).
- 2) Source capacity of active wells, in MGD (stand-by or offline sources not included).
- 3) 10 Year (WY 2011 - WY 2020) Water System Maximum Day Demand, in million gallons per day (MGD), as per CA Waterworks Standards (§ 64554).
- 4) Tahoe Keys Water Company population increases to over 7,300 during the summer.

Table 8-4. Minimum water level targets for active production wells within the TVS Subbasin. Red line indicates drawdown required to reach a condition where the MDD could not be met.

Well I.D.	Water System	Top of Screen (ft bgs)	Bottom of Screen (ft bgs)	Depth to Water ¹ (ft bgs)	Transmissivity (gpd/ft)	Expected Drawdown (ft)	Specific Capacity ² (gpm/ft)	Water Level Min Target ³ (ft bgs)	Freeboard ⁴ (ft)	Source Capacity (MGD)	Cum. Red. Source Cap. (MGD)
Glenwood Well #5	STPUD	150	180	32	25,544	111	9	39	7	1.4933	23.7053
Al Tahoe Well #2	STPUD	110	140	33	67,649	55	51	61	27	3.6000	20.1053
SUT No. 3	STPUD	70	90	19	18,805	23	37	47	28	1.2240	18.8813
LBWC No. 1	LBWC	132	182	20	12,342	82	11	50	30	1.2960	17.5853
Elks Club Well #2	STPUD	110	160	23	3,652	55	6	55	33	0.4320	17.1533
Valhalla Well	STPUD	110	170	27	14,713	37	16	73	45	0.8640	16.2893
Helen Ave. Well #2	STPUD	90	150	20	15,237	17	14	73	53	0.3485	15.9408
LBWC No. 5	LBWC	132	182	20	12,342	57	11	75	55	0.8928	15.0480
Bakersfield Well	STPUD	130	170	29	55,569	38	38	92	63	2.0880	12.9600
TKWC No. 2	TKWC	138	188	20	12,342	54	7	84	64	0.5760	12.3840
TKWC No. 1	TKWC	125	312	20	46,159	39	26	86	66	1.4400	10.9440
Paloma Well	STPUD	188	248	44	39,996	78	23	110	66	2.6280	8.3160
Bayview Well	STPUD	180	300	29	65,308	74	49	106	77	5.1840	3.1320
Arrowhead Well #3	STPUD	250	280	48	14,534	110	7	140	92	1.1160	2.0160
TKWC No. 3	TKWC	175	300	20	30,855	46	18	129	109	1.1520	0.8640
Sunset Well	STPUD	275	430	23	31,506	59	11	221	193	0.8640	0.0000

Notes

1. Based on average WY 2011 – WY 2020 measurements. Bold values are estimates based on nearby wells.
2. Bold values represent directly measured specific capacity at well capacity. Other values are calculated using Cooper and Jacob (1946) equation.
3. Water level minimum threshold based on top of screen - expected drawdown at full well capacity.
4. Freeboard is defined as Water level target - depth to water.

8.1.1.5 **Monitoring and Reporting**

The sustainability indicator (source capacity) will be reconsidered every five years as part of the periodic review for all of the community water system wells operating in the TVS Subbasin and provided in the Annual Report. Trends in source capacity will then be compared to the minimum threshold to determine whether any actions are required to prevent undesirable results from occurring within the TVS Subbasin. Based on the District's annual monitoring, the District will update and submit its Alternative Plan to the DWR every five years as required by SGMA.

There is no indication that groundwater levels are on a long-term downward trend in the TVS Subbasin and therefore are not expected to threaten the ability of groundwater sources (community water system wells) to meet water system demands. The current source capacity is 11.032 MGD more than the MDD which provides a relatively large buffer to allow water levels to fluctuate. In addition, under current conditions water supply wells have freeboard distances of 7 to 193 feet. Only one well (Glenwood Well #5) has a freeboard distance of less than 10 feet.

8.1.2 **Reduction of Groundwater Storage**

- Sustainability Goal: To maintain groundwater storage reserves to ensure a sustainable supply of groundwater.
- Undesirable Result: A groundwater overdraft condition causing water levels to trend downward making it more difficult to extract sufficient groundwater for water supply purposes.
- Sustainability Indicator: Cumulative changes in groundwater storage.
- Minimum Threshold: Cumulative groundwater storage change of negative 32,050 AF relative to WY 2005, which indicates undesirable results.

8.1.2.1 **Sustainability Goal**

The sustainability goal for groundwater storage is to maintain groundwater storage reserves to ensure a sustainable supply of groundwater.

8.1.2.2 **Undesirable Result – Reduction of Groundwater Storage**

Long-term reductions in groundwater storage indicate an overdraft condition. When a groundwater basin is in an overdraft condition, water levels will trend downward making it more difficult to extract for water supply purposes.

Given that the TVS Subbasin is in a surplus state, undesirable results related to reductions in groundwater storage would occur if there were significant reductions in precipitation and drastic increases in groundwater pumping. Regardless of the cause of storage reductions, the threshold can be derived based on the associated groundwater level declines that would result in a reduction of source capacity. From Table 8-4, the minimum drawdown relative to WY 2005 water levels required to cause a well to go offline is seven feet. Assuming a seven-foot reduction

in water levels for the entire TVS Subbasin, a corresponding reduction in storage can be calculated as the area of all MODFLOW model grid cells falling within the TVS Subbasin, multiplied by seven feet and the specific yield for each grid cell (0.3 in most cells). The result is a reduction in storage of 32,050 AF, which is defined as the minimum threshold. Because the loss of only one production well will not result in an inability to meet the MDD, this threshold is quite conservative.

Long-term reductions in groundwater storage are not occurring within the TVS Subbasin as evidenced by stable groundwater levels and average annual groundwater storage changes as calculated by the STGM that are near zero. Minor groundwater storage changes do occur in response to climate variability and changes in groundwater extraction rates. Therefore, it is important to understand the magnitude of groundwater storage changes that occur due to climate variability versus more serious long-term declines.

8.1.2.3 **Sustainability Indicator**

The sustainability indicator will be cumulative changes in groundwater storage (either positive or negative) as calculated using the STGM. The storage change calculations will be performed for the TVS Subbasin only, as opposed to the larger South Tahoe area that makes up the model domain. Since groundwater storage can be calculated directly within the modeling framework, there is no need to specify a surrogate indicator.

8.1.2.4 **Minimum Threshold**

The minimum threshold for groundwater storage changes is a cumulative groundwater storage change of negative 32,050 AF relative to WY 2005, which indicates falling water levels. This value is based on expected groundwater level declines during a long-term drought that would not allow total source capacity to be met.

As average inflows to the TVS Subbasin are more than three times greater than the amount of groundwater extracted, the TVS Subbasin is highly resilient to interannual climate variations. As shown in Figure 5-22 and Figure 5-23, groundwater storage reductions occur during drought periods (Hagan's Meadow experiences less than 31 inches of precipitation) and is replenished during normal and above normal precipitation years.

Cumulative change in storage for all climate scenarios is shown in Figure 5-25. Baseline climate scenario results (average present recharge conditions) indicate that a cumulative storage change of negative 52,000 AF will not occur over the planning horizon of 50 years. Assuming worst case scenario Q2 (hot and dry) climate conditions, the storage threshold would be reached in 17 years. As the Q2 scenario simulates predicted climate change for 2075–2099 beginning immediately, the likelihood of a 17-year drought of this magnitude occurring over the 50-year planning horizon is quite low. However, if this were to occur, water level declines could lead to well failures and other undesirable results.

8.1.2.5 **Monitoring and Reporting**

Changes in groundwater storage will be accounted on an annual basis using the STGM. Cumulative changes in groundwater storage will be compared to the minimum threshold to determine whether any actions are required to prevent undesirable results from occurring within the TVS Basin. Based on the District's annual monitoring, the District will update and resubmit its Alternative Plan to the DWR every five years as required by SGMA.

The historical state of groundwater storage for the TVS Subbasin is shown in Figure 5-22. Figure 5-22 shows that groundwater storage varies according to pumping and climate but is not near the specified threshold of negative 32,050 AF. The changes in groundwater storage have not reached the level of a significant and undesirable result, as indicated by its current level above the minimum threshold.

8.1.3 **Land Subsidence**

Section 5.6.2 provides a detailed assessment of land subsidence within the TVS Subbasin. The analysis presented in Section 5.6.2 demonstrates that the target water levels previously defined in Section 8.1.1 (Chronic Lowering of Groundwater Levels), are more restrictive than the thresholds defined for land subsidence.

Assuming undesirable results would occur if subsidence would be more than one foot, the minimum threshold is defined as a negative change in static water levels of more than 100 feet compared to groundwater elevations measured in Basin Monitoring Network observation wells in May 2015. To evaluate this minimum threshold, groundwater elevations between May 2015 and May 2020 were compared and differences calculated for each observation well. Review of these results show that over the preceding five-year period, most observation wells showed a positive change in static water levels. Only four wells showed a negative change, each on the order of less than one foot: EX-1 (-0.65 ft), Industrial Well No. 2 (-0.85 ft), South Upper Truckee Well No. 3 (-0.75 ft), and USGS TCF-3 (-0.06 ft).

Table 8-5 shows the water level thresholds that would result to ensure subsidence magnitudes of less than one foot. In all but two wells (Sunset and Tahoe Keys #3), the target water levels defined in Section 8.1.1 (Chronic Lowering of Groundwater Levels) are more restrictive than the thresholds defined for land subsidence due to groundwater level declines.

Table 8-5. Water levels targets for land subsidence and chronic lowering of water levels.

Well I.D.	Water System	Depth to Water ¹ (ft bgs)	Subsidence Water Level Threshold (ft bgs)	Water Level Min Target ² (ft bgs)
Al Tahoe Well #2	District	33	133	61
Bakersfield Well	District	29	129	92
Bayview Well	District	29	129	106
Elks Club Well #2	District	23	123	55
Glenwood Well #5	District	32	132	39
Helen Ave. Well #2	District	18	118	73
Paloma Well	District	44	144	110
Sunset Well	District	23	123	221
SUT No. 3	District	19	119	47
Valhalla Well	District	27	127	73
Arrowhead Well #3	District	48	148	140
TKWC No. 1	TKWC	20	120	86
TKWC No. 3	TKWC	20	120	129
TKWC No. 2	TKWC	20	120	84
LBWC No. 1	LBWC	20	120	50
LBWC No. 5	LBWC	20	120	75

Notes

1. Based on average WY 2011 – WY 2020 measurements. Bold values are estimates based on nearby wells.
2. Water level minimum threshold based on top of screen - expected drawdown at full well capacity.

8.2

BMO #2: Maintain and Protect Groundwater Quality

Groundwater in the TVS Subbasin is typically of excellent quality; however, there is a legacy of groundwater contamination from regulated industrial and commercial chemicals (Section 6.2.4), which continues to impair water supplies (Section 6.3). The nature of the aquifer makes it highly vulnerable to groundwater contamination as evidenced by these impacts.

The purpose of BMO #2 is to implement measures to maintain and protect groundwater quality to sustain the beneficial use of groundwater within the TVS Subbasin. These measures would address contamination from manmade contaminants and not natural constituents intrinsic to the aquifer. This would include setting measurable goals and continuing proactive measures to protect groundwater quality.

8.2.1 **Seawater Intrusion**

The TVS Subbasin sits at close to 6,250 feet above sea level in the Sierra Nevada Mountains. The closest source of seawater is close to 200 miles away. Therefore, seawater intrusion is not an issue for the TVS Subbasin and as such a minimum threshold was not developed for this groundwater condition.

8.2.2 **Water Quality**

- **Sustainability Goal:** To ensure that groundwater quality is maintained to support continued extraction for water supply purposes.
- **Undesirable Result:** Degraded water quality threatens the ability to produce groundwater of sufficient quality and quantity to meet the demands of the community.
- **Sustainability Indicator:** The total source capacity of community water supply wells.
- **Minimum Threshold:** Degraded water quality concerns within the TVS Subbasin should not rise to a level that threatens the ability of groundwater sources to meet MDD.

8.2.2.1 **Sustainability Goal**

The sustainability goal for this groundwater condition is to maintain a sustainable long-term groundwater quality. The goal is to implement measures to manage the groundwater quality for long-term sustainability and reliability of the water supply for all users within the TVS Subbasin. If groundwater quality degrades over long periods, this is an indication of contamination. Though this is not the present case in the TVS Subbasin, the goal is to ensure that groundwater quality is maintained to support continued extraction for drinking water use.

Current water use estimates indicate that more than 95 percent of drinking water used in the TVS Subbasin is from groundwater sources (District, 2016). Of this amount, more than 90 percent is produced from community water system wells, about 3 percent is produced from non-

community water system wells, about 2 percent is produced from domestic wells, and about 1 percent is produced from State Small Water System and non-transient non-community water system wells (Figure 8-1).

8.2.2.2 **Undesirable Result – Degraded Water Quality**

The high reliance on groundwater necessitates that active wells have sufficient source capacity to meet water demands within the TVS Subbasin. To remain active, groundwater sources must be able to produce water of acceptable water quality, in accordance with federal and state maximum contaminant levels (MCLs). Degraded water quality in the TVS Subbasin, primarily from pollutants, threatens the ability to produce groundwater of sufficient water quality and has resulted in impairment of some groundwater sources within the TVS Subbasin.

8.2.2.3 **Sustainability Indicator**

Because of the high reliance on groundwater to meet the drinking water needs of the beneficial users in the TVS Subbasin, the vulnerability of the groundwater basin to contamination, and the impact of degraded water quality on a water system's capacity to produce groundwater, the sustainability indicator for degraded water quality concerns is the total source capacity of community water supply wells that meet all state and federal water quality standards in the TVS Subbasin.

The data requirements for this sustainability indicator include the source capacity of the active water supply wells operated by the District, TKWC, and LBWC water systems. Source capacity values for current community water system wells operating in the TVS Subbasin are provided in Table 8-1. Current source capacity for all three water systems is 25.199 MGD.

Reasons for selection of this sustainability indicator for degraded water quality are as follows:

1. The data required for this sustainability indicator is readily available from each of the community water systems.
2. The source capacities of the community water system wells are sensitive to degraded water quality problems that threaten the beneficial users of groundwater within the TVS Subbasin. As such, it is believed to be representative of degraded water quality conditions within the groundwater basin.
3. The source capacities of community water system wells are significantly changed by degraded water quality and the subsequent actions needed to address this undesirable result. The rate of these changes can be quantified, and improvements can be detected over relatively short periods (less than 5 years).
4. The source capacities of the community water system wells are relatively independent from the sustainable yield of the basin but are somewhat dependent on groundwater levels and changes in groundwater storage. However, the level of dependence on other indicators is not significant within the TVS Subbasin and does not diminish its utility as an independent indicator of degraded water quality.

5. Trends in source capacities of community water system wells can inform policy decisions in evaluating the impacts of degraded water quality on groundwater sources operating within the basin. Source capacity can also be used as a performance measure to evaluate the effectiveness of management decisions to mitigate degraded water quality concerns affecting beneficial users within the basin.

8.2.2.4 **Minimum Threshold**

In accordance with the sustainability goal advanced at the beginning of this section, degraded water quality concerns within the TVS Subbasin should not rise to a level that threatens the ability of groundwater sources (i.e., community water system wells) to meet water system demands. Demand requirements for community water systems are calculated in accordance with methods described under Section 64554 of the California Waterworks Standards. Under these standards, a community water system's water sources shall have the capacity to meet the system's MDD calculated using water system's daily, monthly, or annual water use data, as available. These standards also include a water system's peak hourly demand requirements; however, these requirements are directed toward the adequacy of the water system's distribution system to provide sufficient flows. Therefore, only the MDD calculated for the community water systems reliant on groundwater will be used to establish a minimum threshold for degraded water quality in the TVS Subbasin.

The data required for calculating the minimum threshold is the monthly water production data for the active wells in the District, TKWC, and LBWC water systems. The LPA is primarily reliant on surface water to meet its water system demands. LPA has one active well (LPA Well #3). This well is used as a back-up source to augment or help temporarily replace surface water supplies. As the LPA is generally regarded as a surface water system and LPA Well #3 is rarely used, production from the LPA Well #3 is not included in the minimum threshold calculations.

The MDD for the District, TKWC, and LBWC are calculated using the month with the highest water usage (maximum month) for each water system over the preceding 10-years (WY 2011 – WY 2020). The maximum month is divided by the number of days within that month to derive an average daily usage for the maximum month. This value is then multiplied by a peaking factor which is the quotient of the average daily use for the maximum month and the average daily use for that year. For the minimum threshold calculation, peaking factors for each water system were derived for each year and then averaged over the 10-year period. Average peaking factors over the 10-year period for the District, TKWC, and LBWC water systems were 1.68, 2.28, and 1.86, respectively.

As indicated in Figure 8-1, approximately 93 percent of the total water demand is satisfied by the community water system wells operated by the District, TKWC, and LBWC water systems. To account for the beneficial users of groundwater not connected to these water systems, a 10 percent safety factor is added to the MDD derived for these water systems to determine the minimum threshold for the TVS Subbasin. Results of these calculations show that the current minimum threshold is 14.166 MGD (Table 8-3).

Reasons for selection of this minimum threshold for degraded water quality are as follows:

1. The data required for this minimum threshold is readily available from each of the community water systems.
2. The minimum threshold is calculated in a manner that is consistent with California Waterworks Standards and is representative of the volume of water needed to satisfy the water demands of the beneficial users of groundwater within the TVS Subbasin.
3. The minimum threshold is based on direct water use data which is sensitive to changes in population and water use in the TVS Subbasin. Therefore, it can be easily adjusted to reflect current beneficial user needs.
4. The volumes used for the degraded water quality sustainability indicator and accompanying minimum threshold are the same for ease of comparison.
5. The water demand minimum threshold is completely independent of the source capacity sustainability indicator.

8.2.2.5 **Monitoring and Reporting**

The sustainability indicator (source capacity) will be determined every five years as part of the periodic review for all community water system wells operating in the TVS Subbasin and provided in the Annual Report. Trends in source capacity will then be compared to the minimum threshold for degraded water quality to determine whether any actions are required to undesirable results – degraded source water quality – from occurring within the TVS Subbasin. Based on the District’s annual monitoring, the District will update and submit its Alternative Plan to the DWR every five years as required by SGMA.

The current state of the TVS Subbasin is shown below in Figure 8-2. There is a sufficient supply of high-quality water (source capacity) adequate to meet the drinking water needs of the beneficial users of groundwater in the TVS Subbasin. The trend in source capacity has declined since 2015, due to well impairments from degraded water quality. However, these impairments have not reached the level of an undesirable result, as indicated by its current level above the minimum threshold for degraded water quality.

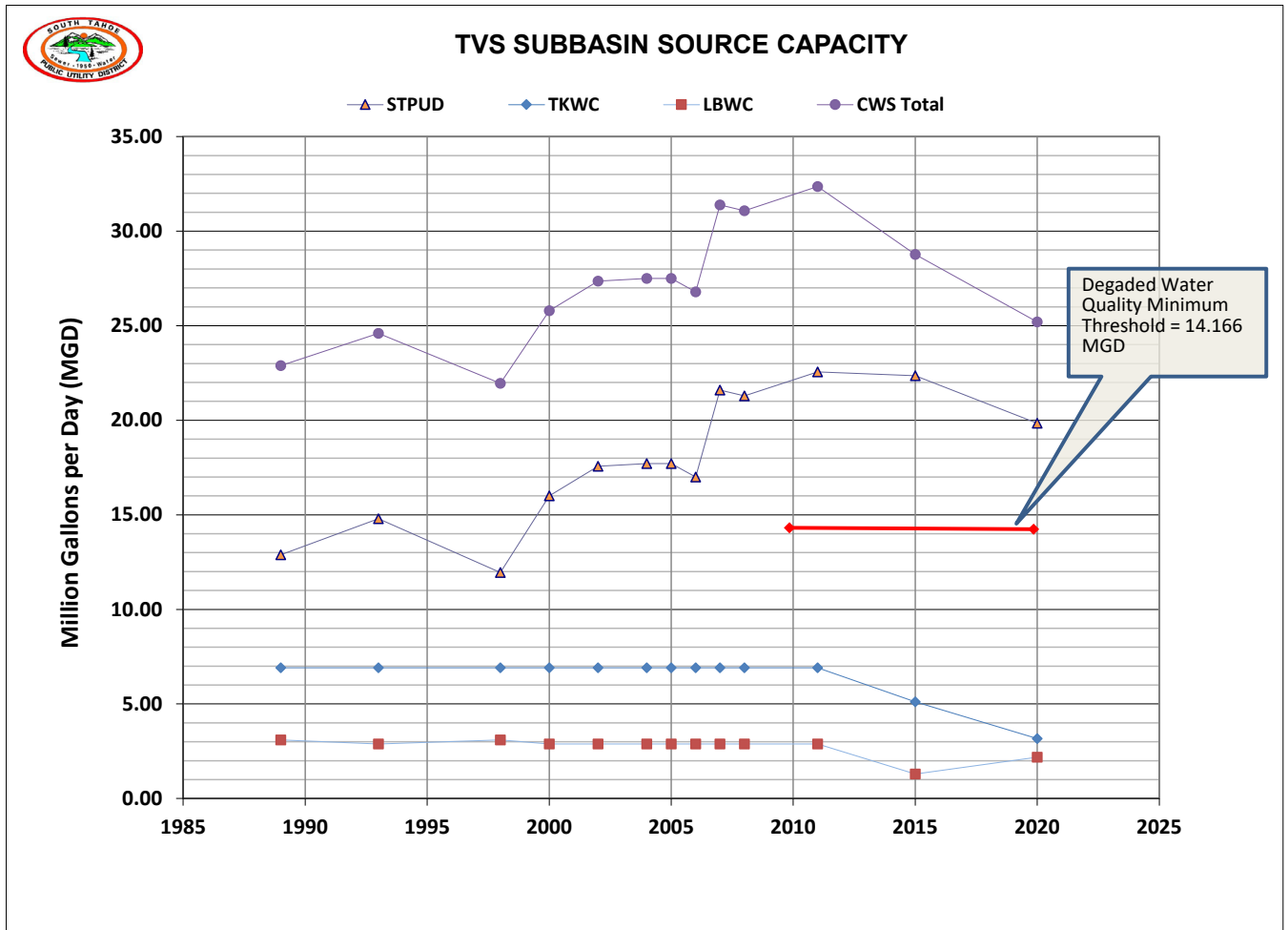


Figure 8-2. Source capacity trends for community water system wells in the TVS Subbasin and the minimum threshold (in MGD) for degraded water quality.

8.3 BMO #5: Assess the Interaction of Water Supply Activities on Environmental Conditions

The TVS Subbasin is in a unique environmental setting. Water supply operations using groundwater may affect environmental conditions or be affected by changes in the environment. Groundwater interactions with Lake Tahoe and the rivers and streams within the TVS Subbasin contribute to both groundwater discharge and recharge, depending on the location and the time of year (Rowe and Allander 2000). Understanding groundwater-surface water interactions is necessary to sound groundwater management of the TVS Subbasin.

Groundwater in the TVS Subbasin is inextricably linked to environmental conditions, and management of groundwater resources will affect both GDEs and interconnected surface flows. The purpose of BMO #5 is to implement measures to maintain and protect the ecological communities – both plants and animals – that are dependent on in-stream surface flows and shallow groundwater.

8.3.1 **Interconnected Surface Waters**

- Sustainability Goal: To maintain spatial and temporal continuity of surface flows to support existing beneficial uses.
- Undesirable Result: Reduction of flow sufficient to negatively impact wildlife.
- Sustainability Indicator: USGS gaged discharge in streams within the TVS Subbasin.
- Minimum Threshold: Both the 10-year average annual discharge and 10-year average late season (Aug-Sept-Oct) discharge are maintained within the range of historical variability (defined as ± 25 percent of historical mean discharge), and statistically significant negative trends in discharge are not induced by groundwater pumping.

8.3.1.1 **Sustainability Goal**

Fish and wildlife species frequently rely on groundwater contributions to streams to provide the water that they need to thrive (CDFW 2019). Published guidance on in-stream flow requirements in Trout Creek and the Upper Truckee River is available from California DFW (California Department of Fish and Game 2008). This guidance is based on habitat modeling of salmonid species in the Tahoe Basin (Department of Fish and Game 1987) and considers spawning and rearing flow requirements for rainbow trout, brown trout, brook trout, and kokanee salmon. Lahontan cutthroat trout are also present in the TVS subbasin (Rohde et al. 2019). All of these salmonid species require cooler water temperatures (<79 °F; 26 °C) year-round (Rohde et al. 2019). Groundwater contributions to streams, i.e., baseflow, help to maintain suitable temperatures for these species. The sustainability goal for interconnected surface waters is therefore to maintain sufficient baseflow in streams to provide spatially and temporally continuous flows at the water temperatures required to support the needs of fish and wildlife species in the basin.

8.3.1.2 **Undesirable Result – Interaction of Water Supply Activities on Environmental Conditions**

Numerous fish and wildlife species depend on in-stream flows in interconnected surface waters. During the spring melt, these flows are fed by surface runoff and drainage from the soil zone. In the late summer and fall, flow in these streams is provided by baseflow, i.e., groundwater moving into the stream from a connected shallow aquifer. The baseflow contributions also regulate higher temperatures in the summer and fall. When these flows are interrupted, in either time or space, the species that depend on the flows are impacted. This BMO seeks to avoid negative impacts to the five salmonid species listed above, and by extension to recreational uses of surface waters (which are largely focused on angling).

8.3.1.3 **Sustainability Indicator**

The sustainability indicator will be the measured flow at three active USGS gages within the TVS Subbasin: the Upper Truckee River at Highway 50 above Meyers, CA (USGS Gage No.

103366092); the Upper Truckee River at South Lake Tahoe, CA (USGS Gage No. 10336610); and Trout Creek near Tahoe Valley, CA (USGS Gage No. 10336780). Streams are naturally integrative features, so these sustainability indicators will be influenced by processes outside of the bounds of the TVS Subbasin. Similarly, the discharge in a stream is affected by numerous environmental processes that are outside the scope of groundwater management.

Whereas salmonid species require cool water temperatures, water temperatures in streams are regulated by baseflow. Two of the above-listed USGS gages (Trout Creek and the Upper Truckee River at South Lake Tahoe) monitor water temperatures as well as discharge, the temperature records are shorter in duration (less than ten years) than the discharge records. During WY 2015 – WY 2021, water temperatures in Trout Creek have not exceeded the 79 °F (26 °C) habitat limit for LCT. Water temperatures in the Upper Truckee River at South Lake Tahoe have exceeded that limit during just seven days in July 2021, and only when discharges were particularly low. For this reason, the discharge threshold is assumed to simultaneously serve as a threshold for water temperature.

Reasons for selection of this indicator for interconnected surface waters are as follows:

1. The data required for this indicator are readily available from existing USGS stream gages.
2. The Upper Truckee River and Trout Creek drain the two largest watersheds in the South Lake Tahoe area accounting for about seventy-five percent of average annual run-off (see Table 2-1)
3. Discharges and temperatures in the Upper Truckee River and Trout Creek and associated impacts on salmonid species have been specifically evaluated by the California Department of Fish and Game (now California Department of Fish and Wildlife; CDFG 2008). As such, the measured discharges are likely to be representative of the effect of interconnected surface waters on wildlife within the TVS Subbasin.
4. Discharges in the Upper Truckee River and Trout Creek are changed significantly by adjacent shallow groundwater levels and the subsequent actions needed to address this undesirable result. The rate of these changes can be quantified, and improvements can be detected over relatively short periods (five to ten years).
5. Discharges in the Upper Truckee River and Trout Creek are independent from the sustainable yield of the TVS Subbasin, but are somewhat dependent on changes in groundwater storage. However, the level of dependence on these other indicators is not critical and does not diminish its utility as an independent indicator of interconnected surface waters.
6. Trends in discharges in the Upper Truckee River and Trout Creek can inform policy decisions in evaluating the impacts of baseflow depletion in interconnected surface waters. It can also be used as a performance measure to evaluate the effectiveness of management decisions to mitigate baseflow depletion affecting beneficial users within the TVS Subbasin.

8.3.1.4 Minimum Threshold

Stream discharge in the TVS subbasin exhibits both high seasonality and high interannual variability. To account for the seasonality of measured discharge, multiple thresholds have been developed for each stream gage, representing in-stream flows occurring during different times of the year. To account for the interannual variability of measured discharge, the minimum thresholds are based on a ten-year average (or thirty-year median) of discharge measurements rather than a single year.

For each monitored USGS gage, DFW guidance is provided for three time periods: 1 October – 31 March (winter), 1 April – 15 July (peak), and 16 July – 30 September (late season). Daily average flows over the last 30 years are shown, along with the DFW recommended seasonal thresholds in 8-3. As the figure indicates, late-season (16 July – 30 September) flows at both Upper Truckee River gages often fall below the DFW-recommended discharge.

For the winter and peak seasons, as well as late season flows in Trout Creek, the minimum thresholds are set at the flows specified in the DFW guidance. For late-season flows in the Upper Truckee River, where DFW guidance is historically unlikely to be achieved under normal conditions, the minimum threshold is set as the 30-year median late-season discharge at each gage, rounded up in each case to 10 cfs. Minimum thresholds for each season and gage are shown below in 6.

During each time, the average annual discharge over the previous ten years must be greater than the minimum threshold. The 10-year average flows for each season shown in Table 8-6 cover WY 2011 – WY 2020 and are currently well above the seasonal thresholds. Currently, there are no statistically significant trends in annual or late season discharge at any of the three gages. A Mann-Kendall trend test (Mann 1945; Kendall 1976) was performed for each season of each gage on both a 30-year and a 10-year timescale.

Table 8-6. Threshold discharges and current (WY 2011 – WY 2020) 10-year average flows in cfs for each season and gage.

Gage No.	Location	1 October – 31 March		1 April- 15 July		16 July – 30 September	
		Threshold	10-yr Mean	Threshold	10-yr Mean	Threshold	10-yr Mean
103366092	Upper Truckee River above Meyers	30	42.8	80	194.4	10	17.6
10336610	Upper Truckee River at South Lake Tahoe	40	61.3	140	226.8	10	19.3
10336780	Trout Creek	15	23.0	30	77.2	15	24.9

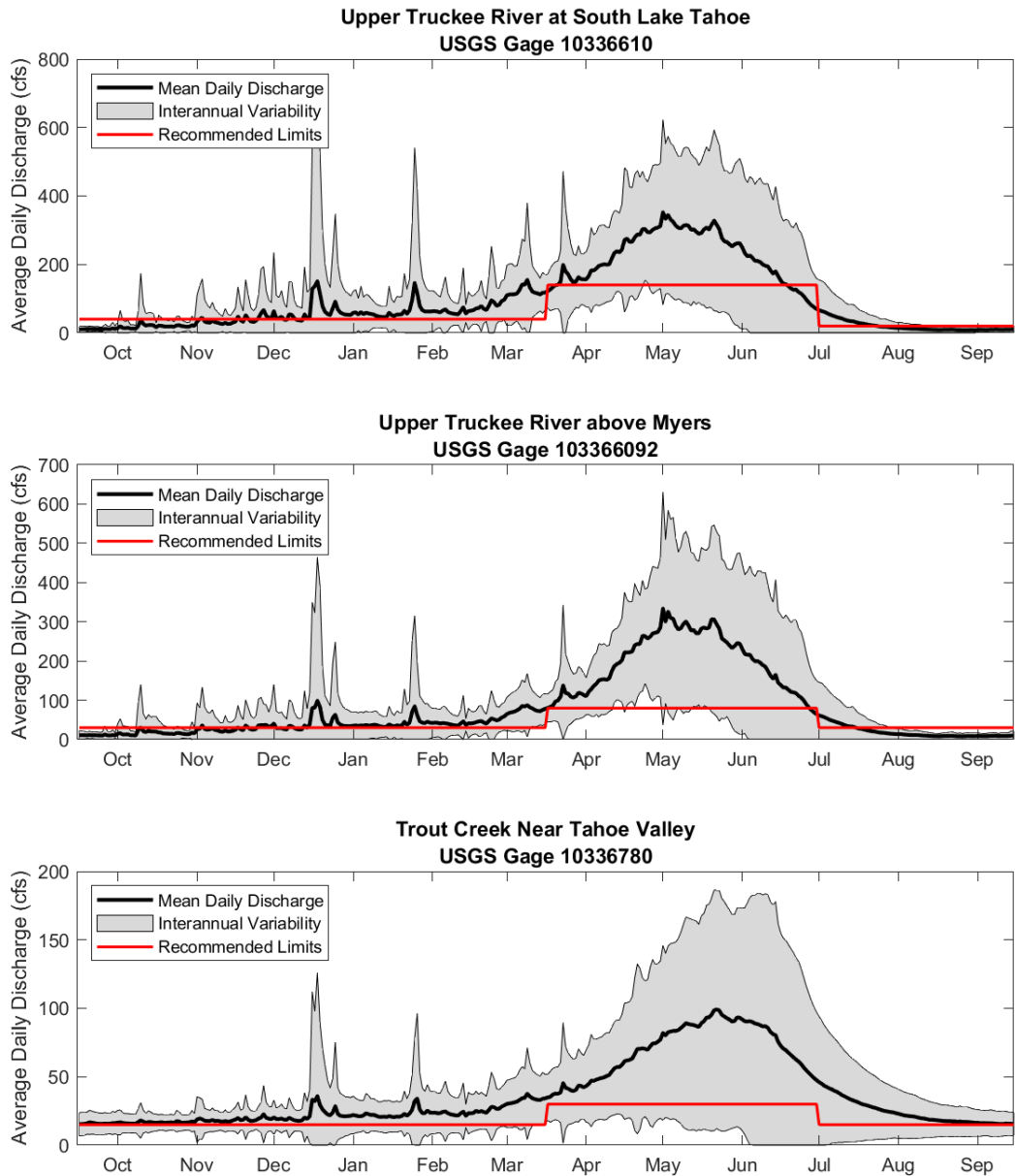


Figure 8-3. Average daily flows, WY 1991 – WY 2020 at each USGS stream gage along with the DFW-recommended daily threshold values. The indicated interannual variability (the shaded gray area) represents ± 1 standard deviation from the mean flow.

Reasons for selection of this minimum threshold are as follows:

1. The data required for this minimum threshold is readily available from long-term records at existing USGS stream gages.

2. The minimum threshold is calculated in a manner that is consistent with maintaining flows within the range of historical variability and is representative of baseflow contributions to interconnected surface waters in the TVS Subbasin.

3. The minimum threshold is based on directly measured discharge data which is sensitive to changes in baseflow in the TVS Subbasin. Therefore, it can be easily adjusted to reflect current needs of beneficial users.

4. The discharges used for the sustainability indicator and accompanying minimum threshold are the same for ease of comparison.

5. The range of historical variability in measured discharge is completely independent of future baseflow contributions.

6. Groundwater levels in the shallow aquifers respond to drought periods on an annual timescale. However, the minimum threshold defined above relies on a multi-year record of measured discharge and thus should be relatively insensitive to water year type, except in cases of prolonged drought.

7. The minimum threshold defined for interconnected surface waters would also be a useful indicator for GDEs, and to a lesser extent groundwater levels. For example, if the minimum threshold for interconnected surface water was violated this would also indicate that groundwater in shallow aquifers is less accessible to the vegetation communities comprising GDEs. If measured discharge declines were such that the threshold could not be met, this would likely indicate a reduction in groundwater storage in the shallow aquifer.

8.3.1.5 **Monitoring and Reporting**

The ten-year average gaged discharge will be evaluated every five years as part of the periodic review of groundwater conditions. For each gage and each season, the 10-year mean discharge will be calculated and compared to the thresholds noted in Table 8-6 above. If the 10-year average discharge at any gage falls below the minimum threshold, the threshold has been exceeded.

To provide an early warning that the threshold may be exceeded in the future, Mann-Kendall trend tests will be performed on the most recent five years of discharge at each gage. The shorter timescale allows for the detection of a trend well before the threshold might be exceeded. If any gage shows a statistically significant, negative trend, additional investigation will be undertaken to determine how much groundwater pumping may be affecting that gaged discharge. This investigation will be based on a comparison between the current STGM (updated annually) and a no-pumping groundwater model scenario that matches recent climate conditions. For each model scenario, the baseflow contribution to the stream in question will be extracted and compared to the baseflow contribution from the baseline model. If the no-pumping scenario indicates a decline in baseflow contribution similar to the current STGM, the exceedance of the threshold is likely driven by climate and may not be effectively mitigated through groundwater management actions. If the baseflow contribution in the no-pumping model is significantly greater than that of the current model, then groundwater management is playing a role in reduced

discharge and it will be necessary to explore management options to mitigate that effect and to return discharges above the minimum threshold.

8.3.1.5.1 **Provisional Groundwater Management Area**

As noted in Section 2, a GSA may designate management areas within a basin for which the GSP or Alternative identifies different minimum thresholds, measurable objectives, monitoring, or projects and management actions based on differences in water use sector, water source type, geology, aquifer characteristics, or other factors (23 Cal. Code Regs., § 351 (r)). A provisional management area, shown in Figure 2-2, was defined to support future investigations into interconnected surface waters.

In 2017, additional analysis of the TVS Subbasin hydrologic system was performed using hydrologic modeling tools developed by DRI to define a potential, provisional management area where additional pumping may result in significant depletions of interconnected surface waters. As part of this effort, DRI created capture maps using two versions of the steady-state STGM, representing baseline and Q2 (hot and dry) climate conditions. Groundwater capture is defined as the change in inflow or outflow from a groundwater system caused by groundwater pumping (Barlow and Leake, 2012). Capture maps are generated by running a model with a hypothetical pumping well in one model grid cell and comparing the resultant flow budget to a model that did not simulate the hypothetical pumping well. This is done iteratively for every grid cell in the model. The difference in flow budgets is equivalent to the pumping rate at the hypothetical well, and the capture fraction at each grid cell can then be defined as the fraction of that pumping rate removed from each flow budget component. For the steady-state STGM, pumping at a well results in a reduction of outflow to Lake Tahoe and local streams. Areas where the capture fraction for streams exceeded 0.5 (indicating that more than half of pumped water was captured from streams rather than from Lake Tahoe) delineate the provisional management area. Results from the baseline model were used to determine the boundaries of the provisional management area because baseline figures indicated a slightly larger and more conservative area than the Q2 (hot and dry) model and streamflow in the Q2 model was reduced due to the simulated effects of climate change.

One limitation of this method is that steady-state models do not simulate changes in storage, therefore a simulated pumping well cannot capture from storage. Instead, results show long-term equilibrium and capture fractions that occur after a pumping well creates a new static head field. It could take many years for this condition to occur, especially for a well situated far from a stream. Therefore, the timing of streamflow depletions for a hypothetical well in each grid cell cannot be determined by this method.

To ensure that local streams have sufficient groundwater to sustain Groundwater Dependent Ecosystems (GDEs), the depletion analysis was also used to recommend a maximum total groundwater extraction rate for the area south of the Lake Tahoe Airport. To apply this groundwater extraction rate as a minimum threshold within the TVS Subbasin, a provisional management area was established in the Alternative Plan to allow for the spatially varying application of pumping thresholds. Over the next five years, the District will evaluate the utility of formally establishing a management area with separate minimum thresholds to protect interconnected surface water in the area south of the Lake Tahoe Airport. For the purposes of

this first five-year update to this Alternative Plan, the sustainability indicators, representative monitoring sites and minimum thresholds for this provisional management area are the same as the entire TVS Subbasin, as described in Section 8.3.2 below.

8.3.2 **Groundwater Dependent Ecosystems**

- Sustainability Goal: To maintain a shallow water table that supports riparian vegetation in areas where riparian vegetation currently exists.
- Undesirable Result: Replacement of riparian vegetation by upland vegetation and loss of associated ecosystem services.
- Sustainability Indicator: Water table elevation.
- Minimum Threshold: Having average groundwater elevations within the interquartile range of historical variability.

8.3.2.1 **Sustainability Goal**

The sustainability goal for GDEs is to maintain GDEs (i.e., riparian communities) where they currently exist. This goal allows for some changes to the communities as they adapt to changing climate. It focuses on the ecosystem services provided by riparian ecosystems in general, rather than the persistence of any particular ecosystem.

8.3.2.2 **Undesirable Result: GDEs**

GDEs provide a wide range of ecosystem services. These services are largely driven by the riparian vegetation that occurs within the GDEs, but they do not depend on any particular riparian ecosystem structure. To maintain its riparian character, the ecosystem must have access to shallow groundwater such that the vegetation can access more water than is available to upland communities. If the riparian vegetation is succeeded by upland vegetation, those ecosystem services are lost and are unlikely to be regained.

8.3.2.3 **Sustainability Indicator**

Because GDEs are defined by their access to shallow groundwater, the sustainability indicator is the depth to groundwater. In addition to this threshold, TRPA monitors a wide range of biotic and abiotic properties of SEZs throughout the Tahoe Basin. These publicly available data may be used to provide additional environmental context and to inform management decisions.

Reasons for selection of this indicator for GDEs are as follows:

1. The data required for this indicator are sometimes available from cooperating agencies, and GDEs in locations without existing data sources can be prioritized for monitoring.

2. Groundwater levels in the shallow aquifers determine whether plant communities have direct access to groundwater as a supplementary water source. As such, it is believed to be representative of the status of GDEs within the TVS Subbasin.

3. Groundwater levels in the shallow aquifers are significantly affected by changes to GDE communities and the subsequent actions needed to address this undesirable result. The rate of these changes can be quantified, and improvements can be detected over relatively short periods (five to ten years).

4. Groundwater levels in the shallow aquifers are independent from the sustainable yield of the TVS Subbasin but are somewhat dependent on changes in groundwater storage and baseflow contributions to interconnected surface waters. However, the level of dependence on these other indicators is not critical and does not diminish its utility as an independent indicator of interconnected surface waters.

5. Trends in groundwater levels in the shallow aquifers can inform policy decisions in evaluating the impacts of groundwater management on GDEs. Groundwater levels and trends can also be used as a performance measure to evaluate the effectiveness of management decisions to mitigate undesirable results affecting beneficial users within the TVS Subbasin.

8.3.2.4 **Minimum Threshold**

Because groundwater levels exhibit interannual variability, this minimum threshold is based on a ten-year average of measurements rather than a single year. For each monitored GDE, the ten-year average groundwater elevation and the ten-year average late-season (Aug-Sept-Oct) groundwater elevation must be greater than 25th percentile of the historical record.

There are few, if any, existing wells with a 30-year record that can be used to establish average conditions. However, the historical STGM can be used to identify GDEs that may be vulnerable to degradation. Three different tests provide a baseline for the analysis of the status of TVS Subbasin GDEs:

1. Mann-Kendall trend test over the last 30 years (long-term trend),
2. Mann-Kendall trend test over the last 10 years (short-term test), and
3. Comparison of ten-year average water level to historical variability.

Like interconnected surface waters, the trend tests and comparisons can be performed observations over the full year or over the late season. Because groundwater changes more slowly than surface water, tests were run using the full year of data. None of the 47 GDEs within the TVS Subbasin have statistically significant negative trends in groundwater level on either a 30-year or a 10-year timescale. In each of the 47 GDEs within the TVS Subbasin, the mean groundwater elevation over the last ten years is greater than the 25th percentile over the 30-year record.

Reasons for selection of this minimum threshold are as follows:

1. The data required for this indicator are sometimes available from cooperating agencies, and GDEs in locations without existing data sources can be prioritized for monitoring.
2. The minimum threshold is calculated in a manner that is consistent with guidance prepared by The Nature Conservancy and the state of California (Rohde et al. 2018; Rohde et al. 2020) for monitoring GDEs and is representative of GDEs in the TVS Subbasin.
3. The minimum threshold is based on directly water levels which are sensitive to changes in GDEs in the TVS Subbasin. Therefore, it can be easily adjusted to reflect current needs of beneficial users.
4. The water levels used for the sustainability indicator and accompanying minimum threshold are the same for ease of comparison.
5. The range of historical variability in measured discharge is completely independent of the condition of GDEs going forward.
6. Groundwater levels in the shallow aquifers respond to drought periods on an annual timescale. However, the minimum threshold defined above relies on a multi-year record of measured discharge and thus should be relatively insensitive to water year type, except in cases of prolonged drought.
7. The minimum threshold defined for GDEs would also be a useful indicator for interconnected surface waters, and to a lesser extent groundwater levels. For example, if the minimum threshold for GDEs was violated this would also indicate that groundwater in shallow aquifers is less available to contribute to streams as baseflow. If shallow aquifer water level declines were such that the threshold could not be met, this would likely indicate a reduction in groundwater storage in the shallow aquifer.

8.3.2.5 **Monitoring and Reporting**

Since none of the 47 GDEs were identified as “vulnerable” in the above analysis, a further analysis considered future vulnerabilities. Using the baseline future scenario (i.e., assuming no change in precipitation or temperature), water levels were simulated over the 50-year planning period. Approximately half of the GDEs in the TVS Subbasin exceeded the threshold within the 50-year planning horizon (Figure 8-4). The time in which they exceeded the threshold, however, varied: a few GDEs would exceed the threshold by 2030 while others would take until 2070. Those simulated GDEs that exceeded the threshold value first are priorities for monitoring.

There are few established monitoring wells with the long-term record needed to establish historical variability of the shallow groundwater that sustains GDEs. Local stakeholders, including the California Tahoe Conservancy and USFS LTBMU, are actively monitoring groundwater levels in and around GDEs, and have provided monitoring data to the District. The data from these wells will provide the initial basis for monitoring GDEs. Because these wells have relatively short time series of data (typically 3-4 years), observed water levels will be regressed against simulated water levels to determine a mathematical relationship between the observed and simulated data. This regression relationship will be used to establish the 25th

percentile threshold by converting the simulated 25th percentile for the well to an equivalent observed water level.

Calculations will be performed every five years as part of the District's periodic evaluation of groundwater conditions. The ten-year average water level will be recalculated in each monitoring well and compared to the previously established 25th percentile values. If the 10-year average at any well falls below the 25th percentile established with the regression, the threshold has been exceeded. To provide an early warning that the threshold may be exceeded in the future, Mann-Kendall trend tests will be performed on the most recent five years of annual average water levels. The shorter timescale allows the detection of a trend well before the threshold might be exceeded.

If any monitoring well shows a statistically significant, negative trend, additional investigation will be undertaken to determine how much groundwater pumping may be affecting that well. This will compare the groundwater elevation in the current STGM (updated annually) to the groundwater elevation in the no-pumping groundwater model scenario that most closely matches the recent climate conditions. If the modeling indicates that groundwater pumping is contributing to the negative trend, the model can then be used to explore management options to minimize this contribution and avoid exceeding the threshold.

As additional data are collected, the 25th percentiles can be updated. During each subsequent review period, recently collected data will be compared to modeled data and the historical record in order to more accurately establish the 25th percentile threshold values.

As other stakeholders continue to collect data in these wells, the collected data can be compared to simulated data to determine whether the model accurately represents the near-surface groundwater that supports GDEs. At the same time, the monitoring data collected in these wells will be examined to identify existing wells with an acceptable water level record as candidates for addition to the existing TVS Subbasin Monitoring Network. At these locations groundwater level monitoring would continue, and long-term trends would be evaluated as is done for other wells in the network.

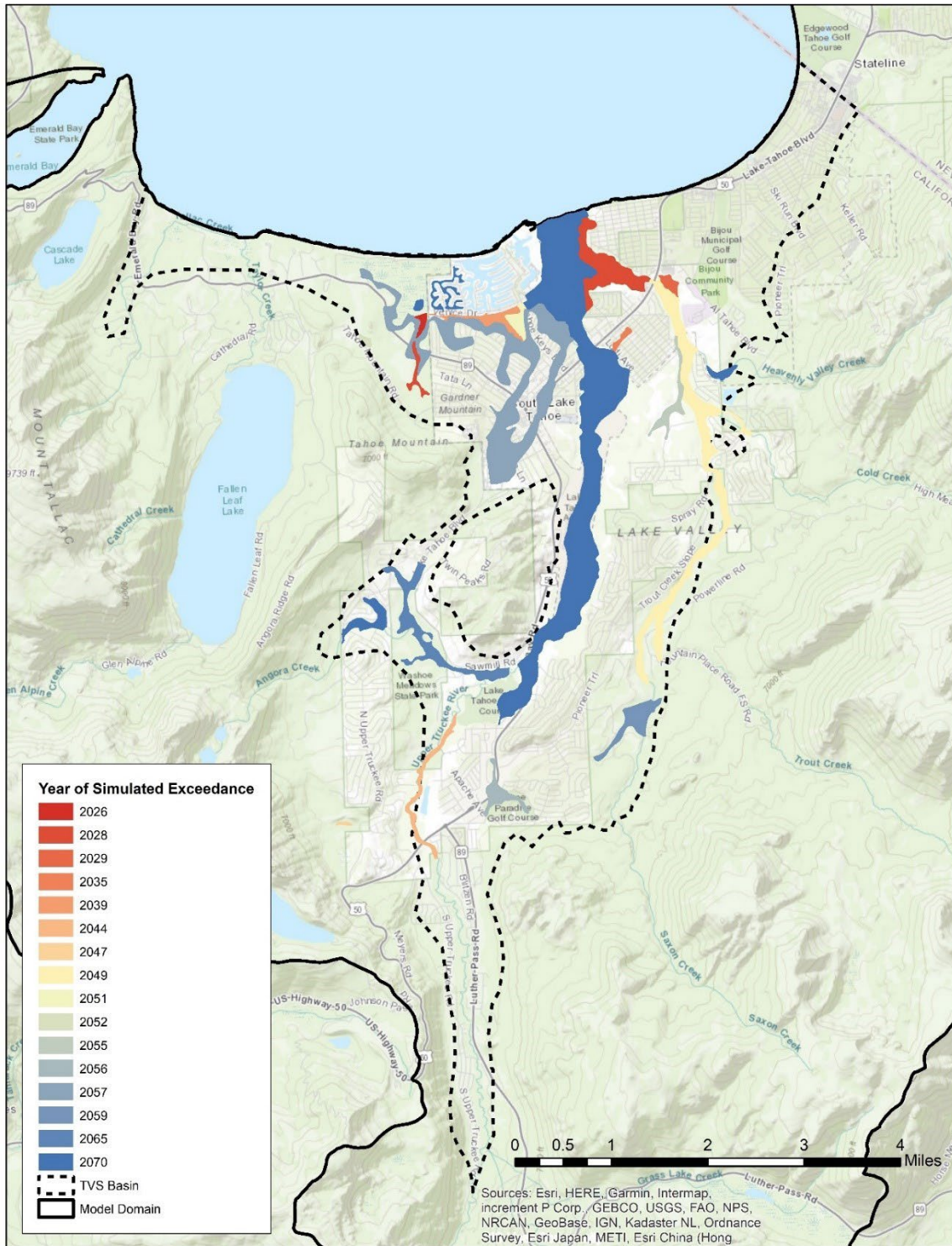


Figure 8-4. Based on baseline simulations, the GDEs (as mapped by TRPA) indicated here are vulnerable to exceeding the threshold value in the timeframe indicated by their color. Mapping is for general use only, requiring verification at the individual parcel scale.

SECTION 9: GROUNDWATER MONITORING

The following section describes the monitoring network, monitoring objectives, monitoring protocols, and data reporting used to assess groundwater conditions in the TVS Subbasin. Monitoring protocols are described in the Groundwater Elevation Monitoring Plan (Bergsohn, 2011) provided in Appendix K.

9.1 Groundwater Monitoring

The District currently has in place various monitoring programs that fulfill SGMA requirements. This section briefly describes the types of data collected and how and where they are acquired. As part of the Basin Monitoring Plan, the District will reach out to other water purveyors and other governmental agencies about sharing data within the TVS Subbasin. The District will work with other agencies to identify data that will help support the Basin Monitoring Program for all stakeholders.

Since 2001, the District has collected groundwater level data in the fall and spring of each year from a standard set of wells which comprise the monitoring network within the District's service area (Figure 9-1). These data were initially used to monitor groundwater production well operations, evaluate groundwater level trends, and develop a dataset for future STGM calibration. Prior to 2001, the District collected spot readings of static and pumping water levels to monitor District production well operations.

In 2010, the District submitted to DWR a Notice of Intent (NOI) to volunteer to be a monitoring entity within the California Statewide Groundwater Elevation Monitoring Program (CASGEM) (District, 2010). The District received monitoring entity designation under the CASGEM program in December 2011 (DWR, 2011). Since 2011, the District has monitored and reported groundwater level elevations to DWR in accordance with the approved Groundwater Level Elevation Monitoring Plan for the TVS Subbasin (Appendix K). The objective of the CASGEM monitoring program is to provide elevation data capable of demonstrating seasonal and long-term groundwater elevation trends. To satisfy this objective, the District reports static groundwater elevation data collected from observation wells within the monitoring network semi-annually to DWR. The District will transition its reporting of groundwater elevation data from CASGEM to the Groundwater Sustainability Plan Reporting System starting in 2022.

Under SGMA, GSAs are required to develop a monitoring network capable of collecting sufficient data to demonstrate short-term, seasonal, and long-term trends in groundwater and related surface conditions and yield representative information about groundwater conditions as necessary to evaluate Plan implementation (23 Cal. Code Regs. § 354.34 (a)). Since adoption of the 2014 GWMP, the District has used groundwater level data collected from the monitoring network to prepare Annual Reports assessing groundwater conditions and has submitted these reports to DWR, in satisfaction of GSA reporting requirements (Wat. Code § 10728), for WY 2017, WY 2018, WY 2019 and WY 2020.

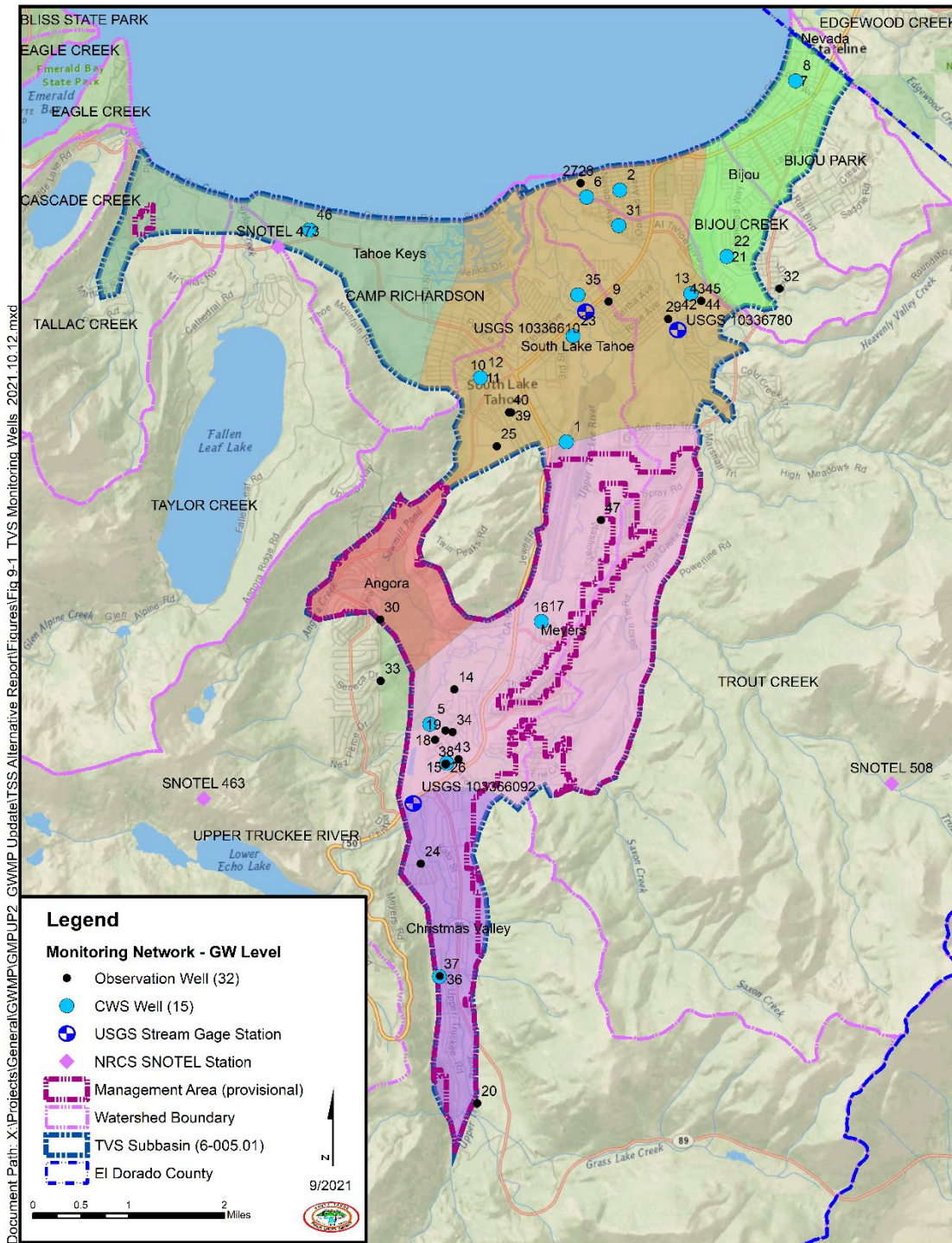


Figure 9-1. Locations of wells used in the TVS Subbasin monitoring network, USGS stream gage stations and NRCS snow telemetry stations

9.1.1

Monitoring Network

Groundwater levels are regularly measured in 47 wells located throughout the TVS Subbasin. The monitoring network includes 32 observation wells and 15 CWS wells (Figure 9-1). The majority of CWS wells (11 of 15) are actively used for groundwater production; three wells are on stand-by status, and one well is currently inactive. The observation wells include monitoring wells, sentinel wells, test wells and former drinking water supply wells that have been removed from service and converted to observation wells. Construction details for selected wells for which hydrographs are regularly provided in Annual Reports are set forth in Table 9-1. Elevation ranges of the perforated intervals for all wells in the monitoring network are depicted in Figure 9-2.

Table 9-1. Screen intervals for selected monitoring wells presented in the Annual Reports for the TVS Subbasin. Hydrographs for these wells showing groundwater level trends within each subarea are presented in Section 5.2 and included in Appendix L.

Well	Subarea	Reference Point Elevation (ft AMSL)	Top of Screen Depth (ft bgs)	Bottom of Screen Depth (ft bgs)
Mountain View	Angora	6313.14	95	164
Blackrock Well #1	Bijou	6242.72	168	180
Glenwood Well #3	Bijou	6261.68	112	192
Henderson OW	Christmas Valley	6369.78	79 142	100 205
Bakersfield	Meyers	6310.50	130 180	170 240
Elks Club Well #1	Meyers	6284.63	110	142
Washoan OW	Meyers	6307.84	102 165 207 249	144 186 228 270
CL-1	South Lake Tahoe	6278.37	104	114
CL-3	South Lake Tahoe	6278.49	39	49
Paloma	South Lake Tahoe	6267.10	188 268	248 408
Sunset	South Lake Tahoe	6249.00	275	430
Martin OW	South Lake Tahoe	6262.42	95 125 160 200	115 145 180 240
USGS TCF-1-1	South Lake Tahoe	6296.48	325	340
USGS TCF-1-2	South Lake Tahoe	6296.47	245	260
USGS TCF-1-3	South Lake Tahoe	6296.65	158	163
USGS TCF-1-4	South Lake Tahoe	6296.63	130	140

Well	Subarea	Reference Point Elevation (ft AMSL)	Top of Screen Depth (ft bgs)	Bottom of Screen Depth (ft bgs)
USGS TCF-1-5	South Lake Tahoe	6296.63	88	98
Lily OW	South Lake Tahoe	6236.08	35	37.5
Valhalla	Tahoe Keys	6256.50	110	170

NOTES:

feet AMSL: Elevation in feet above mean sea level (NAVD88).

ft bgs: Depth in feet below ground surface.

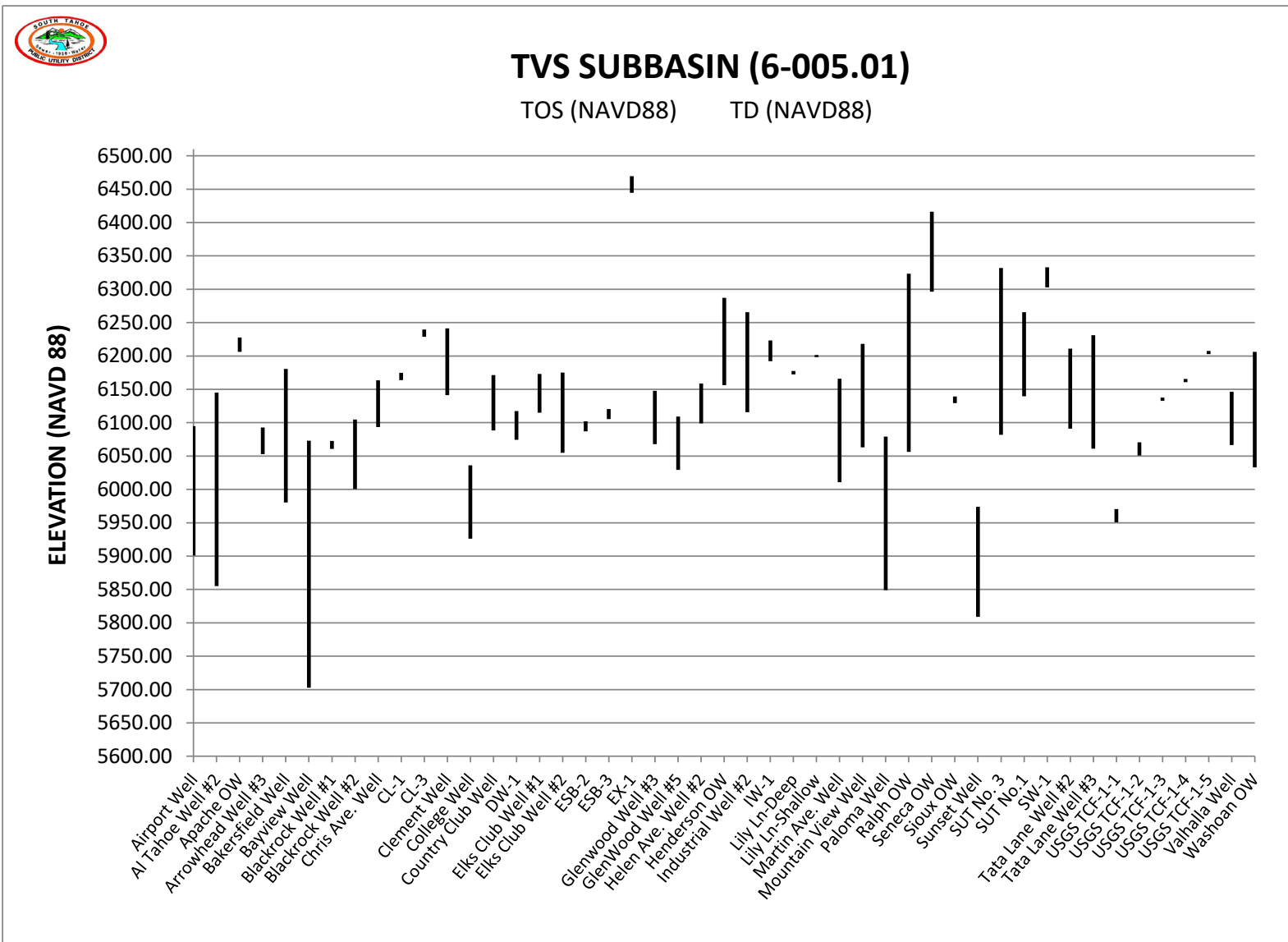


Figure 9-2. Elevation ranges of the perforated intervals for all wells included in the monitoring network for the TVS Subbasin

9.1.2 Monitoring Protocols

Groundwater conditions in the TVS Subbasin are assessed using various climate, groundwater level, groundwater extraction and water use data. The District uses the STGM to calculate annual water budget terms (e.g., inflows, outflows and change in groundwater storage) and generate modeled seasonal high and low isocontours of groundwater levels across the TVS Subbasin.

9.1.2.1 Water Year Type

Water year type is categorized using total precipitation measurements collected at the National Resources Conservation Service (NRCS) Hagans Meadow SNOTEL Site 508 (Figure 9-1). Precipitation records for this site date back to 1978. This site has the best correlation between precipitation at one station and groundwater recharge extracted from the STGM (Figure 9-3). For this reason, it is used as a reference station to classify water year type for the South Lake Tahoe area including the TVS Subbasin (Pohll et al, 2016).

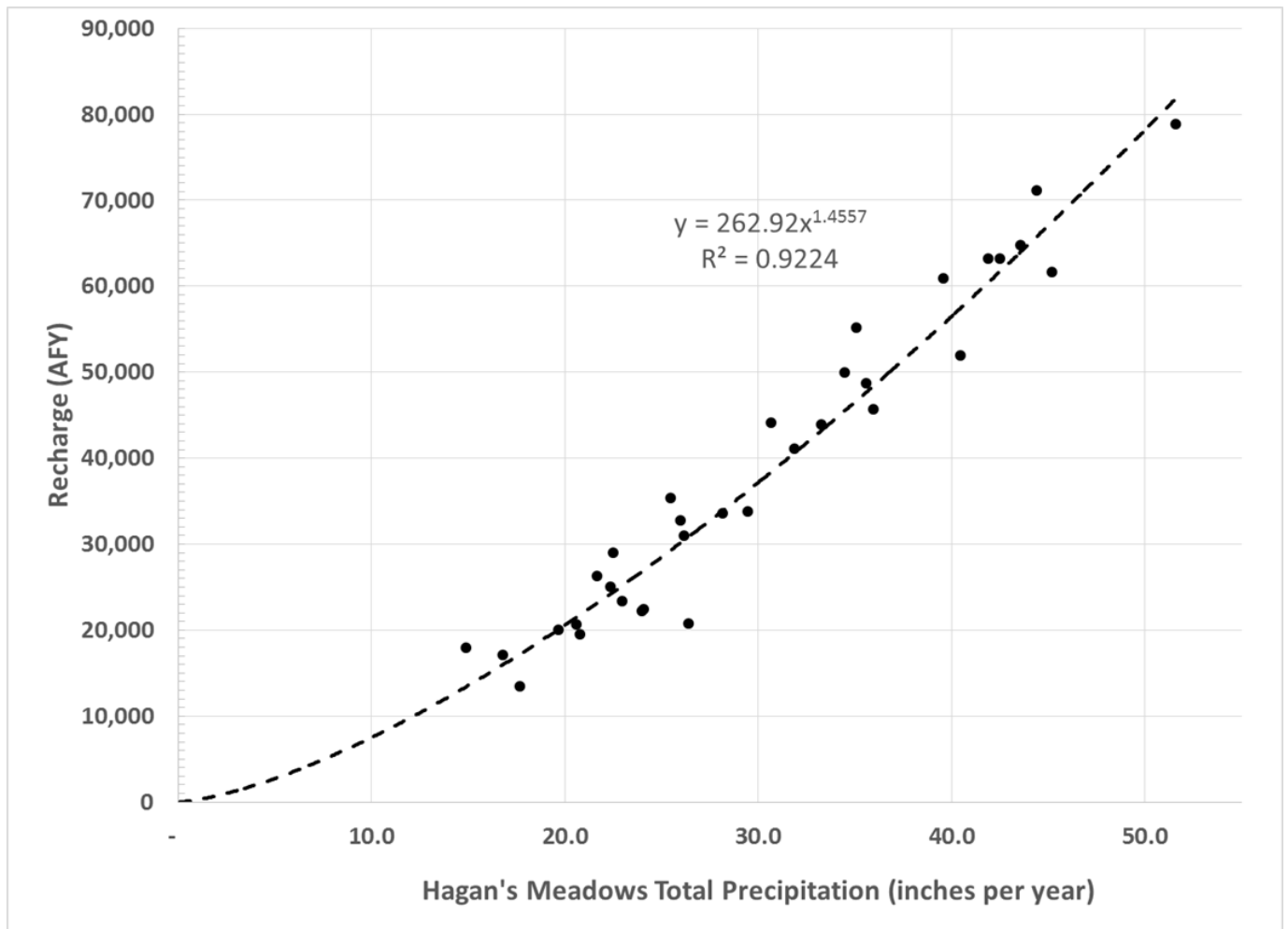


Figure 9-3. Hagans Meadow, CA SNOTEL 508 annual precipitation versus modeled groundwater recharge within the South Lake Tahoe area (G. Pohll et al., 2016).

For water year type classification, water years 1979–2017 were categorically defined by assuming a normal distribution in precipitation and establishing ranges based on the z-statistics (Table 9-2). To allow more flexibility in water year type, seven categories were established: (1) very wet, (2) wet, (3) above normal, (4), normal, (5) below normal, (6) dry, and (7) critical. The very wet periods are indicated by a z-statistic greater than 1.5 and occur in WY 1982, WY 2011 and WY 2017. Critical water years are indicated by a z-statistic of negative 1.5 and occur when total accumulated precipitation is less than 14 inches. For reporting purposes, water year type is identified using the total precipitation measured at SNOTEL site 508 and the precipitation ranges presented in Table 9-2.

Table 9-2. Classification system for water year type based on observed accumulated precipitation at Hagan’s Meadows, CA, SNOTEL 508. Upper bound of z-statistic and ranges in precipitation (inches) (Adapted from Carroll *et al.*, 2016b)

WY Type	z (upper)	Precipitation (in) (1979-2017)		Count (1979 -2020)
		>	≤	
Very Wet	>	49	-	3
Wet	1.5	43	49	4
Above	1	37	43	5
Normal	0.5	26	37	13
Below	-0.5	20	26	13
Dry	-1.0	14	20	4
Critical	-1.5	0	14	0

9.1.2.2 Groundwater Levels

The District uses groundwater level data collected from the monitoring network to assess seasonal, annual, and long-term trends in groundwater conditions. Hydrographs represent long-term groundwater elevation trends and are regularly updated for presentation in the Annual Report (see Appendix L). The District uses hand readings collected during seasonal high groundwater conditions to define annual basin conditions as being either normal, above normal, or below normal with respect to the record of groundwater levels collected during a specified 10-year base period (WY 2001–WY 2010) (Figure 9-4). The District also calculates year-to-year differences in seasonal high groundwater readings to show average annual changes in groundwater elevation.

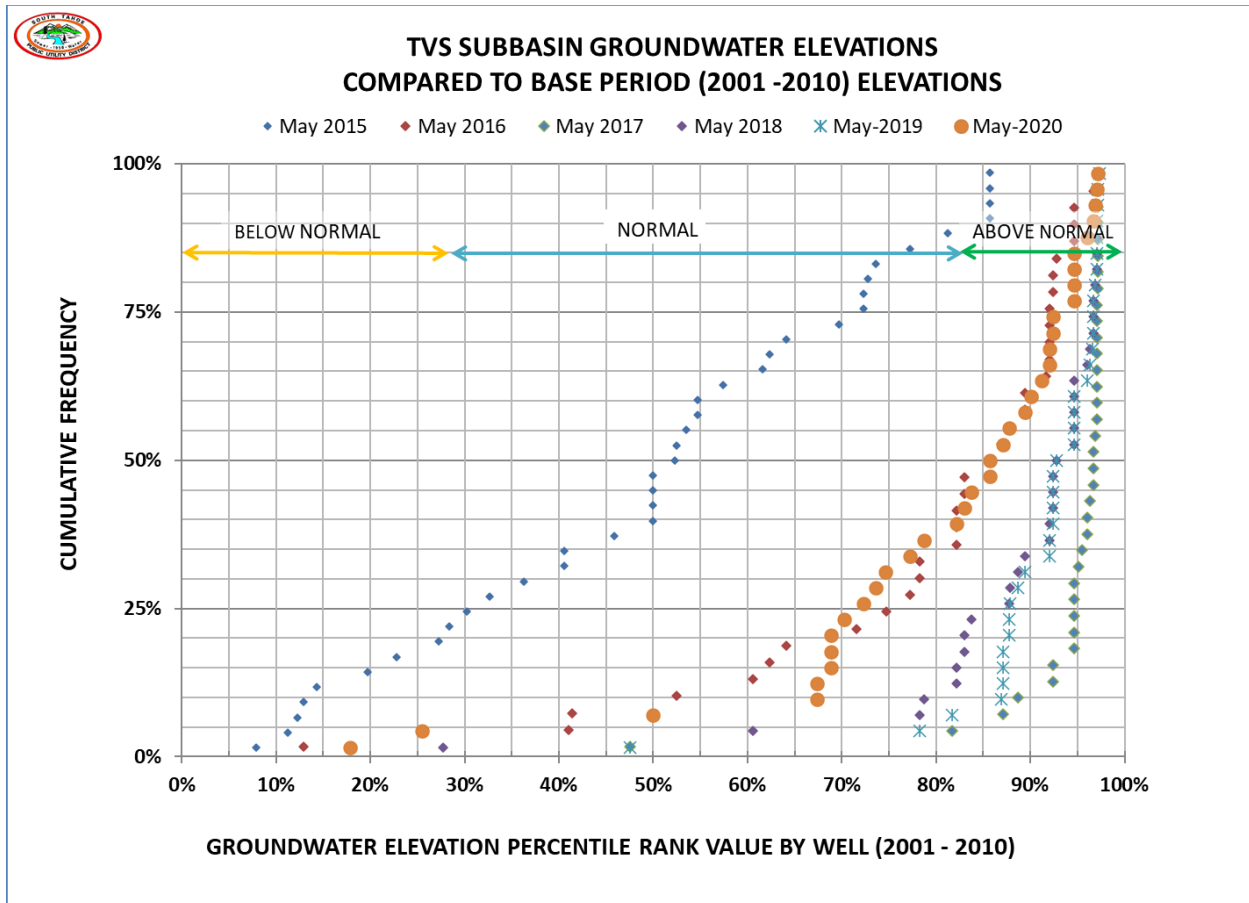


Figure 9-4. Hand readings collected during the May groundwater elevation monitoring event for WY2015 through WY 2020 compared to the record of hand readings for the same wells collected during WY 2001 through WY 2010 base period for groundwater elevations.

The District uses both hand and continuous readings to monitor groundwater elevation trends. Hand readings are collected from each of the groundwater elevation monitoring wells in the fall and spring of each water year. Hand readings from active CWS wells are collected a minimum of 12 hours after well pumps are turned-off for static water level measurements. May and November are optimal for water level readings because these months generally coincide with seasonal high and low groundwater elevations and District water demands are low, allowing production wells to be shut-off for a minimum 12-hour recovery time prior to data collection. These readings are recorded in bound field books and on standard field sheets. Following each measuring event, the District reviews the collected depth-to-water field readings, checking for errors, and enters them into a District MS-excel worksheet. The worksheet is used to convert the field readings to NAVD88 elevations and update water-level hydrographs for each well. The District compares field readings to verify the accuracy of the automated readings.

The District collects pressure head readings on a daily (12-hour frequency) basis from thirteen (13) observation wells in the monitoring network with submersible pressure transducers with internal data loggers. Pressure and barometric head readings from the well transducers are routinely downloaded at least once per year during the summer or early fall. These electronic

files are stored on the District's server and combined to derive compensated head readings and NAVD88 groundwater elevations, which the District uses to update electronic records of long-term groundwater elevations and generate hydrographs for the TVS Subbasin.

Monitoring protocols including the frequency and timing of groundwater elevation readings; data collection and reporting methods are detailed in the Groundwater Elevation Monitoring Plan (District, 2011) A copy of this plan is provided in Appendix K.

9.1.2.3 **Groundwater Flow Directions**

The District updates the STGM annually to simulate changes in groundwater levels and flux due to annual changes in precipitation and groundwater pumpage. The model is used to generate isocontours of groundwater elevations during October and May of each water year to show the general groundwater flow directions across the TVS Subbasin during seasonal low (October) and seasonal high (May) groundwater conditions. (Figure 9-5). These maps are presented in the Annual Report each year.

9.1.2.4 **Groundwater Extractions**

Groundwater extractions from the TVS Subbasin are primarily from CWS wells used for drinking water uses (Section 3.3.5). TKWC, LBWC, and LPA annually share groundwater pumpage for active CWS wells in their water systems with the District to update the STGM, to monitor changes in the spatial distribution of groundwater pumping, and to monitor water system groundwater production trends. These data are included in the Annual Reports.

9.1.2.5 **Groundwater Use**

Pumping from District CWS wells accounts for most of the groundwater pumped from the TVS Subbasin. The District's metered data from its customer service database, therefore, shows the general pattern of water use by water use type. These data are presented in the Annual Reports.

9.1.2.6 **Groundwater Recharge**

Groundwater recharge largely depends on annual precipitation (Figure 9-3) and is a main component of the water budget. Recharge is defined as the model computed excess water leaving the unsaturated root or soil zone and after accounting for abstractions of interception, sublimation, surface runoff and evapotranspiration (Pohll et al., 2016). The STGM calculates water budgets for the Mountain Block and the TVS Subbasin, including the quantity of groundwater recharge. Change in groundwater recharge for the TVS Subbasin is reported in the Annual Reports.

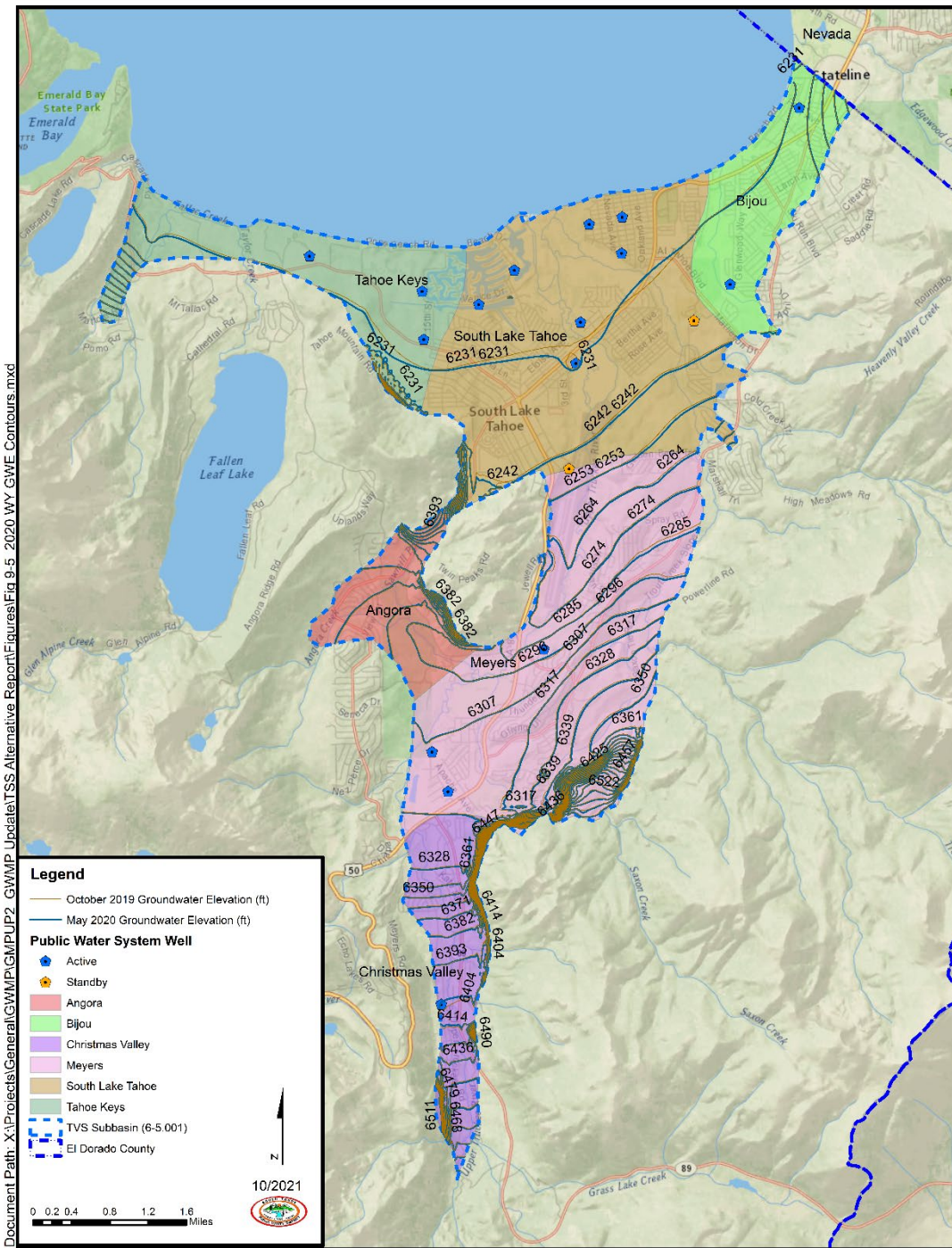


Figure 9-5. Model simulated groundwater elevations (upper 300 ft), representing seasonal low (October 2019) and seasonal high (May 2020) groundwater conditions. Contour interval is 10 ft.

9.1.2.7 **Groundwater Storage**

The District monitors annual change in groundwater in storage using the water budget as calculated by the STGM. The main components of the water budget include groundwater recharge; groundwater discharge to streams (baseflow); groundwater flux to Lake Tahoe; and groundwater pumpage. Change in annual groundwater storage is calculated for the Mountain Block and for the TVS Subbasin from the differences in total inflow (recharge) and total outflows (baseflow, flux to Lake Tahoe and groundwater pumping) to each spatial zone over a specified period (Carroll, *et al.*, 2016b). Change in groundwater in storage for the TVS Subbasin is reported in the Annual Reports.

9.1.2.8 **Seawater Intrusion**

The TVS Subbasin sits at an elevation of more than 6,250 feet above sea level in the Sierra Nevada Mountains. Seawater intrusion is not a sustainability indicator monitored in the TVS Subbasin.

9.1.2.9 **Degraded Water Quality**

Groundwater is typically of excellent quality, however there are known areas of degraded water quality which are regarded as groundwater quality issues within the TVS Subbasin (see Section 6.3). The LRWQCB is primarily responsible for the enforcement and oversight of groundwater clean-up of these sites, except for the Meyers Landfill site which is a federal CERCLA site under the direction of the USFS. Groundwater quality monitoring is conducted by responsible parties, where contamination concerns exist but are not identified by the LRWQCB. Groundwater quality data collected from these sites is available in site investigation reports and chemical data stored in SWRCB-GeoTracker. To monitor degraded water quality, the District relies on current information shared by SAG member agencies and water purveyors during SAG workshops and on groundwater quality data reviewed and evaluated every five-years. A summary of major groundwater contaminant investigations and clean-up activities within the TVS Subbasin are presented in the Annual Reports.

9.1.2.10 **Land Subsidence**

At least one foot of land subsidence would occur if groundwater levels were to decline on the order of 100 feet (Section 8.1.3). Protocols used for measuring groundwater levels from the monitoring network can recognize changes in groundwater levels in increments of 0.10 feet. Groundwater elevation data collected from the monitoring network (Section 9.1.1) during the spring monitoring event are compared to May 2015 water levels at each well to identify significant and unreasonable declines in groundwater level elevations (see Section 8.1.3).

9.1.2.11 **Depletion of Interconnected Surface Water**

The Alternative Plan provides information identifying where interconnected surface water conditions exist, estimates on the quantity and timing of depletions of surface waters, and sustainable management criteria to avoid significant and unreasonable depletion of interconnected surface water caused by groundwater pumping (Sections 5.3; 5.6.1; 8.3.1.5.1; 8.3). Methods to monitor potential changes in flow conditions, temporal change in conditions

due to variations in stream discharge and groundwater pumping are discussed below in Section 9.2.2.

9.2 Identification and Description of Data Gaps

The following section evaluates data gaps in the monitoring network identified during periodic review and assessment of the Alternative Plan. Objectives for the monitoring network include demonstrating progress toward achieving measurable objectives described in the Alternative Plan (Section 8.0), monitoring impacts to beneficial uses or users of groundwater, monitoring changes in groundwater conditions relative to measurable objectives and minimum thresholds, and quantifying annual changes in water budget components. The monitoring network currently achieves these objectives for all sustainability indicators (chronic lowering of groundwater levels, reduction of groundwater storage and land subsidence) except degraded water quality and depletions of interconnected surface water.

9.2.1 Monitoring for Degraded Water Quality

To ensure that water quality of drinking water is maintained, the Water Code includes a requirement that water purveyors regularly monitor groundwater quality at each drinking water source (i.e., well). The Water Code requires monitoring of a suite of constituents, including various inorganic chemicals, radioactivity, and organic chemicals. This section describes the monitoring performed by District and by other entities extracting water from the TVS Subbasin.

The District collects groundwater quality samples from fifteen (15) active wells on at least an annual basis (from June to August) and submits those samples for analysis of the full suite of Title 22 analytes. Sampling procedures and laboratory analyses meet all Title 22 requirements. At present, the District has not requested water quality data from for active wells operated by LBWC, TKWC and LPA or for active wells regulated under the El Dorado County Small Water System Program (see Section 4.3.3). Stormwater quality data collected through the Stormwater Management and Monitoring Program (see Section 4.3.3) may also be helpful, should the list of analytical methods used in these programs be expanded to include selected constituents of concern important to protecting drinking water quality within the TVS Subbasin. Regular compilation and review of these local data could be used to augment groundwater quality datasets currently used to evaluate groundwater quality within the TVS Subbasin (see Section 6.1.2).

9.2.2 Monitoring for Depletions of Interconnected Surface Water

Undesirable effects of depletion of interconnected surface water take one of two forms: reduction or interruption in streamflow or harm to groundwater dependent ecosystems (GDEs). Reductions in streamflow are monitored using existing USGS stream gages within the TVS. Impacts to GDEs are monitored using selected wells within the existing monitoring network.

9.2.2.1 Depletion of Surface Flows

Surface water is monitored by the USGS at three gaging stations managed by the Nevada Water Science Center - Carson City, NV. Two of these stations (USGS # 103366092; USGS # 1033610) are located on the Upper Truckee River; the third gaging station (USGS # 10336780)

is located on Trout Creek (Figure 9-1). The minimum thresholds for depletion of surface flows refer to gaged discharge at each of the three USGS gages. For each gage, the 10-year average discharge over three seasonal timeframes will be calculated and compared to the seasonal thresholds shown in Table 8-2 in the preceding section. If the 10-year average at any gage falls below the indicated threshold, that threshold has been exceeded.

To provide an early warning that the threshold may be exceeded in the future, Mann-Kendall trend tests (Mann 1945; Kendall 1975) will be performed on the most recent five years of seasonal discharge at each gage. The relatively short timescale is intended to allow the detection of a trend well before the threshold might be exceeded. If any gage shows a statistically significant, negative trend, additional investigation will be undertaken to determine how much groundwater pumping may be affecting that gaged discharge.

This investigation, previously described in Section 8.3.1.5, will compare the baseflow contribution in the current STGM (updated annually) to the baseflow contribution of the no-pumping groundwater model scenario that most closely matches the recent climate conditions. If the modeling indicates that groundwater pumping is contributing to the negative trend, the model can then be used to explore management options to minimize this contribution and avoid exceeding the threshold.

The provisional groundwater management area previously described in Section 8.3.1.5.1, will be used to explore potential mitigation approaches if a threshold is exceeded or is likely to be exceeded. The provisional management area includes an area in which the current STGM indicates that any increased pumping is likely to affect interconnected surface waters. While that model is based on the best available climate projections, it still includes a great deal of uncertainty, especially in projected precipitation. Over the next five years, refined climate projections are expected to become available that can better constrain the model, enabling more reliable predictions of the effect of groundwater extraction. Prior to the next update of this Alternative Plan, the District and the SAG will re-evaluate the need for the provisional management area and determine whether to make it a permanent part of the Alternative Plan. If the provisional management area is implemented permanently, the District and the SAG will develop sustainable management criteria for that area. Groundwater management in the provisional management area would likely include a mix of approaches that may involve promoting projects that would enhance groundwater replenishment, water conservation, and land use development limitations to mitigate the need for new pumping.

9.2.2.2 **Groundwater Dependent Ecosystems**

The District will monitor GDEs on an annual basis using hydrographs observed in selected monitoring wells. After the end of each water year, the ten-year average water level will be recalculated in each monitoring well and compared to the previously established 25th percentile values. If the 10-year average at any well falls below the 25th percentile, the threshold has been exceeded.

Monitoring wells will be selected based on their proximity to delineated GDEs. Monitoring wells may be located within or near priority GDEs identified in Section 8.3.1.5 (i.e., the GDEs shown in Figure 8-4 as likely to exceed the minimum threshold between now and

2070). Data from existing shallow monitoring wells has been provided by stakeholders, but these wells generally have short time series of data and will require a statistical reconciliation to the model to be used as a threshold. As more data become available for these wells, the regression to the model can be refined to improve the threshold calculation; after enough data has been collected, the regression can be abandoned and the time series of monitoring data used on its own.

To provide an early warning that the threshold may be exceeded in the future, Mann-Kendall trend tests will be performed on the most recent five years of annual average water levels. The shorter timescale allows detection of a trend well before the threshold might be exceeded.

If any monitoring well shows a statistically significant, negative trend, additional investigation will be undertaken to determine how much groundwater pumping may be affecting that well. In this investigation, the District will compare the groundwater elevation in the current STGM (updated annually) to the groundwater elevation in the no-pumping groundwater model scenario that most closely matches the recent climate conditions. If the modeling indicates that groundwater pumping is contributing to the negative trend, the model can then be used to explore management options to minimize this contribution and avoid exceeding the threshold.

As additional data are collected in monitoring wells, the 25th percentiles can be refined. During each plan update, recently collected data will be compared to modeled data and the historical record in order to more accurately establish the 25th percentile threshold values.

SECTION 10: IMPLEMENTATION PLAN

This section summarizes implementation of the Alternative Plan, including a schedule of proposed projects and management actions organized by BMO and related to the sustainable management criteria developed for the TVS Subbasin (Appendix M). Over the past five years, implementation costs for the Alternative Plan have averaged about \$415,000 per annum (Section 10.2). A general description of funding options for future implementation of the Alternative Plan are discussed below in Section 10.2.

10.1 Projects and Management Actions

The implementation plan is a list of management actions and projects developed from status review of the 2014 GWMP Implementation Plan and assessment of new information developed for the Alternative Plan. The management actions and projects in Appendix M are presented in terms of on-going, short term (over the next five-year assessment period) and long-term (more than the next five years) activities. On-going activities include actions required to monitor groundwater conditions and usage, update and maintain the groundwater budget, and satisfy reporting requirements for the Alternative Plan. Short-term activities are new actions to be implemented over the next five-year assessment period to address Recommended Actions and projects to address current groundwater concerns: quality and impacts to GDEs. Long-term activities are new actions to be implemented in a period of time exceeding five years and will assess groundwater conditions compared to current projections and the need for modifications to sustainable management presented in the Alternative Plan.

10.1.1 Circumstances for Implementation

The District has implemented groundwater management plans successfully for over three decades. The projects and management actions described in this section and Appendix M continue of those efforts. The District will continue management of groundwater in the TVS Subbasin under the Alternative Plan pursuant to the sustainable management criteria presented in Section 8. Currently, certain conditions, such as groundwater contamination and interaction of groundwater pumping on GDEs, warrant short-term management activities to improve groundwater management and avoid undesirable results. These actions are detailed in Appendix M.

There are also more than 300 active private small water system and domestic wells providing drinking water for individual water systems within the TVS Subbasin (Section 3.3.3). These private well owners represent an important stakeholder group that should be more engaged in groundwater management. Short-term activities under BMO #3 includes actions to expand outreach to private well owners and recruitment of a private well owner representative to the SAG.

10.1.2 Approval of Implementation Actions

Permitting and approval requirements may vary depending on each specific project or management action. The District will comply with all applicable law and District policies in approving and obtaining permits for implementation actions.

10.1.3 **Expected Benefits**

Groundwater is the primary source of drinking water within the TVS Subbasin. Continued efforts to mitigate and prevent groundwater contamination and migration will protect the supply for beneficial use.

On-going monitoring and assessment of groundwater conditions within the TVS Subbasin is essential to identify both immediate and long-term groundwater issues that may develop over time as a result of groundwater pumping, groundwater quality degradation, and climate change. Monitoring allows for development of responsive and adaptive management actions to prevent local pumping impacts and the occurrence of undesirable results. Responsive management preserves a sustainable source of drinking water for all beneficial users and uses of groundwater within the TVS Subbasin. Monitoring activities will improve the proposed short-term and long-term groundwater management actions described in Appendix M and allow for the continued evaluation and refinement of sustainable management criteria.

10.2 **Funding Alternative Plan Implementation**

The following section describes the funding mechanisms that have been utilized to implement the 2014 GWMP and additional potential opportunities for future implementation efforts.

10.2.1 **Budget and Funding for Past Groundwater Projects**

Implementation costs for the Alternative Plan are presented in the TVS Subbasin Annual Reports. The total cost of implementation for the past five years was approximately \$2.075 million. Slightly over 50 percent was expended on consultants for groundwater investigations, development of hydrologic models and performance of complex model evaluations. The next two largest expenses were District labor (26 percent) and legal counsel time (18 percent). The remaining 5 percent went towards other expenses (such as temporary workers employed for the well owner survey), water quality analysis, permitting, equipment and supplies.

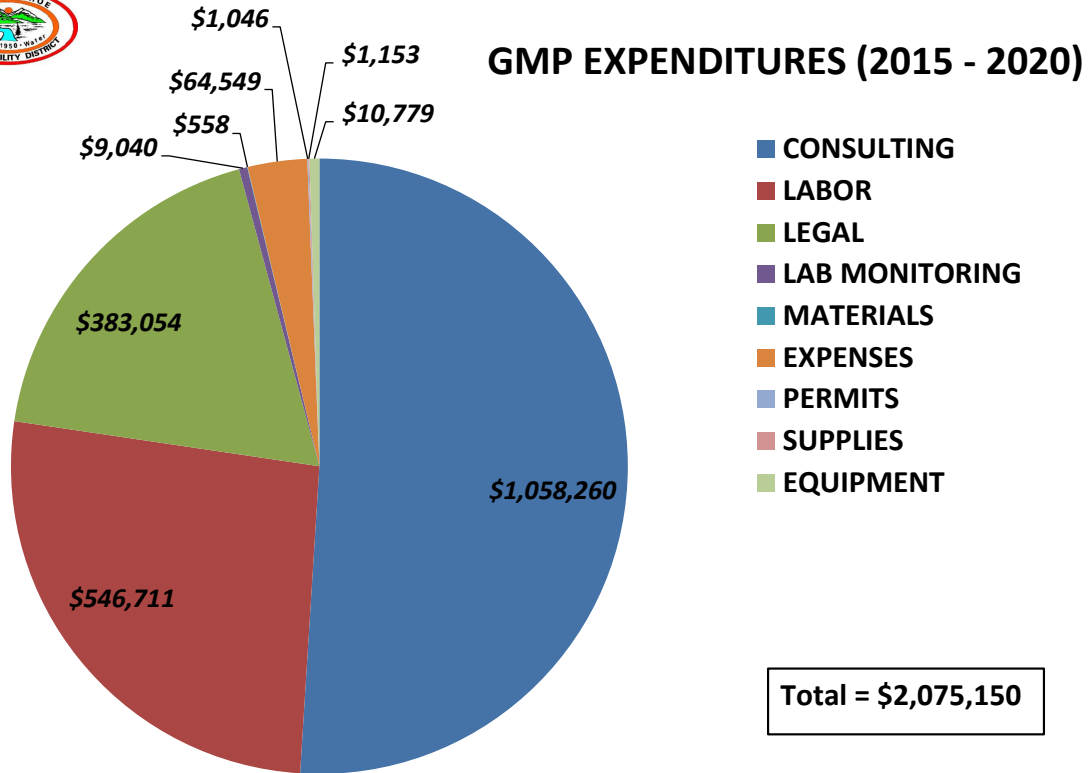


Figure 10-1. Expended costs for groundwater management in the TVS Subbasin through December 2020.

A breakdown of the funding sources and amounts used to support groundwater management in the TVS Subbasin through December 2020 is presented below in Table 10-1. Major sources of funding include the District’s Water Enterprise Fund, EDWA Cost Share Program, and State Grants (used for the South Y Feasibility Study).

Table 10-1. Funding sources and amounts used to support groundwater management through December 2020.

FUNDING SOURCE	AMOUNT (\$)
District Water Enterprise Fund	964,000
EDWA Cost Share Grant Program	681,000
State Grants	430,000
Total	2,075,000

The District’s Water Enterprise Fund finances water operations through user charges, property tax receipts, and other income. The District’s metered water rates are approximately structured with a 75 percent fixed component and 25 percent variable component. Water consumption revenues currently represent only 10.1 percent of the District’s 2020 combined water and sewer service charge revenue and 6.7 percent of total revenues; therefore, fluctuations

in actual usage do not materially impact operating income. Water consumption fees will become a larger portion of the District's revenues as the District continues to install meters to comply with the state mandate requiring water systems to be completely metered by 2025.

The EDWA Cost Share Grant Program assists in funding eligible projects under Section 96-11 of the El Dorado EDWA Act and Board Expenditure Priority Policy (No. B-1003). District activities (including groundwater management) that are not associated with standard operations or direct funding of capital projects are eligible. EDWA Cost Share Grants typically provide 50 percent matching funds. Since adoption of the 2014 GWMP, funding through EDWA Cost Share Grant Program has supported about one-third of the District's total expenditures on groundwater management for the TVS Subbasin. Although EDWA funding is limited, EDWA prioritizes activities with additional state or federal funding, as described in EDWA's Communications and Advocacy Program (see Section 4.3.4).

Proposition 1 (The Water Quality, Supply, and Infrastructure Improvement Act of 2014, Chapter 10 Groundwater Sustainability) included \$900 million in grants and loans for projects that clean up or prevent contamination of groundwater that serves or has served as a source of drinking water. During WY 2016, the District, in collaboration with the SAG, identified potential projects to address the PCE groundwater contamination in the South "Y" Area that might qualify for Proposition 1 funding. The District, in partnership with the LBWC and Tahoe Keys Property Owners Association, prepared pre-applications and a full proposal (FAAST # 36772) requesting funding through the Proposition 1 Groundwater Sustainability Program to conduct an engineering feasibility study of remedial alternatives to mitigate PCE groundwater contamination in the South "Y" Area. On March 30, 2017, the District received notice of preliminary grant award of up to \$294,270.00, conditioned on the successful negotiation of an agreement with DOFA. On May 18, 2017, the District's Board of Directors adopted Resolution No. 3059-17 accepting the grant award. Following adoption of Resolution No. 3059-17, the District entered negotiations with DOFA staff regarding changes to the scope of work and budget presented in the proposal. To facilitate negotiations, the District provided current groundwater quality data for the South "Y" Plume and developed a Pre-Design Investigation, which was subsequently added to the scope of work. The Pre-Design Investigation installed a test well to identify the vertical extent of PCE contamination. The test well could be used for additional field tests to define aquifer properties for engineering design. Inclusion of the Pre-Design Investigation increased total project budget to \$1,008,590.00, consisting of a \$504,295.00 grant request and a 50 percent funding match. The District met its 50 percent matching obligation using funds set aside for technical studies, including funds received from the EDWA Cost Share Grant Program funding.

10.2.2 **Projected Budget and Future Funding Opportunities**

The preceding Section 10.2.1 demonstrates that the District expended significant resources on implementation of the Alternative Plan. Since 2015, annual implementation costs have ranged from \$312,900 to as much as \$591,500, depending on the intensity of groundwater investigations being conducted in a particular year. The first five-year average cost of implementation for the Alternative Plan (2015–2020) is \$415,000 per annum. The District projects a base future cost for groundwater management in the TVS Subbasin to be 25 percent of the first five-year average cost of implementation (\$104,000) for normal years and 35 percent of the first five-year average cost of implementation (\$145,000) every fifth year to account for

added reporting needed for periodic review and assessment. The base cost for groundwater management in the TVS Subbasin assumes minimal groundwater investigations will be needed to inform future groundwater management actions for the subbasin. The District may utilize any funding opportunities available through the District's existing authority or SGMA's fee provisions to fund implementation as necessary.

10.2.2.1 **District Funding Authority**

The Public Utility District Act permits the District to charge a fee for commodities or services. (Pub. Util. Code § 16467.)

The District may impose special taxes for a specific purpose pursuant to Article 3.5 (commencing with Section 50075) of Chapter 1 of Part 1 of Division 1 of Title 5 of the Government Code. (Cal. Pub. Util. Code § 16641.5.) The proposed tax must be submitted to the voters and only upon approval of two-thirds of the votes cast may the District levy the tax. (Gov. Code § 50077(a).)

The District may elect to use county assessments and take them as the basis for taxation. (Pub. Util. Code § 16648.) An election pursuant to Cal. Pub. Util. Code § 16648 is effective the next February 1 after the certified copy is filed. (Pub. Util. Code § 16649.)

10.2.2.2 **SGMA Fees**

A GSA may raise revenue to fund groundwater projects through its own powers as a local agency or through a special provision in SGMA allowing for fees on the extraction of groundwater.

SGMA divides a GSA's financial fee authority into powers (1) granted to a GSA prior to adoption of a GSP (referred to as "Pre-Adoption Fees"), and (2) reserved for after a GSA adopts a GSP (referred to as "Post-Adoption Fees"). (Wat. Code §§ 10730, 10730.2.)

SGMA authorizes a GSA to "impose fees, including, but not limited to, permit fees and fees on groundwater extraction or other regulated activity" to fund the development of a groundwater sustainability program. (Wat. Code § 10730(a).) SGMA describes development of a groundwater sustainability program to include "preparation, adoption, and amendment of a [GSP], and investigations, inspections, compliance assistance, enforcement, and program administration, including a prudent reserve." (Wat. Code § 10730(a).) Water Code section 10730 requires a GSA to follow specific procedures prior to imposing a Pre-Adoption Fee, including noticing and holding a public meeting, making public data upon which the Pre-Adoption Fee is based, and adopting an ordinance or resolution.

Once a GSP or Alternative is adopted, SGMA authorizes a GSA that adopts a GSP (or an Alternative) to impose Post-Adoption Fees on "the extraction of groundwater from the basin to fund the costs of groundwater management[.]" (Water Code § 10730.2(a).) The costs of groundwater management include, but are not limited to, the costs of the following:

- (1) Administration, operation, and maintenance, including a prudent reserve.

- (2) Acquisition of lands or other property, facilities, and services.
- (3) Supply, production, treatment, or distribution of water.
- (4) Other activities necessary or convenient to implement the plan.

(Water Code § 10730.2(a).) Although Post-Adoption Fees are authorized to cover broader costs than Pre-Adoption Fees, Post-Adoption Fees may only be imposed on the “extraction of groundwater.” (Water Code § 10730.2(a).) Specifically, a fee on the “extraction of groundwater” may include “fixed fees and fees charged on a volumetric basis, including, but not limited to, fees that increase based on the quantity of groundwater pumped annually, the year in which the production of groundwater commenced from a groundwater extraction facility, and impacts to the basin.” (Water Code § 10730.2(d).)

Fees authorized by SGMA must comply with both the procedural and substantive requirements set forth in SGMA as well as those imposed by the California Constitution, specifically Subsections C and D of Article XIII (respectively “Proposition 26” and “Proposition 218”).

10.3 **Reporting**

GSA with approved Alternatives are required to submit annual reports and resubmit their Alternatives for periodic review every five-years. The following section describes the Annual Report submitted by the District to DWR to meet its reporting requirements under SGMA regulations (23 Cal. Code Regs. §356). At the end of this section, information needed for regular update of the resubmitted Alternative Plan is provided to assist periodic review by DWR.

10.3.1 **Annual Report**

As part of its obligations under the Alternative Plan, the District prepares annual reports of basin conditions and a summary of groundwater management activities that occurred during the preceding water year. The Annual Reports contain groundwater elevation data, annual aggregated groundwater pumpage, total water usage and change in groundwater storage for the preceding water year in accordance with GSA reporting requirements (Wat. Code § 10728).

Since 2016, the District has regularly submitted its Annual Report to DWR by April 1 electronically through the DWR SGMA Portal. Annual Reports are also presented to the District’s Board of Directors at a public hearing and posted on the District’s Groundwater Web Page. In 2020, DWR waived the reporting deadline and accepted Annual Reports for WY 2019 late in response to ongoing health and safety concerns caused by the COVID-19 Public Health Emergency. The District electronically submitted the WY 2019 Annual Report to DWR on April 8, 2020.

10.3.2 **5-Year Assessment and Resubmittal**

The Alternative Plan is a living document, requiring periodic review and assessment to evaluate how well management actions and objectives are meeting sustainability goals. As a GSA, the District must resubmit the Alternative Plan to DWR by January 1 every five years to

ensure the Alternative Plan remains in compliance with the objectives of SGMA (23 Cal. Code Regs. § 355.6). The District will periodically review the Alternative Plan and rely on groundwater information collected over the preceding five-year period to:

- 1) Update descriptions and assessments of current and historical groundwater conditions, changes in groundwater storage, groundwater quality, groundwater-surface water interactions and potential impacts to GDEs.
- 2) Present historical and updated projected water budgets, sustainable yield and an assessment of potential overdraft issues.
- 3) Update assessments, as needed, of potential impacts from climate change; and
- 4) Update the characterization of undesirable results to identify any potential exceedances of minimum thresholds and to assess the impact of those exceedances on the District's ability to stay in conformance with the sustainability goal for the TVS Subbasin.

The District will modify its implementation plan (Appendix M) in response to data gaps identified during periodic review. Appendix N provides a table listing the component requirements of written assessments of the Alternative Plan required for periodic evaluation by DWR (23 Cal. Code Regs. § 356.4).

REFERENCES

2ND NATURE, 2006. Detention Basin Treatment of Hydrocarbon Compounds in Urban Stormwater, South Lake Tahoe, California. March 17, 2006.

2nd Nature. 2010. Quantification and Characterization of Trout Creek Restoration Effectiveness; Focused Development of a Stream Load Reduction Methodology (SLRT), Appendix A of Quantifying the Benefits of Stream Restoration Efforts in the Lake Tahoe Basin: FINAL REPORT, prepared for USDA Forest Service Pacific Southwest Research Station.

2ND NATURE, 2011. Synthesis of Existing Information, Infiltration BMP Design & Maintenance Study Tahoe Regional Planning Agency. Final August 2011.

117th Congress, 2021. H.R. 2467, July 22, 2021.

Belby B., M. Rudd, and C. Krofta. 2009. Presentation of the Upper Truckee River Restoration, Lake Tahoe, California; City of South Lake Tahoe and California Tahoe Conservancy.

Bergsohn, I., 2011. Groundwater Elevation Monitoring Plan – Tahoe Valley South (Basin No. 6-5.01), version 1.0, report prepared by South Tahoe PUD, December 2011.

Birkeland, P. W. 1962. Pleistocene history of the Truckee area, north of Lake Tahoe, California. Stanford, California, Stanford University.

Burch, GJ, ID Moore and J Burns, 1989. Soil hydrophobic effects on infiltration and catchment runoff. *Hydrological Processes*, 3(3): 211-222. doi: 10.1002/hyp.3360030302.

Burnett, J.L. 1971. Geology of the Lake Tahoe basin, California and Nevada: *California Geology*, v. 24, no.7, p. 119-127

California Department of Fish and Game (DFG), 1987. Instream Flow Requirements Lake Tahoe Basin, Stream Evaluation Report 87-1, 100 pp.

California Department of Water Resources (DWR), 2019. Annual Inventory Of Water Use, Lake Tahoe & Truckee River Basins, Calendar Year 2018, September 21, 2019.

California Environmental Protection Agency Office of Environmental Health Hazard Assessment, 2021. Notice to Interested Parties July 30, 2021.

California Regional Water Quality Control Board (CRWQCB), 1995 Water Quality Control Plan for the Lahontan Region, North and South Basins, last amended 2019.

California State Parks. Upper Truckee River Restoration and Golf Course Reconfiguration. Available: <https://restoreuppertruckee.net/background/>. Accessed August 25, 2020.

Coats, R., 2010. Climate change in the Tahoe basin: Regional trends, impacts and drivers, *Climatic Change*, 102, 435–466.

Collins, M., M.M. Arienzo, Z. Harrold, Z. Bradford, and E. Frey. 2019. Case Study on Developing a Citizen Science Protocol for Microplastics in Lake Tahoe. American Geophysical Union, Fall Meeting 2019, abstract #H43O-2283.

Crippen, J.R. and B.R. Pavelka, 1970. The Lake Tahoe Basin, California-Nevada, U.S. Geological Survey Water-Supply Paper 1972, U.S. Geological Survey, Washington, D.C., 62p.

Datry, T., F. Malard, and J. Gibert (2004), Dynamics of solutes and dissolved oxygen in shallow urban groundwater below a stormwater infiltration basin, *Science of the Total Environment*, 329(1-3), 215–229.

Davidson, J.M., M.M. Arienzo, and Z. Harrold. 2019. Microplastic presence in seasonal snow from the Sierra Nevada. American Geophysical Union, Fall Meeting 2019, abstract #H43O-2284.

Dettinger, M., H. Alpert, J. Battles, J. Kusel, H. Saford, D. Fougères, C. Knight, L. Miller, S. Sawyer. 2018. Sierra Nevada Summary Report. California’s Fourth Climate Change Assessment. Publication number: SUM-CCCA4-2018-004.

Division of Drinking Water and Environmental Management, California Department of Health Services (DDWEM-CDHS), 1999. Drinking Water Source Assessment and Protection Program, January 1999.

DFG, 2008. Flow Recommendations to the State Water Resources Control Board. May 27 2008, 31 pp. Available: https://www.waterboards.ca.gov/waterrights/water_issues/programs/instream_recommendations/docs/dfw_ifr.pdf, accessed November 9 2021.

DWR, 2003. California’s Groundwater, California Department of Water Resources Bulletin 118- Update 2003, 265p.

DWR, 2015. Perspectives and Guidance for Climate Change Analysis. California Department of Water Resources, Climate Change Technical Advisory Group. August 2015.

DWR, 2018. Climate Action Plan Phase 2: Climate Change Analysis. California Department of Water Resources.

DWR, 2020. Climate Action Plan Phase 1: Greenhouse Gas Emissions Reduction Plan. California Department of Water Resources.

El Dorado County (EDC), 2000. MtBE Ordinance No. 4553, passed by the El Dorado County Board of Supervisors on March 28, 2000.

Engineering/Remediation Resources Group, Inc. (ERRG), 2019. Final Workplan for Remedial Investigation/Feasibility Study of Groundwater (Operable Unit 2) at Meyers Landfill, Lake Tahoe Basin management Unit, El Dorado County, California. September 2019.

Environmental Protection Agency (EPA), 2018. Gasoline Composition in the U.S. from Three Datasets 1976 – 2017, EPA/600/R-18/258, August 2018.

Eyring, V., Bony, S., Meehl, G. A., Senior, C. A., Stevens, B., Stouffer, R. J., and Taylor, K. E. 2016. Overview of the Coupled Model Intercomparison Project Phase 6 (CMIP6) experimental design and organization, *Geosci. Model Dev.*, 9, 1937-1958, doi:10.5194/gmd-9-1937-2016.

El Dorado Water Agency (EDWA), 2019. Water Resources Development and Management Plan, October 21, 2019.

Flannigan M, AS Cantin, WJ de Groot, M Wotton, A Newberry, and LM Gowman. 2012. Global wildland fire season severity in the 21st century. *Forest Ecology and Management*, 294: 54-61. doi: 10.1016/j.foreco.2012.10.022.

Fogg, G., E. LaBolle, J. Trask, L. Roll, and I. Bergsohn, 2007. Development of Groundwater Resources in the Presence of Contaminant Plumes, South Lake Tahoe, CA, Final Project Report, prepared for California Department of Water Resources, Division of Planning and Local Assistance, 100p.

Fugro Consultants, Inc., 2014. Site Investigation Completion Report Tahoe Meadows Groundwater Investigation, South Lake Tahoe, California, January 2014.

GEI Consultants, 2016a. Results of PCE Investigation for Tahoe Keys Property Owners Association, South Y Area, South Lake Tahoe, California, GEI Project No. 1604010, August 15, 2016.

GEI Consultants, 2016b. South Tahoe Public Utility District South Y Extraction Well Suitability Investigation, GEI Project No. 1601030, June 29, 2016.

Geosyntec Consultants (Geosyntec), 2020. PFAS in Stormwater What We Know, May 2020

Golder Associates Inc. (Golder), 2012. PFAS Monitoring Results, Meyers Landfill, South Lake Tahoe, California, February 15, 2021.

Harrill, J.R., 1977. Hydrologic map, South Lake Tahoe quadrangle: Nevada Bureau of Mines and Geology Urban Map Series, Map 2Af, scale 1:24,000.

Huffman, EL, LH MacDonald and JD Stednick. Strength and persistence of fire-induced soil hydrophobicity under ponderosa and lodgepole pine, Colorado Front Range. *Hydrological Processes*, 15(15): 2877-2892. doi: 10.1002/hyp379.

Huntington, J.L., and R.G. Niswonger, 2012. Role of surface-water and groundwater interactions on projected summertime streamflow in snow dominated regions : An integrated modeling approach, *Water Resources Research*, vol 48, W11524, doi:10.1029/2012WR012319 .

Hyne, N.J., P. Chelminski, P. Court, J. Gorsline, and C.R. Goldman. 1972. Quaternary History of Lake Tahoe, California-Nevada. *Geological Society of America Bulletin* 83; 5, 1435-1448.

Interstate Technology Regulatory Council (ITRC), 2020. History and Use of Per- and Polyfluoroalkyl Substances (PFAS), April 2020.

Kendall, M.G., (1976). *Rank Correlation Methods*. 4th Ed. Griffin.

Kennedy-Jenks, 2019. Final Pre-Design Investigation Report for Remedial Alternatives to Mitigate Tetrachloroethylene Contamination (D1712508), July 10, 2019.

Kennedy Jenks, 2020. Water Demand Analysis in Support of Supplemental Information for the South Tahoe Public Utility District's Application No. A023393, the North Tahoe Public Utility District's Applications No. A024257, A023475, and A023727, and the Tahoe City Public Utility District's Application No. A023479, January 28, 2020.

Kennedy Jenks Consultants, 2021. Final 2020 Urban Water Management Plan, June 30, 2021.

Lahontan Regional Water Quality Control Board (LRWQCB), 2017. Cleanup And Abatement Order (CAO) R6T-2017-0022 Requiring Remediation And Additional Investigation Of PCE Groundwater Contamination, Lake Tahoe Laundry Works, South Lake Tahoe, California, Site Cleanup Program Case T6S043, May 12, 2017.

Lahontan Regional Water Quality Control Board (LRWQCB), 2018. Water Analysis Results for Tahoe Meadows Subdivision, South Lake Tahoe, El Dorado County, SCP Case No. T6S067, July 12, 2018.

Lahontan Regional Water Quality Control Board (LRWQCB), 2021. Notice of Violation, Former Big O Tire Store, 1961 Lake Tahoe Boulevard, South Lake Tahoe, El Dorado County, Site Cleanup Program Case No. T6S034, Geotracker Global ID SL0601729739, August 13, 2021.

Mann, H.B., (1945). Nonparametric tests against trend. *Econometrica: Journal of the Econometric Society*, 13(3): 245-259.

Mansilha, C, A Carvalho, P Guimaraes, and J Espina Marques. 2014. Water quality concerns due to forest fires: polycyclic aromatic hydrocarbons (PAH) contamination of groundwater from mountain areas. *Journal of Toxicology and Environmental Health Part A*, 77: 806-815. doi: 10.1080/15287394.2014.909301.

Markovich, K., H, Manning, A. H., Condon, L. E., & McIntosh, J. C. (2019). Mountain-block recharge: A review of current understanding. *Water Resources Research*, 55. <https://doi.org/10.1029/2019WR025676> .

Martin, DA and JA Moody. 2001. Comparison of soil infiltration rates in burned and unburned mountainous watersheds. *Hydrological Processes*, 15(15): 2893-2903. doi: 10.1002/hyp.380.

Natural Resources Conservation Service, (NRCS), 2021. United States Department of Agriculture. Web Soil Survey, CA693 v.3 (Spatial Version, 9/16/2019). Available online at <http://websoilsurvey.nrcs.usda.gov/>. Accessed December 10, 2016.

Pearson, C., M.B. Hausner, C. Morton, and J.L. Huntington. 2021. Development of Remote Sensing Analyses to Support Management of Mountain Meadows in the Lake Tahoe Basin. Publication No. 41282, Desert Research Institute Division of Hydrologic Sciences, Reno, Nevada.

Plume, R.W., Tumbusch, M.L., and Welborn, T.L., 2009, Hydrogeology of the Lake Tahoe Basin, California and Nevada: U.S. Geological Survey Scientific Investigations Map 3063, 1 sheet.

Pohll, G., I. Bergsohn, and S. Bacon. 2016. Analysis of Basin Conditions Tahoe Valley South (6-5-01) Groundwater Basin, California.

Pohll, G., S. Rajagopal, R. Carroll, and S. Rybarski., 2018. Addressing Basin Management Objectives for the Tahoe Valley South (TVS – 6.5.01) Groundwater Basin. Desert Research Institute, February 5, 2018, 48p.

PRBO Conservation Science. 2011. Projected Effects of Climate Change in California: Ecoregional Summaries Emphasizing Consequences for Wildlife. Version 1.0. <https://nrm.dfg.ca.gov/FileHandler.ashx?DocumentID=27195&inline> (Accessed May 17, 2021).

Robichaud, Peter R. 2000. Fire effects on infiltration rates after prescribed fire in northern Rocky Mountain forests, USA. *Journal of hydrology*. 231-232(1-4): 220-229.

Rohde, M.M., S. Matsumoto, J. Howard, S. Liu, L. Riege, and E.J. Remson. 2018. Groundwater Dependent Ecosystems under the Sustainable Groundwater Management Act: Guidance for Preparing Groundwater Sustainability Plans. The Nature Conservancy, San Francisco, California.

Rohde M.M., L. Saito, and R. Smith. 2020. Groundwater Thresholds for Ecosystems: A Guide for Practitioners. Global Groundwater Group, The Nature Conservancy.

Rohde M.M., B. Seapy, R. Rogers, and X. Castañeda, editors. 2019. Critical Species Look Book: A compendium of California's threatened and endangered species for sustainable groundwater management. The Nature Conservancy, San Francisco, California.

Rowe, T.G., and K.K. Allander. 2000. Surface- and Ground-Water Characteristics in the Upper Truckee River and Trout Creek Watersheds, South Lake Tahoe, California and Nevada, July-December 1996. U.S. Geological Survey Water-Resources Investigations Report 00-4001. 39 p.

Saucedo, G.J, 2008. GIS Data for the Geologic Map of the Lake Tahoe Basin, California and Nevada Department of Conservation, California Geological Survey.

Selmon, M., A. Schwarz, and P. Coombe. 2019. Climate Action Plan, Phase 3: Climate Change Vulnerability Assessment. California Department of Water Resources.

Tahoe Regional Planning Agency, 2020. Lake Tahoe Stream Environment Zone (SEZ) Baseline Conditions Assessment, https://gis.trpa.org/TahoeSEZViewer/SEZ%20baseline%20condition%20assessment_v8.pdf

Singleton, M. J., and J. E. Moran, 2010. Dissolved noble gas and isotopic tracers reveal vulnerability of groundwater in a small, high elevation catchment to predicted climate change, *Water Resources Research*, 46, W00F06, doi:10.1029/2009WR008718.

South Tahoe Public Utility District (District), 2000. Groundwater Management Plan, added as Division 7, Sections 7.1 through 7.13 to the Administrative Code Pursuant to Ordinance No. 477-00, South Tahoe Public Utility District, South Lake Tahoe, CA, 32p.

South Tahoe Public Utility District (District), 2016. Memorandum of Understanding between the South Tahoe Public Utility District and the El Dorado County EDWA, September 15, 2016.

South Tahoe Public Utility District (District), 2017. Amended and Restated Memorandum of Understanding between the South Tahoe Public Utility District and the El Dorado County EDWA, June 15, 2017.

South Tahoe Public Utility District (District), 2018. Tahoe Valley South Subbasin (6-5.01) Annual Report, 2017 Water Year, March 30, 2018.

South Tahoe Public Utility District (District), 2020a. Second Amended and Restated Memorandum of Understanding, June 4, 2020.

South Tahoe Public Utility District (District), 2020b. Groundwater Management Plan Update for the Tahoe South Subbasin, November 23, 2020.

State Water Resources Control Board (SWRCB), 1978. Water Right Decision 1485, Sacramento-San Joaquin Delta and Suisun Marsh, August 1978.

State Water Resources Control Board (SWRCB), 1979. Report on Water Use and Water Rights, Lake Tahoe Basin, October 1979.

Tague, C.; S. Valentine; M. Kotchen. 2008. Effect of geomorphic channel restoration on streamflow and groundwater in a snowmelt-dominated watershed. *Water Resources Research*, Vol. 44.

Tahoe Regional Planning Agency (TRPA), 2012. TRPA Regional Plan, Chapter 2, Land Use Element, Adopted December 12, 2012.

Tahoe Regional Planning Agency (TRPA), 2021. Tahoe Regional Planning Agency Code of Ordinances, Chapter 60.3 Source Water Protection, Effective February 9, 2013, Amended April 28, 2021.

Thodal, C.E., 1997. Hydrogeology of the Lake Tahoe Basin, California and Nevada, and Results of a Ground-Water Quality Monitoring Network, Water Years 1990-92, U.S. Geological Survey Water- Resources Investigations Report 97-4072, U.S. Geological Survey, Carson City, NV, 58p.

United States Environmental Protection Agency (EPA), 2012. Report to Congress: Radon in Drinking Water Regulations, EPA 815-R-12-0002 May 2012.

United States Environmental Protection Agency (EPA), 2020a. Recommendations from the PFAS NPDES Regional Coordinators Committee Interim Strategy for Per-and Polyfluoroalkyl Substances in Federally Issued National Pollutant Discharge Elimination Systems Permits, November 22, 2020.

United States Environmental Protection Agency (EPA), 2020b. Revisions to the Unregulated Contaminant Monitoring Rule (UCMR 5) for Public Water Systems, Fact Sheet for the Proposed Rule. Office of Water (MS-140) EPA 815-F-20-004, December 2020.

United States Forest Service (USFS), 2007. Technical Guide to Managing Ground Water Resources, United States Department of Agriculture Forest Service Minerals and Geology Management Watershed, Fish, Wildlife, Air, and Rare Plants Engineering FS-881, May 2007.

United States Forest Service (USFS), 2008. Forest Service Manual 2800 – Minerals and Geology, Chapter 2880 Geologic Resources, Hazards, and Services (Amendment 2800-2008-1), September 2008.

United States Forest Service, (USFS) 2013. Meyers Landfill Fact Sheet, Update on Remedial Activities and Supplemental Groundwater Investigation, May 2013.

United States Forest Service (USFS), 2014. Proposed Groundwater Management Directive - Forest Service Manual (FSM) 2500 – Watershed and Air Management, Chapter 2560 – Groundwater Resource Management, draft directive for public comment issued May 6, 2014.

U.S. Army Corps of Engineers, 2003. Lake Tahoe Basin Framework Study, Groundwater Evaluation, Lake Tahoe Basin, California, and Nevada, prepared for Lake Tahoe Basin Framework Implementation Study by U.S. Army Corps of Engineers, Sacramento District, Sacramento, CA, 327p.

U.S. Environmental Protection Agency (EPA), 2010. Final Lake Tahoe Maximum Daily Load Report, November, 2010.

U.S. Forest Service Lake Tahoe Basin Management Unit, California Tahoe Conservancy, El Dorado County. 2009. Proposed Action for the Upper Truckee River (Sunset Reach) Restoration Project.

U.S. Geological Survey (California Geological Survey and Nevada Bureau of Mines and Geology), 2006. Quaternary fault and fold database for the United States, accessed December 22, 2016, from USGS web site: <http://earthquakes.usgs.gov/hazards/qfaults/>.

Weiss Associates (Weiss), 2019. Letter to Patty Kouyoumdijan, Executive Officer, Lahontan Regional Water Quality Control Board, RE: South Y Basin Aquifer PCE, South Lake Tahoe, California, Weiss Project No. 489-2135, December 20, 2019.

Weston Solutions, 2012. Final Interim Groundwater Characterization Report, Meyers Landfill, El Dorado County, California, July 2012.

Weston Solutions, 2018. Updated Interim Groundwater Characterization Report, Meyers Landfill, El Dorado County, California, February 2018.

South Tahoe Public Utility District
TVS Subbasin (6-005.01) 2022 Alternative Plan
References and Technical Studies (§ 354.4(b))

Index of journal articles cited in the first five-year update to the Alternative Plan for the Tahoe Valley South Subbasin (6-005.01) but not in the public domain. Articles are named according to the in-text citations (e.g., [First author] et al. 2021).

Burch, GJ, ID Moore and J Burns, 1989. Soil hydrophobic effects on infiltration and catchment runoff. *Hydrological Processes*, 3(3): 211-222. doi: 10.1002/hyp.3360030302.

Coats, R., 2010. Climate change in the Tahoe basin: Regional trends, impacts and drivers, *Climatic Change*, 102, 435–466.

Datry, T., F. Malard, and J. Gibert (2004), Dynamics of solutes and dissolved oxygen in shallow urban groundwater below a stormwater infiltration basin, *Science of the Total Environment*, 329(1-3), 215–229.

Eyring, V., Bony, S., Meehl, G. A., Senior, C. A., Stevens, B., Stouffer, R. J., and Taylor, K. E. 2016. Overview of the Coupled Model Intercomparison Project Phase 6 (CMIP6) experimental design and organization, *Geosci. Model Dev.*, 9, 1937-1958, doi:10.5194/gmd-9-1937-2016.

Flannigan M, AS Cantin, WJ de Groot, M Wotton, A Newberry, and LM Gowman. Global wildland fire season severity in the 21st century. *Forest Ecology and Management*, 294: 54-61. doi: 10.1016/j.foreco.2012.10.022.

Huffman, EL, LH MacDonald and JD Stednick. Strength and persistence of fire-induced soil hydrophobicity under ponderosa and lodgepole pine, Colorado Front Range. *Hydrological Processes*, 15(15): 2877-2892. doi: 10.1002/hyp379.

Huntington, J.L., and R.G. Niswonger, 2012. Role of surface-water and groundwater interactions on projected summertime streamflow in snow dominated regions: An integrated modeling approach, *Water Resources Research*, vol 48, W11524, doi:10.1029/2012WR012319.

Mann, H.B., (1945). Nonparametric tests against trend. *Econometrica: Journal of the Econometric Society*, 13(3): 245-259.

Mansilha, C, A Carvalho, P Guimaraes, and J Espina Marques. 2014. Water quality concerns due to forest fires: polycyclic aromatic hydrocarbons (PAH) contamination of groundwater from mountain areas. *Journal of Toxicology and Environmental Health Part A*, 77: 806-815. doi: 10.1080/15287394.2014.909301.

Markovich, K., H, Manning, A. H., Condon, L. E., & McIntosh, J. C. (2019). Mountain-block recharge: A review of current understanding. *Water Resources Research*, 55. <https://doi.org/10.1029/2019WR025676>

Martin, DA and JA Moody. 2001. Comparison of soil infiltration rates in burned and unburned mountainous watersheds. *Hydrological Processes*, 15(15): 2893-2903. doi: 10.1002/hyp.380.

Robichaud, Peter R. 2000. Fire effects on infiltration rates after prescribed fire in northern Rocky Mountain forests, USA. *Journal of hydrology*. 231-232(1-4): 220-229.

Singleton, M. J., and J. E. Moran, 2010. Dissolved noble gas and isotopic tracers reveal vulnerability of groundwater in a small, high elevation catchment to predicted climate change, *Water Resources Research*, 46, W00F06, doi:10.1029/2009WR008718.

Tague, C.; S. Valentine; M. Kotchen. 2008. Effect of geomorphic channel restoration on streamflow and groundwater in a snowmelt-dominated watershed. *Water Resources Research*, Vol. 44.

SOIL HYDROPHOBIC EFFECTS ON INFILTRATION AND CATCHMENT RUNOFF

G. J. BURCH

Bureau of Rural Resources, Department of Primary Industries and Energy, Canberra, A.C.T. 2600, Australia

I. D. MOORE

Department of Agricultural Engineering, University of Minnesota, St Paul, Minnesota 55108, U.S.A.

AND

J. BURNS

Division of Water Resources, CSIRO, G.P.O. Box 1666, Canberra, A.C.T., 2601, Australia

ABSTRACT

After dry summers or drought, eucalypt forest soils at two sites in southeastern Australia developed hydrophobic or non-wetting surface characteristics that reduced infiltration, measured using a sprinkling infiltrometer. At one site the development of hydrophobic conditions caused the rainfall to runoff conversion efficiency of a forested catchment to increase from 5 per cent to 15 per cent. Under non-hydrophobic conditions at this site, grassland always generated more runoff than forest. However, one major rainfall-runoff was recorded at a time of highly hydrophobic forest soil conditions and this storm generated greater runoff on the forested catchment than the grassland catchment.

At the second site forest soils have naturally highly conductive surface layers because of a dense network of macropores and pathways for preferential flow. Hydrophobic conditions produced by drought caused soil water movement to be confined to only a few of the larger macropores exposed to surface ponded water. Even so, infiltration rates remained relatively high so that the impacts of hydrophobic soils were not translated into increased catchment runoff as at the first site.

KEY WORDS Catchment runoff Water-repellent soils Preferential flow Hydrophobicity Infiltration

INTRODUCTION

Infiltration in undisturbed and disturbed forest catchments is a major determinant of runoff responses. Physical disturbance or land clearing has been shown to reduce the permeability of forest soils and modify their runoff response (Burch *et al.*, 1987; Moore *et al.*, 1986b). The development of surface water repellency has also been observed to reduce infiltration and modify catchment runoff, but these effects are temporally highly variable, less predictable, and have been poorly quantified.

Numerous plants contribute to the development of water repellency in soils (McGhie and Posner, 1981). Jamison (1942) associated non-wetting soils with citrus, Bond (1968) with perennial pastures, De Bano (1969) with chaparral brush and Gilmour (1965) with dry sclerophyll eucalypt and pine forests. Many eucalypts produce litter and exudate that create water repellent soils, usually attributed to plant residues physically coating soil particles (McGhie and Posner, 1980). This coating has a high wetting angle. Other causative agents such as fire (De Bano, 1969) or fungi in decaying plant matter (Bond, 1969) have been described. However, these studies have considered only localized reductions in infiltration and little information is available describing catchment scale responses to transient changes in soil wettability. The objective of the studies reported in this paper was to investigate the effects of water repellent soils on the infiltration and runoff responses of forest and grassland catchments in southeastern Australia.

EXPERIMENTAL DETAILS

Study areas

Catchments in two geographically different locations were studied; at Puckapunyal (37°S, 145°E) in central Victoria, and in Yambulla State Forest (37°S, 150°E), 50 km inland from Eden on the southeast coast of New South Wales (Figure 1). Two small experimental catchments at Puckapunyal were established to investigate the effects of clearing native eucalypt forest on the hydrology of upland terrain. One is vegetated by remnant eucalypt forest (5.0 ha) and the other, which was completely cleared of forest 80 years ago, is maintained in grassland (7.8 ha). The soils are red or yellow podzolics (Dr 2.21, Dy 3.21—Northcote, 1979), characterized by gravelly surface horizons over red or yellow clay subsoils. These soils fall within the U.S. Soil Taxonomy suborder Xeralf. At Yambulla, a single forest catchment (Geebung Creek, 79.6 ha) was under study prior to treatment by conventional logging practices for woodchip production. Details of the catchments are described by Burch *et al.* (1987) and Moore *et al.* (1986a, b), respectively.

At Puckapunyal, rainfall averages 596 mm per year (70 year record; range, 270–1078 mm) and is seasonally distributed, with monthly rainfall in winter being about double that of summer. Infrequent summer storms occur as short duration, high intensity events that present a serious erosion threat, particularly if drought or excessive grazing has exposed the soil surface. In contrast, winter events commonly have intensities of less than 8 mm h⁻¹. Geebung Creek catchment is located in the South Coast Meteorological Division of New South Wales (Bureau of Meteorology, 1981–1987), which has an average rainfall of 945 mm per year (116 year record). Monthly rainfall is highest during summer and early autumn (90 mm per month in January, February and March) and lowest during mid-winter to early spring (56 mm per month in July, August, and September). Much of the rainfall occurs as long-duration storms associated with stationary depressions off the New South Wales coast, although high intensity summer storms are also common.

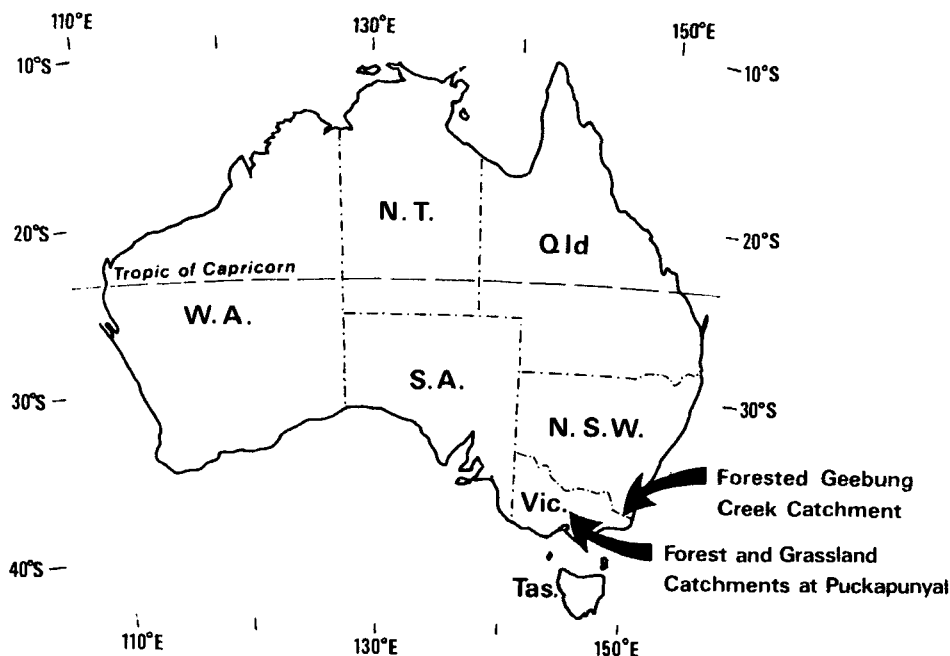


Figure 1. Location of the forest and grassland catchments at Puckapunyal and the forested Geebung Creek catchment

Catchment and Soil measurements

Surface runoff was measured at Puckapunyal between 1981 and 1985 for the grassland, and between 1982 and 1985 for the forest, using identical 0.45 m H-flumes in both catchments. At Geebung Creek streamflow was measured between 1979 and 1986 using a 140° V-notch weir with a rated head of 1.0 m. At both locations RIMCO float recorders and tipping bucket pluviometers were used to record stream stage and precipitation, respectively. Total runoff was partitioned into quickflow (stormflow) and baseflow when required for hydrological analysis using a digital filtering algorithm (program BASUM) following the procedure outlined by O'Loughlin *et al.* (1982).

The soil water status was monitored at both Puckapunyal and Geebung Creek using the neutron attenuation technique (Greacen, 1981). The instrument was calibrated in the field at both locations. At Puckapunyal, regular measurements of the water content of the soil profile (0–0.8 m deep) at five slope positions on transects between the crests and valleys of both catchments recorded successive wetting and drying cycles over a 44 month period. The slope positions instrumented were the depressions (d), lower slopes (ls), midslopes (ms), upper slopes (us), and crests (c). At Geebung Creek periodic soil water measurements (0–1.0 m deep) at 30 locations on two different sites on a single hillslope in the catchment commenced in February 1985.

Water repellency tests, adapted from the method described by Letey (1969), were conducted to detect soil hydrophobicity on the two Puckapunyal catchments. Water containing increasing concentrations of ethanol was applied in drop form to the soil surface (loose litter removed) until a concentration was reached where immediate infiltration occurred. At this concentration the aqueous ethanol drop has a sufficiently small surface tension to overcome the surface water repellency restriction to infiltration. If a high concentration of ethanol is required for incipient infiltration, say above 7 per cent by volume it is indicative of hydrophobic soil. These hydrophobicity tests were conducted at all slope positions (i.e. d, ls, ms, us, and c) in November 1982 and February 1983 during drought conditions. Tests were conducted on soils at two hillslope sites in the Geebung Creek catchment on 20 August 1986.

Infiltration was measured at Puckapunyal and Geebung Creek using a trailer-mounted sprinkling infiltrometer, similar to that described by Morin and Cluff (1980). Rainfall was applied to 1 m × 1 m plots for 20 and 50 minutes, depending on the infiltration and runoff response, at intensities ranging from 26 to 68 mm h⁻¹. Runoff was collected via a flume at 2 minute intervals after flow initiation. Surface ponding was detected using a ceramic tensiometer coupled to a pressure transducer. The tensiometer was placed beneath any loose leaf material but on top of the Ao-horizon.

At Puckapunyal, infiltration was measured under hydrophobic conditions when the soil was dry in April, September, and November 1982, and under non-hydrophobic conditions when the soil was moist in June 1983 and March 1984. Replicated tests were conducted at ms and ls/d hillslope positions. Infiltration sites in the two catchments were chosen to give similar gradients for each slope position. Vegetative cover changed very little in either catchment during 1982 as a result of drought. At Geebung Creek, infiltration was measured in April 1986 under hydrophobic conditions on undisturbed forest sites.

A second series of experiments was conducted at ms positions on the Puckapunyal catchments in November 1982 to examine the effect of repeated wetting on soil hydrophobicity and infiltration. Four wetting cycles (25.6 mm h⁻¹ for 40 minutes) were applied to each site, the interval between each cycle ranged from 6 to 17 hours.

RESULTS

Puckapunyal soils and catchments

The experimental period at Puckapunyal included a severe drought from 1982 to 1983. Annual rainfall for 1981 and 1982 was 619 mm and 270 mm, respectively. This was followed by a wet autumn in 1983 and a total rainfall for that year of 800 mm. Measurements of soil water status at ms locations in both catchments are presented in Figure 2. Pronounced drying of soils occurred each year during the summer, especially in the 1982–1983 drought period. Forest and grassland ms soils had total water storage

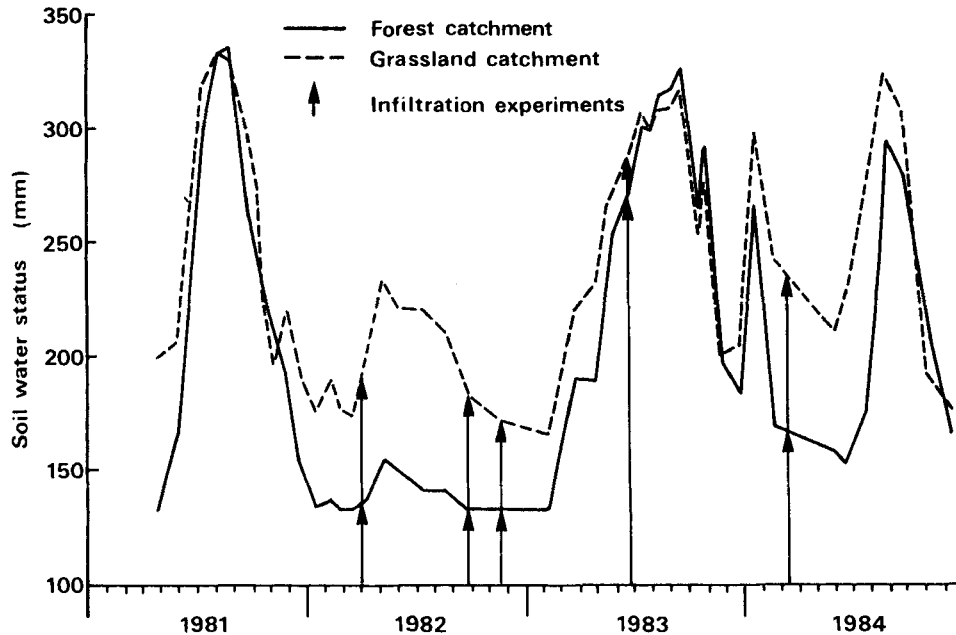


Figure 2. Soil water status versus time at mid-slope positions on the forest and grassland catchments at Puckapunyal

capacities of about 336 mm and 332 mm, respectively. Variations in ms soil water status are indicative of those recorded at higher slope positions (i.e. us and c) but forest depression areas remained wetter overall and stored around 70 mm more water than equivalent grassland soils (Burch *et al.*, 1983).

Ethanol tests for water repellency were conducted at all slope positions in November 1982 and February 1983, during the driest period of record (Figure 2). Results of these tests yielded mean concentrations (percent by volume) of ethanol (\pm one standard deviation) for forest soils of 24.3 ± 5.8 and 16.4 ± 9.7 , respectively, and for grassland soils of 5.9 ± 6.9 and 8.3 ± 7.5 , respectively, for November 1982 and February 1983. Forest soils were consistently hydrophobic on both occasions whereas grassland soils were less hydrophobic. Tests conducted during a wetter period on 29 April 1983 (see Figure 2) yielded values of 1.8 ± 5.7 and 1.1 ± 3.7 for forest and grassland soils, respectively, indicating non-hydrophobic conditions.

Infiltration data for midslope (ms) and lower slope/depression (ls/d) soils of the Puckapunyal catchments are presented in Table I for hydrophobic (September 1982) and non-hydrophobic (June 1983) conditions. Relative infiltration rate (infiltration rate/application rate) versus time curves for hydrophobic and non-hydrophobic conditions at ls/d positions on the forest catchment are compared in Figure 3. Data are presented from single infiltration tests to illustrate the magnitude of the differences in the infiltration responses under hydrophobic and non-hydrophobic conditions.

Infiltration data for hydrophobic soils at ms positions given repeated wetting in November 1982 are summarized in Table II. These data indicate that repeated wetting of the surface soil over a short time produces little reduction in water repellancy of Puckapunyal forest soils but a slight reduction in repellancy of grassland soils.

Irrespective of hydrophobicity effects, relatively low infiltration rates were measured on ls/d soils on the grassland catchment. These soils lacked well-developed macropores and exhibited compacted and impermeable surface layers unlike their forest counterparts which were more porous. Infiltration responses for ls/d soils remained consistent with the usual non-hydrophobic hydrological behaviour of the two catchments reported by Burch *et al.* (1987).

Additional infiltration tests in April 1982 (hydrophobic conditions) and in March 1984 (non-hydrophobic conditions) produced data similar to Table I. Relative infiltration volumes for April 1982

Table I. Mean infiltration characteristics under hydrophobic and non-hydrophobic conditions at midslope (ms) and lower slope/depression (ls/d) positions on the Puckapunyal catchments

Catchment and position	Antecedent soil water content (kg kg ⁻¹)	Rainfall intensity (mm h ⁻¹)	Final infiltration rate (mm h ⁻¹)	Infiltration vol./rainfall vol. (mm mm ⁻¹)	Wetting depth (mm)
Hydrophobic conditions (September 1982)					
Forest					
ms (2)*	0.050	25.6 [‡]	0.75 ± 0.21 [†]	0.22 ± 0.02	16.0 ± 5.0
ls/d(2)	0.057	25.6	1.9 ± 1.6	0.34 ± 0.04	11.0 ± 2.1
Grassland					
ms (2)	0.050	25.6	5.3 ± 0.6	0.56 ± 0.05	21.5 ± 0.7
ls/d(2)	0.046	25.6	2.6 ± 1.2	0.33 ± 0.04	9.9 ± 2.3
Non-hydrophobic conditions (June 1983)					
Forest					
ms (2)	0.21	36.0 [§]	7.9 ± 5.2	0.44 ± 0.09	16.8 ± 2.6
ls/d(3)	0.27	36.0	14.0 ± 6.2	0.67 ± 0.17	42.5 ± 11.5
Grassland					
ms (2)	0.22	36.0	13.4 ± 8.9	0.71 ± 0.17	51.0 ± 14.9
ls/d(3) [¶]	0.20	36.0	2.9 ± 2.5	0.29 ± 0.17	26.3 ± 21.1

*Number in parentheses are the number of replications.

[†] ± one standard deviation.

[‡]Rainfall duration = 50 minutes; rainfall volume = 21.3 mm.

[§]Rainfall duration = 30 minutes; rainfall volume = 18.0 mm.

[¶]For two replicates the rainfall duration was 20 minutes.

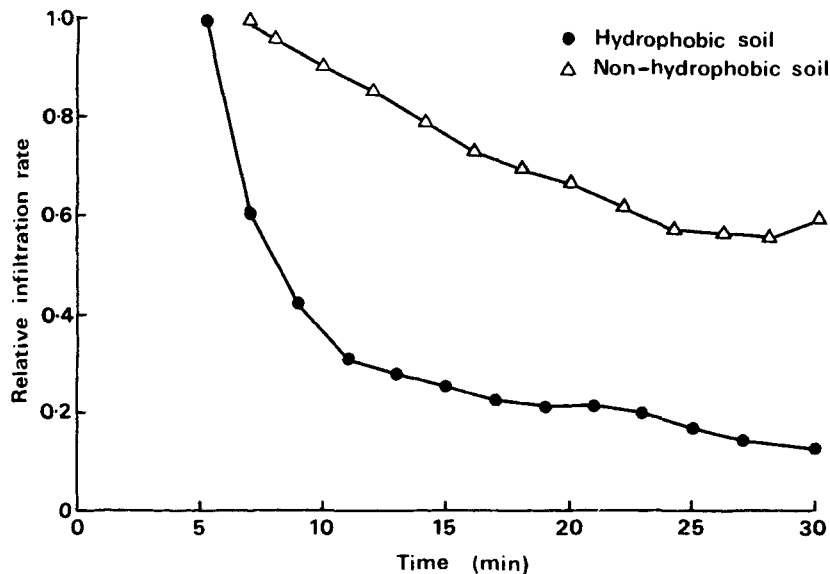


Figure 3. Typical measured relative infiltration rate (infiltration rate/rainfall intensity) versus time relationships of a lower slope/depression site under hydrophobic and non-hydrophobic conditions on the forest catchment at Puckapunyal

Table II. Infiltration behaviour of hydrophobic soils under repeated wetting (25.6 mm h^{-1} for 40 minute durations, at intervals of 6 to 17 hours) at midslope positions on the forest and grassland catchments in November 1982 at Puckapunyal

Run no.	Time between applications (hours)	Time to ponding (s)	Final infiltration rate (mm h^{-1})	Infiltration vol./rainfall vol. (mm mm^{-1})	Wetting depth (mm)
Forest [†]					
1	—	335	1.7	0.37 (0.37)*	9
2	17	298	0.4	0.25 (0.31)	11
3	6	330	0.2	0.22 (0.28)	16
4	17	270	0.2	0.21 (0.26)	17
Grassland [†]					
1	—	965	1.2	0.71 (0.71)	8
2	16	500	0.4	0.39 (0.55)	25
3	7	510	2.4	0.49 (0.53)	27
4	16	390	1.4	0.45 (0.51)	27

*Cumulative values for all previous events in parentheses.

[†]Initial soil water content (0–100 mm soil depth) was 0.061 kg kg^{-1} .

were 0.39 and 0.28 for forest ms and ls/d soils and 0.57 and 0.36 for grassland ms and ls/d soils, respectively. In March 1984, only forest ls/d soils were tested and the relative infiltration volume was 0.65, which is similar to the June 1983 result for non-hydrophobic soils (Table I).

Hydrographs for three consecutive storm events in August 1985 for the two Puckapunyal catchments are presented in Figure 4. Total rainfall for the three storms was 60.3 mm. Forest and grassland catchments yielded 21.8 mm and 63.5 mm of runoff, respectively. Runoff exceeds rainfall for the grassland catchment because of sustained baseflow following 78 mm of rain over the period 4–17 August 1985, just prior to these three events. Substantially higher runoff from the grassland catchment was consistent with catchment responses obtained during seasonally wet autumn and winter periods in years with average or below average rainfall (1985 rainfall was 495 mm). However, catchment runoff responses become similar (both in terms of peak runoff rates and runoff volumes) once forest soils approach saturation, i.e. soil water status exceeds 60 per cent of the available storage capacity (Burch *et al.*, 1987).

An exception to this pattern occurred during a major summer storm event in January 1984 at a time when forest soils were hydrophobic. Catchment hydrographs for this event are presented in Figure 5.

Table III. Infiltration characteristics of hydrophobic and non-hydrophobic soils at Geebung Creek

Site	Slope (%)	Water content (kg kg^{-1})		Rainfall intensity (mm h^{-1})	Duration (min.)	Infiltration rate (mm h^{-1})		Infiltration vol./rainfall vol. (mm mm^{-1})
		Initial	Final			Final	Minimum	
Undisturbed hillslope								
Hydrophobic soils (Type B*)								
2-1	20.7	0.044	—	33.8	30	28.4	26.9	0.85
2-2	20.7	—	0.175	67.6	40	56.1	42.8	0.79
3	20.0	0.055	0.165	67.6	40	51.8	39.0	0.71
Non-hydrophobic soils (Type C*)								
4	18.3	0.216	0.349	67.6	40	55.6	55.0	0.84

*Type B and C soils are described in the text.

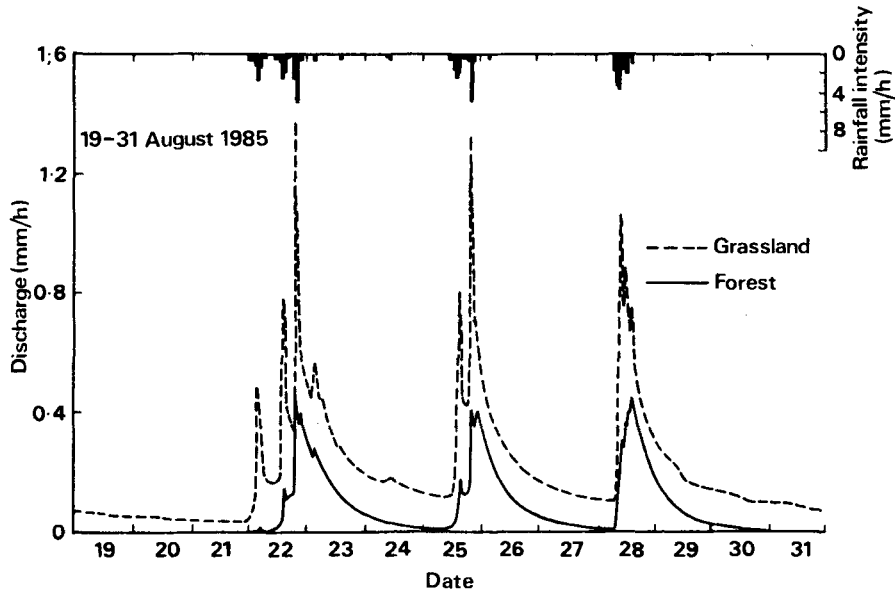


Figure 4. Recorded rainfall-runoff response of the forest and grassland catchments at Puckapunya for three consecutive storm events in August 1985, under non-hydrophobic conditions. Runoff from the grassland and forest catchments was 63.5 and 21.8 mm, respectively

Rainfall for the event was 75 mm and forest grassland runoff was 11.5 mm and 6.8 mm, respectively. The early runoff response was greater from the grassland catchment. However, as rainfall intensified (reaching a maximum intensity of 42 mm h^{-1}) the forest catchment runoff rate rose well above that of the grassland catchment and receded more slowly as the rain eased and stopped (Figure 5). This response is opposite to the usual catchment behaviour described above and illustrated in Figure 4. Under non-hydrophobic conditions the forest runoff is delayed, lower in peak volume, and recedes more quickly than runoff responses from grassland.

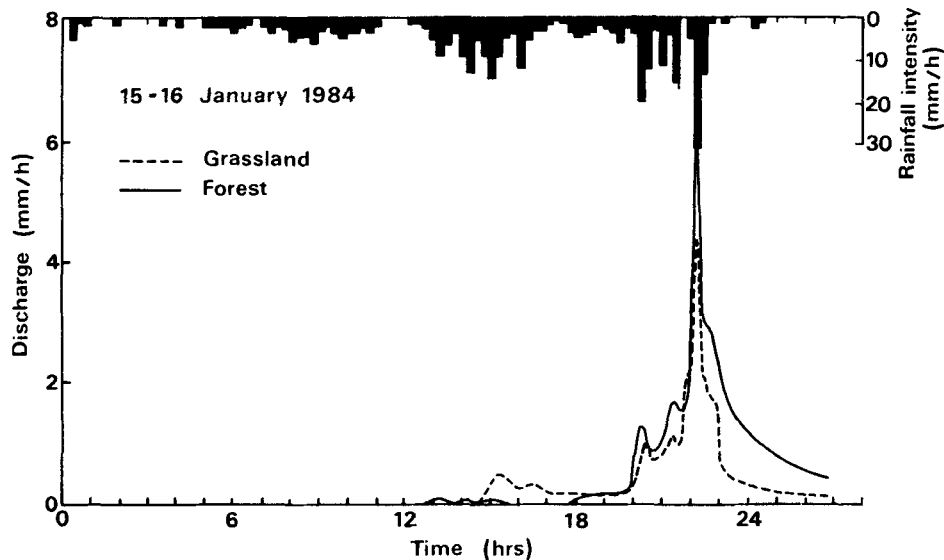


Figure 5. Recorded rainfall-runoff response of the forest and grassland catchments at Puckapunya for the January 1984 storm event when the forest soils were highly hydrophobic. Runoff from the grassland and forest catchments was 6.8 and 11.5 mm, respectively

Two rainfall-runoff events reported in the data presented by Burch *et al.* (1987) in their Table 5, can be compared with the runoff behaviour that was observed in January 1984. These events occurred in May 1983 and August 1984. Ethanol dilution tests conducted on 29 April 1983 showed that the soils were dry, but non-hydrophobic for the May 1983 event. The August 1984 event occurred after a wet winter and no water repellency would have remained. Rainfall recorded for the events in May 1983 and August 1984 was 47.4 mm and 104.8 mm, respectively. Runoff conversion efficiencies for the grassland and forest catchments were 35.4 per cent and 0.1 per cent for May 1983, respectively; 9.1 per cent and 15.3 per cent for January 1984, respectively; and 46.1 per cent and 5.4 per cent for August 1984, respectively. Furthermore, the maximum rainfall intensity was highest for the May 1983 event and lowest for the August 1984 event. Therefore, under non-hydrophobic conditions the grassland runoff conversion efficiency is about an order of magnitude greater than that for the forest catchment. For the January 1984 event this trend is reversed.

Geebung Creek soils and catchment

Between September and December 1985, inclusive, the total rainfall at Geebung Creek was 618 mm, which is 206 per cent of the average (300 mm). This was followed by a very dry period leading up to the infiltration measurements on the catchment in April 1986. The four month rainfall between January and April 1986 was 176 mm, which is only 49 per cent of the average (357 mm). This dry period continued until July. Between January and July 1986, inclusive, the rainfall was 271 mm or 46 per cent of the average (587 mm).

The changing soil water status in the top metre of soil at two locations corresponding to Type B and C soils is presented in Figure 6. Moore *et al.* (1986b) divided the soils on the instrumented Geebung Creek

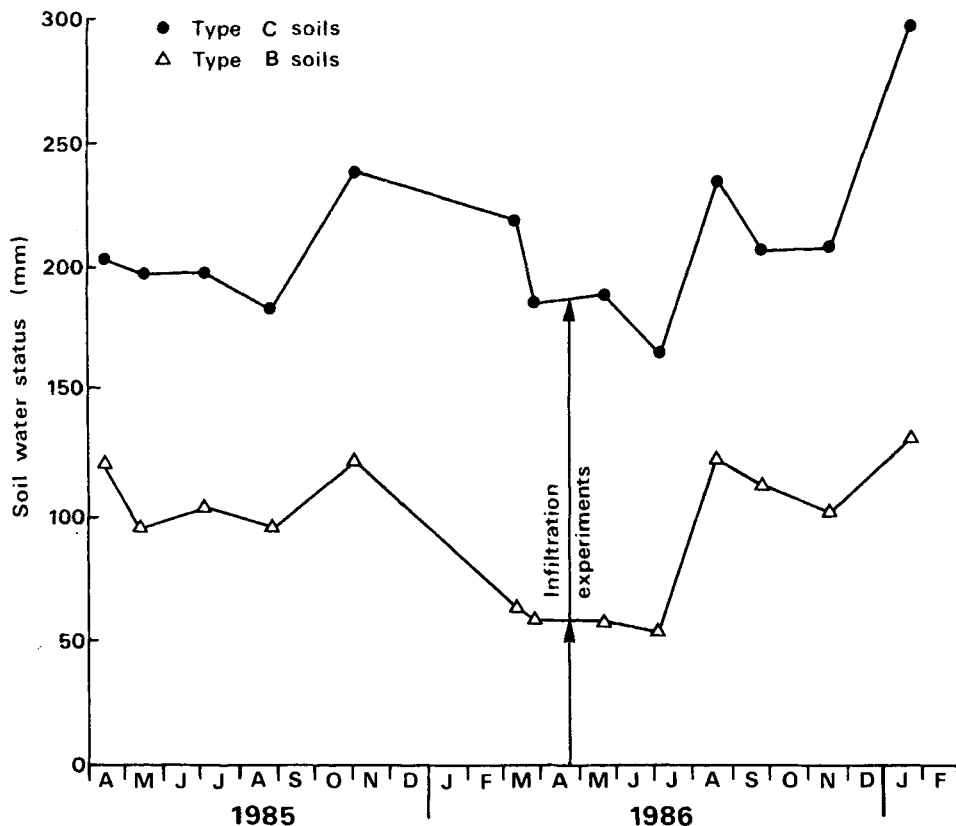


Figure 6. Soil water status versus time at two sites on the instrumented hillslope at Geebung Creek, characteristic of the Type B and Type C soils

hillslope into four groups and defined the Type B soils as: 'yellow duplex soils (Dy2.71–Northcote, 1979) with a loamy-sand A-horizon and a yellow sandy-clay B-horizon'. Type C soils are defined as: 'yellow duplex soils (Dy3.11–Northcote, 1979) with a sandy-clay A-horizon and a mottled medium clay B-horizon'. All soils on the hillslope fall within the U.S. soil taxonomy suborder Aqualf. Figure 6 shows Type B soils retain less water than Type C soils. Type B soils drain downslope towards Type C soils and this accounts for the differences in their response.

Infiltration measurements made in April 1986 on the undisturbed forested hillslope are summarized in Table III. Figure 7 presents the relative infiltration rate (infiltration rate/rainfall intensity) versus time curves for these events. Infiltration Runs 2-1, 2-2, and 3 were conducted on Type B soils, while Run 4 was conducted on a Type C soil. Type B soils were noticeably water repellent, whereas Type C soils were non-hydrophobic. Water repellent Type B soils (Figure 7, Runs 2-1, 2-2, 3) display the following common characteristic, immediately after surface ponding relative infiltration rates rapidly decrease, followed by a gradual recovery to about 0.82. In contrast, the Type C soil (Run 4), gave the usual non-hydrophobic response of a gradual decrease in relative infiltration after ponding, asymptotically approaching a steady-state value. Importantly, both hydrophobic and non-hydrophobic soils approached a similar steady-state relative infiltration rate (0.82).

Following each infiltration event a trench was dug on one side of the plot and the soil water distribution pattern photographed. Figure 8 is a photograph of the pattern observed for plot 3 (hydrophobic soil). It shows a thin surface zone in which there has been little water penetration into the soil profile. This effect is produced by a hydrophobic surface layer restricting water intake into the soil matrix. Superimposed on this pattern is a zone in which relatively deep penetration of water has occurred along channels that are connected to the soil surface.

A rainfall–runoff event on 8–10 July 1986, followed an extended dry period from January to July 1986 and produced no measurable runoff. Rainfall–runoff characteristics of six subsequent events are summarized in Table IV. Runoff conversion efficiencies (runoff volume/gross rainfall \times 100) ranged from 2.0 to 17.2 per cent and quickflow conversion efficiencies ranged from 1.0 to 5.5 per cent. These lie at the lower end of the range of runoff conversion efficiencies previously reported by Moore *et al.* (1986a) for the same catchment. If soil water repellency had an impact on catchment runoff it would be expected that runoff and quickflow conversion efficiencies of the first storm of 4–11 August 1986 would be high. However, they were the lowest of the six storms recorded in Table IV, being only 2.0 per cent and 1.0 per cent, respectively. Ethanol dilution tests for soil water repellency on 20 August indicated no hydrophobicity remained at either soil site tested for infiltration in April 1986.

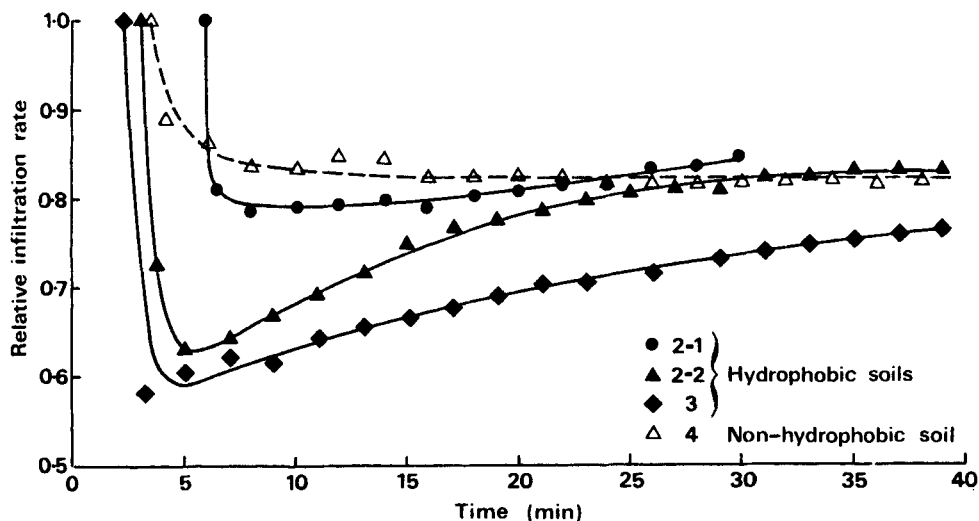


Figure 7. Measured relative infiltration rate (infiltration rate/rainfall intensity) versus time relationships for hydrophobic Type B soils and non-hydrophobic Type C soils on the Geebung Creek catchment



Figure 8. Distribution of infiltrated water in the soil profile of a hydrophobic Type B soil on the Geebung Creek catchment following a simulated rainfall event (Run 3)

Table IV. Rainfall–runoff response of the Geebung Creek catchment following the hydrophobicity inducing dry period between January and July 1986

Events in 1986	Gross rainfall (mm)	Discharge (mm)	Quickflow (mm)	Baseflow (mm)
8–10 July	26.7	—	—	—
4–11 August	66.1	1.3 (2.0)*	0.7 (1.0)	0.6 (1.0)
14–23 August	44.6	3.7 (8.4)	2.1 (4.8)	1.6 (3.6)
12–17 Sept.	57.0	3.1 (5.4)	1.7 (3.0)	1.4 (2.4)
18–26 Sept.	15.4	2.6 (17.2)	0.8 (5.5)	1.8 (11.7)
26–30 Sept.	11.9	1.0 (8.5)	0.3 (2.7)	0.7 (5.8)
2–9 Oct.	23.5	3.4 (14.4)	1.3 (5.4)	2.1 (9.0)

*Numbers in parentheses are the percentage runoff conversion efficiencies (runoff/gross rainfall \times 100).

DISCUSSION

A 5-year record of discharge for the forest and grassland catchments at Puckapunyal shows a consistent pattern of forest producing lower peak discharges and significantly less runoff than grassland (Burch *et al.*, 1987). However, the behaviour of the catchments during the January 1984 event produced the opposite response. Extensively distributed and persistent hydrophobic soils in the forest catchment is believed to be the only possible explanation for this runoff behaviour. On 15 January 1984, 21 mm of low

intensity rain fell intermittently over a 12 hour period prior to the start of the intense runoff producing rainfall. Because no runoff occurred during this time, the amount of rainfall did not exceed the capacity of the infiltration, interception, detention and depression storages for either catchment. As the rainfall intensity increased runoff began, but to sustain the reversal in runoff response for the duration of the entire storm would have required forest soils to remain water repellent throughout.

Infiltration tests indicated that the greatest reductions in permeability occurred with water repellent forest ls/d soils. These soils surround and form the drainage channels that conduct runoff from upslope areas to the catchment outlet. Therefore, they act as important contributory areas for runoff generation if they develop hydrophobic surfaces or become saturated. Crockford and Topalides (personal communication) have recorded similar hydrophobic induced runoff responses in eucalypt forests near Canberra, Australia. Their studies also show water repellency to be more persistent after rainfall in summer than in winter and to reappear more rapidly after drying in summer.

Water repellent soils on the Geebung Creek catchment similarly reduced infiltration. However, infiltration rates at Geebung Creek were an order of magnitude larger than those for Puckapunyal forest soils. In addition, hydrophobic effects were not as persistent as at Puckapunyal (Figure 7), with infiltration rapidly recovering as soil surfaces became saturated. A major difference between the locations was the failure to translate hydrophobic soil effects into increased runoff from the Geebung Creek catchment.

At Geebung Creek the infiltration is controlled by preferential flow through root holes. Figure 8 shows that these macropores provide major conduits for water entry into soils irrespective of water repellency effects. Table III and Figure 7 indicate that macropores alone were conducting water into Type B and C soils at rates of up to 55 mm h^{-1} . Rainfall intensities at Geebung Creek are rarely this high. Hence, for Geebung Creek catchment infiltration via macropores possibly masked any hydrophobicity effects on catchment runoff.

Adopting conventional infiltration theory (Mein and Larson, 1973), that neglects macropore flow, should give similar rates of steady-state infiltration for all three runs presented in Figure 7. This should produce a steady-state relative infiltration rate for Run 2-1 double that of Runs 2-2 and 3. However, they are approximately the same (0.82, see Figure 7). This can occur for varying rainfall intensities only if the area contributing to runoff is constant and virtually impervious, and all water from the remaining area infiltrates. Hydrophobic surface soils with uniform spatial distributions of surface connected macropores (and surrounding areas draining to the macropores) would satisfy this condition. We can, therefore, infer that spatial distributions of surface connected macropores for Runs 2-1, 2-2, and 3 were similar, and that slightly less than 82 per cent of total plot area drained into macropores.

CONCLUSIONS

At Puckapunyal, persistent water repellency greatly reduced infiltration on the naturally more permeable lower slope/depression areas of a forest catchment. Such changes in infiltration behaviour were considered responsible for a reversal in the comparative runoff response of forest and grassland catchments for a summer storm in 1984.

At Geebung Creek infiltration was dominated by macropores and water repellency mainly reduced initial infiltration rates which then recovered. Relatively few macropores would be able to infiltrate the maximum rainfall intensities experienced at this location, even when highly hydrophobic surface conditions exist. As a result, hydrophobic soils have no measurable impact on catchment runoff at this site.

ACKNOWLEDGEMENTS

The authors wish to thank Mr R. Bath, Mr P. Wallbrink, Mr T. Dowling, and Mr J. Brophy, CSIRO, for assistance in obtaining the infiltration data, and Mr R. Bath and Mr J. Margules for digitizing the rainfall and runoff records. Financial assistance for this work was provided in part by the Australian Defence

Department, the Division of Water Resources, CSIRO, Australia, and the College of Agriculture, University of Minnesota, U.S.A. Published as Paper No. 15,638 of the scientific journal series of the Minnesota Agricultural Experiment Station on research conducted under Minnesota Agricultural Experiment Station Project MIN-12-055 and Southern Regional Research Project MIN-12-056 (S-211).

REFERENCES

- Bond, R. D. 1968. 'Water repellent sands', *9th Int. Cong. Soil Sci. Trans., Adelaide*, 339-347.
- Bond, R. D. 1969. 'Factors responsible for water repellence of soils', in De Bano L. F. and Letey J. (Eds), *Water Repellent Soils*, Proc. Symp. on Water Repellent Soils, Univ. Calif. Riverside, 259-264.
- Burch, G. J., Bath, R. K., Moore, I. D., and O'Loughlin, E. M. 1987. 'Comparative hydrological behaviour of forested and cleared catchments in southeastern Australia', *J. Hydrol.*, **90**, 19-42.
- Burch, G. J., Bath, R. K., Spate, A. P., Nicholls, A. O., and O'Loughlin, E. M. 1983. 'Soil water store, infiltration and runoff characteristics of forest and grassland catchments at Puckapunyal in central Victoria', in *Hydrol. Water Resour. Symp. Inst. Eng., Aust. Nat. Conf. Publ.*, **83**(13), 293-299.
- Bureau of Meteorology (Australia) 1981-1987. *Monthly Weather Review, New South Wales*, Department of Science and Technology.
- De Bano L. F. 1969. 'Water repellent soils: a worldwide concern in management of soil and vegetation', *Agric. Sci. Rev.*, **7**, 11-18.
- Gilmour, D. A. 1965. *Hydrological Investigation of Soil and Vegetation Types in the Lower Cotter Catchment*, Unpublished M.Sc. Thesis, Australian National University, Canberra, Australia.
- Greacen, E. L. (Ed.) 1981. *Soil Water Assessment by the Neutron Method*, CSIRO, Melbourne, 98 pp.
- Jamison, V. C. 1942. 'The slow reversible drying of sandy surface soils beneath citrus trees in central Florida', *Soil Sci. Soc. Am. Proc.*, **7**, 36-41.
- Letey, J. 1969. 'Measurement of contact angle, water drop penetration time, and critical surface tension', in De Bano, L. F. and Letey, J. (Eds), *Water Repellent Soils*, Proc. Symp. on Water Repellent Soils, Univ. Calif., Riverside, 43-47.
- McGhie, D. A. and Posner, A. M. 1980. 'Water repellence of a heavy-textured Western Australian surface soil', *Aust. J. Soil Res.*, **18**, 309-323.
- McGhie, D. A. and Posner, A. M. 1981. 'The effect of plant top material on the water repellence of fired sands and water repellent soils', *Aust. J. Agric. Res.*, **32**, 609-620.
- Mein, R. G. and Larson, C. L. 1973. 'Modelling infiltration during a steady rain', *Water Resour. Res.*, **9**, 384-394.
- Moore, I. D., Mackay, S. M., Wallbrink, P. J., Burch, G. J., and O'Loughlin, E. M. 1986a. 'Hydrologic characteristics and modelling of a small forested catchment in southeastern New South Wales. Pre-logging condition', *J. Hydrol.*, **83**, 307-335.
- Moore, I. D., Burch, G. J. and Wallbrink, P. J. 1986b. 'Preferential flow and hydraulic conductivity of forest soils', *Soil Sci. Soc. Am. J.*, **50**, 876-881.
- Morin, J. and Cluff, C. B. 1980. 'Runoff calculation on semi-arid watersheds using a rotadish rainulator', *Water Resour. Res.*, **16**, 1085-1093.
- Northcote, K. H. 1979. *A Factual Key for the Recognition of Australian Soils* (4th Ed.), Rellim Technical Publishers, Adelaide, South Australia, 124 pp.
- O'Loughlin, E. M., Cheney, N. P., and Burns, J. 1982. 'The Bushrangers experiment: hydrological response of a eucalypt catchment to fire', *First Nat. Symp. For. Hydrol., Inst. Eng., Aust. Nat. Conf. Publ.*, **82**(6), 132-138.

Climate change in the Tahoe basin: regional trends, impacts and drivers

Robert Coats

Received: 26 September 2008 / Accepted: 25 August 2009 / Published online: 22 April 2010
© The Author(s) 2010. This article is published with open access at Springerlink.com

Abstract The purpose of this study was to quantify the decadal-scale time trends in air temperature, precipitation phase and intensity, spring snowmelt timing, and lake temperature in the Tahoe basin, and to relate the trends to large-scale regional climatic trends in the western USA. Temperature data for six long-term weather stations in the Tahoe region were analyzed for trends in annual and monthly means of maximum and minimum daily temperature. Precipitation data at Tahoe City were analyzed for trends in phase (rain versus snow), decadal standard deviation, and intensity of rainfall. Daily streamflow data for nine gaging stations in and around the Tahoe basin were examined for trends in snowmelt timing, by two methods, and an existing record for the temperature of Lake Tahoe was updated. The results for the Tahoe basin, which contrast somewhat with the surrounding region, indicate strong upward trends in air temperature, a shift from snow to rain, a shift in snowmelt timing to earlier dates, increased rainfall intensity, increased interannual variability, and continued increase in the temperature of Lake Tahoe. Two hypotheses are suggested that may explain why the basin could be warming faster than surrounding regions. Continued warming in the Tahoe basin has important implications for efforts to manage biodiversity and maintain clarity of the lake.

1 Introduction

On a global scale, the general pattern of climate change is by now well documented, and is no longer scientifically controversial (Oreskes 2004). At the regional and local

R. Coats
Department of Environmental Science and Policy, University of California,
Davis, CA 95616, USA

R. Coats (✉)
2512 9th St., Ste. 7, Berkeley, CA 94710, USA
e-mail: rncoops@ucdavis.edu, coats@hydroikos.com

scales, however, there is considerable variation in the rates of climate change and its hydrologic and ecological impacts (Cohen 1990).

Lake Tahoe is a large ultra-oligotrophic lake lying at an elevation of 1,898 m in the central Sierra Nevada on the California–Nevada border (Fig. 1). The lake is renowned for its deep blue color and clarity. Due to concerns about progressive eutrophication and loss of clarity, the lake has been studied intensively since the mid-

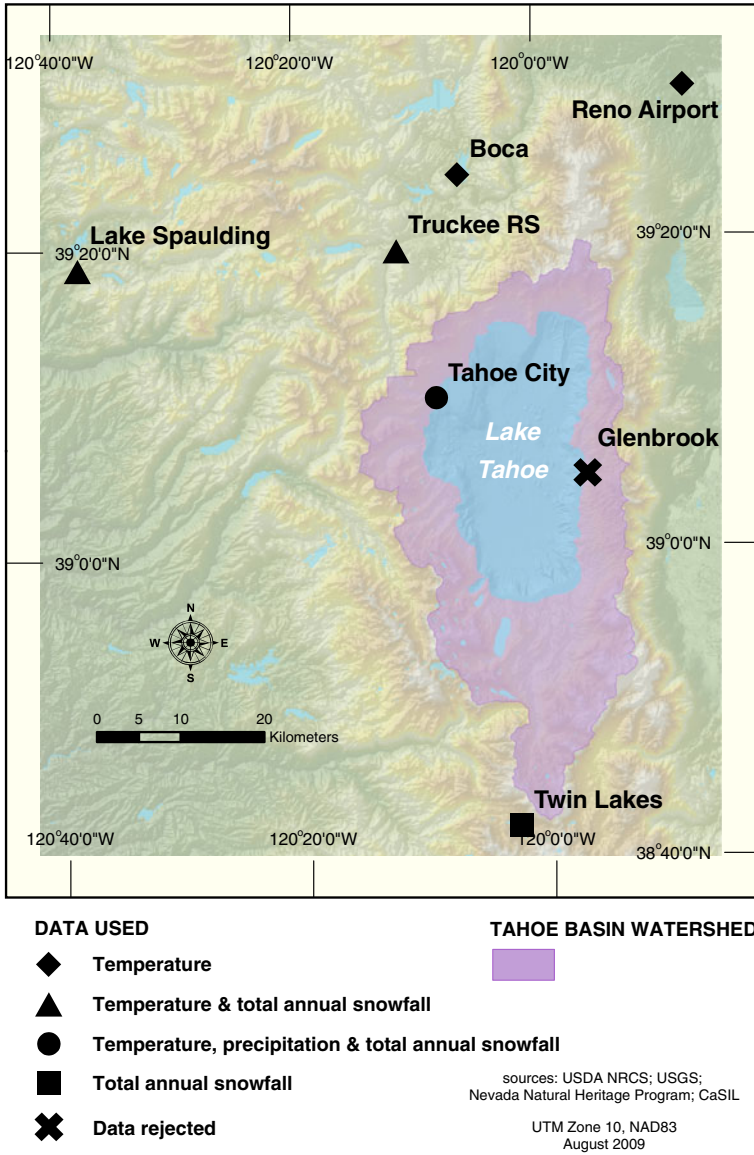


Fig. 1 Map of the Tahoe region, showing locations of weather stations used in this study

1960s, and has been the focus of major efforts to halt the trends in clarity and trophic status. Previous work on the effects of climate change on the lake (Coats et al. 2006) has shown (1) that the lake is warming at an average rate of about $0.015^{\circ}\text{C year}^{-1}$; (2) the warming trend in the lake is driven primarily by increasing air temperature, and secondarily by increased downward long-wave radiation; (3) the warming trend on monthly and annual time scales is correlated with the Pacific decadal oscillation (PDO) and (to a lesser extent) with El Niño–southern oscillation (ENSO); (4) the warming of the lake is modifying its thermal structure, and increasing its resistance to deep mixing.

Recent work on climate change impacts in the western USA has focused attention on the shift in snowmelt timing toward earlier dates (Aguado et al. 1992; Dettinger et al. 2004; Cayan et al. 2001; Dettinger and Cayan 1995; Johnson et al. 1999; Stewart et al. 2005), the shift from snow to rain (Knowles et al. 2006; Regonda et al. 2005), the earlier onset of spring (Cayan et al. 2001); and the effect that these changes will have on water supply in California and throughout the western USA (Hamlet et al. 2005; Barnett et al. 2008; Mote et al. 2005). Pierce et al. (2008) showed that about half of the observed decline in western USA springtime snowpack (1950–1999) results from climate changes forced by anthropogenic greenhouse gases (GHGs), ozone and aerosols. In 2007, the catastrophic Angora Fire in the Tahoe basin showed how legacy vegetation changes can interact with climate change to increase fire hazard, and provided a stunning illustration of the increasing risk of wildfire in the western USA (Westerling et al. 2006; Running 2006; Brown et al. 2004).

Although these trends in climate are largely attributable to increasing atmospheric concentrations of GHGs (Bonfils et al. 2008a), recent modeling work has drawn attention to the role of soot (which is mostly black carbon, or BC) in modifying climate by reducing snow albedo. Hansen and Nazarenk (2004) showed that soot may reduce snow and ice albedo in Northern Hemisphere land areas by as much as 3%, resulting in a climate forcing of $+0.3 \text{ W m}^{-2}$. They found that due to positive feedbacks, the “efficacy” (change in air temperature per unit forcing) of soot is about twice that of CO_2 . Flanner et al. (2007), using a different model, found that the efficacy of BC/soot forcing is more than three times that of CO_2 , since the maximum forcing (due to aging of the snowpack and concentration of soot near the snow surface) coincides with the onset of snowmelt.

The purpose of this study is to document the long-term changes in temperature and precipitation in the Tahoe basin, place those changes in a regional context, and show how climate change is affecting watershed hydrology and the lake itself. A wide variety of issues related to water quality management, including the potential for invasion by exotic species, design of long-term and costly stormwater planning strategies, and restoration of stream environment zones all depend on a more complete understanding of the impact of climate change in the basin.

2 Data sources and methods

Analysis of climatic and hydrologic data in this study includes (a) annual average temperature trends at 6 stations, for the available periods of record; (b) trends in monthly averages of maximum (T_{\max}) and minimum (T_{\min}) daily temperature at 6 stations, 1956–2005; (c) trends in snowmelt timing at nine streamflow gages in and

around the Tahoe basin; (d) the trend in the fraction of precipitation falling as snow at Tahoe City, 1910–2007; (e) the trend in exceedances of the 95th percentile daily rainfall amount at Tahoe City; (f) trends in the average annual and deseasonalized average daily temperature of Lake Tahoe; (g) the statistical relationships between local climatic variables and the PDO and ENSO. The climatic and hydrologic variables were selected for their likely importance to the future condition of Lake Tahoe.

2.1 Air temperature

Daily temperature (maximum, minimum and average), and precipitation data were obtained from the Western Regional Climate Center (WRCC 2008) for 16 stations within 35 km of Lake Tahoe, and screened for length and completeness of record. Of these, six stations (shown in Table 1) were selected for detailed analysis. Figure 1 shows the weather station locations, and the type of data used from each.

Three of the selected stations—Reno, Tahoe and Lake Spaulding—are part of the US Historical Climatology Network (HCN), with records through 2005 available online (Williams et al. 2008). For these stations, the monthly and annual precipitation records have been adjusted to remove the time-of-observation bias, “discontinuous inhomogeneities” resulting from station moves and changes in instrumentation, and effects of urbanization. The adjustment for inhomogeneities requires creating a difference series between a station and its neighbors, and using the Wilcoxon rank-sum test to identify inhomogeneities and calculate adjustment parameters (Karl and Williams 1987).

The adjustment for the effects of urbanization is based on a power relationship (developed for the entire USA, for four seasons) between the urban–rural temperature difference and population, and uses census data to adjust the HCN monthly averages of T_{\max} and T_{\min} through 2005 (Karl et al. 1988). The urbanization effect at individual stations will of course vary from the regression-derived adjustment, and temperature trends from rapidly urbanizing areas must still be reviewed with caution. Comparing the raw monthly data with the “de-urbanized” data for Tahoe City shows an estimated maximum urbanization effect (by 2005) in the average temperature of 0.14°C in winter, 0.11°C in spring, and 0.16°C in summer and fall.

Table 1 Weather stations used in the analysis of regional trends

Station	Coop ID No.	Lat.	Long.	Elev. (m)	Period of record used	HCN?
Reno	266779	39°30' N	119°47' W	1,341	1889–2005	Yes
Boca	040931	39°06' N	120°06' W	1,699	1937–2006	No
Truckee RS	049043	39°20' N	120°11' W	1,829	1935–2006	No
Tahoe	048758	39°10' N	120°08' W	1,900	1910–2005	Yes
Lake Spaulding	044713	39°19' N	120°38' W	1,573	1914–2005	Yes
Sierra average, WRCC	–	–	–	–	1895–2007	–

Data from the Glenbrook station (263205) were analyzed but discarded due to an effect of station relocation. WRCC refers to the Western Regional Climate Center, Reno, NV

For the non-HCN stations (Boca, Truckee Ranger Station and Glenbrook), copies of the Station History Reports, were obtained from the National Climate Data Center, and reports from NOAA's Multi-Network Metadata System (National Climate Data Center 2008) were obtained on-line. These reports aided in interpretation of possible effects of station moves and bias introduced by changes in the time of observation.

In addition, monthly and annual averages of T_{\max} and T_{\min} for the Sierra region, 1895–2007 were obtained from the Western Regional Climate Center (2008). The Cooperative (coop) station data for the 21 Sierra stations from which the averages were derived have been screened for outliers, and values adjusted for inhomogeneities. The stations are located between latitudes 36.48° N and 39.57° N, longitudes 118.83° W and 121.93° W, and elevations ranging from 397 m to 2140 m.

The reported ground elevation of the Truckee Ranger Station (RS) weather station changed 4 times between, 1933 and, 1983, varying between 1824 m and 1835 m, but the records show no change in latitude and longitude in this period (reported as 39.33333° N, 120.18330° W). Beginning in 1991, the location was reported as “Truckee RS Workyard”, which is located 1.53 km southwest of the Ranger Station. In 2000 the weather station was apparently moved 700 m northeast, with the elevation remaining at 1,835 m. Both the Workyard and the Ranger Station are located on gently sloping to flat terrain, above the valley floor. In December 2006 the weather station was moved to the new Workyard location at an elevation of 1,775 m, near the Truckee River. This new location may be more influenced by cold air drainage and intense nighttime inversions than the previous locations, but data from the new location were not used here.

There is a gap in the Truckee RS data from, 1920–1934. During the period 1904–1919, the station was moved several times, and the T_{\max} and T_{\min} temperature records for that period show standard deviations more than twice those of the 1935–2006 period. The US Weather Bureau's Station History Report for 1920 characterized the record as “poor”, and the station was closed. Data from the 1904–1920 period were not used in calculating annual average temperatures.

The time of observation at Truckee RS is not given in the station history reports, but the Forest Service staff has used a hygrothermograph as back-up for the max–min thermometer. Up to May 2007 T_{\max} and T_{\min} were read from the chart trace when the thermometer could not be read at the designated time.

For Truckee RS, about 560 T_{\max} and T_{\min} values were missing in the daily temperature record for the period 1956–2005. Of these, 520 were filled in by linear regression with records from nearby Donner Memorial State Park (5.3 km WSW; $R^2 = 0.95$ and 0.91 , and $SE = 2.1^\circ\text{C}$ and 1.9°C , respectively, for T_{\max} and T_{\min}), and an additional 40 values were filled in by seasonal (winter, spring, summer, fall) regressions with the temperature record at Tahoe City (18.5 km SSE, $R^2 = 0.82$ – 0.93 , $SE = 1.6$ – 2.7°C).

Since December, 1936 the Boca station has been located at the Bureau of Reclamation office, about 600 m south of the Boca Reservoir dam. The elevation decreased by 3 m in 1982, and is now at an elevation of 1,700 m. The Station History Report does not give the time of observation. Boca holds the record for the lowest temperature ever recorded in California: -45°F (-42.8°C) on January 20, 1937.

The history of the Glenbrook station suggests possible problems in the data. From 1950 to 1972, the station was located in a small saddle, about 500 m east of and 52 m above the lake. In 1972 it was moved about 250 m south, and 6 m higher. In 1975 it was moved to its present location 800 m south and 330 m east of its initial location, and 37 m above the lake. Furthermore, the first location was somewhat sheltered from direct wind off the lake by a small knoll to the west, whereas since 1972, the station has been more exposed to afternoon wind, and possibly to increased night-time cold air drainage. To complicate matters, the instrument type was changed from a max–min mercury thermometer to a digital maximum–minimum temperature system (MMTS) in 1983, which is currently located in a lawn that is irrigated twice daily during summer months. The time of observation was changed from 6:00 PM to 5:00 PM in 1960, and from 5:00 PM to 4:00 PM in 1975. Changes in the time of observation are known to introduce bias in a temperature record (Redmond 1991, 1992; Karl et al. 1986). In order to measure the consistency of long-term temperature records, I installed carefully-calibrated temperature loggers at the pre-1975 and present instrument sites, and measured temperature at 15 min intervals from early July to early September, 2008.

Preliminary plotting and inspection of the long-term trends showed upward trends in annual averages of T_{\max} and/or T_{\min} at most sites, but a cooling trend in maximum daily temperature from the mid-1930s to the mid-1950s at some sites. For this reason, the half-century period, 1956–2005, with its generally monotonic increases and more reliable data, was selected for detailed analysis of time trends in monthly average air temperature.

With the Glenbrook data discarded due to the possible effect of station relocation, I tested the annual averages of T_{\max} and T_{\min} over the available period of record for time trends, using the non-parametric Kendall trend test. This test is widely used for testing time trends in environmental variables; it has advantages over ordinary least squares (OLS) regression in that normality of the residuals is not required, and it is more resistant to leveraging by extreme events. (Helsel et al. 2005; Helsel and Frans 2006). The Kendall test calculates the “Theil slope” as the median of slopes of all possible lines between data pairs.

Time series data often show significant autocorrelation, which can increase the likelihood of rejecting the null hypothesis (that is, that there is no trend), when it should be accepted (von Storch 1999). To address this problem, I calculated T_0 , the “time between effectively independent observations”, using a simple approximation given by Trenberth (1984). Where necessary, I then “pruned” the data, discarding enough so that the time between observations was $\geq T_0$.

Using the same test, the annual series of monthly averages of T_{\max} and T_{\min} were tested for time trends at each of the five sites. As with the annual averages, I tested for serial correlation, and pruned the data where necessary. The monthly averages of T_{\max} showed very little serial correlation, but most of the monthly averages of T_{\min} for spring, summer and fall from Reno, Truckee and Tahoe City showed correlation coefficients exceeding 0.20, with a T_0 of 1.5–2.5 years.

It would be useful to know if the trends in monthly temperature are consistent across the region, and across months. I used the method given by van Belle and Hughes (1984) to test for homogeneity of trends between months, between sites, and for the interaction between sites and months in the trends. This nonparametric (χ^2) test uses Z values from the Kendall test, and is formatted like an analysis of variance (ANOVA).

2.2 Precipitation and snowmelt

The total snowfall water equivalent at Tahoe City was calculated for each year by summing the precipitation that occurred on days with average temperature below freezing. The slope of the time trend in snowfall as fraction of total annual precipitation was estimated (and its significance tested) using the Kendall test. Some modeling studies (e.g. Hamlet et al. 2005) have used thresholds at -0.5°C and $+0.5^{\circ}\text{C}$ for partitioning precipitation between rain and snow, with a linear change between the thresholds for days with mixed rain and snow. It seems unlikely, however, that this more nuanced approach would make much difference in the time trend.

An increase in the intensity of rainfall may be at least as important as a trend in the annual amount, especially with regard to erosion potential. Kim (2005) modeled the effect of increasing CO_2 concentrations on the 95th percentile of daily rainfall in the northern Sierra, that is, the amount equaled or exceeded on 5% of the rainy days. In the relatively small watersheds of the Tahoe basin, the duration of rainfall that controls flood frequency is on a time scale of hours, and the largest floods are associated with rain-on-snow events. Unfortunately, hourly rainfall data for the basin are not available over a long enough time period to examine trends. To test for a time trend in daily rainfall intensity, I found the 95th percentile rainfall amount (1910–2007), and compared it to the 2-year annual maximum daily rainfall. I then counted the number of times per half-decade that the 95th percentile value is equaled or exceeded, and tested for a time trend with the Kendall test.

There are over 20 streamflow gages currently in operation in the Tahoe basin, but only five of these (with continuous or near-continuous records dating from 1972 or earlier) are useful for analyzing trends in snowmelt timing. These are the most downstream gages on Ward, Blackwood, Trout and Third Creeks, and the Upper Truckee River. For each station, I identified the date of the maximum discharge in April through July in the five streams, and then scrolled through the record for Blackwood Creek (the watershed with the highest mean annual precipitation) to find sharp runoff peaks that appeared to result from rainstorms. Two suspicious peaks were found and checked against rainfall in the Tahoe City record. The dates for these peaks at all stations were then replaced as needed by peaks not influenced by rainfall.

Since wet (heavy snowfall) years generally have later snowmelt peak timing (SMPT) than dry (low snowfall) years, I removed the effect of total annual snowfall with locally weighted scatterplot smoothing (LOWESS; Helsel and Hirsch 1995) of the plot of SMPT versus total annual snowfall, and then tested for time trends in the residuals, using the Kendall test (with data pruning where T_0 exceeded 1.5 years). I then averaged the Theil slopes of the time trend for the five streams, to estimate the average rate of shift in SMPT. I also tried total annual discharge as the ancillary variable, but it was not as effective as total annual snowfall, possibly because a shift from snow to rain is uncoupling the relationship between timing of the snowmelt and total annual precipitation.

For comparison of shift in SMPT for streams inside and outside of the Tahoe basin, I searched for nearby gaging stations outside of the Tahoe basin that are snow-dominated, have records at least as long as the Tahoe basin streams, and are relatively unaffected by dams and diversions. The stations best meeting these criteria are Sagehen Creek (north of Truckee), the South Fork Yuba River (east of Lake Spaulding), and the East and West Forks of the Carson River (south of the Tahoe

basin). For total annual snowfall (the ancillary variable in the Kendall trend test), I used the Truckee record for Sagehen Creek, the Lake Spaulding record for the S. Fk. Yuba, and the record for twin lakes (coop ID no. 49105) for the Carson tributaries.

Four of the five Tahoe basin streams showed monotonic trends toward earlier SMPT, but Blackwood Creek, with unusually early snowmelt in the period 1961–1970, was an exception. Blackwood Canyon was subjected to much heavier logging during the 1950s and early 1960s than the other four watersheds, and it is possible that the opening of the forest canopy accelerated snowmelt, shifting it toward earlier dates. At the near-by Central Sierra Snow Laboratory, the rate of snowmelt over an entire melt season averaged 75% higher in a clearing than in the forest; in years with long-lasting snowpack, the average melt rate after May 1 was 25 mm day⁻¹ in the open vs. 15 mm day⁻¹ in the forest (Kattelmann 1991). Re-growth of the forest canopy in Blackwood Canyon could thus delay snowmelt, offsetting the effect of a warming trend. For this reason, the period 1961–1970 for Blackwood Creek was not considered in the analysis.

In 1960, 10.5% of the catchment of Sagehen Creek upstream of the USGS gaging station was burned in the 45,000 ac Donner Ridge Fire (Johnson and Needham 1966). Reforestation and regrowth since then could have played a minor role in retarding snowmelt, although the fire was so intense in some areas that re-growth has been slow.

A number of studies on snowmelt timing in the West have used the “center timing”, or date of the centroid of the annual hydrograph (Barnett et al. 2008; Stewart et al. 2005). This is calculated as the discharge-weighted mean day in the water year (WY), that is: $CT = \sum (t_i q_i) / \sum (q_i)$, where t_i = the i th day in the water year, and q_i = discharge on the i th day. To provide a basis for comparison with other regional studies, I calculated the annual CT for all nine gaging stations in the sample (both inside and outside of the basin).

2.3 Lake temperature and thermal structure

Previous calculations of average temperature of Lake Tahoe ran from December, 1969 to October 2002 (Coats et al. 2006). Using an identical methodology the record for the Lake was updated through August 2007. This included calculating the temperature at 400 m, indices of lake stability, the volume-averaged daily lake temperature, the monthly average lake temperature, and the annual maximum, minimum and average lake temperature. The trend in the latter was tested with the Seasonal Kendall test, with data pruning where necessary.

2.4 Influence of the Pacific decadal oscillation and El Niño/southern oscillation

Several studies have shown that ocean circulation and temperature patterns, particularly the Pacific decadal oscillation (PDO) and El Niño/southern oscillation (ENSO) are statistically related to warming trends in the western USA (Arhonditsis et al. 2004; Mantua et al. 1997; LaDochy et al. 2007), the earlier onset of snowmelt runoff (Cayan et al. 2001; Dettinger and Cayan 1995; Stewart et al. 2005), the shift in precipitation from snow to rain (Knowles et al. 2006; Regonda et al. 2005), declining snowpacks (Mote et al. 2005; Hamlet et al. 2005), and earlier onset of spring (Cayan et al. 2001). To examine the relationship between these large-scale climatic

Table 2 Local climatic and hydrologic variables tested by regression against the Pacific decadal oscillation (PDO) and mean ENSO index (MEI)

Dependent variable	PDO	MEI
Monthly ave. of deseasonalized T_{\max} and T_{\min}	Monthly values	Monthly values
April–June deseasonalized T_{\max} and T_{\min} (1914–2002)	Apr–June monthly values	MARAPR–MAYJUN
Percent of annual water year (WY) precip. as snow	Ave. of Nov–Mar values	Ave. of OCTNOV–FEBMAR
Day of peak snowmelt discharge	Ave. of Apr–Jun values	Ave. of MARAPR–MAYJUN
Monthly ave. of deseasonalized daily lake temp, lagged 1, 2 and 3 months	Monthly values	Monthly values

Adjusted P values were calculated from the pruned data set, to account for serial correlation (see Section 2.1)

descriptors and the dependent climate variables in the Tahoe basin, I used OLS regression to test (1) deseasonalized monthly average T_{\max} and T_{\min} air temperature at Tahoe City, (2) water year percent precipitation as snow; (3) SMPT, adjusted for total annual snowfall, and averaged over the five basin streams; and (4) monthly average of deseasonalized volume-averaged lake temperature. For the latter, lake temperature was lagged 1, 2, and 3 months behind PDO and MEI, since the lake would not be expected to respond instantly to large-scale atmospheric and ocean temperature patterns.

Monthly values of the PDO were obtained from the Joint Institute for the Study of the Atmosphere and Ocean (JISAO 2008). For the ENSO, I used the bimonthly values of the Multivariate ENSO Index (NOAA 2008). Table 2 shows the explanatory dependent variables used in the tests. Since the PDO and MEI values are somewhat correlated ($r = 0.57$), simple multiple regression would not be helpful.

3 Results

3.1 Air temperature trends

The slope of the trends in T_{\max} and T_{\min} depends on the period of record, and varies with location. Figure 2a–f shows the time trends in annual averages at five stations, along with the regional average for the Sierra Region. Table 3 shows the results of the Kendall trend tests for significance of slopes. The adjusted P values are based on the Kendall test using pruned data, to eliminate the “over-rejection” problem associated with serial correlation.

The strongest upward trends in annual averages over the available periods of record were in T_{\max} at Reno, and T_{\min} at Tahoe City. Truckee and Boca showed significant upward trends in both T_{\max} and T_{\min} . At Lake Spaulding, there was no significant time trend in either T_{\max} or T_{\min} over the period of record (1914–2005).

The data from the temperature loggers installed at the pre- and post-1975 Glenbrook sites showed that T_{\max} averaged 0.53°C cooler, and T_{\min} 1.36°C cooler at the current site than at the pre-1975 site (P by one-tailed paired t tests $<10^{-7}$), for the period July 2 to September 5, 2008. The lower T_{\max} is probably explained by lawn

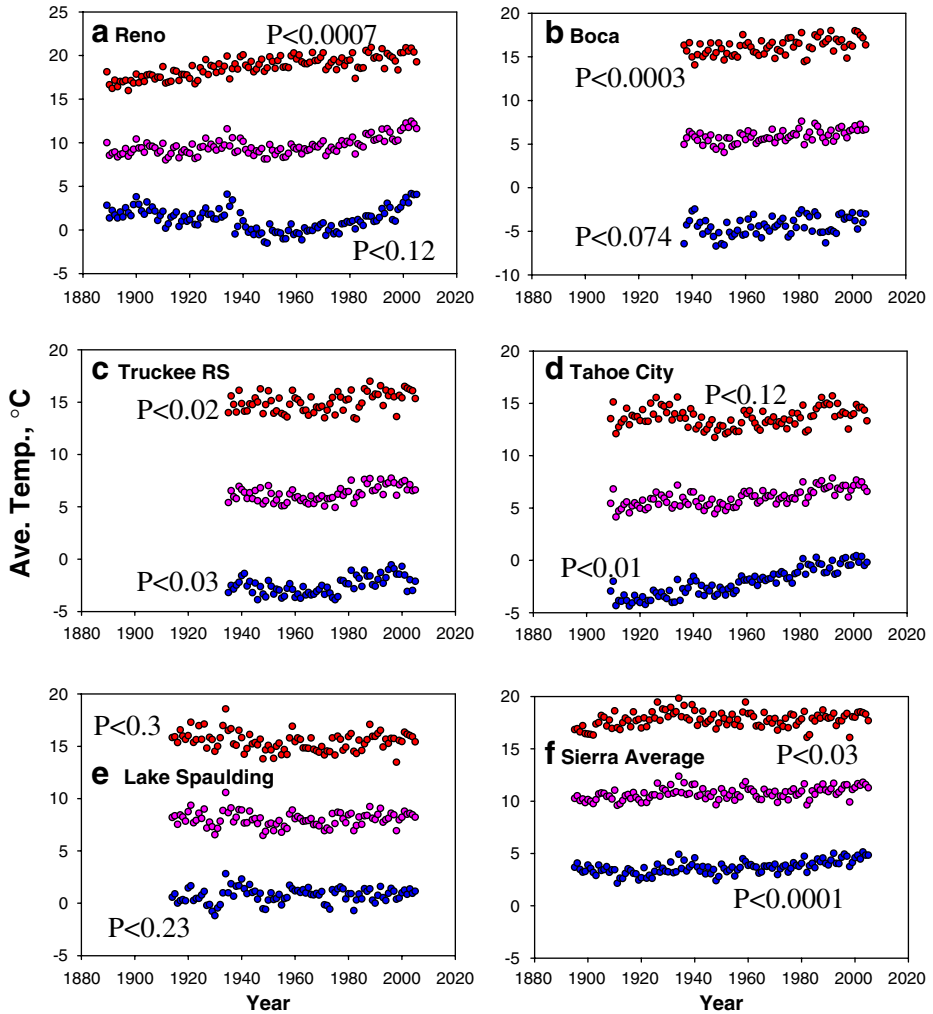


Fig. 2 Annual average air temperatures (T_{max} [red], T_{ave} [pink] and T_{min} [blue]) at **a** Reno, 189–2005; **b** Boca, 1935–2005; **c** Truckee Ranger Station, 1935–2006; **d** Tahoe City, 1909–2005; **e** Lake Spaulding, 1945–2005; and **f** average for Sierra Nevada, 1914–2005, from WRCC. See Table 3 for trend test results

irrigation, and the lower T_{min} by greater exposure to cold air drainage. The long-term record for Glenbrook is considered unusable.

Annual averages, however, may conceal some interesting differences in trends by month. Figure 3a–f show the Theil slopes and significance level by month, at five stations (Reno, Boca, Truckee, Tahoe City and Lake Spaulding) along with the monthly slopes for the Sierra Region, for the period 1956–2005. As shown by the results of the test for homogeneity of trend slopes of these 5 stations (Table 4), for T_{min} there were highly significant differences among sites across months, and among months across sites, but there was no consistent month-site interaction. For T_{max} ,

Table 3 Kendall trend test results on annual averages of T_{\max} and T_{\min} , for period of record

Station	Corr. Coeff.	Theil Slope (°C year ⁻¹)	$P <$	Adj. $P <$
For ann. ave. of T_{\max}				
Reno AP	0.588	0.029	0.00005	0.0007
Boca	0.330	0.024	0.0001	0.0003
Truckee RS	0.252	0.018	0.0017	0.018
Tahoe	0.107	0.006	0.12	–
Lake Spaulding	–0.075	–0.003	0.289	–
Sierra average	0.139	0.005	0.017	0.030
For ann. ave. of T_{\min}				
Reno AP	–0.098	–0.007	0.116	–
Boca	0.224	0.019	0.006	0.074
Truckee RS	0.273	0.018	0.0007	0.030
Tahoe	0.734	0.047	0.00005	0.009
Lake Spaulding	0.089	0.003	0.23	–
Sierra average	0.438	0.012	0.00005	0.00005

the trend slopes for months were heterogeneous when averaged across sites, but the trend slopes for sites were homogeneous when averaged over months, and there was no significant site-month interaction.

The strongest warming trends in the period 1956–2005 were in T_{\min} at Reno and Tahoe, especially in summer months. These stations also showed some upward trends in T_{\max} , but these were not as strong as the trends in night-time temperature. At Truckee and Boca, both T_{\max} and T_{\min} trended upward, especially in winter and spring. In contrast to Reno and Tahoe, warming rates were lower in the summer and minimal in the fall. Lake Spaulding showed cooling trends in both T_{\max} and T_{\min} in December, but these are offset by increases in spring and summer in both T_{\max} and T_{\min} .

3.2 Precipitation and snowmelt timing

Analysis of the precipitation and temperature records at Tahoe City (1910–2007) shows that the percent of total annual precipitation falling as snow (defined here as precipitation falling on a day with average temperature at or below freezing) is decreasing. Figure 4 shows the trend. The OLS regression slope is -0.19% year⁻¹ and the Theil slope is -0.18% year⁻¹, with $P < 0.0004$ and insignificant serial correlation. Such a shift has important implications for erosion and sediment transport in the Tahoe basin, since these processes tend to be more active in a rainfall regime than in a snowfall regime.

The total annual precipitation at Tahoe City (1910–2007) seems to trend slightly upward, (0.13 cm year⁻¹) but the apparent trend is not statistically significant ($P < 0.21$). The interannual variability, however does seem to be increasing. For the decadal standard deviation, the tau correlation coefficient is 0.42, with $P < 0.1$), suggesting that wet years are getting wetter, and dry years getting drier. This has important implications for vegetation and soil erosion. Vegetation stressed (or burned) during drought years will provide less protection against soil erosion during wet years.

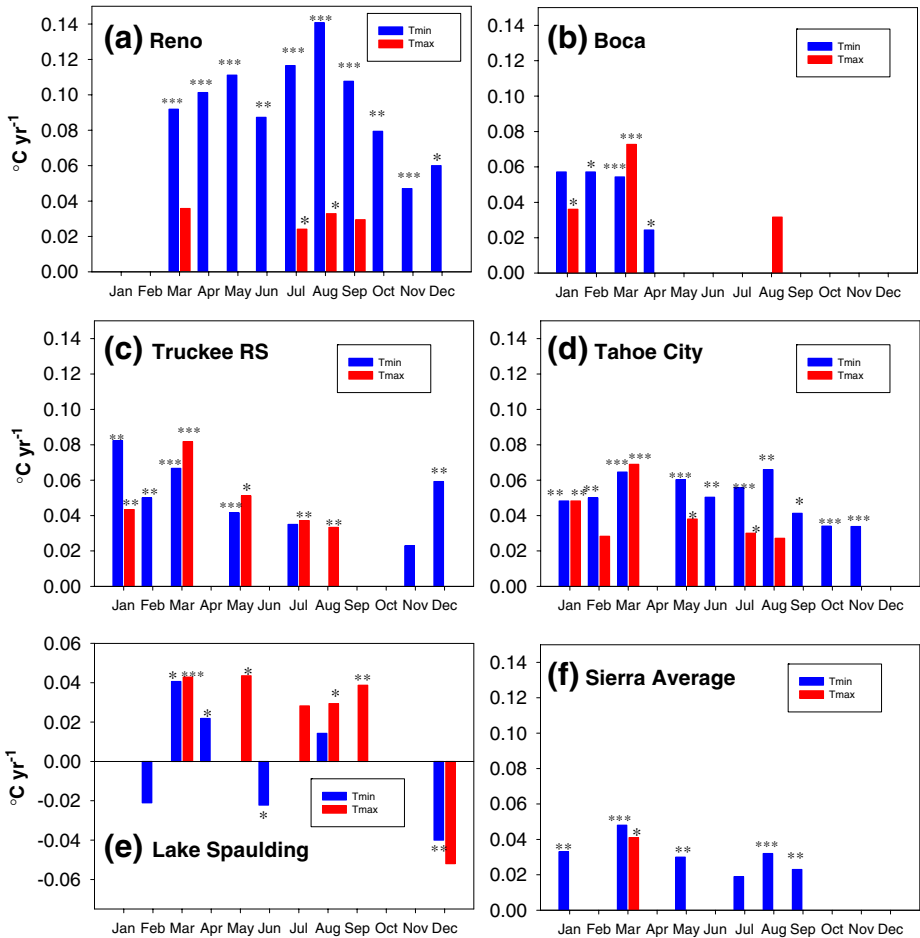


Fig. 3 Theil slope of trend in monthly averages of T_{max} and T_{min} at five stations in the Tahoe region, 1956–2005. Reno, Tahoe City and Lake Spaulding are part of the Historical Climatology Network (HCN). Sierra average (*f*) is from data of the Western Regional Climate Center. *** $P < 0.01$; ** $P = 0.01-0.05$; * $P = 0.05-0.10$; no asterisk $P = 0.15-0.1$. No results are shown for months where $P > 0.15$

Not only are the extremes in annual precipitation increasing, but the frequency of intense rainfall is also increasing. Figure 5 shows the time trend in the number of days per semi-decade that the 95th percentile value for daily rainfall amount—3.9 cm—was exceeded. For comparison, the annual maximum daily 2-year rainfall amount is 6.3 cm, based on a log-Pearson type III analysis, and 3.9 cm was equaled or exceeded (as an annual maximum) in 75 of the 98 years of record examined. Of the 221 events exceeding the 95th percentile daily amount, 91% occurred in the months Nov. through May, when there is likely to be snow on the ground. This suggests a possible increase in rain-on-snow flooding. Mean annual rainfall by semi-decade explains 87% of the variance in number of events >3.9 cm per semi-decade.

The Kendall test for trend in the number of exceedances per half-decade showed a tau correlation coefficient of 0.34, with $P < 0.045$. The rate of increase in frequency

Table 4 Partition of Sums of Squares for Trend Homogeneity test (van Belle and Hughes 1984)

Source	χ^2	df	P <
Monthly average of T_{max}			
Total	120	60	10^{-5}
Homogeneity	58	59	–
Monthly	37	11	10^{-4}
Site	6	4	ns
Site × month	14	44	ns
Trend	62	1	–
Monthly average of T_{min}			
Total	505	60	10^{-6}
Homogeneity	233	59	–
Monthly	49	11	10^{-6}
Site	136	4	10^{-6}
Site × month	47	44	ns
Trend	272	1	–

of daily rainfall exceeding 3.9 cm is about one event per decade. This increase may be related to increases in the strength of ENSO events. The average January–June MEI shows a highly significant ($P < 0.001$, $R^2 = 0.12$) upward trend between 1950 and 2005. The years 1983, 1995 and 1997 were especially strong Niño years, and this is reflected in the data.

The striking thing about Fig. 5 is not just the upward trend in exceedance frequency for the 95th percentile daily amount, but also the apparent increase, beginning in 1975, of large positive and negative deviations from the upward trend. The increasing interannual variability in heavy rainfall events is consistent with the increasing variance in total annual rainfall.

The timing of snowmelt in the western USA is of major concern because of its implications for water supply. In the Tahoe basin, a shift in snowmelt timing may have implications for lake clarity and water quality. The analysis of SMPT in the

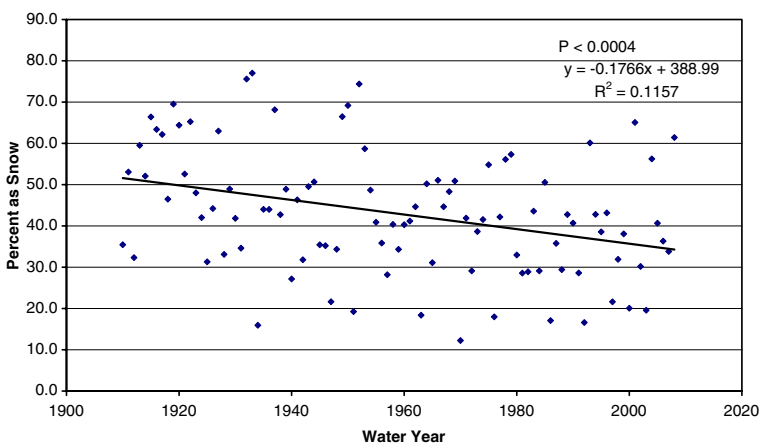


Fig. 4 Percent of total annual precipitation as snow at Tahoe City

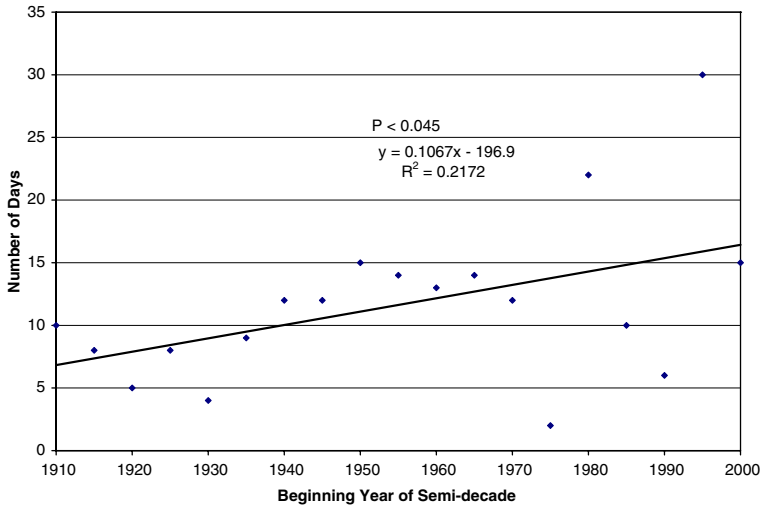


Fig. 5 Number of days per semi-decade that daily rainfall at Tahoe City exceeded 3.9 cm, the 95th percentile value for days with rain

Tahoe basin shows a significant shift toward earlier dates in four of the five streams. Table 5 shows the results of the Kendall tests on the trend in SMPT after removal of the “total snowfall effect” for each water year and stream with the LOWESS smoothing. For the five Tahoe basin streams, the average shift toward earlier dates of the snowmelt peak is about 0.4 days year⁻¹, with Theil slopes ranging from -0.205

Table 5 Results of the Kendall trend test on snowmelt peak timing (SMPT)^a

Stream	USGS Sta. No.	Area (km ²)	Period used	n	Theil Slope	Tau Corr. Coef.	P <
Tahoe basin streams							
Ward Creek	10336676	25.2	1973–2005	33	-0.419	-0.220	0.075
Blackwood Cr.	10336660	28.7	1971–2005	35	-0.205	-0.137	0.187
Upper Truckee	10336610	139.9	1972–2005	31	-0.421	-0.273	0.032
Trout Creek	10336780	95.1	1961–2005	45	-0.465	-0.333	0.001
Third Creek	10336698	15.6	1972–2005	33	-0.453	-0.223	0.070
Average	-	-	-	-	-0.393	-0.149	-
Non-Tahoe basin streams							
Sagehen Creek	10343500	27.2	1961–2005	45	0.086	0.063	0.550
S. Fk Yuba R.	11414000	134.2	1949–1994	46	-0.116	-0.067	0.520
E. Fk Carson R.	10308200	714.8	1961–2004	44	-0.089	-0.066	0.537
W. Fk. Carson R.	10310000	169.4	1960–2004	45	0.144	0.079	0.451

^aThe effects of differences in total snowfall for each water year were removed by treating total water year snowfall as an ancillary variable, and testing the time trends of the LOWESS residuals (Helsel et al. 2005). For Sagehen Creek, snowfall at Truckee was used, for the S. Fk. Yuba, snowfall at Lake Spaulding, and for the forks of the Carson River, snowfall at the Coop Station at Twin Lakes (49105) was used.

to -0.465 for the five creeks. Figure 6 shows the gaging station locations, trend slopes and significance level for both the in-basin and out-of-basin streams.

Figure 7 shows the trend in the average SMPT, for the five Tahoe basin streams. In this plot, the total snowfall effect was removed by OLS regression of SMPT vs. total water-year snowfall, and the residuals have been converted to date. This trend line has a slightly lower slope than the Theil slope from the Kendall test. Serial correlation is negligible ($r = 0.08$). On average, the timing of the spring snowmelt peak discharge (1961–2005) has shifted toward earlier dates at a rate of about 0.4 days year $^{-1}$.

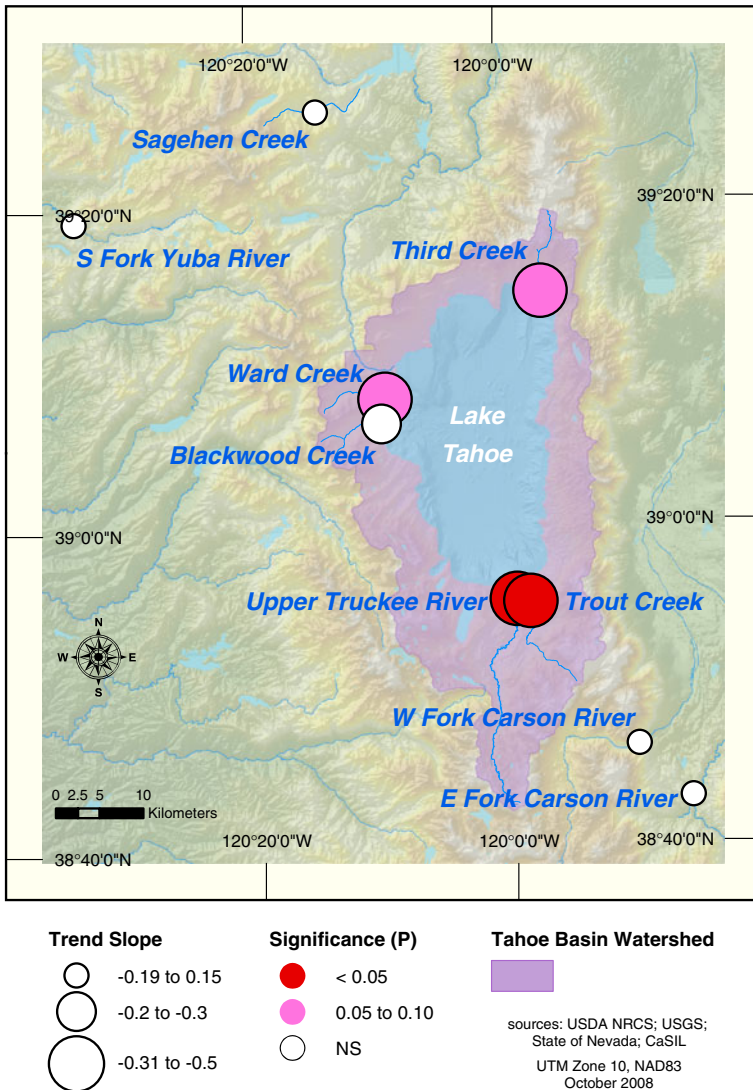


Fig. 6 Trend slopes, significance level and locations of gaging stations used in analysis of the shift in snowmelt timing

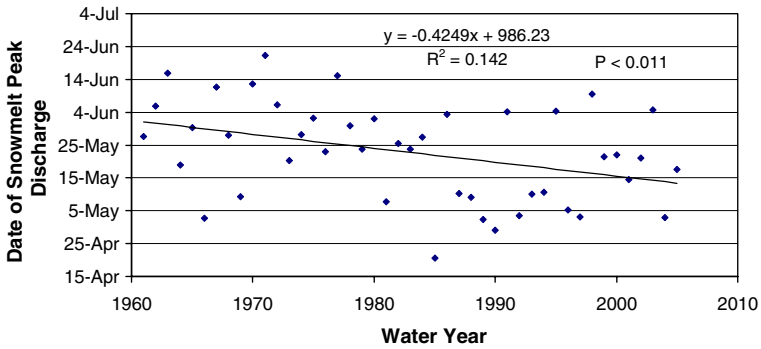


Fig. 7 Average date of snowmelt peak discharge for five streams in the Tahoe Basin, after removal of total annual snowfall effect

The SMPT for the four out-of-basin streams, however, showed no significant time trends. And surprisingly, the centroid timing (CT) for only one of the nine streams—the South Fork Yuba, for the period 1943 to 1994—showed a significant trend, with a tau correlation coefficient of -0.20 , a slope of -0.32 days year $^{-1}$, and $P < 0.034$.

3.3 Changes in lake temperature and thermal structure

Since the average temperature of Lake Tahoe was last calculated through 2002 (Coats et al. 2006), the lake’s annual minimum temperature has continued to increase, reaching its highest level ever in late February–early March, 2007. The annual maximum temperature, however, has not increased over the same period. Figure 8 shows the annual maximum, minimum and average of the daily volume-averaged lake temperature. Although the data used run through October 2007, they capture both the 2007 minimum lake temperature (in early spring) and annual maximum (in fall).

Figure 9 shows the temperature measured monthly at 400 ± 20 m depth. The sharp drop in spring of 2007 resulted from deep mixing, probably to the lake bottom. This mixing event was unusual in that it occurred during a warm and early spring.

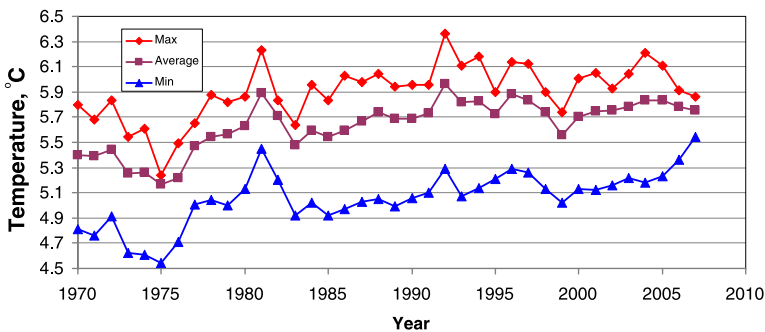
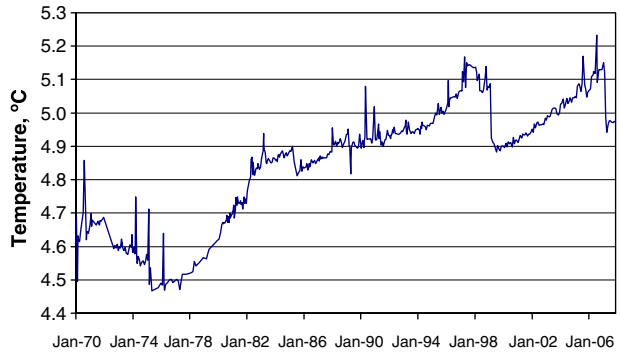


Fig. 8 Annual maximum, average, and minimum of volume-averaged daily water temperature of Lake Tahoe, 1970–2006

Fig. 9 Temperature at 400 m in Lake Tahoe



The spring and summer of 2006, however, were unusually cool, and the lake never warmed enough to create the usual degree of stratification. Apparently the slight cooling in late winter of 2007 was then sufficient to trigger a deep mixing event.

Figure 10 shows the deseasonalized average daily lake temperature. The low point in 2006 (relative to seasonal norm) was reached on September 18, as a result of the unusually cool summer. The large drop in, 1982–1983, is thought to be a result of the eruption of El Chichón in Mexico, March 1982.

The Seasonal Kendall Test for trend in the monthly average lake temperature found a tau correlation coefficient of 0.54, a Theil slope of $0.013^{\circ}\text{C yr}^{-1}$, and $P < 5 \times 10^{-5}$.

3.4 The role of the Pacific decadal oscillation and El Niño/southern oscillation

Table 6 summarizes the results of regression tests of the climatic and hydrologic variables against the PDO and MEI. Some of the climatic-driven variables are

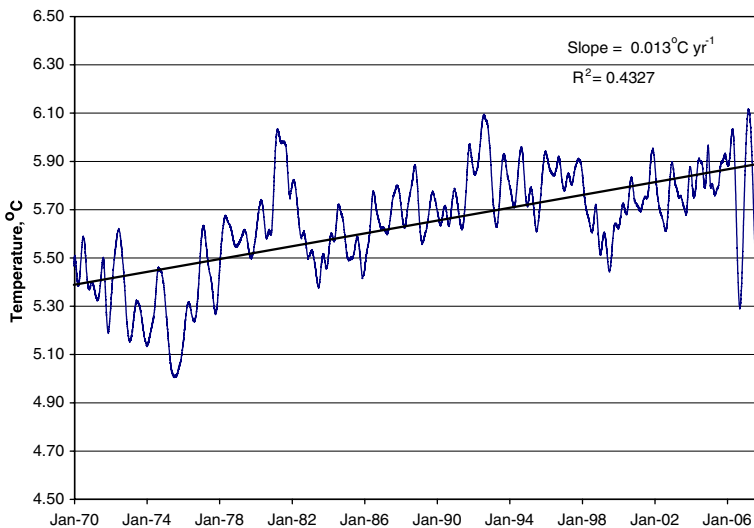


Fig. 10 Volume-averaged daily temperature of Lake Tahoe, de-seasonalized

Table 6 Results of regression of air temperature, snowfall percent, day of snowmelt peak (SMPT) and lake temperature with indices of the Pacific decadal oscillation and El Niño/southern oscillation

Dependent variable	PDO		MEI		
	R^2	$P <$	R^2	$P <$	
Monthly ave. of deseasonalized T_{max}	0.019	10^{-5}	–	NS	
Monthly ave. of deseasonalized T_{min}	0.035	10^{-9}	0.03	1.5×10^{-6}	
Ave. April–June deseasonalized T_{max}	0.08	0.0076	–	NS	
Ave. April–June deseasonalized T_{min}	0.07	0.013	0.12	2×10^{-6}	
Percent of annual WY precip. as snow	–	NS	–	NS	
Day of peak snowmelt discharge, after removal of tot. ann. snowfall effect (with spring PDO and MEI)	0.18	0.0004	0.06	0.11	
Monthly ave. of deseasonalized daily lake temp, lagged 1 month	0.12	5×10^{-14}	0.1	6×10^{-12}	
Seasonal ave. of deseasonalized daily lake temp, lagged 1 month	Spring	0.17	4×10^{-6}	0.07	5×10^{-3}
	Summer	0.21	2.5×10^{-7}	0.13	8×10^{-5}
	Fall	0.05	0.008	0.10	7×10^{-4}
	Winter	0.08	0.001	0.11	4×10^{-4}

statistically related to both the PDO and the MEI. For deseasonalized monthly average of T_{max} and T_{min} at Tahoe City (1909–2005), the PDO explained only 1.9% and 3.5% of the variance, although the effects were highly significant ($P < 10^{-5}$ and 10^{-9} , respectively). T_{min} but not T_{max} is related to the MEI, for monthly averages. For spring air temperature (T_{max} and T_{min}), the PDO connection is significant, but only the spring T_{min} temperatures are related to the MEI. There was no apparent effect of the average winter PDO or MEI on the percent of precipitation falling as snow (1909–2005), but there was a highly significant ($P < 0.0004$) relationship between the average spring (April–June) PDO and the SMPT. This relationship is shown in Fig. 11. When the residuals from the OLS regression are then regressed against date, there is no significant time trend ($P < 0.24$). The regression of SMPT versus average spring MEI was not quite significant ($P < 0.11$).

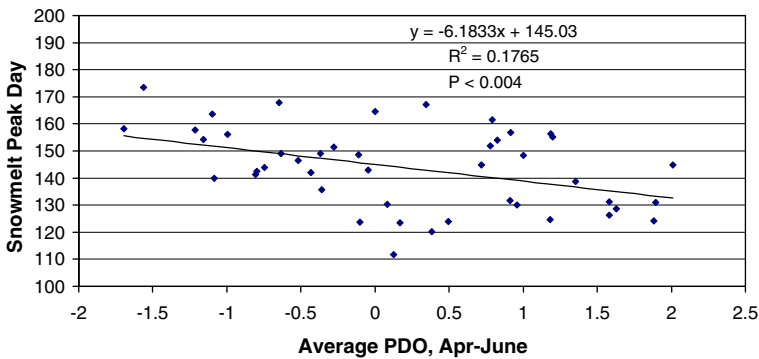


Fig. 11 Annual snowmelt peak Julian day vs. average April–June PDO. Snowmelt peak is average of 5 streams in the Tahoe Basin, after removal of total annual snowfall effect

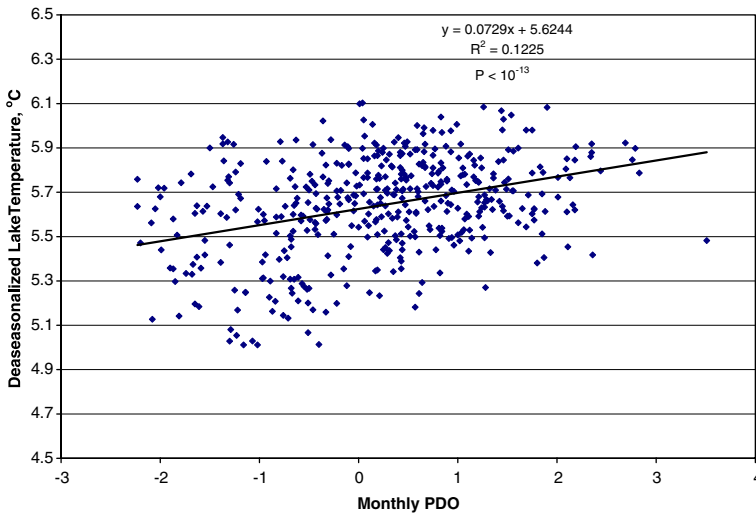


Fig. 12 Monthly average of deseasonalized lake temperature vs. PDO in previous month, 1970–2007

The warming trend in the lake also seems to be linked to both the PDO and ENSO, with each explaining about 10% of the variance in monthly average of deseasonalized average daily lake temperature. Figure 12 shows relationship for the PDO. When the residuals from this regression are heavily pruned to eliminate the effect of serial correlation, the Kendall test shows that remaining time trend is still highly significant, with $P < 0.006$. The Theil slope of the remaining trend is $0.0156^{\circ}\text{C year}^{-1}$, which is close to the slope of the original deseasonalized data. The lake temperatures seem to be a little more closely related to the spring and summer PDO than to the fall and winter PDO, but the relationship between lake temperature and the MEI does not vary with season (see Table 6). Lagging the lake temperature 1–2 months behind the PDO makes only a slight difference in the regression results.

4 Discussion

4.1 Air temperature trends

The warming trends shown here—both annual (for the useable period of record at each station) and monthly (1956–2005)—are generally consistent with much of the research on warming trends in the western USA. In a study on declining snowpack in western North America, Mote et al. (2005) found “overwhelmingly positive” trends in mean November–March temperatures for the periods 1930–1997 and 1950–1997, with the highest warming rates in the more recent period. Bonfils et al. (2008b) found seasonal increases in temperature in California as high as 2.0°C during the 1950–1999 period, with faster warming in late winter and spring, and less rapid warming in summer and fall. Warming rates are generally higher at night (T_{\min}) than in daytime (T_{\max}).

The warming rate in California varies considerably by region, however, with the highest rates in northwest, south coast, and southeast desert climatic divisions, a lower rate in the central valley and central coast, and a slight cooling trend in the NE interior basins. LaDochy et al. (2007) suggest that some of these differences may be due to urbanization, and question the notion of uniform climatic controls over the climatic divisions. My study area falls near and over the western edge of the NE interior basins division.

At some of our stations and in some months, the results are surprising. The extraordinary warming trend at Reno in T_{\min} , especially in the summertime (up to $0.14^{\circ}\text{C year}^{-1}$) may be due the rapid growth in landscape and agricultural irrigation. The desert valley around Reno has been developed rapidly since the mid-1950s, using both surface water from the Truckee River, and groundwater supplies. Christy et al. (2006) found that the night-time temperatures in the San Joaquin Valley of California are increasing faster than in the foothills and Sierras. They attributed the difference primarily to the darkening and moistening of the soil surface, which decreases albedo and increases heat storage capacity, and secondarily to increased night-time humidity. Note that the monthly averages of T_{\max} at Reno in this study showed significant increases ($P < 0.10$) only in the months of July and August, possibly due (as suggested by Bonfils et al. 2008b) to a cooling effect of irrigation on daytime temperatures.

In a study of regional temperature trends in agricultural areas of California, Lobell and Bonfils (2008) found by regression analysis that irrigation caused substantial cooling in T_{\max} , but T_{\min} trends were more positive for non-irrigated than for irrigated sites. Spatial analysis indicated that the upward trends in T_{\min} previously attributed to irrigation could best be attributed to urbanization. It must be noted, however, that urbanization in the arid valleys of California and Nevada generally includes significant increases in landscape irrigation.

The Reno temperature record is part of the Historical Climatology Network, and the data have been adjusted for urbanization on the basis of population growth. The data used in the adjustment, however, were drawn almost entirely from temperature records in the central and eastern USA, with very few stations in the arid West. (Karl et al. 1988). Kalnay and Cai (2003) found that the mean surface warming rate due to land use changes in the USA is at least twice as high as previous estimates based on urbanization alone. The Reno data suggest that if the goal is to determine air temperature trends on a regional or global scale, then some additional adjustment may be necessary in arid regions where land use change has been rapid.

The warming trends at Boca, Truckee and Tahoe City present an interesting contrast. At Boca and Truckee, the warming trends in T_{\max} and T_{\min} are highest during winter and spring, and decrease to a minimum in the fall. This is consistent with the results of Abatzoglou and Redmond (2007), who found that trends in spring circulation patterns over the western USA tend to enhance regional warming, whereas autumn circulation patterns counteract it.

At Tahoe City, however, warming rates (especially in T_{\min}) are high through the summer, and decrease only slightly in the fall. The Tahoe City T_{\min} trend slopes are second only to the slopes at Reno. Since the relatively minor effect of urbanization at Tahoe City has been removed in the HCN monthly average data, and there is no agricultural and little landscape irrigation, we must look for another explanation for locally-enhanced warming. Two hypotheses are presented below, in Section 4.2.

The temperature trends at Lake Spaulding present a slightly different pattern from other stations, with higher T_{\max} than T_{\min} warming rates in late summer, and significant cooling in both T_{\max} and T_{\min} in December. The station is on west side of the Pacific Crest, and may be more influenced by climate trends in the Sacramento Valley.

4.2 Precipitation and snowmelt

Declining snowpacks in the western USA have been the source of a number of recent studies, using both empirical analysis of data and climate modeling (Mote et al. 2005; Barnett et al. 2008; Dettinger and Cayan 1995; Hamlet et al. 2005; Stewart et al. 2004). The results of these studies have raised considerable alarm among water managers, since much of the water supply in the west is dependent on a snowpack that persists into late spring or early summer. In California, the projected severe reduction in the summer snowpack will mean the loss of the largest storage reservoir in the state. At Lake Tahoe as elsewhere in the Sierra Nevada, the declining snowpack on April 1 results from both a shift from snow to rain, and a shift in the timing of snowmelt toward earlier dates.

Knowles et al. (2006) measured the percent of annual precipitation falling as snow for 207 stations in the western USA, for the period 1949–2004. They found that for stations with a significant time trend (tested by the Kendall test) 84% showed a decline in the fraction of precipitation falling as snow. The strongest declines were at lower elevation sites in the Sierra Nevada and the Pacific Northwest. The average rate of decline in snow water equivalent (SWE) for all stations as percent of total precipitation was $0.16\% \text{ year}^{-1}$, slightly less than the rate of $0.19\% \text{ year}^{-1}$ found in this study for Tahoe City, during the period 1910–2005.

The sensitivity of the snowpack to the effects of climate warming (for a given latitude) is strongly related to elevation. A climate modeling study by Knowles and Cayan (2004) found that in the northern Sierra, 85% of the losses in the April snow water equivalent (SWE) by 2060 will occur in between elevations 1300 and 2200 m. About 53.4% of the Tahoe basin lies between 1900 and 2200 m elevation. For the northern Sierra, Knowles and Cayan projected a reduction in the April SWE volume of about 38% by 2060. Johnson et al. (1999) found (on the basis of snow survey data for the Sierra Nevada) trends toward less snow accumulation and earlier melt at elevations below 2400 m, and trends toward higher accumulation and earlier melt at higher elevations.

A number of methods and data sets have been used to measure the trends in snowmelt timing in the western USA. The metrics used have included the monthly and/or fractional seasonal flows (Roos 1991; Stewart et al. 2005), the date of the beginning of spring snowmelt runoff pulse (Cayan et al. 2001; Stewart et al. 2005), and date of the annual hydrograph centroid (CT; Stewart et al. 2005; Barnett et al. 2008). Table 7 summarizes the trends that the various studies have found for the different metrics and time periods used. The shift in snowmelt timing in the Tahoe basin of $0.4 \text{ days year}^{-1}$ as measured by the date of snowmelt peak runoff (SMPT) in this study is on the high side compared with the published results for other areas around the west. Stewart et al. (2005) found an average shift toward earlier dates for CT of $0.13 \text{ days year}^{-1}$ for the western USA. For 73% of their snow-dominated stream

Table 7 Comparison of the shift in timing of snowmelt toward earlier dates, from studies in western North America

Region, data set	Period of record	Metric	Trend	Reference
Tahoe basin, average of five streams	1961–2005	Day of peak snowmelt runoff (SMPT)	0.4 days year ⁻¹	This study
Sacramento R. index	1905–1990	AMJJ ^a	0.13 pct. year ⁻¹	Roos (1991)
Kings and San Joaquin Rivers	1900–1990	AMJJ	0.09 pct. year ⁻¹	Roos (1991)
84 gages, west cent. Canada	varies	Day of peak snowmelt runoff (SMPT)	25% >=0.38 days year ⁻¹	Burn (1994)
Eight rivers index ^b	1948–1990	AMJJ	Ca. 0.26 pct. year ⁻¹	Dettinger and Cayan (1995)
American River	1948–1990	AMJJ	Ca. 0.32 pct. year ⁻¹	Dettinger and Cayan (1995)
Columbia R. at The Dalles	1950–1999	CT ^c	0.17 days year ⁻¹	Barnett et al. (2008); Hidalgo, pers. comm., (2008)
110 rivers in western USA	1957–1994	Onset of spring snowmelt pulse ^d	0.2 days year ⁻¹	Cayan et al. (2001)
294 gages in western N. America	1948–2002	AMJJ	81% of gages with shift toward earlier dates	Stewart et al. (2005)
294 gages in western N. America	1948–2002	Onset of spring snowmelt pulse	66% of gages with shift >0.05 days year ⁻¹	Stewart et al. (2005)
294 gages in western N. America	1948–2002	CT	73% of gages with shift >0.05 days year ⁻¹	Stewart et al. (2005)
89 gages in western USA	1950–1999	50% date ^e	5.6% of gages with shift ≥ 0.3 days year ⁻¹ , most in Pac. NW	Regonda et al. (2005)

^aAMJJ is the fraction (or percent) of total annual flow passing the gage in April through July

^bUnimpaired flow of the Sacramento, Feather, Yuba, American, Tuolumne, Stanislaus, San Joaquin and Merced Rivers

^cCenter timing, or hydrograph centroid (CT) is calculated by $\sum (t_i q_i) / \sum (q_i)$, where t_i = day in the water year, and q_i = discharge on the i th day.

^dDefined as the day when the cumulative departure from mean annual flow is most negative

^eThe date by which 50% of the annual flow has passed the gage

gages around the West, the shift toward earlier CT dates was at least 0.05 days year⁻¹. Only 5% of their gages showed a shift of 0.40 days year⁻¹ or more, and none of these were in California (Stewart-Frey, pers. comm. 2008). In Burn's (1994) data set, only 25% of the gages showed a shift in SMPT \geq 0.38 days year⁻¹.

It is instructive to compare the snowmelt timing shift for in-basin and out-of-basin streams, for the two metrics used here. The time trend for in-basin streams by the SMPT method is clear, while the out-of-basin streams show no such trend. However, the drainages of the East and West Forks of the Carson river cover a larger elevation range than the in-basin streams, so the apparent spring runoff peaks there could be affected by rain in the lower basin. In a study based on 30 years of snow survey data (1966–1996) from 260 snow courses in the Sierra Nevada, Johnson et al. (1999) found that the Tahoe basin had the highest loss—54%—in May SWE of any of the 21 river basins studied.

It may seem paradoxical that only one of the nine streams—the South Fork Yuba—showed a significant trend in CT. But timing of CT and the SMPT respond to different factors in the annual runoff cycle. Figure 13 shows the annual hydrographs for two contrasting water years at Blackwood Creek. In 1982, large winter rainstorms resulted in an early CT date, 56 days ahead of the SMPT. In 2002 (a relatively dry year), there were no major winter rainstorms, but there was a rapid onset of spring thaw, so the SMPT actually preceded the CT date by 15 days. The CT date thus reflects the entire water year (including fall and winter rainstorms), whereas the SMPT (with the snowfall effect removed) responds primarily to spring air temperatures. Since spring air temperatures in the northern Sierra are increasing faster than fall air temperatures, it is reasonable to expect to find time trends in the SMPT for some streams where there is no trend in CT.

Both the air temperature and snowmelt timing results suggest that the Tahoe basin is warming faster than the surrounding region. Two hypotheses (not mutually exclusive) are suggested to explain why. The first is the “lake climate change enhancement hypothesis”. Rouse et al. (2005), working in northern Canada, showed how large lakes (such as Great Slave Lake) can influence a regional energy budget. With a low albedo and high heat storage capacity relative to the land surface, much of the short-wave energy striking the lake surface is stored (25–75% for Great Slave Lake) and released later as latent and sensible heat, and long-wave (LW) radiation. The outgoing LW energy from the lake (and overlying atmospheric boundary layer) is thus greater than it would be absent the lake. The MODIS satellite images of Tahoe in Fig. 14, from July and August 2007, show the contrast between the lake and surrounding land for daytime reflected radiation, and nighttime emitted longwave radiation. Greenhouse gases (GHGs) should intercept the same fraction of outgoing LW radiation from the lake surface as from the land surface, and over time, as GHGs increase, the fraction intercepted should increase. If the LW radiation emission rate of the lake exceeds that of the land, then in absolute terms, the atmospheric energy absorption (and the air temperature) over the lake should increase faster than over the land. This hypothesis could best be tested with a regional climate model coupled to the existing Lake Tahoe temperature model, and embedded in a GCM (Cohen 1990).

The second hypothesis is the “snow albedo perturbation hypothesis”. Qian et al. (2009) modeled soot deposition and its effects on snow albedo, climate and hydrology in the western USA, using chemistry and regional climate configurations of the weather research and forecasting model (WRF) and NOAA land surface model

Fig. 13 Hydrographs for two contrasting water years, Blackwood Creek, showing the relationship between hydrograph centroid (CT) and snowmelt peak timing (SMPT). Vertical lines indicate the CT date

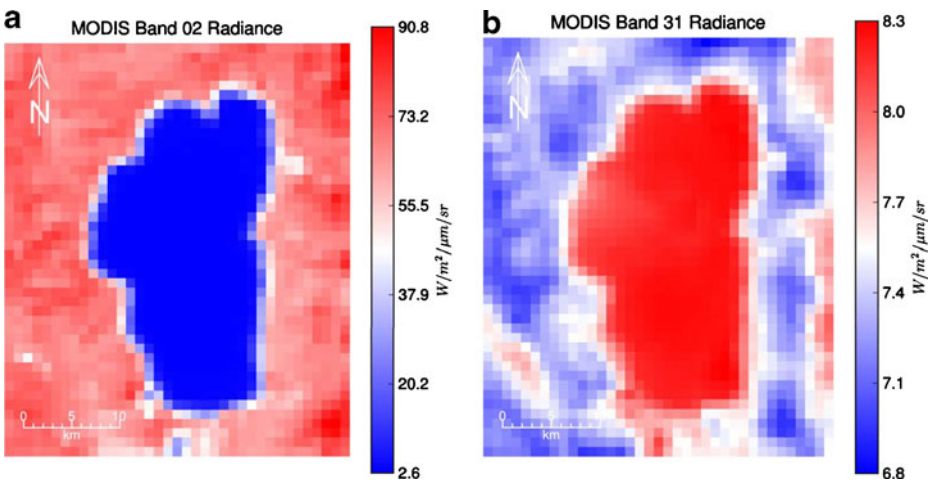
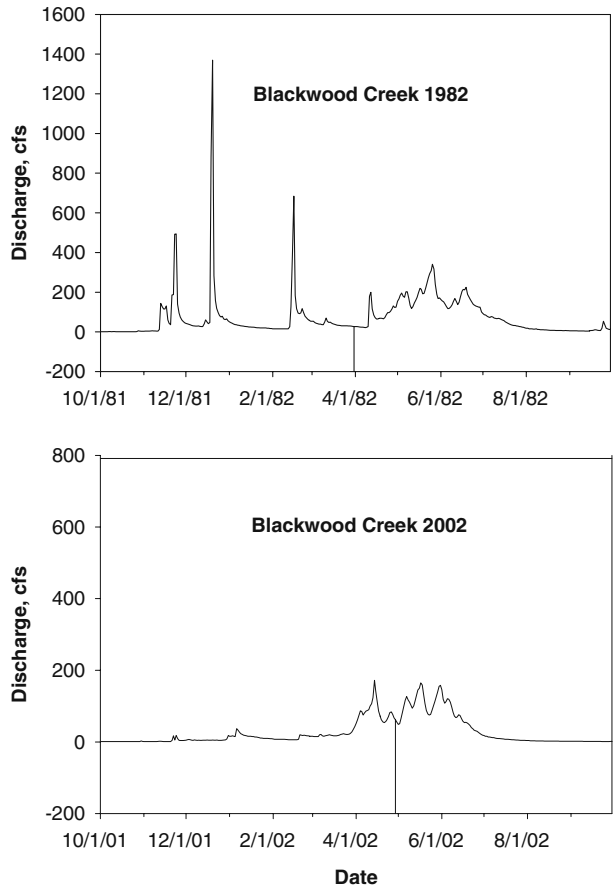


Fig. 14 MODIS satellite images of Lake Tahoe, day and night, at mid-summer. **a** Reflected Near-IR radiation, 0.84–0.85 μm , at 10:50 AM PST, 7/31/2007. **b** Outward Long wave radiation, 10.8–11.3 μm , at 10:10 PM PST, 8/5/2007. Source: Todd Steissberg, Univ. California at Davis

(LSM). They found that soot-induced albedo perturbation (at realistic emissions levels) not only causes a shift in snowmelt timing toward earlier dates, but also (as a result of several positive feedback mechanisms) causes higher air temperatures and a shift from snowfall to rain—trends that seem to be occurring more intensely in the Tahoe Basin than the surrounding region. For the Sierra Nevada, their modeling results showed that the reduction in snow water equivalent (SWE) was greatest in April, amounting to 1.4 mm, or -1.6% . February runoff in the Sierra Nevada increased by 1.0%, and May runoff decreased by 0.6%. The spatial scale of the model used, however, cannot account for emission “hot spots” or the steep climatic gradients that are typical in mountainous terrain (Dobrowski et al. 2009)

The Tahoe basin has abundant winter-time emission sources of soot, most of which is black carbon. Many homes are heated with wood-burning stoves, and traffic during the ski season is heavy at times. Although there are no data on the black carbon (BC) content of snow in the basin, air quality data are available for a station at South Lake Tahoe (SLT), and at Bliss State Park (BSP), on the west shore (IMPROVE 2009). Figure 15 shows the time trends in annual water-year average of near-surface concentration of Fine Total Elemental Carbon ($<2.5 \mu\text{m}$, December, January and February), compared with values at Lassen Volcanic National Park (LVNP). SLT is the most urbanized area of the basin and had the highest Elemental Carbon concentrations, averaging $2.02 \mu\text{g m}^{-3}$. BSP is less influenced by local sources, but like the rest of the basin is down-wind from major metropolitan areas in Sacramento Valley and Bay Area. The average concentration was $0.16 \mu\text{g m}^{-3}$. LVNP (220 km NNW of SLT) is more remote and less affected by in-state sources, and thus had lower BC concentrations than the Tahoe stations, averaging $0.076 \mu\text{g m}^{-3}$. The percentiles for concentrations at SLT, BSP and LVNP in the IMPROVE data base for the entire USA (DJF, $n = 31,043$) were respectively 99.2, 52 and 27. The correlation between BSP and LVNP ($R^2 = 0.74$, $P < 10^{-4}$) suggests a remote background source, possibly in Asia (Tollefson 2009).

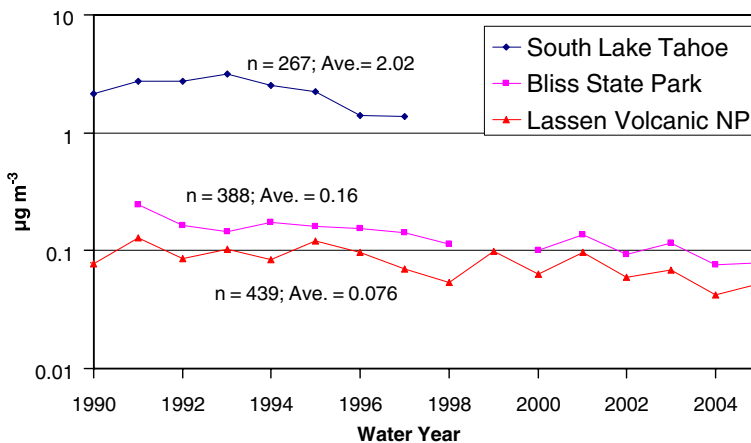


Fig. 15 Annual averages of near-surface atmospheric fine total elemental carbon concentration ($<2.5 \mu\text{m}$), December, January and February, at South Lake Tahoe, Bliss State Park and Lassen Volcanic National Park

Efforts to test the snow albedo perturbation hypothesis might include intensive snowpack energy budget studies, together with sampling and measurement of BC concentrations in the spring snowpack throughout the basin. The California Cooperative Snow Surveys (CCSS; see <http://cdec.water.ca.gov/snow/>) play an important role in the management of California's water resources. It would be appropriate for the CCSS to begin monitoring the black carbon concentration in the snowpack at selected snow survey courses in the Sierra Nevada.

The impacts of hydrologic changes on the lake will depend not just on timing of snowmelt and average runoff, but also on changes in the magnitude/frequency relationship of extreme events. The streamflow and precipitation records for the Tahoe basin are not long enough to permit an analysis of time trends in extreme events, but the daily precipitation record at Tahoe City provides a basis for comparing the historic trend in moderate rainfall amounts with modeled estimates of future changes. Kim (2005) modeled the changes that may occur in the relative magnitude of the 95th percentile wet day precipitation (the amount exceeded by 5% of the days with rainfall >0.5 mm) in the northern Sierra in response to a one percent year⁻¹ rate of increase in atmospheric CO₂ from, 1990. His model results showed that by 2040–2049, the increase at an elevation of 1900 m will amount to 1.6 times as much rainfall, and 2.6 to 2.8 times as much discharge in large river basins, compared the control (stationary CO₂). The measured increase in the frequency of rainfall events that equal or exceed Kim's 95th percentile criterion indicates that rainfall intensity in the basin is already increasing, at an average rate of about one event per decade. This is not a large change in frequency for events that are already relatively frequent, but may reflect a concomitant increase in larger, less frequent rainfall events. Such an increase, combined with the shift from snowfall to rainfall, will increase the frequency and magnitude of rain-on-snow events, which account for the largest floods in the Tahoe basin. Although we do not have data to measure changes in the frequency of rare and short-duration events, it seems likely that increases in rainfall intensity (alternating with periods of drought, with low soil moisture and poor plant growth) are accelerating channel and surface erosion, and the transport of fine sediment to the Lake (Cooke and Reeves 1976).

4.3 Role of the PDO and ENSO

There do seem to be connections between both the Pacific decadal oscillation and ENSO (as measured by the multivariate ENSO index, or MEI), and some the climatic variables examined for the Tahoe basin. For monthly air temperature, the relationship between PDO the monthly average temperature is slight, but statistically significant for both T_{\max} and T_{\min} ; for the MEI, it is significant only for T_{\min} . For average spring temperature, the relationship between air temperature and the PDO is stronger (Table 6). However, the residuals after removing the effect of the PDO by OLS regression from the average spring T_{\min} still show a strong upward trend with time ($R^2 = 0.32$; $P < 10^{-8}$). This is important in interpreting the relationship between the shift in snowmelt timing and the PDO.

The shift in timing of peak snowmelt (SMPT) is linked to the PDO, with $R^2 = 0.20$ and $P < 0.0022$. It is also linked to the MEI, but to a lesser degree, with $R^2 = 0.08$ and $P < 0.06$. When the residuals of the SMPT versus PDO regression are regressed against year, there is no significant time trend. This cannot be interpreted to mean

that the snowmelt timing shift is driven by the ocean temperature variables expressed in the PDO rather than by a long-term global warming trend, for two reasons. First, the hydrologic record used in the analysis of snowmelt timing spans the 1976–1977 step-change in the PDO from negative to positive values, which could exaggerate the importance of the PDO (Stewart et al. 2005). Second, the long-term T_{\min} record shows a strong upward trend even after the PDO effect is removed. Since snow melts faster in a warm spring, the long-term trend in air temperature (independent of the PDO) must be an important factor in the shift in snowmelt timing.

As Fig. 12 and Table 6 show, the monthly average deseasonalized lake temperature is slightly related to the PDO, most strongly in spring and summer. But when the PDO effect is removed, and the data pruned to reduce serial correlation, the Kendall test shows that the upward time trend in the residuals is still significant ($P < 0.006$). As with the factors driving the shift in snowmelt timing, it seems that the long-term upward temperature trend in air temperature (presumably forced by GHG emissions) is the engine of change in the Tahoe basin, and the PDO and ENSO are part of the drive train.

4.4 Changes in Lake temperature and thermal structure: biological and water quality implications

Although there is clearly a long-term upward trend in the temperature of Lake Tahoe, the pattern of temperature change in since 2004 has been unusual in that the maximum annual temperature has declined while the minimum has increased (see Fig. 8). The recent decline in annual maximum is probably due in part to deep mixing that occurred in both 2007 and 2008 (Schladow 2009), when heat transported downward by eddy diffusion was released to the atmosphere. The continued upward trend in minimum temperature may be due to a series of mild winters.

The most significant effect of the warming trend in the lake is not its direct biological effect on organisms (though that may eventually become important) but rather its effect on the thermal stability of the lake. Coats et al. (2006) calculated the Schmidt Stability, Birge Work and Total Work, for the period, 1970–2002. These metrics relate to the work required to mix a thermally-stratified lake to an isothermal state, and the external energy required to produce a given degree of stratification. The upward trend in all three parameters was highly significant.

More recently, Winder et al. (2009) calculated annual and monthly average values of the Brunt–Väisälä frequency as an indicator of stratification strength. They found a significant increase in the intensity of stratification (1980–2006) in the 2–60 m depth interval ($P < 0.008$), and a tendency toward increased shoaling (decreasing depth) of the thermocline during stratification ($P < 0.08$). They were able to relate changes in phytoplankton populations to increasing stratification, finding that reduced vertical mixing is providing a competitive advantage to small-bodied diatoms and other algae that are relatively buoyant and have lower sinking velocities. The less-buoyant species tend to sink below the photic zone, and with reduced mixing, are unable to return.

Over a time scale of several decades, however, temperature changes may directly affect the growth and competitive advantage of organisms in the lake. In the late 1980s largemouth bass (*Micropterus salmoides*) and bluegill (*Lepomis macrochirus*) showed up in a shallow lagoon at the southern end of the lake, probably as a result of

illegal introductions by anglers. They are now spreading into shallow lagoons around the margins of the lake, and are competing with and consuming native fish (Kamerath et al. 2008). Using the regional climate model (RegCM 2.5) of Snyder and Sloan (2005), together with an empirical model of lake surface temperature, Ngai (2008) showed that surface water temperatures in the lake may increase by as much as 3.0°C by 2080–2099 in the open lake, with larger increases in marinas and other shallow lagoons. She concluded that the warming trend will make the lagoons and ultimately the open lake more hospitable to the bass and bluegill. Increased populations of these fish could have important consequences for food web structure, nutrient recycling and lake water quality.

The changes in the lake's thermal structure may interact with changes in basin hydrology in ways that are difficult to predict. An important variable that influences the impact of sediment-rich stream discharge on water clarity is the "insertion depth". Streams entering the lake do so at the depth where the density of the stream water is equal to the density of the lake. The former is influenced by the timing of snowmelt and storm runoff, and by the suspended sediment concentration, and the latter by the seasonal cycle of warming, stratification and mixing. Additional modeling may help to sort out the interaction between stream runoff, lake thermal structure and water clarity, but it seems likely that increased inflow of fine sediment (from more intense rainfall, drought and wildfires) will interact with increasing thermal stability to prolong the period of reduced water clarity that follows periods of heavy runoff (Jassby et al. 1999).

An important question not yet resolved is: what will be the long-term effect of decreased mixing combined with on-going eutrophication on the concentration of dissolved oxygen (DO) at the bottom of the lake? If reduced mixing suppresses the downward flux of DO enough to cause anoxia at the sediment–water interface, the reduction of ferric to ferrous iron would trigger a release of phosphorus to the water column. The result could be a rapid state-change for the lake, from a ultra-oligotrophic and blue, to mesotrophic and green. Additional modeling and careful measurement of DO profiles are needed to resolve this question.

5 Summary and conclusions

This study analyzed air temperature, precipitation, lake temperature and stream discharge data at daily to decadal time scale for sites in and around the Tahoe basin. The major findings are as follows:

1. Annual and monthly averages of air temperature records show upward trends, with the strongest trends for monthly T_{\min} at Tahoe City and Reno. Monthly trends are generally strongest in spring, and weakest in the fall.
2. At some air temperature stations, anomalous trends may be explained by local microclimatic effects or changes in station location.
3. The air temperature and precipitation data for Tahoe City show a shift from snow to rain, a decline in the number of winter days below freezing, and an increase in the intensity of rainfall over the period 1910–2007.
4. Streamflow records in the Tahoe basin show a shift toward earlier dates in the peak of snowmelt runoff, for the period 1961–2005. A similar shift was not found for four streams outside of the Tahoe basin.

5. The annual hydrograph centroid (CT) for nine stream gaging stations (both within and outside the Tahoe basin) showed a trend toward earlier dates only for the South Fork Yuba River, 1949–94.
6. Lake Tahoe warmed at an average rate of about $0.013^{\circ}\text{C year}^{-1}$ during the period 1970–2007. The warming is increasing the lake's thermal stability and resistance to mixing, with important biological and biogeochemical implications and impacts.
7. The trends in air temperature, snowmelt timing and lake temperature (1970–2007) are statistically linked to the Pacific decadal oscillation, and to a lesser extent to El Niño–Southern Oscillation, but these large-scale climatic oscillations can explain only a small part of the variance in descriptors of Tahoe basin climate and hydrology.
8. The air temperature and streamflow records for stations in and around the Tahoe basin suggest that the lake itself may be enhancing the effect of GHGs on warming trends in the basin. This “lake enhancement” hypothesis is supported by work in Canada on the regional climatic effect of large lakes.
9. Atmospheric deposition of black carbon in the Tahoe basin may be implicated in the shift in snowmelt timing, increasing air temperature and the shift from snowfall to rain. Snowpack energy budget studies together with analysis of snowpack black carbon concentrations are needed to test this “snow albedo perturbation” hypothesis. Monitoring of black carbon in snow should be added to routine water quality monitoring in the Tahoe basin, and to the California Cooperative Snow Surveys.
10. Modeling studies that link the lake processes to basin hydrology and regional climate may be useful in understanding the likely long-term impacts of climate change on water quality and biota of Lake Tahoe, and how the lake's heat budget interacts with the basin's climate. A high resolution climate model for the Tahoe basin embedded in a GCM is needed to investigate the interactions between the lake and the regional climate.
11. In relocating coop stations, the National Weather Service needs to pay more attention to the microclimatic effects of large water bodies, topography and landscape irrigation.

Acknowledgements I thank John Reuter, Iris Stewart-Frey and Monika Winder, Gayle Dana and one anonymous reviewer for discussion, encouragement and/or thoughtful review of the manuscript; Scott Hackley, for help with installing and operating data loggers at Glenbrook; Norman Hansen and the crew at Station 5, for access to the old and current Glenbrook instrument locations, Todd Steissberg for providing the MODIS figures, Patricia Arneson for data stewardship, Janet Brewster for cartography, and Charles Goldman and Geoffrey Schladow for support and encouragement over many years. This research was supported in part by grant #08-DG-11272170-101 from the USDA Forest Service Pacific Southwest Research Station using funds provided by the Bureau of Land Management through the sale of public lands as authorized by the Southern Nevada Public Land Management Act.

Open Access This article is distributed under the terms of the Creative Commons Attribution Noncommercial License which permits any noncommercial use, distribution, and reproduction in any medium, provided the original author(s) and source are credited.

References

- Abatzoglou JT, Redmond KT (2007) Asymmetry between trends in spring and autumn temperature and circulation regimes over western North America. *Geophys Res Lett* 34:1–5
- Aguado E, Cayan D, Riddle L, Roos M (1992) Climatic fluctuations and the timing of west coast streamflow. *J Clim* 5:1468–1483
- Arhonditsis GB, Brett MT, DeGasperi CL, Schindler DL (2004) Effects of climatic variability on the thermal properties of Lake Washington. *Limnol Oceanogr* 49:256–270
- Barnett TP, Pierce DW, Hidalgo HG, Bonfils C, Santer BD, Das T, Gala G, Wood AW, Nozawa T, Mirin AA, Cayan DR, Dettinger MD (2008) Human-induced changes in the hydrology of the Western United States. *Sci Express* 319:1080–1083
- Bonfils C, Santer BD, Pierce DW, Hidalgo HG, Bala G, Das T, Barnett TP, Cayan DR, Doutriaux C, Wood AW, Mirin A, Nozawa T (2008a) Detection and attribution of temperature changes in the mountainous western United States. *J Clim* 21:6404–6424
- Bonfils C, Duffy P, Santer B, Wigley T, Lobell D, Phillips T, Doutriaux C (2008b) Identification of external influences on temperatures in California. *Clim Change* 87:S43–S55
- Brown TJ, Hall BL, Westerling AL (2004) The impact of twenty-first century climate change on wildland fire danger in the western United States: an applications perspective. *Clim Change* 62:365–388
- Burn DH (1994) Hydrologic effects of climate change in west-central Canada. *J Hydrol* 160:53–70
- Cayan DR, Kammerdiener S, Dettinger M, Caprio J, Peterson D (2001) Changes in the onset of spring in Western United States. *Bull Am Meteorol Soc* 82:319–415
- Christy J, Norris W, Redmond KT, Gallo K (2006) Methodology and results of calculating Central California surface temperature trends: Evidence of human-induced climate change? *J Clim* 19:548–563
- Coats RN, Perez-Losada J, Schladow G, Richards R, Goldman CR (2006) The warming of Lake Tahoe. *Clim Change* 76:121–148
- Cohen S (1990) Bringing the global warming issue closer to home: the challenge of regional impact studies. *Bull Am Meteorol Soc* 71:520–526
- Cooke RU, Reeves RW (1976) Arroyos and environmental change in the American Southwest. Oxford University Press, New York, 226 pp
- Dettinger MD, Cayan DR (1995) Large-scale atmospheric forcing of recent trends toward early snowmelt runoff in California. *J Clim* 8:606–623
- Dettinger MD, Cayan DR, Knowles N, Westerling A, Tyree M (2004) Recent projections of 21st-century climate change and watershed responses in the Sierra Nevada. USDA Forest Service Gen Tech Rep PSW-GTR-193, pp 43–46
- Dobrowski SAJ, Greenberg J, Schladow G (2009) How much influence does landscape-scale physiography have on air temperature in a mountain environment? *Agric For Meteorol* 49:1751–1758
- Flanner M, Zender C, Randerson J, Rasch P (2007) Present-day climate forcing and response from black carbon in snow. *J Geophys Res* 112:D11202. doi:10.1029/2006JD008003
- Hamlet AF, Mote PW, Clark MP, Lettenmaier DP (2005) Effects of temperature and precipitation variability on snowpack trends in the Western United States. *J Clim* 18:4545–4561
- Hansen J, Nazarenk L (2004) Soot forcing via snow and ice albedos. *Proc Natl Acad Sci* 101:423–428
- Helsel DR, Frans ML (2006) Regional Kendall test for trend. *Environ Sci Technol* 40:4066–4073
- Helsel DR, Hirsch RM (1995) Statistical methods in water resources. Elsevier, New York
- Helsel DR, Mueller DK, Slack JR (2005) Computer program for the Kendall family of trend tests. US Geol. Surv. Scientific Investigations Rep. 2005-5275, Reston, VA, 4 pp. <http://pubs.usgs.gov/sir/2005/5275/>
- IMPROVE (2009) Data resources. Interagency monitoring of protected visual environment. <http://vista.cira.colostate.edu/IMPROVE/>. Accessed 21 Jan 2009
- Jassby AD, Goldman CR, Reuter JE, Richards RC (1999) Origins and scale dependence of temporal variability in the transparency of Lake Tahoe, California–Nevada. *Limnol Oceanogr* 44:282–294
- JISAO (2008) The Pacific decadal oscillation. Joint Institute for the Study of the Atmosphere and Environment. <http://jisao.washington.edu/pdo/>. Accessed 16 Sept 2008
- Johnson CM, Needham PR (1966) Ionic composition of Sagehen Creek, California following an adjacent fire. *Ecology* 47:636–639

- Johnson T, Dozier J, Michaelsen J (1999) Climate change and Sierra Nevada snowpack. In: Interactions between the cryosphere, climate and greenhouse gases. Proc. IUGG 99 Symp. HS2, IAHS, Birmingham, pp 63–70
- Kalnay E, Cai M (2003) Impact of urbanization and land-use change on climate. *Nature* 423:528–531
- Kamerath M, Chandra S, Allan B (2008) Distribution and impacts of warm water invasive fish in Lake Tahoe. *Aquatic Invasions* 3:35–41
- Karl TR, Williams CN (1987) An approach to adjusting climatological time series for discontinuous inhomogeneities. *J Clim Appl Meteorol* 26:1744–1763
- Karl TR, Williams CN Jr, Young PJ, Wendland WM (1986) A model to estimate the time of observation bias associated with monthly mean maximum, minimum and mean temperatures for the United States. *J Clim Appl Meteorol* 25:145–160
- Karl TR, Diaz HF, Kukla G (1988) Urbanization: its detection and effect in the United States climate record. *J Clim* 1:1099–1123
- Kattelmann R (1991) Peak flows from snowmelt runoff in the Sierra Nevada, USA. In: Snow Hydrology and Forests in High Alpine Areas, IAHS, Vienna, pp 203–211
- Kim J (2005) A projection of the effects of the climate change induced by increased CO₂ on extreme hydrologic events in the western U.S. *Clim Change* 68:153–168
- Knowles N, Cayan D (2004) Elevational dependence of projected hydrologic changes in the San Francisco estuary and watershed. *Clim Change* 62:319–336
- Knowles N, Dettinger M, Cayan D (2006) Trends in snowfall versus rainfall in the western United States. *J Clim* 19:4545–4559
- LaDochy S, Medina R, Patzert W (2007) Recent California climate variability: spatial and temporal patterns in temperature trends. *Clim Res* 33:159–169
- Lobell D, Bonfils C (2008) The effect of irrigation on regional temperatures: a spatial and temporal analysis of trends in California, 1934–2003. *J Clim* 21:2063–2071
- Mantua NJ, Hare SR, Zhang Y, Wallace JM, Francis RC (1997) A Pacific interdecadal climate oscillation with impacts on salmon production. *Bull Am Meteorol Soc* 78:1069–1079
- Mote PW, Hamlet AF, Clark M, Lettenmaier D (2005) Declining mountain snowpack in western North America. *Bull Am Meteorol Soc* 86:19–49
- National Climate Data Center (2008) System access—MMS. http://mi3.ncdc.noaa.gov/mi3_access. Accessed 16 Sept 2008
- Ngai KLC (2008) Potential effects of climate change on the invasion of largemouth bass (*Micropterus salmoides*) in Lake Tahoe, California-Nevada. MS Thesis, Graduate Dept. of Zoology (118 pp). University of Toronto, Toronto, Canada
- NOAA (2008). Multivariate ENSO Index (MEI). Earth System Research Laboratory. <http://www.cdc.noaa.gov/people/klaus.wolter/MEI/mei.html>. Accessed 16 Sept 2008
- Pierce DW, Barnett TP, Hidalgo H, Das T, Bonfils C, Santer B, Bala G, Dettinger M, Cayan D, Mirin A, Wood A, Nozawa T (2008) Attribution of declining western U.S. snowpack to human effects. *J Clim* 21:6425–6444
- Qian Y, Gustafson W, Leung LR, Ghan S (2009) Effects of soot-induced snow albedo change on snowpack and hydrological cycle in western U.S. based on weather research and forecasting chemistry and regional climate simulations. *J Geophys Res* 114:DO3108. doi:10.1029/2008JD011039
- Oreskes N (2004) The scientific consensus on climate change. *Science* 306:1686
- Redmond K (1991) Effects of time of observation bias on temperature time series. Conference on Applied Climatology (6 pp). Salt Lake City, UT
- Redmond K (1992) Effects of observation time on interpretation of climatic time series—a need for consistency. In: Redmond KT (ed) Eighth Annual Pacific Climate (PACLIM) Workshop, pp 141–150. California Dept. Water Resour Interagency Ecological Studies Program for the Sacramento–San Joaquin Estuary, Asilomar CA
- Regonda S, Rajagopalan B, Clark M, Pitlick J (2005) Seasonal cycle shifts in hydroclimatology over the western United States. *J Clim* 18:372–384
- Roos M (1991) A trend of decreasing snowmelt runoff in northern California. 59th Western Snow Conference, pp 29–36. Western Snow Conf, Juneau AK
- Rouse WR, Oswald CJ, Binyamin J, Spence C, Schertzer W, Blanken P, Bussieres N, Duguay C (2005) The role of northern lakes in a regional energy balance. *J Hydrometeorol* 6:291–305
- Running S (2006) Is global warming causing more, larger wildfires? *Sci Express* 313:927–928
- Schladow SG (ed) (2009) Tahoe: state of the lake report 2009. UC Davis Tahoe Environmental Research Center Technical Report, Davis, CA

- Snyder MA, Sloan LC (2005) Transient future climate over the western United States using a regional climate model. *Earth Interact* 9(11):1–21
- Stewart IT, Cayan D, Dettinger M (2004) Changes in snowmelt runoff timing in western North America under a ‘business as usual’ climate change scenario. *Clim Change* 62:217–232
- Stewart IT, Cayan DR, Dettinger M (2005) Changes toward earlier streamflow timing across western North America. *J Clim* 18:1136–1155
- Tollefson J (2009) Climate’s smoky spectre. *Nature* 460:29–32
- Trenberth KE (1984) Some effects of finite sample size and persistence on meteorological statistics. Part I: autocorrelations. *Mon Weather Rev* 112:2359–2368
- van Belle G, Hughes J (1984) Nonparametric tests for trend in water quality. *Water Resour Res* 20:127–136
- von Storch H (1999) Misuses of statistical analysis in climate research. In: von Storch H, Navarra A (eds) *Analysis of climate variability*. Springer-Verlag, New York, pp 11–26
- Westerling AL, Hidalgo HG, Cayan DR, Swetnam T (2006) Warming and earlier spring increases western U.S. forest wildfire activity. *Sci Express* 313:940–943
- Western Regional Climate Center (2008) Historical climate information. <http://www.wrcc.dri.edu>. Accessed 16 Sept 2008
- Williams CN Jr, Menne MJ, Vose RS, Easterling DR (2008) Long-term daily and monthly climate records for stations across the contiguous United States. <http://cdiac.ornl.gov/epubs/ndp/ushcn/newushcn.html>. Accessed 16 Sept 2008
- Winder M, Reuter JR, Schladow SG (2009) Lake warming favors small-sized planktonic diatom species. *Proc R Soc B* 276:427–435



Dynamics of solutes and dissolved oxygen in shallow urban groundwater below a stormwater infiltration basin

T. Datry*, F. Malard, J. Gibert

UMR CNRS 5023, Ecologie des Hydrosystèmes Fluviaux, Université Claude Bernard Lyon 1, Bât. Forel 403,
43 Bd 11 Novembre 1918, F-69622 Villeurbanne Cedex, France

Received 22 September 2003; received in revised form 24 February 2004; accepted 28 February 2004

Abstract

Artificial recharge of urban aquifers with stormwater has been used extensively in urban areas to dispose of stormwater and compensate for reduced groundwater recharge. However, stormwater-derived sediments accumulating in infiltration beds may act as a source of dissolved contaminants for groundwater. Concentrations of hydrocarbons, heavy metals, nutrients and dissolved oxygen (DO) were monitored at multiple depths in shallow groundwater below a stormwater infiltration basin retaining large amounts of contaminated organic sediments. Multilevel wells and multiparameter loggers were used to examine changes in groundwater chemistry occurring over small spatial and temporal scales. Rainfall events produced a plume of low-salinity stormwater in the first 2 m below the groundwater table, thereby generating steep vertical physico-chemical gradients that resorbed during dry weather. Heavy metals and hydrocarbons were below reference concentrations in groundwater and aquifer sediments, indicating that they remained adsorbed onto the bed sediments. However, mineralization of organic sediments was the most probable cause of elevated concentrations of phosphate and DOC in groundwater. DO supply in groundwater was severely limited by bed respiration which increased with temperature. Cold winter stormwater slightly re-oxygenated groundwater, whereas warm summer stormwater lowered DO concentrations in groundwater. Among several results provided by this study, it is recommended for management purposes that infiltration practices should minimize the contact between inflow stormwater and organic sediments retained in infiltration basins.

© 2004 Elsevier B.V. All rights reserved.

Keywords: Urban stormwater; Infiltration basins; Groundwater recharge; Nutrients; Heavy metals; Hydrocarbons

1. Introduction

Induced infiltration of urban stormwater into the ground is increasingly used as an alternative to its direct disposal to streams (Pitt et al., 1999; Dechesne, 2002; Fischer et al., 2003). Stormwater

infiltration basins are expected to compensate for reduced groundwater recharge caused by the sealing of the urban landscape and are designed to promote the retention and degradation of contaminants in the soil and vadose zone (Chocat, 1997; Fujita, 1997; Mason et al., 1999). Moreover, recharge of groundwater with oxic stormwater can increase the flux of dissolved oxygen (DO), thereby re-oxygenating shallow water-table aquifers that often exhibit low DO concentrations (Starr and

*Corresponding author. Tel.: +33-4-72-43-29-45; fax: +33-4-72-43-15-23.

E-mail address: datry@univ-lyon1.fr (T. Datry).

Gillham, 1993; Malard and Hervant, 1999; Chappelle, 2000).

Although urban runoff waters are known to transport a variety of contaminants including heavy metals, hydrocarbons and nutrients (Chebbo et al., 1995; Pitt et al., 1999; Dechesne, 2002; Fischer et al., 2003), few studies have examined the influence of induced stormwater infiltration on the physico-chemistry of underlying groundwater. Because most metals and hydrocarbons in stormwater are associated with suspended solids they can readily be retained by physical filtration in the beds of infiltration basins (Legret et al., 1988; Chebbo et al., 1995; Mason et al., 1999; Pitt et al., 1999; Baveye et al., 2000). However, stormwater sediments accumulating in infiltration beds may act as a source of nutrients. Datry et al. (2003a) have demonstrated that oxidation of organic carbon contained in the bed sediments of a stormwater infiltration basin consumed DO in inflow stormwater and released ammonium, phosphate and dissolved organic carbon (DOC). Where the groundwater table is closed to the surface, the residence time of water in the vadose zone may be insufficient to allow microbial degradation of DOC and re-oxygenation of infiltrating stormwater. In this case, groundwater below stormwater infiltration basins may become temporarily anoxic in response to the input of weakly oxygenated stormwater and oxygen consumption caused by the microbial degradation of DOC.

The dynamics of solutes and DO in shallow groundwater below a stormwater infiltration basin that has accumulated considerable amounts of organic sediments contaminated with heavy metals and hydrocarbons have been examined. Detailed information on the physico-chemical characteristics of sediments and water in the infiltration bed have been reported by Datry et al. (2003a,b). Groundwater sampling and continuous measurements of DO were carried out at multiple depths below the groundwater table using two clusters of short screen monitoring wells; one was located below the stormwater infiltration basin, the other at a nearby reference site which was not influenced by induced stormwater infiltration. The objectives of the present study were to (1) identify contaminants transported by stormwater into the ground-

water; (2) delineate the thickness of the groundwater layer physico-chemically affected by stormwater inputs; and (3) determine changes in the DO dynamics of shallow groundwater artificially recharged with stormwater.

2. Site description

The stormwater infiltration basin, located on the campus of the University Claude Bernard, Lyon, France, has a surface area of 750 m² and a storage capacity of approximately 4000 m³ (Fig. 1a). The catchment is 2.5 ha in area and comprises teaching and research buildings, car parks, roads and lawns. The coefficient of imperviousness is approximately 0.9. The infiltration bed is a 2-m thick layer of cobbles, which were spread over local fluvial sediments (Fig. 1b). Because the basin has been in operation for more than 30 years, the cobble layer has retained considerable amounts of organic stormwater sediments contaminated with hydrocarbons and heavy metals.

Due to the long-term accumulation of stormwater sediment, the cobble layer is partially clogged and permanently retains water (Fig. 1b). The water table in the infiltration bed was 1.2 m below the ground surface during dry periods and rose rapidly during rainfall events in response to the inputs of stormwater. Return to pre-event water levels usually took less than 4 days. Aquifer sediments consisted of sand and gravel, the thickness and hydraulic conductivity of which ranged from 13 m to 20 m and from $3 \cdot 10^{-3}$ m/s to $9 \cdot 10^{-2}$ m/s, respectively (Horizon, 2000). Groundwater was recharged with Rhône River water and flowed south-westward (Fig. 1a). The groundwater table fluctuated between 2.5 and 3.5 m below the surface of the infiltration bed. Therefore, the thickness of the unsaturated layer of sediments between the bottom of the infiltration bed and the regional groundwater table varied from 0.8 to 1.3 m. The reference site, whose groundwater was not artificially recharged with stormwater, was located at a distance of 1100 m from the infiltration basin (Fig. 1a). The groundwater table at the reference site fluctuated between 6 and 7 m below the soil surface (Fig. 1b).

3. Materials and methods

3.1. Monitoring wells

Six monitoring wells were positioned at regular intervals along a 1-m diameter circle, the centre of which was located at a distance of 1.6 m from the main stormwater inlet (Fig. 1a). The well casing was made of transparent Plexiglas® with an internal/external diameter of 54/60 mm. Transparent casing was used to examine in situ groundwater sediments and animals by means of a downhole viewer (Datry et al., 2003c). All wells were hermetically closed with a cap to prevent direct input of stormwater. The wells were screened at their lower end over a height of only 0.5 m and were successively installed at depths of 2, 3, 4, 5, 6 and 7 m below the surface of the infiltration bed (Fig. 1b). Well 1 was used for sampling stormwater circulating within the infiltration bed, whereas wells 3, 4, 5 and 6 were used to collect groundwater at depths of 1, 2, 3 and 4 m below the groundwater table. Well 2, which intersected the contact zone between the lowermost part of the infiltration bed and fluvial sediments, remained dry during the study period (November 2001–September 2002). Wells 7, 8 and 9 were installed at the reference site to obtain groundwater samples at depths of approximately 1.5, 3 and 4 m below the groundwater table. The screen height of well 7 was 2.5 m instead of 0.5 m because there was little information about the fluctuations of the groundwater table when the wells were installed.

3.2. Sediment sampling

Sediments were sampled to investigate the potential accumulation of dissolved components on fluvial sediments located below the infiltration bed. A mixture of water and sediment was extracted using a hand piston pump from piezometers 1, 2, 3, 4, 5, 6 and 7. Because piezometer 2 was dry, sediment was obtained by repeatedly injecting and pumping water. After decanting, 3 sediment subsamples were collected for each well in polypropylene bottles and brought to the laboratory for analysis of particulate organic carbon (POC), par-

ticulate nitrogen (PN), particulate phosphorus (PP), heavy metals (Cd, Cr, Cu, Ni, Pb and Zn) and total hydrocarbons.

3.3. Groundwater sampling

Subsurface water samples were collected from wells 1 to 9 during 3 dry weather periods (5 November 2001, 8 March 2002 and 18 November 2002) and 3 rainfall events (30 November 2001, 15 March 2002 and 28 June 2002) (Fig. 2). During rainfall events, a stormwater sample was collected at the outlet of the stormwater inlet pipe. The first, second and third rainfall events resulted in an input of 517 m³, 560 m³ and 598 m³ of stormwater, respectively. Groundwater was sampled 12 h after the end of the rain. In addition, groundwater samples were collected 32, 80 and 108 h after the end of the third rainfall (28 June 2002) to examine changes in physico-chemistry during recharge (i.e. 4 days). Water was pumped from each piezometer at a discharge rate of 10 l/min with a suction piston pump (Bou and Rouch, 1967). The first 50 l of pumped water were discarded as rinse. Then, water was collected in burned 0.05-l glass bottles for the determination of DOC, in 2-l polypropylene bottles for the analysis of metals (Cd, Cr, Cu, Ni, Pb and Zn) and dissolved non-metallic constituents (Ca²⁺, Mg²⁺, Na⁺, K⁺, HCO₃⁻, SO₄²⁻, Cl⁻, PO₄³⁻, NO₃⁻, NO₂⁻, NH₄⁺ and SiO₂), and in 1-l glass bottles for the analysis of total hydrocarbons. Water samples were stored at 4 °C, brought within 4 h to the laboratory, and filtered through a 0.45 µm membrane filter (except for hydrocarbons). Depth of the water table was measured in each well with an OTT contact gauge. Specific conductance (WTW LF 330), DO (WTW OXI 330) and pH (WTW pH 330) were measured in the field. Sediment (grain size < 2 mm) and water analyses were performed by the Health and Environmental Laboratory of Lyon following standard methods (Clesceri et al., 1998; AFNOR, 1999). A detailed description of all analytical methods is given by Datry et al. (2003a). The average charge balance error for water samples ($n=75$) was $1.35 \pm 1.96\%$ (min. = -3.69; max. = 4.48) and the linear correlation coefficient between the sum of charge equivalents and specific conductance was $r=0.98$.

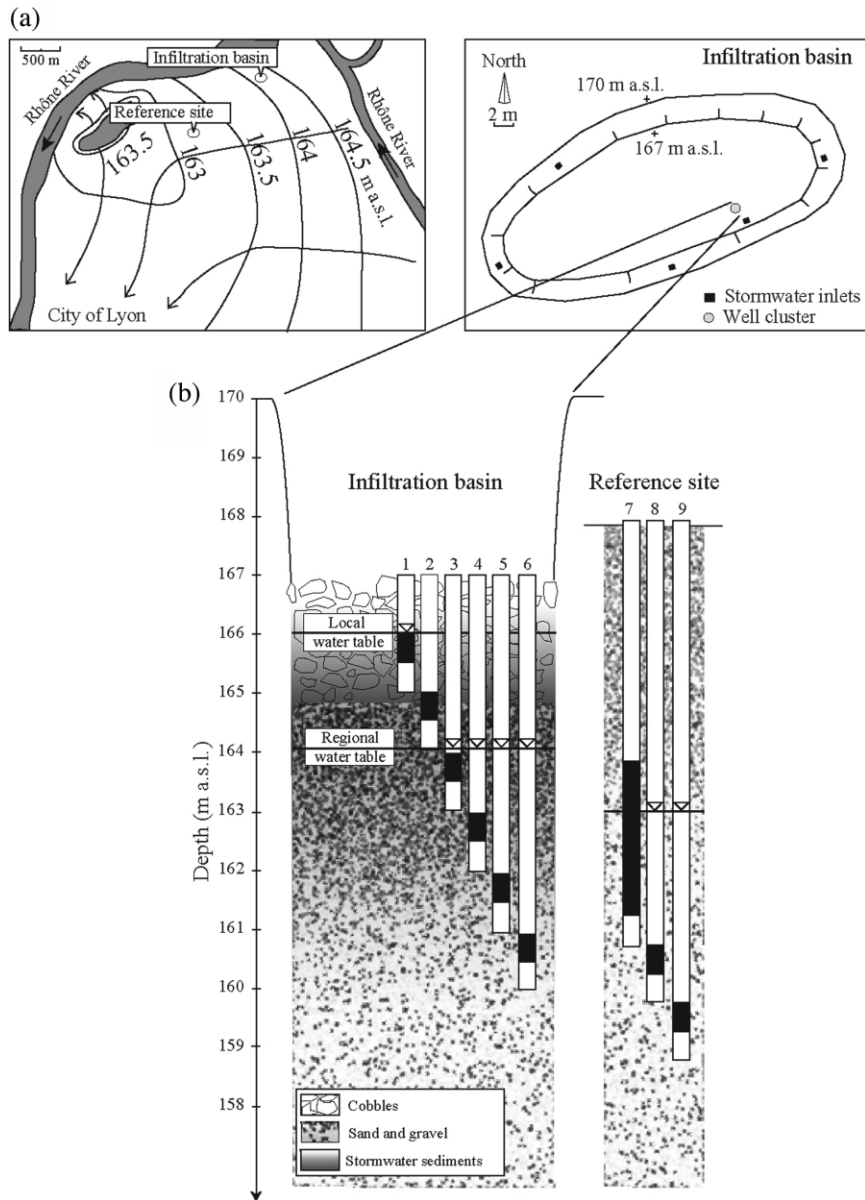


Fig. 1. Location of the stormwater infiltration basin and reference site (a) and description of well clusters used for sampling groundwater at multiple depths below the water table (b). Arrows in panel A indicate the regional groundwater flow direction.

3.4. Continuous measurements of specific conductance, temperature and DO

From October 2001 to September 2002, depth of the water table, specific conductance, temperature and DO were recorded in wells 1–9 using

YSI 600 XLM multi-parameter loggers. Based on manufacturer information, the accuracy and resolution of the probes were 0.12 and 0.001 m for water depth, $\pm 2\%$ and $1 \mu\text{S}/\text{cm}$ for specific conductance, $\pm 0.15\%$ and 0.01°C for temperature and $\pm 2\%$ and $0.01 \text{ mg}/\text{l}$ for DO, respectively.

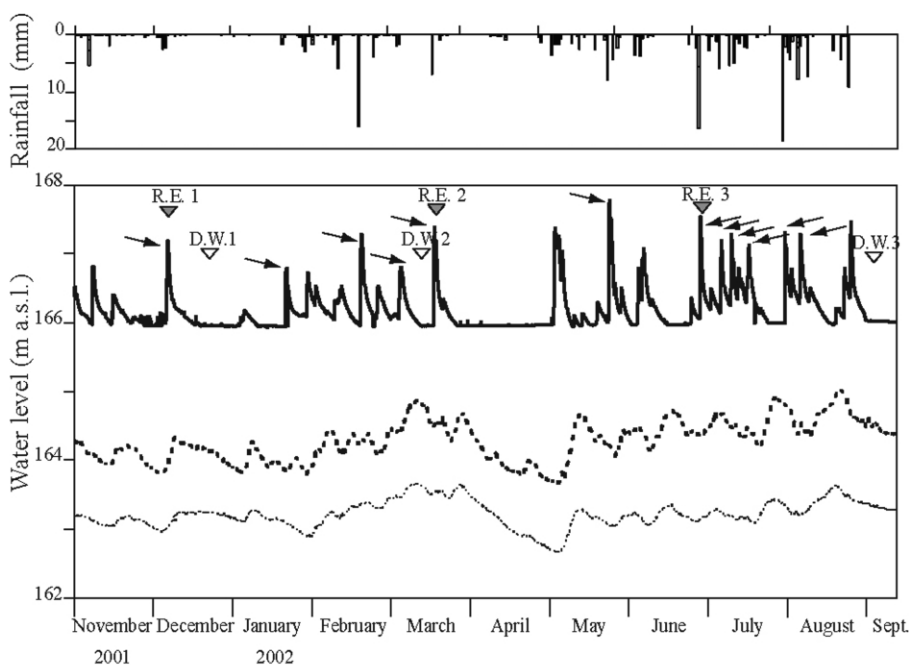


Fig. 2. Rainfall and fluctuations of the local water table in the infiltration bed (thick continuous line) and regional groundwater table at the infiltration site (thick broken line) and reference site (thin broken line). Grey and white arrows indicate sampling dates during rainfall events (R.E.) and dry weather (D.W.), respectively. Leaning black arrows indicate cold (December–May, $n=6$) and warm (July–August, $n=6$) rainfall events used for the analysis of DO dynamics in groundwater.

Parameters were measured at 1 h intervals and the loggers were transported to the laboratory every 15 days for data transfer, data examination, probe maintenance and calibration. Data were downloaded onto a computer and each series was checked for inconsistencies (i.e. drift, erroneous values). Loggers were placed in a water bath to test for differences between readings provided by the individual loggers and those provided by calibrated portable meters. When differences greatly exceeded the manufacturer accuracy, a correction factor was applied to the data derived from the loggers. Then, specific conductance and dissolved oxygen were calibrated and differences between measurements from the individual loggers were tested before deploying the loggers into the wells. On several occasions, measurements provided by the loggers were checked against those made on groundwater samples collected from the wells. Rainfall data (1 h intervals) were obtained from the nearest station of the Meteorological Survey

of the city of Lyon, 200 m from the infiltration basin.

4. Data analysis

Three-way analysis of variance (ANOVA) and multiple comparison tests (Scheffé tests) were used to test for differences in solute concentrations between sites, depths and hydrological phases (i.e. dry weather vs. rainfall events). Concentrations measured at depths of 1 and 2 m in groundwater below the infiltration basin were compared with those measured at a depth of 1.5 m in groundwater at the reference site. Solute concentrations were $\log_{10}(x+1)$ transformed prior to statistical analysis to satisfy the assumption of homoscedasticity. Three-way ANOVAs were performed on data recorded during 6 cold rain and 6 warm rain events in order to test for differences in specific conductance, temperature and DO concentration between sites, depths and time (i.e. before vs. after rain)

(Fig. 2). Cold and warm rains, which, respectively, decreased and increased water temperature of the infiltration bed, were treated separately because they appeared to have a dissimilar effect on DO concentration of groundwater. For each rainfall event, the following were calculated: (1) the average of DO values recorded during the 12 h preceding the beginning of the rain (i.e. before the rain); (2) the average of DO values recorded during the 12 h following the lowest specific conductance measured in groundwater (i.e. after the rain). Specific conductance was used as a tracer of stormwater infiltration because it was much lower in stormwater (130 $\mu\text{S}/\text{cm}$) than in groundwater (540 $\mu\text{S}/\text{cm}$).

A two-end member mixing model based on recorded values of specific conductance was used: (i) to determine vertical variation in the proportion of inflow stormwater in groundwater; and (ii) to measure the amount of DO consumed between two consecutive depths during rainfall events. Water sampled at each depth below the water table was assumed to be a mix of (i) pre-event groundwater and (ii) stormwater water percolating downward into the saturated zone. The relative proportion at depth x of water from depth $x-1$ was calculated using the following formula:

$$f(x-1) = (C_x - C_{g_x}) / (C_{x-1} - C_{g_x})$$

where $f(x-1)$ is the proportion at depth x of water from depth $x-1$, and C_x , C_{g_x} and C_{x-1} represent the specific conductance values of water collected at depth x during rainfall events (i.e. average of values recorded during the 12 h following the lowest specific conductance measured in groundwater), pre-event groundwater at depth x (i.e. average of values recorded during the 12 h preceding the beginning of the rain), and water collected at depth $x-1$, respectively. Specific conductance measured in runoff water collected from the main inlet pipe was used to calculate the proportion of stormwater at a depth of 1 m below the groundwater table. For checking the validity of the mixing model, differences in the proportion of inflow stormwater calculated at each depth were tested by using specific conductance and chloride as conservative tracers. To determine the amount of

DO consumed between two consecutive depths, predicted concentrations of DO (simple mixing of water sources) were plotted against measured concentrations. Predicted vs. measured concentrations were compared using a Wilcoxon paired test. Significance for all statistical analyses was accepted at $\alpha=0.05$. Statistical analyses were performed using the Statistica 6[®] software package (Statsoft Inc., Tulsa, Oklahoma, USA).

5. Results

5.1. Concentrations of nutrients, heavy metals and hydrocarbons in sediments

Stormwater sediments collected in the infiltration bed (well 1) had high concentrations of nutrients, hydrocarbons and heavy metals (Table 1). Ammonium nitrogen represented only 9% of total nitrogen, indicating that nitrogen was essentially present in an organic form. Zinc, lead and copper were by far the most abundant metals, representing 95% of the total metal concentration in stormwater sediments. Concentrations of nutrients, hydrocarbons and heavy metals were markedly reduced at a depth of 0.5 m below the bottom of the infiltration bed (well 2). Concentrations in fluvial sediments collected at depths of 1–3 m below the infiltration bed (wells 3–5) were not statistically higher (T -tests, $n=3$ sub-samples per well, $P>0.05$) than those measured in sediments of the reference site (well 7).

5.2. Patterns of solute concentrations

Water retained in the infiltration bed during dry-weather periods was enriched in solutes relative to the chemical composition of stormwater collected from the inlet pipe (Table 2). Whereas stormwater was near DO saturation, near-anoxic conditions prevailed in the infiltration bed during dry weather. Dissolved nitrogen was present exclusively as ammonium in the infiltration bed, whereas nitrate was the dominant form in stormwater. The average concentration of ammonium nitrogen in the infiltration bed (1.9 mg/l $\text{NH}_4^+ - \text{N}$) exceeded the concentration of nitrate nitrogen in stormwater (1 mg/l $\text{NO}_3^- - \text{N}$). Phosphate concentrations in the

Table 1

Concentrations (per kg sediment dry weight) of particulate organic carbon (POC), nitrogen (PN), phosphorous (PP), ammonium (NH_4^+), heavy metals, and total hydrocarbons in sediments

	Infiltration basin						Reference site
	Well 1 (n=3)	Well 2 (n=2)	Well 3 (n=3)	Well 4 (n=3)	Well 5 (n=3)	Well 6 (n=1)	Well 7 (n=3)
Nutrients (g/kg)							
POC	108.73 ± 11.50	6.05 ± 0.07	1.87 ± 0.47	1.73 ± 0.25	1.90 ± 0.35	1.60	1.27 ± 0.31
PP(P_2O_5)	5.40 ± 0.87	0.60 ± 0.00	0.37 ± 0.06	0.37 ± 0.06	0.43 ± 0.06	0.40	0.53 ± 0.06
PN	5.94 ± 1.11	0.25 ± 0.07	<0.1	<0.1	<0.1	<0.1	<0.1
NH_4^+	0.68 ± 0.10	<0.1	<0.1	<0.1	<0.1	<0.1	<0.1
Hydrocarbons (mg/kg)	3686 ± 1835	185 ± 37	<10	<10	<10	<10	<10
Heavy metals (mg/kg)							
Cd	25 ± 12	2 ± 1	<0.5	<0.5	<0.5	<0.5	<0.5
Cr	94 ± 21	15 ± 5	9 ± 2	10 ± 2	16 ± 8	16	13 ± 7
Cu	374 ± 118	20 ± 6	<2	<2	<2	2	<2
Ni	67 ± 13	7 ± 1	5 ± 1	6 ± 1	5 ± 1	8	8 ± 3
Pb	952 ± 159	60 ± 22	<5	<5	<5	<5	<5
Zn	2350 ± 626	159 ± 71	14 ± 4	14 ± 1	16 ± 1	18	14 ± 3

infiltration bed averaged 3.9 mg/l, against concentrations of 0.3 mg/l in stormwater. The concentration of hydrocarbons averaged 0.7 mg/l in water of the infiltration bed, whereas they were not detected in stormwater samples. Metals were never detected in stormwater or in the water of the infiltration bed. Specific conductance and the concentration of most solutes decreased as the infiltration bed was replenished with stormwater during rainfall events (Table 2). Discharge of stormwater into the infiltration bed increased the concentrations of DO (from 0.8 to 4.6 mg/l O_2), nitrate (from 0.1 to 4.5 mg/l NO_3^-) and DOC (from 3.1 to 4.3 mg/l).

There were no differences in solute concentrations between depths at the reference site (Fig. 3). Specific conductance and the concentrations of bicarbonate and calcium in groundwater below the infiltration basin did not differ from those measured at the reference site during dry weather but they were statistically lower during rainfall events ($P < 0.001$) (Table 2, Fig. 3). Sulfate, chloride, silica, magnesium and sodium concentrations were always lower ($P < 0.0001$) at the infiltration site, although differences between sites were typically more pronounced during rainfall events. Metals were never detected in groundwater. The concentration of hydrocarbons averaged 0.9 ± 1.3 mg/l at

the reference site during dry weather whereas they were never detected in groundwater below the infiltration basin. Groundwater recharged with stormwater was enriched in DOC and phosphate ($P < 0.001$) during both dry weather periods and rainfall events (Table 2, Fig. 3).

There were steep vertical gradients of concentration in groundwater below the infiltration basin during rainfall events (Fig. 3). Differences in solute concentrations between sites were highly significant ($P < 0.0001$, multiple comparison tests) at depths of 1 and 2 m below the groundwater table, whereas there were either little or no differences between sites at depths of 3 and 4 m. Vertical gradients of bicarbonate, nitrate and DOC were greatest 12 h after the end of rain (Fig. 4). Differences in concentration between depths progressively resorbed over time although they were still apparent 108 h after the end of the rain. Phosphate concentration exhibited a different pattern with highest differences between depths at the end of a recharge event.

5.3. Time series of specific conductance, temperature and DO during rainfall events

Temporal changes (1-h intervals) in temperature, specific conductance and DO of water in the

Table 2

Solute concentrations (\pm S.D., $n=3$) in inflow stormwater, water in the infiltration bed, groundwater below the infiltration basin, and groundwater at the reference site during dry weather (D.W.) and rainfall events (R.E.)

	Storm water	Infiltration bed		Ground water			
		D.W.	R.E.	Below basin		Reference site	
				D.W.	R.E.	D.W.	R.E.
Sp. conductance (μ S/cm)	129.0 \pm 7.5	321.0 \pm 94.0	183.0 \pm 47.0	543.8 \pm 61.3	370.8 \pm 46.3	553.3 \pm 9.9	515.7 \pm 52.0
Temperature ($^{\circ}$ C)	15.5 \pm 7.2	14.4 \pm 4.5	15.0 \pm 6.3	14.6 \pm 2.8	14.7 \pm 3.9	15.3 \pm 0.2	15.6 \pm 0.5
pH	7.2 \pm 0.1	7.3 \pm 0.1	7.4 \pm 0.0	7.3 \pm 0.2	7.4 \pm 0.2	7.3 \pm 0.1	7.4 \pm 0.0
HCO ₃ ⁻ (mg/l)	61 \pm 6.1	158.6 \pm 48.8	103.7 \pm 54.9	274.5 \pm 30.5	201.3 \pm 24.4	262.3 \pm 6.1	268.4 \pm 6.1
SO ₄ ²⁻ (mg/l)	5.8 \pm 0.5	9.8 \pm 7.8	10.5 \pm 6.4	33.7 \pm 14.4	25.1 \pm 8.4	42.8 \pm 1.4	44.0 \pm 2.2
SiO ₂ (mg/l)	2.0 \pm 0.2	6.0 \pm 0.8	4.0 \pm 2.2	6.4 \pm 0.5	5.1 \pm 0.6	9.3 \pm 0.5	9.5 \pm 0.7
Ca ²⁺ (mg/l)	23.8 \pm 1.3	43.3 \pm 14.7	35.3 \pm 16.2	90.5 \pm 10.4	68.9 \pm 10.1	90.2 \pm 3.2	92.5 \pm 4.4
Mg ²⁺ (mg/l)	0.5 \pm 0.2	2.5 \pm 1.4	1.4 \pm 1.3	5.1 \pm 1.1	3.8 \pm 0.5	7.2 \pm 0.4	7.3 \pm 0.4
Na ⁺ (mg/l)	0.4 \pm 0.8	5.7 \pm 4.0	1.8 \pm 3.1	6.4 \pm 1.9	4.7 \pm 2.1	9.9 \pm 1.0	10.3 \pm 1.3
K ⁺ (mg/l)	1.4 \pm 0.4	4.3 \pm 1.6	2.8 \pm 1.5	2.8 \pm 0.5	2.8 \pm 0.4	2.5 \pm 0.4	2.5 \pm 0.2
Cl ⁻ (mg/l)	1.5 \pm 0.7	6.6 \pm 5.4	3.0 \pm 2.8	10.4 \pm 2.8	6.1 \pm 1.6	16.1 \pm 1.9	15.4 \pm 2.0
PO ₄ ³⁻ (mg/l)	0.3 \pm 0.2	3.9 \pm 1.1	0.9 \pm 0.9	0.8 \pm 0.8	0.8 \pm 1.2	<0.05	<0.05
NO ₃ ⁻ (mg/l)	4.4 \pm 2.8	0.1 \pm 0.1	4.5 \pm 2.1	10.9 \pm 3.7	10.8 \pm 2.4	10.1 \pm 0.3	10.2 \pm 0.5
NO ₂ ⁻ (mg/l)	0.2 \pm 0.0	<0.02	<0.02	<0.02	<0.02	<0.02	<0.02
NH ₄ ⁺ (mg/l)	0.1 \pm 0.1	2.4 \pm 1.8	0.4 \pm 0.6	<0.05	<0.05	<0.05	<0.05
DOC (mg/l)	3.6 \pm 0.5	3.1 \pm 0.3	4.9 \pm 1.7	1.2 \pm 0.3	1.7 \pm 1.0	0.5 \pm 0.1	0.5 \pm 0.1
DO (mg/l)	9.5 \pm 1.2	0.8 \pm 0.4	4.6 \pm 0.8	3.5 \pm 0.5	4.7 \pm 1.8	3.9 \pm 0.9	3.6 \pm 1.1
Hydrocarbons (mg/l)	<0.02	0.7 \pm 0.9	0.7 \pm 0.6	<0.02	<0.02	0.9 \pm 1.3	0.2 \pm 0.3
Cd (μ g/l)	<1	<1	<1	<1	<1	<1	<1
Cr (μ g/l)	<10	<10	<10	<10	<10	<10	<10
Cu (μ g/l)	<50	<50	<50	<50	<50	<50	<50
Ni (μ g/l)	<10	<10	<10	<10	<10	<10	<10
Pb (μ g/l)	<10	<10	<10	<10	<10	<10	<10
Zn (μ g/l)	<50	<50	<50	<50	<50	<50	<50

infiltration bed, groundwater below the infiltration basin (i.e. 1 m below the water table), and groundwater at the reference site during a cold and a warm rain are shown in Fig. 5. These cold and warm rains resulted in a discharge of 535 m³ and 598 m³ of stormwater into the infiltration bed, respectively. Groundwater at the reference site showed no variation in specific conductance, temperature and DO. Less than 1 h after the beginning of both rains, the inflow stormwater resulted in a sharp decrease in specific conductance in the infiltration bed. Specific conductance of groundwater started to decline 10 h after the beginning of rain. Temperature decreased from 13 to 10 $^{\circ}$ C in the infiltration bed and from 15 to 12 $^{\circ}$ C in groundwater during the cold rain. The warm rain elevated temperature of the infiltration bed from 20 to 24 $^{\circ}$ C and that of groundwater from 16 to

19 $^{\circ}$ C. During both rainfall events, DO concentration in the infiltration bed rose with the input of stormwater. However, the increase in DO concentration occurred 19 h after that of specific conductance during the warm rain. This lag difference between the pulses of specific conductance and DO was only observed during warm rainfall events. DO concentration of groundwater increased during the cold rain (from 3.8 to 4.7 mg/l O₂), whereas it decreased during the warm rain (from 3.6 to 1.9 mg/l O₂).

5.4. Vertical gradients of specific conductance, temperature and DO

Specific conductance, temperature and DO concentration showed no variation with depth at the reference site either before or after the cold and

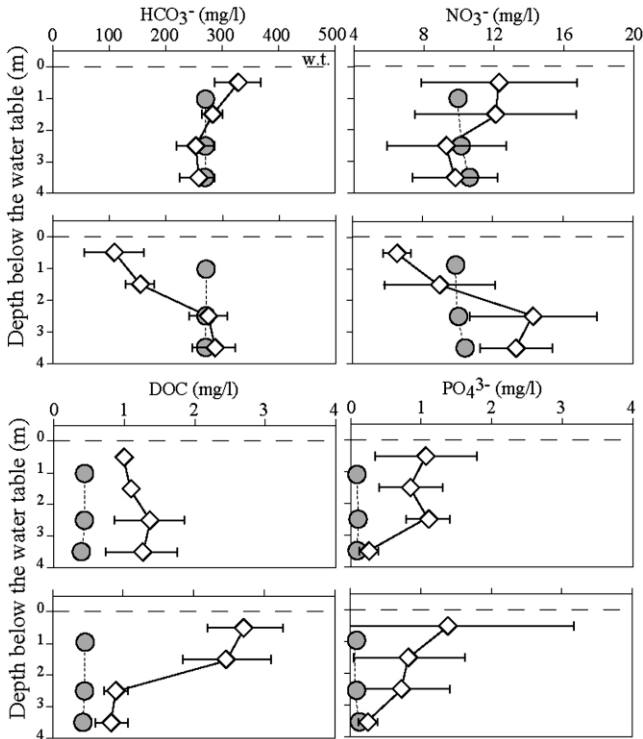


Fig. 3. Vertical gradients of bicarbonates, nitrates, dissolved organic carbon and phosphates in groundwater at the reference site (gray circles) and infiltration site (white diamonds) during dry weather (upper panels, mean \pm S.D.; $n=3$) and rainfall events (lower panels, $n=3$).

warm rains (Fig. 6). Groundwater recharge with stormwater resulted in a marked increasing gradient of specific conductance with depth. Specific conductance at depths of 1, 2 and 3 m below the water table was significantly lower after the rain. There were no differences in specific conductance before and after the rain at a depth of 4 m below the water table. Cold and warm rains, respectively, decreased and increased groundwater temperature at depths of 1 and 2 m below the water table (Fig. 6). Temperature measured after the rain at depths of 3 and 4 below the water table did not differ from that measured before the rain. There were no differences in DO concentration between depths before the rain. Post-event DO concentration decreased with depth during cold rains, whereas it increased during warm rains. Recharge with storm-

water elevated DO concentration at depths of 1, 2 and 3 m below the water table during cold rains, whereas it decreased DO concentration at depths of 1 and 2 m during warm rains. There were no significant changes in DO concentration at a depth of 4 m during cold rains and at depths of 3 and 4 m during warm rains.

5.5. DO consumption

Wilcoxon matched pairs test indicated no difference ($P=0.078$) between the proportions of stormwater calculated with the mixing models based on chloride concentration and specific conductance (Fig. 7, $n=3$ rainfall events). Calculation made using specific conductance as a conservative tracer revealed that 84.6 ± 5.6 and $71.0 \pm 7.0\%$ ($n=12$ rainfall events) of groundwater at depths of 1 and 2 m below the water table was composed of newly infiltrating stormwater. The relative proportion of stormwater dropped to $6.6 \pm 5.7\%$ and 0% at depths of 3 m and 4 m below the water table, respectively. Measured concentrations of DO were significantly lower ($P<0.001$) than predicted concentrations at a depth of 1 m below the water table (Fig. 8a). However, there were no differences between measured and predicted concentrations at depths of 2, 3 and 4 m below the water table. The difference between measured and predicted concentrations of DO at a depth of 1 m below the water table was much higher during warm rainfall events than during cold rainfall events and increased linearly with water temperature in the infiltration bed (Fig. 8b).

6. Discussion

6.1. Stormwater flow pattern

The transit of water in the catchment of the infiltration basin was rapid as stormwater started to discharge into the infiltration bed only 15 min after the beginning of rains (Datry et al., 2003a). Because of the reduced thickness of the vadose zone (<3 m) and high permeability of fluvial sediments ($K=5 \cdot 10^{-2}$ m/s), the transit of water from the infiltration bed to the groundwater table should have been a matter of minutes. However,

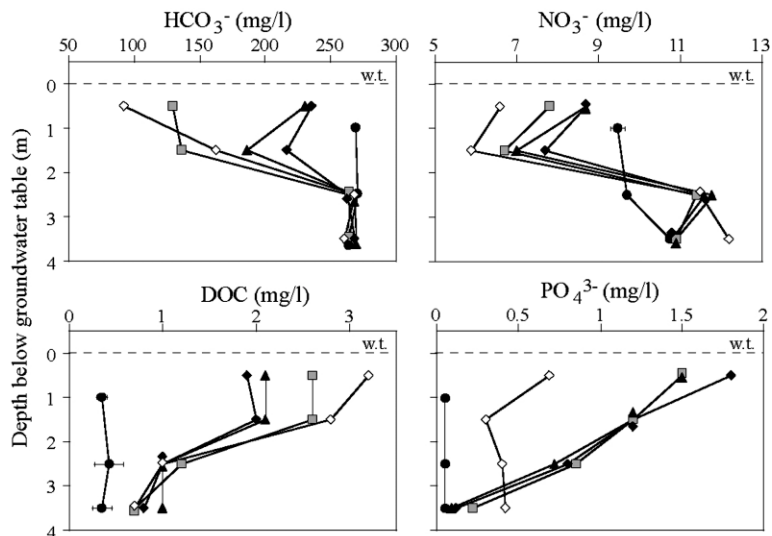


Fig. 4. Vertical gradients of bicarbonates, nitrates, dissolved organic carbon and phosphates in groundwater below the infiltration basin 12 h (white diamonds), 32 h (gray squares), 80 h (gray triangles) and 108 h (black diamonds) after the end of a rain (28 June 2002). Black circles show mean concentrations (\pm S.D.; $n=4$) at the reference site during the same rainfall event.

specific conductance of groundwater was found to decrease only 10 h after the beginning of rains. This long time lag strongly suggested that clogging of the infiltration bed prevented the downward flow of stormwater through the vadose zone in the vicinity of monitoring wells. Well 2, whose screen intersected the contact zone between the infiltration bed and fluvial sediments, remained dry during the study period. Video-logging carried out in transparent wells revealed that the pores of the cobble layer were entirely filled with fine stormwater sediments (particle size $<100 \mu\text{m}$) from a depth of 1.4 m below the surface of the infiltration bed (Datry et al., 2003c). Therefore, stormwater followed subhorizontal pathways in the upper part of the cobble layer prior to infiltration through permeable areas of the infiltration bed. The bulk of stormwater probably percolated downward at the edges of the infiltration bed because stormwater sediments were found to extend over most of the bed area (BURGEAP, 2002). Spatial heterogeneity in the infiltration of stormwater is probably a common phenomenon because infiltration basins without decanting pre-treatment accumulate

considerable amounts of low permeability sediments over time (Chebbo et al., 1995; Marsalek and Marsalek, 1997; Baveye et al., 2000; Dechesne, 2002).

Stormwater input to the water table resulted in a low-salinity plume that extended vertically and horizontally into the aquifer. During rainfall events, the water level in the shallowest well was on average 8 cm higher than that of the deepest well, indicating a downward flow of water. The vertical velocity of stormwater in the upper layers of the saturated zone was approximately 0.7 m/h because the time lag between the lowest specific conductance values measured at depths of 1 and 2 m below the groundwater table averaged 1.5 h ($n=9$ rainfall events). Groundwater at a depth of 1 m below the water table consisted almost exclusively of stormwater. However, the plume of low specific conductance water was restricted to the upper part of the aquifer: stormwater did not appear to penetrate at depths greater than 3 m below the water table. Appleyard (1993) has demonstrated that stormwater recharge through infiltration basins receiving runoff from large

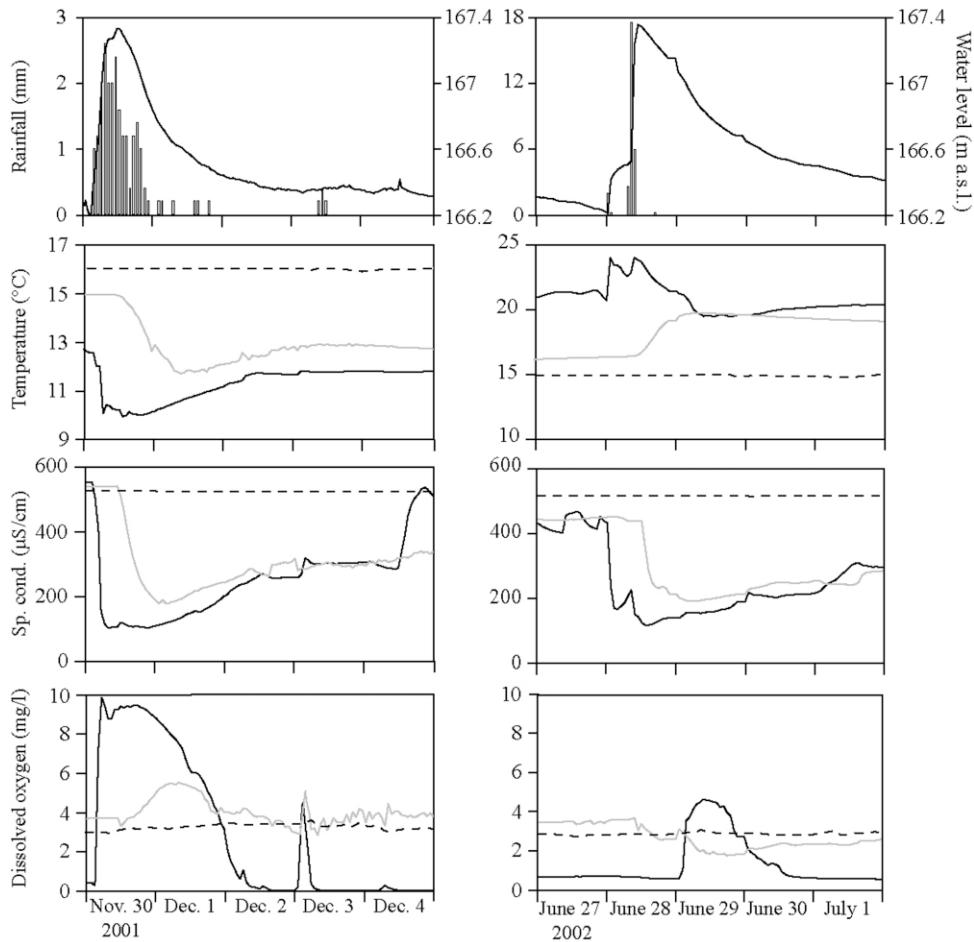


Fig. 5. Rainfall, temporal changes in water level in the infiltration bed (upper panels) and corresponding temporal series (1-h intervals) of temperature, specific conductance and DO of water in the infiltration bed (black continuous line), groundwater below the infiltration basin (1 m below the water table, gray continuous line), and groundwater at the reference site (black broken line) during a cold (left panels) and a warm (right panels) rain.

impervious catchments of the Perth metropolitan area, Australia, caused a marked reduction in total dissolved salts to depths of more than 10 m below the groundwater table. Return to pre-event water level in the infiltration bed took less than 4 days but the low specific conductance plume persisted for longer in groundwater (7 days). Therefore, vertical gradients of specific conductance and temperature were maintained in the absence of stormwater infiltration when rainfall events succeeded

over short time intervals (e.g. thunderstorms in July and August).

6.2. Effects of stormwater infiltration on nutrient concentrations in groundwater

Clogging of the infiltration bed favoured the contact between stormwater and organic sediments stored in the cobble matrix. Indeed, clogging not only increased the residence time of inflow storm-

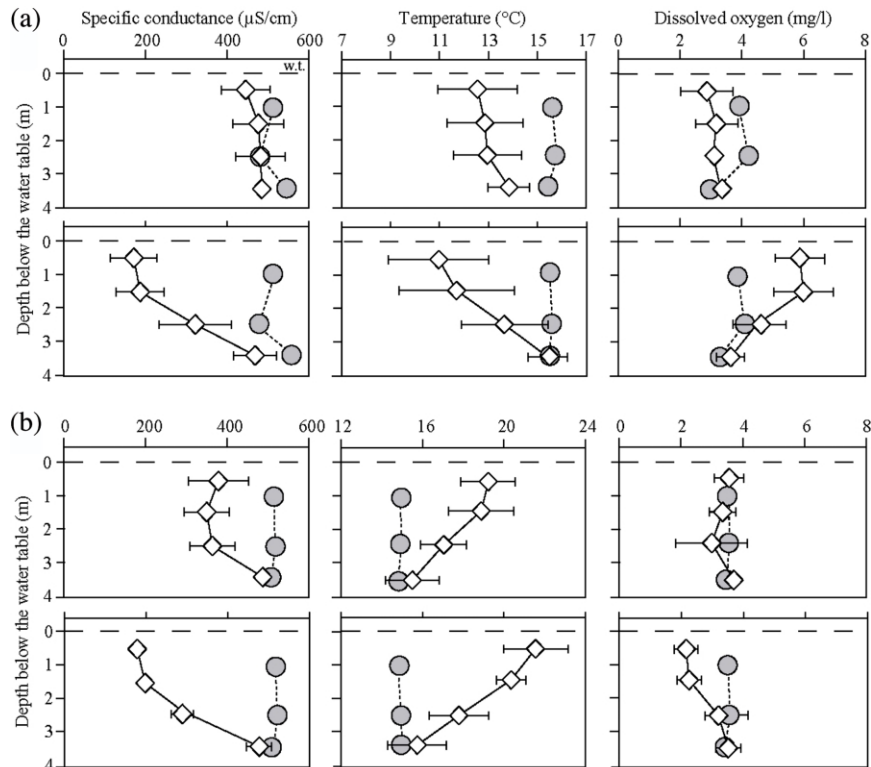


Fig. 6. (a) Vertical gradients of specific conductance, temperature and dissolved oxygen in groundwater at the reference site (gray circles) and infiltration site (white diamonds) before (upper panels) and after (lower panels) cold rainfall events (mean \pm S.D.; $n=6$ rainfall events). (b) Same as in (a) but for warm rainfall events ($n=6$).

water during recharge events but also caused a permanent retention of water. Assuming a thickness of water-saturated cobble matrix of 1 m, an estimated volume of 280 m³ of stormwater was retained in the infiltration bed between successive rains. Differences in chemistry between inflow stormwater and water collected in the infiltration bed during dry weather showed that microbial respiration of organic matter produced ammonium and phosphates, which accumulated in solution in the absence of dissolved oxygen. Datry et al. (2003a) have measured average concentrations of ammonium and phosphate as high as 12.0 ± 2.6 mg/l NH₄⁺ ($n=30$ samples) and 9.2 ± 1.7 mg/l PO₄³⁻ during a dry weather. Based on the results of field sampling and slow filtration column experiments, these authors also demonstrated that particulate organic matter stored in the infiltration bed

released DOC through leaching and/or enzymatic hydrolysis. Therefore, we expected stormwater infiltration to result in elevated concentrations of DOC, phosphates and ammonium in groundwater. This assumption was partly supported by the present study.

During rainfall events, DOC and phosphate concentrations were higher in groundwater below the infiltration basin and decreased with increasing depth below the water table. The average concentration of DOC at depths of 1 and 2 m below the water table (2.52 ± 0.17 mg/l) was 4.8 times higher than that measured at the reference site (0.52 ± 0.07 mg/l). However, DOC concentration in groundwater was less than that measured in inflow stormwater. Therefore, the results did not conclusively determine whether the main source of DOC was from particulate organic matter

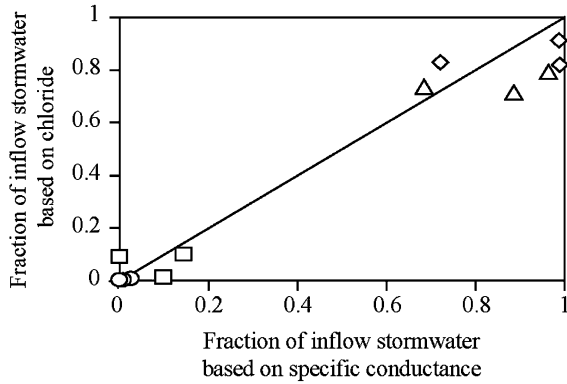


Fig. 7. Comparison between the proportions of inflow stormwater at depths of 1 m (diamond), 2 m (triangle), 3 m (square) and 4 m (circle) below the groundwater table calculated with the mixing models based on chloride concentration and specific conductance ($n=3$ rainfall events). The line indicates 1:1 equivalence relationships.

trapped in the infiltration bed or from inflow stormwater. In contrast, dissolved phosphate measured in groundwater was necessarily produced within the infiltration bed because it appeared at a concentration higher than that measured in inflow stormwater. The migration of phosphates might occur preferentially towards the end of each recharge event when stormwater in the infiltration bed become anoxic. Although ammonium was the dominant nitrogen species in the infiltration bed during dry weather, it was not detected in groundwater. Ammonium was probably oxidized to nitrate when the bed was replenished with oxic inflow stormwater. Nitrification is a rapid process shown to cause the disappearance of ammonium in a number of fast infiltration basins (Summer et al., 1998; Mason et al., 1999). Because stormwater contained 2.5 times less nitrate than pre-event groundwater, induced infiltration caused a marked reduction in nitrate concentration in the upper part of the saturated zone. Heavy metals and hydrocarbons were never detected in groundwater despite their high concentrations in bed sediments; despite shallow water table conditions (<3 m), groundwater was not impacted by either metal or hydrocarbons contamination. Particulate materials to which metals bind were retained by physical filtration in the infiltration bed. Moreover, the five

metals measured in this study are known to adsorb strongly onto particle surfaces such as clay minerals and oxides under the pH range in the infiltration bed (pH approx. 7.5) (Hermann and Neuman-Mahlkau, 1985; Legret et al., 1988). A total of 15 polycyclic aromatic hydrocarbons were identified in the bed sediments (Datry et al., 2003a), all of which (except naphtalene) had a very solubility in water (solubility $\ll 1$ mg/l, Montgomery, 1996). Results of sediment analyses also suggested that metals and hydrocarbons did not migrate at depth into underlying gravely and sandy sediments. In contrast, Mason et al. (1999) have reported that zinc, lead and chromium contained in roof runoff migrated downward to a depth of 1.6 m in unsaturated soil sediments of a

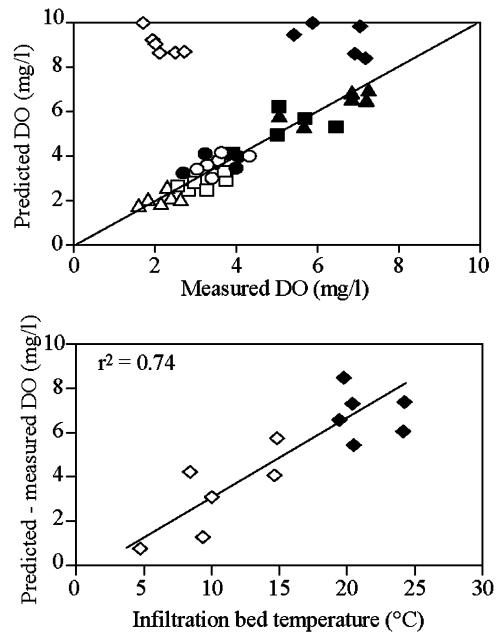


Fig. 8. Upper panel: Predicted concentrations from the two-end member mixing model based on specific conductance vs. concentrations of DO measured at depths of 1 m (diamond), 2 m (triangle), 3 m (square) and 4 m (circle) below the groundwater table at the infiltration site. Black and white symbols correspond to cold ($n=6$) and warm ($n=6$) rainfall events, respectively. The line indicates 1:1 equivalence relationships. Lower panel: Relation between DO deficit in groundwater (i.e. predicted minus measured DO concentrations) at a depth of 1 m below the water table and water temperature in the infiltration bed.

2-year old infiltration site. In the present study, metals and hydrocarbons were restricted to the first 50 cm of sediments, which consisted of a mixture of fine stormwater particles and natural gravel and sands.

6.3. DO dynamics in groundwater below the infiltration bed

Induced infiltration of stormwater is expected to replenish urban groundwater with DO, as runoff water is usually near DO saturation. Appleyard (1993) showed that infiltration of urban runoff water into groundwater of the Perth metropolitan area, Australia, elevated DO concentration and resulted in the oxidation of free ferrous iron. In contrast, Fischer et al. (2003) measured lower dissolved oxygen concentrations compared to background levels in groundwater below 16 stormwater basins in southern New Jersey, USA. In the present study, stormwater infiltration induced only a moderate (2 mg/l) and short-duration (less than 2 days) increase in DO concentration of groundwater during cold rains. DO concentration of groundwater even decreased during warm rainfall events. Results strongly suggest that the dynamics of DO in groundwater is mainly controlled by variation in the rate of microbial respiration in the infiltration bed. Indeed, differences in oxygen deficit between depths (predicted minus measured DO concentrations) showed that DO was consumed during the transit of inflow stormwater from the infiltration bed to the first meter below the groundwater table. DO concentration in inflow stormwater was substantially reduced by microbial respiration of organic sediments stored in the infiltration bed. Microbial respiration was stimulated by the increase in temperature, thereby leading to higher oxygen deficit in summer. During warm rains, microbial respiration was high enough to maintain near anoxic conditions in the infiltration bed during most of the recharge period. The transit time of infiltrating water in the vadose zone was probably too short for inducing a substantial re-oxygenation of infiltrating water. Thus, the strong oxygen deficit measured at a depth of 1 m below the groundwater table was more likely due

to the input of deoxygenated stormwater rather than to the biological degradation of DOC in groundwater. This observation was supported by the fact that the input of DOC had no detectable influence on DO consumption at depths of 2, 3 and 4 below the groundwater table. Although additional analyses are needed to determine the composition of DOC, this might indicate that a large fraction of dissolved organic matter reaching groundwater was refractory.

7. Conclusions

Shallow water-table groundwater artificially recharged with urban runoff stormwater exhibited a strong temporal and vertical heterogeneity in physico-chemistry. Hence, multilevel wells and multiparameter loggers were essential for examining changes in groundwater chemistry occurring over small spatial and temporal scales below infiltration basin. Rainfall events resulted in a plume of low-specific conductance water in the uppermost layers of the aquifer (2 m below the groundwater table), thereby generating steep vertical physico-chemical gradients, which progressively resorbed when infiltration ceased. Heavy metals and hydrocarbons were either not detected or below reference concentrations in groundwater and aquifer sediments indicating that they remained adsorbed onto stormwater sediments stored in the infiltration bed. However, mineralization of organic sediments appeared to be the most probable cause of elevated concentrations of phosphate and DOC in groundwater below the infiltration basin. The influence of mineralization processes on nutrient concentration of infiltrating stormwater was all the more pronounced as bed clogging considerably increased the contact time of inflow stormwater with organic sediments. Similarly, microbial respiration strongly reduced DO in inflow stormwater, thereby severely limiting DO supply in groundwater. Because DO uptake in the infiltration bed increased with increasing temperature, the effect of stormwater infiltration on DO concentration of groundwater varied seasonally. Cold winter stormwater slightly re-oxygenated groundwater, whereas warm summer stormwater lowered DO concentra-

tion in groundwater. In a previous paper (Datry et al., 2003a), it has been suggested that there could be a discrepancy between the expected effects of runoff water infiltration evaluated from the analysis of nutrients and DO concentrations in inflow water and the risk resulting from the percolation of inflow water through a layer of stormwater sediment. This assumption was supported by the results of the present study. It is recommended that stormwater infiltration practices should minimize the contact between inflow stormwater and organic sediments retained in infiltration basins.

Acknowledgments

This work was part of the OTHU project (Experimental Observatory for Urban Hydrology) and was funded by the urban community of Lyon (COURLY) and the Rhône-Alpes Region. We are indebted to G. Bouger and L. Vitry for their most dedicated help with the field and laboratory work. We also thank Chris Robinson and one anonymous reviewer for their comments and meticulous editing that improved the final version of this paper.

References

- Appleyard SJ. Impact of stormwater infiltration basins on groundwater quality, Perth metropolitan region, Western Australia. *Environ Geol* 1993;2:227–236.
- A.F.N.O.R. La qualité de l'eau. Association Française de Normalisation, Paris, 1999.
- Baveye P, Vandevivere P, Hoyle BL, Deleo PC, Sanchez de Lozada D. Environmental impact and mechanisms of the biological clogging of saturated soils and aquifer materials. *Crit Rev Environ Sci Technol* 2000;28:123–191.
- Bou C, Rouch R. Un nouveau champ de recherche sur la faune aquatique souterraine. *Compte Rendus Acad Sci* 1967;265:369–370.
- Burgeap. Prospection géophysique du bassin d'infiltration de l'IUT. Villeurbanne (69). RLy.861/A.9394/C.902071, 2002; p. 14.
- Chapelle FH. Groundwater microbiology and geochemistry. New York: John Wiley & Sons, 2000. p. 468
- Chebbo G, Mouchel JM, Saget A, Gousailles M. La pollution des rejets urbains par temps de pluie: flux, nature et impacts. *Tech Sci Méthod* 1995;11:796–804.
- Chocat B. Aménagement urbain et hydrologie. *La Houille Blanche* 1997; 7: pp. 12–19.
- Clesceri LS, Greenberg AE, Eaton AD, editors. Standard methods for the examination of water and wastewater. Washington: American Public Health Association, 1998.
- Datry T, Malard F, Hervant F, Vitry L, Gibert J. Solute dynamics in the bed of a rapid infiltration storm water basin. *J Hydrol* 2003a;273:217–233.
- Datry T, Hervant F, Malard F, Vitry L, Gibert J. Dynamics and adaptive responses of invertebrates to suboxia in contaminated sediments of a stormwater infiltration basin. *Arch Hydrobiol* 2003b;156(3):339–359.
- Datry T, Malard F, Niedereitter R, Gibert J. Video logging for examining biogenic structures in deep heterogeneous subsurface sediments. *Compte Rendus Acad Sci: Biol* 2003c;326(6):589–597.
- Dechesne M. Connaissance et modélisation du fonctionnement des bassins d'infiltration d'eaux de ruissellement urbain pour l'évaluation des performances techniques et environnementales sur le long terme. Thesis INSA Lyon, 2002; p. 277.
- Fischer D, Charles EG, Baehr AL. Effects of stormwater infiltration on quality if groundwater beneath retention and detention basins. *J Environ Eng* 2003;129(5):464–471.
- Fujita S. Measures to promote stormwater infiltration. *Water Sci Technol* 1997;36:289–293.
- Horizon. Synthèse hydrogéologique et thermique des forages pompes à chaleurs. Lyon-Villeurbanne (69). Etude DH160, 2000; p. 32.
- Hermann R, Neuman-Mahlkau P. The mobility of zinc, copper, lead and arsenic in groundwater as a function of redox potential and pH. *Sci Total Environ* 1985;43:1–12.
- Legret M, Divet L, Juste C. Migration et spéciation des métaux lourds dans un sol soumis à des épandages de boues de station d'épuration à très forte charge en Cd et Ni. *Water Res* 1988;22(8):953–959.
- Malard F, Hervant F. Oxygen supply and the adaptations of animals in groundwater. *Freshwater Biol* 1999;41:1–30.
- Marsalek J, Marsalek PM. Characteristic of sediments from a stormwater management pond. *Water Sci Technol* 1997;36(8–9):117–122.
- Mason Y, Amman A, Ulrich A, Sigg L. Behavior of heavy metals nutrients and major components during roof runoff infiltration. *Environ Sci Technol* 1999;33:1588–1597.
- Montgomery JH. Groundwater chemicals: desk reference. New York: Lewis Publishers, 1996. p. 1345
- Pitt R, Clark S, Field R. Groundwater contamination potential from stormwater infiltration practices. *Urban Water* 1999;1:217–236.
- Starr RC, Gillham RW. Denitrification and organic carbon availability in two aquifers. *Ground Water* 1993;31:934–947.
- Summer DM, Rolston DE, Bradner LA. Nutrient transport and transformation beneath an infiltration basin. *Water Environ Res* 1998;70:997–1004.



Overview of the Coupled Model Intercomparison Project Phase 6 (CMIP6) experimental design and organization

Veronika Eyring¹, Sandrine Bony², Gerald A. Meehl³, Catherine A. Senior⁴, Bjorn Stevens⁵, Ronald J. Stouffer⁶, and Karl E. Taylor⁷

¹Deutsches Zentrum für Luft- und Raumfahrt (DLR), Institut für Physik der Atmosphäre, Oberpfaffenhofen, Germany

²Laboratoire de Météorologie Dynamique, Institut Pierre Simon Laplace (LMD/IPSL), CNRS, Université Pierre et Marie Curie, Paris, France

³National Center for Atmospheric Research (NCAR), Boulder, CO, USA

⁴Met Office Hadley Centre, Exeter, UK

⁵Max-Planck-Institute for Meteorology, Hamburg, Germany

⁶Geophysical Fluid Dynamics Laboratory/NOAA, Princeton, NJ, USA

⁷Program for Climate Model Diagnosis and Intercomparison (PCMDI), Lawrence Livermore National Laboratory, Livermore, CA, USA

Correspondence to: Veronika Eyring (veronika.eyring@dlr.de)

Received: 3 December 2015 – Published in Geosci. Model Dev. Discuss.: 14 December 2015

Revised: 15 April 2016 – Accepted: 27 April 2016 – Published: 26 May 2016

Abstract. By coordinating the design and distribution of global climate model simulations of the past, current, and future climate, the Coupled Model Intercomparison Project (CMIP) has become one of the foundational elements of climate science. However, the need to address an ever-expanding range of scientific questions arising from more and more research communities has made it necessary to revise the organization of CMIP. After a long and wide community consultation, a new and more federated structure has been put in place. It consists of three major elements: (1) a handful of common experiments, the DECK (Diagnostic, Evaluation and Characterization of Klima) and CMIP historical simulations (1850–near present) that will maintain continuity and help document basic characteristics of models across different phases of CMIP; (2) common standards, coordination, infrastructure, and documentation that will facilitate the distribution of model outputs and the characterization of the model ensemble; and (3) an ensemble of CMIP-Endorsed Model Intercomparison Projects (MIPs) that will be specific to a particular phase of CMIP (now CMIP6) and that will build on the DECK and CMIP historical simulations to address a large range of specific questions and fill the scientific gaps of the previous CMIP phases. The DECK and CMIP historical simulations, together with the use of CMIP

data standards, will be the entry cards for models participating in CMIP. Participation in CMIP6-Endorsed MIPs by individual modelling groups will be at their own discretion and will depend on their scientific interests and priorities. With the Grand Science Challenges of the World Climate Research Programme (WCRP) as its scientific backdrop, CMIP6 will address three broad questions:

- How does the Earth system respond to forcing?
- What are the origins and consequences of systematic model biases?
- How can we assess future climate changes given internal climate variability, predictability, and uncertainties in scenarios?

This CMIP6 overview paper presents the background and rationale for the new structure of CMIP, provides a detailed description of the DECK and CMIP6 historical simulations, and includes a brief introduction to the 21 CMIP6-Endorsed MIPs.

1 Introduction

The Coupled Model Intercomparison Project (CMIP) organized under the auspices of the World Climate Research Programme's (WCRP) Working Group on Coupled Modelling (WGCM) started 20 years ago as a comparison of a handful of early global coupled climate models performing experiments using atmosphere models coupled to a dynamic ocean, a simple land surface, and thermodynamic sea ice (Meehl et al., 1997). It has since evolved over five phases into a major international multi-model research activity (Meehl et al., 2000, 2007; Taylor et al., 2012) that has not only introduced a new era to climate science research but has also become a central element of national and international assessments of climate change (e.g. IPCC, 2013). An important part of CMIP is to make the multi-model output publicly available in a standardized format for analysis by the wider climate community and users. The standardization of the model output in a specified format, and the collection, archival, and access of the model output through the Earth System Grid Federation (ESGF) data replication centres have facilitated multi-model analyses.

The objective of CMIP is to better understand past, present, and future climate change arising from natural, unforced variability or in response to changes in radiative forcings in a multi-model context. Its increasing importance and scope is a tremendous success story, but this very success poses challenges for all involved. Coordination of the project has become more complex as CMIP includes more models with more processes all applied to a wider range of questions. To meet this new interest and to address a wide variety of science questions from more and more scientific research communities, reflecting the expanding scope of comprehensive modelling in climate science, has put pressure on CMIP to become larger and more extensive. Consequently, there has been an explosion in the diversity and volume of requested CMIP output from an increasing number of experiments causing challenges for CMIP's technical infrastructure (Williams et al., 2015). Cultural and organizational challenges also arise from the tension between expectations that modelling centres deliver multiple model experiments to CMIP yet at the same time advance basic research in climate science.

In response to these challenges, we have adopted a more federated structure for the sixth phase of CMIP (i.e. CMIP6) and subsequent phases. Whereas past phases of CMIP were usually described through a single overview paper, reflecting a centralized and relatively compact CMIP structure, this GMD special issue describes the new design and organization of CMIP, the suite of experiments, and its forcings, in a series of invited contributions. In this paper, we provide the overview and backdrop of the new CMIP structure as well as the main scientific foci that CMIP6 will address. We begin by describing the new organizational form for CMIP and the pressures that it was designed to alleviate (Sect. 2). It also

contains a description of a small set of simulations for CMIP which are intended to be common to all participating models (Sect. 3), details of which are provided in the Appendix. We then present a brief overview of CMIP6 that serves as an introduction to the other contributions to this special issue (Sect. 4), and we close with a summary.

2 CMIP design – a more continuous and distributed organization

In preparing for CMIP6, the CMIP Panel (the authors of this paper), which traditionally has the responsibility for direct coordination and oversight of CMIP, initiated a 2-year process of community consultation. This consultation involved the modelling centres whose contributions form the substance of CMIP as well as communities that rely on CMIP model output for their work. Special meetings were organized to reflect on the successes of CMIP5 as well as the scientific gaps that remain or have since emerged. The consultation also sought input through a community survey, the scientific results of which are described by Stouffer et al. (2015). Four main issues related to the overall structure of CMIP were identified.

First, we identified a growing appreciation of the scientific potential to use results across different CMIP phases. Such approaches, however, require an appropriate experimental design to facilitate the identification of an ensemble of models with particular properties drawn from different phases of CMIP (e.g. Rauser et al., 2014). At the same time, it was recognized that an increasing number of Model Intercomparison Projects (MIPs) were being organized independent of CMIP, the data structure and output requirements were often inconsistent, and the relationship between the models used in the various MIPs was often difficult to determine, in which context measures to help establish continuity across MIPs or phases of CMIP would also be welcome.

Second, the scope of CMIP was taxing the resources of modelling centres making it impossible for many to consider contributing to all the proposed experiments. By providing a better basis to help modelling centres decide exactly which subset of experiments to perform, it was thought that it might be possible to minimize fragmented participation in CMIP6. A more federated experimental protocol could also encourage modelling centres to develop intercomparison studies based on their own strategic goals.

Third, some centres expressed the view that the punctuated structure of CMIP had begun to distort the model development process. Defining a protocol that allowed modelling centres to decouple their model development from the CMIP schedule would offer additional flexibility, and perhaps encourage modelling centres to finalize their models and submit some of their results sooner on their own schedule.

Fourth and finally, many groups expressed a desire for particular phases of CMIP to be more than just a collection of

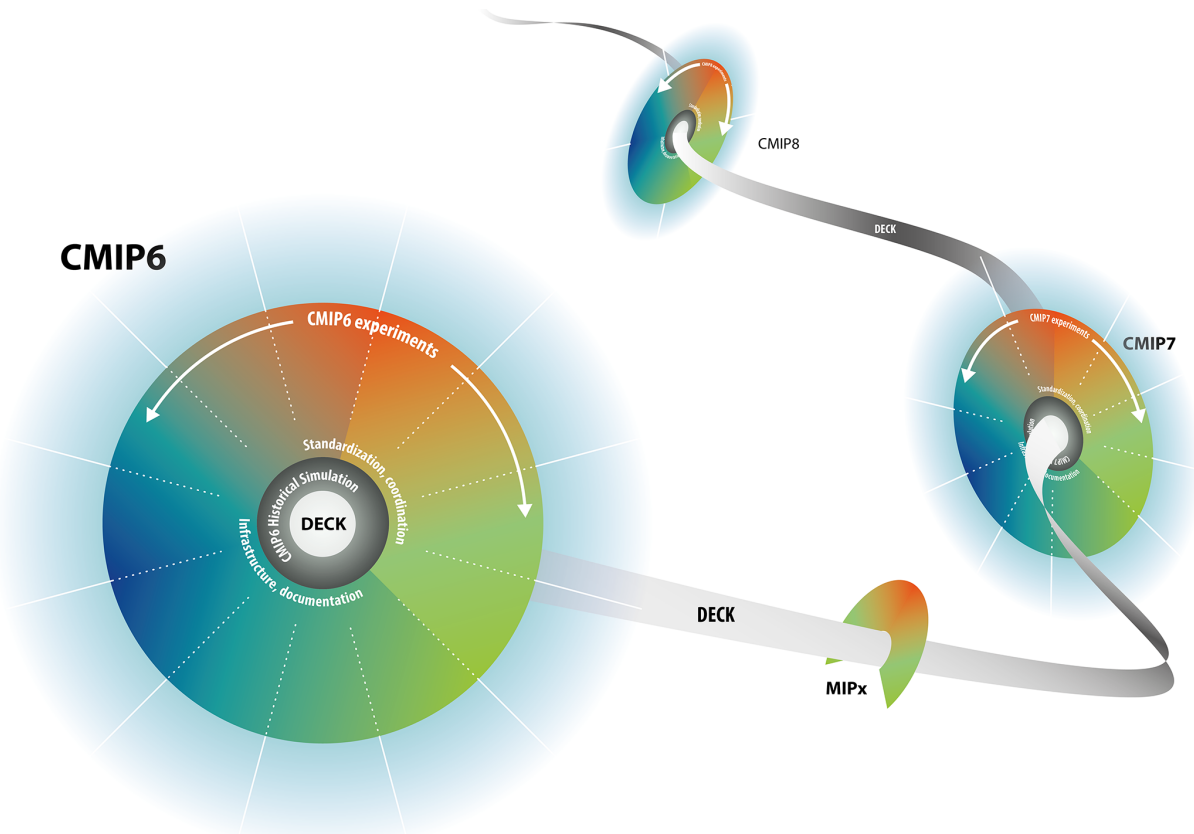


Figure 1. CMIP evolution. CMIP will evolve but the DECK will provide continuity across phases.

MIPs, but rather to reflect the strategic goals of the climate science community as, for instance, articulated by WCRP. By focusing a particular phase of CMIP around specific scientific issues, it was felt that the modelling resources could be more effectively applied to those scientific questions that had matured to a point where coordinated activities were expected to have substantial impact.

A variety of mechanisms were proposed and intensely debated to address these issues. The outcome of these discussions is embodied in the new CMIP structure, which has three major components. First, the identification of a handful of common experiments, the Diagnostic, Evaluation and Characterization of Klima (DECK) experiments (*klima* is Greek for “climate”), and CMIP historical simulations, which can be used to establish model characteristics and serves as its entry card for participating in one of CMIP’s phases or in other MIPs organized between CMIP phases, as depicted in Fig. 1. Second, common standards, coordination, infrastructure, and documentation that facilitate the distribution of model outputs and the characterization of the model ensemble, and third, the adoption of a more federated structure, building on more autonomous CMIP-Endorsed MIPs.

Realizing the idea of a particular phase of CMIP being centred on a collection of more autonomous MIPs required

the development of procedures for soliciting and evaluating MIPs in light of the scientific focus chosen for CMIP6. These procedures were developed and implemented by the CMIP Panel. The responses to the CMIP5 survey helped inform a series of workshops and resulted in a draft experiment design for CMIP6. This initial design for CMIP6 was published in early 2014 (Meehl et al., 2014) and was open for comments from the wider community until mid-September 2014. In parallel to the open review of the design, the CMIP Panel distributed an open call for proposals for MIPs in April 2014. These proposals were broadly reviewed within WCRP with the goal to encourage and enhance synergies among the different MIPs, to avoid overlapping experiments, to fill gaps, and to help ensure that the WCRP Grand Science Challenges would be addressed. Revised MIP proposals were requested and evaluated by the CMIP Panel in summer 2015. The selection of MIPs was based on the CMIP Panel’s evaluation of ten endorsement criteria (Table 1). To ensure community engagement, an important criterion was that enough modelling groups (at least eight) were willing to perform all of the MIP’s highest priority (Tier 1) experiments and providing all the requested diagnostics needed to answer at least one of its leading science questions. For each of the selected CMIP6-Endorsed MIPs it turned out that at least ten mod-

Table 1. Main criteria for MIP endorsement as agreed with representatives from the modelling groups and MIPs at the WGCM 18th Session in Grainau, Germany in October 2014.

No.	MIP endorsement criterion
1	The MIP and its experiments address at least one of the key science questions of CMIP6.
2	The MIP demonstrates connectivity to the DECK experiments and the CMIP6 historical simulations.
3	The MIP adopts the CMIP modelling infrastructure standards and conventions.
4	All experiments are tiered, well defined, and useful in a multi-model context and do not overlap with other CMIP6 experiments.
5	Unless a Tier 1 experiment differs only slightly from another well-established experiment, it must already have been performed by more than one modelling group.
6	A sufficient number of modelling centres (~ 8) are committed to performing all of the MIP's Tier 1 experiments and providing all the requested diagnostics needed to answer at least one of its science questions.
7	The MIP presents an analysis plan describing how it will use all proposed experiments, any relevant observations, and specially requested model output to evaluate the models and address its science questions.
8	The MIP has completed the MIP template questionnaire.
9	The MIP contributes a paper on its experimental design to the GMD CMIP6 special issue.
10	The MIP considers reporting on the results by co-authoring a paper with the modelling groups.

elling groups indicated their intent to participate in Tier 1 experiments at least, thus attesting to the wide appeal and level of science interest from the climate modelling community.

3 The DECK and CMIP historical simulations

The DECK comprises four baseline experiments: (a) a historical Atmospheric Model Intercomparison Project (*amip*) simulation, (b) a pre-industrial control simulation (*piControl* or *esm-piControl*), (c) a simulation forced by an abrupt quadrupling of CO₂ (*abrupt-4×CO2*) and (d) a simulation forced by a 1% yr⁻¹ CO₂ increase (*1pctCO2*). CMIP also includes a historical simulation (*historical* or *esm-hist*) that spans the period of extensive instrumental temperature measurements from 1850 to the present. In naming the experiments, we distinguish between simulations with CO₂ concentrations calculated and anthropogenic sources of CO₂ prescribed (*esm-piControl* and *esm-hist*) and simulations with prescribed CO₂ concentrations (all others). Hereafter, models that can calculate atmospheric CO₂ concentration and account for the fluxes of CO₂ between the atmosphere, the ocean, and biosphere are referred to as Earth System Models (ESMs).

The DECK experiments are chosen (1) to provide continuity across past and future phases of CMIP, (2) to evolve as little as possible over time, (3) to be well established, and incorporate simulations that modelling centres perform anyway as part of their own development cycle, and (4) to be relatively independent of the forcings and scientific objectives of a specific phase of CMIP. The four DECK experiments and the CMIP historical simulations are well suited for quantifying and understanding important climate change response characteristics. Modelling groups also commonly perform simulations of the historical period, but reconstructions of the external conditions imposed on historical runs (e.g. land-

use changes) continue to evolve significantly, influencing the simulated climate. In order to distinguish among the historical simulations performed under different phases of CMIP, the historical simulations are labelled with the phase (e.g. “CMIP5 *historical*” or “CMIP6 *historical*”). A similar argument could be made to exclude the AMIP experiments from the DECK. However, the AMIP experiments are simpler, more routine, and the dominating role of sea surface temperatures and the focus on recent decades means that for most purposes AMIP experiments from different phases of CMIP are more likely to provide the desired continuity.

The persistence and consistency of the DECK will make it possible to track changes in performance and response characteristics over future generations of models and CMIP phases. Although the set of DECK experiments is not expected to evolve much, additional experiments may become enough well established as benchmarks (routinely run by modelling groups as they develop new model versions) so that in the future they might be migrated into the DECK. The common practice of including the DECK in model development efforts means that models can contribute to CMIP without carrying out additional computationally burdensome experiments. All of the DECK and the historical simulations were included in the core set of experiments performed under CMIP5 (Taylor et al., 2012), and all but the *abrupt-4×CO2* simulation were included in even earlier CMIP phases.

Under CMIP, credentials of the participating atmosphere–ocean general circulation models (AOGCMs) and ESMs are established by performing the DECK and CMIP historical simulations, so these experiments are required from all models. Together these experiments document the mean climate and response characteristics of models. They should be run for each model configuration used in a CMIP-Endorsed MIP. A change in model configuration includes any change that might affect its simulations other than noise expected from

different realizations. This would include, for example, a change in model resolution, physical processes, or atmospheric chemistry treatment. If an ESM is used in both CO₂-emission-driven mode and CO₂-concentration-driven mode in subsequent CMIP6-Endorsed MIPs, then both emission-driven and concentration-driven control, and historical simulations should be done and they will be identical in all forcings except the treatment of CO₂.

The forcing data sets that will drive the DECK and CMIP6 historical simulations are described separately in a series of invited contributions to this special issue. These articles also include some discussion of uncertainty in the data sets. The data will be provided by the respective author teams and made publicly available through the ESGF using common metadata and formats.

The historical forcings are based as far as possible on observations and cover the period 1850–2014. These include:

- emissions of short-lived species and long-lived greenhouse gases (GHGs),
- GHG concentrations,
- global gridded land-use forcing data sets,
- solar forcing,
- stratospheric aerosol data set (volcanoes),
- AMIP sea surface temperatures (SSTs) and sea ice concentrations (SICs),
- for simulations with prescribed aerosols, a new approach to prescribe aerosols in terms of optical properties and fractional change in cloud droplet effective radius to provide a more consistent representation of aerosol forcing, and
- for models without ozone chemistry, time-varying gridded ozone concentrations and nitrogen deposition.

Some models might require additional forcing data sets (e.g. black carbon on snow or anthropogenic dust). Allowing model groups to use different forcing¹ data sets might better sample uncertainty, but makes it more difficult to assess the uncertainty in the response of models to the best estimate of the forcing, available to a particular CMIP phase. To avoid conflating uncertainty in the response of models to a given forcing, it is strongly preferred for models to be integrated with the same forcing in the entry card historical simulations, and for forcing uncertainty to be sampled in supplementary

¹Here, we distinguish between an applied input perturbation (e.g. the imposed change in some model constituent, property, or boundary condition), which we refer to somewhat generically as a “forcing”, and radiative forcing, which can be precisely defined. Even if the forcings are identical, the resulting radiative forcing depends on a model’s radiation scheme (among other factors) and will differ among models.

simulations that are proposed as part of DAMIP. In any case it is important that all forcing data sets are documented and are made available alongside the model output on the ESGF. Likewise to the extent modelling centres simplify forcings, for instance by regridding or smoothing in time or some other dimension, this should also be documented.

For the future scenarios selected by ScenarioMIP, forcings are provided by the integrated assessment model (IAM) community for the period 2015–2100 (or until 2300 for the extended simulations). For atmospheric emissions and concentrations as well as for land use, the forcings are harmonized across IAMs and scenarios using a similar procedure as in CMIP5 (van Vuuren et al., 2011). This procedure ensures consistency with historical forcing data sets and between the different forcing categories. The selection of scenarios and the main characteristics are described elsewhere in this special issue, while the underlying IAM scenarios are described in a special issue in Global Environmental Change.

An important gap identified in CMIP5, and in previous CMIP phases, was a lack of careful quantification of the radiative forcings from the different specified external forcing factors (e.g. GHGs, sulphate aerosols) in each model (Stouffer et al., 2015). This has impaired attempts to identify reasons for differences in model responses. The effective radiative forcing or ERF component of the Radiative Forcing MIP (RFMIP) includes fixed SST simulations to diagnose the forcing (RFMIP-lite), which are further detailed in the corresponding contribution to this special issue. Although not included as part of the DECK, in recognition of this deficiency in past phases of CMIP we strongly encourage all CMIP6 modelling groups to participate in RFMIP-lite. The modest additional effort would enable the radiative forcing to be characterized for both historic and future scenarios across the model ensemble. Knowing this forcing would lead to a step change in efforts to understand the spread of model responses for CMIP6 and contribute greatly to answering one of CMIP6’s science questions.

An overview of the main characteristics of the DECK and CMIP6 historical simulations appears in Table 2. Here we briefly describe these experiments. Detailed specifications for the DECK and CMIP6 historical simulations are provided in Appendix A and are summarized in Table A1.

3.1 The DECK

The AMIP and pre-industrial control simulations of the DECK provide opportunities for evaluating the atmospheric model and the coupled system, and in addition they establish a baseline for performing many of the CMIP6 experiments. Many experiments branch from, and are compared with, the pre-industrial control. Similarly, a number of diagnostic atmospheric experiments use AMIP as a control. The idealized CO₂-forced experiments in the DECK (*abrupt-4×CO2* and *1pctCO2*), despite their simplicity, can reveal fundamental forcing and feedback response characteristics of models.

Table 2. Overview of DECK and CMIP6 historical simulations providing the experiment short names, the CMIP6 labels, brief experiment descriptions, the forcing methods, as well as the start and end year and minimum number of years per experiment and its major purpose. The DECK and CMIP6 historical simulation are used to characterize the CMIP model ensemble. Given resource limitations, these entry card simulations for CMIP include only one ensemble member per experiment. However, we strongly encourage model groups to submit at least three ensemble members for the CMIP historical simulation as requested in DAMIP. Large ensembles of AMIP simulations are also encouraged. In the “forcing methods” column, “All” means “volcanic, solar, and anthropogenic forcings”. All experiments are started on 1 January and end on 31 December of the specified years.

Experiment short name	CMIP6 label	Experiment description	Forcing methods	Start year	End year	Minimum no. years per simulation	Major purpose
DECK experiments							
AMIP	<i>amip</i>	Observed SSTs and SICs prescribed	All; CO ₂ concentration prescribed	1979	2014	36	Evaluation, variability
Pre-industrial control	<i>piControl</i> or <i>esm-piControl</i>	Coupled atmosphere–ocean pre-industrial control	CO ₂ concentration prescribed or calculated	n/a	n/a	500	Evaluation, unforced variability
Abrupt quadrupling of CO ₂ concentration	<i>abrupt-4×CO2</i>	CO ₂ abruptly quadrupled and then held constant	CO ₂ concentration prescribed	n/a	n/a	150	Climate sensitivity, feedback, fast responses
1 % yr ⁻¹ CO ₂ concentration increase	<i>1pctCO2</i>	CO ₂ prescribed to increase at 1 % yr ⁻¹	CO ₂ concentration prescribed	n/a	n/a	150	Climate sensitivity, feedback, idealized benchmark
CMIP6 historical simulation							
Past ~ 1.5 centuries	<i>historical</i> or <i>esm-hist</i>	Simulation of the recent past	All; CO ₂ concentration prescribed or calculated	1850	2014	165	Evaluation

For nearly 3 decades, AMIP simulations (Gates et al., 1999) have been routinely relied on by modelling centres to help in the evaluation of the atmospheric component of their models. In AMIP simulations, the SSTs and SICs are prescribed based on observations. The idea is to analyse and evaluate the atmospheric and land components of the climate system when they are constrained by the observed ocean conditions. These simulations can help identify which model errors originate in the atmosphere, land, or their interactions, and they have proven useful in addressing a great variety of questions pertaining to recent climate changes. The AMIP simulations performed as part of the DECK cover at least the period from January 1979 to December 2014. The end date will continue to evolve as the SSTs and SICs are updated with new observations. Besides prescription of ocean conditions in these simulations, realistic forcings are imposed that should be identical to those applied in the CMIP historical simulations. Large ensembles of AMIP simulations are encouraged as they can help to improve the signal-to-noise ratio (Li et al., 2015).

The remaining three experiments in the DECK are premised on the coupling of the atmospheric and oceanic circulation. The pre-industrial control simulation (*piControl* or *esm-piControl*) is performed under conditions chosen to be

representative of the period prior to the onset of large-scale industrialization, with 1850 being the reference year. Historically, the industrial revolution began in the 18th century, and in nature the climate in 1850 was not stable as it was already changing due to prior historical changes in radiative forcings. In CMIP6, however, as in earlier CMIP phases, the control simulation is an attempt to produce a stable quasi-equilibrium climate state under 1850 conditions. When discussing and analysing historical and future radiative forcings, it needs to be recognized that the radiative forcing in 1850 due to anthropogenic greenhouse gas increases alone was already around 0.25 W m⁻² (Cubasch, 2013) although aerosols might have offset that to some extent. In addition, there were other pre-1850 secular changes, for example, in land use (Hurtt et al., 2011), and as a result, global net annual emissions of carbon from land use and land-use change already were responsible in 1850 for about 0.6 Pg C yr⁻¹ (Houghton, 2010). Under the assumptions of the control simulation, however, there are no secular changes in forcing, so the concentrations and/or sources of atmospheric constituents (e.g. GHGs and emissions of short-lived species) as well as land use are held fixed, as are Earth’s orbital characteristics. Because of the absence of both naturally occurring changes in forcing (e.g. volcanoes, orbital or solar changes) and human-

induced changes, the control simulation can be used to study the unforced internal variability of the climate system.

An initial climate spin-up portion of a control simulation, during which the climate begins to come into balance with the forcing, is usually performed. At the end of the spin-up period, the *piControl* starts. The *piControl* serves as a baseline for experiments that branch from it. To account for the effects of any residual drift, it is required that the *piControl* simulation extends as far beyond the branching point as any experiment to which it will be compared. Only then can residual climate drift in an experiment be removed so that it is not misinterpreted as part of the model's forced response. The recommended minimum length for the *piControl* is 500 years.

The two DECK climate change experiments branch from some point in the 1850 control simulation and are designed to document basic aspects of the climate system response to greenhouse gas forcing. In the first, the CO₂ concentration is immediately and abruptly quadrupled from the global annual mean 1850 value that is used in *piControl*. This *abrupt-4×CO2* simulation has proven to be useful for characterizing the radiative forcing that arises from an increase in atmospheric CO₂ as well as changes that arise indirectly due to the warming. It can also be used to estimate a model's equilibrium climate sensitivity (ECS, Gregory et al., 2004). In the second, the CO₂ concentration is increased gradually at a rate of 1 % per year. This experiment has been performed in all phases of CMIP since CMIP2, and serves as a consistent and useful benchmark for analysing model transient climate response (TCR). The TCR takes into account the rate of ocean heat uptake which governs the pace of all time-evolving climate change (e.g. Murphy and Mitchell, 1995). In addition to the TCR, the 1 % CO₂ integration with ESMs that include explicit representation of the carbon cycle allows the calculation of the transient climate response to cumulative carbon emissions (TCRE), defined as the transient global average surface temperature change per unit of accumulated CO₂ emissions (IPCC, 2013). Despite their simplicity, these experiments provide a surprising amount of insight into the behaviour of models subject to more complex forcing (e.g. Bony et al., 2013; Geoffroy et al., 2013).

3.2 CMIP historical simulations

In addition to the DECK, CMIP requests models to simulate the historical period, defined to begin in 1850 and extend to the near present. The CMIP historical simulation and its CO₂-emission-driven counterpart, *esm-hist*, branch from the *piControl* and *esm-piControl*, respectively (see details in Sect. A1.2). These simulations are forced, based on observations, by evolving, externally imposed forcings such as solar variability, volcanic aerosols, and changes in atmospheric composition (GHGs and aerosols) caused by human activities. The CMIP historical simulations provide rich opportunities to assess model ability to simulate climate, includ-

ing variability and century timescale trends (e.g. Flato et al., 2013). These simulations can also be analysed to determine whether climate model forcing and sensitivity are consistent with the observational record, which provides opportunities to better bound the magnitude of aerosol forcing (e.g. Stevens, 2015). In addition they, along with the control run, provide the baseline simulations for performing formal detection and attribution studies (e.g. Stott et al., 2006) which help uncover the causes of forced climate change.

As with performing control simulations, models that include representation of the carbon cycle should normally perform two different CMIP historical simulations: one with prescribed CO₂ concentration and the other with prescribed CO₂ emissions (accounting explicitly for fossil fuel combustion). In the second, CO₂ concentrations are predicted by the model. The treatment of other GHGs should be identical in both simulations. Both types of simulation are useful in evaluating how realistically the model represents the response of the carbon cycle anthropogenic CO₂ emissions, but the prescribed concentration simulation enables these more complex models to be evaluated fairly against those models without representation of carbon cycle processes.

3.3 Common standards, infrastructure, and documentation

A key to the success of CMIP and one of the motivations for incorporating a wide variety of coordinated modelling activities under a single framework in a specific phase of CMIP (now CMIP6) is the desire to reduce duplication of effort, minimize operational and computational burdens, and establish common practices in producing and analysing large amounts of model output. To enable automated processing of output from dozens of different models, CMIP has led the way in encouraging adoption of data standards (governing structure and metadata) that facilitate development of software infrastructure in support of coordinated modelling activities. The ESGF has capitalized on this standardization to provide access to CMIP model output hosted by institutions around the world. As the complexity of CMIP has increased and as the potential use of model output expands beyond the research community, the evolution of the climate modelling infrastructure requires enhanced coordination. To help in this regard, the WGCM Infrastructure Panel (WIP) was set up, and is now providing guidance on requirements and establishing specifications for model output, model and simulation documentation, and archival and delivery systems for CMIP6 data. In parallel to the development of the CMIP6 experiment design, the ESGF capabilities are being further extended and improved. In CMIP5, with over 1,000 different model/experiment combinations, a first attempt was also made to capture structured metadata describing the models and the simulations themselves. Based upon the Common Information Model (CIM, Lawrence et al., 2012), tools were provided to capture documentation of models and simula-

tions. This effort is now continuing under the banner of the international ES-DOC activity, which establishes agreements on common Controlled Vocabularies (CVs) to describe models and simulations. Modelling groups will be required to provide documentation following a common template and adhering to the CVs. With the documentation recorded uniformly across models, researchers will, for example, be able to use web-based tools to determine differences in model versions and differences in forcing and other conditions that affect each simulation. Further details on the CMIP6 infrastructure can be found in the WIP contribution to this special issue.

A more routine benchmarking and evaluation of the models is envisaged to be a central part of CMIP6. As noted above, one purpose of the DECK and CMIP historical simulations is to provide a basis for documenting model simulation characteristics. Towards that end an infrastructure is being developed to allow analysis packages to be routinely executed whenever new model experiments are contributed to the CMIP archive at the ESGF. These efforts utilize observations served by the ESGF contributed from the obs4MIPs (Ferraro et al., 2015; Teixeira et al., 2014) and ana4MIPs projects. Examples of available tools that target routine evaluation in CMIP include the PCMDI metrics software (Gleckler et al., 2016) and the Earth System Model Evaluation Tool (ESMValTool, Eyring et al., 2016), which brings together established diagnostics such as those used in the evaluation chapter of IPCC AR5 (Flato et al., 2013). The ESMValTool also integrates other packages, such as the NCAR Climate Variability Diagnostics Package (Phillips et al., 2014), or diagnostics such as the cloud regime metric (Williams and Webb, 2009) developed by the Cloud Feedback MIP (CFMIP) community. These tools can be used to broadly and comprehensively characterize the performance of the wide variety of models and model versions that will contribute to CMIP6. This evaluation activity can, compared with CMIP5, more quickly inform users of model output, as well as the modelling centres, of the strengths and weaknesses of the simulations, including the extent to which long-standing model errors remain evident in newer models. Building such a community-based capability is not meant to replace how CMIP research is currently performed but rather to complement it. These tools can also be used to compute derived variables or indices alongside the ESGF, and their output could be provided back to the distributed ESGF archive.

4 CMIP6

4.1 Scientific focus of CMIP6

In addition to the DECK and CMIP historical simulations, a number of additional experiments will colour a specific phase of CMIP, now CMIP6. These experiments are likely

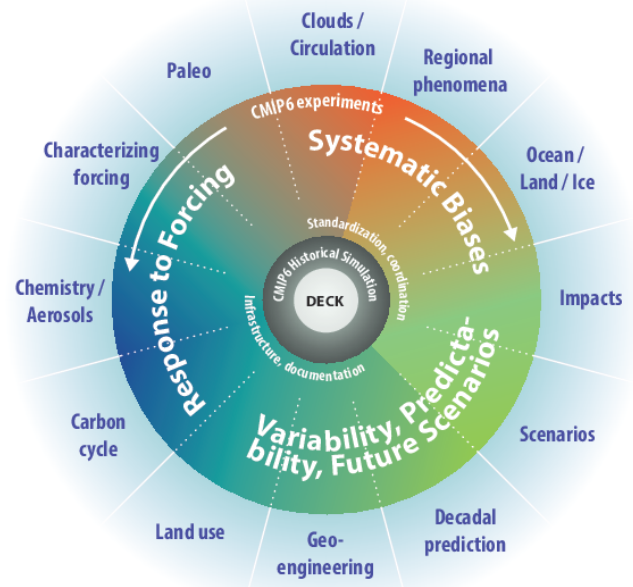


Figure 2. Schematic of the CMIP/CMIP6 experiment design. The inner ring and surrounding white text involve standardized functions of all CMIP DECK experiments and the CMIP6 historical simulation. The middle ring shows science topics related specifically to CMIP6 that are addressed by the CMIP6-Endorsed MIPs, with MIP topics shown in the outer ring. This framework is superimposed on the scientific backdrop for CMIP6 which are the seven WCRP Grand Science Challenges.

to change from one CMIP phase to the next. To maximize the relevance and impact of CMIP6, it was decided to use the WCRP Grand Science Challenges (GCs) as the scientific backdrop of the CMIP6 experimental design. By promoting research on critical science questions for which specific gaps in knowledge have hindered progress so far, but for which new opportunities and more focused efforts raise the possibility of significant progress on the timescale of 5–10 years, these GCs constitute a main component of the WCRP strategy to accelerate progress in climate science (Brasseur and Carlson, 2015). They relate to (1) advancing understanding of the role of clouds in the general atmospheric circulation and climate sensitivity (Bony et al., 2015), (2) assessing the response of the cryosphere to a warming climate and its global consequences, (3) understanding the factors that control water availability over land (Trenberth and Asrar, 2014), (4) assessing climate extremes, what controls them, how they have changed in the past and how they might change in the future, (5) understanding and predicting regional sea level change and its coastal impacts, (6) improving near-term climate predictions, and (7) determining how biogeochemical cycles and feedback control greenhouse gas concentrations and climate change.

These GCs will be using the full spectrum of observational, modelling and analytical expertise across the WCRP, and in terms of modelling most GCs will address their specific science questions through a hierarchy of numerical models of different complexities. Global coupled models obviously constitute an essential element of this hierarchy, and CMIP6 experiments will play a prominent role across all GCs by helping to answer the following three CMIP6 science questions: How does the Earth system respond to forcing? What are the origins and consequences of systematic model biases? How can we assess future climate change given internal climate variability, climate predictability, and uncertainties in scenarios?

These three questions will be at the centre of CMIP6. Science topics related specifically to CMIP6 will be addressed through a range of CMIP6-Endorsed MIPs that are organized by the respective communities and overseen by the CMIP Panel (Fig. 2). Through these different MIPs and their connection to the GCs, the goal is to fill some of the main scientific gaps of previous CMIP phases. This includes, in particular, facilitating the identification and interpretation of model systematic errors, improving the estimate of radiative forcings in past and future climate change simulations, facilitating the identification of robust climate responses to aerosol forcing during the historical period, better accounting of the impact of short-term forcing agents and land use on climate, better understanding the mechanisms of decadal climate variability, along with many other issues not addressed satisfactorily in CMIP5 (Stouffer et al., 2015). In endorsing a number of these MIPs, the CMIP Panel acted to minimize overlaps among the MIPs and to reduce the burden on modelling groups, while maximizing the scientific complementarity and synergy among the different MIPs.

4.2 The CMIP6-Endorsed MIPs

Close to 30 suggestions for CMIP6 MIPs have been received so far, of which 21 MIPs were eventually endorsed and invited to participate (Table 3). Of those not selected some were asked to work with other proposed MIPs with overlapping science goals and objectives. Of the 21 CMIP6-Endorsed MIPs, 4 are diagnostic in nature, which means that they define and analyse additional output, but do not require additional experiments. In the remaining 17 MIPs, a total of around 190 experiments have been proposed resulting in 40 000 model simulation years with around half of these in Tier 1. The CMIP6-Endorsed MIPs show broad coverage and distribution across the three CMIP6 science questions, and all are linked to the WCRP Grand Science Challenges (Fig. 3).

Each of the 21 CMIP6-Endorsed MIPs is described in a separate invited contribution to this special issue. These contributions will detail the goal of the MIP and the major scientific gaps the MIP is addressing, and will specify what is new compared to CMIP5 and previous CMIP phases. The con-

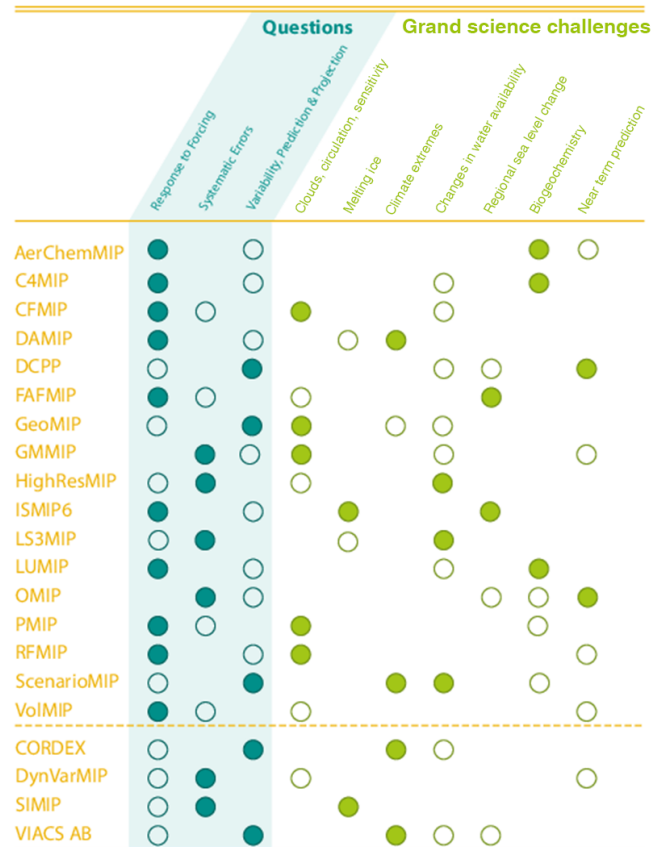


Figure 3. Contributions of CMIP6-Endorsed MIPs to the three CMIP6 science questions and the WCRP Grand Science Challenges. A filled circle indicates highest priority and an open circle, second highest priority. Some of the MIPs additionally contribute with lower priority to other CMIP6 science questions or WCRP Grand Science Challenges.

tributions will include a description of the experimental design and scientific justification of each of the experiments for Tier 1 (and possibly beyond), and will link the experiments and analysis to the DECK and CMIP6 historical simulations. They will additionally include an analysis plan to fully justify the resources used to produce the various requested variables, and if the analysis plan is to compare model results to observations, the contribution will highlight possible model diagnostics and performance metrics specifying whether the comparison entails any particular requirement for the simulations or outputs (e.g. the use of observational simulators). In addition, possible observations and reanalysis products for model evaluation are discussed and the MIPs are encouraged to help facilitate their use by contributing them to the obs4MIPs/ana4MIPs archives at the ESGF (see Sect. 3.3). In some MIPs, additional forcings beyond those used in the DECK and CMIP6 historical simulations are required, and these are described in the respective contribution as well.

Table 3. List of CMIP6-Endorsed MIPs along with the long name of the MIP, the primary goal(s) and the main CMIP6 science theme as displayed in Fig. 2. Each of these MIPs is described in more detail in a separate contribution to this special issue. MIPs marked with * are diagnostic MIPs.

Short name of MIP	Long name of MIP	Primary goal(s) in CMIP6	Main CMIP6 science theme
AerChemMIP	Aerosols and Chemistry Model Intercomparison Project	(a) Diagnosing forcings and feedback of tropospheric aerosols, tropospheric ozone precursors and the chemically reactive WMGHGs; (b) documenting and understanding past and future changes in the chemical composition of the atmosphere; (c) estimating the global-to-regional climate response from these changes.	Chemistry/ Aerosols
C ⁴ MIP	Coupled Climate Carbon Cycle Model Intercomparison Project	Understanding and quantifying future century-scale changes in the global carbon cycle and its feedback on the climate system, making the link between CO ₂ emissions and climate change.	Carbon cycle
CFMIP	Cloud Feedback Model Intercomparison Project	Improving assessments of cloud feedback via (a) improved understanding of cloud-climate feedback mechanisms and (b) better evaluation of clouds and cloud feedback in climate models. Also improving understanding of circulation, regional-scale precipitation, and non-linear changes.	Clouds/ Circulation
DAMIP	Detection and Attribution Model Intercomparison Project	(a) Estimating the contribution of external forcings to observed global and regional climate changes; (b) observationally constraining future climate change projections by scaling future GHG and other anthropogenic responses using regression coefficients derived for the historical period.	Characterizing forcings
DCPP	Decadal Climate Prediction Project	Predicting and understanding forced climate change and internal variability up to 10 years into the future through a coordinated set of hindcast experiments, targeted experiments to understand the physical processes, and the ongoing production of skilful decadal predictions.	Decadal prediction
FAFMIP	Flux-Anomaly-Forced Model Intercomparison Project	Explaining the model spread in climate projections of ocean climate change forced by CO ₂ increase, especially regarding the geographical patterns and magnitude of sea level change, ocean heat uptake, and thermal expansion.	Ocean/Land/ Ice
GeoMIP	Geoengineering Model Intercomparison Project	Assessing the climate system response (including on extreme events) to proposed radiation modification geoengineering schemes by evaluating their efficacies, benefits, and side effects.	Geoengineering
GMMIP	Global Monsoons Model Intercomparison Project	(a) Improving understanding of physical processes in global monsoons system; (b) better simulating the mean state, interannual variability, and long-term changes of global monsoons.	Regional phenomena
HighResMIP	High-Resolution Model Intercomparison Project	Assessing the robustness of improvements in the representation of important climate processes with weather-resolving global model resolutions (~ 25 km or finer), within a simplified framework using the physical climate system only with constrained aerosol forcing.	Regional phenomena
ISMIP6	Ice Sheet Model Intercomparison Project for CMIP6	Improving confidence in projections of the sea level rise associated with mass loss from the ice sheets of Greenland and Antarctica.	Ocean/Land/ Ice
LS3MIP	Land Surface, Snow and Soil Moisture	Providing a comprehensive assessment of land surface, snow, and soil moisture-climate feedback, and diagnosing systematic biases in the land modules of current ESMs using constrained land-module-only experiments.	Ocean/Land/ Ice
LUMIP	Land-Use Model Intercomparison Project	Quantifying the effects of land use on climate and biogeochemical cycling (past–future), and assessing the potential for alternative land management strategies to mitigate climate change.	Land use

Table 3. Continued.

OMIP	Ocean Model Intercomparison Project	Providing a framework for evaluating, understanding, and improving ocean, sea ice, and biogeochemical, including inert tracers, components of climate and Earth system models contributing to CMIP6. Protocols are provided to perform coordinated ocean/sea ice/tracer/biogeochemistry simulations forced with common atmospheric data sets.	Ocean/Land/Ice
PMIP	Paleoclimate Modelling Intercomparison Project	(a) Analysing the response to forcings and major feedback for past climates outside the range of recent variability; (b) assessing the credibility of climate models used for future climate projections.	Paleo
RFMIP	Radiative Forcing Model Intercomparison Project	(a) Characterizing the global and regional effective radiative forcing for each model for historical and $4\times\text{CO}_2$ simulations; (b) assessing the absolute accuracy of clear-sky radiative transfer parameterizations; (c) identifying the robust impacts of aerosol radiative forcing during the historical period.	Characterizing forcings
ScenarioMIP	Scenario Model Intercomparison Project	(a) Facilitating integrated research on the impact of plausible future scenarios over physical and human systems, and on mitigation and adaptation options; (b) addressing targeted studies on the effects of particular forcings in collaboration with other MIPs; (c) help quantifying projection uncertainties based on multi-model ensembles and emergent constraints.	Scenarios
VolMIP	Volcanic Forcings Model Intercomparison Project	(a) Assessing to what extent responses of the coupled ocean–atmosphere system to strong volcanic forcing are robustly simulated across state-of-the-art coupled climate models; (b) identifying the causes that limit robust simulated behaviour, especially differences in their treatment of physical processes	Characterizing forcings
CORDEX*	Coordinated Regional Climate Downscaling Experiment	Advancing and coordinating the science and application of regional climate downscaling (RCD) through statistical and dynamical downscaling of CMIP DECK, CMIP6 <i>historical</i> , and ScenarioMIP output.	Impacts
DynVarMIP*	Dynamics and Variability Model Intercomparison Project	Defining and analysing diagnostics that enable a mechanistic approach to confront model biases and understand the underlying causes behind circulation changes with a particular emphasis on the two-way coupling between the troposphere and the stratosphere.	Clouds/Circulation
SIMIP*	Sea Ice Model Intercomparison Project	Understanding the role of sea ice and its response to climate change by defining and analysing a comprehensive set of variables and process-oriented diagnostics that describe the sea ice state and its atmospheric and ocean forcing.	Ocean/Land/Ice
VIACS AB*	Vulnerability, Impacts, Adaptation and Climate Services Advisory Board	Facilitating a two-way dialogue between the CMIP6 modelling community and VIACS experts, who apply CMIP6 results for their numerous research and climate services, towards an informed construction of model scenarios and simulations and the design of online diagnostics, metrics, and visualization of relevance to society.	Impacts

A number of MIPs are developments and/or continuation of long-standing science themes. These include MIPs specifically addressing science questions related to cloud feedback and the understanding of spatial patterns of circulation and precipitation (CFMIP), carbon cycle feedback, and the understanding of changes in carbon fluxes and stores (C^4 MIP), detection and attribution (DAMIP) that newly includes 21st-century GHG-only simulations allowing the projected responses to GHGs and other forcings to be separated and scaled to derive observationally constrained projections, and

paleoclimate (PMIP), which assesses the credibility of the model response to forcing outside the range of recent variability. These MIPs reflect the importance of key forcing and feedback processes in understanding past, present, and future climate change and have developed new experiments and science plans focused on emerging new directions that will be at the centre of the WCRP Grand Science Challenges. A few new MIPs have arisen directly from gaps in understanding in CMIP5 (Stouffer et al., 2015), for example, poor quantification of radiative forcing (RFMIP), better understanding of

ocean heat uptake and sea level rise (FAFMIP), and understanding of model response to volcanic forcing (VolMIP).

Since CMIP5, other MIPs have emerged as the modelling community has developed more complex ESMs with interactive components beyond the carbon cycle. These include the consistent quantification of forcings and feedback from aerosols and atmospheric chemistry (AerChemMIP), and, for the first time in CMIP, modelling of sea level rise from land ice sheets (ISMIP6).

Some MIPs specifically target systematic biases focusing on improved understanding of the sea ice state and its atmospheric and oceanic forcing (SIMIP), the physical and biogeochemical aspects of the ocean (OMIP), land, snow and soil moisture processes (LS3MIP), and improved understanding of circulation and variability with a focus on stratosphere–troposphere coupling (DynVarMIP). With the increased emphasis in the climate science community on the need to represent and understand changes in regional circulation, systematic biases are also addressed on a more regional scale by the Global Monsoon MIP (GMMIP) and a first coordinated activity on high-resolution modelling (High-ResMIP).

For the first time, future scenario experiments, previously coordinated centrally as part of the CMIP5 core experiments, will be run as an MIP ensuring clear definition and well-coordinated science questions. ScenarioMIP will run a new set of future long-term (century timescale) integrations engaging input from both the climate science and integrated assessment modelling communities. The new scenarios are based on a matrix that uses the shared socioeconomic pathways (SSPs, O'Neill et al., 2015) and forcing levels of the Representative Concentration Pathways (RCP) as axes. As a set, they span the same range as the CMIP5 RCPs (Moss et al., 2010), but fill critical gaps for intermediate forcing levels and questions, for example, on short-lived species and land use. The near-term experiments (10–30 years) are coordinated by the decadal climate prediction project (DCPP) with improvements expected, for example, from the initialization of additional components beyond the ocean and from a more detailed process understanding and evaluation of the predictions to better identify sources and limits of predictability.

Other MIPs include specific future mitigation options, e.g. the land use MIP (LUMIP) that is for the first time in CMIP isolating regional land management strategies to study how different surface types respond to climate change and direct anthropogenic modifications, or the geoengineering MIP (GeoMIP), which examines climate impacts of newly proposed radiation modification geoengineering strategies.

The diagnostic MIP CORDEX will oversee the downscaling of CMIP6 models for regional climate projections. Another historic development in our field that provides, for the first time in CMIP, an avenue for a more formal communication between the climate modelling and user community is the endorsement of the vulnerability, impacts, and adaptation and climate services advisory board (VIACS AB). This

diagnostic MIP requests certain key variables of interest to the VIACS community be delivered in a timely manner to be used by climate services and in impact studies.

All MIPs define output streams in the centrally coordinated CMIP6 data request for each of their own experiments as well as the DECK and CMIP6 historical simulations (see the CMIP6 data request contribution to this special issue for details). This will ensure that the required variables are stored at the frequency and resolution required to address the specific science questions and evaluation needs of each MIP and to enable a broad characterization of the performance of the CMIP6 models.

We note that only the Tier 1 MIP experiments are overseen by the CMIP Panel, but additional experiments are proposed by the MIPs in Tiers 2 and 3. We encourage the modelling groups to participate in the full suite of experiments beyond Tier 1 to address in more depth the scientific questions posed.

The call for MIP applications for CMIP6 is still open and new proposals will be reviewed at the annual WGCM meetings. However, we point out that the additional MIPs suggested after the CMIP6 data request has been finalized will have to work with the already defined model output from the DECK and CMIP6 historical simulations, or work with the modelling group to recover additional variables from their internal archives. We also point out that some experiments proposed by CMIP6-Endorsed MIPs may not be finished until after CMIP6 ends.

5 Summary

CMIP6 continues the pattern of evolution and adaptation characteristic of previous phases of CMIP. To centre CMIP at the heart of activities within climate science and encourage links among activities within the World Climate Research Programme (WCRP), CMIP6 has been formulated scientifically around three specific questions, amidst the backdrop of the WCRP's seven Grand Science Challenges. To meet the increasingly broad scientific demands of the climate-science community, yet be responsive to the individual priorities and resource limitations of the modelling centres, CMIP has adopted a new, more federated organizational structure.

CMIP has now evolved from a centralized activity involving a large number of experiments to a federated activity, encompassing many individually designed MIPs. CMIP6 comprises 21 individual CMIP6-Endorsed MIPs and the DECK and CMIP6 historical simulations. Four of the 21 CMIP6-Endorsed MIPs are diagnostic in nature, meaning that they require additional output from models, but not additional simulations. The total amount of output from CMIP6 is estimated to be between 20 and 40 petabytes, depending on model resolution and the number of modelling centres ultimately participating in CMIP6. Questions addressed in the MIPs are wide ranging, from the climate of distant past to the response of turbulent cloud processes to radiative forc-

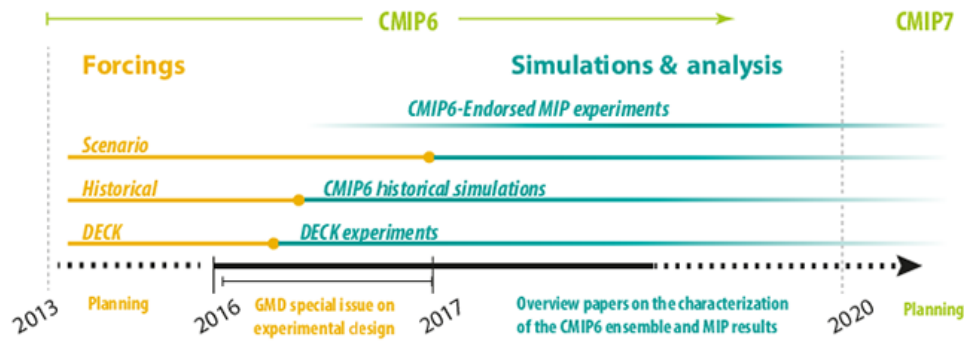


Figure 4. CMIP6 timeline for the preparation of forcings, the realization of experiments and their analysis.

ing, from how the terrestrial biosphere influences the uptake of CO₂ to how much predictability is stored in the ocean, from how to best project near-term to long-term future climate changes while considering interdependence and differences in model performance in the CMIP6 ensemble, and from what regulates the distribution of tropospheric ozone, to the influence of land-use changes on water availability.

The last 3 years have been dedicated to conceiving and then planning what we now call CMIP6. Starting in 2016, the first modelling centres are expected to begin performing the DECK and uploading output on the ESGF. Forcings for the DECK and CMIP6 historical simulations will be ready before mid-2016 so that these experiments can be started, and by the end of 2016 the diverse forcings for different scenarios of future human activity will become available. Past experience suggests that most centres will complete their CMIP6 simulations within a few years while the analysis of CMIP6 results will likely go on for a decade or more (Fig. 4).

Through an intensified effort to align CMIP with specific scientific questions and the WCRP Grand Science Challenges, we expect CMIP6 to continue CMIP's tradition of major scientific advances. CMIP6 simulations and scientific achievements are expected to support the IPCC Sixth Assessment Report (AR6) as well as other national and international climate assessments or special reports. Ultimately scientific progress on the most pressing problems of climate variability and change will be the best measure of the success of CMIP6.

Data availability

The model output from the DECK and CMIP6 historical simulations described in this paper will be distributed through the Earth System Grid Federation (ESGF) with digital object identifiers (DOIs) assigned. As in CMIP5, the model output will be freely accessible through data portals after registration. In order to document CMIP6's scientific impact and enable ongoing support of CMIP, users are obligated to acknowledge CMIP6, the participating modelling groups, and the ESGF centres (see details on the CMIP Panel website at <http://www.wcrp-climate.org/index.php/wgcm-cmip/about-cmip>). Further information about the infrastructure supporting CMIP6, the metadata describing the model output, and the terms governing its use are provided by the WGCM Infrastructure Panel (WIP) in their invited contribution to this special issue. Along with the data, the provenance of the data will be recorded, and DOIs will be assigned to collections of output so that they can be appropriately cited. This information will be made readily available so that published research results can be verified and credit can be given to the modelling groups providing the data. The WIP is coordinating and encouraging the development of the infrastructure needed to archive and deliver this information. In order to run the experiments, data sets for natural and anthropogenic forcings are required. These forcing data sets are described in separate invited contributions to this special issue. The forcing data sets will be made available through the ESGF with version control and DOIs assigned.

Appendix A: Experiment specifications

A1 Specifications for the DECK

Here we provide information needed to perform the DECK, including specification of forcing and boundary conditions, initialization procedures, and minimum length of runs. This information is largely consistent with but not identical to the specifications for these experiments in CMIP5 (Taylor et al., 2009).

The DECK and CMIP6 historical simulations are requested from all models participating in CMIP. The expectation is that this requirement will be met for each model configuration used in the subsequent CMIP6-Endorsed MIPs (an entry card). For CMIP6, in the special case where the burden of the entry card simulations is prohibitive but the scientific case for including a particular model simulation is compelling (despite only partial completion of the entry card simulations), an exception to this policy can be granted on a model-by-model basis by the CMIP Panel, which will seek advice from the chairs of the affected CMIP6-Endorsed MIP.

CMIP6 is a cooperative effort across the international climate modelling and climate science communities. The modelling groups have all been involved in the design and implementation of CMIP6, and thus have agreed to a set of best practices proposed for CMIP6. Those best practices include having the modelling groups submit the DECK experiments and the CMIP6 historical simulations to the ESGF, as well as any CMIP6-Endorsed MIP experiments they choose to run. Additionally, the modelling groups decide what constitutes a new model version. The CMIP Panel will work with the MIP co-chairs and the modelling groups to ensure that these best practices are followed.

A1.1 AMIP simulation

As in the first simulations performed under the Atmospheric Model Intercomparison Project (AMIP, Gates et al., 1999), SSTs and SICs in AMIP experiments are prescribed consistent with observations (see details on this forcing data set in the corresponding contribution to this special issue). Land models should be configured as close as possible to the one used in the CMIP6 historical simulation including transient land use and land cover. Other external forcings including volcanic aerosols, solar variability, GHG concentrations, and anthropogenic aerosols should also be prescribed consistent with those used in the CMIP6 historical simulation (see Sect. A2 below). Even though in AMIP simulations models with an active carbon cycle will not be fully interactive, surface carbon fluxes should be archived over land.

AMIP integrations can be initialized from prior model integrations or from observations or in other reasonable ways. Depending on the treatment of snow cover, soil water content, the carbon cycle, and vegetation, these runs may require a spin-up period of several years. One might establish quasi-

equilibrium conditions consistent with the model by, for example, running with ocean conditions starting earlier in the 1970s or cycling repeatedly through year 1979 before simulating the official period. Results from the spin-up period (i.e. prior to 1979) should be discarded, but the spin-up technique should be documented.

For CMIP6, AMIP simulations should cover at least the period from January 1979 through December 2014, but modelling groups are encouraged to extend their runs to the end of the observed period. Output may also be contributed from years preceding 1979 with the understanding that surface ocean conditions were less complete and in some cases less reliable then.

The climate found in AMIP simulations is largely determined by the externally imposed forcing, especially the ocean conditions. Nevertheless, unforced variability (noise) within the atmosphere introduces some non-deterministic variations that hamper unambiguous interpretation of apparent relationships between, for example, the year-to-year anomalies in SSTs and their consequences over land. To assess the role of unforced atmospheric variability in any particular result, modelling groups are encouraged to generate an ensemble of AMIP simulations. For most studies, a three-member ensemble, where only the initial conditions are varied, would be the minimum required, with larger size ensembles clearly of value in making more precise determination of statistical significance.

A1.2 Multi-century pre-industrial control simulations

Like laboratory experiments, numerical experiments are designed to reveal cause and effect relationships. A standard way of doing this is to perform both a control experiment and a second experiment where some externally imposed experiment condition has been altered. For many CMIP experiments, including the rest of the experiments discussed in this Appendix, the control is a simulation with atmospheric composition and other conditions prescribed and held constant, consistent with best estimates of the forcing from the historical period.

Ideally the pre-industrial control (*piControl*) experiment for CMIP would represent a near-equilibrium state of the climate system under the imposed conditions. In reality, simulations of hundreds to many thousands of years would be required for the ocean's depths to equilibrate and for biogeochemical reservoirs to fully adjust. Available computational resources generally preclude integrations long enough to approach equilibrium, so in practice shorter runs must suffice. Usually, a *piControl* simulation is initialized from the control run of a different model or from observations, and then run until at least the surface climate conditions stabilize using 1850 forcings (see Stouffer et al., 2004, for further discussion). This spin-up period can be as long as several hundred years and variables that can document the spin-up behaviour should be archived (under the experiment labels *piControl*-

spinup or *esm-piControl-spinup*). At the very least the length of the spin-up period should be documented.

Although equilibrium is generally not achieved, the changes occurring after the spin-up period are usually found to evolve at a fairly constant rate that presumably decreases slowly as equilibrium is approached. After a few centuries, these drifts of the system mainly affect the carbon cycle and ocean below the main thermocline, but they are also manifest at the surface in a slow change in sea level. The climate drift must be removed in order to interpret experiments that use the pre-industrial simulation as a control. The usual procedure is to assume that the drift is insensitive to CMIP experiment conditions and to simply subtract the control run from the perturbed run to determine the climate change that would occur in the absence of drift.

Besides serving as controls for numerical experimentation, the *piControl* and *esm-piControl* are used to study the naturally occurring, unforced variability of the climate system. The only source of climate variability in a control arises from processes internal to the model, whereas in the more complicated real world, variations are also caused by external forcing factors such as solar variability and changes in atmospheric composition caused, for example, by human activities or volcanic eruptions. Consequently, the physical processes responsible for unforced variability can more easily be isolated and studied using the control run of models, rather than by analysing observations.

A DECK control simulation is required to be long enough to extend to the end of any perturbation runs initiated from it so that climate drift can be assessed and possibly removed from those runs. If, for example, a historical simulation (beginning in 1850) were initiated from the beginning of the control simulation and then were followed by a future scenario run extending to year 2300, a control run of at least 450 years would be required. As discussed above, control runs are also used to assess model-simulated unforced climate variability. The longer the control, the more precisely can variability be quantified for any given timescale. A control simulation of many hundreds of years would be needed to assess variability on centennial timescales. For CMIP6 it is recommended that the control run should be at least 500 years long (following the spin-up period), but of course the simulation must be long enough to reach to the end of the experiments it spawns. It should be noted that those analysing CMIP6 simulations might also require simulations longer than 500 years to accurately assess unforced variability on long timescales, so modelling groups are encouraged to extend their control runs well beyond the minimum recommended number of years.

Because the climate was very likely not in equilibrium with the forcing of 1850 and because different components of the climate system differentially respond to the effects of the forcing prior to that time, there is some ambiguity in deciding on what forcing to apply for the control. For CMIP6

we recommend a specification of this forcing that attempts to balance conflicting objectives to

- minimize artificial climate responses to discontinuities in radiative forcing at the time a historical simulation is initiated, and
- minimize artefacts in sea level change due to thermal expansion caused by unrealistic mismatches in conditions in the centennial-scale averaged forcings for the pre- and post-1850 periods. Note that any preindustrial multi-centennial observed trend in global-mean sea level is most likely to be due to slow changes in ice-sheets, which are likely not to be simulated in the CMIP6 model generation.

The first consideration above implies that radiative forcing in the control run should be close to that imposed at the beginning of the CMIP historical simulation (i.e. 1850). The second implies that a background volcanic aerosol and time-averaged solar forcing should be prescribed in the control run, since to neglect it would cause an apparent drift in sea level associated with the suppression of heat uptake due to the net effect of, for instance, volcanism after 1850, and this has implications for sea level changes (Gregory, 2010; Gregory et al., 2013). We recognize that it will be impossible to entirely avoid artefacts and artificial transient effects, and practical considerations may rule out conformance with every detail of the control simulation protocol stipulated here. With that understanding, here is a summary of the recommendations for the imposed conditions on the spin-up and control runs, followed by further clarification in subsequent paragraphs:

- Conditions must be time invariant except for those associated with the mean climate (notably the seasonal and diurnal cycles of insolation).
- Unless indicated otherwise (e.g. the background volcanic forcing), experiment conditions (e.g. greenhouse gas concentrations, ozone concentration, surface land conditions) should be representative of Earth around the year 1850.
- Orbital parameters (eccentricity, obliquity, and longitude of the perihelion) should be held fixed at their 1850 values.
- Land use should not change in the control run and should be fixed according to reconstructed agricultural maps from 1850. Due to the diversity of model approaches in ESMs for land carbon, some groups might deviate from this specification, and again this must be clearly documented.
- The solar constant should be fixed at its mean value (no 11-year solar cycle) over the first two solar cycles of the historical simulation (i.e. the 1850–1873 mean).

- A background volcanic aerosol should be specified that results in radiative forcing matching, as closely as possible, that experienced, on average, during the historical simulation (i.e. 1850–2014 mean).
- Models without interactive ozone chemistry should specify the pre-industrial ozone fields from a data set produced from a pre-industrial control simulation that uses 1850 emissions and a mean solar forcing averaged over solar cycles 8–10, representative of the mean mid-19th century solar forcing.
- For models with interactive chemistry and/or aerosols, the CMIP6 pre-industrial emissions dataset of reactive gases and aerosol precursors should be used. For models without internally calculated aerosol concentrations, a monthly climatological dataset of aerosol physical and optical properties should be used.

In the CO₂-concentration-driven *piControl*, the value of the global annual mean 1850 atmospheric CO₂ concentration is prescribed and held fixed during the entire experiment. There are some special considerations that apply to control simulations performed by emission-driven ESMs (i.e. runs with atmospheric concentrations of CO₂ calculated prognostically rather than being prescribed). In the *esm-piControl* simulation, emissions of CO₂ from both fossil fuel combustion and land-use change are prescribed to be zero. In this run any residual drift in atmospheric CO₂ concentration that arises from an imbalance in the exchanges of CO₂ between the atmosphere and the ocean and land (i.e. by the natural carbon cycle in the absence of anthropogenic CO₂ emissions) will need to be subtracted from perturbation runs to correct for a control state not in equilibrium. It should be emphasized that the *esm-piControl* is an idealized experiment and is not meant to mimic the true 1850 conditions, which would have to include a source of carbon of around 0.6 Pg C yr⁻¹ from the already perturbed state that existed in 1850.

Due to a wide variety of ESMs and the techniques they use to compute land carbon fluxes, it is hard to make statements that apply to all models equally well. A general recommendation, however, is that the land carbon fluxes in the emission and concentration-driven control simulations should be stable in time and in approximate balance so that the net carbon flux into the atmosphere is small (less than 0.1 Pg C yr⁻¹). Further details on ESM experiments with a carbon cycle are provided in the C⁴MIP contribution to this special issue.

The historical time-average volcanic forcing stipulated above for the control run is likely to approximate the much longer term mean. The volcanic aerosol radiative forcing estimates of Crowley (2000) for the historical period and the last millennium are -0.18 and -0.22 W m⁻², respectively. Because the mean volcanic forcing between 1850 and 2014 is small, the discontinuity associated with transitioning from a mean forcing to a time-varying volcanic forcing is also expected to be small. Even though this is the design objective, it

is likely that it will be impossible to eliminate all artefacts in quantities such as historical sea level change. For this reason, and because some models may deviate from these specifications, it is recommended that groups perform an additional simulation of the historical period but with only natural forcing included. With this additional run, which is already called for under DAMIP, the purely anthropogenic effects on sea level change can be isolated.

The forcing specified in the *piControl* also has implications for simulations of the future, when solar variability and volcanic activity will continue to exist, but at unknown levels. These issues need to be borne in mind when designing and evaluating future scenarios, as a failure to include volcanic forcing in the future will cause future warming and sea level rise to be over-estimated relative to a *piControl* experiment in which a non-zero volcanic forcing is specified. This is accounted for by introducing a time-invariant non-zero volcanic forcing (e.g. the mean volcanic forcing for the *piControl*) into the scenarios. This is further specified in the ScenarioMIP contribution to this special issue.

These issues, and the potential of different modelling centres adopting different approaches to account for their particular constraints, highlight the paramount importance of adequately documenting the conditions under which this and the other DECK experiments are performed.

A1.3 Abruptly quadrupling CO₂ simulation

Until CMIP5, there were no experiments designed to quantify the extent to which forcing differences might explain differences in climate response. It was also difficult to diagnose and quantify the feedback responses, which are mediated by global surface temperature change (Sherwood et al., 2015). In order to examine these fundamental characteristics of models – CO₂ forcing and climate feedback – an abrupt 4×CO₂ simulation was included for the first time as part of CMIP5. Following Gregory et al. (2004), the simulation branches in January of the CO₂-concentration-driven *piControl* and abruptly the value of the global annual mean 1850 atmospheric CO₂ concentration that is prescribed in *piControl* is quadrupled and held fixed. As the system subsequently evolves toward a new equilibrium, the imbalance in the net flux at the top of the atmosphere can be plotted against global temperature change. As Gregory et al. (2004) showed, it is then possible to diagnose both the effective radiative forcing due to a quadrupling of CO₂ and also effective equilibrium climate sensitivity (ECS). Moreover, by examining how individual flux components evolve with surface temperature change, one can learn about the relative strengths of different feedback, notably quantifying the importance of various feedback associated with clouds.

In the *abrupt-4×CO2* experiment, the only externally imposed difference from the *piControl* should be the change in CO₂ concentration. All other conditions should remain as they were in the *piControl*, including any background vol-

canic aerosols. By changing only a single factor, we can unambiguously attribute all climatic consequences to the increase in CO₂ concentration.

The minimum length of the simulation should be 150 years, but longer simulations would enable investigations of longer-timescale responses. Also there is value, as in CMIP5, in performing an ensemble of short (~5-year) simulations, all prescribing global annual mean 1850 atmospheric CO₂ concentration but initiated at different times throughout the year (in addition to the *abrupt-4×CO2* simulation initiated from the *piControl* in January). Such an ensemble would reduce the statistical uncertainty with which the effective CO₂ radiative forcing could be quantified and would allow more detailed and accurate diagnosis of the fast responses of the system under an abrupt change in forcing (Bony et al., 2013; Gregory and Webb, 2008; Kamae and Watanabe, 2013; Sherwood et al., 2015). Different groups will be able to afford ensembles of different sizes, but in any case each realization should be initialized in a different month and the months should be spaced evenly throughout the year.

A1.4 1 % CO₂ increase simulation

The second idealized climate change experiment was introduced in the early days of CMIP (Meehl et al., 2000). It is designed for studying model responses under simplified but somewhat more realistic forcing than an abrupt increase in CO₂. In this *1pctCO2* experiment, the simulation is branched from the *piControl*, and the global annual mean CO₂ concentration is gradually increased at a rate of 1 % yr⁻¹ (i.e. exponentially), starting from its 1850 value that is prescribed in the *piControl*. A minimum length of 150 years is requested so that the simulation goes beyond the quadrupling of CO₂ after 140 years. Note that in contrast to previous definitions, the experiment has been simplified so that the 1 % CO₂ increase per year is applied throughout the entire simulation rather than keeping it constant after 140 years as in CMIP5. Since the radiative forcing is approximately proportional to the logarithm of the CO₂ increase, the radiative forcing linearly increases over time. Drawing on the estimates of effective radiative forcing (for definitions see Myhre et al., 2013) obtained in the *abrupt-4×CO2* simulations, analysts can scale results from each model in the 1 % CO₂ increase simulations to focus on the response differences in models, largely independent of their forcing differences. In contrast, in CMIP6 historical simulations (see Sect. A2), the forcing and response contributions to model differences in simulated climate change cannot be easily isolated.

As in the *abrupt-4×CO2* experiment, the only externally imposed difference from the *piControl* should be the change in CO₂ concentration. The omission of changes in aerosol concentrations is the key to making these simulations easier to interpret.

Models with a carbon cycle component will be driven by prescribed CO₂ concentrations, but terrestrial and marine

surface fluxes and stores of carbon will become a key diagnostic from which one can infer emission rates that are consistent with a 1 % yr⁻¹ increase in model CO₂ concentration. This DECK baseline carbon cycle experiment is built upon in C⁴MIP to diagnose the strength of model carbon climate feedback and to quantify contributions to disruption of the carbon cycle by climate and by direct effects of increased CO₂ concentration.

A2 The CMIP6 historical simulations

CMIP6 historical simulations of climate change over the period 1850–2014 are forced by common data sets that are largely based on observations. They serve as an important benchmark for assessing model performance through evaluation against observations. The historical integration should be initialized from some point in the control integration (with *historical* branching from the *piControl* and the *esm-hist* branching from *esm-piControl*) and be forced by varying time, externally imposed conditions that are based on observations. Both naturally forced changes (e.g. due to solar variability and volcanic aerosols) and changes due to human activities (e.g. CO₂ concentration, aerosols, and land use) will lead to climate variations and evolution. In addition, there is unforced variability which can obscure the forced changes and lead to expected differences between the simulated and observed climate variations (Deser et al., 2012).

The externally imposed forcing data sets that should be used in CMIP6 cover the period 1850 through the end of 2014 and are described in detail in various other contributions to this special issue. In the CO₂-concentration-driven historical simulations, time-varying global annual mean concentrations for CO₂ and other long-lived greenhouse gases are prescribed. If a modelling center decides to represent additional spatial and seasonal variations in prescribed greenhouse gas forcings, this needs to be adequately documented.

Recall from Sect. A1.2 that the conditions in the control should generally be consistent with the forcing imposed near the beginning of the CMIP historical simulation. This should minimize artificial transient effects in the first portion of the CMIP historical simulation. An exception is that for the CO₂-emission-driven experiments, the zero CO₂ emissions from fossil fuel and the land-use specifications for 1850 in the *esm-piControl* could cause a discontinuity in land carbon at the branch point.

As described in Sect. A1.2, the 1850 *esm-piControl* should be developed for an idealized case that is stable in time and balance so that the net carbon flux into the atmosphere is small. Meanwhile, the start of the *esm-hist* in 1850 should be as realistic as possible and attempt to account for the fact the land surface was not in equilibrium in 1850 due to prior land-use effects (Houghton, 2010; Hurtt et al., 2011). Some modelling groups have developed methods to achieve these twin goals in a computationally efficient manner, for example, by performing pre-1850 off-line land model simulations

Table A1. Specifications in the DECK and CMIP6 historical simulations.

Experiment	Volcanic stratospheric aerosol	Solar variability	Anthropogenic forcings
<i>amip</i>	Time-dependent observations	Time-dependent observations	Time-dependent observations
<i>piControl</i>	Background volcanic aerosol that results in radiative forcing matching, as closely as possible, that was experienced, on average, during the historical simulation (i.e. 1850–2014 mean)	Fixed at its mean value (no 11-year solar cycle) over the first two solar cycles of the historical simulation (i.e. the 1850–1873 mean)	Given that the historical simulations start in 1850, the <i>piControl</i> should have fixed 1850 atmospheric composition, not true pre-industrial
<i>esm-piControl</i>	As in <i>piControl</i>	As in <i>piControl</i>	As in <i>piControl</i> but with CO ₂ concentration calculated, rather than prescribed. CO ₂ from both fossil fuel combustion and land-use change are prescribed to be zero.
<i>abrupt-4×CO2</i>	As in <i>piControl</i>	As in <i>piControl</i>	As in <i>piControl</i> except CO ₂ that is 4 times that of <i>piControl</i>
<i>lpctCO2</i>	As in <i>piControl</i>	As in <i>piControl</i>	As in <i>piControl</i> except CO ₂ that is increasing at 1 % yr ⁻¹
<i>historical</i>	Time-dependent observations	Time-dependent observations	Time-dependent observations
<i>esm-hist</i>	As in <i>historical</i>	As in <i>historical</i>	As in <i>historical</i> but with CO ₂ emissions prescribed and CO ₂ concentration calculated (rather than prescribed)

to account for the land carbon cycle disequilibrium before 1850 and to adequately simulate carbon stores at the start of the historical simulation (Sentman et al., 2011). Due to the wide diversity of modelling approaches for land carbon in the ESMs, the actual method applied by each group to account for these effects will differ and needs to be well documented.

As discussed earlier, there will be a mismatch in the specification of volcanic aerosols between control and historical simulations that especially affect estimates of ocean heat uptake and sea level rise in the historical period. This can be minimized by prescribing a background volcanic aerosol in the pre-industrial control that has the same cooling effect as the volcanoes included in the CMIP6 historical simulation. Any residual mismatch will need to be corrected, which requires a special supplementary simulation (see Sect. A1.2) that should be submitted along with the CMIP6 historical simulation.

For model evaluation and for detection and attribution studies (the focus of DAMIP) there would be considerable value in extending the CMIP6 historical simulations beyond the nominal 2014 ending date. To include the more recent observations in model evaluation, modelling groups are encouraged to document and apply forcing data sets representing the post-2014 period. For short extensions (up to a few years) it may be acceptable to simply apply forcing from one of the future scenarios defined by ScenarioMIP. To distinguish between the portion of the historical period when all models will use the same forcing data sets (i.e. 1850–2014) from the extended period where different data sets might be

used, the experiment for 1850–2014 will be labelled *historical* (*esm-hist* in the case of the emission-driven run) and the period from 2015 through near-present will likely be labelled *historical-ext* (*esm-hist-ext*).

Even if the CMIP6 historical simulations are extended beyond 2014, all future scenario simulations (called for by ScenarioMIP and other MIPs) should be initiated from the end of year 2014 of the CMIP6 historical simulation since the “future” in CMIP6 begins in 2015.

Due to interactions within and between the components of the Earth system, there is a wide range of variability on various time and space scales (Hegerl et al., 2007). The timescales vary from shorter than a day to longer than several centuries. The magnitude of the variability can be quite large relative to any given signal of interest depending on the time and space scales involved and on the variable of interest. To more clearly identify forced signals emerging from natural variability, multiple model integrations (comprising an ensemble) can be made where only the initial conditions are perturbed in some way which should be documented. A common way to do this is to simply branch each simulation from a different point in the control run. Longer intervals between branch points will ensure independence of ensemble members on longer timescales. By averaging many different ensemble members together, the signal of interest becomes clear because the natural variations tend to average out if the ensemble size and averaging period are long enough. If the variability in the models is realistic, then the spread of the ensemble members around the ensemble average is caused

by unforced (i.e. internal) variability. To minimize the number of years included in the entry card simulations, only one ensemble member is requested here. However, we strongly encourage model groups to submit at least three ensemble members of their CMIP historical simulation as requested in DAMIP.

Acknowledgements. We thank the scientific community for their engagement in the definition of CMIP6 and for the broad participation in the CMIP5 survey in 2013. We thank the co-chairs and steering committee members of the CMIP6-Endorsed MIPs for their continuous engagement in defining CMIP6, and the modelling groups and wider community for reviewing the CMIP6 design and organization. We thank the WGCM Infrastructure Panel (WIP) for overseeing the CMIP6 infrastructure, Martin Jukes for taking the lead in preparing the CMIP6 data request, and the group of scientists who are producing forcing datasets for CMIP6. Thanks to Jonathan Gregory for raising awareness about the treatment of volcanic forcing in the pre-industrial control experiment and its consequence for sea level changes, and to Pierre Friedlingstein, George Hurtt, Chris Jones, and David Lawrence for help in defining carbon cycle and land-use specifications in the DECK experiments and CMIP6 historical simulations. Norbert Noreiks is thanked for help in drafting the figures. Thanks to our topical editor Julia Hargreaves, to Gavin Schmidt and the other two anonymous reviewers, and to everyone who contributed to the open discussions for constructive comments. GM and KET were supported by the Regional and Global Climate Modeling Program (RGCM) of the U.S. Department of Energy's Office of Biological & Environmental Research (BER) (through Cooperative Agreement no. DE-FC02-97ER62402 for GM), and GM received additional support from the U.S. National Science Foundation. The National Center for Atmospheric Research is sponsored by the National Science Foundation.

The article processing charges for this open-access publication were covered by a Research Centre of the Helmholtz Association.

Edited by: J. Hargreaves

References

- Bony, S., Bellon, G., Klocke, D., Sherwood, S., Fermepin, S., and Denvil, S.: Robust direct effect of carbon dioxide on tropical circulation and regional precipitation, *Nat. Geosci.*, 6, 447–451, 2013.
- Bony, S., Stevens, B., Frierson, D. M. W., Jakob, C., Kageyama, M., Pincus, R., Shepherd, T. G., Sherwood, S. C., Siebesma, A. P., Sobel, A. H., Watanabe, M., and Webb, M. J.: Clouds, circulation and climate sensitivity, *Nat. Geosci.*, 8, 261–268, 2015.
- Brasseur, G. and Carlson, D.: Future directions for the World Climate Research Programme, *Eos, Transactions American Geophysical Union*, 96, doi:10.1029/2015EO033577, 2015.
- CMIP Panel: WCRP Coupled Model Intercomparison Project (CMIP), available at: <http://www.wcrp-climate.org/index.php/wgcm-cmip/about-cmip>, 2016.
- Crowley, T. J.: Causes of climate change over the past 1000 years, *Science*, 289, 270–277, 2000.
- Cubasch, U., Wuebbles, D., Chen, D., Facchini, M. C., Frame, D., Mahowald, N., and Winther, J.-G.: Introduction, in: *Climate Change 2013: The Physical Science Basis. Contribution of Working Group I to the Fifth Assessment Report of the Intergovernmental Panel on Climate Change*, edited by: Stocker, T. F., Qin, D., Plattner, G.-K., Tignor, M., Allen, S. K., Boschung, J., Nauels, A., Xia, Y., Bex, V., and Midgley, P. M., Cambridge University Press, Cambridge, UK and New York, NY, USA, 2013.
- Deser, C., Knutti, R., Solomon, S., and Phillips, A. S.: Communication of the role of natural variability in future North American climate, *Nat. Clim. Change*, 2, 775–779, 2012.
- Eyring, V., Righi, M., Lauer, A., Evaldsson, M., Wenzel, S., Jones, C., Anav, A., Andrews, O., Cionni, I., Davin, E. L., Deser, C., Ehbrecht, C., Friedlingstein, P., Gleckler, P., Gottschaldt, K.-D., Hagemann, S., Jukes, M., Kindermann, S., Krasting, J., Kunert, D., Levine, R., Loew, A., Mäkelä, J., Martin, G., Mason, E., Phillips, A. S., Read, S., Rio, C., Roehrig, R., Senftleben, D., Sterl, A., van Ulft, L. H., Walton, J., Wang, S., and Williams, K. D.: ESMValTool (v1.0) – a community diagnostic and performance metrics tool for routine evaluation of Earth system models in CMIP, *Geosci. Model Dev.*, 9, 1747–1802, doi:10.5194/gmd-9-1747-2016, 2016.
- Ferraro, R., Waliser, D. E., Gleckler, P., Taylor, K. E., and Eyring, V.: Evolving obs4MIPs to Support the Sixth Coupled Model Intercomparison Project (CMIP6), *B. Am. Meteorol. Soc.*, doi:10.1175/BAMS-D-14-00216.1, online first, 2015.
- Flato, G., Marotzke, J., Abiodun, B., Braconnot, P., Chou, S. C., Collins, W., Cox, P., Driouech, F., Emori, S., Eyring, V., Forest, C., Gleckler, P., Guilyardi, E., Jakob, C., Kattsov, V., Reason, C., and Rummukainen, M.: Evaluation of Climate Models, in: *Climate Change 2013: The Physical Science Basis. Contribution of Working Group I to the Fifth Assessment Report of the Intergovernmental Panel on Climate Change*, edited by: Stocker, T. F., Qin, D., Plattner, G.-K., Tignor, M., Allen, S. K., Boschung, J., Nauels, A., Xia, Y., Bex, V., and Midgley, P. M., Cambridge University Press, Cambridge, UK and New York, NY, USA, 2013.
- Gates, W. L., Boyle, J. S., Covey, C., Dease, C. G., Doutriaux, C. M., Drach, R. S., Fiorino, M., Gleckler, P. J., Hnilo, J. J., Marlais, S. M., Phillips, T. J., Potter, G. L., Santer, B. D., Sperber, K. R., Taylor, K. E., and Williams, D. N.: An Overview of the Results of the Atmospheric Model Intercomparison Project (AMIP I), *B. Am. Meteorol. Soc.*, 80, 29–55, 1999.
- Geoffroy, O., Saint-Martin, D., Olivie, D. J. L., Voldoire, A., Bellon, G., and Tyteca, S.: Transient Climate Response in a Two-Layer Energy-Balance Model. Part I: Analytical Solution and Parameter Calibration Using CMIP5 AOGCM Experiments, *J. Climate*, 26, 1841–1857, 2013.
- Gleckler, P. J., Doutriaux, C., Durack, P. J., Taylor, K. E., Zhang, Y., Williams, D. N., Mason, E., and Servonnat, J.: A More Powerful Reality Test for Climate Models, *Eos Trans. AGU*, doi:10.1029/2016EO051663, 2016.
- Gregory, J. and Webb, M.: Tropospheric adjustment induces a cloud component in CO₂ forcing, *J. Climate*, 21, 58–71, 2008.
- Gregory, J. M.: Long-term effect of volcanic forcing on ocean heat content, *Geophys. Res. Lett.*, 37, L22701, doi:10.1029/2010gl045507, 2010.
- Gregory, J. M., Ingram, W. J., Palmer, M. A., Jones, G. S., Stott, P. A., Thorpe, R. B., Lowe, J. A., Johns, T. C., and Williams, K. D.: A new method for diagnosing radiative forcing and climate sensitivity, *Geophys. Res. Lett.*, 31, L03205, doi:10.1029/2003gl018747, 2004.
- Gregory, J. M., Bi, D., Collier, M. A., Dix, M. R., Hirst, A. C., Hu, A., Huber, M., Knutti, R., Marsland, S. J., Meinshausen, M., Rashid, H. A., Rotstayn, L. D., Schurer, A., and Church, J. A.: Climate models without preindustrial volcanic forcing underes-

- imate historical ocean thermal expansion, *Geophys. Res. Lett.*, 40, 1600–1604, 2013.
- Hegerl, G. C., Zwiers, F. W., Braconnot, P., Gillett, N. P., Luo, Y., Marengo Orsini, J. A., Nicholls, N., Penner, J. E., and Stott, P. A.: Understanding and Attributing Climate Change, in: *Climate Change 2007: The Physical Science Basis. Contribution of Working Group I to the Fourth Assessment Report of the Intergovernmental Panel on Climate Change*, edited by: Solomon, S., Qin, D., Manning, M., Chen, Z., Marquis, M., Averyt, K. B., Tignor, M., and Miller, H. L., Cambridge University Press, Cambridge, UK and New York, NY, USA, 2007.
- Houghton, R. A.: How well do we know the flux of CO₂ from land-use change?, *Tellus B*, 62, 337–351, 2010.
- Hurt, G. C., Chini, L. P., Frolking, S., Betts, R. A., Feddema, J., Fischer, G., Fisk, J. P., Hibbard, K., Houghton, R. A., Janetos, A., Jones, C. D., Kindermann, G., Kinoshita, T., Goldewijk, K. K., Riahi, K., Shevliakova, E., Smith, S., Stehfest, E., Thomson, A., Thornton, P., van Vuuren, D. P., and Wang, Y. P.: Harmonization of land-use scenarios for the period 1500–2100: 600 years of global gridded annual land-use transitions, wood harvest, and resulting secondary lands, *Climatic Change*, 109, 117–161, 2011.
- IPCC: *Climate Change 2013: The Physical Science Basis. Contribution of Working Group I to the Fifth Assessment Report of the Intergovernmental Panel on Climate Change*, Cambridge University Press, Cambridge, UK and New York, NY, USA, 2013.
- Kamae, Y. and Watanabe, M.: Tropospheric adjustment to increasing CO₂: its timescale and the role of land-sea contrast, *Clim. Dynam.*, 41, 3007–3024, 2013.
- Lawrence, B. N., Balaji, V., Bentley, P., Callaghan, S., DeLuca, C., Denvil, S., Devine, G., Elkington, M., Ford, R. W., Guilyardi, E., Lautenschlager, M., Morgan, M., Moine, M.-P., Murphy, S., Pascoe, C., Ramthun, H., Slavin, P., Steenman-Clark, L., Tossaint, F., Treshansky, A., and Valcke, S.: Describing Earth system simulations with the Metafor CIM, *Geosci. Model Dev.*, 5, 1493–1500, doi:10.5194/gmd-5-1493-2012, 2012.
- Li, C., Stevens, B., and Marotzke, J.: Eurasian winter cooling in the warming hiatus of 1998–2012, *Geophys. Res. Lett.*, 42, 8131–8139, 2015.
- Meehl, G. A., Boer, G. J., Covey, C., Latif, M., and Stouffer, R. J.: Intercomparison makes for a better climate model, *Eos, Transactions American Geophysical Union*, 78, 445–451, 1997.
- Meehl, G. A., Boer, G. J., Covey, C., Latif, M., and Stouffer, R. J.: The Coupled Model Intercomparison Project (CMIP), *B. Am. Meteorol. Soc.*, 81, 313–318, 2000.
- Meehl, G. A., Covey, C., Taylor, K. E., Delworth, T., Stouffer, R. J., Latif, M., McAvaney, B., and Mitchell, J. F. B.: THE WCRP CMIP3 Multimodel Dataset: A New Era in Climate Change Research, *B. Am. Meteorol. Soc.*, 88, 1383–1394, 2007.
- Meehl, G. A., Moss, R., Taylor, K. E., Eyring, V., Stouffer, R. J., Bony, S., and Stevens, B.: Climate Model Intercomparisons: Preparing for the Next Phase, *Eos Trans. AGU*, 59, 77, doi:10.1002/2014EO090001, 2014.
- Moss, R. H., Edmonds, J. A., Hibbard, K. A., Manning, M. R., Rose, S. K., van Vuuren, D. P., Carter, T. R., Emori, S., Kainuma, M., Kram, T., Meehl, G. A., Mitchell, J. F. B., Nakicenovic, N., Riahi, K., Smith, S. J., Stouffer, R. J., Thomson, A. M., Weyant, J. P., and Wilbanks, T. J.: The next generation of scenarios for climate change research and assessment, *Nature*, 463, 747–756, 2010.
- Murphy, J. M. and Mitchell, J. F. B.: Transient-Response of the Hadley-Center Coupled Ocean-Atmosphere Model to Increasing Carbon-Dioxide. 2. Spatial and Temporal Structure of Response, *J. Climate*, 8, 57–80, 1995.
- Myhre, G., Shindell, D., Breion, F.-M., Collins, W., Fuglestedt, J., Huang, J., Koch, D., Lamarque, J.-F., Lee, D., Mendoza, B., Nakajima, T., Robock, A., Stephens, G., Takemura, T., and Zhang, H.: Anthropogenic and Natural Radiative Forcing, in: *Climate Change 2013: The Physical Science Basis. Contribution of Working Group I to the Fifth Assessment Report of the Intergovernmental Panel on Climate Change*, edited by: Stocker, T. F., Qin, D., Plattner, G.-K., Tignor, M., Allen, S. K., Boschung, J., Nauels, A., Xia, Y., Bex, V., and Midgley, P. M., Cambridge University Press, Cambridge, UK and New York, NY, USA, 2013.
- O'Neill, B. C., Kriegler, E., Ebi, K. L., Kemp-Benedict, E., Riahi, K., Rothman, D. S., van Ruijven, B. J., van Vuuren, D. P., Birkmann, J., Kok, K., Levy, M., and Solecki, W.: The roads ahead: Narratives for shared socioeconomic pathways describing world futures in the 21st century, *Global Environ. Chang.*, doi:10.1016/j.gloenvcha.2015.01.004, online first, 2015.
- Phillips, A. S., Deser, C., and Fasullo, J.: Evaluating Modes of Variability in Climate Models, *Eos Trans. AGU*, 95, 453–455, 2014.
- Rauscher, F., Gleckler, P., and Marotzke, J.: Rethinking the Default Construction of Multimodel Climate Ensembles, *B. Am. Meteorol. Soc.*, 96, 911–919, 2014.
- Sentman, L. T., Shevliakova, E., Stouffer, R. J., and Malyshev, S.: Time Scales of Terrestrial Carbon Response Related to Land-Use Application: Implications for Initializing an Earth System Model, *Earth Interact.*, 15, 1–16, 2011.
- Sherwood, S. C., Bony, S., Boucher, O., Bretherton, C., Forster, P. M., Gregory, J. M., and Stevens, B.: Adjustments in the Forcing-Feedback Framework for Understanding Climate Change, *B. Am. Meteorol. Soc.*, 96, 217–228, 2015.
- Stevens, B.: Rethinking the Lower Bound on Aerosol Radiative Forcing, *J. Climate*, 28, 4794–4819, 2015.
- Stott, P. A., Mitchell, J. F. B., Allen, M. R., Delworth, T. L., Gregory, J. M., Meehl, G. A., and Santer, B. D.: Observational constraints on past attributable warming and predictions of future global warming, *J. Climate*, 19, 3055–3069, 2006.
- Stouffer, R. J., Weaver, A. J., and Eby, M.: A method for obtaining pre-twentieth century initial conditions for use in climate change studies, *Clim. Dynam.*, 23, 327–339, 2004.
- Stouffer, R. J., Eyring, V., Meehl, G. A., Bony, S., Senior, C., Stevens, B., and Taylor, K. E.: CMIP5 Scientific Gaps and Recommendations for CMIP6, *B. Am. Meteorol. Soc.*, submitted, 2015.
- Taylor, K. E., Stouffer, R. J., and Meehl, G. A.: A Summary of the CMIP5 Experiment Design, available at: http://cmip.llnl.gov/cmip5/docs/Taylor_CMIP5_design.pdf (last access: 13 May 2016), 2009.
- Taylor, K. E., Stouffer, R. J., and Meehl, G. A.: An Overview of Cmp5 and the Experiment Design, *B. Am. Meteorol. Soc.*, 93, 485–498, 2012.
- Teixeira, J., Waliser, D., Ferraro, R., Gleckler, P., Lee, T., and Potter, G.: Satellite Observations for CMIP5: The Genesis of Obs4MIPs, *B. Am. Meteorol. Soc.*, 95, 1329–1334, 2014.

- Trenberth, K. and Asrar, G.: Challenges and Opportunities in Water Cycle Research: WCRP Contributions, *Surv. Geophys.*, 35, 515–532, 2014.
- van Vuuren, D. P., Edmonds, J., Kainuma, M., Riahi, K., Thomson, A., Hibbard, K., Hurtt, G. C., Kram, T., Krey, V., Lamarque, J. F., Masui, T., Meinshausen, M., Nakicenovic, N., Smith, S. J., and Rose, S. K.: The representative concentration pathways: an overview, *Climatic Change*, 109, 5–31, 2011.
- Williams, D. N., Balaji, V., Cinquini, L., Denvil, S., Duffy, D., Evans, B., Ferraro, R., Hansen, R., Lautenschlager, M., and Trenham, C.: A Global Repository for Planet-Sized Experiments and Observations, *B. Am. Meteorol. Soc.*, doi:10.1175/bams-d-15-00132.1, online first, 2015.
- Williams, K. and Webb, M.: A quantitative performance assessment of cloud regimes in climate models, *Clim. Dynam.*, 33, 141–157, 2009.



Global wildland fire season severity in the 21st century [☆]

Mike Flannigan ^{a,*}, Alan S. Cantin ^b, William J. de Groot ^b, Mike Wotton ^c, Alison Newbery ^b,
Lynn M. Gowman ^b

^a University of Alberta, Dept. of Renewable Resources, 51 General Services Building, Edmonton, AB, Canada T6G 2H1

^b Canadian Forest Service, Natural Resources Canada, 1219 Queen St. East, Sault Ste. Marie, ON, Canada P6A 2E5

^c Natural Resources Canada-Canadian Forest Service, Faculty of Forestry, University of Toronto, 33 Willcocks St, Toronto, ON, Canada M5S 3B3

ARTICLE INFO

Article history:

Available online 5 January 2013

Keywords:

Wildland fire
Climate change
Fire severity
Fire season length
Fire weather
Fire management

ABSTRACT

We used Cumulative Severity Rating (CSR), a weather-based fire danger metric, to examine the potential influence of climate change on global fire season severity. The potential influence of climate change on fire season length was also addressed. We used three General Circulation Models (GCMs) and three emission scenarios to calculate the CSR and fire season length for mid-century (2041–2050) and late century (2091–2100) relative to the 1971–2000 baseline. Our results suggest significant increases in the CSR for all models and scenarios. Increases were greatest (more than three times greater than the baseline CSR) for the Northern Hemisphere at the end of the century. Fire season length changes were also most pronounced at the end of the century and for northern high latitudes where fire season lengths will increase by more than 20 days per year. The implications from this study are that fire seasons will be more severe in future and that conventional fire management approaches may no longer be effective.

Crown Copyright © 2012 Published by Elsevier B.V. All rights reserved.

1. Introduction

Wildland fire is a widespread and critical aspect of the earth system (Bond and Keeley, 2006). Estimates of annual area burned range between 300 and 450 Mha (van der Werf et al., 2006) which is comparable to the size of India. Over 80% of the global area burned occurs in grasslands and savannas, primarily in Africa and Australia but also in South Asia and South America. Globally fires are frequent over most of the earth except in areas of sparse vegetation (e.g., North Africa) and near the poles (Mouillot and Field, 2005). Wildland fires are a continuous and global feature with fire occurring all year long in the northern or southern or both hemispheres. We do not know how many fires are started each year but human activities are responsible for the vast majority; lightning is the other common ignition cause for wildland fires. Many billions of dollars are spent on fire management and fire suppression every year.

Fire activity is strongly influenced by four factors: fuels, climate-weather, ignition agents and people (Flannigan et al., 2005). Fuel amount, type, continuity, structure, and moisture level are critical elements of fire occurrence and spread. For fires to spread there needs to be fuel continuity; some suggest that at least 30% of the landscape needs to have fuel for a fire to spread (Har-

grove et al., 2000). This is important in many drier parts of the world where a certain amount of precipitation is required prior to the fire season for plant growth to provide sufficient fuel buildup that allows continuous fire spread on the landscape (Swetnam and Betancourt, 1998; Meyn et al., 2007). Fuel structure can also be important in fire dynamics. For example, understory trees and shrubs in a forest can act as ladder fuels that carry a surface fire up into tree crowns and thereby generate a faster moving and much more intense fire. Although the amount of fuel, or fuel load, affects fire activity because a minimum amount of fuel is required for fire to start and spread, fuel moisture largely determines fire behaviour, and has been found to be an important factor in the amount of area burned.

Weather and climate – including temperature, precipitation, wind, and atmospheric moisture – are critical aspects of fire activity (Flannigan and Harrington, 1988; Swetnam, 1993). Some examples that highlight the role of weather and climate include Cary et al. (2006) who found that weather and climate best explained the amount of area burned using landscape fire models, as compared with variation in terrain and fuel pattern. Carcaillet et al. (2001) found that climate was the key process triggering fire over the eastern boreal forest during the Holocene. Prasad et al. (2008) found that mean annual temperature and average precipitation of the warmest quarter of the year were among the variables that best explained fire occurrence in southern India.

The global climate is warming and this may have a profound and immediate impact on wildland fire activity. Some suggest that wildland fire activity has already increased due to climate change.

[☆] Presented at Exploring the Mega-Fire Reality 2011 Conference 14–17 November 2011, Tallahassee, FL, USA.

* Corresponding author. Tel.: +1 780 248 2033; fax: +1 780 492 4323.

E-mail address: mike.flannigan@ualberta.ca (M. Flannigan).

Gillett et al. (2004) suggest that the increase in area burned in Canada over the past four decades is due to human-caused increases in temperatures. Flannigan et al. (2009a) in a review of global wildland fire activity found numerous research papers that suggests area burned and fire occurrence will increase with a warmer climate and fire seasons will be longer. The results were more mixed with respect to fire severity and intensity with some studies suggesting increase and some suggesting no changes or decreases. The objective of this paper is to examine future global fire season severity using the Daily Severity Rating (DSR) of the Canadian Forest Fire Danger Rating System (CFFDRS). These results provide insights into future fire intensity, which is important in terms of fire management. For example, as average fire intensity increases, wildfire suppression resource requirements will exceed available resource levels with greater frequency, resulting in greater area burned. Additionally, we will calculate future fire season length for the globe as an additional indicator of future fire management challenges since longer fire seasons will translate into more fire starts and more opportunities for fires to escape control.

2. Data and methods

This study used components of the Canadian Forest Fire Weather Index (FWI) System. The FWI System is used by many countries around the world, and the FWI component itself (of the FWI System) is commonly used as a general indicator of fire danger and fire intensity at the landscape level (Van Wagner, 1987). The FWI System is a weather-based system that models fuel moisture using a dynamic bookkeeping system that tracks the drying and wetting of distinct fuel layers in the forest floor. There are three moisture codes that represent the moisture content of fine fuels (Fine Fuel Moisture Code, FFMC), loosely compacted organic material (Duff Moisture Code, DMC) and a deep layer of compact organic material (Drought Code, DC). The drying time lags for these three fuel layers are 2/3 of a day, 15 days and 52 days respectively for the FFMC, DMC and DC under normal conditions (temperature 21.1 °C, relative humidity 45%). These moisture indexes are combined to create a generalised index of the availability of fuel for consumption (Buildup Index, BUI); the FFMC is combined with wind to estimate the potential spread rate of a fire (Initial Spread Index, ISI). The BUI and ISI are combined to create the FWI which is an estimate of the

potential intensity of a spreading fire. The daily severity rating (DSR) is a simple power function of the FWI intended to increase the weight of higher values of FWI in order to compensate for the exponential increase in area burned with fire diameter (Williams, 1959; Van Wagner, 1970).

The FWI was designed as a scaled analogue of Byram (1959) fireline intensity. Fireline intensity is used operationally in many jurisdictions around the world to evaluate the potential effectiveness of different resources to contain and control wildland fire for the environmental conditions on a given day. It was recognised early in the development of fire danger rating that the appropriate scale of operationally useful fire danger indexes (i.e. the FWI) did not reflect the difficulty of control or work required for suppression of a fire under given conditions (Williams, 1959). The Daily Severity Rating (DSR) was conceived to indicate fire suppression difficulty in the Canadian danger rating system and is essentially a simple power function of the FWI (with an exponent of 1.77). With this scaling, the DSR is intended to reflect the non-linear increase in difficulty of control as the fire grows (Van Wagner, 1970) and as such is the index used when seasonal summaries of fire severity are generated.

Typically, the average DSR over an entire fire season (the Seasonal Severity Rating, SSR) is used to provide a general summary of the potential difficulty of fire control over an entire season. It is used when regionally contrasting potential fire control difficulty for seasons over multiple years. A simple seasonal average, however, may not be the best relative indicator of changes in control difficulty in scenarios where a trend to a lengthening of the fire season exists. In such scenarios, increased number of days of high and extreme potential suppression difficulty may be obscured in the average by increased number of days overall; days which, in the shoulders of the season, are likely to be more benign. For this study, to try to capture the changes in control difficulty across fire seasons with potentially changing lengths, we chose to rely on the sum of DSR values over the season as our indicator of fire season severity (the Cumulative Severity Rating, CSR). In a region with an unchanging fire season duration, SSR and CSR are essentially the same (CSR simply being SSR unscaled by the number of days in the fire season). By not scaling the CSR by season length, however, it provides what can be thought of as a weighted count of number of severe days in the fire season, and thus will be a better indicator of the absolute numbers of challenging (in terms of fire

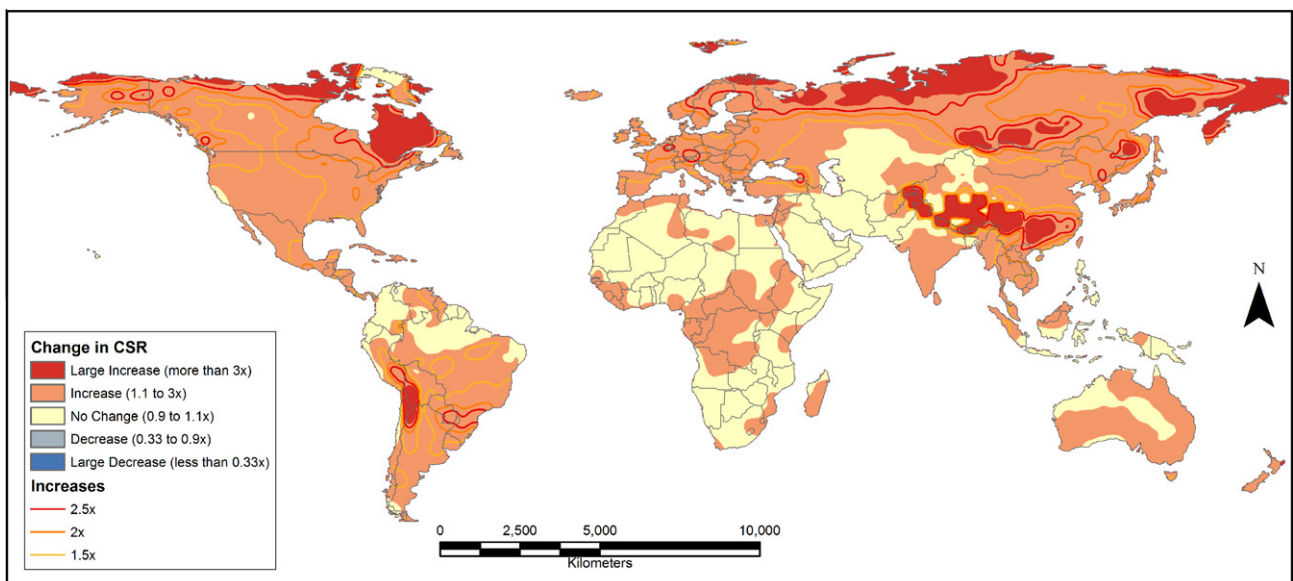


Fig. 1. CSR anomalies for the IPSL-CM4 A2 for 2041–2050 relative to the 1971–2000 base period.

control) days across fire seasons. The fire season length was calculated using a straightforward temperature approach similar to that used by Wotton and Flannigan (1993). The beginning of the season was defined as 3 consecutive days of 9 °C or greater, and the end of the fire season was defined as three consecutive days of 2 °C or lower. These values are lower than what Flannigan and Wotton used but this study used mean temperature as opposed to 1200 LST temperature in the previous study.

For the observational weather data required to calculate the CSR, we used the NCEP Reanalysis I data from 1971 to 2000, which was provided by NOAA/OAR/ESRL PSD, in Boulder Colorado. The raw data was analysed using a $2.5^\circ \times 2.5^\circ$ grid for daily mean surface RH, air temperature, U-wind vector and V-wind vector. Wind speed was calculated as the magnitude of the sum of these two vectors. The 6 h precipitation rate was analysed on T63 Gaussian grid then interpolated to the $2.5^\circ \times 2.5^\circ$ grid and assumed to fall uniformly over the 6 h interval. This hourly precipitation was then

accumulated for the 24 h prior to noon local time each day, and together with the other three weather variables, was combined into one large dataset, sorted by date and grid point, and then used to calculate daily FWI System outputs.

We selected three GCMs for this study: (1) the CGCM3.1 from the Canadian Centre for Climate Modelling and Analysis, (2) the HadCM3 from the Hadley Centre for Climate Prediction in the United Kingdom, and (3) the IPSL-CM4 from France. For the Canadian model, there were two resolutions available: T47 and T63. T47 was chosen as it was more complete than T63. These three models were selected to provide us a range of warming with the Canadian model being the smallest increase in monthly mean temperatures and the Hadley having the largest increase in monthly mean temperature.

There are four families of emission scenarios to choose from for this analysis; A1, A2, B1, and B2. A1 is described by a world of very rapid economic growth, with the global population peaking

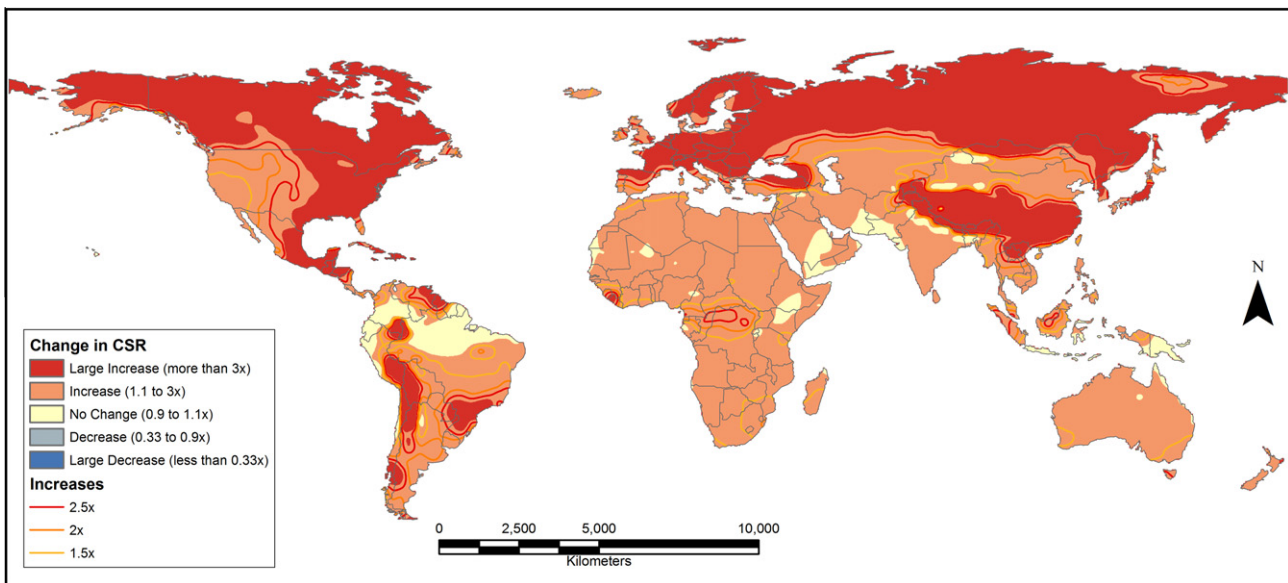


Fig. 2. CSR anomalies for the IPSL-CM4 A2 for 2091–2100 relative to the 1971–2000 base period.

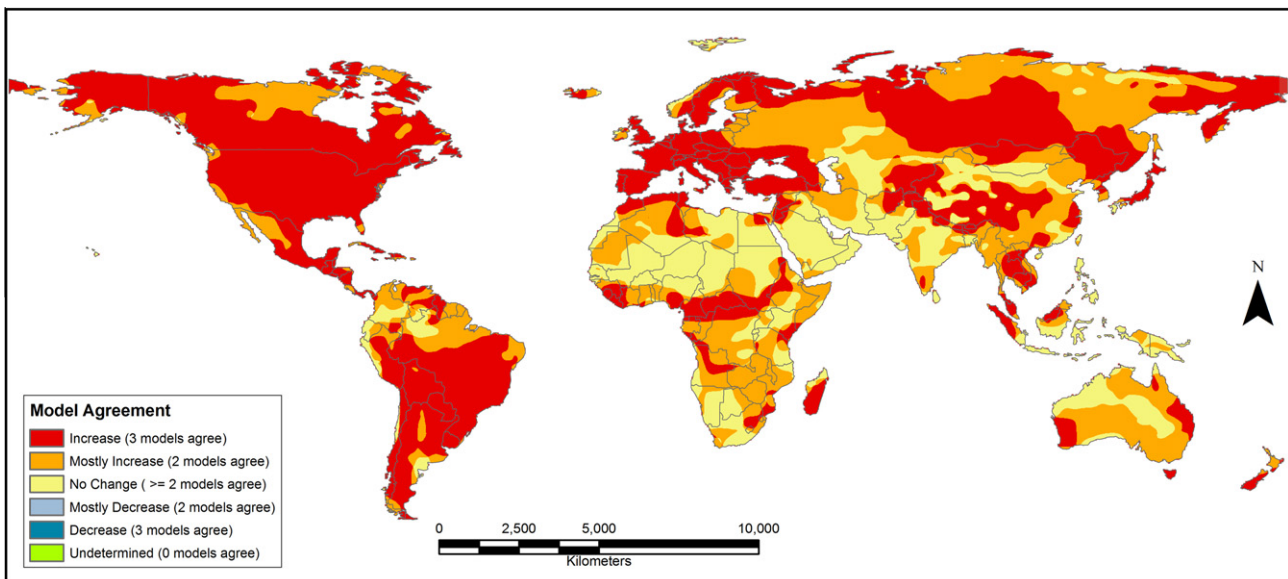


Fig. 3. Composite CSR anomaly map for the A2 scenario 2041–2050 relative to the 1971–2000 base period.

mid-century. In this scenario, there is a rapid introduction of new and more efficient technologies. A1 is further divided into three groups. A1F1 is fossil-fuel intensive, A1T assumes non-fossil energy resource use, and A1B is a balance across all energy sources. A2 is a world with increased population growth, slow economic development and slow technological change. B1 shares the same population trend as A1, but has a more rapid change in economic structure, moving towards service and information technology. Lastly, B2 has an intermediate population and economic growth. It emphasises local solutions to economic, social and environmental sustainability. We selected three scenarios for evaluation in this study: A1B, A2 and B1.

We downloaded the historical or baseline monthly data for air temperature, precipitation rate, U-wind vector and V-wind vector variables for each GCM. For CGCM3.1 and IPSL-CM4 models, specific humidity was downloaded and converted to relative humidity; for HadCM3, relative humidity was downloaded directly. We

calculated 30-year monthly averages for each variable. We then downloaded monthly data for the 21st century for all three GCMs and all three emission scenarios (A1B, A2 and B1). The CSR and fire season lengths were calculated using the modified NCEP daily data to be representative of future decades. Because the GCM grids were different from the NCEP Reanalysis, we interpolated all GCM data to the same NCEP $2.5^\circ \times 2.5^\circ$ grid. We used XConv/convsh 1.91 (Cole, 2009) which allowed us to easily interpolate from one grid format to any other grid format using an area weighted interpolation.

For all scenarios and models, we calculated the decadal monthly means for all the variables and for all decades in the 21st century (2001–2010 to 2091–2100). The GCM 30-year baseline monthly averages for air temperature, relative humidity and wind speed were subtracted from the future decadal monthly averages and the result was added to the NCEP baseline daily data, by month. The resulting new daily weather was used to calculate the start

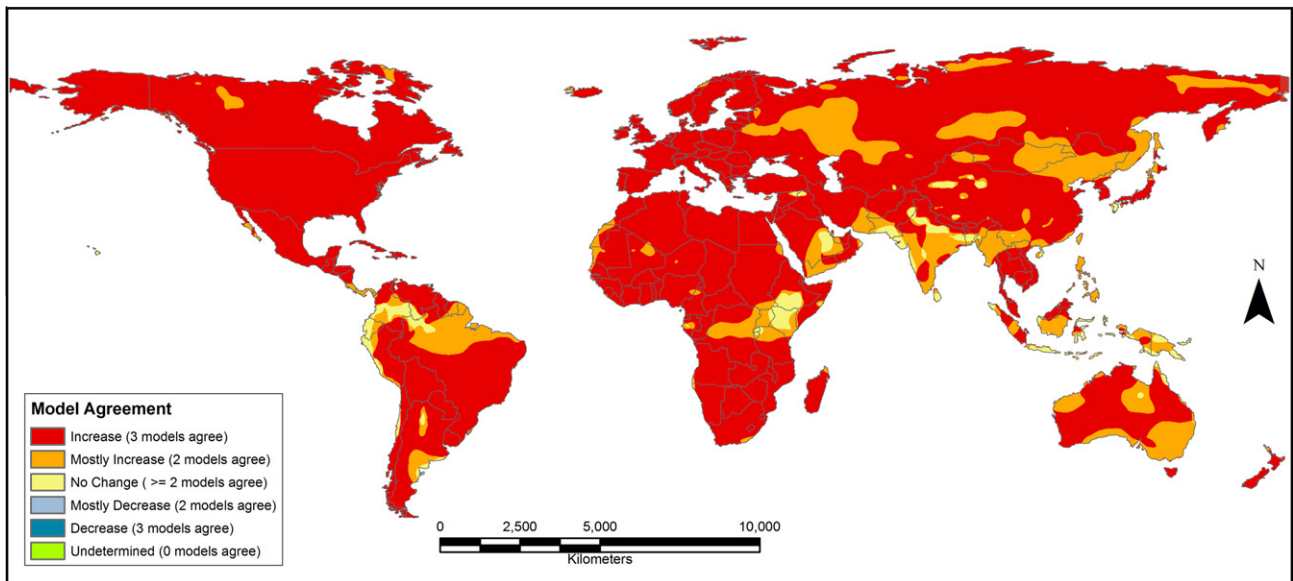


Fig. 4. Composite CSR anomaly map for the A2 scenario 2091–2100 relative to the 1971–2000 base period.

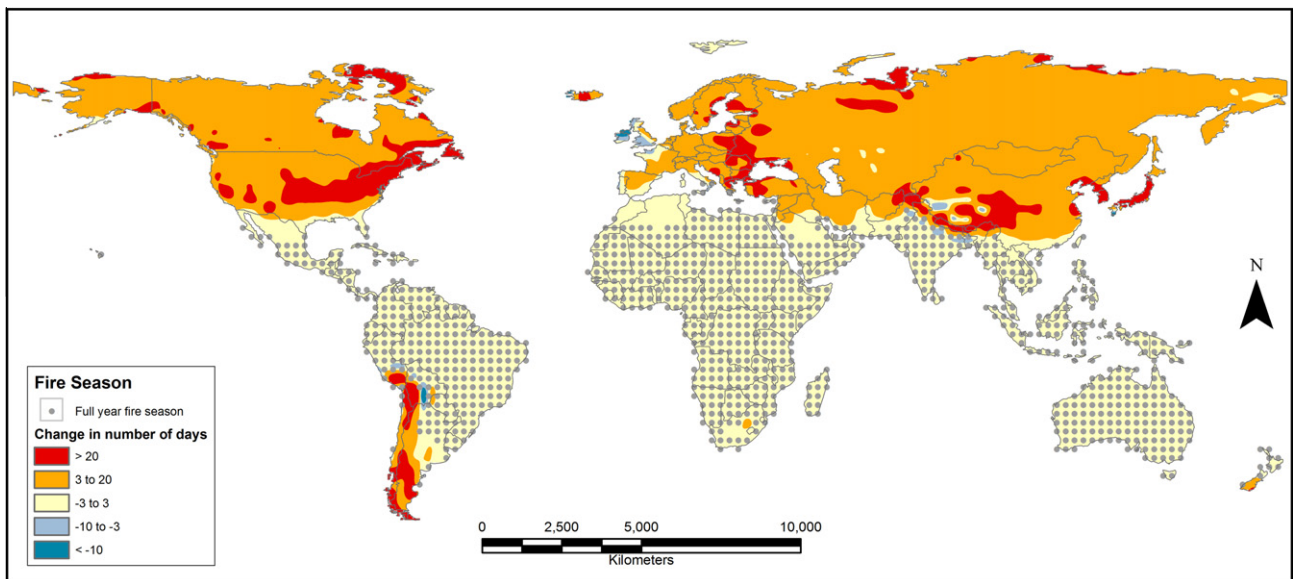


Fig. 5. Fire season length anomaly maps for 2041–2050 for Hadley CM3 B1 scenario relative to the 1971–2000 base period.

and end dates of the fire season and calculate the FWI System components, and ultimately the CSR over the resulting fire season. For example, if the average May temperature was 2 °C warmer in a future decade than in the GCM 1971–2000 period at a particular grid point then all the daily May temperatures in the NCEP baseline data at that grid point were increased by 2 °C. For precipitation, the decadal future monthly GCM averages were divided by the 30-year GCM monthly baselines to get a ratio of future precipitation over baseline precipitation. This ratio was used as a multiplier to the daily precipitation amount in the NCEP baseline. Thus the CSR and fire season length were calculated using the modified NCEP daily data to be representative of future decades. CSR anomaly maps (ratios of future CSR over baseline 1971–2100 CSR values) were created for the 2041–2050 and 2091–2100 periods for all GCMs and all emission scenarios. For this study, we used the entire land surface of the earth except Antarctica but there are other regions that are sparsely vegetated where fire is currently absent

or infrequent. There were nine maps for each decade (3 GCMs × 3 scenarios). Fire season length anomaly maps were created for the 2041–2050 and 2091–2100 periods for each GCM and each scenario (nine maps for each decade) in the same fashion as the CSR maps.

All the analyses were conducted using R (R development Core Team, 2011).

3. Results

Figs. 1 and 2 show examples of CSR for the IPSL model and the A2 scenario for 2041–2050 and for 2091–2100. These examples (Figs. 1 and 2) are representative of all the GCMs and scenarios maps that show a significant world-wide increase in CSR especially for the northern hemisphere. The increases relative to the base period of 1971–2000 are observed across the entire world at the end

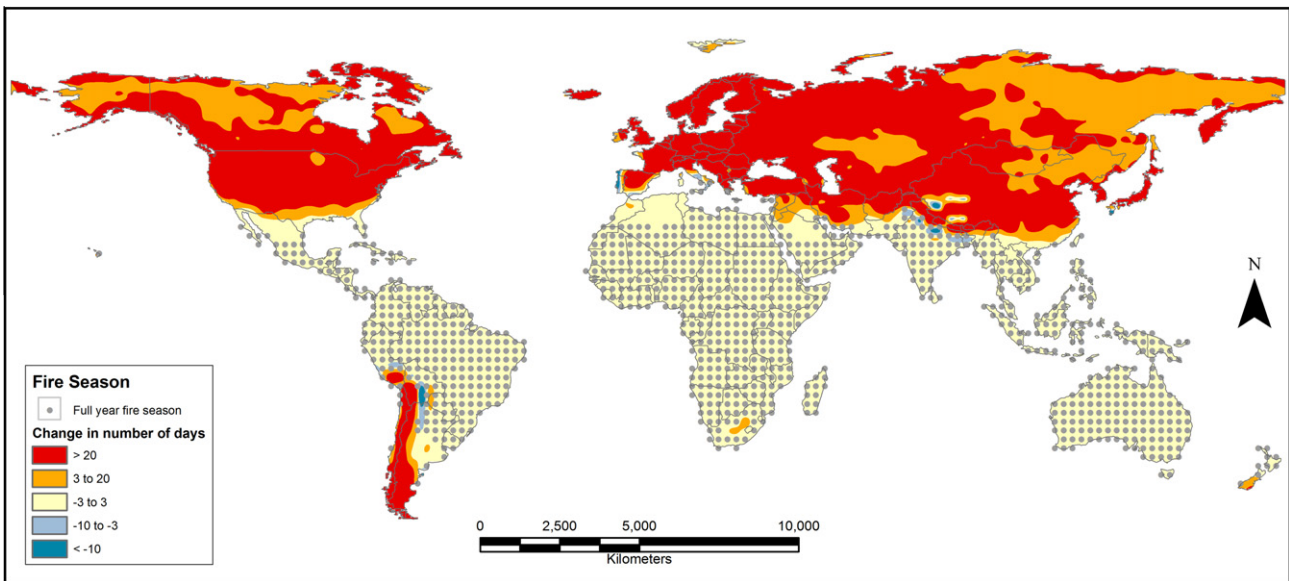


Fig. 6. Fire season length anomaly maps for 2091–2100 for Hadley CM3 B1 scenario relative to the 1971–2000 base period.

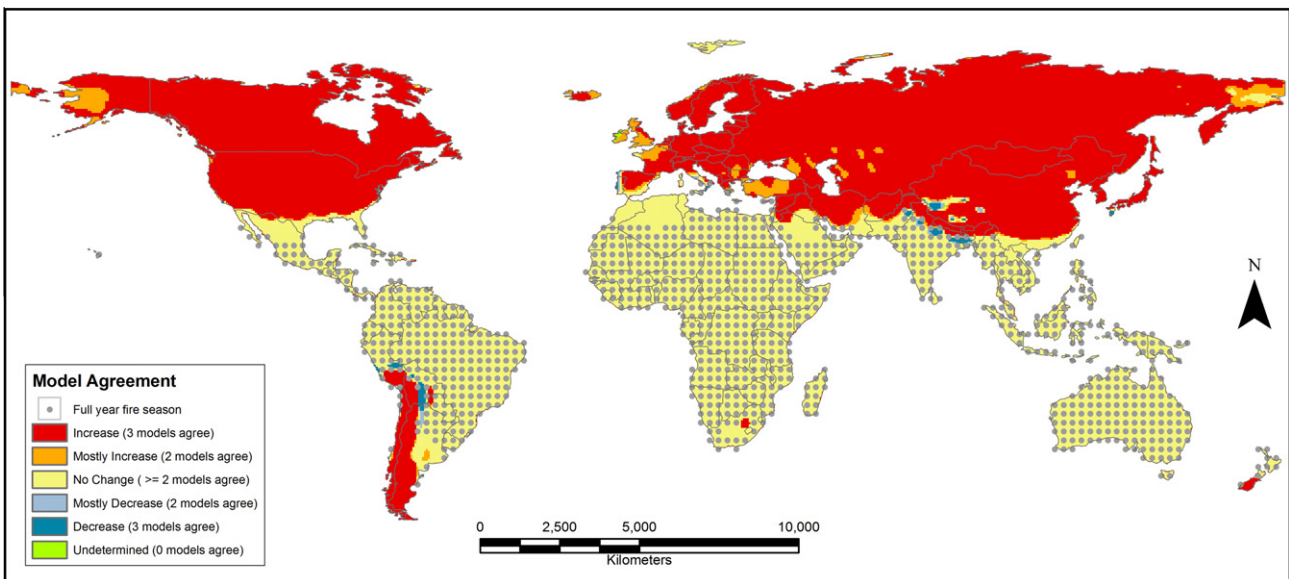


Fig. 7. Fire season length anomaly maps for the B1 scenario 2041–2050.

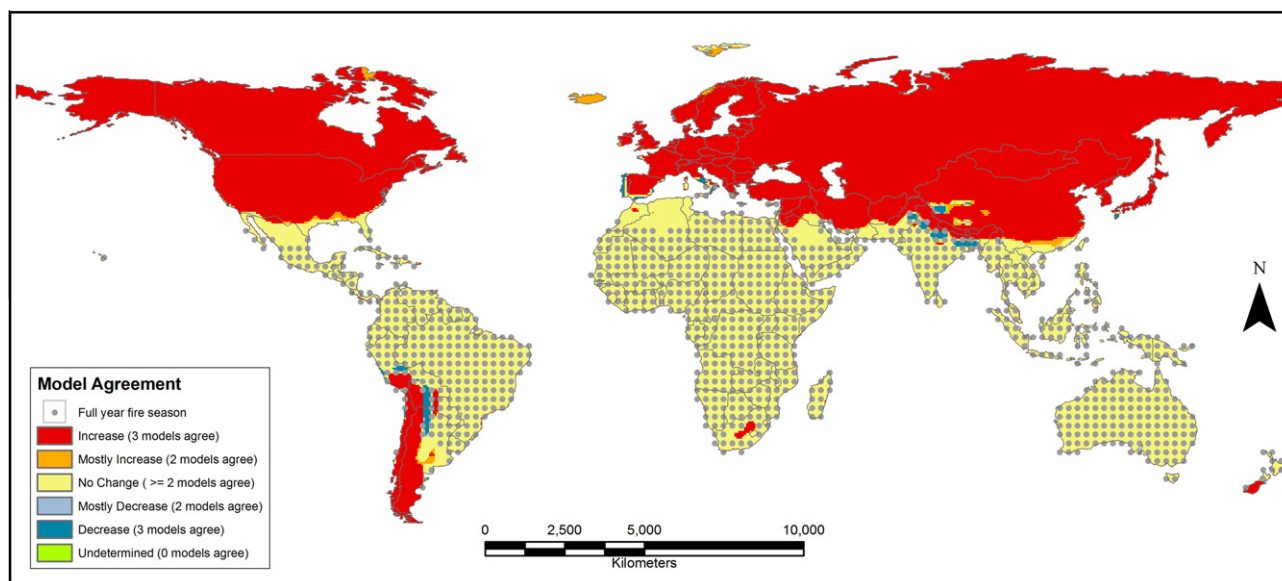


Fig. 8. Fire season length anomaly maps for the B1 scenario 2091–2100.

of the century with some of the increases exceeding three times the baseline value which are very significant.

Composite CSR anomaly maps were made for 2041–2050 and 2091–2100 that show how well GCMs agreed for each emission scenario (Figs. 3 and 4 show the A2 scenario which is very similar to A1B and B1 that are not shown). In these maps, agreement was made on whether it was in the same category; we used three categories, decrease, no change and increase. These figures highlight that there is good agreement across the models and there is good agreement across scenarios (not shown). Large parts of the earth are showing increases in CSR for all three GCMs for mid-century and the increases are even more pronounced at the end of the century. There are no areas where models suggest a decrease in CSR. There are some regions where the consensus is no change but these areas are not large and become almost insignificant by the end of the century.

The anomaly maps showed the change in number of days in fire season per year. Figs. 5 and 6 show examples of fire season length for the Hadley model and the B1 scenario for 2041–2050 and 2091–2100. These maps were combined to show how well the models agreed across scenarios for each time period (Figs. 7 and 8 for the B1 scenario but these are very similar to A1B and A2 that are not shown).

These results suggest significant increases in CSR across most of the earth with very pronounced increases initially at high northern latitudes but encompassing most of the earth by the end of the century. With these increases we expect more area burned, increased fire occurrence, and greater fire intensity that will result in more severe fire seasons and increased fire control difficulty. The fire season length shows significant parts of the globe such as tropical areas and the Mediterranean region have a full year fire season already. The increases in fire season length are modest overall, and are largest at higher latitudes and later in the century.

4. Discussion

Our climate is warming and this may have a dramatic and rapid impact on wildland fire activity. The consistency in the results suggesting significant increases over most of the earth may be attributed to the role temperature plays in fire activity. Almost the entire

globe is expected to warm over this century and our results may be a reflection of this temperature increase. Numerous studies suggest that temperature is the most important variable affecting annual wildland fire activity, with warmer temperatures leading to increased fire activity (Parisien et al., 2011). Gillett et al. (2004) suggest that the increase in area burned in Canada over the past four decades is due to human-caused increases in temperatures. The reason for the positive relationship between temperature and wildland fire is threefold. First, warmer temperatures will increase evapotranspiration, as the ability for the atmosphere to hold moisture increases rapidly with higher temperatures, thereby lowering water table position and decreasing fuel moisture unless there are significant increases in precipitation. Second, warmer temperatures translate into more lightning activity that generally leads to increased ignitions (Price and Rind, 1994). Third, warmer temperatures may lead to a lengthening of the fire season (Westerling et al., 2006). While testing the sensitivity of landscape fire models to climate change and other factors, Cary et al. (2006) found that area burned increased with higher temperatures. This increase was present even when precipitation was increased, although the increase in area burned was greatest for the warmer and drier scenario. The bottom line is that we expect more fire in a warmer world. Precipitation also has an important influence on fire activity but timing of precipitation during the fire season rather than the amount is usually the most important aspect (Flannigan and Harrington, 1988). In this study, we did not change the timing of the precipitation but only the amount and this probably does have some bearing on our results. If some regions have fewer days of precipitation in the future, this would probably enhance the predicted increases in fire activity; alternatively, if some regions have greater precipitation frequency, this could offset some of the predicted fire activity increases. Our results are somewhat similar to Liu et al. (2010) who found potentially significant increases in future wildfire potential in many parts of world using the Keetch–Byram Drought Index. Our results differ from Liu et al. (2010) in the circumboreal region (Russia, Canada, Alaska) where we found very significant increases. The results from this study do not agree with the findings from Krawchuk et al. (2009) who suggest that there may be many regions of the world with decreasing fire activity. However, most of the research suggests that we should expect increases in area burned and number of fires in a warmer world

(Flannigan et al., 2009a). Hansen et al. (2012) show that the likelihood of extreme seasonal mean temperatures has increased significantly since the 1951–1980 base period and suggests that the extreme anomalies in Russia 2010 and Texas and Oklahoma in 2011 are a consequence of global warming. It is interesting to note that extreme fire activity was associated with this period of extreme heat in Russia and central USA. Also, Dai (2012) demonstrates that increasing drought has been observed, and some models suggest more severe and widespread droughts in the future under global warming. As mentioned earlier, fuels, ignitions, weather and people are key factors affecting fire activity but in many regions it is weather, and in particular temperature, that is the primary factor explaining much of the variance in regional area burned (Balshi et al., 2009; Parisien et al., 2011). In many parts of the world, ignitions are not limiting as people are widely distributed across the landscape. The fuel factor is more complicated and may indeed be a constraint for fire activity in extremely sparsely vegetated parts of the world during some time periods. However, many fire-prone biomes like the circumboreal (de Groot et al., 2013) have little or no fuel constraints. The bottom line is that a warmer world will have more fire over most of the earth according to the simulations in this study.

If fire activity is determined by fuels, ignitions and weather, then this influences our response to the potential impact of climate warming on wildland fire activity. We can't change the weather and we can't modify lightning activity in any significant way. Our remaining options are to reduce human-caused ignitions and to modify fuels. Human-caused ignitions can be reduced through education programs, restricting or excluding the use of fire, and through proper enforcement of existing policies. Treating fuels at the global scale is not possible but treating fuels at the local scale near areas of high value can be done. A number of programs already exist that promote the fuel reduction or modification approach as one way to help protect communities and other values at risk.

Using three GCMs and three emission scenarios, our results suggest an increase in fire season length in regions where the fire season is not a full year already. Wotton and Flannigan (1993) found that the fire season length in Canada increased by an average of 22% or 30 days using the Canadian GCM $2 \times \text{CO}_2$ scenario. Our results suggest similar numbers by the end of the century rather than mid-century. In a study of wildfire in the western USA, Westerling et al. (2006) found that the fire season length has increased by over 2 months since 1980s. These results suggest a more dramatic change than our results are showing but this could be due to coarse spatial scale in our global study and the influence of snow and mountains in the Westerling study.

The substantial CSR predicted across climate change scenarios by the end of this century are truly noteworthy for wildland fire managers. Increases of up to 300% in cumulative DSR, particularly in the northern circumpolar region, will place unprecedented demands on fire suppression resources. Some of the CSR increase is due to longer fire seasons (about 20–30 days); however the DSR on low and even moderate days (the most frequent days in the fire season) is quite small relative to DSR values on high and extreme days and thus the vast majority of the increase is due to the increase in potential fire intensity and subsequent control difficulty. Fire suppression action most often fails during high intensity crown fires (Stocks et al., 2004), and the climate change scenarios of this study indicate that this type of fire behaviour will occur with greater frequency in the future. Many countries of the world operate highly efficient fire management organisations that have a high fire control success rate. However, climate change may cause a disproportionate increase in uncontrolled fires because it is thought that most modern fire management organisations already operate at near to optimum efficiency; thus any further increase in

fire control difficulty will force many more fires beyond a threshold of suppression capability (cf Flannigan et al., 2009b; Podur and Wotton, 2010). Perhaps we are already experiencing what is to come with recent disastrous fires in Australia in 2009, Russia in 2010 and Texas and other states in the USA in 2011. Increased wildland fire on the landscape in the future will force fire management agencies to re-assess policy and strategy. All wildland areas cannot be protected from fire, and many high value areas managed with a policy of fire exclusion will be threatened by wildfire. To protect those key areas, early warning systems based on fire danger will be critical to prevent or mitigate disaster fires (de Groot et al., 2010). The international fire community recognises that greater demands will be placed on fire management as fire season severity increases in the future. Fire early warning systems, one component of A Strategy to Enhance International Cooperation in Fire Management (FAO, 2006), will assist in pre-suppression preparedness and support greater international resource-sharing during periods of extreme fire activity.

Acknowledgements

We acknowledge the modeling groups, the Program for Climate Model Diagnosis and Intercomparison (PCMDI) and the WCRP's Working Group on Coupled Modelling (WGCM) for their roles in making available the WCRP CMIP3 multi-model dataset. Support of this dataset is provided by the Office of Science, U.S. Department of Energy. NCEP Reanalysis data provided by the NOAA/OAR/ESRL PSD, Boulder, Colorado, USA, from their Web site at <<http://www.esrl.noaa.gov/psd/>>. We also want to thank Dennis Quintilio who introduced us to the Cumulative Severity Rating concept.

References

- Balshi, M.S., McGuire, A.D., Duffy, P., Flannigan, M., Walsh, J., Melillo, J., 2009. Assessing the response of area burned to changing climate in western boreal North America using a multivariate adaptive regression splines (MARS) approach. *Global Change Biol.* 15, 578–600. <http://dx.doi.org/10.1111/j.1365-2486.2008.01679.x>.
- Bond, W.J., Keeley, J.E., 2006. Fire as a global 'herbivore': the ecology and evolution of flammable ecosystems. *Trends Ecol. Evol.* 20, 387–394.
- Byram, G.M., 1959. Combustion of forest fuels. In: Davis, K.P. (Ed.), *Forest Fire: Control and Use*. McGraw-Hill, New York, pp. 61–89.
- Carcaillet, C., Bergeron, Y., Richard, P.J.H., Fréchette, B., Gauthier, S., Prairie, Y.T., 2001. Change of fire frequency in the eastern Canadian boreal forests during the Holocene: does vegetation composition or climate trigger the fire regime? *J. Ecol.* 89, 930–946.
- Cary, G.J., Keane, R.E., Gardner, R.H., Lavorel, S., Flannigan, M.D., Davies, I.D., Li, C., Lenihan, J.M., Rupp, T.S., Mouillot, F., 2006. Comparison of the sensitivity of landscape-fire-succession models to variation in terrain, fuel pattern, climate and weather. *Landscape Ecol.* 21, 121–137.
- Cole, J., 2009. Xconv/Convsh (Version 1.91). Software. <<http://badc.nerc.ac.uk/help/software/xconv/>>.
- Dai, A., 2012. Increasing drought under global warming: observations and models. *Nat. Climate Change*. <http://dx.doi.org/10.1038/NCLIMATE1633>.
- de Groot W.J., Goldammer, J.G., Justice, C.O., Lynham, T.J., Csiszar, I.A., San-Miguel-Ayanz, J., 2010. Implementing a global early warning system for wildland fire. In: Viegas, D.X. (Ed.), *Proceedings of the VI International Conference on Forest Fire Research, ADAI/CEIF, Univ. Coimbra, Portugal (CD ROM)*.
- de Groot, W.J., Cantin, A.S., Flannigan, M.D., Soja, A.J., Gowman, L.M., Newbery, A., 2013. A Comparison of Canadian and Russian Boreal Forest Fire Regimes. *For. Ecol. Manage.* 294, 23–34.
- FAO, 2006. *Fire Management Review: International Cooperation*. Fire Management Working Paper 18. Food and Agriculture Organization, United Nations. Rome.
- Flannigan, M.D., Harrington, J.B., 1988. A study of the relation of meteorological variables to monthly provincial area burned by wildfire in Canada 1953–80. *J. Appl. Meteorol.* 27, 441–452.
- Flannigan, M.D., Krawchuk, M.A., de Groot, W.J., Wotton, B.M., Gowman, L.M., 2009a. Global wildland fire and climate change. *Int. J. Wildland Fire* 18, 483–507.
- Flannigan, M.D., Logan, K.A., Amiro, B.D., Skinner, W.R., Stocks, B.J., 2005. Future area burned in Canada. *Climatic Change* 72, 1–16.
- Flannigan, M.D., Stocks, B.J., Turetsky, M.R., Wotton, B.M., 2009b. Impacts of climate change on fire activity and fire management in the circumboreal forest. *Global Change Biol.* 15, 549–560.
- Gillett, N.P., Weaver, A.J., Zwiers, F.W., Flannigan, M.D., 2004. Detecting the effect of climate change on Canadian forest fires. *Geophys. Res. Lett.* 31, L18211.

- Hansen, J., Sato, M., Ruedy, R., 2012. Perception of climate change. In: Proceedings of the National Academy of Sciences. <http://dx.doi.org/10.1073/pnas.1205276109>.
- Hargrove, W.W., Gardner, R.H., Turner, M.G., Romme, W.H., Despain, D.G., 2000. Simulating fire patterns in heterogeneous landscapes. *Ecol. Model.* 135, 243–263.
- Krawchuk, M.A., Moritz, M.A., Parisien, M.-A., Van Dorn, J., Hayhoe, K., 2009. Global pyrogeography: macro-scaled models for understanding the current and future distribution of fire. *Public Libr. Sci. (PLOS One)* 4. <http://dx.doi.org/10.1371/journal.pone.0005102>.
- Liu, Y., Stanturf, J., Goodrick, S., 2010. Trends in global wildfire potential in a changing climate. *Forest Ecol. Manage.* 259, 686–697.
- Meyn, A., White, P.S., Buhk, C., Jentsch, A., 2007. Environmental drivers of large, infrequent wildfires: the emerging conceptual model. *Prog. Phys. Geogr.* 31, 287–312.
- Mouillot, F., Field, C.B., 2005. Fire history and the global carbon budget: A $1^\circ \times 1^\circ$ fire history reconstruction for the 20th century. *Global Change Biol.* 11, 398–420.
- Parisien, M.-A., Parks, S.A., Krawchuk, M.A., Flannigan, M.D., Bowman, L.M., Moritz, M.A., 2011. Scale-dependent controls on the area burned in the boreal forest of Canada, 1980–2005. *Ecol. Appl.* 21, 789–805.
- Podur, J., Wotton, B.M., 2010. Will climate change overwhelm fire management capacity? *Ecol. Model.* 221, 1301–1309.
- Prasad, V.K., Badarinath, K.V.S., Eaturu, A., 2008. Biophysical and anthropogenic controls of forest fires in the Deccan Plateau. *India J. Environ. Manage.* 86, 1–13.
- Price, C., Rind, D., 1994. Possible implications of global climate change on global lightning distributions and frequencies. *J. Geophys. Res.* 99 (D5), 10,823–10,831.
- R Development Core Team, 2011. R: A Language and Environment for Statistical Computing. R Foundation for Statistical Computing, Vienna, Austria. ISBN 3-900051-07-0. <<http://www.R-project.org/>>.
- Stocks, B.J., Alexander, M.E., Lanoville, R.A., 2004. Overview of the international crown fire modelling experiment (ICFME). *Can. J. For. Res.* 34, 1543–1547.
- Swetnam, T.W., 1993. Fire history and climate change in giant sequoia groves. *Science* 262, 885–889.
- Swetnam, T.W., Betancourt, J.L., 1998. Mesoscale disturbance and ecological response to decadal climatic variability in the American southwest. *J. Clim.* 11, 3128–3147.
- van der Werf, G.R., Randerson, J.T., Giglio, L., Collatz, G.J., Kasibhatla, P.S., Arellano Jr., A.F., 2006. Interannual variability in global biomass burning emissions from 1997 to 2004. *Atmos. Chem. Phys.* 6, 3423–3441.
- Van Wagner, C.E., 1970. Conversion of Williams severity rating for use with the fire weather index. *Can. Dep. Fish. For., Can. For. Serv., Rep. PS-X-21*. Petawawa, ON.
- Van Wagner, C.E., 1987. Development and structure of the Canadian Forest Fire Weather Index System. *Can. For. Serv., For. Tech. Rep. 35*, Ottawa, ON.
- Westerling, A.L., Hidalgo, H.G., Cayan, D.R., Swetnam, T.W., 2006. Warming and earlier spring increase western U.S. forest wildfire activity. *Science* 313, 940–943.
- Williams, D.E., 1959. Fire Season Severity Rating. Department of Northern Affairs and National Resources, Forestry Branch, Headquarters. Forest Research Division Technical Note 73. Ottawa, ON.
- Wotton, B.M., Flannigan, M.D., 1993. Length of the fire season in a changing climate. *Forest. Chron.* 69, 187–192.

Strength and persistence of fire-induced soil hydrophobicity under ponderosa and lodgepole pine, Colorado Front Range

Edward L. Huffman,¹ Lee H. MacDonald^{2*} and John D. Stednick²

¹ Boulder Ranger District, Arapaho-Roosevelt National Forest, USDA Forest Service, Boulder, CO, USA

² Department of Earth Resources, Colorado State University, Fort Collins, CO 80523-1482, USA

Abstract:

Fire-induced soil hydrophobicity is presumed to be a primary cause of the observed post-fire increases in runoff and erosion from forested watersheds in the Colorado Front Range, but the presence and persistence of hydrophobic conditions has not been rigorously evaluated. Hence the goals of this study were to: (1) assess natural and fire-induced soil hydrophobicity in the Colorado Front Range, and (2) determine the effect of burn severity, soil texture, vegetation type, soil moisture, and time since burning on soil hydrophobicity.

Five wild and prescribed fires ranging in age from 0 to 22 months were studied. Each fire had four study sites in ponderosa pine forests that had been burned at high, moderate, or low severity, and three sites were in unburned areas. Additional sites were established in lodgepole pine stands and an area with unusually coarse-textured soils. At each site the soil hydrophobicity was assessed in two pits using the water drop penetration time (WDPT) and the critical surface tension (CST). Measurements were made at the mineral soil surface and depths of 3, 6, 9, 12, 15, and 18 cm.

In sites burned at moderate or high severity the soils were often strongly hydrophobic at 0, 3, and 6 cm. Unburned sites or sites burned at low severity were typically hydrophobic only at the surface. Although soil hydrophobicity generally strengthened with increasing burn severity, statistically significant differences in soil hydrophobicity were difficult to detect because of the high variability within and between sites. Hydrophobicity also increased with increasing percent sand and was not present when soil moistures exceeded 12–25%. There were no significant differences in soil hydrophobicity between ponderosa and lodgepole pine stands, regardless of burn severity.

Repeat measurements on one fire suggest a weakening of fire-induced soil hydrophobicity after 3 months. Comparisons between fires suggest that fire-induced soil hydrophobicity persists for at least 22 months. Overall, CST values were more consistent and more highly correlated with the independent variables than the WDPT, and the CST is recommended for assessing soil hydrophobicity rather than the more commonly used WDPT. Copyright © 2001 John Wiley & Sons, Ltd.

KEY WORDS soil hydrophobicity; water repellency; burn severity; soil texture; Colorado Front Range; critical surface tension; ponderosa pine; lodgepole pine

INTRODUCTION

Soil hydrophobicity is a naturally occurring phenomenon (DeBano, 1981; Doerr *et al.*, 2000). This natural hydrophobicity usually is found at the mineral soil surface, and it is caused by the leaching of hydrophobic compounds, such as aliphatic hydrocarbons, from the litter and humus layers. Under unburned conditions the presence of hydrophobicity below the soil surface is commonly associated with fungal mycelia (Savage *et al.*, 1969).

The heat of a fire vaporizes hydrophobic compounds in the litter, humus, and soil organic matter (DeBano *et al.*, 1967). These compounds can escape into the atmosphere, or move into the soil atmosphere and condense

*Correspondence to: L. H. MacDonald, Department of Earth Resources, Colorado State University, Fort Collins, CO 80523-1482, USA.
E-mail: leemac@cnr.colostate.edu

on cooler soil particles at or below the soil surface (DeBano, 1981; Crockford *et al.*, 1991; Doerr *et al.*, 1996). The condensation of these compounds forms a hydrophobic coating on the soil particles (DeBano and Krammes, 1966; Savage, 1974).

In most forested areas the natural hydrophobicity is too weak and discontinuous to hinder infiltration and initiate infiltration-excess overland flow. Flow is mostly subsurface and the runoff and erosion rates are correspondingly low (DeBano, 1981). The formation of a strong hydrophobic layer after natural or prescribed fires can inhibit infiltration (Meeuwig, 1971; Scott and van Wyk, 1990). Once the ash and soil above the hydrophobic layer becomes saturated, any additional precipitation will become runoff. Hence the rate of runoff from forested areas can increase by more than an order of magnitude after burning, and this surface runoff, when combined with the loss of the protective litter layer, can cause even larger increases in surface erosion and catchment-scale sediment yields (e.g. Helvey, 1980; Scott and van Wyk, 1990).

Fire-induced soil hydrophobicity is believed to be the primary cause of the observed increases in runoff and erosion from forested watersheds after wildfires (DeBano and Krammes, 1966; DeBano, 1981; Wohlgemuth *et al.*, 1996). Fire is an important element in the ponderosa and lodgepole pine forests in Colorado's Front Range (Brown *et al.*, 1999), and increasing development means that an increase in runoff or erosion can threaten lives and property. The observed large increases in runoff and erosion after recent wildfires in Colorado have been ascribed to post-fire soil hydrophobicity (Colorado Water Conservation Board, 1997), but there has been no rigorous assessment of the extent and persistence of post-fire soil hydrophobicity in the fire-prone ponderosa and lodgepole pine forests of the Colorado Front Range.

A number of factors are believed to control the strength of soil hydrophobicity, and the most important of these are burn severity, vegetation type, soil texture, soil moisture, and time since burning. Burn severity is often cited as a primary control on the strength and extent of fire-induced soil hydrophobicity (DeBano and Krammes, 1966; DeBano, 1981), as high-severity fires vaporize more organic compounds and thereby generate a stronger and more continuous hydrophobic layer (Tiedemann *et al.*, 1979; DeBano, 1981).

Vegetation type also affects the formation and strength of a hydrophobic layer (DeBano, 1981; Imeson *et al.*, 1992; Doerr *et al.*, 1998; Scott, 2000). The amount of fuel affects burn severity, whereas the amount and types of hydrophobic compounds in plant materials control the potential strength of a hydrophobic layer. Most studies on fire-induced soil hydrophobicity in the USA have been done in chaparral (e.g. DeBano and Krammes, 1966), and a few studies have documented the formation of a water-repellent layer in *Pinus radiata* (radiata pine), *Pinus ponderosa* (ponderosa pine), *Pinus contorta* (lodgepole pine), and other forests dominated by the *Pinaceae* family (Meeuwig, 1971; Dyrness, 1976; Campbell *et al.*, 1977; Helvey, 1980; Doerr *et al.*, 1996).

Soil texture also affects the strength of the hydrophobic layer (DeBano, 1981). Since coarse-textured soils have a lower specific surface than fine-textured soils, a given amount of hydrophobic compounds will cause more hydrophobicity—both naturally and following burning—in coarse-textured soils (Meeuwig, 1971; DeBano, 1981).

Over time a hydrophobic soil will wet up due to the strong hydraulic gradient and movement of water vapour (DeBano, 1981). Once a hydrophobic soil begins to wet there is usually a soil moisture threshold at which these soils cease to be hydrophobic (Crockford *et al.*, 1991; Dekker and Ritsema, 1994; Doerr and Thomas, 2000). This soil moisture threshold ranges from 1.75% in dune sands (Dekker and Ritsema, 1994) to 28% in soils under eucalyptus (Doerr and Thomas, 2000). Upon drying, the hydrophobic conditions can be re-established (Shakesby *et al.*, 1993).

The persistence of a post-fire hydrophobic layer will depend on the strength and extent of hydrophobic chemicals after burning and the many physical and biological factors that can aid in breakdown (DeBano, 1981). Soil hydrophobicity usually returns to pre-burn conditions in no more than 6 years (Dyrness, 1976; DeBano, 1981), and several studies have documented a much more rapid recovery (e.g. DeByle, 1973; Reeder and Jurgensen, 1979).

The goal of this study was to characterize natural and post-fire soil hydrophobicity in ponderosa and lodgepole pine forests in the central and northern Colorado Front Range. The specific objectives were to:

(1) measure the strength of soil hydrophobicity at different soil depths in both burned and unburned ponderosa and lodgepole pine forests; (2) relate the observed hydrophobicity to burn severity, vegetation type, soil texture, soil moisture, and time since burning; and (3) develop a model to predict those areas that are most likely to be strongly hydrophobic after a forest fire.

STUDY AREAS

Five wild and prescribed fires in the northern and central Colorado Front Range were selected for study (Table I; Figure 1). The time since burning ranged from 0 to 22 months. All five fires contained sites burned at high, moderate, and low severities as well as unburned areas. Ponderosa pine was the dominant vegetation type, although the Bobcat and Lower Flowers fires also burned areas dominated by lodgepole pine. The Bobcat and Hi Meadows wildfires were tested immediately after burning, and the sites in the Bobcat wildfire were retested 3 months after burning. Hydrophobicity was tested 4 months, 7 months, and 22 months after burning in the Dadd Bennett, Lower Flowers, and Crosier Mountain prescribed fires respectively. All fieldwork was conducted from May to September 2000. Each fire was tested in a 1–2 week period, depending on the number of sites.

Soil textures ranged from sand to loam, with the majority of soils classified as sandy loams (Table I). Soil types ranged from Typic Argicryolls to Ustic Haplocryalfs (E. Kelly, Colorado State University, personal communication, 2001).

METHODS

Site selection

Within each fire the sample sites were stratified by burn severity, vegetation type, and soil texture. A set of approximately 15 sites was established for each fire, each vegetation type, and each soil texture. For each set of 15 sites, four sites each were in areas burned at high, moderate, and low severity, and three sites were in unburned areas.

Table I. Fires selected for study, date of each fire, time since burning when hydrophobicity was tested, vegetation types within each fire, the type of fire, mean soil texture of the top 12 cm, and the number of sites tested for each fire. Percent sand, silt, and clay were calculated for the fine fraction (<2 mm). Standard deviations are in parentheses

Name of fire	Date of fire	Time since burning when tested (months)	Vegetation type(s)	Prescribed or wildfire	>2 mm (%)	Sand (%)	Silt (%)	Clay (%)	No. of sites
Bobcat	June 2000	0	Ponderosa and lodgepole pine	Wildfire	10.8 (7.7)	64.3 (9.9)	28.8 (8.0)	6.9 (3.5)	45
	June 2000	3							45
Hi Meadows	June 2000	0	Ponderosa pine	Wildfire	43.0 (5.5)	66.2 (4.2)	25.9 (4.0)	7.9 (1.4)	14
Dadd Bennett	February 2000	4	Ponderosa pine	Prescribed fire	20.5 (7.4)	69.6 (3.7)	22.5 (3.8)	7.9 (1.9)	15
Lower Flowers	November 1999	7	Ponderosa and lodgepole pine	Prescribed fire	21.2 (6.9)	72.8 (5.8)	21.6 (4.8)	5.6 (1.3)	30
Crosier Mountain	August 1998	22	Ponderosa pine	Prescribed fire	21.8 (10.2)	65.4 (3.2)	27.3 (2.9)	7.3 (1.2)	12

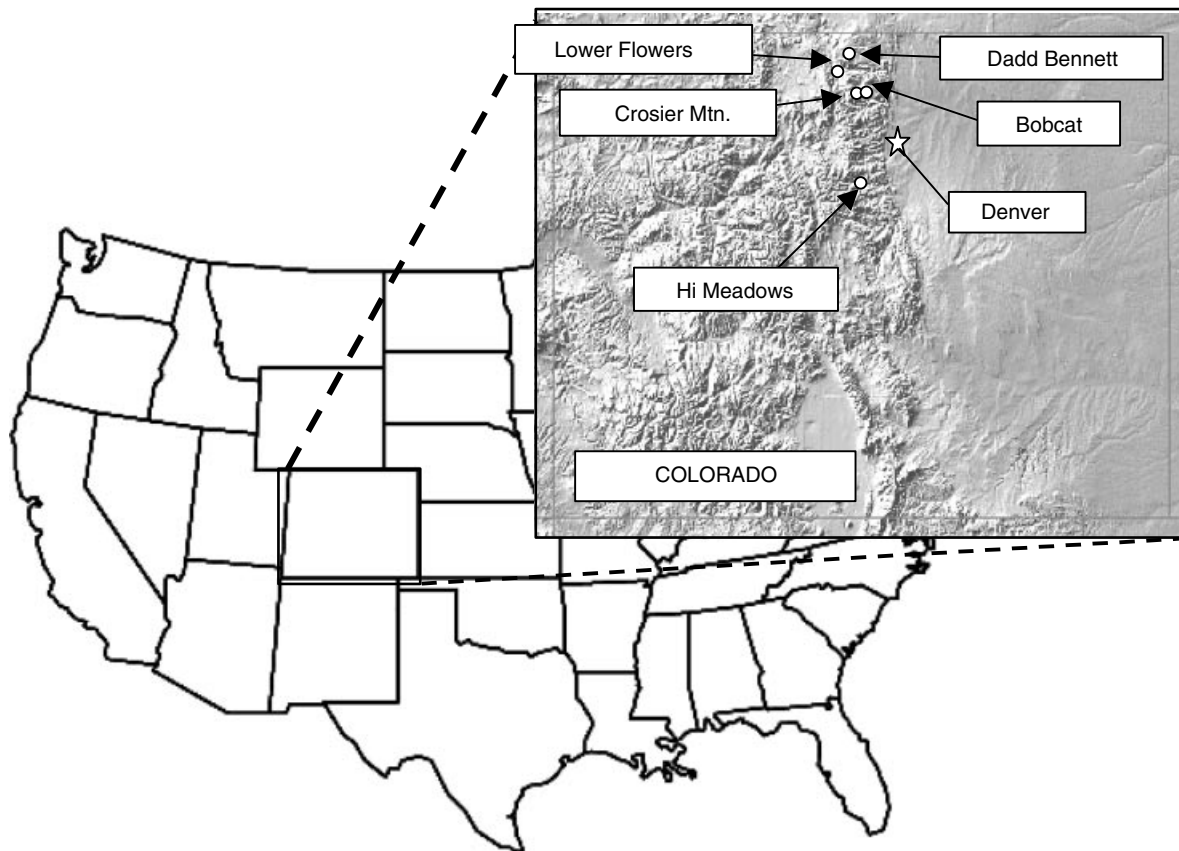


Figure 1. Location of the fires used in this study

Ponderosa pine sites were tested in all five fires, and complete sets of 15 sites were also established in lodgepole pine in the Bobcat and Lower Flowers fires (Table I). Large differences in soil texture were only present in the Bobcat fire, and an additional 15 sites were sampled in a ponderosa pine forest with unusually coarse soil textures. Sites in the same vegetation and burn severity class were always separated by at least 50 m. There were a total of 161 sites.

Burn severity was determined qualitatively at each site following the USDA Forest Service (1995) criteria. High-severity sites were identified by the complete combustion of organic matter, leaving only black or white ash. In moderate-severity sites most of the organic matter was consumed; ash and scorching was found on the mineral soil surface. At low-severity sites most of the organic matter was not consumed, but the litter surface was at least charred. In these sites the duff layer below the unconsolidated litter was still intact and there were no visible effects of the fire at the mineral soil surface.

At each site two pits were located approximately 30 cm apart. Pits were located under the drip line of the canopy where the soil hydrophobicity was stronger (Huffman, 2001). When the Bobcat fire was retested new pits were dug at each site.

Hydrophobicity assessment

At each pit the litter, duff, and ash were carefully swept aside. Soil hydrophobicity was assessed at the mineral soil surface and at depths of 3, 6, 9, 12, 15, and 18 cm. Soil hydrophobicity was tested in the field by measuring the water drop penetration time (WDPT) and the critical surface tension (CST). These two

measures are the most widely used tests for assessing soil hydrophobicity (Wallis and Horne, 1992). The WDPT is the time needed for a drop of de-ionized water to be absorbed into the soil (Letey, 1969). In this study the WDPT was replicated ten times at each depth in each pit. Observations were continued for a maximum of 360 s, and the median time was used as the WDPT for that depth. The median WDPT was averaged between pits to generate a mean site WDPT for each depth.

The CST, also known as the 90° surface tension, was determined by placing drops of varying concentrations of de-ionized water and pure ethanol on the soil surface (Letey, 1969). Surface tension decreases with increasing ethanol concentrations, and the 13 solutions used in this study were 0, 1, 3, 5, 9, 14, 19, 24, 34, 48, 60, 72, and 80% ethanol. Beginning with pure water, at least five drops were applied at each depth. If the drops were not absorbed within 5 s, drops with successively greater concentrations of ethanol were applied until all the drops were absorbed within 5 s (Watson and Letey, 1970). The CST of the last solution used was averaged between pits to generate a mean site CST for each depth. Lower CST values indicate stronger soil hydrophobicity (Watson and Letey, 1970). Surface tensions were corrected for the effect of air temperature at the time of sampling (Weast, 1983).

Soil moisture and particle-size analysis

At each pit one soil sample was taken from 0–3 cm ('surface') and another from 9–12 cm ('10 cm'). Each sample was weighed, dried, and weighed again to determine percent moisture (Gardner, 1986).

The two samples from each pit were combined after drying; approximately 50 g of the combined sample was used to determine the particle-size distribution by the hydrometer method (Gee and Bauder, 1986). The fraction greater than 2 mm was determined by sieving the sample used for the particle-size analysis (Gee and Bauder, 1986). Data from the two pits were averaged to obtain mean values for each site. Soil textures were classified according to the USDA classification scheme (Soil Survey Division Staff, 1993).

Data analysis

The soil hydrophobicity within fires was compared by depth and burn severity. The soil hydrophobicity was compared between fires by depth and burn severity. The soil hydrophobicity between vegetation types was compared by depth and burn severity for both the Bobcat and Lower Flowers fires. Each of these comparisons was analyzed by the Ryan, Einot, Gabriel, Welsch (REGWQ) test (Gabriel, 1978) to control for maximum experiment-wise error at $\alpha = 0.05$. Pairwise *t*-tests were used to compare hydrophobicity by depth and burn severity for the sites on the Bobcat fire that were retested after 3 months.

The effect of soil texture and soil moisture on hydrophobicity was analyzed by testing the dependence of WDPT and CST on percent sand, percent clay, percent mass >2 mm, and percent soil moisture for each burn severity and depth. Plots of soil moisture content against WDPT and CST for each burn severity and depth were used to determine whether there was a sudden reduction in soil hydrophobicity with increasing percent soil moisture.

The significant predictors of WDPT and CST at each depth were identified using Mallows' C_p selection method (Ott, 1993). Burn severity was assigned values of 1 (unburned) through 4 (high severity). Similarly, ponderosa and lodgepole pine were assigned the categorical values of 1 and 2 respectively. WDPT and CST values were transformed to natural logarithms to control decreasing variance with depth and improve the normality of their distributions. General linear models (GLMs) were then constructed from the significant predictors identified using Mallows' C_p . In contrast to the regression procedure used for predictor selection, GLMs can use both discrete and continuous variables (Ott, 1993).

RESULTS

The CST and WDPT values were strongly correlated ($r = -0.652$ to -0.999) at all depths (Table II). The strongest correlations were at 12–18 cm because there was less hydrophobicity and hence less variability

at these depths (Figure 2). In general, there was considerable variation in soil hydrophobicity between pits, between similar sites within a fire, and between comparable sites from different fires (Table III, Figure 3). In some cases the soils in one pit exhibited little or no hydrophobicity at 0, 3, and 6 cm, whereas the soils in the adjacent pit were strongly hydrophobic at these depths. The CST values had a mean coefficient of variation (CV) between pits of 4%, and the mean CV between sites stratified by fire, burn severity and depth was 9%. Individual CVs ranged from 0 to 53%. Because the CST values had much lower CVs than the WDPT and the CST values were more strongly related to the independent variables, only the CST values are reported here.

A plot of CST values versus depth for all sites shows strong hydrophobicity at shallow depths in sites burned at high and moderate severity (Figure 2a and b). There was some evidence of hydrophobicity at the mineral soil surface in the sites burned at low severity, and only very weak hydrophobicity at the surface of the unburned sites. From 9–18 cm only a few sites exhibited much hydrophobicity. Two pits in an unburned

Table II. Correlations between CST and WDPT from the soil surface (0 cm) to a depth of 18 cm. All correlation (r) are significant at $p < 0.0001$

Depth (cm)	0	3	6	9	12	15	18
	-0.685	-0.730	-0.684	-0.652	-0.771	-0.9997	-0.893

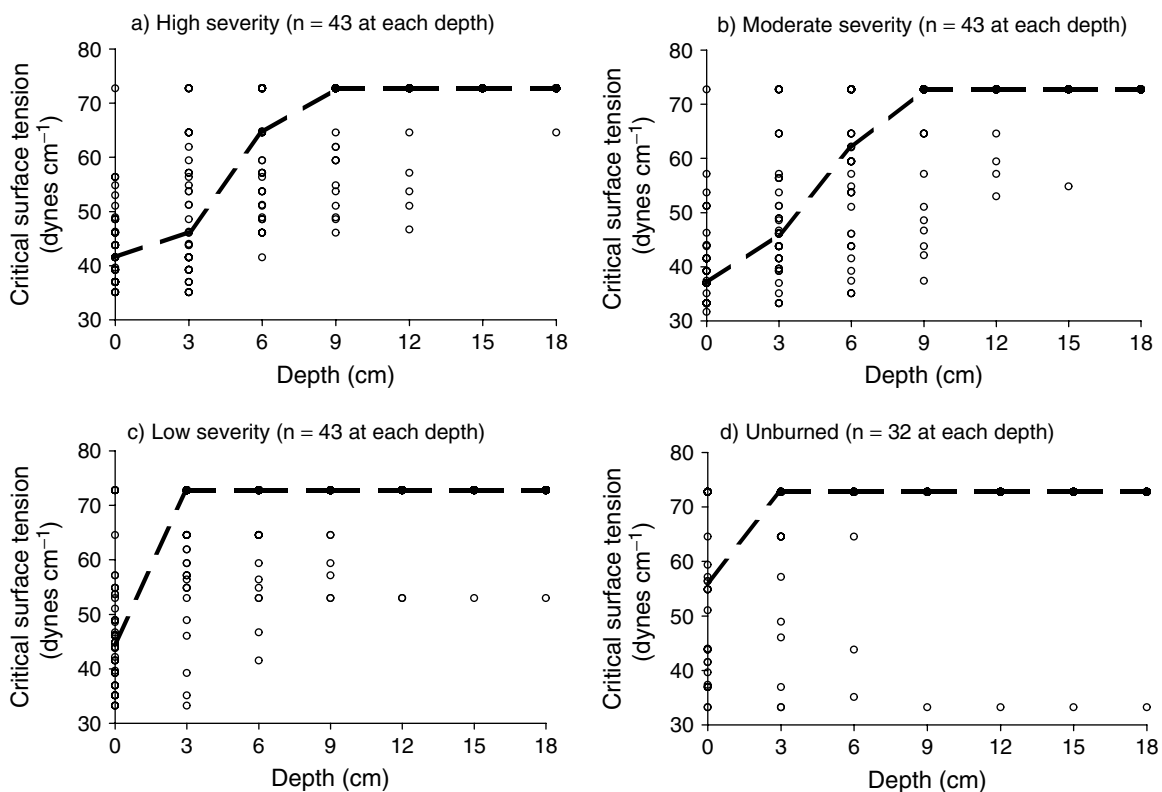


Figure 2. CSTs for (a) high severity, (b) moderate severity, (c) low severity, and (d) unburned sites. Each circle represents the average value at a site. Because so many values are overlapping, the median value for all sites is plotted as a dashed line. A decrease in CST indicates stronger hydrophobicity

Table III. Mean CST values for each fire and fire severity class at the mineral soil surface and depths of 3 and 6 cm. The horizontal comparisons are between fire severity classes within each fire and these are designated by the letters a, b, and c. The vertical comparisons are between fires within each fire severity class and these are designated by the letters x, y, and z. Values with the same letter are not significantly different at $p \leq 0.05$. Standard deviations are shown in parentheses

Fire/(months since burning)		High severity	Moderate severity	Low severity	Unburned
<i>Mineral soil surface</i>					
Bobcat	0	41.7 (6.1) b x	38.9 (2.6) b x,y	47.8 (10.9) b x	59.2 (13.9) a x
	3	47.3 (10.4) b x	46.7 (11.4) b x	52.9 (11.9) a,b x	62.4 (13.2) a x
Hi Meadows	0	46.2 (1.9) b x	39.2 (1.9) b x,y	54.7 (12.2) a,b x	64.6 (11.6) a x
Dadd Bennett	4	39.8 (5.8) a x	33.2 (0) a y	37.2 (3.0) a x	49.8 (19.9) a x
Lower Flowers	7	38.8 (4.5) a x	35.2 (2.9) a y	40.0 (7.1) a x	47.4 (17.1) a x
Crosier Mountain	22	45.4 (5.9) a,b x	35.7 (2.1) b x,y	43.0 (3.5) a,b x	52.4 (9.6) a x
<i>3 cm below the soil surface</i>					
Bobcat	0	51.5 (11.5) a x,y	50.8 (11.3) a x	61.6 (9.8) a x	63.2 (14.7) a x
	3	55.8 (14.4) a x,y	52.9 (15.2) a x	67.6 (11.3) a x	65.7 (13.4) a x
Hi Meadows	0	46.9 (12.7) b y	54.7 (3.9) b x	72.75 (0) a x	72.75 (0) a x
Dadd Bennett	4	40.5 (4.6) c y	39.0 (5.4) c x	60.3 (5.0) b x	70.0 (4.7) a x
Lower Flowers	7	44.5 (4.3) b y	47.0 (11.8) b x	57.0 (14.5) a,b x	63.4 (15.3) a x
Crosier Mountain	22	67.3 (9.5) a x	52.4 (19.8) a x	72.75 (0) a x	72.75 (0) a x
<i>6 cm below the soil surface</i>					
Bobcat	0	63.1 (9.8) a x,y,z	64.3 (9.6) a x	67.9 (7.5) a x	68.6 (9.7) a x
	3	69.9 (6.8) a x,y	65.0 (13.1) a x	70.6 (5.5) a x	72.75 (0) a x
Hi Meadows	0	60.0 (8.6) a x,y,z	72.75 (0) a x	68.7 (4.7) a x	72.75 (0) a x
Dadd Bennett	4	54.1 (8.4) b z	48.9 (12.5) b x	70.7 (4.1) a x	72.75 (0) a x
Lower Flowers	7	55.4 (8.3) a y,z	51.4 (8.3) a x	62.1 (13.1) a x	66.5 (15.4) a x
Crosier Mountain	22	72.75 (0) a x	61.0 (20.4) a x	72.75 (0) a x	72.75 (0) a x

site and one pit in a site burned at low severity had strong hydrophobic conditions at all depths (Figure 2c and d), and this is probably due to abundant fungal mycelia from symbiotic mycorrhizae. As most of the observed soil hydrophobicity was at 0, 3 and 6 cm, the data analysis will focus on these depths.

There were no significant differences in CST values between ponderosa and lodgepole pine for any depth or burn severity class in either the Bobcat or the Lower Flowers fires. Because there also were no significant correlations between the CST values and vegetation type, the data from the two vegetation types were pooled.

Soil hydrophobicity by fire and burn severity

The patterns of hydrophobicity in the Bobcat fire immediately after burning (Figure 3a) are similar to the CST values for all fires when stratified by burn severity (Figure 2). For this fire, the soil hydrophobicity immediately after burning generally decreased with decreasing burn severity and increasing depth (Figure 3a). The moderate- and high-severity sites at the soil surface had the lowest CST values (strongest hydrophobicity). The soil surface in the burned areas was significantly more hydrophobic than the soil surface in the unburned areas, but the surface hydrophobicity in the burned sites did not vary significantly among the three burn severity classes (Table III). The CST values at 3 cm were lower in the sites burned at high and moderate severity than unburned and low-severity sites, but the differences were not significant with respect to burn severity class or between burned and unburned sites. Similarly, there was some evidence for stronger hydrophobicity at 6 cm in sites burned at high and moderate severity than in unburned and low-severity sites (Figure 3a), but the differences were not significant (Table III).

A comparison of Figure 3a and b suggests that the soil hydrophobicity in the Bobcat fire was slightly weaker 3 months after burning than immediately after the fire. In particular, the CST values at 6 cm for the sites burned at moderate and high severity showed less evidence of hydrophobicity. The sites burned at low severity also had higher CST values (weaker hydrophobicity) at the soil surface and at a depth of 3 cm

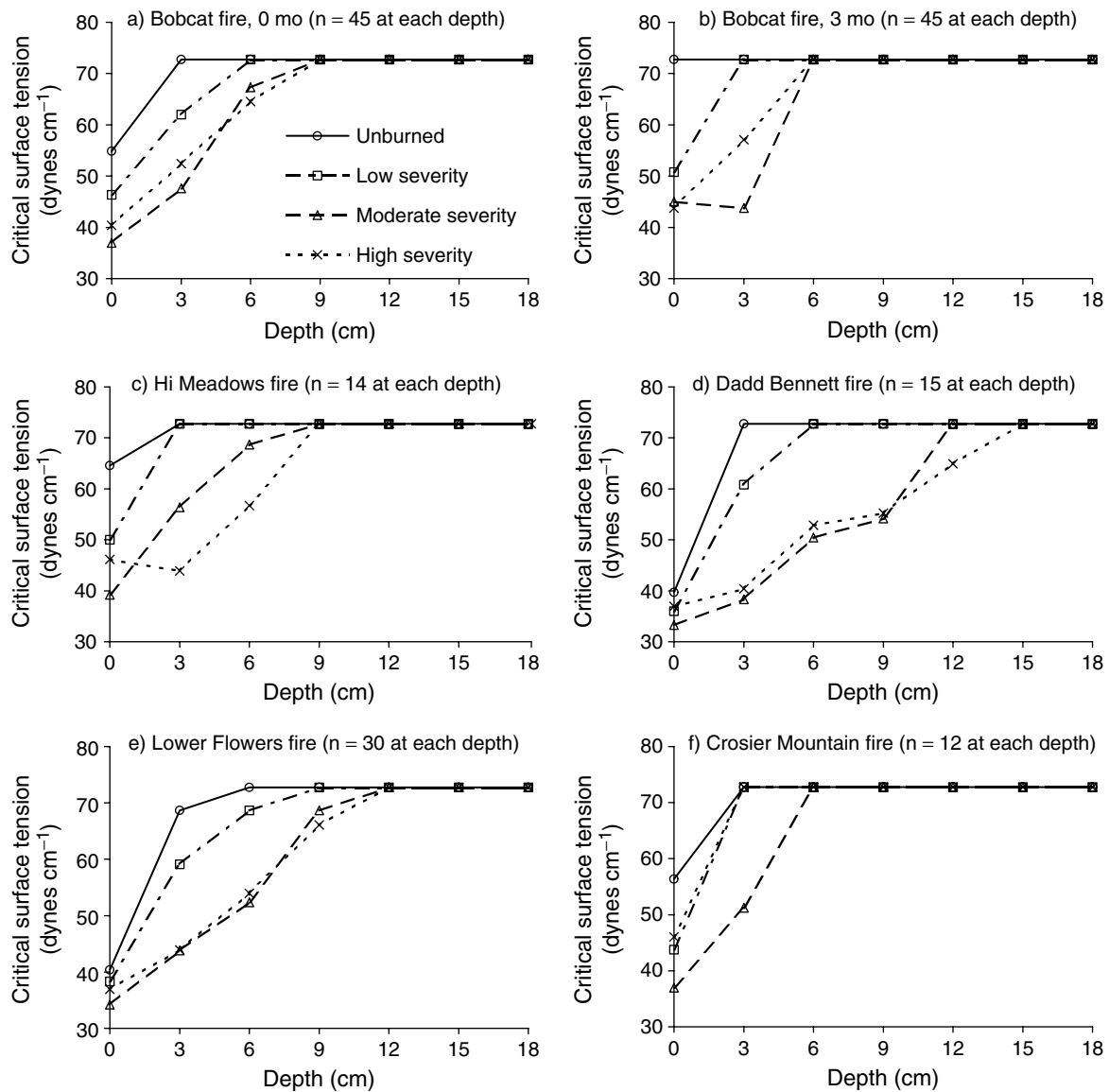


Figure 3. CST for high severity, moderate severity, low severity, and unburned sites in the (a) Bobcat fire shortly after burning, (b) Bobcat fire 3 months after burning, (c) Hi Meadows fire, (d) Dadd Bennett fire, (e) Lower Flowers fire, and (f) Crosier Mountain fire. Each symbol represents the median value at a given depth. The legend in (a) applies to all figures

than 3 months earlier. The unburned sites also had weaker hydrophobicity at the soil surface. However, the multiple comparisons test indicated that there were no significant differences in CST values between the two sampling dates for any depth or burn severity (Table III). The comparisons by depth and burn severity for this sampling time showed that, as in the case of the Bobcat fire immediately after burning, the only significant difference was that the sites burned at high and moderate severity were significantly more hydrophobic at the soil surface than the unburned sites (Table III).

The Hi Meadows wildfire also burned in June 2000, and the overall trends in hydrophobicity were similar to the Bobcat fire (Figure 3c). The strongest hydrophobicity was at 0 and 3 cm in the sites burned at high

and moderate severity, and there was little evidence of hydrophobicity at or below 9 cm. Unburned sites were weakly hydrophobic only at the soil surface. The sites burned at high and moderate severity had significantly stronger hydrophobicity at the soil surface and at 3 cm than the unburned sites (Table III). The soils at 3 cm in the moderate- and high-severity sites were significantly more hydrophobic than the soils at 3 cm in the low severity sites (Table III). Sites burned at low severity had intermediate or low levels of hydrophobicity and were not statistically different from the unburned sites.

The hydrophobicity at 3 cm in severely burned sites appeared to be substantially stronger in the Hi Meadows fire than the Bobcat fire (Figure 3a–c). However, the high variability between sites meant that none of the differences in hydrophobicity between the Bobcat and Hi Meadows fires was statistically significant (Table III).

In the Dadd Bennett prescribed fire the soil was hydrophobic to a greater depth in sites burned at high and moderate severity than in any of the other four fires. There was evidence of soil hydrophobicity from the soil surface to a depth of 12 cm in the sites burned at high severity, and to a depth of 9 cm in the sites burned at moderate severity (Figure 3d). The strength of the observed hydrophobicity was very similar between the high- and moderate-severity sites.

Both the unburned sites and the sites burned at low severity were strongly hydrophobic at the soil surface, and there were no significant differences in the CST values at the soil surface with burn severity (Table III). However, the sites burned at moderate and high severity were significantly more hydrophobic at 3 cm than the sites burned at low severity, and the sites burned at low severity were significantly more hydrophobic at 3 cm than the unburned sites. At 6 cm the sites burned at high and moderate severity were significantly more hydrophobic than the low-severity and unburned sites (Table III).

The soils in the high- and moderate-severity sites in the Dadd Bennett fire were more hydrophobic than the corresponding sites in the Bobcat and Hi Meadows fires, but these differences were generally not significant (Table III). However, comparisons with the Bobcat fire 3 months after burning showed that the moderate-severity sites in the Dadd Bennett prescribed fire were more strongly hydrophobic at the soil surface, and the high-severity sites had significantly stronger hydrophobicity at 6 cm.

The values and overall patterns of soil hydrophobicity in the Lower Flowers prescribed fire were similar to the Dadd Bennett fire, even though soil hydrophobicity was tested 7 months after burning as opposed to 4 months in the case of the Dadd Bennett fire (Table I). The surface soils in the Lower Flowers fire were hydrophobic at all sites, and there were no significant differences between the CST values with burn severity (Table III). At 3 cm the sites burned at high and moderate severity were significantly more hydrophobic than the unburned sites, whereas the sites burned at low severity had intermediate CST values. At 6 cm there were no significant differences in hydrophobicity with burn severity, even though the CST values in high- and moderate-severity sites were lower than in the low-severity and unburned sites (Table III).

The CST values from the Lower Flowers fire suggest slightly weaker hydrophobicity in sites burned at high and moderate severity relative to the Dadd Bennett fire, and stronger hydrophobicity than the Hi Meadows and Bobcat fires. Although most of these differences were not significant at $p < 0.05$, the moderate-severity sites in the Lower Flowers fire had significantly stronger surface hydrophobicity than the corresponding sites in the Bobcat fire 3 months after burning.

Hydrophobicity was measured in the Crosier Mountain prescribed fire 22 months after burning, and the CST values indicate relatively little hydrophobicity except at the soil surface in the burned sites (Figure 3f). The only significant difference was that the hydrophobicity at the soil surface in sites burned at moderate severity was significantly stronger than the unburned sites (Table III). The sites burned at moderate severity also had the strongest hydrophobicity at 3 and 6 cm, but the differences in hydrophobicity with burn severity were not statistically significant at either of these depths.

Comparisons between fires showed that the sites burned at high severity at Crosier Mountain were significantly less hydrophobic at 3 cm than the corresponding sites in the Hi Meadows, Dadd Bennett, and Lower Flowers fires (Table III). Similarly, the hydrophobicity at 6 cm in sites burned at high severity at Crosier Mountain was significantly weaker than in the Dadd Bennett and Lower Flowers prescribed fires.

Table IV. Correlations between each independent variable and measured CST values at depths of 0, 3 and 6 cm. The first number for a given correlation is the correlation coefficient r and the number in parentheses is the p value. Values in bold are significant at $p \leq 0.05$

Variable	CST		
	Depth = 0 cm	Depth = 3 cm	Depth = 6 cm
Fire severity	-0.179 (0.0235)	-0.308 (<0.0001)	-0.161 (0.0418)
Vegetation type	0.087 (0.27)	-0.025 (0.75)	-0.057 (0.47)
Time since burning	-0.130 (0.10)	0.108 (0.17)	-0.008 (0.92)
Surface soil moisture	0.382 (<0.0001)	0.349 (<0.0001)	0.266 (0.0007)
Percent >2 mm	0.116 (0.14)	0.016 (0.84)	-0.074 (0.35)
Percent sand	-0.295 (0.0001)	-0.398 (<0.0001)	-0.418 (<0.0001)
Percent clay	0.175 (0.026)	0.300 (0.0001)	0.244 (0.0018)

Effect of soil texture

Of the 161 soil samples, 152 had more than 50% sand and 145 had less than 10% clay. The soil samples from the Lower Flowers and Dadd Bennett fires had significantly more sand than the soil samples from the Bobcat and Crosier Mountain fires (Table I). The soils in Lower Flowers' also had significantly less clay than the soils from the other fires.

When all the data were pooled, there was a significant increase in soil hydrophobicity at 0, 3 and 6 cm with increasing percent sand ($p < 0.001$). Percent clay was negatively correlated with soil hydrophobicity at the same three depths (Table IV). For each depth the correlation between percent sand and the CST values was stronger than the correlation between percent clay and the CST values. The percent mass >2 mm was not significantly correlated with the CST values (Table IV).

When stratified by burn severity the relationship between percent sand and CST values was significant at $p < 0.05$ at the soil surface for low- and moderate-severity sites, and at 3 cm for unburned, low-severity, and moderate-severity sites. In each case the R^2 decreased with increasing burn severity.

Effect of soil moisture

An increase in soil moisture was generally associated with a decrease in hydrophobicity at 0, 3 and 6 cm (Table IV). The correlations between CST values at these three depths and surface soil moisture were all significant at $p < 0.001$. Surface soil moisture explained more of the variability in CST values at the soil surface than burn severity or any of the soil texture variables. However, the R^2 was low owing to the variability in CST values and the lack of a true linear relationship between surface soil moisture and CST values. Percent soil moisture at 10 cm was not significantly correlated with the CST values at 9, 12, 15, or 18 cm, and this is probably due to the absence of much hydrophobicity at these depths.

Persistence of fire-induced soil hydrophobicity

There were no significant differences in hydrophobicity at the soil surface between the different fires for the sites burned at high severity, but there were significant differences in the CST values among the different fires at 3 and 6 cm (Table III). In high severity sites the soil hydrophobicity was significantly weaker at 3 cm in the 22-month-old Crosier Mountain prescribed fire than the corresponding sites in the Hi Meadows fire immediately after burning, the 4-month-old Dadd Bennett fire, or the 7-month-old Lower Flowers fire (Table III). Similarly, soil hydrophobicity was significantly weaker in high-severity sites at 6 cm in the Bobcat fire 3 months after burning and the 22-month-old Crosier Mountain fire than in the 4-month-old Dadd Bennett fire. Soil hydrophobicity at 6 cm in the sites burned at high severity in the Crosier Mountain fire was significantly weaker than in the 7-month-old Lower Flowers fire (Table III).

In sites burned at moderate severity the surface hydrophobicity was significantly weaker in the Bobcat fire 3 months after burning than in the 4-month-old Dadd Bennett and the 7-month-old Lower Flowers fires. Between-fire comparisons showed no other significant differences in hydrophobicity for sites burned at moderate severity. There were no significant differences in CST values between fires for the sites burned at low severity or the unburned sites.

For the Bobcat fire, the more sensitive pairwise comparisons showed significantly weaker surface hydrophobicity 3 months after burning in high- ($p = 0.02$) and moderate-severity ($p = 0.03$) sites. At a depth of 3 cm there were no significant differences in hydrophobicity between the two sets of measurements. At 6 cm, the hydrophobicity in sites burned at high severity was significantly weaker 3 months after burning than immediately after the fire ($p = 0.02$).

There was no significant correlation between time since burning and CST (Table IV). This is probably due to the low CST values in high- and moderate-severity sites in the 4- and 7-month-old fires relative to the 3- and 22-month-old fires.

Predicting soil hydrophobicity

The significant variables for predicting CST values at 0, 3 and 6 cm were burn severity, percent sand, and percent soil moisture (Table V). These three variables explained 38% of the variability in CST values at the soil surface and 41% of the variability in CST values at 3 cm. At 6 cm the predictive model uses the soil moisture at 10 cm rather than surface soil moisture, and the overall model R^2 drops to 30%.

The general linear models indicate stronger soil hydrophobicity with increasing burn severity and increasing percent sand, and weaker soil hydrophobicity with increasing percent soil moisture. Burn severity was the most significant variable at the soil surface, but this declined in importance with increasing depth (Table V). Percent sand became progressively more important with increasing depth. Percent soil moisture was the least significant variable at all three depths (Table V).

DISCUSSION

Assessing soil hydrophobicity

The strong correlations between CST and WDPT in this study are consistent with previous work (Crockford *et al.*, 1991; Dekker and Ritsema, 1994; Harper and Gilkes, 1994; Scott, 2000). A recent study compared five different methods for measuring hydrophobicity: WDPT, CST, water repellency index, liquid–solid contact angle, and apparent advancing contact angle. All five measures were strongly correlated with one another and only the CST was recommended for future use (Scott, 2000). Crockford *et al.* (1991) concluded that the reproducibility of WDPT was poor, providing further evidence for using CST rather than the more common WDPT. We found that the CST had much lower variability and was faster to measure. For these reasons the CST is recommended for assessing soil hydrophobicity.

Table V. R^2 , F , and p values for the overall model to predict the natural logarithm of CST values, and the statistics for each significant variable. The soil moisture at the surface was used for predicting \ln CST at 0 and 3 cm, whereas the model for \ln CST at 6 cm uses the soil moisture at 10 cm

	Depth = 0 cm			Depth = 3 cm			Depth = 6 cm		
	R^2	F	p	R^2	F	p	R^2	F	p
Overall model	0.38	18.87	<0.0001	0.41	21.46	<0.0001	0.30	13.36	<0.0001
Burn severity		16.71	<0.0001		17.68	<0.0001		9.12	<0.0001
Soil moisture		9.78	0.0021		7.57	0.0066		7.0	0.009
Percent sand		12.91	0.0004		22.81	<0.0001		20.61	<0.0001

Burn severity

The amount of soil heating in prescribed fires is often assumed to be less than in wildfires (Robichaud and Hungerford, 2000). However, in upper Michigan there was no difference in the fire-induced water repellency between wildfires and prescribed fires (Reeder and Jurgensen, 1979).

The data from our study showed stronger soil hydrophobicity in the Dadd Bennett and Lower Flowers prescribed fires than the two recent wildfires (Table III), even though the prescribed fires were tested 4 and 7 months after burning. Stronger hydrophobicity after prescribed fires could be due to higher fuel loads, a slower rate of spread (Pyne *et al.*, 1996), and the tendency for prescribed fires to stay on the ground rather than become crown fires (Pyne *et al.*, 1996). Data on pre-burn fuel loadings are not available for the Bobcat or Hi Meadows wildfires, but the rate of spread was much slower for the Dadd Bennett and Lower Flowers prescribed fires than the Bobcat and Hi Meadows wildfires.

A difference in the natural hydrophobicity prior to burning might also affect the degree of soil hydrophobicity after burning. In this study there were no significant differences in soil hydrophobicity between fires for unburned and low-severity sites (Table III). This suggests that the different fires are comparable, and the between-fire differences in soil hydrophobicity in high- and moderate-severity sites are not due to differences in hydrophobicity prior to burning.

Vegetation

There were no significant differences in the CST values between ponderosa and lodgepole pine sites when stratified by burn severity and depth. This implies that these two species have similar types and amounts of hydrophobic compounds in their litter. Different species in the *Pinaceae* family have been shown to have a similar extractive content in their litter (Shafizadeh *et al.*, 1977). Although the amount of litter will vary with site conditions and forest age, the similarity in extractive compounds suggests a similar heat content and chemical composition, and hence a similar propensity for pre- and post-fire soil hydrophobicity.

Both ponderosa and lodgepole pine have large ranges in North America, suggesting that there may be large differences in site productivity, decomposition rates, and fuel loadings. Since the depth of fire-induced soil hydrophobicity is believed to be a function of soil heating (DeBano, 1981), the amount of fuel will affect the depth and strength of the hydrophobic layer. Lodgepole pine sites in Oregon that burned at high or moderate severity had a strongly hydrophobic layer from 5 to 15 cm below the soil surface, whereas in unburned sites the soils were moderately hydrophobic from the soil surface to a depth of 5 cm (Dyrness, 1976). The greater depth of hydrophobicity in lodgepole pine sites in Oregon may stem from the higher productivity of lodgepole pine forests in Oregon than Colorado. Differences in productivity should be considered when comparing or extrapolating the results of our study to other areas.

Soil texture

Like many previous studies (DeBano *et al.*, 1970; Campbell *et al.*, 1977; DeBano, 1981; Crockford *et al.*, 1991), we found stronger fire-induced and natural soil hydrophobicity in coarser-textured soils. The stronger hydrophobicity in the Dadd Bennett and Lower Flowers fires may be partly due to the significantly higher percent sand in these two fires relative to the Bobcat and Crosier Mountain fires. Pre-burn data on soil moisture and fuel loadings are needed to more clearly identify the effect of soil texture on fire-induced soil hydrophobicity.

Soil moisture

Soil moisture is assigned a linear relationship with the natural logarithm of CST in the general linear models, but a plot of the data by burn severity indicates that there may be a soil moisture threshold rather than a linear relationship (Huffman, 2001). Any change in soil moisture below this threshold will not necessarily alter the strength of soil hydrophobicity (Doerr and Thomas, 2000).

To more accurately determine the effect of soil moisture on soil hydrophobicity more tests should be done when soil moisture levels are in the range 15–30%. This would help determine whether there is a threshold where hydrophobic soils become easily wettable. Alternatively, one could dry soil samples in the laboratory and compare the potential water repellency of dried soils with the actual water repellency as measured in the field under varying soil moisture conditions (Dekker and Ritsema, 1994). Dekker *et al.* (1998) concluded that the most reliable estimate of soil hydrophobicity was from undried samples collected during dry periods.

The effect of soil moisture on soil hydrophobicity means that runoff from spring snowmelt should be less affected by soil hydrophobicity than runoff from summer rainstorms. The slow rate of snowmelt should wet the soil above the soil moisture threshold and allow meltwater to infiltrate readily. High-intensity summer convective storms are more likely to occur when the soil surface is dry and the hydrophobic layer is more likely to limit infiltration. This means that mid- and late-summer precipitation events are of greatest concern for increasing runoff from burned watersheds in Colorado.

Persistence of fire-induced soil hydrophobicity

The time since burning was not a significant predictor of fire-induced soil hydrophobicity, because the differences in hydrophobicity between fires of similar ages were almost as great as the differences between fires of different ages. Hydrophobicity was stronger in the Dadd Bennett and Lower Flowers prescribed fires than in the two younger fires and the much older Crosier Mountain fire.

The short-term nature of this study means that we cannot reliably determine the persistence of fire-induced soil hydrophobicity in the pine forests of the Colorado Front Range. However, the data suggest a weakening of fire-induced soil hydrophobicity in the Bobcat fire after 3 months, and still weaker hydrophobicity in the Crosier Mountain fire 22 months after burning. The high-severity sites in the Crosier Mountain fire had the highest (i.e. least hydrophobic) CST values at 3 and 6 cm, and the CST values in these sites were not significantly different than unburned sites. Limited testing showed no evidence of fire-induced soil hydrophobicity at any depth for the Buffalo Creek fire 4 years after burning, or for the 1994 Hourglass fire 5 years after burning (Huffman, 2001).

In contrast, fire-induced soil hydrophobicity persisted for 6 years in lodgepole pine stands in the upper Cascades of Oregon (Dyrness, 1976), and about 4 years in ponderosa pine stands in Arizona (Campbell *et al.*, 1977). In upper Michigan over 50% of the burned sites that were initially classified as water repellent were no longer water repellent within 1 year after burning (Reeder and Jurgensen, 1979). In conifer forests in Montana the post-fire water repellency also disappeared within 1 year (DeByle, 1973).

This variability means that the persistence of post-fire hydrophobicity cannot be readily extrapolated between regions (Doerr *et al.*, 2000). The persistence of fire-induced soil hydrophobicity should be determined by repeated testing on individual fires in different regions while controlling for variables such as soil moisture, burn severity, and soil texture.

Scale implications

In hydrophobic soils the water flow is generally limited to preferential flow paths or finger flow (Dekker and Ritsema, 1994). Even if large areas within a fire are hydrophobic, infiltration can occur at some locations through finger flow (Imeson *et al.*, 1992), root channels, rodent burrows (Ferreira *et al.*, 2000), or other preferential flow paths. Since infiltration rates in most forest soils are relatively high, a few preferential flow paths or scattered areas with weak hydrophobicity can significantly reduce runoff at the hillslope scale.

Preliminary testing for soil hydrophobicity indicated that fire-induced soil hydrophobicity was stronger under the drip line than in intercanopy areas (Huffman, 2001). Stands with high tree densities will have less intercanopy area and hence a potentially greater continuity of areas with hydrophobic soils, whereas less dense stands should have more areas where runoff can infiltrate.

In addition to stand density, the proportion of area burned at high and moderate severity will also affect post-fire increases in runoff. The Bobcat and Hi Meadows wildfires had a higher proportion of area burned

at high or moderate severity than the three prescribed fires. This means that the proportion of the area that is hydrophobic in a prescribed fire may be lower than for a wildfire, and there would be more non-hydrophobic areas for overland flow to infiltrate (Tiedemann *et al.*, 1979). Runoff and erosion from prescribed fires might, therefore, be much less than for wildfires, even though a prescribed fire could have similar or even stronger fire-induced soil hydrophobicity in sites burned at high or moderate severity.

CONCLUSIONS

CST was less variable than the WDPT when stratified by fire, burn severity and depth. CST was also better correlated with the variables measured in this study than the WDPT. Since CST is also quicker and easier to measure, the CST should be used for assessing soil hydrophobicity in the field.

In sites burned at high and moderate severity the soils were generally hydrophobic from the soil surface to a depth of 6 cm. In low-severity and unburned sites the soils were generally hydrophobic only at the soil surface, and this surface hydrophobicity was generally weaker than in sites burned at high and moderate severity. Soil hydrophobicity was often stronger and deeper in the prescribed fires than the wildfires, but the effect of hydrophobicity on runoff is likely to be less in prescribed fires because they are usually smaller and have less area burned at high and moderate severity. Three of the 161 sites tested in this study had strong natural hydrophobicity to a depth of 18 cm, and this was associated with fungal mycelia.

Burn severity and percent sand are the most significant predictors of fire-induced soil hydrophobicity in ponderosa and lodgepole forests in the central and northern Colorado Front Range. Together with soil moisture, these factors explained approximately 40% of the variability in soil hydrophobicity at the soil surface and a depth of 3 cm. The time since burning was not a significant predictor of soil hydrophobicity, and this is probably due to the variability of fire-induced soil hydrophobicity between fires. There was some evidence that hydrophobic soils become hydrophilic when soil moisture levels exceed 12 to 25%. Fire-induced and natural soil hydrophobicity were not significantly different between lodgepole and ponderosa pine stands.

Repeated measurements suggest that fire-induced soil hydrophobicity weakens within 3 months after burning. Hydrophobicity measurements 22 months after burning showed little evidence of fire-induced soil hydrophobicity at 3 and 6 cm in sites burned at high and moderate severity. However, the soil surface was significantly more hydrophobic in sites burned 22 months earlier at moderate severity than in unburned sites.

ACKNOWLEDGEMENTS

We are grateful to Don Brady and Dwight Atkinson of the US Environmental Protection Agency and Dr Neil Berg of the USDA Forest Service for helping fund this research through Grant No. PSW-99-0008CA, and to Dave Gloss and Carl Chambers of the Arapaho–Roosevelt National Forest for providing support through Agreement No. 00-CS-11021000-038. Dr Philip Chapman graciously provided advice on the statistical analyses. We are also grateful to the three anonymous reviewers and John Munn for their constructive comments.

REFERENCES

- Brown PM, Kaufmann MR, Shepperd WD. 1999. Long-term, landscape patterns of past fire events in a montane ponderosa pine forest of central Colorado. *Landscape Ecology* **14**: 513–532.
- Campbell RE, Baker MB, Folliott PF, Larson FR, Avery CC. 1977. *Wildfire effects on a ponderosa pine ecosystem: an Arizona case study*. USDA Forest Serv. Res. Paper RM-191, Rocky Mountain Forest and Range Exp. Stn., Fort Collins, CO; 12.
- Colorado Water Conservation Board. 1997. *Emergency response, flood hazard mitigation, and flood hazard awareness for residents of Buffalo Creek, Colorado*. Department of Natural Resources, Denver, Colorado; 18.
- Crockford H, Topalidis S, Richardson DP. 1991. Water repellency in a dry sclerophyll eucalypt forest—measurements and processes. *Hydrological Processes* **5**: 405–420.

- DeBano LF. 1981. *Water repellent soils: a state-of-the-art*. Gen. Tech. Rep. PSW-46, illus. Pacific Southwest Forest and Range Exp. Stn., Forest Serv., US Dep. Agric.: Berkeley, CA; 21.
- DeBano LF, Krammes JS. 1966. Water repellent soils and their relation to wildfire temperatures. *Bulletin of the International Association of Scientific Hydrology* **11**(2): 14–19.
- DeBano LF, Osborn JF, Krammes JS, Letey J. 1967. *Soil wettability and wetting agents: our current knowledge of the problem*. USDA For. Serv. Res. Pap. PSW-43; 13.
- DeBano LF, Mann LD, Hamilton DA. 1970. Translocation of hydrophobic substances into soil by burning organic litter. *Soil Science Society of America Proceedings* **34**: 130–133.
- DeByle NV. 1973. Broadcast burning of logging residues and the water repellency of soils. *Northwest Science* **47**: 77–87.
- Dekker LW, Ritsema CJ. 1994. Fingering flow: the creator of sand columns in dune and beach sands. *Earth Surface Processes and Landforms* **19**: 153–164.
- Dekker LW, Ritsema CJ, Oostindie K, Boersma OH. 1998. Effect of drying temperature on the severity of soil water repellency. *Soil Science* **163**(10): 780–796.
- Doerr SH, Thomas AD. 2000. The role of soil moisture in controlling water repellency: new evidence from forest soils in Portugal. *Journal of Hydrology* **231–232**: 134–147.
- Doerr SH, Shakesby RA, Walsh RPD. 1996. Soil hydrophobicity variations with depth and particle size fraction in burned and unburned *Eucalyptus globulus* and *Pinus pinaster* forest terrain in the Aqedada Basin, Portugal. *Catena* **27**: 25–47.
- Doerr SH, Shakesby RA, Walsh RPD. 1998. Spatial variability of soil hydrophobicity in fire-prone eucalyptus and pine forests, Portugal. *Soil Science* **163**: 313–324.
- Doerr SH, Shakesby RA, Walsh RPD. 2000. Soil water repellency: its causes, characteristics and hydro-geomorphological significance. *Earth-Science Reviews* **51**: 33–65.
- Dyrness CT. 1976. *Effect of wildfire on soil wettability in the high Cascades of Oregon*. USDA For. Serv. Res. Pap. PNW-202; 18.
- Ferreira AJD, Coelho COA, Walsh RPD, Shakesby RA, Ceballos A, Doerr SH. 2000. Hydrological implications of soil water-repellency in *Eucalyptus globulus* forests, north-central Portugal. *Journal of Hydrology* **231–232**: 165–177.
- Gabriel KR. 1978. A simple method of multiple comparisons of means. *Journal of the American Statistical Association* **73**(364): 724–729.
- Gardner WH. 1986. Water content. In *Methods of Soil Analysis: Part 1*, Klute A (ed.). American Society of Agronomy: Madison, WI; 493–507.
- Gee GW, Bauder JW. 1986. Particle-size analysis. In *Methods of Soil Analysis: Part 1*, Klute A (ed.). American Society of Agronomy: Madison, WI; 383–411.
- Harper RJ, Gilkes RJ. 1994. Soil attributes related to water-repellency and the utility of soil survey for predicting its occurrence. *Australian Journal of Soil Research* **32**: 1109–1124.
- Helvey JD. 1980. Effects of a north central Washington wildfire on runoff and sediment production. *Water Resources Bulletin* **16**(4): 627–634.
- Huffman EL. 2001. *Fire-induced soil hydrophobicity under ponderosa and lodgepole pine, Colorado Front Range*. MSc Thesis. Department of Earth Resources, Colorado State University, Fort Collins, CO; 186.
- Imeson AC, Verstraten JM, van Mulligan EJ, Sevink J. 1992. The effects of fire and water repellency on infiltration and runoff under Mediterranean type forest. *Catena* **19**: 345–361.
- Letey J. 1969. Measurement of contact angle, water drop penetration time, and critical surface tension. In *Proceedings of a Symposium on Water Repellent Soils*, DeBano LF, Letey J (eds), University of California, Riverside, 6–10 May, 1968; 43–47.
- Meeuwig RO. 1971. *Infiltration and water repellency in granitic soils*. Research Paper INT-111, illus. Intermountain Forest and Range Experiment Station, Forest Serv., US Dep. Agric.: Ogden, UT; 20.
- Ott RL. 1993. *An Introduction to Statistical Methods and Data Analysis*, 4th edn. Wadsworth Publishing Company: Belmont, CA; 1051.
- Pyne SJ, Andrews PL, Laven RD. 1996. *Introduction to Wildland Fire*, 2nd edn. John Wiley and Sons, Inc.: New York. 769.
- Reeder CJ, Jurgensen MF. 1979. Fire-induced water repellency in forest soils of upper Michigan. *Canadian Journal of Forestry Research* **9**: 369–373.
- Robichaud PR, Hungerford RD. 2000. Water repellency by laboratory burning of four northern Rocky Mountain forest soils. *Journal of Hydrology* **231–232**: 207–219.
- Savage SM. 1974. Mechanism of fire-induced water repellency in soil. *Soil Science Society of America Proceedings* **38**: 652–657.
- Savage SM, Martin JP, Letey J. 1969. Contribution of some soil fungi to natural and heat-induced water repellency in sand. *Soil Science Society of America Proceedings* **33**: 405–409.
- Scott DF. 2000. Soil wettability in forested catchments in South Africa; as measured by different methods and as affected by vegetation cover and soil characteristics. *Journal of Hydrology* **231–232**: 87–104.
- Scott DF, van Wyk DB. 1990. The effects of wildfire on soil wettability and hydrological behavior of an afforested catchment. *Journal of Hydrology* **121**: 239–256.
- Shafizadeh F, Chin PPS, DeGroot WF. 1977. Effective heat content of green forest fuels. *Forest Science* **23**(1): 81–89.
- Shakesby RA, Coelho COA, Ferreira AD, Terry JP, Walsh RPD. 1993. Wildfire impacts on soil erosion and hydrology in wet Mediterranean forest, Portugal. *International Journal of Wildland Fire* **3**(2): 95–110.
- Soil Survey Division Staff. 1993. *Soil Survey Manual*. US Department of Agriculture Handbook No. 18; 437.
- Tiedemann AR, Conrad CE, Dietrich JH, Hornbeck JW, Megahan WF, Viereck LA, Wade DD. 1979. *Effects of fire on water: a state-of-knowledge review*. General Technical Report WO-10, Forest Service, US Department of Agriculture; 28.
- USDA Forest Service. 1995. *Burned-Area Emergency Rehabilitation Handbook*. FSH 2509.13-95-6 USDA: Washington, DC; Chapter 20, 8.
- Wallis MG, Horne DJ. 1992. Soil water repellency. In *Advances in Soil Science*, Vol. 20, Stewart BA (ed.). Springer: New York; 91–146.
- Watson CL, Letey J. 1970. Indices for characterizing soil-water repellency based upon contact angle–surface tension relationships. *Soil Science Society of America Proceedings* **34**: 841–844.
- Weast RC (ed.). 1983. *CRC Handbook of Chemistry and Physics*, 1983–1984, 64th edn. CRC Press: Boca Raton, FL; F-33.

Wohlgemuth PM, Conard SG, Wakeman CD, Beyers JL. 1996. Postfire hillslope erosion and recovery in chaparral: variability in responses and effects of postfire rehabilitation treatments. Presented at: *13th Conference on Fire and Forest Meteorology*, 27–31 October, 1996, Lorne, Australia; 19.

Role of surface-water and groundwater interactions on projected summertime streamflow in snow dominated regions: An integrated modeling approach

Justin L. Huntington¹ and Richard G. Niswonger²

Received 25 April 2012; revised 31 August 2012; accepted 1 October 2012; published 17 November 2012.

[1] Previous studies indicate predominantly increasing trends in precipitation across the Western United States, while at the same time, historical streamflow records indicate decreasing summertime streamflow and 25th percentile annual flows. These opposing trends could be viewed as paradoxical, given that several studies suggest that increased annual precipitation will equate to increased annual groundwater recharge, and therefore increased summertime flow. To gain insight on mechanisms behind these potential changes, we rely on a calibrated, integrated surface and groundwater model to simulate climate impacts on surface water/groundwater interactions using 12 general circulation model projections of temperature and precipitation from 2010 to 2100, and evaluate the interplay between snowmelt timing and other hydrologic variables, including streamflow, groundwater recharge, storage, groundwater discharge, and evapotranspiration. Hydrologic simulations show that the timing of peak groundwater discharge to the stream is inversely correlated to snowmelt runoff and groundwater recharge due to the bank storage effect and reversal of hydraulic gradients between the stream and underlying groundwater. That is, groundwater flow to streams peaks following the decrease in stream depth caused by snowmelt recession, and the shift in snowmelt causes a corresponding shift in groundwater discharge to streams. Our results show that groundwater discharge to streams is depleted during the summer due to earlier drainage of shallow aquifers adjacent to streams even if projected annual precipitation and groundwater recharge increases. These projected changes in surface water/groundwater interactions result in more than a 30% decrease in the projected ensemble summertime streamflow. Our findings clarify causality of observed decreasing summertime flow, highlight important aspects of potential climate change impacts on groundwater resources, and underscore the need for integrated hydrologic models in climate change studies.

Citation: Huntington, J. L., and R. G. Niswonger (2012), Role of surface-water and groundwater interactions on projected summertime streamflow in snow dominated regions: An integrated modeling approach, *Water Resour. Res.*, 48, W11524, doi:10.1029/2012WR012319.

1. Introduction

[2] There is growing consensus that increased greenhouse gas (GHG) concentrations in the global atmosphere are causing long-term changes to the Earth's climate [Christensen *et al.*, 2007]. The combination of rising GHG forcings, ongoing natural-climate variability, and uncertainty in climate model projections make future climates more uncertain for water resource managers [Brekke *et al.*, 2008]. Additionally, the fact that hydrologic processes,

such as runoff, recharge, and evapotranspiration (ET), all covary in time and space, and are correlated to each other, makes it difficult to analyze cause and effects for any one hydrologic process without an integrated framework to model all these processes simultaneously. In environments where summertime streamflow and groundwater discharge is critical for water resources and biological demands, an accurate understanding of the causality of historical and future hydrologic change during these periods is especially important.

[3] The mechanisms causing observed historical and projected hydrologic change in high-elevation catchments is poorly understood, especially regarding surface water/groundwater interactions (SW/GW). For example, streamflow records across the Western United States indicate predominantly decreasing summertime flow [Kim and Jain, 2010], and 25th percentile annual flows [Luce and Holden, 2009] where groundwater discharge is a major component of the total streamflow. These opposing trends could be

¹Division of Hydrologic Sciences, Desert Research Institute, Reno, Nevada, USA.

²U.S. Geological Survey, Carson City, Nevada, USA.

Corresponding author: J. L. Huntington, Division of Hydrologic Sciences, Desert Research Institute, 2215 Raggio Pkwy., Reno, NV 89512, USA. (justinh@dri.edu)

viewed as paradoxical, given that several studies suggest that increased annual precipitation will equate to increased annual groundwater recharge, and therefore high summertime flow [Jyrkama and Sykes, 2007; Allen et al., 2010]. Many hydrologic modeling studies support observed decreases in summertime flow, asserting that earlier snowmelt and runoff is the primary cause [Hamlet and Lettenmaier, 1999; Wilby and Dettinger, 2000; Dettinger et al., 2004; Scibek et al., 2007; Mantua et al., 2010; Maurer et al., 2010]. Although these modeling studies provide an explanation of decreasing summertime flow, shifts in snowmelt and runoff timing alone are not complete explanations. Additional clarification on the causality of decreasing summertime flow, and ties to changes in hydrologic timing are needed to assess historical and future trends [Luce and Holden, 2009]. A thorough understanding of the linkage between changes in snowmelt timing and SW/GW interactions will help address an important question in hydroclimate research, that is, how do changes in snowmelt and streamflow timing impact groundwater resources and groundwater-derived surface water resources?

[4] Recent findings show significant shifts in the timing of snowmelt and observed streamflow in several watersheds in the Sierra Nevada [Coats, 2010], and vulnerability of groundwater to changing climate in the region [Singleton and Moran, 2010]. The purpose of this work is to develop a process-based explanation for decreasing summertime flows that have been reported by previous investigators by using an integrated modeling framework to analyze changing SW/GW interactions. We show that decreased summertime flow is likely part of a broader hydrologic change that is occurring due to earlier onset of the snowmelt pulse and the resulting earlier seasonal drainage in these watersheds. Six different climate model projections are used to force the hydrologic model and demonstrate that projections of earlier snowmelt recession results in decreased summertime flow over a wide range in projected precipitation amounts, including both decreasing and increasing long-term precipitation trends. The use of multiple climate projections are important for providing greater evidence for our explanation of why summertime flows are decreasing because the period of record for these watersheds is short, and thus the climate projections provide greater credence to the statistical significance of decadal or longer trends in the historical streamflow data.

[5] To simulate the effects of earlier snowmelt runoff on watershed drainage and SW/GW interactions, we rely on the integrated SW/GW interactions model, GSFLOW. Both observed historical data, as well as climate model projections for the 21st century are used to evaluate the significance and implications of decreased summertime flow in the Sierra Nevada. Projections of future hydrologic conditions complement the historical simulations by allowing for a longer simulation period to discern persistent shifts in hydrologic conditions. Models are constructed for three snow-dominated watersheds of the eastern Sierra Nevada tributary to Lake Tahoe and Truckee Meadows hydrographic areas of California and Nevada (Figure 1). The study area is of special interest with regard to water resources because it is representative of many low-permeability bedrock snow-dominated mountainous regions of the Western United States that provide primary water supplies to nearby developed watersheds. The study area is representative of the greater Sierra Nevada because topography, geology, climate,

and hydrology are similar over much of the upland regions, where precipitation is the greatest. Important characteristics that are shared among the upland (i.e., >2000 m) watersheds of the Sierra Nevada are the large topographic relief and relatively impermeable shallow bedrock that accentuate the dominance of shallow groundwater-flow paths in the regional system. Because the alluvial aquifers are small and have limited storage, the alluvial aquifers are likely to be more sensitive to climate fluctuations than large valley aquifers. There is additional interest in the drainage processes within the Incline and Third Creek watersheds because these watersheds transport sediment and nutrients to Lake Tahoe, which is nationally recognized for its clarity and recreational value.

1.1. Modeling Background

[6] Due to model limitations and computing constraints, simulating climate change effects on groundwater hydrology typically has been done with compartmentalized models, in which SW/GW interactions are decoupled or neglected [Vaccaro, 1992; Middelkoop et al., 2001; Scibek et al., 2007; Jyrkama and Sykes, 2007; Tague and Grant, 2009; Allen et al., 2010]. In these studies, if the unsaturated zone is explicitly considered, it is represented as a soil column through which water flows independently of the underlying water table. These models calculate recharge independently of dynamic groundwater levels and SW/GW interactions. Furthermore, the important interplay between snowmelt-derived streamflow and SW/GW interactions are not simulated in a coupled manner, which we will show is a key process that must be considered to evaluate climate-change impacts on summertime flow in snow-dominated regions. In short, the effects of climate on the interactions between SW/GW and resulting summertime flow are not fully understood due to various compartmental model limitations and assumptions [Scibek et al., 2007].

[7] Recently, with the development of sophisticated computer codes, several studies have applied integrated models to simulate climate change effects on water resources [Maxwell and Kollet, 2008; Ferguson and Maxwell, 2010; Sulis et al., 2011]. These models have provided greater insight into climate change effects on watershed hydrologic processes due to their ability to more realistically simulate feedback between hydrologic processes that occur above and below land surface. Here, we add to these past works by calibrating over a longer period to evaluate the model's ability to simulate low-frequency variations in summertime flow that are associated with groundwater storage, considering climate projections from six climate models and two GHG scenarios, and projecting hydrologic conditions over the next century to assess the combined effects of low-frequency weather cycles and future climate change. Natural climate variability will be an important component of future climate conditions, and a good representation of these historical cycles allows for more realistic projections of water availability and the severity of climate extremes. Researchers have observed both interdecadal and intradecadal periodicities in precipitation and streamflow [Hanson et al., 2006; Perry, 2006], and groundwater levels [Hanson et al., 2006; Laque-Espinar et al., 2007]. These low-frequency signals have been linked to Quasi-Biannual Oscillation (QBO), El Niño Southern Oscillation (ENSO), Pacific Decadal Oscillation (PDO), tidal, and solar cycles [Barco et al., 2010;

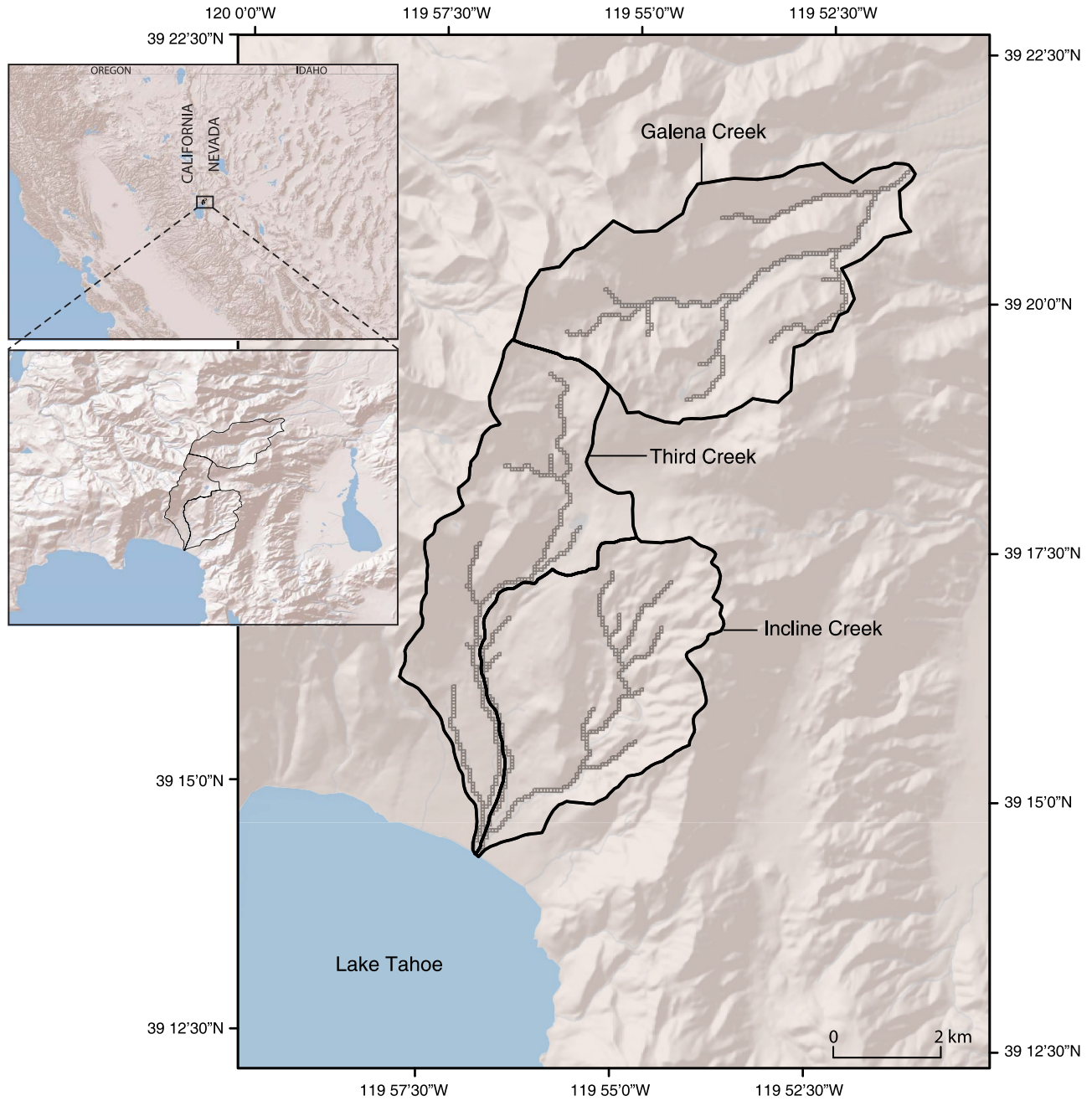


Figure 1. Study area illustrating Incline Creek, Third Creek, and Galena Creek watersheds and model domain (thick black line indicating watershed boundaries).

Burroughs, 2003]. Accurately predicting historical low-frequency responses is central to predicting future low-frequency responses in groundwater storage, discharge to streams and springs, and water-dependent biota. Integrated models that are calibrated to historical interactions of SW/GW over wet and dry periods, and are forced with future climate data over many decades, are better suited to assess how climate change might affect water resources, and in particular, groundwater resources.

1.2. Model Description

[8] GSFLOW was used to simulate all near-surface and groundwater hydrologic processes within three watersheds

of the eastern Sierra Nevada (Figures 1 and 2). GSFLOW simultaneously accounts for climatic conditions, runoff across the land surface, variably saturated subsurface flow and storage, plus connections among terrestrial systems, streams, lakes, wetlands, and groundwater. Runoff and interflow (shallow subsurface flow) cascade to receiving streams or lakes, while including effects of saturation-excess runoff caused by shallow water table conditions. GSFLOW and its precursors have been applied in several basins across the United States to simulate SW/GW interactions [e.g., Hunt et al., 2008; Markstrom et al., 2008; Niswonger et al., 2008; Doherty and Hunt, 2009; Koch et al., 2011].

A.

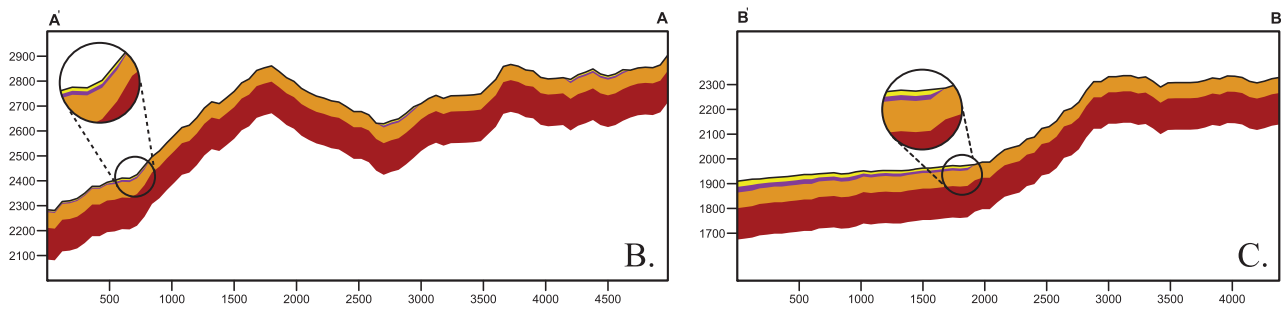
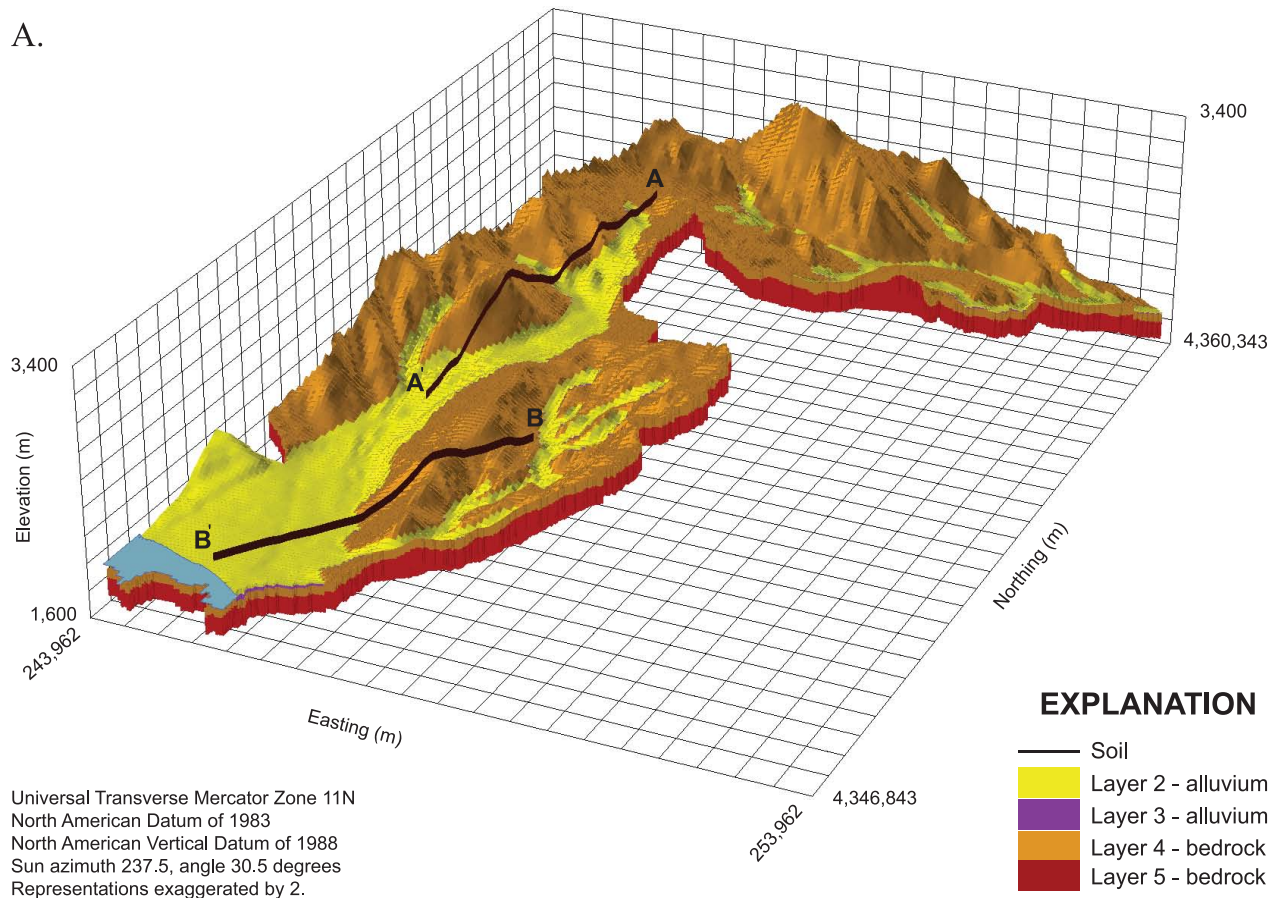


Figure 2. Three dimensional and cross section representation of the hydrogeologic framework model illustrating vertical and horizontal model discretization and hydrogeologic units.

[9] GSFLOW is the integration of the Precipitation Runoff Modeling System (PRMS) and the Modular Groundwater Flow model (MODFLOW). Integration of PRMS and MODFLOW was facilitated by an implicit iterative coupling approach using the Newton linearization method [Niswonger et al., 2011]. Markstrom et al. [2008] and Niswonger et al. [2011] provide a complete description of GSFLOW and its theory, and only a broad description is provided herein. PRMS is a modular deterministic, distributed-parameter, physical-process watershed model used to simulate precipitation, climate, and land use on watershed response [Leavesley et al., 1983]. PRMS simulates snowpack processes using a distributed two-layered system that is maintained and modified on both a water equivalent basis and as a dynamic heat reservoir. PRMS simulates snowmelt- and rain-generated runoff in a fully distributed sense,

where runoff can cascade among four neighboring surface grid cells, infiltrate, or flow to a stream. The soil zone is represented by coupled continuity equations with storages that represent different components of soil porosity (i.e., dead-end versus kinematic and macropore porosity), conceptualized in PRMS as the preferential, gravity, and capillary reservoirs. Water in the soil zone can percolate into the deeper unsaturated zone (MODFLOW), flow horizontally to a receiving grid cell or stream, or evapotranspire to the atmosphere. In areas where the water table is above the base of the soil zone, groundwater can seep into the soil zone. Additionally, groundwater discharge occurs to the surface in areas where groundwater heads are above land surface.

[10] ET is derived from the vegetation canopy and land surface (sublimation from the snowpack and evaporation

off of land surface), within the soil zone, and the deeper unsaturated and saturated zones. Evaporation also can be simulated from surface water, such as from the surfaces of lakes and streams. ET is simulated as a function of the potential (PET), water storage in the vegetation canopy and in the soil zone. Beneath the soil zone, ET is a function of the PET that is not satisfied from the soil zone, root available water content in the deeper unsaturated zone, and water table elevation in the deeper saturated zone. If the water table elevation is above the root depth (i.e., extinction depth) and the PET is not met by the soil and unsaturated zones, then ET is removed directly from groundwater using the formulation developed in the MODFLOW ET Package [McDonald and Harbaugh, 1988]. There are three options in GSFLOW for calculating PET. These formulas are empirical and rely on climate data including, air temperature, solar radiation, and elevation. For this work, the Jensen and Haise [1963] solar radiation-temperature empirical formulation for calculating PET was used. Markstrom *et al.* [2008] provide further details, including the distribution of climate data on the landscape and calculations of energy-budget components.

[11] Flow beneath the base of the soil zone is simulated by MODFLOW, including vertical unsaturated flow, groundwater flow, and with a wide variety of boundary conditions that represent streams, lakes, groundwater development, and many other hydrologic processes. Vertical unsaturated flow is simulated by MODFLOW using the Unsaturated-Zone Flow (UZF1) Package [Niswonger *et al.*, 2006], in which unsaturated flow is simulated using the kinematic-wave equation. The relation between the unsaturated hydraulic conductivity and water content in the unsaturated zone is defined on the basis of the Brooks-Corey function [Brooks and Corey, 1966]. The version of MODFLOW used in this application of GSFLOW is called MODFLOW-NWT, which is a Newton formulation of MODFLOW-2005 that provides capabilities to simulate drying and wetting of groundwater cells [Harbaugh, 2005; Bedekar *et al.*, 2011; Niswonger *et al.*, 2011]. MODFLOW simulates three-dimensional (3-D) confined and unconfined groundwater flow using the conservative form of the continuity equation that is discretized using block-centered finite differences; groundwater head is calculated at the cell center, and flows are calculated at the interface between cells [Harbaugh, 2005]. Following the approach of MODFLOW for solving the 3-D unconfined groundwater-flow equation, the water table is resolved at the subgrid scale that allows a coarse vertical discretization of the subsurface without degradation of the unconfined solution. Similarly, unsaturated flow is simulated using the method of characteristics solution of the kinematic-wave equation that is not dependent on grid-cell thickness [Smith, 1983; Niswonger and Prudic, 2004; Niswonger *et al.*, 2006]. Thus, vertical discretization of GSFLOW models is guided by geologic information rather than constraints associated with numerical stability and accuracy. However, the equations used in GSFLOW are more approximate than full 3-D Richards' equation, which results in some error that must be balanced against errors in parameterization. All surface water in GSFLOW, other than overland runoff, is simulated by MODFLOW packages, including the modified lake (LAK7) and streamflow routing (SFR2) packages [Merritt and Konikow, 2000; Niswonger and Prudic, 2005]. Readers are

referred to Markstrom *et al.* [2008] for details regarding SW/GW interactions, including groundwater interactions with overland flow and lakes.

2. Methods

2.1. Model Setup

[12] Gridded datasets of elevation, geology, vegetation, soils, and land use were used to discretize and parameterize GSFLOW. Model cells were set to a 60×60 m spatial resolution over the 54-km² model domain. Climate was distributed spatially across the model (1,900–3,000 m above Mean Sea Level AMSL) based on the Parameter-elevation Regression on Independent Slopes Model (PRISM) mean monthly precipitation patterns [Daly *et al.*, 1994], and daily temperature and precipitation recorded at the Natural Resource Conservation Service (NRCS) Mt. Rose SNOTEL station located at 2700 m elevation, and the Tahoe City National Oceanic and Atmospheric Administration (NOAA) cooperative-observer weather station, located within 20 km of the model domain at 1900 m elevation (AMSL). Mean annual precipitation within the model domain ranges from 380 to 1650 mm, with 90% of the precipitation occurring between November and March. Monthly average extreme temperatures range from 30°C in August to –10°C in January. Vegetation consists of subalpine and conifer forest, with some deciduous riparian and meadows association.

[13] Mountain block geology is composed of granodiorite and andesite, overlain with glacial moraines and stream deposits in low-elevation areas making up the alluvial aquifers, while soils generally are shallow and derived from parent rock consisting of mostly sand. Plume *et al.* [2009] recently compiled and evaluated geologic, geophysical, and hydrogeologic data for the study area for examining the extent and characteristics of the hydrogeologic units that comprise the aquifers. Spatial hydrogeologic and stratigraphic data reported by Plume *et al.* [2009] were used to develop the conceptual hydrogeologic framework model (HFM) and vertical and horizontal model discretization (Figure 2). Alluvium in these watersheds consists primarily of decomposed granite, glacial outwash, and stream deposits. Accordingly, the alluvial layers increase in thickness around the streams and toward Lake Tahoe [Plume *et al.*, 2009]. Figure 2c illustrates a cross section of the HFM for the Incline Village area, starting at the mountain block and ending near the Lake Tahoe shore line. The thickness of the layers representing the alluvium follows values provided by well logs and geophysical data, and was linearly interpolated on the basis of distance from a stream channel and valley bottom in order to define areas between data locations. Based on hydrogeologic and stratigraphic data reported by Plume *et al.* [2009], Incline, Third, and Galena Creek watersheds were discretized vertically into five layers, and horizontally into approximately 16,500 grid cells per layer, for a total of 83,000 active cells. The model was divided into four basic geologic units, including topsoil, alluvium, weathered bedrock, and less-weathered bedrock. Coarse (three layers) and fine (eight layers) vertical layering models also were developed to test the effects of vertical discretization on hydrologic response, while keeping geologic units the same for all models. The five-layer

model produced similar results as the eight-layer model, and thus, the five-layer model was adopted for this work.

[14] Drainage in these watersheds occurs rapidly due to the great topographic relief and relatively shallow, permeable aquifers that sit on the low-permeable bedrock. The main stem and tributary stream channels drain the shallow soils and alluvial aquifers such that nearly all recharge within the Third and Incline Creek watersheds discharges to streams before entering Lake Tahoe, as indicated by observed shallow groundwater gradients at the base of the watershed. This process also was supported by simulation results that showed that subsurface groundwater flowing to the lake was negligible over a broad range in model parameters. Recharge in Galena Creek watershed partially drains as groundwater beneath the stream valley and alluvial fans that extend east to the valley bottom. Based on the steep topography near the watershed divides, no-flow boundary conditions were assigned along the edges of the model domain that coincide with watershed divides. Head-dependent flux boundary conditions were set where a portion of the model extended into Lake Tahoe, and where the streams crossed the model boundary at the outlets of the model domain. Lake Tahoe water surface elevation was used to represent the head-dependent boundary condition for the portion of the lake in the model. Land surface slopes were used to define groundwater gradients at the boundary conditions beneath where the stream crossed the model boundary. The upper soil and alluvial layers (layers 1–3) were assigned a zero thickness where there were no soils or where bedrock outcropped at land surface.

[15] The stream network was divided into 861 stream reaches, where a stream reach is the length of a stream that is contained within a single model grid cell. Streams were delineated using a geographic information system according to the contributing area method, where a minimum threshold was used to define streams that correlated with field observations and stream delineations from 1:24,000 topographic maps. Streams were delineated in order to define their subgrid geometries; however, defining a stream reach does not require that water flows in the reach. Stream reaches naturally flow and dry depending on whether there is runoff or subsurface flow entering the reach. Generally, all streams are perennial in the study area and serve as drains for shallow aquifers, except in the upper reaches where flow is intermittent. Stream cross-sectional geometries, slopes, and lengths for each reach were estimated from surveys using a differential global positioning system and a 10 m digital elevation model. Runoff that occurs on a grid cell that does not contain a stream reach is assumed to flow as surface flow or interflow according to the overland-flow routing equations in PRMS.

[16] In many surface water model parameterizations, shrub and tree root depths, which affect plant available soil water and ET, generally are assumed to be between 0.4 and 2 m, but limited to the depth of the soil zone [Leavesley *et al.*, 1983; Liang *et al.*, 1994; Flerchinger *et al.*, 1996]. However, it has been documented that roots extend beneath the soil zone and into weathered bedrock and bedrock fractures [Stone and Kalisz, 1991; Canadell *et al.*, 1996; Hubbert *et al.*, 2001]. In the Sierra Nevada, at least 70% of the water used by the forest during the growing season is extracted from weathered bedrock and bedrock fractures

from at least 3.5 m [Witty *et al.*, 2003], as this unsaturated zone stores more than twice as much plant-available water by virtue of its greater thickness as compared to the soil layer [Hubbert *et al.*, 2001]. For these reasons, and given the ability to model ET derived from the deeper weathered bedrock and bedrock unsaturated and saturated zones using the Unsaturated Zone Flow Package (UZFI) in GSFLOW [McDonald and Harbaugh, 1988; Niswonger *et al.*, 2006], and on the basis of calibration, roots were assumed to extend to a maximum of 4 m below land surface.

[17] Calibration of the integrated model followed two different conceptual models (CM1 and CM2) in order to determine the most accurate conceptualization of drainage from these watersheds on the basis of the analytically derived water balance, observed streamflows, and groundwater heads. CM1 proposed that the major watershed drainage mechanism consists of snowmelt recharging shallow alluvial aquifers that drain to streams. Because alluvium is shallow and overlays bedrock, saturation excess runoff is likely to occur in response to the water table rising to land surface, particularly near streams and wetlands. CM1 relies on the unconfined groundwater-flow equation solved by MODFLOW to simulate most of the lateral subsurface flow, whereas the soil zone has very low storage and smaller capability to conduct water to streams. CM2 assumes that most of the lateral subsurface flow occurs through macropores in the soil zone. In this case, the soil zone has significant storage and conductance, and is represented by the kinematic-wave formulation to simulate lateral subsurface stormflow, as calculated by PRMS [Beven, 1981; Markstrom *et al.*, 2008]. Saturation excess runoff is assumed to play a lesser role in CM2 due to the ability of the soil zone to conduct water laterally, resulting in faster drainage of shallow groundwater. During snowmelt periods, macropore flow was observed around eroded boulders and holes within the shallow soils and decomposed granite. Furthermore, overland runoff outside of the channels and wetlands was mostly nonexistent.

2.2. Calibration

[18] For calibration purposes, the model was forced with historical temperature and precipitation observations from Mt. Rose SNOTEL and Tahoe City NOAA weather stations, in which streamflow was simulated during an 18 year historical period (1992–2008). The model was calibrated using a 3 step process. For the first step of the calibration process, PRMS was calibrated independent of MODFLOW for the 18 year period by matching observed streamflows. PRMS was manually calibrated and a separate calibration was performed for each conceptual model (CM1 and CM2). This was done by running PRMS for 1 year as a “spin-up” period to establish initial storages in the soil zone. The calibration procedure consisted of a multiobjective, stepwise procedure where PRMS is calibrated first by adjusting parameters that affect the distribution of solar radiation and potential ET in order to match the average flow of water through the watershed and observed annual water balance. Simulated snow covered area (SCA) was then compared to SCA estimated from satellite remote sensing data derived from the MODIS Terra instrument to verify the simulated timing and spatial distribution snow pack development and melt. Some adjustment of the PRMS

snowpack module parameters was required to better simulate the timing of snowmelt, specifically the parameters that determine the shape of the snowpack areal depletion curve for each grid cell. Following calibration of the snowpack module, parameters that affect the timing and magnitude of runoff and shallow subsurface flow were then adjusted until the model provided a good fit between the simulated and observed daily streamflow. Goodness of fit between the simulated and observed daily streamflow was assessed using the Nash-Sutcliffe statistic [Nash and Sutcliffe, 1970].

[19] For the second step of the calibration process, MODFLOW was run independent of PRMS (MODFLOW-only) using a steady state stress period (i.e., storage terms in the groundwater-flow equations were set to 0). Long-term average recharge rates estimated by the PRMS-only simulations were used for the steady state recharge distribution. The steady state recharge rates were scaled until there was a good correspondence between the simulated steady state flows in streams and the 18 year average of the observed summertime flow in the streams. The steady state groundwater simulation was calibrated by adjusting aquifer hydraulic conductivity values and matching groundwater levels, summertime flow, and the locations of springs in the watersheds. Mapped wetland and spring areas were used to calibrate the steady state groundwater model by comparing the surface elevations of wetland spring areas to the spatial distribution of simulated heads that were within 1 m of the land surface. For the third step of the calibration process, GSFLOW was run in integrated mode, and the aquifer storage parameters were adjusted to match observed variations in observed low flows and to match dominant frequencies in climate signals exhibited in the streamflow data (i.e., 6 month, 1, 2, 3, and 11 year periods). Additionally, further refinement was done by adjusting parameters that affect the timing and rates of runoff and subsurface flows to the stream. The integrated model calibration was assessed on the basis of the goodness of fit between simulated and observed streamflow on the basis of the Nash-Sutcliffe statistic and root-mean-square error of groundwater heads and wetland areas.

2.3. Future Climate Forcing

[20] To assess future hydrologic change and to extend the simulation period, bias-corrected and spatially disaggregated general circulation model (GCM) projections of daily temperature and precipitation were used as direct input to GSFLOW. The projections came from six different GCMs that contributed to the Intergovernmental Panel on Climate Change (IPCC) Fourth Assessment [Christensen *et al.*, 2007], considering the Special Report on Emissions Scenarios A2 and B1 scenarios. We used data from six climate models and for two greenhouse gas (GHG) emission scenarios to consider uncertainty in future hydrologic conditions [Hay and Clark, 2003; Prudhomme *et al.*, 2003; Wilby and Harris, 2006]. Downscaled projections of temperature and precipitation from 2010 to 2100 at 12 km resolution were developed from the bias-corrected spatial disaggregation (BCSD) method [Maurer and Hidalgo, 2008; Cayan *et al.*, 2009] for GCMs of CNRM CM3.0, GFDL CM2.1, MIROC3.2 (med), MPI ECHAM5, NCAR CCSM3, NCAR PCM1, responding to B1 and A2 GHG

scenarios. Specifically, climate model projections were taken from two 12 km grid cells that were coincident with the Mt. Rose SNOTEL and Tahoe City NOAA weather stations. These projections were further interpolated to the Mt. Rose SNOTEL and Tahoe City NOAA weather stations using a quantile-quantile mapping approach [Panofsky and Brier, 1968] to account for biases in temperature and precipitation due to elevation differences between 12 km GCM projections and weather-station elevations. Comparison between the 12 km GCM projected climate and the historical climate observed from the climate station clearly indicated the need for this second level of bias correction. The final resolution of climate data after bias correction and spatial distribution using average spatial relations provided by PRISM was equal to the hydrologic model grid cells (60 m). Hydrologic simulations were run using daily time steps on 12 desktop computers, one for each GCM forcing. The steady state, 18 year historical, and 100 year projections required approximately 10 s, 12 h, and 3 days of computational time, respectively.

3. Results

3.1. Calibration

[21] Results of the steady state groundwater-model calibration indicate that the groundwater model was able to simulate the limited amount of observed heads and the locations and extent of small wetlands and spring areas within the watershed, without defining any structural features or heterogeneities in our hydraulic conductivity fields beyond the original HFM (i.e., additional geologic heterogeneities or faults that act as barriers or conduits for flow), indicating that nearly all springs and wetlands in these watersheds are topographically derived (Figure 3). However, the model did not predict groundwater discharge to land surface for two of the mapped springs. These springs are not topographically controlled like the other springs in these watersheds. For these two springs, CFC-estimated apparent ages are more than 15 years older than other springs and near-stream seepage faces that were sampled, and have apparent ages older than samples from wells screened about 200 m below land surface. CFC apparent ages of the two springs that are not considered to be topographically controlled were 38 and 41 years, whereas the apparent ages of all other springs were less than 15 years. Adjustments to the model input were not made to better simulate these two structurally controlled springs because of uncertainties in their origin and because structurally controlled springs that originate from deep groundwater are considered less important for this study relative to shallow groundwater-discharge areas.

[22] Using spring and wetland locations to constrain the steady state calibration proved very useful. For example, Figure 3 shows a sensitivity analysis that demonstrates the tightly constrained aquifer hydraulic conductivity (K) values. The spatial distribution of heads within 1 m or above land surface was plotted for K distributions that were scaled by factors of 0.1 and 10 of the calibrated K values. For a factor of 0.1 (Figure 3a), it is evident that the model overpredicts heads, as it would only be expected to have heads within 1 m or above land surface around springs, wetlands, and perennial streams. For a factor of 10 (Figure 3b), it is

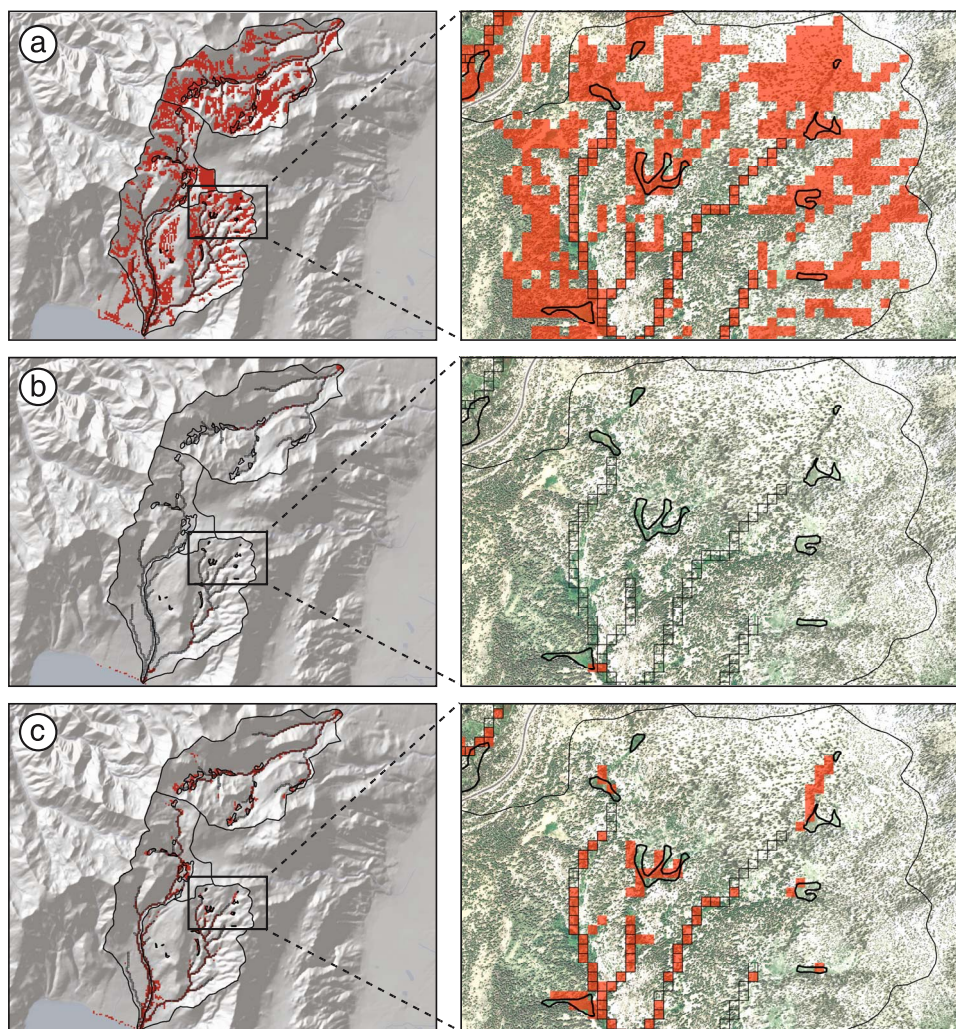


Figure 3. Spatial distribution of groundwater heads within 1 m of land surface shown as red-transparent grid cells where the hydraulic conductivity was varied by (a) a factor of 0.1 lower than calibrated values for all layers, (b) a factor of 10 greater than calibrated values for all layers, and (c) calibrated values for all layers. Black hallow grid cells are specified stream cells, and thick black polygons illustrate mapped springs and wetlands. The optimally calibrated case (Figure 3c) illustrates that the water table intersects the land surface in areas that coincide with mapped streams, springs, and wetlands.

evident that the model underpredicts heads in the upland areas and does not provide shallow groundwater levels around springs, wetlands, and perennial streams. Clearly, the calibrated K distribution provides the most accurate representation of wetland, spring, and perennial stream areas. Figure 4 shows simulated versus observed heads in wells, and land-surface elevations for spring and wetland areas. The 1-to-1 plot (Figure 4a) shows that the model simulates the head distribution accurately over a wide range in head values, with RMSE and normalized RMSE values of 3.2 m and 0.4%, respectively. A small normalized RMSE (i.e., RMSE/total head loss) as shown in this work indicates that model errors are only a small part of the overall model response [Anderson and Woessner, 1992]. The errors in simulated heads (Figure 4b) indicate that there is a slight bias in overpredicting the groundwater heads observed in wells, while underpredicting the heads in spring and wetland areas. Adding further complexity to the model to better match heads was not warranted given the model

scale and uncertainty in these observation data. Most of the wells in the study are located in steep terrain, making direct comparisons between simulated and measured heads in these wells difficult due to the grid scale. Additionally, errors in simulated wetland heads are acceptable given the subgrid variability in land surface from which the wetland observation heads were derived. Water levels in wetland areas are not always at land surface, but near land surface and within the root zone of identified wetland areas. Thus, a bias toward underpredicting the wetland heads is consistent with our conceptualization of groundwater levels in the wetland areas. Additionally, annual average water balance calculations using observed streamflow and precipitation data were used to further constrain simulated ET values. The calibrated steady state water budget corresponded well with the 18 year annual average water budget; precipitation and streamflow were 350,000 and 158,000 $\text{m}^3 \text{d}^{-1}$, and 350,000 and 155,000 $\text{m}^3 \text{d}^{-1}$ for the simulated and observed values, respectively. The ratio of streamflow to precipitation

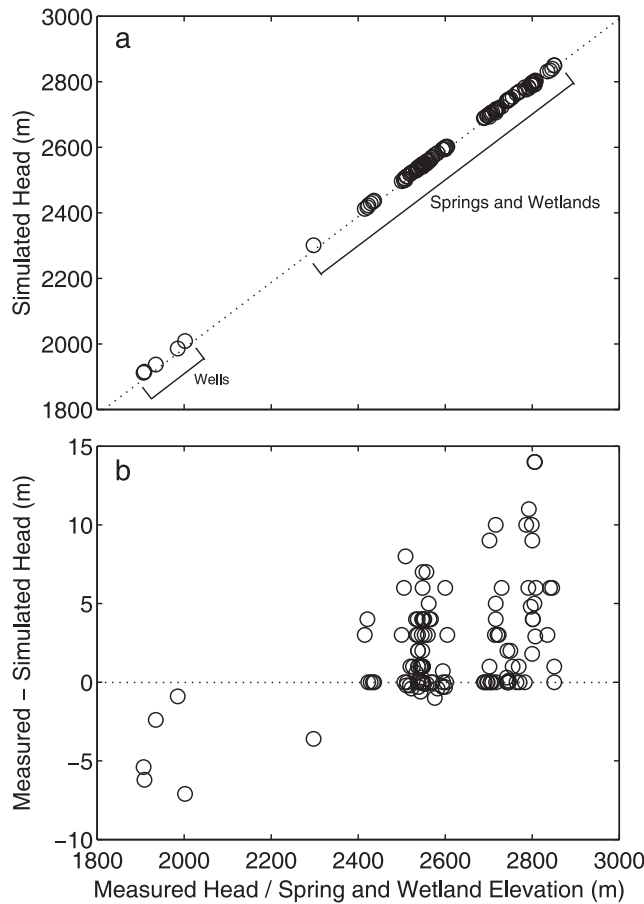


Figure 4. (a) Observed and simulated groundwater head, and (b) residual head error relative to the observed head.

for these watersheds is 45%, indicating that 55% of the precipitation in these watersheds is lost to ET. As previously discussed, groundwater flowing out of these basins through the subsurface is an insignificant component of the water budget. These results compare well with ET derived from recent watershed modeling, chloride mass balance, and Darcian flux estimates of water yield (i.e., runoff + mountain front recharge) in adjacent watersheds with similar geology, vegetation, and precipitation magnitudes [Maurer *et al.*, 1996; Maurer and Berger, 1997; Jeton and Maurer, 2007].

[23] In accordance with the conceptual model developed for these basins, calibration results favored decreases in

K with depth and there is a large contrast in K at the interface between the alluvium and shallow bedrock. Calibrated values for K decrease from 21.5 m d⁻¹ for shallow soils to 1.4 m d⁻¹ for the alluvium, and from 1.4 m d⁻¹ to 0.005 m d⁻¹ at the alluvium/bedrock interface (Table 1). Calibrated anisotropy (K_h/K_v) values for the alluvium are equal to 3.5 and the bedrock was assumed to be isotropic. Calibration results strongly favored CM2, suggesting that most of the lateral subsurface flow occurs through macropores within the soil zone (represented as an equivalent porous media in the model). A good fit to the streamflow hydrograph could not be attained for CM1 because saturation excess runoff occurred over all reasonable ranges in model parameters and this resulted in a hydrograph that had flows that changed much too abruptly relative to the observed streamflows. Thus, parameterizing the soil zone to represent a mixture of macropore and matrix flow provided the best fit to observed streamflows. Table 1 lists calibrated saturated and unsaturated zone hydraulic properties. The calibration of hydraulic properties is robust as determined from many simulations that were run, despite the many input parameters that are required in the integrated model. This was mostly due to the large amount of relief in these watersheds and the distribution of groundwater-discharge areas that constrain aquifer K values (Figure 3c). Additionally, the character of the hydrograph and the gross water balance calculations put tight constraints on parameters that control flow and storage in the soil zone. However, despite observation constraints on model input, there is uncertainty around the estimated parameter values, especially K . The effects of uncertainty in K were assessed with regards to simulated streamflow using sensitivity analysis, as shown in climate projection section.

[24] Results of the calibrated integrated model (i.e., PRMS + MODFLOW) indicate that historical daily streamflows are well simulated, with an average Nash-Sutcliffe value [Nash and Sutcliffe, 1970] of 0.73 (0.77 for log streamflow; 1.0 indicating a perfect fit), as are 6 month, 1–3 year, and 11 year periodicities exhibited in simulated streamflow for the 18 year period of record, where the 11 year cycle is the most notable of the cycles greater than 1 year (Figures 5a and 5b). The 6 month period in observed and modeled streamflow shown in Figure 5b is the result of October–November rain and snowmelt runoff along with later spring runoff that typically occurs about 6 months later, and is evident by close inspection of Figure 5a. The 11 year period in observed summertime flow is a result of

Table 1. Major Hydraulic Properties Used for GSFLOW Model^a

	Soils ^b	Shallow Alluvium ^c	Deep Alluvium ^c	Shallow Weathered Bedrock ^c	Deeper Weathered Bedrock ^c
Horizontal hydraulic conductivity (m d ⁻¹)	21.5	2.8	1.4	0.005	0.001
Vertical hydraulic conductivity (m d ⁻¹)	11.5	0.8	0.4	0.005	0.001
Specific storage (m ⁻¹)	–	1 × 10 ⁻⁶	1 × 10 ⁻⁶	1 × 10 ⁻⁶	1 × 10 ⁻⁶
Specific yield (unitless)	0.18	0.18	0.10	0.005	0.005
Brooks-Corey exponent (unitless)	–	4.0	4.0	4.0	4.0
Saturated water content (unitless)	0.23–0.48	0.35	0.35	0.006	0.006
Air entry pressure (m)	–	–0.15	–0.15	–0.15	–0.15

^aThe specific storage, Brooks-Corey exponent, and air-entry pressure were not required for layer 1.

^bFlow in this layer is calculated using a kinematic wave formulation in PRMS.

^cFlow in this layer is calculated using the groundwater flow equation in MODFLOW.

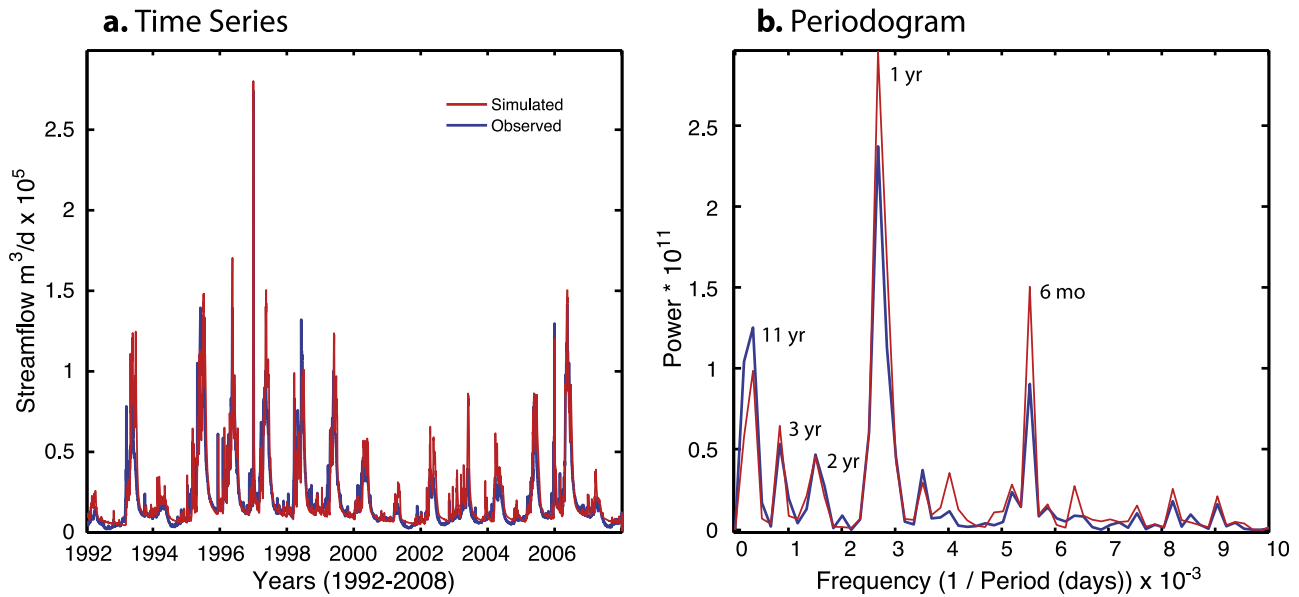


Figure 5. Simulated and observed (a) daily streamflow and (b) periodograms for Incline Creek.

precipitation and groundwater-recharge cycles and associated distributions of residence times of water flowing through the subsurface, effectively resembling the hydraulic memory of the watershed governed by climate, geology, and geomorphology [Smakhtin, 2001]. Periods of wet climate on the order of 2–4 years sustain increases in summertime flow, and seem to contribute to the strong 11 year period in streamflow. It is recognized that the statistical significance of the 11 year cycle in observed and simulated streamflow shown in Figure 5b is low given the limited period of record of only 18 years. However, after analyzing many long-term streamflow records in the region, the 11 year cycle is a common attribute and is statistically significant at the 95% confidence level when tested against red noise [Gilman *et al.*, 1963]. Given that the model produces an 11 year cycle from the input precipitation, suggests that this cycle has significance, even if it is not statistically significant due to the short period of record.

[25] Spatial distributions of groundwater recharge during the winter (Figure 6a), early spring (Figure 6b), and late spring (Figure 6c) indicate that the greatest groundwater-recharge rates occur near stream channels, mountain fronts, and across the alluvial aquifers, where the alluvium is relatively permeable as compared to the upland bedrock areas. Recharge occurs in the upland bedrock areas; however, deep percolation in these areas is restricted by the relatively low vertical hydraulic conductivity of the weathered bedrock. These results are consistent with recent findings from a noble gas and isotopic tracer study of recharge in a nearby high-elevation catchment with similar geology, which suggests that most groundwater recharge to the alluvial aquifer occurs on the lower slopes of the catchment [Singleton and Moran, 2010].

[26] Recharge in the alluvial areas occurs quickly following the onset of snowmelt because of shallow water tables and high rates of deep percolation. Shallow water tables also result in saturated-excess runoff and subsurface

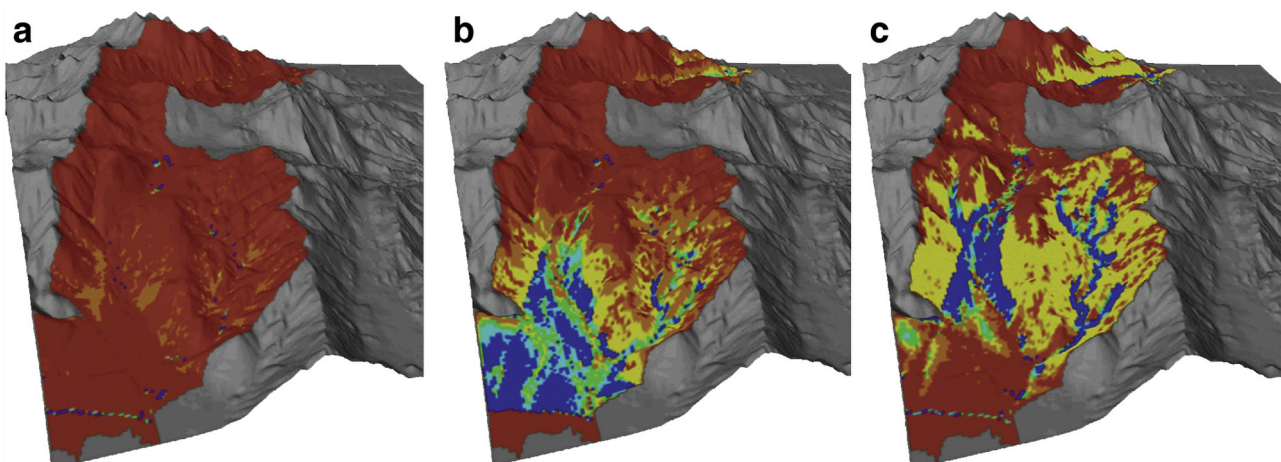


Figure 6. Spatial distributions of groundwater recharge (a) during winter, (b) early spring, and (c) late spring of 2005. Red grid cells indicate negligible recharge, where yellow, green, and blue grid cells indicate low, moderate, and high groundwater recharge, respectively.

stormflow near streams and groundwater discharge areas due to the lack of storage for deep percolation. Accordingly, during peak runoff, the simulated relative proportion of presnowmelt and postsnowmelt event water is dominated by postsnowmelt event water. This result is supported by observed $\delta^{18}\text{O}$ in snowmelt, streamflow, and spring samples taken from Third Creek and springs within the watershed. Figure 7 shows a time series of $\delta^{18}\text{O}$ from Third Creek for a 1 year period. The large proportion of snowmelt derived water in the stream is illustrated by the large change in stream $\delta^{18}\text{O}$ following the onset of the spring snowmelt period and the resulting peak flow in the stream. Following the hydrograph recession, $\delta^{18}\text{O}$ in the stream is representative of groundwater, as represented by spring flow and summertime streamflow $\delta^{18}\text{O}$ values (Figure 7).

3.2. Climate and Hydrologic Projections

[27] Climate-change simulations run with GSFLOW indicate that projected temperatures and precipitation strongly influence all water budget components. Daily average temperatures are projected for the study watershed from 2°C to 4°C for the B1 and A2 GHG scenarios, respectively, during 2010–2100 relative to the base period of 1950–2010. Long-term changes in projected precipitation also are apparent during the next century. For GHG scenario A2, four GCMs predict a steady decrease in annual precipitation, while the other two predict a steady increase in precipitation (Figure 8a1). For GHG scenario B1, five GCMs predict a steady decrease in precipitation, while one predicts a decrease up to about year 2040 and then an increase in precipitation for the remainder of the century (Figure 8b1). The ensemble 30 year annual average precipitation from 2010–2040 to 2070–2100 changes by -5 and -9% for the A2 and B1 climate scenarios, respectively. Discrepancies among

GCMs in their projections of precipitation over the next century suggest a large amount of uncertainty in precipitation for these basins. Variations in long-term precipitation trends presented by Coats [2010] for various watersheds in the Sierra Nevada are consistent with variations in projected precipitation among GCM projections of precipitation. Thus, by using several GCM climate projections, we are able to (1) utilize a long period of record that cannot be developed using historical data alone, and (2) evaluate the mechanisms for decreasing summertime flow that is consistent across many watersheds in the Sierra Nevada that are experiencing disparate trends in precipitation.

[28] Similar to recent PRMS simulations using future climate for many watersheds across the U.S. [Hay et al., 2011; Markstrom et al., 2012], our results indicate that annual snow water content is projected to decrease for all GCMs and GHG scenarios due to increased temperature, snowmelt rates, and precipitation falling as rain (Figures 8a2–8b2). Annual streamflow projections mimic precipitation projections, with a majority indicating decreases (Figures 8a3–8b3). In analyzing projected streamflow, attributes of a 6 month streamflow cycle are common among GCMs; however, a 7 year cycle is most clearly evident among the projected streamflow results. Although less pronounced than in observed data, the streamflow simulated on the basis of the CNRM CM3.0 climate projection exhibited an 11 year signal that most closely corresponds to the observed streamflow in the area. GCMs do show some ability to project realistic weather cycles; however, improving the GCMs ability to better simulate these decadal weather cycles would make their projections and subsequent seasonal and decadal hydrologic responses more realistic.

[29] Annual overland runoff (i.e., infiltration excess and saturation excess overland flow) generally increases or remains steady for A2 and B1 scenarios, respectively (Figures 8a4–8b4). The increase in runoff is caused by more precipitation falling as rain, higher frequency of rain-on-snow events, and increased snowmelt rates, and has been well documented in snow dominated regions [Barnett et al., 2005]. Overland runoff typically is the fastest pathway to a stream, and increased overland runoff could result in larger peak streamflow rates and a greater occurrence of flooding, which has been previously pointed out for the region [Hayhoe et al., 2004].

[30] Annual groundwater recharge, groundwater storage, and groundwater discharge to streams exhibit a decreasing trend in four of the six A2 climate scenarios (Figures 8a5–8b7). Annual streambed losses increase for all simulations with decreased precipitation as a result of decreased groundwater heads beneath streams (Figures 8a7–8b7). Annual groundwater discharge and streambed losses generally are steady for the A2 MPI ECHAM5 and NCAR PCM1 GCMs (Figures 8a7–8a8), despite large increases in annual groundwater storage (Figure 8a6), which reflects the earlier drainage of the watersheds and decreased groundwater heads beneath streams following snowmelt recession. In summary, as annual precipitation, streamflow, and groundwater recharge decrease, so does the annual groundwater storage and discharge to streams, while at the same time, streambed losses to the aquifer increase. These results illustrate the important interplay between surface water and groundwater and underscore the need to run long-term simulations within an integrated modeling framework when making inferences about the effects of

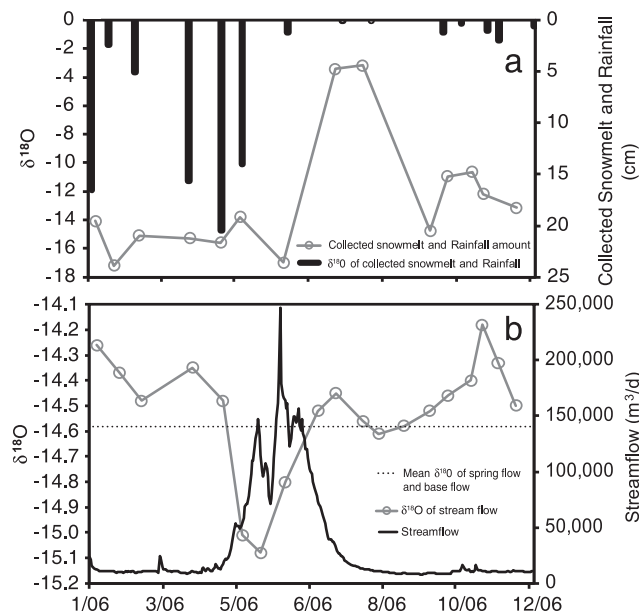


Figure 7. Time series of (a) collected snowmelt and rainfall amount and $\delta^{18}\text{O}$, and (b) streamflow volume and $\delta^{18}\text{O}$ for Third Creek. Mean summertime flow and spring $\delta^{18}\text{O}$ also are shown for reference, which illustrates that the spring hydrograph is mostly composed of snowmelt.

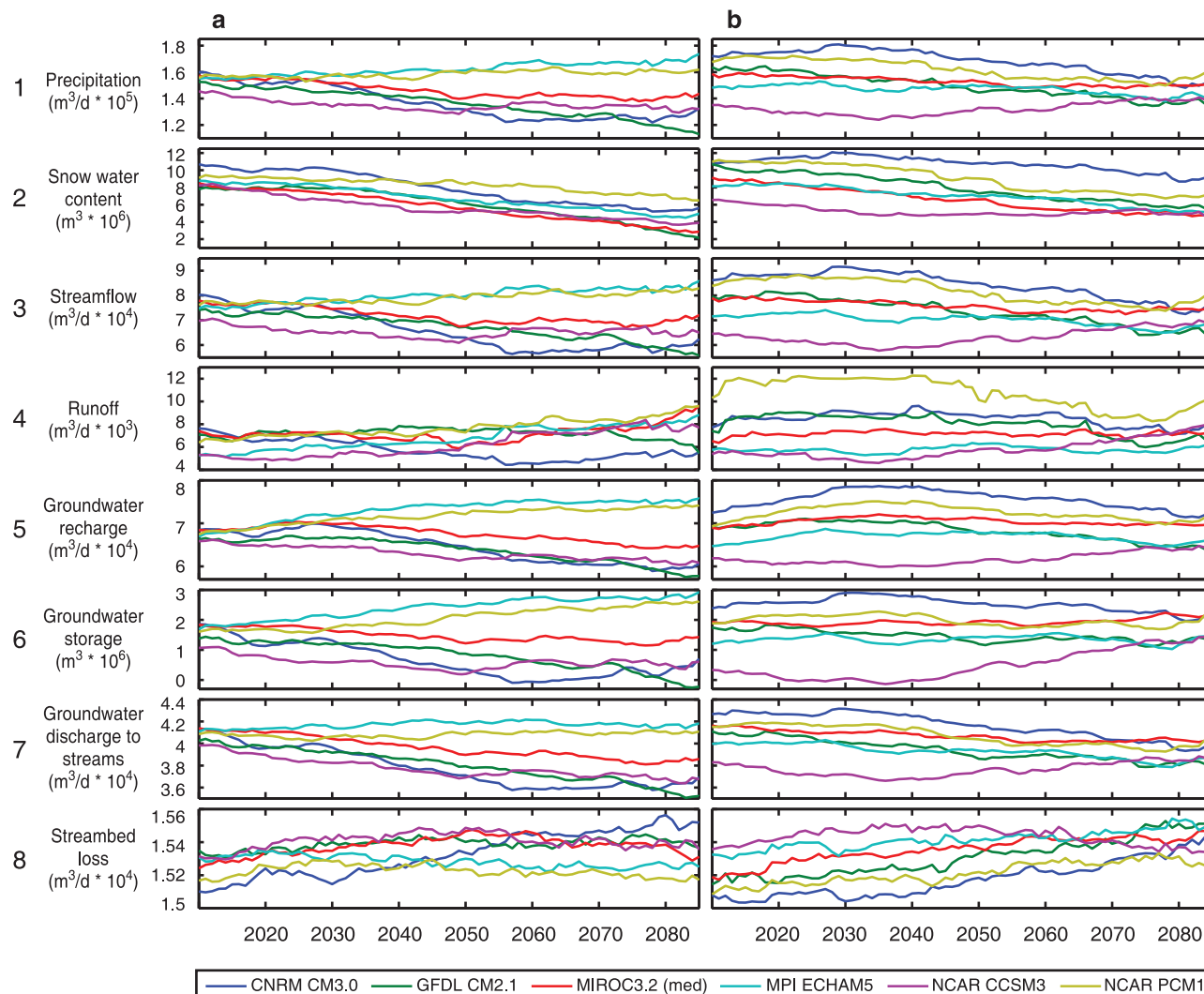


Figure 8. Time series of simulated yearly average hydrologic variables. Simulated hydrologic variables for different GCMs (colored lines) and greenhouse gas emission scenarios (a) A2 and (b) B1. Time series were smoothed using a 30 year moving average. Hydrologic variables included (1) precipitation, (2) snow water content, (3) streamflow, (4) runoff, (5) groundwater recharge, (6) groundwater storage relative to initial conditions, (7) groundwater discharge to streams, and (8) streambed loss.

climate change on surface water and groundwater resources. Long-term simulations are important for these analyses because of the long-term autocorrelation exhibited in hydrologic variables that are related to groundwater storage.

[31] Broadly speaking, results in Figure 8 suggest that changes in annual precipitation drive changes in annual groundwater fluxes; however, seasonal variations in groundwater fluxes are driven by the timing of snowmelt runoff, and more directly by the depth of flow in streams. The effects of increased air temperature on the hydrology of these basins become clear when streamflow components are analyzed on a seasonal basis. To better demonstrate the interplay of seasonal stream gains and losses, Figure 9 illustrates simulations of these variables on a daily basis during a selected 2 year time period (2027–2028) for the CNRM CM3.0 climate model and A2 GHG scenario. The net groundwater discharge to streams is significantly reduced during peak snowmelt runoff due to the bank storage effect [Cooper and Rorabaugh, 1963; Pinder

and Sauer, 1971]. The bank storage effect is important in these watersheds due to rapid runoff and interflow that elevates the stream head more abruptly than the rise in groundwater head near streams. Elevated stream head increases streambed losses to the groundwater and suppresses groundwater discharge to streams, effectively reducing the net groundwater discharge to streams (black line in Figure 9). Earlier snowmelt and streamflow increases the period of time during which groundwater drains to streams, where a longer groundwater-drainage period causes a decrease in July–October streamflow. These results indicate that there is an asymmetric shift toward earlier snowmelt recession that is not completely compensated by earlier onset of snowmelt, thus resulting in a longer period of groundwater drainage to streams during each year.

[32] Figure 10 was developed on the basis of the simulated results, and illustrates our conceptualization of the seasonal drainage of these watersheds. During winter, the snowpack builds, and cold conditions result in negligible

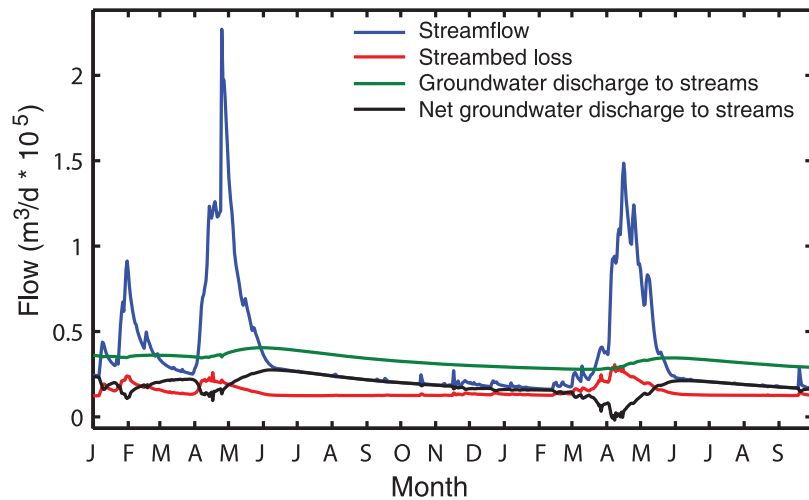


Figure 9. Selected 2 year time series from 2027–2028 of projected streamflow, streamflow loss to groundwater, groundwater discharge to streams, and net groundwater discharge to streams (i.e., groundwater discharge to streams minus streamflow loss to groundwater), illustrating the seasonality of surface and groundwater interactions.

recharge, groundwater storage is at minima from previous summer and autumn drainage, and streamflow (i.e., groundwater discharge) is at a minima (Figure 10a). During the spring snowmelt period, runoff and interflow fill the stream channels and elevate the stream head, suppressing groundwater discharge to the stream that causes the stream to lose water to the streambanks and deeper subsurface (Figure 10b). Higher stream head during the snowmelt period increases horizontal flow parallel to the stream in the down valley direction. Following the peak snowmelt runoff period, the stream head subsides and bank storage and regional groundwater seeps into the stream, resulting in peak groundwater seepage to the stream (Figure 10c). Shallow aquifers surrounding the stream are then drained and groundwater discharge to the stream decreases and reaches a minimum during summer and early autumn that is exacerbated by riparian ET (Figure 10d). The transition from a gaining to a losing stream during high flows (Figure 10b) is caused by bank storage and groundwater suppression and is a well-documented process [Cooper and Rorabaugh, 1963; Pinder and Sauer, 1971]. This process is clearly evident in our simulations of streambed losses and groundwater discharge to streams. Due to similar climatic, geologic, and geomorphologic characteristic among other basins, the drainage process illustrated in Figure 10 likely represent drainage processes in many snow-dominated mountain block watersheds.

[33] When evaluating projected hydrologic change on a seasonal basis, as expected, model results clearly show that increased temperatures projected for these watersheds result in significant timing shifts. Although the GCM ensemble of precipitation (Figures 11a–11b1) shows little change among the 30 year time periods (i.e., 2010–2040, 2040–2070, and 2070–2100), increased temperatures result in an overall decrease in the snowpack, expressed as snow-water equivalent (Figures 11a2–11b2). The earlier snowmelt (Figures 11a3–11b3) cascades through the hydrologic system and impacts the timing of all other important hydrologic processes, including streamflow, groundwater recharge, and groundwater discharge to streams (Figures 11a4–11b6). As

our simulated hydrograph separation and conceptual illustrations suggest (Figures 9 and 10), groundwater discharge to streams is inversely correlated to streamflow (Figures 11a4–11b4 and Figures 11a6–11b6). Additionally, groundwater discharge peaks approximately 1 month later than recharge, further indicating that the timing of peak groundwater discharge to streams follows the timing of streamflow recession rather than the timing of recharge (Figures 11a5–11b6).

[34] Increased air temperatures and earlier snowmelt also greatly affect soil moisture. Increased air temperatures reduce soil moisture in two ways, directly by providing more energy to drive the ET process, and indirectly by causing earlier snowmelt and drainage from the soil zone. The 30 year annual average ensemble soil moisture from 2010–2040 to 2070–2100 is decreased by 13 and 7% as compared to precipitation being decreased by 5 and 9% for the A2 and B1 climate scenarios, respectively. Seasonal variations in soil moisture show that the decrease in soil moisture occurs during April–November. Soil moisture is largely unchanged during winter and early spring, while the soil zone is at its water-holding capacity. Drier conditions during April–November significantly reduce ET from early to late century, and more than compensate for late century increased ET during December–May that is associated with high air temperatures. Accordingly, the 30 year annual average ensemble ET from 2010–2040 to 2070–2100 is reduced by 5 and 4% for the A2 and B1 scenarios, respectively, due to reduced growing-season soil moisture. Saturated zone ET that occurs near springs and wetlands increases over the next century indicating that groundwater levels near springs and wetlands do not change appreciably in these simulations.

[35] With regards to projected changes in ET, the two main competing processes affecting ET are high temperatures, increasing PET, and reduced soil moisture, which decreases ET below the PET. The relative impact of these two processes is further revealed by 30 year running means of precipitation, total ET, and saturated zone ET for each GCM climate projection. Trends in annual basin wide total

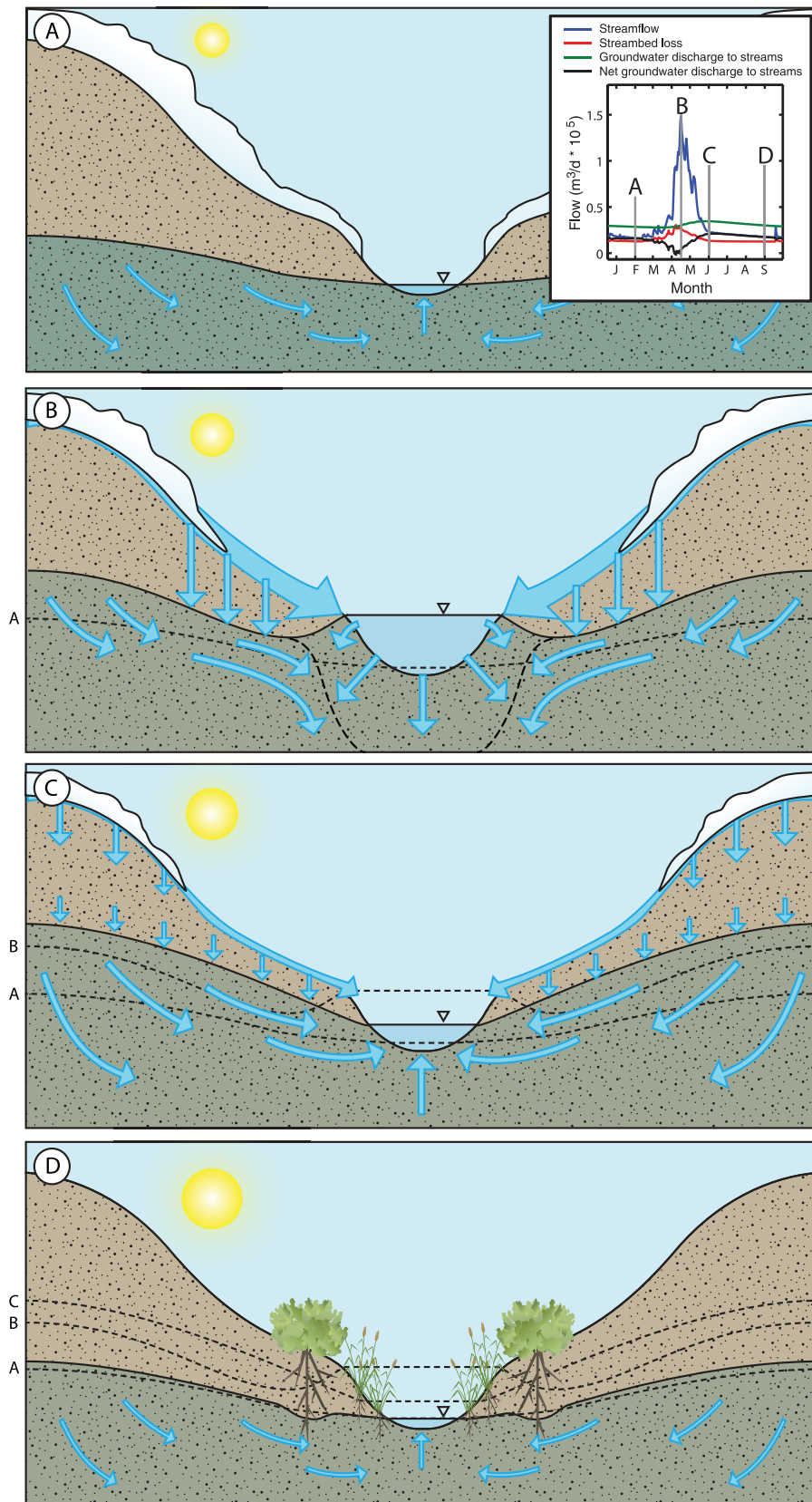


Figure 10. Conceptualization of the seasonal drainage of a snowmelt dominated stream – aquifer system for, (a) early winter with negligible recharge, groundwater storage, and groundwater discharge, (b) spring snowmelt with elevated the stream head, seepage losses to bank storage and shallow aquifers, and suppressed shallow aquifer heads, (c) summer stream recession with peak shallow and regional groundwater discharge to the stream, and (d) late autumn recession of groundwater discharge to the stream.

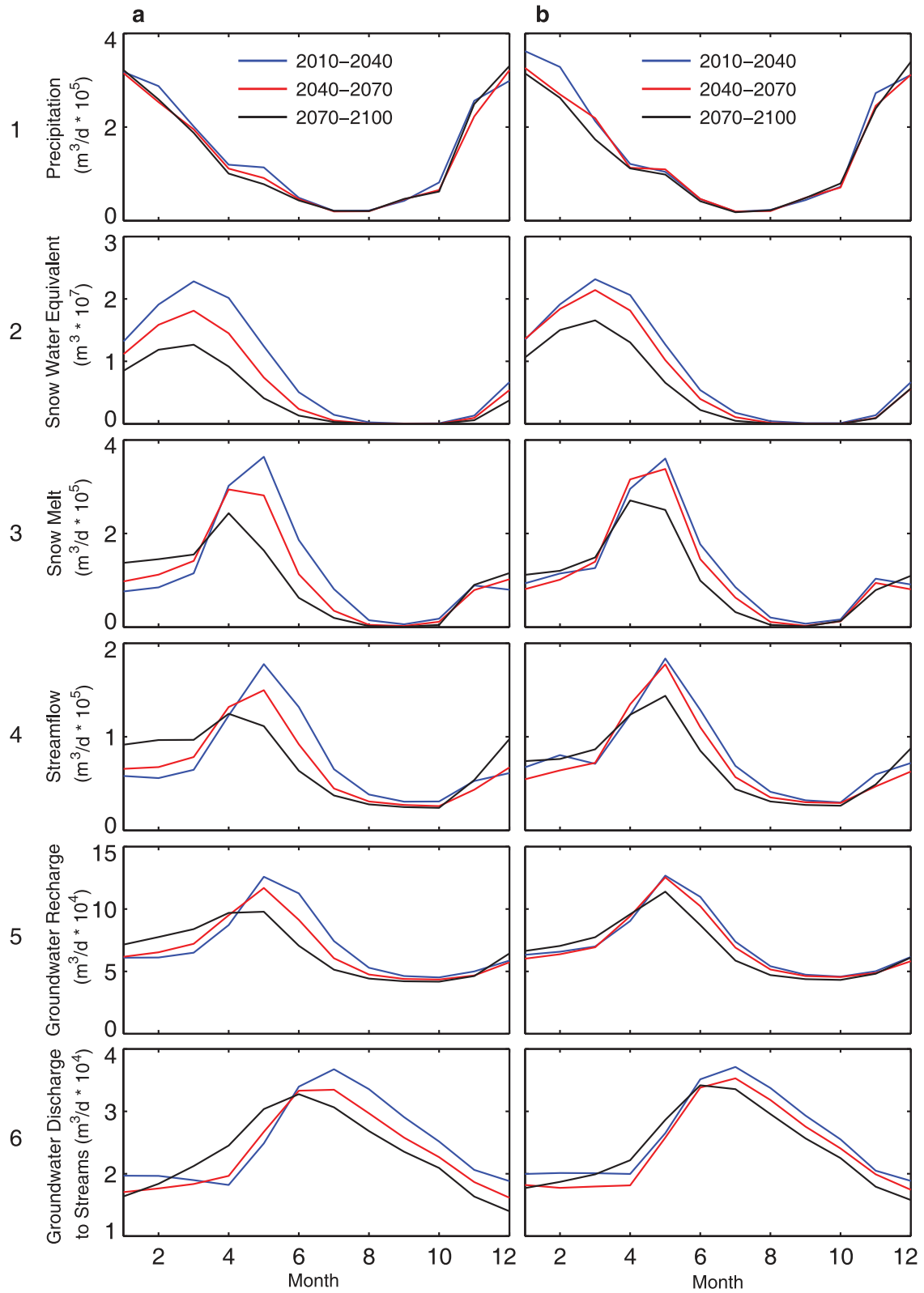


Figure 11. (1) Mean monthly precipitation, (2) snow water equivalent, (3) snow melt, (4) streamflow, (5) groundwater recharge, and (6) groundwater discharge to streams for different time periods and greenhouse gas emission scenarios (a) A2 and (b) B1.

ET correlate well with annual precipitation, which indicates that total ET is limited by water availability. Increases in ET are dampened for GCM models that project increases in precipitation. For example, the NCAR PCM1 A2 scenario projects an increase in precipitation; however, total ET for this projection remains relatively constant over the next century. Similarly, the NCAR CCSM3 A2 scenario projects an increase in precipitation during 2050–2080, whereas ET decreases during this period. These results illustrate the impact of the earlier snowmelt and earlier drainage of soil water, causing drier conditions in the summer that limit and/or decrease annual ET.

[36] Figure 12 illustrates average July–October soil moisture, total ET, net groundwater discharge to streams, and streamflow shown as a 30 year running average. By focusing on the warm season period, the dramatic decreases in soil moisture, total ET, net groundwater discharge, and streamflow are clearly evident. Decreased net groundwater discharge to streams, along with increases in saturated zone ET surrounding riparian areas and stream zones, decrease streamflow during the hottest months of the year, despite projected increases in annual precipitation, groundwater recharge, and groundwater storage by some GCMs (Figure 8).

[37] To test the sensitivity of the model with respect to climate change, a simple sensitivity analysis was conducted, in which hydraulic conductivity (K) was perturbed by $\pm 50\%$ from calibrated values, and the model was run with the GCM NCAR PCM1, A2 climate scenario, in which annual precipitation is projected to increase. This sensitivity analysis was used to analyze the July–October streamflow sensitivity to scaled hydraulic conductivity distributions. Figure 13 illustrates the sensitivity of July–October streamflows to changes in K , where streamflow decrease even for the perturbed K simulations. Thus, the major results of this paper that July–October streamflows are projected to decrease is a robust result, despite uncertainty in K . It should be noted that under prediction of shallow groundwater heads could result in incorrect seepage rates (and directions) under some sections of the streams. However, because the streams act as drains within these shallow aquifers, greater aquifer drainage would occur if simulated groundwater heads were greater. Thus the effect of earlier drainage on summertime flow would still occur as shown here.

4. Discussion

[38] An important discussion point that is highlighted in many hydrologic studies, and is the driver of this work, is the principle cause of historical and projected changes in summertime flow in small mountainous watersheds of the Sierra Nevada. Several studies point out that increased conceptual understanding, derived from better observations and increased model structure, is needed to better understand observed and projected decreases in summertime flow and groundwater dominated flows [Scibek and Allen, 2006; Luce and Holden, 2009; Kim and Jain, 2010; Maurer et al., 2010]. As indicated by these studies, primary deficiencies in observations are limited headwater precipitation and groundwater-monitoring networks. The primary model structural deficiency in snow-dominated basins is the simulation of transient SW/GW interactions, starting

with snowpack development and melt, groundwater recharge and storage, and linking these states and fluxes with in stream SW/GW interactions, as done in the simulations presented herein. While considering all of these coupled processes, our results indicate that summertime streamflows decrease in the model over all reasonable ranges in precipitation and recharge values, indicating that decreased summertime flow is independent of precipitation and recharge, and is a result of temperature changes and the resulting shift in the snowmelt recession. Furthermore, summertime streamflows decrease in simulations with perturbed hydraulic conductivity distributions indicating that these results are robust given uncertainties in hydraulic conductivity. Future work should focus on making frequent and spatially distributed head measurements in streams and adjacent shallow aquifers to provide verification of the strong relationship between the timing of snowmelt recession and peak groundwater discharge to streams that is illustrated by simulations presented herein.

[39] Our results demonstrate the important inverse relation between streamflow and groundwater discharge to streams that is caused by the effects of elevated stream depths during snowmelt runoff that suppresses groundwater discharge to streams, often referred to as the bank storage effect. Furthermore, the timing of peak groundwater discharge is not correlated to the timing of recharge, indicating that snowmelt recession is the dominant mechanisms controlling summertime flow as compared to the timing of groundwater recharge. This distinction is important because if summertime flow were correlated to the timing recharge then the effects of earlier snowmelt recession would be compensated by earlier snowmelt onset and earlier recharge. Earlier snowmelt recession decreases stream depths, which allows the shallow aquifers to drain to streams earlier in the season, thereby decreasing the amount of groundwater discharge to streams during the summer months (Figures 14a3–14b3). This explanation is in contrast with previous explanations that attributed earlier drainage of aquifers to earlier aquifer recharge, and that summertime flows are expected to increase with increased groundwater recharge [Jyrkama and Sykes, 2007; Allen et al., 2010]. Our results suggest the opposite, where simulated groundwater discharge to streams and summertime flow decrease for all GCM climate projections, even those with increased annual precipitation and groundwater recharge. These results are consistent with observations of decreasing summertime flow and dry year annual flows [Luce and Holden, 2009; Kim and Jain, 2010] coincident with increasing trends of annual and winter time precipitation [Groisman and Easterling, 1994; Karl and Knight, 1998; Mote et al., 2005; Coats, 2010].

[40] The mechanisms for reduced summertime flow are indeed linked to increasing atmospheric temperatures and the resulting changes in the timing of snowmelt, as previously suggested [Eckhardt and Ulbrich, 2003; Scibek and Allen, 2006; Maurer et al., 2010]; however, we highlight strong evidence for a direct mechanism, the shift in the timing of groundwater discharge, which is dependent on the stream stage and timing of streamflow recession (i.e., the timing of hydraulic gradient reversals between the stream and underlying groundwater). Due to numerous similarities in physical characteristics of other watersheds to those studied in this research (i.e., climate, geology, topography,

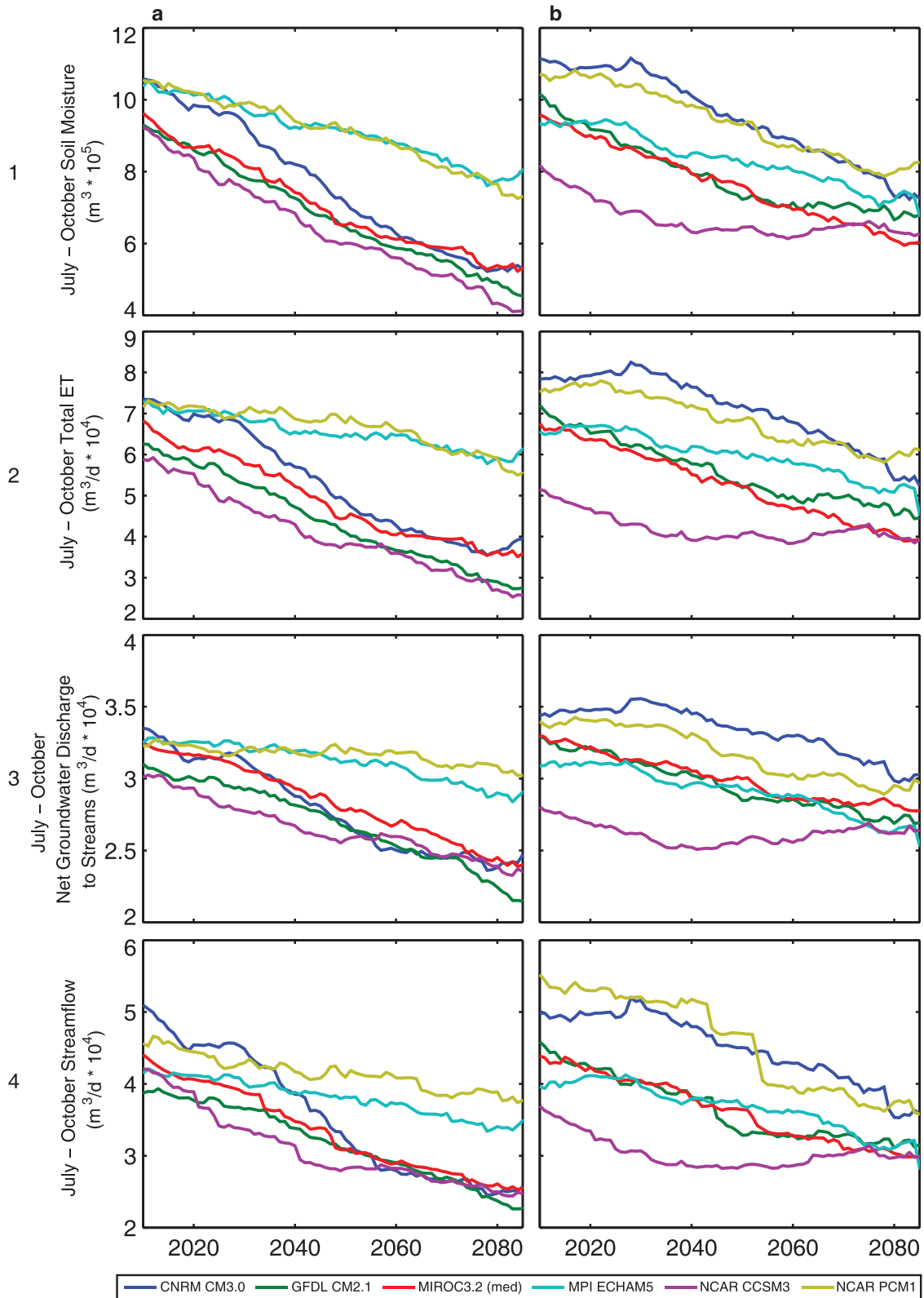


Figure 12. Time series of 30 year moving average July–October (late summer and early autumn) (1) soil moisture, (2) total ET, (3) net groundwater discharge, and (4) streamflow for different GCMs (colored lines) and greenhouse gas emission scenarios (a) A2 and (b) B1. Note the July–October net groundwater discharge and streamflow decreases even if annual precipitation and groundwater recharge increases for GCMs NCAR PCM1 and MPI ECHAM5 (Figures 8).

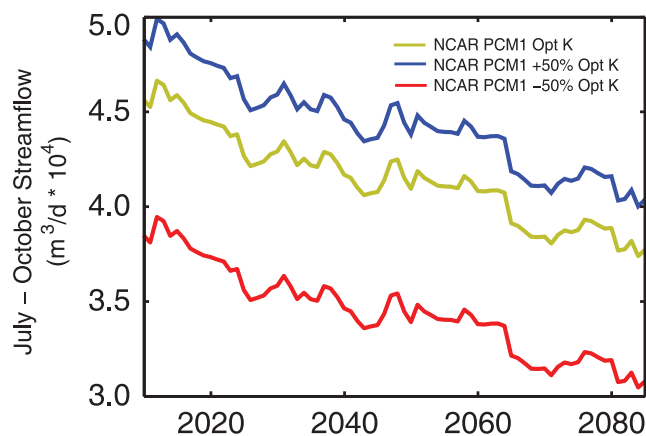


Figure 13. Time series of 30 year moving average July–October streamflow for GCM NCAR PCM1, A2 climate scenario, for different values of K, illustrating the sensitivity of summertime flows to changes in K.

vegetation), we propose that the results from this study would most likely extend to other mountainous, snow-dominated basins. This generalization is confirmed by our results being congruent with observations, that is, summertime flow that decreases even during periods when annual precipitation and groundwater recharge increases.

[41] The model informs us of a plausible process-based explanation of what may be occurring in these watersheds in response to earlier snowmelt. More field measurements are required to verify our explanation of decreased summertime flow, including distributed measurements of streamflow and streambed hydraulic gradients observed during a snowmelt cycle. However, it is difficult to compare field-scale measurements to watershed-scale response that is exhibited by the model. The model indicates that SW/GW interactions are highly variable in time and space and that a large proportion of seepage through the streambed consists of water that is recycled in and out of the stream. Complex topography causes streams to gain and lose over short reaches and large variations in streamflow causes time variable hydraulic gradients. Capturing this variability with field measurements remains a challenge, especially with regards to upscaling field measurements to infer broader scale SW/GW interactions. The model, however, could be used to guide field measurements to better understand the transient and spatial nature of SW/GW interactions and how these interactions affect or control watershed drainage.

5. Summary and Conclusions

[42] Results suggest that high temperatures have an indirect and compounding effect on groundwater storage, discharge, and streambed losses, due to interactions between surface water and groundwater. Hydraulic gradients between the stream and underlying groundwater become neutral or reversed from earlier snowmelt, streamflow, and groundwater discharge to streams. Accordingly, groundwater is depleted during the summer and there is less water to flow to streams, resulting in low summertime flow. Simulations show that the timing of peak groundwater discharge to the stream is inversely correlated to snowmelt runoff and

groundwater recharge due to the bank storage effect and reversal of hydraulic gradients between the stream and underlying groundwater. That is, groundwater flow to streams peak following the decrease in stream depth caused by snowmelt recession. These changes in SW/GW interactions result in more than a 30% decrease in summertime flow when averaged across all GCM projections. Based on these results, similar snow-dominated watersheds may become more arid during the hottest part of the year, and dry season water stresses will likely become more severe even if annual precipitation increases.

[43] Groundwater will be pivotal for future water supplies, yet our current understanding of climate change impacts on groundwater is extremely limited. These findings clarify causality of decreasing summertime flow and dry year annual flows, and highlight important aspects of potential climate change impacts on groundwater resources, while explicitly considering interactions between groundwater and surface water in an integrated modeling framework.

[44] **Acknowledgments.** Support for the first author was provided by the NV State Engineer's Office and the Bureau of Reclamation NV Water Resources Evaluation Program, funded by a grant under Public Law 109-103, section 2.8(a), Cooperative Agreement 06FC204044. Support for the second author was provided by the U.S. Geological Survey's (USGS) Groundwater Resources Program through the Office of Groundwater. The authors would like to thank Mary Tiree, Scripps Institution of Oceanography, and Mike Dettinger, USGS, for their help in obtaining GCM data, and Dave Prudic, USGS emeritus, for his help with conceptual model development, Steve Regan, Steve Markstrom, and Paul Barlow, USGS, for their help with model development, and Toby Welborn for help with figure illustration. The authors also would like to thank Greg Pohl, John Mejia, and Darko Koracin, Desert Research Institute, for their ideas and input, Lisa Wable and Anna Knust, Desert Research Institute for their illustration and editing efforts, and Jim Thomas and Simon Poulson from the Desert Research Institute and University of NV Reno for financial assistance and isotopic analysis.

References

- Allen, D. M., A. J. Cannon, M. W. Toews, and J. Scibek (2010), Variability in simulated recharge using different GCMs, *Water Resour. Res.*, *46*, W00F03, doi:10.1029/2009WR008932.
- Anderson, M. P., and W. W. Woessner (1992), *Applied Groundwater Modeling: Simulation of Flow and Advective Transport*, 2nd edition, Academic, San Diego, Calif.
- Barco, J., T. S. Hogue, M. Giroto, D. R. Kendall, and M. Putti (2010), Climate signal propagation in southern California aquifers, *Water Resour. Res.*, *46*, W00F05, doi:10.1029/2009WR008376.
- Barnett, T. P., J. C. Adam, and D. P. Lettenmaier (2005), Potential impacts of a warming climate on water availability in snow-dominated regions, *Nature*, *438*, 303–309.
- Bedekar, V., R. G. Niswonger, K. Kipp, S. Panday, M. Tonkin (2011), Approaches to the simulation of unconfined flow and perched groundwater flow in MODFLOW, *Ground Water*, *50*, 1745–6584.
- Beven, K. (1981), Kinematic subsurface stormflow, *Water Resour. Res.*, *17*(5), 1419–1424, doi:10.1029/WR017i005p01419.
- Brekke, L. D., M. D. Dettinger, E. P. Maurer, and M. Anderson (2008), Significance of model credibility in estimating climate projection distributions for regional hydroclimatological risk assessments, *Clim. Change*, *89*, 371–394.
- Brooks, R. H., and A. T. Corey (1966), Properties of porous media affecting fluid flow, *J. Irrig. Drain.*, *101*, 85–92.
- Burroughs, W. J. (2003), *Weather Cycles, Real or Imaginary?*, 2nd edition, Cambridge Univ., Cambridge, U. K.
- Canadell, J., R. B. Jackson, J. R. Ehleringer, H. A. Mooney, O. E. Sala, and E.-D. Schulze (1996), Maximum rooting depths of vegetation types at the global scale, *Oecologia*, *108*, 583–595.
- Cayan, D., M. Tyree, M. Dettinger, H. Hidalgo, T. Das, E. Maurer, P. Bromirski, N. Graham, and R. Flick (2009), Climate change scenarios and sea level rise estimates for the California 2009 Climate Change

- Scenarios Assessment, in *Publ. CEC-500-2009-014-F*, 64 p. Calif. Clim. Change Cent., Scripps Inst. Oceanogr., La Jolla, Calif.
- Christensen, J. H., et al. (2007), Regional climate projections, in *Climate Change 2007: The Physical Science Basis. Contribution of Working Group I to the Fourth Assessment Report of the Intergovernmental Panel on Climate Change*, edited by S. Solomon et al., Cambridge Univ., New York.
- Coats, R. (2010), Climate change in the Tahoe basin: Regional trends, impacts and drivers, *Clim. Change*, 102, 435–466.
- Cooper, H. H., and M. I. Rorabaugh (1963) Ground-water movements and bank storage due to flood stages in surface streams, *U.S. Geol. Surv. Water Suppl. Pap.*, 1536-J, 30 p.
- Daly, C., R. P. Neilson, and D. L. Phillips (1994), A statistical-topographic model for mapping climatological precipitation over mountainous terrain, *J. Appl. Meteorol.*, 33, 140–158.
- Dettinger, M. D., D. R. Cayan, M. K. Meyer, and A. E. Jeton (2004), Simulated hydrologic responses to climate variations and change in the Merced, Carson, and American River Basins, Sierra Nevada, California, 1900–2009, *Clim. Change*, 62, 283–317.
- Doherty, J., and R. J. Hunt (2009), Two statistics for evaluating parameter identifiability and error reduction, *J. Hydrol.*, 366, 119–127.
- Eckhardt, K., and U. Ulbrich (2003), Potential impacts of climate change on groundwater recharge and streamflow in a central European low mountain range, *J. Hydrol.*, 284(1–4), 244–252.
- Ferguson, I. M., and R. M. Maxwell (2010), Role of groundwater in watershed response and land surface feedbacks under climate change, *Water Resour. Res.*, 46, W00F02, doi:10.1029/2009WR008616.
- Flerchinger, G. N., C. L., Hanson, and J. R. Wight (1996), Modeling evapotranspiration and surface energy budgets across a watershed, *Water Resour. Res.* 32, 2539–2548.
- Gilman, D. L., F. J. Fuglister, and J. M. Mitchell Jr. (1963), On the power spectrum of red noise, *J. Atmos. Sci.*, 20(2), 182–184.
- Groisman, P. Y., and D. R. Easterling (1994), Variability and trends of total precipitation and snowfall over the United States and Canada, *J. Clim.*, 7, 184–205.
- Hamlet, A. F. and D. P. Lettenmaier (1999), Effects of climate change on hydrology and water resources in the Columbia River Basin, *J. Am. Water Resour. Assoc.*, 35(6), 1597–1623.
- Hanson, R. T., M. D. Dettinger, and M. W. Newhouse (2006), Relations between climatic variability and hydrologic time series from four alluvial basins across the southwestern United States, *Hydrogeol. J.*, 14, 1122–1146.
- Harbaugh, A. W. (2005), *MODFLOW-2005, the U.S. Geological Survey modular ground-water model—The ground-water flow process*, Tech. Methods, Book 6, Chap. A16, U.S. Geol. Surv., Reston, Va.
- Hay, L. E., and M. P. Clark (2003), Use of statistically and dynamically downscaled atmospheric model output for hydrologic simulations in three mountainous basins in the western United States, *J. Hydrol.*, 282, 56–75.
- Hay, L. E., S. L. Markstrom, and C. Ward-Garrison (2011), Watershed-scale response to climate change through the twenty-first century for selected basins across the United States, *Earth Interact.*, 15(17), 1–37.
- Hayhoe, K., et al. (2004), Emissions pathways, climate change, and impacts on California, *Proc. Natl. Acad. Sci.*, 101, 12,422–12,427.
- Hubbert, K. R., R. C. Graham, and M. A. Anderson (2001), Soil and weathered bedrock: Components of a Jeffrey pine plantation substrate, *Soil Sci. Soc. Am. J.*, 65, 1255–1262.
- Hunt, R. J., D. E. Prudic, J. F. Walker, and M. P. Anderson (2008), Importance of unsaturated zone flow for simulating recharge in a humid climate, *Ground Water*, 46(4), 551–560.
- Jensen, M. E., and H. R. Haise (1963), Estimation evapotranspiration from solar radiation, *J. Irrig. Drain. Div.*, 89, 15–41.
- Jeton, A. E., and D. K. Maurer (2007), Precipitation and runoff simulations of the Carson Range and Pine Nut Mountains, and updated estimates of ground-water inflow and the ground-water budget for basin-fill aquifers of Carson Valley, Douglas County, Nevada, and Alpine County, California, *U.S. Geol. Surv. Sci. Invest. Rep. 2007-5205*, 56 p.
- Jyrkama, M. I., and J. F. Sykes (2007), The impact of climate change on spatially varying groundwater recharge in the Grand River watershed (Ontario), *J. Hydrol.*, 338, 237–250.
- Karl, T. R., and R. W. Knight (1998), Secular trends of precipitation amount, frequency, and intensity in the United States, *Bull. Am. Meteorol. Soc.*, 79(2), 231–241.
- Kim, J. S., and S. Jain (2010), High-resolution streamflow trend analysis applicable to annual decision calendars: A western United States case study, *Clim. Change*, 102, 699–707.
- Koch, J. C., D. M. McKnight, and R. M. Neupauer (2011), Simulating unsteady flow, anabranching, and hyporheic dynamics in a glacial melt-water stream using a coupled surface water routing and groundwater flow model, *Water Resour. Res.*, 47, W05530, doi:10.1029/2010WR009508.
- Laque-Espinar, J. A., M. Chica-Olmo, and E. Pardo-Iguzquiza (2007), Climatological cycles in groundwater levels in a detritic aquifer, in *Climate Change and Groundwater*, edited by W. Dragoni, and B. S. Sukhija, *Geol. Soc., London, Special Pub.*, 288, 79–98.
- Leavesley, G. H., R. W. Lichty, B. M. Troutman, and L. G. Saindon (1983), Precipitation-runoff modeling system: User's manual, *U.S. Geol. Surv. Water Resour. Invest. Rep.*, 83-4238, 207 p.
- Liang, X., D. Lettenmaier, E. F. Wood, and S. J. Burges (1994), A simple hydrologically based model of land surface water and energy fluxes for general circulation models, *J. Geophys. Res.*, 99(14), 415–428.
- Luce, C. H., and Z. A. Holden (2009), Declining annual streamflow distributions in the Pacific Northwest United States, 1948–2006, *Geophys. Res. Lett.*, 36, L16401, doi:10.1029/2009GL039407.
- Mantua, N., I. Tohver, and A. Hamlet (2010), Climate change impacts on streamflow extremes and summertime stream temperature and their possible consequences for freshwater salmon habitat in Washington State, *Clim. Change*, 102, 187–223.
- Markstrom, S. L., R. G. Niswonger, R. S. Regan, D. E. Prudic, and P. M. Barlow (2008), GSFLOW-Coupled Ground-water and Surface-water FLOW model based on the integration of the Precipitation-Runoff Modeling System (PRMS) and the Modular Ground-Water Flow Model (MODFLOW-2005), *U.S. Geol. Surv. Tech. Methods*, 6-D1, 240 p.
- Markstrom, S. L., et al. (2012), Integrated watershed-scale response to climate change for selected basins across the United States: *U.S. Geol. Surv. Sci. Invest. Rep.*, 2011-5077, 143 p.
- Maurer, D. K., and D. L. Berger (1997), Subsurface flow and water yield from watersheds tributary to Eagle Valley Hydrographic area, west-central Nevada, *U.S. Geol. Surv. Water Resour. Invest. Rep.*, 97-4191, 56 p.
- Maurer, D. K., D. L. Berger, and D. E. Prudic (1996), Subsurface flow to Eagle Valley from Vicee, Ash, and Kings Canyons, Carson City, Nevada, estimated from Darcy's law and the chloride-balance method, *U.S. Geol. Surv. Water Resour. Invest. Rep.*, 96-4088, 74 p.
- Maurer, E. P., and H. G. Hidalgo (2008), Utility of daily vs. monthly large-scale climate data: An intercomparison of two statistical downscaling methods, *Hydrol. Earth Syst. Sci.*, 12, 551–563.
- Maurer, E. P., L. D. Brekke, and T. Pruitt (2010), Contrasting lumped and distributed hydrology models for estimating climate change impacts on California Watersheds, *J. Am. Water Resour. Assoc.*, 46(5), 1024–1035.
- Maxwell, R. M., and S. J. Kollet (2008), Interdependence of groundwater dynamics and land energy feedbacks under climate change, *Nat. Geosci.*, 1, 665–669.
- McDonald, M. G., and W. W. Harbaugh (1988), A modular three-dimensional finite-difference ground-water flow model, Book 6, Chapter A1, *U.S. Geol. Surv. Tech. Water Resour. Invest.*, 586 p.
- Merritt, M. L., and L. F. Konikow (2000), Documentation of a computer program to simulate lake-aquifer interaction using the MODFLOW groundwater flow model and the MOC3D solute-transport model, *U.S. Geol. Surv. Water Resour. Invest. Rep. 00-4167*, 146 pp.
- Middelkoop, H., K. Daamen, D. Gellens, W. Grabs, J. C. J. Kwadijk, H. Lang, B. W. A. H. Parmet, B. Schadler, J. Schulla, and K. Wilke (2001), Impact of climate change on hydrological regimes and water resources management in the Rhine Basin, *Clim. Change*, 49, 105–128.
- Mote, W. P., A. F. Hamlet, M. P. Clark, and D. P. Lettenmaier (2005), Declining mountain snowpack in western North America, *Bull. Am. Meteorol. Soc.*, 86, 39–49.
- Nash, J. E., and J. V. Sutcliffe (1970), River flow forecasting through conceptual models part 1-A discussion of principles, *J. Hydrol.*, 10(3), 282–290.
- Niswonger, R. G., and D. E. Prudic (2004), Modeling variably saturated flow using kinematic waves in MODFLOW, in *Groundwater Recharge in a Desert Environment—The Southwestern United States*, *Water Sci. Appl.*, vol. 9, edited by J. F. Hogan, F. M. Phillips, and B. R. Scanlon, pp. 101–112, AGU, Washington, D. C.
- Niswonger, R. G., and D. E. Prudic (2005), Documentation of the streamflow-routing (SFR2) package to include unsaturated flow beneath streams—A modification to SFR1, *U.S. Geol. Surv. Tech. Methods*, 6-A13, 51 p.
- Niswonger, R. G., D. E. Prudic, and R. S. Regan (2006), Documentation of the Unsaturated-Zone Flow (UZFI) Package for modeling unsaturated flow between the land surface and the water table with MODFLOW-2005, *U.S. Geol. Surv. Tech. Methods*, Book 6, Chap. A19, 62 pp.

- Niswonger, R. G., D. E. Prudic, G. E. Fogg, D. A. Stonestrom, and E. M. Buckland (2008), Method for estimating seepage loss and streambed hydraulic conductivity in intermittent and ephemeral streams, *Water Resour. Res.*, *44*, W05418, doi:10.1029/2007WR006626.
- Niswonger, R. G., S. Panday, and I. Motomu (2011), MODFLOW-NWT, A Newton formulation for MODFLOW-2005, *U.S. Geol. Surv. Tech. Methods*, *6-A37*, 44 p.
- Panofsky, H. A., and G. W. Brier (1968), *Some Applications of Statistics to Meteorology*, Pennsylvania State University, University Park, 224 pp.
- Perry, C. A. (2006), Midwestern streamflow, precipitation, and atmospheric vorticity influenced by Pacific sea-surface temperatures and total solar-irradiance variations, *Int. J. Clim.*, *26*(2), 207–218.
- Pinder, G. F., and S. P. Sauer (1971), Numerical simulation of flood wave modification due to bank storage effects, *Water Resour. Res.*, *7*(1), 63–70.
- Plume, R. W., M. L. Tumbusch, and T. L. Welborn (2009), Hydrogeology of the Lake Tahoe Basin, California and Nevada, *U.S. Geol. Surv. Sci. Invest. Map*, *3063*, 1 sheet.
- Prudhomme, C., D. Jakob, and C. Svensson (2003), Uncertainty and climate change impact on the flood regime of small UK catchments, *J. Hydrol.*, *277*(1–2), 1–23.
- Scibek, J., and D. M. Allen (2006), Modeled impacts of predicted climate change on recharge and groundwater levels, *Water Resour. Res.*, *42*, W11405, doi:10.1029/2005WR004742.
- Scibek, J., D. M. Allen, A. J. Cannon, and P. H. Whitfield (2007), Groundwater-surface water interaction under scenarios of climate change using a high-resolution transient groundwater model, *J. Hydrol.*, *333*, 165–181.
- Singleton, M. J., and J. E. Moran (2010), Dissolved noble gas and isotopic tracers reveal vulnerability of groundwater in a small, high elevation catchment to predicted climate change, *Water Resour. Res.*, *46*, W00F06, doi:10.1029/2009WR008718.
- Smakhtin, V. U. (2001), Low flow hydrology: A review, *J. Hydrol.*, *240*, 147–186.
- Smith, R. E. (1983), Approximate sediment water movement by kinematic characteristics, *Soil Sci. Soc. Am., J.*, *47*, 3–8.
- Stone, E. L., and P. J. Kalisz (1991), On the maximum extent of tree roots, *For. Ecol. Manage.*, *46*(1–2), 59–102.
- Sulis, M., C. Paniconi, C. Rivard, R. Harvey, and D. Chaumont (2011), Assessment of climate change impacts at the catchment scale with a detailed hydrological model of surface-subsurface interactions and comparison with a land surface model, *Water Resour. Res.*, *47*, W01513, doi:10.1029/2010WR009167.
- Tague, C., and G. E. Grant (2009), Groundwater dynamics mediate low-flow response to global warming in snow dominated alpine regions, *Water Resour. Res.*, *45*, W07421, doi:10.1029/2008WR007179.
- Vaccaro, J. J. (1992), Sensitivity of groundwater recharge estimates to climate variability and change, Columbia Plateau, Washington, *J. Geophys. Res.*, *97*(D3), 2821–2833.
- Wilby, R. L., and M. D. Dettinger (2000), Streamflow changes in the Sierra Nevada, California, simulated using statistically downscaled general circulation model output, in *Linking Climate Change to Land Surface Change*, *Adv. Global Change Res.*, vol. 6, edited by S. McLaren and D. Kniveton, pp. 99–121, Kluwer Acad., New York.
- Wilby, R. L., and I. Harris (2006), A framework for assessing uncertainties in climate change impacts: Low-flow scenarios for the River Thames, UK, *Water Resour. Res.*, *42*, W02419, doi:10.1029/2005WR004065.
- Witty, J. H., R. C. Graham, K. R. Hubbert, J. A. Doolittle, and J. A. Wald (2003), Contributions of water supply from the weathered bedrock zone to forest soil quality, *Geoderma*, *114*, 389–400.

Nonparametric Tests Against Trend

Author(s): Henry B. Mann

Source: *Econometrica*, Jul., 1945, Vol. 13, No. 3 (Jul., 1945), pp. 245-259

Published by: The Econometric Society

Stable URL: <https://www.jstor.org/stable/1907187>

REFERENCES

Linked references are available on JSTOR for this article:

https://www.jstor.org/stable/1907187?seq=1&cid=pdf-reference#references_tab_contents

You may need to log in to JSTOR to access the linked references.

JSTOR is a not-for-profit service that helps scholars, researchers, and students discover, use, and build upon a wide range of content in a trusted digital archive. We use information technology and tools to increase productivity and facilitate new forms of scholarship. For more information about JSTOR, please contact support@jstor.org.

Your use of the JSTOR archive indicates your acceptance of the Terms & Conditions of Use, available at <https://about.jstor.org/terms>



The Econometric Society is collaborating with JSTOR to digitize, preserve and extend access to *Econometrica*

JSTOR

NONPARAMETRIC TESTS AGAINST TREND¹

By HENRY B. MANN

1. INTRODUCTION

The function of a statistical test is usually to decide between two or more courses of action. A test consists in dividing the n -dimensional space into several regions W_1, \dots, W_m (m may also be infinite). A sample of n measurements (X_1, \dots, X_n) is then taken and if (X_1, \dots, X_n) lies in W_i a certain action A_i ($i=1, \dots, m$) is taken. The action A_i is the appropriate action if a certain hypothesis H_i is true. In case of two regions we shall say that we test the hypothesis H_1 against the hypothesis H_2 .

It is the purpose of the present paper to discuss tests of randomness against trend. In terms of distribution functions the hypothesis H_1 of randomness states that the sample (X_1, \dots, X_n) is a random sample of n independent variables each with the same continuous distribution function. The hypothesis of a downward trend may be defined in the following way: The sample is still a random sample but X_i has the continuous cumulative distribution function f_i and $f_i(X) < f_{i+k}(X)$ for every i , every X , and every $k > 0$. An upward trend is similarly defined with $f_i(X) > f_{i+k}(X)$.

In testing the hypothesis H_1 of randomness against some class H_2 of alternatives it is customary to fix $P[(X_1, \dots, X_n) \subset W_1 | H_1]$ where $P(E|H)$ denotes the probability of the event E if H is the true situation. The reason for fixing $P[(X_1, \dots, X_n) \subset W_1 | H_1]$ is that in this way we can fix the cost of testing, as long as H_1 is the true situation. In quality control, for instance, this means that we fix the cost of controlling a production process that is under statistical control. $1 - P[(X_1, \dots, X_n) \subset W_1 | H_1]$ is called the size of the critical region.

In proposing a test we usually define for every n a region W_{1n} in the n -dimensional space such that $P[(X_1, \dots, X_n) \subset W_{1n} | H_1]$ is a fixed constant. Such a test is called consistent with respect to the hypothesis H_2 if, for every alternative B of H_2 , $\lim_{n \rightarrow \infty} P[(X_1, \dots, X_n) \subset W_{1n} | B] = 0$.

A test of the hypothesis H_1 against the hypothesis H_2 is called unbiased if for any alternative B of H_2 we have $P[(X_1, \dots, X_n) \subset W_{1n} | B] \leq P[(X_1, \dots, X_n) \subset W_{1n} | H_1]$. Unbiasedness is for all practical purposes a more important requirement than consistency. Suppose, for instance, that a test is biased and an alternative B is true for which $P[(X_1, \dots, X_n) \subset W_{1n} | B] > P[(X_1, \dots, X_n) \subset W_{1n} | H_1]$, then the action A_2 is less likely to be taken under the situation B than under

¹ Research under a grant of the Research Foundation of Ohio State University.

TABLE 1*
PROBABILITY OF OBTAINING A PERMUTATION WITH $T \leq \bar{T}$ IN PERMUTATIONS OF n VARIABLES.

$\bar{T} \backslash n$	0	1	2	3	4	5	6	7	8	9	10	11	12	13	14	15	16	17	18	19	20	21	
3	167	500	833																				
4	042	167	375	625	833	958																	
5	008	042	117	242	408	592	758	883	958	992													
6	001	008	028	068	136	235	360	500	500	640	765	864	932	972	992	999							
7	000	001	005	015	035	068	119	191	281	386	500	500	614	719	809	881	932	965	985	995	999		
8	000	000	001	003	007	016	031	054	089	138	199	274	360	452									
9	000	000	000	000	001	003	006	012	022	038	060	090	130	179	238	306	381	460					
10	000	000	000	000	000	000	001	002	005	008	014	023	036	054	078	108	146	190	242	300	364	431	
$P(c)$	000	000	000	000	001	001	002	004	006	010	016	025	037	054	076	105	142	186	237	296	360	429	

* Tabular values should be divided by 1000.

$$P(c) = \frac{1}{\sqrt{2\pi}} \int_{-\infty}^{-c} e^{-x^2/2} dx, \quad c = \left(\frac{n(n-1)}{4} - T - \frac{1}{2} \right) / \sqrt{\frac{2n^3 + 3n^2 - 5n}{72}}, \quad n = 10.$$

TABLE 2
PROBABILITY OF OBTAINING A PERMUTATION WITH $K \leq \bar{K}$ IN PERMUTATIONS OF n VARIABLES.

$\bar{K} \backslash n$	1	2	3	4	5	6	7
3	0.1667	0.5000					
4	0.0417	0.2083	0.5000				
5	0.0083	0.0667	0.2083	0.5000			
6	0.0014	0.0181	0.0792	0.2083	0.5000		
7	0.0002	0.0042	0.0246	0.0792	0.2083	0.5000	
8	0.0000	0.0008	0.0066	0.0284	0.0792	0.2083	0.5000
9	0.0000	0.0002	0.0016	0.0086	0.0284	0.0792	0.2083

the situation H_1 although it should not be taken if H_1 is the true situation. In quality control, for instance, in testing against trend the action A_2 may consist in inspecting machinery to find the causes of a trend. But if a biased test is used then there exist situations when a periodical inspection of machinery would be preferable in deciding the action to be taken. In other words, a biased test is in certain cases not only useless but even worse than no test at all.

In this paper we shall propose two tests against trend and find sufficient conditions for their consistency and unbiasedness. Both tests are based on ranks. The advantages and disadvantages of restricting oneself to tests based on ranks have been discussed in a paper by H. Scheffé.² To the advantages of such tests one may add that they may also be used if the quantities considered cannot be measured, as long as it is possible to rank them. Intensity of sensory impressions, pleasure, and pain, are examples of such quantities. In this paper tests against downward trend will be discussed. A test against upward trend can then always be made by testing $-X_1, \dots, -X_n$ against downward trend.

2. THE T-TEST

Let X_{i_1}, \dots, X_{i_n} be a permutation of the n distinct numbers X_1, \dots, X_n . Let T count the number of inequalities $X_{i_k} < X_{i_l}$ where $k < l$. One such inequality will be called a reverse arrangement. If X_1, \dots, X_n all have the same continuous distribution, then the probability of obtaining a sample with T reverse arrangements is proportional to the number of permutations of the variables $1, 2, \dots, n$ with T reverse arrangements.

The statistic T was first proposed by M. G. Kendall³ for testing independence in a bivariate distribution. Kendall also derived the recursion formula (1), tabulated the distribution of T for $T \leq 10$, and proved that the limit distribution of T is normal. Table 1, however, seems more convenient to use for our purpose. The proof of the normality of the limit distribution of T given in the present paper seems simpler than Kendall's and the method employed may be of general interest.

We now propose the following test against a downward trend: We determine \bar{T} so that $P(T \leq \bar{T} | H_1) = \alpha$, where H_1 is the hypothesis of randomness and α the size of the critical region. If in our sample we obtain a value $T \leq \bar{T}$ we shall proceed as if the sample came from a

² Henry Scheffé, "On a Measure Problem Arising in the Theory of Non-Parametric Tests," *Annals of Mathematical Statistics*, Vol. 14, September, 1943, pp. 227-233.

³ M. G. Kendall, "A New Measure of Rank Correlation," *Biometrika*, Vol. 30, June, 1938, pp. 81-93.

downward trend. If $T > \bar{T}$ we shall proceed as if H_1 were true. It will be shown that under a mild additional restriction on the sequence f_1, f_2, \dots, f_n in the alternative H_2 the T -test is a consistent test against trend.

3. THE DISTRIBUTION OF T

Let $P_n(T)$ be the number of permutations of $1, 2, \dots, n$ with T reverse arrangements. Consider first the permutations of $2, 3, \dots, n$. We can obtain each permutation of $1, 2, \dots, n$ exactly once by putting 1 into n different places of all permutations of $2, 3, \dots, n$. In doing this we increase the number of reverse arrangements by $0, 1, \dots, n-1$ according to the position into which 1 is placed. Hence

$$(1) \quad P_n(T) = P_{n-1}(T) + P_{n-1}(T - 1) + \dots + P_{n-1}(T - n + 1),$$

if $P_n(T) = 0$ for $T < 0$.

Formula (1) permits tabulation of $P_n(T)$ for small values of n . In Table 1 are given the cumulative probabilities of obtaining a permutation with T or fewer reverse arrangements, when every permutation occurs with probability $1/n!$

Since, under the hypothesis of randomness, $P(X_i > X_k) = 1/2$, we have $E(T) = n(n-1)/4$.

To obtain higher moments of T we multiply (1) by $[T - n(n-1)/4]^i = X_n^i$. Denoting by $E_n[f(X)]$ the expectation of $f(X_n)$ in permutations of n variables, we obtain

$$(2) \quad \begin{aligned} E_n(X^i) = & \frac{1}{n} \left\{ E_{n-1} \left[\left(X - \frac{n-1}{2} \right)^i \right] \right. \\ & + E_{n-1} \left[\left(X - \frac{n-3}{2} \right)^i \right] + \dots \\ & \left. + E_{n-1} \left[\left(X + \frac{n-1}{2} \right)^i \right] \right\}. \end{aligned}$$

Since the distribution of X is symmetric, $E_n(X^{2i+1}) = 0$, ($i = 0, 1, \dots$). From (2) we obtain

$$(3) \quad E_n(X^{2i}) = E_{n-1}(X^{2i}) + \binom{2i}{2} B_n^{(2)} E_{n-1}(X^{2i-2}) + \dots + B_n^{(2i)},$$

where

$$(4) \quad B_n^{(2i)} = \frac{1}{n} \sum_{k=0}^{k=n-1} \left(\frac{n-1}{2} - k \right)^{2i}.$$

We now put $nB_n^{(2i)} = f^{(2i)}(n)$ and $f^{(2i)}(1) = f^{(2i)}(0) = 0$; then $f^{(2i)}(n)$ satisfies for $n = 0, 1, \dots$, the difference equation

$$(5) \quad f^{(2j)}(n+2) - f^{(2j)}(n) = 2 \left(\frac{n+1}{2} \right)^{2j}$$

with the initial condition $f^{(2j)}(1) = f^{(2j)}(0) = 0$. For $j=1$ a solution of (5) is $(n^3-n)/12$. Hence we have $B_n^{(2)} = (n^2-1)/12$. For $j=2$ we obtain $B_n^{(4)} = (3n^4-10n^2+7)/240$. Hence for $i=1$, (3) becomes

$$E_n(X^2) = E_{n-1}(X^2) + \frac{n^2-1}{12}.$$

From this we obtain

$$(6) \quad E_n(X^2) = \sigma_n^2(T) = \frac{2n^3 + 3n^2 - 5n}{72}.$$

In a similar manner we obtain

$$(7) \quad E_n(X^4) = \frac{100n^6 + 228n^5 - 455n^4 - 870n^3 + 625n^2 + 372n}{43,200}.$$

Formula (6) can also be obtained in a different manner. Let, for $i < j$,

$$(8) \quad y_{ij} = \begin{cases} 1 & \text{if } X_i < X_j, \\ 0 & \text{if } X_i > X_j. \end{cases}$$

Then if the continuous function f is the distribution function of X_i for $i=1, 2, \dots$, we have

$$\begin{aligned} E(y_{ij}) &= \frac{1}{2}, & \sigma^2(y_{ij}) &= \frac{1}{4}, \\ E(y_{ij}y_{jk}) &= P(X_i < X_j < X_k) = \frac{1}{6}, \\ \sigma(y_{ij}y_{jk}) &= -\frac{1}{12}. \end{aligned}$$

Similarly we obtain $\sigma(y_{ij}y_{ik}) = \sigma(y_{ij}y_{kj}) = 1/12$, while $\sigma(y_{ij}y_{kl}) = 0$ if i, j, k, l are distinct. For these results (5) can easily be obtained.

We proceed to prove that the limit distribution of T is normal. From (5) and the initial conditions of (5) it follows that $B_n^{(2j)}$ is given by a polynomial in n of degree $2j$. To see this we first determine a polynomial $f^{(2j)}(n)$ of degree $2j+1$ satisfying (5) and the initial condition $f^{(2j)}(0) = 0$. It may then be shown by induction that $f^{(2j)}(n) = -f^{(2j)}(-n)$ for all even n . But this is only possible if $f^{(2j)}(n) = -f^{(2j)}(-n)$ for all n . From (5) it follows that $f^{(2j)}(1) = f^{(2j)}(-1)$. Hence we must also have $f^{(2j)}(1) = 0$. Thus there exists a polynomial of degree $2j+1$ satisfying (5) and its initial conditions. We proceed to show by induction that $E_n(X^{2i})$ is given by a polynomial in n of degree $3i$ and first coefficient $[(2i-1)(2i-3) \dots 3 \cdot 1]/36^i$.

From (3) we have

$$(9) \quad E_n(X^{2i}) - E_{n-1}(X^{2i}) = \binom{2i}{2} \frac{(n^2 - 1)}{12} E_{n-1}(X^{2i-2}) + \binom{2i}{4} B_n^{(4)} E_{n-1}(X^{2i-4}) + \dots + B_n^{(2i)}.$$

From the hypothesis of the induction it follows that the j th term on the right-hand side of (9) is of degree $3i - j$ in n . Hence only the first term is of degree $3i - 1$. Since the first difference of $E_n(X^{2i})$ is a polynomial of degree $3i - 1$ it follows that $E_n(x^{2i})$ is a polynomial of degree $3i$. Hence we may put $E_n(X^{2i}) = a_0 n^{3i} + \dots$. Using again the hypothesis of our induction we obtain on comparing coefficients in (9)

$$(10) \quad 3ia_0 = \frac{(2i - 3) \dots 3 \cdot 1}{36^{i-1} \cdot 12} \frac{2i(2i - 1)}{2}, \quad a_0 = \frac{(2i - 1) \dots 3 \cdot 1}{36^i}.$$

From (10) and (6) we have

$$\lim_{n \rightarrow \infty} \frac{E_n(X^{2i})}{\sigma_n^{2i}(X)} = (2i - 1) \dots 3 \cdot 1.$$

It follows by a well-known theorem that $X/\sigma_n(X)$ is in the limit normally distributed with variance 1. From Table 1 it may be seen that the approach to normality is remarkably rapid.

4. CONDITIONS FOR CONSISTENCY AND UNBIASEDNESS OF THE T-TEST

Let us assume now that some alternative situation (not necessarily a trend) is true. Let, for $i < k$, $P(X_i < X_k) = \frac{1}{2} + \epsilon_{ik}$. Let further y_{ij} be defined by (8) and let $\sum_i \sum_{i < k} \epsilon_{ik} = \lambda_n n(n - 1)/2$. Then

$$T = \sum_i \sum_{i < k} y_{ik},$$

$$E(T) = \frac{n(n - 1)}{4} + \sum_i \sum_{i < k} \epsilon_{ik} = \frac{n(n - 1)}{4} (1 + 2\lambda_n).$$

Moreover we shall assume that X_i is independent of X_j for $i \neq j$ so that $\sigma(y_i y_{kl}) = 0$ if i, j, k, l are distinct. We proceed to compute $\sigma^2(T)$ under the alternative hypothesis. To simplify the notation the symbol \sum without further specification will denote summation over all values for which the summands have been defined. We have

$$(11) \quad \sigma^2(T) = E[(T - E(T))^2] = \sum \sigma^2(y_{ik}) + 2 \sum \sigma(y_i y_{jk}) + \sum \sigma(y_{kj} y_{ij}) + \sum \sigma(y_{ik} y_{il}).$$

We have

$$(12) \quad \sigma^2(y_{ik}) = \frac{1}{4} - \epsilon_{ik}^2, \quad \sigma(y_{i,j,k}) \leq 0.$$

The second of these two statements can be proved as follows: Let f_1, f_2, f_3 be three continuous functions, then:

$$\begin{aligned} \left[\int_{-\infty}^{X_1} df_2(X_2) \int_{-\infty}^{X_2} df_3(X_3) \right] \int_{X_1}^{\infty} df_2(X_2) \\ \leq \int_{-\infty}^{X_1} df_2(X_2) \int_{X_1}^{\infty} df_2(X_2) \int_{-\infty}^{X_1} df_3(X_3) \\ \leq \int_{-\infty}^{X_1} df_2(X_2) \left[\int_{X_1}^{\infty} df_2(X_2) \int_{-\infty}^{X_2} df_3(X_3) \right]. \end{aligned}$$

Adding

$$\int_{-\infty}^{X_1} df_2(X_2) \left[\int_{-\infty}^{X_1} df_2(X_2) \int_{-\infty}^{X_2} df_3(X_3) \right]$$

to both sides of this inequality we obtain

$$\int_{-\infty}^{X_1} df_2(X_2) \int_{-\infty}^{X_2} df_3(X_3) \leq \int_{-\infty}^{X_1} df_2(X_2) \int_{-\infty}^{+\infty} df_2(X_2) \int_{-\infty}^{X_2} df_3(X_3).$$

Integrating both sides with respect to X_1 we obtain

$$\begin{aligned} \int_{-\infty}^{+\infty} df_1(X_1) \int_{-\infty}^{X_1} df_2(X_2) \int_{-\infty}^{X_2} df_3(X_3) \\ \leq \left[\int_{-\infty}^{+\infty} df_1(X_1) \int_{-\infty}^{X_1} df_2(X_2) \right] \left[\int_{-\infty}^{+\infty} df_2(X_2) \int_{-\infty}^{X_2} df_3(X_3) \right] \end{aligned}$$

or $P(X_1 > X_2 > X_3) \leq P(X_1 > X_2)P(X_2 > X_3)$. From this result the inequality in (12) follows easily.

We further have

$$\begin{aligned} \sigma(y_{ik}y_{il}) &= P(y_{ik} = y_{il} = 1) - E(y_{ik})E(y_{il}) \\ &= P(y_{ik} = y_{il} = 1) - \left(\frac{1}{2} + \epsilon_{ik}\right)\left(\frac{1}{2} + \epsilon_{il}\right), \end{aligned}$$

$$P(y_{ik} = y_{il} = 1) = \int_{-\infty}^{+\infty} (1 - f_k)(1 - f_l)df_i \leq \frac{1}{2} + \min(\epsilon_{ik}, \epsilon_{il}).$$

Hence

$$(13) \quad \sigma(y_{ik}y_{il}) \leq \frac{1}{2} + \min(\epsilon_{ik}, \epsilon_{il}) - \left(\frac{1}{2} + \epsilon_{ik}\right)\left(\frac{1}{2} + \epsilon_{il}\right) \leq \frac{1}{4} - \epsilon_{ik}\epsilon_{il}.$$

Similarly

$$(14) \quad \sigma(y_{kj}y_{lj}) \leq \frac{1}{4} - \epsilon_{kj}\epsilon_{lj}.$$

From (11), (12), (13), and (14) we obtain

$$\sigma^2(T) \leq \frac{n(n-1)}{4} + \frac{n(n-1)(n-2)}{6} - \sum_{i=1}^n \left[\sum_k \epsilon_{ik}^2 + \sum_{k \neq j} \epsilon_{ik} \epsilon_{ij} + \sum_{k \neq j} \epsilon_{ki} \epsilon_{ji} \right].$$

We put $\sum_{k=i+1}^{k=n} \epsilon_{ik} = L_{i.}$, $\sum_{i=1}^{i=k-1} \epsilon_{ik} = L_{.k}$; then

$$\begin{aligned} \sum_i \left(\sum_k \epsilon_{ik}^2 + \sum_{k \neq j} \epsilon_{ik} \epsilon_{ij} + \sum_{k \neq j} \epsilon_{ki} \epsilon_{ji} \right) &= \sum_i L_{i.}^2 + \sum_j L_{.j}^2 - \sum_i \sum_j \epsilon_{ij}^2. \end{aligned}$$

Since $\epsilon_{ij}^2 \leq \frac{1}{4}$ we obtain

$$(15) \quad \sigma^2(T) \leq \frac{3n(n-1)}{8} + \frac{n(n-1)(n-2)}{6}.$$

If all ϵ_{ij} have the same sign then $L_{i.}^2 \geq \sum_j \epsilon_{ij}^2$ and $\sum_i L_{.j}^2 \geq \lambda_n^2 n^2 (n-1)/4$. We can then improve (15) to the form

$$(15') \quad \sigma^2(T) \leq \frac{n(n-1)}{4} + \frac{n(n-1)(n-2)}{6} - \lambda_n^2 \frac{n^2(n-1)}{4}.$$

If the critical region is given by $T \leq \bar{T}$ then the power of the T test with respect to the hypothesis H is given by $P(T \leq \bar{T} | H)$.

If the size of the critical region is fixed then $\bar{T} = n(n-1)/4 - t_n \sqrt{(2n^3 + 3n^2 - 5n)/72}$, where $\lim_{n \rightarrow \infty} t_n = t$ and $\int_{-\infty}^{-t} e^{-x^2/2} dx$ equals the size of the critical region.

Consider now the case that $\lambda_n < 0$ and $n(n-1)(1+2\lambda_n)/4 < \bar{T} + 1$ then by Tchebycheff's theorem we have

$$(16) \quad P(T \leq \bar{T} | H) \geq 1 - \frac{\sigma^2(T)}{\left[\bar{T} + 1 - \frac{n(n-1)}{4} (1 + 2\lambda_n)^2 \right]}.$$

We may also use

$$(16') \quad \begin{aligned} &P(T \leq \bar{T} | H) \\ &\geq 1 - \frac{\sigma^2(T)}{\left(\lambda_n \frac{n(n-1)}{2} + t_n \sqrt{\frac{2n^3 + 3n^2 - 5n}{72}} \right)^2} \end{aligned}$$

for

$$\lambda_n \frac{n(n-1)}{2} \leq -t_n \sqrt{\frac{2n^3 + 3n^2 - 5n}{72}}.$$

For large values of n we may replace t_n by t . From (15), (16'), and the fact that $\lim_{n \rightarrow \infty} t_n = t$, it can be seen that the T -test is consistent whenever $\lim_{n \rightarrow \infty} \sqrt{n}\lambda_n = -\infty$.

In case the alternative H is a downward trend, we have $f_i(X) < f_j(X)$ if $i < j$ and

$$P(X_i < X_j) = \int (1 - f_j)df_i < \int (1 - f_i)df_i = \frac{1}{2};$$

hence ϵ_{ij} is always negative and (15') may be used as an upper bound of $\sigma^2(T)$ in (16) or (16').

Another estimate of $P(T \leq \bar{T})$, which for small values of n gives better results than (16), can be obtained as follows:

If X is always positive and $E(X) = A$, then

$$P(X > B) = \int_{B+\epsilon}^{\infty} df(X) \leq \frac{1}{B'} \int_{B+\epsilon}^{\infty} Xdf(X) \leq \frac{A}{B'},$$

$$\int_{B+\epsilon}^{\infty} dg = \lim_{\epsilon \rightarrow \infty} \int_{B+\epsilon}^{\infty} dg, \quad \epsilon > 0,$$

where B' is the lower bound of all values B'' for which $\int_{B+\epsilon}^{B''} df(X) > 0$. Thus

$$P(X \leq B) \geq 1 - \frac{A}{B'} = \frac{B' - A}{B'}.$$

Hence

$$(17) \quad P(T \leq \bar{T} | H) \geq \frac{\bar{T} + 1 - \frac{n(n-1)}{4} (1 + 2\lambda_n)}{\bar{T} + 1}.$$

We may also use

$$(17') \quad P(T \leq \bar{T}) \geq \frac{-2\lambda_n n(n-1) - 4t_n \sigma_0}{n(n-1) - 4t_n \sigma_0},$$

where $\sigma_0 = \sqrt{(2n^3 + 3n^2 - 5n)/72}$, and may for large n replace t_n by t . Thus, for instance, for $n = 20$, $\lambda_n = 0.25$, $t_{20} = 1.64$, (17') yields $P(T \leq \bar{T}) \geq 0.326$. A much better result is obtained from (16') if the distribution of T under the alternative H is approximately normal as is probably the case under a wide class of alternatives.

If the size of the critical region, that is to say, $1 - P[(X_1, \dots, X_n) \subset W_1 | H_1] = \alpha$, then the test is unbiased with respect to H_2 if $P(T \leq \bar{T} | B) \geq \alpha$ for every B in H_2 . This is, according to (17), the case if

$$\frac{\bar{T} + 1 - \left(\frac{n(n-1)}{4} + \lambda_n \frac{n(n-1)}{2} \right)}{\bar{T} + 1} \geq \alpha$$

or

$$(18) \quad -\lambda_n \geq \frac{1}{2} - \frac{(1-\alpha)2(\bar{T}+1)}{n(n-1)}.$$

For instance, if $n=5$, $\alpha=5/120$, then $\bar{T}+1=2$, and we obtain from (18), $-\lambda_n \geq 0.31$. If n is large enough to use the normal approximation for determining the size of the critical region we obtain with $\sigma_0 = \sqrt{(2n^3 + 3n^2 - 5n)/72}$

$$(18') \quad -\lambda_n \geq \frac{\alpha}{2} + \frac{(1-\alpha)t2\sigma_0}{n(n-1)}.$$

Thus, for example, if $n=10$, $\alpha=0.05$, then $t=1.64$, and we find from (18') that the T -test is certainly unbiased if $-\lambda_n \geq 0.218$ [the value obtained from (18) is 0.205]. For $n=20$, $\alpha=0.05$, $t=1.64$, we obtain from (18'), $-\lambda_{20} \geq 0.154$, which seems satisfactory.

Summary of Section 4: The T -test is consistent with respect to any sequence of random variables X_1, \dots, X_n for which

1. $P(X_i > X_j) = \frac{1}{2} + \epsilon_{ij}$, for $i < j$;
2. $P(X_i > X_j | X_k > X_l) = P(X_i > X_j)$, if i, j, k, l are distinct;
3. $\lim_{n \rightarrow \infty} (\sqrt{n} \sum \epsilon_{ij}/n^2) = -\infty$.

The T -test is unbiased with respect to any set of random variables X_1, \dots, X_n , if $\lambda_n = 2 \sum \epsilon_{ij}/n(n-1)$ satisfies the inequality (18), which for large n may be replaced by (18'). Lower bounds for the power of the T -test are given by (16), (16') and (17), (17') where the primed inequalities are convenient for larger values of n .

5. ALTERNATIVES WITH RESPECT TO WHICH THE T-TEST IS MOST POWERFUL

Let $z_k = i$ if exactly $i-1$ of the X 's are larger than X_k . Let $T(i_1, \dots, i_n)$ be the number of nonreverse arrangements in the permutation i_1, \dots, i_n . $T(i_1, \dots, i_n)$ is equal to the number of reverse arrangements in the sequence of the X 's. Further let us restrict ourselves to tests based on ranks.

Whenever an alternative B is such that $T(i_1, \dots, i_n) \geq T(j_1, \dots, j_n)$ implies $P(z_1 = i_1, \dots, z_n = i_n) \leq P(z_1 = j_1, \dots, z_n = j_n)$, then the T -test

will be most powerful with respect to the alternative B among all tests based on ranks.

We shall as a special case consider a particular alternative B , defined as follows: The probability that, among the set X_i, X_{i+1}, \dots, X_n , X_i will be the first, second, \dots in magnitude, is, if B is true, given by $a_i, a_i p, \dots, a_i p^{n-i-1}$ ($p < 1$), $a_i = 1/(1 + p + \dots + p^{n-i-1})$ independently of the ranks of the first $i-1$ variables.

Thus, if B is true,

$$P(z_i = k \mid z_1 = j_1, \dots, z_{i-1} = j_{i-1}) = \begin{cases} 0 & \text{if one } j_\alpha = k, \\ a_i p^{k-l_i-1} & \text{otherwise,} \end{cases}$$

where l_i is the number of j_α 's which are $< k$.

Then

$$(19) \quad \begin{aligned} P(z_1 = i_1, z_2 = i_2, \dots, z_n = i_n) &= a_1 p^{i_1-1} a_2 p^{i_2-l_2-1} \dots a_n p^{i_n-l_n-1} \\ &= \left(\prod_{i=1}^{i=n} a_i \right) p^{n(n-1)/2 - \sum l_i} = \left(\prod_{i=1}^{i=n} a_i \right) p^{T(i_1, \dots, i_n)}. \end{aligned}$$

Hence $P(z_1 = i_1, \dots, z_n = i_n) < P(z_1 = j_1, \dots, z_n = j_n)$ whenever $T(i_1, \dots, i_n) > T(j_1, \dots, j_n)$. Thus the T -test has maximum power with respect to the alternative B . It is, however, not known whether B can result if the X 's are independently distributed.

As a side result we obtain from (19) the characteristic function of T . We have

$$\begin{aligned} \prod_{i=1}^{i=n} a_i &= [1(1+p) \dots (1+p+\dots+p^{n-1})]^{-1} \\ &= \frac{(p-1)^n}{(p-1)(p^2-1) \dots (p^n-1)}. \end{aligned}$$

Summing (19) over all permutations, we obtain

$$\frac{1}{n!} \sum P_n(T) p^T = \frac{(p^n-1)(p^{n-1}-1) \dots (p-1)}{(p-1)^n}.$$

This is an identity in p . Hence $f_T(\theta)$, the characteristic function of T , is given by

$$f_T(\theta) = \sum \frac{1}{n!} P_n(T) e^{iT\theta} = \frac{(e^{in\theta} - 1) \dots (e^{i\theta} - 1)}{(e^{i\theta} - 1)^n}.$$

6. THE K-TEST

If $P(X_i > X_j)$ increases rapidly with $j-i$, then another test is more powerful than the T -test. This test is carried out as follows:

Determine for the sample X_0, X_1, \dots, X_{n-1} the smallest value of K for which the following set of inequalities is fulfilled:

$$\begin{aligned}
 & X_0 > X_k, X_0 > X_{k+1}, \dots, X_0 > X_{n-1}, \\
 (20) \quad & X_1 > X_{k+1}, \dots, X_1 > X_{n-1}, \\
 & \dots \dots \dots \dots \dots \\
 & X_{n-k-1} > X_{n-1}.
 \end{aligned}$$

Determine \bar{K} so that $P(K \leq \bar{K} | H_1)$ is equal to the size of the critical region. If $K \leq \bar{K}$, proceed as if H_2 were true; if $K > \bar{K}$, proceed as if H_1 were true.

Let X_0, X_1, \dots, X_{n-1} be the sample in the order taken. Consider the $n!$ points $(Y_0, Y_1, \dots, Y_{n-1})$ where $Y_0 = X_{i_0}, \dots, Y_{n-1} = X_{i_{n-1}}$ for every permutation i_0, \dots, i_{n-1} of the numbers $0, 1, \dots, n-1$. Let $Q_n(\bar{K})$ be the number of points (Y_0, \dots, Y_{n-1}) that satisfy the \bar{K} th set of inequalities. We arrange every point in order of decreasing magnitude so that to every point Y_0, Y_1, \dots, Y_{n-1} we have a sequence of inequalities $Y_{i_0} > \dots > Y_{i_{n-1}}$. Thus every point is mapped into a permutation i_0, \dots, i_{n-1} . In order that the point with the permutation i_0, \dots, i_{n-1} fulfill the \bar{K} th set of inequalities, it is necessary and sufficient that in the permutation i_0, i_1, \dots, i_{n-1} no number α be preceded by any of the numbers $\alpha + \bar{K}, \alpha + \bar{K} + 1, \dots, n-1$. Hence the number of points fulfilling the \bar{K} th set of inequalities is equal to the number of permutations in which no number α is preceded by any of the numbers $\alpha + \bar{K}, \alpha + \bar{K} + 1, \dots, n-1$.

We have $Q_n(1) = 1$. A permutation in which no α is preceded by any number larger than $\alpha + 1$ can have the number 0 only at the first or the second place. Hence such a permutation must either be of the type $0, i_1, \dots, i_{n-1}$, or of the type $1, 0, i_2, \dots, i_{n-1}$; and $i_1, \dots, i_{n-1}; i_2, \dots, i_{n-1}$ respectively must fulfill the \bar{K} th set of inequalities with $\bar{K} = 2$. Hence we have the recursion

$$(21) \quad Q_n(2) = Q_{n-1}(2) + Q_{n-2}(2).$$

In using this relation we must put $Q_n(\bar{K}) = 0$ for $n < 0$, $Q_n(n+j) = n!$ for $j \geq 0, n \geq 0$. To obtain a similar recursion for $\bar{K} = 3$ we observe that a permutation in which α is never preceded by any number larger than $\alpha + 2$ can be only of one of the following types:

- $0, i_1, \dots, i_{n-1}; 1, 0, i_2, \dots, i_{n-1}; 2, 0, 1, i_3, \dots, i_{n-1};$
- $2, 0, 3, 1, i_4, \dots, i_{n-1}; 1, 2, 0, i_3, \dots, i_{n-1}; 2, 1, 0, i_3, \dots, i_{n-1}.$

Hence we have the recursion

$$(22) \quad Q_n(3) = Q_{n-1}(3) + Q_{n-2}(3) + 3Q_{n-3}(3) + Q_{n-4}(3).$$

Let $P_n(\bar{K})$ be the probability of obtaining a permutation satisfying the \bar{K} th set of inequalities. For $n \leq 2\bar{K}$ some of the variables are not involved in the inequalities (20). We therefore have⁴

$$(23) \quad P_n(n - \bar{K}) = P_{2\bar{K}}(\bar{K}) \quad \text{for } n \geq 2\bar{K}.$$

We shall show below that $P_8(4) = 0.0284$, $P_9(4) = 0.0086$, $P_{10}(5) = 0.0098$. These values and the relations (21), (22), and (23) permit tabulation of $P_n(\bar{K})$ for $n \leq 9$. From (23) and Table 2 we further obtain:

$$(24) \quad \begin{aligned} P_n(n - 5) &= P_{10}(5) = 0.0098 \dots & \text{for } n \geq 10; \\ P_n(n - 4) &= P_8(4) = 0.0284 \dots & \text{for } n \geq 8; \\ P_n(n - 3) &= P_6(3) = 0.0792 \dots & \text{for } n \geq 6; \\ P_n(n - 2) &= 0.2083 \dots & \text{for } n \geq 4; \\ P_n(n - 1) &= 0.5 & \text{for } n \geq 2. \end{aligned}$$

It is clear that (24) contains for $n \geq 10$ all critical regions possible for the K -test between size 0.0098 and 0.5. Regions smaller than 0.0098 are not likely to occur in practical problems. Hence within a range which is of interest to the practical statistician we shall have all regions available for the K -test if we compute $P_8(4)$, $P_9(4)$, and $P_{10}(5)$. It is a disadvantage of the K -test that we are rather limited in the choice of the size of the critical region.

We shall derive the following two relations: Let $R_n(\bar{K})$ be the subset of the n -dimensional Euclidean space given by (20) and let f be the common cumulative distribution function of the X_i ; then for $n \geq 2\bar{K}$, as we shall prove below,

$$(25) \quad \begin{aligned} P_n(n - \bar{K}) &= P_{2\bar{K}}(\bar{K}) = \int_{R_{2\bar{K}}(\bar{K})} df(X_0) \dots df(X_{2\bar{K}-1}) \\ &= \sum \{ (j_1 + 1) [\max(j_1, j_2) + 2] \dots [\max(j_1, \dots, j_{\bar{K}}) + \bar{K}] \}^{-1}, \end{aligned}$$

where \sum denotes summation over all permutations $j_1, \dots, j_{\bar{K}}$ of $1, \dots, \bar{K}$. Further let $\bar{\max}(i_1, \dots, i_l) = \min[\max(i_1, \dots, i_l), \bar{K} - 1]$; then

$$(26) \quad \begin{aligned} P_9(4) &= \int_{R_9(4)} df(X_0), \dots, df(X_8) \\ &= \sum' \{ [\bar{\max}(j_1) + 1] [\bar{\max}(j_1, j_2) + 2] \\ &\quad \dots [\bar{\max}(j_1, \dots, j_6) + 5] \}^{-1}, \end{aligned}$$

⁴ For typographical reasons it was not possible to use \bar{K} in subscripts and exponents. Every K in subscripts and exponents in this section should be read as \bar{K} .

where \sum' denotes summation over all permutations j_1, \dots, j_k of $1, \dots, k$ for which 1 precedes k .

Since the integral in (25) is independent of f , we may assume that f is a rectangular distribution between 0 and 1. We consider the integral in (25). For X_0, X_1, \dots, X_{k-1} fixed, X_k varies from 0 to X_0 ; X_{k+1} from 0 to $\min(X_0, X_1)$; X_{k+2} from 0 to $\min(X_0, X_1, X_2)$; and so forth; hence we obtain

$$P_{2k}(\bar{K}) = \int_0^1 \dots \int_0^1 X_0 \min(X_0, X_1) \dots \min(X_0, X_1, \dots, X_{k-1}) dX_0 \dots dX_{k-1}.$$

We split this integral into the $\bar{K}!$ parts $X_{i_1} < X_{i_2} < \dots < X_{i_k}$; then for any permutation i_1, \dots, i_k of $0, \dots, \bar{K}-1$ we have to compute

$$(27) \int_0^1 dX_{i_k} \int_0^{X_{i_k}} dX_{i_{k-1}} \dots \int_0^{X_{i_2}} dX_{i_1} X_0 \min(X_0, X_1) \dots \min(X_0, \dots, X_{k-1}).$$

Consider the exponent of X_{i_α} in (27). In the factors under the integral sign X_{i_α} occurs for the first time in $\min(X_0, X_1, \dots, X_{i_\alpha})$. From then on it occurs in every factor. If $i_\beta < i_\alpha$ for $\beta < \alpha$, then none of the factors in (27) will be equal to X_{i_α} . If $\min(i_1, \dots, i_{\alpha-1}) = i_\beta > i_\alpha$ ($\alpha > 1$), then the factors $\min(X_0, \dots, X_{i_\alpha})$, $\min(X_0, \dots, X_{i_{\alpha+1}})$, \dots , $\min(X_0, \dots, X_{i_{\beta-1}})$ will be equal to X_{i_α} . In both cases the exponent of X_{i_α} may be written as $\min(i_1, \dots, i_{\alpha-1}) - \min(i_1, \dots, i_\alpha)$. For $\alpha = 1$, we shall have $\min(X_0, \dots, X_{i_1}) \dots \min(X_0, \dots, X_{k-1})$ equal to X_{i_1} . Hence (27) becomes

$$(28) \int_0^1 dX_{i_k} X_{i_k}^{\min(i_1, \dots, i_{k-1}) - \min(i_1, \dots, i_k)} \dots \int_0^{X_{i_2}} dX_{i_2} X_{i_2}^{i_1 - \min(i_1, i_2)} \int_0^{X_{i_2}} dX_{i_1} X_{i_1}^{k - i_1}.$$

Integrating out the last integral we obtain under the next to the last integral sign

$$\frac{1}{\bar{K} - i_1 + 1} X_{i_2}^{k - i_1 + 1} X_{i_2}^{i_1 - \min(i_1, i_2)} = (\bar{K} - i_1 + 1)^{-1} X_{i_2}^{k - \min(i_1, i_2) + 1}.$$

When this process is continued (28) finally becomes

$$(29) (\bar{K} - i_1 + 1)^{-1} [\bar{K} - \min(i_1, i_2) + 2]^{-1} \dots [\bar{K} - \min(i_1, \dots, i_k) + \bar{K}]^{-1}.$$

Putting $\bar{K} - i_\alpha = j_\alpha$ and summing over all permutations i_1, \dots, i_K , we obtain (25).

In the integral in (26) we have X_5 varying from 0 to $\min(X_0, X_1)$; X_6 from 0 to $\min(X_0, X_1, X_2)$; and so forth, hence

$$(30) \quad P_9(4) = \int_0^1 \cdots \int_0^1 \int_0^{X_0} \min(X_0, X_1) \cdots \min(X_0, X_1, \dots, X_4) dX_4 \cdots dX_0.$$

Now for every subset $X_{i_1} < \dots < X_{i_5}$ where i_1, \dots, i_5 is a permutation of the numbers 0, 1, 2, 3, 4, we obtain

$$\begin{aligned} & \int_0^1 \int_0^{X_{i_1}} \cdots \int_0^{X_{i_5}} \min(X_0, X_1) \cdots \min(X_0, \dots, X_4) dX_{i_1} \cdots dX_{i_5} \\ &= \int_0^1 \int_0^{X_{i_1}} \cdots \int_0^{X_{i_5}} X_{i_1}^{5-\max(i_1,1)} X_{i_2}^{\max(i_1,1)-\max[\min(i_1,i_2),1]} \\ & \quad \cdots X_{i_5}^{\max[\min(i_1,i_2,i_3,i_4),1]-\max[\min(i_1,i_2,i_3,i_4,i_5),1]} \\ & \quad \quad \quad dX_{i_1} \cdots dX_{i_5}, \end{aligned}$$

from which (26) follows by an obvious extension of the argument used in the proof of (25).

By the use of (25) and (26) the values $P_8(4)$, $P_{10}(5)$, and $P_9(4)$ have been computed. It may be remarked that the labor involved was not at all excessive since in carrying out the computations a great many short cuts offer themselves freely.

It is easy to construct trends for which the K -test has maximum power at some fixed level of significance. Let the critical value of K be \bar{K} and consider alternatives where $P(X_i > X_{K+i+j}) = 1$ for $j \geq 0$. It is easy to find trends for which this is true. The K -test has then clearly the power 1 with respect to such trends. The power of the K -test is also high with respect to trends for which $P(X_1 > X_{i+K+j})$ is close to 1 for $j \geq 0$. Such alternatives do quite frequently occur in practical work. The fact that the K -test is most powerful with respect to a fairly wide class of alternatives seems worth noting. It is very often said that in using a test based on ranks, one is "throwing away information." In using the K -test an even larger "amount of information" is "thrown away," nevertheless it is a most powerful test with respect to a substantial class of alternatives.

The Ohio State University

WATER QUALITY CONCERNS DUE TO FOREST FIRES: POLYCYCLIC AROMATIC HYDROCARBONS (PAH) CONTAMINATION OF GROUNDWATER FROM MOUNTAIN AREAS

C. Mansilha^{1,2}, A. Carvalho^{3,4}, P. Guimarães³, J. Espinha Marques^{3,4}

¹National Institute of Health Doutor Ricardo Jorge, R. Alexandre Herculano 321, Porto, Portugal

²Requimte, University of Porto, Porto, Portugal

³Department of Geosciences, Environment and Territorial Planning, Faculty of Sciences, University of Porto, Porto, Portugal

⁴Geology Centre of the University of Porto (CGUP), Porto, Portugal

Water quality alterations due to forest fires may considerably affect aquatic organisms and water resources. These impacts are cumulative as a result of pollutants mobilized from fires, chemicals used to fight fire, and postfire responses. Few studies have examined post-fire transport into water resources of trace elements, including the polycyclic aromatic hydrocarbons (PAH), which are organic pollutants produced during combustion and are considered carcinogenic and harmful to humans. PAH are also known to adversely affect survival, growth, and reproduction of many aquatic species. This study assessed the effects of forest wildfires on groundwater from two mountain regions located in protected areas from north and central Portugal. Two campaigns to collect water samples were performed in order to measure PAH levels. Fifteen of 16 studied PAH were found in groundwater samples collected at burned areas, most of them at concentrations significantly higher than those found in control regions, indicating aquifer contamination. The total sum of PAH in burned areas ranged from 23.1 to 95.1 ng/L with a median of 62.9 ng/L, which is one- to sixfold higher than the average level measured in controls (16.2 ng/L). In addition, in control samples, the levels of light PAH with two to four rings were at higher levels than heavy PAH with five or six rings, thus showing a different profile between control and burned sites. The contribution of wildfires to groundwater contamination by PAH was demonstrated, enabling a reliable assessment of the impacts on water quality and preparation of scientifically based decision criteria for postfire forest management practices.

Wildfires, both natural and synthetic, are a major international concern with a tremendous impact on environment, the economy, tourism, society, and human health.

Portugal faces the risk of wildfires every summer, and the situation is getting worse due to heat waves, dry weather, and erratic rains. In 2013, seven firefighters died, dozens were injured, and hundreds of individuals were evacuated and severely affected socially and economically. In response to the risks of forest fire, it is therefore important to have integrated

strategies and policies capable for forest fire prevention and remediation (Forest Europe Liaison Unit Oslo, 2010; European Forest Fire Information System [EFFIS], 2013).

Natural waters are severely affected by wildfires. Erosion, ash deposition, soil hydrophobicity, landslides, and flooding are some of the biggest concerns after a fire that alters the quality of water. Independent of fire type and intensity, the combustion process generates vast amounts of carbon dioxide and several groups of pollutants, including

dioxins, dibenzofurans, and polycyclic aromatic hydrocarbons (PAH) (Austin et al, 2001; Lemieux, 2004). Due to their potential adverse effects on humans and wildlife, PAH are registered on European and American lists of priority pollutants that need to be monitored in the environment (U.S. Environmental Protection Agency [EPA], 2008). There is concern regarding PAH relating to toxicity, carcinogenicity, environmental long-term persistence, widespread occurrence, long-range transportation, and tendency to bioaccumulate (Smith et al., 2011a; International Agency for Research on Cancer [IARC] and World Health Organization [WHO], 2010), which resulted in classification as persistent organic pollutants (POP). It is also important to consider that in natural waters, PAH may undergo various transformations such as volatilization and photochemical degradation; these physicochemical properties are responsible for different interactions with suspended matter, sediments, and biota.

Regarding water quality, PAH were firstly considered priority hazardous substances by Decision No. 2455/2001/EC of the European Parliament and of the Council of 20 November 2001, which became Annex X of the Water Framework Directive (2000/60/EC). This list was replaced by Annex II of the Directive on Environmental Quality Standards (Directive 2008/105/EC), also known as the Priority Substances Directive, subsequently reviewed by the European Commission (EC) in 2012 (COM(2011) 876 final). The European Commission proposal concerned evaluation of the list of priority substances in the field of water policy, where chemicals were identified among those presenting a significant risk to or via the aquatic environment at European Union (EU) level.

In environmental water analysis, one of the most critical steps involved in determination of these contaminants is sample pre-treatment, which needs to include an accurate procedure for extraction, isolation, and concentration of the analytes. Currently, there are several "environmentally friendly" extraction procedures available, but solid-phase extraction (SPE) continues to be one of the

most reliable methodologies, allowing for high enrichment factors. Therefore, SPE coupled with gas chromatography/mass spectrometry (GC/MS) is commonly accepted as one of the most powerful techniques for organic pollutants analysis, even in the nanogram (ng) range (Alder et al., 2006; Viglino et al, 2008). In this study, a multiresidue method for detection and quantification of trace levels of PAH in water matrices was optimized and validated following international recommendations (International Conference on Harmonisation [ICH], 1995, 1997, 2005; Food and Drug Administration [FDA], 2001; National Committee for Clinical Laboratory Standards [NCCLS], 2002; Clinical and Laboratory Standards Institute [CLSI], 2006). Unequivocal analytical data require a specific set of validation criteria and method performance verification to ensure international acceptance of analytical results. Matrix-standard calibration solutions were used to avoid matrix-induced chromatographic response enhancement. It is noteworthy that verified heteroscedasticity was supplanted by a weighted least-squares linear regression model application (WLSLR) (Mansilha et al., 2010; Miller and Miller, 2005) that provides unbiased estimative for prediction, calibration, and optimization when standard deviations of data random errors are not constant across all levels of the explanatory variables.

Several studies demonstrated the influence of forest fires on air quality (Okuda et al., 2002), sediments and soil (Kim et al., 2011; Vergnoux et al., 2011), and riverine waters (Olivella et al, 2006), but, to the best of our knowledge, there are few investigations on the impact of extensive forest fires on groundwater contamination by PAH, as well as on the influence of climatic conditions and time elapsed since the last fire.

The aim of this study was to determine levels of PAH in groundwater samples from two sectors located in mountain regions of two Portuguese protected areas where forest wildfires exerted a devastating effect (Figures 1 and 2): Serra da Estrela (Central Portugal) and Serra do Gerês (North Portugal). Unburned areas were also selected for water sampling and considered as controls.

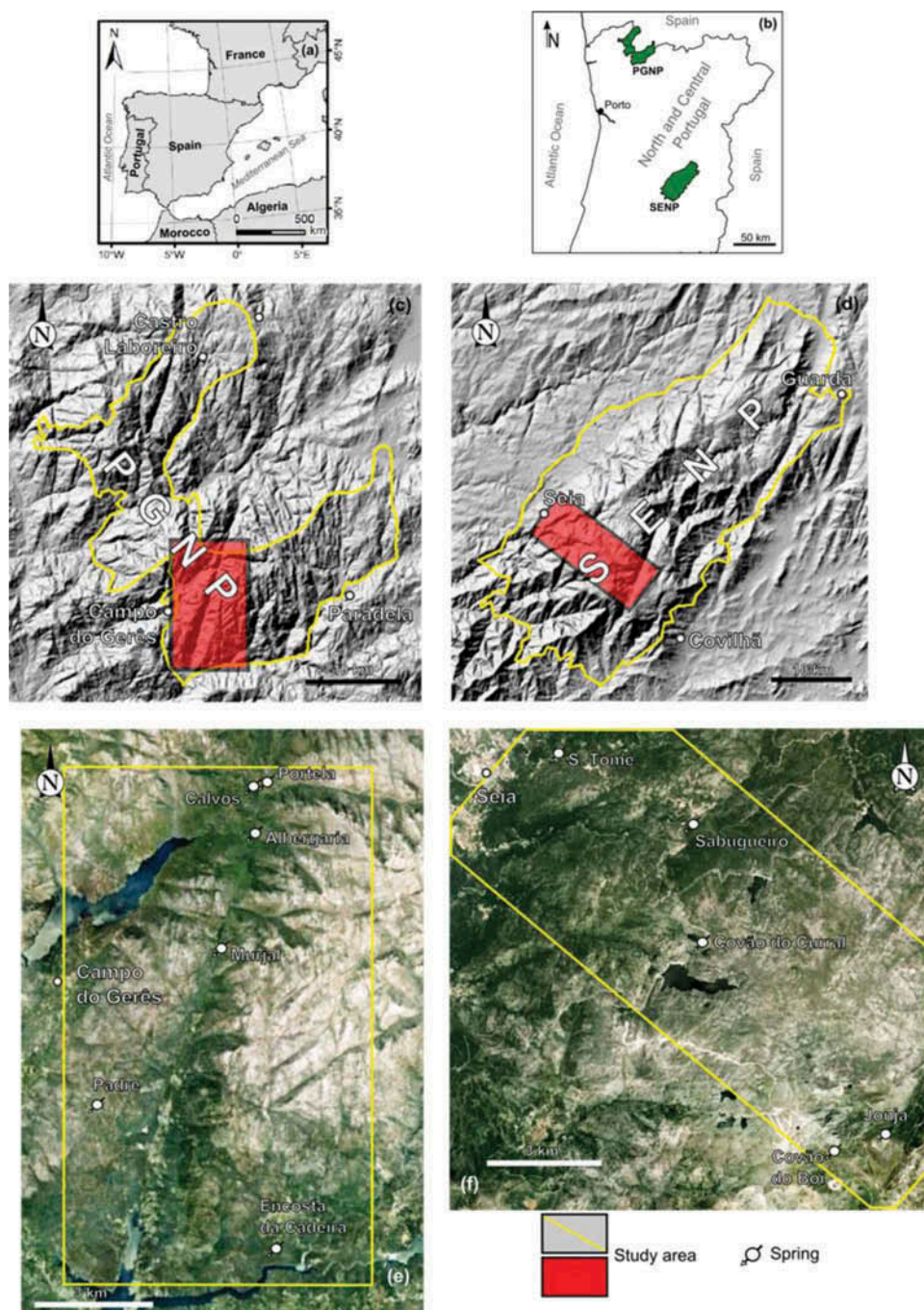


FIGURE 1. Location of the PGNP and SENP protected areas (a, b, c, and d). Location of the studied sectors (c, d, e, and f). Location of the water points (e and f). (Satellite images from Google Earth.)

MATERIAL AND METHODS

Chemicals and Reagents

PAH calibration mix (naphthalene, Nap; acenaphthylene, Acy; acenaphthene, Ace; fluorene, Flu; phenanthrene, Phe;

anthracene, Ant; fluoranthene, Flt; pyrene, Pyr; benz[a]anthracene, BaA; chrysene, Chr; benzo[b]fluoranthene, BbF; benzo[k]fluoranthene (BkF); benzo[a]pyrene, BaP; dibenz[a,h]anthracene, DahA; benzo[ghi]perylene, BghiP; and indeno[1,2,3-cd]pyrene,

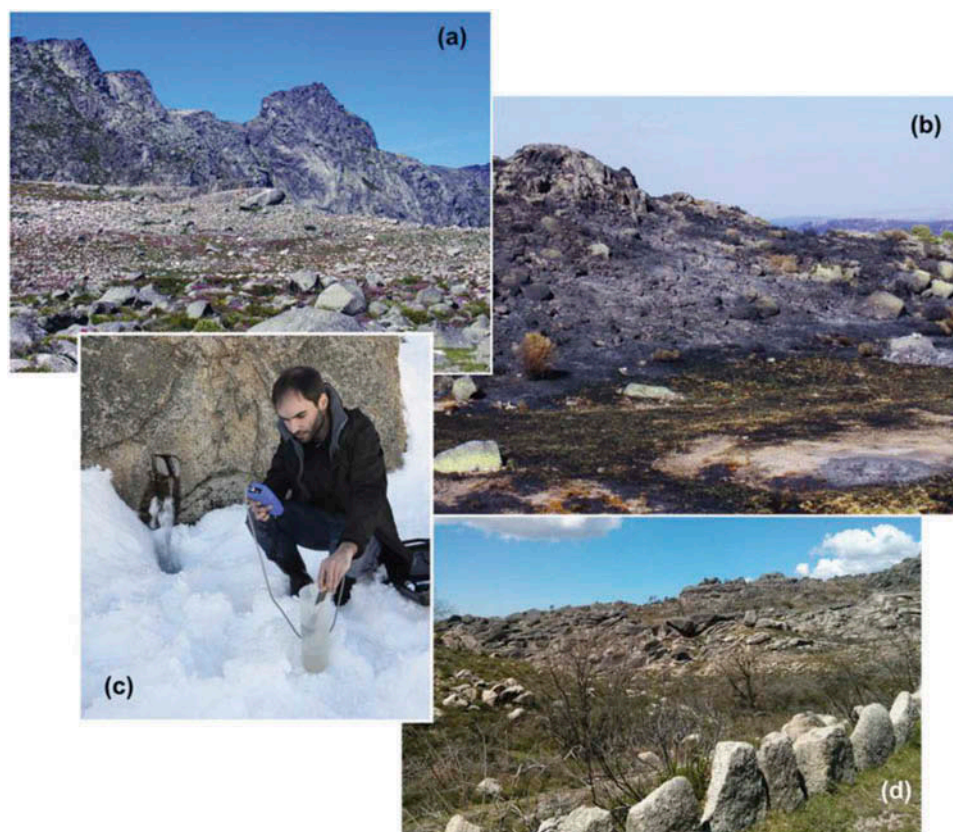


FIGURE 2. Some aspects from the study sites: landscape from Serra da Estrela showing loss of vegetation as a consequence of recurrent wildfires (a); recently burned slope at Serra da Estrela (b); field measurements at Covão do Boi spring (c); vegetation cover recovery in a burned area at Serra do Gerês (d).

TABLE 1. Quantitation and Identification Ions for the GC-MS Analyses of Selected PAHs

	RT (min)	Quantitation ions (m/z)	Identification ions (m/z)
Naphthalene (Nap)	5.293	128	127; 128; 129
Acenaphthylene (Acy)	6.933	152	151; 152; 153; 154
Acenaphthene (Ace)	7.153	154	151; 152; 153; 154
Fluorene (Flu)	7.973	166	165; 166; 167
Phenanthrene (Phe)	9.927	178	176; 178; 179
Anthracene (Ant)	10.033	178	176; 178; 179
Fluoranthene (Flt)	12.220	202	101; 202; 203
Pyrene (Pyr)	12.615	202	101; 202; 203
Benz[a]anthracene (BaA)	14.733	228	226; 228; 229
Chrysene (Chr)	14.790	228	226; 228; 229
Benzo[b]fluoranthene (BbF)	16.716	252	126; 252; 253
Benzo[k]fluoranthene (BkF)	16.784	252	126; 252; 253
Benzo[a]pyrene (BaP)	17.457	252	126; 252; 253
Indeno[1,2,3-cd]pyrene (Ind)	19.886	276	138; 139; 276; 277; 278
Dibenz[a,h]anthracene (DahA)	19.986	278	138; 139; 276; 277; 278
Benzo[ghi]perylene (BghiP)	20.493	276	138; 139; 276; 277; 278

Note. RT, retention time.

TABLE 2. Method Validation Data With Calibration Parameters

	<i>b</i>	<i>a</i>	<i>r</i>	$\sum\%ER$	LD (ng/L)	LQ (ng/L)
Naphthalene (Nap)	710.6	1356.0	0.9998	12.2	0.9	3.1
Acenaphthylene (Acy)	1337.6	2327.5	0.9992	15.8	2.9	9.6
Acenaphthene (Ace)	903.2	1048.2	0.9999	4.7	1.1	3.7
Fluorene (Flu)	1130.0	1397.1	0.9999	4.5	1.0	3.3
Phenanthrene (Phe)	1978.2	48683.5	0.9998	6.7	1.6	5.3
Anthracene (Ant)	1588.2	-3195.9	0.9999	4.5	1.0	3.4
Fluoranthene (Flt)	2332.2	7156.2	0.9997	9.9	2.1	6.9
Pyrene (Pyr)	2464.5	4428.4	0.9998	6.9	4.2	13.9
Benz[a]anthracene (BaA)	1306.5	-6476.7	0.9999	4.4	0.9	2.9
Chrysene (Chr)	1472.9	665.8	0.9997	6.1	1.0	3.4
Benzo[b]fluoranthene (BbF)	1091.3	-5893.0	0.9997	9.8	1.8	5.9
Benzo[k]fluoranthene (BkF)	1121.4	-2839.0	0.9998	5.0	0.8	2.7
Benzo[a]pyrene (BaP)	1204.7	-5774.1	0.9999	8.5	1.1	3.6
Dibenz[a,h]anthracene (DahA)	834.0	-6032.8	0.9998	8.8	1.5	5.0
Benzo[ghi]perylene (BghiP)	960.9	-7693.7	0.9999	8.0	0.7	2.3
Indeno[1,2,3-cd]pyrene (Ind)	819.0	-5047.0	0.9997	12.8	1.6	5.3

Note. *b*, Slope; *a*, weighted intercept; *r*, weighted correlation coefficient; $\sum\%ER$, sum of relative errors; *LOD*, limit of detection of the method; *LOQ*, limit of quantification of the method.

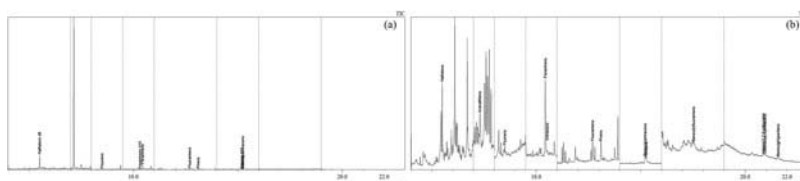


FIGURE 3. Chromatographic profiles of two samples collected in Serra da Estrela, in an unburned area (a) and in a burned one (b).

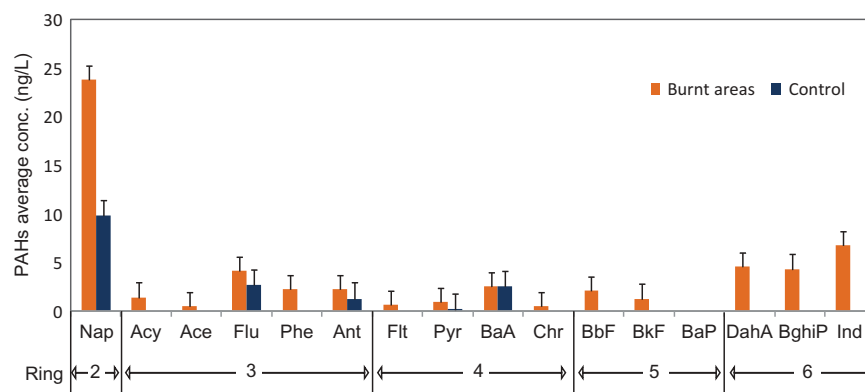


FIGURE 4. Average concentrations of PAH (individual fractions) in the burned ($n = 9$) and unburned (control) areas ($n = 2$).

Ind) was purchased from Sigma-Aldrich (Steinheim, Germany) (Figure 3). Methanol, dichloromethane, and acetonitrile were organic trace analysis grade SupraSolv and were obtained from Merck (Darmstadt, Germany). Ultrapure water was highly purified

by a Milli-Q gradient system (18.2 $m\Omega$ -cm) from Millipore (Milford, MA).

For calibration purposes, a stock standard solution was prepared in acetonitrile by dilution of PAH mixture to a concentration of 1000 $\mu\text{g/L}$. Matrix-standard calibration solutions

(residue-free matrix spiked with standards), at concentration levels ranging from 0.01 $\mu\text{g/L}$ to 0.1 $\mu\text{g/L}$ per compound, were prepared by spiking 500 ml water with different volumes of the 1000 $\mu\text{g/L}$ stock solution just before extraction.

SPE-GC/MS Conditions

SPE was conducted in an SPE vacuum manifold system using Strata PAH cartridges from Phenomenex (Torrance, CA). SPE conditions were as follows: (a) conditioning step, by the sequential addition of 10 ml dichloromethane, 10 ml methanol, and 20 ml Milli-Q water at a flow rate of 1 ml/min; (b) loading step, by passing the sample/standard through the cartridges at a flow rate of 5 ml/min; (c) washing step, by rinsing the cartridge with 3 ml water/methanol 1:1 and dried by vacuum pressure during approximately 30 s; and (d) elution performed with 2×3 ml dichloromethane, at a flow of 1 ml/min. After elution, the organic phase was transferred to a new tube, evaporated to dryness in a rotative evaporator (Buchi/Brinkman Rotavapor RE-111 and Water Bath B-461), and reconstituted within acetonitrile to a final volume of 500 μl .

Chromatographic analyses were carried out in a Shimadzu GCMS-QP2010 gas chromatograph mass spectrometer equipped with an auto injector AOC-5000. Injections (1 μl) were conducted in the splitless mode with a 1-min purge-off time and injector temperature set at 280°C. Helium (99.9999%) at a constant flow rate of 1.5 ml/min was used as the carrier gas.

Samples were analyzed using a fused-silica capillary column, Zebron ZB-5MS (30 m \times 0.25 mm ID, 0.25 μm film thickness), with the following oven program temperature: initial temperature 70°C (held for 2 min), increased by 25°C/min to 180°C (held for 2 min), increased by 15°C/min to 280°C (held for 2 min), and increased again by 10°C/min to 300°C, and held at this temperature for 5 min.

Positive fragment ions (m/z , ions mass/charge ratio) were analyzed over 45–500 m/z mass range in full scan mode and in selected-ion monitoring (SIM) mode.

Instrument control and mass spectrometry data were managed by a personal computer running the LabSolutions GCMS software (2.50 SU3 version). The optimized methodology was applied for environmental water samples analysis.

Samples Collection

Two campaigns to collect water samples were performed in order to measure PAH concentrations with time. The studied sectors are located in the so-called Iberian Massif (Farias et al., 1987, Ribeiro et al., 2007): Serra do Gerês sector is located in the Galicia Trás-os-Montes Zone and Serra da Estrela sector is located in the Central-Iberian Zone. In both cases, geological setting is dominated by occurrence of variscan granitic rocks, with minor areas corresponding to metasedimentary rocks and sedimentary cover (Ferreira et al., 1987; Dias et al., 1998).

The altitude of the Serra do Gerês sector varies from around 400 m above sea level (a.s.l.) to 1200 m a.s.l. According to the Köppen–Geiger climate classification, this region has a Csb climate (warm temperate, with dry and warm summers), the same as north-western Iberia (AEMET-IM, 2011). Information regarding air temperature and precipitation is scarce. The annual precipitation at the Gerês meteorological station (370 m a.s.l.) is around 2994 mm; at the Albergaria meteorological station (800 m a.s.l.) it reaches 3300 mm, while in the upper areas of the mountain it may reach 3500 mm/yr (Daveau et al., 1977; Mendes and Bettencourt, 1980; INMG, 1990). The mean annual air temperature at the Gerês station is 14°C; in August the mean is 21°C and in January the mean is 8°C (Mendes and Bettencourt, 1980). Daveau et al. (1985) estimated that in the upper area of the mountain, the mean minimal air temperature was under 1°C during the coldest month. For the same area, the mean maximal air temperature of the warmest month was less than 23°C.

The altitude of the Serra da Estrela sector ranges from 500 m a.s.l. to 1993 m a.s.l.

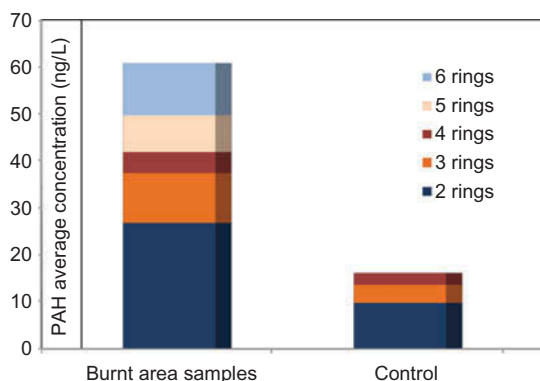


FIGURE 5. Average PHA profiles of the samples collected in burned and control areas according to their structural composition (number of benzene rings).

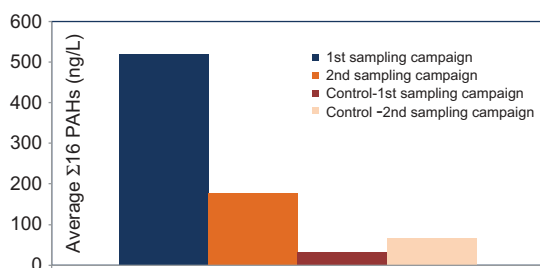


FIGURE 6. Temporal variations on PAHs concentrations (average $\Sigma 16$ PAHs).

According to the Köppen–Geiger climate classification, the Serra da Estrela region has a Csb climate (warm temperate, with dry and warm summers; AEMET-IM, 2011). Yet the southern part of the mountain has a climate influence

of Csa subtype (warm temperate, with dry and hot summers). Mean annual precipitation is approximately 2500 mm in the uppermost areas, and mean annual air temperatures are below 7°C in most of the plateau area (Daveau et al., 1997, Espinha Marques et al., 2011). Mean annual air temperature may be as low as 4°C near the summit.

The sampling points (Figure 1) consisted of springs from water-table aquifers from areas affected by wildfires (5 in Serra do Gerês and 4 in Serra da Estrela)—hence the interest in determining the content of the 16 PAH listed by the U.S. EPA as priority pollutants. Samples from unburned areas (Murjal Spring and Covão do Boi Spring) were also collected and used as control. The criteria to select the groundwater points were that (i) water needs to flow throughout the year and (ii) springs need to be located far from industrial or residential areas and upstream from roads, in order to avoid PAH contamination from road traffic.

Sampling took place in spring 2011 in Serra da Estrela and in summer 2012 in Serra do Gerês. A second sampling campaign was performed with a year interval, after intense precipitation conditions. Water samples were collected in glass amber bottles (Figure 2) and refrigerated at 4°C until analysis. Water pH, electrical conductivity, and temperature were measured in situ at the moment of sampling.

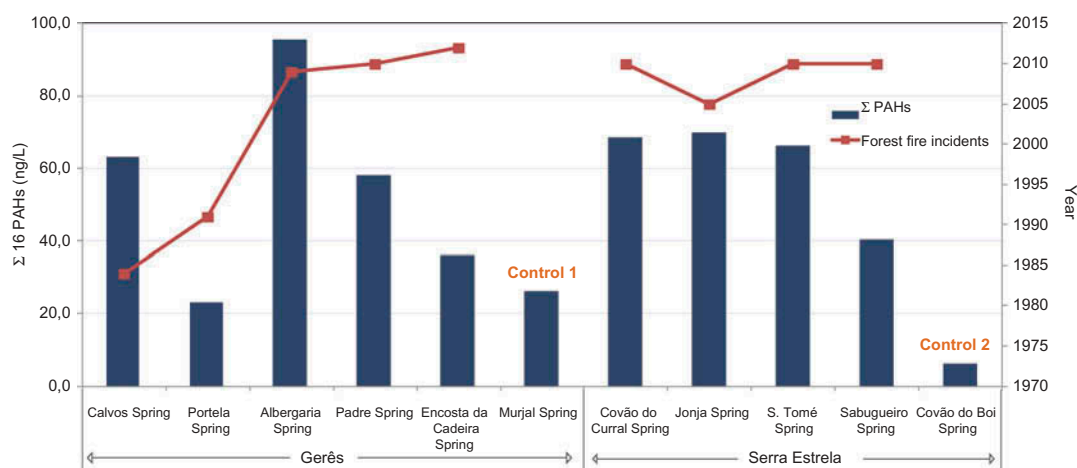


FIGURE 7. Sum of PAHs concentrations in samples collected at Serra da Estrela and Serra do Gerês and time elapsed since the last fire.

RESULTS AND DISCUSSION

Optimization and validation of the methodology for PAH analysis were conducted and results presented were according to method performance acceptability criteria. Analytes were identified by both their chromatographic characteristics, as retention time (RT), and through their specific fragmentation. Programs were developed in the SIM mode based on detection of selected ions for each analyte (Table 1). A multiresidue method was selected to enable simultaneous analysis of several compounds.

Specificity and selectivity were evaluated by comparing the chromatograms of matrix-blank samples with an aqueous solution of analytes at concentrations near the limits of quantification (LOQ). No significant interferences were detected at RT of the analyzed PAH. Selectivity was also assessed by comparison of the analytes mass spectra with spectra from libraries. Calibration parameters are presented in Table 2.

Fifteen of the 16 PAH were found in groundwater samples collected in burned areas, most of them at concentrations significantly higher than those present in control areas, which indicates aquifer contamination (Figure 3). Average PAH concentrations (individual fractions) are shown in Figure 4. As noted, the PAH Nap, Flu, Ant, BaA, DahA, BghiP, and Ind appeared to be the predominant pollutants produced.

Regarding the total sum of PAH ($\Sigma 16$ PAH) in burned areas, values ranged from 23.1 to 95.1 ng/L, with a median of 62.9 ng/L, values that were one- to sixfold higher than the average level measured in controls (16.2 ng/L). In addition in control samples, the levels of light PAH with two to four rings were markedly higher than for heavy PAHs with five or six rings, with Nap the most abundant compound (60% of the total concentrations). In forest fires samples, Nap contributed 41%, while DahA, BghiP, and Ind contributed approximately 27%, thus showing a different profile in chemicals between burned and control locations (Figure 5).

Temporal variations on PAH concentration were also evaluated. A second campaign took place 1 year after the first one after heavy rainfalls that occurred 2–3 months earlier and results are shown in Figure 6. The decline of PAH with time, ranging from 10 to 30.5 ng/L, may be attributed to a dilution effect rather than biodegradation, since these compounds are known to be persistent. Similar results were found by Olivella et al. (2006) with respect to PAH in riverine waters. These data are in agreement with values found at each sampling site taking into account time elapsed since the last fire (Figure 7).

The contribution of wildfires to the content of PAH in groundwater was demonstrated, as well as climatic conditions as a confounding factor on PAH levels detected. As water supplies may be vulnerable to disruption, increasing knowledge on water quality alterations due to forest fires is essential for development of decision criteria into management practices. This would enable scientists and stakeholders to work together to formulate effective management practices (Smith et al., 2011a, 2011b). These studies allow for a definition and presentation of a more accurate official list of organic pollutants, which is essential to propose new mechanisms for water treatment, in order to ensure quality and permit new environmental remediation strategies and human health promotion.

REFERENCES

- AEMET-IM. 2011. *Iberian climate atlas, air temperature and precipitation (1971–2000)*. http://www.ipma.pt/resources.www/docs_pontuais/ocorrencias/2011/atlas_clima_iberico.pdf
- Alder, L., Greulich, K., Kempe, G., and Vieth, B. 2006. Residue analysis of 500 high priority pesticides: Better by GC-MS or LC-MS/MS? *Mass Spectrom. Rev.* 25: 838–865.
- Austin, C. C., Wang, D., Ecobichon D. J., and Dussault, G. 2001. Characterization of volatile organic compounds in smoke at municipal structural fires. *J. Toxicol. Environ. Health A* 63: 437–458.

- Clinical and Laboratory Standards Institute. 2006. Statistical quality control for quantitative measurement procedures: Principles and definitions. Approved guideline, 3th ed., C24–A3. CLSI. http://shopping.netsuite.com/c.1253739/site/Sample_pdf/C24A3_sample.pdf
- Daveau, S., Coelho, C., Costa, V. G., and Carvalho, L. 1977. Répartition et rythme des précipitations au Portugal (Distribution and rhythm of precipitation in Portugal). Lisbon, Portugal: CEG [in French].
- Dias, G., Leterrier, J., Mendes, A., Simões, P., and Bertrand, J. 1998. U-Pb zircon and monazite geochronology of post-collisional Hercynian granitoids from the Central Iberian Zone (northern Portugal). *Lithos* 45: 349–369.
- Espinha Marques, J., Samper, J., Pisani, B., Alvares, D., Carvalho, J. M., Chaminé, H. I., Marques, J. M., Vieira, G. T., Mora, C., and Borges, F. S. 2011. Evaluation of water resources in a high-mountain basin in Serra da Estrela, central Portugal, using a semi-distributed hydrological model. *Environ. Earth Sci.* 62:1219–1234.
- European Forest Fire Information System. 2013. European Forest Fire Information System Supporting the Member States in forecasting forest fire danger and assessing fire damage. <http://ies.jrc.ec.europa.eu/our-activities/support-for-member-states/forest-fire-information.html> (accessed 15 October 15, 2013).
- Food and Drug Administration. 2001. *Guidance for industry—Bioanalytical method validation*. Washington, DC: U.S. Department of Health and Human Services.
- Farias, P., Gallastegui, G., Gonzalez Lodeiro, F., Marquinez, J., Martin Parra, L. M., Martínez Catalan, J. R., de Pablo Maciá, J. G., and Rodriguez Fernandez, L. R. 1987. Aportaciones al conocimiento de la litoestratigrafía y estructura de Galicia Central. In *IX Reunião de Geologia do Oeste Peninsular, Porto, 1985. Mem. Mus. Labor. miner. geol. Fac. Ciênc. Univ. Porto 1*, 411–431.
- Ferreira, N., Iglésias, M., Noronha, F., Pereira, E., Ribeiro, A., and Ribeiro, M. L. 1987. Granitóides da Zona Centro Ibérica e seu enquadramento geodinâmico. In *Geología de los Granitoides y Rocas Asociadas del Macizo Hesperico*, ed. F. Bea, A. Carnicero, J. Gonzalo, M. Lopez Plaza, and M. Rodriguez Alonso, 37–51. Madrid, Spain: Editorial Rueda, Madrid, Libro de Homenaje a L.C. García de Figuerola.
- Forest Europe Liaison Unit Oslo. 2010. *Assessment of forest fire risks and innovative strategies for fire prevention*. Workshop report, Ministerial Conference on the Protection of Forests in Europe. 4–6 May 2010 Rhodes, Greece.
- International Agency for Research on Cancer (IARC) and World Health Organization (WHO). 2010. *Some non-heterocyclic polycyclic aromatic hydrocarbons and some related exposures*. IARC Working Group on the Evaluation of Carcinogenic Risks to Humans, vol. 92. Geneva, Switzerland.
- International Conference on Harmonisation. 1995. Validation of analytical methods definitions and terminology, Q2A guideline. <http://www.fda.gov/Drugs/GuidanceComplianceRegulatoryInformation/Guidances/ucm065005.htm>
- International Conference on Harmonisation. 1995. Validation of analytical procedures: methodology (CPMP/ICH/281/95) Q2B. <http://www.fda.gov/Drugs/GuidanceComplianceRegulatoryInformation/Guidances/ucm065005.htm>
- International conference on harmonisation. 2005. Harmonised tripartite guideline. Validation of analytical procedures: Text and methodology Q2(R1). <http://www.fda.gov/Drugs/GuidanceComplianceRegulatoryInformation/Guidances/ucm065005.htm>
- Kim, E. J., Choi, S. D., and Chang, Y. S. 2011. Levels and patterns of polycyclic aromatic hydrocarbons (PAHs) in soils after forest fires in South Korea. *Environ. Sci. Pollut. Res.* 18:1508–1517.
- Lemieux, P. M. 2004. United States Environmental Protection Agency Project Summary. Center for Environmental Research Information. Cincinnati, OH45268. Emissions of organic air toxics from open burning. Project

- Summary. National Risk Management Research Laboratory. Research and Development, EPA/600/SR-02/076.
- Mansilha, C., Melo, A., Rebelo, H., Ferreira, I. M. P. L. V. O., Pinho, O., Domingues, V., Pinho, C., and Gameiro, P. 2010. Quantification of endocrine disruptors and pesticides in water by gas chromatography-tandem mass spectrometry. Method validation using weighted linear regression schemes. *J. Chromatogr. A* 1217: 6681–6691.
- Mendes, J. C., and Bettencourt, M. L. 1980. Contribuição para o estudo do balanço climatológico de água no solo e classificação climática de Portugal Continental. In *O Clima de Portugal*, (ed. Inst. Nac. Met. Geof.), 24: 1–289, Lisbon.
- Miller, J. N., and Miller, J. C. 2005. *Statistics and chemometrics for analytical chemistry*, 5th ed. Essex, England: Pearson Education Limited.
- National Committee for Clinical Laboratory Standards. 2002. Approved guideline, C43-A. Gas chromatography/mass spectrometry (GC/MS) confirmation of drugs. <http://clsi.org>
- Okuda, T., Kumata, H., Zakaria, M. P., Naraoka, H., Ishiwatari, R., and Takada, H. 2002. Source identification of Malaysian atmospheric polycyclic aromatic hydrocarbons nearby forest fires using molecular isotopic compositions. *Atmos. Environ.* 36: 611–618.
- Olivella, M. A., Ribalta, T. G., Febrer, A. R., Mollet, J. M., and Heras, F. X. C. 2006. Distribution of polycyclic aromatic hydrocarbons in riverine waters after Mediterranean forest fires. *Sci. Total Environ.* 355: 156–166.
- Ribeiro, A., Munhá, J., Dias, R., Mateus, A., Pereira, E., Ribeiro, L., Fonseca, P. E., Araújo, A., Oliveira, J. T., Romão, J., Chaminé, H. I., Coke, C., and Pedro, J. 2007. Geodynamic evolution of the SW Europe Variscides. *Tectonics* 26(TC6009): 1–24. doi:10.1029/2006TC002058
- Smith, H. G., Sheridan G. J., Lane, P. N. J., Nymana, P., and Haydon, S. 2011a. Wildfire effects on water quality in forest catchments: A review with implications for water supply. *J. Hydrol.* 396: 170–192.
- Smith, H., Cawson, J., Sheridan, G., and Lane, P. 2011b. Impact of bushfires on water quality for the Australian government. Department of Sustainability, Environment, Water, Population and Communities. <http://www.environment.gov.au/resource/desktop-review-impact-bushfires-water-quality>
- U.S. Environmental Protection Agency. 2008. *PAH*. Washington, DC: U.S. EPA.
- Vergnoux, A., Malleret, L., Asia, L., Doumenq, P., and Theraulaz, F. 2011. Impact of forest fires on PAH level and distribution in soils. *Environ. Res.* 11: 193–198.
- Viglino, L., Aboulfadl, K., Prevost, M., and Sauve, S. 2008. Analysis of natural and synthetic estrogenic endocrine disruptors in environmental waters using online preconcentration coupled with LC-APPI-MS/MS. *Talanta* 76: 1088–1096.

Water Resources Research



REVIEW ARTICLE

10.1029/2019WR025676

Key Points:

- Mountain-block recharge confirmed as important source of recharge to basin aquifers in a variety of climatic and geologic settings globally
- Recent work advanced understanding of fundamental controls on mountain-block recharge and somewhat improved methods for characterization
- Future research should aim to acquire subsurface data in mountain block and at the mountain front

Correspondence to:

K. H. Markovich,
 khmarkovich@email.arizona.edu

Citation:

Markovich, K., H. Manning, A. H., Condon, L. E., & McIntosh, J. C. (2019). Mountain-block recharge: A review of current understanding. *Water Resources Research*, 55, 8278–8304. <https://doi.org/10.1029/2019WR025676>





Received 29 MAY 2019

Accepted 16 SEP 2019

Accepted article online 16 OCT 2019

Published online 11 NOV 2019

Mountain-Block Recharge: A Review of Current Understanding

Katherine H. Markovich¹ , Andrew H. Manning² , Laura E. Condon¹ , and Jennifer C. McIntosh¹ 

¹Department of Hydrology and Atmospheric Sciences, University of Arizona, Tucson, AZ, USA, ²U.S. Geological Survey, Denver, CO, USA

Abstract Mountain-block recharge (MBR) is the subsurface inflow of groundwater to lowland aquifers from adjacent mountains. MBR can be a major component of recharge but remains difficult to characterize and quantify due to limited hydrogeologic, climatic, and other data in the mountain block and at the mountain front. The number of MBR-related studies has increased dramatically in the 15 years since the last review of the topic was conducted by Wilson and Guan (2004), generating important advancements. We review this recent body of literature, summarize current understanding of factors controlling MBR, and provide recommendations for future research priorities. Prior to 2004, most MBR studies were performed in the southwestern United States. Since then, numerous studies have detected and quantified MBR in basins around the world, typically estimating MBR to be 5–50% of basin-fill aquifer recharge. Theoretical studies using generic numerical modeling domains have revealed fundamental hydrogeologic and topographic controls on the amount of MBR and where it originates within the mountain block. Several mountain-focused hydrogeologic studies have confirmed the widespread existence of mountain bedrock aquifers hosting considerable groundwater flow and, in some cases, identified the occurrence of interbasin flow leaving headwater catchments in the subsurface—both of which are required for MBR to occur. Future MBR research should focus on the collection of high-priority data (e.g., subsurface data near the mountain front and within the mountain block) and the development of sophisticated coupled models calibrated to multiple data types to best constrain MBR and predict how it may change in response to climate warming.

1. Introduction

Hydrologists have long recognized the importance of mountains to global water resources (Bales et al., 2006; Viviroli et al., 2011; Wilson & Guan, 2004). Mountains receive disproportionately large amounts of precipitation due to the orographic effect and deliver this water via streamflow to populated areas at lower elevations. Often, mountain precipitation is stored in snowpack and glaciers, and meltwater maintains critical streamflows during warmer and drier months. What is less well understood, but equally important, is how mountain systems recharge lowland aquifers via mountain-front recharge (MFR) and mountain-block recharge (MBR) processes (Wilson & Guan, 2004). While the specific definitions of MFR and MBR vary in the literature, MFR is generally defined as all water that enters a lowland aquifer with its source in the mountain block. MBR, a component of MFR, is the subsurface inflow of groundwater to the lowland aquifer that comes directly from the mountain block. These sources of recharge can be significant, and in arid regions, MFR is the dominant source of recharge to lowland aquifers (Earman et al., 2006; Scanlon et al., 2006). Despite its importance, MFR estimates are usually poorly constrained, particularly the MBR component, because subsurface hydrogeologic data are limited within mountain blocks and often nonexistent at the mountain front itself.

MBR was first described by Feth (1964), who referred to it as “hidden recharge.” Feth (1964) observed that hydraulic head contours in a basin aquifer in northern Utah, USA, paralleled the adjacent Wasatch Range front, that basin wells near the mountain block exhibited chemistry similar to high elevation springs as opposed to local surface waters, and that water level response in these wells mimicked discharge fluctuations in a nearby mine tunnel. In the decades following, a handful of studies attempted to quantify mountain system recharge, often with conflicting definitions of MFR and MBR, very sparse data, and questionable assumptions. Wilson and Guan (2004) provided a parsimonious set of definitions of MFR, MBR, and their

©2019. The Authors.

This is an open access article under the terms of the Creative Commons Attribution License, which permits use, distribution and reproduction in any medium, provided the original work is properly cited.

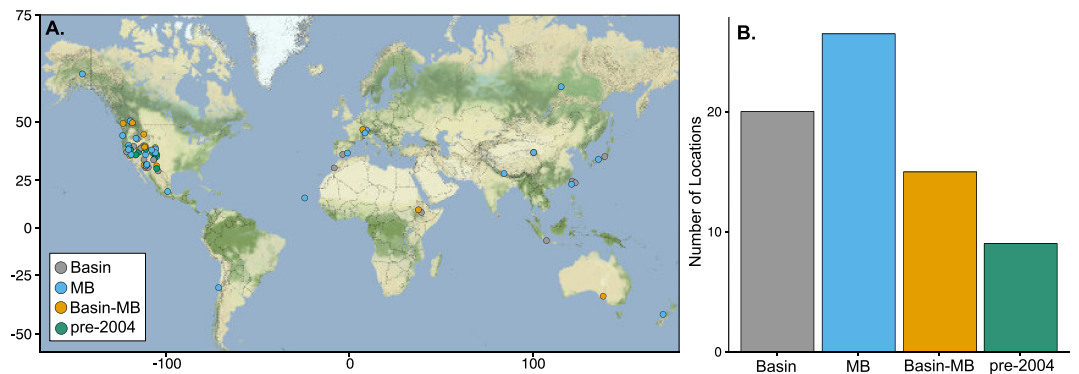


Figure 1. (a) Map of pre- and post-2004 mountain-block recharge studies, colored by type of study: basin-focused (Basin), mountain block-focused (MB), and combined basin-mountain block studies (Basin-MB). (b) Bar chart showing the number of studies by type.

components and compiled and reviewed the handful of MBR estimates published as of 2004. These early MBR estimates were predominantly basin focused (as opposed to mountain focused; see section 3.2), carried large uncertainties, and were all located in the western United States. Since then, numerous MBR-related studies have been performed around the world (Figure 1). Several of these have detected and quantified MBR utilizing a broader and more robust set of methods, confirming that MBR is not a limited regional phenomenon but instead an important component of recharge to many lowland aquifers globally.

Our motivation for presenting an updated review of MBR research is twofold. First, a considerable amount of work has occurred since the MFR review paper by Wilson and Guan (2004), leading to important advances in our understanding of MBR. A need exists to synthesize this work and summarize our current understanding in order to better focus future research efforts. Second, there is a growing urgency to understand and predict how climate and land use change is altering the timing and amount of recharge from mountain systems (Beniston et al., 1997; Meixner et al., 2016; Niraula et al., 2017a, 2017b; Viviroli et al., 2011). To date, the focus of research aimed at understanding the effects of climate change on mountain hydrology has largely been on surface water resources, where peak flows are shifting earlier (Barnett et al., 2005; Cayan et al., 2001; Cayan et al., 2008; Christensen et al., 2004; Stewart et al., 2005) and snowpack and streamflow volumes are on the decline (Luce & Holden, 2009; Mote et al., 2005; Musselman et al., 2017; Zapata-Rios et al., 2016). Studies of potential impacts to mountain groundwater are more limited but suggest that projected warming and reduction of snowpack will likely decrease recharge to many mountain aquifers (e.g., Manning et al., 2012; Meixner et al., 2016). This decrease could clearly impact MBR, though uncertainties in specific mountain recharge processes, potential feedbacks, and routing of groundwater through the mountain block mean that the magnitude and timescales of such impacts remain largely unknown. Distinguishing MBR from other MFR contributions infiltrating at lower elevation directly through the basin fill has always been necessary for developing effective groundwater source protection strategies for lowland aquifers. However, distinguishing these different MFR components has recently taken on yet greater importance because the different infiltration locations and residence times of these components mean that they could respond very differently to changing future mountain hydrologic conditions.

2. Conceptual Background and Definitions

A consistent conceptualization of MBR and associated set of definitions are important to allow scientists to effectively communicate and build on existing work. We believe the conceptual framework and definitions put forward by Wilson and Guan (2004) generally remain relevant and should continue to be applied in future work. We therefore describe them below only briefly, with the exception of some definition modifications discussed in more detail.

A *mountain block* is an area of topographically elevated and rugged terrain where soils and unconsolidated sediment are thin to nonexistent, such that the shallow subsurface is composed predominantly of bedrock. A mountain block is thus topographically and geologically distinct from adjacent lowland areas, which are relatively flat and underlain by thick unconsolidated to semiconsolidated sediments (henceforth “basin fill”) that often form highly productive aquifers. Note that a mountain block consists of both bedrock and

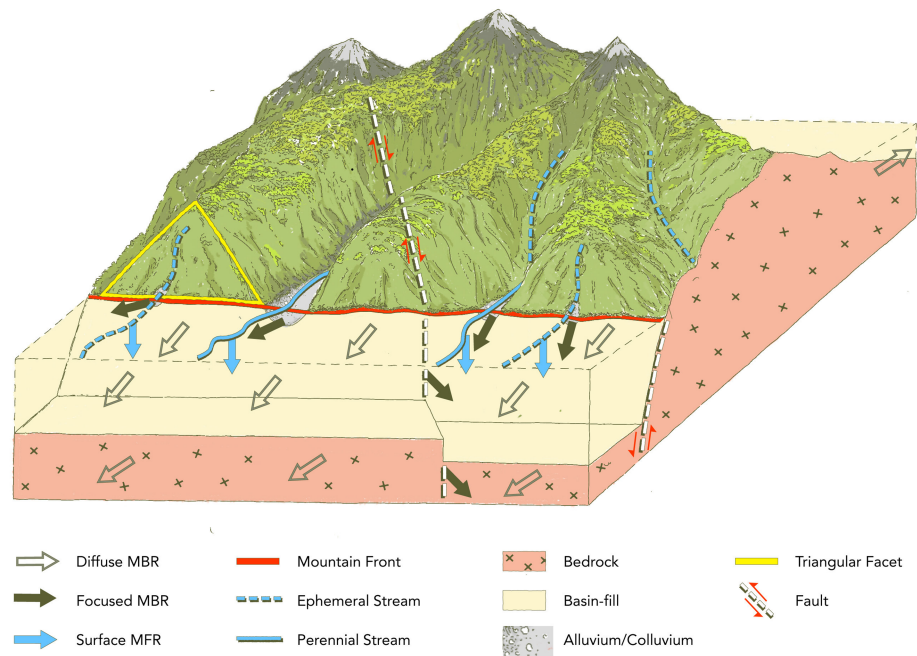


Figure 2. Conceptual diagram showing two mountain fronts: a sedimentary contact (far side) between the mountain block and basin fill and a fault-controlled contact (near side). Different components of mountain-front recharge (MFR) and mountain-block recharge (MBR) are also shown, including surface MFR or infiltration through the basin fill from a mountain-sourced perennial or ephemeral stream; focused MBR, which occurs either through discrete faults and fracture zones or underneath mountain-sourced streams; and diffuse MBR, which occurs widely across the mountain front.

all directly overlying colluvium/alluvium, soils, and vegetation. Mountain blocks can form as a result of multiple geological processes, the most common being uplift in extensional tectonic settings through normal faulting, uplift in compressional tectonic settings through thrust/reverse faulting, and emplacement of igneous rocks through volcanic eruptions.

We define the *mountain front* as the surface trace of the geologic contact between the mountain block and the adjacent basin fill. In other words, it is a linear feature defined by the intersection of two planar features, these being (1) the ground surface and (2) the subsurface geologic contact between the bedrock of the mountain block and the adjacent basin fill. Note that we consider shallow fingers/lenses of alluvium underlying mountain streams to be part of the mountain block (not the basin fill) where they overlie and extend into the mountain block. Our definition of mountain front differs somewhat from that of Wilson and Guan (2004), who define it as the piedmont zone between the mountains and the valley floor. While the transition from mountains to piedmont is in most cases relatively well defined, the transition from piedmont to basin floor may be poorly defined in many basins, particularly those with more human development and heavy vegetation. We therefore believe our definition is preferable because it is conceptually simpler and more easily applied across a wide range of mountain/basin settings. The mountain front may be either fault controlled or a depositional contact, a classic example of these two types being the east and west sides, respectively, of the Sierra Nevada mountain block in California, USA.

MFR is all water that enters a basin-fill aquifer with its source in the mountain block. MFR is composed of two components: surface MFR and MBR. *Surface MFR* is infiltration through the basin fill of mountain-sourced perennial and ephemeral stream water after these streams exit the mountain block (Figure 2). Surface MFR is equivalent to the “focused near-surface” component of MFR as defined by Wilson and Guan (2004) with the modification explained in the following paragraph. Infiltration from mountain-sourced streams occurs near the mountain front because this is where the basin-fill aquifer water table (WT) is commonly well below the land surface (see plate 3 in Wilson & Guan, 2004). We consider the maximum distance from the mountain front that surface MFR can occur to be the point where the WT is

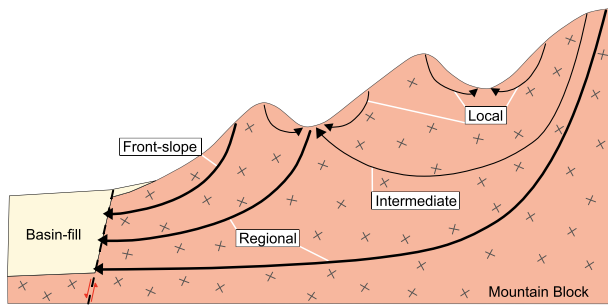


Figure 3. Conceptual diagram showing the four major flowpaths in mountain-block systems: (1) local, which discharges within the same subcatchment as where recharge occurred; (2) intermediate, which bypasses the local stream and discharges at a higher-order stream within the mountain block (often flowing largely perpendicular to the cross-section shown); (3) regional, which bypasses all mountain streams and exits the mountain block in the subsurface, becoming mountain-block recharge; and (4) front-slope flow, which recharges immediately above the mountain front and becomes mountain-block recharge. The mountain-block recharge flowpaths are shown in bold.

no longer predominantly below stream level—that is, where the stream ceases to be predominantly a losing stream. *Mountain-block recharge* is groundwater inflow to a lowland aquifer from an adjacent mountain block. *Diffuse MBR* is spatially broadly distributed and occurs widely across the mountain front. *Focused MBR* occurs through discrete permeable geologic features in the mountain block, such as steeply dipping fault zones or high-permeability sedimentary rock units that strike at a high angle to the mountain front (Figure 2). Focused MBR may also occur near the point where a mountain stream exits the mountain block (or “watershed mouth”) in the unconsolidated material or shallow bedrock underneath the stream. Our consideration of shallow subsurface inflow beneath streams to be MBR is a break from Wilson and Guan (2004), who considered this a component of “focused near-surface” MFR, not MBR. We feel including this component as MBR provides a more logically consistent definition of MBR—that is, MBR is all groundwater that enters the basin aquifer from the mountain block (where the mountain block includes immediately overlying shallow colluvium/alluvium). Further, most studies characterizing MBR do not distinguish deep from shallow flowpaths, so this definition is more in line with current research methods.

A common mistake in the literature is to refer to all recharge that occurs within the mountain block as MBR. As illustrated in Figure 3, groundwater within the mountain block can follow different flowpaths of potentially widely varying depth and length, and importantly, not all flowpaths contribute to MBR. We define four types of flow paths, expanding upon the three types (local, intermediate, and regional) defined by Tóth (1963) and applied to mountain topography in Wilson and Guan (2004) and Gleeson and Manning (2008). Local flow is groundwater that discharges to the nearest stream within the same subwatershed where it recharged. Intermediate flow is groundwater that exits the subwatershed where it recharged through the subsurface and discharges to a lower-elevation stream of higher order than the subwatershed where it recharged. Importantly, intermediate and local flowpaths discharge to the surface system *within* the mountain block and thus do not contribute to MBR. For this reason, we refer to all recharge to mountain aquifers as *mountain aquifer recharge* to distinguish it from MBR. Regional flow follows yet longer flowpaths than intermediate flow and exits the mountain block in the subsurface, thus becoming MBR. Here, we propose a fourth type of flow, *front-slope flow*, which is recharged on the slopes immediately above the mountain front between the mouths of major mountain watersheds (i.e., within triangular facets, Figure 2) and flows directly to the basin-fill aquifer as MBR. A unique definition for this flow path is justified because it does not neatly fall within one of the other three definitions above, and recent modeling studies suggest that it may be a major contributor to MBR (Welch & Allen, 2012; Manning & Solomon, 2005). In summary, regional and front-slope flows contribute to MBR, but local and intermediate flows do not.

3. MBR Review

A literature search revealed >200 studies since 2004 that mention MBR and/or cite the review by Wilson and Guan (2004). We refined this group (also adding some studies) by selecting those that attempt to distinguish, characterize, or quantify MBR or that conduct research directly related to it (e.g., estimating deep percolation and interbasin flow in headwater catchments). This resulted in 74 MBR studies, falling in four categories: (1) model-based conceptual studies; (2) basin-focused studies, which rely mainly on the relative wealth of data from wells in the basin-fill aquifer to estimate MBR; (3) mountain-focused studies, which directly examine mountain aquifers, mountain aquifer recharge, and mountain-block groundwater flow; and (4) combined mountain-basin studies. Here, we provide an updated review of MBR studies published since 2004, organized by the aforementioned categories, as well as an overview of studies addressing potential human impacts to MBR. All quantitative MBR estimates presented in these studies are presented in Table 1.

3.1. Conceptual Studies

Gleeson and Manning (2008) used an integrated hydrologic model of a three-dimensional mountainous domain to test how different topographic and hydrogeologic variables affect the relative proportions of

Table 1
Mountain Block Recharge Estimates Organized by Type of Study

Location	Authors	Type	Method	MBR amount		Climate ^a	Dominant MB lithology
				Acquifer-scale estimate	Mountain aquifer recharge		
Spanish Springs Valley, NV, USA	Schaefer et al. (2007)	Basin	MODFLOW	13.5%	—	Cold semiarid	Metasedimentary and intrusive
Eagle Springs Valley, NV, USA	Schaefer et al. (2007)	Basin	MODFLOW	28%	—	Cold semiarid	Metasedimentary and intrusive
Grenchen Basin, Switzerland	Althaus et al. (2009)	Basin	NGTs, SIs, and age tracers	—	9% (0–91%)	Temperate oceanic	Karst
Southeastern Española Basin, NM, USA	Manning (2011)	Basin	NGTs and radiocarbon	—	24% (0–50%)	Cold semiarid	Metasedimentary and intrusive
Kanto Plain, Japan	Liu and Yamanaka (2012)	Basin	SIs and chemistry	—	22% (0–100%) ^b	Humid subtropical	Sedimentary
Middle Rio Grande Basin, NM, USA	Bexfield et al. (2016)	Basin	MODFLOW	6–25%	—	Cold semiarid	Intrusive and metamorphic overlain by karst
Langyang Plain, Taiwan	Peng et al. (2016)	Basin	SIs and chemistry	—	12% (0–35%)	Humid subtropical	Metasedimentary
Eastern Coastal Plain, Taiwan	Peng et al. (2018)	Basin	SIs and chemistry	—	33% (22–54%) ^c	Humid subtropical	Metamorphic
Dry Creek Watershed, ID, USA	Aishlin and McNamara (2011)	MB	Chloride mass balance	—	—	Cold semiarid	Intrusive
Qilian Mountains, China	Yao et al. (2017)	MB	MODFLOW	—	—	Humid continental	Metamorphic and volcanic
Salt Lake Valley, UT, USA	Manning and Solomon (2005)	Basin-MB	FEMWATER	27–62%	—	Cold semiarid	Intrusive and metasedimentary
Tobacco Root Mountains, MT, USA	Magruder et al. (2009)	Basin-MB	Biome-BGC and MODFLOW	36%	—	Cold semiarid	Metamorphic and intrusive
Northern Utah Valley, UT, USA	Gardner (2009)	Basin-MB	MODFLOW	46%	—	Cold semiarid	Sedimentary and metasedimentary
Central Valley, CA, USA	Brush et al. (2013)	Basin-MB	IWFEM	10–13%	—	Mediterranean	Intrusive
Northwestern South Park Basin, CO, USA	Ball et al. (2014)	Basin-MB	FEFLOW	60%	—	Cold semiarid	Metamorphic and intrusive overlain by sedimentary
Gibsons Basin, BC, Canada	Doyle et al. (2015)	Basin-MB	NGTs and MODFLOW	45%	—	Humid coastal	Metasedimentary and metavolcanic
Gidabo River Basin, Ethiopia	Mechal et al. (2016)	Basin-MB	MODFLOW	35%	—	Subtropical highland	Volcanic
San Joaquin Valley, CA, USA	Gilbert and Maxwell (2017)	Basin-MB	ParFlow-CLM	7.7–23%	—	Mediterranean	Intrusive

Note. IWFEM = Integrated Water Flow Model; MB = mountain block; MBR = mountain-block recharge; NGT = noble gas temperatures; SIs = stable water isotopes.
^aAccording to the Köppen-Geiger climate classification system (Peel et al., 2007). ^bRange is for means from different aquifer sectors—individual well estimate values not provided. ^cMean is approximate, estimated from well MBR fractions reported in a plot, not a table.

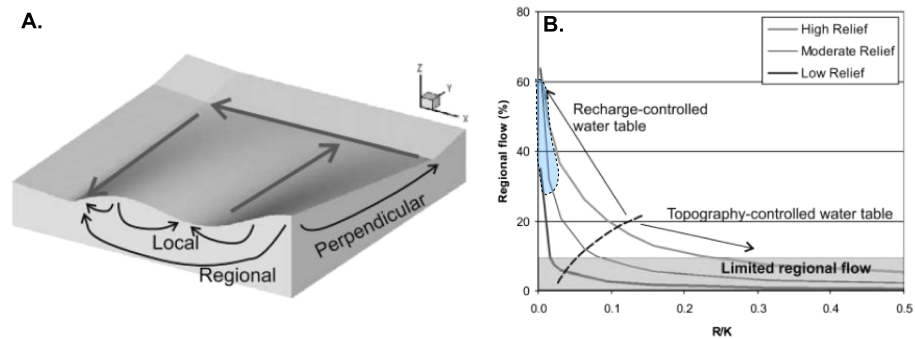


Figure 4. Modeling results from Gleeson and Manning (2008). (a) Base domain indicating local, perpendicular (intermediate), and regional flow paths. (b) Relationship between the proportion of regional flow (as a fraction of total recharge) and the ratio of recharge to mountain-block hydraulic conductivity (R/K). Low R/K ratios result in a deep “recharge-controlled” water table (WT) and higher proportions of regional flow, and high R/K ratios result in a shallow “topography-controlled” WT and lower proportions of regional flow. The dashed black line differentiates between the two types of WTs using the definition in Haitjema and Mitchell-Bruker (2005). The dashed blue area indicates R/K ratios commonly associated with first-order streams being within the unsaturated zone (perennial). High-, moderate-, and low-relief terrains were tested with topographies characteristic of the Himalaya, Rocky Mountains, and Appalachian Mountains, respectively.

regional and local groundwater flow (Figure 4). The study is essentially a three-dimensional extension of Tóth's (1963) seminal regional groundwater flow study applicable to mountainous areas. Their model domain contained connected first-, second-, and third-order drainage basins with representative mountain topography, and they defined regional groundwater flow as water that recharges in the first- or second-order basin and discharges in the third-order basin (Figure 4a). Although their model did not explicitly include a mountain front, their results are directly relevant to MBR because, as stated by the authors, their simulated regional flow would be equivalent to MBR if the third-order (lowest-elevation) watershed in the model domain contained sedimentary fill. They found that regional flow is mainly controlled by the mountain-block WT elevation (Figure 4b). Their work adopted the WT classification of Haitjema and Mitchell-Bruker (2005), which defined two fundamental types of WTs: (1) a topography-controlled WT resulting from high recharge (R) and/or low hydraulic conductivity (K), producing a WT high enough to sustain perennial streamflow in mountain catchments, and (2) a recharge-controlled WT resulting from low R and/or high K , producing a WT below mountain stream beds. For topography-controlled WTs, which should be more common in mountains (given typically low fractured-rock K s), they found a theoretical maximum regional flow fraction of about 20% of total model recharge. This suggests that the mountain WT must be recharge controlled (i.e., deeper, so more deep circulation) for large fractions of MBR to originate from parts of the mountain block farther back from the mountain front. For topography-controlled WTs, they also found that less deeply incised stream drainage networks promote larger regional flow fractions, because a deeper level of incision draws more local flow to the streams. Finally, they confirmed that higher mountain elevation above the basin and greater mountain aquifer thickness both promote larger regional flow fractions.

Welch and Allen (2012) conducted a similar theoretical study of mountain groundwater flow paths using a larger-scale, three-dimensional numerical model that included complete mountain watershed systems with multiple tributaries. They varied the topographic configuration to explore a variety of plausible mountain groundwater unit geometries. A mountain groundwater unit is defined by a regional-scale mountain surface watershed, containing a dominant stream valley, with the important exception that it also includes the adjacent triangular facets immediately above the mountain front (Figure 5), these being a common geomorphological feature (Figure 2). Welch and Allen (2012) assumed a mountain aquifer thickness of 100 m, typical for fractured crystalline rock, with a relatively low K of 10^{-8} m/s at greater depth. They found that the majority of flow paths generating MBR (73–97%) are front-slope flow, originating on the triangular facets, shown in Figure 5 as the red pathlines. This was consistent with the findings of Manning and Solomon (2005), whose modeling of the Wasatch Range, UT, found that 90% of MBR was front-slope flow for the case of an aquifer thickness of 200 m. However, the modeling of Welch and Allen (2012) provided evidence that this was a common and widespread, rather than just a local, phenomenon. Manning and

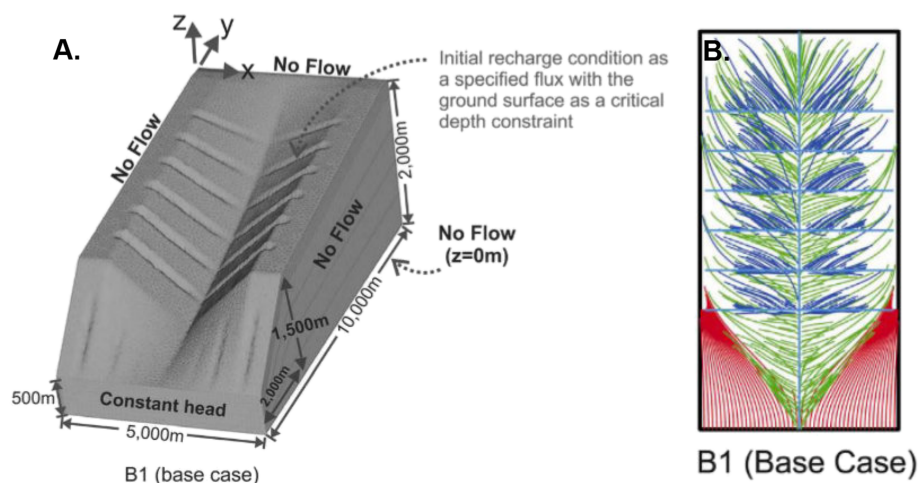


Figure 5. Modeling results from Welch and Allen (2012). (a) Base-case model space including a single mountain groundwater unit. (b) Reverse pathlines taken from $z = 75$ m for base case model, where red lines indicate mountain-block recharge, green lines indicate groundwater contributions to the dominant stream, and blue lines indicate groundwater contributions to the small perpendicular tributary streams. The light blue lines indicate streams. Modified from Welch and Allen (2012).

Solomon (2005) showed decreases in the fraction of MBR originating from front-slope flow with increasing aquifer thickness (43% for a thickness of 2,000+ m) but noted that such large circulation depths are probably uncommon. Welch and Allen (2012) also found that changing the mountain-block drainage and/or topographic configuration did not substantially change MBR, and they attributed this to the triangular facet topography varying little. Finally, their modeling provided further support for the hypothesis put forward by Gleeson and Manning (2008) that less stream incision promotes larger MBR contributions from areas behind the facets farther back from the mountain front.

In summary, these conceptual studies found that more MBR can be expected in mountain systems with higher K , greater aquifer thickness (modestly high K to greater depth), deeper WTs, less stream incision, and higher elevation above the adjacent basin (Gleeson & Manning, 2008; Welch & Allen, 2012). They also found that MBR is most inclined to originate closer to the mountain front, particularly as front-slope flow from triangular facets (Welch & Allen, 2012).

3.2. Basin-Focused Studies

Basin-focused studies primarily use models for observations from the basin-fill system to estimate MBR. In the case of models, this involves treating the contact between the basin fill and the mountain block as a boundary and estimating MBR as a flux across this boundary. For observational studies, this involves using groundwater chemistry, tracer, and age data from wells located mainly within the basin-fill aquifer to estimate the source and amount of recharge. These studies take advantage of the large number of wells in basin-fill aquifers compared to mountain blocks and the resulting abundance of hydrogeologic information, such as measurements of hydraulic conductivity, WT elevation, aquifer storage properties, and water chemistry. Prior to 2004, most MBR studies were basin focused, and almost all were located in the intermountain basins of the southwestern United States (Figure 1). These studies mainly utilized water balance methods, calibrated numerical basin-aquifer models, and Darcy flow calculations. As Wilson and Guan (2004) pointed out, each of these methods carried large uncertainties due to uncertainties in evapotranspiration, model nonuniqueness, and homogeneity assumptions, to name a few. Since then, numerous basin-focused studies have been performed in mountain areas around the world. Though model nonuniqueness and difficulties in distinguishing MBR from surface MFR remain major challenges, many of these more recent basin-focused studies employ new methodologies that show promise for reducing MBR estimate uncertainties.

In several of the observational basin-focused studies we reviewed, MBR was inferred primarily based on stable isotopes of water (Blasch & Bryson, 2007; Earman et al., 2006; Kohfahl et al., 2008; Eastoe & Towne, 2018). However, a major limitation of this approach is that, although stable water isotopes effectively identify a high-elevation precipitation source, they do not distinguish the elevation where this water actually

recharged (i.e., whether the water is MBR or surface MFR). For example, Blasch and Bryson (2007) used stable water isotopes in an elevation-weighted mixing model to determine the likeliest elevations contributing precipitation to recharge in the Verde River Basin, AZ, and found that the great majority of recharge originated as mountain precipitation (MFR). They then inferred substantial MBR to the basin-fill aquifer, but this conclusion relied largely on ancillary climatic and geologic information regarding the apparent favorability of different parts of basin and mountain block for infiltration. Further, many of these stable water isotope studies do not appear to consider the significant potential variability and uncertainty in isotopic signature of precipitation from a single elevation. Studies have demonstrated large variation within storms (McDonnell et al., 1990), based on aspect (Dahlke & Lyon, 2013), based on seasonal storm-track variations (Pape et al., 2010), and over the course of a snowpack melting (Taylor et al., 2002, 2001). Finally, Eastoe and Towne (2018) demonstrated how depleted isotopic signatures may represent paleorecharge as opposed to high elevation recharge in some intermountain basins in Arizona. In short, the numerous studies relying primarily on stable isotope ratios have identified MFR to basin-fill aquifers with some degree of confidence, but their conclusions regarding MBR contributions, specifically, remain highly speculative.

Other basin-focused studies inferring the presence of MBR have applied a broader sampling approach, combining stable isotopes with water chemistry and groundwater age tracers. Bouchaou et al. (2008), Gillespie et al. (2012), and Wahi et al. (2008) combined stable water isotopes with groundwater age information from radiocarbon and tritium data to assess recharge sources in the Souss-Massa Basin, Morocco; the Snake and Spring Valley Basins, UT and NV; and in the Upper San Pedro Basin, AZ, respectively. All three studies report large MFR fractions in the basin aquifer based on depleted stable isotopic signatures combined with groundwater ages being younger closer to the mountain front. They further state that at least some of this MFR is likely MBR given apparently high mountain-block permeability based on geologic evidence (extensive carbonates) or measurements in mountain-block wells. Although these studies provide stronger evidence for high MFR fractions than those relying primarily on stable isotope data, conclusions regarding MBR contributions remain highly speculative. Hopkins et al. (2014) characterized recharge sources to wells completed in a shallow unconfined and a deeper confined aquifer in the San Pedro Basin, AZ, using stable isotopes, water chemistry, age tracers, and numerical modeling. They were able to distinguish MBR from surface MFR by examining isotopic signatures and water age in both deep and shallow wells, attributing the combination of high-elevation stable isotopic signatures and long residence times in the deep confined aquifer to MBR and short residence times in the shallow unconfined aquifer to surface MFR. Longer residence times are to be expected in a confined aquifer and do not necessarily indicate MBR; however, the geochemical and numerical flow path modeling employed by Hopkins et al. (2014), further informed by some wells screened within the mountain block, allowed for a robust evaluation of recharge pathways. This study demonstrates the importance and utility of sampling from a range of well depth completions in the basin fill, particularly if perched and confined aquifers are present.

Several basin-focused studies have stepped beyond simply inferring the presence of MBR and have attempted to quantify MBR with the use of either endmember mixing analysis (EMMA) or noble gas recharge temperatures (NGT). EMMA relies on the assumption that the chemical signatures of endmembers can be characterized, are distinct, and either do not vary or that variations are considered (Buttle, 1994; Klaus & McDonnell, 2013; Liu et al., 2008). Liu and Yamanaka (2012) used deuterium and chloride to quantify the proportions of recharge from low-elevation precipitation, surface MFR from a mountain-sourced river, and MBR to wells in the Ashikaga area of central Japan. They found MBR contributed 40–100% of recharge to wells in a portion of the basin adjacent to a synclinal structure in the mountains, which they believed promoted subsurface flow in the mountain block. Importantly, they found much lower MBR contributions (down to 0%) in other wells, with a mean contribution of 22%, which points to a large spatial variability in MBR tied to geologic features within the mountain block. Such local variability in MBR is often overlooked when quantifying basin-wide estimates but is clearly evident in Table 1 for studies like Liu and Yamanaka (2012) and others discussed below that report MBR contributions for individual wells. Peng et al. (2016) attributed a modest mean fraction (12%) of total recharge to the Langyang alluvial fan aquifer in Taiwan to MBR using stable isotopes and electrical conductivity (EC) in an EMMA model. They later applied this same approach in the eastern coastal plain of Taiwan and found more significant fractions of MBR (22–54%) that correlated with mountain-block geology (Peng et al., 2018). These studies demonstrate the potential of EMMA to quantify MBR, based on the often unique combined isotopic and chemical signatures of recharge from low-elevation precipitation on the basin floor, surface MFR, and MBR. However, all three studies relied

on a limited number of samples from mountain springs and/or shallow wells to identify the signature of MBR and did not rigorously address potential spatial or temporal variability in endmember signatures.

To date, the most effective method for distinguishing MBR from surface MFR in basin-fill aquifers is using groundwater dissolved noble gas concentrations to determine the shallow ground temperature at the recharge location (NGT). NGTs can be used to estimate a recharge elevation when a relationship between shallow ground temperature and elevation is assumed or derived for the study area (Aeschbach-Hertig et al., 1999; Manning & Solomon, 2003). Surface MFR will typically have a relatively warm NGT, reflecting low-elevation recharge, whereas MBR will typically have a cooler NGT, reflecting recharge at higher elevation. Building on the suggestion of Aeschbach-Hertig et al. (1999) that noble gases might be applied as recharge elevation tracers, Manning and Solomon (2003) further developed this approach and used NGTs to detect MBR in a proof of concept study in the eastern Salt Lake Valley, UT. They first used NGTs from mountain springs and mine tunnels to derive a local recharge temperature lapse rate, which they found to be similar to the local atmospheric temperature lapse rate as theoretically expected. They then used NGTs from basin aquifer wells to place constraints on the MBR fraction in the basin-fill aquifer, finding >50% MBR in 17 of 22 wells in the southeastern part of the valley. Later studies have demonstrated the use of NGTs with stable isotopes and age tracers to provide both qualitative and quantitative estimates of MBR. Althaus et al. (2009) measured all of these tracers in the Grenchen aquifer system, Switzerland, and found an absence of MBR from the adjacent Jura Mountains in most wells (though not all) based largely on warm, low-elevation NGTs. Manning (2011) used NGTs and radiocarbon ages to determine minimum MBR fractions of 0–50%, with a mean of 24%, for the southeastern Española Basin, NM. The radiocarbon ages further revealed that the majority of MBR likely enters the basin-fill aquifer near watershed mouths. Manning (2011) also found much cooler NGTs in samples of Pleistocene age (>12,000 years old), as expected given the cooler climate during the Pleistocene epoch, and cautioned that radiocarbon ages should be collected along with noble gases in basins where very old groundwater may be present. Gardner and Heilweil (2014) applied a similar approach as Manning (2011) for a large number of springs and wells in the Snake Valley area of the north-eastern Great Basin, NV and UT. They found that the NGTs and radiocarbon ages suggest that most recharge within the study area is MBR from the Snake Range. Thoma et al. (2011) measured NGTs in Treasure Valley, Idaho, and identified the presence of MBR from the adjacent Boise Front Range. They also measured some unexpectedly warm NGTs exceeding the mean annual air temperature at the well location and applied an infiltration-weighted recharge model to determine that the likely cause was infiltration of summer irrigation water in the valley. Their work underscores the importance of taking into account possible NGT variations at a given elevation due to seasonally shallow WT when deriving local NGT lapse rates. Overall, NGTs have proved to be a reliable method for distinguishing surface MFR from MBR, but their effectiveness requires a significant difference in recharge elevation between these two components. Distinguishing low-elevation MBR, which might be focused beneath streams exiting the mountain block or front-slope flow (Figure 2), from surface MFR using environmental tracers remains a challenge.

Some basin-focused studies have addressed the important issue of major faults near the mountain front potentially acting to either impede or enhance MBR. Fault-zone architecture commonly includes a clay-rich core, which can impede cross-fault groundwater flow, surrounded by a highly fractured damage zone, which can enhance fault-parallel groundwater flow (Caine et al., 1996). Because the process of mountain building often involves significant tectonism and crustal deformation, mountain blocks commonly contain and/or are bounded by major faults. Theoretically, range-bounding faults, which accommodated uplift of the mountain block, could act as barriers to MBR because they are generally oriented at a high angle to MBR flow—that is, MBR must flow across them to enter the basin-fill aquifer. Conversely, major faults within the mountain block oriented more parallel to MBR flow paths could act as conduits for MBR, particularly regional flow. Chowdhury et al. (2008) used stable water isotopes, radiocarbon, and tritium to explore recharge processes in a normal-fault-bounded basin in West Texas. They interpret the deep WT in the basin fill near the fault combined with low tritium and low percent modern carbon in water samples from the same location as evidence that the fault impedes flow and that modern MBR is minimal. A steep head gradient across the mountain front is a common line of evidence used to support faults impeding flow; however, this can also simply be the result of the high-K basin fill juxtaposed against the lower-K mountain block, as discussed by Bresciani et al. (2018). Delinom (2009) came to a similar conclusion regarding the range-bounding Lembang fault, which appears to impede MBR to the Bandung Basin, Indonesia, based on hydraulic head, stable isotopes, and salinity. Kebede et al. (2008) conducted a thorough hydrogeological, hydrochemical,

and groundwater age assessment of basin wells in two transects within the Ethiopian rift having distinctly different structural characteristics. The first transect includes transverse faults that crosscut the mountain front at a high angle, whereas the second transect does not include such faults and also has fault-controlled grabens paralleling the mountain front at the foot of the mountain block. They interpret the presence of isotopically depleted and older groundwater in the first transect as evidence that the transverse faults provide permeable conduits for MBR. However, the isotopic and age data show little evidence of MBR in the second transect, suggesting that the mountain-front-parallel faults in the rift generally act as barriers to MBR. Caine et al. (2017) performed a detailed field examination of mountain-front faults near the foot of the Sangre de Cristo mountain block along the eastern margin of the Española Basin, NM, characterizing their brittle structure and possible hydraulic influence. They found that the faults are largely discontinuous when mapped in detail and are thus unlikely to significantly impede MBR. Taken together, the above studies provide evidence that faults can indeed either impede or enhance MBR, depending largely on their orientation, but also that mountain-front-parallel faults probably do not systematically and significantly impede MBR to such a degree as to render MBR a rare exception, rather than a common phenomenon. This general finding is thus consistent with the other widespread evidence of MBR found by other basin-focused studies.

Another widely used method for quantifying MBR in basin-focused studies is numerical groundwater flow modeling. Modeling studies generally treat the mountain block as a boundary in one of two ways: (1) assuming MBR is negligible and assigning a no-flow boundary or (2) initializing MBR based on results from other modeling or observational studies and adjusting it to match observations from the basin-fill aquifer during calibration. Basin-focused modeling studies of the second type thus essentially use head data and K estimates from the basin-fill aquifer to further constrain or revise prior independent MBR estimates. The first approach of assuming the mountain block is impermeable (no-flow mountain-front boundary) has historically been the most common (Bolger et al., 2011; Faunt, 2009; Mason & Bota, 2006). A major impediment to determining whether this no-flow assumption is appropriate is the typical scarcity of K data in the mountain block, particularly near the mountain front. Though treating the mountain front as a no-flow boundary may be justified in some cases, this assumption should be made with caution given the growing number of studies that find appreciable rates of groundwater flow in mountain fractured-bedrock aquifers, even in crystalline rock (see section 3.3). In basin-fill aquifers where MFR and MBR are suspected to be substantial portions of recharge, such as in intermountain basins in the arid and semiarid western United States, the second approach of specifying and calibrating MBR is more common. Siade et al. (2015) estimated natural MFR to the Antelope Valley, CA, with a groundwater flow model calibrated to both observed head and subsidence data. Their estimate of MFR included both surface MFR and MBR components, but they did not report separate results for the two. Their inverse calibration allowed for confidence intervals to be placed around MFR rates, as well as the ability to evaluate “reasonableness” of prior or higher recharge estimates. Schaefer et al. (2007) relied on prior MBR estimates from Maurer and Thodal (2000) to specify the lateral boundaries to their MODFLOW model of Eagle Valley and Spanish Springs Valley, NV. They computed MBR fractions of 28% and 13.3%, respectively, for the two basins, these being somewhat lower than the estimates of Maurer and Thodal (2000). Bexfield et al. (2016) relied on previous modeling and groundwater age-based estimates of subsurface inflow to specify MBR fluxes as lateral boundary conditions to their MODFLOW model of the Middle Rio Grande Basin, NM. Their calibration resulted in a slight increase of MBR in predevelopment (25% of recharge) and modern (6% of recharge) conditions compared to previous studies. Note that the postdevelopment decrease in MBR in their study is a relative decrease due to the addition of canal and crop irrigation seepage to basin-fill aquifer recharge.

Regardless of the chosen approach, using basin-focused groundwater flow models to estimate MBR or distinguish it from surface MFR is inherently uncertain due to poor constraints on K and resulting nonunique combinations of R and K that can reproduce observed head data in the basin during calibration (Wilson & Guan, 2004). Not distinguishing MBR from surface MFR in these models introduces bias to the hydrogeologic conceptualization and limits the robustness of prediction. Multiple studies have demonstrated the feasibility of calibrating basin-centered groundwater flow models to age tracers in addition to heads to reduce this uncertainty (Bexfield et al., 2016; Sanford, 2011; Sanford et al., 2004). However, establishing useful tracer-based age constraints for samples from long-screened production wells (short-screened monitoring wells are rarely available; McCallum et al., 2015) and realistically modeling age dispersion related to subsurface heterogeneity (Engdahl et al., 2012; Fogg & Zhang, 2016) remain major challenges to calibrating numerical models with age tracer data.

Despite their data advantage, basin-focused studies still produce MBR estimates that carry considerable uncertainty largely due to difficulty in distinguishing MBR from surface MFR, especially studies relying heavily on stable water isotopes or traditional calibration of groundwater flow models. Combined approaches, particularly those using stable water isotopes, age tracers, and NGTs, are the most robust and hold the greatest promise for distinguishing and quantifying MBR. Regardless of the uncertainties in MBR estimates, these studies as a group strongly argue that substantial MBR to lowland aquifers (5–50% of total recharge; Table 1) is common throughout the world. This is the case even for basins bounded by crystalline-rock mountain blocks of apparently low permeability. Importantly, some of these studies have also found an absence of MBR in some basins (or parts of basins), and most attribute this to major range-bounding faults, though the actual role of mountain-block faults in impeding (or enhancing) MBR remains largely speculative.

3.3. Mountain-Focused Studies

Mountain-focused studies directly examine mountain aquifers and processes related to groundwater flow in the mountain block. Wilson and Guan (2004) stated that MFR-related work up to that time had employed mainly “basin-centered approaches” and declared that “the mountain-block hydrologic system is ripe for new studies” (p. 18). Many researchers agreed, and by far the largest category of MBR-related papers published since 2004 has been mountain-focused studies, taking full advantage of a growth in instrumented watersheds with wells, advances in numerical modeling, and the novel application of tracers. As a result, the hydrology community has confirmed that mountain bedrock aquifers are an important component of the mountain hydrologic system, often having recharge rates as large as 10–50% of precipitation (30–300 mm/year; e.g., Andreu et al., 2011; Carrera-Hernández & Gaskin, 2008; Kormos et al., 2015) and contributing substantially to mountain streamflow (e.g., Hale & McDonnell, 2016; Hale et al., 2016; Gabrielli et al., 2018; Kosugi et al., 2006). Here, we review recent studies of mountain-block hydrogeology and mountain groundwater flow that are directly relevant to MBR, though this list should not be considered comprehensive.

The hydraulic conductivity (K) distribution within the mountain block and active circulation depth of groundwater, or depth to which groundwater circulates on human rather than geologic timescales, are first-order controls on the rate and distribution of MBR (Gleeson & Manning, 2008; Welch & Allen, 2012; Wilson & Guan, 2004). The multiple geological factors potentially controlling mountain-block K are discussed by Wilson and Guan (2004), and Welch and Allen (2014) present a compilation of fractured-bedrock K measurements and estimates for mountainous terrain. In general, K decreases with depth in fractured rocks owing to the decreasing influence of weathering (Worthington et al., 2016) and the decreasing aperture and number of open fractures and pores due to increasing overburden loads and mineral precipitation (Manning & Ingebritsen, 1999; Saar & Manga, 2004; Stober & Bucher, 2007; St. Clair et al., 2015; Voekler & Allen, 2012). As reviewed in detail in Welch and Allen (2014) and Manning and Caine (2007), multiple lines of evidence presented in pre- and post-2004 studies have contributed to the development of a now widely invoked general conceptual model for mountain groundwater flow systems, in which a higher- K “active” zone (the aquifer) overlies a deep low- K zone (relatively impermeable bedrock). Some flow within the deep low- K zone still occurs but is on average small relative to mountain hydrologic budgets and is not spatially pervasive, instead limited to a few discrete features such as deeply penetrating major faults. Available data suggest general K ranges of 10^{-8} to 10^{-6} m/s for the active fractured bedrock zone and $<10^{-8}$ m/s for the deep low- K zone (Katsura et al., 2009; Welch & Allen, 2014).

Welch and Allen (2014) propose the following more specific vertical K zones for fractured crystalline-rock mountain systems based on their compilation, as illustrated in Figure 6: soil (0 to 3 m), saprolite and highly weathered bedrock (0 to 10 m), fractured bedrock (10 to 100–200 m), and deep low- K bedrock (>100 –200 m). Although available data converge on a depth estimate of 100–200 m for active circulation in crystalline rocks, the number of study locations remains relatively small, and this depth may vary widely depending on local tectonic history, specific lithology, and climate. Frisbee et al. (2017) used the quartz-silica geothermometer on mountain spring and well waters in the Rio Hondo watershed, Sangre de Cristo Mountains, NM, which is underlain by crystalline metamorphic rocks, to estimate active circulation depths upward of 1,000 m, though the substantial assumptions required for such geothermometers make them less than ideal for this application. Multiple studies have observed active groundwater circulation to depths of 500–1,500 m within steeply dipping faults and discrete fracture zones in tunnels and mines in the mountain block, as evidenced by modern recharge and hydraulic head data (Ofterdinger et al., 2014; Oyarzún et al., 2019;

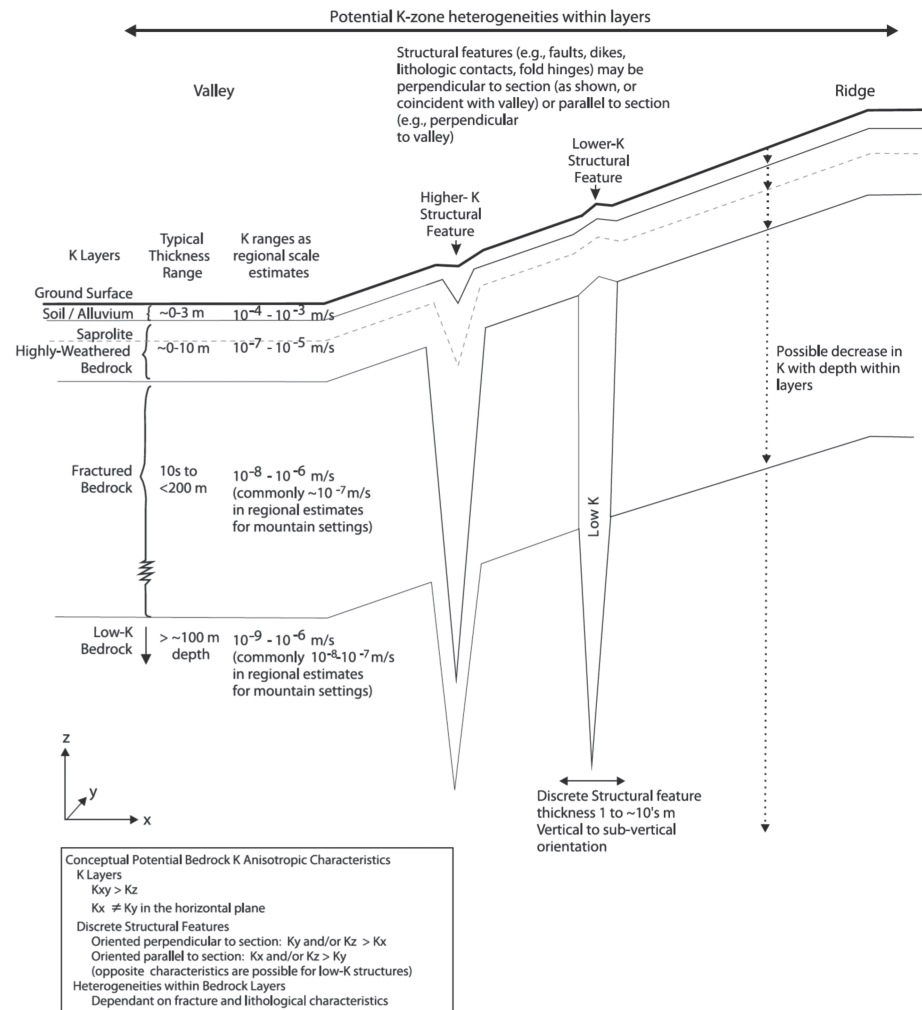


Figure 6. Conceptual model of catchment-scale vertical hydraulic conductivity (K) zones typical of fractured crystalline rock mountain aquifer systems, reproduced from Welch and Allen (2014).

Tomonaga et al., 2017; Wilson & Guan, 2004). However, whether or not these structures hosted active flow prior to tunnel or mine installation (which induces draining) and, if so, whether cumulative flow within them was sufficient to extend the active zone down to the tunnel/mine depth remain major unanswered questions. St. Clair et al. (2015) combined information from seismic refraction and electrical resistivity geophysical surveys for transects in three Critical Zone Observatory watersheds (Gordon Gulch, CO; Calhoun, SC; and Pond Branch, MD), all underlain by crystalline metamorphic rocks and were able to discern a zone of unweathered bedrock with low water content below a depth of approximately 40 m and a zone of fractured bedrock with high water content above. They concluded that circulation depths of <100 m may not be unusual in watersheds underlain by crystalline rocks. However, this conclusion assumes a close correlation between water content and K, and no corroborating subsurface data from boreholes or wells were presented. Nevertheless, St. Clair et al. (2015) demonstrated that ground geophysical surveys may be a useful screening tool for determining circulation depth over broad areas.

Regional-scale coupled heat and groundwater flow models of sedimentary basins and volcanic terrains compiled by Manning and Ingebritsen (1999) show $K_s > 10^{-8}$ m/s typically extending to depths of 2 km, suggesting that active circulation depths considerably greater than 100–200 m may be common in noncrystalline sedimentary and volcanic rocks. Available studies involving mountain blocks composed of volcanic rock appear to support such deep circulation. Saar and Manga (2004) derive a permeability-depth relationship for the volcanic rocks composing the Oregon Cascade Range based on hydrogeologic, thermal, seismic, and magmatic modeling constraints and find that $K_s > 10^{-8}$ m/s extends to depths of roughly 3 km. Heilweil

et al. (2012) use a coupled heat and fluid flow model combined with NGTs to constrain recharge rates and K_s for a volcanic island aquifer rising to 2,000 m above sea level in the Cape Verde Islands and report WT depths of 600–1,000 m and K_s on the order of 10^{-8} m/s to a depth of 2 km below the central caldera. Frisbee et al. (2017) apply the same previously mentioned quartz-silica geothermometer method in the Saguache Creek watershed in the San Juan Mountains, CO, which is underlain by volcanic rocks, and estimate active circulation depths of 900–1,700 m. In the only recent study, we are aware of examining circulation depth for a sedimentary rock mountain block; Lazear (2006) reports K_s on the order of 10^{-8} m/s extending to a depth of 1,500 m derived from a regional heat and groundwater flow model of the Tongue Creek watershed, Grand Mesa, CO. However, Mayo et al. (2003) and Mayo and Koontz (2000) used groundwater temperature, chemistry, and age data from mines and springs to estimate a circulation depth of only 150–300 m for very similar packages of sedimentary rocks in Colorado and Utah. This discrepancy might be explained by the model of Lazear (2006) failing to include K anisotropy, which can commonly cause vertical K to be 2–3 orders of magnitude less than horizontal K in sedimentary rocks, thus substantially reducing circulation depth.

Although the number of mountain K measurements is growing, estimates of active mountain groundwater circulation depth are typically very poorly constrained, even in well-instrumented watersheds, and circulation depth remains in general perhaps the most uncertain characteristic of mountain groundwater flow. The primary reason for this uncertainty is a continued scarcity of mountain wells of sufficient depth to penetrate below the active zone and allow direct observation of the transition from the active zone to the deep low- K zone.

A growing number of studies are attempting to determine the amount of mountain aquifer recharge that becomes baseflow within the same subwatershed (local flow) versus the amount that is lost to interbasin (intermediate and regional) flow (Figure 3). This interbasin flow has also been referred to as the “headwater groundwater subsidy” to the parent watershed (Ameli et al., 2018), and basins have been classified as “exporters” (recharge is greater than streamflow) and “importers” (streamflow is greater than recharge; Fan & Schaller, 2009). The portion of mountain aquifer recharge that becomes interbasin flow does not necessarily become MBR, though it is available to become MBR. Thus, these studies directly inform efforts to estimate and identify sources of MBR. Welch et al. (2012) explored interbasin flow using 3-D groundwater flow models of both generic and real (Daves Creek, Canada) mountain watershed configurations. They found that interbasin flow is a standard component of mountain groundwater flow systems and should be considered in studies of mountain streamflow generation. However, the amount of interbasin flow and the time scale on which it changes in response to changing mountain aquifer recharge are highly variable, depending on detailed characteristics of mountain watershed topography and recharge rates. Kormos et al. (2015) developed a spatially distributed soil-water infiltration method for estimating deep drainage from the bottom of the soil layer to the bedrock. They estimate roughly 34% of precipitation becomes “bedrock infiltration” in the ephemeral headwater Treeline catchment in the Dry Creek Experimental watershed, ID, which they define as water that leaves the catchment boundaries through subsurface drainage (i.e., interbasin flow). This estimate is in agreement with a prior estimate of 22–34% of precipitation for headwater catchments of the Dry Creek watershed based on chloride mass balance (Aishlin & McNamara, 2011). Installation of bedrock wells in the M8 catchment of the Maimai Experimental watershed, New Zealand, allowed for estimation of local versus interbasin bedrock groundwater flow through a combination of modeling and field measurements of WT depth and residence time (Ameli et al., 2018; Gabrielli et al., 2018). These studies concluded that roughly 50% of groundwater recharge in the headwater catchments becomes intermediate flow and subsidizes the parent watershed. Ameli et al. (2018) also perform model experiments to determine the sensitivity of the interbasin flow fraction to R and find that it increases markedly with decreasing R (as the WT falls), thus providing a real-world example supporting the findings of Gleeson and Manning (2008) that interbasin flow should generally increase with a progressively deeper WT (Figures 4 and 7). Such large interbasin flow fractions are consistent with other studies that have identified deep, old groundwater contributions to mountain streams, as well as increases in these old-water contributions with increasing watershed scale regardless of the underlying geology (Ameli et al., 2018; Frisbee et al., 2017; Hale & McDonnell, 2016; Hale et al., 2016). However, these large fractions appear in conflict with the theoretical maximum of about 25% interbasin flow (intermediate plus regional) found by Gleeson and Manning (2008) for first-order watersheds with a topography-controlled WT (observed WT depths are <10 m in the M8 headwater catchment).

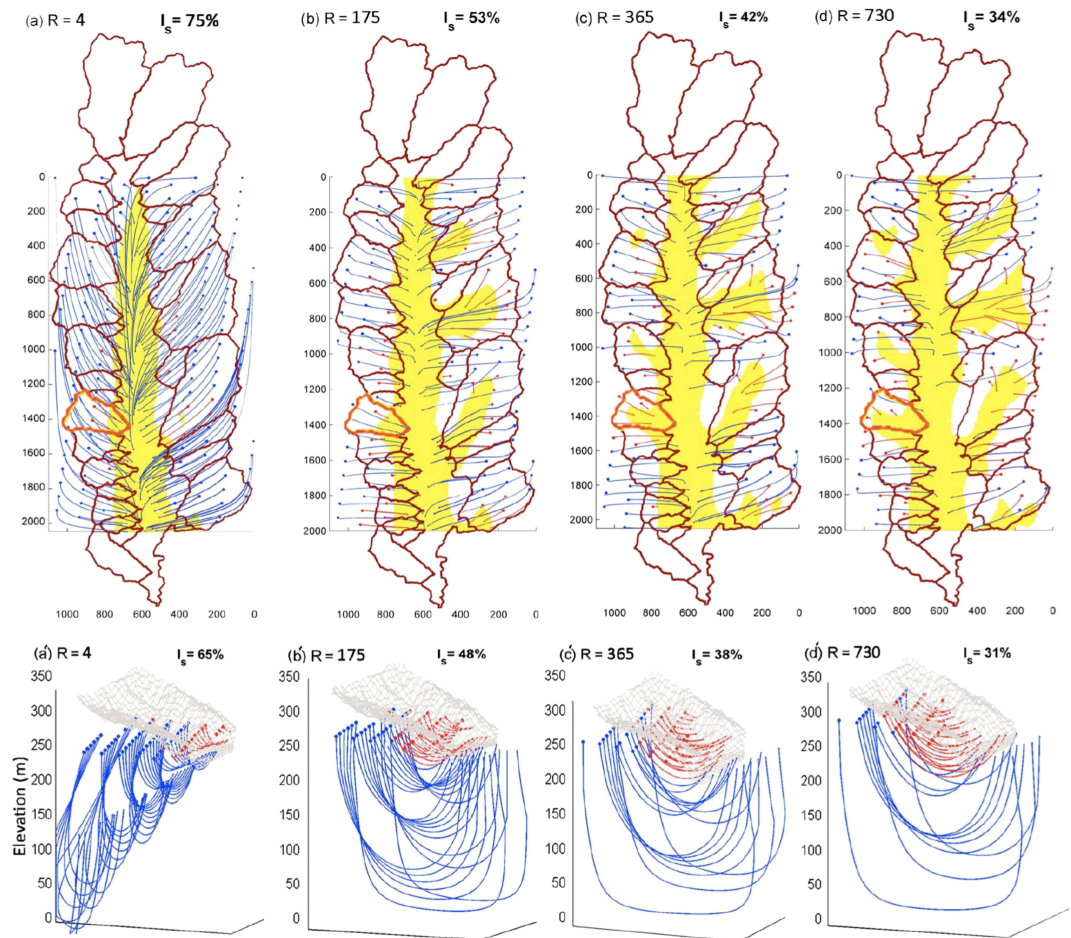


Figure 7. Modeled groundwater flow pathline results from Ameli et al. (2018) demonstrating the dependence of the amount and distribution of intermediate flow (blue pathlines) on recharge rate (R , in mm/year). I_s is the percentage of headwater catchment recharge that becomes intermediate flow. (a)–(d) show results for the entire Maimai Experimental watershed, and (a')–(d') show results for the heavily instrumented M8 headwater catchment. Decreasing R increases the amount of intermediate flow relative to local flow (red pathlines), as the WT drops farther below the land surface. These results provide a real-world example supporting the finding of Gleeson and Manning (2008) that the interbasin flow fraction increases as the water table drops from a higher- to a lower-elevation position (see Figure 4).

The discrepancy could be explained by complicating factors, such as perched WTs in the studied headwater catchments (the regional WT could be deeper and recharge controlled), or by real-world complexities in topography and bedrock K distribution not included in the idealized modeling of Gleeson and Manning (2008).

In contrast to the above studies, others employing tracer-based and modeling methods have estimated only very small amounts of interbasin flow from headwater catchments. For example, two studies using NGTs and groundwater age tracers in two different watersheds in the Sierra Nevada, CA (Martis Valley and Olympic Valley), found that groundwater from headwater catchments probably contributes little to the parent watershed (Segal et al., 2014; Singleton & Moran, 2010). This conclusion was based mainly on NGTs for groundwater samples collected from wells in the parent watershed being inconsistent with high-elevation (cold) recharge in the headwater catchments. Voeckler et al. (2014) calibrated a specified head outlet in a numerical coupled surface water and groundwater model of the Upper Pentiction Creek, BC, and estimated that only 7% of recharge leaves the catchment in the subsurface and becomes interbasin flow. Two studies in Marshall Gulch, AZ, obtained very small estimates (1–2% of precipitation) for bedrock groundwater recharge in this headwater catchment based on a storage-discharge function (Ajami et al., 2011) and base-flow recession analysis (Dwivedi et al., 2019), though neither studies had access to bedrock wells for their analysis. Sandoval et al. (2018) applied a similar approach as Ajami et al. (2011) and estimated bedrock recharge to be 1–4% of precipitation in the Punitaqui Basin of northern Chile. The low bedrock recharge

estimates in these three studies indicate small absolute interbasin flow rates and are not surprising for these arid mountain regions. However, these studies did not discern relative amounts of local versus interbasin flow, and it remains possible (if not probable, given the results of Gleeson & Manning, 2008, and Ameli et al., 2018) that relative interbasin flow fractions are large.

Of the mountain-focused studies we considered, relatively few attempted to quantify MBR, specifically. Kao et al. (2012) estimated MBR in the Choushui-Wu River basin, Taiwan, from mountain aquifer recharge estimates and stream gage data. They estimated mountain aquifer recharge using two independent methods: modeled rainfall infiltration estimates over the mountain block and baseflow separation from gaging stations in catchments hosting perennial streamflow. They then applied these recharge rates over the entire mountain block (including areas without perennial streamflow) and subtracted streamflow to obtain two separate MBR estimates which agreed well (though these were never presented as a percentage of mountain aquifer recharge or basin-fill aquifer recharge). However, this approach carries significant uncertainty due to well-established difficulties in accurately estimating baseflow and mountain water budget components (particularly evapotranspiration [ET]) as discussed by Wilson and Guan (2004). Aishlin and McNamara (2011) used chloride mass balance to estimate interbasin flow leaving the Dry Creek Experimental watershed, ID, in the subsurface. They estimated that 14% of precipitation, or 40% of mountain aquifer recharge, becomes interbasin flow, which likely then becomes MBR to the adjacent Boise valley aquifer. They found larger percentages of interbasin flow (22–34% of precipitation) leaving the smaller headwater subcatchments of the Dry Creek watershed in the subsurface, in agreement with Kormos et al. (2015), but some of this water discharges as springflow or baseflow lower down on the mountain block and does not become MBR. However, applying chloride mass balance in mountain systems requires satisfying several major assumptions including (1) inert behavior of chloride, (2) accurate estimation of precipitation and chloride deposition rates, (3) no endogenous sources of chloride, and (4) chloride concentration values representative of groundwater for the entire mountain block. Wilson and Guan (2004), Bresciani et al. (2014), Guan et al. (2010a), and Guan et al. (2010b) present thorough examinations of where these assumptions may be violated or confounded in heterogeneous and shallow-soiled mountain systems. Yao et al. (2017) constructed a MODFLOW model of the Qilian Mountains in China to estimate MBR to adjacent valleys in which they assumed a prescribed rate of K decay with depth, a recharge rate of 20% of precipitation, and a head-dependent boundary at the mountain front. They calibrated the model to mountain stream baseflows and estimated that approximately 35% of mountain aquifer recharge becomes MBR, with the rest contributing to baseflow. However, they found that the MBR fraction ranged from 30% to 70% of mountain aquifer recharge when the rate of K decay (on which they had no independent constraint) was varied within reasonable limits. This study therefore clearly demonstrates the large uncertainty of model-based MBR estimates that result from highly limited subsurface K data.

Overall, the surge of mountain-focused studies since 2004 has helped advance our understanding of mountain-block hydrogeology, supporting the existence of mountain aquifers with considerable recharge rates, K values, and contributions to streamflow. The large increase in the number of bedrock monitoring wells in mountain watersheds has played a central role in this advancement, as well as the number of studies taking advantage of deep tunnels. Multiple studies have converged on active zone K values of 10^{-8} to 10^{-6} m/s and on active circulation depths of 100–200 m in fractured crystalline bedrock, an important advancement given the widespread occurrence of crystalline rock in mountain systems. Active circulation depths in mountain blocks composed of volcanic rocks are likely greater and commonly may be deeper for sedimentary rock mountain blocks as well, but the number of studies addressing active circulation depth in noncrystalline rock mountain blocks remains highly limited. Finally, estimates for the amount of interbasin flow (this being potential MBR) originating from mountain headwater catchments are in some cases considerable (up to 50% of catchment recharge) but also can be negligible, and the degree to which these large site-to-site variations stem from inherent uncertainty in the interbasin flow estimates (rather than real variations in watershed hydrogeology) remains unclear.

3.4. Combined Basin-Mountain Studies

Studies that combine the mountain block and basin are a considerable step forward from the basin-focused studies that predominated prior to 2004. The majority of combined basin-mountain studies employ numerical modeling to simulate MBR processes and are thus challenged by the difficulty of calibrating and/or validating model “correctness,” especially at the regional scale. Most of these modeling studies have addressed this through varying levels of sophistication in representing physically based recharge (Ball et al.,

2014; Gilbert & Maxwell, 2017; Magruder et al., 2009) and by employing NGTs, age tracers, and temperature data (Doyle et al., 2015; Manning & Solomon, 2005), in addition to heads and stream flows, for model calibration.

Mountain aquifer recharge estimates are typically uncertain, leading to large inherited uncertainties in MBR estimates. However, major advances in the acquisition of distributed precipitation and evapotranspiration data over the mountains using remote sensing, as well as advancements in coupled and integrated hydrologic models, have led to improved parameterization and estimation of MBR. Ball et al. (2014) developed a groundwater flow model of the South Park Basin, CO, and surrounding mountains, including spatially and temporally varying recharge and a K distribution representing complex geologic structures. They estimated that 17% of recharge to the mountain aquifer in the dominant mountain range bounding the basin (Mosquito Range) becomes MBR, accounting for 60% of recharge to the adjacent basin-fill aquifers in the northern part of the basin. They also found that most of the MBR originates from watersheds closer to the mountain front rather than the highest part of the range (~70% of groundwater flow in the mountain block circulates <1 km), in general agreement with the conceptual modeling studies discussed in section 3.1. Gardner (2009) constructed a MODFLOW model of the northern Utah Valley, UT, including the adjacent mountain blocks, and used a detailed spatially distributed water balance model to estimate mountain aquifer recharge using the Recharge Package (Harbaugh et al., 2000). They estimate that 17–33% of mountain precipitation becomes MBR, with MBR contributing 46% of basin-fill aquifer recharge, and this estimate is further supported by groundwater ages and NGTs presented by Cederberg et al. (2009) indicating substantial MBR fractions in the basin aquifer. Importantly, the substantial fractions of MBR in the Utah Valley are likely controlled by the presence of carbonate rocks with known karst development in the mountain block (Cederberg et al., 2009; Gardner, 2009). Brush et al. (2013) acknowledged the importance of surface and subsurface inflow from small, ungaged watersheds adjacent to the Central Valley, CA, and included these fluxes in their Integrated Water Flow Model of the basin. They estimated MBR in the small stream watershed percolation module—a simple water budget model that utilizes monthly distributed precipitation and evapotranspiration data to estimate streamflow and subsurface inflow to the basin. They found that this MBR accounted for 13%, 10%, and 12% of total groundwater recharge to the basin for the 1922–1929, 1960–1969, and 2000–2009 time periods, respectively. Magruder et al. (2009) estimated mountain aquifer recharge using an ecohydrologic process model and then subtracted surface water runoff to arrive at an MBR estimate of 19% of mountain precipitation (48% of mountain aquifer recharge). They then applied this MBR as a boundary condition to a groundwater flow model of the adjacent basin-fill aquifer in the Tobacco Root Basin, MT, and found that MBR accounts for 36% of basin-fill aquifer recharge. Similarly, Mechal et al. (2016) estimated recharge to the Gidabo River Basin in the Ethiopian rift valley using a semidistributed soil water model and then applied those values as recharge to a groundwater flow model. They estimate MBR composes 35% of recharge to the rift basin and found that including faults acting as both flow barriers and conduits improved model fit.

Integrated hydrologic models such as HydroGeoSphere (Brunner & Simmons, 2012) and ParFlow-CLM (Maxwell & Miller, 2005) reduce process uncertainty by simulating distributed recharge and allowing for seamless integration between the surface processes governing recharge and groundwater flow within underlying aquifers receiving this recharge. Gilbert and Maxwell (2017) developed a ParFlow-CLM model of the San Joaquin River Valley, CA, and estimated MBR to the Central Valley, applying a manual sensitivity analysis for mountain-block bedrock K. They found that MBR ranged from 7.7% of total recharge for a mountain-block bedrock K of 10^{-7} m/s to 23% for a K of 10^{-3} m/s. They also found this MBR contribution to be temporally constant despite the seasonality of snowmelt recharge in the Sierra Nevada. This result is important, given that other widely used models of the Central Valley aquifer system assume negligible MBR from the adjacent dominantly granitic Sierran mountain block (Bolger et al., 2011; Faunt, 2009). The combination of a sensitivity analysis of bedrock K with model fluxes rigorously validated to observational, remotely sensed and satellite data makes this study an important advancement in using models to estimate MBR.

While traditional validation (e.g., to fluxes and heads) increases confidence in model parameterization, it typically still results in substantial model solution nonuniqueness in groundwater flow models (Schilling et al., 2019). To reduce this nonuniqueness, two studies have employed the use of nontraditional sources of information to constrain and validate combined basin-mountain models. Manning and Solomon (2005) attempted to constrain MBR, as well as active circulation depth, in the Wasatch mountain block, UT, by calibrating a coupled heat and groundwater flow model of the mountain block and adjacent southeastern Salt Lake Valley to mountain stream baseflow, groundwater temperature, and groundwater age. In the 38

model runs combining varying mountain bedrock aquifer K , effective porosity, and thickness, temperature data constrained the upper limit of MBR to 62% of basin-fill aquifer recharge and groundwater age data constrained the lower limit of MBR to 27% of basin-fill aquifer recharge. These constraints substantially reduced the range of possible MBR rates based on previous studies, but the modeling methodology was not successful in constraining the circulation depth. Notably, while this study found MBR to contribute an important fraction of basin-fill aquifer recharge, the estimated MBR range was lower than previous estimates for the basin derived from numerical models calibrated using traditional hydraulic data. Doyle et al. (2015) were the first to use NGTs as calibration targets for a groundwater flow model, simulating MBR to a coastal alluvial aquifer in British Columbia, Canada. Backward particle tracking from basin wells in the numerical model allowed for direct calibration to the NGT-based estimated recharge elevation, and R and K values were iteratively updated to match observed recharge elevations. They estimate MBR composes 45% of basin-fill aquifer recharge. Overall, these studies demonstrate the importance and feasibility of combining independent sources of information to constrain model estimates of MBR.

Combining substantial independent data sets from both the mountains and adjacent basin-fill aquifer is not only useful for reducing uncertainty in numerical models of basin-mountain systems but may also be an effective data-driven approach in MBR studies. A recent study combined stable water isotopes, groundwater age tracers, and chloride data from the layered Adelaide Plains aquifer system, Australia, and adjoining mountain block to examine aquifer recharge sources and rates (Batlle-Aguilar et al., 2017). The authors conclude that nearly all recharge to the deep confined aquifers is MBR based on the following lines of evidence: (1) Old groundwater is present near the top of the deep aquifers (inconsistent with substantial downward leakage), and groundwater age within them increases with depth and distance from the mountain front; (2) chloride in the shallow aquifer is often higher than in the deep confined aquifers (suggesting minimal vertical leakage); and (3) mountain aquifer recharge rates estimated from chloride mass balance roughly agree with Darcy groundwater flow velocities calculated from groundwater age gradients in the deep confined aquifers (meaning MBR alone can account for all deep flow). A follow-up study of the same aquifer system leveraged long-term and spatially extensive data sets of hydraulic head and groundwater EC from both the mountain block and the basin to determine the fraction of MBR versus surface MFR in shallow and deep aquifers (Bresciani et al., 2018). The head and EC data suggest that surface MFR predominates over MBR in both the shallow and deep aquifers based on relatively well-defined WT highs and EC lows underneath streams exiting the mountain block. Furthermore, head data in the mountain aquifer indicate predominantly local flow toward streams rather than regional flow toward the mountain front. These results are inconsistent with the conclusion of Batlle-Aguilar et al. (2017) that recharge to the deep aquifers is nearly all MBR, and surface MFR is minor. Two possible explanations for this discrepancy include the following: (1) The spatial resolution of EC data examined by Bresciani et al. (2018) is far greater than the chloride data examined by Batlle-Aguilar et al. (2017) and is thus better able to resolve spatial patterns relative to streams traversing the mountain front; or (2) MBR is indeed the dominant recharge source for the deep aquifers, but it is focused MBR leaving the mountain block mainly under streams and thus cannot be easily distinguished from surface MFR based on head and EC data. Repeat studies in other basins have led to substantial revisions in MBR estimates based on improved methods and more targeted or comprehensive sampling (e.g., the MBR range estimated by Manning & Solomon, 2005, for the southeast Salt Lake Valley was 50–100% of the prior estimate by Lambert, 1995), but these two studies reaching nearly opposite conclusions is unusual and clearly merits further work. Despite their conflicting results, these two studies demonstrate that extensive hydraulic and geochemical data sets collected from both the basin fill and adjacent mountain block may by themselves yield valuable information regarding MBR, and the abundance of hydraulic head and EC data in mountain-front systems around the world makes this approach potentially widely applicable.

Numerical-model-based combined basin-mountain studies appear to be the most promising for characterizing and quantifying MBR. This is particularly true when these studies also utilize novel calibration targets and sophisticated surface-process models for estimating mountain aquifer recharge. Combined basin-mountain models also have the greatest potential for successfully predicting MBR and MFR under future warming climate conditions. However, characteristic mountain-block K distributions and active circulation depths for various mountain geologic settings will have to be better constrained through field observations before these models can be considered truly predictive.

3.5. Studies Addressing Human Impacts

Human-induced changes in land use and land cover (LU/LC) and climate are rapidly changing the boundary conditions of mountain groundwater flow systems and thus could significantly influence mountain aquifer recharge and MBR. Since 2004, there has been a surge in studies seeking to understand how climate and LU/LC change may impact groundwater recharge. Here, we review studies that either specifically address impacts to MFR and MBR or have findings directly relevant to potential impacts. Comprehensive reviews of potential effects of climate and LU/LC change impacts on groundwater recharge in general are provided by Green et al. (2011), Taylor et al. (2013), and Smerdon (2017).

Global projections of climate change impacts to groundwater recharge are uncertain due to limited representation of groundwater in global climate models and poorly resolved precipitation trends (Green et al., 2011; Taylor et al., 2013). Projected future changes in precipitation in mountainous areas are especially uncertain due to complications introduced by local orographic effects (Beniston et al., 1997). That said, some regional and watershed-scale studies have substantially contributed to our understanding of how climate change could potentially influence mountain aquifer recharge and MBR. Regional studies reporting declining base-flows in mountain streams over recent decades (e.g., Rood et al., 2008), combined with studies indicating a close link between snowpack volume and mountain aquifer recharge rate (e.g., Manning et al., 2012), suggest that future mountain aquifer recharge rates are likely to decline in response to continued declines in snowpack in many areas. Meixner et al. (2016) synthesized regional climate change projection studies and expert knowledge to estimate recharge component shifts for eight aquifer systems in the western United States. They found that the MFR component (including MBR) would likely decrease across much of the region due to declining snowpack and increased ET, although they also note that this decrease may be less in more humid higher-latitude areas due to projected increases in total precipitation. As emphasized by Meixner et al. (2016), in mountainous systems, snowmelt commonly composes a disproportionately large fraction of mountain aquifer recharge compared to rainwater (e.g., Ajami et al., 2012; Earman et al., 2006), making mountain aquifer recharge potentially sensitive to an increasing rain/snow ratio due to warming alone. Snowpack declines will be greatest at lower elevations (Stewart, 2009), though the magnitude of decrease will vary since the snow rain transition elevation is different across mountainous regions. This is particularly concerning for MBR from crystalline-rock mountain blocks because, as discussed in section 3.1, much of this MBR may originate from lower-elevation areas closer to the mountain front (Welch & Allen, 2012).

The effect of decreasing snowpack on mountain aquifer recharge and MBR could vary widely across different mountain block zones composed of different lithologies. For example, Markovich et al. (2016) performed numerical climate change experiments using a low-K and higher-K hillslope, representing fractured crystalline and volcanic rock settings, respectively, and found large recharge reductions in the higher-K hillslope and relatively slight recharge reductions in the low-K hillslope. This suggests a mountain aquifer permeability threshold below which absolute MBR rates may be insensitive to warming and associated declines in precipitation available for infiltration. Other studies have found that recharge to mountain aquifers composed of fractured crystalline rock (i.e., lower K) commonly may be permeability limited rather than precipitation limited (Carroll et al., 2019; Flint et al., 2008; Manning & Solomon, 2005). Furthermore, Manning (2011) concluded that the absolute MBR rate from the crystalline-rock Sangre de Cristo Mountains, New Mexico, USA, probably decreased little from the cooler, wetter Pleistocene to warmer, drier Holocene epochs based on NGTs and radiocarbon ages from wells in the adjacent Española Basin. The manner in which climate-change-related shifts in mountain aquifer recharge would impact flow path partitioning within the mountain block and the relative importance of MBR versus surface MFR also remains largely unknown. For example, a decrease in mountain aquifer recharge could lead to lower WTs in the mountain block that could result in more regional versus local groundwater flow. This could in turn increase the relative amount of MBR compared to surface runoff/MFR, thus increasing the MBR fraction in the basin aquifer (though both the total recharge and absolute MBR rate would decrease). However, this shifting balance in the relative importance of MBR versus surface MBR could be buffered by increasing extreme precipitation events that might increase surface MFR but not MBR.

Most studies of climate change impacts to mountain aquifer recharge have focused on snowmelt, and few have addressed potential near-term and long-term changes in recharge resulting from glacier and permafrost melt. Alpine glaciers are melting rapidly across the world (Zekollari et al., 2019), and many are drained by permeable streambeds which, depending on the style of connection to the WT, can potentially conduct substantial amounts of recharge to mountain aquifers. Through a combination of stream loss gaging and glacier

mass balance, Liljedahl et al. (2017) found that glacier melt contributed disproportionately to stream runoff and that headwater streams lost up to 56% of annual runoff to mountain aquifer recharge in the Tanana River watershed, AK. This suggests that, while recharge in these headwaters may increase in the short term due to accelerated melting, it could substantially decrease in the long-term due to glacier loss. Permafrost melt may increase recharge to mountain aquifers in two ways: (1) increasing the active layer depth, or unfrozen zone, thereby increasing mountain aquifer thickness (Lamontagne-Hallé et al., 2018); and (2) direct contribution of permafrost melt to groundwater storage (Hiyama et al., 2013). Importantly, glacier and permafrost melt are generally not captured by current precipitation networks or recharge calculations, and so the quantification of this added component at the mountain-block scale remains a major uncertainty in climate change projections.

Historical LU/LC change in basins has been dominated by land conversion for agriculture. This has resulted in well-documented increases in direct recharge over the basin due to irrigation losses (Scanlon et al., 2006; Scanlon et al., 2005). Consequently, the fraction of MBR in overall basin-fill aquifer recharge has decreased in basins with high agricultural activity (Bexfield et al., 2016; Brush et al., 2013). However, the recent development and adoption of precision water application has led to a decrease in the “loss” of irrigation water to recharge and ET (Ward & Pulido-Velazquez, 2008), decreasing total basin-fill aquifer recharge in areas where this practice is applied and perhaps increasing the relative fraction of MBR toward predevelopment levels. The dominant LU/LC change in mountain blocks has been within forests. Studies have found that deforestation generally leads to increases in recharge and vice versa (Jobbágy & Jackson, 2004; Scanlon et al., 2006). Forest thinning (Roche et al., 2018) and tree die-off due to climate-exacerbated insect infestation (Bearup et al., 2014) have been shown to reduce ET and augment runoff and recharge during certain times of year. However, increases in total annual runoff and mountain aquifer recharge remain uncertain and may be compensated by increased snow sublimation (due to decreased canopy cover; Biederman et al., 2015), longer growing seasons (Mankin et al., 2018), and migrating treelines (Goulden & Bales, 2014). Finally, there have been documented increases in both runoff (Seibert et al., 2010; Wine et al., 2018) and baseflow (Kinoshita & Hogue, 2015) following fire disturbance in mountain headwater catchments.

Taken together, available studies suggest that LU/LC and climate change have the potential to significantly impact MBR. These studies indicate that LU/LC and climate change are currently driving, and will continue to drive, changes in factors directly linked to mountain aquifer recharge, such as decreasing snow fractions in precipitation, melting glaciers and permafrost, increasing ET, longer growing seasons, and increased fire frequency and intensity. These trends point to decreased mountain aquifer recharge in many regions, though uncertainties in precipitation projections, subsurface hydrogeologic characteristics, and system feedbacks limit our confidence in making specific projections regarding the extent or degree of changes in a particular mountain system. Projecting LU/LC and climate change impacts to absolute and relative MBR rates is yet more uncertain, further exacerbated by major gaps in our understanding of mountain-block hydrogeology outlined in sections above. Meaningful projections of future MBR rates and basin-fill aquifer water budgets will only be possible with improved precipitation projections, more comprehensive knowledge of MBR itself, and the development of sophisticated numerical models that represent both surface and subsurface conditions/processes at an appropriate level of detail.

4. Current Understanding of Controls on MBR

The studies reviewed above demonstrate that MBR can be an important fraction of recharge to basin-fill aquifers around the world, even in the case of apparently low-K mountain blocks. Here, we summarize our current understanding of the fundamental factors controlling where and how much MBR might be occurring.

First, MBR requires the existence of a mountain-block aquifer that hosts active groundwater flow. As discussed in section 3.3, apparent thresholds to produce active mountain groundwater flow are $K > 10^{-8}$ m/s and recharge rates greater than roughly 10 mm/year. If neither of these conditions are satisfied, MBR is probably negligible. If either is satisfied, then there is likely some MBR, with the caveat that MBR still could be locally obstructed by mountain-front parallel faults (Caine et al., 2017; Chowdhury et al., 2008; Delinon, 2009; Kebede et al., 2008).

If active mountain bedrock groundwater flow exists, making MBR possible, the next consideration is the depth of active circulation (i.e., mountain aquifer thickness). If the active circulation depth is less than the

approximate scale of topographic relief in the headwater catchments (commonly hundreds of meters), then MBR will mainly originate from slopes immediately above the mountain front as front-slope flow (Welch & Allen, 2012) and perhaps also enter the basin near the mouths of mountain watersheds immediately below streams (Figure 2). For many mountain systems, slopes immediately above the mountain front compose a small percentage of the total mountain-block terrain, so MBR rates will be more limited but could still be an important recharge component for the basin aquifer. If the active circulation depth is greater than the scale of topographic relief in the headwater catchments, MBR can potentially originate farther back in the mountain block and MBR rates will thus be higher (Manning & Solomon, 2005). In crystalline-rock mountain blocks, circulation depths appear to generally extend to depths of 100–200 m (Welch & Allen, 2014), though this contact may be highly variable (Clair et al., 2015; Frisbee et al., 2017). This aquifer thickness is substantially less than the topographic relief of typical mountain headwater catchments and has been shown to produce MBR predominantly near the front of the mountain block as front-slope flow (Manning & Solomon, 2005; Welch & Allen, 2012). Mountain-block faults may promote deeper (>500 m) active circulation in crystalline rocks (Ofterdinger et al., 2014; Tomonaga et al., 2017), but the volumetric significance of these localized fault-hosted flows relative to basin-fill total recharge rates remains unclear. Greater active circulation depths (>1,000 m) are likely in mountain blocks composed of volcanic rocks (Frisbee et al., 2017; Saar & Manga, 2004) and could be common in sedimentary rock mountain blocks as well (Lazear, 2006), but studies addressing circulation depth in such noncrystalline mountain blocks are limited.

If the mountain-block circulation depth is greater than the scale of the topographic relief in the headwater catchments, the WT position relative to the land surface in the mountain block becomes the primary control on the relative proportions of local versus interbasin (potential MBR) flow. If the regional WT is lower than the streambeds in the headwater catchments, such that headwater stream channels are dominantly ephemeral (recharge-controlled WT), a larger fraction of mountain groundwater is inclined to follow a regional flow path toward the mountain front and become MBR. If the regional WT is higher and headwater streams are dominantly perennial (topography-controlled WT), a larger fraction of mountain groundwater will discharge locally in the headwater streams, and a smaller fraction will become MBR (Bresciani et al., 2018; Gleeson & Manning, 2008). It should be kept in mind, however, that large fractions of regional flow in the mountain block do not necessarily equate with large absolute MBR rates to the adjacent basin. In other words, if the mountain-block regional WT position is very low due to very low mountain aquifer recharge rates (as could be the case in arid mountains), absolute MBR rates would also be low. The highest absolute MBR rates will occur when, in addition to the mountain-block WT being recharge controlled, the active zone K is high and the mountain-block WT remains as high as possible relative to the adjacent basin elevation (maximizing the head gradient between the mountain block and the basin)—a situation that can only occur if mountain aquifer recharge rates are high as well. Mountain WTs will be higher relative to the adjacent basin if the mountain topography is high relative to the basin surface and if the mountain stream network is less deeply incised (Gleeson & Manning, 2008; Welch & Allen, 2012). Finally, geologic heterogeneity could complicate the above general rules by producing perched aquifers, barriers, and conduits for interbasin flow, and more work is needed to explore how the presence of common types of heterogeneity would affect the proportion of local, intermediate, and regional flow paths.

In summary, higher mountain aquifer K and recharge rates, deeper mountain groundwater circulation, recharge-controlled mountain WTs, and higher mountains with less incised stream networks all promote greater MBR. The clarifications of the fundamental factors controlling MBR in conceptual studies, as well as their validation in some real-world case studies, are important advances in our understanding of MBR. However, significant challenges remain in the application of these governing principles to real, heterogeneous systems to successfully constrain and predict MBR. These conceptual studies also clearly demonstrate the close link between mountain aquifer recharge rates and MBR, underscoring the importance of understanding the effects of LU/LC and climate change on mountain aquifer recharge if we are to successfully forecast future MBR rates.

5. Conclusions and Future Research Priorities

Our understanding of MBR has advanced significantly in the 15 years since Wilson and Guan (2004), driven by a surge in MBR studies applying a broadening range of methodologies around the world. We believe that the hydrologic community has accomplished the first hurdle of confirming that MBR is a real and often substantial component of recharge to lowland aquifer systems in a variety of climatic and geologic

settings. The second hurdle lies in developing and validating robust methodologies for quantifying MBR (including its spatial distribution) and fully understanding controlling processes. Toward this end, we have made major progress through new observational techniques, technological and analytical advances, and well-conceived research programs. However, data limitations still impart large uncertainties in our estimates of MBR, particularly subsurface data from the mountain block and mountain front.

A major advancement since Wilson and Guan (2004) has been in our understanding of groundwater flow in mountain headwater catchments, driven by investment in surface and relatively shallow subsurface (<50 m deep) observational infrastructure aimed at understanding near-surface hydrological, chemical, and biological processes within the catchment. However, if we are to make significant further advancements in understanding MBR, we now need to apply a similar level of investment to directly investigating and characterizing larger-scale interbasin groundwater flow in the mountain block and lower-elevation front-slope flow. Thus far, studies attempting to characterize interbasin and front-slope flow have mainly done so using numerical flow models based on limited subsurface information between shallow depths in headwater catchments and the mountain front (Ameli et al., 2018; Doyle et al., 2015; Gilbert & Maxwell, 2017; Gleeson & Manning, 2008). Thus, there is a high-priority need for deep (>100 m) research monitoring wells and deep-imaging geophysical surveys located at different strategic positions in the mountain block, including near the mountain front, that would allow us to determine bedrock properties (particularly K) through a range of depths and to access and sample groundwater following deeper flow paths. Boreholes drilled for deep well installation should be logged using standard downhole geophysical logging tools and should be completed with multilevel well screens to better enable discrete-depth groundwater sampling. Airborne and surface geophysical surveys capable of discerning deep subsurface geologic framework (and potentially porosity and permeability) such as airborne time domain electromagnetic surveys (Vittecoq et al., 2019) and nuclear magnetic resonance (Legchenko et al., 2002) should be performed. These methods become yet more powerful when combined with downhole geophysical logs and drill core from a local deep borehole (Flinchum et al., 2018; Orlando et al., 2016; Vittecoq et al., 2019). Because installing wells and performing such surveys can be prohibitively expensive for individual researchers or institutions, we advocate for funding strategies that involve pooling investment in observational infrastructure and that lever existing infrastructure to the greatest degree possible. For example, the existing Critical Zone Observatory network could be targeted for deep well installation, since they already possess important infrastructure and are located in a range of climatic and lithologic settings around the world (Anderson et al., 2008), and expanded to include lower-elevation research sites farther down potential MBR flow paths. Also, transportation and water diversion tunnels and active mining operations (which often include monitoring well networks) have been largely underutilized in MBR studies and could provide valuable additional hydrogeologic data when combined with newly installed research monitoring wells.

Investment in subsurface observations in the mountain block and at the mountain front is key for advancing our understanding of MBR to the quantitative and predictive stage. We believe this stage is most likely to be reached if, in parallel, the following four major questions are prioritized in future field and modeling research efforts.

1. What are the active circulation depths in different systems? Of the primary factors controlling the amount of MBR, active circulation depth (i.e., the K vs. depth relationship) in the mountain block remains in general the most uncertain. Available studies point to a typical active circulation depth of 100–200 m for fractured crystalline rock settings, but the number of direct subsurface measurements at depths >100 m remains relatively few. These measurements are even more rare in other lithologies, such as volcanic and sedimentary rock systems. The deeper subsurface data obtained from wells and geophysical surveys discussed above would significantly tighten constraints on active circulation depth estimates for specific sites. These estimates could then be used to increase knowledge of characteristic circulation depths for different lithologies that have undergone different weathering and tectonic histories, which in turn could substantially improve our ability to predict MBR.
2. What is the spatial distribution of MBR in different systems? Several studies have identified a high degree of spatial variability in MBR (Table 1), but few have directly linked these variations with specific changes in geologic, topographic, or climatic characteristics of the mountain block. Furthermore, we are aware of no studies that have quantified how much MBR occurs as shallow focused flow near watershed mouths versus front-slope flow versus deep diffuse or focused flow (Figures 2 and 3). A clear need therefore exists to better understand the geologic, topographic, and climatic controls on the spatial distribution of MBR and

the relative importance of different MBR components. This includes a better understanding of the roles of structural and tectonic features in enhancing or impeding different MBR flowpaths. A potential approach for examining the spatial distribution of MBR with current methodological capabilities could be the installation of multiple monitoring wells distributed along the mountain front adjacent to different representative sections/features of the mountain block (e.g., at the mouth of a watershed composed of intrusive rocks, beneath a triangular facet composed of carbonates). Multiple different types of discrete-depth observations (temperature measurements, groundwater chemistry and age, NGTs, etc.) could then be combined with numerical modeling to elucidate and potentially quantify relative fluxes of different MBR pathways and link these to specific variations in the mountain block.

3. What is the relative fraction of MBR and surface MFR in different systems? Distinguishing MBR from surface MFR is critical for producing reliable MBR estimates. However, many studies still do not convincingly distinguish between these two sources, and challenges in doing so continue to contribute substantial uncertainty to most MBR estimates. This review covered some effective methods that could be more widely applied, and efforts should continue in developing new and improved methods for distinguishing MBR from surface MFR. As previously emphasized, combined approaches hold the greatest promise. For example, the approach of Bresciani et al. (2018) of using large and spatially extensive EC and hydraulic head measurements could be used in combination with EMMA (Liu & Yamanaka, 2012; Peng et al., 2018) and/or NGTs to detect the presence or absence of MBR in the basin-fill aquifer, distinguish it from surface MFR, and quantify its relative magnitude with reasonable confidence. Note that this approach would be yet more effective with the existence of deep monitoring wells at the mountain front.
4. How will MBR shift in response to climate and land use change? Available studies, though few, provide reason for concern that MBR could generally decrease in response to climate and LU/LC change. However, the magnitude of this decrease and the extent to which it may be locally buffered by factors discussed in section 3.5 (or perhaps even increase) are uncertain. This uncertainty is partially attributable to uncertainty in regional precipitation projections but is mostly due to our inability to confidently quantify and predict MBR under varying conditions. Thus, addressing the above three questions is essential for producing useful MBR projections. Physically based integrated hydrologic models are most capable of projecting MBR response to climate and LU/LC change, as they can capture feedbacks between temperature, ET, precipitation phase, and recharge (Markovich et al., 2016). Furthermore, advances in running large models with high-performance computing indicate the feasibility of large-scale integrated simulations (Maxwell et al., 2015). Though calibrating and validating these parameter dense models remains a major challenge, the development of multitarget calibration strategies including nontraditional calibration targets (temperature, groundwater age, and NGTs) have shown great promise in reducing model nonuniqueness and increasing our confidence in model projections (Schilling et al., 2019).

The “hidden” nature of MBR initially described by Feth (1964) has continued to present major challenges in its characterization and quantification over the past 15 years since the review of Wilson and Guan (2004). However, we believe answering the above questions is within reach given the current methodological and technological capabilities of the hydrologic community, provided there is a coordinated and significant investment in deeper subsurface data from the mountain block and near the mountain front. Thus, clearing the second hurdle of confidently quantifying MBR and reaching the important stage of useful prediction is possible. Given the importance of basin-fill aquifers as water resources globally and the potential for declines in MBR in the face of climate warming and LU/LC, the need for this progress is now pressing.

Acknowledgments

We thank B. Scanlon, P. Gardner, and four anonymous reviewers whose thoughtful and constructive comments greatly improved our manuscript. The first author was supported by an NSF EAR Postdoctoral Fellowship (EAR-1806383). The NSF Santa Catalina Mountains and Jemez River Basin Critical Zone Observatory (EAR-1331408) also provided support for this study. The information and R code used to produce Figure 1 is available online (<https://doi.org/10.5281/zenodo.3387776>). The authors declare no conflict of interest. Any use of trade, firm, or product names is for descriptive purposes only and does not imply endorsement by the U.S. Government.

References

- Aeschbach-Hertig, W., Peeters, F., Beyerle, U., & Kipfer, R. (1999). Interpretation of dissolved atmospheric noble gases. *Water Resources Research*, 35(9), 2779–2792. <https://doi.org/10.1029/1999WR900130>
- Aishlin, P., & McNamara, J. P. (2011). Bedrock infiltration and mountain block recharge accounting using chloride mass balance. *Hydrological Processes*, 25(12), 1934–1948. <https://doi.org/10.1002/hyp.7950>
- Ajami, H., Meixner, T., Dominguez, F., Hogan, J., & Maddock, T. (2012). Seasonalizing mountain system recharge in semiarid basins—Climate change impacts. *Ground Water*, 50(4), 585–597. <https://doi.org/10.1111/j.1745-6584.2011.00881.x>
- Ajami, H., Troch, P. A., Maddock, T., Meixner, T., & Eastoe, C. (2011). Quantifying mountain block recharge by means of catchment-scale storage-discharge relationships. *Water Resources Research*, 47, W04504. <https://doi.org/10.1029/2010WR009598>
- Althaus, R., Klump, S., Onnis, A., Kipfer, R., Purtschert, R., Stauffer, F., & Kinzelbach, W. (2009). Noble gas tracers for characterisation of flow dynamics and origin of groundwater: A case study in Switzerland. *Journal of Hydrology*, 370(1), 64–72. <https://doi.org/10.1016/j.jhydrol.2009.02.053>
- Ameli, A., Gabrielli, C., Morgenstern, U., & McDonnell, J. J. (2018). Groundwater subsidy from headwaters to their parent water watershed: A combined field-modeling approach. *Water Resource Research*, 54, 5110–5125. <https://doi.org/10.1029/2017WR022356>

- Anderson, S. P., Bales, R. C., & Duffy, C. J. (2008). Critical Zone Observatories: Building a network to advance interdisciplinary study of Earth surface processes. *Mineralogical Magazine*, 72(1), 7–10. <https://doi.org/10.1180/minmag.2008.072.1.7>
- Andreu, J. M., Alcalá, F. J., Vallejos, Á., & Pulido-bosch, A. (2011). Recharge to mountainous carbonated aquifers in SE Spain: Different approaches and new challenges. *Journal of Arid Environments*, 75(12), 1262–1270. <https://doi.org/10.1016/j.jaridenv.2011.01.011>
- Bales, R. C., Molotch, N. P., Painter, T. H., Dettinger, M. D., Rice, R., & Dozier, J. (2006). Mountain hydrology of the western United States. *Water Resources Research*, 42, W08432. <https://doi.org/10.1029/2005WR004387>
- Ball, L. B., Caine, J. S., & Ge, S. (2014). Controls on groundwater flow in a semiarid folded and faulted intermountain basin. *Water Resources Research*, 50, 6788–6809. <https://doi.org/10.1002/2013WR014451>
- Barnett, T. P., Adam, J. C., & Lettenmaier, D. P. (2005). Potential impacts of a warming climate on water availability in snow-dominated regions. *Nature*, 438, 303–309. <https://doi.org/10.1038/nature04141>
- Battle-Aguilar, J., Banks, E. W., Batelaan, O., Kipfer, R., Brennwald, M. S., & Cook, P. G. (2017). Groundwater residence time and aquifer recharge in multilayered, semi-confined and faulted aquifer systems using environmental tracers. *Journal of Hydrology*, 546, 150–165. <https://doi.org/10.1016/j.jhydrol.2016.12.036>
- Bearup, L., Maxwell, R., Clow, D., & McCray, J. (2014). Hydrological effects of forest transpiration loss in bark beetle-impacted watersheds. *Nature Climate Change*, 4(6), 481–486. <https://doi.org/10.1038/NCLIMATE2198>
- Beniston, M., Diaz, H. F., & Bradley, R. S. (1997). Climatic change at high elevation sites: An overview. *Climatic Change*, 36, 233–251. <https://doi.org/10.3406/rga.2005.2342>
- Bexfield, B. L. M., Heywood, C. E., Kauffman, L. J., Rattray, G. W., & Vogler, E. T. (2016). Hydrogeologic setting and groundwater flow simulation of the Middle Rio Grande Basin Regional Study Area, New Mexico. In S. Eberts (Ed.), *in Hydrogeologic settings and groundwater-flow simulations for regional investigations of the transport of anthropogenic and natural contaminants to public-supply wells—Investigations begun in 2004*: Reston, VA pp. 21–261: U.S. Geological Survey Professional Paper 1737—B.
- Biederman, J. A., Somor, A. J., Harpold, A. A., Gutmann, E. D., Breshears, D. D., Troch, P. A., et al. (2015). Recent tree die-off has little effect on streamflow in contrast to expected increases from historical studies. *Water Resource Research*, 51, 9775–9789. <https://doi.org/10.1002/2015WR017401>
- Blasch, K. W., & Bryson, J. R. (2007). Distinguishing sources of ground water recharge by using ^2H and ^{18}O . *Ground Water*, 45(3), 294–308. <https://doi.org/10.1111/j.1745-6584.2006.00289.x>
- Bolger, B. L., Park, Y. J., Unger, A. J., & Sudicky, E. A. (2011). Simulating the pre-development hydrologic conditions in the San Joaquin Valley, California. *Journal of Hydrology*, 411(3–4), 322–330. <https://doi.org/10.1016/j.jhydrol.2011.10.013>
- Bouchaou, L., Michelot, J. L., Vengosh, A., Hsissou, Y., Qurtobi, M., Gaye, C. B., et al. (2008). Application of multiple isotopic and geochemical tracers for investigation of recharge, salinization, and residence time of water in the Souss Massa aquifer, southwest of Morocco. *Journal of Hydrology*, 352, 267–287. <https://doi.org/10.1016/j.jhydrol.2008.01.022>
- Bresciani, E., Cranswick, R. H., Banks, E. W., Battle-aguilar, J., Cook, P. G. & Batelaan, O. (2018). Using hydraulic head, chloride and electrical conductivity data to distinguish between mountain-front and mountain-block recharge to basin aquifers. *Hydrology and Earth System Sciences*, 22, 1629–1648. <https://doi.org/10.5194/hess-22-1629-2018>
- Bresciani, E., Ordens, C. M., Werner, A. D., Batelaan, O., Guan, H., & Post, V. E. (2014). Spatial variability of chloride deposition in a vegetated coastal area: Implications for groundwater recharge estimation. *Journal of Hydrology*, 519, 1177–1191. <https://doi.org/10.1016/j.jhydrol.2014.08.050>
- Brunner, P., & Simmons, C. T. (2012). Hydrogeosphere: A fully integrated, physically based hydrological model. *Groundwater*, 50(2), 170–176. <https://doi.org/10.1111/j.1745-6584.2011.00882.x>
- Brush, C. F., Dogrul, E. C., & Tariq, N. K. (2013). Development and calibration of the California Central Valley groundwater-surface water simulation model (C2VSim), Version 3.02-CG (*Technical Memorandum p. 196*): California Department of Water Resources, Bay-Delta Office.
- Buttle, J. (1994). Isotope hydrograph separations and rapid delivery of pre-event water from drainage basins. *Progress in Physical Geography*, 18(1), 16–41. <https://doi.org/10.1177/030913339401800102>
- Caine, J., Evans, J., & Forster, C. (1996). Fault zone architecture and permeability structure. *Geology*, 1025–1028. <https://doi.org/10.1130/0091-7613>
- Caine, J. S., Minor, S. A., Grauch, V., Budahn, J. R., & Keren, T. T. (2017). A comprehensive survey of faults, breccias, and fractures in and flanking the eastern Española basin, Rio Grande Rift, New Mexico. *Geosphere*, 13(5), 1566–1609. <https://doi.org/10.1130/ges01348.1>
- Carrera-Hernández, J. J., & Gaskin, S. J. (2008). Spatio-temporal analysis of potential aquifer recharge: Application to the basin of Mexico. *Journal of Hydrology*, 353(3–4), 228–246. <https://doi.org/10.1016/j.jhydrol.2008.02.012>
- Carroll, R. W., Deems, J. S., Niswonger, R., Schumer, R., & Williams, K. H. (2019). The importance of interflow to groundwater recharge in a snowmelt-dominated headwater basin. 46, 5899–5908. <https://doi.org/10.1029/2019GL02447>
- Cayan, D. R., Kammerdiener, S. a., Dettinger, M. D., Caprio, J. M., & Peterson, D. H. (2001). Changes in the onset of spring in the western United States. *Bulletin of the American Meteorological Society*, 82(3), 399–415. [https://doi.org/10.1175/1520-0477\(2001\)082<2265:CAACOC>2.3.CO;2](https://doi.org/10.1175/1520-0477(2001)082<2265:CAACOC>2.3.CO;2)
- Cayan, D. R., Maurer, E. P., Dettinger, M. D., Tyree, M., & Hayhoe, K. (2008). Climate change scenarios for the California region. *Climatic Change*, 87(S1), 21–42. <https://doi.org/10.1007/s10584-007-9377-6>
- Cederberg, J., Gardner, P., & Thiros, S. (2009). Hydrology of northern Utah Valley, Utah County, Utah, 1975–2005: U.S. Geological Survey Scientific Investigations Report, 2008–5197.
- Chowdhury, A. H., Uliana, M., & Wade, S. (2008). Ground water recharge and flow characterization using multiple isotopes. *Ground Water*, 46(3), 426–436. <https://doi.org/10.1111/j.1745-6584.2008.00443.x>
- Christensen, N. S., Wood, A. W., Voisin, N., Lettenmaier, D. P., & Palmer, R. N. (2004). The effects of climate change on the hydrology and water resources of the Colorado River basin. *Climatic Change*, 62(1), 337–363. <https://doi.org/10.1023/B:CLIM.0000013684.13621.1f>
- Dahlke, H. E., & Lyon, S. W. (2013). Early melt season snowpack isotopic evolution in the Tarfala Valley, northern Sweden. *Annals of Glaciology*, 54(62), 149–156. <https://doi.org/10.3189/2013AoG62A232>
- Delinon, R. M. (2009). Structural geology controls on groundwater flow: Lembang Fault case study, West Java, Indonesia. *Hydrogeology Journal*, 17(4), 1011–1023. <https://doi.org/10.1007/s10040-009-0453-z>
- Doyle, J. M., Gleeson, T., Manning, A. H., & K. Ulrich Mayer (2015). Using noble gas tracers to constrain a groundwater flow model with recharge elevations: A novel approach for mountainous terrain. *Water Resources Research*, 51, 8094–8113. <https://doi.org/10.1002/2015WR017274>
- Dwivedi, R., Meixner, T., Mcintosh, J. C., Ferré, P. A. T., Dwivedi, R., Eastoe, C. J., et al. (2019). Hydrologic functioning of the deep critical zone and contributions to streamflow in a high-elevation catchment: Testing of multiple conceptual models. *Hydrological Processes*, 33, 476–494. <https://doi.org/10.1002/hyp.13363>

- Earman, S., Campbell, A. R., Phillips, F. M., & Newman, B. D. (2006). Isotopic exchange between snow and atmospheric water vapor: Estimation of the snowmelt component of groundwater recharge in the southwestern United States. *Journal of Geophysical Research*, *111*, D09302. <https://doi.org/10.1029/2005JD006470>
- Eastoe, C., & Towne, D. (2018). Regional zonation of groundwater recharge mechanisms in alluvial basins of Arizona: Interpretation of isotope mapping. *Journal of Geochemical Exploration*, *194*, 134–145. <https://doi.org/10.1016/j.gexplo.2018.07.013>
- Engdahl, N. B., Ginn, T. R., & Fogg, G. E. (2012). Non-Fickian dispersion of groundwater age. *Water Resources Research*, *48*, W07508. <https://doi.org/10.1029/2012WR012251>
- Fan, Y., & Schaller, M. F. (2009). River basins as groundwater exporters and importers: Implications for water cycle and climate modeling. *Journal of Geophysical Research Atmospheres*, *114*, D04103. <https://doi.org/10.1029/2008JD010636>
- Faunt, C. (2009). Groundwater availability of the Central Valley aquifer, California, U.S. *Geological Survey Professional Paper*, *1766*, 225.
- Feth, J. H. (1964). Hidden recharge. *Groundwater*, *2*(4), 14–17. <https://doi.org/10.1111/j.1745-6584.1964.tb01780.x>
- Flinchum, B. A., Holbrook, W. S., Rempe, D., Moon, S., Riebe, C. S., Carr, B. J., et al. (2018). Critical zone structure under a granite ridge inferred from drilling and three-dimensional seismic refraction data. *Journal of Geophysical Research: Earth Surface*, *123*(6), 1317–1343. <https://doi.org/10.1029/2017jf004280>
- Flint, A. L., Flint, L. E., & Dettinger, M. D. (2008). Modeling soil moisture processes and recharge under a melting snowpack. *Vadose Zone Journal*, *7*(1), 350. <https://doi.org/10.2136/vzj2006.0135>
- Fogg, G. E., & Zhang, Y. (2016). Debates—stochastic subsurface hydrology from theory to practice: A geologic perspective. *Water Resources Research*, *52*, 9235–9245. <https://doi.org/10.1002/2016WR019699>
- Frisbee, M. D., Tolley, D. G., & Wilson, J. L. (2017). Field estimates of groundwater circulation depths in two mountainous watersheds in the western U.S. and the effect of deep circulation on solute concentrations in streamflow. *Water Resource Research*, *53*, 2693–2715. <https://doi.org/10.1002/2016WR019553>
- Gabrielli, C., Morgenstern, U., Stewart, M. K., & McDonnell, J. J. (2018). Contrasting groundwater and streamflow ages at the Maimai Watershed. *Water Resource Research*, *54*, 3937–3957. <https://doi.org/10.1029/2017WR021825>
- Gardner, P. (2009). Three-dimensional numerical model of ground-water flow in northern Utah Valley, Utah County, Utah, U.S: Geological Survey Scientific Investigations Report 2008-5049. p. 95.
- Gardner, P. M., & Heilweil, V. M. (2014). A multiple-tracer approach to understanding regional groundwater flow in the Snake Valley area of the eastern Great Basin, USA. *Applied Geochemistry*, *45*, 33–49. <https://doi.org/10.1016/j.apgeochem.2014.02.010>
- Gilbert, J. M., & Maxwell, R. M. (2017). Examining regional groundwater-surface water dynamics using an integrated hydrologic model of the San Joaquin River basin. *Hydrology and Earth System Sciences*, *21*(2), 923–947. <https://doi.org/10.5194/hess-21-923-2017>
- Gillespie, J., Nelson, S. T., Mayo, A. L., & Tingey, D. G. (2012). Why conceptual groundwater flow models matter: A trans-boundary example from the arid Great Basin, western USA. *Hydrogeology Journal*, *20*(6), 1133–1147. <https://doi.org/10.1007/s10040-012-0848-0>
- Gleeson, T., & Manning, A. H. (2008). Regional groundwater flow in mountainous terrain: Three-dimensional simulations of topographic and hydrogeologic controls. *Water Resources Research*, *44*, W10403. <https://doi.org/10.1029/2008WR006848>
- Goulden, M. L., & Bales, R. C. (2014). Mountain runoff vulnerability to increased evapotranspiration with vegetation expansion. *Proceedings of the National Academy of Sciences*, *111*(39), 14,071–14,075. <https://doi.org/10.1073/pnas.1319316111>
- Green, T. R., Taniguchi, M., Kooi, H., Gurdak, J. J., Allen, D. M., Hiscock, K. M., et al. (2011). Beneath the surface of global change: Impacts of climate change on groundwater. *Journal of Hydrology*, *405*(3–4), 532–560. <https://doi.org/10.1016/j.jhydrol.2011.05.002>
- Guan, H., Love, A. J., Simmons, C. T., Hutson, J., & Ding, Z. (2010a). Catchment conceptualisation for examining applicability of chloride mass balance method in an area with historical forest clearance. *Hydrology and Earth System Sciences*, *14*(7), 1233–1245. <https://doi.org/10.5194/hess-14-1233-2010>
- Guan, H., Love, A. J., Simmons, C. T., Makhnin, O., & Kayaalp, A. S. (2010b). Factors influencing chloride deposition in a coastal hilly area and application to chloride deposition mapping. *Hydrology and Earth System Sciences*, *14*(5), 801–813. <https://doi.org/10.5194/hess-14-801-2010>
- Haitjema, H. M., & Mitchell-Bruker, S. (2005). Are water tables a subdued replica of the topography? *Groundwater*, *43*(6), 781–786. <https://doi.org/10.1111/j.1745-6584.2005.00090.x>
- Hale, V. C., & McDonnell, J. J. (2016). Effect of bedrock permeability on stream base flow mean transit time scaling relations: 1. A multiscale catchment intercomparison. *Water Resources Research*, *52*, 1358–1374. <https://doi.org/10.1002/2014WR016124>
- Hale, V. C., McDonnell, J. J., Stewart, M. K., Solomon, D. K., Doolittle, J., Ice, G. G., & Pack, R. T. (2016). Effect of bedrock permeability on stream base flow mean transit time scaling relationships: 2. Process study of storage and release. *Water Resources Research*, *52*, 1375–1397. <https://doi.org/10.1002/2015WR017660>
- Harbaugh, A. W., Banta, E. R., Hill, M. C., McDonald, M. G., Groat, C. G., Harbaugh, B. A. W., et al. (2000). MODFLOW-2000, the U.S. Geological Survey modular ground-water model: User guide to modularization concepts and the ground-water flow process: U.S. Geological Survey Open-File Report 00-92. p. 127.
- Heilweil, V. M., Healy, R. W., & Harris, R. N. (2012). Noble gases and coupled heat/fluid flow modeling for evaluating hydrogeologic conditions of volcanic island aquifers. *Journal of Hydrology*, *464*–465, 309–327. <https://doi.org/10.1016/j.jhydrol.2012.07.019>
- Hiyama, T., Asai, K., Kolesnikov, A. B., & Gagarin, L. A. (2013). Estimation of the residence time of permafrost groundwater in the middle of the Lena River basin, eastern Siberia. *Environmental Research Letters*, *8*(3), 35040. <https://doi.org/10.1088/1748-9326/8/3/035040>
- Hopkins, C. B., McIntosh, J. C., Eastoe, C., Dickinson, J. E., & Meixner, T. (2014). Evaluation of the importance of clay confining units on groundwater flow in alluvial basins using solute and isotope tracers: The case of Middle San Pedro Basin in southeastern Arizona (USA). *Hydrogeology Journal*, *22*(4), 829–849. <https://doi.org/10.1007/s10040-013-1090-0>
- Jobbágy, E. G., & Jackson, R. B. (2004). Groundwater use and salinization with grassland afforestation. *Global Change Biology*, *10*(8), 1299–1312. <https://doi.org/10.1111/j.1365-2486.2004.00806.x>
- Kao, Y. H., Liu, C. W., Wang, S. W., & Lee, C. H. (2012). Estimating mountain block recharge to downstream alluvial aquifers from standard methods. *Journal of Hydrology*, *426*–427, 93–102. <https://doi.org/10.1016/j.jhydrol.2012.01.016>
- Katsura, S., Kosugi, K., Mizutani, T., & Mizuyama, T. (2009). Hydraulic properties of variously weathered granitic bedrock in headwater catchments. *Vadose Zone Journal*, *8*(3), 557. <https://doi.org/10.2136/vzj2008.0142>
- Kebede, S., Travi, Y., Asrat, A., Alemayehu, T., Ayenew, T., & Tessema, Z. (2008). Groundwater origin and flow along selected transects in Ethiopian rift volcanic aquifers. *Hydrogeology Journal*, *16*(1), 55–73. <https://doi.org/10.1007/s10040-007-0210-0>
- Kinoshita, A. M., & Hogue, T. S. (2015). Increased dry season water yield in burned watersheds in Southern California. *Environmental Research Letters*, *10*(1), 14003. <https://doi.org/10.1088/1748-9326/10/1/014003>
- Klaus, J., & McDonnell, J. J. (2013). Hydrograph separation using stable isotopes: Review and evaluation. *Journal of Hydrology*, *505*, 47–64. <https://doi.org/10.1016/j.jhydrol.2013.09.006>

- Kohfahl, C., Sprenger, C., Benavente, J., Meyer, H., & Ferna, F. (2008). Recharge sources and hydrogeochemical evolution of groundwater in semiarid and karstic environments: A field study in the Granada Basin (Southern Spain). *Applied Geochemistry*, 23, 846–862. <https://doi.org/10.1016/j.apgeochem.2007.09.009>
- Kormos, P. R., McNamara, J. P., Seyfried, M. S., Marshall, H. P., Marks, D., & Flores, A. N. (2015). Bedrock infiltration estimates from a catchment water storage-based modeling approach in the rain snow transition zone. *Journal of Hydrology*, 525, 231–248. <https://doi.org/10.1016/j.jhydrol.2015.03.032>
- Kosugi, K., Katsura, S., Katsuyama, M., & Mizuyama, T. (2006). Water flow processes in weathered granitic bedrock and their effects on runoff generation in a small headwater catchment. *Water Resources Research*, 42, W02414. <https://doi.org/10.1029/2005WR004275>
- Lambert, P. (1995). Numerical simulation of ground-water flow in basin-fill material in Salt Lake Valley: Tech. Publ. Utah Dep. Nat. Resour., 110-B, p. 58.
- Lamontagne-Hallé, P., McKenzie, J. M., Kurylyk, B. L., & Zipper, S. C. (2018). Changing groundwater discharge dynamics in permafrost regions. *Environmental Research Letters*, 13(084017). <https://doi.org/10.1088/1748-9326/aad404>
- Lazear, G. D. (2006). Evidence for deep groundwater flow and convective heat transport in mountainous terrain, Delta County, Colorado, USA. *Hydrogeology Journal*, 14(8), 1582–1598. <https://doi.org/10.1007/s10040-006-0058-8>
- Legchenko, A., Baltassat, J. M., Beauce, A., & Bernard, J. (2002). Nuclear magnetic resonance as a geophysical tool for hydrogeologists. *Journal of Applied Geophysics*, 50(1-2), 21–46. [https://doi.org/10.1016/S0926-9851\(02\)00128-3](https://doi.org/10.1016/S0926-9851(02)00128-3)
- Liljedahl, A. K., Gädeke, A., O'Neel, S., Gatesman, T. A., & Douglas, T. A. (2017). Glacierized headwater streams as aquifer recharge corridors, subarctic Alaska. *Geophysical Research Letters*, 44, 6876–6885. <https://doi.org/10.1002/2017GL073834>
- Liu, F., Bales, R. C., Conklin, M. H., & Conrad, M. E. (2008). Streamflow generation from snowmelt in semi-arid, seasonally snow-covered, forested catchments, Valles Caldera, New Mexico. *Water Resources Research*, 44, W12443. <https://doi.org/10.1029/2007WR006728>
- Liu, Y., & Yamanaka, T. (2012). Tracing groundwater recharge sources in a mountain-plain transitional area using stable isotopes and hydrochemistry. *Journal of Hydrology*, 464–465, 116–126. <https://doi.org/10.1016/j.jhydrol.2012.06.053>
- Luce, C. H., & Holden, Z. A. (2009). Declining annual streamflow distributions in the Pacific Northwest, United States, 1948–2006. *Geophysical Research Letters*, 36, L16401. <https://doi.org/10.1029/2009GL039407>
- Magruder, I. A., Woessner, W. W., & Running, S. W. (2009). Ecohydrologic process modeling of mountain block groundwater recharge. *Ground Water*, 47(6), 774–785. <https://doi.org/10.1111/j.1745-6584.2009.00615.x>
- Mankin, J. S., Williams, A. P., Seager, R., Smerdon, J. E., & Horton, R. M. (2018). Blue water trade-offs with vegetation in a CO₂-enriched climate. *Geophysical Research Letters*, 45, 3115–3125. <https://doi.org/10.1002/2018GL077051>
- Manning, A. H. (2011). Mountain-block recharge, present and past, in the eastern Española Basin, New Mexico, USA. *Hydrogeology Journal*, 19(2), 379–397. <https://doi.org/10.1007/s10040-010-0696-8>
- Manning, A. H., & Caine, J. S. (2007). Groundwater noble gas, age, and temperature signatures in an Alpine watershed: Valuable tools in conceptual model development. *Water Resources Research*, 43, W04404. <https://doi.org/10.1029/2006WR005349>
- Manning, A. H., Clark, J. F., Diaz, S. H., Rademacher, L. K., Earman, S., & Plummer, L. N. (2012). Evolution of groundwater age in a mountain watershed over a period of thirteen years. *Journal of Hydrology*, 460–461, 13–28. <https://doi.org/10.1016/j.jhydrol.2012.06.030>
- Manning, C. E., & Ingebritsen, S. E. (1999). Permeability implications of the continental of geothermal data crust and metamorphic systems. *Reviews of Geophysics*, 37(1), 127–150.
- Manning, A. H., & Solomon, D. K. (2003). Using noble gases to investigate mountain-front recharge. *Journal of Hydrology*, 275(3-4), 194–207. [https://doi.org/10.1016/S0022-1694\(03\)00043-X](https://doi.org/10.1016/S0022-1694(03)00043-X)
- Manning, A. H., & Solomon, D. K. (2005). An integrated environmental tracer approach to characterizing groundwater circulation in a mountain block. *Water Resources Research*, 41, W12412. <https://doi.org/10.1029/2005WR004178>
- Markovich, K. H., Maxwell, R. M., & Fogg, G. E. (2016). Hydrogeological response to climate change in alpine hillslopes. *Hydrological Processes*, 30(18), 3126–3138. <https://doi.org/10.1002/hyp.10851>
- Mason, D., & Bota, L. (2006). Regional groundwater flow model of the Tucson Active Management Area, Tucson, Arizona: Simulation and application. Modeling Report No. 13. Phoenix, Arizona: Arizona Department of Water Resources, Hydrology Division, p. 159.
- Maurer, D., & Thodal, C. (2000). Quantity and chemical quality of recharge, and updated water budgets, for the basin-fill aquifer in Eagle Valley, Western Nevada, U.S. *Geological Survey Scientific Investigations Report*, 2014-5103, 46.
- Maxwell, R. M., Condon, L. E., & Kollet, S. J. (2015). A high-resolution simulation of groundwater and surface water over most of the continental US with the integrated hydrologic model ParFlow v3. *Geoscientific Model Development*, 8(3), 923–937. <https://doi.org/10.5194/gmd-8-923-2015>
- Maxwell, R. M., & Miller, N. L. (2005). Development of a coupled land surface and groundwater model. *Journal of Hydrometeorology*, 6, 233–247. <https://doi.org/10.1175/JHM422.1>
- Mayo, A. L., & Koontz, W. (2000). Fracture flow and groundwater compartmentalization in the Rollins Sandstone, Lower Mesaverde Group, Colorado, USA. *Hydrogeology Journal*, 8(4), 430–446. <https://doi.org/10.1007/s100400000056>
- Mayo, A. L., Morris, T. H., Peltier, S., Petersen, E. C., Payne, K., Holman, L. S., et al. (2003). Active and inactive groundwater flow systems: Evidence from a stratified, mountainous terrain. *GSA Bulletin*, 115(12), 1456–1472. <https://doi.org/10.1130/B25145.1>
- McCallum, J. L., Cook, P. G., & Simmons, C. T. (2015). Limitations of the use of environmental tracers to infer groundwater age. *Groundwater*, 53(S1), 56–70. <https://doi.org/10.1111/gwat.12237>
- McDonnell, J. J., Bonell, M., Stewart, M. K., & Pearce, J. A. (1990). Deuterium variations in storm rainfall: Implications for stream hydrograph separation. *Water Resources Research*, 26(3), 455–458. <https://doi.org/10.1029/WR026i003p00455>
- Mechal, A., Birk, S., Winkler, G., Wagner, T., & Mogessie, A. (2016). Characterizing regional groundwater flow in the Ethiopian Rift: A multi-model approach applied to Gidabo River Basin. *Austrian Journal of Earth Sciences*, 109(1), 68–83. <https://doi.org/10.17738/ajes.2016.0005>
- Meixner, T., Manning, A. H., Stonestrom, D. A., Allen, D. M., Ajami, H., Blasch, K. W., et al. (2016). Implications of projected climate change for groundwater recharge in the western United States. *Journal of Hydrology*, 534, 124–138. <https://doi.org/10.1016/j.jhydrol.2015.12.027>
- Mote, P. W., Hamlet, A. F., Clark, M. P., & Lettenmaier, D. P. (2005). Declining mountain snowpack in western North America. *Bulletin of the American Meteorological Society*, 86(1), 39–50. <https://doi.org/10.1175/BAMS-86-1-39>
- Musselman, K. N., Clark, M. P., Liu, C., Ikeda, K., & Rasmussen, R. (2017). Slower snowmelt in a warmer world. *Nature Climate Change*, 7(3), 214–219. <https://doi.org/10.1038/nclimate3225>
- Niraula, R., Meixner, T., Ajami, H., Rodell, M., Gochis, D., & Castro, C. L. (2017a). Comparing potential recharge estimates from three land surface models across the western US. *Journal of Hydrology*, 545, 410–423. <https://doi.org/10.1016/j.jhydrol.2016.12.028>
- Niraula, R., Meixner, T., Dominguez, F., Bhattarai, N., Rodell, M., Ajami, H., et al. (2017b). How might recharge change under projected climate change in the western US? *Geophysical Research Letters*, 44, 10,407–10,418. <https://doi.org/10.1002/2017GL075421>

- Oftefinger, U. S., Renard, P., & Loew, S. (2014). Hydraulic subsurface measurements and hydrodynamic modelling as indicators for groundwater flow systems in the Rotondo granite, Central Alps (Switzerland). *Hydrological Processes*, 278, 255–278. <https://doi.org/10.1002/hyp.9568>
- Orlando, J., Comas, X., Hynes, S. A., Buss, H. L., & Brantley, S. L. (2016). Architecture of the deep critical zone in the Rio Icacos watershed (Luquillo Critical Zone Observatory, Puerto Rico) inferred from drilling and ground penetrating radar (GPR). *Earth Surface Processes and Landforms*, 41(13), 1826–1840. <https://doi.org/10.1002/esp.3948>
- Oyarzún, J., Núñez, J., Fairley, J. P., Tapia, S., Alvarez, D., Maturana, H., et al. (2019). Groundwater recharge assessment in an arid, coastal, middle mountain copper mining district, Coquimbo Region, north-central Chile. *Mine Water and the Environment*, 38(2), 226–242. <https://doi.org/10.1007/s10230-019-00603-7>
- Pape, J. R., Banner, J. L., Mack, L. E., Musgrove, M., & Guilfoyle, A. (2010). Controls on oxygen isotope variability in precipitation and cave drip waters, central Texas, USA. *Journal of Hydrology*, 385(1), 20–215. <https://doi.org/10.1016/j.jhydrol.2010.02.021>
- Peel, M. C., Finlayson, B. L., & McMahon, T. A. (2007). Updated world map of the Koppen-Geiger climate classification. *Hydrology and Earth System Sciences*, 11(5), 1633–1644. <https://doi.org/10.5194/hess-11-1633-2007>
- Peng, T.-R., Huang, C.-C., & Chen, J.-E. (2016). Evaluating the relative importance of groundwater recharge sources in a subtropical alluvial plain using tracer-based ternary end member mixing analysis (EMMA). *Water Resources Management*, 30, 3861–3878. <https://doi.org/10.1007/s11269-016-1393-8>
- Peng, T.-R., Zhan, W.-J., Tong, L.-T., Chen, C.-T., Liu, T.-S., & Lu, W.-C. (2018). Assessing the recharge process and importance of montane water to adjacent tectonic valley-plain groundwater using a ternary end-member mixing analysis based on isotopic and chemical tracers. *Hydrogeology Journal*, 26, 2041–2055. <https://doi.org/10.1007/s10040-018-1741-2>
- Roche, J. W., Goulden, M. L., & Bales, R. C. (2018). Estimating evapotranspiration change due to forest treatment and fire at the basin scale in the Sierra Nevada, California. *Ecohydrology*, 11(7), 1–10. <https://doi.org/10.1002/eco.1978>
- Rood, S. B., Pan, J., Gill, K. M., Franks, C. G., Samuelson, G. M., & Shepherd, A. (2008). Declining summer flows of Rocky Mountain rivers: Changing seasonal hydrology and probable impacts on floodplain forests. *Journal of Hydrology*, 349(3-4), 397–410. <https://doi.org/10.1016/j.jhydrol.2007.11.012>
- Saar, M. O., & Manga, M. (2004). Depth dependence of permeability in the Oregon Cascades inferred from hydrogeologic, thermal, seismic, and magmatic modeling constraints. *Journal of Geophysical Research B*, 109, B04204. <https://doi.org/10.1029/2003JB002855>
- Sandoval, E., Baldo, G., Núñez, J., Oyarzún, J., Fairley, J. P., Ajami, H., et al. (2018). Groundwater recharge assessment in a rural, arid, mid-mountain basin in north-central Chile. *Hydrological Sciences Journal*, 63(13-14), 1873–1889. <https://doi.org/10.1080/02626667.2018.1545095>
- Sanford, W. (2011). Calibration of models using groundwater age. *Hydrogeology Journal*, 19, 13–16. <https://doi.org/10.1007/s10040-010-0637-6>
- Sanford, W., Plummer, L., McAda, D., Bexfield, L., & Anderholm, S. (2004). Use of environmental tracers to estimate parameters for a predevelopment ground-water-flow model of the Middle Rio Grande Basin, New Mexico, U.S. *Geological Survey Water-Resources Investigations Report*, 03-4286, 110.
- Scanlon, B. R., Keese, K. E., Flint, A. L., Flint, L. E., Gaye, B., Cheikh, W. M. E., & Simmers, I. (2006). Global synthesis of groundwater recharge in semiarid and arid regions. *Hydrological Processes*, 20, 3335–3370. <https://doi.org/10.1002/hyp.6335>
- Scanlon, B. R., Levitt, D. G., Reedy, R. C., Keese, K. E., & Sully, M. J. (2005). Ecological controls on water-cycle response to climate variability in deserts. *Proceedings of the National Academy of Sciences of the United States of America*, 102(17), 6033–8. <https://doi.org/10.1073/pnas.0408571102>
- Schaefer, D. H., Green, J. M., & Rosen, M. R. (2007). Hydrogeologic settings and ground-water flow simulations of the Eagle Valley and Spanish Springs Valley Regional Study Areas, Nevada. In S. Paschke (Ed.), *in Hydrogeologic settings and ground-water flow simulations for regional studies of the transport of anthropogenic and natural contaminants to public-supply wells—Studies begun in 2001* pp. 38: U.S. Geological Survey Professional Paper 1737–A.
- Schilling, O. S., Cook, P. G., & Brunner, P. (2019). Beyond classical observations in hydrogeology: The advantages of including exchange flux, temperature, tracer concentration, residence time, and soil moisture observations in groundwater model calibration. *Reviews of Geophysics*, 57(1), 146–182. <https://doi.org/10.1029/2018RG000619>
- Segal, D. C., Moran, J. E., Visser, A., Singleton, M. J., & Esser, B. K. (2014). Seasonal variation of high elevation groundwater recharge as indicator of climate response. *Journal of Hydrology*, 519, 3129–3141. <https://doi.org/10.1016/j.jhydrol.2014.10.051>
- Seibert, J., McDonnell, J. J., & Woodsmith, R. D. (2010). Effects of wildfire on catchment runoff response: A modelling approach to detect changes in snow-dominated forested catchments. *Hydrology Research*, 41(5), 378–390. <https://doi.org/10.2166/nh.2010.036>
- Siade, A., Nishikawa, T., & Martin, P. (2015). Natural recharge estimation and uncertainty analysis of an adjudicated groundwater basin using a regional-scale flow and subsidence model (Antelope Valley, California, USA). *Hydrogeology Journal*, 23(6), 1267–1291. <https://doi.org/10.1007/s10040-015-1281-y>
- Singleton, M. J., & Moran, J. E. (2010). Dissolved noble gas and isotopic tracers reveal vulnerability of groundwater in a small, high-elevation catchment to predicted climate changes. *Water Resources Research*, 46, W00F06. <https://doi.org/10.1029/2009WR008718>
- Smerdon, B. D. (2017). A synopsis of climate change effects on groundwater recharge. *Journal of Hydrology*, 555, 125–128. <https://doi.org/10.1016/j.jhydrol.2017.09.047>
- Stewart, I. T. (2009). Changes in snowpack and snowmelt runoff for key mountain regions. *Hydrological Processes*, 23, 78–94. <https://doi.org/10.1002/hyp.7128>
- Stewart, I. T., Cayan, D. R., & Dettinger, M. D. (2005). Changes toward earlier streamflow timing across western North America. *Journal of Climate*, 18, 1136–1155. <https://doi.org/10.1175/JCLI3321.1>
- St. Clair, J., Moo, S., Holbrook, W. S., Perron, J. T., Riebe, C. S., Martel, S. J., et al. (2015). Geophysical imaging reveals topographic stress control of bedrock weathering. *Science*, 350(6260), 534–539. <https://doi.org/10.1126/science.aab2210>
- Stober, I., & Bucher, K. (2007). Hydraulic properties of the crystalline basement. *Hydrogeology Journal*, 15(8), 1643–1643. <https://doi.org/10.1007/s10040-007-0214-9>
- Taylor, S., Feng, X., Kirchner, J. W., Osterhuber, R., Klaue, B., & Renshaw, C. E. (2001). Isotopic evolution of a seasonal snowpack and its melt. *Water Resources Research*, 37, 3, 759–769. <https://doi.org/10.1029/2000WR900341>
- Taylor, S., Feng, X., Williams, M., & McNamara, J. (2002). How isotopic fractionation of snowmelt affects hydrograph separation. *Hydrological Processes*, 16(18), 3683–3690. <https://doi.org/10.1002/hyp.1232>
- Taylor, R. G., Scanlon, B. R., Doll, P., Rodell, M., van Beek, R., Wada, Y., et al. (2013). Ground water and climate change. *Nature Geoscience*, 3, 322–329. <https://doi.org/10.1038/NCLIMATE1744>
- Thoma, M. J., McNamara, J. P., Gribb, M. M., & Benner, S. G. (2011). Seasonal recharge components in an urban/agricultural mountain front aquifer system using noble gas thermometry. *Journal of Hydrology*, 409(1-2), 118–127. <https://doi.org/10.1016/j.jhydrol.2011.08.003>

- Tomonaga, Y., Marzocchi, R., Pera, S., Pfeifer, H.-R., Kipfer, R., Decrouy, L., & Vennemann, T. (2017). Using noble-gas and stable-isotope data to determine groundwater origin and flow regimes: Application to the Ceneri Base Tunnel. *Journal of Hydrology*, *545*, 395–409. <https://doi.org/10.1016/j.jhydrol.2016.11.043>
- Tóth, J. (1963). A theoretical analysis of groundwater flow in small drainage basins. *Journal of Geophysical Research*, *68*(16), 4795–4812. <https://doi.org/10.1029/JZ068i016p04795>
- Vittecoq, B., Reninger, P. A., Lacquement, F., Martelet, G., & Violette, S. (2019). Hydrogeological conceptual model of andesitic watersheds revealed by high-resolution airborne geophysics. *Hydrology and Earth System Sciences*, *23*(5), 2321–2338. <https://doi.org/10.5194/hess-23-2321-2019>
- Viviroli, D., Archer, D. R., Buytaert, W., Fowler, H. J., Greenwood, G. B., Hamlet, A. F., et al. (2011). Climate change and mountain water resources: Overview and recommendations for research, management and policy. *Hydrology and Earth System Sciences*, *15*(2), 471–504. <https://doi.org/10.5194/hess-15-471-2011>
- Voeckler, H., & Allen, D. M. (2012). Estimating regional-scale fractured bedrock hydraulic conductivity using discrete fracture network (DFN) modeling. *Hydrogeology Journal*, *20*(6), 1081–1100. <https://doi.org/10.1007/s10040-012-0858-y>
- Voeckler, H. M., Allen, D. M., & Alila, Y. (2014). Modeling coupled surface water-groundwater processes in a small mountainous headwater catchment. *Journal of Hydrology*, *517*, 1089–1106. <https://doi.org/10.1016/j.jhydrol.2014.06.015>
- Wahi, A. K., Hogan, J. F., Ekwurzel, B., Baillie, M. N., & Eastoe, C. J. (2008). Geochemical quantification of semiarid mountain recharge. *Ground Water*, *46*(3), 414–425. <https://doi.org/10.1111/j.1745-6584.2007.00413.x>
- Ward, F. A., & Pulido-Velazquez, M. (2008). Water conservation in irrigation can increase water use. *Proceedings of the National Academy of Sciences*, *105*(47), 220. <https://doi.org/10.1073/pnas.0805554105>
- Welch, L. A., & Allen, D. M. (2012). Consistency of groundwater flow patterns in mountainous topography: Implications for valley bottom water replenishment and for defining groundwater flow boundaries. *Water Resources Research*, *48*, W05526. <https://doi.org/10.1029/2011WR010901>
- Welch, L. A., Allen, D. M., & van Meerveld, H. J. (2012). Topographic controls on deep groundwater contributions to mountain headwater streams and sensitivity to available recharge. *Canadian Water Resources Journal*, *37*(4), 349–371. <https://doi.org/10.4296/cwrj2011-907>
- Welch, L. A., & Allen, D. M. (2014). Hydraulic conductivity characteristics in mountains and implications for conceptualizing bedrock groundwater flow. *Hydrogeology Journal*, *22*(5). <https://doi.org/10.1007/s10040-014-1121-5>
- Wilson, J. L., & Guan, H. (2004). Mountain-block hydrology and mountain-front recharge In F. Phillips, J. Hogan, & B. Scanlon (Eds.), *in Groundwater recharge in a desert environment, The southwestern United States*. Washington, DC: AGU. <https://doi.org/10.1029/009WSA08>
- Wine, M. L., Cadol, D., & Makhnin, O. (2018). In ecoregions across western USA streamflow increases during post-wildfire recovery. *Environmental Research Letters*, *13*(1). <https://doi.org/10.1088/1748-9326/aa9c5a>
- Worthington, S. R., Davies, G. J., & Alexander, E. C. (2016). Enhancement of bedrock permeability by weathering. *Earth-Science Reviews*, *160*, 188–202. <https://doi.org/10.1016/j.earscirev.2016.07.002>
- Yao, Y., Zheng, C., Andrews, C., Zheng, Y., Zhang, A., & Liu, J. (2017). What controls the partitioning between baseflow and mountain block recharge in the Qinghai-Tibet Plateau? *Geophysical Research Letters*, *44*, 8352–8358. <https://doi.org/10.1002/2017GL074344>
- Zapata-Rios, X., Brooks, P. D., Troch, P. A., McIntosh, J., & Rasmussen, C. (2016). Influence of climate variability on water partitioning and effective energy and mass transfer in a semi-arid critical zone. *Hydrology and Earth System Sciences*, *20*, 1103–1115. <https://doi.org/10.5194/hess-20-1103-2016>
- Zekollari, H., Huss, M., & Farinotti, D. (2019). Modelling the future evolution of glaciers in the European Alps under the EURO-CORDEX RCM ensemble. *Cryosphere*, *13*(4), 1125–1146. <https://doi.org/10.5194/tc-13-1125-2019>

Comparison of soil infiltration rates in burned and unburned mountainous watersheds

Deborah A. Martin^{1*} and John A. Moody²

¹US Geological Survey, 3215 Marine Street, Suite E-127, Boulder, CO 80303, USA

²US Geological Survey, Mail Stop 413, Denver Federal Center, Lakewood, CO 80225, USA

Abstract:

Steady-state infiltration measurements were made at mountainous sites in New Mexico and Colorado, USA, with volcanic and granitic soils after wildfires and at comparable unburned sites. We measured infiltration in the New Mexico volcanic soils under two vegetation types, ponderosa pine and mixed conifer, and in the Colorado granitic soils under ponderosa pine vegetation. These measurements were made within high-severity burn areas using a portable infiltrometer with a 0.017 m² infiltration area and artificial rainfall rates ranging from 97 to 440 mm h⁻¹. Steady-state infiltration rates were less at all burned sites relative to unburned sites. The volcanic soil with ponderosa pine vegetation showed the greatest difference in infiltration rates with a ratio of steady-state infiltration rate in burned sites to unburned soils equal to 0.15. Volcanic soils with mixed conifer vegetation had a ratio (burned to unburned soils) of at most 0.38, and granitic soils with ponderosa pine vegetation had a ratio of 0.38. Steady-state infiltration rates on unburned volcanic and granitic soils with ponderosa pine vegetation are not statistically different. We present data on the particle-size distribution at all the study sites and examples of wetting patterns produced during the infiltration experiments. Published in 2001 by John Wiley & Sons, Ltd.

KEY WORDS wildfire; infiltration; New Mexico; Colorado

INTRODUCTION

Wildfires alter the infiltration response of burned watersheds by changing both the physical and chemical characteristics of the watersheds. The most significant effects are evident in watersheds subjected to high-severity burns, characterized by the combustion of all of the organic forest floor material, the presence of a deep ash layer, the alteration of the soil-mineral layer, and charring of the organic matter in the soils (Miller, 1994). The unburned forest floor consists of a litter layer (uppermost layer of the forest floor with recognizable leaves, needles, fine twigs, bark flakes, matted dead grass, mosses and lichens, O1 soil horizon; USFS, 2001) and a duff layer (partially decomposed remnants of the material in the litter layer, O2 soil horizon; Brown and Smith, 2000). These layers absorb most of the rainfall, provide ample storage, and obstruct the flow of water. The combustion process converts the litter and duff layers into ash and charcoal. Ash and small soil particles can seal soil pores (Morin and Benyamini, 1977; Neary *et al.*, 1999), decreasing the infiltration rate (Fuller *et al.*, 1955; Barfield *et al.*, 1981) and increasing potential runoff and erosion. When the charcoal and ash are removed from the hillslope by post-fire runoff or wind, the soil is left bare soil to rain splash and overland flow.

Chemical changes that affect infiltration may be as significant as physical changes. Combustion of organic matter during fire can produce volatile organic gasses that coat soil particles with water-repellant substances, thereby reducing infiltration rates (DeBano, 1981). This effect is thought to be more pronounced in coarser-grained soils where pore sizes are larger than in finer-grained soils (DeBano *et al.*, 1970; Doerr *et al.*, 1996).

*Correspondence to: D. A. Martin, US Geological Survey, 3215 Marine Street, Suite E-127, Boulder, CO 80303, USA. E-mail: damartin@usgs.gov

However, laboratory tests have shown that this is not a consistent pattern (Robichaud and Hungerford, 2000). A greater quantity of water-repellent substances may be produced when areas with greater fuel loads are burned or when certain vegetation types, like chaparral, are burned (DeBano, 1981), though naturally occurring water-repellent soil conditions have been observed in unburned soils. Burning reduces soil organic matter, alters the soil pH, and impinges on soil microbiological communities (Clark, 1994), all of which will have an effect on infiltration rates. Heat-induced changes in infiltration rates have been measured in the laboratory (Burgy and Scott, 1952; Robichaud and Hungerford, 2000), after prescribed fire (Arend, 1941; Zwolinski, 1971; Scott, 1993; Robichaud, 2000), and at various times after wildfires (Krammes and DeBano, 1965; Imeson *et al.*, 1992; Pradas *et al.*, 1994; Kutiel *et al.*, 1995; Benavides-Solorio and MacDonald, 2001). Measurements of infiltration rates after wildfire are often limited to rainfall simulations in areas accessible by roads.

In this study we measured infiltration rates using a portable rainfall simulator that allowed us access to remote sites. Our objective was to quantify differences in infiltration rates due to wildfire in two mountainous watersheds with different soil types: a volcanic soil near Los Alamos, New Mexico, burned by the Cerro Grande Fire, and a granitic soil near Pine, Colorado, burned by the Hi Meadow Fire.

Background

The Cerro Grande Fire near Los Alamos, New Mexico (Figure 1), occurred on the eastern flank of the Jemez Mountains and the western side of the Parajito Plateau, and burned nearly 1700 ha in May 2000 (BAER, 2000). Volcanic rocks, either welded or non-welded tuffs or andesite flows, underlie both the Jemez Mountains and the Parajito Plateau (Griggs, 1964). The area is in a semi-arid environment with a summer monsoon wet season from July through September, and covers an elevational range from about 2200 to 3000 m. Los Alamos

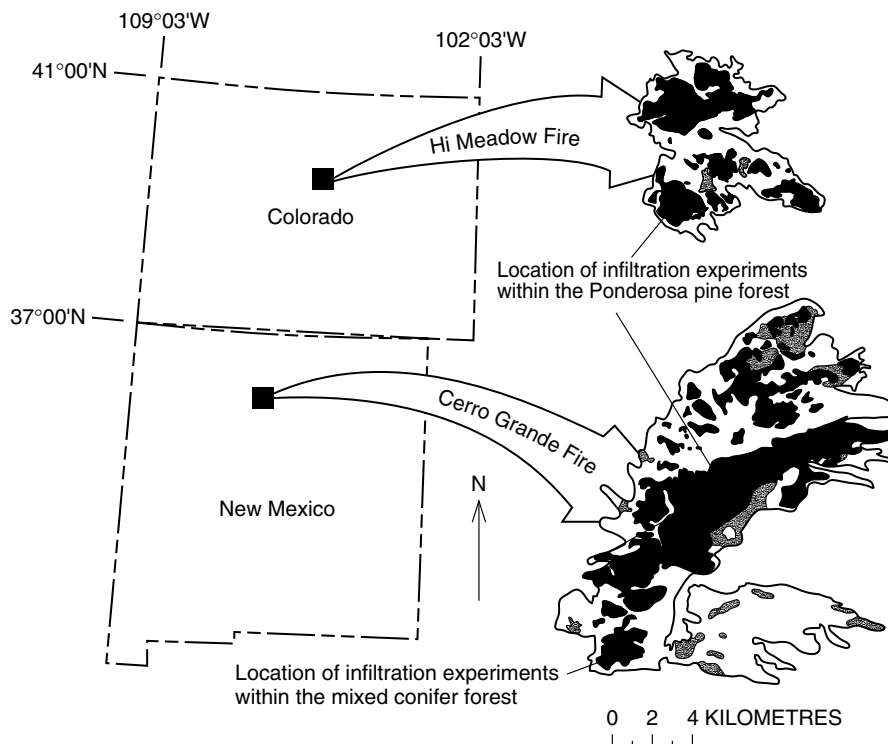


Figure 1. Locations of two wildfires that burned in 2000 and the respective study sites. The black areas were classified as high-burn severity, the crosshatched areas as moderate-burn severity, and the white areas as low-burn severity on the basis of BAER (2000), and Hart (2000)

is at 2259 m and receives 490 mm of mean annual precipitation (Nyhan *et al.*, 1978). Three major overstory vegetation types occurred in the burned area: (1) ponderosa pine forest (*Pinus ponderosa*); (2) mixed conifer forest consisting of four species: ponderosa pine (*P. ponderosa*), white fir (*Abies concolor*), Douglas-fir (*Pseudotsuga menziesii*), and aspen (*Populus tremuloides*); and (3) piñon–juniper forest consisting of one-seed juniper (*Juniperus monosperma*) and piñon (*Pinus edulis*) (Balice *et al.*, 1997). From visual observations within the Cerro Grande fire perimeter, we estimated that the stem density, a measure of the fuel loading, was about 3000 stems ha⁻¹ in the ponderosa pine and mixed conifer forests. These estimates are of the same order of magnitude as measurements in the same area by Balice *et al.* (2000). Before the fire litter and duff layers in these forests were between 0.5 and 3 cm thick.

The Hi Meadow fire near Pine, Colorado, southwest of Denver (Figure 1) burned 450 ha in June 2000 (Hart, 2000). The area is underlain by the Pikes Peak batholith that weathers to grös or decomposed granite a few centimetres to several metres thick (Moore, 1992). The burned area covers an elevational range of about 2100 to 2700 m and receives about 430 mm of mean annual precipitation (based on data for Bailey, Colorado; Colorado Climate Center, 2001). The predominant overstory vegetation type within the burn perimeter was ponderosa pine forest (*P. ponderosa*). Our visual estimate of the stem density within the Hi Meadow fire area was 400 stems ha⁻¹. The total thickness of the pre-fire litter and duff layers was usually less than 1 cm.

METHODS

We made infiltration measurements in three areas within 1 to 4 months after each wildfire was contained. Burned study areas were selected within the ponderosa pine forest in Rendija Canyon (Cerro Grande fire), the mixed conifer forest in Frijoles Canyon (Cerro Grande fire), and the ponderosa pine forest in Beaver Gulch (Hi Meadow fire). Measurements were also made at the closest unburned sites as a control to determine the effects of wildfire on the infiltration rate. The slopes of the study areas ranged from 6 to 16°. At the Cerro Grande fire, we made infiltration measurements in June 2000 at the severely burned and adjacent unburned sites in both the ponderosa pine and mixed conifer forests, and repeated the measurements at the ponderosa pine forest sites in September 2000. For the Hi Meadow fire, we completed one set of measurements in July 2000.

Equipment

We used a portable rainfall-simulator infiltrometer (McQueen, 1963) for the infiltration measurements (Figure 2). McQueen (1963) lists the main components of the device as (1) a reservoir and control unit, (2) a rainulator, (3) a supporting tripod and wind screen, (4) a base unit containing a splash screen, and (5) a system for measuring runoff water and sediment (a 0.05 m diameter plastic tube with a machined conical tip, calibrated to measure volume in millilitres). We modified the infiltrometer to include an extra strut to stabilize the wind screen further, used silicence cement to seal the cylindrical base unit to the soil (rather than bentonite as specified in the original design), and cut a small notch in the base unit to allow the surface runoff and sediment to drain from the soil *via* a flat metal spout into a container from which we aspirated the runoff into a measuring tube.

The reservoir and control unit permit the application and measurement of controlled volumes of water to the infiltration plot, which is circular in shape and has an area of 0.017 m². The rainulator produces raindrops 5.6 mm in diameter. These raindrops, falling the distance from the rainulator to the ground surface (approximately 1.5 m), have an energy value of 0.137 J cm⁻² cm⁻¹ at the normal application rate of about 100 mm h⁻¹. McQueen (1963) estimates that this application rate approximates that of a natural storm with an intensity of about 48 mm h⁻¹.

A major limitation of the McQueen (1963) portable rainfall-simulator infiltrometer is the size of the infiltration plot (0.017 m²). On the other hand, the size of the equipment and the amount of water needed for the infiltration experiments allowed us to access otherwise inaccessible sites. Issues of scaling up plot-scale

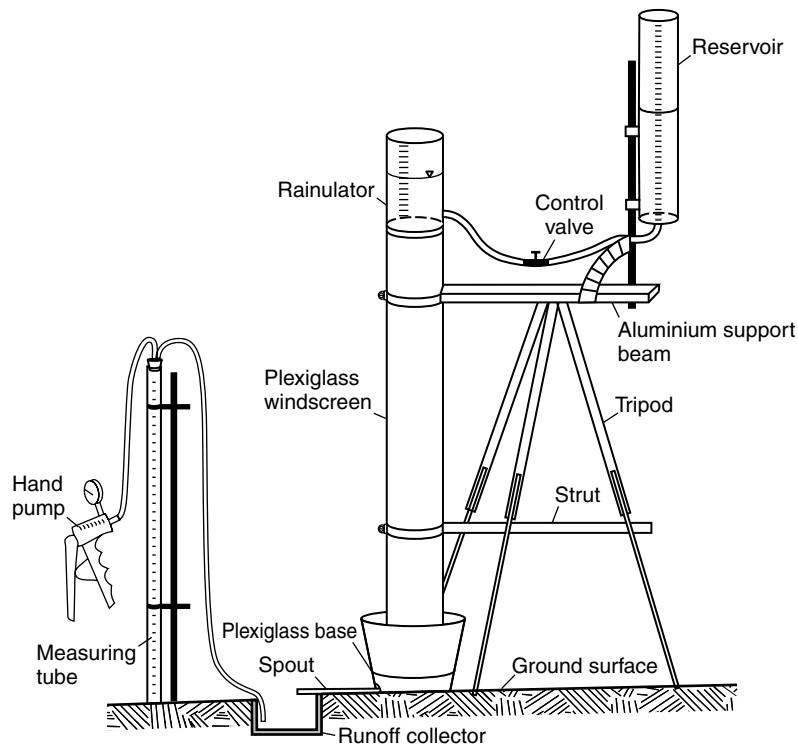


Figure 2. Diagram of the portable rainfall-simulator infiltrometer [modified from McQueen (1963)]

measurements to the watershed scale have been addressed elsewhere, for example by Kirkby *et al.* (1996), Newman *et al.* (1997), and Hendrayanto *et al.* (2000).

The infiltration experiments

We chose study areas to represent the general conditions throughout the rest of the area of interest. At each study area, we selected three to eight replicate sites. An initial infiltration experiment showed that a considerable amount of the applied water was absorbed either by the ash at the burned areas or by the litter and duff in the unburned areas. Therefore, we carefully removed the ash or litter and duff prior to each experiment and collected these materials for further studies. After scraping away the surface material, the base unit and spout were carefully cemented to the ground. While the cement dried we positioned the tripod and windscreen over the infiltration plot and filled both the reservoir and control unit with distilled water. Distilled water was used to minimize variations among experiments due to the chemistry of the local water source. The rain rate from the rainulator was adjusted before the unit was put in place over the windscreen.

Our target was to produce less than 5 mm of runoff per minute once we reached steady-state infiltration rates based on the capacity of the runoff measuring tube, but we did not know *a priori* the steady-state infiltration at a site, nor the variability among replicates. Rainfall rates ranged from 97 to 440 mm h⁻¹ in the ponderosa pine forest sites in Rendija Canyon, from 240 to 400 mm h⁻¹ in the mixed conifer forest sites in Frijoles Canyon, and from 160 to 300 mm h⁻¹ in the ponderosa pine forest sites in Beaver Gulch. We selected rainfall rates iteratively at each site. At the unburned mixed conifer site on volcanic soils we did not produce runoff for two of the replicates because a thick mycorrhizal mat below the soil–duff interface absorbed all of the water applied during our experiment.

Infiltration experiments were conducted for 15 to 20 min, enough time for the infiltration rates to reach steady-state conditions (George Leavesley, USGS, personal communication). We define steady state as that part

of the infiltration curve that varies little with time during the experiment. Infiltration rates rapidly decreased to steady-state conditions within 2–3 min. The application rate of the water was adjusted to a steady rate throughout the experiment by modifying the flow rate from the control unit. We recorded the water levels in both the reservoir and control unit. The runoff from the collector draining the infiltration plot was aspirated through an aspiration tube, which was connected through a stopper to the measuring tube. A vacuum was applied to the aspiration tube with a hand pump that was connected to the stopper by a separate tube. The volumes in the measuring tube were also recorded. The data were recorded at 1 min intervals. The temperature of the water was recorded at the beginning and end of the experiment.

The data for the steady-state period were used to calculate an average steady-state infiltration rate for each experiment. Minor variations above and below the steady-state part of the curve reflect the inherent uncertainties in reading the volume marks on the infiltrometer reservoir and control unit. Data for each replicate site were averaged and 95% confidence limits were calculated based on the Student-*t* distribution. Because the infiltration rate is inversely proportional to water viscosity, we adjusted all field measurements made at different temperatures to a constant temperature of 10 °C (CRC, 1987).

Following the experiment, we examined the surface and sub-surface pattern of wetting. The base unit was removed from the plot and measurements of the shape and size of the surface-wetting front were recorded. Starting at the downhill end of the infiltration plot, we excavated vertical slices through the zone wetted by the experiment. Any rocks, roots, or irregularities in the wetting pattern were noted, and a sketch of the pattern at the middle section of the infiltration plot was produced.

Soil characteristics

In order to evaluate the effects of particle-size distribution on infiltration rates, we collected a soil core at each replicate infiltration site. Cores were 0.048 m in diameter and either 0.05 or 0.10 m deep. The soil was dried overnight at 105 °C and the dry sediment sieved by whole ϕ intervals ($\phi = -\log_2$ of the particle size diameter in millimetres; Krumbein, 1934). We averaged the results for each site and calculated D_{16} , D_{50} , D_{84} , and dispersion. Dispersion is a dimensionless number (geometric standard deviation, $\sigma = \sqrt{D_{84}/D_{16}}$, where D_{84} and D_{16} are the diameters at which 84% and 16% of the sediment are finer than the specified diameter; Inman, 1952) that measures the spread of the particle-size distribution and is equal to 1.0 for a distribution with one particle-size class. We created particle-size distribution curves by fitting the data to a third-order polynomial using a cubic spline (Robert Stallard, USGS, personal communication).

RESULTS

Infiltration rates

Steady-state infiltration rates were smaller at all burned sites than at unburned sites (Table I and Figure 3). The volcanic soil in the ponderosa pine forest showed the greatest difference in steady-state infiltration rate. This is highlighted by the ratios of infiltration rates on burned versus unburned soils: 0.15 for ponderosa pine on volcanic soils, at most 0.38 for mixed conifer forest on volcanic soils, and 0.38 for the granitic soil. This ratio provides a relative measure of the effects of burning on infiltration and is useful for comparing disparate sites. Steady-state infiltration rates on unburned volcanic and granitic soils with ponderosa pine forest are not statistically different. The infiltration rate for unburned volcanic soil with mixed conifer forest can only be considered as a lower limit because we were unable to produce runoff at two replicates at this site.

Wetting patterns

Excavation of the infiltration sites indicated a variety of patterns for the wetting profile but, in general, did not indicate any major lateral migration of water. At some infiltration sites, some of the subsurface particles in the volcanic soils were on the order of 10 cm in diameter and represented a significant portion of the infiltration

Table I. Particle-size characteristics and steady-state infiltration rates for volcanic and granitic soils in unburned and burned sites (95% confidence limits are given after the \pm symbol)

Location	Forest	Condition	D_{50} (mm)	Dispersion, σ	Bulk density (kg m^{-3})	Number of runs	Infiltration rate at 10°C (mm h^{-1})
<i>Volcanic soil—Cerro Grande fire</i>							
Rendija Canyon	Ponderosa pine	Unburned	0.73	12.6	1150 ± 160	5	170 ± 80
Rendija Canyon	Ponderosa pine	Burned	0.25	5.6	1010 ± 110	8	26 ± 15
Frijoles Canyon	Mixed conifer	Unburned	0.50	11.2	1000 ± 120	3	>260
Frijoles Canyon	Mixed conifer	Burned	0.75	9.8	960 ± 90	3	97 ± 70
<i>Granitic soil—Hi Meadow fire</i>							
Beaver Gulch	Ponderosa pine	Unburned	1.3	7.7	1210 ± 260	3	120 ± 130
Beaver Gulch	Ponderosa pine	Burned	1.7	8.3	1400 ± 140	3	45 ± 16

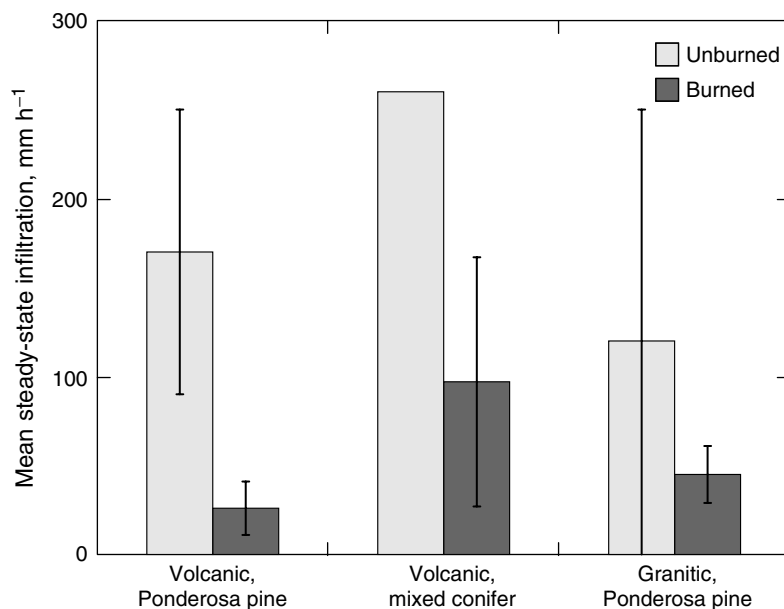


Figure 3. Steady-state infiltration rate in unburned and burned sites

area of 0.017 m^2 . These large particles undoubtedly affected the infiltration rate. The wetting profiles often showed pockets of non-wetted soil (Figure 4). Other authors have documented spatial variability of wetting fronts in both unburned and burned soil (Meeuwig, 1971; Imeson *et al.*, 1992; Ritsema *et al.*, 1998).

Surface particle-size distribution

Unburned, volcanic soils were finer (average $D_{50} = 0.62 \text{ mm}$) than unburned, granitic soils ($D_{50} = 1.3 \text{ mm}$) and had a much greater dispersion than the granitic soil (Table I). Both the unburned volcanic soils representing the average of three samples collected from the top 0–0.10 m of soil have a tri-modal distribution with peaks near 0.09 and 1 mm and the largest peak between 8 and 16 mm (Figure 5). The first two peaks of the tri-modal distribution are more pronounced in one sample collected from the top 0–0.05 m and the third peak is much reduced. The differences represent some of the spatial variability of the soils. The 0–0.10 m samples contained soil closer to the weathered bedrock and thus had some larger sizes than the 0–0.05 m sample.

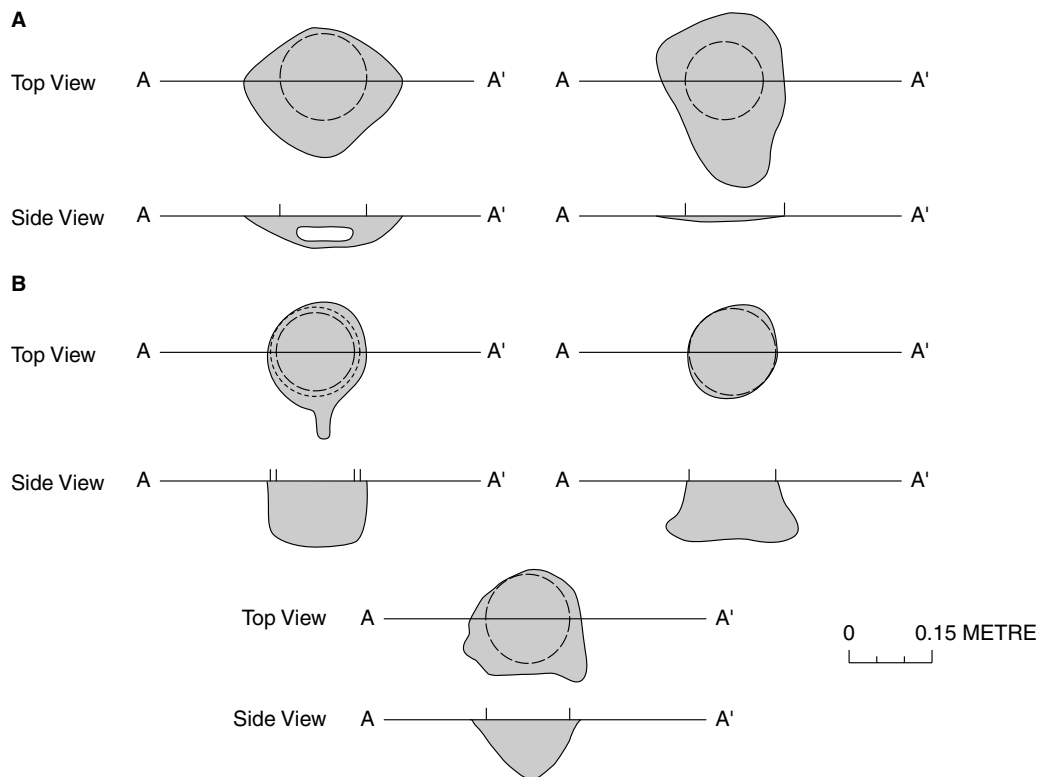


Figure 4. Wetting-front patterns after infiltration measurements. (A) Examples of wetting-front patterns with lateral spreading dominant over vertical penetration. (B) Examples of wetting-front patterns with vertical penetration dominant over lateral spreading. The circles with the dashed line represent the diameter of the rainulator, 15 cm

Unburned granitic soil samples of the top 0–0.10 m were quite different than the volcanic soils and had only one relatively broad peak between 2 and 8 mm (Figure 5B) similar to other unburned granitic soils collected from sites in the adjacent Buffalo Creek fire area (Martin and Moody, 2001; Moody and Martin, 2001). Samples from the top 0–0.05 m were almost identical to the 0–0.10 m samples, and field observations indicated that the weathering profile was thicker on the granitic bedrock than on the volcanic bedrock.

During our infiltration experiments, we observed that surficial ash acts as a storage reservoir for rainfall and initially prevents runoff. Once this storage capacity is exceeded, however, or the ash is washed off, subsequent rainfall may produce runoff. The ash layer often appears black in aerial photographs of burned areas, and a shift toward a lighter colour in subsequent photographs reflects the removal of this ash. The storage effect of the ash was not a factor in the infiltration experiments because we removed it, as well as the litter and duff layer at the unburned sites, so that we only measured the steady-state infiltration rate of the bare soil.

DISCUSSION

Infiltration

Burned volcanic soils with ponderosa pine vegetation show the greatest relative reduction in steady-state infiltration rates. Though we limited our studies to areas classified as high severity (BAER, 2000; Hart, 2000), we think the burn severity of the ponderosa pine site in the Cerro Grande fire was much greater than the burn severity of the mixed conifer volcanic site or granitic site in the Hi Meadow fire as a result of higher

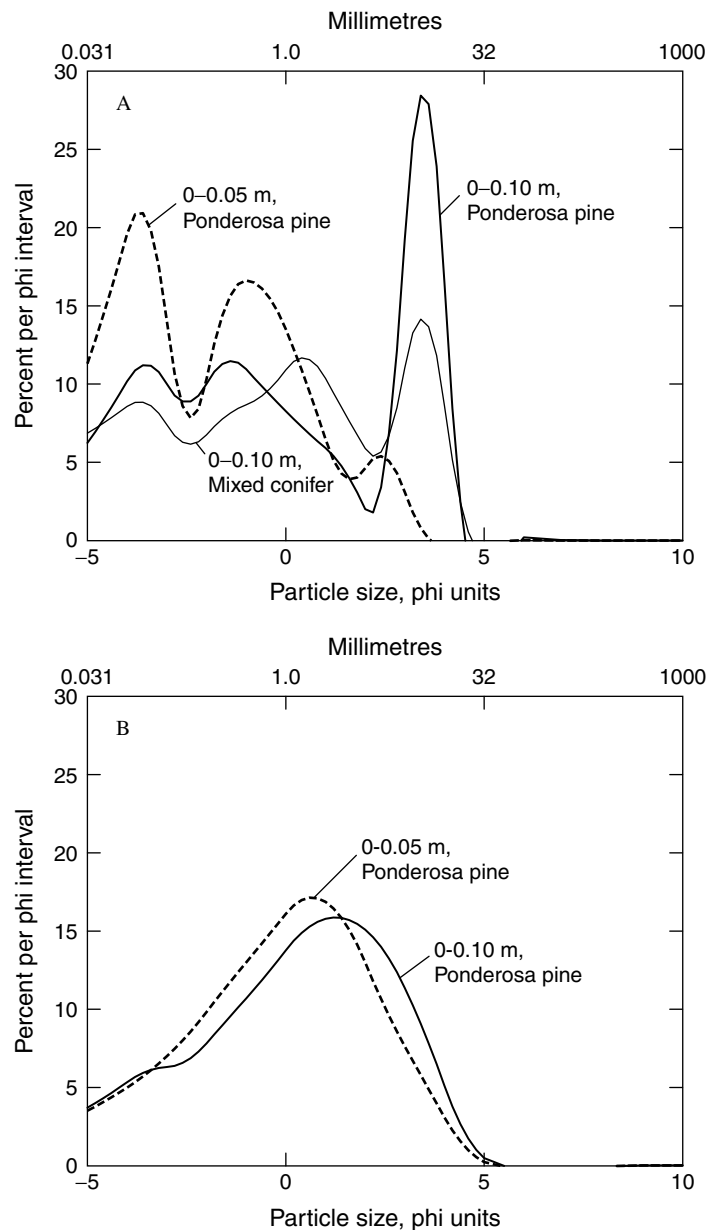


Figure 5. Particle-size distributions for unburned soils. (A) Volcanic soils in two forest types and for 0–0.05 m below the soil surface and 0–0.10 m below the soil surface. (B) Granitic soil for 0–0.05 m below the soil surface and 0–0.10 m below the soil surface

fuel loads. Fuel loadings were higher in the forests burned by the Cerro Grande Fire than those burned by the Hi Meadow fire. The litter and duff layers in the ponderosa pine forest of the Cerro Grande fire were completely combusted, leaving a layer of ash that was white in some locations, indicating hotter temperatures than those areas with black ash (Raison *et al.*, 1990). The litter and duff layers in the high-severity sites of the Hi Meadow fire were incompletely combusted, with partially burned needles and no obvious deposits of white ash. Similar observations were noted within the mixed conifer forest site in the Cerro Grande fire

and may explain why post-fire steady-state infiltration rates (97 mm h^{-1}) in this area were higher than in the ponderosa pine forest (26 mm h^{-1}). The litter and duff layers in the unburned mixed conifer forest site were thicker (3 cm) than any sites we studied and had a thick mat of mycorrhizal growth below the duff layer. Even the burned soil at the mixed conifer site had the remains of the mycorrhizal mat, which indicated that the heat pulse to the soil was not great enough to combust this organic matter.

Multiple factors bring about the reduction in infiltration rates in burned soils relative to their unburned counterparts. Certainly, fire-induced water repellency is a factor that may contribute to a reduction in infiltration rates, though all of our unburned sites exhibited some naturally occurring water repellency based on water drop penetration tests (Doerr *et al.*, 1996). Sealing may also be a factor that reduces surface porosity by the action of raindrop impact on the ash and fine-grained particles. A sealing component was incorporated by Leavesley *et al.* (1989) to model the infiltration rates observed in volcanic soils after the eruption of Mount St Helens in southern Washington, where they measured steady-state infiltration rates of 2 to 5 mm h^{-1} . The sealing process requires a source of fine-grained material. Wildfire produces this in the form of ash, which may swell and clog soil pores (Etiégni and Campbell, 1991). Wildfire may also alter the soil porosity by combusting organic material that binds soil aggregates together (Neary *et al.*, 1999).

The particle-size distribution of soil surface layers is a key factor in controlling infiltration rates. The granitic soils were distinctly coarser than the volcanic soils (Table I). Soil water studies on the Pajarito Plateau (Newman *et al.*, 1997) indicated that the presence of a homogeneous soil with a well-developed Bt horizon was more important than vegetation type in controlling the flux of water to deeper layers. The effect of wildfire on surface soils with different porosities, organic matter contents, and particle-size distributions is still not well characterized. Discussions by DeBano *et al.* (1970) and Doerr *et al.* (1996) on the one hand, and by Robichaud and Hungerford (2000) on the other hand present conflicting evidence about the magnitude of the effects of wildfire, particularly fire-induced water repellency, on coarse-grained versus finer-grained soils.

Very few measurements of steady-state infiltration rates after a wildfire have been made in mountainous terrain with similar forests. Kutiel *et al.* (1995) measured infiltration rates of 29 mm h^{-1} on burned plots in a pine forest and oak shrubland located in the Mediterranean mountainous region near Haifa, Israel. Imeson *et al.* (1992) measured infiltration rates of 15 to 20 mm h^{-1} in oak forests of northeastern Spain with relatively flat terrain. Both sets of measurements are comparable to those at the burned site of the ponderosa pine forest in the volcanic terrain of Rendija Canyon. The ratio of infiltration rates for burned and unburned sites in the Mediterranean mountains was 0.9, indicating relatively little change, but this ratio ranged from 0.3 to 0.5 for the sites in Spain.

Several experiments have measured effects on infiltration due to prescribed fires. Rates measured on burned and unburned plots in an oak forest in the Missouri Ozarks (Arend, 1941) had a ratio of 0.6. Sites in northern Arizona (Fuller *et al.*, 1955) had a ratio of 0.16, which is similar to the ratio for the ponderosa pine site in Rendija Canyon (0.15).

Wetting-front patterns

Wetting-front patterns varied considerably (Figure 4), reflecting both the presence of stones and unwetted zones. Some wetting patterns demonstrated more lateral spreading and had shallow vertical penetration. Others were more confined horizontally with deeper vertical penetration. We were unable to place wetting patterns in generalized categories based on soils, vegetation type, or burn status. By contrast, Meeuwig (1971), while acknowledging that no two wetting patterns were exactly alike, classified wetting-front patterns in granitic soil into eight categories. Imeson *et al.* (1992) nicely depict two examples of complex wetting patterns in $1 \text{ m} \times 0.5 \text{ m}$ plots under a burned and unburned soil. Non-continuous zones of water-repellent soil and zones of penetration exist in a complex pattern in response to variations in macropores, vegetation, and both fire-induced and naturally occurring water-repellent soil conditions. Based on the wetting-front patterns we observed after our infiltration experiments, no continuous water-repellent layer was present in the burned soils we studied.

CONCLUSIONS

Our measurements of steady-state infiltration rates after wildfire provide an estimate of the reduction in infiltration compared with rates in adjacent unburned soils. The use of the ratio of steady-state infiltration rates in burned sites to those in comparable unburned soils is an effective method to compare disparate sites. In our studies, volcanic soils with ponderosa pine vegetation showed the greatest reduction in infiltration rates, and this may be a reflection of the burn severity. Qualitatively, we think the New Mexico site with volcanic soils and ponderosa pine vegetation was the most severely burned site we studied, with a ratio of steady-state infiltration rates in burned soils to unburned soils equal to 0.15. The infiltration rates on granitic soils in Colorado with ponderosa pine vegetation were less affected, with a ratio of steady-state infiltration rates in burned soils to unburned soils equal to 0.38. Because the mycorrhizal mat in unburned volcanic soils at the mixed conifer site in New Mexico soaked up all the rainfall we applied, it is difficult to quantify the reduction in infiltration rates, but the ratio is at most 0.38. We measured no statistical differences in infiltration rates on unburned volcanic and granitic soils with ponderosa pine vegetation. Though limited by the small plot size and uncertainties in scaling up from the plot scale to the watershed scale, these ratios provide comparative data that may be useful in empirically based hillslope runoff and erosion models to predict the increase in runoff and erosion as a consequence of wildfires in mountainous terrain.

REFERENCES

- Arend JL. 1941. Infiltration rates of forest soils in the Missouri Ozarks as affected by burning and litter removal. *Journal of Forestry* **39**: 726–728.
- BAER. 2000. *Cerro Grande fire, burned area emergency rehabilitation (BAER) plan*. Interagency BAER Team, US Forest Service Region 3, June 9, 2000; 416 pp. plus GIS maps.
- Balice RG, Ferran SG, Foxx TS. 1997. *Preliminary land cover classification for the Los Alamos region*. LA-UR-97-4627, Los Alamos National Laboratory: Los Alamos, NM.
- Balice RG, Miller JD, Oswald BP, Edminster C, Yool SR. 2000. *Forest surveys and wildfire assessment in the Los Alamos region; 1998–1999*. LA-13714-MS, Los Alamos National Laboratory: Los Alamos, NM.
- Barfield BJ, Warner RC, Haan CT. 1981. *Applied Hydrology and Sedimentology for Disturbed Areas*. Technical Press: Stillwater, OK; 603.
- Benavides-Solorio J, MacDonald LH. 2001. Post-fire runoff and erosion from simulated rainfall on small plots, Colorado Front Range. *Hydrological Processes* **15**: 2931–2952.
- Brown JK, Smith JK (eds). 2000. *Wildland fire in ecosystems: effects of fire on flora*, vol. 2, General Technical Report RMRS-GTR-42, US Department of Agriculture, Forest Service, Rocky Mountain Research Station: Ogden, UT; 257.
- Burgy RH, Scott VH. 1952. Some effects of fire and ash on the infiltration capacity of soils. *Transactions, American Geophysical Union* **33**: 405–416.
- Clark B. 1994. Soils, water, and watersheds. In *Fire Effects Guide*, Miller M (ed.). NFES 2394/PMS 481, National Wildfire Coordinating Group, National Interagency Fire Center: Boise, ID; V-1–V-14.
- Colorado Climate Center. 2001. <http://ulysses.atmos.colostate.edu/>.
- CRC. 1987. *Handbook of Chemistry and Physics*, 70th edn. CRC Press: Boca Raton, FL; F-40.
- DeBano LF. 1981. *Water repellent soils: a state of the art*. General Technical Report PSW-46. US Department of Agriculture, Forest Service, Pacific Southwest Forest and Range Experiment Station; 21.
- DeBano LF, Mann LD, Hamilton DA. 1970. Translocation of hydrophobic substances into soil by burning organic litter. *Soil Science Society of America Proceedings* **34**: 130–133.
- Doerr SH, Shakesby RA, Walsh RPD. 1996. Soil hydrophobicity variations with depth and particle size fraction in burned and unburned *Eucalyptus globulus* and *Pinus pinaster* forest terrain in the Águeda Basin, Portugal. *Catena* **27**: 25–47.
- Etiégni L, Campbell AG. 1991. Physical and chemical characteristics of wood ash. *Bioresource Technology* **37**: 173–178.
- Fuller WN, Shannon S, Burgess PS. 1955. Effect of burning on certain forest soils of Northern Arizona. *Forest Science* **1**: 44–50.
- Griggs RL. 1964. Geology and ground-water resources of the Los Alamos area, New Mexico. *US Geological Survey Water-Supply Paper 1753*; 107 pp. plus maps.
- Hart S. 2000. *Hi Meadow incident; narrative summary and discussion of incident management operations, June 13–22, 2000*. Rocky Mountain Interagency Incident Management Team, State of Colorado, Park County, Jefferson County, South Platte Ranger District, Pike and San Isabel National Forests; 18 pp. plus attachments.
- Hendrayanto, Kosugi K, Mizuyama T. 2000. Scaling hydraulic properties of forest soils. *Hydrological Processes* **14**: 521–538.
- Imeson AC, Verstrate JM, van Mulligen EJ, Sevink J. 1992. The effects of fire and water repellency on infiltration and runoff under Mediterranean type forest. *Catena* **19**(3–4): 345–361.
- Inman DL. 1952. Measures for describing the size distribution of sediments. *Journal of Sedimentary Petrology* **22**(3): 125–145.
- Kirkby MJ, Imeson AC, Bergkamp G, Cammeraat LH. 1996. Scaling up processes and models from the field plot to the watershed and regional areas. *Journal of Soil and Water Conservation* **51**: 391–396.

- Krammes JS, DeBano LF. 1965. Soil wettability: a neglected factor in watershed management. *Water Resources Research* **1**(2): 283–286.
- Krumbein WC. 1934. Size frequency distribution of sediments. *Journal of Sedimentary Petrology* **4**: 65–77.
- Kutiel P, Lavee H, Segev M, Benyamini Y, Poesen J. 1995. The effect of fire-induced surface heterogeneity on rainfall–runoff–erosion relationships in an eastern Mediterranean ecosystem, Israel: special issue. In *Experimental Geomorphology and Landscape Ecosystem Changes; Proceedings of the Memorial Symposium Prof. Jan de Ploey*, Govers G, Goossens D (eds). Catena-Verlag Rohdenburg: Cremlingen-Destedt, Germany; 77–87.
- Leavesley GH, Lusby GC, Lichty RW. 1989. Infiltration and erosion characteristics of selected tephra deposits from the 1980 eruption of Mount St. Helens, Washington, USA. *Hydrological Sciences* **34**(3): 339–353.
- Martin DA, Moody JA. 2001. The flux and particle-size distribution of sediment collected in hillslope traps after a Colorado wildfire. In *Proceedings 7th Federal Interagency Sedimentation Conference*, March 26–29, 2001, Reno, NV; III-40–III-47.
- McQueen IS. 1963. Development of a hand portable rainfall-simulator infiltrometer. *US Geological Survey Circular* **482**; 16.
- Meeuwig RO. 1971. *Infiltration and water repellency in granitic soils*. Forest Service Research Paper; INT-111. US Department of Agriculture Intermountain Forest and Range Experiment Station: Ogden, UT; 20.
- Miller M (ed.). 1994. *Fire Effects Guide*. NFES 2394/PMS 481. National Wildfire Coordinating Group, National Interagency Fire Center: Boise, ID; II-12.
- Moody JA, Martin DA. 2001. Hydrologic and sedimentologic response of two burned watersheds. *US Geological Survey Water-Resources Investigation Report* **01-4122**.
- Moore R. 1992. *Soil survey of Pike National Forest, eastern part, Colorado; parts of Douglas, El Paso, Jefferson, and Teller counties*. US Department of Agriculture, Forest Service and Soil Conservation Service; 106.
- Morin J, Benyamini Y. 1977. Rainfall infiltration into bare soils. *Water Resources Research* **13**(5): 813–817.
- Neary DG, Klopatek CC, DeBano LF, Ffolliott PF. 1999. Fire effects on below ground sustainability: a review and synthesis. *Forest Ecology and Management* **122**: 51–71.
- Newman BD, Campbell AR, Wilcox BP. 1997. Tracer-based studies of soil water movement in semi-arid forests of New Mexico. *Journal of Hydrology* **196**: 251–270.
- Nyhan JW, Hacker LW, Calhoun TE, Young DL. 1978. *Soil survey of Los Alamos county, New Mexico*. Informal Report LA-6779-MS; 102.
- Pradas M, Imeson A, Van Mulligen E. 1994. The infiltration and runoff characteristics of burnt soils in NE-Catalonia and the implications for erosion. In *Soil Erosion and Degradation as a Consequence of Forest Fires*, Sala M, Rubio JL (eds). Geofoma Ediciones; 229–240.
- Raison RJ, Keith H, Khanna PK. 1990. Effects of fire on the nutrient-supplying capacity of forest soils. In *Impact of Intensive Harvesting on Forest Site Productivity*. Proceedings IEA/BE A3 Workshop, South Island, New Zealand, March 1989. IEA/BE T6/A6 Report No. 2. Forest Research Institute Bulletin. New Zealand Forest Service **159**: 39–54.
- Ritsema CJ, Dekker LW, Nieber JL, Steenhuis TS. 1998. Modeling and field evidence of finger formation and finger recurrence in a water repellent sandy soil. *Water Resources Research* **34**(4): 555–567.
- Robichaud PR. 2000. Fire effects on infiltration rates after prescribed fire in Northern Rocky Mountain forests, USA. *Journal of Hydrology* **231–232**: 220–229.
- Robichaud PR, Hungerford RD. 2000. Water repellency by laboratory burning of four northern Rocky Mountain forest soils. *Journal of Hydrology* **231–232**: 207–219.
- Scott DF. 1993. The hydrological effects of fire in South African mountain catchments. *Journal of Hydrology* **150**: 409–432.
- USFS. 2001. Fire Effects Information System. U.S. Department of Agriculture, Forest Service, Rocky Mountain Research Station, Fire Sciences Laboratory, Online: <http://www.fs.fed.us/database/feis/>.
- Zwolinski MJ. 1971. Effects of fire on water infiltration rates in a ponderosa pine stand. *Hydrology and Water Resources in Arizona and the Southwest* **1**: 107–112.

Fire effects on infiltration rates after prescribed fire in Northern Rocky Mountain forests, USA

P.R. Robichaud

USDA-Forest Service, Rocky Mountain Research Station, Forestry Science Laboratory, 1221 South Main Street, Moscow, ID 83843, USA

Received 3 October 1998; accepted 11 May 1999

Abstract

Infiltration rates in undisturbed forest environments are generally high. These high infiltration rates may be reduced when forest management activities such as timber harvesting and/or prescribed fires are used. Post-harvest residue burning is a common site preparation treatment used in the Northern Rocky Mountains, USA, to reduce forest fuels and to prepare sites for natural and artificial tree regeneration. Prescribed burn operations attempt to leave sites with the surface condition of a low-severity burn. However, some of the areas often experience surface conditions associated with a high-severity burn which may result in hydrophobic or water repellent conditions. In this study, infiltration rates were measured after logging slash was broadcast burned from two prescribed burns. The two sites were in Northern Rocky coniferous forests of Douglas-fir/lodgepole pine and ponderosa pine/Douglas-fir. Simulated rainfall was applied to one-square meter plots in three, 30-min applications at 94 mm h^{-1} within the three surface conditions found after the burn: unburned-undisturbed areas, low-severity burn areas and high-severity burn areas.

Runoff hydrographs from the rainfall simulations were relatively constant from the plots that were in unburned-undisturbed areas and in areas subjected to a low-severity burn. These constant runoff rates indicate constant hydraulic conductivity values for these surface conditions even though there was variation between plots. Hydrographs from the rainfall simulation plots located within areas of high-severity burn indicate greater runoff rates than the plots in low-severity burn areas especially during the initial stages of the first rainfall event. These runoff rates decreased to a constant rate for the last 10 min of the event. These results indicate hydrophobic or water repellent soil conditions, which temporarily cause a 10–40% reduction in hydraulic conductivity values when compared to a normal infiltrating soil condition. Since variability was high for these forest conditions, cumulative distribution algorithms of hydraulic conductivity provide a means to account for the inherent variability associated with these hillslopes and different surface conditions cause by fire. Published by Elsevier Science B.V.

Keywords: Water repellent; Rainfall simulation; Forest fire; Hydraulic conductivity

1. Introduction

Water infiltration is defined as the flow of water from the soil surface into the soil profile. The rate at which water is transmitted through soil is highly dependent upon the surface conditions. In forest

environments, various surface conditions can exist and it is important to characterize these conditions and their effect on infiltration.

Runoff from harvested and burned hillslopes varies from extensive to minor. The major determining factor is the amount of disturbance to the surface material which is usually organic debris (commonly referred to as duff or forest floor) that protects the underlying mineral soil. Disturbance may be from

E-mail address: probichaud@fs.fed.us
(P.R. Robichaud).

tree harvesting operations, road building, or fire. All of these activities may impact the protective duff layer. Adverse effects on the duff layer by burning depend upon the severity of fire (Robichaud et al., 1993; Robichaud and Waldrop, 1994; Robichaud, 1996). Post-fire condition of the surface horizons are important because they determine the amount of mineral soil exposed to raindrop splash, overland flow and the development of water repellent soil conditions (DeBano, 1981). Observations from previous studies (Robichaud et al., 1993) suggest there are four different surface/hydrologic conditions to monitor which affect infiltration. These conditions are: (1) areas subjected to high-severity burns (possibly hydrophobic); (2) areas subjected to low-severity burns; (3) areas with bare soil due to log dragging, log landings, skid trails, or roads; and (4) unburned-undisturbed areas.

Numerous observations of water repellent soil conditions have been reported throughout the western USA and the world. Water repellency caused by wildfires has received the most attention in southern California chaparral (DeBano et al., 1967; DeBano and Rice, 1973), although it has been reported after forest wildfires (Megahan and Molitor, 1975; Dyrness, 1976; Campbell, 1977) and on rangelands (Richardson and Hole, 1978; Soto et al., 1994).

In burned soils, severity of water repellency not only depends on soil texture, but is also related to fire intensity, antecedent soil-water content and fuel conditions (DeBano et al., 1976; Robichaud and Hungerford, 2000; Robichaud, 1996). Under field conditions, the water-repellent layer is usually not continuous, so irregular wetting patterns are common (Bond, 1964; Meeuwig, 1971; DeBano, 1981; Dekker and Ritsema, 1995, 1996). Water repellency induced by a low-to-moderate severity prescribed burn is usually of short duration. For example, in southwestern Oregon, soil wettability resulting from a late spring wildfire burn returned to near normal levels after the fall rains began (McNabb et al., 1989). After a late summer wildfire in the Oregon Cascade Mountains, Dyrness (1976) found that soil wettability in stands of lodgepole pine (*Pinus contorta*) experiencing burns of low-severity recovered more rapidly than soils experiencing burns of high-severity. By the sixth year after the

fire, wettability of the soils that experienced both low- and high-severity burns approached that of unburned soil.

The most apparent hydrologic effect of hydrophobic soil conditions is the reduction of infiltration which can induce erosion by overland flow (DeBano et al., 1967). Infiltration curves reflect increasing wettability over time once the soil is placed in contact with water. Infiltration increases with time because the hydrophobic substances responsible for water repellency are slightly water soluble and slowly dissolve, thereby increasing wettability (DeBano, 1981). Researchers have documented persistence of hydrophobic conditions from weeks to years (DeBano et al., 1967; Holzhey 1969). In general, hydrophobicity is broken up, or is sufficiently washed away, within one to two years after a fire.

The objective of this study was to determine infiltration characteristics of forest soils burned at different severities. These calculated hydraulic conductivity values provide important input parameters for use in current erosion prediction models that describe hydrologic responses for various surface conditions typically encountered in forest environments.

2. Methods

2.1. Field sites

The first site, Slate Point (7 ha), was located on the West Fork Ranger District of the Bitterroot National Forest in western Montana, USA. This location has a Douglas-fir (*Pseudotsuga menziesii*)/lodgepole pine (*Pinus contorta*) forest. The habitat type is Douglas-fir/twinflower (*Linnaea borealis*) (Pfister et al., 1977). Slopes within the study area range from 30 to 70% with a northern aspect. Elevation range from 1620 to 1780 m. The soils (83% sand, 12% silt, 5% clay with 33% gravel component) consist of a loamy skeletal mixed Typic Cryoboralf and a loamy skeletal mixed Dystric Cryochrept. Both were formed from weathered rhyolite.

The second site, Hermada (9 ha), was located on the Idaho City Ranger District of the Boise National Forest in central Idaho, USA. This location has a ponderosa pine (*Pinus ponderosa*)/Douglas-fir forest.

Table 1
Selected fire behavior parameters from the Slate Point and the Hermada prescribed fires

Measurement	Slate Point	Hermada
Litter temp. (°C)	633–837	429–915
Duff temp. (°C)	69–612	187–217
Mineral soil surface temp. (°C)	n.a. ^a	119–187
3 mm below mineral soil interface (°C)	38	n.a.
22 mm below mineral soil interface (°C)	30	37–112
Lower duff moisture content (%)	72 ^b	39 ^c
Upper duff moisture content (%)	42	71
Fine fuel moisture content (%)	9	18
Flame length (m)	2–6	1–3
Fireline intensity ^d (kW m ⁻¹)	1160–12,600	260–2800
Ambient temperature (°C)	23	12
Wind speed (km h ⁻¹)	8–11	0–8
Wind direction	N	SE
Relative humidity (%)	22	36

^a n.a. indicates data not available.

^b N = 20 at the Slate Point site.

^c N = 30 at the Hermada site.

^d Fireline intensity is calculated as: $258 \times \text{flame length}^{2.17}$.

The habitat type is Douglas-fir/ninebark (*Physocarpus malvaceus*) (Steele et al., 1981). Slopes within the study area range from 40 to 75% with northeasterly and southeasterly aspects. Elevations range from 1760

to 1880 m. The predominant soil (85% sand, 13%, 2% clay with 12% gravel component) is Typic Cryum-brept, loamy skeletal mixed derived from granitic parent material.

2.2. Field experiment

Duff and fuel characteristics were measured with a geostatistical sampling scheme prior to each burn (Robichaud, 1996; Robichaud and Miller, 2000). The geostatistical sampling scheme used about three-quarters of the sampling points on a grid basis and the remaining sampling points were located close to the grid sampling points to obtain shorter distances between sampling points. To estimate duff thickness and duff reduction by the fire, eight steel pins (200 mm in length) were installed flush with the duff layer (forest floor surface) located in the corners and midpoints of an imaginary 1-m square centered at each sampling point. There were 20 sampling points at the Slate Point site and 30 at the Hermada site. The duff consumed during the fire was determined from the differences between the two surveys (pre- and post-burn measurement).

After the spring burn at the Slate Point site, the area had a mosaic surface pattern indicating variable fire severity. Selected fire behavior parameters are provided in Table 1. This mosaic pattern gave a

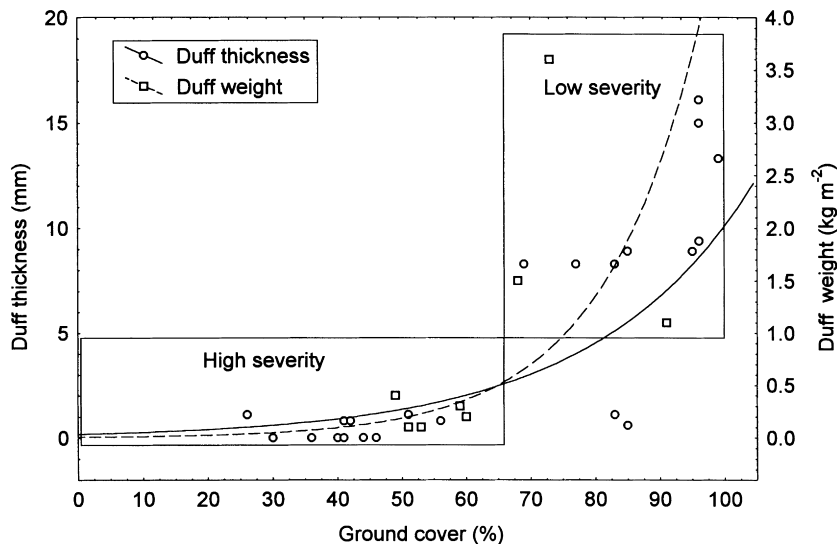


Fig. 1. Ground cover amounts and duff thickness used to classify areas as low- and high-severity burns (Robichaud, 1996).

Table 2

Surface conditions, areas, total runoff and hydraulic conductivity values for the Slate Point and Hermada sites

Surface condition	Total area (%)	No. of plots	Total runoff (mm)			Hydraulic conductivity (mm h^{-1})	
			Event 1	Event 2	Event 3	$K_{\text{for}}^{\text{a}}$	$K_{\text{hydrobi}}^{\text{b}}$
<i>Slate Point</i>							
Unburned-undisturbed	20	2	4	4	4	77–81	
Low severity burn	65	8	15	9	8	60–89	
High severity burn	15	4	12	14	11		
Non-hydrophobic		2				30–84	
Hydrophobic		4 ^c					23–55
<i>Hermada</i>							
Unburned-undisturbed	40	3	15	17	16	36–62	
Low severity burn	55	3	24	24	22	10–63	
High severity burn	5	5	26	22	20		
Non-hydrophobic		2				22–74	
Hydrophobic		3					15–40

^a Hydraulic conductivity values fitted from the rainfall simulation hydrographs during rain event 3.

^b Hydraulic conductivity for hydrophobic soil conditions fitted from the rainfall simulation hydrographs during the first 10 min of Event 1.

^c Two of the four plots that were hydrophobic were located in areas subjected to the low-severity burns. All others were in areas subjected to high-severity burns.

variety of surface conditions from white ashy (complete combustion) to blackened appearance with minimal destruction of the duff layer, indicating a moderate to light ground char fire as described by Ryan and Noste (1983), or a low- to high-severity burn as described by Phillips and Abercrombie (1987). The fall fire did not burn as expected at the Hermada site. The southern aspect was dryer than the northern aspect but fuel loadings and duff thickness were very variable spatially, thus making it more difficult to carry the fire. After burning the Hermada site, small areas appeared ashy white, whereas the majority of the burn area had a black appearance indicating light ground char (Ryan and Noste, 1983) or low-severity burn (Phillips and Abercrombie, 1987). Surface conditions after the burn were classified on type and severity of disturbance. The four surface conditions were unburned-undisturbed, burns of a low-severity (65–100% ground cover remaining and a duff thickness between 5 and 20 mm), burns of high-severity (0–65% ground cover remaining and a duff thickness less than 5 mm) and skid trails (high disturbance) areas (Robichaud et al., 1993; Robichaud, 1996) (Fig. 1). Skid trails were not used in this analysis.

2.3. Rainfall simulation

Rainfall simulation plots were located randomly in each surface/hydrologic condition area several days after the burn. Fourteen rainfall simulation plots were located at Slate Point site and 11 at the Hermada site (Table 2). Adjustments to plot locations were made for access to water supply and electrical power. Because of fiscal and logistical constraints, rainfall simulation could not take place at each geostatistical sampling location. Since variability within each surface condition was high, as many repetitions as possible were completed as permitted by time and weather. At the Hermada site, most of the area was subjected to a low-severity burn, efforts were made to locate a few plots in areas subjected to high-severity burn to be able to determine the effects of the different surface conditions.

Simulated rainfall events were applied to 1 m^2 plots with the USDA-Forest Service oscillating nozzle rainfall simulator. These plots were bordered by 150 mm wide sheet metal inserted vertically 50 mm into the mineral soil. The simulator produced a mean rainfall intensity of 94 mm h^{-1} ($\text{SD} = 5.5 \text{ mm h}^{-1}$). Each plot received three 30-min rainfall events. Event 1 (dry) was conducted with existing soil moisture condition. After Event 1, the plots were covered with plastic

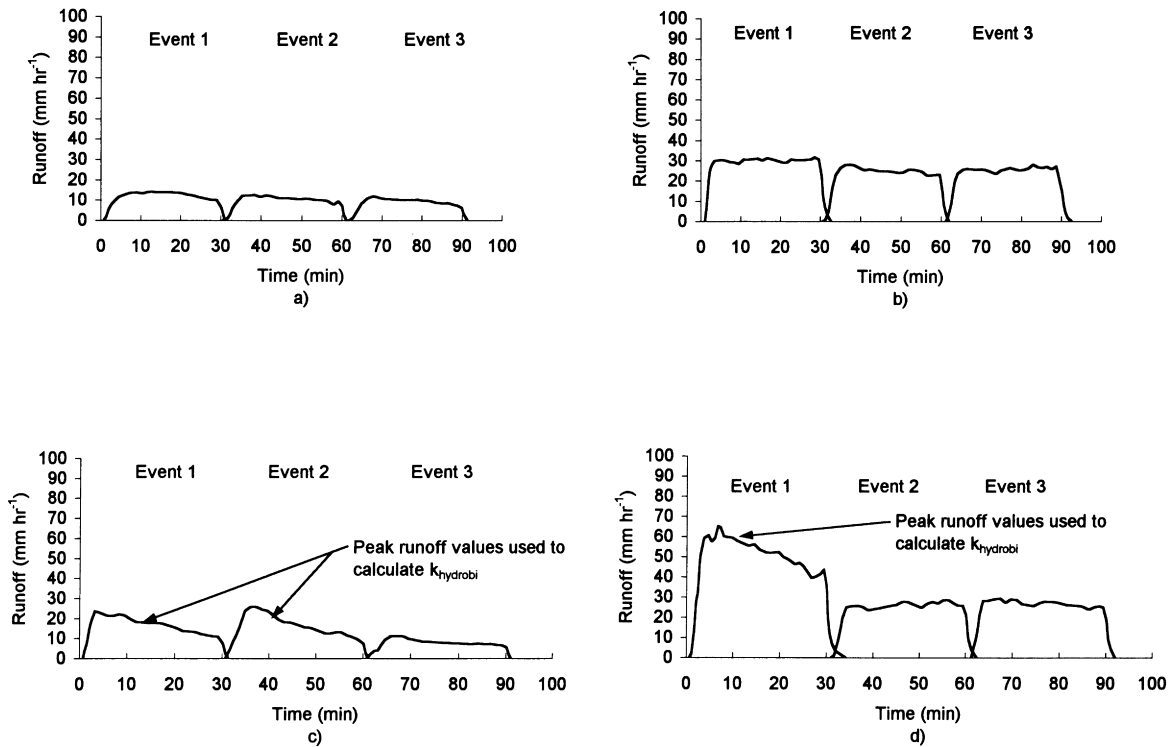


Fig. 2. Hydrographs from the Slate Point site that were within: (a) areas that were unburned-undisturbed; (b) areas subjected to a low-severity burn; (c) areas subjected to a high-severity burn with a slight hydrophobic response; and (d) areas subjected to a high-severity burn with a hydrophobic response.

sheeting and Event 2 (wet) was conducted the following day. Event 3 (very wet) was conducted about 30 min after Event 2. This procedure provided three distinct antecedent moisture conditions. A covered trough at the lower end of each plot carried runoff (water and sediment) through an outlet tube for timed volume samples, collected manually in 500 ml bottles. These data were used to develop hydrographs, total runoff volumes and sediment yields (Robichaud, 1996).

2.4. Analysis methods

Hydrographs show the temporal variation in runoff rate (mm h^{-1}) collected at the outlet of the 1 m^2 plot for three 30-min rainfall events. Runoff amounts can be calculated by the integration of the hydrograph. These hydrographs were used to calculate hydraulic conductivity values by the methods of Luce and Cundy (1994) which determine parameter values for

kinematic wave-Philip's infiltration overland flow equation from the runoff hydrographs. The best fit equation minimizes the error between the observed and synthetic hydrographs by an iterative process of adjusting the values for the sorptivity, conductivity and time to ponding under constant rainfall rate and duration, plot slope and size, and moisture contents. Inputs to saturated hydraulic conductivity (K_{for}) values were fitted from the very wet events when the soil was saturated, since these estimates are more reliable than from the dry or wet events. However, hydraulic conductivity values were also estimated near the beginning of the first rainfall event for determining the hydrophobic hydraulic conductivity (K_{hydrobi}) when the hydrograph had a peaked shape (Figs. 2c,d and 3). When this occurred, the synthetic hydrograph was fitted to the peaked portion of the runoff hydrograph to estimating K_{hydrobi} .

Mean hydraulic conductivity values between the surface conditions were compared by the least

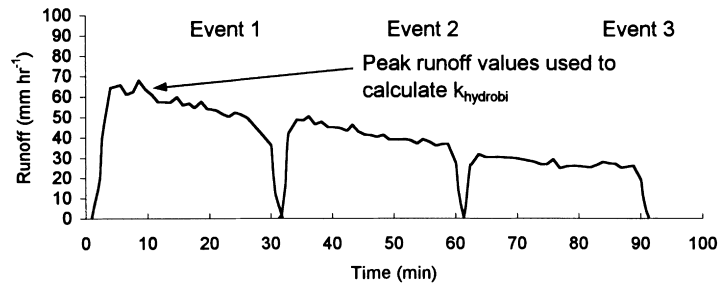


Fig. 3. Hydrographs from the Hermada site that were within areas that were subjected a high-severity burn with a hydrophobic response.

significant difference (LSD) at $\alpha = 0.05$ (StatSoft, 1995). Probability distribution functions were also used to define probabilities of occurrence for values of hydraulic conductivity for each site. Best-fit distribution algorithms were determined by testing various distribution functions (normal, gamma and exponential with an $\alpha = 0.05$) and various number of categories using the Kolmogorov–Smimov one-sample test for goodness-of-fit (McCuen and Snyder, 1986; StatSoft, 1995). This tests the null hypothesis that the cumulative distribution of a variable agrees with the cumulative distribution of some specified probability function at specified α -levels.

3. Results and discussion

3.1. Fire descriptions

Ignition techniques, fuel moisture and weather during the Slate Point burn produced an intense fire concentrated in the center of the unit, whereas the Hermada burn produced a low intensity fire (Table 1). Maximum temperatures within the duff were 69–612°C lasting 3–8 min at the Slate Point site, whereas at the Hermada site maximum temperatures were only 119–187°C in the duff. Spatially varied surface conditions occurred after both prescribed burns. Duff depths averaged 47 mm prior to the fire and 19 mm following the burn at the Slate Point site. Duff depths averaged 36 mm prior to the burn and 29 mm following the burn at the Hermada site. At the Hermada site, the harvest unit did not burn well due to high moisture conditions (71%) of the upper duff, high humidity (36%) and higher fine fuel moisture content (18%) (Table 1).

The fires created mosaic patterns of duff consumption and some unburned areas. These spatial patterns are described in detail in Robichaud and Miller (2000) and Robichaud (1996). The burn sites were divided into three surface conditions: unburned, low severity and high severity surface conditions for rainfall simulation plot locations. The areas subjected to a low-severity burn retained 65–100% of its original ground cover. The area subjected to a high-severity burn retained 0–65% of its original ground cover (Fig. 1). At the Slate Point site, approximately 65% of the area was subjected to a low-severity burn and 15% of the area was subjected to high-severity burn at the top of the slope, where the heat generated during the fire consumed most of the duff layer. Whereas at the Hermada site, approximately 55% of the area was subjected to a low-severity burn and only 5% of the area was subjected to a high-severity burn which occurred on a southern aspect drainage depression (Table 2).

3.2. Slate Point

On the unburned-undisturbed areas, runoff was minimal and constant (4 mm for each event) (Table 2 and Fig. 2a). This low runoff rate resulted because the protective layer of duff (100% ground cover) covering the mineral soil remained intact. The intact duff layer protects the mineral soil from both overland flow and raindrop impact, thereby preventing erosion and increasing infiltration. The duff provided detention storage by allowing water to be released slowly into the underlying mineral soil resulting in high hydraulic conductivity values (77–81 mm h⁻¹). The duff material also acted as a lateral flow path for water moving downslope.

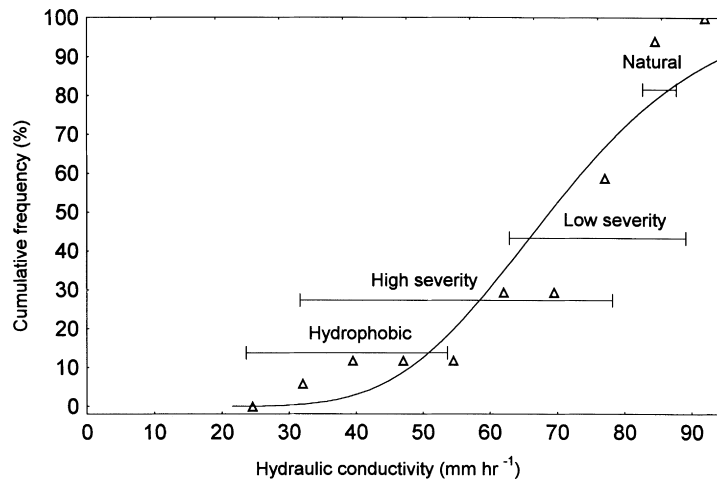


Fig. 4. Cumulative distribution function for hydraulic conductivity at the Slate Point site. Kolmogorov–Smirnov $d = 0.27$ at the $\alpha = 0.05$ level.

An example of a hydrograph from a low-severity burn area indicates a relatively constant runoff rate for all three 30-min rain events (Fig. 2b). Hydraulic conductivity was calculated as 72 mm h^{-1} during Event 3. Total runoff collected, calculated from the area under the hydrograph, were 14, 12 and 12 mm for each successive rainfall event. In contrast, a hydrograph from areas subjected to a high-severity burn indicate high runoff rates during Event 1, decreasing to a constant rate for the last 10 min of each event (Fig. 2c). The shape of a second hydrograph indicates a hydrophobic soil condition was present because runoff decreases with time. Another hydrograph from the same site and surface condition indicates a similar hydrophobic response with a greater magnitude of runoff during the initial portion of the simulated rainfall event and the final runoff rate (Fig. 2d).

3.3. Hermada

Portions of the Hermada site provided another example of a hydrophobic response to simulated rainfall with runoff decreasing with each successive rain event (Fig. 3). Runoff quickly reaches 67 mm h^{-1} and then drops to 30 mm h^{-1} at the end of Event 3. Hydraulic conductivity was estimated at 62 mm h^{-1} at the end of Event 3. At the onset of rain, the hydrophobic hydraulic conductivity was estimated at 35 mm h^{-1} . Thus we can see how hydrophobic

conditions vary as the soil profile becomes wetted and eventually responds as a normal infiltrating soil.

Normal infiltration theory indicates that downward infiltration in an initially unsaturated soil generally occurs under the combined influence of suction and gravity gradients. As the water penetrates deeper and the wetted part of the profile lengthens, the average suction gradient decreases, since the overall difference in the pressure head divides itself along an ever-increasing distance. This trend continues until eventually the suction gradient in the upper part of the profile becomes negligible, leaving the constant gravitational gradient as the only force moving water downward. Since the gravitational head gradient has the value of unity (the gravitational head decreasing at the rate of 1 mm with each millimeter of vertical depth below the surface), it follows that the flux tends to approach the hydraulic conductivity as a limiting value (Hillel, 1982).

3.4. Hydrophobic response

When analyzing a hydrograph such as in Figs. 2c,d and 3, hydraulic conductivity was determined from Event 3, where runoff and infiltration are fairly constant. Data from the beginning of Event 1 represents the hydrophobic hydraulic conductivity. The difference between initial (hydrophobic) hydraulic conductivity and the final hydraulic conductivity when hydrophobic conditions were present. The

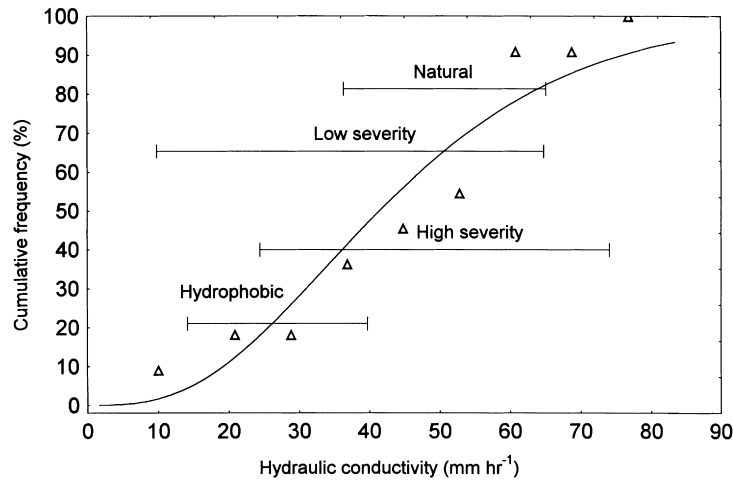


Fig. 5. Cumulative distribution function for hydraulic conductivity at the Hermada site. Kolmogorov–Smimov $d = 0.16$ at the $\alpha = 0.05$ level.

hydrophobic hydraulic conductivity values were 10–40% of normal saturated hydraulic conductivity. Only 4 out of 14 plots indicated hydrophobicity from Slate Point, and 3 out of 11 plots from Hermada thus indicating that hydrophobic conditions were not extensive especially since only 5% of the total area at the Hermada site was subjected to a high-severity burn. Since hydrophobic substances are water soluble, they can be broken down and destroyed with water, as evident by the declining hydrographs during the third rain event (Figs. 2c,d and 3). The timing or persistence of the hydrophobicity was not measured in this experiment, i.e. repeated rainfall simulation over weeks or months on the same plots was not performed. Researchers have documented persistence from weeks to years. In general, the hydrophobicity is broken up or is sufficiently washed away within one to two years after the fire.

3.5. Cumulative distribution of hydraulic conductivity

Hydraulic conductivity varies within each surface condition (Table 2) and the means were not significantly different by LSD method at $\alpha = 0.05$. For example at the Slate Point site, there was little variation for the unburned-undisturbed hydraulic conductivity; a range of 60–89 mm h⁻¹ for the surface conditions with a low-severity burn; and a range of 30–84 mm h⁻¹ for the surface conditions with a high-severity burn. Therefore, best-fit cumulative

distribution algorithms were used to describe the range of hydraulic conductivity by using all measured hydraulic conductivity for a given field site excluding hydrophobic response conditions (Figs. 4 and 5). Cumulative distribution algorithms combined with spatial distribution (Robichaud and Monroe, 1997) provide methods for estimates of runoff and erosion from spatially-varied forest conditions. This agrees with the finding of Smith and Hebbert (1979), Moore and Clarke (1981) and Hawkins and Cundy (1987) that a single value for hydraulic conductivity for a site is not appropriate for forest conditions.

Hydraulic conductivity values at the Hermada site had larger variations for all treatments and means were significantly smaller by the LSD method when compared with Slate Point (Table 2; Figs. 4 and 5). The differences were due to larger post-fire site variation since much of the site did not burn well as previously described. Overall lower values are probably due to some surface crusting and sealing which have been reported for these soil types. This thin crust can be developed by the beating action of the raindrops, or as a result of the spontaneous slaking and breakdown of the soil aggregates during wetting (Hillel, 1982). This was common on south aspects which have thinner duff. Thus, a single cumulative distribution algorithm for each site should provide reasonable estimates of hydraulic conductivity.

Water drop penetration times, WDPT, (DeBano, 1981) were measured during this study (Robichaud,

1996) using the same geostatistical design described in Robichaud and Miller (2000). These results showed greater repellency in areas subjected to high-severity burns (Robichaud, 1996). Since WDPT were not measured prior to each rainfall simulation, no relations can be made on the expected reduction in infiltration throughout the site based on WDPT. Thus, the reduction in infiltration described here needs additional field evaluation to determine its spatial distribution.

4. Conclusions

Variable surface conditions are common in forest environments especially after prescribed fires. Small-scale rainfall simulation techniques provide a reliable method to determine hydraulic conductivity for these various surface conditions. Two prescribed burns were conducted and both produced variable infiltration rates related to burn severity. When hydrophobic conditions were present, marked changes in the runoff hydrographs over time allowed for the determination of a hydrophobic hydraulic conductivity. When hydrophobic conditions occurred after a high-severity burn, the saturated hydraulic conductivity was reduced between 10 and 40% during the onset of simulated rainfall, thus $K_{\text{hydrobi}} = 0.1\text{--}0.4K_{\text{sat}}$. These hydrophobic hydraulic conductivity values recovered to near saturated hydraulic conductivity values by the third simulated rainfall event for all plots.

In a forest environment, hydraulic conductivity varies by surface condition which is a function of the type and severity of disturbance. Within each surface condition there is also variability. Cumulative distribution algorithms provide a means to account for the inherent variability associated with these hillslopes and surface conditions. Cumulative distribution algorithms and spatial distributions of hydraulic conductivity should be used with erosion prediction models to predict surface runoff and erosion from forest environments.

References

- Bond, R.D., 1964. The influence of the microflora on the physical properties of soils. II. Field studies on water repellent sands. *Aust. J. Soil Res.* 2, 111–122.
- Campbell, I.A., 1977. Stream discharge, suspended sediment and erosion rates in the Red Deer River basin, Alberta, Canada. *Int. Assoc. Hydrol. Sci.* 122, 244–259.
- DeBano, L.F., 1981. Water repellent soils: a state of the art. Gen. Tech. Rpt. PSW-46. USDA For. Serv., Pacific Southwest Forest and Range Exp. Sta., Berkeley, CA, 21pp.
- DeBano, L.F., Rice, R.M., 1973. Water repellent soils: their implications in forestry. *J. Forestry* 71, 220–223.
- DeBano, L.F., Osborn, J.F., Krammes, J.S., Letey, J., Jr., 1967. Soil wettability and wetting agents...our current knowledge of the problem. Gen. Tech. Rpt. PSW-43. USDA For. Serv., Pacific Southwest Forest and Range Exp. Sta., Berkeley, CA, 13pp.
- DeBano, L.F., Savage, S.M., Hamilton, D.A., 1976. The transfer of heat and hydrophobic substances during burning. *Soil Sci. Soc. Am. J.* 40, 779–782.
- Dekker, L.W., Ritsema, C.J., 1995. Fingerlike wetting patterns in two water-repellent loam soils. *J. Environ. Qual.* 24, 324–333.
- Dekker, L.W., Ritsema, C.J., 1996. Preferential flow paths in a water repellent clay soil with grass cover. *Water Resour. Res.* 32, 1239–1249.
- Dyrness, C.T., 1976. Effect of wildfire on soil wettability in the High Cascades of Oregon. Res. Paper PNW-202. USDA For. Serv., Pacific Northwest Forest and Range Exp. Sta. Portland, OR, 18pp.
- Hawkins, R.H., Cundy, T.W., 1987. Steady-state analysis of infiltration and overland flow for spatially-varied hillslopes. *Water Resour. Bull.* 23, 251–256.
- Hillel, D., 1982. *Introduction to Soil Physics*, Academic Press, San Diego, CA (364pp.).
- Holzhey, C.S., 1969. Water-repellent soil in Southern California. In: DeBano, L.F., Letey, J. (Eds.), *Water-Repellent Soils: Proceedings*, Riverside, CA, pp. 31–41.
- Luce, C.H., Cundy, T.W., 1994. Parameter identification for a runoff model for forest roads. *Water Resour. Res.* 30, 1057–1069.
- McCuen, R.H., Snyder, W.M., 1986. *Hydrologic Modeling: Statistical Methods and Applications*, Prentice-Hall, Newark, NJ (568pp.).
- McNabb, D.H., Gaweda, F., Froehlich, H.A., 1989. Infiltration, water repellency, and soil moisture content after broadcast burning a forest site in southwest Oregon. *J. Soil Water Conserv.* 44, 87–90.
- Meeuwig, R.O., 1971. Infiltration and water repellency in granitic soils. Res. Paper INT-111. USDA For. Serv., Intermountain Res. Sta., Ogden, UT, 10pp.
- Megahan, W.F., Molitor, D.C., 1975. Erosional effects of wildfire and logging in Idaho. *Watershed Management Symposium*. Am. Soc. Civil Eng. Irrigation and Drainage Div., Logan, UT, pp. 423–444.
- Moore, R.J., Clarke, R.T., 1981. A distribution function approach to rainfall runoff modeling. *Water Resour. Res.* 17, 1367–1382.
- Pfister, R.D., Kovalchik, B.L., Arno, S.F., Presby, R.C., 1977. Forest habitat types of Montana. Gen. Tech. Rpt. INT-GTR-34. USDA For. Serv., Intermountain Forest and Range Exp. Sta., Ogden, UT, 174pp.
- Phillips, D.R., Abercrombie, J.A., 1987. Pine–hardwood mixtures—a new concept in regeneration. *Southern J. Appl. Forestry* 11 (4), 192–197.

- Richardson, J.L., Hole, F.D., 1978. Influence of vegetation on water repellency in selected western Wisconsin soils. *Soil Sci. Soc. Am. J.* 42, 465–467.
- Robichaud, P.R., 1996. Spatially-varied erosion potential from harvested hillslopes after prescribed fire in the Interior Northwest. PhD Diss., University of Idaho, Moscow, ID, 219pp.
- Robichaud, P.R., Hungerford, R.D., 2000. Water repellency by laboratory burning of four northern Rocky Mountain forest soils. *J. Hydrol.* 231–232, 207–219.
- Robichaud, P.R., Miller, S.M., 2000. Spatial simulations to describe duff consumption of prescribed fire. *Int. J. Wildland Fire* (in press).
- Robichaud, P.R., Monroe, T.M., 1997. Spatially-varied erosion modeling using WEPP for timber harvested and burned hillslopes. ASAE paper No. 97-5015. Amer. Soc. Agric. Eng., Minneapolis, MN, 8pp.
- Robichaud, P.R., Waldrop, T.A., 1994. A comparison of surface runoff and sediment yields from low- and high-severity site preparation burns. *Water Resour. Bull.* 30, 27–34.
- Robichaud, P.R., Luce, C.H., Brown, R.E., 1993. Variation among different surface conditions in timber harvest sites in the Southern Appalachians. International workshop on soil erosion: Proc. Moscow, Russia. Purdue University, West Lafayette, IN, pp. 231–241.
- Ryan, K.C., Noste, N.V., 1983. Evaluating prescribe fires. In: Lotan, J.E., Kilgore, B.M., Fischer, W.C., Mutch, R.W. (Tech. Coord.), Symposium and Workshop of Wilderness Fire: Proc. Gen. Tech. Rpt. INT-182. USDA For. Serv., Intermountain Res. Sta., Ogden, UT, pp. 230–238.
- Smith, R.E., Hebbert, H.B., 1979. A Monte Carlo analysis of the hydrologic effects of spatial variability of infiltration. *Water Resour. Res.* 15, 419–429.
- Soto, B., Basanta, R., Benito, E., Perez R., Diaz-Fierros, F., 1994. Runoff and erosion from burnt soils in northwest Spain. In: Sala, M., Rubio, J.L. (Eds.), *Soil Erosion and Degradation as a Consequence of Forest Fires: Proc. Barcelona, Spain*, pp. 91–98.
- StatSoft, 1995. *Statistica for Windows*. Version 5.1. StatSoft Inc., Tulsa, OK.
- Steele, R., Pfister, R.D., Ryker, R.A., Kittams, J.A., 1981. Forest habitat types of Central Idaho. Gen. Tech. Rpt. INT-GTR-114. USDA For. Serv., Intermountain Res. Sta., Ogden, UT, 138pp.

Dissolved noble gas and isotopic tracers reveal vulnerability of groundwater in a small, high-elevation catchment to predicted climate changes

Michael J. Singleton¹ and Jean E. Moran²

Received 30 September 2009; revised 22 July 2010; accepted 26 August 2010; published 4 December 2010.

[1] Noble gas concentrations and multiple isotopic tracers in groundwater and stream water at a small, high-elevation catchment of the Sierra Nevada Mountains constrain recharge conditions and subsurface residence times of different groundwater components. We identify three sources that contribute to groundwater flow: (1) seasonal groundwater recharge with short travel times, (2) water with elevated radiogenic ⁴He that has experienced longer flow paths, and (3) upwelling of deep fluids that have “magmatic” helium and carbon isotope signatures. Results from our study illuminate two important aspects of the hydrological system that will have a direct impact on how this system responds to climate change: (1) recharge to the alluvial aquifer occurs primarily on the lower slopes of the catchment and is therefore sensitive to changes in snowline elevation and (2) deep groundwater in the western part of the aquifer is very young and provides very little buffering capacity. Although apparent groundwater ages indicate residence times range from less than a year to several decades, the water that recharges seasonally dominates the alluvial aquifer. Noble gas recharge temperatures are close to mean annual air temperature, and are 5°–11° higher than would be expected for direct influx of snowmelt. Excess air concentrations, indicating entrapment of air bubbles during recharge, are lower than would be expected for recharge through bedrock fractures. Instead, recharge likely occurs over vegetated areas on the lower slopes, as indicated by $\delta^{13}\text{C}$ -dissolved inorganic carbon values that are consistent with incorporation of CO₂ from soil respiration.

Citation: Singleton, M. J., and J. E. Moran (2010), Dissolved noble gas and isotopic tracers reveal vulnerability of groundwater in a small, high-elevation catchment to predicted climate changes, *Water Resour. Res.*, 46, W00F06, doi:10.1029/2009WR008718.

1. Introduction

[2] Predicted changes in the climate will have profound impacts on water resources and water management. Future climate changes in the western United States are likely to include a decrease in the percentage of precipitation that falls as snow; earlier onset of snowpack melting; an increase in number of rain on snow events; and changes in humidity, air temperature, and soil moisture [Dettinger and Cayan, 1995; Howat and Tulaczyk, 2005; Maurer and Duffy, 2005; Melack et al., 1997]. Snowmelt is an important component of groundwater recharge in high-elevation watersheds of the western United States [e.g., Earman et al., 2006]. In these watersheds, the predicted climate change impacts on snowmelt will likely alter the amount and timing of groundwater recharge, which may lead to reduced groundwater production, declining water tables, and reduced base flow to streams.

[3] Groundwater aquifers in alpine and subalpine basins play a critical role by storing and releasing snowmelt as base flow to streams long after seasonal precipitation and the disappearance of the snowpack and in this manner significantly impact streamflow and water temperature. Furthermore, geochemical hydrograph separations have shown that groundwater may supply a majority of alpine streamflow during peak snowmelt conditions [Liu et al., 2004]. Mountain-block aquifers can also provide significant recharge to mountain-front and basin-fill aquifers [Manning and Solomon, 2003; Manning and Solomon, 2005]. Despite being an important part of the water supply system, the recharge mechanisms, storage capacity, and residence times of high-elevation groundwater aquifers are poorly understood. The net change in recharge to mountain aquifers due to alterations in the timing of snowpack melting is not known in sign or magnitude, making it difficult to predict the response of these hydrological systems to climate change.

[4] Dissolved gas and isotope studies have given insights into the residence times and recharge processes operating in high-elevation watersheds. Manning and Caine [2007] used dissolved noble gas analyses to characterize groundwater recharge and residence times in a high-elevation (3300–3900 m above sea level [asl]) alpine watershed in Colorado. They determined that permeability decreases with depth and that aquifer parameters are relatively uniform throughout

¹Chemical Sciences Division, Physical and Life Sciences Directorate, Lawrence Livermore National Laboratory, Livermore, California, USA.

²Department of Earth and Environmental Science, California State University East Bay, Hayward, California, USA.

much of the watershed, with mean residence times between 8 and 11 years. *Plummer et al.* [2001] use dissolved gases to examine groundwater residence time in a mountainous region in Shenandoah National Park, VA. They found the shallow groundwater system to be dominated by young (<3 years) water and observed seasonally varying recharge temperatures, indicating shallow, seasonal recharge. In a study over a much larger geographic area, *Manning and Solomon* [2005] used dissolved noble gas results to examine mountain block recharge and subsurface flow to an adjacent basin. *Rademacher et al.* [2001] found that the apparent groundwater ages of springs in the Sagehen Basin, a small catchment approximately 27 km north of our study site, ranged from 1 to 36 years, and based on the chemical evolution of spring and creek waters, inferred that base flow to the local creek was dominated by moderately old groundwater [*Rademacher et al.*, 2005]. Also in the Sagehen Basin, *Blumhagen and Clark* [2008] used carbon isotope compositions to show that dissolved inorganic carbon (DIC) in spring waters was inherited from respiration of CO₂ in the soil zone.

[5] In alpine basins, the large gradients in altitude and temperature, which control gas solubility, make dissolved gases especially well suited to examining recharge processes and groundwater transport. Dissolved noble gases provide a snapshot of recharge water temperature and physical processes at the time of recharge and are transported conservatively in saturated media, providing a long-term record. Dissolved inorganic carbon concentrations, in combination with carbon isotope compositions, are useful for delineating the location of recharge and mixing of different water sources. When combined with measurements of tritium, helium isotopes provide a means of quantifying apparent groundwater subsurface residence time, or groundwater age, over a time scale relevant to the interaction between shallow groundwater and streamflow.

[6] In this paper the power of dissolved gas data to evaluate the vulnerability of water resources in high-elevation, snow-dominated watersheds is demonstrated in a small basin likely to experience altered runoff and recharge under warmer climate scenarios. Specifically, the questions that are addressed using dissolved gas and isotopic analyses are: What are the temperatures and time periods over which recharge takes place? Does water infiltrate through a soil layer or through fractures? What is the range in aquifer residence times for the bulk of the groundwater and for the groundwater most likely to contribute to stream base flow? One of the challenges in mountain hydrology is that many potential field sites lack access to adequate groundwater sampling points, such as monitoring wells. The research reported here takes advantage of the numerous monitoring wells and production wells in the Olympic Valley groundwater basin.

2. Study Site

[7] The Olympic Valley catchment is located 150 km east of Sacramento, CA, near Lake Tahoe in the Sierra Nevada, and has an area of approximately 22 km² including alpine and subalpine zones. An alluvial aquifer extends eastward 4 km from the base of Granite Chief, a 2750 m peak that forms the center of Squaw Valley ski area, to the northward flowing Truckee River (Figure 1). The valley is drained by Squaw Creek, which is formed at the confluence of two

major tributaries at the west margin of the basin at elevation 1898 m, entering the Truckee River at 1853 m. The groundwater basin is underlain by Cretaceous granites of the Sierra Nevada batholith, Jurassic metasediments, and Pliocene volcanics that also form the surrounding peaks. Glacial, lacustrine, and fluvial sediments fill the valley to a maximum thickness of 55 m near the center of the 0.8 km wide valley [*Gasch and Associates*, 1973]. A terminal moraine at the eastern end of the basin near the confluence of Squaw Creek and the Truckee River acted as a sediment dam throughout the Quaternary period.

[8] The hydrogeology of the valley has been examined through drill core logs and surface exposures [*Hydrometrics-LLC*, 2007; *Kleinfelder and Associates*, 1987; *West-Yost and Associates*, 2003]. The unconsolidated valley-fill sediments act as an unconfined aquifer (dotted line on Figures 1a and 1b) except where laterally discontinuous fine-grained lacustrine deposits create semiconfined conditions. Three hydrostratigraphic units are loosely defined: a shallow unit consisting of fine-grained lake sediments and stream deposits, a middle unit of glacial sands and gravels, and a deep unit comprising fine-grained glacial lake sediments. Coarse-grained materials predominate in the western portion of the basin upstream of the production wells and are highly permeable. Sediments become less permeable in the downstream portion of the basin, and at the terminal moraine, groundwater occurrence is minimal. Estimates of hydraulic conductivity based on well tests range from 0.002 to 0.514 cm/s, averaging 0.067 cm/s [*Kleinfelder Inc.*, 2000]. Groundwater also occurs in the crystalline rocks, with fractures providing secondary permeability. Four faults have been mapped across the valley based on surface exposures [*Nevada Bureau of Mines and Geology*, 2000], one of which is coincident with a spring (“Upwelling” spring on Figure 1) near monitoring wells 304/305.

[9] Precipitation in Olympic Valley occurs mainly in the form of snow in the winter months, with a smaller amount of precipitation occurring as rain during spring, summer, and fall. A U.S. Department of Agriculture SNOTEL site (site #784) located at 2447 m elevation in the catchment recorded an average annual precipitation of 1684 mm for the 1982–2008 water years (<http://www.wcc.nrcs.usda.gov/snotel/>). Estimated isohyets [*Di Luzio et al.*, 2008] show mean annual precipitation increasing from 1016 mm in the east to 1650 mm in higher elevations to the west.

[10] Olympic Valley is uniquely suited to a study of alpine and subalpine groundwater because of its relatively simple geometry and because many wells are available for sampling. However, the natural hydrologic cycle is altered through groundwater pumping and possibly because of channelization of the Squaw Creek streambed. Groundwater is extracted to supply the needs of valley residents and businesses (approximately 6.2×10^5 m³/yr), additional resorts, private residences and the ski area (extraction unknown), snow-making (8.5×10^4 m³/yr), and for irrigation of a golf course that fills a portion of the meadow surrounding Squaw Creek (2.5×10^5 m³/yr) [*Hydrometrics-LLC*, 2007]. The total average annual groundwater extraction by known sources was 8.9×10^5 m³/yr for the years 1992–2004. Peak water demand occurs from July to October and is about twice the wintertime demand. The peak demand corresponds to the driest months of the year and may contribute to water table

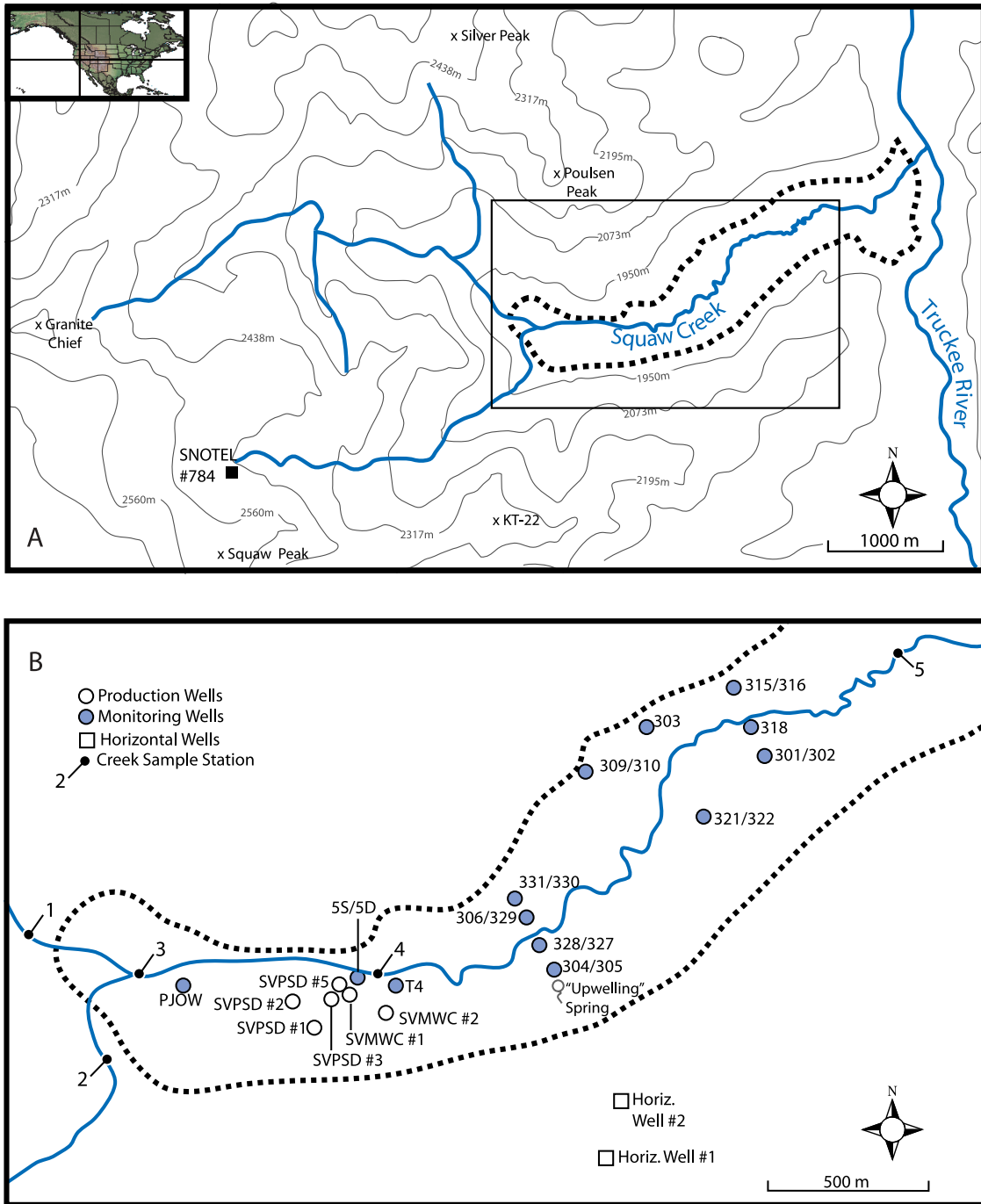


Figure 1. Topographic map of (a) the study area and (b) locations of the spring, wells, and faults discussed in the text. The outline of the alluvial aquifer is shown as a dotted line [after *Hydrometrics-LLC*, 2007]. Stream sampling sites as labeled in Table 1 are (1) Shirley Canyon, (2) South Fork, (3) Confluence, (4) Trapezoid, and (5) Squaw Creek Rd Bridge.

declines (Figure 2). The main production wells are located in a cluster in the western portion of the basin (Figure 1). Although the total groundwater discharge due to pumping is a small fraction of the annual precipitation that falls in the catchment (<3%), the cluster of production wells in the upstream portion of the alluvium does capture water that would contribute to down-gradient flow or to base flow in Squaw Creek. Fifteen monitoring well pairs are located on and around a golf course in the meadow that covers the

lower valley. A small number of horizontal wells drilled into bedrock produce water at about 190 L/min, which is about 10% of the flow rate of the production wells in valley alluvium. Export of wastewater and increased evapotranspiration during irrigation cause a small net water loss to the catchment due to human activity. Total discharge from Squaw Creek is approximately $2 \times 10^7 \text{ m}^3/\text{yr}$ [*West-Yost and Associates*, 2003], representing about 57% of the annual precipitation.

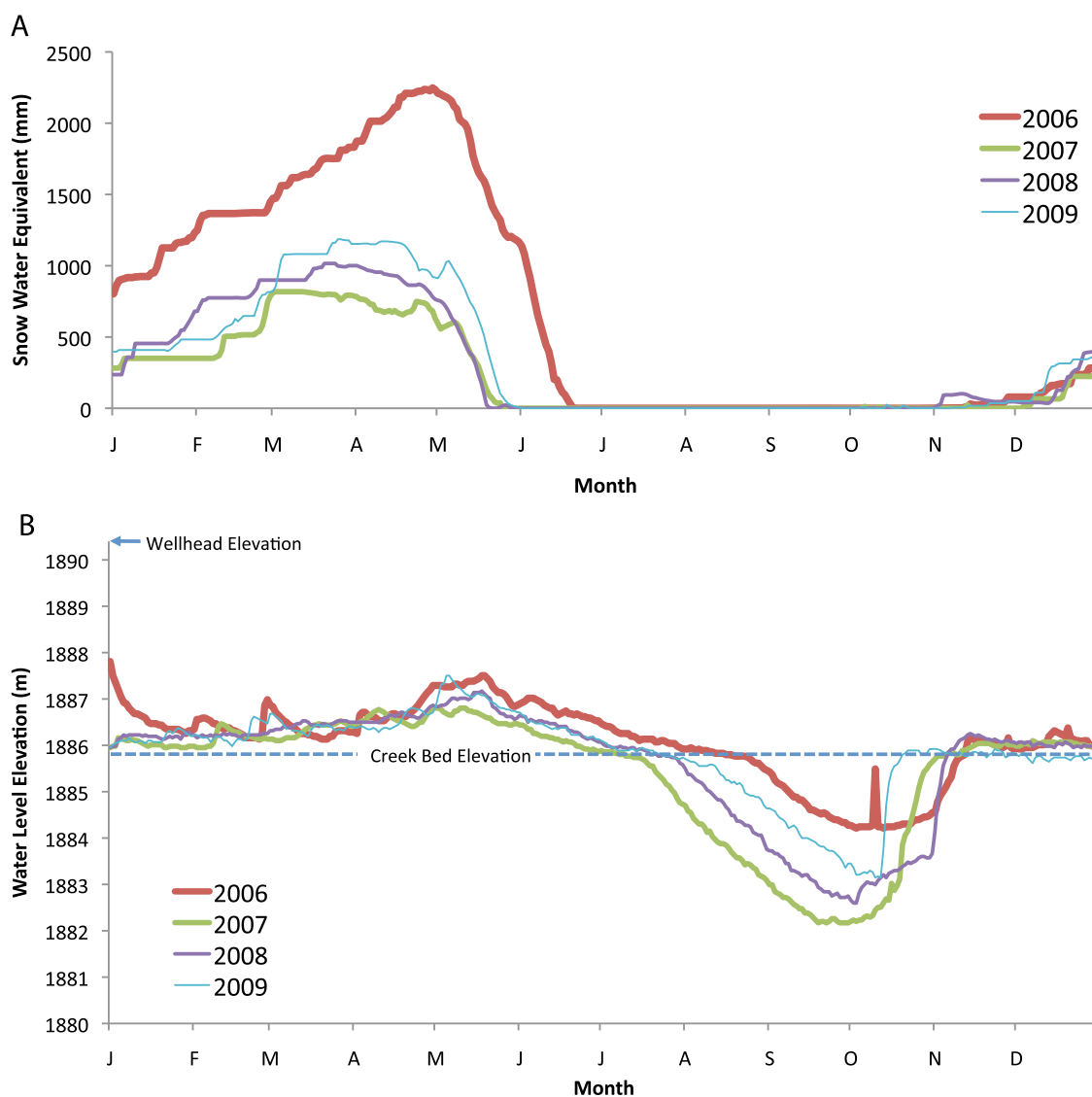


Figure 2. (a) Daily snow water equivalent at SNOTEL Station #784 located at an elevation of 2447 m in the study area (<http://www.wcc.nrcs.usda.gov/snotel/>). (b) Maximum daily water level elevation during pumping at SVPSD Well 2 (<http://www.svpsd.org/scada/aquiferwebdata.html>). A dashed line shows the elevation of the Squaw Creek Bed where it passes near Well 2.

[11] Interaction between the groundwater production wells and streamflow is of concern because of the potential for adversely affecting habitat of brown trout and other fauna. The creek is gaining throughout the annual period of substantial streamflow (November–June), as indicated by water levels (Figure 2) and stream gauging stations monitored by SVPSD. During the summer months, when streamflow decreases to $<0.05 \text{ m}^3/\text{s}$, the groundwater elevation recorded in pumping production wells adjacent to the stream falls below the elevation of the creek bed (Figure 2). Hydrographs in production wells recorded during pumping since 1997 show total water level ranges of approximately 2.4m, with seasonal lows in late fall and highs in late spring [West-Yost and Associates, 2003]. Water level contours roughly mirror topography, with flows parallel to Squaw Creek in the center of the basin, and flow toward the creek along the margins of the basin. Head differences in paired monitoring wells show a general trend of slight downward

gradients in the western portion of the meadow and upward gradients in the eastern portion [West-Yost and Associates, 2003]. During the year in which the study was carried out, the upper reach of the creek became dry by late summer, but deep pools and low flow persisted in the lower reach.

3. Methods

[12] This study includes results from eight production wells, including two horizontal wells located about 100 m above the valley floor, 22 monitoring wells, and 5 stream sampling sites (Figure 1 and Table 1). Samples for DIC were passed through a $0.45 \mu\text{m}$ filter and stored in 40 mL dark glass vials with no headspace. The DIC samples were kept cold in the field and stored in a refrigerator until analysis. Tritium samples were collected in 1 L glass containers with plastic caps. Dissolved noble gas samples (He, Ne, Ar, Kr, Xe) were collected using clear Tygon tubing to

Table 1. Measurements of Dissolved Gas and Isotopic Compositions From Horizontal Wells (HW), Monitoring Wells (MW), Production Wells (PW), a Spring (SP), and Stream Waters (SW)^a

Sample Site	Collection Date	Sample Type	Screen Depth (m)	Approximate Bedrock Depth (m)	DIC (mg/L C)	$\delta^{13}\text{C}$ (‰Vienna Pee Dee)	^3H (pCi/L)	$^3\text{He}/^4\text{He}$ (10^{-6})	^4He ($10^{-8} \text{ cm}^3 \text{ STP/g}$)	Ar ($10^{-4} \text{ cm}^3 \text{ STP/g}$)	Kr ($10^{-8} \text{ cm}^3 \text{ STP/g}$)	Ne ($10^{-8} \text{ cm}^3 \text{ STP/g}$)	Xe ($10^{-8} \text{ cm}^3 \text{ STP/g}$)
Horizontal Well 1	06/19/2008	HW			26	-17.5	11.9 ± 0.5	1.64 ± 0.05	6.49 ± 0.21	4.00 ± 0.08	8.99 ± 0.27	28.33 ± 0.57	1.25 ± 0.04
Horizontal Well 2	06/19/2008	HW			32	-17.6	19.8 ± 1.2	1.77 ± 0.06	6.07 ± 0.19	4.15 ± 0.08	9.22 ± 0.28	27.64 ± 0.55	1.28 ± 0.04
MW 301	05/13/2008	MW	3-5	34	38	-15.7	8.4 ± 0.6	1.65 ± 0.01	3.56 ± 0.07	3.42 ± 0.07	7.75 ± 0.23	19.78 ± 0.40	1.15 ± 0.03
MW 302	05/13/2008	MW	12-14	34	40	-14.9	8.3 ± 0.4	2.09 ± 0.02	6.79 ± 0.14	3.39 ± 0.07	7.66 ± 0.23	21.11 ± 0.42	1.08 ± 0.03
MW 303	06/18/2008	MW	3-5	30	20	-18.8	10.5 ± 1.3	1.46 ± 0.04	6.67 ± 0.13	3.53 ± 0.07	7.78 ± 0.23	24.93 ± 0.50	1.12 ± 0.03
MW 304	05/14/2008	MW	3-5	12	73	-7.7	6.1 ± 0.6	2.19 ± 0.02	95.29 ± 1.91	3.85 ± 0.08	8.39 ± 0.25	28.02 ± 0.56	1.24 ± 0.04
MW 305	05/14/2008	MW	11-13	12	72	-8.1	6.2 ± 0.6	2.15 ± 0.02	101.83 ± 2.04	3.87 ± 0.08	8.53 ± 0.26	26.42 ± 0.53	1.20 ± 0.04
MW 306	05/14/2008	MW	2-3	23	21	-20.8	10.3 ± 1.2	1.52 ± 0.01	5.74 ± 0.11	4.11 ± 0.08	9.09 ± 0.27	29.85 ± 0.60	1.31 ± 0.04
MW 309	06/18/2008	MW	3-5	24	22	-14.4	16.2 ± 1.3						
MW 310	06/18/2008	MW	11-12	24	22	-20.9	9.6 ± 1.2	1.64 ± 0.05	5.30 ± 0.11	3.75 ± 0.08	8.19 ± 0.25	26.67 ± 0.53	1.18 ± 0.04
MW 315	06/18/2008	MW	2-3	24	77	4.2	11.1 ± 1.0						
MW 316	06/18/2008	MW	8-10	24	66	-16.6	9.5 ± 1.3						
MW 318	05/13/2008	MW	3-5	41	67	-0.7	16.2 ± 1.1						
MW 321	05/14/2008	MW	3-5	34	29	-17.5	9.8 ± 1.2	1.68 ± 0.01	5.28 ± 0.11	3.33 ± 0.07	7.61 ± 0.23	24.06 ± 0.48	1.08 ± 0.03
MW 322	05/14/2008	MW	17-18	34	21	-18.1	13.2 ± 1.3	1.65 ± 0.01	7.06 ± 0.14	3.82 ± 0.08	8.58 ± 0.26	26.64 ± 0.53	1.24 ± 0.04
MW 327	05/14/2008	MW	11-13	15	83	-8.1							
MW 328	05/14/2008	MW	3-5	15	23	-18.3	11.3 ± 1.3	1.42 ± 0.01	5.37 ± 0.11	3.68 ± 0.07	8.67 ± 0.26	29.56 ± 0.59	1.25 ± 0.04
MW 329	05/14/2008	MW	13-15	23	203	-5.7	0.3 ± 0.6	2.77 ± 0.03	290.88 ± 5.82	4.26 ± 0.09	8.95 ± 0.27	31.69 ± 0.63	1.32 ± 0.04
MW 330	05/13/2008	MW	8-9	32	222	-4.7	-0.5 ± 0.8						
MW 331	05/13/2008	MW	2-3	32	20	-17.1	11.5 ± 0.9	1.51 ± 0.01	6.19 ± 0.12	3.50 ± 0.07	8.02 ± 0.24	21.29 ± 0.43	1.14 ± 0.03
MW 5D	05/13/2008	MW	12-14	34	18	-19.3	8.4 ± 0.6	1.36 ± 0.01	7.38 ± 0.15	3.63 ± 0.07	7.95 ± 0.24	25.76 ± 0.52	1.14 ± 0.03
MW 5D	08/12/2008	MW	12-14	34	16	-18.8	9.0 ± 0.9	1.39 ± 0.08	6.74 ± 0.55	3.53 ± 0.07	8.03 ± 0.24	25.16 ± 0.50	1.12 ± 0.03
MW 5S	05/13/2008	MW	6-8	34	28	-19.6	11.0 ± 0.7	1.37 ± 0.01	4.84 ± 0.10	3.81 ± 0.08	8.58 ± 0.26	22.91 ± 0.46	1.16 ± 0.03
MW 5S	08/12/2008	MW	6-8	34	25	-19.2	11.6 ± 1.0	1.37 ± 0.08	4.54 ± 0.37	3.20 ± 0.06	7.39 ± 0.22	20.77 ± 0.42	1.03 ± 0.03
MW-PJOW	05/13/2008	MW	24-26	?	11	-13.0	9.8 ± 0.9	1.38 ± 0.01	4.74 ± 0.09	3.43 ± 0.07	8.47 ± 0.25	18.67 ± 0.37	1.24 ± 0.04
MW-PJOW	08/12/2008	MW	24-26	?	11	-12.9	9.2 ± 0.9	1.36 ± 0.08	4.59 ± 0.37	3.48 ± 0.07	8.65 ± 0.26	20.08 ± 0.40	1.26 ± 0.04
MW T4	09/26/2008	MW	16-48	44	22	-12.5	8.3 ± 0.5	1.54 ± 0.02	15.67 ± 0.31	3.72 ± 0.07	8.36 ± 0.25	26.36 ± 0.53	1.15 ± 0.04
MWC Well 1	04/25/2008	PW	18-30	38	22	-18.4	9.6 ± 0.4	1.37 ± 0.01	NM	3.69 ± 0.07	8.22 ± 0.25	24.84 ± 0.50	1.14 ± 0.03
MWC Well 1	08/12/2008	PW	18-30	38	23	-19.1	11.0 ± 0.9	1.43 ± 0.08	5.67 ± 0.46	3.57 ± 0.07	8.12 ± 0.24	23.68 ± 0.47	1.16 ± 0.03
MWC Well 2	04/25/2008	PW	11-30	38	30	-19.0	9.7 ± 0.4	1.36 ± 0.01	NM	3.83 ± 0.08	8.22 ± 0.25	23.06 ± 0.46	1.23 ± 0.04
MWC Well 2	08/12/2008	PW	11-30	38	25	-19.0	11.5 ± 0.9	1.37 ± 0.04	5.34 ± 0.17	3.64 ± 0.07	8.30 ± 0.25	24.06 ± 0.48	1.14 ± 0.03
SVPSD Well1	04/25/2008	PW	23-34	37	21	-16.9	9.3 ± 0.4						
SVPSD Well1	06/18/2008	PW	23-34	37	21	-16.5	9.1 ± 2.4	1.41 ± 0.04	7.50 ± 0.15	3.64 ± 0.07	8.29 ± 0.25	22.49 ± 0.45	1.19 ± 0.04
SVPSD Well1	08/12/2008	PW	23-34	37	20	-16.4	8.3 ± 0.8	1.41 ± 0.08	7.99 ± 0.65	3.75 ± 0.07	8.96 ± 0.27	23.99 ± 0.48	1.24 ± 0.04
SVPSD Well2	04/25/2008	PW	10-23	24	17	-17.2	10.9 ± 0.5						
SVPSD Well2	06/18/2008	PW	10-23	24	17	-16.7	9.9 ± 0.9	1.44 ± 0.04	5.77 ± 0.12	3.65 ± 0.07	8.49 ± 0.25	22.59 ± 0.45	1.23 ± 0.04
SVPSD Well2	08/12/2008	PW	10-23	24	16	-18.1	10.4 ± 0.5	1.41 ± 0.08	5.56 ± 0.45	3.50 ± 0.07	8.49 ± 0.25	21.15 ± 0.42	1.19 ± 0.04
SVPSD Well3	04/25/2008	PW	22-35	46	17	-17.4	10.0 ± 0.4	1.35 ± 0.01	NM	3.65 ± 0.07	7.95 ± 0.24	21.47 ± 0.43	1.18 ± 0.04
SVPSD Well3	06/18/2008	PW	22-35	46	18	-16.9	10.3 ± 1.0	1.41 ± 0.04	5.43 ± 0.11	3.56 ± 0.07	8.29 ± 0.25	21.76 ± 0.44	1.20 ± 0.04
SVPSD Well5	04/25/2008	PW	22-39	46	17	-18.3	9.9 ± 0.4	1.36 ± 0.01	5.75 ± 0.11	3.63 ± 0.07	7.97 ± 0.24	22.78 ± 0.46	1.19 ± 0.04
SVPSD Well5	06/18/2008	PW	22-39	46	17	-17.9	14.3 ± 2.4	1.39 ± 0.04	5.88 ± 0.12	3.74 ± 0.07	8.21 ± 0.25	25.82 ± 0.52	1.16 ± 0.03
SVPSD Well5	08/12/2008	PW	22-39	46	16	-17.3	12.6 ± 1.0	1.40 ± 0.04	5.49 ± 0.18	3.49 ± 0.07	7.99 ± 0.24	22.04 ± 0.44	1.17 ± 0.04
Upwelling	04/25/2008	SP			33	-16.5							
Upwelling	05/14/2008	SP			33	-15.6	10.2 ± 0.9						
Upwelling	08/12/2008	SP			26	-18.0							
Confluence	04/25/2008	SW			7	-10.2	9.5 ± 0.4						
Confluence	05/14/2008	SW			4	-4.8	11.2 ± 0.7						

Table 1. (continued)

Sample Site	Collection Date	Sample Type	Screen Depth (m)	Approximate Bedrock Depth (m)	DIC (mg/L C)	$\delta^{13}\text{C}$ (%Vienna Pee Dee Belemnite)	^3H (pCi/L)	$^3\text{He}/^4\text{He}$ (10^{-6})	^4He (10^{-8} cm ³ STP/g)	Ar (10^{-4} cm ³ STP/g)	Kr (10^{-8} cm ³ STP/g)	Ne (10^{-8} cm ³ STP/g)	Xe (10^{-8} cm ³ STP/g)
Confluence	06/19/2008	SW			4	-3.4							
Shirley Canyon	04/25/2008	SW			5	-5.3	9.5 ± 0.4						
Shirley Canyon	05/14/2008	SW			4	-4.8	11.5 ± 0.6						
Shirley Canyon	06/18/2008	SW			3	-2.7							
South Fork at Bridge	04/25/2008	SW			6	-7.5	11.2 ± 0.5						
South Fork at Bridge	05/14/2008	SW			4	-6.0							
South Fork at Bridge	06/18/2008	SW			5	-2.6							
Squaw Creek Rd bridge	04/25/2008	SW			8	-10.2	11.0 ± 0.5						
Squaw Creek Rd bridge	05/14/2008	SW			4	-7.3							
Squaw Creek Rd bridge	06/19/2008	SW			5	-5.9							
Squaw Creek Rd bridge	08/12/2008	SW			11	-11.0							
Squaw Creek Rd bridge	09/25/2008	SW			13	-10.1	9.2 ± 0.5						
Trapezoid	04/25/2008	SW			7	-8.8	11.5 ± 0.5						

^aNM, Measurement failed.

connect the sample vessel (8 mm inner diameter copper tubing, 250 mm long) to the wellhead of operating production wells or monitoring wells pumped by a Grundfos® submersible pump. Horizontal wells drilled into bedrock were likewise sampled at the wellhead. Water flowed for several minutes to purge air from the sample tube. The copper tubing was tapped lightly to dislodge bubbles and a visual inspection for bubbles was made. Close attention was paid to maintaining sufficient pressure in the sampling apparatus, and backpressure was applied when necessary to prevent escape of dissolved gas. Steel clamps pinched the copper tubing flat in two locations to secure the water sample.

[13] All analyses were performed at Lawrence Livermore National Laboratory (LLNL). Dissolved inorganic carbon and its carbon isotope composition were determined using the automated DIC-dissolved organic carbon-isotope ratio mass spectrometry technique [St-Jean, 2003] consisting of an OI Analytical Model 1030 Carbon analyzer and a Micromass (now Isoprime Ltd) IsoPrime isotope ratio mass spectrometer. Carbon isotope compositions ($^{13}\text{C}/^{12}\text{C}$) are reported as delta values in per mil relative to the Vienna Pee Dee Belemnite reference, with an analytical uncertainty of $\pm 0.3\%$. Copper tube samples for noble gas analysis were mounted on a multiport gas handling manifold under vacuum. Reactive gases were removed with multiple reactive metal getters. Known quantities of isotopically enriched ^{22}Ne , ^{86}Kr , and ^{136}Xe were added to provide internal standards. The isotope dilution protocol used for measuring noble gas concentrations is insensitive to potential isotopic composition variation in dissolved gases (especially Ne) due to diffusive gas exchange. Noble gases were separated from one another using cryogenic adsorption. Helium was analyzed using a VG-5400 noble gas mass spectrometer. Other noble gas isotopic compositions were measured using a quadrupole mass spectrometer. The Ar abundance was determined by measuring the total noble gas sample pressure using a high-sensitivity capacitance manometer. The procedure was calibrated using water samples equilibrated with the atmosphere at a known temperature and air standards spiked with known quantities of the noble gases. Tritium concentrations were determined on 500 g subsamples by the ^3He in-growth method (approximately 25 day accumulation time). Analytical uncertainties are approximately 1% for $^3\text{He}/^4\text{He}$; 2% for He, Ne, and Ar; and 3% for Kr and Xe. Errors for derived parameters such as groundwater age and recharge temperature are propagated using analytical errors for the individual measured quantities (Table 2). A detailed description of the data reduction routine is reported in the report by *Ekwurzel* [2004].

4. Results and Discussion

[14] A total of 34 samples from 25 wells were analyzed for noble gas, and 50 samples from wells and surface water were analyzed for tritium (Table 1). Samples were collected between April and September of 2008. A total of 60 DIC samples were collected from 30 wells, 1 spring, and 5 stream sampling sites (Table 1).

4.1. Excess Air

[15] The concentration of dissolved noble gases in groundwater is virtually always greater than equilibrium solubility. The portion of gas in excess of equilibrium solubility is termed "excess air" because of its compositional similarity to

Table 2. Calculations Based on Noble Gas Concentrations and Isotope Ratios^a

Well Name	Date	Screen Depth (m)	ΔNe	$^4\text{He}_{\text{rad}}$ (10^{-9} cm ³ STP/g)	NGRT ^b (°C)	χ^2	Age ^c	% Pre-modern	Group
<i>Upper Valley MWs</i>									
MW-PJOW	5/13/08	24–26	17%	4.5 ± 1.6	5.5 ± 0.6	1.0	1 ± 1	<20%	1
MW-PJOW	8/12/08	24–26	24%	<2	5.3 ± 0.6	3.1	<1 ± 1	<20%	1
MW 5D	5/13/08	12–14	38%	11.8 ± 4.1	9.2 ± 0.9	0.3	15 ± 5	52%	2
MW 5D	8/12/08	12–14	37%	6.3 ± 3.8	9.5 ± 0.9	0.8	11 ± 9	36%	2
MW 5S	5/13/08	6–8	30%	<2	8.2 ± 0.7	11.0	<1 ± 1	<10%	1
MW 5S	8/12/08	6–8	25%	<2	11.4 ± 0.8	0.5	<1 ± 1	<10%	1
MW T4	9/26/08	16–48	37%	94.0 ± 4.8	8.8 ± 0.9	0.4	49 ± 3	98%	2
<i>Production Wells</i>									
SVPSD Well1	6/18/08	23–34	27%	22.3 ± 2.8	7.2 ± 0.7	0.4	23 ± 4	75%	2
SVPSD Well1	8/12/08	23–34	31%	23.2 ± 3.4	6.2 ± 0.7	1.2	23 ± 6	73%	2
SVPSD Well2	6/18/08	10–23	27%	4.8 ± 2.8	6.4 ± 0.7	0.0	11 ± 4	21%	2
SVPSD Well2	8/12/08	10–23	23%	5.8 ± 2.3	7.1 ± 0.7	1.3	11 ± 6	31%	2
SVPSD Well3	4/25/08	22–35	23%	NM	7.3 ± 0.7	3.0	<1 ± 1	<10%	1
SVPSD Well3	6/18/08	22–35	25%	3.2 ± 2.5	6.8 ± 0.7	0.1	4 ± 2	16%	1
SVPSD Well5	4/25/08	22–39	28%	3.8 ± 2.9	7.3 ± 0.7	1.3	<1 ± 1	<10%	1
SVPSD Well5	6/18/08	22–39	37%	<2	8.6 ± 0.8	0.5	1 ± 1	<10%	1
SVPSD Well5	8/12/08	22–39	27%	2.7 ± 2.6	7.7 ± 0.7	0.8	3 ± 1	<10%	1
MWC Well 1	4/25/08	18–30	27%	<2	8.6 ± 0.8	4.1	<1 ± 1	<10%	1
MWC Well 1	8/12/08	18–30	32%	<2	8.1 ± 0.8	0.2	6 ± 6	<10%	1
MWC Well 2	4/25/08	11–30	22%	<2	6.2 ± 0.7	7.5	<1 ± 1	<10%	1
MWC Well 2	8/12/08	11–30	31%	<2	8.7 ± 0.8	1.4	<1 ± 1	<10%	1
<i>Horizontal Wells</i>									
Horizontal Well 1	6/19/08		41%	<2	6.5 ± 0.8	0.6	15 ± 2	<10%	1
Horizontal Well 2	6/19/08		40%	<2	5.6 ± 0.8	3.5	17 ± 2	<10%	1
<i>Shallow Lower Valley MWs (2–5 m BGS)</i>									
MW 301	5/13/08	3–5	16%	<2	7.7 ± 0.7	0.7	17 ± 1	60%	1
MW 303	6/18/08	3–5	37%	6.2 ± 3.7	9.5 ± 0.8	1.0	10 ± 2	45%	2
MW 304	5/14/08	3–5	43%	885 ± 18	7.0 ± 0.9	2.0	³ He excess	NA	3
MW 306	5/14/08	2–3	43%	<2	5.6 ± 0.8	0.1	13 ± 1	35%	1
MW 321	5/14/08	3–5	32%	<2	10.3 ± 0.8	2.6	21 ± 2	67%	1
MW 328	5/14/08	3–5	44%	<2			4 ± 1	<10%	1
MW 331	5/13/08	2–3	24%	11.8 ± 2.3	8.2 ± 0.7	0.4	12 ± 1	58%	2
<i>Deep Lower Valley MWs (11–18 m BGS)</i>									
MW 302	5/13/08	12–14	24%	18.0 ± 2.3	9.7 ± 0.7	0.4	38 ± 1	97%	2
MW 305	5/14/08	11–13	39%	954 ± 20	7.7 ± 0.8	0.4	³ He excess	NA	3
MW 310	6/18/08	11–12	40%	<2	8.2 ± 0.9	0.5	19 ± 3	62%	1
MW 322	5/14/08	17–18	38%	7.3 ± 4.5	6.7 ± 0.8	0.3	19 ± 1	61%	2
MW 327	5/14/08	11–13	75%	803 ± 25	9.2 ± 2.5	0.1	³ He excess	NA	3
MW 329	5/14/08	13–15	49%	2832 ± 57	5.9 ± 0.9	0.8	³ He excess	NA	3

^aFor date, read 5/13/08 as 13 May 2008.

^bAn elevation of 1950 m used to determine pressure, except at the two horizontal wells, where an elevation of 2050 m is applied.

^cA crustal ³He/⁴He ratio of 6×10^{-7} is used in the age determination for samples with $[\text{He}_{\text{meas}} - (\text{He}_{\text{sol}} + \text{He}_{\text{xs air}})] > 2 \times 10^{-9}$ cm³ STP/g.

air [Aeschbach-Hertig et al., 2000; Holocher et al., 2002]. During transport through the unsaturated zone, infiltrating water may entrain or trap air bubbles that subsequently dissolve in groundwater. Air bubbles may also become trapped in groundwater during fluctuations in water table elevation. The concentration of excess air provides unique information about recharge processes, including the degree to which infiltrating water incorporates unsaturated zone gas. For dissolved noble gases, addition of excess air has the greatest relative impact on He and Ne concentrations because the equilibrium solubility components of these gases are relatively small.

[16] The total measured concentration of dissolved gas i , $C_{i,m}$, is the sum of multiple components [Lehmann et al., 1993]:

$$C_{i,m} = C_{i,\text{eq}} + C_{i,\text{exc}} + C_{i,\text{rad}} + C_{i,\text{ter}}, \quad (1)$$

where subscripts exc, rad, and ter refer to excess air, radiogenic, and terrigenic components, respectively. The equilibrium component for each gas is determined from Henry's law. Radiogenic and terrigenic contributions to Ne, Ar, Kr, and Xe are assumed to be negligible in the study area.

[17] A common way to represent the amount of excess air is as percent excess Ne, or ΔNe (excess Ne relative to equilibrium component; Table 2). Neon concentrations are used in determining excess air because Ne can be assumed to derive solely from the atmosphere and because Ne is measured with high precision. Excess air may be fractionated during the recharge process (whereby lighter gases are depleted relative to heavier gases) and Aeschbach-Hertig et al. [1999], and later Cey et al. [2008], examined optimization models to treat fractionated excess air and calculate noble gas recharge temperatures. For samples from Olympic

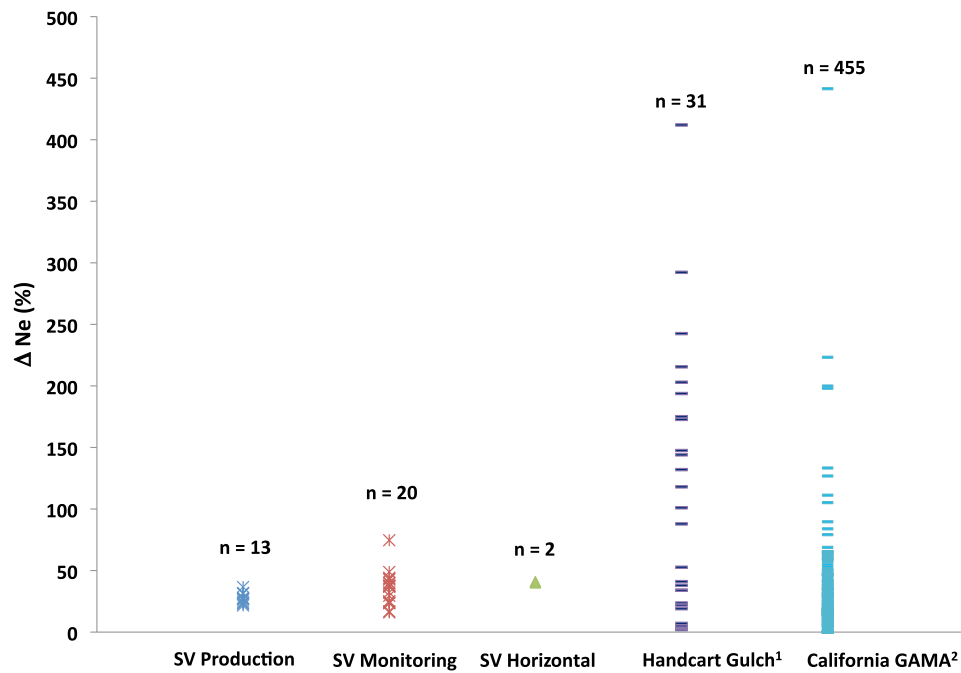


Figure 3. Observed ranges in excess air, expressed as ΔNe , for samples from Olympic Valley (categorized by well type), samples from the alpine watershed Handcart Gulch, and a large number of samples from around California sampled under the GAMA program. Handcart Gulch after *Manning and Caine* [2007]; California GAMA after *Cey et al.* [2008].

Valley, gas concentration ratios (e.g., He/Ne versus Ar/Ne) indicate that addition of excess air above equilibrium solubility is with gas of very nearly atmospheric composition, and therefore, the unfractionated excess air model was used to evaluate the noble gas concentration results. Use of one of the other excess air models would result in changes to calculated groundwater ages and recharge temperatures of not more than +2 years and +1°C, respectively.

[18] The total concentration of gas i as given by the unfractionated air model is [*Heaton and Vogel*, 1981]:

$$C_{i,m} = C_{i,eq} + A_d \cdot z_i, \quad (2)$$

where A_d is concentration of dry air dissolved, and z_i is the volume fraction of gas i in dry air (volume fraction composition of dry air from *Ozima and Podosek* [1983]). Additional equations and solubility coefficients used to calculate equilibrium solubility and excess air components are given in the report by *Ekwurzel* [2004].

[19] Recently, *Cey et al.* [2008] interpreted over 900 analyses of excess air in groundwater samples from the major groundwater basins in California. Results for over 400 samples not affected by artificial recharge (which can greatly increase excess air due to rapid changes in hydraulic head and water table height) are shown in Figure 3, compared with excess air results for 35 samples from Olympic Valley and 31 wells from Handcart Gulch, an alpine watershed in Colorado [*Manning and Caine*, 2007]. Excess air in alpine basins is relatively unexplored, but *Manning and Caine* [2007] find high excess air concentrations, as shown in Figure 3, associated with bedrock wells, and attribute the high values to recharge through fractures. Similarly, *Plummer et al.* [2001] found higher concentrations of excess air in

groundwater from wells in fractured rock compared to other wells in Shenandoah National Park. The highly dynamic fluctuations in water table elevation during recharge through fractured rock lead to elevated excess air concentrations [*Ingram et al.*, 2007]. Very low excess air concentrations are expected where an unsaturated zone is not present, as for continuous stream recharge where the water table intersects the surface [*Beyerle et al.*, 1999; *Kipfer et al.*, 2002]. If an unsaturated zone is present between the stream and the water table, somewhat higher excess air concentrations are expected.

[20] Excess air concentrations in Olympic Valley wells range from ΔNe of 16%–75%, with an average value of 34% and a median value of 31%, in line with the median value of 28% for the large California data set. These values argue against substantial recharge through fractures. The observed range for Olympic Valley samples suggests that groundwater recharges through an unsaturated zone but not under conditions of high hydraulic head, large fluctuations in water table height, or very high infiltration rates. Interestingly, this observation holds true for horizontal well samples, which are drilled into fractured bedrock, indicating that recharge through soils overlying the bedrock is likely even at higher elevation in this basin. The moderate average excess air concentrations observed in Olympic Valley wells also argue against stream recharge as the predominant recharge mechanism, since lower excess air values would be expected where there was a direct connection between the stream and the water table. Water table elevations in the western part of the aquifer are typically higher than the elevation of Squaw Creek during periods of creek flow (Figure 2), so recharge through an unsaturated zone under the creek is unlikely.

4.2. Recharge Temperature

[21] Solubilities of the noble gases in fresh water vary as a function of temperature and pressure according to Henry's law and are well-known from theoretical and empirical studies [Andrews, 1992]. The strong temperature dependence, especially for the heavy gases, makes it possible to determine the temperature at the water table at the time of recharge [Stute and Schlosser, 1999]. Cey *et al.* [2009] demonstrate that recharge temperatures determined from noble gas concentrations are very close to measured water table temperatures. Using inverse modeling, the recharge temperature and pressure are determined from noble gas concentrations. However, simultaneous estimation of both temperature and pressure results in a poorly resolved solution because these two parameters are strongly correlated. In general, pressure (or elevation) is more easily constrained by geographic conditions; once an elevation is estimated, temperature is well constrained. In wells producing water of mixed age, noble gas recharge temperatures (NGRTs) represent mean, integrated values for the mixtures.

[22] NGRTs are calculated from Xe concentrations, after subtraction of the excess air component, using a polynomial fit to the Xe-temperature solubility curve. Xenon is used to calculate NGRTs because Xe solubility has the strongest temperature dependence. Equilibrium concentrations of Ar and Kr are then calculated using a polynomial that gives a concentration based on the recharge temperature determined from Xe, multiplied by a pressure fraction, which is based on the assumed recharge elevation.

[23] The calculated Ar and Kr values are compared with the measured values and used to check the goodness of fit between measured and modeled values, which is reported as χ^2 (Table 2). This situation has 2 d.f. so a χ^2 value >6 corresponds to a probability (p) value of <0.05 . The p value is the probability that the deviation between modeled recharge temperatures and their true values is solely due to the 1 sigma measurement error. The data reduction procedure for calculating NGRTs and examining the goodness of fit is given in the report by *Ekwurzel* [2004].

[24] For this sample set, χ^2 values have a mean of 1.54, and for 27 out of 35 samples, χ^2 values are <2 (Table 2); thus, the model for recharge temperature calculation describes these data adequately. Four samples with somewhat higher χ^2 values are included, but their calculated NGRTs have higher associated uncertainties. NGRTs, calculated assuming a recharge elevation of 1950 m, range from $5.3^\circ\text{C} \pm 0.6^\circ\text{C}$ to $11.4^\circ\text{C} \pm 0.8^\circ\text{C}$, with an average value of 7.7°C . The assumed recharge elevation of 1950 m is close to the break in slope between the surrounding mountainous area and the valley floor, and about 50 m above wellhead elevations, which is a likely elevation of recharge for the basin groundwaters.

[25] Increasing the elevation in the recharge calculations will lead to lower calculated NGRTs. We can therefore calculate a minimum recharge temperature by assuming that the sample was recharged at the very top of the catchment (2750 m asl). Assuming the maximum recharge elevation for the catchment results in a minimum recharge temperature of $3.0^\circ\text{C} \pm 0.6^\circ\text{C}$. The highest recharge temperature, assuming maximum elevation, is $8.9^\circ\text{C} \pm 0.7^\circ\text{C}$, and the mean of all the samples is lowered to 5.4°C . It is unlikely that any significant proportion of the groundwater is recharged at this high elevation given the very small area available. A wider range of

recharge elevations that covers much of the surface area, from 2300 to 1950 m, gives a mean recharge temperature that ranges from 6.7°C to 7.7°C . Given that this difference is close to the analytical uncertainty for most measurements, we use 1950 m as an estimate for elevation when calculating recharge temperatures for most wells. We use a recharge elevation of 2050 m for the horizontal wells, since they are located approximately 100 m above the valley floor.

[26] Even the minimum possible recharge temperatures calculated for the Olympic Valley wells are significantly higher than the melting point of snow and ice. If we assume that most recharge originates as snowmelt, then the water temperature must have increased prior to reaching the water table. This observation would indicate that an unsaturated zone is present during recharge rather than a direct connection between groundwater and the land surface and that the infiltrating water has a residence time that allows for equilibration with the shallow ground temperature.

[27] In general, soil temperatures near the surface show a damped version of surface temperature variations, but deeper in the unsaturated zone, temperatures approach the mean annual air temperature (MAAT) [e.g., Cey *et al.*, 2009; Kipfer *et al.*, 2002]. Flint *et al.* [2008] measured soil temperatures at a site near Yosemite at a similar elevation (2130 m asl) to the Olympic Valley and found that soil temperatures were fairly stable and increased with depth from approximately 1°C at 10 cm to approximately 3°C at 72 cm under a melting snowpack. Once the snowpack disappeared, Flint *et al.* [2008] observed rapid increases in soil temperatures of approximately 8°C – 23°C , with the 10 cm depth showing diurnal temperature fluctuations.

[28] The recharge temperatures calculated for Olympic Valley wells fall close to or slightly above the long-term MAATs reported for the nearby Tahoe City NASA GISS Climate Station (http://data.giss.nasa.gov/gistemp/station_data/), which is located approximately 7 km to the southeast of Olympic Valley at an elevation of 1899 m (Figure 4). In most cases shallow ground temperatures are slightly greater (1°C – 2°C) than the MAAT, so it is common for NGRTs to be slightly greater than MAAT [Kipfer *et al.*, 2002]. The average maximum recharge temperature for groundwater samples (7.7°C) falls very close to the long-term average air temperature for May (7.8°C), when there is significant snowmelt (Figure 4c). The higher recharge temperatures fall closer to the long-term mean air temperature in June (11.4°C). This overlap between recharge temperatures and monthly mean air temperatures is consistent with recharge taking place over a 2–3 month period during the snowmelt season. However, a seasonal signal in the recharge temperatures would only be recorded if water table depths in recharge areas were shallow enough to be influenced by seasonal temperature. It is equally possible that the recharge temperatures primarily reflect MAAT, with some locally higher temperatures due to shallow water table depths. There is no discernable trend toward higher or lower recharge temperature values with apparent age (Figure 4b). However, the large range in NGRTs observed in samples with mean apparent ages ≤ 1 year (discussed in the next section) likely shows the effects of seasonal recharge, with lower temperatures reflecting recharge at the beginning of the melting period and higher temperatures reflecting late season recharge. In wells sampled more than once, only two wells show a significant seasonal change in

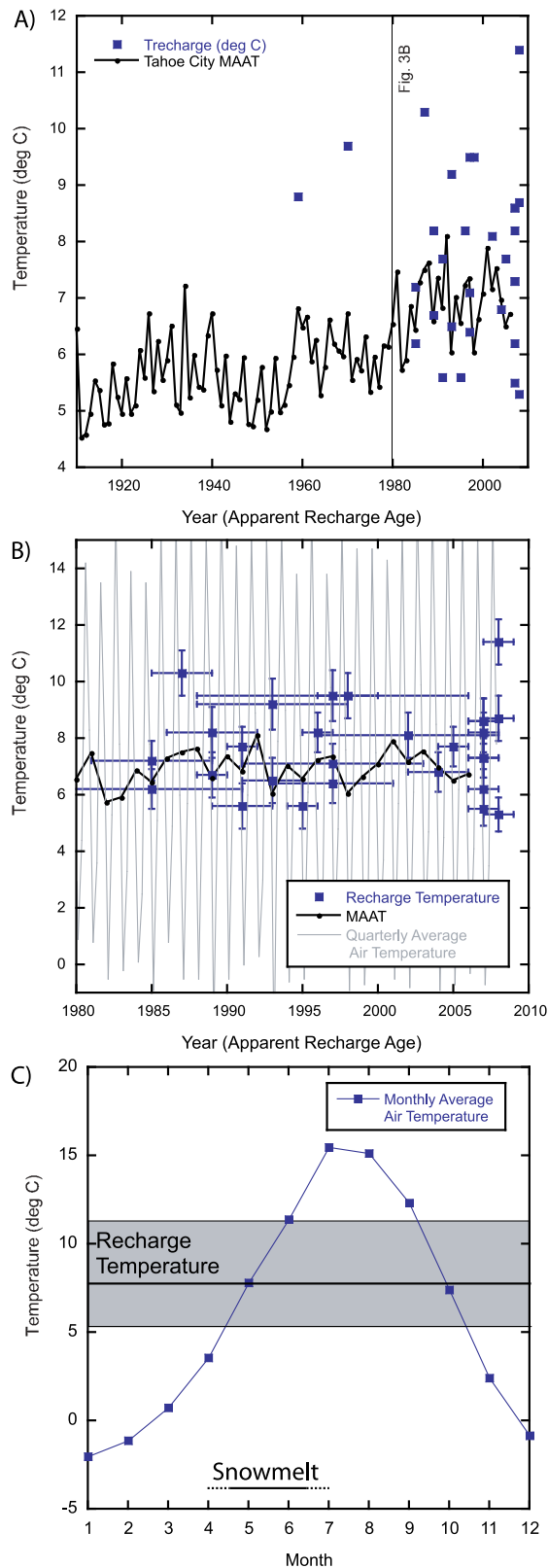


Figure 4. Noble gas recharge temperatures and apparent groundwater ages shown with (a) mean annual air temperature, (b) quarterly air temperature, and (c) average monthly air temperature at the NASA/Goddard Institute for Space Studies station at Tahoe City, CA. The range (shaded) and average (horizontal line) of recharge temperatures, along with the typical snowmelt season are shown on Figure 4c.

recharge temperature (Table 2). The shallow well directly adjacent to the creek (Well 5S), changed from $8.2^{\circ}\text{C} \pm 0.7^{\circ}\text{C}$ on 13 May to $11.4^{\circ}\text{C} \pm 0.8^{\circ}\text{C}$ on 12 August, and the MWC Well 2 production well changed from $6.2^{\circ}\text{C} \pm 0.7^{\circ}\text{C}$ on 25 April to $8.7^{\circ}\text{C} \pm 0.8^{\circ}\text{C}$ on 12 August.

4.3. Tritium Concentrations and Groundwater Ages

[29] All but two of the samples have tritium (^3H ; half-life 12.32 years) concentrations above the detection limit of approximately 1 pCi/L (Table 1), signaling the presence of groundwater recharged within the last 50 years. Most of the tritium concentrations overlap with the expected range for modern day precipitation, which limits the utility of tritium concentrations alone for determining ages. This range also overlaps with the tritium concentrations measured in Squaw Creek, which ranged from 9.2 to 11.5 pCi/L, with a mean for eight measurements of 10.6 pCi/L (Table 1). Well values at the high end of the observed range are the result of a contribution from global fallout from nuclear testing, while observed low values are the result of decay, and/or dilution with older, tritium-free water.

[30] Mean apparent groundwater ages, calculated from tritium and tritiogenic ^3He concentrations, are shown in Table 2. In order to determine tritiogenic ^3He , the measured ^3He and ^4He must be adjusted for contributions from the atmosphere (equilibrium solubility and excess air) and from subsurface sources [Cook and Solomon, 1997; Ekwurzel *et al.*, 1994; Schlosser *et al.*, 1989; Schlosser *et al.*, 1988]. A significant buildup of radiogenic ^4He due to decay of U and Th in crustal rocks takes place as the saturated zone residence time increases [Andrews *et al.*, 1985; Torgersen and Clarke, 1985]. Radiogenic ^4He is the portion of measured ^4He remaining after subtracting solubility and excess air components. In addition, magmatic fluids can contribute dissolved helium that has a much higher $^3\text{He}/^4\text{He}$ ratio than atmospheric or crustal sources. The observed tritium and dissolved helium compositions indicate that all of these components are present and will be considered in the analysis of Olympic Valley groundwater.

[31] Wells with long screens typically sample water of differing ages. In examining samples with a mixture of ages, it is useful to determine the fraction of the mixture that recharged before about 1950 (the time of large increases in global atmospheric ^3H due to nuclear weapons testing). The reported tritium-helium age is the mean apparent age of the portion of the sample that contains tritium above the detection limit. A rough estimate of the “percent pre-modern” is determined by comparing the initial ^3H in a sample (i.e., measured $^3\text{H} + ^3\text{He}_{\text{tritiogenic}}$) with the ^3H in precipitation at the time and location of recharge (Figure 5). The nearest International Atomic Energy Agency GNIP stations where ^3H in precipitation data were collected are Santa Maria, CA, and Menlo Park, CA (http://www-naweb.iaea.org/napc/ih/GNIP/IHS_GNIP.html), but these are incomplete records in very different physiographic settings than Olympic Valley. Figure 5 shows an exponential fit to mean annual averaged data for Western North America, along with measured values from two cities with long records. Several points for groundwater samples from Olympic Valley with apparent ages older than 10 years fall below the curve. The percentage of pre-modern water (Table 2) is calculated according to the difference between the expected value on the curve,

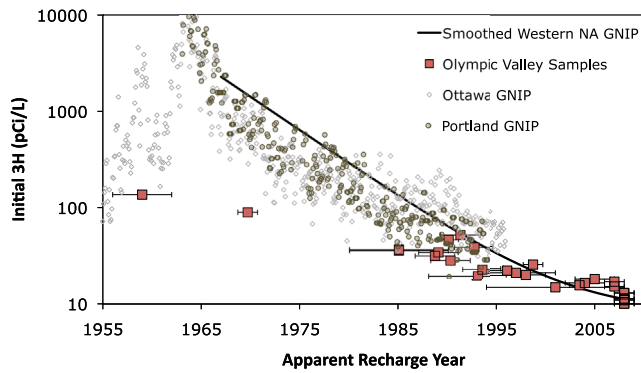


Figure 5. Tritium concentrations measured in precipitation at two locations where long International Atomic Energy Agency GNIP records exist, along with an exponential curve that approximates mean annual values from western North America. Results for Olympic Valley well samples are plotted according to the calculated apparent tritium helium age (recharge year) and the measured tritium + tritogenic ³He (initial ³H). Points that fall well below the curve contain a significant component of pre-modern water.

and the observed value below the curve. This approach assumes that the sample is a binary mixture between pre-modern water and modern water of a single age and that no mixing of groundwater with different ages occurs during transport (i.e., “piston flow”). For exponential mixing of post-bomb pulse peak water [Cook and Böhlke, 1999], the initial ³H curve is generally somewhat higher than the

smoothed curve, so larger pre-modern percentages would be calculated. In any case, samples with the oldest tritium-helium ages are mixed with a significant component of pre-modern water.

[32] Olympic Valley groundwater samples fall into three groupings: (1) samples with very young (≤ 1 year) to young (1–17 years) mean apparent ages and little pre-modern water; (2) samples with a component of relatively young (<50 years), tritiated water mixed with older, pre-modern water containing radiogenic ⁴He; and (3) samples with a smaller component of young water, mixed with older water and affected by gasses from a magmatic source.

[33] The three groups are distinguishable on a plot of ³He/⁴He versus Ne/He (Figure 6). On this plot, Ne and He concentrations are adjusted by subtracting the excess air component of each. For comparison, values for air saturated water at 8°C are also shown. Ne has only an atmospheric source, whereas He may be affected by the buildup of crustal He, accumulation of tritogenic ³He, or addition of magmatic He. Crustal He can contribute both ³He (via an α, n reaction on ⁶Li) and ⁴He (via α decay of natural U and Th); the effect is insignificant for ³He but can be very large for ⁴He, so an increase in crustal He results in a decrease in Ne/He. Magmatic He sources have high ³He/⁴He and typically high He concentrations. On Figure 6, samples with magmatic He stand out as having high ³He/⁴He and low Ne/He, whereas samples with a component of radiogenic ⁴He have Ne/He ratios lower than air saturated water (corresponding to wells with radiogenic ⁴He concentrations $> 2 \times 10^{-9}$ cm³ STP/g H₂O in Table 2). Addition of tritogenic ³He due to decay of ³H causes an increase in ³He/⁴He above values expected for atmospheric sources of He.

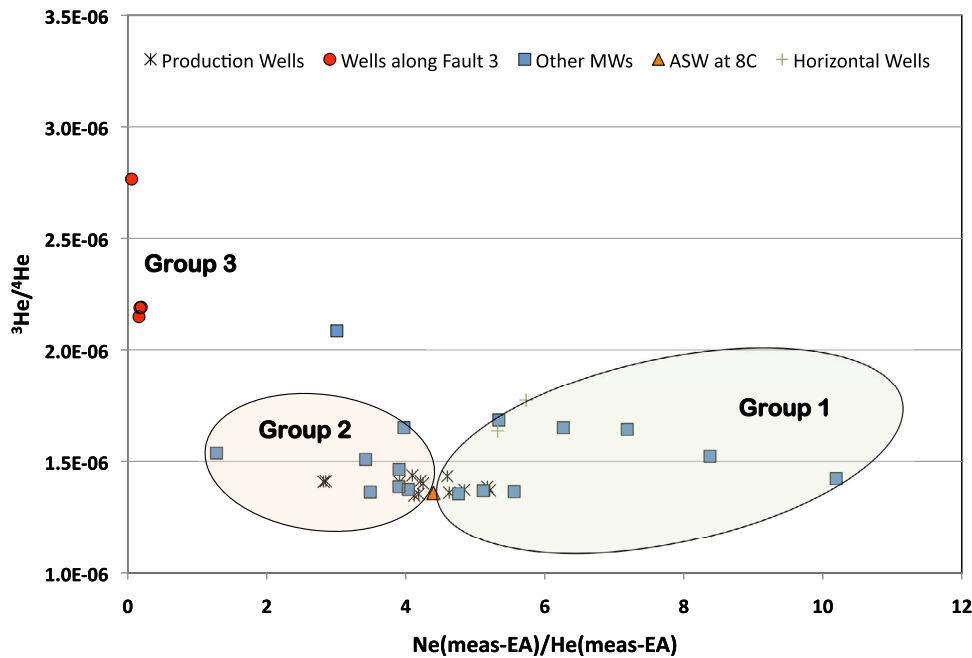


Figure 6. A plot of the ratio of Ne/He (measured concentration minus amount due to excess air) versus the measured ³He/⁴He ratio. Samples in Group 1 with very young ages are close to solubility values; significant amounts of tritogenic ³He bring some samples above the solubility ratio of 1.364×10^{-6} . Group 2 samples are affected by crustal He, which results in a decrease in Ne/He and by tritogenic ³He. Group 3 samples are affected by magmatic He. Orange triangle represents air saturated water (ASW) at 8°C.

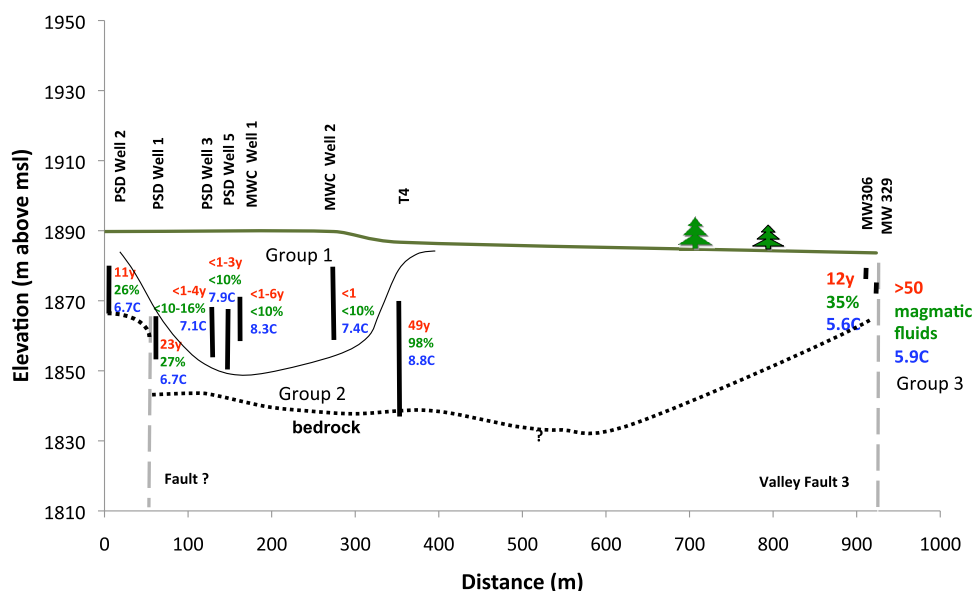


Figure 7. Schematic cross section through Olympic Valley running along Squaw Creek, showing the approximate locations of the major faults and the depth to bedrock as based on well logs [West-Yost and Associates, 2003] and seismic profiling [Gasch and Associates, 1973]. Solid vertical lines represent screened intervals for wells on or close to the cross section, with labels indicating the mean apparent tritium-helium groundwater age (year), percentage of pre-modern water, and noble gas recharge temperature ($^{\circ}\text{C}$). A curved line separates the wells in Group 1 with recent recharge from wells in Group 2 that are screened into bedrock and sample water with longer flow paths. Vertical exaggeration is 5.

4.3.1. Recent Recharge

[34] Group 1 (Figure 6) includes two monitoring wells and four production wells that yield water with a mean apparent age of less than 1 year (with a 2 sigma analytical uncertainty of about 1 year) and no detectable pre-modern water. Groundwater ages of 1 year or less in long screened, high-flow wells are unusual; fewer than 2% of drinking water wells ($n = 1317$) examined under California's Groundwater Ambient Monitoring and Assessment (GAMA) program (<http://www.swrcb.ca.gov/gama/>) have apparent tritium-helium ages ≤ 1 year. The wells producing very recent recharge are located in the western portion of the basin where coarse-grained glacial and fluvial sediments prevail, which exhibit high hydraulic conductivity (estimates are 0.07–0.51 cm/s in the area of the main production wells [Kleinfelder Inc., 2000]). In addition, the extraction of water from the production wells may lead to younger ages by drawing shallow groundwater deeper into the aquifer. However, results from well MW-PJOW indicate that Group 1, seasonally recharged waters already dominate the aquifer upgradient and outside the influence of the production wells. The production wells were sampled on different dates, and for three of the four production wells, mean apparent groundwater ages increased from <1 year for the April sampling to 3 years (SVPSD well 5), 4 years (SVPSD well 3), and 6 years (SV MWC well 2) when sampled during later summer months (Table 2). By contrast, ages in production wells producing older groundwater did not change between sampling dates. This finding suggests that during the dry season, the seasonal recharge (0–1 year) has moved through the aquifer and the wells draw in water that recharged in prior years, having taken longer flow paths to well capture zones.

[35] The vigorous flow system sampled by wells in Group 1 is recharged on a short time scale (≤ 1 year) and over a limited spatial extent (given the short time period for saturated zone transport). The production wells in this group have screened intervals from 11 to 20 m long at depths of 11–39 m but do not reach depths near the bedrock basement (Figure 7). Although the creek is not likely a major source of recharge to these wells (based on the excess air and carbon isotopes results in this study), the predominance of young groundwater in the alluvial aquifer suggests that it is this young component that likely provides much of the potential base flow to the stream. Under climate change scenarios with earlier snowmelt and runoff, this groundwater reservoir will be depleted earlier, providing less base flow and possible extreme low flows in the creek during summer and fall.

[36] Several of the lower valley monitoring wells and the two horizontal wells (Figure 8) exhibit somewhat older $^3\text{H}-^3\text{He}$ apparent ages. The apparent groundwater ages calculated for these wells give the groundwater age histogram its bimodal character (Figure 8). These wells are grouped with wells dominated by relatively recent recharge because they do not share dissolved gas characteristics associated with bedrock groundwater. The wells do not produce groundwater containing radiogenic ^4He , but they have higher concentrations of tritiogenic ^3He than samples with <1 year ages (Figure 6). In contrast to the production wells with <1 year mean ages, many of these wells are screened in lower permeability media, which includes near surface fine-grained sediments in the lower valley and near surface fractured rock (in the case of the two horizontal wells). This older component may contribute to stream base flow in the lower reaches of Squaw Creek, given its occurrence in

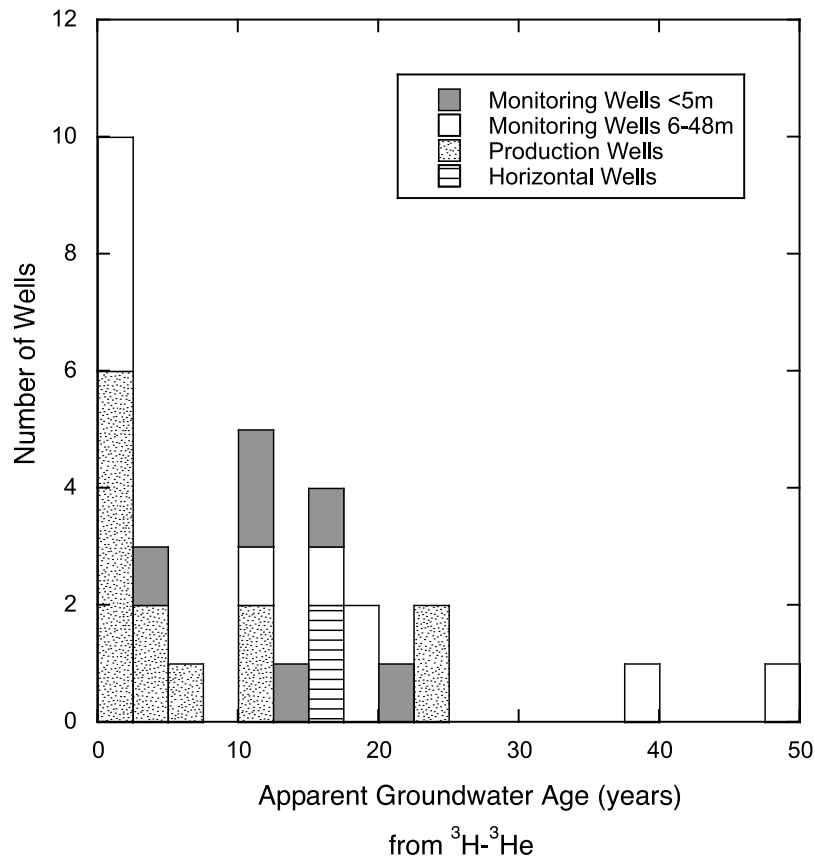


Figure 8. Histogram of apparent groundwater ages.

shallow monitoring wells adjacent to the creek. Significant flow and deep pools are observed in downstream reaches of the creek later in the water year than in upstream reaches.

4.3.2. Long Flow Paths

[37] The remaining production wells (SVPSD Well 1, SVPSD Well 2), well T4, MW 5D, and five of the valley monitoring wells fall into Group 2, drawing a component of significantly older groundwater as evidenced by a concentration of radiogenic ^4He greater than $2 \times 10^{-9} \text{ cm}^3 \text{ STP/g}$ and high pre-modern fractions (Table 2). These wells produce mixed aged water (21%–98% pre-modern), as they also all contain tritium and have mean apparent groundwater ages (for the portion of the water containing tritium) of less than 50 years. All of these wells tap the deeper flow system associated with bedrock that underlies the alluvial fill, either being partially screened in bedrock or being situated near a major fault (Figure 7).

[38] Granitic rocks have comparatively high U and Th concentrations, which can result in a relatively high radiogenic ^4He production rate [Andrews *et al.*, 1989]. In addition, glacial tills and weathered granites have been shown to exhibit high ^4He release rates into circulating groundwater [Beyerle *et al.*, 1999; Van der Hoven *et al.*, 2005]. Nonetheless, radiogenic ^4He concentrations in affected Olympic Valley wells are low in comparison to production wells affected by crustal He in bedrock wells elsewhere [Holocher *et al.*, 2001; Manning and Caine, 2007] and in deep supply wells elsewhere in California [Hudson *et al.*, 2002; Moran *et al.*, 2002; Moran *et al.*, 2005]. This component is not

observed in many of the production and monitoring wells screened exclusively in alluvium, which may be a reflection of the shorter residence time for water in the alluvium. Alternatively, the crustal fluid may not be produced within the alluvium but rather may be related to diffusion of ^4He from low permeability bedrock at the base of the alluvial aquifer. Although present at depth, and clearly affecting wells that directly tap bedrock groundwater or are affected by focused flow along faults (Figure 7), this component is minor in comparison to the very young groundwater component and is not likely to play a significant role in stream interaction or base flow to the stream.

4.3.3. Deep Upwelling Fluids

[39] Samples that fall into Group 3 have smaller components of recent recharge, along with an older component containing crustal He, and a component of dissolved gases from a magmatic source. Recently, Kulongoski *et al.* [2005] and Saar *et al.* [2005] have presented methods for quantifying mixing proportions for groundwaters that have crustal, magmatic, and tritogenic components, as revealed by examination of the isotopic composition of dissolved helium. Compared to samples from those studies, Olympic Valley groundwater samples have much smaller magmatic and crustal components. The ^3He in Olympic Valley samples is predominantly from atmospheric equilibrium, dissolved excess air, and from the decay of ^3H . However, because the magmatic $^3\text{He}/^4\text{He}$ ratio is drastically different from the $^3\text{He}/^4\text{He}$ ratio for other helium sources, the presence of a small component of magmatic helium in four of

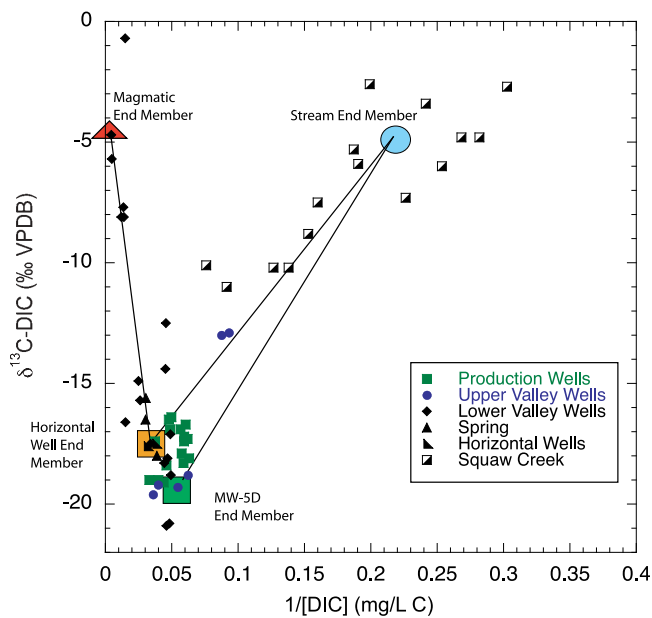


Figure 9. Stable carbon isotope compositions ($\delta^{13}\text{C-DIC}$) and inverse concentration of DIC for wells, a spring, and creek water in the Olympic Valley study area. Mixing lines are plotted between two potential end-members for groundwater recharge through soils, a magmatic water end-member, and a stream end-member.

the samples makes determination of a $^3\text{H-}^3\text{He}$ age highly unconstrained (age labeled as “ ^3He excess” in Table 2). These samples lie along a transect that lines up with an active fault, Valley Fault 3 (Figure 1 and Figure 7), and are clearly affected by gases that emanate from a deep, magmatic source. One of these samples, MW 329, contains less than 1 pCi/L ^3H and thus is a mixture of only magmatic and crustal components. A simple linear mixing calculation for this sample (using $^3\text{He}/^4\text{He}_{\text{magmatic}} = 1.22 \times 10^{-5}$ [Graham, 2002] and $^3\text{He}/^4\text{He}_{\text{crustal}} = 6 \times 10^{-7}$ (Lawrence Livermore National Laboratory, unpublished data, 2010)) results in estimates for the magmatic component of only 7%. The other three wells along Valley Fault 3 contain tritium, and tritiogenic ^3He , and are complex mixtures of relatively recent recharge, older water with a significant radiogenic ^4He component, and magmatic gases that reach shallow groundwater via the active fault. One additional monitoring well sample from the lower valley (MW302) is likewise affected by magmatic He.

4.4. Determination of Recharge Sources Based on DIC

[40] Water samples from the horizontal and production wells contain 16–32 mg/L C as DIC with $\delta^{13}\text{C-DIC}$ values that range from -19.1‰ to -16.4‰ . The lower valley monitoring wells have $\delta^{13}\text{C-DIC}$ values that range from -20.9‰ to 4.2‰ , with concentrations from 20 to 222 mg/L C. Stream waters are low in DIC concentration (3–13 mg/L C) and have $\delta^{13}\text{C}$ values that range from -11.0‰ to -2.6‰ .

[41] The carbon isotope values for the production well groundwater samples ($\delta^{13}\text{C-DIC}$ of -19.1‰ to -16.4‰) are consistent with the incorporation of soil CO_2 during recharge [e.g., Blumhagen and Clark, 2008; Cerling *et al.*,

1991], which reflects a mix of respiration CO_2 and atmospheric CO_2 sources. The incorporation of soil CO_2 in the production well groundwater suggests that recharge occurs in subalpine areas with developed soils such as the vegetated slopes surrounding the valley, as opposed to the bare rock exposures that are prevalent over the highest elevation areas surrounding the valley.

[42] When plotted against $1/[\text{DIC}]$, the $\delta^{13}\text{C-DIC}$ values indicate mixing between three dominant sources (Figure 9): (1) groundwater recharged through the soil zone, (2) recharge from Squaw Creek, and (3) upwelling of deep groundwater containing carbon derived from a magmatic source. The compositions of these end-members are discussed below.

4.4.1. Recharge Through the Soil Zone

[43] The concentration and isotopic composition of soil CO_2 vary in relation to the respiration rate [Cerling *et al.*, 1991]. Consequently, recharge through soils with a range of soil respiration rates might be expected to result in a range of DIC concentrations and isotopic compositions. For this reason we selected two potential end-members for groundwaters recharged through the soil zone. In both cases, wells with moderate groundwater ages (11–17 years) were selected to avoid wells that might receive significant recharge from the creek. The average values of $[\text{DIC}]$ (29 mg/L C) and $\delta^{13}\text{C-DIC}$ (-17.5‰) for the Horizontal Wells were selected as the first groundwater end-member. The Horizontal wells are influenced by recharge through soils over higher elevations than the valley monitoring wells. Monitoring well MW-5D was selected as the second groundwater end-member, and has an average $[\text{DIC}]$ of 17.2 mg/L C and an average $\delta^{13}\text{C-DIC}$ value of -19.1‰ . These end-members will be used to constrain recharge sources discussed below.

4.4.2. Magmatic Carbon

[44] The monitoring wells have a very broad range of DIC concentrations and isotopic compositions. Many of the monitoring wells have DIC compositions that are similar to those observed in the production wells. However, wells along Valley Fault #3 have much higher concentrations of DIC (50–222 mg/L C) and appear to be influenced by a carbon source with $\delta^{13}\text{C}$ values close to -5‰ . Similar $\delta^{13}\text{C}$ values and high $[\text{DIC}]$ have been linked to upwelling of magmatic fluids and seismic activity along faults around Mammoth Mountain in California [Sorey *et al.*, 1998]. A contribution from a magmatic source is also consistent with the $^3\text{He}/^4\text{He}$ ratios discussed previously. Well MW-330 was chosen as an end-member to represent groundwater that has interacted with a magmatic source of fluids. Well MW-330 was selected because it has the highest $[\text{DIC}]$ of 222 mg/L C and has no detectable tritium (<1 pCi/L).

4.4.3. Recharge From Squaw Creek

[45] The concentrations and isotopic compositions of DIC observed in the stream water samples are generally consistent with DIC derived from equilibration with atmospheric CO_2 , which has a $\delta^{13}\text{C}$ value of approximately -8‰ . Some of the stream $\delta^{13}\text{C-DIC}$ values are slightly higher than the $\delta^{13}\text{C}$ value of air, suggesting that perhaps some of the stream DIC is derived from mineral weathering. An end-member for Squaw Creek was defined by the average value of samples collected at the lower ends of the southern and northern tributaries to Squaw Creek, above the confluence (sites 1 and 2 in Figure 1), which have an average $[\text{DIC}]$ of 4.6 mg/L C, and an average $\delta^{13}\text{C-DIC}$ value of -4.8‰ .

[46] The downstream sampling sites tend to have lower $\delta^{13}\text{C}$ -DIC values and higher concentrations than the upper parts of the creek, which likely indicates an influx of groundwater along the stream channel (also indicated by water level and stream gauge observations, as noted above). A more detailed study quantifying the groundwater influx to the stream is ongoing and will not be discussed further here.

[47] On the basis of the end-members defined above, Squaw Creek does not appear to be a dominant source of recharge for most of the wells sampled in this study. The lone exception is the monitoring well MW-PJOW, which was the uppermost valley well sampled. On the basis of the samples collected in May and August, the [DIC] and $\delta^{13}\text{C}$ -DIC in MW-PJOW appears to be derived from between 50% and 70% creek water. The low recharge temperatures calculated for MW-PJOW may indicate that the creek recharge occurs during the cold, high-flow conditions during snowmelt runoff. As an alternative, well MW-PJOW may receive recharge from the prominent rock escarpment to the west. Recharge through bare rock fractures would have essentially identical [DIC] and $\delta^{13}\text{C}$ -DIC values to creek water.

[48] In general, the production wells have much higher [DIC] and much lower $\delta^{13}\text{C}$ -DIC values than Squaw Creek. This contrast between the isotopic compositions and concentrations of DIC in the production wells and DIC in stream water suggests that these waters have different sources and indicates that Squaw Creek is not a dominant source of recharge to the production wells. However, based on the end-members defined above, samples from production wells SVPSS Well # 1, 2, and 3 fall within the range of [DIC] and $\delta^{13}\text{C}$ -DIC values that potentially indicate between 10% and 30% of produced water is from Squaw Creek. Quantifying such small contributions of the stream water is highly uncertain due to a strong dependence on the defined compositions of end-members. Given the older apparent ages of SVPSS Wells 1 and 2, it is unlikely that they receive significant recharge from the creek. As discussed above, the slightly higher $\delta^{13}\text{C}$ -DIC values may also indicate the presence of water that was recharged over bare rock. On the basis of the mixing analysis of DIC, the majority of water from the production wells recharged through a soil zone where respiration was active. It is unlikely that an unsaturated zone between the creek and the water table could impart the carbon isotope compositions of the production wells, since CO_2 respiration would not take place. The carbon isotope results demonstrating a lack of significant recharge from Squaw Creek are in agreement with the interpretation of excess air and recharge temperature results and with stream and well hydrograph observations.

4.5. Implications of Predicted Changes in Climate

[49] Climate models predict that our study site in the Sierra Nevada Mountains is likely to see a decrease in the percentage of precipitation that falls as snow; earlier onset of snowpack melting; an increase in the number of rain on snow events; and changes in humidity, air temperature, and soil moisture [Dettinger and Cayan, 1995; Howat and Tulaczyk, 2005; Maurer and Duffy, 2005; Melack et al., 1997]. It is still uncertain whether these changes will be accompanied by a decrease in total precipitation [Hayhoe et al., 2004]. Data from our study illuminate two impor-

tant aspects of the hydrological system in Olympic Valley both of which will have a direct impact on how this system responds to climate change: (1) that recharge to the alluvial aquifer occurs primarily on the lower slopes of the catchment and (2) that deep groundwater in the western part of the aquifer is very young. In this section we review the evidence for these conclusions and consider their potential impact on the response of the hydrologic system to climate change effects.

4.5.1. Recharge on Lower Slopes

[50] Groundwater sampled for this study is primarily recharged on the lower elevation slopes that surround the alluvial valley where soils are thicker and vegetation is common, rather than in upper elevation areas of exposed bedrock. Evidence for lower elevation recharge comes from NGRTs, excess air concentrations, carbon isotope compositions, and groundwater ages in the deeper alluvial aquifer. NGRTs are similar to MAATs and much higher than would be expected for direct recharge of snowmelt through fractured rock. Excess air concentrations are relatively low compared with other mountainous areas where recharge in fractured rock has been shown to lead to high excess air entrapment. Carbon isotope compositions and concentrations of DIC in the groundwater also indicate recharge through a vegetated soil zone where soil respiration is active. These carbon isotope compositions are not consistent with recharge through exposed rock or with recharge from Squaw Creek. Finally, groundwater ages in the western portion of the basin are very young; younger than ages found in horizontal wells drilled into bedrock at higher elevation. The short residence time for much of the groundwater precludes a significant contribution of recharge to these wells from distant high-elevation locations.

[51] Under the current seasonal snowmelt scenario most of the water is transported during a short snowmelt period in the spring, and much of the potential infiltration is diverted to overland flow as recharge areas become saturated. With increased temperatures, the snow line is likely to move to higher elevations in the catchment. If we assume that total precipitation remains the same, then this would mean more rain for the lower parts of the catchment where most recharge occurs. Therefore, an increase in the snow line elevation could alter the infiltration mechanisms for a significant portion of the recharge areas that feed the valley aquifer. Infiltration would change from a seasonal peak during snowmelt to a more episodic pattern spread over a longer time period during winter rainstorms.

[52] The impact of an increasing snow line elevation on recharge to the aquifer will depend to some extent on the precipitation rate during these winter storms. Winter storms with higher precipitation rates than the current snowpack melting rates are likely to cause an increase in runoff at the expense of infiltration. Whereas, precipitation rates that are lower than the current snowpack melting rate (approximately 20–50 mm/d) would spread the infiltration events out over a longer time period, providing the opportunity for more of the precipitation to infiltrate rather than run off as overland flow. From Figure 2, it appears that under current conditions, the melt rate of the snowpack generally outpaces the accumulation of precipitation as snow water equivalent during the winter. If winter precipitation were to fall as rain rather than snow, but at a similar amount and rate, it could lead to more infiltration. However, other factors such as an

earlier growing season, which might increase evapotranspiration could counteract an increase in recharge. Furthermore, rain on snow events would magnify the precipitation rate and would likely exceed the current snowmelt rates over a short period of time, leading to increased overland flow and decreased infiltration.

4.5.2. Young Groundwater

[53] Groundwater ages from this study show that near the production wells, the top 10–40 m of the aquifer is dominated by seasonal snowmelt. Once the snowmelt season is over and water levels drop, these wells capture older water that infiltrated in previous years. With a decrease in infiltration, this shift would likely happen earlier resulting in an earlier onset of decreased creek flow and groundwater availability in that portion of the basin. An extremely dry winter would impact that year's water budget with little buffering by groundwater storage in the aquifer from previous years. For the same reasons, earlier onset of snowpack melting would lead to an earlier drop in water levels with little buffering from recharge of previous years. In this scenario, the detrimental effect of little to no flow in the late summer on fish and other fauna would be almost immediate. Even the moderately older groundwater ages (average MW age of 17 years) observed in the eastern portion of the basin offer only a decadal time period during which the downstream portions of Squaw Creek may be buffered against predicted changes in runoff by groundwater inflow.

[54] A decrease in total precipitation would undoubtedly lead to less groundwater recharge and less overland flow. However, because of the seasonal nature of flow in the aquifer, such changes would very quickly affect the availability of groundwater and the groundwater contribution to streamflow. This scenario is analogous to the changes observed between the very wet 2006–2007 El Niño year and the following 3 years with much lower winter precipitation (Figure 2). In 2006, the snowpack persisted for approximately 1 month longer than it did in the following 3 years. Likewise, the water level in SVPSD Well 2 remained higher than the Squaw Creek bed elevation for approximately 1 month longer in 2006 than in the following 3 years.

5. Summary and Conclusions

[55] Dissolved gas tracers provide a powerful toolset to evaluate the vulnerability of high-altitude aquifers to climate change impacts because they address key questions about recharge location and subsurface residence time. The extent to which individual catchments are vulnerable to climate change will depend largely on the specifics of geology, topography, and climate. The dissolved gas toolset used for this study can be applied under a wide range of potential settings but is especially useful in high-elevation areas because of the steep gradients in precipitation and temperature and because active recharge and vigorous flow results in relatively young apparent groundwater ages, dateable by the tritium-helium method.

[56] NGRTs constrain the location and timing of recharge and correspond to air temperatures at the time of snowmelt. Recharge occurs mainly through soil zones where the water incorporates CO₂ from respiration and recharging water is thermally equilibrated within the unsaturated zone. Recharge through fractures and recharge from the creek is of lesser importance in this catchment. Predicted climate change

effects such as an increase in snow line elevation and an increase in rain-on-snow events will cause the greatest impacts to the accumulation of snowpack and timing of recharge at the lower elevations of Olympic Valley. The alluvial aquifer is therefore highly susceptible to changes in climate because, as we have shown, the lower elevation areas are important for groundwater recharge. Long-term monitoring of recharge temperatures may provide a means to gauge watershed response to climate changes such as an earlier onset of snowmelt and an increase in mean air temperature.

[57] Young groundwater dominates the most permeable part of the alluvial aquifer in Olympic Valley and likely accounts for much of the potential base flow to Squaw Creek. This groundwater has an apparent age of less than one year and is therefore vulnerable to climate change over short time scales. Mixed age components also need to be considered in studies of alpine and subalpine groundwater residence time. In this study the bedrock aquifer underlying the valley fill contributes an older component that has accumulated radiogenic ⁴He. In addition, helium and carbon isotopes show the influence of magmatic fluids in shallow groundwater, especially in the area of an active fault.

[58] The major findings with respect to groundwater residence times in Olympic Valley, i.e., that the alluvial aquifer experiences rapid flushing of seasonal recharge and that significantly older fluids are found at the bedrock interface that underlies the alluvium are similar to the major findings of *Beyerle et al.* [1999] in the Lisenthal aquifer of Switzerland and *Plummer et al.* [2001] in the Blue Ridge Mountains. The changes in recharge, groundwater availability, and streamflow due to predicted climate change that are outlined here are likely for other small mountain catchments. Similar studies are needed in much larger mountain watersheds to determine whether an increase in scale may decrease the dominance of young waters.

[59] **Acknowledgments.** The authors wish to gratefully acknowledge assistance with field sampling and sample analysis by Brad Esser, Sarah Roberts, Darren Hillemonds, Mike Sharp, and Carl Gustafson. Well access and logistical support were provided by Squaw Valley Public Services District, Friends of Squaw Creek, The Resort at Squaw Creek, Squaw Valley Mutual Water Company, and Derrick Williams (HydroMetrics LLC). Funding for this work was provided by LLNL Laboratory Directed Research and Development, Climate Initiative. Jean Moran received support from the Joan Sieber research award at California State University, East Bay. We are grateful to three WRR reviewers whose comments led to improvements in the text. This work was performed under the auspices of the U.S. Department of Energy by Lawrence Livermore National Laboratory under contract DE-AC52-07NA27344.

References

- Aeschbach-Hertig, W., F. Peeters, U. Beyerle, and R. Kipfer (1999), Interpretation of dissolved atmospheric noble gases in natural waters, *Water Resour. Res.*, 35(9), 2779–2792, doi:10.1029/1999WR900130.
- Aeschbach-Hertig, W., F. Peeters, U. Beyerle, and R. Kipfer (2000), Palaeotemperature reconstruction from noble gases in ground water taking into account equilibration with entrapped air, *Nature*, 405(6790), 1040–1044, doi:10.1038/35016542.
- Andrews, J. N. (1992), Mechanisms for noble gas dissolution by groundwaters, in *Isotopes of Noble Gases as Tracers in Environmental Studies*, pp. 87–110, Int. At. Energy Agency, Vienna.
- Andrews, J. N., G. B. Wilson, M. J. Youngman, J. E. Goldbrunner, W. G. Darling, P. J. Hooker, L. Eichinger, W. Rauert, and W. Stichler (1985), A Radiochemical, hydrochemical and dissolved gas study of groundwaters in the Molasse basin of Upper Austria, *Earth Planet. Sci. Lett.*, 73, 317–332, doi:10.1016/0012-821X(85)90080-9.

- Andrews, J. N., N. Hussain, and M. J. Youngman (1989), Atmospheric and radiogenic gases in ground waters from the Stripa granite, *Geochim. Cosmochim. Acta*, 53, 1831–1841, doi:10.1016/0016-7037(89)90304-9.
- Beyerle, U., W. Aeschbach-Hertig, M. Hofer, D. M. Imboden, H. Baur, and R. Kipfer (1999), Infiltration of river water to a shallow aquifer investigated with $^3\text{H}/^3\text{He}$, noble gases and CFCs, *J. Hydrol. Amsterdam*, 220(3–4), 169–185, doi:10.1016/S0022-1694(99)00069-4.
- Blumhagen, E. D., and J. F. Clark (2008), Carbon sources and signals through time in an Alpine groundwater Basin, Sagehen California, *Appl. Geochem.*, 23(8), 2284–2291, doi:10.1016/j.apgeochem.2008.03.010.
- Cerling, T. E., D. K. Solomon, J. Quade, and J. R. Bowman (1991), On the isotopic composition of carbon in soil carbon dioxide, *Geochim. Cosmochim. Acta*, 55(11), 3403–3405, doi:10.1016/0016-7037(91)90498-T.
- Cey, B. D., G. B. Hudson, J. E. Moran, and B. R. Scanlon (2008), Impact of artificial recharge on dissolved noble gases in groundwater in California, *Environ. Sci. Technol.*, 42(4), 1017–1023, doi:10.1021/es0706044.
- Cey, B. D., G. B. Hudson, J. E. Moran, and B. R. Scanlon (2009), Evaluation of noble gas recharge temperatures in a shallow unconfined aquifer, *Ground Water*, 47(5), 646–659, doi:10.1111/j.1745-6584.2009.00562.x.
- Cook, P. G., and J. K. Böhlke (1999), Determining timescales for groundwater flow and solute transport, in *Environmental Tracers in Subsurface Hydrology*, edited by P. G. Cook and A. L. Herczeg, pp. 1–30, Kluwer Acad., Boston, Mass.
- Cook, P. G., and D. K. Solomon (1997), Recent advances in dating young groundwater—Chlorofluorocarbons, $^3\text{H}/^3\text{He}$ and ^{85}Kr , *J. Hydrol.*, 191(1–4), 245–265, doi:10.1016/S0022-1694(96)03051-X.
- Dettinger, M. D., and D. R. Cayan (1995), Large-scale atmospheric forcing of recent trends toward early snowmelt runoff in California, *J. Clim.*, 8(3), 606–623, doi:10.1175/1520-0442(1995)008<0606:LSAFOR>2.0.CO;2.
- Di Luzio, M., G. L. Johnson, C. Daly, J. K. Eischeid, and J. G. Arnold (2008), Constructing Retrospective gridded daily precipitation and temperature datasets for the conterminous United States, *J. Appl. Meteorol. Climatol.*, 47(2), 475–497, doi:10.1175/2007JAMC1356.1.
- Earman, S., A. R. Campbell, F. M. Phillips, and B. D. Newman (2006), Isotopic exchange between snow and atmospheric water vapor: Estimation of the snowmelt component of groundwater recharge in the southwestern United States, *J. Geophys. Res.*, 111, D09302, doi:10.1029/2005JD006470.
- Ekwurzel, B. (2004), LLNL Isotope Laboratories Data Manual, *Rep. UCRL-TM-203316*, 133 pp., Lawrence Livermore Natl. Lab, Livermore, Calif.
- Ekwurzel, B., P. Schlosser, W. M. Smethie, L. N. Plummer, E. Busenberg, R. L. Michel, R. Weppernig, and M. Stute (1994), Dating of shallow groundwater—comparison of the transient tracers $^3\text{H}/^3\text{He}$, chlorofluorocarbons, and ^{85}Kr , *Water Resour. Res.*, 30(6), 1693–1708, doi:10.1029/94WR00156.
- Flint, A. L., L. E. Flint, and M. D. Dettinger (2008), Modeling soil moisture processes and recharge under a melting snowpack, *Vadose Zone J.*, 7(1), 350, doi:10.2136/vzj2006.0135.
- Gasch and Associates (1973), Squaw Valley geophysical investigation, *Rep. Proj. GA318*, 8 pp., Squaw Valley Public Serv. Dist., Squaw Valley, Calif.
- Graham, D. W. (2002), Noble gas isotope geochemistry of mid-ocean ridge and ocean island basalts: Characterization of mantle source reservoirs, *Rev. Mineral. Geochem.*, 47(1), 247, doi:10.2138/rmg.2002.47.8.
- Hayhoe, K., D. Cayan, C. Field, P. Frumhoff, E. Maurer, N. Miller, S. Moser, S. Schneider, K. Cahill, and E. Cleland (2004), Emissions pathways, climate change, and impacts on California, *Proc. Natl. Acad. Sci. U. S. A.*, 101(34), 12,422, doi:10.1073/pnas.0404500101.
- Heaton, T. H. E., and J. C. Vogel (1981), Excess air in groundwater, *J. Hydrol.*, 50(1–3), 201–206, doi:10.1016/0022-1694(81)90070-6.
- Holocher, J., V. Matta, W. Aeschbach-Hertig, U. Beyerle, M. Hofer, R. Peeters, and R. Kipfer (2001), Noble gas and major element constraints on the water dynamics in an alpine floodplain, *Ground Water*, 39(6), 841–852, doi:10.1111/j.1745-6584.2001.tb02472.x.
- Holocher, J., F. Peeters, W. Aeschbach-Hertig, M. Hofer, M. Brennwald, W. Kinzelbach, and R. Kipfer (2002), Experimental investigations on the formation of excess air in quasi-saturated porous media, *Geochim. Cosmochim. Acta*, 66(23), 4103–4117, doi:10.1016/S0016-7037(02)00992-4.
- Howat, I. M., and S. Tulaczyk (2005), Climate sensitivity of spring snowpack in the Sierra Nevada, *J. Geophys. Res.*, 110, F04021, doi:10.1029/2005JF000356.
- Hudson, G. B., J. E. Moran, and G. F. Eaton (2002), Interpretation of Tritium- ^3He groundwater ages and associated dissolved noble gas results from public water supply wells in the Los Angeles Physiographic Basin, *Rep. UCRL-AR-151447*, 26 pp., Lawrence Livermore Natl. Lab., Livermore, Calif.
- Hydrometrics-LLC (2007), Olympic valley groundwater management plan, report, 104 pp., Squaw Valley Public Serv. Dist., Placer County, Calif.
- Ingram, R., K. Hiscock, and P. Dennis (2007), Noble gas excess air applied to distinguish groundwater recharge conditions, *Environ. Sci. Technol.*, 41(6), 1949–1955, doi:10.1021/es061115r.
- Kipfer, R., W. Aeschbach-Hertig, F. Peeters, and M. Stute (2002), Noble gases in lakes and ground waters, *Rev. Mineral. Geochem.*, 47(1), 615, doi:10.2138/rmg.2002.47.14.
- Kleinfelder and Associates (1987), Basin water quality investigation, report, Resort at Squaw Creek, Squaw Valley, Calif.
- Kleinfelder Inc. (2000), Technical memorandum, Squaw Valley groundwater background data, Squaw Valley, California, report, Resort at Squaw Creek, Squaw Valley, Calif.
- Kulongoski, J. T., D. R. Hilton, and J. A. Izbicki (2005), Source and movement of the eastern Morongo groundwater Basin: The influence of regional tectonics on crustal and mantle helium fluxes, *Geochim. Cosmochim. Acta*, 69(15), 3857–3872, doi:10.1016/j.gca.2005.03.001.
- Lehmann, B. E., S. N. Davis, and J. T. Fabryka-Martin (1993), Atmospheric and subsurface sources of stable and radioactive nuclides used for groundwater dating, *Water Resour. Res.*, 29(7), 2027–2040, doi:10.1029/93WR00543.
- Liu, F., M. W. Williams, and N. Caine (2004), Source waters and flow paths in an alpine catchment, Colorado Front Range, United States, *Water Resour. Res.*, 40, W09401, doi:10.1029/2004WR003076.
- Manning, A. H., and J. S. Caine (2007), Groundwater noble gas, age, and temperature signatures in an Alpine watershed: Valuable tools in conceptual model development, *Water Resour. Res.*, 43, W04404, doi:10.1029/2006WR005349.
- Manning, A. H., and D. K. Solomon (2003), Using noble gases to investigate mountain-front recharge, *J. Hydrol.*, 275(3–4), 194–207, doi:10.1016/S0022-1694(03)00043-X.
- Manning, A. H., and D. K. Solomon (2005), An integrated environmental tracer approach to characterizing groundwater circulation in a mountain block, *Water Resour. Res.*, 41, W12412, doi:10.1029/2005WR004178.
- Maurer, E. P., and P. B. Duffy (2005), Uncertainty in projections of streamflow changes due to climate change in California, *Geophys. Res. Lett.*, 32, L03704, doi:10.1029/2004GL021462.
- Melack, J. M., J. Dozier, C. R. Goldman, D. Greenland, A. M. Milner, and R. J. Naiman (1997), Effects of climate change on inland waters of the Pacific Coastal Mountains and Western Great Basin of North America, *Hydrol. Processes*, 11(8), 971–992, doi:10.1002/(SICI)1099-1085(19970630)11:8<971::AID-HYP514>3.0.CO;2-Y.
- Moran, J. E., G. B. Hudson, G. F. Eaton, and R. Leif (2002), A contamination vulnerability assessment for the Livermore-Amador and Niles Cone groundwater basins: Report to the California State Water Resources Control Board, *Rep. UCRL-AR-148831*, 25 pp., Lawrence Livermore Natl. Lab, Livermore, Calif.
- Moran, J. E., G. B. Hudson, G. F. Eaton, and R. Leif (2005), A contamination vulnerability assessment for the Sacramento Valley and northern Volcanic Provinces: Report to the California State Water Resources Control Board, *Rep. UCRL-TR-209191*, 71 pp., Lawrence Livermore Natl. Lab, Livermore, Calif.
- Nevada Bureau of Mines and Geology (2000), Preliminary Map of Pleistocene to Holocene Faults in the Lake Tahoe Basin, California and Nevada, scale 1:100,000, *U.S. Geol. Surv. Open File Rep.*, 2000-4.
- Ozima, M., and F. Podosek (1983), *Noble Gas Geochemistry*, 367 pp., Cambridge Univ. Press, New York.
- Plummer, L. N., E. Busenberg, J. K. Bohlke, D. L. Nelms, R. L. Michel, and P. Schlosser (2001), Groundwater residence times in Shenandoah National Park, Blue Ridge Mountains, Virginia, USA: A multi-tracer approach, *Chem. Geol.*, 179(1–4), 93–111, doi:10.1016/S0009-2541(01)00317-5.
- Rademacher, L. K., J. F. Clark, G. B. Hudson, D. C. Erman, and N. A. Erman (2001), Chemical evolution of shallow groundwater as recorded by springs, Sagehen basin; Nevada County, California, *Chem. Geol.*, 179(1–4), 37–51, doi:10.1016/S0009-2541(01)00314-X.
- Rademacher, L. K., J. F. Clark, D. W. Clow, and G. B. Hudson (2005), Old groundwater influence on stream hydrochemistry and catchment response times in a small Sierra Nevada catchment: Sagehen Creek, California, *Water Resour. Res.*, 41, W02004, doi:10.1029/2003WR002805.
- Saar, M. O., M. C. Castro, C. M. Hall, M. Manga, and T. P. Rose (2005), Quantifying magmatic, crustal, and atmospheric helium contributions to volcanic aquifers using all stable noble gases: Implications for magma-

- tism and groundwater flow, *Geochem. Geophys. Geosyst.*, 6, Q03008, doi:10.1029/2004GC000828.
- Schlosser, P., M. Stute, H. Doerr, C. Sonntag, and K. O. Muennich (1988), Tritium/³He dating of shallow groundwater, *Earth Planet. Sci. Lett.*, 89(3–4), 353–362, doi:10.1016/0012-821X(88)90122-7.
- Schlosser, P., M. Stute, C. Sonntag, and K. O. Muennich (1989), Tritogenic ³He in shallow groundwater, *Earth Planet. Sci. Lett.*, 94(3–4), 245–256, doi:10.1016/0012-821X(89)90144-1.
- Sorey, M. L., W. C. Evans, B. M. Kennedy, C. D. Farrar, L. J. Hainsworth, and B. Hausback (1998), Carbon dioxide and helium emissions from a reservoir of magmatic gas beneath Mammoth Mountain, California, *J. Geophys. Res.*, 103(B7), 15,303–15,323, doi:10.1029/98JB01389.
- St-Jean, G. (2003), Automated quantitative and isotopic (C-13) analysis of dissolved inorganic carbon and dissolved organic carbon in continuous-flow using a total organic carbon analyser, *Rapid Commun. Mass Spectrom.*, 17(5), 419–428, doi:10.1002/rcm.926.
- Stute, M., and P. Schlosser (1999), Atmospheric noble gases, in *Environmental Tracers in Subsurface Hydrology*, edited by P. G. Cook and A. L. Herczeg, pp. 349–377, Kluwer Acad., Boston, Mass.
- Torgersen, T., and W. B. Clarke (1985), Helium accumulation in groundwater: I. An evaluation of sources and the continental flux of crustal ⁴He in the Great Artesian Basin, Australia, *Geochim. Cosmochim. Acta*, 49(5), 1211–1218, doi:10.1016/0016-7037(85)90011-0.
- Van der Hoven, S. J., R. E. Wright, D. A. Carstens, and K. C. Hackley (2005), Radiogenic helium 4 as a conservative tracer in buried-valley aquifers, *Water Resour. Res.*, 41, W11414, doi:10.1029/2004WR003857.
- West-Yost and Associates (2003), Squaw Valley groundwater development and utilization feasibility study update, report, Squaw Valley Public Serv. Dist., Squaw Valley, Calif.
-
- J. E. Moran, Department of Earth and Environmental Science, California State University East Bay, 25800 Carlos Bee Blvd., Hayward, CA 94542, USA. (jean.moran@csueastbay.edu)
- M. J. Singleton, Chemical Sciences Division, Physical and Life Sciences Directorate, Lawrence Livermore National Laboratory, 7000 East Ave., L-231, Livermore, CA 94550, USA. (singleton20@llnl.gov)

Effect of geomorphic channel restoration on streamflow and groundwater in a snowmelt-dominated watershed

Christina Tague,¹ Scott Valentine,² and Matthew Kotchen¹

Received 7 August 2007; revised 3 July 2008; accepted 29 July 2008; published 22 October 2008.

[1] Reengineering of stream channels is a common approach used to restore hydrologic function in degraded landscapes, but there has been little published research analyzing its effectiveness. A key challenge for impact assessment is disentangling the effects of restoration from climate variability. Trout Creek, near Lake Tahoe, California, was reengineered to reestablish hydrologic connectivity between the stream and its former floodplain. Gauges located above and below the site, along with groundwater well measurements, were used to analyze prerestoration and postrestoration hydrology. Results show that restoration has a seasonal impact with statistically significant increases in streamflow during the summer recession period and decreased groundwater table depths across a wide range of streamflow conditions. Paired gauges and statistical models that are robust to serial autocorrelation demonstrate a feasible approach for assessing hydrologic restoration in regions where climate patterns lead to substantial within-year and between-years variation in streamflow.

Citation: Tague, C., S. Valentine, and M. Kotchen (2008), Effect of geomorphic channel restoration on streamflow and groundwater in a snowmelt-dominated watershed, *Water Resour. Res.*, 44, W10415, doi:10.1029/2007WR006418.

1. Introduction

[2] The alteration of riparian and stream ecosystems through urban and agricultural land use practices has prompted widespread and costly restoration projects [Palmer *et al.*, 2005; Bernhardt *et al.*, 2005; Booth, 2005]. Most of these projects involve engineered alteration of streamflow and groundwater to support the restoration of aquatic and riparian ecosystem structure and function. It is therefore critical that assessment of the effectiveness of restoration efforts include consideration of changes to both streamflow regimes and groundwater dynamics [Booth, 2005; Ward *et al.*, 2002].

[3] Undesirable human-induced changes to the hydrology of riparian areas and streams can arise through a variety of mechanisms and can occur across a range of scales. Associated restoration strategies reflect the type and scale of impacts associated with different land use practices. Common examples of relatively local impacts include overgrazing and construction in riparian zones, channelization of streams as part of agricultural and urban conveyance systems, and down cutting of stream channels leading to dewatering of riparian areas [Mant and Janes, 2005; National Research Council (NRC), 1992]. In these cases, stream restoration activities often seek to directly modify stream channel and riparian zone surface and subsurface drainage properties.

[4] There is a variety of stream modification techniques designed to enhance hydrologic function. These techniques

range from approaches that focus largely on altering the channel itself to more geomorphically based approaches that include consideration of surrounding floodplain or riparian area [NRC [1992]; De Laney [1995]; Poff *et al.* [1997]; Hillman [1998]; Swanson *Hydrology and Geomorphology (SHG)* [2004]; D. S. Lindquist and J. Wilcox, New concepts for meadow restoration in the northern Sierra Nevada, Feather River coordinated resource management, 2000, accessed 27 February 2006 at <http://www.feather-river-crm.org/publications/abstracts/ieca.htm> (hereinafter referred to as Lindquist and Wilcox, 2000); U.S. Forest Service, Lake Tahoe Basin Management Unit, Draft environmental assessment Big Meadow Creek: Cookhouse Meadow stream restoration project, 2004]. Recently, biotechnical restoration techniques are replacing older restoration methods involving “hard” engineering solutions such as riprap, concrete, sheet piling, dams, and levies [Goodwin *et al.*, 1997; NRC, 1992]. Biotechnical approaches, which incorporate natural materials such as rock, root wads, and native vegetation, can often times perform the same functions as hard engineering techniques with arguably improved hydrologic, ecologic, and aesthetic results [SHG, 2004]. Preliminary studies in stream and meadow restoration projects have indicated that reengineered channels utilizing biotechnical techniques can successfully raise groundwater levels and reconnect channels with their floodplains [SHG, 2004]; see also Lindquist and Wilcox (2000). Nevertheless, inadequate monitoring and evaluation continues to be one of the major criticisms of river restoration projects, and further research is needed to assess the response of streamflow and groundwater regimes to channel modifications [Ralph and Poole, 2002; Reeve *et al.*, 2006; Palmer *et al.*, 2005]. Studies are needed across a broad range of geographic settings, and explicit consideration of interactions between hydroclimatic processes and restoration

¹Bren School of Environmental Science and Management, University of California, Santa Barbara, California, USA.

²Department of Geography, Lake Tahoe Community College, Lake Tahoe, California, USA.

effects are needed to support generalization of monitoring results. This study provides an assessment of the restoration impacts on both streamflow and groundwater dynamics for Trout Creek in the Sierra Nevada. Restoration of Trout Creek used a biotechnical approach and was designed to improve connectivity between channel and floodplain through infilling of an incised channel coupled with a significant reworking of the surrounding floodplain. Hydroecologic goals of the Trout Creek project included reducing flood flow and nutrient loading by increasing overbank flow, decreasing channel erosion and restoring riparian vegetation by improving summer groundwater availability [Wigart, 2004].

[5] Estimating changes to hydrologic regimes following restoration is often confounded by multiple and interacting variables that shape observable hydrologic behavior, such as streamflow and groundwater table elevations. Disentangling the impacts of restoration from natural variation due to climate can be particularly challenging. Trout Creek is situated in a region where spring snowmelt and warm dry summers are the primary hydroclimatologic controls on hydrologic processes. Flow regimes (especially those in snowmelt-dominated watersheds) exhibit large interannual and intra-annual variations due to these seasonal changes [Wohl *et al.*, 2005; Poff *et al.*, 1997; Smakhtin, 2001]; see also Lindquist and Wilcox (2000). Groundwater measurements are rarely available for more than a few years. Stream gauge measurements may be available for longer periods, on the order of decades at some sites. However, even with longer-term data sets, climate shifts may make subtle changes due to restoration difficult to detect or lead to a misidentification of the effects. In the western United States, for example, recent studies have shown trends toward lower summer base flows for many streams in the Oregon Cascades and Sierras, due to climate-driven reductions in snow accumulation and melt [Knowles and Cayan, 2002; Bales *et al.*, 2006]. Given the potential interaction between climate-driven changes and the impacts of restoration efforts, assessment strategies are needed that can disentangle these effects.

[6] Paired catchment studies have been widely used to separate the effects of climate variability and land use change, particularly in studies that analyze the affects of logging on streamflow (reviewed by Bosch and Hewlett [1982] and Best *et al.* [2003]). The application of a paired catchment approach requires that the two watersheds be both proximal and similar and that the control catchment not change over the course of the analysis. Similarity is generally defined in terms of climate, geology, vegetation, topography, and land use. Critiques of the paired catchment approach often center on whether the degree of similarity is sufficient to distinguish changes of interest from changes due to climate [Best *et al.*, 2003].

[7] In the case of channel modification and near stream restoration, a refinement of the paired catchment approach is to use two gauges on the same stream—one upstream and one downstream of the restoration site. Given that a substantial proportion of the contributing area will be shared by both gauges, this approach should maximize similarity. In this study, we take advantage of this modified version of the paired catchment approach or paired gauge approach, using longitudinal stream gauges to assess the impact of channel

reconstruction for Trout Creek. We compare the gain in discharge, measured between gauges upstream and downstream of the restoration site, for prerestoration and post-restoration periods. We use streamflow gain defined at a daily time step in order to examine seasonal variation in the impact of stream restoration. We also compare relationships between groundwater well observations and streamflow for prerestoration and postrestoration periods.

[8] The Trout Creek Stream Restoration and Wildlife Enhancement Project in South Lake Tahoe was completed in 2001. Over 3000 m of channel was excavated and most of the original channel infilled followed by significant reworking of floodplain to construct a new channel. The new stream alignment exhibited enhanced sinuosity, a raised channel elevation, reduced slope, and an overall increase in channel length. Parts of the old channel were infilled to reduce the likelihood of stream recapture, while other segments (expected to fill in time by natural processes) were left to enhance diversity and function as small oxbow lakes. Bioengineering techniques were used during construction to maximize the biologic recovery of the stream corridor, improve stream habitat, and to allow for increased hydrologic connectivity between the stream channel and the floodplain.

[9] Changes to the channel and floodplain were designed to raise local groundwater tables, lower channel gradients, increase riparian zone storage, and increase transit time in the channel. Given the seasonality of flow regimes, the impact of these changes on streamflow and groundwater would be expected to differ during winter, snowmelt recession, and summer and early fall base flow periods. Specifically, we made the following hypotheses.

[10] 1. Following occasional large autumn rainfall events and in the early to peak snowmelt recharge period, restoration will lead to a decrease in the gain in streamflow measured between gauges above and below the restoration site. During these recharge periods, channel modifications should reduce channel flood flows, particularly if opportunities for overbank flow are increased. Restoration should also increase the storage in the riparian area and further support reduced streamflow downstream of the restored site (relative to flow at the upstream gauge).

[11] 2. During the recession period following peak snowmelt recharge, streamflow downstream of the restored site will increase, relative to upstream site, supported by the slower draining riparian groundwater system. Groundwater levels will also be elevated relative to prerestoration conditions.

[12] 3. Later in the summer and early fall, we hypothesize that higher riparian groundwater levels will persist but their influence on streamflow will diminish. High groundwater in late summer may also increase riparian evapotranspiration and potentially decrease summer base flow. In fact, increased evapotranspiration was one of the implicit goals of the project, designed to reduce the dewatering of riparian vegetation due to channel incision.

[13] We used available streamflow and groundwater measurements to test whether the hypothesized effects took place. More generally, our analysis tests whether changes to the hydrograph described above take place and thus support our conceptual model of potential restoration effects on

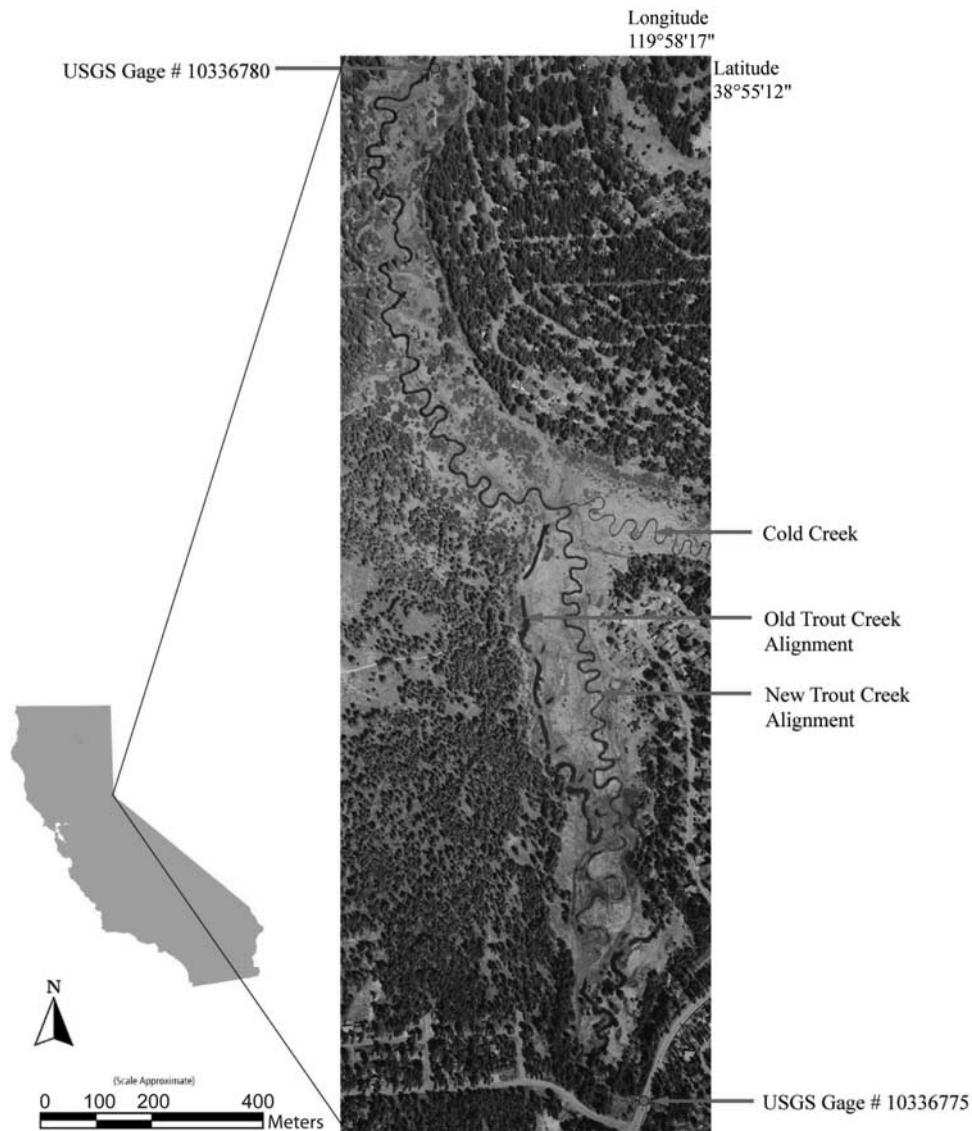


Figure 1. Location map of Trout Creek.

streamflow and groundwater dynamics in this snowmelt-dominated system.

2. Methods

2.1. Site Description

[14] Trout Creek watershed is located in the southern portion of the Lake Tahoe Basin in El Dorado County, California. Trout Creek has a drainage area of 106 km², and the main channel length is approximately 19.5 km long. The watershed ranges from a high of 3317 m above mean sea level at Freel Peak to a low of approximately 1897 m, where it enters Lake Tahoe. In the Lake Tahoe area, most precipitation occurs in the winter as snowfall, and summer drought is typical. Mean annual precipitation ranges from 50 cm to 100 cm, and approximately 94% of the annual precipitation occurs between late November and mid-May.

[15] The Trout Creek study site lies just north of Pioneer Trail and south of Martin Avenue in the City of South Lake Tahoe. The two gauges used in this study are located at

the upper and downstream ends of a riparian meadow (Figure 1). Snowmelt at the meadow generally occurs from mid-May to mid-June, and a vast majority of the snow in the upper watershed has usually melted by late July. Although summer thunderstorms do occur, they are infrequent and seldom contribute to significant streamflow pulses. The meadow substrate comprises well-sorted alluvial and glacial deposits, and the study site comprises vegetation typical of high-altitude montane environments in the Sierra Nevada. Plant community structure varies throughout the meadow system and includes a variety of riparian vegetation bounded by dryer upland vegetation communities. Meadow vegetation comprises sedges, rushes, grasses, annual and perennial forbs, and a variety of willow species. Dominant meadow species include *Carex nebrascensis*, *Juncus balticus*, *Muhlenbergia richardsonis*, *Poa pratensis*, *Arnica chamissonis*, *Aster occidentalis*, *Achillea millefolium*, *Lupinus polyphyllus*, and *Salix lutea*. Upland species adjacent to the meadow are primarily coniferous

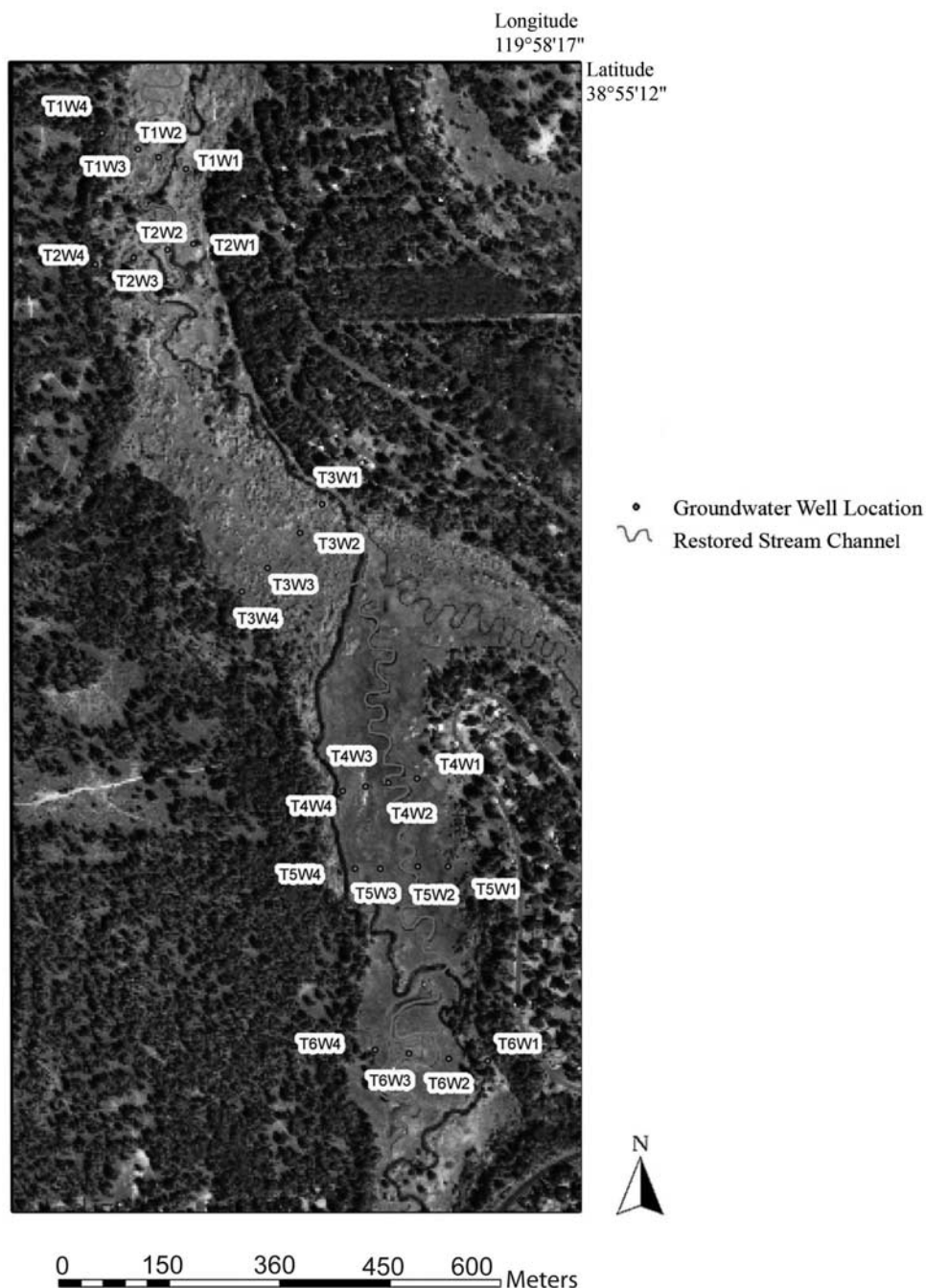


Figure 2. Map showing groundwater well locations and preretoration and postrestoration stream alignments.

trees, including *Abies concolor*, *Pinus contorta*, *Pinus jeffrey*, and *Pinus ponderosa*.

[16] The U.S. Geological Survey (USGS) has operated a streamflow gauging station on Trout Creek continuously since 1 October 1960 (station number 10336780). The gauge is located just downstream of the project site at the Martin Avenue crossing. A second USGS gauge (station number 10336775) is located upstream of the project site, and approximately 1 km upstream of first gauge, at the Pioneer Trail crossing. This gauge has been providing continuous streamflow data since 1 October 1990. There is a small tributary, Cold Creek, which intersects Trout

Creek between the two gauges. No significant land cover changes occurred in the Cold Creek watershed throughout the study period and flow contributions from Cold Creek are relatively small. Groundwater data was collected by the City of South Lake Tahoe from 24 wells situated within the meadow. The monitoring wells were installed in October of 1999 and were arranged in 6 transects oriented perpendicular to the stream channel. Transect and well locations can be seen in Figure 2. Piezometers were constructed out of perforated PVC pipe 1.8 m in length, and monitored by lowering a hydrolight until the water table was detected.

Groundwater readings were taken on a bimonthly basis from November 1999 to June 2003.

2.2. Data Analysis

[17] In order to assess the effect of restoration on streamflow, we use a paired gauge comparison. We examine the relative difference in daily streamflow between the upper and lower gauges at a daily time step for the preperiod (1990–2000) and postperiod (2001–2004). As discussed above, both the effect of restoration and the relative difference between the upper and lower gauges are expected to vary seasonally.

[18] Using the daily streamflow data for both gauges over the entire period from 1990 to 2004, we define proportional streamflow gain as

$$\Delta q_{rel} = (q_{upper} - q_{lower})/q_{upper}, \quad (1)$$

where q_{upper} and q_{lower} are measured discharge at the upper and lower gauges averaged for each day. It follows that Δq_{rel} represents the daily increase in discharge between the two gauges as a proportion of streamflow at the upper gauge. Differencing the data in this way takes out any effects that are common to both gauges, such as interannual variation in the timing and magnitude of snowmelt. Our aim is to determine whether restoration has any effect on proportional streamflow gain and whether the effect differs by time of year.

[19] In order to identify the potential restoration effect by month, we estimate a regression model with the following specification:

$$\Delta q_{rel} = \alpha + \beta' \mathbf{m}_t + \delta' \mathbf{R}_t \mathbf{m}_t + \theta wydev_t + \varepsilon_t, \quad (2)$$

where \mathbf{m}_t is a vector of 12 binary dummy variables, one for each month January through December, R_t is a binary dummy variable indicating whether the observation is during the postrestoration period, $wydev_t$ is the annual deviation from the annual mean streamflow at the upper gauge, and ε_t is a random error term. Annual streamflow is computed by water year, which is defined as October through September. Deviation is computed as the difference between annual streamflow in each water year and the long-term mean annual streamflow over the period of record. Deviation from mean annual streamflow is included to control for year-to-year variation in atmospheric conditions (temperature and precipitation) that may drive differences between streamflow at the upper and lower gauges. Since water inputs are dominated by spring snowmelt, annual (water year) streamflow should provide a good surrogate for the magnitude of primary water input throughout the melt season and into the summer.

[20] The vector of coefficients β will provide estimates of the monthly differences between gauges before restoration. As required whenever including a set of mutually exclusive categorical variables in a regression model (i.e., 12 months in a year), one category must be omitted to avoid perfect multicollinearity. We omit the month of May, meaning that the estimated coefficients in β are interpreted as the average difference in proportional streamflow gain between the corresponding month and May for the period 1990 through 2000. The coefficients δ , which are of primary concern, are

interpreted as the differences in the monthly averages for the years 2001 through 2005. In other words, the estimates of δ are interpreted as the monthly effects of restoration on the proportional streamflow gain.

[21] A potential concern with the model specified by equation (2) is that Δq_{rel} is highly serially correlated, which implies that the error term ε_t is serially correlated. Not accounting for serial correlation poses a problem for making statistical inference. Serial correlation is a ubiquitous problem in streamflow analysis [Worrall *et al.*, 2003]. Temporal aggregation (e.g., using monthly or annual streamflow rather than daily values) is a commonly used approach to avoid problems associated with serial correlation. Aggregation, however, is problematic when data are limited and sample variation is high, as is the case here. Aggregation also smoothes the data, thereby reducing the information content at finer time scales that may be important when the effect (of restoration) varies at relatively fine time scales. Parametric autoregressive models are another widely used approach, such as specifying an AR1 process for the error term [e.g., Worrall *et al.*, 2003], but these require the researcher to assume a specific functional form of the serial correlation.

[22] Here we use a nonparametric approach that allows for robust statistical inference. Specifically, we report Newey and West [1987] standard errors that enable statistical inference that is robust to both heteroskasticity and any form serial correlation up to a specified lag. Reporting these standard errors is a commonly used approach in the economics literature to account for serial correlation [Wooldridge, 2002]. The relative advantage of the Newey-West approach is that it does not require any assumptions about the structure of the serial correlation, but rather, assumes the number of time periods over which serial correlation will be accounted for. For comparison purposes, we use lags of 15 and 30 days, which should cover the window over which serial correlation is a concern for our streamflow data. To demonstrate the effect of this approach, we compare the Newey-West standard errors and consequent statistical significance with those corresponding to standard ordinary least squares (OLS) estimation. Note that OLS is used to estimate the only set of coefficients that we report, as the Newey-West standard errors are derived using postestimation methods and do not affect the coefficient estimates.

[23] In addition to streamflow data, we compare groundwater table elevations in the prerestoration and postrestoration periods. Figure 2 illustrates the piezometer locations. As with streamflow, groundwater elevation is expected to vary with atmospheric conditions; however, changes in the relationship between groundwater elevation and streamflow are likely to reflect changes directly due to restoration. In order to examine this relationship at our study site, we estimate the following regression model:

$$gwlevel_{it} = \lambda q_{upper} + \phi R_t + \gamma R_t q_{upper} + \rho distance_{it} + \nu_i + v_{it}, \quad (3)$$

where $gwlevel_{it}$ is the depth to groundwater table (meters of depth below the surface) for well i at time t , the variables q_{upper} and R_t are defined the same as above, $distance_{it}$ is the distance (in meters) from well i to the channel at time t , the term ν_i is a unique intercept for each well, and v_{it} is an error

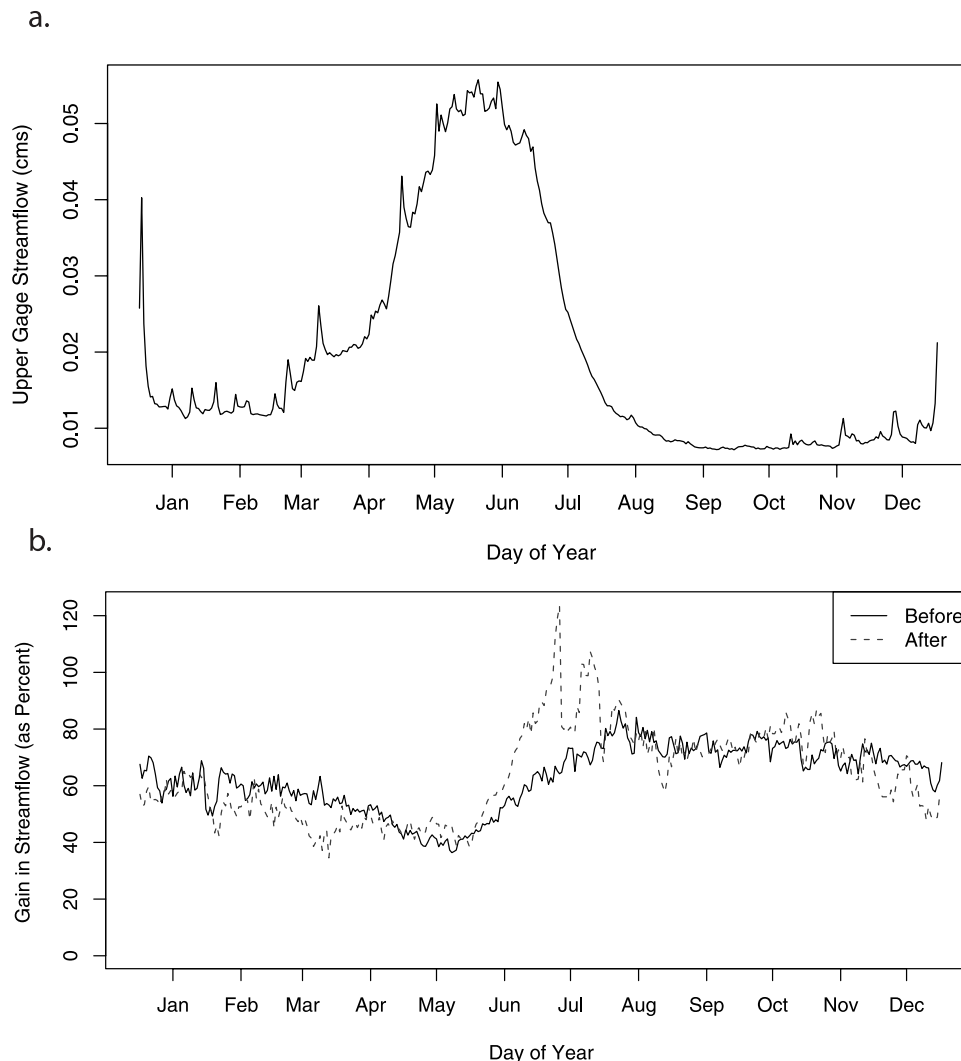


Figure 3. (a) Daily streamflow for the upper gauge (q_{upper}) averaged by day of year over water years 1990–2004 and (b) proportional difference (Δq_{rel}) in daily streamflow, averaged by day of year, for prerestoration and postrestoration periods.

term. The control variables specified in (3) have several advantages. The unique intercept term for each well, or fixed effect, enables us to control for any time-invariant, unobserved heterogeneity that explains the groundwater elevation at each well. The inclusion of $distance_{it}$ controls for changes in groundwater elevation that may be due to changes in the distance of the channel from each well after restoration. This is important because the position of individual wells relative to the stream channel changed following restoration, with the average distance to the channel decreasing by 30 m. We note that lateral distance is an approximation of groundwater flow path distance [Woessner, 2000]; however, it was the only readily available measure for the study site. Finally, the inclusion of q_{upper} accounts for the effect of streamflow on groundwater depth that is not due to either restoration or distance.

[24] The coefficients φ and γ are of primary interest, as they will provide estimates of the restoration effect on the overall groundwater depth at all wells and on the relationship between streamflow and groundwater depth. Once again, we account for serial correlation by reporting stan-

dard errors that are clustered on each well. As with the Newey-West approach described above, the clustering is robust to any form of potential serial correlation. But in this case, we assume a lag that covers the entire study period. We also experimented with specifications that included further interaction terms with distance (i.e., to determine whether the relationship with streamflow and the restoration effect varied with distance), but we do not report these models because none of the interactions yielded coefficients that were statistically significant.

3. Results and Discussion

3.1. Effects of Restoration on Streamflow

[25] Figure 3a shows mean streamflow by day of year for the upper gauge and depicts the seasonality of flow. Snowmelt-dominated flow begins in early March with the peak snowmelt period falling between mid-May and mid-June. Snowmelt recharge supports recession flow through July and into August, followed by a base flow period extending into late October. Periodic rainfall (or snowmelt) events do

Table 1. Linear Regression Results for Monthly Changes in Streamflow^a

Variable	Coefficient	OLS SE ^c	Newey-West SE ^b	
			15-Day Lag	30-Day Lag
β_{Jan}	0.211	0.015***	0.028***	0.032***
β_{Feb}	0.183	0.015***	0.027***	0.031***
β_{Mar}	0.165	0.015***	0.038***	0.044***
β_{Apr}	0.095	0.015***	0.030***	0.034***
β_{Jun}	0.116	0.015***	0.034***	0.037***
β_{Jul}	0.277	0.014***	0.048***	0.056***
β_{Aug}	0.363	0.014***	0.060***	0.074***
β_{Sep}	0.322	0.014***	0.044***	0.052***
β_{Oct}	0.334	0.015***	0.028***	0.031***
β_{Nov}	0.295	0.015***	0.023***	0.026***
β_{Dec}	0.262	0.015***	0.021***	0.023***
δ_{Jan}	-0.028	0.017	0.028	0.031
δ_{Feb}	-0.067	0.018***	0.029**	0.034*
δ_{Mar}	-0.110	0.017***	0.042***	0.047*
δ_{Apr}	-0.037	0.018**	0.041	0.048
δ_{May}	0.035	0.018**	0.027	0.028
δ_{Jun}	0.112	0.019***	0.059*	0.062*
δ_{Jul}	0.240	0.018***	0.102**	0.124*
δ_{Aug}	-0.009	0.018	0.069	0.082
δ_{Sep}	-0.002	0.019	0.058	0.070
δ_{Oct}	0.028	0.017	0.054	0.064
δ_{Nov}	0.034	0.018*	0.037	0.041
δ_{Dec}	-0.094	0.017***	0.021***	0.018*
θ_{wydev}	0.010	0.004**	0.014	0.018
Constant	0.408	0.010***	0.018***	0.020***
Observations	6179			
R ²	0.281			

^aThe dependent variable is Δq_{rel} . May is the omitted category for the month dummies. Single asterisk indicates significant at 90% level; double asterisk indicates significant at 95% level; triple asterisk indicates significant at 99% level.

^bNewey and West [1987] standard error.

^cOrdinary least squares standard error.

occur throughout the November to March period. While these effects are smoothed through multiyear averaging in this seasonal hydrograph, increased flow associated with several large December and January rain and rain-on-snow events can be seen.

[26] Figure 3b depicts the proportional gain in streamflow between upper and lower gauges for pre and post restoration periods, averaged by day of year. As expected, the effects of restoration differ seasonally and there are distinct responses during the peak snowmelt recharge period (mid-May through mid-June), the initial snowmelt recession period (June–July), and the late summer and early fall period (August–October). Changes in streamflow gain during the winter and peak snowmelt recharge periods show the expected tendency toward lower values (supporting hypothesis 1) in February–April and November–December. The largest relative changes in streamflow occur during the snowmelt recession period. Increased streamflow in the lower gauge relative to the upper gauge during this period is consistent with our hypothesis 2 that increased riparian storage and reduced riparian channel gradients support higher flow during snowmelt recession. These increases diminish throughout the summer and early fall base flow periods (hypothesis 3). Note that late summer and early fall base flow patterns are likely to combine two effects: First, toward the tail of the streamflow recession period, the impact of increased storage and slower drainage remains although it diminishes relative to June–July increases. Second, during this late summer and early fall period, higher groundwater levels may support increased

evapotranspiration losses leading to reduced flow. The combination of remaining effects of increased storage support for base flow and increases in evapotranspiration may effectively cancel each other leading to no observed change in late season base flow.

[27] We use the regression model represented by equation (2) to test whether the seasonal effects evident in Figure 3b are statistically significant. Table 1 reports the estimated coefficients. As noted above, coefficients δ denote changes in monthly differences between gauges following restoration and are the primary focus of the analysis. The coefficients β provide estimates of the monthly differences between gauges that are constant from 1990 to 2004. Coefficients β differ across months and are statistically significant for all months. Monthly differences show that there are seasonal differences in the relationship between the upper and lower gauges. It is also worth noting that year-to-year differences in the timing and magnitude of snowmelt inputs, as reflected in the deviation of total water year streamflow from the norm ($wydev_t$), do not have a significant effect on relative streamflow differences.

[28] The estimated coefficients δ support the hypothesis (hypothesis 2) that during the recession period the relative gain in flow between the upper and lower gauges will increase. There is a statistically significant increase in percent gain for both June and July following restoration, and the July increase is the largest monthly effect. The magnitudes of these increases are substantial: the increase in flow at the lower gauge, relative to the upper gauge, is 11% in June and 24% in July. Note in Figure 3b that June and July are high-

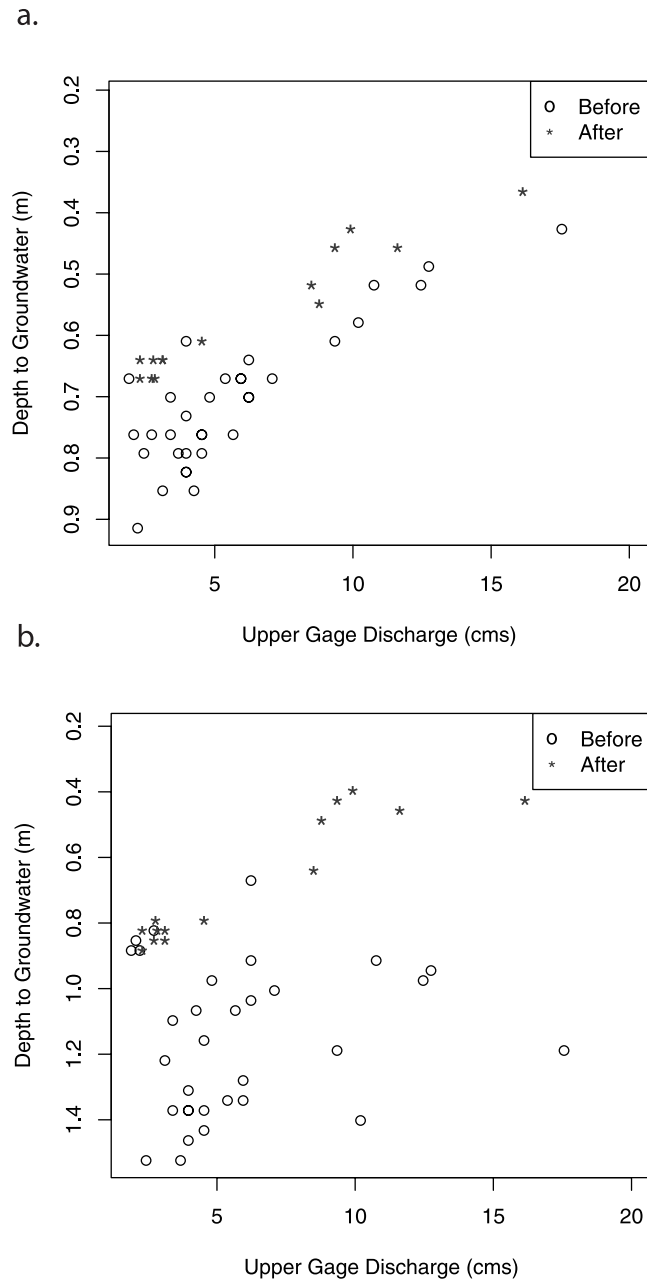


Figure 4. Depth to groundwater versus discharge at the upper gauge for prerestoration and postrestoration periods for (a) groundwater well T1W2 and (b) groundwater well T5W3.

flow periods; thus these relative increases correspond to substantial changes in absolute flow volumes.

[29] Accounting for serial autocorrelation using with the Newey-West standard errors decreases the level of statistical significance of the changes in June and July, from 99% to 95% or 90%, depending on the size of the lag. We assume that a significance level greater than 90% reflects a meaningful change in streamflow behavior, and thus the estimated changes in streamflow for June and July are robust to the effects of serial autocorrelation.

[30] During the winter and early snowmelt periods, relative streamflow generally decreases, as predicted by hypothesis 1, although the coefficients are not always statistically significant. The decrease in streamflow is statistically significant in February and March, even with the

30-day lag to account for serial correlation. In August through October, there is no statistically significant effect of restoration on streamflow.

3.2. Effects of Restoration on Groundwater

[31] Figure 4 shows the relationship between depth to groundwater and discharge for two wells, T1W2 and T5W3, for which the distance to the channel increased (22 to 40 m) and decreased (48 to 28 m) respectively following restoration. As expected, overall depth to groundwater decreases, and depth to groundwater values for a given streamflow value are lower following restoration. The slope of the discharge-groundwater relationship, however, does not appear to change. A high groundwater table (lower depth)

Table 2. Linear Regression Results for Changes in Groundwater Levels^a

Variable	Coefficient	OLS SE ^b	Clustered SE
$\lambda_{q_{upper}}$	-0.027	0.003***	0.005***
φ_R	-0.324	0.029***	0.052***
$\gamma_{Rq_{upper}}$	0.003	0.003	0.004
$\rho_{distance}$	0.0001	0.0003	0.0002
Constant	1.144	0.029***	0.065***
Well fixed effects (18)	yes		
Observations	842		
R^2 (within)	0.47		

^aThe dependent variable is $gwlevel_{it}$. Single asterisk indicates significant at 90% level; double asterisk indicates significant at 95% level; triple asterisk indicates significant at 99% level.

^bOLS SE, ordinary least squares standard error.

following restoration is consistent with our conceptual model that restoration increases storage in the riparian zone.

[32] Table 2 reports the results of regression model (3) applied using all available groundwater wells (as shown in Figure 2). As expected, depth to groundwater is significantly related to streamflow, with lower streamflow corresponding to greater groundwater depths. Depth to groundwater also increases with increasing distance from the channel, although this effect is not statistically significant. The depth to groundwater decreases significantly with restoration (R_t), but there is no significant change in the relationship between streamflow and groundwater table elevation ($R_t q_{upper}$). The decrease in depth to groundwater is substantial. For example, mean August base flow is 0.01 cm. At this August base flow value, for a well 0.5 m from the channel, the model estimates a decrease from 1.1 to 0.8 m in groundwater depth following restoration. Mean depth to groundwater for all sample dates and wells prior to restoration was 1.4 m, and 1.0 m following restoration.

[33] Riparian and aquatic ecosystems are dependent on the timing and magnitude of groundwater levels and streamflow. Thus changes to hydrologic regimes have been shown to impact specific organisms as well as overall ecosystem health [Poff *et al.*, 1997; Kauffman *et al.*, 1997]. Our analysis of paired gauge streamflow and groundwater well measurements provides evidence of a strongly seasonal pattern of hydrologic impacts of restoration for the snowmelt-dominated Trout Creek. Changes in streamflow, particularly the statistically significant increases in recession flow during June and July, indicate that restoration has led to greater storage and slower drainage of near-channel areas. This interpretation is further supported by significant decreases in depth to groundwater in riparian zone wells. The seasonal pattern of results suggests that the primary impact of restoration on streamflow regimes occurs during the snowmelt recession period. Increases during the recession period (both absolute and relative) diminish as flow magnitude decreases throughout the summer.

[34] Changes to groundwater dynamics, however, are maintained throughout the summer period. One of the primary goals of channel restoration projects, including Trout Creek, is to reduce the dewatering of riparian areas and the associated impacts on the structure and function of riparian ecosystems. Decreases in depth to groundwater across a range of discharge conditions in Trout Creek suggest that restoration has successfully improved riparian

water availability for vegetation. In a report by *Western Botanical Services, Inc.* [2003], a general trend toward a wetter, more hydric plant community was observed throughout the Trout Creek meadow, and most of the mesic species present before restoration exhibited declines in cover values. By the time the vegetative survey had been completed in 2002 vegetative cover of native perennial forbs had almost doubled. An increase in plant diversity and vigor had occurred despite droughtlike conditions in the preceding years. At the time of the survey, willow densities had not changed, but were still expected to increase as the new cuttings grew and matured. Initial postproject evaluation also found evidence of increases in invertebrate and fish populations [SHG, 2004; Wigart, 2004]. We note that the restoration of Trout Creek was an intensive undertaking that included reworking of both the channel and riparian zone was guided by geomorphic principles. Other less intensive restoration projects which focus solely on the stream channel may not yield comparable changes in hydrologic regimes.

[35] Underlying variability in hydrologic and climatic processes coupled with inadequate monitoring, infrequent reporting, and the relatively low number of adequate restoration sites continues to limit the availability of data to support restoration research [Moerke and Lamberti, 2004]. In an analysis of a restoration project in Idaho, for example, Klein *et al.* [2007] found no statistically significant changes to several hydrologic variables following restoration. They attribute the lack of statistical significance to small sample size and high interannual variability. These are common problems in postrestoration assessment, where monitoring data is limited and climate drivers of hydrologic variables tend to show significant interannual and seasonal variation. Aggregation of streamflow data into monthly or annual time scales further limits data availability. Aggregation, however, is often necessary in order to avoid the problem of serial autocorrelation in discharge measurements. In this study, the use of the Newey-West approach supported the use of daily data by accounting for autocorrelation. This study demonstrates the utility of the Newey-West nonparametric approach for robust statistical inference and offers an alternative to autoregressive methods commonly used in hydrologic science to account for serial autocorrelation. Unlike autoregressive methods, Newey-West does not require assumptions to be made about the form of the serial autocorrelation and thus is likely to be robust across a wider variety of situations. Assessment in this study was also supported by the availability of paired gauges above and below the restoration site. Paired gauges are not routinely included in restoration assessment planning, and this study demonstrates the potential utility of the approach.

4. Conclusions

[36] One of the primary objectives of reengineering the channel in Trout Creek was to improve ecologic function by increasing summer water availability in riparian areas. Analysis of streamflow and groundwater data in this study suggests that restoration did alter the relevant hydrologic processes and that these effects were significant, even given substantial climatic variation. Restoration projects such as the Trout Creek are likely to continue to be one of the main thrusts of restoration activities. Snowmelt-dominated envi-

ronments, where human impacts were once limited, have experienced significant development pressures in the past decades. Restoration projects will likely continue to receive significant public and private funding in these areas and the need for monitoring and assessment will continue [Cobourn, 2006; Bernhardt et al., 2005]. Statistical techniques that increase extractable information from available data are important assessment tools. This study demonstrates the utility of paired gauge instrumentation and the Newey-West approach to account for serial autocorrelation, in addition to documenting postrestoration hydrologic change across a wide range of flow conditions. Further studies are still needed to provide a foundation of research on hydrologic effects of channel restoration in a wide range of geographic settings.

References

- Bales, R. C., N. P. Molotch, T. H. Painter, M. D. Dettinger, R. Rice, and J. Dozier (2006), Mountain hydrology of the western United States, *Water Resour. Res.*, *42*, W08432, doi:10.1029/2005WR004387.
- Bernhardt, E. S., et al. (2005), Ecology: Synthesizing U.S. river restoration efforts, *Science*, *308*(5722), 636–637, doi:10.1126/science.1109769.
- Best, A., L. Zhang, T. McMahon, A. Western, and R. Vertessy (2003), A critical review of paired catchment studies with reference to seasonal flows and climatic variability, in *CSIRO Land Water Tech. Rep. 25/3*, Murray-Darling Basin Comm. and Commonw. Sci. Ind. Res. Organ., Melbourne, Victoria, Australia.
- Booth, D. B. (2005), Challenges and prospects for restoring urban streams: A perspective from the Pacific Northwest of North America, *J. North Am. Benthol. Soc.*, *24*(3), 724–737.
- Bosch, J. M., and J. D. Hewlett (1982), A review of catchment experiments to determine the effects of vegetation changes on water yield and evapotranspiration, *J. Hydrol.*, *55*, 3–23, doi:10.1016/0022-1694(82)90117-2.
- Cobourn, J. (2006), How riparian ecosystems are protected at Lake Tahoe, *J. Am. Water Resour. Assoc.*, *42*(1), 35–43, doi:10.1111/j.1752-1688.2006.tb03821.x.
- De Laney, T. A. (1995), Benefits to downstream flood attenuation and water quality as a result of constructed wetlands in agricultural landscapes, *J. Soil Water Conserv.*, *50*(6), 620–626.
- Goodwin, C. N., C. P. Hawkins, and J. L. Kershner (1997), Riparian restoration in the western United States: Overview and perspective, *Restor. Ecol.*, *5*(4S), 4–14, doi:10.1111/j.1526-100X.1997.00004.x.
- Hillman, G. R. (1998), Flood wave attenuation by a wetland following a beaver dam failure on a second-order boreal stream, *Wetlands*, *18*(1), 21–34.
- Kauffman, J. B., R. L. Beschta, N. Otting, and D. Lytjen (1997), An ecological perspective of riparian and stream restoration in the western United States, *Fisheries*, *22*(5), 12–24, doi:10.1577/1548-8446(1997)022<0012:AEPORA>2.0.CO;2.
- Klein, L., S. R. Clayton, J. R. Alldredge, and P. Goodwin (2007), Long-term monitoring and evaluation of the lower Red River Meadow restoration project, Idaho, U.S.A., *Restor. Ecol.*, *15*(2), 223–239, doi:10.1111/j.1526-100X.2007.00206.x.
- Knowles, N., and D. Cayan (2002), Potential effects of global warming on the Sacramento/San Joaquin watershed and the San Francisco estuary, *Geophys. Res. Lett.*, *29*(18), 1891, doi:10.1029/2001GL014339.
- Mant, J., and M. Janes (2005), Restoration of rivers and floodplains, in *Restoration Ecology: The New Frontier*, edited by J. van Andel and J. Aronson, pp. 141–157, Blackwell, Malden, Mass.
- Moerke, A. H., and G. A. Lamberti (2004), Restoring stream ecosystems: Lessons from a midwestern state, *Restor. Ecol.*, *12*(3), 327–334, doi:10.1111/j.1061-2971.2004.0340.x.
- National Research Council (NRC) (1992), *Restoration of Aquatic Ecosystems: Science, Technology, and Public Policy*, Natl. Acad. Press, Washington, D.C.
- Newey, W. K., and K. D. West (1987), A simple, positive semi-definite heteroskedasticity and autocorrelation consistent covariance matrix, *Econometrica*, *55*, 703–708, doi:10.2307/1913610.
- Palmer, M. A., et al. (2005), Standards for ecologically successful river restoration, *J. Appl. Ecol.*, *42*, 208–217, doi:10.1111/j.1365-2664.2005.01004.x.
- Poff, N. L., J. D. Allan, M. B. Bain, J. R. Karr, K. L. Prestegard, B. D. Richter, R. E. Sparks, and J. C. Stromberg (1997), The natural flow regime, *BioScience*, *47*(11), 769–784, doi:10.2307/1313099.
- Ralph, S. C., and G. C. Poole (2002), Putting monitoring first: Designing accountable ecosystem restoration and management plans, in *Restoration of Puget Sound Rivers*, edited by D. R. Montgomery, S. Bolton, D. B. Booth, and L. Wall, pp. 226–245, Univ. of Wash. Press, Seattle.
- Reeve, T., J. Lichatwoich, W. Towey, and A. Duncan (2006), Building science and accountability into community-based restoration: Can a new funding approach facilitate effective and accountable restoration?, *Fisheries*, *31*(1), 17–24, doi:10.1577/1548-8446(2006)31[17:BSAaic]2.0.CO;2.
- Smakhtin, V. U. (2001), Low flow hydrology: A review, *J. Hydrol.*, *240*, 147–186, doi:10.1016/S0022-1694(00)00340-1.
- Swanson Hydrology and Geomorphology (SHG) (2004), Trout Creek meadow restoration: Geomorphic monitoring final report 2001–2003, Santa Cruz, Calif.
- Ward, J. V., K. Tockner, D. B. Arscott, and C. Claret (2002), Riverine landscape diversity, *Freshwater Biol.*, *47*, 517–539, doi:10.1046/j.1365-2427.2002.00893.x.
- Western Botanical Services, Inc. (2003), *Post construction vegetation monitoring report: Trout Creek stream restoration and wildlife enhancement project*, prepared for the city of South Lake Tahoe, Reno, Nev.
- Wigart, R. (2004), Trout Creek final report summary. City of South Lake Tahoe.
- Woessner, W. W. (2000), Stream and fluvial plain ground water interactions: Re-scaling hydrogeologic thought, *Ground Water*, *38*(3), 423–429, doi:10.1111/j.1745-6584.2000.tb00228.x.
- Wohl, E., P. L. Angermeier, B. Bledsoe, G. M. Kondolf, L. MacDonnell, D. M. Merritt, M. A. Palmer, N. L. Poff, and D. Tarboton (2005), River restoration, *Water Resour. Res.*, *41*, W10301, doi:10.1029/2005WR003985.
- Wooldridge, J. M. (2002), *Econometric Analysis of Cross Section and Panel Data*, MIT Press, Cambridge, Mass.
- Worrall, F., W. T. Swank, and T. P. Burt (2003), Changes in stream nitrate concentrations due to land management practices, ecological succession, and climate: Developing a systems approach to integrated catchment response, *Water Resour. Res.*, *39*(7), 1177, doi:10.1029/2000WR000130.

M. Kotchen and C. Tague, Bren School of Environmental Science and Management, University of California, Santa Barbara, Santa Barbara, CA 93106, USA. (kotchen@bren.ucsb.edu; ctague@bren.ucsb.edu)

S. Valentine, Department of Geography, Lake Tahoe Community College, Lake Tahoe, CA 96150, USA. (valentine@lccc.edu)